Magmatic and metamorphic evolution of the Stolzburg Block, Barberton Granitoid-Greenstone Terrain

by

Moritz Mühlberg

Dissertation presented for the degree of Doctor of Philosophy in the Faculty of Science at Stellenbosch University. This dissertation has also been presented at UJM St. Etienne in terms of a joint degree agreement.

The financial assistance of the National Research Foundation (NRF) towards this research is hereby acknowledged. Opinions expressed and conclusions arrived at, are those of the author and are not necessarily to be attributed to the NRF.

Supervisor: Dr Gary Stevens, Stellenbosch University (South Africa)

Co-supervisor: Dr Jean-François Moyen, Université de Saint-Étienne (France)

Co-supervisor: Dr Alex Kisters, Stellenbosch University (South Africa)

December 2022

DECLARATION

By submitting this dissertation electronically, I declare that the entirety of the work contained therein is my own, original work, that I am the sole author thereof (save to the extend explicitly otherwise stated), that reproduction and publication thereof by Stellenbosch University will not infringe any third-party rights and that I have not previously in its entirety or in part submitted it for obtaining any qualification. This dissertation has also been presented at Université Jean Monnet, Saint-Étienne in terms of a joint-degree agreement.

This dissertation includes one original paper published in a peer-reviewed journal and one manuscript in preparation for submission to a peer-reviewed journal. The development and writing of the papers (published and unpublished) were the principal responsibility of myself and, for each of the cases where this is not the case, a declaration is included in the dissertation indicating the nature and extent of the contributions of co-authors. Translation of the abstract into French was performed by Hugo Dominguez and into Afrikaans by Suné Butler.

Date: December 2022

Abstract

The processes that formed and shaped the first stable continents in the Archean are poorly constrained for various reasons, including the scarcity of well-preserved, unaltered rock sequences and the lack of modern equivalents of lithologies that are typical for the Archean. This has led to the emergence of various geodynamic models that try to explain the unique features of the Archean crust, but too often rely on assumptions on the thermal state of the crust, in particular of the felsic crust.

This thesis is an investigation of the igneous and metamorphic history of the Stolzburg Block, an area comprised of tonalite-trondhjemite-granodiorite (TTG) and amphibolite-facies supracrustal rocks, located in the Barberton Granitoid Greenstone Terrain (BGGT) in South Africa. The thermal history of a well-preserved piece of felsic Archean crust is studied through a combination of field work and geochemical, geochronological and petrological analyses on TTG and related rocks, with the aim of providing robust constraints on the thermal state of the Archean crust to improve geodynamic models.

Uranium-lead (U-Pb) thermochronology on apatite grains has revealed four distinct groups of $^{207}Pb/^{206}Pb$ ages that are present throughout the Stolzburg Block. The three oldest groups of U-Pb apatite ages overlap with the time of emplacement of TTG plutons (~3450 Ma), of regional metamorphism (~3230-3200 Ma) and of intrusion of granitic plutons (~3105 Ma), while the ~2820 Ma group indicates a previously undiscovered thermal event. The preservation of the ~3450 Ma apatite ages indicates that the Stolzburg Block has not been heated above ~400-500 °C after the emplacement of TTG plutons – at least not for a prolonged period.

Trace-element and strontium isotope analyses of the dated apatite grains show homogenous compositions regardless of age and $^{87}Sr/^{86}Sr$ ratios that are within uncertainty identical to the initial $^{87}Sr/^{86}Sr$ ratio of the respective bulk rock, and these features are being interpreted as primary igneous signatures. This indicates that the different groups of U-Pb apatite ages are not the result of new growth but rather of partial resetting of the U-Pb systematics through heating. Zirconium-in-titanite and titanium-in-zircon thermometry gives temperatures of ~700 °C for magmatic titanite and ~650 °C for metamorphic titanite and zircon from TTG samples, which is in the same range as the reported metamorphic conditions recorded by the associated supracrustal rocks at ~3230-3200 Ma. While no chronological constraints are available for the temperature estimates of the TTG rocks, a shared history between TTG plutons and greenstones can be inferred from the intrusive relationship between the two. The preservation of ~3450 Ma U-Pb signatures in apatite grains shows that, regardless of the timing of heating to ~650 °C, the heating was very short-lived (< 1 million years).

This work demonstrates that the felsic Archean crust – at least the section preserved in the BGGT – was relatively cool and stable, and that any heating of the TTG plutons was short-lived. The results of this study argue against a prolonged radiogenic heating of TTG crust and a partial convective overturn of the Archean crust, as proposed by some geodynamic models.

Résumé

Les processus responsables de la formation des premiers continents stables de l'Archéen sont mal connus pour diverses raisons, notamment la rareté des séquences rocheuses bien préservées et le manque d'équivalents modernes des lithologies typiques de l'Archéen. Ceci a conduit à l'émergence de divers modèles géodynamiques qui tentent d'expliquer les caractéristiques de la croûte archéenne, mais qui reposent souvent sur des hypothèses concernant l'état thermique de la croûte, en particulier de la croûte felsique.

Cette thèse investigue l'histoire ignée et métamorphique du bloc de Stolzburg, une zone composée de roches supracrustales de faciès tonalite-trondhjemite-granodiorite (TTG) et amphibolite, située dans le Barberton Granitoid Greenstone Terrain (BGGT) en Afrique du Sud. L'histoire thermique d'un morceau bien préservé de croûte archéenne felsique est étudiée par une combinaison de travaux de terrain et d'analyses géochimiques, géochronologiques et pétrologiques sur les TTG et les roches adjacentes, dans le but de fournir des contraintes robustes sur l'état thermique de la croûte archéenne pour améliorer les modèles géodynamiques.

La thermochronologie à l'uranium-plomb (U-Pb) sur les grains d'apatite a révélé quatre groupes distincts d'âges $^{207}Pb/^{206}Pb$ qui sont présents dans tout le bloc de Stolzburg. Les trois groupes les plus anciens d'apatite chevauchent avec la mise en place des plutons de TTG (~3450 Ma), du métamorphisme régional (~3230-3200 Ma) et de l'intrusion de plutons granitiques (~3105 Ma), tandis que le groupe ~2820 Ma indique un événement thermique décrit pour la première fois. La préservation des âges d'apatite de ~3450 Ma indique que le bloc de Stolzburg n'a pas atteint une température supérieure à ~400-500 °C après la mise en place des plutons de TTG, du moins pas pendant une période prolongée.

Les analyses isotopiques des éléments traces et du strontium des grains d'apatite datés montrent des compositions homogènes indépendamment de l'âge et des rapports $^{87}Sr/^{86}Sr$ qui sont, dans la limite de l'incertitude, identiques au rapport $^{87}Sr/^{86}Sr$ initial de la roche totale, et ces caractéristiques sont interprétées comme des signatures ignées primaires. Ceci indique que les différents groupes d'âges U-Pb de l'apatite reflètent une réinitialisation thermique partielle du système U-Pb. La thermométrie du zirconium dans le sphène et du titane dans le zircon donne des températures de ~700 °C pour le sphène magmatique et de ~650 °C pour le sphène et le zircon métamorphiques des échantillons de TTG. Ces températures sont dans la même gamme que les conditions métamorphiques préservées par les roches supracrustales associées à ~3230-3200 Ma. La préservation des signatures U-Pb de ~3450 Ma dans les grains d'apatite montre que, quel que soit le moment de l'anomalie thermique à ~650 °C, celui-ci a été de très courte durée (< 1 million d'années).

Ce travail démontre que la croûte archéenne felsique - du moins la section préservée dans le BGGT - était relativement fraîche et stable, et que toutes anomalies thermiques des plutons de TTG étaient de courte durée. Les résultats de cette étude plaident contre un apport thermique radiogénique prolongé de la croûte TTG et un renversement convectif partiel de la croûte archéenne, comme le proposent certains modèles géodynamiques.

Opsomming

Die prosesse wat die eerste stabiele kontinente in die Argeaanse tydperk gevorm het, is om verskeie redes swak beperk, insluitend die skaarsheid van goed gepreserveerde, onveranderde rotsreekse en die gebrek aan moderne ekwivalente van kenmerkende litologieë vir die Argeaanse tydperk. Dit het gelei tot die ontstaan van verskeie geodinamiese modelle wat poog om die unieke kenmerke van die Argeaanse kors te verduidelik, maar wat te dikwels staatmaak op aannames oor die termiese toestand van die kors, in die besonder van die felsiese kors.

Hierdie tesis is 'n ondersoek na die stollings- en metamorfiese geskiedenis van die Stolzburgblok, 'n gebied wat bestaan uit tonaliet-trondhjemiet-granodioriet (TTG) plutone en amfiboliet-facies suprakrustalgesteentes, geleë in die Barberton Granitoïed Groensteen Terrein (BGGT) in Suid-Afrika. Die termiese geskiedenis van 'n goed bewaarde stuk felsiese Argeaanse kors word bestudeer deur 'n kombinasie van veldwerk en geochemiese, geochronologiese en petrologiese ontledings van TTG en verwante gesteentes, met die doel om robuuste beperkings op die termiese toestand van die Argeaanse kors vas te stel en sodoende geodinamiese modelle te verbeter.

Uraan-lood (U-Pb) termochronologie op apatietkorrels het vier afsonderlike groepe van $^{207}Pb/^{206}Pb$ ouderdomme aan die lig gebring wat regdeur die Stolzburg-blok teenwoordig is. Die drie oudste groepe van U-Pb apatiet ouderdomme oorvleuel met die tyd van indringing van TTG plutone (~3450 Ma), van streeksmetamorfose (~3230-3200 Ma) en die indringing van granitiese plutone (~3105 Ma), terwyl die ~2820 Ma groep op 'n voorheen onontdekte termiese gebeurtenis dui. Die preservering van die ~3450 Ma apatiet ouderdomme dui aan dat die Stolzburg Blok nie bo ~400-500 °C verhit is na die plasing van TTG-plutone nie – ten minste nie vir 'n lang tydperk nie.

Spoorelement- en strontiumisotoopontledings van die gedateerde apatietkorrels toon homogene samestellings ongeag ouderdom en $^{87}Sr/^{86}Sr$-verhoudings wat binne onsekerheid identies is aan die aanvanklike $^{87}Sr/^{86}Sr$-verhouding van die onderskeie heelrots, en hierdie kenmerke word geïnterpreteer as primêre stollingseienskappe. Dit dui daarop dat die verskillende groepe U-Pb apatiet ouderdomme nie die gevolg is van nuwe groei nie, maar liewer die gedeeltelike terugstelling van die U-Pb sistematiek deur verhitting. Sirkonium-in-titaniet en titanium-in-sirkon termometrie gee temperature van ~700 °C vir magmatiese titaniet en ~650 °C vir metamorfiese titaniet en sirkoon van TTG-monsters, wat in dieselfde omvang is as die metamorfiese toestande wat deur die geassosieerde suprakrustale gesteentes by ~3230-3200 Ma geraporteer word.

Alhoewel geen chronologiese beperkings beskikbaar is vir die temperatuurskattings van die TTG-gesteentes nie, kan 'n gedeelde geskiedenis tussen TTG-plutone en groenstene afgelei word uit die indringende verhouding tussen die twee. Die preservering van ~3450 Ma U-Pb-eienskappe in apatietkorrels toon dat, ongeag die tyd van verhitting tot ~650 °C, was die verhitting baie kortstondig (< 1 miljoen jaar).

Hierdie werk demonstreer dat die felsiese Argeaanse kors – ten minste die gedeelte wat in die BGGT bewaar is – relatief koel en stabiel was, en dat enige verhitting van die TTG-plutone van korte duur was. Die resultate van hierdie studie argumenteer teen 'n langdurige radiogene verhitting van TTG-kors en 'n gedeeltelike konvektiewe omslag van die Argeaanse kors, soos voorgestel word deur sommige geodinamiese modelle.

Acknowledgements

I owe my deepest gratitude to my supervisors, Gary Stevens, Jean-François (Jeff) Moyen and Alex Kisters, for giving me the opportunity to take on this project under their supervision. A big thank you to Gary for coming up with the project, for giving me the freedom to take this project into the direction I feel the most comfortable in, for discussions and for always being optimistic. Thank you, Jeff, for giving me the best introduction to the Barberton geology I could have wished for, for discussions and for your encouragements. And thank you, Alex, for discussions. I would like to thank all three of you for your patience with me.

The biggest thank you goes to my wife Suné: Thank you for your continuous support, for always believing in me and for giving me the strength to go on. Thank you for your help with translating the abstract into Afrikaans. And thank you for being my best friend and my life partner. For being the perfect match. For being you. I could not have done this without you.

I would like to thank my mother for her emotional and financial support, and for all the delicious recipes that make any place feel like home. Thank you to my father for his love and support.

I also would like to thank my brothers Felix and Igor for the distractions and for begrudgingly accepting whenever I did not have time for you.

At Stellenbosch University, I would like to thank Mareli Grobbelaar-Moolman, Madeleine Frazenburg and Riana Rossouw for all your help with sample preparation and analyses. A big thank you to Jeanne Taylor for your assistance with my zircon analyses and for giving me the opportunity to join you for field work in Eswatini. Thank you to Laura Bracciali for all your help with Iolite. I also would like to thank the administrative and technical staff at the Department of Earth Sciences, namely Loxie Conradie, Gillian Strydom, George Olivier and Fiazel Timmey, and at the International Office, namely Dorothy Stevens, Linda Uys and Grant Leukes.

On the Brazilian side, I would like to thank Cris Lana for giving me the opportunity to experience Ouro Preto, and Cris and Ana Alkmin for all the analyses. Thank you to Guilherme “Marcha” de Oliveria Gonçalves for setting me up with a room at UPA for my stay at UFOP, to Mathias Schannor and Kai for letting me experience the night life of Ouro Preto and to Rafael Barbosa for his assistance during field work.

On the French side, I would like to thank Oscar Laurent for discussions in the field and for taking me to that infamous derby, igniting a green fire inside of me. I would like to thank the

ASSE for actually playing a decent season while I was there and the GA92 for the incredible atmosphere. Thank you to Lucas Cassini for many discussions and nights out in Sainté. I also want to thank Laurance Chaugne at Le Littré for setting me up with a room to stay in during my time in St. Etienne and for all her assistance. A big thank you to Emilie Bruand for her guidance and for giving me the opportunity to come to Clermont-Ferrand. Thank you to Jean-Marc Hénot and Jean-Luc Devidal for your assistance with the analytical instruments. I would like to thank Hugo Dominguez for translating the abstract into French and also thank Gautier Nicoli and Hugo for reviewing the grammar on my poster.

A massive thank you to Matthew (Matt) Mayne for making me feel welcome and accepted in Stellenbosch from day one, for introducing me to the night life in Stellenbosch and to many lovely people, for hikes big and small, for endless discussions about geology and far beyond, and simply for being a good friend. Thank you to Matt, Arnu and Tom for Canyon.

I would like to thank my old housemates James and Chantelle for the perfect accommodation, for braais and beers and especially for Kitty, Benji and Frank the Tank. Thank you to the Keens for letting me join their family Christmas. Thank you Eben, Govind and Hugo for being good housemates.

Last but not least a big thank you to everybody whom I forgot to mention here.

This research was carried out as part of the France-South Africa scientific collaboration IPR BuCoMO, a collaborative research project funded by the French Centre national de la recherche scientifique (CNRS) and the South African National Research Foundation (NRF). Financial support was provided by NRF funding to Gary Stevens via the SARChI program, as well as through a PhD bursary granted to me for three years and three months, a further five months of departmental bursary granted from the Stellenbosch University Department of Earth Sciences, and Campus France funding for the duration of my stays in Saint-Étienne.

Table of Contents

Page

List of Figures

List of Tables

Chapter 6

Chapter 7

Chapter 1: General introduction

1.1 TTG petrogenesis and Archean geodynamics

There is an ongoing debate on the nature of geodynamic processes that shaped Earth's first stable continents. The Hadean zircon record indicates that felsic crust may have already existed in the first few 100 million years of Earth's history (e.g. Blichert-Toft and Albarède, 2008; Faltys and Wielicki, 2020; Harrison, 2009). However, these oldest remnants are only found as detrital zircons (e.g. Cavosie et al., 2004; Compston and Pidgeon, 1986) and their source rocks have not been preserved. The oldest preserved rock found to date has formed at the Hadean-Paleoarchean transition (Bowring and Williams, 1999) and most of the oldest preserved stable continental nuclei have formed during the Eo- to Paleoarchean (e.g. Amelin et al., 2000; Kröner et al., 2018; Nutman et al., 1999). These Archean cratons are typically defined by (predominantly mafic) volcanosedimentary successions comprised of a series of predominantly mafic supracrustal rocks arranged in greenstone belts and of tonalite-trondhjemite-granodiorite (TTG) rocks. Greenstone belts and TTGs are arranged in a so called dome-and-keel pattern (Kisters and Anhaeusser, 1995). The supracrustal rocks of the greenstone belts are defined by greenschist- to amphibolite-facies metamorphism and are often heavily folded.

The TTG rocks can range from pristine plutons through gneisses to migmatitic banded gneisses (Moyen and Martin, 2012), with the latter being the most common and only rare instances of preserved primary TTG plutons. The petrogenesis of TTG rocks in the Archean is not fully understood. Based on experimental petrology, it is generally assumed that TTGs form through the melting of metamorphosed basalt in the garnet stability field, i.e. garnet-amphibolite or eclogite, at depth (Moyen and Martin, 2012). Based on geochemistry, Moyen (2011) identified three subgroups of TTG rocks that are thought to have been generated at different depths of melting: low-pressure (P) TTGs corresponding to melting of a plagioclase-rich garnet-amphibolite at ca. 10-12 kbar, medium-P TTGs generated through melting of plagioclase-free, garnet-rich amphibolite at ca. 15 kbar, and high-P TTGs corresponding to melting of rutile-bearing eclogite at ≥20 kbar.

According to Moyen and Martin (2012), a dehydration melting triggered by the destabilization of hydrous minerals in a water-absent system is "*the most commonly investigated scenario, as the general consensus is that fluid-present melting at >10 kbar (i.e. garnet stability field) is unlikely in nature*", but petrological experiments and numerical modeling have demonstrated that water-saturated melting of an eclogite at depth can produce a melt composition akin to high-P TTG (Laurie and Stevens, 2012) and is possible at hotter Archean mantle temperatures (Laurie et al., 2013). On the other hand, it has recently been shown by Mayne et al., (2020) that water-fluxed melting of quartz and plagioclase in a K-feldspar-free assemblage can also

produce considerable volumes of trondhjemitic melt at low temperatures (ca. 710-750 °C). However, all of the melting scenarios mentioned above have been derived under the assumption that TTG rocks represent the melt composition at source. An alternative model was recently proposed by Laurent et al. (2020), in which the TTG rocks represent plagioclase cumulates that have been drained of interstitial melt by silicic volcanism. Based on this proposed genetic link between TTG and coeval felsic volcanic rocks, Laurent et al. (2020) suggest that the "*compositional diversity of TTGs could derive from the upper crustal differentiation of a single, tonalitic magma*" formed though intracrustal melting.

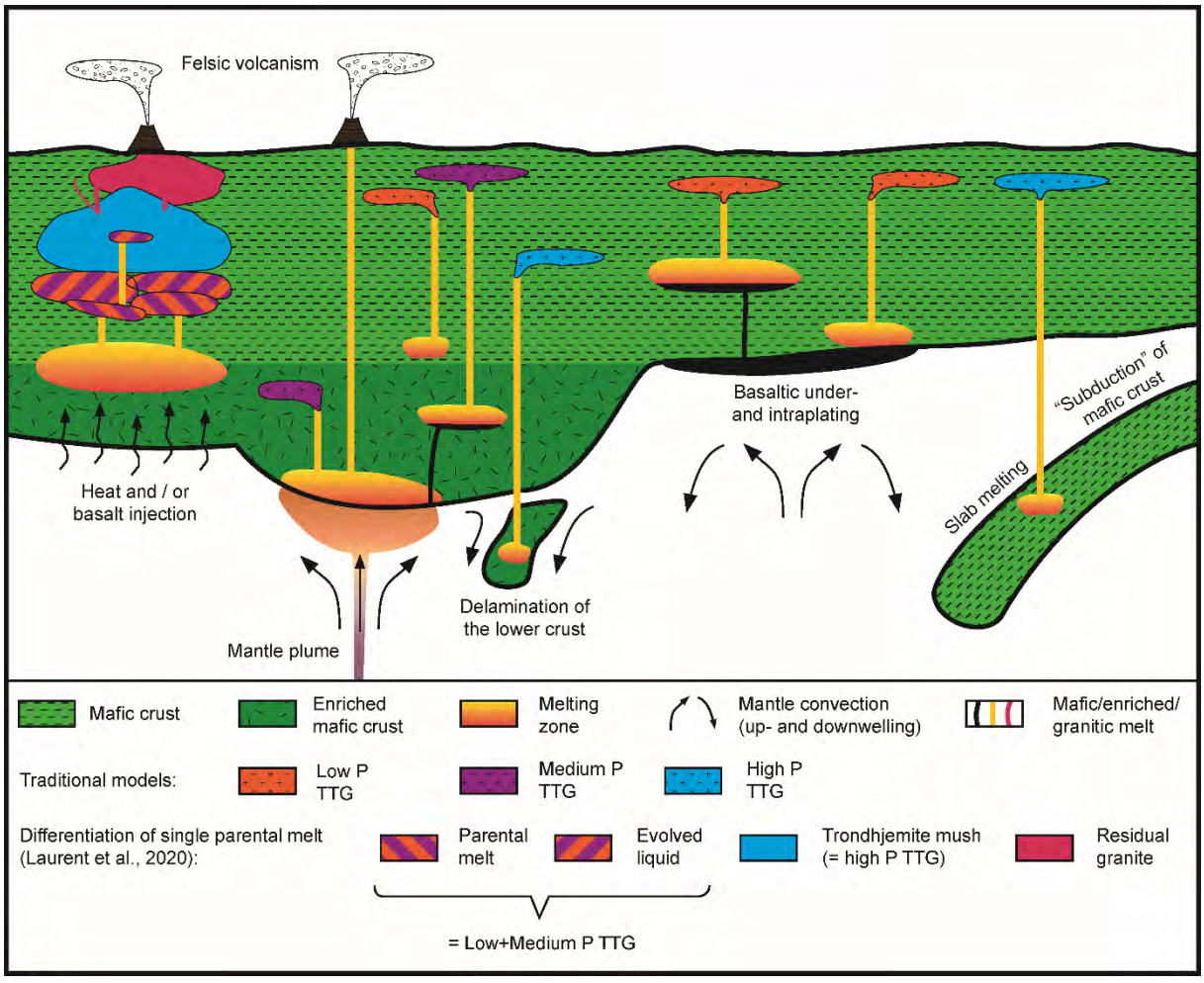

Fig. 1.1. Compilation of different ways of generating tonalite-trondhjemite-granodiorite (TTG) crust. See text for details and references.

A schematic illustration of different ways of generating TTG melts is given in Figure 1.1. In-situ melting of the crust can occur via heat injection through basaltic under- and intraplating (e.g. Fig. 11a of Van Kranendonk et al., 2015), via (post)orogenic processes, rifting or via plume activity, generating low- and medium-P TTGs and felsic volcanism. The burial of mafic crust to facilitate the generation of high-P TTGs can be ascribed to subduction (s.l.) (e.g. Moyen and

Laurent, 2018) or to delamination of the dense lower crust (e.g. Rudnick, 1995). Alternatively, differentiation of a single parental melt may generate all types of TTG and felsic volcanism in a succession of fractionation and loss of interstitial liquid (Laurent et al., 2020).

The difficulties of understanding and reconstructing the Archean geodynamic processes lie in the rarity of well-preserved Archean rock sequences and in the fact that most Archean volcanosedimentary successions are typically defined by greenschist- to amphibolite-facies metamorphic grades, which are not characteristic of a specific tectonic context. This uncertainty has led to a debate which traditionally focused on two “endmembers”, uniformitarian (“horizontal”) and static lid (“vertical”) models.

The distinct features of Archean cratons have led many researchers to pursue non-uniformitarian geotectonic models. For example, in the vertical tectonic model of partial convective (crustal) overturn (PCO), the juxtaposition of greenstone belts and TTGs is driven by gravitational instability of the middle to upper crust. As proposed by Van Kranendonk et al. (2015), the mafic to ultra-mafic rocks of the greenstone belts are continuously stacked on top of each other in a volcanic plateau-type setting. This thick volcanic plateau would insulate the buried felsic crust until radiogenic heating aided by a hotter mantle would produce sufficient heat to facilitate a widespread partial melting. The partially molten felsic crust would buoyantly rise as granite domes, while the denser, cold greenstones would sink in between the rising diapirs (Fig. 1.2a), each taking a P-T path that is distinct from the other (Fig. 1.2c). Similar non-uniformitarian models have been proposed by other authors (Barnes and Van Kranendonk, 2014; Bédard, 2006; Bouhallier et al., 1993; Chardon et al., 2002, 1998; Choukroune et al., 1995; Collins et al., 1998; Collins and Van Kranendonk, 1999; Schmitz and Heubeck, 2021; Smithies et al., 2007, 2009; Van Kranendonk, 2011, 2007; Van Kranendonk et al., 2014, 2007, 2004). In these models, the strain pattern of a specific part of the crust is assumed to be representative of the global tectonic regime.

It has on the other hand been suggested by some authors some form of subduction was already active in the Paleoarchean. Some greenstone successions from this era have been compared to ophiolite complexes (de Wit, 2004; de Wit et al., 1987; Furnes et al., 2015, 2009, 2007; Grosch and Slama, 2017), Paleoarchean garnet-amphibolites have been suggested to represent an Archean blueschist equivalent (Moyen et al., 2006; Palin and Dyck, 2018; Palin and White, 2016) and the trondhjemite and tonalite rocks that are characteristic for the Archean have been interpreted as magmas that formed through subduction processes (De Ronde and Kamo, 2000; de Wit et al., 2011; Kisters et al., 2003; Laurie et al., 2013; Martin, 1999, 1986; Martin and Moyen, 2002; Moyen et al., 2006). An example for such a model as proposed by Moyen and Laurent (2018) is illustrated in Figure 1.2b. Mafic crust formed by extrusive

volcanism thickens and becomes more dense at the base. The dense base of the crust “peels off” from the overlying layer and sinks into the mantle in a subduction-like manner (Fig. 1.2b1). The “subducted” “slab” begins to melt and granitoids are emplaced in the mafic crust, marking the beginning of felsic crust formation. This proto-subduction is very unstable and short-lived (Fig. 1.2b1). Over time, continental nuclei are formed and start focusing mantle convection (Fig. 1.2b2). They “drift” and collide with each other, with the mafic crust in between the cratons being partially buried in a subduction-like setting, although still short-lived (Fig. 1.2b2).

Fig. 1.2. (a) Schematic illustration of a gravity-driven partial convective overturn of the crust as proposed by some authors. See text for details. Modified after Van Kranendonk et al. (2015). (b) Model of short-lived proto-subduction of Moyen and Laurent (2018). See text for details. (c) Pressure-temperature paths invoked for the tectonic scenarios depicted in (a) and (b). Paths for the blue circles after Van Kranendonk et al. (2015) and for the red circle modified after Cutts et al. (2014), Diener et al. (2005), Kato et al. (2018) and Nédélec et al. (2012).

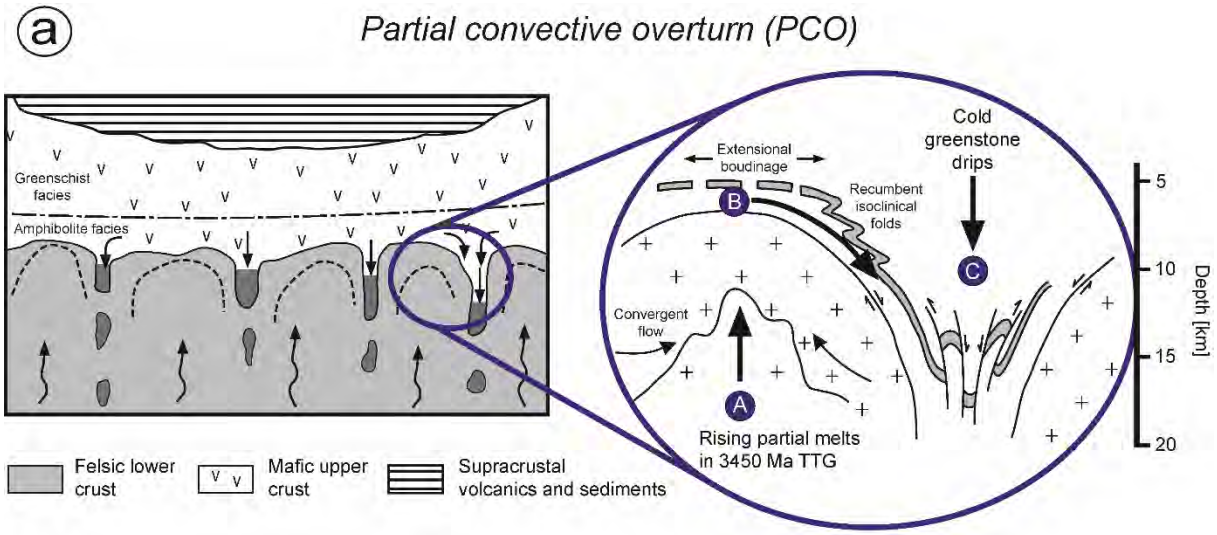

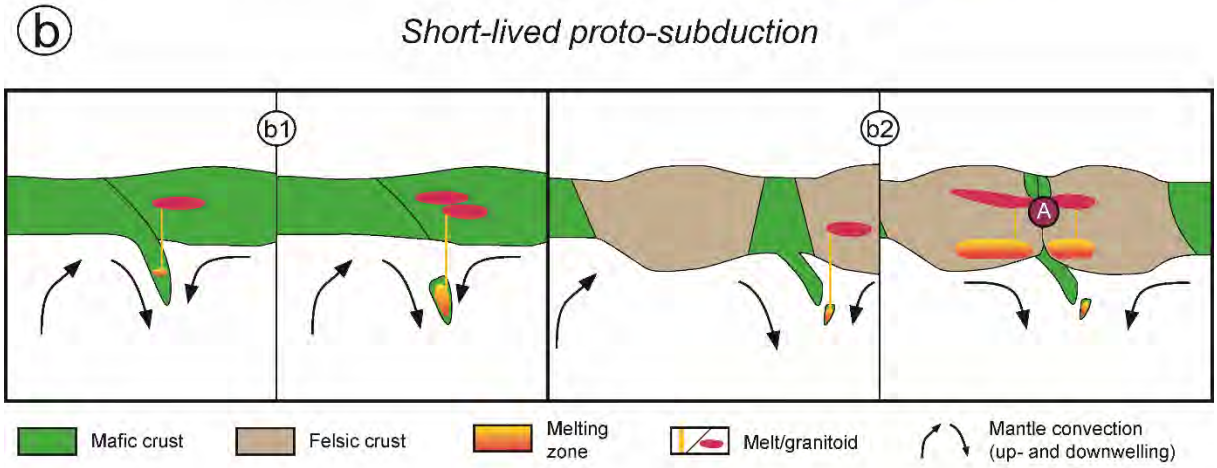

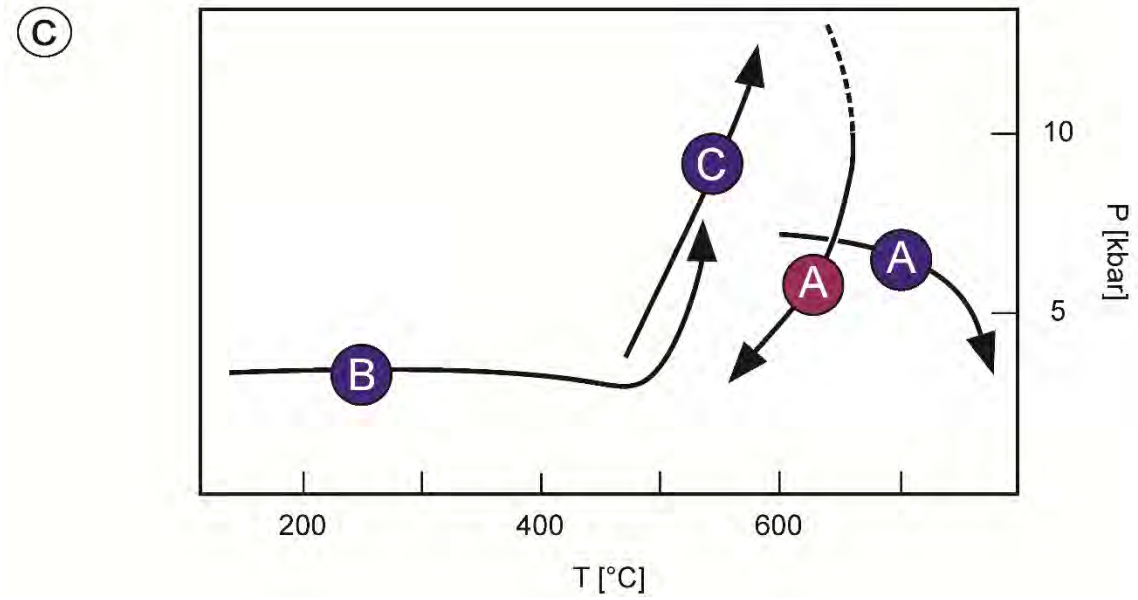

However, this dichotomy that views mechanisms as strictly “on” or “off” has been a hinderance in advancing the understanding of Archean geodynamics. With recent advancements in numerical modelling (Debaille et al., 2013; Duclaux et al., 2007; Halla et al., 2009; Moyen and van Hunen, 2012; O’Neill et al., 2015, 2007; Rey et al., 2014; Sizova et al., 2018, 2015; van Hunen and Moyen, 2012) it has become evident that the contraposition of a “horizontal” and a “vertical” endmember is likely not an appropriate basis for understanding Archean tectonic processes. Regional horizontal crustal movement, with locally divergent (“rift”) and convergent (“subduction”) domains, does not require a global system of plate boundaries (Hansen and Willis, 1996; Harris and Bédard, 2015; Piskorz et al., 2014). Furthermore, there is no simple connection to be made between the strain regime observed in a crustal segment and the large-scale tectonic system in which the crust evolved. In the present-day Colorado plateau, the crust evolves in (or near) the absence of external stresses under a hot geotherm, which is achieved through delamination of lower crust (Levander et al., 2011). Though it is here occurring in the context of modern plate tectonics, the process of crustal delamination is also evoked in stagnant lid models for the Archean (Bédard, 2006). A hot and rheologically weak crust is unable to support significant thickening under compressive stress, instead accommodating collisional processes by collapse and lateral flow of the crust in a so-called “hot orogen” (Cagnard et al., 2006a, 2006b; Chardon et al., 2009; Fossen et al., 2017). These hot orogens commonly show pervasive fabrics indicating whole-scale ductile flow of the crust, smooth metamorphic gradients and the absence of high-pressure rocks that would indicate a deep burial. Still, hot orogens develop under a tectonic regime involving horizontal movement and, more precisely, compression of a deformation zone between two stiffer blocks, be it part of a global system of interlinked plate boundaries or not (Harris and Bédard, 2015, 2014).

Based on the above, it is a vain endeavor to try and reconstruct a global tectonic style based solely on the description of regional strain. It is more purposeful to investigate the thermal evolution of the crust as a function of time and ideally also pressure. Such data, if obtained with sufficient resolution in space and time, will give a robust indication on which geodynamic processes are plausible for the Archean crust. Constraints on the mafic crust are “readily” available, but not so much for the felsic/TTG crust. Models have been proposed for the geodynamic evolution during the Archean based on assumptions on the thermal state of the felsic crust (see e.g. Fig. 1.2c). As stated by Van Kranendonk et al. (2015), “*studies of P-T conditions of metamorphism in granitic rocks, as a counterpart to greenstones*” are required. To help improve the understanding of the crustal conditions in the Archean, this thesis aims to constrain the thermal state of the Archean felsic crust. This is done primarily by means of apatite petrochronology (section 1.2) on samples from the Paleo- to Mesoarchean Barberton Granitoid Greenstone Terrain (section 1.3).

1.2 Apatite as a thermo- and petrochronological tool

Thermochronology is a method of estimating the cooling history of a rock by means of geochronology. This is either done by measuring parent and daughter isotopes, or by counting the number of “marks” left behind on the crystal by the α-particles emitted from a radioactive element as a result of its decay into the daughter element (fission tracks). The main principle behind it is the closure temperature (T_C), as first described by Dodson (1973). A mineral containing radioactive elements in its crystal lattice is formed at or heated up to elevated temperature through igneous or metamorphic processes (Fig. 1.3a). The radioactive elements/isotopes decay into their corresponding daughter elements/isotopes (Fig. 1.3b). As long as the mineral is at elevated temperature, the radiogenic daughter elements will diffuse out of the mineral (Fig. 1.3c), either because they are incompatible with the mineral’s crystal lattice or because the mineral strives for isotopic equilibrium with its surroundings. Diffusion stops once the mineral has cooled below a certain temperature, the closure temperature T_C (Fig. 1.3d). The age obtained for this mineral by means of isotopic analysis of parent and daughter elements corresponds for the time when the mineral has cooled down below T_C (Fig. 1.3e). In the case of fission tracks, above T_C the crystal lattice is able to self-anneal the radiation damage, below T_C the fission tracks remain (Fig. 1.3f). Because diffusion depends on the mineral and elements involved, the closure temperature is specific for each mineral – decay-system pair (Fig. 1.4). Furthermore, it is important to note that T_C is not a set temperature, but rather a temperature range, with the “exact” temperature depending on grain size and heating/cooling rate (Fig. 1.5).

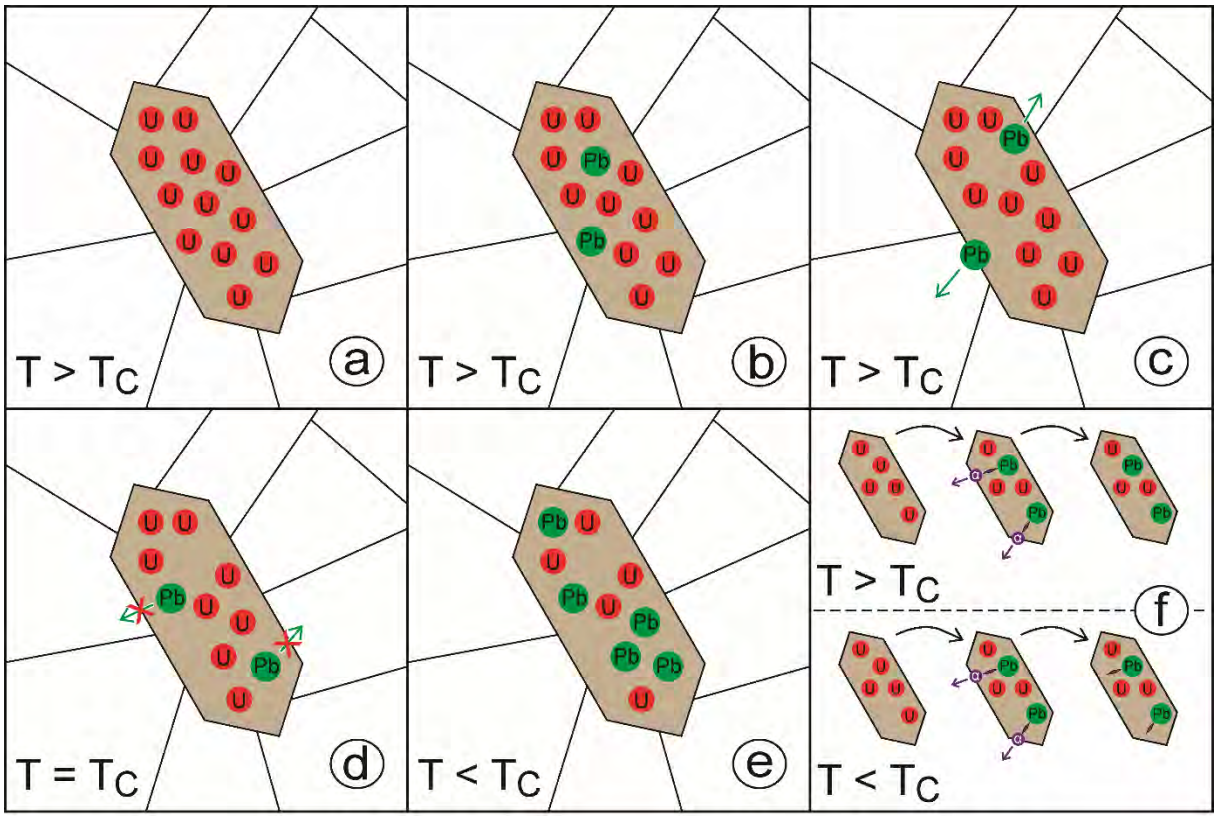

Fig. 1.3. Schematic illustrations of (a-e) thermal diffusion in a crystal above and below the closure temperature (T_C) and (f) self-annealing of radiation damage (fission tracks) caused by α-decay of U in zircon above T_C, and preservation of fission tracks below T_C. See text for details.

While thermochronology deals with the cooling history of a rock, it is by itself a very limited approach to the often very complex igneous and/or metamorphic history of a given rock sample. The term *petrochronology* has been coined recently to describe a more integrated method of investigating the protracted history of a rock sample (Engi et al., 2017). For this, geochronology of igneous and/or metamorphic and/or sedimentary mineral and rock samples is combined with petrological and geochemical methods to link "*time (i.e. ages or duration) with specific rock-forming processes and their physical conditions*" (Engi et al., 2017).

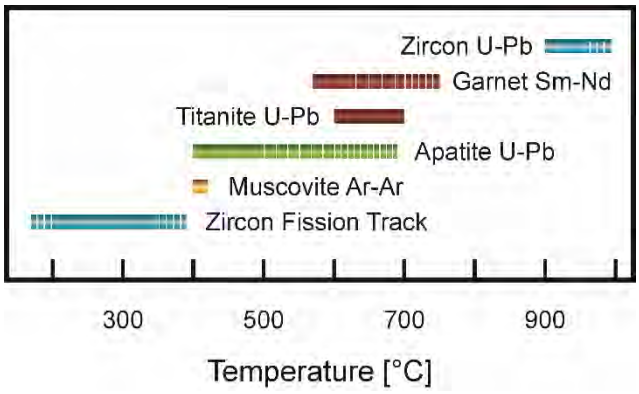

Fig. 1.4. Comparison of closure temperatures for different thermochronometers. Closure temperature ranges after Chamberlain and Bowring, (2000) and Cherniak et al. (1991) (apatite), Hensen and Zhou (1995) and Mezger et al. (1992) (garnet), Harrison et al. (2009) (muscovite), Scott and St-Onge (1995) (titanite), Bernet, (2009), Tagami et al. (1996) and Yamada et al. (1995) (zircon fission track) and Cherniak and Watson (2001) and Lee et al. (1997) (zircon U-Pb).

Apatite is a popular thermochronometer for mid-crustal processes due to its closure temperature of typically 400 to 550 °C for U-Pb (Fig. 1.4). Its potential as a tool to study petrogenetic processes has been introduced by Sha and Chappell (1999) and Belousova et

al. (2002), showing that the trace-element composition of apatite is characteristic for a given rock type. Subsequent studies have further explored the use of apatite petrology (Antoine et al., 2020; Bruand et al., 2020, 2017, 2016; Henrichs et al., 2018; Sullivan et al., 2020; Webster and Piccoli, 2015; Zirner et al., 2015).

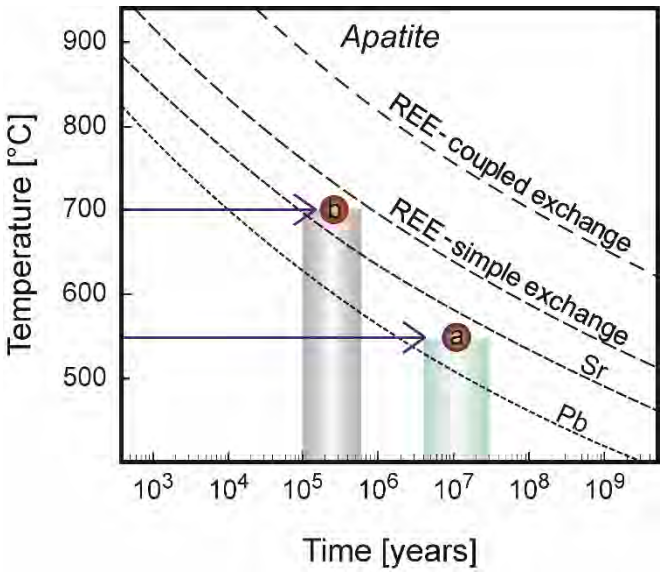

Fig. 1.5. Summary of diffusion constraints for Pb, Sr and REE in apatite (modified after Cherniak et al., 2000). The lines indicate the T-t conditions, above which the original composition of a spherical apatite grain of 250 µm will be lost even at the core. Example (a) represents a hypothetical sample, in which the apatite shows a reset of U-Pb isotope systematics, but still preserves the initial $^{87}Sr/^{86}Sr$ ratio. The metamorphic temperature determined for the sample by traditional geothermometry is 550 °C, resulting in a heating duration of ca. 4 to 30 million years. Example (b) indicates a hypothetical sample, in which matrix apatites yield younger U-Pb ages and more evolved $^{87}Sr/^{86}Sr$ ratios compared to apatite inclusions in zircon, but identical $^{143}Nd/^{144}Nd$ ratios. The Zr-in-titanite temperature determined for a metamorphic titanite rim is 700 °C, resulting in a heating duration of ca. 100,000 to 600,000 years.

The parameters for thermal diffusion of elements in apatite have been determined experimentally (Cherniak, 2005, 2000; Cherniak et al., 1991; Cherniak and Ryerson, 1993). The temperature above which the original composition of an apatite grain is lost through diffusion differs from element to element (or group of chemically similar elements). The diffusion constraints for Pb, Sr and REE in apatite are shown in Figure 1.5. Of these, Pb is the least resistant to diffusion. As a consequence, it is possible that a sample is sufficiently heated to that the U-Pb systematics in apatite are (partially) reset, while the original REE or Sr (isotopic) compositions are still preserved. Such a decoupling of U-Pb and REE has been recently reported by Antoine et al. (2020) for apatite grains from the Acasta Gneiss Complex, Canada. In the samples of Antoine et al. (2020), the U-Pb systematics of matrix apatite had been completely reset by an orogenic event. However, some matrix apatites were still able to preserve primary magmatic trace-element characteristics that are identical to those from inclusions of primary apatite in zircon that had been protected from Pb loss.

As apatite does incorporate Sr into its crystal structure but only negligible amounts of Rb, it can potentially preserve the initial $^{87}Sr/^{86}Sr$ ratio of the magma or fluid from which it has

crystallized (e.g. Creaser and Gray, 1992). On the other hand, the Sr isotopic composition of apatite can also be affected by thermal resetting. Emo et al. (2018) report that matrix apatites from the Acasta Gneiss Complex show an altered Sr isotopic composition, while apatite inclusions in zircon preserve the apparent initial $^{87}Sr/^{86}Sr$ ratio. However, while the initial composition will be lost, a reset of Sr isotope systematics in apatite does also give insight into the sample's history, especially if coupled with U-Pb and REE analyses. Because Pb is more susceptible to diffusion than Sr (Fig. 1.5), the U-Pb age can reflect the time of reset of Sr isotopic composition. The REE are much more resistant to diffusion than Pb and Sr (Fig. 1.5) and the preservation of primary REE signatures in apatites with altered Pb and Sr can give an upper limit to the thermal conditions. When combined with an applicable geothermometer, the duration of heating can be estimated dependent on which elements have been affected by thermal diffusion (see examples in Fig. 1.5).

In summary, the compositional dependence on rock type, well constrained diffusion parameters, a moderate closure temperature for U-Pb and the relative abundance in a variety of rock types make apatite a powerful tool for investigating the igneous and metamorphic history of a given sample.

1.3 Regional Geology

1.3.1 The Barberton Granitoid Greenstone Terrain

The Barberton Granitoid Greenstone Terrain (BGGT) is located in southern Africa, covering some 7500 km^2 of north-eastern South Africa and western Eswatini (Fig. 1.6). It contains some of Earth's oldest crustal remnants, which are remarkably well preserved in comparison to other localities and are superbly exposed (Fig. 1.7). The BGGT is comprised of the ca. 3.5 to 3.2 Ga Paleoarchean supracrustal sequence of the Barberton Greenstone Belt (BGB) and surrounding ca. 3.5 to 3.2 Ga TTG rocks (Fig. 1.6). Younger, granodiorite-monzogranite-syenite (GMS) plutons and batholiths, ranging in age from ca. <3.22 to 2.70 Ga but peaking around ca. 3.1 Ga, surround the BGGT. A review of these younger rocks was recently given by Kröner et al. (2019) and will not be repeated here because these units are well beyond the scope of this thesis. The features of the BGGT most relevant to this thesis will be summarized in the following sections. More detailed reviews can be found in Byerly et al. (2019) for the supracrustal rocks of the BGB and in Kröner et al. (2019) and Moyen et al. (2019) for the surrounding granitoids.

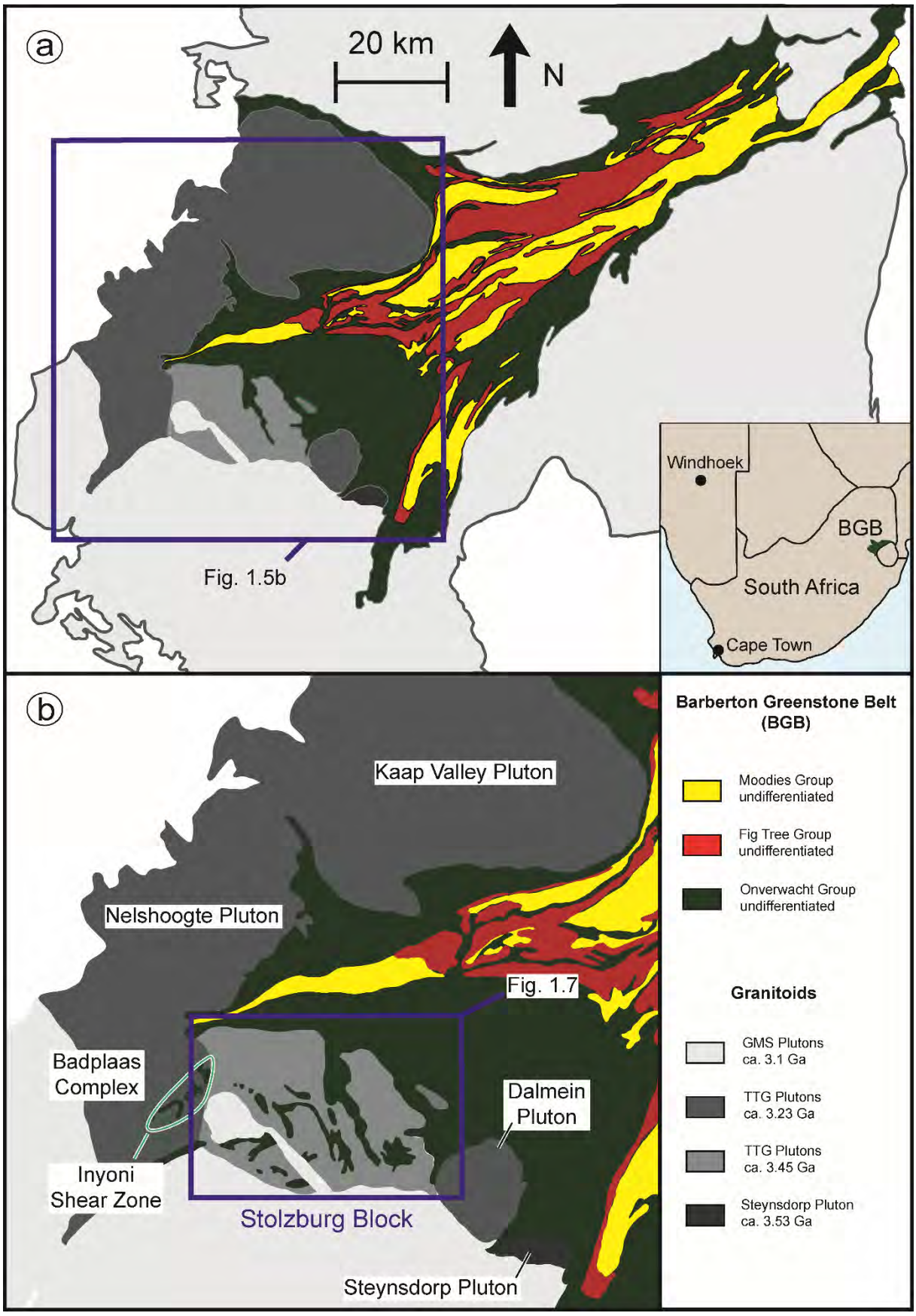

Fig. 1.6. Simplified geological map of the Barberton granitoid greenstone terrain (BGGT), showing the important units of the Baberton Greenstone Belt (BGB) and surrounding granitoids. Inset in (a) shows the location of the BGB in the context of southern Africa. Modified after Anhaeusser et al. (1981).

1.3.1.1 The supracrustal rocks of the BGB

The supracrustal rocks of the BGB are traditionally divided into three major lithographic units: The Onverwacht, Fig Tree and Moodies groups (Lowe et al., 2012; Lowe and Byerly, 1999; Viljoen and Viljoen, 1969). The oldest is the ca. 3538 to 3270 Ma Ga Onverwacht Group., consisting of the following formations (oldest to youngest). The ca. 3538 to <3511 Ma, amphibolite-facies Theespruit and Sandspruit formations will be described in detail in section 1.3.2 and are separated from the ca. 3480 Ma (Dann, 2000) greenschist facies (Cloete, 1994) Komati Formation by the Komati Fault (Armstrong et al., 1990; Kisters et al., 2003). The ca. 3472 to 3438 Ma (Armstrong et al., 1990; Kröner et al., 2013; Kröner and Todt, 1988) Hooggenoeg Formation (Viljoen and Viljoen, 1969) is comprised of basalts interlayered with cherts, overlain by felsic intrusives and tuffs, and is followed by the ca. 3334 Ma (Byerly et al., 1996) mafic to ultramafic sequence of the Kromberg Formation and the ca. 3298 Ma (Byerly et al., 1996) basalts and komatiites of the Mendon Formation.

The Onverwacht Group is unconformably overlain by the Fig Tree Group (FTG), followed by the Moodies Group. Detailed reviews of the different lithological units of the Fig Tree and Moodies groups are given by Byerly et al. (2019) and Drabon and Lowe (2021) and will not be repeated here as it is well beyond the scope of this thesis. Only the features of these groups that are pertinent to this thesis will be summarized here. The ca. 3260 to 3225 Ma (Drabon and Lowe, 2021, and references therein) volcaniclastic strata of the FTG mark the onset of deposition of clastic sediments derived from the uplifting Onverwacht Group (Byerly et al., 2019). The FTG shows an upwards coarsening trend and a change from regional to local provenance in its stratigraphy and has recently been interpreted to represent "*deposition in a foreland basin that experienced progressive accretion of crustal terranes onto a northward prograding fold-and-thrust belt*" (Drabon and Lowe, 2021). The FTG is followed by the ca. 3225 to 3220 Ma continentally derived coarse-clastic sediments and sandstones of the Moodies Group. Some conglomerates of the Moodies Group contain granitic clasts which have been dated to ca. 3565 Ma down to ca. 3226 Ma (Kröner et al., 2018; Sanchez-Garrido et al., 2011). These granite clasts are unique in the BGGT, and their existence indicates that crustal reworking by melting of subducted sediments may have already been happening in the Paleoarchean (Sanchez-Garrido et al., 2011). Their source rock has not been preserved; Kröner et al. (2018) suggested that it has been exhumed and eroded during an unroofing event at ca. 3.2 Ga.

The nature of the BGB stratigraphy is under debate. The traditional view is that the supracrustal rocks of the BGB form a continuous stratigraphy (see Byerly et al. (2019) and references therein). The Onverwacht Group is regarded as a continuous pile that was formed in a volcanic plateau-type setting (Van Kranendonk et al., 2015). Recent publications have challenged this

traditional framework. It was proposed by de Wit et al. (2011). that "*at least seven major shear zones and an unconformity separate the rocks of the southern Barberton Greenstone Belt into seven units with different geological histories*" and that the formations and groups should rather be referred to as complexes and suites, respectively. For example, the felsic top unit of the Hooggenoeg Formation has been redefined as the Noisy Complex (de Wit et al., 2011) and was described by Grosch et al. (2011) as remnants of the earliest tectonic basin in the BGB. A study on the Kromberg Formation has reported that this unit contains no contamination from the underlying units and thereby likely represents juvenile oceanic crust that was tectonically thrusted over the older units (Grosch and Slama, 2017). However, the timing of deposition of many of the supracrustal units of the BGB is still poorly constrained due to the absence of reliably datable minerals in some of them and, where datable minerals can be obtained, due to the large uncertainties that are unavoidable when dealing with rocks of this age, particularly with the increasingly common LA-ICP-MS dating that is more easily accessible but less precise than SHRIMP or TIMS analyses.

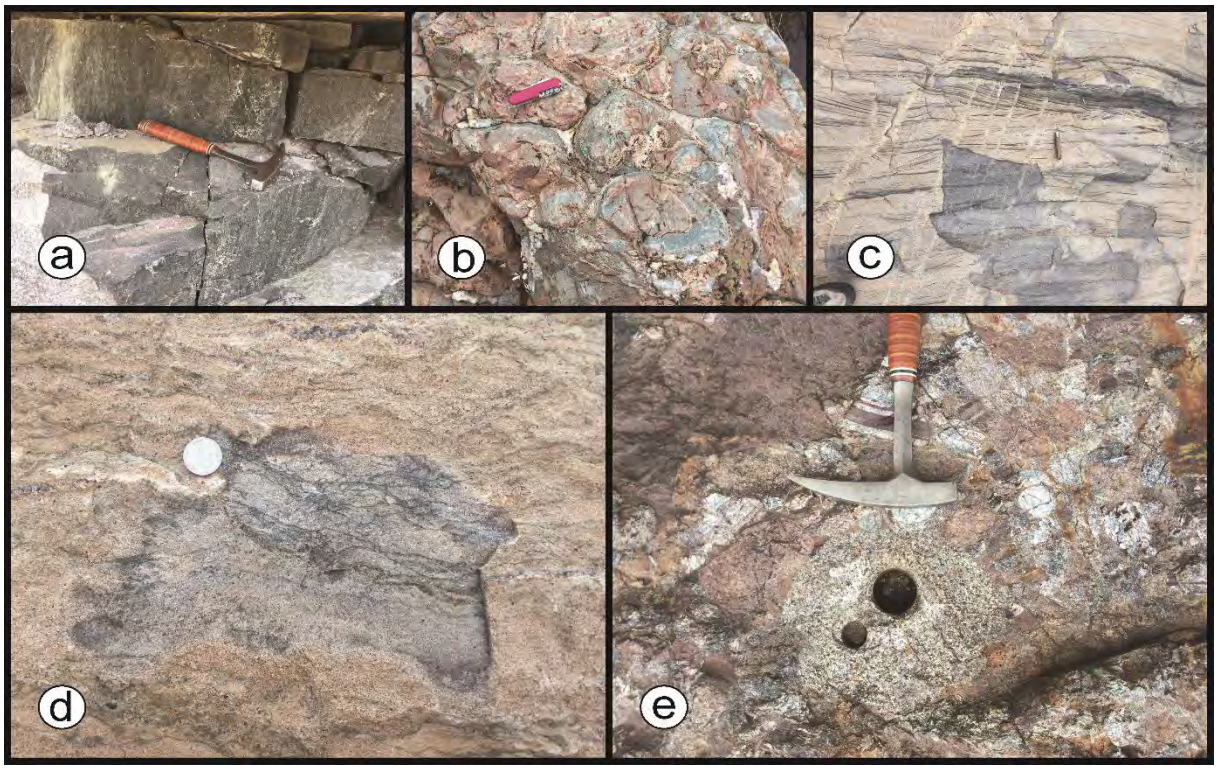

Fig. 1.7. Field photos from the Barberton Greenstone Belt (BGB). (a) Theespruit Formation xenolith in trondhjemite of the Theespruit Pluton. (b) Komati Formation pillow lava. (c) Tidal sandstones of the Moodies Group. (d) Fossilized remains of ca. 3220 Ma microbial mats in Moodies Group sandstone. (e) Granite clast in Moodies Group conglomerate.

1.3.1.2 TTG plutons

The BGB is surrounded by a series of ca. 3518 to 3215 Ma TTG rocks (Fig. 1.6b). The ca. 3518-3502 Ma (Kamo and Davis, 1994; Kröner et al., 1996; Schoene et al., 2008) Steynsdorp gneisses (Kisters and Anhaeusser, 1995; Lana et al., 2010a) are the oldest and most deformed of these TTG rocks. They are "*characterized by a pervasively developed gneissosity and parallel compositional banding, which mimics the convex shape of the pluton*" (Kisters and Anhaeusser, 1995). No intrusive contact between the Steynsdorp gneisses and the greenstones of the lower Onverwacht formation can be observed, but a locally developed granitic phase of the gneisses has been reported to intrude the greenstones and greenstone xenoliths can also be found within the Steynsdorp Pluton (Kisters and Anhaeusser, 1995). The second oldest TTG rocks are found in the south of the BGGT (Fig. 1.6b). These have been dated to ca. 3460 to 3445 Ma (Kamo and Davis, 1994; Lana et al., 2010b; Laurent et al., 2020; Schoene et al., 2008; Wang et al., 2019) and are much less deformed compared to the Steynsdorp gneisses, preserving igneous rock textures (Cutts et al., 2015; Moyen et al., 2019). The ca. 3.45 Ga TTG plutons are in intrusive contact with the Theespruit and Sandspruit formations of the lower Onverwacht Group. These ca. 3.45 Ga plutons and associated greenstones are collectively referred as Stolzburg Block. The Stolzburg Block is the focus of this study and will be described in detail in section 1.3.2 and chapter 2.

The Badplaas Complex in the south-west of the BGGT (Fig. 1.6b) consists of several compositionally, texturally and geochronologically distinct phases, that were dated to ca. 3272 to 3230 Ma (Kisters et al., 2010). A detailed review of the geology of the Badplaas Complex was recently given by Moyen et al. (2019) and will not be repeated here as it is beyond the scope of this thesis. The border between the Badplaas Complex and the Stolzburg Block to the east is marked by the ca. 3 km wide high-strain Inyoni shear zone (ISZ) (Kato et al., 2018; Moyen et al., 2006; Van Kranendonk et al., 2014). The ISZ is comprised of gneisses, amphibolites, intrusive TTG phases and subordinate metasediments, and shows a steeply dipping and north-northeast striking gneissosity (Kato et al., 2018; Kisters et al., 2010; Moyen et al., 2019, 2006). Two different varieties of gneisses can be identified in the ISZ: an undated, migmatitic trondhjemitic gneiss (Van Kranendonk et al., 2014) that might represent an enclave of the adjacent Stolzburg Pluton (Moyen et al., 2019), and ca. 3282 to 3238 Ma TTG gneisses resembling those of the Badplaas Complex (Kisters et al., 2010). The amphibolites of the ISZ record peak metamorphic conditions of ca. 550 to 650 °C at ca. 8 to 10 kbar and retrograde metamorphic conditions of ca. 500 °C at 5 kbar (Cutts et al., 2021; Kato et al., 2018). Timing of metamorphism was constrained to ca. 3200 Ma by Sm-Nd garnet geochronology (Cutts et al., 2021). A banded iron formation (BIF) from the ISZ yields peak metamorphic conditions of ca. 600 to 680 °C at >10 kbar and retrograde metamorphic conditions of 510 to 540 °C at 8-

11 kbar through to <500 °C at 4 kbar (Kato et al., 2018). The geodynamic setting driving the metamorphism of the supracrustal rocks of the ISZ has been interpreted to be either cool greenstone drips sinking between rising TTG domes in a partial convective overturn (Van Kranendonk et al., 2014), or arc-continent collision in a plate tectonic-style regime (Kato et al., 2018; Kisters et al., 2010; Moyen et al., 2006).

The Nelshoogte and Kaap Valley plutons in the north-west of the BGGT are the two youngest and largest TTG plutonic bodies of the BGGT. The mainly tonalitic Kaap Valley Pluton was emplaced at ca. 3227 Ma (Kamo and Davis, 1994) at pressures of 1 to 2 kbar (Matsumura, 2014). The compositionally heterogenous Nelshoogte Pluton was emplaced at ca. 3235 to 3215 Ma (Guitreau et al., 2012; Matsumura, 2014; Schoene et al., 2008; Zeh et al., 2009) at pressures of 2 to 5 kbar (Matsumura, 2014). Both late TTG plutons are in intrusive contact with the supracrustal rocks of the BGB (De Ronde and Kamo, 2000; Moyen et al., 2019).

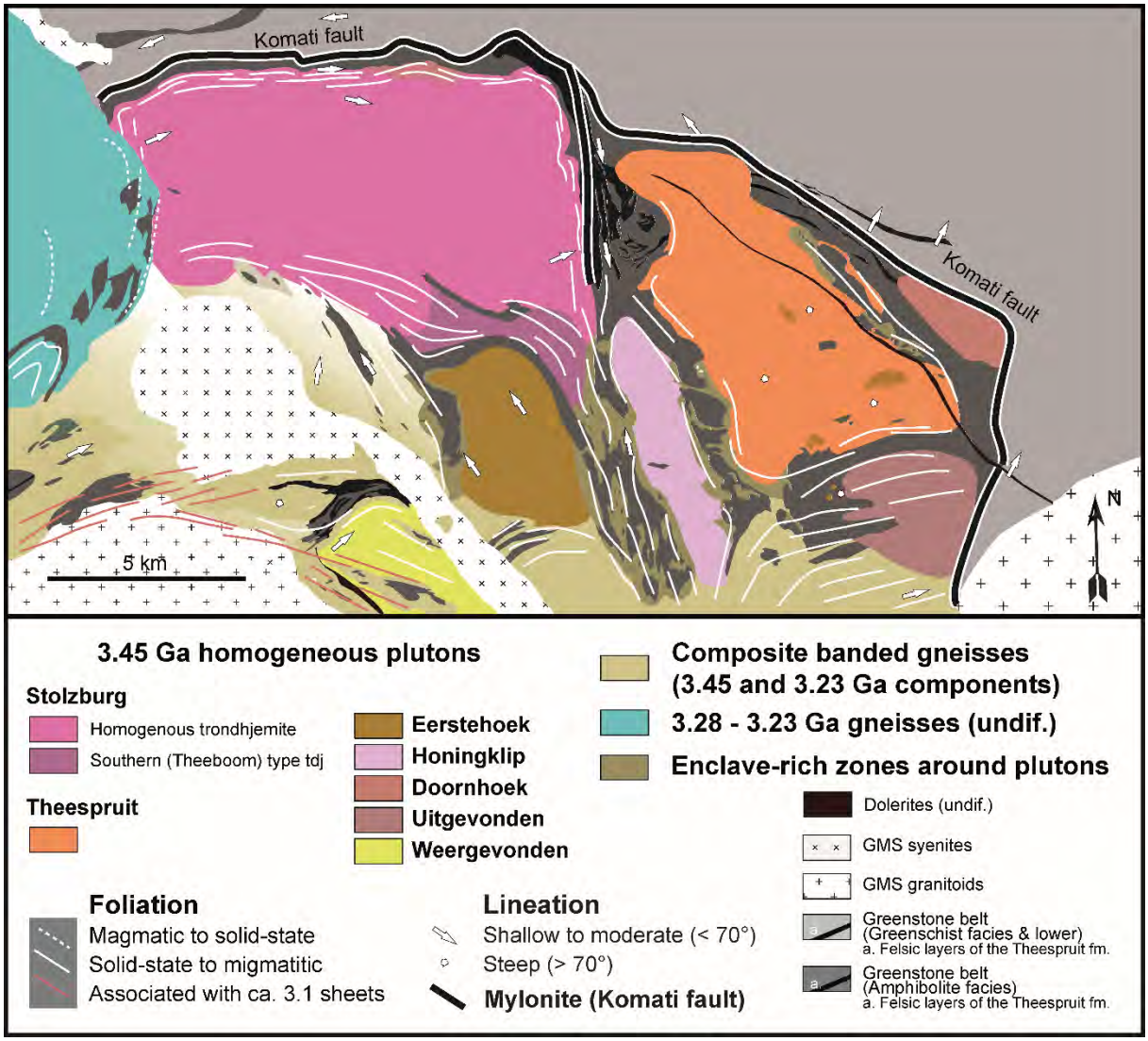

Fig. 1.8. Geological map of the Stolzburg Block, showing the important units. Modified after Moyen et al. (2019).

1.3.2 The Stolzburg Block

The Stolzburg Block in the south of the BGGT is the field area of this thesis (Fig. 1.8). It is comprised of two main lithologies: the ca. 3.5 Ga amphibolite-facies supracrustal rocks of the Theespruit and formations of the lower Onverwacht Group and ca. 3.45 Ga, primarily trondhjemitic plutonic rocks (Fig. 1.8). The contact between the two is intrusive (e.g. Moyen et al., 2019, and references therein).

The rocks of the Theespruit and Sandspruit formations are mainly mafic to ultramafic metavolcanic rocks, with subordinate felsic volcanic metavolcanic rocks and clastic sediments derived from the volcanic rocks (Dziggel et al., 2002; Viljoen and Viljoen, 1969). These supracrustal rocks occur in the Stolzburg Block as larger consecutive units around and in between the TTG plutons, e.g. in the Schapenburg schist belt, and also as remnants and xenoliths within the plutons. Igneous zircon grains from the felsic metavolcanic rocks from both the Theespruit and Sandspruit formations yield ages of ca. 3530 Ma, indicating that the two are contemporaneous and were formed in a single volcanic event (Kröner et al., 2016). Detrital zircon ages of ca. 3540 to 3510 Ma were obtained for an impure arkose (Dziggel et al., 2002). The rocks of the lower Onverwacht Group have experienced multiple metamorphic events. Rocks from the north-eastern margin of the Stolzburg Block records metamorphic conditions of ca. 550 °C and ca. 4.5 kbar at 3436 ± 18 Ma and ca. 550 °C and ca. 7 kbar at ca. 3230 Ma (Cutts et al., 2014). For the Schapenburg schist belt, conditions of ca. 550 to 600 °C and ca. 7.5 to 8.5 kbar at ca. 3230 Ma (Cutts et al., 2014; Diener et al., 2005). Greenstone remnants from the south-western margin of the Stolzburg Pluton yield peak metamorphic conditions of ca. 650 to 700 °C and ca. 8 to 11 kbar (Dziggel et al., 2002) at ca. 3230 Ma (Dziggel et al., 2005). The P-T conditions recorded for the ca. 3230 Ma metamorphic event in the Stolzburg Block are in the same range as those reported for the ISZ (see section 1.3.1).

The Stolzburg Block is separated from the BGB by the Komati fault (Armstrong et al., 1990; de Wit et al., 1983; Kisters et al., 2003) (Fig. 1.8), which also forms a break in metamorphic grade from amphibolite facies in the Stolzburg Block (see above) to greenschist facies in the BGB (Cloete, 1994). The Komati Fault is ca. 1 km wide and records Stolzburg Block upwards, greenstone belt downwards kinematics (Kisters et al., 2003; Van Kranendonk et al., 2009).

The TTG rocks of the Stolzburg Block are comprised in a number of plutonic bodies of different sizes (Fig. 1.8), of which the Stolzburg and Theespruit plutons are the most well studied. A summary of the published information of the important lithologies follows here and a detailed description of the different plutonic bodies based on my own fieldwork can be found in Chapter 2.

The Stolzburg Pluton is mainly made up of homogenous, undeformed trondhjemite, locally occuring in a fine- and a coarse-grained variety, with a smooth transition between the two varieties (Moyen et al., 2019). The trondhjemite of the Stolzburg Pluton has yielded U-Pb zircon ages of ca. 3455 to 3440 Ma (Kamo and Davis, 1994; Kröner et al., 1991; Schoene et al., 2008; Wang et al., 2019; Zeh et al., 2009). On the southern margin of the Stolzburg Pluton, a unique phase named Theeboom Gneisses crops out (Fig. 1.8). There, the trondhjemite is banded and highly deformed, and contains greenstone xenoliths (Schoene et al., 2008). A U-Pb zircon age of ca. 3460 to 3455 Ma was obtained for the banded trondhjemite (Kamo and Davis, 1994; Schoene et al., 2008) and of ca. 3212 Ma for a deformed felsic dyke cutting both gneiss and greenstone (Schoene et al., 2008). Kamo and Davis (1994) also report U-Pb zircon ages of ca. 3255 to 3237 Ma and a U-Pb titanite age of ca. 3200 Ma for a trondhjemite phase from the same outcrop, which the authors interpreted to reflect a (hydro)thermal event based on the very low Th/U ratios of the analyzed grains (ca. 0.00 to 0.11).

The Theespruit Pluton is made up of a similar homogenous trondhjemite to the Stolzburg Pluton. However, some compositional zoning can be observed in the Theespruit Pluton (Moyen et al., 2019). The U-Pb zircon ages published for the Theespruit Pluton range from 3460 to 3437 Ma (Armstrong et al., 1990; Kamo and Davis, 1994; Laurent et al., 2020). In the western margin, the trondhjemite of the Theespruit Pluton is in intrusive contact with the supracrustal rocks of the lower Onverwacht Group. In this locality, both the trondhjemite and the greenstone are cut by a set of felsic dykes. However, the time of emplacement of these cross-cutting dykes is not well constrained (Moyen et al., 2019).

Apart from the Stolzburg and Theespruit pluton, a number of smaller plutonic bodies occur in the Stolzburg Block (Fig. 1.8). These bodies were mapped by Anhaeusser et al. (1981) as plutons, but in many cases such an interpretation is not accurate as they can show quite a variety in lithologies and textures. The Doornhoek in the north-east of the Stolzburg Block has yielded an U-Pb zircon age of 3448 ± 4 Ma (Kamo and Davis, 1994). The Uitgevonden, south of the Theespruit Pluton, is distinct from the homogenous, weakly deformed trondhjemite of the Stolzburg and Theespruit plutons. The Uitgevonden gneisses show a strong foliation and "*compositional layering defined by alternating decimeter-wide grey, granodioritic bands and white felsic bands*" (Lana et al., 2010b). A U-Pb zircon age of ca. 3432 ± 10 Ma has been obtained for a gneiss sample from the Uitgevonden (Lana et al., 2010b). Wang et al., (2019) report a U-Pb zircon age of 3225 ± 4 Ma for a trondhjemite sample from the Honingklip and U-Pb zircon ages of 3454 ± 8 Ma and 3225 ± 4 Ma for a trondhjemite and quartz diorite sample from the Weergevonden, respectively. So far, no geochronological constraints are available for the Eerstehoek and Nederland.

The occurrence of ca. 3.2 Ga TTG rocks has been used to invoke a partial melting of the TTG rocks of the Stolzburg Block at that time (Van Kranendonk, 2011; Van Kranendonk et al., 2015). However, the extent of ca. 3.2 Ga felsic magmatism in the Stolzburg Block and the degree to which the ca. 3.45 Ga TTG rocks were affected by it is not well constrained.

1.4 Structure of the thesis

I attempt to further the current knowledge on the evolution of the southern BGGT and on the thermal state of Earth's first stable continental crust, by investigating the igneous and metamorphic history of granitoid and metasedimentary rock samples from the Stolzburg Block. I herein present the work in three parts through the compilation of two manuscripts, one published and one in preparation for submission, and a chapter in which I combine the two papers with additional, unpublished data in an attempt to reconstruct the geodynamic history of the southern BGGT. These three parts can be summarized as follows:

(1) The first manuscript presents the thermal history of the Stolzburg Block. In this paper, I investigated the emplacement age of different granitoid phases from the Stolzburg Block using U-Pb zircon geochronology and constrained the thermal state of the Archean crust using apatite thermochronology. The magmatic age of the trondhjemite rocks that make up the bulk of the Stolzburg Block is ca. 3450 Ma, cross-cutting TTG dykes intruded the margins of the trondhjemite plutons at ca. 3200 Ma, and a diorite phase has been dated to 3221 ± 2 Ma. The apatite grains record four groups of U-Pb ages, at ca. 3442 ± 7, 3212 ± 3, 3104 ± 6 and 2819 ± 5 Ma. The preservation of magmatic U-Pb apatite ages shows that the whole Stolzburg Block has not been subjected to any prolonged heating events after the emplacement of TTG plutons at ca. 3450 Ma. The findings of this paper strongly argue against partial convective overturn as a mechanism for ca. 3200 Ma metamorphism of the Stolzburg Block.

(2) The second manuscript is focused on the cryptic metamorphic history of the granitoids of the Stolzburg Block. In this paper, I investigated the chemical composition of apatite, titanite and zircon grains. The apatite grains dated in the first manuscript show a de-coupling of their U-Pb, trace-element and Sr isotope systematics: in all but one sample, all analyzed apatite grains preserve their igneous trace-element and Sr isotope signatures, while the U-Pb isotopic composition has been affected by metamorphic events. Titanite grains show metamorphic rims and alteration of igneous zones. Zirconium-in-titanite temperature estimates are ca. 700 °C for igneous zones and ca. 650 °C for metamorphic ones. This shows that the metamorphic temperatures recorded by the TTG rocks of the Stolzburg Block are comparable to those of the metamafic

lithologies. The findings of this study argue for rapid burial and exhumation of the Stolzburg Block in the Paleo- to Mesoarchean, potentially by a mechanism similar to modern plate tectonics.

(3) The final part combines the research papers with additional, unpublished data that were beyond the scope of the two manuscripts and is an attempt to reconstruct the history of the Stolzburg Block from emplacement of TTG plutons at ca. 3450 Ma to the last metamorphic event recorded by the apatite grains at ca. 2820 Ma.

References

Amelin, Y., Lee, D.C., Halliday, A.N., 2000. Early-middle Archaean crustal evolution deduced from Lu-Hf and U-Pb isotopic studies of single zircon grains. Geochim. Cosmochim. Acta 64, 4205–4225. https://doi.org/10.1016/S0016-7037(00)00493-2

Anhaeusser, C.R., Robb, L.J., Viljoen, M.J., 1981. Provisional geological map of the Barberton Greenstone Belt and surrounding granitic terrane.

Antoine, C., Bruand, E., Guitreau, M., Devidal, J.L., 2020. Understanding Preservation of Primary Signatures in Apatite by Comparing Matrix and Zircon-Hosted Crystals From the Eoarchean Acasta Gneiss Complex (Canada). Geochemistry, Geophys. Geosystems 21. https://doi.org/10.1029/2020GC008923

Armstrong, R.A., Compston, W., de Wit, M.J., Williams, I.S., 1990. The stratigraphy of the 3.5-3.2 Ga Barberton Greenstone Belt revisited: a single zircon ion microprobe study. Earth Planet. Sci. Lett. 101, 90–106. https://doi.org/10.1016/0012-821X(90)90127-J

Barnes, S.J., Van Kranendonk, M.J., 2014. Archean andesites in the east Yilgarn craton, Australia: Products of plume-crust interaction? Lithosphere 6, 80–92. https://doi.org/10.1130/L356.1

Bédard, J.H., 2006. A catalytic delamination-driven model for coupled genesis of Archaean crust and sub-continental lithospheric mantle. Geochim. Cosmochim. Acta 70, 1188–1214. https://doi.org/10.1016/j.gca.2005.11.008

Belousova, E.A., Griffin, W.L., O'Reilly, S.Y., Fisher, N.I., 2002. Apatite as an indicator mineral for mineral exploration: Trace-element compositions and their relationship to host rock type. J. Geochemical Explor. 76, 45–69. https://doi.org/10.1016/S0375-6742(02)00204-2

Bernet, M., 2009. A field-based estimate of the zircon fission-track closure temperature. Chem. Geol. 259, 181–189. https://doi.org/10.1016/j.chemgeo.2008.10.043

Blichert-Toft, J., Albarède, F., 2008. Hafnium isotopes in Jack Hills zircons and the formation of the Hadean crust. Earth Planet. Sci. Lett. 265, 686–702. https://doi.org/10.1016/j.epsl.2007.10.054

Bouhallier, H., Choukroune, P., Ballèvre, M., 1993. Diapirism, bulk homogeneous shortening and transcurrent shearing in the Archaean Dharwar craton: the Holenarsipur area, southern India. Precambrian Res. 63, 43–58. https://doi.org/10.1016/0301-9268(93)90004-L

Bowring, S.A., Williams, I.S., 1999. Priscoan (4.00-4.03 Ga) orthogneisses from northwestern Canada. Contrib. to Mineral. Petrol. 134, 3–16.

https://doi.org/10.1007/s004100050465

Bruand, E., Fowler, M., Storey, C., Darling, J., 2017. Apatite trace element and isotope applications to petrogenesis and provenance. Am. Mineral. 102, 75–84. https://doi.org/10.2138/am-2017-5744

Bruand, E., Fowler, M., Storey, C., Laurent, O., Antoine, C., Guitreau, M., Heilimo, E., Nebel, O., 2020. Accessory mineral constraints on crustal evolution: Elemental fingerprints for magma discrimination. Geochemical Perspect. Lett. 13, 7–12. https://doi.org/10.7185/geochemlet.2006

Bruand, E., Storey, C., Fowler, M., 2016. An apatite for progress: Inclusions in zircon and titanite constrain petrogenesis and provenance. Geology 44, 91–94. https://doi.org/10.1130/G37301.1

Byerly, G.R., Kröner, A., Lowe, D.R., Todt, W., Walsh, M.M., 1996. Prolonged magmatism and time constraints for sediment deposition in the early Archean Barberton greenstone belt: evidence from the Upper Onverwacht and Fig Tree groups. Precambrian Res. 78, 125–138. https://doi.org/10.1016/0301-9268(95)00073-9

Byerly, G.R., Lowe, D.R., Heubeck, C., 2019. Geologic Evolution of the Barberton Greenstone Belt - A Unique Record of Crustal Development, Surface Processes, and Early Life 3.55-3.20 Ga, in: Van Kranendonk, M.J., Bennett, V.C., Hoffmann, J.E. (Eds.), Earth's Oldest Rocks. pp. 569–613.

Cagnard, F., Brun, J., Gapais, D., 2006a. Modes of thickening of analogue weak lithospheres. Tectonophysics 421, 145–160. https://doi.org/10.1016/j.tecto.2006.04.016

Cagnard, F., Durrieu, N., Gapais, D., Brun, J.P., Ehlers, C., 2006b. Crustal thickening and lateral flow during compression of hot lithospheres, with particular reference to precambrian times. Terra Nov. 18, 72–78. https://doi.org/10.1111/j.1365-3121.2005.00665.x

Cavosie, A.J., Wilde, S.A., Liu, D., Weiblen, P.W., Valley, J.W., 2004. Internal zoning and U-Th-Pb chemistry of Jack Hills detrital zircons: A mineral record of early Archean to Mesoproterozoic (4348-1576 Ma) magmatism. Precambrian Res. 135, 251–279. https://doi.org/10.1016/j.precamres.2004.09.001

Chamberlain, K.R., Bowring, S.A., 2000. Apatite – feldspar U – Pb thermochronometer : a reliable , mid-range (~ 450°C), diffusion-controlled system. Chem. Geol. 172, 173–200.

Chardon, D., Choukroune, P., Jayananda, M., 1998. Sinking of the Dharwar Basin (South India): implications for Archaean tectonics. Precambrian Res. 91, 15–39. https://doi.org/10.1016/S0301-9268(98)00037-0

Chardon, D., Gapais, D., Cagnard, F., 2009. Flow of ultra-hot orogens: A view from the Precambrian, clues for the Phanerozoic. Tectonophysics 477, 105–118. https://doi.org/10.1016/j.tecto.2009.03.008

Chardon, D., Peucat, J.J., Jayananda, M., Choukroune, P., Fanning, C.M., 2002. Archean granite-greenstone tectonics at Kolar (South India): Interplay of diapirism and bulk inhomogeneous contraction during juvenile magmatic accretion. Tectonics 21. https://doi.org/10.1029/2001TC901032

Cherniak, D.J., 2005. Uranium and manganese diffusion in apatite. Chem. Geol. 219, 297–308. https://doi.org/10.1016/j.chemgeo.2005.02.014

Cherniak, D.J., 2000. Rare earth element diffusion in apatite. Geochim. Cosmochim. Acta 64, 3871–3885. https://doi.org/10.1016/S0016-7037(00)00467-1

Cherniak, D.J., Lanford, W.A., Ryerson, F.J., 1991. Lead diffusion in apatite and zircon using ion implantation and Rutherford Backscattering techniques. Geochim. Cosmochim. Acta 55, 1663–1673. https://doi.org/10.1016/0016-7037(91)90137-T

Cherniak, D.J., Ryerson, F.J., 1993. A study of strontium diffusion in apatite using Rutherford backscattering spectroscopy and ion implantation. Geochim. Cosmochim. Acta 57, 4653–4662. https://doi.org/10.1016/0016-7037(93)90190-8

Cherniak, D.J., Watson, E.B., 2001. Pb diffusion in zircon. Chem. Geol. 172, 5–24. https://doi.org/10.1016/S0009-2541(00)00233-3

Choukroune, P., Bouhallier, H., Arndt, N.T., 1995. Soft lithosphere during periods of Archaean crustal growth or crustal reworking. Geol. Soc. Spec. Publ. 95, 67–86. https://doi.org/10.1144/GSL.SP.1995.095.01.05

Cloete, M., 1994. Aspects of Vocanism and Metamorphism of the Onverwacht Group lavas in the South-Western portion of the Barberton Greenstone Belt. University of the Witwatersrand.

Collins, W.J., Van Kranendonk, M.J., 1999. Model for the development of kyanite during partial convective overturn of Archean granite-greenstone terranes: The Pilbara Craton, Australia. J. Metamorph. Geol. 17, 145–156. https://doi.org/10.1046/j.1525-1314.1999.00187.x

Collins, W.J., Van Kranendonk, M.J., Teyssier, C., 1998. Partial convective overturn of Archaean crust in the east Pilbara Craton, Western Australia: Driving mechanisms and tectonic implications. J. Struct. Geol. 20, 1405–1424. https://doi.org/10.1016/S0191-8141(98)00073-X

Compston, W., Pidgeon, R.T., 1986. Jack Hills, evidence of more very old detrital zircons in Western Australia. Nature 321, 766–769. https://doi.org/10.1038/321766a0

Creaser, R.A., Gray, C.M., 1992. Preserved initial 87Sr86Sr in apatite from altered felsic igneous rocks: A case study from the Middle Proterozoic of South Australia. Geochim. Cosmochim. Acta 56, 2789–2795. https://doi.org/10.1016/0016-7037(92)90359-Q

Cutts, K.A., Maneiro, K.A., Stevens, G., Baxter, E.F., 2021. Metamorphic evolution for the Inyoni shear zone: Investigating the geodynamic evolution of a 3.20 Ga terrane boundary in the Barberton granitoid greenstone terrane, South Africa. South African J. Geol. 124, 163–180. https://doi.org/10.25131/sajg.124.0009

Cutts, K.A., Stevens, G., Hoffmann, J.E., Buick, I.S., Frei, D., Münker, C., 2014. Paleo- to Mesoarchean polymetamorphism in the Barberton Granite- Greenstone Belt , South Africa : Constraints from U-Pb monazite and Lu- Hf garnet geochronology on the tectonic processes that shaped the belt 251–270. https://doi.org/10.1130/B30807.1

Cutts, K.A., Stevens, G., Kisters, A., 2015. Reply to “ Paleo- to Mesoarchean polymetamorphism in the Barberton granite-greenstone belt , South Africa : Constraints from U-Pb monazite and Lu-Hf garnet geochronology on the tectonic processes that shaped the belt : Discussion ” by M . Brown 1558–1563. https://doi.org/10.1130/B31304.1

Dann, J.C., 2000. The 3.5 Ga Komati Formation, Barberton Greenstone Belt, South Africa, Part I: New maps and magmatic architecture. South African J. Geol. 103, 47–68. https://doi.org/10.2113/103.1.47

De Ronde, C.E.J., Kamo, S.L., 2000. An Archaean arc-arc collisional event: a short-lived (ca 3 Myr) episode, Weltevreden area, Barberton greenstone belt, South Africa. J. African Earth Sci. 30, 219–248.

de Wit, M.J., 2004. Archean Greenstone Belts Do Contain Fragments of Ophiolites. Dev. Precambrian Geol. 13, 599–614. https://doi.org/10.1016/S0166-2635(04)13018-1

de Wit, M.J., Fripp, R.E.P., Stanistreet, I.G., 1983. Tectonic and stratigraphic implications of new field observations along the southern part of the Barberton greenstone belt. Spec. Publ. Geol. Soc. South Africa 21–29.

de Wit, M.J., Furnes, H., Robins, B., 2011. Geology and tectonostratigraphy of the Onverwacht Suite, Barberton Greenstone Belt, South Africa. Precambrian Res. 186, 1–27. https://doi.org/10.1016/j.precamres.2010.12.007

de Wit, M.J., Hart, R.A., Hart, R.J., 1987. The Jamestown Ophiolite Complex, Barberton mountain belt: a section through 3.5 Ga oceanic crust. J. African Earth Sci. 6, 681–730. https://doi.org/10.1016/0899-5362(87)90007-8

Debaille, V., O'Neill, C., Brandon, A.D., Haenecour, P., Yin, Q.Z., Mattielli, N., Treiman, A.H., 2013. Stagnant-lid tectonics in early Earth revealed by 142Nd variations in late Archean rocks. Earth Planet. Sci. Lett. 373, 83–92. https://doi.org/10.1016/j.epsl.2013.04.016

Diener, J.F.A., Stevens, G., Kisters, A.F.M., Poujol, M., 2005. Metamorphism and exhumation of the basal parts of the Barberton greenstone belt , South Africa : Constraining the rates of Mesoarchaean tectonism 143, 87–112. https://doi.org/10.1016/j.precamres.2005.10.001

Dodson, M.H., 1973. Closure temperature in cooling geochronological and petrological systems. Contrib. to Mineral. Petrol. 40, 259–274. https://doi.org/10.1007/BF00373790

Drabon, N., Lowe, D.R., 2021. Progressive accretion recorded in sedimentary rocks of the 3.28−3.23 Ga Fig Tree Group, Barberton Greenstone Belt. GSA Bull. 1–19. https://doi.org/10.1130/b35973.1

Duclaux, G., Rey, P., Guillot, S., Ménot, R.P., 2007. Orogen-parallel flow during continental convergence: Numerical experiments and archean field examples. Geology 35, 715–718. https://doi.org/10.1130/G23540A.1

Dziggel, A., Armstrong, R.A., Stevens, G., Nasdala, L., 2005. Growth of zircon and titanite during metamorphism in the granitoid-gneiss terrane south of the Barberton greenstone belt, South Africa. Mineral. Mag. 69, 1019–1036.

Dziggel, A., Stevens, G., Poujol, M., Anhaeusser, C.R., Armstrong, R.A., 2002. Metamorphism of the granite-greenstone terrane south of the Barberton greenstone belt, South Africa: An insight into the tectono-thermal evolution of the "lower" portions of the Onverwacht Group. Precambrian Res. 114, 221–247. https://doi.org/10.1016/S0301-9268(01)00225-X

Emo, R.B., Smit, M.A., Schmitt, M., Kooijman, E., Scherer, E.E., Sprung, P., Bleeker, W., Mezger, K., 2018. Evidence for evolved Hadean crust from Sr isotopes in apatite within Eoarchean zircon from the Acasta Gneiss Complex. Geochim. Cosmochim. Acta 235, 450–462. https://doi.org/10.1016/j.gca.2018.05.028

Engi, M., Lanari, P., Kohn, M.J., 2017. Significant Ages - An Introduction to Petrochronology, in: Kohn, M.J., Engi, M., Lanari, P. (Eds.), Petrochronology: Methods and Applications. pp. 1–12.

Faltys, J.P., Wielicki, M.M., 2020. Inclusions in impact-formed zircon as a tracer of target rock lithology: Implications for Hadean continental crust composition and abundance. Lithos 376–377, 105761. https://doi.org/10.1016/j.lithos.2020.105761

Fossen, H., Cavalcante, G.C., de Almeida, R.P., 2017. Hot Versus Cold Orogenic Behavior: Comparing the Araçuaí-West Congo and the Caledonian Orogens. Tectonics 36, 2159–

2178. https://doi.org/10.1002/2017TC004743

Furnes, H., De Wit, M., Staudigel, H., Rosing, M., Muehlenbachs, K., 2007. A vestige of earth's oldest ophiolite. Science (80-.). 315, 1704–1707. https://doi.org/10.1126/science.1139170

Furnes, H., Dilek, Y., De Wit, M., 2015. Precambrian greenstone sequences represent different ophiolite types. Gondwana Res. 27, 649–685. https://doi.org/10.1016/j.gr.2013.06.004

Furnes, H., Rosing, M., Dilek, Y., de Wit, M., 2009. Isua supracrustal belt (Greenland)-A vestige of a 3.8 Ga suprasubduction zone ophiolite, and the implications for Archean geology. Lithos 113, 115–132. https://doi.org/10.1016/j.lithos.2009.03.043

Grosch, E.G., Kosler, J., Mcloughlin, N., Drost, K., Slama, J., Pedersen, R.B., 2011. Paleoarchean detrital zircon ages from the earliest tectonic basin in the Barberton Greenstone Belt , Kaapvaal craton , South Africa. Precambrian Res. 191, 85–99. https://doi.org/10.1016/j.precamres.2011.09.003

Grosch, E.G., Slama, J., 2017. Evidence for 3.3-billion-year-old oceanic crust in the Barberton greenstone belt, South Africa. Geology. https://doi.org/10.1177/0964663912467814

Guitreau, M., Blichert-Toft, J., Martin, H., Mojzsis, S.J., Albarède, F., 2012. Hafnium isotope evidence from Archean granitic rocks for deep-mantle origin of continental crust. Earth Planet. Sci. Lett. 337–338, 211–223. https://doi.org/10.1016/j.epsl.2012.05.029

Halla, J., van Hunen, J., Heilimo, E., Hölttä, P., 2009. Geochemical and numerical constraints on Neoarchean plate tectonics. Precambrian Res. 174, 155–162. https://doi.org/10.1016/j.precamres.2009.07.008

Hansen, V.L., Willis, J.J., 1996. Structural analysis of a sampling of tesserae: Implications for Venus geodynamics. Icarus 123, 296–312. https://doi.org/10.1006/icar.1996.0159

Harris, L.B., Bédard, J.H., 2015. Interactions between continent-like "drift", rifting and mantle flow on Venus: Gravity interpretations and Earth analogues. Geol. Soc. Spec. Publ. 401, 327–356. https://doi.org/10.1144/SP401.9

Harris, L.B., Bédard, J.H., 2014. Crustal Evolution and Deformation in a Non-Plate-Tectonic Archaean Earth: Comparisons with Venus, in: Dilek, Y., Furnes, H. (Eds.), Evolution of Archean Crust and Early Life. Springer, pp. 215–291. https://doi.org/10.1007/978-94-007-7615-9_9

Harrison, T.M., 2009. The hadean crust: Evidence from >4 Ga Zircons. Annu. Rev. Earth Planet. Sci. 37, 479–505. https://doi.org/10.1146/annurev.earth.031208.100151

Harrison, T.M., Célérier, J., Aikman, A.B., Hermann, J., Heizler, M.T., 2009. Diffusion of 40Ar in muscovite. Geochim. Cosmochim. Acta 73, 1039–1051. https://doi.org/10.1016/j.gca.2008.09.038

Henrichs, I.A., O'Sullivan, G., Chew, D.M., Mark, C., Babechuk, M.G., McKenna, C., Emo, R., 2018. The trace element and U-Pb systematics of metamorphic apatite. Chem. Geol. 483, 218–238. https://doi.org/10.1016/j.chemgeo.2017.12.031

Hensen, B.J., BO. Zhou, 1995. Retention of isotopic memory in garnets partially broken down during an overprinting granulite-facies metamorphism: implications for the Sm-Nd closure temperature. Geology 23, 225–228. https://doi.org/10.1130/0091-7613(1995)023<0225:ROIMIG>2.3.CO;2

Kamo, S.L., Davis, D.W., 1994. Reassessment of Archean crustal development in the

Barberton Mountain Land, South Africa, based on U-Pb dating. Tectonics 13, 167–192.

Kato, D., Aoki, K., Komiya, T., Yamamoto, S., Sawaki, Y., Asanuma, H., Sato, T., Tsuchiya, Y., Shozugawa, K., Matsuo, M., Windley, B.F., 2018. Constraints on the P–T conditions of high-pressure metamorphic rocks from the Inyoni shear zone in the mid-Archean Barberton Greenstone Belt, South Africa. Precambrian Res. 315, 1–18. https://doi.org/10.1016/j.precamres.2018.06.018

Kisters, A F M, Anhaeusser, C.R., 1995. Emplacement features of Archean TTG plutons along the southern margin of the Barberton greenstone belt, South Africa. Precambrian Res. 75, 1–15. https://doi.org/10.1016/0301-9268(95)00003-N

Kisters, A. F.M., Anhaeusser, C.R., 1995. The structural significance of the Steynsdorp pluton and anticline within the tectono-magmatic framework of the Barberton Mountain Land. South African J. Geol. 98, 43–51.

Kisters, A.F.M., Belcher, R.W., Poujol, M., Dziggel, A., 2010. Continental growth and convergence-related arc plutonism in the Mesoarchaean : Evidence from the Barberton granitoid-greenstone terrain , South Africa. Precambrian Res. 178, 15–26. https://doi.org/10.1016/j.precamres.2010.01.002

Kisters, A.F.M., Stevens, G., Dziggel, A., Armstrong, R.A., 2003. Extensional detachment faulting and core-complex formation in the southern Barberton granite-greenstone terrain, South Africa: Evidence for a 3.2 Ga orogenic collapse. Precambrian Res. https://doi.org/10.1016/j.precamres.2003.08.002

Kröner, A., Anhaeusser, C.R., Hoffmann, J.E., Wong, J., Geng, H., Hegner, E., Xie, H., Yang, J., Liu, D., 2016. Chronology of the oldest supracrustal sequences in the Palaeoarchaean Barberton Greenstone Belt, South Africa and Swaziland. Precambrian Res. 279, 123–143. https://doi.org/10.1016/J.PRECAMRES.2016.04.007

Kröner, A., Byerly, G.R., Lowe, D.R., 1991. Chronology of early Archaean granite-greenstone evolution in the Barberton Mountain Land, South Africa, based on precise dating by single zircon evaporation. Earth Planet. Sci. Lett. 103, 41–54. https://doi.org/10.1016/0012-821X(91)90148-B

Kröner, A., Elis Hoffmann, J., Xie, H., Wu, F., Münker, C., Hegner, E., Wong, J., Wan, Y., Liu, D., 2013. Generation of early Archaean felsic greenstone volcanic rocks through crustal melting in the Kaapvaal, craton, southern Africa. Earth Planet. Sci. Lett. 381, 188–197. https://doi.org/10.1016/j.epsl.2013.08.029

Kröner, A., Hegner, E., Wendt, J.I., Byerly, G.R., 1996. The oldest part of the Barberton granitoid-greenstone terrain, South Africa: Evidence for crust formation between 3.5 and 3.7 Ga. Precambrian Res. 78, 105–124. https://doi.org/10.1016/0301-9268(95)00072-0

Kröner, A., Hoffmann, J.E., Wong, J.M., Geng, H.-Y., Schneider, K.P., Xie, H., Yang, J.-H., Nkleko, N., 2019. Archean Crystalline Rocks of the Eastern Kaapvaal Craton, in: Kröner, A., Hofmann, A. (Eds.), The Archean Geologz of the Kaapvaal Craton, Southern Africa. Springer, pp. 1–32. https://doi.org/https://doi.org/10.1007/978-3-319-78652-0

Kröner, A., Todt, W., 1988. Single Zircon Dating Constraining the Maximum Age of the Barberton Greenstone Belt, Southern Africa. J. Geophys. Res. 93, 15,329-15,337.

Kröner, A., Wong, J., Xie, H., 2018. The oldest granite clast in the moodies conglomerate, barberton greenstone belt, South Africa, and its likely origin. South African J. Geol. 121, 43–50. https://doi.org/10.25131/sajg.121.0001

Lana, C., Kisters, A., Stevens, G., 2010a. Exhumation of Mesoarchean TTG gneisses from the middle crust: Insights from the Steynsdorp core complex, Barberton granitoid-greenstone terrain, South Africa. Bull. Geol. Soc. Am. 122, 183–197.

https://doi.org/10.1130/B26580.1

Lana, C., Tohver, E., Cawood, P., 2010b. Quantifying rates of dome-and-keel formation in the Barberton granitoid-greenstone belt, South Africa. Precambrian Res. 177, 199–211. https://doi.org/10.1016/j.precamres.2009.12.001

Laurent, O., Björnsen, J., Wotzlaw, J.F., Bretscher, S., Pimenta Silva, M., Moyen, J.F., Ulmer, P., Bachmann, O., 2020. Earth's earliest granitoids are crystal-rich magma reservoirs tapped by silicic eruptions. Nat. Geosci. https://doi.org/10.1038/s41561-019-0520-6

Laurie, A., Stevens, G., 2012. Water-present eclogite melting to produce Earth's early felsic crust. Chem. Geol. 314–317, 83–95. https://doi.org/10.1016/j.chemgeo.2012.05.001

Laurie, A., Stevens, G., Van Hunen, J., 2013. The end of continental growth by TTG magmatism. Terra Nov. 25, 130–136. https://doi.org/10.1111/ter.12015

Lee, J.K.W., Williams, I.S., Ellis, D.J., 1997. Pb, U and Th diffusion in natural zircon. Lett. to Nat. 390, 159–162.

Levander, A., Schmandt, B., Miller, M.S., Liu, K., Karlstrom, K.E., Crow, R.S., Lee, C.T.A., Humphreys, E.D., 2011. Continuing Colorado plateau uplift by delamination-style convective lithospheric downwelling. Nature 472, 461–465. https://doi.org/10.1038/nature10001

Lowe, D.R., Byerly, G.R., 1999. Stratigraphy of the west-central part of the Barberton greestone belt, in: Lowe, D.R., Byerly, G.R. (Eds.), Geologic Evolution of the Barberton Greenstone Belt. Geological Society of America, pp. 1–36.

Lowe, D.R., Byerly, G.R., Heubeck, C., 2012. Geologic Map of the West-Central Barberton Greenstone Belt, South Africa.

Martin, H., 1999. Adakitic magmas: Modern analogues of Archaean granitoids. Lithos 46, 411–429. https://doi.org/10.1016/S0024-4937(98)00076-0

Martin, H., 1986. Effect of steeper Archean geothermal gradient on geochemistry of subduction-zone magmas. Geology 753–756. https://doi.org/10.1130/0091-7613(1986)14<753

Martin, H., Moyen, J.F., 2002. Secular changes in tonalite-trondhjemite-granodiorite composition as markers of the progressive cooling of Earth. Geology 30, 319–322. https://doi.org/10.1130/0091-7613(2002)030<0319:SCITTG>2.0.CO;2

Matsumura, R., 2014. The petrogenesis of the Nelshoogte pluton: The youngest and most compositionally variable TTG plutons in the Barberton Granit-Greenstone Terrain. Stellenbosch University.

Mayne, M.J., Stevens, G., Moyen, J.F., 2020. A phase equilibrium investigation of selected source controls on the composition of melt batches generated by sequential melting of an average metapelite. Geol. Soc. Spec. Publ. 491, 223–241. https://doi.org/10.1144/SP491-2018-121

Mezger, K., Essene, E.J., Halliday, A.N., 1992. Closure temperatures of the SmNd system in metamorphic garnets. Earth Planet. Sci. Lett. 113, 397–409. https://doi.org/10.1016/0012-821X(92)90141-H

Moyen, J.-F., Stevens, G., Kisters, A.F.M., Belcher, R.W., Lemirre, B., 2019. TTG Plutons of the Barberton Granitoid-Greenstone Terrain, South Africa, in: Van Kranendonk, M.J., Bennett, V.C., Hoffmann, J.E. (Eds.), Earth's Oldest Rocks. pp. 615–653.

Moyen, J.F., 2011. The composite Archaean grey gneisses: Petrological significance, and

evidence for a non-unique tectonic setting for Archaean crustal growth. Lithos 123, 21–36. https://doi.org/10.1016/j.lithos.2010.09.015

Moyen, J.F., Laurent, O., 2018. Archaean tectonic systems: A view from igneous rocks. Lithos. https://doi.org/10.1016/j.lithos.2017.11.038

Moyen, J.F., Martin, H., 2012. Forty years of TTG research. Lithos. https://doi.org/10.1016/j.lithos.2012.06.010

Moyen, J.F., Stevens, G., Kisters, A.F.M., 2006. Record of mid-Archaean subduction from metamorphism in the Barberton terrain , South Africa. Nature 442, 559–562. https://doi.org/10.1038/nature04972

Moyen, J.F., van Hunen, J., 2012. Short-term episodicity of Archaean plate tectonics. Geology 40, 451–454. https://doi.org/10.1130/G322894.1

Mühlberg, M., Hegner, E., Klemd, R., Pfänder, J.A., Kaliwoda, M., Biske, Y.S., 2016. Late Carboniferous high-pressure metamorphism of the Kassan Metamorphic Complex (Kyrgyz Tianshan) and assembly of the SW Central Asian Orogenic Belt. Lithos 264, 41–55. https://doi.org/10.1016/j.lithos.2016.08.008

Nédélec, A., Chevrel, M.O., Moyen, J.F., Ganne, J., Fabre, S., 2012. TTGs in the making: Natural evidence from Inyoni shear zone (Barberton, South Africa). Lithos 153, 25–38. https://doi.org/10.1016/j.lithos.2012.05.029

Nutman, A.P., Bennett, V.C., Friend, C.R.L., Norman, M.D., 1999. Meta-igneous (non-gneissic) tonalites and quartz-diorites from an extensive ca. 3800 Ma terrain south of the Isua supracrustal belt, southern West Greenland: Constraints on early crust formation. Contrib. to Mineral. Petrol. 137, 364–388. https://doi.org/10.1007/s004100050556

O'Neill, C., Jellinek, A.M., Lenardic, A., 2007. Conditions for the onset of plate tectonics on terrestrial planets and moons. Earth Planet. Sci. Lett. 261, 20–32. https://doi.org/10.1016/j.epsl.2007.05.038

O'Neill, C., Lenardic, A., Condie, K.C., 2015. Earth's punctuated tectonic evolution: Cause and effect. Geol. Soc. Spec. Publ. 389, 17–40. https://doi.org/10.1144/SP389.4

Palin, R.M., Dyck, B., 2018. Metamorphic consequences of secular changes in oceanic crust composition and implications for uniformitarianism in the geological record. Geosci. Front. 9, 1009–1019. https://doi.org/10.1016/j.gsf.2018.04.004

Palin, R.M., White, R.W., 2016. Emergence of blueschists on Earth linked to secular changes in oceanic crust composition. Nat. Geosci. 9, 60–64. https://doi.org/10.1038/ngeo2605

Piskorz, D., Elkins-Tanton, L.T., Smrekar, S.E., 2014. Coronae formation on Venus via extension and lithospheric instability. J. Geophys. Res. Planets 119, 2568–2582. https://doi.org/10.1002/2014JE004636

Rey, P.F., Coltice, N., Flament, N., 2014. Spreading continents kick-started plate tectonics. Nature 513, 405–408. https://doi.org/10.1038/nature13728

Rudnick, R.L., 1995. Making continental crust. Nature 378, 571–578. https://doi.org/10.1038/378571a0

Sanchez-Garrido, C.J.M.G., Stevens, G., Armstrong, R.A., Moyen, J.F., Martin, H., Doucelance, R., 2011. Diversity in earth's early felsic crust: Paleoarchean peraluminous granites of the Barberton Greenstone Belt. Geology 39, 963–966. https://doi.org/10.1130/G32193.1

Schmitz, M., Heubeck, C., 2021. Constraints on deformation mechanisms of the Barberton

Greenstone Belt from regional stratigraphic and structural data of the synorogenic Moodies Group. Precambrian Res. 362, 106177. https://doi.org/10.1016/j.precamres.2021.106177

Schoene, B., de Wit, M.J., Bowring, S.A., 2008. Mesoarchean assembly and stabilization of the eastern Kaapvaal craton: A structural-thermochronological perspective. Tectonics 27, 1–27. https://doi.org/10.1029/2008TC002267

Scott, D.J., St-Onge, M.R., 1995. Constraints on Pb closure temperature in titanite based on rocks from the Ungava orogen, Canada: implications for U-Pb geochronology and P-T-t path determinations. Geology 23, 1123–1126. https://doi.org/10.1130/0091-7613(1995)023<1123:COPCTI>2.3.CO;2

Sha, L.K., Chappell, B.W., 1999. Apatite chemical composition, determined by electron microprobe and laser-ablation inductively coupled plasma mass spectrometry, as a probe into granite petrogenesis. Geochim. Cosmochim. Acta 63, 3861–3881. https://doi.org/10.1016/S0016-7037(99)00210-0

Sizova, E., Gerya, T., Brown, M., Stüwe, K., 2018. What drives metamorphism in early Archean greenstone belts? Insights from numerical modeling. Tectonophysics 746, 587–601. https://doi.org/10.1016/j.tecto.2017.07.020

Sizova, E., Gerya, T., Stüwe, K., Brown, M., 2015. Generation of felsic crust in the Archean: A geodynamic modeling perspective. Precambrian Res. 271, 198–224. https://doi.org/10.1016/j.precamres.2015.10.005

Smithies, R.H., Champion, D.C., Van Kranendonk, M.J., 2009. Formation of Paleoarchean continental crust through infracrustal melting of enriched basalt. Earth Planet. Sci. Lett. 281, 298–306. https://doi.org/10.1016/j.epsl.2009.03.003

Smithies, R.H., Van Kranendonk, M.J., Champion, D.C., 2007. The Mesoarchean emergence of modern-style subduction 11, 50–68. https://doi.org/10.1016/j.gr.2006.02.001

Sullivan, G.O., Chew, D., Kenny, G., Henrichs, I., Mulligan, D., 2020. Earth-Science Reviews The trace element composition of apatite and its application to detrital provenance studies. Earth-Science Rev. 201, 103044. https://doi.org/10.1016/j.earscirev.2019.103044

Tagami, T., Carter, A., Hurford, A.J., 1996. Natural long-term annealing of the zircon fission-track system in Vienna Basin deep borehole samples: Constraints upon the partial annealing zone and closure temperature. Chem. Geol. 130, 147–157. https://doi.org/10.1016/0009-2541(96)00016-2

van Hunen, J., Moyen, J.-F., 2012. Archean Subduction: Fact or Fiction? Annu. Rev. Earth Planet. Sci. 40, 195–219. https://doi.org/10.1146/annurev-earth-042711-105255

Van Kranendonk, M.J., 2011. Cool greenstone drips and the role of partial convective overturn in Barberton greenstone belt evolution. J. African Earth Sci. 60, 346–352. https://doi.org/10.1016/j.jafrearsci.2011.03.012

Van Kranendonk, M.J., 2007. Chapter 8.6 Tectonics of Early Earth. Dev. Precambrian Geol. https://doi.org/10.1016/S0166-2635(07)15086-6

Van Kranendonk, M.J., Collins, W.J., Hickman, A., Pawley, M.J., 2004. Critical tests of vertical vs. horizontal tectonic models for the Archaean East Pilbara Granite-Greenstone Terrane, Pilbara Craton, Western Australia, in: Precambrian Research. pp. 173–211. https://doi.org/10.1016/j.precamres.2003.12.015

Van Kranendonk, M.J., Kröner, A., Hegner, E., Connelly, J., 2009. Age, lithology and structural evolution of the c. 3.53 Ga Theespruit Formation in the Tjakastad area,

southwestern Barberton Greenstone Belt, South Africa, with implications for Archaean tectonics. Chem. Geol. 261, 114–138. https://doi.org/10.1016/j.chemgeo.2008.11.006

Van Kranendonk, M.J., Kröner, A., Hoffman, J.E., Nagel, T., Anhaeusser, C.R., 2014. Just another drip: Re-analysis of a proposed mesoarchean suture from the Barberton mountain land, South Africa. Precambrian Res. 254, 19–35. https://doi.org/10.1016/j.precamres.2014.07.022

Van Kranendonk, M.J., Smithies, R.H., Griffin, W.L., Huston, D.L., Hickman, A.H., Champion, D.C., Anhaeusser, C.R., Pirajno, F., 2015. Making it thick: a volcanic plateau origin of Palaeoarchean continental lithosphere of the Pilbara and Kaapvaal cratons. Geol. Soc. London, Spec. Publ. 389, 83–111. https://doi.org/10.1144/SP389.12

Van Kranendonk, M.J., Smithies, R.H., Hickman, A.H., Champion, D.C., 2007. Chapter 4.1 Paleoarchean Development of a Continental Nucleus: the East Pilbara Terrane of the Pilbara Craton, Western Australia. Dev. Precambrian Geol. https://doi.org/10.1016/S0166-2635(07)15041-6

Viljoen, R.P., Viljoen, M.J., 1969. The Geological and Geochemical Significance of the Upper Formations of the Onverwacht Group. Geol. Soc. South Africa Spec. Publ. 2, 113–152.

Wang, H., Yang, J.H., Kröner, A., Zhu, Y.S., Li, R., 2019. Non-subduction origin for 3.2 Ga high-pressure metamorphic rocks in the Barberton granitoid-greenstone terrane, South Africa. Terra Nov. 31, 373–380. https://doi.org/10.1111/ter.12397

Webster, J.D., Piccoli, P.M., 2015. Magmatic apatite: A powerful, yet deceptive, mineral. Elements 11, 177–182. https://doi.org/10.2113/gselements.11.3.177

Yamada, R., Tagami, T., Nishimura, S., Ito, H., 1995. Annealing kinetics of fission tracks in zircon: an experimental study. Chem. Geol. 122, 249–258. https://doi.org/10.1016/0009-2541(95)00006-8

Zeh, A., Gerdes, A., Barton, J.M., 2009. Archean accretion and crustal evolution of the kalahari craton - The zircon age and Hf isotope record of granitic rocks from barberton/ swaziland to the francistown arc. J. Petrol. 50, 933–966. https://doi.org/10.1093/petrology/egp027

Zirner, A.L.K., Marks, M.A.W., Wenzel, T., Jacob, D.E., Markl, G., 2015. Rare earth elements in apatite as a monitor of magmatic and metasomatic processes: The Ilímaussaq complex, South Greenland. Lithos 228–229, 12–22. https://doi.org/10.1016/j.lithos.2015.04.013

Chapter 2: Field work and samples

The field area of this thesis is the Stolzburg Block in the southern BGGT, spanning an area of ca. 350 km^2 (Figs 1.8 and 2.1). The important lithologies and geochronological constraints of the Stolzburg Block are summarized in Chapter 1.3.2. Field work was performed in 2017 in two blocks. The first field trip (25.03.2017 to 09.04.2017) served as an introduction to the Stolzburg Block and also the broader BGGT geology. Seven days were spent in the southern and nine days in the northern part of the BGGT. Key outcrops in the Stolzburg Block were visited and 27 samples were taken. The second field trip (08.08.2017 to 30.08.2017) focused on field work in the Stolzburg Block. Some key outcrops were revisited and studied more extensively than before. Areas of the Stolzburg Block that had not been visited in the first field trip were explored with the target of mapping the occurrence and distribution of cross-cutting felsic dykes in the ca. 3.45 Ga plutons. An additional 26 samples were taken on the second field trip. In the two field trips combined, samples of 46 granitoids, six supracrustal rocks and one pegmatitic vein were taken from the Stolzburg Block. Short sample and outcrop descriptions and localities are listed in Table 2.1, and the sample localities and the distance covered in the two field trips are shown in Figure 2.1. The results of the field work in the Stolzburg Block are described in the following sections, divided according to the plutonic bodies as per Anhaeusser et al. (1981). The field work in the north of the BGGT is beyond the scope of this thesis and will not be discussed here.

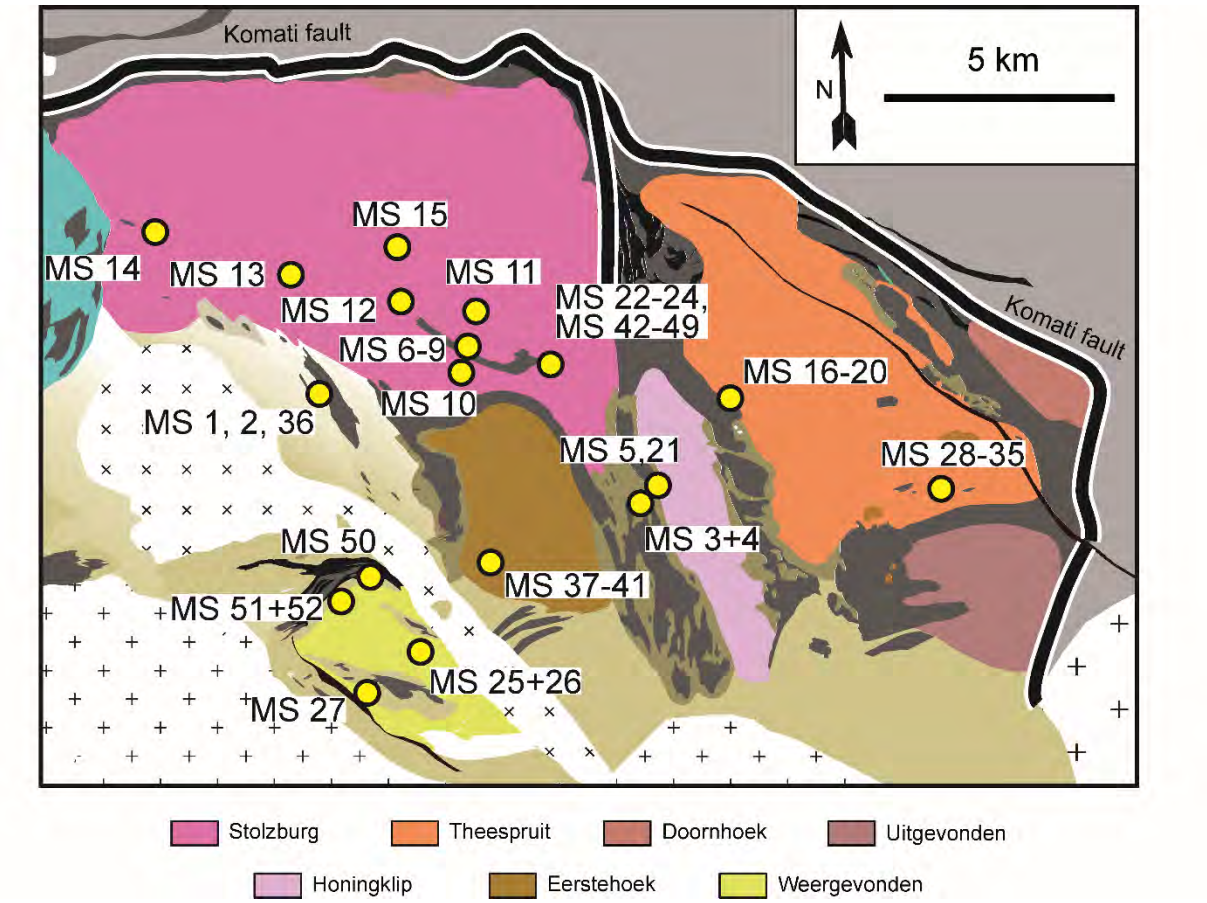

Fig. 2.1. Geological map of the Stolzburg Block showing the sample localities. See Figure 1.8 for the full legend and Table 2.1 for GPS coordinates and descriptions of the sample localities. Modified after Moyen et al. (2019).

Table 2.1 Field descriptions and localities of samples taken from the Stolzburg Block.

Sample	Field description	Locality	Coordinates
Stolzburg Pluton			
MS 1	Undeformed felsic dyke, weathered	Near river; south-western margin of Stolzburg Pluton	26.03086 °S 30.71258 °E
MS 2	Foliated trondhjemite		26.03089 °S 30.71280 °E
MS 36	Ca. 10 cm thick more mafic phase within trondhjemite	Other side of the river from samples MS 1 and MS 2	26.03112 °S 30.71247 °E
MS 6	Foliated grey gneiss to migmatite	Theeboom Gneisses; southern margin of the Stolzburg Pluton	26.02244 °S 30.74375 °E
MS 7	Dark grey felsic dyke?		
MS 8	Light grey felsic dykes		
MS 9			
MS 10	Vertically foliated, weakly laminated grey gneiss	Upstream from samples MS 6 to MS 9	26.02764 °S 30.74306 °E
MS 11	Main Trondhjemite; weak foliation	In a field, ca. 200 m south of R541	26.01578 °S 30.74792 °E
MS 12	Main Trondhjemite; weak foliation	In a field, next to R541	26.01142 °S 30.73742 °E
MS 13	Main Trondhjemite; most weathered sample, semi-fresh inside	In a field, next to R541	26.00675 °S 30.71489 °E
MS 14	Main Trondhjemite; weak foliation	Westernmost visible of the Stolzburg Pluton	25.99689 °S 30.67719 °E
MS 15	Main Trondhjemite; more deformed than samples MS 11 to MS 14	In a field, about halfway between R541 and Tjakastad road	26.00331 °S 30.73664 °E
MS 22	Main Trondhjemite	(Abandoned?) quarry on south-eastern margin of the Stolzburg Pluton	26.02475 °S 30.76181 °E
MS 23	Dark grey granitoid, fine grained; titanite visible in hand specimen		
MS 24	Light grey dyke, cutting both MS 22 and MS 23		
MS 42	Main Trondhjemite		26.02465 °S 30.76195 °E
MS 43	Garnet/cordierite-bearing pegmatite?		n/a
MS 44	Dark grey granitoid, fine grained; no titanite visible in hand specimen		26.02392 °S 30.76065 °E
MS 45	Light grey dyke		26.02505 °S 30.76189 °E
MS 46	Dark grey dyke		26.02440 °S 30.76128 °E
MS 47	Light grey dyke, cutting MS 45		26.02490 °E 30.76191 °E
MS 48	Dark grey dyke, cutting everything except some pegmatitic dykes		26.02489 °E 30.76192 °E
MS 49	Light grey dyke, cutting through everything; pegmatitic in center		26.02552 °S 30.76221 °E

Table 2.1, continued.

Sample	Field description	Locality	Coordinates
Theespruit Pluton			
MS 16	Theesp. Fm. felsic metasediment	Intrusive breccia at the contact of trondhjemite and Theespruit Formation supracrustal rocks at the western margin of the Theespruit Pluton	26.03581 °S 30.80253 °E
MS 17	Main Trondhjemite; sampled in close proximity to contact with greenstones		
MS 18			
MS 19	Fine grained, undeformed felsic dyke, cutting both trondhjemite and greenstone		
MS 20			
MS 28	Greenstone xenoliths	Abandoned quarry on the southern margin of the Theespruit Pluton	26.05583 °S 30.85027 °E
MS 29			26.05587 °S 30.85027 °E
MS 30	Series of Main Trondhjemite samples taken along the top side of the quarry		26.05624 °S 30.85023 °E
MS 31			26.05616 °S 30.85016 °E
MS 32			26.05609 °S 30.85015 °E
MS 33			26.05604 °S 30.85011 °E
MS 34			26.05591 °S 30.85018 °E
MS 35			26.05583 °S 30.85027 °E
Weergevonden Pluton			
MS 25	Dark grey granitoid; titanite visible in hand specimen	Roadcut on R541, east side	
MS 26b	Dark grey granitoid; no titanite visible in hand specimen	Roadcut on R541, west side	26.09008 °S 30.73336 °E
MS 26	Strongly banded grey granitoid; titanite visible in hand specimen	Roadcut on R541, east side	
MS 27	Sheared trondhjemite	Hill on southern margin of Weergevonden Pluton	26.09836 °S 30.72219 °E
MS 50	Foliated trondhjemite	North-wester margin of Weergevonden Pluton	26.07312 °S 30.72350 °E
MS 51	Trondhjemite; weathered	River platform on western margin of Weergevonden Pl.	26.07853 °S 30.71645 °E
MS 52	Dark grey dyke; weathered		

Table 2.1, continued.

Sample	Field description	Locality	Coordinates
Honingklip Pluton?			
MS 3	Fine grained, undeformed dark grey dyke	Pavement next to river	26.05489 °S 30.78208 °E
MS 4	Medium- to coarse-grained, foliated and deformed "grey gneiss"		
MS 21	Garnet-bearing schist, cut by or interlayered with quartz-muscovite-rich phase	Next to river by broken down bridge	26.05250 °S 30.78497 °E
MS 5	Garnet-bearing schist, badly weathered	Continuation of MS 21 up a hill	26.05372 °S 30.78586 °E
Eerstehoek Pluton			
MS 37	Foliated trondhjemite	Pavement next to the road	26.06803 °S 30.74864 °E
MS 38	Garnet/cordierite-bearing pegmatite?	Pavement next to river on the western margin of the Eerstehoek Pluton	26.06904 °S 30.74963 °E
MS 39	Greenstone xenolith		26.06933 °S 30.74875 °E
MS 40	Lightly deformed trondhjemite		26.06938 °S 30.74879 °E
MS 41	Fine-grained felsic dyke		

2.1 Stolzburg Pluton

This study focused primarily on the Stolzburg Pluton, the largest of the plutonic bodies in the Stolzburg Block (Fig. 2.2a). The field work was limited to the central and southern part of the Stolzburg Pluton, due to inaccessibility of the northern part located in a private nature reserve.

The westernmost outcrop of the Stolzburg Pluton is located close to the turnoff from the R541 onto the old Lochiel road. Sample *MS 14* was taken from the largest outcrop on the western margin of the Stolzburg Pluton. The outcrop is dome-shaped body of ~5 m diameter, rising ~1 m above the surrounding soil, and contains only one phase, a sheared trondhjemite. There are a few smaller outcroppings to the west, in which only trondhjemite crops out in all but one. The westernmost of these, ~500 m to the west of the large outcrop, contains a ~10 cm wide leucocratic dyke cutting the Main Trondhjemite.

Outcrops are scarce and limited to flat pavements of the side of the old Lochiel road. On the south-western margin of the Stolzburg Pluton, there is a large outcrop on the Theespruit River. It is found to the west of the old Lochiel road, just before crossing a bridge over the Theespruit River. The outcrop is ~200 x 150 m in size and is dominated by the typical homogenous trondhjemite, though other phases can be found as well. In the north-eastern part of the outcrop, closest to the bridge, some cm- to m-sized greenstone xenoliths occur inside the trondhjemite. The trondhjemite is cut by a North-South trending, ~20 cm thick leucocratic dyke; the dyke is fine grained, with quartz, feldspar, biotite and epidote visible to the naked eye in hand specimen. On the western edge of the outcrop, where sampling with a hammer was

possible, a weathered sample (*MS 1*) was taken from the felsic dyke. Sample *MS 2* was taken from the Main Trondhjemite ~30 m to the east from sample MS 1. A more mafic phase occurs as a roughly North-South trending, ~10 cm thick band within the trondhjemite on the southside of the Theespruit river (Fig. 2.2c); it was sampled as *MS 36*.

The “Zebra outcrop” (Fig. 2.2d) in the Theeboom Gneisses locality has previously been described and studied by Schoene et al. (2008). Here, samples were taken from a foliated grey gneiss as (*MS 6*), a dark grey phase (*MS 7*) and from two light grey felsic dykes (*MS 8* and *MS 9*). A vertically foliated grey gneiss was sampled further upstream as *MS 10*. Samples *MS 11* to *MS 13* were taken of weakly foliated trondhjemite from outcrops next to the R541, along the southern margin of the Stolzburg Pluton, and the stronger foliated trondhjemite sample *MS 15* was taken about halfway between R541 and Tjakastad road, towards the center of the Stolzburg Pluton.

A quarry on SE corner of Stolzburg Pluton, at the T-junction where R541 turns south towards Lochiel, bears witness to the complicated cross-cutting relationship at the pluton margins. The main phase here is sheeted trondhjemite with a steeply dipping lineation (Fig. 2.2e). There is also a second, darker grey phase, seemingly co-genetic with the trondhjemite. The contact between the trondhjemite and the dark grey phase is usually sharp. However, some “xenoliths” of the trondhjemite can be found in the dark grey phase, that show the same orientation of lineation as the massive trondhjemite (Fig. 2.2f). The “dark grey main phase” occurs in two varieties: one with titanite visible in hand-specimen, found in the north-east side of the quarry, and one without visible titanite, found in the west side of the quarry. The trondhjemite was sampled as *MS 22* and *MS 42*, a more leucocratic variety of the trondhjemite as *MS 43* and the dark grey main phase as MS 23 (visible titanite) and MS 44 (no visible titanite). Within the trondhjemite, there are numerous greenstone remnants, ranging from small xenoliths (cm to dm size) to bands of 10s of cm thickness to enclaves of 10s of meters (Fig. 2.2g+h). The trondhjemite is intrusive into the greenstone (Fig. 2.2i). Greenstones, trondhjemite and the dark grey main phase are cut by a series of leucocratic dykes and veins (Fig. 2.2j). At least five major cross-cutting phases were identified and were sampled as *MS 24* and *MS 45* to *MS 49*.

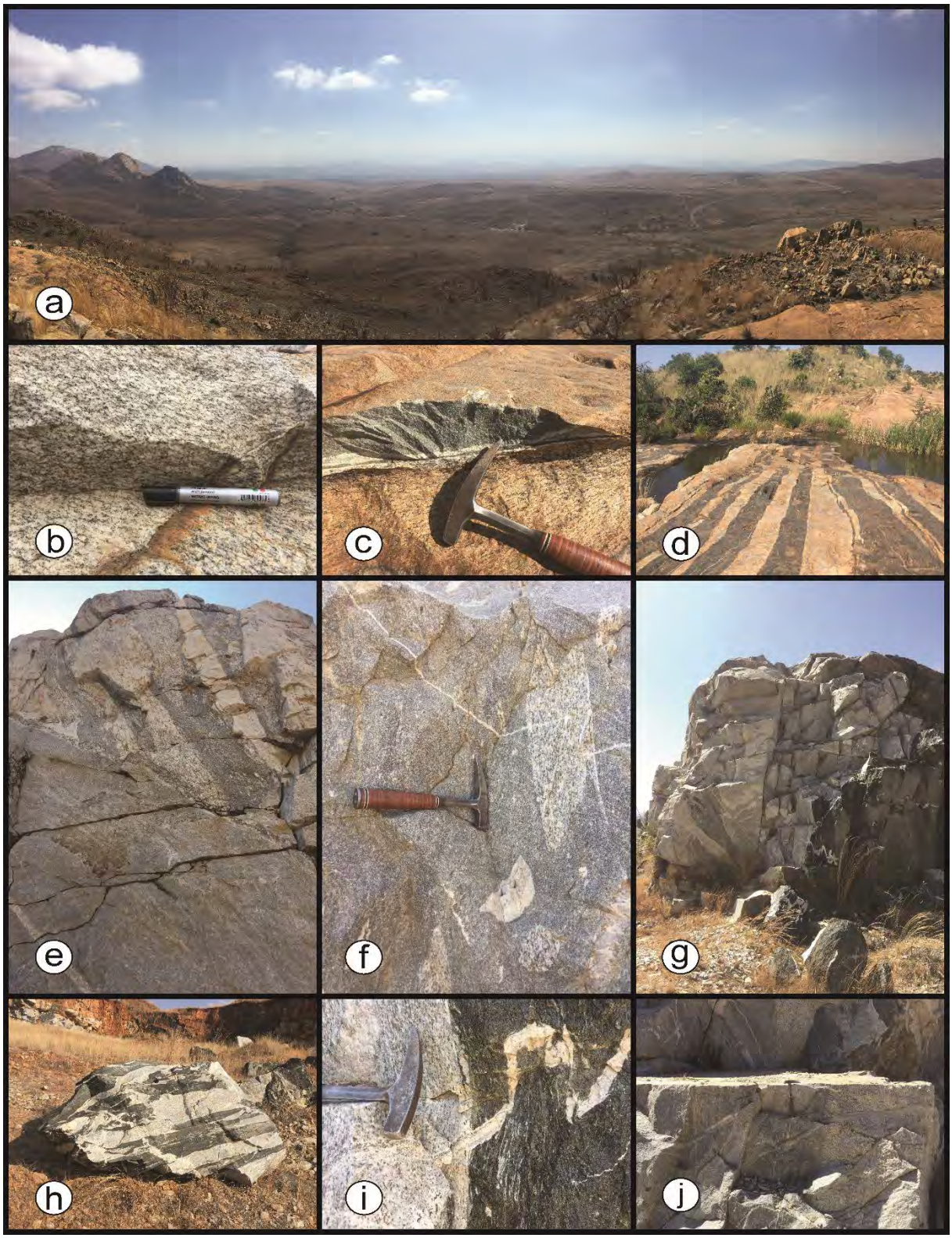

Fig. 2.2. Field photos from the Stolzburg Pluton. (a) The Stolzburg Pluton, as seen from the south. (b) Homogenous foliated trondhjemite of the Stolzburg Pluton. (b) Localized mafic phase within the trondhjemite (sampled as MS 36). (d) “Zebra outcrop” of Theeboom gneisses on the southern margin of the Stolzburg Pluton. (e) and (f) Compositional variety of TTG rocks on the eastern margin of the Stolzburg Pluton. (g) to (i) Variety of greenstone remnants within the Stolzburg Pluton. (j) Multiple generations of felsic dykes cross-cutting the Stolzburg Pluton on the eastern margin.

2.2 Theespruit Pluton

The Theespruit Pluton is in most parts comprised of a similar homogenous foliated trondhjemite to the Stolzburg Pluton. In the west-central part, a dioritic phase can be found. On the western margin of the Theespruit Pluton at the contact with the Theespruit Formation, the trondhjemite is heavily intruding into the greenstone (Fig. 2.3a). Both the trondhjemite and the greenstone are cut by undeformed dykes (Fig. 2.3a+b). In the contact zone of pluton and supracrustal rocks, a Theespruit Formation felsic meta-sediment was sampled as *MS 16*, the trondhjemite close to contact with greenstone as *MS 17* and *MS 18* and dykes as *MS 19* and *MS 20*. In an abandoned quarry on the southern margin of the Theespruit pluton, some m-sized greenstone xenoliths are found in homogenous trondhjemite (Fig. 2.3c). The greenstone was sampled as *MS 28* and *MS 29*, and a series of trondhjemite samples was taken along the topside of the quarry as samples *MS 30* to *MS 35*.

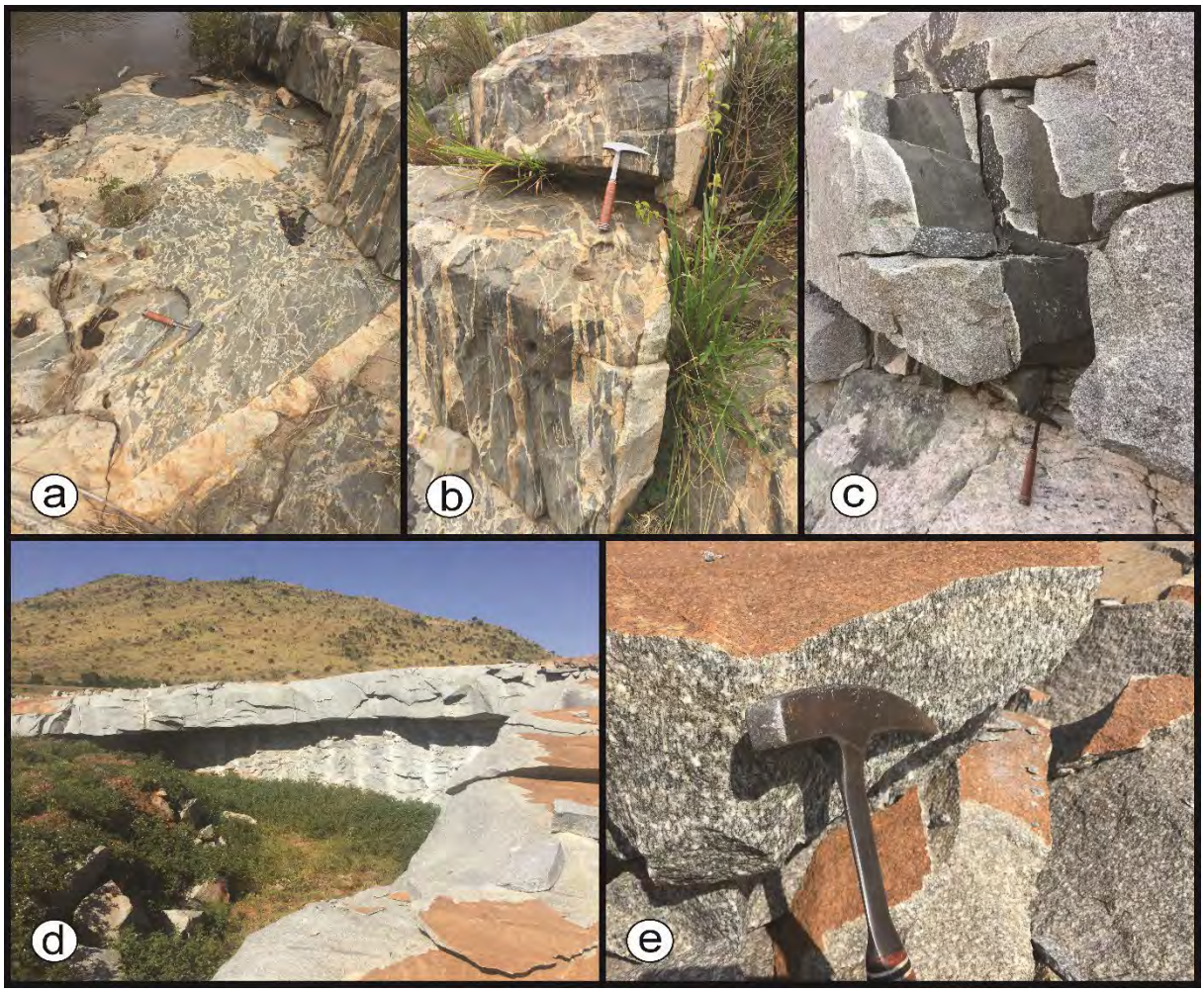

Fig. 2.3. Field photos from the Theespruit Pluton. (a) and (b) Theespruit Formation greenstones intruded by trondhjemite on the western edge of the Theespruit Pluton; both lithologies are cut by younger felsic dykes. (c) Greenstone xenolith of the lower Onverwacht Group in trondhjemite. (d) and (e) Homogenous trondhjemite of the Theespruit Pluton.

2.3 Smaller plutonic bodies

The Doornhoek is the smallest of the plutonic bodies of the Stolzburg Block. It is located in the north-east of the Stolzburg Block. Outcrops are confined to rounded granitoid domes. The trondhjemite of the Doornhoek shows a layering of biotite crystals (Fig. 2.4a), which is perhaps primary igneous layering. The Doornhoek appears fairly homogenous, akin to the Stolzburg and Theespruit plutons. Felsic dykes cross-cutting the Doornhoek trondhjemite are primarily north-south trending. No samples were taken from the Doornhoek.

The Uitgevonden is found south of the Theespruit Pluton and is accessed via a gravel road about halfway between eLukwatini and Mooiplaas. In the south-west, the trondhjemite of the Uitgevonden is intrusive into greenstone lithologies (Fig. 2.4b). The trondhjemite is homogenous and foliated in the north of the Uitgevonden and is cut by felsic dykes (Fig. 2.4c). In the contact zone with the Dalmein Pluton and the Mpuluzi Batholith in the south-east, the trondhjemite is banded and heavily intruded by other felsic plutonic rocks, in places even migmatitic (Fig. 2.4d). Overall, the Uitgevonden is rather heterogenous and should not be referred to as pluton. The more homogenous lithologies could represent an offshoot of the bordering Theespruit Pluton. No samples were taken from the Uitgevonden.

The Honingklip is located between the Theespruit pluton and the Eerstehoek (Fig. 2.1). The north and center of the Honingklip are mostly covered by human settlements. In the south, a homogenous trondhjemite is cut by multiple sets of felsic dykes (Fig. 2.4e+f). Due to the scarcity of outcrops (that are not in somebody's backyard…), it is difficult to comment on the exact nature of the Honingklip and whether it as a whole represents a pluton.

Between the Honingklip and the Eerstehoek is the southern extension of the Schapenburg schist belt. Next to a river within the town of Nhlazatje, a grey gneiss dated to 3532 ± 17 Ma (Moyen, pers. comm.) is found within a weakly foliated granitoid, dated to ca. 3462 ± 17 Ma (Moyen, pers. comm.). The package is cut by at least two sets of felsic dykes (Fig. 2.5a). Near a broken-down bridge, there is an enclave of garnet-bearing schist (Fig. 2.5b+c). The trondhjemite was sampled as *MS 4*, a cross-cutting felsic dyke as *MS 3*. A fresh sample of the garnet-bearing schist was taken next to the river as *MS 21* and the continuation of it on the slope above the river was sampled as *MS 5* from a weathered block.

The Eerstehoek is south of the Stolzburg Pluton and west of the Honingklip. In the north of the Eerstehoek only a few flat pavement outcrops occur on the side of the R541 (Fig. 2.5d). In the eastern part is the town of Nhlazatje. More extensive outcrops are found south of the road connecting the R541 with Nhlazatje, west of the town. Next to the road is a mostly flat pavement of foliated trondhjemite, which is cut by a fine-grained felsic dyke. Both the trondhjemite and the dyke are cut by a m-sized pegmatite and younger quartz-veins (maximum thickness a few

cm). The trondhjemite was sampled as *MS 37* (Fig. 2.5e). Where sampling by hammer is possible, the felsic dyke is too weathered to give a useful sample, so no sample was taken ~~of the dyke~~. Downstream the river south of the road, ca. 3 m thick pegmatite crops out. Nearby, a thinner pegmatitic intrusion bears garnet; some garnet-rich material was sampled as *MS 38*. In the riverbed, greenstone enclaves occur, varying in thickness from 10s of cm to several meters. An intrusive relationship between the greenstone remnants and the trondhjemite can be observed (Fig. 2.5f). Here, trondhjemite and greenstone are again cut by an undeformed felsic dyke. A greenstone remnant was sampled as *MS 39*, the trondhjemite as *MS 40* and a cutting dyke as *MS 41*. South of the town of Nhlazatje, outside of the Eerstehoek proper as defined by Moyen et al. (2019), cross-cutting dykes are found in homogenous foliated trondhjemite. The main rock of Eerstehoek appears to be fairly homogenous and, at least in the northern and western parts, the Eerstehoek might represent a coherent plutonic body.

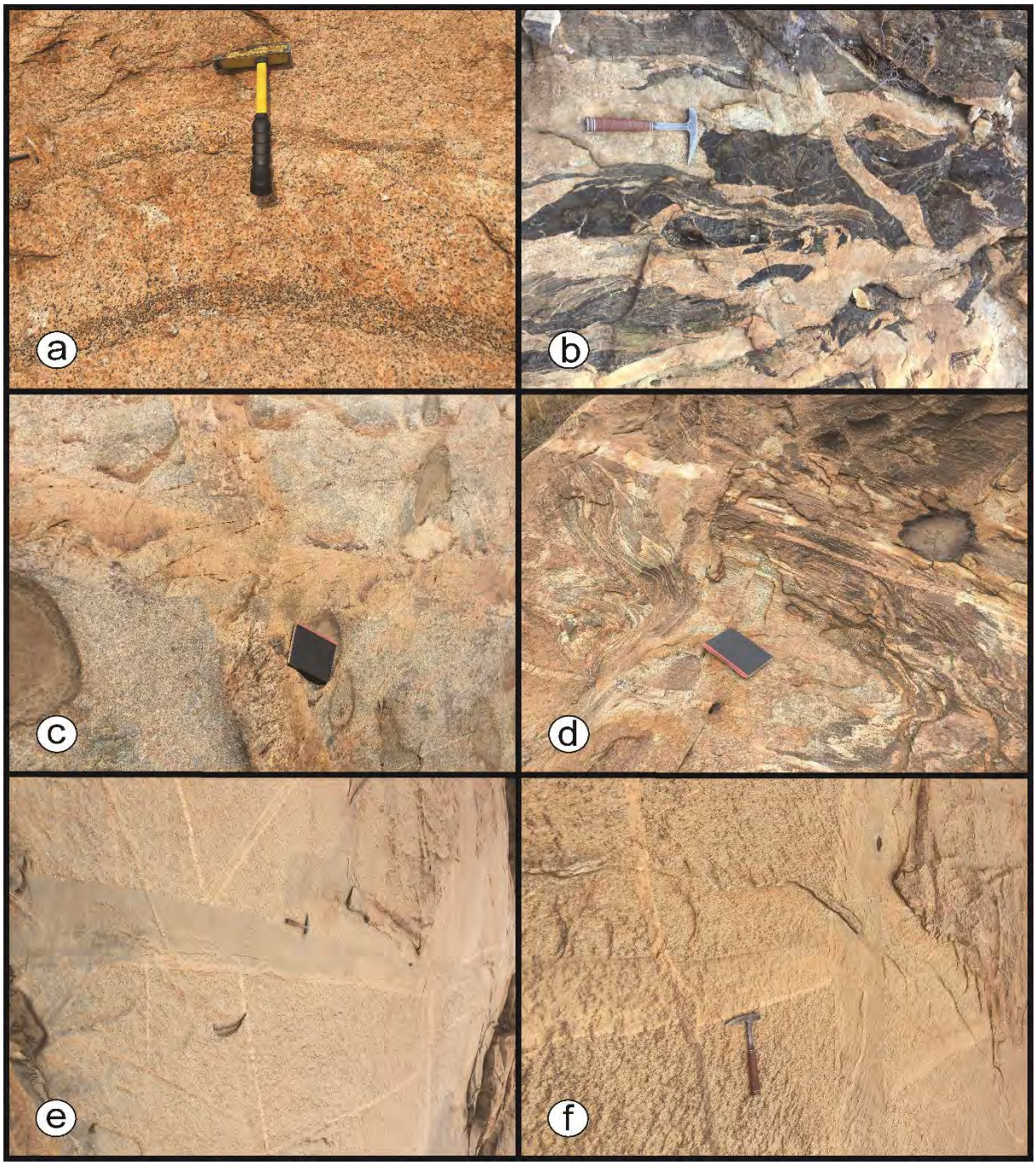

Fig. 2.4. Field photos from the Doornhoek (a) and Uitgevonden (b-d) and Honingklip (e+f) plutons. See text for details.

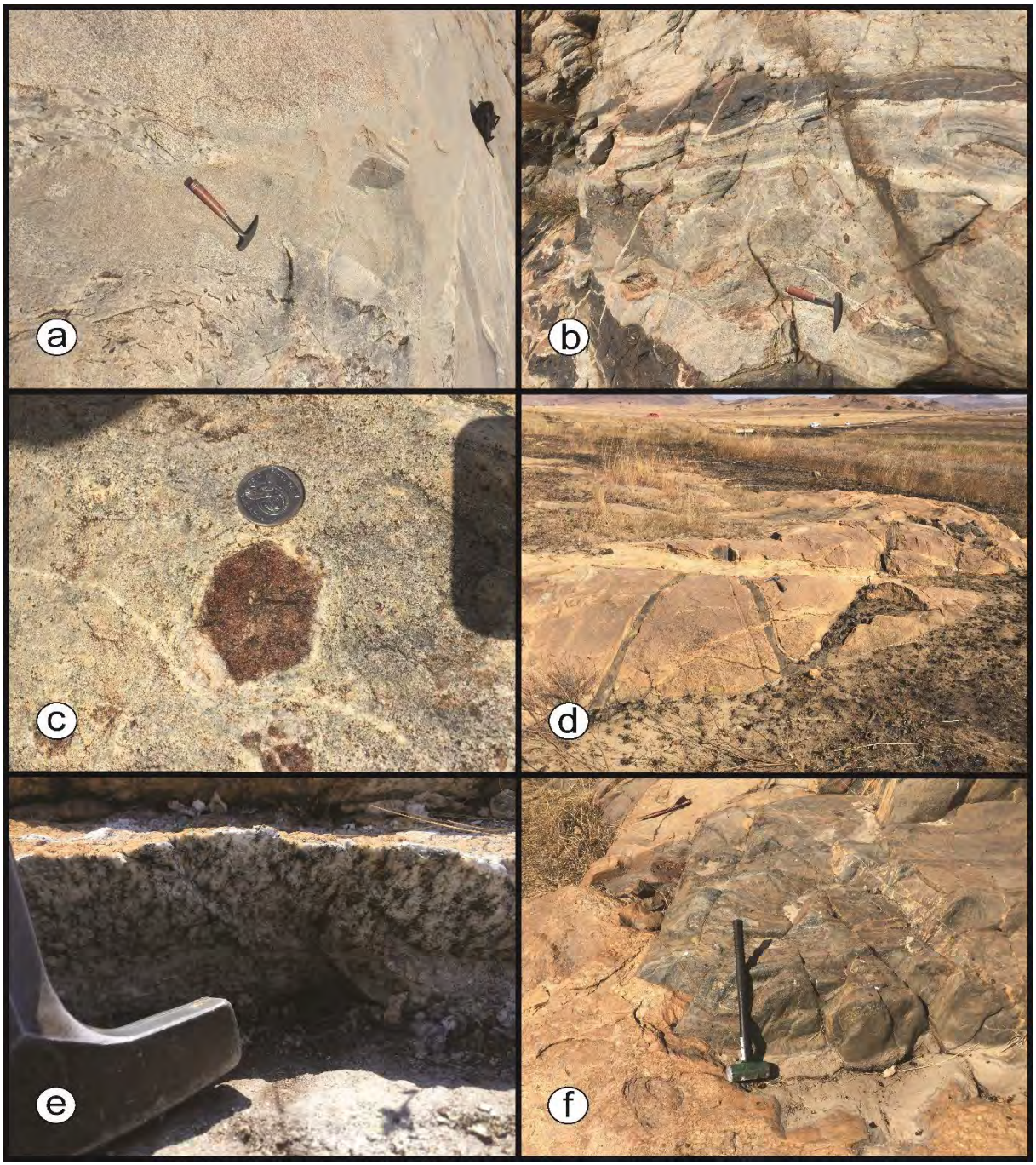

Fig. 2.5. Field photos from the contact zone of the Honingklip Pluton and the Tjakastad schist belt (a-c) and from the Eerstehoek Pluton (d-f). See text for details.

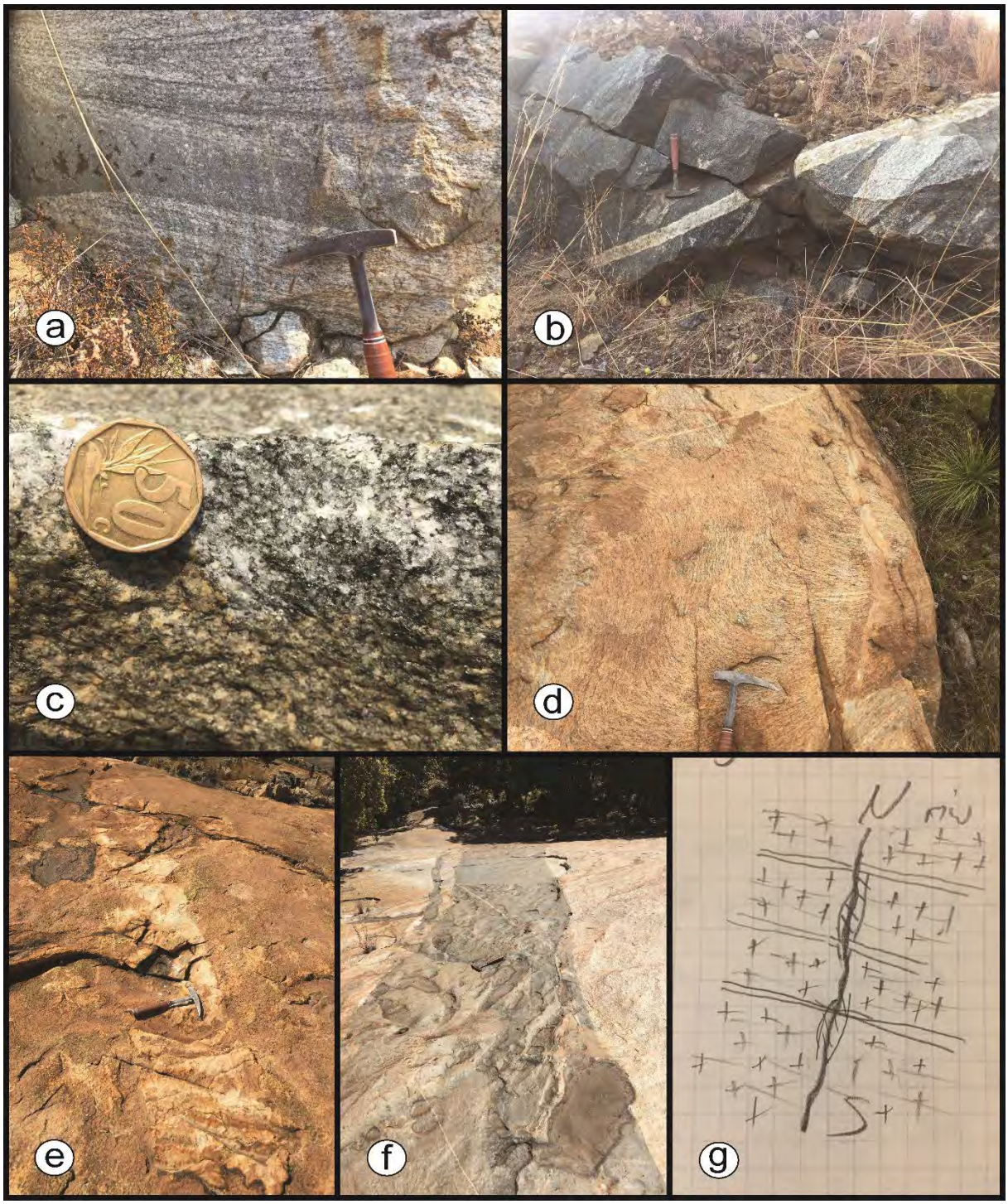

Fig. 2.6. Field photos (a-f) and outcrop sketch (g) from the Weergevonden Pluton. (a) Banded trondhjemite. (b) and (c) Dark grey granitoid with titanite visible in hand specimen cutting the trondhjemite. (d) Sheared trondhjemite on the southern margin of the Weergevonden Pluton. (e) Felsic dyke cutting the trondhjemite of the Weergevonden Pluton on the western margin. (f) Greenstone remnant within trondhjemite on the western margin of the Weergevonden Pluton. (g) Sketch of the outcrop of (f), where a series of ± east-west trending felsic dykes cut the trondhjemite and the ± north-south trending greenstone remnant.

The Weergevonden Pluton is located south of the tail of the Boesmanskop syenite (Fig. 2.1). In the east of the Weergevonden, outcrops are mostly confined to road cuts along the R541. In the first outcrop next to the R541 south of the Boesmanskop syenite, foliated trondhjemite is found, no cross-cutting dykes. About 750 m to the south, several phases are exposed in a road cut. There, the trondhjemite is heavily banded (Fig. 2.6a) and cut by a dark grey granitoid (Fig. 2.6b). On the eastern side of the R541, the dark grey phase has titanite grains visible in hand specimen (Fig. 2.6c), on the western side not. The dark grey granitoid was sampled as *MS 25a+b* and the trondhjemite as *MS 26*. On the southern margin, a foliated and sheared trondhjemite can be found up on a hill next to a farm road, which was sampled as *MS 27* (Fig. 2.6d). At the northern margin of the Weergevonden Pluton, a ca. 2-3 m thick of vertically dipping metasediments is exposed. The Weergevonden trondhjemite appears ca. 200 m south of the greenstone. A semi-fresh trondhjemite sample (*MS 50*) was taken on the foot of a dome-like hill. On the top of the dome, an ESE-NNW trending dyke cuts the trondhjemite (Fig. 2.6e). On the western margin of the Weergevonden Pluton, an up to ca. 1.5 m thick greenstone remnant, striking ± N-S, is found in foliated trondhjemite (Fig. 2.6f). The greenstone remnant goes on for about 15 m, then thins out to the south. Both the greenstone and the trondhjemite are cut by several, ca. 10 cm thick felsic dykes, that all trend ± E-W (Fig. 2.6g). The outcrop is mostly flat pavement or weathered in the riverbed. A weathered trondhjemite was sampled as *MS 51* and a semi-fresh dyke as *MS 52*. The Weergevonden varies from homogenous, weakly foliated trondhjemite in the north and west to banded gneiss in the center to sheared but homogenous trondhjemite in the south.

2.4 Summary

The aims of my field work were to identify the main phases of the TTG plutons in the Stolzburg Block and any younger cross-cutting phases. I found that the TTG plutons are dominated by a homogenous, generally foliated trondhjemite. In the following chapters, this trondhjemite will be referred to as the Main Trondhjemite. In the Stolzburg Pluton, the grain size of the Main Trondhjemite may vary locally; however, the general appearance is the same throughout the pluton. Other, more mafic comagmatic phases are localized and confined to the pluton margin, for example in the quarry on the south-eastern margin of the Stolzburg Pluton. Equally, the occurrence of younger cross-cutting felsic dykes is limited to the pluton margins and the contact zones in between the plutons, while the centers of the plutons are generally free of cross-cutting felsic dykes (Fig. 2.7). Figure 2.7 is also an attempt to map the state of the main rock. While a distinction between syn- and post-magmatic foliation is not easily possible in the field, a weak foliation of a homogenous rock in general can be distinguished from a composite lithology with multiple (cogenetic?) phases and from banded gneisses to migmatites.

Migmatites are rare and like the felsic dykes they are confined to the margins, such as in the Theeboom Gneiss locality on the southern margin of the Stolzburg Pluton and on the south-eastern margin of the Stolzburg Block, in the contact zone between Stolzburg Block, Dalmein Pluton and Mpuluzi Batholith (Fig. 2.4d).

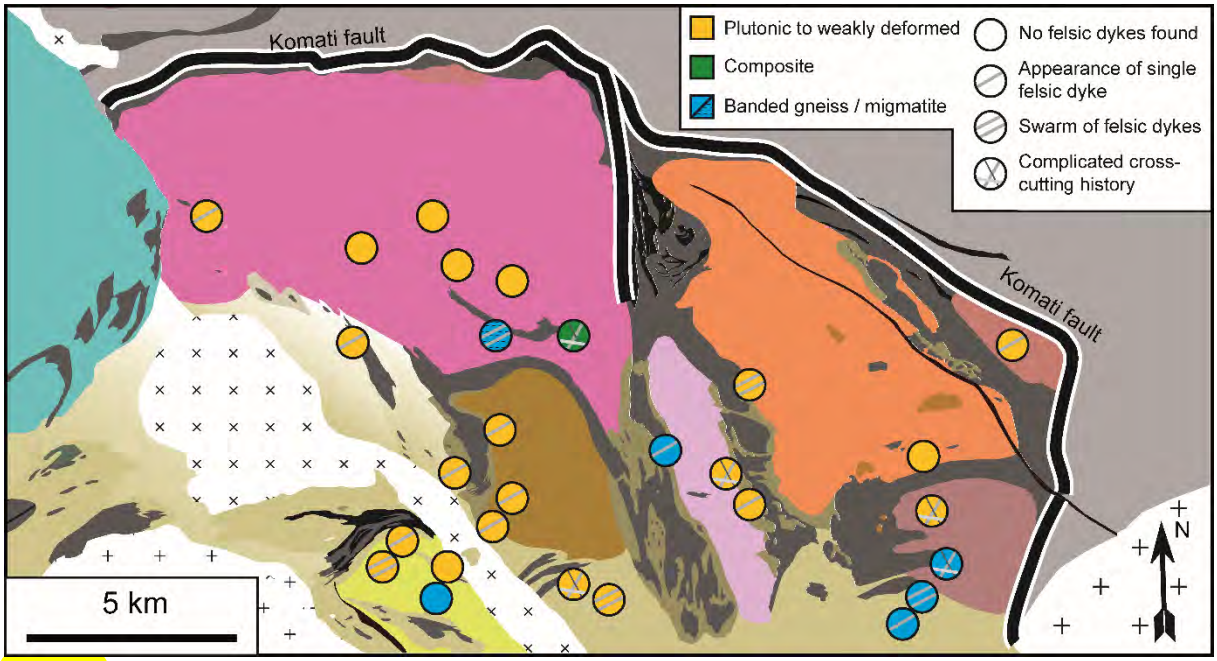

Fig. 2.7. Geological map showing the occurrence and distribution of cross-cutting felsic dykes in the Stolzburg Block. The color-coding indicates the state of the main rock. See Figure 1.8 for the full legend. Modified after Moyen et al. (2019).

References

Anhaeusser, C.R., Robb, L.J., Viljoen, M.J., 1981. Provisional geological map of the Barberton Greenstone Belt and surrounding granitic terrane.

Moyen, J.-F., Stevens, G., Kisters, A.F.M., Belcher, R.W., Lemirre, B., 2019. TTG Plutons of the Barberton Granitoid-Greenstone Terrain, South Africa, in: Van Kranendonk, M.J., Bennett, V.C., Hoffmann, J.E. (Eds.), Earth's Oldest Rocks. pp. 615–653.

Schoene, B., de Wit, M.J., Bowring, S.A., 2008. Mesoarchean assembly and stabilization of the eastern Kaapvaal craton: A structural-thermochronological perspective. Tectonics 27, 1–27. https://doi.org/10.1029/2008TC002267

Chapter 3: Analytical methods

3.1 Sample preparation

In the field, the samples were taken using geologist's hammer, sledgehammer and chisel, and the samples were shipped to Stellenbosch University by air freight. All sample preparation was performed at the Central Analytical Facilities, Stellenbosch University, South Africa.

3.1.1 Cutting, crushing and milling

The larger samples were first cut into pieces suitable for the jaw crusher using a diamond blade saw and weathered surfaces were also removed in the process. For the preparation of thin sections, a fraction of the samples was cut into smaller blocks, that were subsequently cut into thin section-sized blocks. The thin sections were produced externally by Lab Crystals, Lucknow, Uttar Pradesh, India.

The cut samples were crushed with a jaw crusher into cm-sized pieces suitable for milling. For major- and trace-element analyses, the samples were milled into a fine powder using a tungsten-carbide swing mill. In order to obtain a representative aliquot of the fine-grained granitoids, three loads were milled in the swing mill. Each batch was taken from the bulk sample via the coning and quartering method.

For separation of minerals for U-Pb analyses, the leftover material from the jaw crusher that was not used in the swing mill was carefully milled using a disk mill. After each grinding process, the product was sieved using a sieve with 350 µm mesh size to remove the desired grain size and any dust. The material left in the sieve was then again milled in the disk mill at reduced spacing between the disks. The milling and sieving process was repeated multiple times, reducing the spacing between the disks after each step, until all material was ground down to ≤350 µm.

3.1.2 Mineral separation and mounting

The ≤350 µm fraction was first washed in a large beaker to remove the clay fraction. For this, the beaker was filled with water and the sample stirred; once the large grains had settled, the water was poured out. This process was repeated until no more suspended particles were visible and the water was clear.

After washing, the samples were placed on a Super Panner for *gravitational separation*. Inclination of the table and water flow were kept in such a way, that the upper end of the sample stream, in which the heavy minerals were concentrated, stayed static on the table. Once sufficient heavy minerals had concentrated, they were removed from the table using a

disposable pipet and gathered in a petri dish. The petri dishes with the heavy minerals were then placed in an oven to dry.

Once the heavy mineral separates had dried, they were subjected to *magnetic separation*. First, the ferro-magnetic minerals were removed from the samples using a hand magnet. The samples were then separated into magnetic and non-magnetic fractions using a Frantz magnetic separator. The separation was done in three steps, using a chute slope of 20° and a tilt of 25° and a current of 0.4, 0.8 and 1.5 A, respectively, removing the magnetic fraction after each step.

The non-magnetic fraction, containing the desired minerals apatite and zircon, was then further enriched in heavy minerals by *heavy liquid separation*. For this, the samples were poured into a separator funnel containing tetrabromoethane (TBE, ρ = 2.97 gcm^{-3}). The separator funnel was gently shaken and then left for ~30-60 minutes so that the heavy grains could settle at the bottom. Once the grains had completely separated, the heavy fraction was collected in a filter paper. The filter paper containing the heavy mineral separate was placed in a beaker and dried in an oven.

The heavy mineral separate was placed into a petri dish and apatite and zircon were hand-picked from the separate using a needle, thinly coated with petroleum jelly, under an optical microscope. The grains were mounted on a glass plate covered with double-sided tape. Mounts were produced by placing a 1-inch diameter mold ring over the grains and pouring epoxy resin into it. Then the mounting plate was placed in an oven for curing. After the epoxy resin had hardened, the mounts were removed from the plate and polished using a Rotopol-35. Polishing was done in three steps using a 9, 3 and 1 µm polishing pad, respectively, and applicable polishing suspension of the same grain sizes.

3.2 Major- and trace-element analyses of whole-rock samples

Whole-rock major- and trace-element analyses were carried out at the Central Analytical Facilities, Stellenbosch University, South Africa. Fused disks were prepared using 0.7 g of sample powder mixed with 7 g of high purity flux (32.83 % $LiBO_2$, 66.67 % $Li_2B_4O_7$, 0.50 % LiI). Major-element compositions were determined on a PANalytical wavelength dispersive x-ray fluorescence spectrometer. The reference materials used for instrumental calibration are NIM-G and BE-N. Trace-element and REE concentrations were analyzed using an Element E2 on fragments of the glass disks used for ME analysis. Ablation was done with a Resonetics 193nm Excimer laser connected to an Agilent 7700 ICP-MS. Reference materials BHVO-1 and BHVO-2G yielded a typical accuracy of <10 % deviation from the published value, except for Pb (45%

deviation) and Nb (16% deviation), and a precision of <1%, with the exception of Ba (3%), Cr (4.8%), Cu (2.8%), Ni (2.3%), Sr (8.9%), V (6.9%), Zn (2.7%) and Zr (3.1%).

The major- and trace-element data were published in research publication 1 (Chapter 4) and are listed in Table 4.4.

3.3 Electron microscopy

3.3.1 Imaging of accessory minerals

Cathodoluminescence (CL) and back-scattered electron (BSE) images and zircon grains and CL images of apatite grains were obtained at the Central Analytical Facilities, Stellenbosch University, South Africa, using a Zeiss Merlin Scanning Electron Microscope (SEM). The mineral mounts were gold-coated for the imaging. Overview CL and BSE images of zircon grains for selection of grains for geochronological analysis were acquired at an accelerating voltage of 20 kV, a beam current of 12 nA and a working distance of 13.1 (CL) and 13.2 mm (BSE), respectively. High-resolution images of zircon for spot selection for trace-element analyses were taken at an accelerating voltage of 10 kV and a beam current of 12 nA were used at a working distance of 11.8 mm. Beam conditions used for apatite were an accelerating voltage of 20 kV, beam current of 12 nA at a working distance of 6.1 mm. The scanning speed was typically ~1 min/image for all CL images. Overview images of apatite and zircon were taken at a resolution of 1024 by 768 pixels, while high-resolution images of zircon were taken at a resolution of 2048 by 1536 pixels.

Back-scattered electron images of titanite grains were obtained at the University of Clermont-Ferrand in the laboratory Magmas et Volcans (LMV) using a JEOL JSM-5910 LV SEM with an accelerating voltage of 15 kV. The BSE images of titanite were taken at a resolution of 800 by 600 pixels. Images of titanite were taken from carbon-coated thin sections.

3.3.2 Cryo CL

To investigate potential fluid alteration in major minerals, cryo-cathodoluminescence (cryo CL) images were taken of a thin section from sample MS 2. For this, the sample chamber of a Zeiss Merlin SEM was cooled down to ~-196 °C using liquid N_2. The beam conditions used during cryo CL were an acceleration voltage of 12 kV and a beam current of 12 nA at a working distance of 8.1 mm.

3.4 Isotope analyses

3.4.1 Zircon U-Pb isotope analysis

The U-Pb isotopic composition of zircons was measured at the Central Analytical Facilities, Stellenbosch University, South Africa using a Thermo-Fisher Element E2 ICP-MS connected to an ASI Resolution SE Excimer laser operating at a wavelength of 193 nm. The samples were analyzed in a Laurin Technic S-115 dual-volume cell. The parameters of analysis are a spot size of 30 µm, a frequency of 9 Hz, a fluence of 1.4 Jcm^{-2} and gas flows of 800 $mlmin^{-1}$ for He and 900 $mlmin^{-1}$ for Ar. Masses 202, 204, 206, 207, 208, 232, 235 and 238 were measured using a single collector Secondary Electron Multiplier detection system. Each run lasted 21 s and 20 s of background acquisition. Zircon GJ-1 was used as a primary reference material and Plesovice and M-127 were used for quality control.

Data reduction was performed using Iolite reduction software package v.3.5 with VizualAge (Paton et al., 2011). Laser-induced elemental fractionation (LIEF) was modelled within each analytical session on the basis of combined analyses of the primary reference material GJ-1; LIEF correction assumes reference material and samples behave identically. The integration periods for baseline and primary reference material integrations were inspected and a spline was selected, so that as many integrations as possible lie on the selected spline while keeping the spline as smooth as possible; during the inspection of baseline and primary reference material integrations, the 238U, 207Pb, 206Pb, 204Pb and 202Hg input channels were monitored. After inspection of baseline and primary reference material integrations and the selection of a suitable spline, the VizualAge data deduction scheme and a correction for downhole fractionation were applied and the data were crunched. The quality of the primary reference material was checked using the 206Pb/238U age and targeting a mean squared weighted deviation (MSWD) of ~1; if necessary, the spline type was changed. The integrations for secondary reference materials and unknowns were inspected by monitoring the “Final 206-238”, “U238-CPS”, “Pb206-CPS” and “Pb204-CPS” channels. For each analysis, the integration period was adjusted, so that the “Final 206-238” signal is flat over the selected period while keeping as much of the selected period as possible. An analysis was discarded if there were no or too short flat parts in the “Final 206-208” signal or any ^{204}Pb counts above the background. Since any analysis containing ^{204}Pb was discarded, no common Pb correction was applied.

The reduced data were exported from Iolite. Concordia diagrams were plotted in Isoplot (Ludwig, 2012) and age calculations were performed using IsoplotR (Vermeesch, 2018). Repeated analyses of reference materials M-127 and Plesovice yielded weighted mean $^{206}Pb/^{238}U$ ages of 531.2 ± 2.1 Ma (n = 43) and 339.6 ± 0.7 Ma (n = 43), respectively. The full

zircon U-Pb LA ICP-MS metadata are given in Table 4.5. The zircon U-Pb isotope data were published in research paper 1 (Chapter 4) and are given in Table 4.7.

3.4.2 Zircon Lu-Hf isotope analysis

The Lu-Hf isotopic composition of dated zircon grains were measured at Universidade Federal de Ouro Preto (UFOP), Brazil, on the edge and on top of concordant U-Pb spots according to the method of Gerdes and Zeh (2009, 2006). Model ages were calculated based on the depleted mantle (DM) model of Blichert-Toft and Albarède (2008). Analyses of zircon reference materials BB, GJ-1 and Mud Tank yielded $^{176}Hf/^{177}Hf$ ratios of 0.281670 ± 0.0000247 (n = 21), 0.282005 ± 0.000034 (n = 12) and 0.282503 ± 0.000029 (n = 21) (uncertainties stated at 2SD). The zircon Lu-Hf data were published in research paper 1 (Chapter 4) and are given in Table 4.8.

3.4.3 Apatite U-Pb isotope analysis

The U-Pb isotopic composition of apatite grains and the Lu-Hf isotopic composition of zircon grains were determined at UFOP following the method described by Lana et al. (2017) using a ThermoScientific Neptune Plus multi-collector (MC)-ICP-MS connected to a Photon Machines Gs excimer laser operating at a wavelength of 193 nm. The parameters of analysis are a spot size of 20 µm, a frequency of 6 Hz, a fluence of 1.2 Jcm^{-2} and gas flows of 100 $mlmin^{-1}$ for He and 500 $mlmin^{-1}$ for Ar. Masses 232 and 238 were measured using Faraday cups and masses 202, 204, 206, 207 and 208 were measured using Secondary Electron Multiplier/compact discrete ion counters in a multi collector (MC) detection system. Each run lasted 40 s and 15 s of background acquisition. Zircon GJ-1 was used as a primary reference material and apatite reference materials 401, MAD and DUR were used for quality control.

The reduction of the apatite U-Pb data was done using an in-house MS Excel spreadsheet modified from Gerdes and Zeh (2009), see also details in Schneider et al. (2015). The raw data were corrected for: 1) background noise, 2) common Pb, 3) laser-induced element fractionation, 4) instrument mass discrimination, and 5) time-dependent elemental fractionation. The background-corrected ^{204}Pb signal was used for common Pb corrections based on the two-stage evolution model of terrestrial Pb composition (Stacey and Kramers, 1975). The ^{204}Pb was estimated by subtracting the average mass 204 signal of the background, which mostly results from ^{204}Hg in the carrier gas, from the mass 204 signal during sample ablation. All corrections have been applied on the time-resolved data set for each 0.4 s of integration prior to correction of downhole fractionation.

Reference materials 401, MAD and DUR gave $^{206}Pb/^{238}U$ ages of 531. ± 3.5 (n = 22), 481.9 ± 2.7 (n = 33) and 31.93 ± 0.22 Ma (n = 23), respectively. The full laser and gas conditions are given in Table 4.6. The apatite U-Pb data were published in research paper 1 (Chapter 4) and are given in Table 4.9.

3.4.4 Apatite Sr isotope analysis

The Sr isotopic composition of apatite grains was determined at UFOP using a ThermoFisher Neptune Plus LA-MC-ICP-MS connected to a 193 nm HelEx Photone Machine laser ablation system, following the methodology proposed by Wilson et al. (2017) and Yang et al. (2014, 2008). The parameters of analysis are a frequency of 6 Hz, fluence of 4 Jcm^{-2} and gas flows of 500 $mlmin^{-1}$ for He, 800 $mlmin^{-1}$ for Ar and 5 $mlmin^{-1}$ for N_2. On the previously dated zones, a variable spot size of 30 to 85 µm was used to accommodate for their varying size, and a spot size of 85 µm was used on apatite grains of unknown age. Each run lasted 60 s and 30 s of background acquisition. The data reduction was performed on an in-house MS Excel spreadsheet modified from Wilson et al. (2017). The raw data for $^{86}Sr/^{87}Sr$ were corrected for isobaric mass interference by ^{84}Kr and ^{86}Kr on ^{84}Sr and ^{86}Sr using a Kr baseline measurement. A NIST 610 glass was used as a primary reference material to determine the $^{87}Rb/^{85}Rb$ mass bias.

Quality control was done using MIR plagioclase (in-house reference material from Dr. A. Gerdes, Frankfurt) and Durango and Madagascar apatite reference materials. Over the course of the analyses, MIR plagioclase yielded an $^{87}Sr/^{86}Sr$ ratio of 0.70303 ± 12 (2SD, n = 19), within uncertainty identical with the published value of 0.703096 ± 70 (2s, Rankenburg et al., 2004). The $^{87}Sr/^{86}Sr$ ratio obtained for Madagascar apatite of 71181 ± 9 (2SD, n = 6) is within uncertainty in agreement with the value of 0.71179 ± 3 (2SD) of Yang et al., (2014), and the $^{87}Sr/^{86}Sr$ ratio obtained for Durango apatite of 0.70632 ± 35 (2SD, n = 7) is within uncertainty in agreement with the published value of 0.706328 ± 23 (2SD, Yang et al, 2014). The apatite Sr isotope data were used in research paper 2 (Chapter 5) and are listed in Table 5.8.

3.4.5 Whole-rock Pb, Sr and Nd isotope analyses

Whole-rock samples were analyzed for Sr, Nd and Pb isotopes at the University of Cape Town using a NuPlasma HR MC ICP-MS, with the sample being introduced as a solution, obtaining present day $^{87}Sr/^{86}Sr$, $^{143}Nd/^{144}Nd$, $^{208}Pb/^{204}Pb$, $^{207}Pb/^{204}Pb$ and $^{206}Pb/^{204}Pb$ ratios. Reference material JG-2 yields the following ratios: $^{87}Sr/^{86}Sr$ = 0.759423 ± 0.000271 $^{143}Nd/^{144}Nd$ = 0.512231 ± 0.000001, $^{208}Pb/^{204}Pb$ = 39.0378 ± 0.0324, $^{207}Pb/^{204}Pb$ = 15.6448 ± 0.0083 and

$^{206}Pb/^{204}Pb$ = 18.6557 ± 0.0344. A $^{143}Nd/^{144}Nd$ ratio of 0.512115 ± 0.000007 was obtained for reference material JNdi-1, an $^{87}Sr/^{86}Sr$ ratio of 0.710255 for NIST987, and $^{208}Pb/^{204}Pb$, $^{207}Pb/^{204}Pb$ and $^{206}Pb/^{204}Pb$ ratios of 36.7219 ± 0.0044, 15.4963 ± 0.0016 and 16.9405 ± 0.0015, respectively, for NIST981.

Initial Sr and Nd ratios were calculated using an in-house spreadsheet and the whole-rock Rb, Sr, Sm and Nd concentrations (Table 4.4) and sample ages (Table 4.3). Uncertainties on the initial ratios were determined using the uncertainties on the present-day ratios (see Tables 5.3, 6.4 and 6.5) and on the whole-rock trace-element analyses (Rb: 2%, Sr: 5%, Sm: 2%, Nd: 3%). The whole-rock isotope compositions are given in Tables 5.3 (Sr), 6.4 (Pb) and 6.5 (Nd).

3.5 Major- and trace-element analyses of accessory minerals

3.5.1 Apatite and titanite

Major-element and halogen concentrations of apatite and titanite grains were determined at the University of Clermont-Ferrand in the LMV using a Cameca SX 100 electron microprobe. Apatite grains were analyzed in epoxy mounts with a spot size of 10 µm, an accelerating voltage of 20 kV and a beam current of 10 nA. Titanite grains were analyzed in thin sections with a spot size 1 µm, and accelerating voltage of 20 kV and a beam current of 40 nA. The major-element concentrations as well as detection limits and standard deviations are given in Tables 5.4 (apatite) and 5.5 (titanite).

Trace-element concentrations for apatite and titanite grains were determined at the University of Clermont-Ferrand in the LMV using a Thermo Element XR ICP-MS connected to a 193nm Resonetics M-50E laser ablation system. The parameters used are a spot size of 20 µm, a frequency of 2 Hz, a fluence of 2.8 Jcm^{-2} and depending on the day of analysis gas flows of 590 and 650 $mlmin^{-1}$ for He and 7.5 and 7 $mlmin^{-1}$ for N_2. Each run lasted 60 s and 30 s of background acquisition. Each sequence was bracketed by two analyses of GSD-1G (Jochum et al., 2005). Internal normalization for LA ICP-MS data was done using ^{43}Ca and data processing was conducted using the GLITTER software (Griffin, 2008). Hafnium was monitored and any analyses containing Hf concentrations above the background were discarded to account for potential zircon inclusions. The reference materials Durango apatite (Marks et al., 2012) and Khan titanite (Heaman, 2009) were used as a secondary standard for quality control during analysis. The trace-element concentrations as well as their standard deviations and the detection limits are given in Tables 5.4 (apatite) and 5.5 (titanite).

3.5.2 Zircon

The major-element compositions of zircon grains were determined at the CAF at Stellenbosch University using a Zeiss EVO MA15 SEM. Full quantitative analyses were obtained using an Oxford Instruments X-Max 20 mm^2 Energy Dispersive X-Ray Spectrometry (EDS) detector and INCA Oxford software. The beam conditions are an accelerating voltage of 20 kV, probe and specimen currents of 1.1 and 19 nA, respectively, and a working distance of 8.5 mm. The results are listed in Table 5.6.

Trace element concentrations in zircon grains mounted in epoxy resin were determined at the CAF at Stellenbosch University using an Agilent 8800 ICP-MS connected to a Resonetics 193nm Excimer laser ablation system. The parameters of analysis are a spot size of 26 µm, a frequency of 7 Hz, a fluence of 2.5 Jcm^{-2} and gas flows of 400 $mlmin^{-1}$ for He, 800 $mlmin^{-1}$ for Ar and 4 $mlmin^{-1}$ for N_2. Each run lasted 30 s and 20 s of background acquisition. Zircon GJ-1 was used as a primary reference material and BCR-2G glass (Jochum et al., 2005) was used for quality control. Data reduction was done using the Iolite software (Paton et al., 2011). Only data points with stable signal and without spikes were selected to filter for micro-inclusions. The results are given in Table 5.6.

3.6 Thermometry

The Zr-in-titanite and Ti-in-zircon temperatures were calculated using the methods of Hayden et al. (2008) and Ferry and Watson (2007), respectively. Both thermometers require knowledge of the activities of SiO_2 relative to quartz (a_{SiO2}) and of TiO_2 relative to rutile (a_{TiO2}). It is common practice to simply assume a_{TiO2} and a_{SiO2} values, but with advances in computational petrology and thermodynamic modelling, one can estimate more accurate a_{TiO2} and a_{SiO2} values.

In a thermodynamically closed system, the activity of a component (a_A) can be calculated as a function of the chemical potential of the component at the pressure and temperature of interest ($\mu_A^{P,T}$) and the chemical potential of the pure substance at the pressure and temperature of interest ($\mu 0_A^{P,T}$):

$$a_A = e^{\left(\frac{\mu_A^{P,T} - \mu 0_A^{P,T}}{R \times T}\right)}$$

In order to acquire a_{TiO2} for a range of P and T values, this calculation was automated in the phase equilibria modeling tool Rcrust (Mayne et al., 2019, 2016). The chemical potentials are extracted from meemum from Perple_X (Connolly, 2009), first for the pure substance of interest (rutile) and then for the full system considered. In this way, a_{TiO2} is calculated as

$$a_{TiO2} = e^{\left(\frac{\mu_{TiO2}^{P,T} - \mu 0_{Rutile}^{P,T}}{R \times T}\right)}$$

In order to test the assumption that $a_{SiO2} = 1$, a_{SiO2} was also calculated as

$$a_{SiO2} = e^{\left(\frac{\mu_{SiO2}^{P,T} - \mu 0_{Quartz}^{P,T}}{R \times T}\right)}$$

For the purpose of this study, a_{TiO2} and a_{SiO2} values were calculated for a P-T range of 3-15 kbar and 550-850 °C in steps of 0.25 kbar and 10 °C, respectively assuming closed system crystallization. The a_{TiO2} values are listed in Table 5.7.

At an H_2O content of ca. 2 wt. %, the calculation of a_{SiO2} yielded values of 1.00 over the whole modeled P-T range. Increasing the H_2O content decreases the a_{SiO2} value in the low pressure-high temperature corner of the P-T grid down to ca. 0.95 at ca. 5 wt. % H_2O and ca. 0.90 at ca. 7 wt. % H_2O. In the effective range of the obtained temperature estimates (ca. 600-700 °C), the H_2O content has no effect on the a_{SiO2} value.

The calculation of a_{TiO2} gave values of 0.03 to 1.00 over the modeled P-T range; the a_{TiO2} values for the full P-T range and for each modeled sample are listed in Table S.4. The effect of the H_2O content on the a_{TiO2} value appears to be negligible. The temperatures are initially calculated using an a_{TiO2} value of 0.5 and are then refined using the values extracted from Rcrust until the calculated $T_{Zr\text{-}in\text{-}titanite}$ / $T_{Ti\text{-}in\text{-}zircon}$ and the temperature corresponding to the used a_{TiO2} value are equal within a reasonable range (± ca. 10 °C). The uncertainty of the Zr-in-titanite thermometer is given by Hayden et al. (2008) as ca. ± 20 °C. Uncertainties on the Ti-in-zircon temperatures have been calculated by propagating the uncertainties on the Ti analyses. Zirconium saturation temperatures were also calculated after Boehnke et al. (2013) in GCDkit (Janoušek et al., 2006) using whole-rock data given in Table 4.4 and are listed in Table 5.2.

References

Blichert-Toft, J., Albarède, F., 2008. Hafnium isotopes in Jack Hills zircons and the formation of the Hadean crust. Earth Planet. Sci. Lett. 265, 686–702. https://doi.org/10.1016/j.epsl.2007.10.054

Boehnke, P., Watson, E.B., Trail, D., Harrison, T.M., Schmitt, A.K., 2013. Zircon saturation re-revisited. Chem. Geol. 351, 324–334. https://doi.org/10.1016/j.chemgeo.2013.05.028

Connolly, J.A.D., 2009. The geodynamic equation of state: What and how. Geochemistry, Geophys. Geosystems 10. https://doi.org/10.1029/2009GC002540

Ferry, J.M., Watson, E.B., 2007. New thermodynamic models and revised calibrations for the Ti-in-zircon and Zr-in-rutile thermometers. Contrib. to Mineral. Petrol. 154, 429–437. https://doi.org/10.1007/s00410-007-0201-0

Gerdes, A., Zeh, A., 2009. Zircon formation versus zircon alteration - New insights from combined U-Pb and Lu-Hf in-situ LA-ICP-MS analyses, and consequences for the interpretation of Archean zircon from the Central Zone of the Limpopo Belt. Chem. Geol. 261, 230–243. https://doi.org/10.1016/j.chemgeo.2008.03.005

Gerdes, A., Zeh, A., 2006. Combined U-Pb and Hf isotope LA-(MC-)ICP-MS analyses of detrital zircons: Comparison with SHRIMP and new constraints for the provenance and age of an Armorican metasediment in Central Germany. Earth Planet. Sci. Lett. 249, 47–61. https://doi.org/10.1016/j.epsl.2006.06.039

Griffin, W.L., 2008. GLITTER: data reduction software for laser ablation ICP-MS. Laser Ablation ICP-MS Earth Sci. Curr. Pract. Outst. issues 308–311.

Hayden, L.A., Watson, E.B., Wark, D.A., 2008. A thermobarometer for sphene (titanite). Contrib. to Mineral. Petrol. 155, 529–540. https://doi.org/10.1007/s00410-007-0256-y

Heaman, L.M., 2009. The application of U-Pb geochronology to mafic, ultramafic and alkaline rocks: An evaluation of three mineral standards. Chem. Geol. 261, 43–52. https://doi.org/10.1016/j.chemgeo.2008.10.021

Janoušek, V., Farrow, C.M., Erban, V., 2006. Interpretation of whole-rock geochemical data in igneous geochemistry: Introducing Geochemical Data Toolkit (GCDkit). J. Petrol. 47, 1255–1259. https://doi.org/10.1093/petrology/egl013

Jochum, K.P., Willbold, M., Raczek, I., Stoll, B., Herwig, K., 2005. Chemical characterisation of the USGS reference glasses GSA-1G, GSC-1G, GSD-1G, GSE-1G, BCR-2G, BHVO-2G and BIR-1G using EPMA, ID-TIMS, ID-ICP-MS and LA-ICP-MS. Geostand. Geoanalytical Res. 29, 285–302. https://doi.org/10.1111/j.1751-908x.2005.tb00901.x

Ludwig, K.R., 2012. User's Manual for Isoplot 3.75, a geochronological toolkit for Microsoft Excel. Berkeley Geochronol. Cent. Spec. Publ. 5, 1–72.

Marks, M.A.W., Wenzel, T., Whitehouse, M.J., Loose, M., Zack, T., Barth, M., Worgard, L., Krasz, V., Eby, G.N., Stosnach, H., Markl, G., 2012. The volatile inventory (F, Cl, Br, S, C) of magmatic apatite: An integrated analytical approach. Chem. Geol. 291, 241–255. https://doi.org/10.1016/j.chemgeo.2011.10.026

Mayne, M.J., Moyen, J.F., Stevens, G., Kaislaniemi, L., 2016. Rcrust: a tool for calculating path-dependent open system processes and application to melt loss. J. Metamorph. Geol. 34, 663–682. https://doi.org/10.1111/jmg.12199

Mayne, M.J., Stevens, G., Moyen, J.-F., Johnson, T., 2019. Performing process-oriented investigations involving mass transfer using Rcrust: a new phase equilibrium modelling tool. Geol. Soc. London, Spec. Publ. SP491-2018–85. https://doi.org/10.1144/sp491-

2018-85

Paton, C., Hellstrom, J., Paul, B., Woodhead, J., Hergt, J., 2011. Iolite: Freeware for the visualisation and processing of mass spectrometric data. J. Anal. At. Spectrom. 26, 2508–2518. https://doi.org/10.1039/c1ja10172b

Rankenburg, K., Lassiter, J.C., Brey, G., 2004. Origin of megacrysts in volcanic rocks of the Cameroon volcanic chain - Constraints on magma genesis and crustal contamination. Contrib. to Mineral. Petrol. 147, 129–144. https://doi.org/10.1007/s00410-003-0534-2

Schneider, S., Hammerschmidt, K., Rosenberg, C.L., Gerdes, A., Frei, D., Bertrand, A., 2015. U – Pb ages of apatite in the western Tauern Window (Eastern Alps): Tracing the onset of collision-related exhumation in the European plate. Earth Planet. Sci. Lett. 418, 53–65. https://doi.org/10.1016/j.epsl.2015.02.020

Stacey, J.S., Kramers, J.D., 1975. Approximation of terrestrial lead isotope evolution by a two-stage model. Earth Planet. Sci. Lett. 26, 207–221.

Vermeesch, P., 2018. IsoplotR: A free and open toolbox for geochronology. Geosci. Front. 9, 1479–1493. https://doi.org/10.1016/j.gsf.2018.04.001

Wilson, A.H., Zeh, A., Gerdes, A., 2017. In situ Sr isotopes in plagioclase and trace element systematics in the lowest part of the eastern Bushveld Complex: Dynamic processes in an evolving magma chamber. J. Petrol. 58, 327–360. https://doi.org/10.1093/petrology/egx018

Yang, Y.H., Sun, J.F., Xie, L.W., Fan, H.R., Wu, F.Y., 2008. In situ Nd isotopic measurement of natural geological materials by LA-MC-ICPMS. Chinese Sci. Bull. 53, 1062–1070. https://doi.org/10.1007/s11434-008-0166-z

Yang, Y.H., Wu, F.Y., Yang, J.H., Chew, D.M., Xie, L.W., Chu, Z.Y., Zhang, Y. Bin, Huang, C., 2014. Sr and Nd isotopic compositions of apatite reference materials used in U-Th-Pb geochronology. Chem. Geol. 385, 35–55. https://doi.org/10.1016/j.chemgeo.2014.07.012

Chapter 4: Presentation of research paper 1: Thermal evolution of the Stolzburg Block, Barberton granitoid-greenstone terrain, South Africa: Implications for Paleoarchean tectonic processes

This paper, fist authored by Moritz Mühlberg, was accepted for publication in Precambrian Research (http://dx.doi.org/10.1016/j.precamres.2020.106082). The following aspects of the research were done independently by Moritz Mühlberg while receiving standard supervision by his supervisors Gary Stevens, Jean-François Moyen and Alex Kisters: (i) fieldwork and sampling; (ii) sample preparation for whole-rock and mineral analyses; (iii) SEM imaging and acquisition of LA ICP-MS U-Pb data for apatite and zircon grains; (iv) zircon U-Pb LA ICP-MS data reduction; (v) generation of the figures except Figures 4.2 and 4.12 which were generated by Jean-François Moyen; (vi) writing of the manuscript. Preparation of fused disks for whole rock major- and trace-element analyses were done by Herschel Achilles. Whole-rock major-element XRF data acquisition was performed by Mareli Grobbelaar-Moolman and acquisition and reduction of whole-rock trace-element LA ICP-MS data were done by Riana Rossouw. Zircon Lu-Hf data acquisition and apatite U-Pb and zircon Lu-Hf data reduction were performed by Cristiano Lana.

Thermal evolution of the Stolzburg Block, Barberton granitoid-greenstone terrain, South Africa: Implications for Paleoarchean tectonic processes.

Moritz Mühlberg[a,b], Gary Stevens[a]*, Jean-François Moyen[b], Alex F.M. Kisters[a], Cristiano Lana[c]

[a] Department of Earth Sciences, University of Stellenbosch, Private Bag X1, Matieland 7602, South Africa

[b] Université de Lyon, Laboratoire Magmas et Volcans, UJM-UCA-CNRS-IRD, 23 rue Dr. Paul Michelon, 42023 Saint Etienne, France

[c] Departamento de Geologia (DEGEO), Universidade Federal de Ouro Preto, Morro do Cruzeiro, Ouro Preto, Minas Gerais, 35400000, Brazil

* Corresponding author. gs@sun.ac.za

Abstract

The thermal state of the crust controls its rheology and is therefore an important variable in understanding Archean tectonic processes. Thermochronology is a useful tool to track the long-term thermal evolution of the crust, and U-Pb in apatite, with an effective closing temperature for volume diffusion of Pb of ca. 400 – 550 °C, is useful in constraining the temperature-time history of igneous and metamorphic rocks, when apatite contains sufficient U. The Paleo- and Mesoarchean represent time periods in Earth's history where there is little certainty about the geodynamic processes that controlled the movement of crustal blocks. In this study on the Paleoarchean Stolzburg Block of the Barberton Granitoid Greenstone Terrain (BGGT), South Africa, we report new U-Pb apatite and zircon ages, as well as Lu-Hf zircon data for several TTG plutons that are considered to represent the type of felsic crust that formed the nucleus of the proto-Kaapvaal craton. Zircons from the Stolzburg, Theespruit and Weergevonden plutons provide apparent crystallization ages of ca. 3451 Ma in agreement with earlier studies. Felsic dykes concentrated in the deformed margins of the Stolzburg and Theespruit plutons yielded zircon crystallization ages of ca. 3215 Ma, postdating the main 3230-3225 Ma accretionary event in the belt. Zircon εHf_t values were determined to be +1.2 to -0.8. in the 3450 Ma plutons and +0.4 to -2.0 in the 3215 Ma dykes. U-Pb apatite thermochronology for the plutons shows igneous ages of ca. 3445 Ma, but also and multiple subsequent events of apatite growth or recrystallization at ca. 3210, 3105 and 2820 Ma. The preservation of this range of apatite dates indicates that no post-emplacement heating of the granitoids above ca. 600 °C has occurred. The Hf isotopic data show that the ca. 3.2 Ga dykes are less evolved than their host TTG plutons and are not produced by melt extraction following anatexis of the latter or their equivalents. Collectively, this evidence demonstrates that the Stolzburg, Theespruit and Weergevonden plutons have not undergone anatexis and have not been mobilized as anatectic domes at ca. 3.2 Ga, as proposed by some tectonic models.

4.1 Introduction

The nature of the geodynamic processes that shaped the first stable continental nuclei to emerge in the Paleoarchean is poorly constrained. This is due to both the scarcity of well-preserved Archean sequences and the fact that the typically greenschist- to amphibolite-facies grades of metamorphism that characterize most Archean volcanosedimentary successions are not specific to any particular tectonic context. The debate has traditionally revolved around a dichotomy between uniformitarian and static lid models, which, as discussed below, has not been particularly useful in advancing knowledge of Archean geodynamics. For example, it has been suggested that plate tectonics functioned since Paleoarchean times, that some greenstone successions from this era represent ophiolite complexes (de Wit, 2004; de Wit et

al., 1987; Furnes et al., 2015, 2009, 2007; Grosch and Slama, 2017), that some trondhjemites and tonalites represent magmas that were formed as a consequence of Archean subduction processes (De Ronde and Kamo, 2000; de Wit et al., 2011; Kisters et al., 2003; Laurie et al., 2013; Martin, 1999, 1986; Martin and Moyen, 2002; Moyen et al., 2006) and that garnet-amphibolites from this era may represent the Archean equivalents of blueschists (Moyen et al., 2006; Palin and Dyck, 2018; Palin and White, 2016). On the other hand, non-uniformitarian models propose vertical tectonics driven by the gravitational instability of a partially molten felsic crust, below a thick, predominantly mafic volcanoclastic stratigraphy, to explain the deformation and metamorphism of greenstone sequences and the formation of related magmatic rocks, in the same or similar localities (Barnes and Van Kranendonk, 2014; Bédard, 2006; Bouhallier et al., 1993; Chardon et al., 2002, 1998; Choukroune et al., 1995; Collins et al., 1998; Collins and Van Kranendonk, 1999; Smithies et al., 2009, 2007; Van Kranendonk, 2011, 2007; Van Kranendonk et al., 2015, 2014, 2007, 2004). In these vertical tectonic models, a hotter Archean mantle, substantial radiogenic heating of the crust and a protracted period of incubation by the thick overlying supracrustal succession are essential elements in raising the temperature of the buried felsic crust sufficiently to allow for widespread partial melting and granite production. In this traditional view, the strain patterns in specific portions of the crust are interpreted to have formed due to the sinking of greenstone keels between rising granite magma diapirs, and are taken as indicative of the global tectonic pattern.

Recent developments in numerical modelling (Debaille et al., 2013; Duclaux et al., 2007; Halla et al., 2009; Moyen and van Hunen, 2012; O'Neill et al., 2015, 2007; Rey et al., 2014; Sizova et al., 2018, 2015; van Hunen and Moyen, 2012), as well as comparison with evidence for crustal mobility from some telluric planets, have emphasized that the time-honored opposition between "horizontal" and "vertical" tectonics is probably not an appropriate framework to understand Archean tectonic processes. Regional horizontal mobility of the crust, with locally divergent (rift) and convergent ("subduction") domains, does not need to occur within a global system of plate boundaries (Hansen and Willis, 1996; Harris and Bédard, 2015; Piskorz et al., 2014). There is also no simple link between the strain regime recorded by a segment of the crust and the large-scale tectonic system within which the crust evolved. Portions of the modern crust evolve in the absence (or near the absence) of external stresses under hot geotherms (e.g. the present-day Colorado plateau, where the hot geotherm is achieved by delamination of the lower crust – a process more generally envisioned for the Archean (Levander et al., 2011)), even though this has occurred within the context of present day plate tectonics. On the other hand, a rheologically weak crust reacting to a compressive stress field would not be able to support significant thickening and collisional processes are instead accommodated by the collapse and lateral flow of the crust ("hot orogens": Cagnard et al.,

2006a, 2006b; Chardon et al., 2009; Fossen et al., 2017; Gapais et al., 2009). As a result, hot orogens are commonly characterized by pervasive fabrics that indicate the whole-scale ductile flow of the crust, smooth metamorphic gradients and a lack of high-P rocks that would point to deep burial of rocks. They nonetheless develop under a regime with some horizontal mobility and specifically compression of a deformation zone between two stiffer blocks – that may or may not be part of a globally interlinked system of plate boundaries (Harris and Bédard, 2015, 2014).

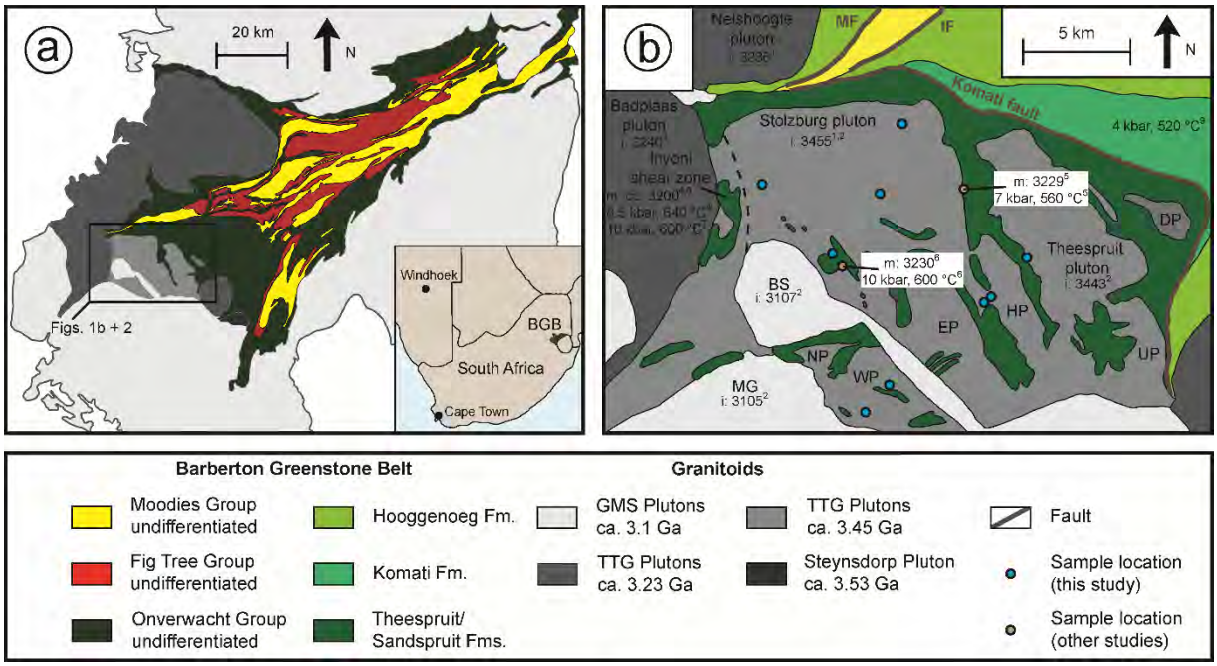

Fig. 4.1. (a) Simplified geological map of the Barberton Greenstone Belt and surrounding granitoid plutons; inset shows the location of the BGB in the context of southern Africa. (b) Geological map of the Stolzburg Block consisting of the Stolzburg, Theespruit and a series of smaller trondhjemite plutons and amphibolite-facies (ultra-) mafic rocks of the Theespruit and Sandspruit formations of the Lower Onverwacht Group. Igneous (i) and metamorphic (m) ages (in Ma) and pressure-temperature conditions after [1]Schoene et al., 2008; [2]Kamo and Davis, 1994; [3]Kisters et al., 2006; [4]Cutts et al., 2014; [5]Diener et al., 2003; [6]Dziggel et al., 2002; [7]Kato et al., 2018; [8]Maneiro et al., 2018; [9]Cloete, 1991. Blue circles indicate the locations of the samples dated in this study. Modified after Anhaeusser et al. (1981) Anhaeusser et al., 1981. BS: Boesmanskop syenite, DP: Doornhoek pluton, EP Eerstehoek pluton, HP: Honingklip pluton, MG: Mpuluzi granite, NP: Nederland pluton, UP: Uitgevonden pluton; IF: Inyoka fault, MF: Moodies fault.

Consequently, it is futile to try and unravel Earth's global tectonic style based on the description of regional strain. What can be done, however, is to quantify the evolution of the thermal state of the crust as a function of time and ideally also pressure. If such data can be obtained with sufficient resolution, particularly in space and time, it will provide robust constraints on what may have been possible or impossible in terms of geodynamic processes in the Archean crust. The rocks of the Barberton Granite Greenstone Terrane (BGGT) (Fig. 4.1a) are exceptionally well suited to contribute further to this debate, because in outcrop pattern the rocks define, particularly along the south-western margin of the greenstone belt, a classic dome and keel pattern (Anhaeusser, 1980), whilst the same area also contains high-pressure mid-amphibolite

facies metasedimentary and metamafic rocks (e.g. Diener et al., 2005; Moyen et al., 2006), that form part of the greenstone keels between the TTG domes. This study has investigated the thermal history of two prominent proposed domes from this area of the greenstone belt, the Theespruit and Stolzburg plutons (Fig. 4.1b), using a combination of LA ICP-MS U-Pb zircon and apatite dating in order to better understand the thermal evolution of these trondhjemite plutons. The Theespruit and Stolzburg plutons intruded the lower units of the Barberton greenstone belt at ca 3.45 Ga (Fig. 4.2) and are proposed to have been exhumed, either by orogenic collapse or diapiric rise and dome formation, at ca. 3.23 Ga. The study also aims to constrain the age of crystallization and possible magmas sources for felsic dykes that crosscut the plutons. To meet these collective aims we present and interpret U-Pb and Lu-Hf zircon data for 14 granitoid samples and U-Pb apatite data for seven granitoid samples and from one metamafic rock.

Fig. 4.2. A summary of the geochronological constrains available on the ages of crystallization of Barberton TTG plutons, as well as on the patterns of age distribution in zircons from clastic sediments and felsic volcanic units from the BGB (after Moyen et al., 2018). (A) Generalized stratigraphy of the Barberton Greenstone Belt (following Lowe and Byerly, 2007) with the zircon U-Pb age density (using KDE: kernel density estimate (Vermeesch, 2012), calculated using R software (Venables and Ripley, 2002)) of the felsic magmatism in the belt (Amelin et al., 2000; Armstrong et al., 1990; Byerly et al., 1996; De Ronde et al., 1991; Heubeck et al., 2013; Kamo and Davis, 1994; Kröner et al., 2016, 2013, 1996; Kröner and Todt, 1988; Van Kranendonk et al., 2009); the detrital zircons from Moodies and Fig Tree groups (Zeh et al., 2013). Probability is plotted on the vertical axis and age, in Ma., is plotted on the horizontal axis. (B) Compilation of ages interpreted as metamorphic or cooling ages; they include a diverse set of minerals and methods such as U-Pb on titanite or apatite, Ar-Ar on amphibole and micas, U-Pb zircon ages interpreted as system opening post-emplacement, etc. (Armstrong et al., 1990; Cutts et al., 2014; Diener et al., 2005; Dziggel et al., 2005, 2002; François et al., 2014; Kamo and Davis, 1994; Kisters et al., 2003; Kröner, 2016; Kröner et al., 2016; Layer et al., 1998; Schoene et al., 2008; and unpulished data by B. Lemirre). (C-H) KDE zircon U-Pb age density plots for each of the six main TTG plutons that are associated with the southern BGB. For individual age values and references see Moyen et al., (2018).

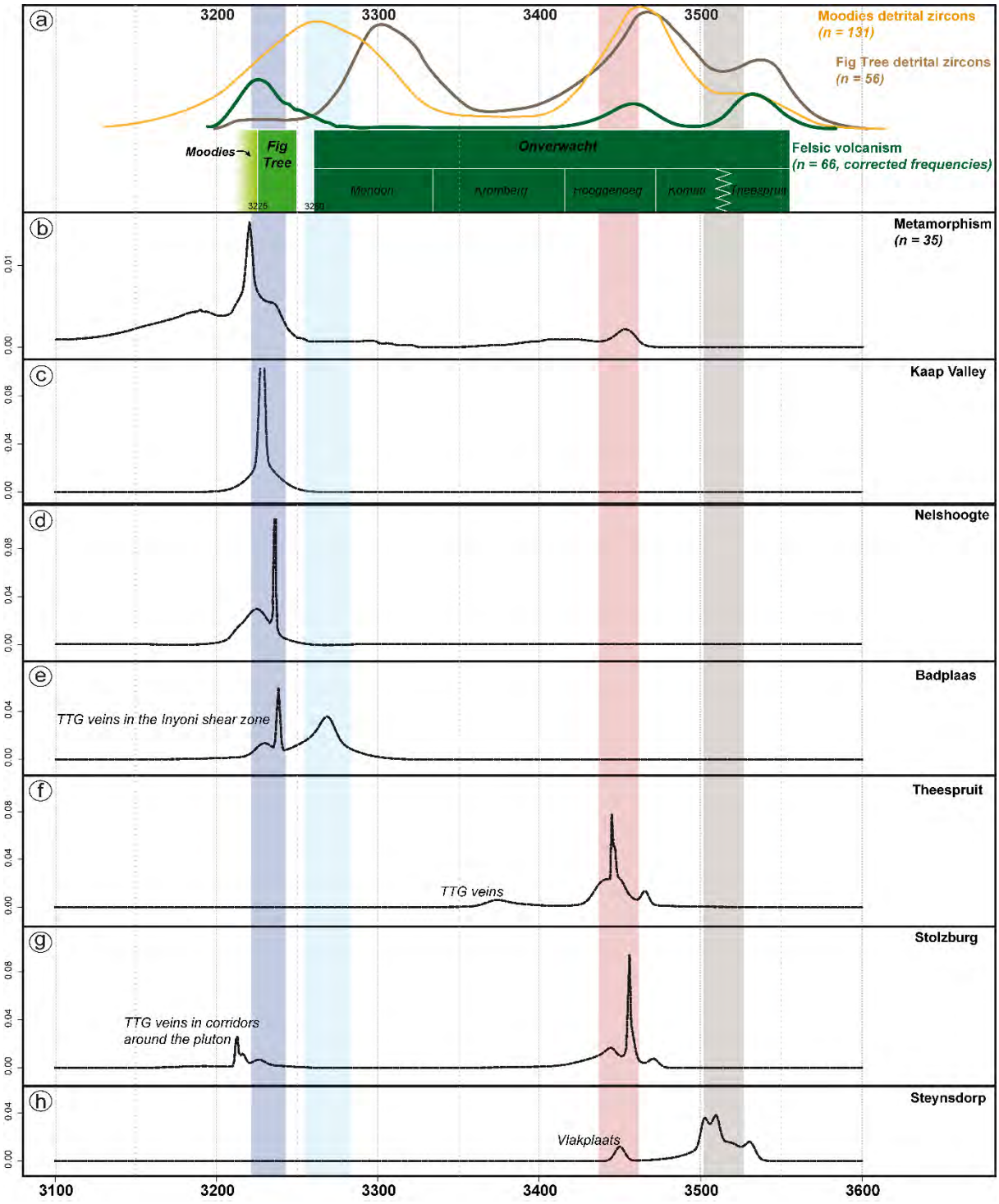

4.2 Geological background

4.2.1 The geology of the Barberton Granitoid Greenstone Terrain

The BGGT (Fig. 4.1a) constitutes the well-preserved and superbly exposed Paleoarchean supracrustal sequence of the Barberton Greenstone Belt (BGB) and the surrounding associated magmatic rocks which crystallized between ca 3.55 Ga and 3.1 Ga (Fig. 4.2). A comprehensive description of the BGB is given by Byerly et al. (2019), whilst the TTG plutons associated with the belt have been recently reviewed by Moyen et al. (2019); the details covered by these previous works won't be repeated here except to point out the elements most relevant to this study. The supracrustal rocks of the BGB consist of three major lithostratigraphic units, the Onverwacht, Moodies and Fig Tree groups (Lowe et al., 2012) (Fig. 1 and 2). In the southern part of the BGB, at the base of the Onverwacht Group (Fig. 4.1), the lowermost Sandspruit and Theespruit formations constitute a lithologically heterogeneous, highly tectonized sequence of felsic and mafic to ultra-mafic volcanic and volcanoclastic rocks. The rocks from these two formations have both been dated at ca. 3530 Ma (Kröner et al., 2016; Moyen et al., 2020), indicating that they are possibly contemporaneous. The amphibolite-facies rocks of the Sandspruit and Theespruit formations (Cloete, 1991; Cutts et al., 2014; Diener et al., 2005; Dziggel et al., 2002; Kato et al., 2018; Van Kranendonk et al., 2009) are separated from the greenschist-facies rocks of the structurally overlying ca. 3482 to 3472 Ma Komati Formation (Cloete, 1991; Grosch, 2018) by the Komati Fault (Armstrong et al., 1990; de Wit et al., 1983; Kisters et al., 2003) (Fig. 4.1).

The rocks of the Theespruit and Sandspruit formations are spatially associated with the oldest TTG plutons in the BGGT. On the south-eastern end of the BGB, the tonalitic Steynsdorp Gneisses, the protolith of which crystalized at ca. 3.52 (e.g. Kröner et al., 1996) form an orthogness dome mantled by the Theespruit Formation in the Steynsdorp anticline (Lana et al., 2010a), whilst the trondhjemitic Theespruit and Stolzburg plutons (Moyen et al., 2019) intruded the rocks of the Theespruit and Sandspruit formations at ca. 3.45 Ma (e.g. Kamo and Davis, 1994; Schoene et al., 2008) in the central and south-western portions of the southern margin of the BGB, respectively, along with several minor predominantly trondhjemitic plutons and cells (Anhaeusser and Robb, 1980) (Fig. 4.3). These oldest TTGs and the rocks of the Theespruit and Stolzburg formations have been defined as a coherent crustal block – generally referred to as the Stolzburg Block - consisting predominantly of rocks older than 3.44 Ga that were metamorphosed under amphibolite facies conditions (Kisters et al., 2003; Moyen et al., 2006).

Progressing from south to north, the western margins of the Stolzburg Block and the southern BGB were intruded by the long-lived Badplaas Complex and the Nelshoogte and Kaap Valley plutons between ca. 3.29 and 3.21 Ga (Fig. 4.1). The composite Badplaas Complex intruded

the Inyoni shear zone which marks the western boundary of the Stolzburg block in between ca. 3.29 and 3.23 Ga (Kisters et al., 2010). The 3236 ± 1 Ma Nelshoogte (De Ronde and Kamo, 2000) and the 3227 ± 1 Ma Kaap Valley (Kamo and Davis, 1994) plutons are relatively shallowly emplaced (Matsumura, 2014) and intrusive into the higher levels of the Onverwacht Group.

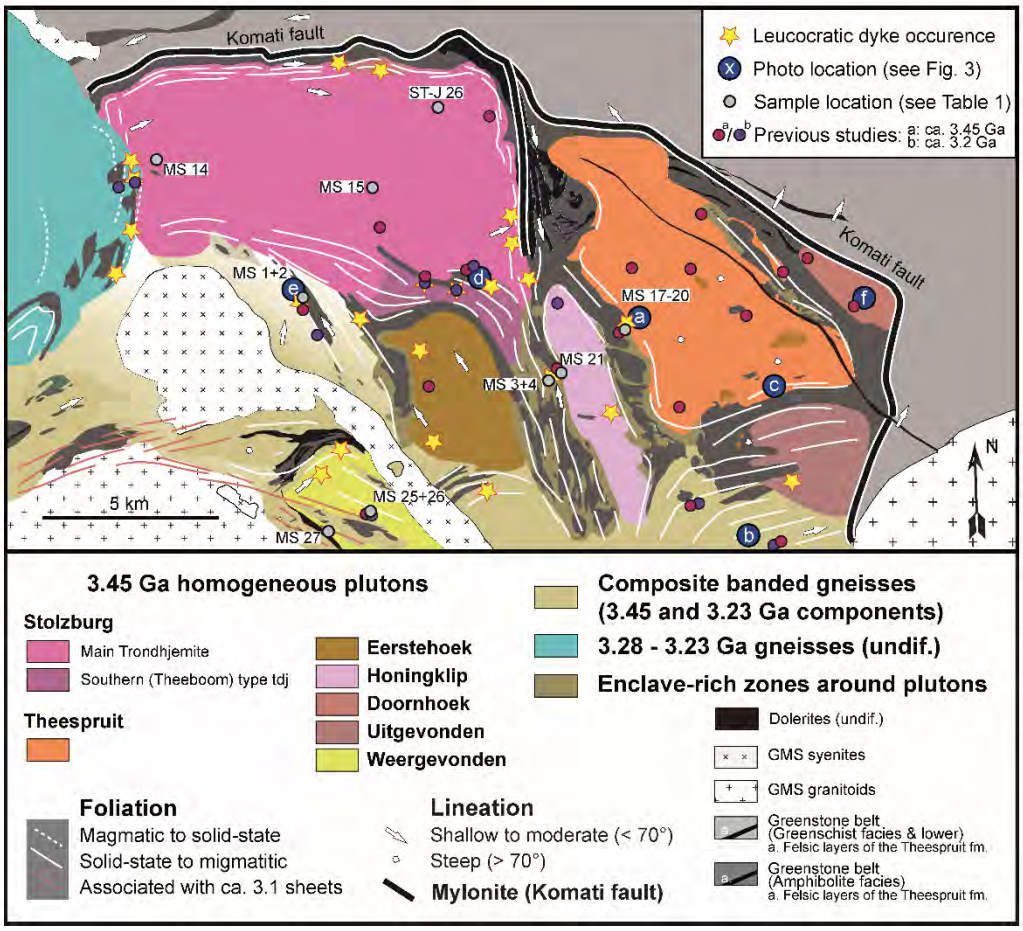

Fig. 4.3. Geological map of the Stolzburg Block. Blue circles show the location of field photos depicted in Figure 3 and grey circles the location of samples dated in this study. Samples from previous U-Pb zircon studies (Amelin et al., 2000; Armstrong et al., 1990; Dziggel et al., 2006, 2002; Kamo and Davis, 1994; Kisters et al., 2010; Kröner et al., 2016, 1991; Lana et al., 2010b; Laurent et al., 2020; Schoene et al., 2008; Van Kranendonk et al., 2014; Wang et al., 2019; Zeh et al., 2009) are indicated by red (ca. 3.45 Ga) and purple (ca. 3.2 Ga) circles, respectively. Modified after Moyen et al. (2019).

4.2.2 The Stolzburg Block

The plutons of the Stolzburg Block show varying degrees of deformation (Anhaeusser and Robb, 1980; Schoene et al., 2008). The cores of the larger plutons are largely undeformed and preserve magmatic textures and fabrics (Anhaeusser, 1980; Moyen et. al., 2019; Laurent et al., 2020), whereas an intermittently developed semi-concentric, steep to vertical solid-state foliation and lineation are developed towards the margins (e.g. Kisters and Anhaeusser, 1995;

Kisters et al., 2003; Lana et al., 2010a) (Fig. 4.3). Despite this deformation, clear intrusive relationships, including injection breccias, exist between the TTG and the hosting Theespruit and Sandspruit formation rocks (Fig. 4.4a - d). The Stolzburg, Theespruit, Weergevonden and Honingklip plutons are characterized by a homogenous coarse-grained trondhjemite, at outcrop scale, that will be referred to as the Main Trondhjemite in the following sections. The Stolzburg Pluton, the largest of the plutons of the Stolzburg Block, also contains localized minor phases that are texturally and/or compositionally distinct from the Main Trondhjemite: Lit-par-lit intrusive relationships with amphibolite-facies greenstone screens characterize the distinct unit of the composite Theeboom Gneisses in the south-eastern margin, while a granodiorite phase is exposed in a quarry on the eastern margin of the Stolzburg pluton (Fig. 4.3). Similarly, the Theespruit Pluton contains minor dioritic bodies (Laurent et al., 2020). Mostly, the trondhjemites are not migmatitic or even gneissose and exhibit well preserved plutonic, igneous textures.

The marginal zones of individual plutons against the greenstone, but also between different plutons of the Stolzburg Block, are intruded by variably deformed sheets of leucocratic dykes (Fig. 4.3, 4.4a). The sheets are leucotrondhjemitic in composition with a typical thickness of 20 to 30 cm and up to 2 to 3 m. The existing age constraints on the emplacement of these felsic dykes are possibly inconclusive. Schoene et al. (2008) dated a deformed dyke from the southern margin of the Stolzburg Pluton at 3212.5 ± 0.8 Ma, while seemingly undeformed dykes from the western margin of the Theespruit Pluton yield a date of ca. 3390 Ma (Moyen et al., 2019). Felsic dykes of similar age have also been reported from the Inyoni shear zone on the western margin of the Stolzburg Pluton (e.g. Wang et al., 2019).

The fabrics in the deformed margins of the Stolzburg block TTG plutons developed simultaneously with similar fabrics in the Theespruit and Sandspruit formation rocks that the TTGs intruded. Metasedimentary and metamafic layers within these greenstone belt rocks of the Stolzburg block record lineations and S-C fabrics (e.g. Fig. 5 of Diener et al., 2005) that are defined by peak metamorphic mineral associations such kyanite + staurolite and staurolite + garnet in metasedimentary rocks and garnet + hornblende + epidote in metamafic rocks. In combination, these assemblages clearly indicate peak metamorphic conditions in the high-pressure, low-temperature portion of the amphibolite facies (Diener et al., 2005; Cutts et al., 2014). These fabrics demonstrate exhumation of the amphibolite facies rocks of the Stolzburg Block relative to the greenschist facies rocks of the remainder of the BGB, from the base of the Hooggenoeg Formation upwards (Kisters et al., 2003; Diener et al., 2005). Deformation associated with this exhumation is prominent in the marginal portions of the plutons and in the greenstone belt rocks of the Stolzburg block, but it is strongly partitioned into the up to 1 km wide Komati Fault (Fig. 4.1b) that records greenstone belt down, Stolzburg Block up kinematics

(Kisters et al., 2003; Van Kranendonk et al., 2009). The break in metamorphic grade at the Komati Fault is substantial. The Sandspruit and Theespruit formation rocks record peak pressures from different localities that range between 8 and 12 kbar at temperatures of 560 to 650 °C (Cloete, 1991; Cutts et al., 2014; Diener et al., 2005; Dziggel et al., 2002; Moyen et al., 2006) corresponding to apparent geothermal gradients of around 15 to 20 °C km^{-1}, comparable to modern orogens (Clemens et al., 2006; Cutts et al., 2014; Diener et al., 2005; Dziggel et al., 2002; Moyen et al., 2006). In contrast, the rocks of the overlying Komati Formation record peak conditions of 350 °C at 3 kbar and considerable higher geothermal gradients of > 35 °C km^{-1} (Cloete, 1991).

The timing of amphibolite-facies metamorphism in the rocks of the lower Onverwacht Group has been constrained by a U-Pb age of 3229 ± 25 Ma on titanite from a metamafic rock of the Theespruit formation from the Tjakastad schist belt between the Stolzburg and Theespruit plutons (Diener et al., 2005). As the peak metamorphic temperature in this area is estimated to be approximately 560 °C, the age is interpreted to represent a crystallization age for the titanite which is aligned with the prominent hornblende lineation in the rocks (Diener et al., 2005). This age is in agreement with a garnet Lu-Hf age of 3233 ± 17 Ma from a garnet-biotite-chlorite schist from the same area (Cutts et al., 2014). However, it is within error different from a monazite U-Pb age of 3191 ± 9 Ma from an aluminous metapelite from the same area (Cutts et al., 2014), which may represent an age of monazite recrystallization due to fluid rock interaction or another pulse of amphibolite facies metamorphism. The possibility of polymetamorphism is supported by garnet Sm-Nd ages of 3201.6 ± 5.2 Ma (2σ, MSWD = 1.12), and 3200.7 ± 5.3 Ma (2σ, MSWD = 0.46) from metamafic rocks in the Inyoni shear zone (Maneiro et al., 2018) which are peak metamorphic ages from the Inyoni structure that are within error identical to the monazite age from the Tjakastad schist belt. Both these Sm-Nd garnet isochron ages yield relatively high Sm/Nd ratios (>0.6) and low Nd concentrations (<0.3 ppm) for garnet, mitigating concerns about age inaccuracy due to mineral inclusions (Maneiro et al., 2018). The older ages coincide with the main phase of deformation in the BGB and the accretion of northern and southern domains in the greenstone belt along the Inyoka fault (De Wit et al., 1992).

The chronological constraints available at present on the metamorphic history of the ca. 3.45 Ga TTG plutons of the Stolzburg block are two sets of TIMS U-Pb apatite dates (on a limited number of grains) of ca. 3100 Ma and ca. 3263 – 3401 Ma, respectively (Schoene et al., 2008) and U-Pb titanite and zircon dates of ca. 3200 Ma interpreted as metamorphic growth (Kamo and Davis, 1994), but the data at hand is insufficient for a reconstruction of the thermal history of the Stolzburg Block.

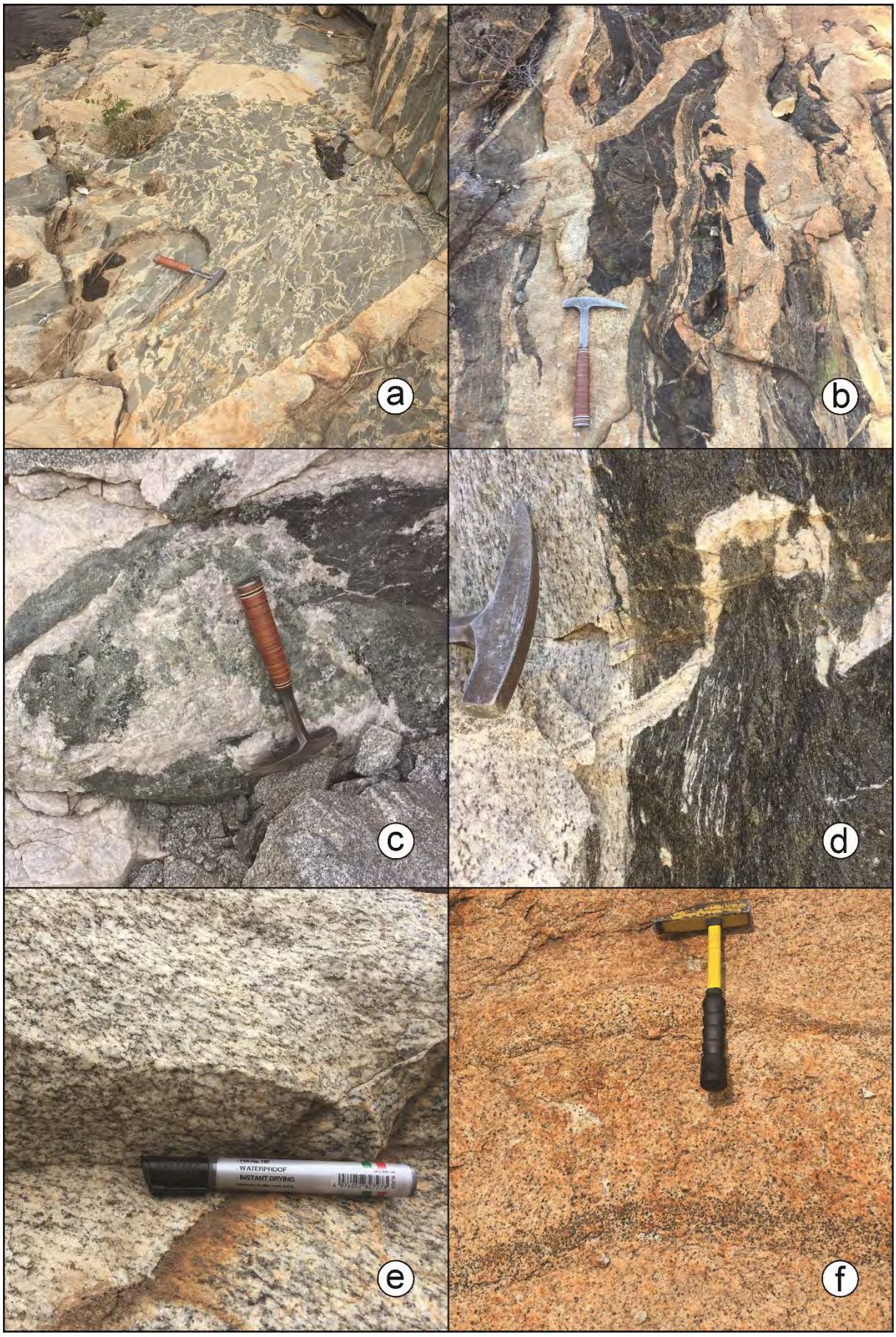

Fig. 4.4. Field photos from the Stolzburg Block. (a-(d) Intrusive contact between trondhjemite plutons and greenstones of the Lower Onverwacht Group. In (a), a later felsic dyke cuts both trondhjemite and greenstone. (e) Homogenous trondhjemite of the Stolzburg pluton. (f) Gravitational layering of biotite in the Doornhoek pluton, interpreted as a primary magmatic feature. See Fig. 2 for photo locations.

Zircon U-Pb ages from the Main Trondhjemite phase of the TTG plutons of the Stolzburg Block are typically in the rage of 3455 to 3440 Ma (Kamo and Davis, 1994; Kröner et al., 1996; Laurent et al., 2020; Schoene et al., 2008; Wang et al., 2019), while younger dates are rare. Kamo and Davis (1994) report dates of 3255 and 3237 ± 6.4 Ma for two zircon grains and a date of 3201 ± 1.6 Ma for a titanite grain from a foliated trondhjemite sample from the southern margin of the Stolzburg pluton, which they, based on the (calculated) low Th/U ratios of the two zircon grains of 0.00 to 0.11, interpreted as metamorphic growth. Wang et al. (2019) obtained a 3225.6 ± 3.9 Ma date for zircons from a granodiorite phase from the eastern margin of the Stolzburg Pluton, a date of 3224.6 ± 4.3 Ma for zircon grains from a quartz diorite phase of the Weergevonden Pluton and dates of 3224.6 ± 8.3 and 3225.0 ± 3.9 for zircon and titanite grains, respectively, for Trondhjemite samples from the northern margin of the Honingklip pluton. With the exception of Wang et al. (2019)'s samples, no backscattered electron or cathodoluminescence images are available for the published samples, making an interpretation of these ca. 3.2 Ga dates difficult. A clear pattern that emerges from the published age data for the granitoids of the Stolzburg Block is that the ca. 3.2 Ga dates are confined to the pluton margins, while no comparable dates are reported for the cores (Fig. 4.2). A more in-depth discussion of the existing geochronological data for the Stolzburg Block is given below in section 5.1.

In this study, samples were taken of the Main Trondhjemite of the Stolzburg Pluton and a more mafic phase confined to its eastern margin, of the Main Trondhjemite of the Theespruit, Weergevonden, Honingklip and Eerstehoek plutons and of felsic dykes cross-cutting the plutons. The sampling strategy was to obtain samples of the Main Trondhjemite from both the centers and the margins of the plutons in order to investigate any potential core-margin differences, focusing mainly on outcrops for which no or no sufficient geochronological data had been published yet. Furthermore, a sample of a garnet-bearing mafic schist xenolith was taken from the Honingklip pluton. Field descriptions and localities of the samples are given in Table 4.1.

Table 4.1. Sample descriptions and localities for dated granitoid and meta-sediment samples from the Stolzburg block.

Sample	Field description	Locality
Stolzburg pluton		
MS 1	Light grey, fine grained felsic dyke, not deformed	26.03086 °S, 30.71258 °E
MS 2	Foliated Trondhjemite	26.03089 °S, 30.71283 °E
MS 14	Weakly foliated Trondhjemite	25.99689 °S, 30.67719 °E
MS 15	Foliated Trondhjemite	26.00331 °S, 30.73664 °E
MS 36	Dark grey dyke or band?	26.03120 °S, 30.71247 °E
ST-J 26		25.97090 °S, 30.75233 °E
Honingklip pluton		
MS 3	Light grey, fine grained felsic dyke, not deformed	26.05489 °S, 30.78208 °E
MS 4	Foliated Trondhjemite	26.05489 °S, 30.78208 °E
Onverwacht Group		
MS 21	Garnet-bearing schist	26.05250 °S, 30.78497 °E
Theespruit pluton		
MS 17	Foliated Trondhjemite	26.03581 °S, 30.80253 °E
MS 18	Foliated Trondhjemite	26.03581 °S, 30.80253 °E
MS 19	Light grey, fine grained felsic dyke, not deformed	26.03581 °S, 30.80253 °E
MS 20	Light grey, fine grained felsic dyke, not deformed	26.03581 °S, 30.80253 °E
Weergevonden pluton		
MS 25	Dark gray dyke	26.09008 °S, 30.73336 °E
MS 26	Foliated Trondhjemite	26.09008 °S, 30.73336 °E
MS 27	Foliated Trondhjemite	26.09836 °S, 30.72219 °E

4.3 Analytical methods

4.3.1 Major- and trace-element analyses

Whole-rock major- and trace-element analyses were carried out at the Central Analytical Facilities, Stellenbosch University, South Africa. Fused disks were prepared using 0.7 g of sample powder mixed with 7 g of high purity flux (32.83 % $LiBO_2$, 66.67 % $Li_2B_4O_7$, 0.50 % LiI). Major-element compositions were determined on a PANalytical wavelength dispersive x-ray fluorescence spectrometer. The reference materials used for instrumental calibration are NIM-G and BE-N. The major-element data were recalculated to anhydrous compositions for data comparison and are listed in Table 4.4.

Trace-element and REE concentrations were analyzed using an Element E2 on fragments of the glass disks used for ME analysis. Ablation was done with a Resonetics 193nm Excimer laser connected to an Agilent 7700 ICP-MS. Reference materials BHVO-1 and BHVO-2G yielded a typical accuracy of <10 % deviation from the published value, except for Pb (45% deviation) and Nb (16% deviation), and a precision of <1%, with the exception of Ba (3%), Cr (4.8%), Cu (2.8%), Ni (2.3%), Sr (8.9%), V (6.9%), Zn (2.7%) and Zr (3.1%). Trace-element data are listed in Table 4.4.

4.3.2 U-Pb and Lu-Hf isotope analyses

For U-Pb analyses of zircon and apatite grains, heavy mineral separates were produced using standard mineral separation methods. Mineral grains were hand-picked, mounted in epoxy resin and polished. Back-scattered electron (BSE) and cathodoluminescence (CL) imaging was used to reveal the internal structure and zonation of apatite and zircon grains. Selected CL images of representative zircon grains are shown in Figures 4.6 and 4.14.

The U-Pb isotopic composition of zircons was measured at the Central Analytical Facilities, Stellenbosch University, South Africa using a Thermo-Fisher Element E2 ICP-MS. Laser and gas conditions are given in Table 4.5. Repeated analyses of reference materials M-127 and Plesovice yielded weighted mean $^{206}Pb/^{238}U$ ages of 531.1 ± 2.1 Ma (n = 43) and 339.6 ± 0.7 Ma (n = 43), respectively.

The U-Pb isotopic composition of apatite grains and the Lu-Hf isotopic composition of zircon grains were determined at UFOP using a ThermoScientific Neptune Plus multi-collector (MC)-ICP-MS following the method described by Lana et al. (2017). We reduced Pb–U apatite data offline, using an in-house MS Excel spreadsheet modified from Gerdes and Zeh (2009), see also details in Schneider et al. (2015). The raw data were corrected for: 1) background noise, 2) common Pb, 3) laser-induced element fractionation, 3) instrument mass discrimination, and 4) time-dependent elemental fractionation. the background-corrected ^{204}Pb signal was used for common Pb corrections based on the two-stage evolution model of terrestrial Pb composition (Stacey and Kramers, 1975). The ^{204}Pb was estimated by subtracting the average mass 204 signal of the background, which mostly results from ^{204}Hg in the carrier gas, from the mass 204 signal during sample ablation. All corrections have been applied on the time-resolved data set for each 0.4 s of integration prior to correction of downhole fractionation. Laser and gas conditions are given in Table 4.6. Reference materials 401 and MAD gave 206Pb/238U ages of 527.6 ± 3.3 (n=11) and 474.2 ± 2.1 Ma (n=11), respectively. Lu-Hf isotopes were measured on the edge and on top of concordant U-Pb spots according to the method of Gerdes and Zeh (2009, 2006). Model ages were calculated based on the depleted mantle (DM) model of Blichert-Toft and Albarède (2008) Analyses of zircon reference materials BB, GJ-1 and Mud Tank yielded 176Hf/177Hf ratios of 0.281670 ± 0.0000247 (n = 21), 0.282005 ± 0.000034 (n = 12) and 0.282503 ± 0.000029 (n = 21) (uncertainties stated at 2SD).

The U-Pb isotope data for zircon and apatite grains are listed in Tables 4.7 and 4.9, respectively, and the Hf isotope data for zircon grains in Table 4.8. The calculated zircon dates and εHft values are given in Table 4.2 and the apatite dates in Table 4.3 are also shown in the respective Concordia diagrams (Figs. 4.6 and 4.9).

4.4 Results

4.4.1 Major- and trace-element compositions

The major- and trace-element compositions have been determined for 37 granitoid samples – 25 samples from the plutons' main phases and twelve samples from cross-cutting dykes – and one mafic schist sample were taken from the Stolzburg Block. The results are listed in Table 4.4 and a classification of the granitoids based on their normative feldspar composition is given in Figure 4.5a. An in-depth description of the geochemical characteristics of the granitoid rocks of the Stolzburg block was recently published by Moyen et al. (2019).

The samples taken from the Main Trondhjemite phase of the Stolzburg, Theespruit, Weergevonden and Honingklip plutons plot in the trondhjemite field of the ternary feldspar diagram of O'Connor (1965) (Fig. 4.5a). Samples MS 23 and MS 36 from more mafic phases of the Stolzburg Pluton, sample MS 17 from the Theespruit Pluton and samples MS 37 and MS 40 from the Eerstehoek Pluton plot in the tonalite field. The cross-cutting dykes in general have a major-element composition comparable to the main trondhjemites, plotting mostly in the trondhjemite field in the ternary feldspar diagram. However, The Yb vs. La/Yb diagram (Fig. 4.5b) reveals slight but systematic differences between the trondhjemite and cross-cutting dyke samples of the Stolzburg Pluton, with the trondhjemites having low Yb concentrations of <0.3 ppm but a broad range of La/Yb ratios (50-180), while the felsic dykes have generally low La/Yb ratios of <50 with Yb concentrations ranging from 0.4 to >1 ppm. This trend can also be seen in samples from the Honingklip and Weergevonden plutons, but not in the samples from the Eerstehoek and Theespruit plutons, for which the main trondhjemites and cross-cutting felsic dykes plot in close proximity to each other.

The Y vs. Sr/Y diagram (Fig. 4.5c) shows a similar trend: The main phases of the plutons have a narrow range of Y concentrations (< ca. 7 ppm) but a large variety of Sr/Y ratios (50-600), while the cross-cutting dykes show variable Y (ca. 5-25 ppm) concentrations and lower Sr/Y ratios (ca. 0-130) compared to the host plutons. Again, the sample from the Eerstehoek Pluton do not follow this trend, all plotting close to each other at 15-20 ppm Y and a Sr/Y ratio of ca. 25. The two trends can also be seen in the database of ca. 190 granitoid samples from the Stolzburg Block (Moyen et al., 2019), with an overlap of the "Main Trondhjemite" and "dyke" fields at intermediate La/Yb and Sr/Y ratios, respectively (Fig. 4.5).

Sample MS 25 and MS25b, cutting the Weergevonden Pluton, has a composition distinct from the other samples analyzed in this study. They have a more intermediate composition, plotting in the Diorite field of the total alkali vs. silica diagram (not shown) with a SiO2 content of ca. 60 wt.% and a Na2O+K2O content of ca. 5.5 wt.%. In the ternary feldspar diagram, MS25 and MS25b plot in the Tonalite field (Fig. 4.5a).

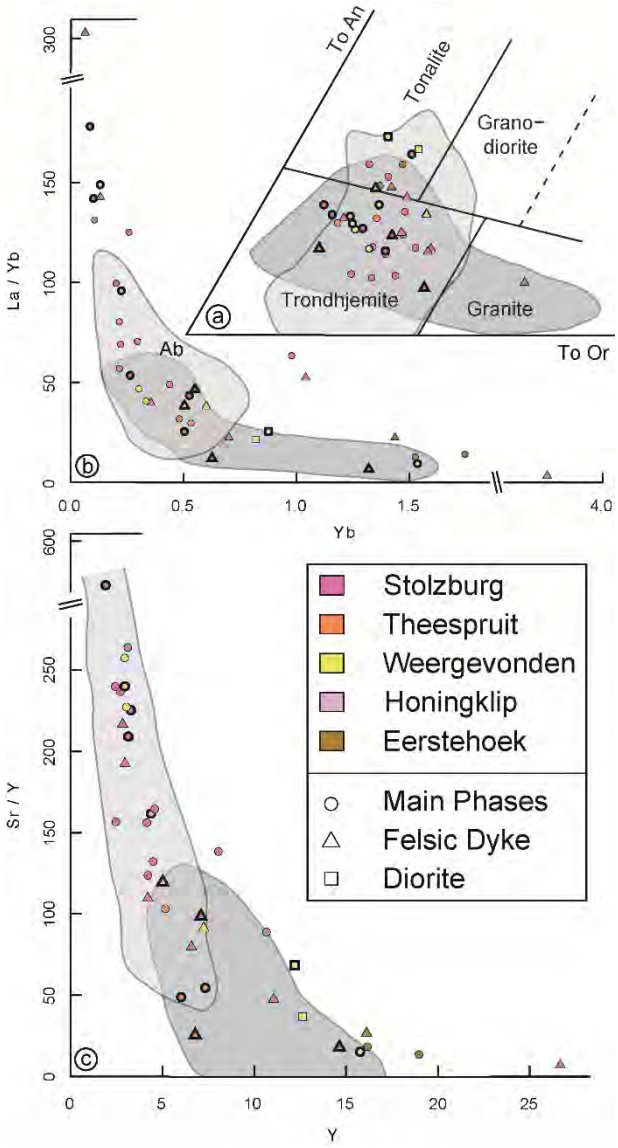

Fig. 4.5. Discriminatory diagrams for granitoid samples from the Stolzburg Block. Samples for which U-Pb zircon ages were obtained as part of this study are marked with a thicker rim. The shaded areas indicate the fields for main plutonic phases (light grey) and cross-cutting dykes (dark grey) from the Stolzburg Block (Moyen et al., 2019). (a) Classification of granitoid samples from the Stolzburg block based on their (CIPW-) normative feldspar composition (after O'Connor, 1965). (b) Yb vs. La/Yb diagram showing a trend of low Yb concentrations at varying La/Yb ratios for the main trondhjemites and of varying Yb concentrations at low La/Yb ratios for the felsic dykes. Yb concentrations in ppm. (c) Y vs. Sr/Y diagram showing a trend of low Y concentrations at varying Sr/Y ratios for the Main Trondhjemite and varying Y concentrations at low Sr/Y ratios for the felsic dykes. Y concentrations in ppm. See Table S.1 for whole-rock major- and trace-element data and text for discussion.

4.4.2 U-Pb systematics zircon

The U-Pb isotopic compositions were determined for zircon grains from samples of the main Trondhjemites and cross-cutting dykes from the Stolzburg (MS 1, 2, 14, 15, ST-J 26), Theespruit (MS 17-20), Honingklip (MS 3, 4) and Weergevonden (MS 25-27) plutons of the Stolzburg Block. The results are listed in Table 4.7 and a summary of relevant dates is given

in Table 4.2. Cathodoluminescence (CL) images of representative zircon grains are shown in Figures 4.6 and 4.14 and Concordia diagrams are shown in Figure 4.7. All dates reported in this section are $^{207}Pb/^{206}Pb$ dates. Ages are calculated as weighted mean $^{207}Pb/^{206}Pb$ ages and the uncertainties given are 2σ. Concordance is given as $^{206}Pb/^{238}U$ vs. $^{207}Pb/^{206}Pb$. As illustrated by the range of data collated in Fig. 4.2, the crystallization ages of the various TTG plutons associated with the southern portion of the Barberton greenstone belt have been the subject of numerous previous studies. Consequently, the zircon U-Pb ages from this study are intended to make it possible to categorize the samples as part of the approximately 3.45 or 3.23 Ga populations. This was readily possible, despite the fact that in some samples an apparent spread of concordant ages exists. This could have a range of possible causes, from a protracted crystallization history to radiogenic Pb loss. The cause of this spread in ages has not been resolved in this study.

The Main Trondhjemite of the Stolzburg Pluton: MS 2, MS 14, MS 15 and ST-J 26

Four samples from the Main Trondhjemite (one from the middle of the pluton, three from nearby the margins) yielded zircon grains with similar characteristics. They show igneous oscillatory zoning in their CL images (Fig. 4.6b, e, f, n). The primary zoning is in many grains partly recrystallized, forming fewer and broader zones, as described by Pidgeon et al. (1998), or replaced by featureless material. The zircon grains are often surrounded by a thin (commonly <1-2 µm) metamorphic rim, most common in samples MS 2 (Fig. 4.6b), MS 14 (Fig. 4.6e) and ST-J 26 (Fig. 4.6n) from the margin of the pluton and less pronounced in sample MS 15 (Fig. 4.6f) from the center. Replacement of igneous zoning by featureless material often originates from the metamorphic rim, indicating that this alteration is contemporaneous with metamorphic overprint. Some zircon grains from the margin show multiple metamorphic rims, appearing white and dark grey in CL images (e.g. Fig. 4.6b #14-16, #60; Fig. 4.6e #60; see also samples MS 2 and MS 14 in Fig. 4.14), indicative of multiple episodes of metamorphic zircon growth.

The Main Trondhjemite samples from the south-western and western margin and from the center of the Stolzburg Pluton all show the same pattern in their U-Pb data, with a continuous spread of concordant to near-concordant dates from ca. 3450 to 3400 Ma and a tail of discordant points. The range of concordant dates most likely points toward to lead loss shortly after emplacement. Extremely slow cooling over 50 Ma would have required higher metamorphic grades in the country rocks than are observed. Similarly, protracted assembly of the pluton by multiple magma batches over 50 Ma appears not to be a good fit with the field relations as the core domain of the Stolzburg Pluton is relatively featureless and displays a simple and homogenous igneous texture. No clear core-rim systematics are observed in igneous zircon domains. Concordant dates younger than ca. 3420 Ga are rare and likely the

result of post-crystallization recrystallization (e.g. Fig. 4.6e spot #53), represent mixed analyses between igneous and recrystallized zones (e.g. Fig. 4.6b spots #13 and #60) or are the product of ancient lead loss, which can be indistinguishable from pristine magmatic dates at those ages due to the low slope of the Concordia curve.

Dates for the Main Trondhjemite of the Stolzburg Pluton were calculated for each sample using concordant (100 ± 3 %) data points at the upper end of the main age cluster, that statistically form a single population (MSWD ≤ 1.0), and the results are listed in Table 4.2 and shown in Figure 4.7. From the south-western margin of the pluton, sample MS 2 (Fig. 4.7a) shows a main population at 3439 ± 5 Ma (MSWD = 0.59; n = 13) and its tail of discordant points has an upper intercept at ca. 3434 Ma and a lower intercept at ca. 970 Ma. Sample MS 14 (Fig. 4.7b) from the western margin has a main population of dates at 3440 ± 6 Ma (MSWD = 0.74; n= 9) and an upper intercept for the discordant points at ca. 3388 Ma and a lower intercept at ca. 820 Ma. One concordant and one discordant spot from recrystallized grains give an upper intercept age of 3202 +21/-18 Ma, which is interpreted as the time of a metamorphic and/or hydrothermal event that triggered recrystallization of zircon and Pb loss. Sample ST-J 26 (Fig. 4.7d), taken near the northern margin, yields a date of 3451 ± 8 Ma (MSWD = 1.02; n = 5), and the tail of discordant data-points has an upper intercept at ca. 3429 Ma and a lower intercept at ca. 950 Ma. The sample also contains a single potential inherited core of 3493 ± 19 Ma. For the core of the Stolzburg Pluton, sample MS 15 (Fig. 4.7c) give a date of 3432 ± 3 Ma (MSWD = 0.88; n = 34), with the tail of discordant spots intersecting the Concordia at ca. 3430 and 400 Ma.

The Main Trondhjemite of the Theespruit Pluton: MS 17 and MS 18

Samples MS 17 (Fig. 4.6g) and MS 18 (Fig. 4.6h) from the Main Trondhjemite of the Theespruit Pluton show a weak oscillatory or no zonation in their CL images. Where present, the oscillatory zoning is often recrystallized into fewer and broader bands, as described by Pidgeon et al. (1998), or featureless patches. Metamorphic rims around the zircon grains are uncommon and often confined to the terminations of the crystals. The U-Pb data for sample MS 17 (Fig. 4.7g) show a range of concordant (100 ± 3 %) dates from 3313 to 3439 Ma, with the main population of dates at 3411 ± 6 Ma (MSWD = 0.43; n = 8) and two older spots, one concordant and one reversely discordant (108 %), at 3444 ± 12 Ma (MSWD = 0.52; n = 2). The latter is interpreted as emplacement age and younger dates are regarded as the result of lead loss or recrystallization. The discordant data-points for samples MS 17 have an upper intercept at ca. 3378 Ma and a lower intercept at ca. 1090 Ma. Sample MS 18 (Fig. 4.7h) has a similar range of concordant (100 ± 3 %) dates from 3336 to 3427 Ma and a main population at 3417 ± 6 Ma (MSWD = 0.58; n = 8). A single discordant (94 %) spot on an oscillatory zoned grain

plots outside the main population at 3438 ± 19 Ma and may indicate the “real” emplacement age, while the majority of the analyzed grains were likely affected by ancient lead loss shifting them towards younger dates. This ca. 3440 Ma data-point is also within error identical with the ca. 3444 Ma date determined for MS 17 from the same outcrop. Three concordant (98 %) to discordant (92 resp. 90 %) spots determined for recrystallized zones yield date of 3204 ± 10 Ma (MSWD = 0.43; n = 3), which give an estimate for the timing of metamorphism/hydrothermal alteration. One inherited core in sample MS 18 gave an age of 3530 ± 19 Ma. Discordant data-points yield intercepts with the Concordia at ca. 3350 and 870 Ma.

Dykes cutting the Stolzburg Pluton: MS 1

Cross-cutting dyke sample MS 1 (Fig. 4.7e) only yielded eight datable grains. The zircons show igneous, oscillatory zoning in their CL images, that is partially recrystallized into less, broader zones (Fig. 4.6a). Oscillatory zoned zircon domains from two grains give a date of 3204 ± 12 (MSWD = 0.25; n = 2), interpreted as emplacement age. Grain #9/10 has a moderately to heavily recrystallized rim with a discordant analysis yielding a 2827 ± 20 Ma date (79%; n = 1). Four concordant (98%) to discordant (96-91%) analyses give a younger date of 3151 ± 9 Ma (MSWD = 5.58; n = 4) and likely represent a lead loss event. One concordant (98%; 3439 ± 19 Ma) and one discordant (93%; 3414 ± 19 Ma) analysis of an oscillatory zoned grain give a date of 3427 ± 12 Ma (MSWD = 4.33; n = 2), while further discordant (94-89%) analyses yield dates of ca. 3371 Ma (see Fig. 4.14 and Table 4.7, analyses #1, 12, 13); the grains show embayment and a CL white rim not present on the ca. 3204 Ma grains and are interpreted as either inheritance or xenocrysts from the Main Trondhjemite.

Dykes cutting the Theespruit Pluton: MS 19 and MS 20

Cross-cutting felsic dyke samples MS 19 and MS 20 (Fig. 4.7i), sampled in close proximity to MS 17 and MS 18 and to each other, only yielded twelve and five datable grains, respectively. The zircon grains are mostly heavily recrystallized, but MS 19 (Fig. 4.6i) and MS 20 (Fig. 4.6j) each contain one oscillatory zoned grain. While the grains have metamict rims, seemingly pristine igneous zones are preserved in the cores, yielding ages of 3211 ± 13 Ma (MSWD = 0.03; n = 2) for MS 19 and 3215 ± 15 Ma (MSWD = 0.04; n = 2) for MS 20 and a combined date of 3213 ± 10 Ma (MSWD = 0.09; n = 4), interpreted as emplacement age for those dykes. Heavily altered grains in samples MS 19 and MS 20 give a date of 3385 ± 9 Ma (MSWD = 0.61; n = 4) and are regarded as either inheritance or xenocrysts taken in from the Main Trondhjemite.

The small plutons south of the Stolzburg Pluton: MS 4 and 3 (Honingklip Pluton)

For the Honingklip Pluton, the CL images of Main Trondhjemite sample MS 4 (Fig. 4.6d) show igneous, oscillatory zoning, that is partially replaced by featureless material, sometimes affecting most of the grain and often originating from the rim; some grains have a thin (<1 µm) metamorphic rim. Inherited cores, some still with oscillatory zoning while others are unzoned, can be identified in the CL images.

The U-Pb data for samples MS 4 shows three main clusters of concordant dates that are interpreted as different populations (Fig. 4.7c). The oldest population, corresponding to inherited cores, yields an age of 3520 ± 8 Ma (MSWD = 0.98; n = 4), the next younger population gives an age of 3439 ± 6 Ma (MSWD = 0.69; n = 9) for oscillatory zoned grains, interpreted as emplacement age. The youngest population of concordant dates yields an age of 3219 ± 6 Ma (MSWD = 1.05; n = 8); this population corresponds mostly to recrystallized zones, although for few data points the microtextures are not clearly indicative of any recrystallization of the igneous zonation. The Th/U ratios for the ca. 3220 Ma data-points are relatively low, ranging from 0.1 to 0.3. Few concordant data points plot outside of these populations and are likely caused by either mixed analyses of igneous and altered zones or by ancient lead loss. Discordant data points form a tail from the youngest age population, with an upper intercept at ca. 3300 Ma and a lower intercept at ca. 890 Ma.

Sample MS 3 from a felsic dyke cross-cutting the Main Trondhjemite of the Honingklip Pluton yielded five datable zircon grains. The CL images (Fig. 4.6c) show weak oscillatory zoning, partially replaced by featureless material originating from the rim and from cracks. Three oscillatory zoned grains gave an age of 3207 ± 7 Ma (MSWD = 0.25; n = 6), interpreted as emplacement age. Analyses of recrystallized zircon domains yield a 3165 ± 10 Ma date (MSWD = 0.28; n = 3). Grain #1/2 has a partially resorbed core surrounded by oscillatory to patchy zoned zircon. Mixed analyses give a 3312 ± 12 Ma date (MSWD = 0.44; n = 2).

The small plutons south of the Stolzburg Pluton: MS 26, MS 27 and MS 25 (Weergevonden Pluton)

For the southernmost pluton of the Stolzburg Block, the Weergevonden Pluton, zircons from Main Trondhjemite samples MS 26 (Fig. 4.6l) and MS 27 (Fig. 4.6m) show oscillatory zoning in their CL images, that is partially replaced by featureless material in some grains, and a thin metamorphic rim. For sample MS 26, the U-Pb data shows a range of concordant (100 ± 3) dates from 3388 to 3458 Ma (Fig. 4.7j), the main population being at 3434 ± 4 Ma (MSWD = 0.86; n = 18), interpreted as emplacement age. Sample MS 27 has a range of dates from 3351 to 3455 Ma (Fig. 4.7l) and yields a main population at 3435 ± 3 Ma (MSWD = 0.78; n = 34),

interpreted as emplacement age. Concordant dates younger than the main population are rare in samples MS 26 and 27 and likely the result of (partial) recrystallization or ancient lead loss. Both samples show a tail of discordant dates with intercepts at ca. 3420 and 910 Ma (MS 26) and ca. 3430 and 660 Ma (MS 27).

The CL images for zircon grains in sample MS 25, cutting the Weergevonden Pluton near sample MS 26, show oscillatory zoning and often a thin metamorphic rim (Fig. 4.6k). Data points for sample MS 25 are mostly concordant and range from 3170 to 3245 Ma (Fig. 4.7k) and few discordant points (92 to 96 %) range from 3108 to 3292 Ma. The main age population is at 3221 ± 2 Ma (MSWD = 0.93; n = 84), interpreted as emplacement age.

Fig. 4.6. Representative cathodoluminescence images of zircon grains from granitoid sample from the Stolzburg Block. Dashed circles indicate the location of the ablation pits. Suffixes behind the $^{207}Pb/^{206}Pb$ dates correspond to the number of analysis in Table 4.7

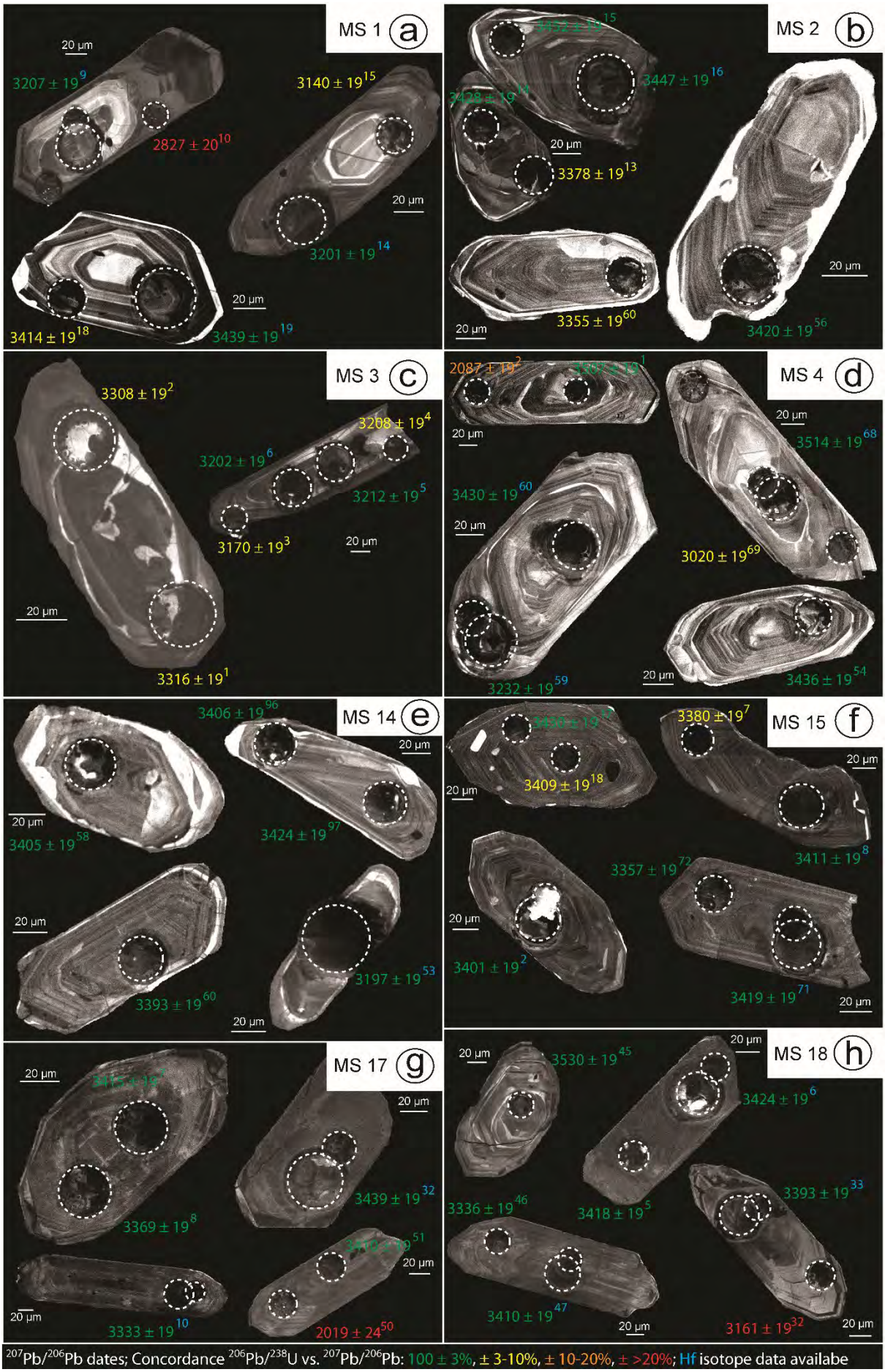

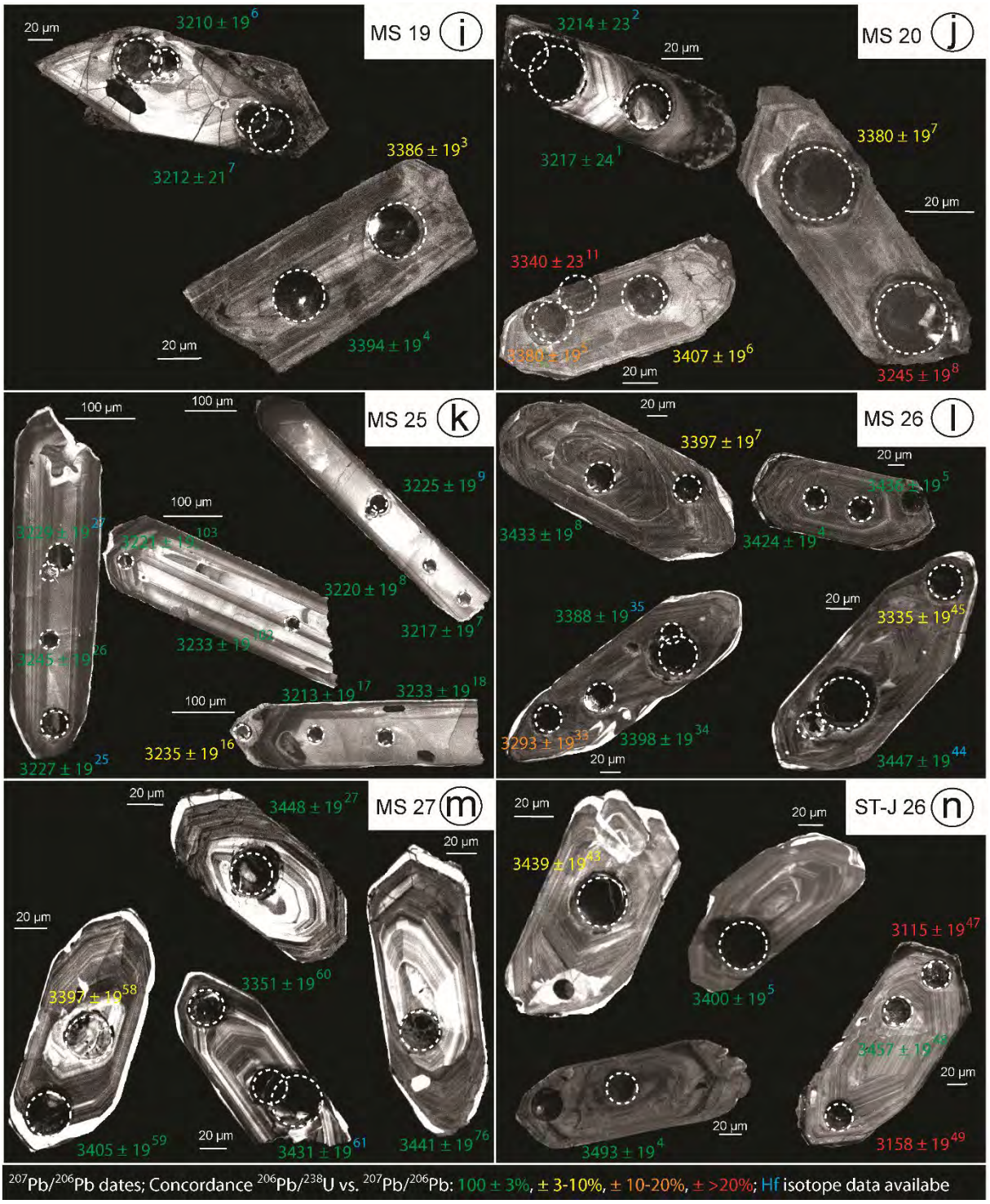

Fig. 4.6, continued.

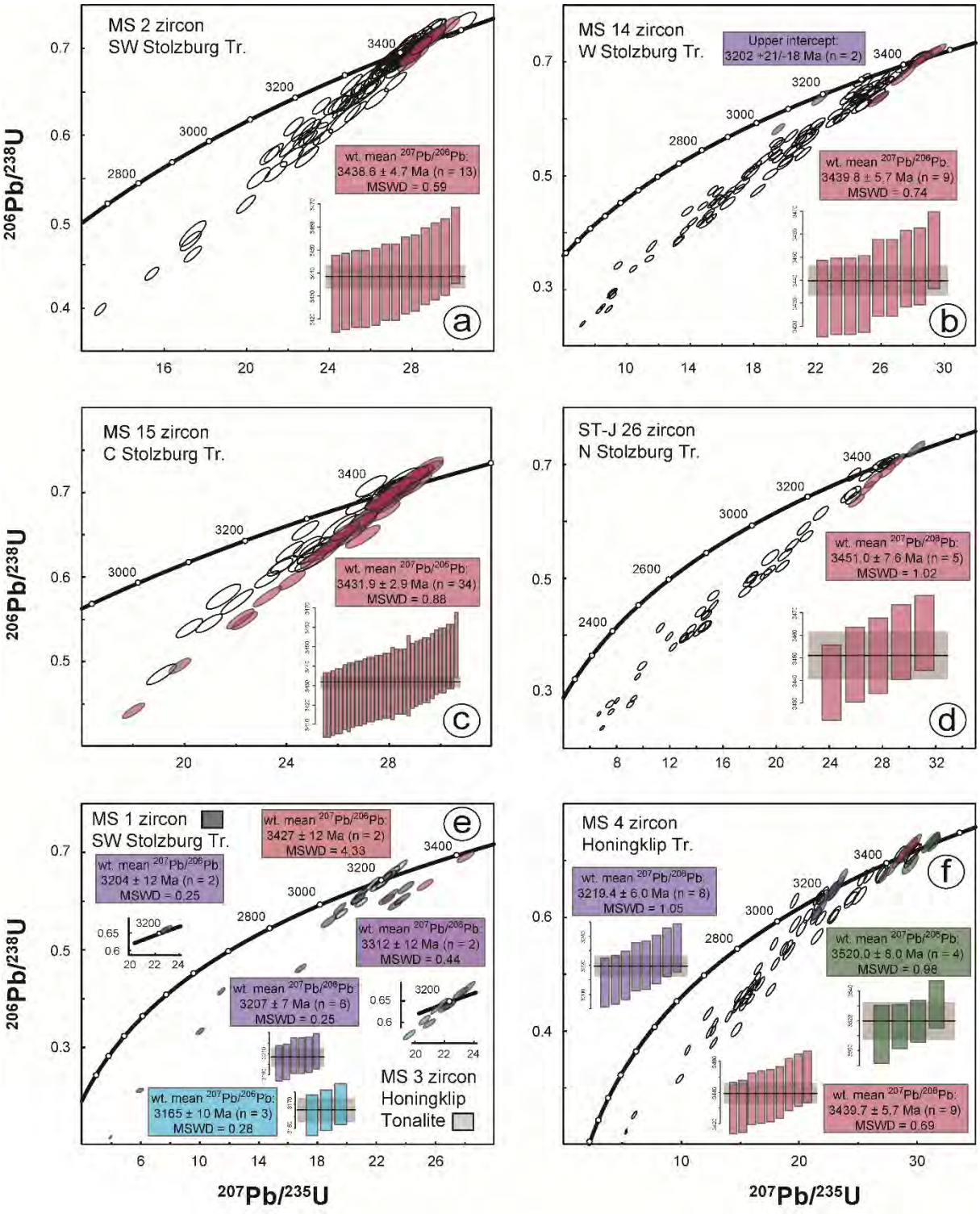

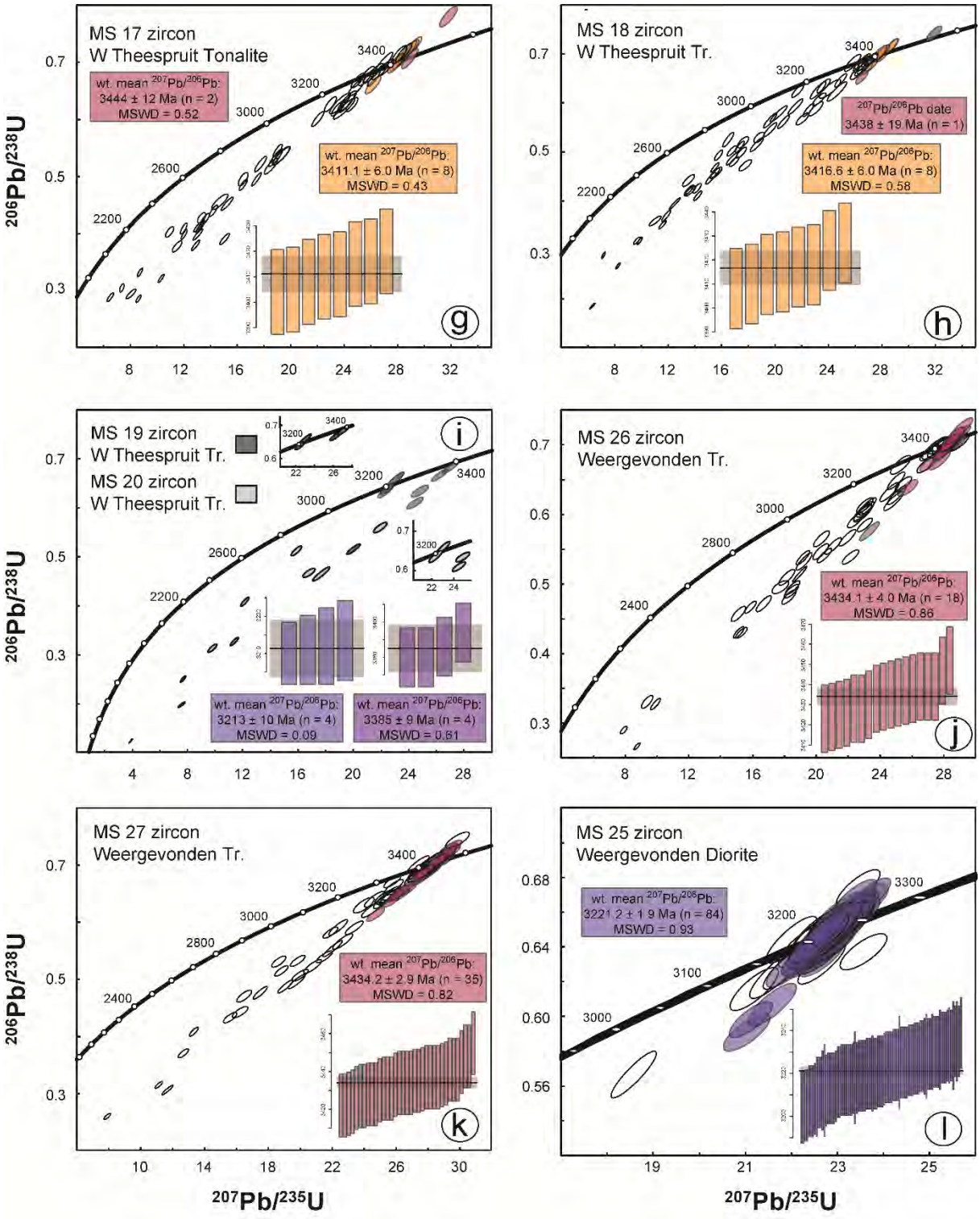

Fig. 4.7, continued.

Table 4.2. Summary of U-Pb zircon dates and Lu-Hf isotope characteristics for TTG samples from the Stolzburg block.

Sample	Field description	Th/U	U-Pb date [Ma]	MSWD	n	$\varepsilon Hf_{(t)}$	T_{DM} [Ga]	n	Interpretation
Stolzburg pluton									
MS 1	Fine-grained felsic dyke, not deformed	0.19–0.48	3204 ± 12 ^{PbPb}	0.3	2	-0.6	3.55	2	Age of intrusion
		0.49	3439 ± 19	--	1	+1.9	3.59	1	Xenocrystal or inheritance
MS 2	Foliated Trondhjemite	0.22–0.96	3436 ± 5 ^{PbPb}	0.6	13	-0.7	3.73	8	Minimum crystallization age
MS 14	Weakly foliated Trondhjemite	0.04–0.32	3202 +21/-18 ^{UI}	--	2	-9.1	4.01	1	Hydrothermal growth/alteration
		0.35–0.87	3440 ± 6 ^{PbPb}	0.7	9	+0.5	3.67	5	Crystallization age
MS 15	Foliated Trondhjemite	0.24–0.88	3432 ± 3 ^{PbPb}	0.9	34	-0.4	3.71	5	Minimum crystallization age
ST-J 26		0.45–1.3	3451 ± 8 ^{PbPb}	1.0	5	+0.1	3.69	4	Minimum crystallization age
		0.74	3493 ± 19	--	1	--	--	--	Inheritance
Honingklip pluton									
MS 3	Fine-grained felsic dyke, not deformed	0.02–0.06	3165 ± 10	0.3	3	-1.2	3.54	1	Hydrothermal growth/alteration
		0.32–0.38	3207 ± 7 ^{PbPb}	0.3	6	+0.4	3.49	3	Age of intrusion
		0.02–0.06	3312 ± 12 ^{PbPb}	0.4	2	--	--	--	Xenocrystal or inheritance
MS 4	Foliated Trondhjemite	0.08–0.30	3219 ± 6 ^{PbPb}	1.1	8	-1.7	3.62	3	Hydrothermal growth/alteration
		0.40–0.77	3440 ± 6 ^{PbPb}	0.7	9	+0.5	3.66	4	Minimum crystallization age
		0.52–0.62	3520 ± 8 ^{PbPb}	1.0	4	+1.8	3.65	3	Inheritance
Theespruit pluton									
MS 17	Foliated Trondhjemite	0.38–0.66	3411 ± 6 ^{PbPb}	0.4	8	-0.5	3.69	5	Minimum crystallization age
		0.63-1.2	3187 ± 13 ^{UI}	1.3	4	--	--	--	Hydrothermal growth/alteration
MS 18	Foliated Trondhjemite	0.37–1.0	3417 ± 6 ^{PbPb}	0.6	8	-0.8	3.72	4	Crystallization age
		0.60	3530 ± 19	--	1	--	--	--	Inheritance
MS 19	Fine-grained felsic dyke	0.43	3211 ± 13 ^{PbPb}	--	2	-1.1	3.58	2	Age of intrusion
MS 20	Fine-grained felsic dyke	0.39	3214 ± 23 ^{PbPb}	--	1	-2.0	3.63	1	Age of intrusion
MS 19+20		0.38-0.47	3385 ± 9 ^{PbPb}	0.6	4	--	--	--	Xenocrystal or inheritance
Weergevonden pluton									
MS 25	Dark grey granitoid	0.05–0.98	3221 ± 2 ^{PbPb}	0.9	84	-1.4	3.61	19	Age of intrusion
MS 26	Foliated Trondhjemite	0.26–0.77	3434 ± 4 ^{PbPb}	0.9	18	-0.3	3.71	4	Crystallization age
MS 27	Foliated Trondhjemite	0.31-1.2	3435 ± 3 ^{PbPb}	0.8	34	+1.2	3.63	7	Crystallization age

Uncertainties are 2σ. Dates of single analyses are $^{207}Pb/^{206}Pb$ dates. UI = upper intercept; PbPb = weighted mean $^{207}Pb/^{206}Pb$ age; MSWD = mean square weighted deviation. $\varepsilon Hf_{(t)} = [(^{176}Hf/^{177}Hf)_{sample(t)} / (^{176}Hf/^{177}Hf)_{CHUR(t)} - 1] * 10^4$. Model ages are calculated using the depleted mantle model of Blichert-Toft and Albarède (2008).

4.4.3 Hf in zircon

The Lu-Hf isotopic composition has been determined for zircon grains from the Stolzburg Block showing concordant (Concordance $^{206}Pb/^{238}U$ vs. $^{207}Pb/^{206}Pb$: 100 ± 5 %) U-Pb dates. The results are listed in Table 4.8 and εHf_t values are given in Table 2. Figure 8 illustrates the $^{177}Hf/^{176}Hf_{(i)}$ and εHf characteristics of the zircon grains and a function of $^{207}Pb/^{206}Pb$ age.

Main Trondhjemite of the Stolzburg block

For the Main Trondhjemite samples, the main population of initial $^{176}Hf/^{177}Hf$ ratios are chondritic to sub-chondritic at ca. 3450 Ma (Fig. 4.8a). The data show a tail of spots with similar initial $^{176}Hf/^{177}Hf$ values but varying apparent ages down to ca. 3180 Ga, likely due to resetting of the U-Pb system that did not affect the Hf isotopic system (Zeh et al., 2009, and references therein). This argues for an ancient (>3 Ga) lead loss as the cause of the spread in (near-) concordant dates seen in all Main Trondhjemite samples rather than protracted emplacement (c.f. 4.4.2). Sample MS 4 contains two distinct groups, the younger one having higher initial $^{176}Hf/^{177}Hf$ values, indicating growth of new metamorphic or igneous zircon. The εHf_t values for the Main Trondhjemite of the Stolzburg block range from +1.2 to -0.8 with model ages of ca. 3.7 Ga (Fig. 4.8b; Table 4.2).

Dykes cross-cutting the Stolzburg Block

The few zircon grains obtained from cross-cutting felsic dykes also yielded chondritic $^{177}Hf/^{176}Hf_{(i)}$ values, but at younger dates of ca. 3.2 Ga (Fig. 4.8a). The εHf_t values for the felsic dykes are from +0.4 to -2.0 with model ages of ca. 3.6 Ga. A single older grain of 3439 ± 19 Ma in sample MS 1 yielded a lower initial $^{176}Hf/^{177}Hf$ ratio that is lower compared to the ca. 3.2 Ga grains in the same sample but similar to the zircon grains in the close-by sample MS 2, indicating that it could be a xenocryst incorporated into sample MS 1 during emplacement.

The initial $^{177}Hf/^{176}Hf$ values determined for diorite sample MS 25 are all sub-chondritic at ca. 3.23 Ga and show little scatter, indicating that the U-Pb system in those grains remained undisturbed (Fig. 4.8a). The $\varepsilon Hf_{3.2Ga}$ value for samples MS 25 is -1.4 with a model age of ca. 3.6 Ga (Fig. 4.8b; Table 4.2).

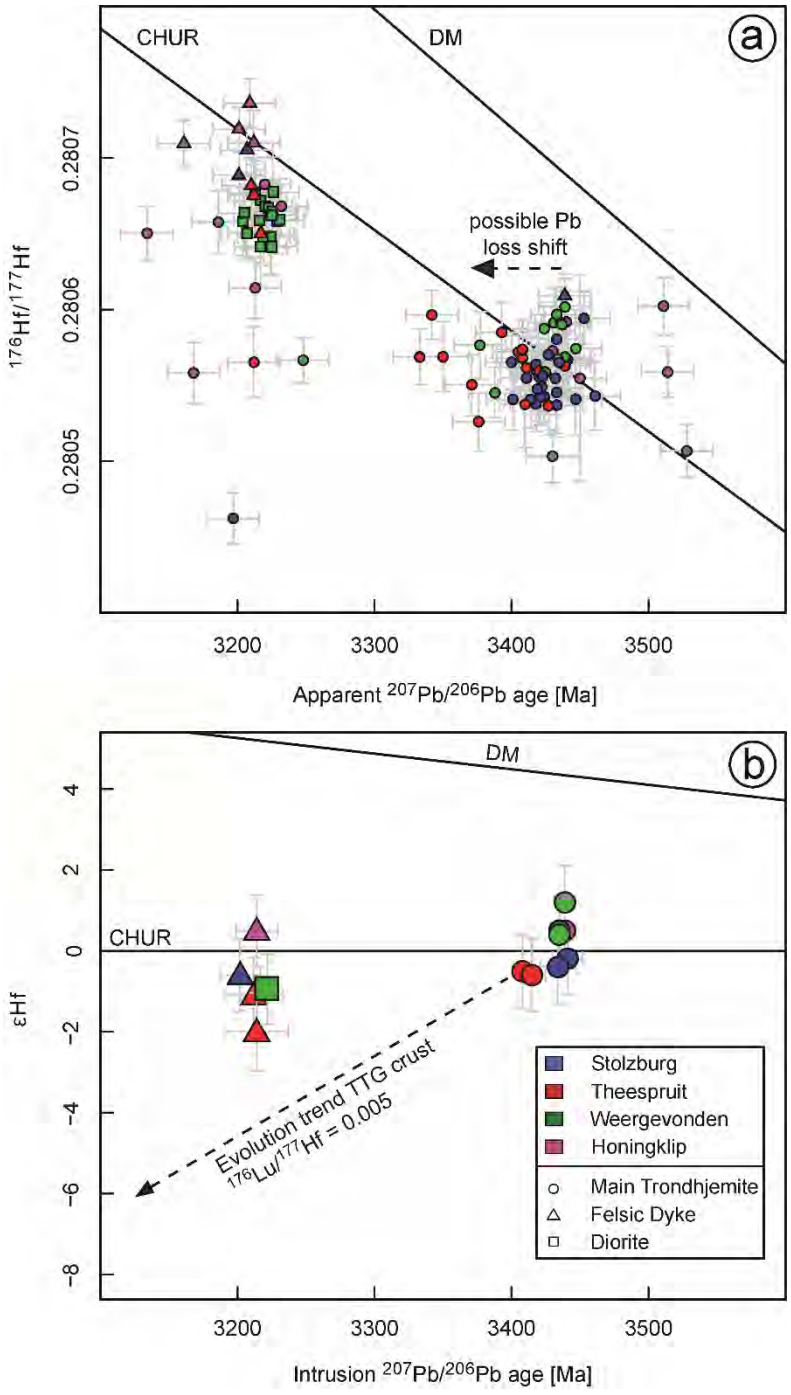

Fig 4.8. $^{176}Hf/^{177}Hf$ vs. Pb-Pb age (a) and εHf vs. age (b) diagrams showing the results of U-Pb and Hf isotope analyses for concordant analyses of zircon grains from Main Trondhjemite (circles), felsic dyke (triangles) and diorite (squares) samples of the Stolzburg block. Single grain analyses are designated with small symbols and averaged analyses of multiple grains with large symbols. The sample's emplacement age was used for averaged data points and the apparent $^{207}Pb/^{206}Pb$ age for single points. See Table 4.2 for εHf_t values and model ages and Table 4.8 for Hf isotopic data. CHUR: chondritic uniform reservoir, DM: depleted mantle (after Blichert-Toft and Albarède, 2008).

4.4.4 U-Pb dates apatite

In an attempt to better constrain the thermochronology of the Stolzburg Block, U-Pb dates were obtained for apatite grains from five trondhjemite and one tonalite sample from the Stolzburg (MS 2, 14, 15, 36) and Honingklip (MS 4) plutons, a diorite sample cutting the Weergevonden Pluton (MS 25), and a garnet-bearing mafic schist from the Honingklip Pluton (MS 21). The results are listed in Table 4.9. Cathodoluminescence images are shown in Figure 4.9 and Concordia diagrams in Figure 10. All apatite dates reported are weighted mean $^{207}Pb/^{206}Pb$ dates, unless stated otherwise, and the uncertainties are at 95% confidence.

The microtexture of the apatite grains from the Stolzburg Block (Fig. 4.9) reveals a complex history of multiple dissolution and precipitation events. Multiple generations can commonly be identified within individual grains, with up to four within a single grain (e.g. Fig. 4.9a #79+80, Fig. 9c #28+29). These different growth zones are rarely euhedral, often in a different orientation compared to the overgrown grain and can show embayment, indicating growth over multiple dissolution and precipitation events. The apatite grains are typically equant in form, which is interpreted as a sign of growth under near-equilibrium conditions (Webster and Piccoli, 2015).

The Main Trondhjemite samples from the Stolzburg Pluton all show multiple apatite age populations (Fig. 4.10a-c, f). The oldest population is at ca. 3.45 Ga, overlapping within error with the emplacement age of the Stolzburg Pluton (cf. section 4.4.2). The younger populations are at ca. 3.22, 3.10 and 2.82 Ga. The four age populations occur in all analyzed samples from the Stolzburg Pluton, with the exception of the ca. 3.1 Ga population, which is absent in sample MS 15 from the center of the pluton. Sample MS 4 from the Honingklip Pluton only shows a single, discordant age group at 2813 ± 9 Ma (MSWD = 1.2; n = 14), but sample MS 21, which was taken ~400 m from sample MS 4, contains the same four age populations as the samples from the Stolzburg Pluton (Fig. 4.10d). Diorite sample MS 25 from the Weergevonden Pluton shows a pattern of apatite ages that is consistent with that of the trondhjemite samples, with an oldest age peak overlapping within error with the emplacement age of the rock (for this sample at 3221 ± 2 Ma, c.f. section 4.4.2), and then younger peaks at ca. 3104 ± 16 (MSWD = 0.31; n = 6) and 2830 ± 15 (MSWD = 1.18; n = 9) Ma (Fig. 4.10e).

The four main age populations at 3442 ± 7 (average of five samples; MSWD = 1.37; n = 25), 3212 ± 4 (average of six samples; MSWD = 0.95; n = 71), 3104 ± 6 (average of five samples; MSWD = 0.37; n = 30) and 2820 ± 5 (average of six samples; MSWD = 1.01; n = 57) Ma are distinct from one another despite the rather large uncertainties of the single analyses of up to 65 Ma (2σ) and are within error identical throughout the Stolzburg Block. There is no spatial or petrological control on the distribution of the younger populations.

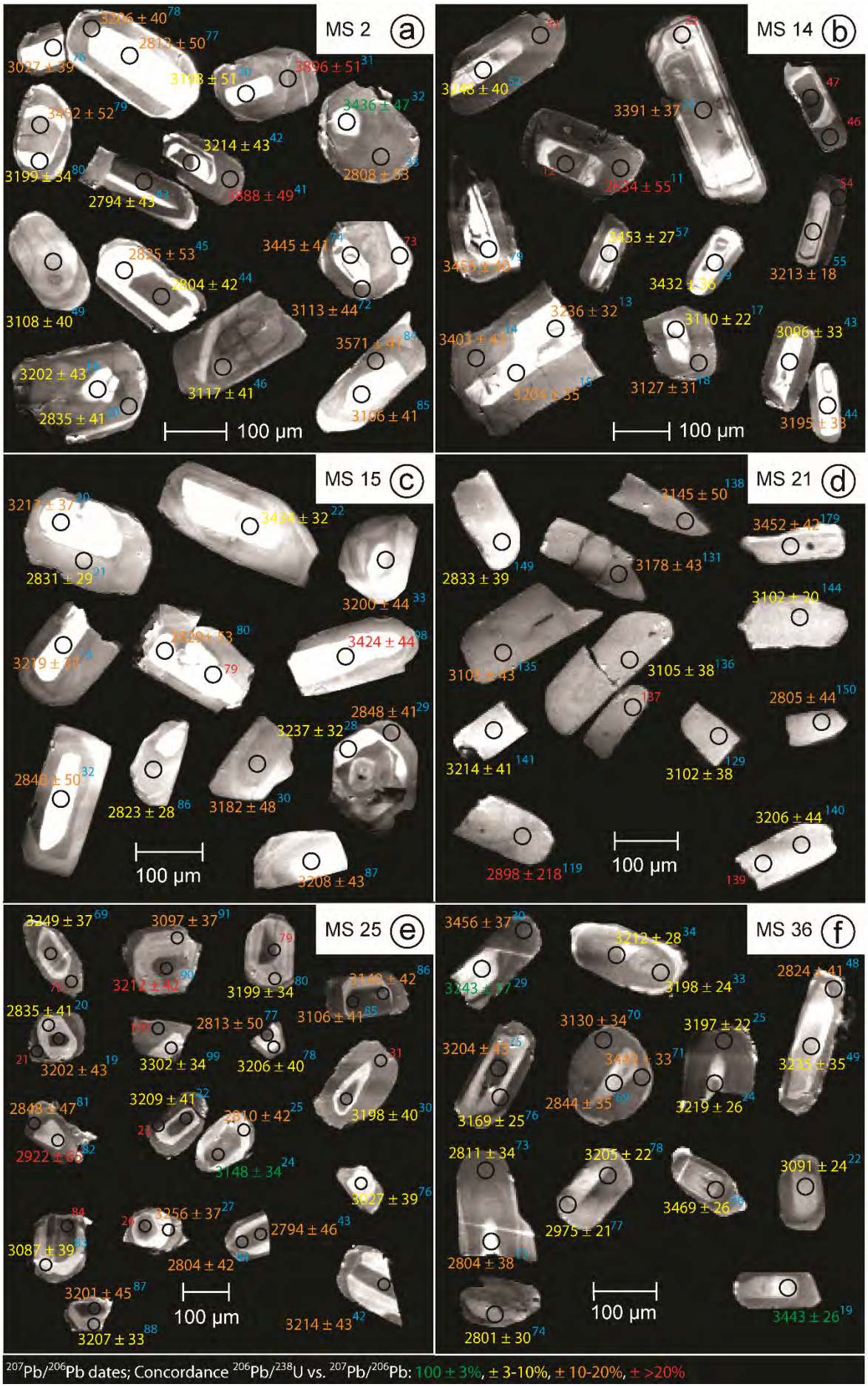

Fig. 4.9. Representative cathodoluminescence images of apatite grains from granitoid (a-c, e, f) and mafic schist (d) samples from the Stolzburg block. Suffixes behind the $^{207}Pb/^{206}Pb$ dates correspond to the number of analysis in Table 4.9.

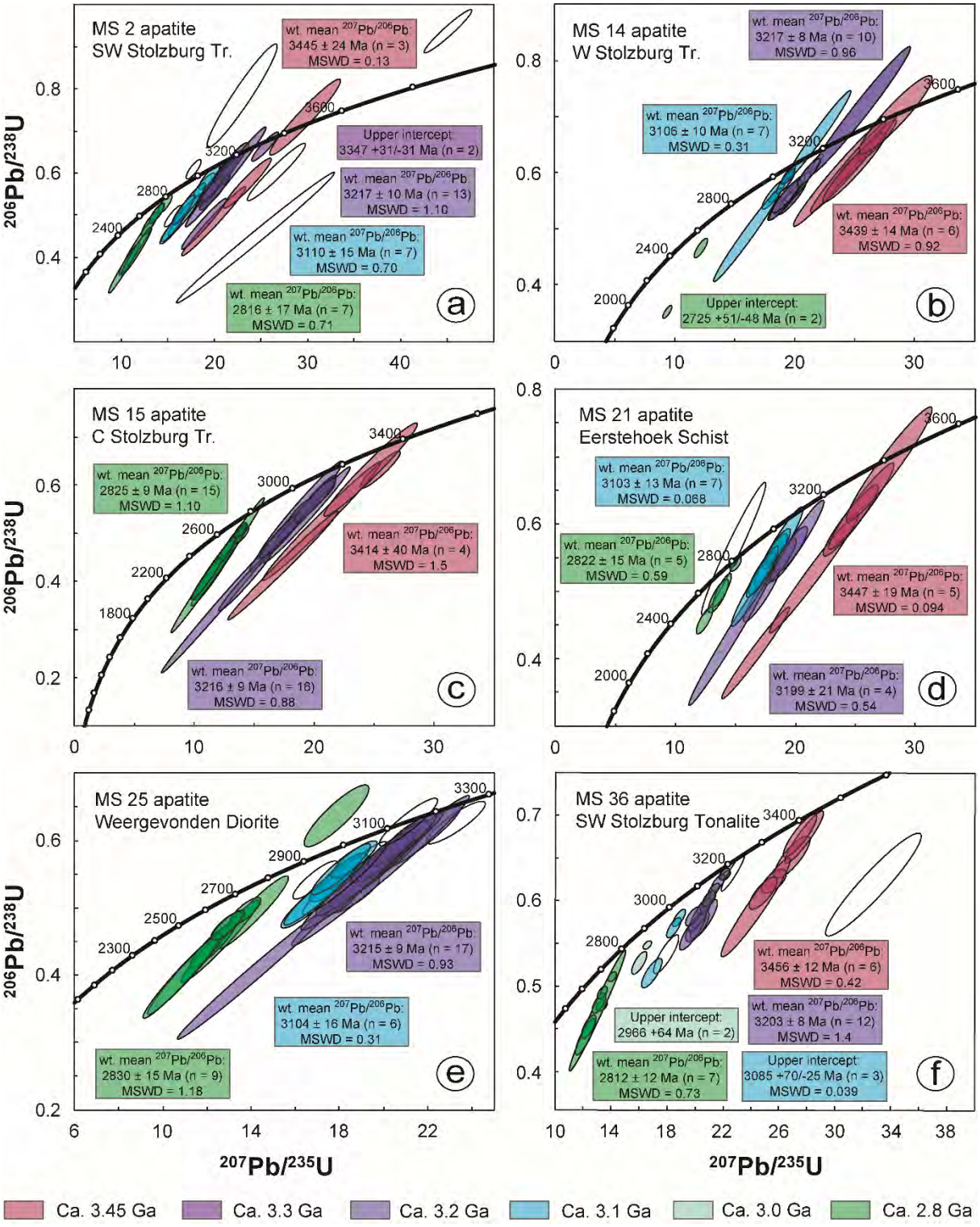

Fig. 4.10. U-Pb Concordia diagrams for apatite grains from granitoid (a-c, e, f) and mafic schist (d) samples from the Stolzburg block. Error ellipses are 2σ. The data used in the plot has been corrected for common Pb. See Table 4.9 for apatite U-Pb isotope data.

Outliers plotting outside of those four age groups are rare. Sample MS 2 contains one concordant and one discordant data-point which give an upper intercept age of 3347 ± 31 Ma (Fig. 4.10a) and sample MS 36 contains two discordant data-points with an upper intercept age of 2966 ± 64 Ma. The geological significance of those dates is questionable, because – other than the four main age groups – they only occur in one sample each and cannot be easily correlated with known regional metamorphic or igneous events. In addition, the recorded ages could be interpreted to represent mixtures of the previously described age populations. Other outliers are reversely discordant or have apparent $^{207}Pb/^{206}Pb$ ages older than the crystallization age of these samples and will be ignored.

The majority of the data points are discordant to varying degrees. For each age cluster, the lower intercept is around zero. As a consequence, this discordant array is interpreted to reflect recent lead loss due to surface alteration. The high uncertainties for some of the $^{206}Pb/^{238}U$ dates are caused by short integration periods (due to small grain size, inclusions or cracks) and some but not all analyses show a correlation of uncertainties with U content.

4.5 Discussion

4.5.1 Interpretation of the emplacement age of trondhjemite plutons and felsic dykes

Main Trondhjemite of the Stolzburg Pluton

The spread in concordant dates from ca. 3460 to ca. 3400 found in all analyzed Main Trondhjemite samples from the Stolzburg Pluton and the occurrence of several phases within the pluton (Fig. 4.3) may be interpreted in different ways. Taken at face value, our U-Pb zircon dates seem to suggest a protracted emplacement through successive magma batches over tens of millions of years, with sample ST-J 26 from the northern margin having its main population at 3451 ± 8 Ma while the samples from the center, western and south-western margin have their main populations of concordant dates at ca. 3435 to 3440 Ma. The northern part of the Stolzburg Pluton would have been emplaced some ten to twenty million years earlier than the main plutonic body. This is indeed a possibility, as evidenced by the protracted construction of the Badplaas Complex (Fig. 4.1) between 3290 and 3230 Ma (Kisters et al., 2010). The Badplaas Complex however contains clear field evidence for the intrusion of older phases by younger magma additions (Kisters et al., 2010). In contrast, magmatic contacts within the Stolzburg Pluton are rare.

Ancient lead loss offers an alternative explanation for the apparent range of crystallization ages as it can obscure the “real” emplacement age by shifting the dates along a Discordia line that is indistinguishable from the Concordia. The Hf isotope systematics illustrated in Figure 8 can be interpreted to indicate a disturbance of the U-Pb system in the seemingly younger zircon

domains. In combination with the field evidence, this is interpreted to reflect ancient lead loss from Stolzburg Pluton zircon grains.

The published U-Pb zircon ages for the Stolzburg Block are on average older than and not overlapping in their uncertainties with the results of this study, except for sample ST-J 26. For the Main Trondhjemite of the Stolzburg Pluton, Kamo and Davis (1994) report an emplacement age of 3460 +5/-4 Ma based on three discordant data-points. Similar, yet slightly younger dates of 3455.9 ± 0.5 and 3455.5 ± 0.6 Ma are given by Schoene et al. (2008) for samples of the Main Trondhjemite from the north-eastern and southern margin of the Stolzburg Pluton, respectively. From the supplementary data of Laurent et al. (2020), we calculated weighted mean 207Pb/206Pb dates of 3453.2 ± 7.3 (MSWD = 0.72; n = 23) Ma for a tonalite sample and 3449.4 ± 3.1 (MSWD = 0.67; n = 41) Ma for a trondhjemite sample from the southern margin of the Stolzburg Pluton. From the eastern margin, Wang et al. (2019) report a date of 3440 ± 8 Ma for a Main Trondhjemite sample and a 3225.6 ± 3.9 Ma date for a granodiorite dyke which, in Fig. S1a of Wang et al. (2019), appears to be approximately 2m thick and clearly crosscutting to the Main Trondhjemite.

The dates reported by Schoene et al. (2008) and Laurent et al. (2020) for samples from the eastern and southern margin are within error identical with our date for sample ST-J 26 and with the oldest dates obtained for all Main Trondhjemite samples from the Stolzburg Pluton (Table 4.7). The agreement of dates from the northern and southern margin and the apparent lead loss as indicated by the Hf-in-zircon systematics suggest that ca. 3455 Ma. Can be considered reasonably representative of the emplacement age of the Stolzburg Pluton. The ca. 3225 Ma date of Wang et al. (2019) for a granodiorite from the eastern margin of the Stolzburg Pluton is similar to the emplacement age of the marginal dykes documented in this study.

Main Trondhjemite of the Theespruit Pluton

The main populations of dates from samples MS 17 and MS 18 from the Main Trondhjemite of the Theespruit Pluton give dates of 3411 ± 6 and 3417 ± 6 Ma, respectively. We regard those dates as affected by ancient lead loss, based on that both samples contain older dates that are statistically different to the main populations at 3444 ± 12 Ma (MS 17; n = 2) and 3438 ± 19 Ma (MS 18; n = 1) and on the lead loss array visible in the Hf data (Fig. 4.8).

The oldest and most precise magmatic dates for the Theespruit Pluton are 3456.33 ± 0.14 and 3456.57 ± 0.11 Ma based on, respectively, seven and five concordant to discordant U-Pb TIMS zircon analyses on samples from the center of the Theespruit Pluton (Laurent et al., 2020), similar to a 3451 ± 7 Ma U-Pb zircon date reported by Zeh et al. (2009) for a sample from the

southern margin. Our dates for the Theespruit are within error identical with those dates, though on average ca. 10 Ma younger. Armstrong et al. (1990), Kamo and Davis, (1994) and Lana et al. (2010) report younger dates at 3437 ± 6, 3434 +4/-3 and 3431.9 ± 9.8 Ma, respectively, for the eastern (Kamo and Davis, 1994) and the southern (Armstrong et al., 1990; Lana et al., 2010a) margin of the Theespruit Pluton. Lana et al. (2010) also found a date of 3234 ± 12 Ma in the same sample, which they interpreted as age of intrusion of the southern Theespruit Pluton, but the low Th/U ratio for those grains suggest that those dates could reflect metamorphic rather than igneous growth.

Those ca. 3435 Ma dates (Armstrong et al., 1990; Kamo and Davis, 1994; Lana et al., 2010a) are within error identical with our dates, but not with those of Laurent et al. (2020) and (Zeh et al., 2009), and are likely the result of the lead loss that is apparent in our samples. The emplacement of the Theespruit Pluton likely happened at as early as ca. 3455 Ma, simultaneous with the Stolzburg Pluton, and no later than ca. 3445 Ma.

Dykes cutting the Stolzburg and Theespruit plutons

Age data for the marginal dykes are scarcer compared to the Main Trondhjemite due to their low zircon yield, but all analyzed samples contain oscillatory zoned zircon grains that yield similar dates. Sample MS 1, cross-cutting the Main Trondhjemite of the Stolzburg Pluton on the southern-western margin close to samples MS 2, yields date of 3204 ± 12 Ma (MSWD = 0.25; n = 2), which we interpret as the emplacement age for this sample, and an older date of 3427 ± 12 Ma (MSWD = 4.33; n = 2) regarded as inherited or assimilated from the Main Trondhjemite. The emplacement age of 3204 ± 12 Ma overlaps within error with a dyke sample from the southern margin of the Stolzburg Pluton, dated at 3212.5 ± 0.8 (Schoene et al., 2008).

For the Theespruit Pluton, samples MS 19 and MS 20, cutting the Main Trondhjemite of the Theespruit Pluton and mafic rocks of the lower Onverwacht formation on the western margin, yield dates of 3211 ± 13 (n = 2) and 3215 ± 15 Ma (n = 2), respectively, and a combined date of 3213 ± 10 Ma (n = 4) for analyses of oscillatory zoned zircon, which we interpret as the emplacement age for these samples. Older dates of 3385 ± 9 Ma are based on their microtexture (Fig. 4.6i, j) regarded as inheritance or xenocrysts taken in from the Main Trondhjemite; they are within error identical with dates of 3387 ± 36 (n = 1) and 3382 ± 11 Ma (n = 10) published for two samples taken from the same outcrop as MS 19 and MS 20 (Moyen et al., 2019). Comparison of samples is difficult as no CL images are available for the samples of Moyen et al. (2019), but we assume those ca. 3385 Ma grain to represent the same inheritance/xenocrysts that are present in samples MS 19 and MS 20.

Contact zone between the Honingklip Pluton and the Tjakastad schist belt

For the contact of the Honingklip Pluton and the Tjakastad schist belt, Main Trondhjemite sample MS 4 yields a date of 3440 ± 6 Ma (n = 9) for pristine, oscillatory zoned grains with Th/U ratios of 0.4 to 0.7. Younger dates from this sample occur in zircon grains, that mostly show in their microtexture signs of recrystallization similar to those described by Pidgeon (1992), and are not considered to reflect a magmatic event; they are characterized by Th/U ratios of 0.1 to 0.3 and yield a date of 3219 ± 6 Ma (n = 8). One single analysis of 3219 ± 19 Ma seems to show seemingly pristine igneous zoning (Table 4.7, analysis #51, see also Fig. 4.14), but its Th/U ratio of 0.12 is in line with the other, more clearly recrystallized grains than with the older, primary igneous grains. Cross-cutting dyke sample MS 3 yields a date of 3207 ± 7 (n = 6) for igneous grains, interpreted as emplacement age for this dyke. Younger analyses at 3165 ± 10 Ma (n = 3) are related to recrystallized zones and show low Th/U ratios of 0.02 to 0.06 indicative of metamorphic growth.

Based on our findings, we interpret the ca. 3440 Ma date as the minimum age of emplacement and the ca. 3220 Ma dates in sample MS 4 as the maximum age of metamorphism/hydrothermal recrystallization. This is in contrast to the findings of Wang et al. (2019), who report a U-Pb date of 3224.6 ± 8.3 for zircon with higher Th/U ratios for a sample from the northern margin of the Honingklip Pluton.

The Weergevonden Pluton

Samples MS 26 and MS 27, taken from the northern (MS 26) and southern (MS 27) margin of the Weergevonden Pluton, yield dates of ca. 3435 Ma for their main populations (Table 4.2; Fig. 4.6 j, k). These dates are ca. 20 Ma younger than the 3453.9 ± 8.0 Ma date reported by Wang et al. (2019) and ca. 10 Ma younger, but within error identical, with a 3445.5 ± 9 Ma (MSWD = 0.27; n = 14) calculated by us using the data of Laurent et al. (2020) for samples from the same outcrop as MS 26. The ca. 3454 Ma date of Wang et al. (2019) is within error identical with the oldest data-points obtained for MS 26 (Table 4.7, analyses #26 and #67) and likely reflects the emplacement age for the Main Trondhjemite of the Weergevonden Pluton, while the younger dates are interpreted to be the result of the ancient lead loss which can also be observed in the Stolzburg and Theespruit plutons. For diorite sample MS 25, cross-cutting the Weergevonden Pluton on the northern margin close to sample MS 26, an emplacement age of 3221 ± 2 Ma was determined for diorite sample MS 25, confirming the 3224.6 ± 4.3 Ma date of Wang et al. (2019).

The findings of this study confirm previously published emplacement ages for the Stolzburg, Theespruit and Weergevonden plutons of the Stolzburg Block. The ca. 3455 Ma dates for the Stolzburg (Schoene et al., 2008), Theespruit (Laurent et al., 2020; Zeh et al., 2009) and Weergevonden (Wang et al., 2019) plutons seem to reflect the “true” emplacement age, while younger dates (Kamo and Davis, 1994; Lana et al., 2010a) are influenced by ancient lead loss. Timing of this lead loss remains enigmatic, but dates obtained for altered/recrystallized grains suggest a lower limit at ca. 3170 Ma. Within the Main Trondhjemite of the Stolzburg Block, dates of ca. 3.2 Ga are confined to hydrothermally altered/recrystallized zircon grains. Later cross-cutting granitoids were emplaced in at least two successive events, starting with the Weergevonden diorite (MS 25) at ca. 3221 Ma. It was followed by injection of felsic dykes on the plutons’ margins at ca. 3215 Ma and potentially as late as ca. 3205 Ma. An age of 3215 to 3205 Ma for the leucocratic dykes implies, that they post-date the Moodies Group and thereby the main accretionary event in the belt.

4.5.2 Comparison of different granitoid phases

For the most part, the plutons of the Stolzburg Block are made up of the homogenous, coarse-grained Main Trondhjemite, but other phases also occur. The most prominent are the leucocratic dykes, cross-cutting the Main Trondhjemite and greenstones at the margins of the plutons. Furthermore, a granodiorite dyke occurs on the eastern margin of the Stolzburg Pluton, dated to ca. 3226 Ma (Wang et al., 2019). On the south-western margin of the Stolzburg Pluton, a ca. 10 cm wide band of a more mafic phase can be found (sample MS 36); no U-Pb zircon dates are were obtained for this sample, but the U-Pb apatite chronology shows dates of ca. 3.45 Ga, indicating that is contemporaneous with the Main Trondhjemite. In the Weergevonden Pluton, a diorite phase is exposed in a road cut, dated to ca. 3221 Ma (Wang et al., 2019; this study). The occurrence of ca. 3.2 Ga phases in the ca. 3.45 Ga plutons has been used as an argument for a ca. 3.2 Ga anatexis of the plutons, with the younger phases constituting the product of recycling of the older ones (Van Kranendonk et al., 2015). It is however very unlikely that partial melting of a trondhjemite would yield a dioritic melt.

The different granitoid phases of the Stolzburg Block are very similar with regard to their major-element composition, plotting in the trondhjemite and tonalite fields of the O’Connor (1965) normative diagram (Fig. 4.5a). While their trace-element patterns show no differences between the different granitoid phases (not shown), a slight but systematic distinction is visible in the Yb vs. La/Yb and Sr/Y vs. Y diagrams (Fig. 4.4b+c; see section 4.4.1). A clearer difference between the ca. 3.45 Ga Main Trondhjemite and the ca. 3.2 dykes can be seen in the Hf-in-zircon systematics (section 4.4.3). The leucocratic dykes yield chondritic values (εHf = ca. +1 to -2) at ca. 3.2 Ga, while their host TTGs also show chondritic values (εHf = ca. +2 to -1), but

at ca. 3.45 Ga (Fig. 4.8b). Similarly, diorite sample MS 25 from the Weergevonden Pluton yields an $\varepsilon Hf_{3.22\ Ga}$ value of -1.5. The projected εHf values for the Main Trondhjemite at ca. 3.2 Ga are in the range of -4 to -5 ± 1 (2σ) and are thereby distinct from those of the younger phases. The model ages for the leucocratic dykes are some 100 Ma younger than those of the Main Trondhjemite (Table 2).

The Hf-in-zircon systematics show, that the dykes are less evolved compared to the Main Trondhjemite and could not have been derived exclusively from partial melting of the Main Trondhjemite (or its equivalent). Instead, they represent the injection of more juvenile magma; a mixing of juvenile melt with melt derived from partial melting of the Main Trondhjemite is theoretically possible, but no field evidence exists to assume such partial melting. The protolith from which the leucocratic dykes were derived was likely similar to that which produced the magmas to form the TTG plutons, as indicated by their fairly similar trace-element characteristics. Diorite samples MS 25 is more distinct from the Main Trondhjemite compared to the dykes in terms of chemical composition, but similar with regards to Hf-in-zircon systematics. With sample MS 25 being some 10 to 20 Ma older than the felsic dykes, it could represent an early product of the same magmatic system that produced the dykes.

4.5.3 Interpretation of apatite ages

Apatite is known to crystalize as a magmatic mineral (Webster and Piccoli, 2015); as a and metamorphic mineral where it crystallizes as a result of subsolidus reactions (Spear and Pyle, 2002); as well as hydrothermally where it crystalizes in rocks undergoing fluid-driven alteration and diagenesis (Chen et al., 2019; Dill, 1994; Lev et al., 1998; Liu et al., 2017; Miller et al., 1989). In this study, apatite crystals of these different origins are respectively referred to as igneous, metamorphic and hydrothermal apatite. U-Pb dates in apatite commonly reflect cooling below the closure temperature (Tc) after crystallization from a magma or as part of a metamorphic assemblage. However, apatite U-Pb dates can reflect apatite crystallization ages for a metamorphic event, or hydrothermal growth at temperatures below Tc. The estimates for Tc are typically in the range of 400 to 500 °C, depending on grain size and cooling rate/duration of the heating event (Chamberlain and Bowring, 2000; Cherniak et al., 1991). The effective diffusive grain radius is ca. 50 µm and in larger grains the diffusion volume is limited by diffusional short circuits such as cleavage planes or fractures (Cherniak et al., 1991). Grains smaller than 50 µm consequently have a lower Tc of ca. 450 °C at fast cooling rates of 100 °C/m.yr. and down to ca. 400 °C for slow cooling rates of 2 °C/m.yr. (Chamberlain and Bowring, 2000; Cherniak et al., 1991). Only in very short-lived (ca. 50 k.yr.) heating events, can the U-Pb systematics in apatite can withstand temperatures of up to 690 °C (Cherniak et al., 1991).

General mineral stability considerations also aid in the interpretation of apatite ages in this study. The preservation of igneous textured biotite and plagioclase within the Main Trondhjemite (e.g. Laurent et al., 2020) argue against significant fluid-rock interaction following ca 3.45 Ga, except perhaps for very localized fluid flow along grain boundaries. The southern portion of the BGGT contains exhumation related ca. 3230 Ma shear fabrics within the greenstone belt metamafic and metapelitic rocks associated with the Stolzburg and Theespruit plutons, and within these rocks fluid ingress along the shear fabrics has facilitated retrogression to greenschist facies assemblages, including the replacement of biotite porphyroblasts by muscovite and chlorite (e.g. Kisters et al., 2003; Diener et al., 2005). The existence of 3230 Ma retrograde greenschist facies assemblages appears to rule out subsequent heating of the BGGT beyond ~ 400 °C.

The apatite grains analyzed in this study typically have a grain size of 100 to 300 µm, with individual internal zones of ca. 30 to 50 µm (Fig. 4.9), resulting in Tc estimates of ca. 450 to 530 °C for these grains (Cherniak et al., 1991). The internal structure confirms multiple apatite growth and/or recrystallization events, whilst the U-Pb apatite geochronology shows multiple groups of dates that broadly correspond to the apatite zonation, with older dates occurring in the inner zones and younger dates mostly in the outer zones. However, not all younger dates are confined to the outer zones (e.g. Fig. 4.9a #77+78). We interpret these cases of younger core ages to be the result of selective recrystallization, which has been described for cores of apatite grains (Kirkland et al., 2018).

Based on the microtextures which generally allow the cores to be identified as older areas and zones mantling these to be demonstrated as younger, we interpret the different age groups of apatite dates as a result of four distinct apatite growth events, happening at ca. 3445, 3210, 3105 and 2820 Ma. We rule out different degrees of partial resetting of the U-Pb system in apatite caused by a single ca. 2820 Ma event as the cause for the different groups, as the age clusters are within error identical throughout the Stolzburg Block and are distinct from one another. In addition, outliers between the four age groups are very rare. The oldest apatite dates are within error identical with the emplacement ages determined for the granitoid plutons of the Stolzburg Block (c.f. section 4.5.2) and reflect magmatic apatite in the granitoid samples and metamorphic growth due to the intrusion of TTG magmas in Tjakastad schist belt sample MS 21. The dates younger than ca. 3.45 Ga are likely the result of dissolution/precipitation around older grains or forming of new grains.

Dates corresponding to the youngest group of apatite dates at ca. 2.8 Ga are uncommon in the eastern Kaapvaal Craton. For a ca. 3640 Ma tonalitic gneiss sample from the Ancient Gneiss Complex (AGC) of Swaziland, ca. 50 km to the east of the Stolzburg Block, Compston

and Kröner (1988) reported a U-Pb zircon regression age of 2867 ± 13 Ma, based on one concordant and six discordant analyses. They interpreted this to be the result of veining and/or hydrothermal activity (Compston and Kröner, 1988) of this age. Apart from this very tenuous link with a largely undefined process, this ca. 2.8 Ga event remains enigmatic, as no other similar dates were reported for the BGGT and the AGC, though so far very few thermochronological studies have been published. Considering options further afield, magmatic zircons of ca. 2.8 Ga were reported for a quartzofeldspathic gneiss from the Northern Marginal Zone of the Limpopo Belt (Tsunogae and Yurimoto, 1995) as well as in granitoids from the Southern Marginal Zone (Laurent et al. 2019), indicating that this event could be of regional significance for the Kaapvaal Craton. This group of ages is interpreted to reflect apatite recrystallization due to minor fluid ingress, possibly associated with sub 400 °C heating.

The next oldest group at ca. 3.1 Ga is contemporaneous with the emplacement of the large granitic Mpuluzi and Heerenveen batholiths to the east and south of the Stolzburg Block and with the intrusion of the Boesmanskop syenite into the Stolzburg Block (Kamo and Davis, 1994). Apatite recrystallization at this time could have been caused by mobilization of fluids within the Stolzburg Block through heating by the plutonism or by external fluids coming in from the crystallizing batholiths. As with the ca 2.8 Ga group, the preservation of igneous minerals that are vulnerable to reaction with hydrothermal fluids, as well as the preservation of low grade but older retrograde metamorphic assemblages in associated greenstones, rules out heating to > 400 °C or substantial fluid ingress. The formation of minor chlorite and sericite in the Main Trondhjemite possibly reflects these fluid ingress events.

4.5.4 Metamorphic history of the Stolzburg Block and the ca. 3.2 Ga event(s)

At ca. 3.2 Ga, the proto-Kaapvaal Craton was affected by major events. The regional deformation event D2 at ca. 3230 to 3225 Ma (De Ronde and De Wit, 1994; Kisters et al., 2003) saw cessation of deposition of terrigenous clastic sediments of the Fig Tree Group and amalgamation of the NW and SE terranes of the BGB along the Inyoka-Saddleback Fault zone (De Ronde and Kamo, 2000). It is contemporaneous with most reported ages of peak metamorphism of the lower Onverwacht Group (Cutts et al., 2014; Diener et al., 2005; Dziggel et al., 2002; Stevens et al., 2002), though potentially younger Sm-Nd garnet dates of, respectively, 3201.6 ± 5.2 and 3200.7 ± 5.3 Ma were reported for a garnet-amphibolite sample from the Inyoni sheer zone (Maneiro et al., 2018). D2 was followed by orogenic uplift, characterized by the sedimentation of the Moodies Group in extensional tectonic basins at ca. 3225 to 3215 Ma (Byerly et al., 2019).

In the apatite chronology, the most prominent age group is at ca. 3210 Ma, occurring in all analyzed samples from the Stolzburg Block. The significance of the ca. 3.2 Ga events can also be seen in the zircon record. The zircon geochronology and microtexture indicate at least one, if not several events where zircon was recrystallized and/or overgrown with featureless material. The metamorphic rims that are present around zircon grains from the Main Trondhjemite of the Stolzburg Block are too small to be analyzed by LA ICP-MS, but some grains show replacement of igneous zoning by featureless material protruding into the grain from the metamorphic rim. Multiple metamorphic rims can be seen around zircon grains from the plutons' margins (samples MS 2, 14 , 27; Fig. 4.5) but seem to be absent in samples MS 15 from the core of the Stolzburg Pluton (Fig. 4.6f), indicating that the second zircon overgrowth event is related to deformation of the marginal rocks. The upper age limit is given by sample MS 25, where 3221 Ma zircon grains show the same metamorphic rim as in the Main Trondhjemite samples (Fig. 4.5k). A ca. 3219 Ma date for recrystallized zircon grains in sample MS 4 (Fig. 4.7f) suggests that the first metamorphic overprint likely happened shortly after emplacement of sample MS 25. Further zircon growth events could have happened at ca. 3200 Ma, as indicated by a ca. 3202 Ma date for recrystallized grains in samples MS 15, and as late as ca. 3170 Ma, as the youngest concordant spot in sample MS 4 suggests. The ca. 3220 to 3200 Ma zircon relates to peak metamorphism of the Stolzburg Block and the emplacement of leucocratic dykes on the plutons' margins. The ca. 3170 zircon could be related to the onset of Pigg's Peak/Mpuluzi plutonism, as also suggested by the age spread obtained by Murphy (2015) in the Mpuluzi batholith: between 3167 and 3104 Ma.

The conservation of the ca. 3.45 Ga dates in the apatite grains in all five samples shows that the granitoid plutons of the Stolzburg Block have not been heated above the closure temperature of the U-Pb system in apatite after emplacement. As outlined in section 4.5.3, the closure temperature is dependent on cooling rate and grain size, and for the grain size of the apatite grains in this study (Fig. 4.9) it ranges between 450 and 690 °C (Chamberlain and Bowring, 2000; Cherniak et al., 1991). The peak temperature estimates for the supracrustal rocks of the Lower Onverwacht Formation at ca. 3.2 Ga (Cutts et al., 2014; Diener et al., 2005; Dziggel et al., 2002; Maneiro et al., 2018) are in the range of 520 to 600 °C for the Tjakastad schist belt (Cutts et al., 2014; Diener et al., 2005) and 600 to 650 °C for the Inyoni shear zone (Kato et al., 2018; Moyen et al., 2006) (Fig. 4.11a). This leads to several different interpretations of the apatite thermochronology with regards to the ca. 3.2 Ga event:

1. The granitoid plutons experienced a "normal" cooling rate of ca. 10 to 30 °C/Ma in the early stage of cooling (Bethune et al., 1999), leading to a Tc of 450 to 550 °C (Chamberlain and Bowring, 2000). In that case, there is a temperature difference of 50 to 200 °C between granitoids and greenstones, which are spatially related and have an intrusive contact (Kisters

and Anhaeusser, 1995) dated to ca. 3.45 Ga (c.f. section 4.5.1). A possible explanation for the difference in temperature is shear heating of the greenstone, which has been reported to cause temperatures 200 °C higher than spatially related rocks outside of the shear zone (Camacho et al., 2001). However, shear heating is commonly highly localized along faults; it is unlikely that localized movement produced the near-vertical foliation in the greenstone rocks, as the margins of the plutons are also deformed, and that localized heating contributed significantly to the metamorphism of the immediately surrounding greenstones.

2. The magmas of the marginal leucocratic dykes are the heat source producing elevated temperatures in the greenstone rocks through advective heating. These dykes are more abundant in the Inyoni shear zone, where temperature estimates are ca. 600 to 650 °C (Dziggel et al., 2002; Kato et al., 2018; Moyen et al., 2006), compared to the Tjakastad schist belt, which records lower temperatures of ca. 520 to 600 °C (Cutts et al., 2014; Diener et al., 2005). The lower end of the temperature estimates for the Tjakastad schist belt of 520 °C (Diener et al., 2005) are lower than the Tc of the U-Pb system in apatite and could represent the actual temperatures of the regional metamorphic event, while the elevated temperatures of 600 to 650 °C reflect local maxima induced by the intruding felsic dykes. In the granitoid plutons, the dykes are confined to the margins and thereby the plutons were not sufficiently heated by the intruding dykes to reach temperatures above Tc, preserving the pre-3.2 Ga apatite dates.

3. The Stolzburg block as a whole experienced the same temperatures of 600 to 650 °C at ca. 3.2 Ga. This would require a very short-lived thermal event of <1 m.yr. (Cherniak et al., 1991) to not erase the ca. 3445 Ma apatite dates. Such a short-lived thermal peak can be achieved through a “hairpin” P-T trajectory, which is commonly associated with rapid burial and exhumation of buoyant material (Compagnoni et al., 1995; Ernst, 1988). The mineral assemblage in the greenstone rocks, with peak metamorphic minerals such as kyanite and staurolite defining exhumation fabrics (Diener et al., 2005), is consistent with immediate exhumation while still forming the peak assemblage. Figure 4.11b shows a proposed schematic rapid heating and cooling path, which allows for peak temperatures of ca. 600 °C in for the rocks of the Stolzburg Block ca. 3.23 Ga while still preserving >3.23 Ga apatite dates.

In either case, the granitoid plutons of the Stolzburg block could not have experienced higher temperatures than the greenstones. Following emplacement at ca. 3.45 Ga, the temperatures in the Stolzburg Block did likely not exceed ca. 600 °C. The apparent discrepancy between the temperature estimates for the greenstone rocks and the results of the apatite thermochronology can be explained by rapid burial and exhumation along a “hairpin” P-T trajectory or by advective heating of the greenstone rocks via the intruding marginal dykes (or a combination of the two). We propose the following timeline for the ca. 3.2 Ga event: (1)

collision and amalgamation of NW and SE terranes of the BGB at ca. 3230 to 3225 Ma, accompanied by TTG plutonism of the Nelshoogte and Kaap Valley plutons and the Badplaas domain; (2) rapid burial of the Stolzburg Block at ca. 3225 to 3220 Ma, accompanied by intrusion of dioritic to granodioritic magmas and immediately followed by while still forming the peak mineral assemblage; (3) injection of felsic dykes in the granitoid plutons and greenstone septa of the Stolzburg Block during the later stages of exhumation and development of regional fabrics at ca. 3215 to 3205 Ma. The magma of the dykes could have served as a lubricant during exhumation, limiting deformation of the plutons.

Fig. 4.11. An illustration of the constraints placed on the pressure-temperature-time evolution of the Stolzburg Pluton and related rocks, by the apatite thermochronology information from this study. (a) P-T diagram showing published P-T paths for Lower Onverwacht Group rocks within the Stolzburg Block ([1]Kato et al., 2018; [2]Moyen et al., 2006; [3]Diener et al., 2003). In the case of the Moyen et al. (2006) study, the path illustrated here utilizes the lower temperature portion of the uncertainty ellipse on their peak metamorphic constraint, as this is most consistent with the findings of this study. The grey arrows the proposed paths for greenstone keels (x) and granitoid domes (y) of the PCO model (Van Kranendonk et al., 2015), with the path for the domes corrected for the fact that it must start in the field of partial melting. Stippled vertical lines represent closure temperatures (T_C) of the U-Pb system in apatite for different cooling rates and the shaded area the maximum Tc range for preserving U-Pb apatite compositions during short-lived thermal events (Chamberlain and Bowring, 2000; Cherniak et al., 1991; Nemchin and Pidgeon, 1999). Granite wet solidus after Hermann (2003).
(b) Temperature-time graph showing the known thermal evolution of the Stolzburg Block in black arrows, as constrained by metamorphic data and the apatite thermochronology from this study (blue line). The ca. 3.23 Ga metamorphic event produced peak temperatures of 600 to 650 °C. The retention of older U-Pb ages in apatite grains during this event indicates rapid heating and cooling, as it is achieved during tectonic burial and exhumation of rock units to produce characteristic hair-pin loops (Compagnoni et al., 1995; Ernst, 1988). This is consistent with peak metamorphic minerals such as kyanite and staurolite defining exhumation fabrics (Diener et al., 2005). Crustal evolution via partial convective overturn at ca. 3.23 Ga (green line) is inconsistent with the preservation of older apatite U-Pb ages in the Stolzburg Block, as heating of the felsic crust below the greenstone belt by radiogenic decay produces a long-lived heating event that would have resulted in complete resetting of all apatite U-Pb ages.
Apatite U-Pb ages at ca. 3.1 and 2.8 Ga are less well constrained in terms of duration and magnitude of heating, but cannot exceed ~400 °C due to the preservation of low-grade greenschist facies retrograde assemblages during the ca. 3.23 Ga event. Metamorphic assemblages relating to these younger apatite ages have not been identified.

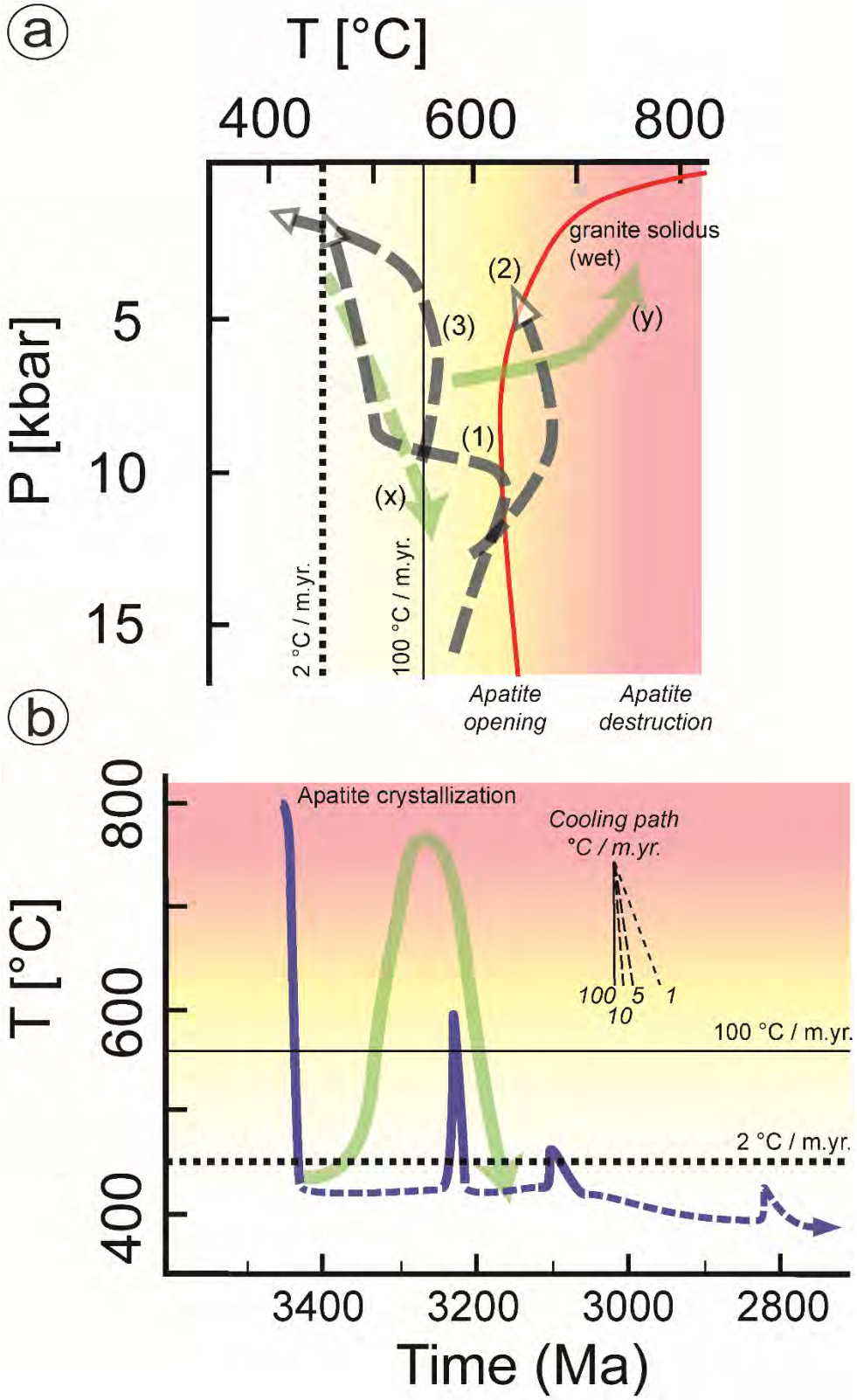

4.5.5 Tectonic implications

A critical aspect of every tectonic model is the thermal state of the crust, as it controls the crustal rheology and thereby the possible modes of deformation and accretion. A key finding of our study is that primary magmatic apatite ages of ca. 3.45 Ga are conserved in the Stolzburg Block. This implies that the Stolzburg Block crust did never exceed 600 °C after ca. 3.45 Ga. In particular, this rules out an excursion towards high (anatectic) temperatures. Such a thermal evolution has been postulated in recent models, which suggest sufficiently elevated crustal temperatures and episodes of extensive partial melting that would significantly lower rheologies and thereby drive a buoyancy-driven partial convective overturn (PCO) of the crust (e.g. Mareschal and West, 1980; Smithies et al., 2007; Van Kranendonk et al., 2015; West and Mareschal, 1979). These models have been suggested for, e.g. the East Pilbara Terrane of the Pilbara Craton, Australia, or the Dharwar Craton in India, to explain the characteristic dome-and-keel geometry of many Archean provinces worldwide (e.g. Chardon et al., 2002, 1998; Collins et al., 1998; François et al., 2014; Thébaud and Rey, 2013; Van Kranendonk et al., 2015).

In the PCO model, a thick volcanic plateau is constructed on top of TTG plutons, burying the granitoids to temperatures are high enough to induce partial melting to such an extent that they could behave as a buoyancy-driven anatectic mush that was juxtaposed against the overlying greenstone rocks to cause the infolding and sinking of denser greenstone keels (Van Kranendonk et al., 2015). The model proposes different PT conditions for greenstone keels and granitoid domes; the sinking greenstones are characterized by a low T, high P trajectory, while the anatectic domes show high T at medium P (Fig. 4.11). For the Stolzburg Block, the time of this PCO event is postulated to be ca. 3.2 Ga, with the ca. 3.2 Ga igneous phases being the product of partial melting of ca. 3.45 Ga granitoids (Van Kranendonk et al., 2015, 2014; Wang et al., 2019).

Figure 4.11a depicts the PT trajectories required by the PCO model along with the published amphibolite facies PT estimates for metamafic rocks of the Stolzburg Block (e.g. Moyen et al., 2006). Figure 4.11b illustrates the likely temperature-time evolution of the Stolzburg pluton, as constrained by apatite U-Pb thermochronology and compares this with the temperature-time history required by PCO. It is clear that the temperatures required to initiate anatectic domes at ca. 3.23 Ma far exceed those that are compatible with the apatite U-Pb systematics of the plutons. Also, the time required for radiogenic heating to facilitate a PCO is in excess of 150 Ma, which would have erased all older apatite ages (Fig. 4.11b). Furthermore, the granitoid plutons with their mostly pristine igneous textures show no signs of post-emplacement reworking and intrusive contacts between TTG plutons and greenstone are clearly older and related to the emplacement of the Main Trondhjemite at ca. 3.45 Ga. The only ca. 3.2 Ga

igneous phases in the Stolzburg Block are shown to be more juvenile compared to the Main Trondhjemite and this rules out the possibility that the dykes are produced solely by melting of the older TTGs; it is theoretically possible that the dykes are a mixture of partial melts of the Main Trondhjemite and more juvenile melts, but there is no field evidence to support this interpretation. Despite their apparently similar map pattern, a key difference between Barberton and Pilbara “granitic domes” is that the plutons of the Stolzburg Block are pristine plutons, preserving igneous features and having undergone no heating/melting event post-emplacement. This is in stark contrast with the migmatitic domes of the Pilbara craton, which are composite gneissic/migmatitic units where the older components are gneissose and partially molten, surrounded by a network of veins, dykes and small plutons of in-situ, in-source or nearly in-source younger anatectic melts.

The evolution of the BGGT is thus largely different from the evolution of the coeval Pilbara craton. Whereas the Pilbara crust was hot (above melting temperature) for large portions of its history, the BGGT lower crust remained solid (below 600 °C) for most of its post-accretion history (Fig. 4.12). This difference in thermal evolution between Barberton and Pilbara echoes the opposition between hot and cold orogens, suggest that both types may have existed simultaneously in the Archean Earth. This duality needs to be taken into account in future geodynamic models.

With a hotter Archean mantle, an apparent cool Barberton crust requires either an insulating mechanism or a way to conduct the heat without significantly rising the temperature of the crust. Insulation could possibly have been achieved by forming of a deep subcontinental lithospheric mantle (SCLM) root underneath the proto-Kaapvaal Craton. We hypothesize that the construction of such a SCLM root could have been facilitated through intermitted and repeated, shallow dipping burial of mafic supracrustal rocks and consequent of imbrication of those micro-slabs underneath the Barberton crust.

Fig. 4.12. Inferred thermal state of the crust during the ca. 3.2 Ga deformation, as inferred from this work. Geochronology: same data as Fig. 1 (and this work) for zircons, this work for apatites. Although some ca. 3.2 Ga ages are published in and around the Stolzburg Pluton (Schoene et al., 2008; Wang et al., 2019), they invariably come from narrow, dyke-rich corridors on the Western (ISZ) and South-Eastern edges of the pluton. Ca. 3.2 Ga dykes are chemically distinct as identified in this work (Fig. 4.5); some of them were dated ca. 3.2 Ga. P-T estimates after Moyen et al., 2006 (M06); Kato et al., 2018 (K18); Diener et al., 2005 (D05); Cloete, 1994 (CL94); Cutts et al., 2014 (C14); Dziggel et al., 2002 (Dz02). The thermal state is inferred to be <600 °C in plutonic cores with preserved apatites, few or no ca. 3.2 Ga zircons and, rarely, actual P-t estimates. It is inferred >600 °C when dykes are abundant, apatites are reset and/or actual P-T estimates confirm it. The Inyoni Shear Zone is the best example of one such zone. The BGB proper, north of the Komati Fault, is greenschist facies (<400 °C), with weak quantitative constrains (Cloete, 1994). The Badplaas Complex, west of ISZ, was of course at magmatic state during its emplacement, in several phases from 3.28 to 3.23 Ga.

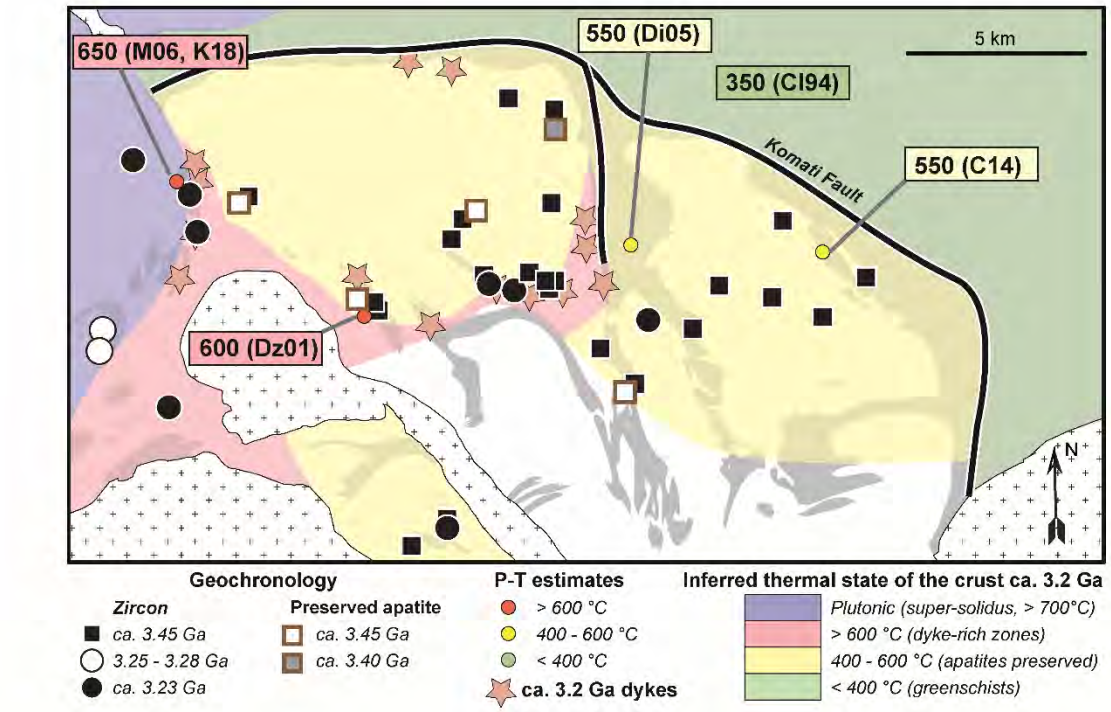

4.6 Conclusions

- The Granitoid plutons of the Stolzburg Block have been emplaced at ca. 3450 Ma.
- Leucocratic dykes crosscut the Stolzburg Block at ca. 3210 Ma.
- Hf-in-zircon data suggests that those dykes are the result of the injection of more juvenile magma, not of in-situ reworking of the 3450 Ma trondhjemites.
- U-Pb apatite dates reveal the polymetamorphic history of the Stolzburg Block with major (hydro-)thermal events at ca. 3210, 3105 and 2820 Ma.
- The preservation of igneous apatite ages indicates that the granitoids of the Stolzburg Block did not reach temperatures higher than ca. 600 °C after emplacement and demonstrates that the rocks did not undergo partial melting to facilitate partial convective overturn of the crust at ca. 3.2 Ga.
- The possible difference in peak temperature between the granitoid plutons and the greenstone remnants of the Inyoni shear zone at ca. 3.2 Ga is explained by the injection of felsic magma into the shear zone at this time.
- The ca. 3.2 Ga event can be split into three phases: accretion at ca. 3230 to 3225 Ma, uplift at ca. 3225 to 3215 Ma and exhumation, aided by the injection of leucocratic magmas, at ca. 3215 to 3205 Ma.

Acknowledgments

This research was supported by NRF funding to GS via the SARChI program. Similarly, support from the CNRS and the NRF under the PROTEA program is gratefully acknowledged by GS and JFM. We would like to thank Mareli Grobbelaar-Moolman and Riana Roussow (CAF Stellenbosch) for providing major- and trace-element analyses, respectively, and Ana Alkmim (UFOP) for assistance during the ICP-MS analysis of apatite and for providing Lu-Hf isotope analyses of zircon. Geochemical plots were created with GCDkit (Janoušek et al., 2006), Concordia diagrams with Isoplot (Ludwig, 2012) and age calculations were done in IsoplotR (Vermeesch, 2018). This is IRP BuCoMO contribution A13 (2021). The authors gratefully acknowledge editorial handling and inputs by Tony Kemp, as well as helpful and constructive reviews by two anonymous reviewers.

Appendix

Table 4.3. U-Pb apatite dates for granitoid and meta-sediment samples from the Stolzburg domain.

Sample	U-Pb date [Ma]	MSWD	n
Stolzburg pluton			
	2816 ± 17	0.7	7
	3110 ± 15	0.7	7
MS 2	3217 ± 10	1.1	13
	3347 +31/-31 ^{UI}	--	2
	3445 ± 24	0.1	3
	2812 ± 12	0.7	7
	2966 ± 64 ^{UI}	--	2
MS 36	3085 +70/-25 ^{UI}	0.1	3
	3203 ± 8	1.4	12
	3456 ± 12	0.4	6
	2725 +51/-48 ^{UI}	--	2
	3106 ± 10	0.3	7
MS 14	3217 ± 9	1.0	10
	3439 ± 14	0.9	6
	2825 ± 9	1.1	15
MS 15	3216 ± 9	0.9	16
	3414 ± 40	1.5	4
Honingklip pluton			
MS 4	2813 ± 9	1.2	14
Onverwacht Group			
	2822 ± 15	0.6	5
MS 21	3103 ± 13	0.1	7
	3199 ± 21	0.5	4
	3447 ± 19	0.1	5
Weergevonden pluton			
	2830 ± 15	1.2	9
MS 25	3104 ± 16	0.3	6
	3215 ± 10	0.9	17

All dates are weighted mean $^{207}Pb/^{206}Pb$ dates, unless stated otherwise, and have been corrected for common Pb. Uncertainties are at 95% confidence level. MSWD = mean square weighted deviation; UI = upper intercept.

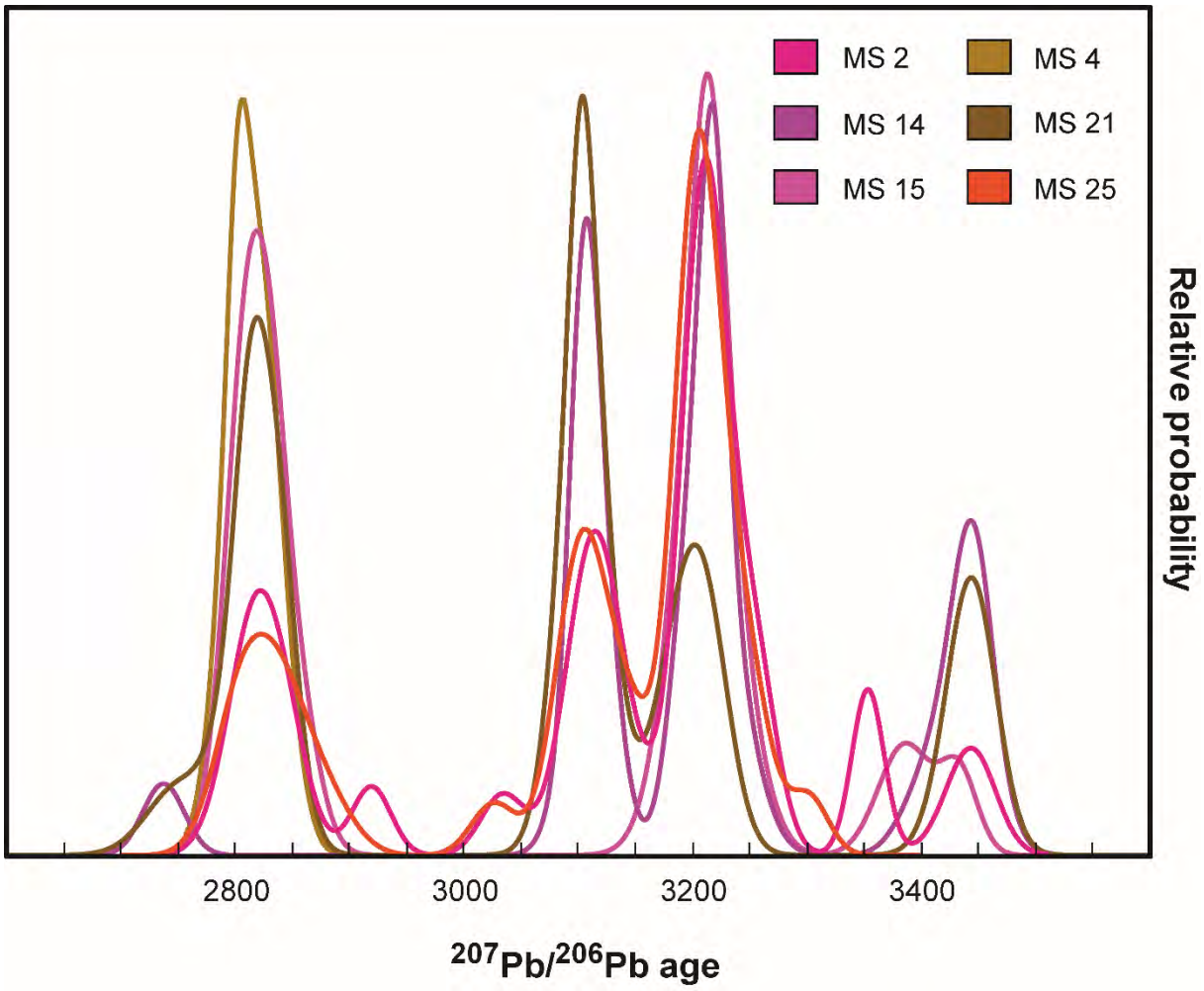

Fig. 4.13. Probability density plot showing the distribution of common Pb corrected $^{207}Pb/^{206}Pb$ apatite ages. The four age groups identified are clear spikes in the graph, with few outliers in between. The ca. 3.2 Ga age component is more pronounced in the samples from the Stolzburg Pluton (MS 2, 14, 15), while the samples from the contact of the Tjakastad schist belt with the granitoids of the Stolzburg Block has a stronger ca. 2.8 Ga component (MS 4, 21). See Table 4.9 for apatite U-Pb isotope data.

References

Amelin, Y., Lee, D.C., Halliday, A.N., 2000. Early-middle Archaean crustal evolution deduced from Lu-Hf and U-Pb isotopic studies of single zircon grains. Geochim. Cosmochim. Acta 64, 4205–4225. https://doi.org/10.1016/S0016-7037(00)00493-2

Anhaeusser, C.R., 1980. A Geological Investigation of the Archean Granite-Greenstone Terrane South of the Boesmanskop Syenite Pluton, Barberton Mountain Land. Trans. Geol. Soc. South Africa 83, 93–106.

Anhaeusser, C.R., Robb, L.J., 1980. Regional and detailed field and geochemical studies of Archean trondhjemitic gneisses, migmatites and greenstone xenoliths in the southern part of the Barberton Mountain Land, South Africa. Precambrian Res. 11, 373–397. https://doi.org/10.1016/0301-9268(80)90073-X

Anhaeusser, C.R., Robb, L.J., Viljoen, M.J., 1981. Provisional geological map of the Barberton Greenstone Belt and surrounding granitic terrane.

Armstrong, R.A., Compston, W., de Wit, M.J., Williams, I.S., 1990. The stratigraphy of the 3.5-3.2 Ga Barberton Greenstone Belt revisited: a single zircon ion microprobe study. Earth Planet. Sci. Lett. 101, 90–106. https://doi.org/10.1016/0012-821X(90)90127-J

Barnes, S.J., Van Kranendonk, M.J., 2014. Archean andesites in the east Yilgarn craton, Australia: Products of plume-crust interaction? Lithosphere 6, 80–92. https://doi.org/10.1130/L356.1

Bédard, J.H., 2006. A catalytic delamination-driven model for coupled genesis of Archaean crust and sub-continental lithospheric mantle. Geochim. Cosmochim. Acta 70, 1188–1214. https://doi.org/10.1016/j.gca.2005.11.008

Bethune, K.M., Villeneuve, M.E., Bleeker, W., 1999. Laser 40Ar/39Ar thermochronology of Archean rocks in Yellowknife Domain, southwestern Slave Province: Insights into the cooling history of an Archean granite-greenstone terrane1. Can. J. Earth Sci. 36, 1189–1206. https://doi.org/10.1139/e99-006

Blichert-Toft, J., Albarède, F., 2008. Hafnium isotopes in Jack Hills zircons and the formation of the Hadean crust. Earth Planet. Sci. Lett. 265, 686–702. https://doi.org/10.1016/j.epsl.2007.10.054

Bouhallier, H., Choukroune, P., Ballèvre, M., 1993. Diapirism, bulk homogeneous shortening and transcurrent shearing in the Archaean Dharwar craton: the Holenarsipur area, southern India. Precambrian Res. 63, 43–58. https://doi.org/10.1016/0301-9268(93)90004-L

Byerly, G.R., Kröner, A., Lowe, D.R., Todt, W., Walsh, M.M., 1996. Prolonged magmatism and time constraints for sediment deposition in the early Archean Barberton greenstone belt: evidence from the Upper Onverwacht and Fig Tree groups. Precambrian Res. 78, 125–138. https://doi.org/10.1016/0301-9268(95)00073-9

Byerly, G.R., Lowe, D.R., Heubeck, C., 2019. Geologic Evolution of the Barberton Greenstone Belt - A Unique Record of Crustal Development, Surface Processes, and Early Life 3.55-3.20 Ga, in: Van Kranendonk, M.J., Bennett, V.C., Hoffmann, J.E. (Eds.), Earth's Oldest Rocks. pp. 569–613.

Cagnard, F., Brun, J., Gapais, D., 2006a. Modes of thickening of analogue weak lithospheres. Tectonophysics 421, 145–160. https://doi.org/10.1016/j.tecto.2006.04.016

Cagnard, F., Durrieu, N., Gapais, D., Brun, J.P., Ehlers, C., 2006b. Crustal thickening and lateral flow during compression of hot lithospheres, with particular reference to precambrian times. Terra Nov. 18, 72–78. https://doi.org/10.1111/j.1365-3121.2005.00665.x

Camacho, A., McDougall, I., Armstrong, R., Braun, J., 2001. Evidence for shear heating, Musgrave Block, central Australia. J. Struct. Geol. 23, 1007–1013. https://doi.org/10.1016/S0191-8141(00)00172-3

Chamberlain, K.R., Bowring, S.A., 2000. Apatite – feldspar U – Pb thermochronometer : a reliable , mid-range (~ 450°C), diffusion-controlled system. Chem. Geol. 172, 173–200.

Chardon, D., Choukroune, P., Jayananda, M., 1998. Sinking of the Dharwar Basin (South India): implications for Archaean tectonics. Precambrian Res. 91, 15–39. https://doi.org/10.1016/S0301-9268(98)00037-0

Chardon, D., Gapais, D., Cagnard, F., 2009. Flow of ultra-hot orogens: A view from the Precambrian, clues for the Phanerozoic. Tectonophysics 477, 105–118. https://doi.org/10.1016/j.tecto.2009.03.008

Chardon, D., Peucat, J.J., Jayananda, M., Choukroune, P., Fanning, C.M., 2002. Archean

granite-greenstone tectonics at Kolar (South India): Interplay of diapirism and bulk inhomogeneous contraction during juvenile magmatic accretion. Tectonics 21. https://doi.org/10.1029/2001TC901032

Chen, M., Bagas, L., Liao, X., Zhang, Z., Li, Q., 2019. Hydrothermal apatite SIMS Th–Pb dating: Constraints on the timing of low-temperature hydrothermal Au deposits in Nibao, SW China. Lithos 324–325, 418–428. https://doi.org/10.1016/j.lithos.2018.11.018

Cherniak, D.J., Lanford, W.A., Ryerson, F.J., 1991. Lead diffusion in apatite and zircon using ion implantation and Rutherford Backscattering techniques. Geochim. Cosmochim. Acta 55, 1663–1673. https://doi.org/10.1016/0016-7037(91)90137-T

Choukroune, P., Bouhallier, H., Arndt, N.T., 1995. Soft lithosphere during periods of Archaean crustal growth or crustal reworking. Geol. Soc. Spec. Publ. 95, 67–86. https://doi.org/10.1144/GSL.SP.1995.095.01.05

Clemens, J.D., Yearron, L.M., Stevens, G., 2006. Barberton (South Africa) TTG magmas: Geochemical and experimental constraints on source-rock petrology, pressure of formation and tectonic setting. Precambrian Res. 151, 53–78. https://doi.org/10.1016/j.precamres.2006.08.001

Cloete, M., 1994. Aspects of Vocanism and Metamorphism of the Onverwacht Group lavas in the South-Western portion of the Barberton Greenstone Belt. University of the Witwatersrand.

Cloete, M., 1991. An overview of metamorphism in the Barberton greenstone belt, in: Two Cratons and an Orogen, Excursion Guidebook and Rewiev Articles for a Field Workshop through Selected Archean Terranes of Swaziland, South Africa and Zimbabwe, IGCP Project. pp. 84–98.

Collins, W.J., Van Kranendonk, M.J., 1999. Model for the development of kyanite during partial convective overturn of Archean granite-greenstone terranes: The Pilbara Craton, Australia. J. Metamorph. Geol. 17, 145–156. https://doi.org/10.1046/j.1525-1314.1999.00187.x

Collins, W.J., Van Kranendonk, M.J., Teyssier, C., 1998. Partial convective overturn of Archaean crust in the east Pilbara Craton, Western Australia: Driving mechanisms and tectonic implications. J. Struct. Geol. 20, 1405–1424. https://doi.org/10.1016/S0191-8141(98)00073-X

Compagnoni, R., Hirajima, T., Chopin, C., 1995. Ultra-high-pressure metamorphic rocks in the Western Aps, in: Coleman, R.G., Wang, X. (Eds.), Ultrahigh Pressure Metamorphism. Cambridge University Press, New York, pp. 206–243.

Compston, W., Kröner, A., 1988. Multiple zircon growth within early Archaean tonalitic gneiss from the Ancient Gneiss Complex, Swaziland. Earth Planet. Sci. Lett. 87, 13–28. https://doi.org/10.1016/0012-821X(88)90061-1

Cutts, K.A., Stevens, G., Hoffmann, J.E., Buick, I.S., Frei, D., Münker, C., 2014. Paleo- to Mesoarchean polymetamorphism in the Barberton Granite- Greenstone Belt , South Africa : Constraints from U-Pb monazite and Lu- Hf garnet geochronology on the tectonic processes that shaped the belt 251–270. https://doi.org/10.1130/B30807.1

De Ronde, C.E.J., Kamo, S., Davis, D.W., de Wit, M.J., Spooner, E.T.C., 1991. Field, geochemical and U-Pb constraints from hypabyssal felsic intrusion within the Barberton greenstone belt, South Africa: Implications for tectonics and the timing of gold mineralization. Precambrian Res. 49, 261–280.

De Ronde, C.E.J., Kamo, S.L., 2000. An Archaean arc-arc collisional event: a short-lived (ca 3 Myr) episode, Weltevreden area, Barberton greenstone belt, South Africa. J. African

Earth Sci. 30, 219–248.

De Ronde, C.E.J. De, De Wit, M.J. De, 1994. Tectonic history of the Barberton greenstone belt, South Africa: 490 million years of Archean crustal evolution. Tectonics 13, 983–1005.

de Wit, M.J., 2004. Archean Greenstone Belts Do Contain Fragments of Ophiolites. Dev. Precambrian Geol. 13, 599–614. https://doi.org/10.1016/S0166-2635(04)13018-1

de Wit, M.J., Fripp, R.E.P., Stanistreet, I.G., 1983. Tectonic and stratigraphic implications of new field observations along the southern part of the Barberton greenstone belt. Spec. Publ. Geol. Soc. South Africa 21–29.

de Wit, M.J., Furnes, H., Robins, B., 2011. Geology and tectonostratigraphy of the Onverwacht Suite, Barberton Greenstone Belt, South Africa. Precambrian Res. 186, 1–27. https://doi.org/10.1016/j.precamres.2010.12.007

de Wit, M.J., Hart, R.A., Hart, R.J., 1987. The Jamestown Ophiolite Complex, Barberton mountain belt: a section through 3.5 Ga oceanic crust. J. African Earth Sci. 6, 681–730. https://doi.org/10.1016/0899-5362(87)90007-8

De Wit, M.J., Roering, C., Hart, R.J., Armstrong, R.A., De Ronde, C.E.J., Green, R.W.E., Tredoux, M., Peberdy, E., Hart, R.A., 1992. Formation of an Archaean continent. Nature 357, 553–562.

Debaille, V., O'Neill, C., Brandon, A.D., Haenecour, P., Yin, Q.Z., Mattielli, N., Treiman, A.H., 2013. Stagnant-lid tectonics in early Earth revealed by 142Nd variations in late Archean rocks. Earth Planet. Sci. Lett. 373, 83–92. https://doi.org/10.1016/j.epsl.2013.04.016

Diener, J.F.A., Stevens, G., Kisters, A.F.M., Poujol, M., 2005. Metamorphism and exhumation of the basal parts of the Barberton greenstone belt , South Africa : Constraining the rates of Mesoarchaean tectonism 143, 87–112. https://doi.org/10.1016/j.precamres.2005.10.001

Dill, H.G., 1994. Can REE patterns and U-Th variations be used as a tool to determine the origin of apatite in clastic rocks? Sediment. Geol. 92, 175–196. https://doi.org/10.1016/0037-0738(94)90105-8

Duclaux, G., Rey, P., Guillot, S., Ménot, R.P., 2007. Orogen-parallel flow during continental convergence: Numerical experiments and archean field examples. Geology 35, 715–718. https://doi.org/10.1130/G23540A.1

Dziggel, A., Armstrong, R.A., Stevens, G., Nasdala, L., 2005. Growth of zircon and titanite during metamorphism in the granitoid-gneiss terrane south of the Barberton greenstone belt, South Africa. Mineral. Mag. 69, 1019–1036.

Dziggel, A., Knipfer, S., Kisters, A.F.M., Meyer, F.M., 2006. P-T and structural evolution during exhumation of high- T, medium-P basement rocks in the Barberton Mountain Land, South Africa. J. Metamorph. Geol. 24, 535–551. https://doi.org/10.1111/j.1525-1314.2006.00653.x

Dziggel, A., Stevens, G., Poujol, M., Anhaeusser, C.R., Armstrong, R.A., 2002. Metamorphism of the granite-greenstone terrane south of the Barberton greenstone belt, South Africa: An insight into the tectono-thermal evolution of the "lower" portions of the Onverwacht Group. Precambrian Res. 114, 221–247. https://doi.org/10.1016/S0301-9268(01)00225-X

Ernst, W.G., 1988. Tectonic history of subduction zones inferred from retrograde blueschist P-T paths. Geology 16, 1081–1084. https://doi.org/10.1130/0091-7613(1988)016<1081:THOSZI>2.3.CO;2

Fossen, H., Cavalcante, G.C., de Almeida, R.P., 2017. Hot Versus Cold Orogenic Behavior: Comparing the Araçuaí-West Congo and the Caledonian Orogens. Tectonics 36, 2159–2178. https://doi.org/10.1002/2017TC004743

François, C., Philippot, P., Rey, P., Rubatto, D., 2014. Burial and exhumation during Archean sagduction in the East Pilbara Granite-Greenstone Terrane. Earth Planet. Sci. Lett. 396, 235–251. https://doi.org/10.1016/j.epsl.2014.04.025

Furnes, H., De Wit, M., Staudigel, H., Rosing, M., Muehlenbachs, K., 2007. A vestige of earth's oldest ophiolite. Science (80-.). 315, 1704–1707. https://doi.org/10.1126/science.1139170

Furnes, H., Dilek, Y., De Wit, M., 2015. Precambrian greenstone sequences represent different ophiolite types. Gondwana Res. 27, 649–685. https://doi.org/10.1016/j.gr.2013.06.004

Furnes, H., Rosing, M., Dilek, Y., de Wit, M., 2009. Isua supracrustal belt (Greenland)-A vestige of a 3.8 Ga suprasubduction zone ophiolite, and the implications for Archean geology. Lithos 113, 115–132. https://doi.org/10.1016/j.lithos.2009.03.043

Gapais, D., Cagnard, F., Gueydan, F., Barbey, P., Ballèvre, M., 2009. Mountain building and exhumation processes through time: Inferences from nature and models. Terra Nov. 21, 188–194. https://doi.org/10.1111/j.1365-3121.2009.00873.x

Gerdes, A., Zeh, A., 2009. Zircon formation versus zircon alteration - New insights from combined U-Pb and Lu-Hf in-situ LA-ICP-MS analyses, and consequences for the interpretation of Archean zircon from the Central Zone of the Limpopo Belt. Chem. Geol. 261, 230–243. https://doi.org/10.1016/j.chemgeo.2008.03.005

Gerdes, A., Zeh, A., 2006. Combined U-Pb and Hf isotope LA-(MC-)ICP-MS analyses of detrital zircons: Comparison with SHRIMP and new constraints for the provenance and age of an Armorican metasediment in Central Germany. Earth Planet. Sci. Lett. 249, 47–61. https://doi.org/10.1016/j.epsl.2006.06.039

Grosch, E.G., 2018. Metamorphic processes preserved in early Archean supracrustal rocks of the Barberton Greenstone Belt , South Africa. Geol. Soc. London, Spec. Publ. 478.

Grosch, E.G., Slama, J., 2017. Evidence for 3.3-billion-year-old oceanic crust in the Barberton greenstone belt, South Africa. Geology. https://doi.org/10.1177/0964663912467814

Halla, J., van Hunen, J., Heilimo, E., Hölttä, P., 2009. Geochemical and numerical constraints on Neoarchean plate tectonics. Precambrian Res. 174, 155–162. https://doi.org/10.1016/j.precamres.2009.07.008

Hansen, V.L., Willis, J.J., 1996. Structural analysis of a sampling of tesserae: Implications for Venus geodynamics. Icarus 123, 296–312. https://doi.org/10.1006/icar.1996.0159

Harris, L.B., Bédard, J.H., 2015. Interactions between continent-like "drift", rifting and mantle flow on Venus: Gravity interpretations and Earth analogues. Geol. Soc. Spec. Publ. 401, 327–356. https://doi.org/10.1144/SP401.9

Harris, L.B., Bédard, J.H., 2014. Crustal Evolution and Deformation in a Non-Plate-Tectonic Archaean Earth: Comparisons with Venus, in: Dilek, Y., Furnes, H. (Eds.), Evolution of Archean Crust and Early Life. Springer, pp. 215–291. https://doi.org/10.1007/978-94-007-7615-9_9

Hermann, J., 2003. Experimental evidence for diamond-facies metamorphism in the Dora-Maira massif. Lithos 70, 163–182. https://doi.org/10.1016/S0024-4937(03)00097-5

Heubeck, C., Engelhardt, J., Byerly, G.R., Zeh, A., Sell, B., Luber, T., Lowe, D.R., 2013. Timing of deposition and deformation of the Moodies Group (Barberton Greenstone Belt , South

Africa): Very-high-resolution of Archaean surface processes. Precambrian Res. 231, 236–262. https://doi.org/10.1016/j.precamres.2013.03.021

Janoušek, V., Farrow, C.M., Erban, V., 2006. Interpretation of whole-rock geochemical data in igneous geochemistry: Introducing Geochemical Data Toolkit (GCDkit). J. Petrol. 47, 1255–1259. https://doi.org/10.1093/petrology/egl013

Kamo, S.L., Davis, D.W., 1994. Reassessment of Archean crustal development in the Barberton Mountain Land, South Africa, based on U-Pb dating. Tectonics 13, 167–192.

Kato, D., Aoki, K., Komiya, T., Yamamoto, S., Sawaki, Y., Asanuma, H., Sato, T., Tsuchiya, Y., Shozugawa, K., Matsuo, M., Windley, B.F., 2018. Constraints on the P–T conditions of high-pressure metamorphic rocks from the Inyoni shear zone in the mid-Archean Barberton Greenstone Belt, South Africa. Precambrian Res. 315, 1–18. https://doi.org/10.1016/j.precamres.2018.06.018

Kirkland, C.L., Yakymchuk, C., Szilas, K., Evans, N., Hollis, J., McDonald, B., Gardiner, N.J., 2018. Apatite: a U-Pb thermochronometer or geochronometer? Lithos 318–319, 143–157. https://doi.org/10.1016/j.lithos.2018.08.007

Kisters, A.F.M., Anhaeusser, C.R., 1995. Emplacement features of Archean TTG plutons along the southern margin of the Barberton greenstone belt, South Africa. Precambrian Res. 75, 1–15. https://doi.org/10.1016/0301-9268(95)00003-N

Kisters, A.F.M., Belcher, R.W., Poujol, M., Dziggel, A., 2010. Continental growth and convergence-related arc plutonism in the Mesoarchaean : Evidence from the Barberton granitoid-greenstone terrain , South Africa. Precambrian Res. 178, 15–26. https://doi.org/10.1016/j.precamres.2010.01.002

Kisters, A.F.M., Stevens, G., Dziggel, A., Armstrong, R.A., 2003. Extensional detachment faulting and core-complex formation in the southern Barberton granite-greenstone terrain, South Africa: Evidence for a 3.2 Ga orogenic collapse. Precambrian Res. https://doi.org/10.1016/j.precamres.2003.08.002

Kröner, A., 2016. In: Badplaas Field Workshop on Archaean Geodynamics, 18-22 August 2016. Southern Barberton Granitoid-Greenstone Terrane. South Africa excursion guidebook.

Kröner, A., Anhaeusser, C.R., Hoffmann, J.E., Wong, J., Geng, H., Hegner, E., Xie, H., Yang, J., Liu, D., 2016. Chronology of the oldest supracrustal sequences in the Palaeoarchaean Barberton Greenstone Belt, South Africa and Swaziland. Precambrian Res. 279, 123–143. https://doi.org/10.1016/J.PRECAMRES.2016.04.007

Kröner, A., Byerly, G.R., Lowe, D.R., 1991. Chronology of early Archaean granite-greenstone evolution in the Barberton Mountain Land, South Africa, based on precise dating by single zircon evaporation. Earth Planet. Sci. Lett. 103, 41–54. https://doi.org/10.1016/0012-821X(91)90148-B

Kröner, A., Hegner, E., Wendt, J.I., Byerly, G.R., 1996. The oldest part of the Barberton granitoid-greenstone terrain, South Africa: evidence for crust formation between 3.5 and 3.7 Ga. Precambrian Res. 78, 105–124. https://doi.org/10.1016/0301-9268(95)00072-0

Kröner, A., Nagel, T.J., E., H.J., Ernst, H., Geng, H., Wong, J., Xie, H., Liu, X., Schneider, K., Kasper, U.H., 2013. High-temperature metamorphism and crustal melting at ca. 3.2 Ga in the eastern Kaapvaal craton, southern Africa. J. Chem. Inf. Model. 53, 1689–1699. https://doi.org/10.1017/CBO9781107415324.004

Kröner, A., Todt, W., 1988. Single Zircon Dating Constraining the Maximum Age of the Barberton Greenstone Belt, Southern Africa. J. Geophys. Res. 93, 15,329-15,337.

Lana, C., Farina, F., Gerdes, A., Alkmim, A., Gonçalves, G.O., Jardim, A.C., 2017. Characterization of zircon reference materials via high precision U–Pb LA-MC-ICP-MS. J. Anal. At. Spectrom. https://doi.org/10.1039/C7JA00167C

Lana, C., Kisters, A., Stevens, G., 2010a. Exhumation of Mesoarchean TTG gneisses from the middle crust: Insights from the Steynsdorp core complex, Barberton granitoid-greenstone terrain, South Africa. Bull. Geol. Soc. Am. 122, 183–197. https://doi.org/10.1130/B26580.1

Lana, C., Tohver, E., Cawood, P., 2010b. Quantifying rates of dome-and-keel formation in the Barberton granitoid-greenstone belt, South Africa. Precambrian Res. 177, 199–211. https://doi.org/10.1016/j.precamres.2009.12.001

Laurent, O., Björnsen, J., Wotzlaw, J.F., Bretscher, S., Pimenta Silva, M., Moyen, J.F., Ulmer, P., Bachmann, O., 2020. Earth's earliest granitoids are crystal-rich magma reservoirs tapped by silicic eruptions. Nat. Geosci. https://doi.org/10.1038/s41561-019-0520-6

Laurie, A., Stevens, G., Van Hunen, J., 2013. The end of continental growth by TTG magmatism. Terra Nov. 25, 130–136. https://doi.org/10.1111/ter.12015

Layer, P.W., Lopez-martinez, M., Kro, A., York, D., Mcwilliams, M., 1998. Thermochronometry and palaeomagnetism of the Archaean Nelshoogte Pluton , South Africa 129–145.

Lev, S.M., McLennan, S.M., Meyers, W.J., Hanson, G.N., 1998. A petrographic approach for evaluating trace-element mobility in a black shale. J. Sediment. Res. 68, 970–980. https://doi.org/10.2110/jsr.68.970

Levander, A., Schmandt, B., Miller, M.S., Liu, K., Karlstrom, K.E., Crow, R.S., Lee, C.T.A., Humphreys, E.D., 2011. Continuing Colorado plateau uplift by delamination-style convective lithospheric downwelling. Nature 472, 461–465. https://doi.org/10.1038/nature10001

Liu, W., Mei, Y., Etschmann, B., Brugger, J., Pearce, M., Ryan, C.G., Borg, S., Wykes, J., Kappen, P., Paterson, D., Boesenberg, U., Garrevoet, J., Moorhead, G., Falkenberg, G., 2017. Arsenic in hydrothermal apatite: Oxidation state, mechanism of uptake, and comparison between experiments and nature. Geochim. Cosmochim. Acta 196, 144–159. https://doi.org/10.1016/j.gca.2016.09.023

Lowe, D.R., Byerly, G.R., 2007. AN OVERVIEW OF THE GEOLOGY OF THE BARBERTON GREENSTONE BELT AND VICINITY : IMPLICATIONS FOR EARLY CRUSTAL DEVELOPMENT, in: Van Kranendonk, M.J., Smithies, R.H., Bennett, V.C. (Eds.), Earth's Oldest Rocks. pp. 481–526. https://doi.org/10.1016/S0166-2635(07)15053-2

Lowe, D.R., Byerly, G.R., Heubeck, C., 2012. Geologic Map of the West-Central Barberton Greenstone Belt, South Africa.

Ludwig, K.R., 2012. User's Manual for Isoplot 3.75, a geochronological toolkit for Microsoft Excel. Berkeley Geochronol. Cent. Spec. Publ. 5, 1–72.

Maneiro, K.A., Cutts, K., Baxter, E.F., Stevens, G., 2018. Earth's Oldest Garnet: 3.20 Ga Garnet Ages Robustly Constrain the Timing of Early Metamorphism.

Mareschal, J.-C., West, G.F., 1980. A model for Archean tectonism. Part 2. Numerical models of vertical tectonism in greenstone belts. Can. J. Earth Sci. 17, 60–71. https://doi.org/10.1139/e80-006

Martin, H., 1999. Adakitic magmas: Modern analogues of Archaean granitoids. Lithos 46, 411–429. https://doi.org/10.1016/S0024-4937(98)00076-0

Martin, H., Moyen, J.F., 2002. Secular changes in tonalite-trondhjemite-granodiorite

composition as markers of the progressive cooling of Earth. Geology 30, 319–322. https://doi.org/10.1130/0091-7613(2002)030<0319:SCITTG>2.0.CO;2

Matsumura, R., 2014. The petrogenesis of the Nelshoogte pluton: The youngest and most compositionally variable TTG plutons in the Barberton Granit-Greenstone Terrain. Stellenbosch University.

Miller, A.R., Cumming, G.L., Kristic, D., 1989. U-Pb, Pb-Pb, and K-Ar isotopic study and petrography of uraniferous phosphate-bearing rocks in the Thelon Formation, Dubawnt Group, Northwest Territories, Canada. Can. J. Earth Sci. 26, 867–880.

Moyen, J.-F., Stevens, G., Kisters, A.F.M., Belcher, R.W., Lemirre, B., 2019. TTG Plutons of the Barberton Granitoid-Greenstone Terrain, South Africa, in: Van Kranendonk, M.J., Bennett, V.C., Hoffmann, J.E. (Eds.), Earth's Oldest Rocks. pp. 615–653.

Moyen, J.F., Stevens, G., Kisters, A.F.M., 2006. Record of mid-Archaean subduction from metamorphism in the Barberton terrain , South Africa. Nature 442, 559–562. https://doi.org/10.1038/nature04972

Moyen, J.F., van Hunen, J., 2012. Short-term episodicity of Archaean plate tectonics. Geology 40, 451–454. https://doi.org/10.1130/G322894.1

Moyen, J.F., Zeh, A., Cuney, M., Dziggel, A., Carrouée, S., 2020. The multiple ways of recycling Archaean crust : a case study from the ca. 3.1 Ga granitoids from the Barberton Greenstone Belt , South Africa. Precambrian Res. 105998. https://doi.org/10.1016/j.precamres.2020.105998

Murphy, R., 2015. Stabilizing a Craton: The Origin and Emplacment of the 3.1 Ga Mpuluzi Batholith. Maquarie University.

Nemchin, A.A., Pidgeon, R.T., 1999. U-Pb ages on titanite and apatite from the Darling Range granite: Implications for Late Archaean history of the southwestern Yilgarn Craton. Precambrian Res. 96, 125–139. https://doi.org/10.1016/S0301-9268(99)00007-8

O'Connor, J.T., 1965. A classification for quartz-rich igneous rocks based on feldspar ratios. US Geol. Surv. Prof. Pap. 252, 79–84.

O'Neill, C., Lenardic, A., Condie, K.C., 2015. Earth's punctuated tectonic evolution: Cause and effect. Geol. Soc. Spec. Publ. 389, 17–40. https://doi.org/10.1144/SP389.4

O'Neill, C., Lenardic, A., Moresi, L., Torsvik, T.H., Lee, C.T.A., 2007. Episodic Precambrian subduction. Earth Planet. Sci. Lett. 262, 552–562. https://doi.org/10.1016/j.epsl.2007.04.056

Palin, R.M., Dyck, B., 2018. Metamorphic consequences of secular changes in oceanic crust composition and implications for uniformitarianism in the geological record. Geosci. Front. 9, 1009–1019. https://doi.org/10.1016/j.gsf.2018.04.004

Palin, R.M., White, R.W., 2016. Emergence of blueschists on Earth linked to secular changes in oceanic crust composition. Nat. Geosci. 9, 60–64. https://doi.org/10.1038/ngeo2605

Pidgeon, R.T., 1992. Recrystallisation of oscillatory zoned zircon: some geochronological and petrological implications. Contrib. to Mineral. Petrol. 110, 463–472. https://doi.org/10.1007/BF00344081

Pidgeon, R.T., Nemchin, A.A., Hitchen, G.J., 1998. Internal structures of zircons from Archaean granites from the Darling Range batholith: Implications for zircon stability and the interpretation of zircon U-Pb ages. Contrib. to Mineral. Petrol. https://doi.org/10.1007/s004100050422

Piskorz, D., Elkins-Tanton, L.T., Smrekar, S.E., 2014. Coronae formation on Venus via

extension and lithospheric instability. J. Geophys. Res. Planets 119, 2568–2582. https://doi.org/10.1002/2014JE004636

Rey, P.F., Coltice, N., Flament, N., 2014. Spreading continents kick-started plate tectonics. Nature 513, 405–408. https://doi.org/10.1038/nature13728

Schneider, S., Hammerschmidt, K., Rosenberg, C.L., Gerdes, A., Frei, D., Bertrand, A., 2015. U – Pb ages of apatite in the western Tauern Window (Eastern Alps): Tracing the onset of collision-related exhumation in the European plate. Earth Planet. Sci. Lett. 418, 53–65. https://doi.org/10.1016/j.epsl.2015.02.020

Schoene, B., de Wit, M.J., Bowring, S.A., 2008. Mesoarchean assembly and stabilization of the eastern Kaapvaal craton: A structural-thermochronological perspective. Tectonics 27, 1–27. https://doi.org/10.1029/2008TC002267

Sizova, E., Gerya, T., Brown, M., Stüwe, K., 2018. What drives metamorphism in early Archean greenstone belts? Insights from numerical modeling. Tectonophysics 746, 587–601. https://doi.org/10.1016/j.tecto.2017.07.020

Sizova, E., Gerya, T., Stüwe, K., Brown, M., 2015. Generation of felsic crust in the Archean: A geodynamic modeling perspective. Precambrian Res. 271, 198–224. https://doi.org/10.1016/j.precamres.2015.10.005

Smithies, R.H., Champion, D.C., Van Kranendonk, M.J., 2009. Formation of Paleoarchean continental crust through infracrustal melting of enriched basalt. Earth Planet. Sci. Lett. 281, 298–306. https://doi.org/10.1016/j.epsl.2009.03.003

Smithies, R.H., Van Kranendonk, M.J., Champion, D.C., 2007. The Mesoarchean emergence of modern-style subduction 11, 50–68. https://doi.org/10.1016/j.gr.2006.02.001

Spear, F.S., Pyle, J.M., 2002. Apatite, monazite, and xenotime in metamorphic rocks (in Phosphates; geochemical, geobiological, and materials importance) Reviews in Mineralogy and Geochemistry. Rev. Mineral. Geochemistry 48, 293–335. https://doi.org/10.2138/rmg.2002.48.7

Stacey, J.S., Kramers, J.D., 1975. Approximation of terrestrial lead isotope evolution by a two-stage model. Earth Planet. Sci. Lett. 26, 207–221.

Stevens, G., Droop, G.T.R., Armstrong, R.A., Anhaeusser, C.R., 2002. Amphibolite facies metamorphism in the Schapenburg schist belt: A record of the mid-crustal response to ~ 3.23 Ga terrane accretion in the Barberton greenstone belt. South African J. Geol. 105, 271–284. https://doi.org/10.2113/1050271

Thébaud, N., Rey, P.F., 2013. Archean gravity-driven tectonics on hot and flooded continents: Controls on long-lived mineralised hydrothermal systems away from continental margins. Precambrian Res. 229, 93–104. https://doi.org/10.1016/j.precamres.2012.03.001

Tsunogae, T., Yurimoto, H., 1995. Single zircon U-Pb geochronology of the Limpopo Belt by secondary ion mass spectrometry. Geochem. J. 29, 197–205. https://doi.org/10.2343/geochemj.29.197

van Hunen, J., Moyen, J.-F., 2012. Archean Subduction: Fact or Fiction? Annu. Rev. Earth Planet. Sci. 40, 195–219. https://doi.org/10.1146/annurev-earth-042711-105255

Van Kranendonk, M.J., 2011. Journal of African Earth Sciences Cool greenstone drips and the role of partial convective overturn in Barberton greenstone belt evolution. J. African Earth Sci. 60, 346–352. https://doi.org/10.1016/j.jafrearsci.2011.03.012

Van Kranendonk, M.J., 2007. Chapter 8.6 Tectonics of Early Earth. Dev. Precambrian Geol. https://doi.org/10.1016/S0166-2635(07)15086-6

Van Kranendonk, M.J., Collins, W.J., Hickman, A., Pawley, M.J., 2004. Critical tests of vertical vs. horizontal tectonic models for the Archaean East Pilbara Granite-Greenstone Terrane, Pilbara Craton, Western Australia, in: Precambrian Research. pp. 173–211. https://doi.org/10.1016/j.precamres.2003.12.015

Van Kranendonk, M.J., Kröner, A., Hegner, E., Connelly, J., 2009. Age, lithology and structural evolution of the c. 3.53 Ga Theespruit Formation in the Tjakastad area, southwestern Barberton Greenstone Belt, South Africa, with implications for Archaean tectonics. Chem. Geol. 261, 114–138. https://doi.org/10.1016/j.chemgeo.2008.11.006

Van Kranendonk, M.J., Kröner, A., Hoffman, J.E., Nagel, T., Anhaeusser, C.R., 2014. Just another drip: Re-analysis of a proposed mesoarchean suture from the Barberton mountain land, South Africa. Precambrian Res. 254, 19–35. https://doi.org/10.1016/j.precamres.2014.07.022

Van Kranendonk, M.J., Smithies, R.H., Griffin, W.L., Huston, D.L., Hickman, A.H., Champion, D.C., Anhaeusser, C.R., Pirajno, F., 2015. Making it thick: a volcanic plateau origin of Palaeoarchean continental lithosphere of the Pilbara and Kaapvaal cratons. Geol. Soc. London, Spec. Publ. 389, 83–111. https://doi.org/10.1144/SP389.12

Van Kranendonk, M.J., Smithies, R.H., Hickman, A.H., Champion, D.C., 2007. Chapter 4.1 Paleoarchean Development of a Continental Nucleus: the East Pilbara Terrane of the Pilbara Craton, Western Australia. Dev. Precambrian Geol. https://doi.org/10.1016/S0166-2635(07)15041-6

Venables, W.N., Ripley, B.D., 2002. Modern applied Statistics with S. Springer.

Vermeesch, P., 2018. IsoplotR: A free and open toolbox for geochronology. Geosci. Front. 9, 1479–1493. https://doi.org/10.1016/j.gsf.2018.04.001

Vermeesch, P., 2012. On the visualisation of detrital age distributions. Chem. Geol. 312–313, 190–194. https://doi.org/10.1016/j.chemgeo.2012.04.021

Wang, H., Yang, J.H., Kröner, A., Zhu, Y.S., Li, R., 2019. Non-subduction origin for 3.2 Ga high-pressure metamorphic rocks in the Barberton granitoid-greenstone terrane, South Africa. Terra Nov. 31, 373–380. https://doi.org/10.1111/ter.12397

Webster, J.D., Piccoli, P.M., 2015. Magmatic apatite: A powerful, yet deceptive, mineral. Elements 11, 177–182. https://doi.org/10.2113/gselements.11.3.177

West, G.F., Mareschal, J.C., 1979. A MODEL FOR ARCHEAN TECTONISM - 1. THE THERMAL CONDITIONS. Can. J. Earth Sci. 16, 1942–1950. https://doi.org/10.1139/e79-181

Zeh, A., Gerdes, A., Barton, J.M., 2009. Archean accretion and crustal evolution of the kalahari craton - The zircon age and Hf isotope record of granitic rocks from barberton/ swaziland to the francistown arc. J. Petrol. 50, 933–966. https://doi.org/10.1093/petrology/egp027

Zeh, A., Gerdes, A., Heubeck, C., 2013. U–Pb and Hf isotope data of detrital zircons from the Barberton Greenstone Belt: constraints on provenance and Archaean crustal evolution. J. Geol. Soc. London. 170, 215–223. https://doi.org/10.1144/jgs2011-162

Chapter 5: Presentation of research paper 2: Thermometry and trace-element composition of accessory minerals record Mesoarchean short-lived MT metamorphism in the Stolzburg Block, BGGT, South Africa

This paper, fist authored by Moritz Mühlberg, is in preparation for submission in Lithos. The following aspects of the research were done independently by Moritz Mühlberg while receiving standard supervision by his supervisors Gary Stevens, Jean-François Moyen and Alex Kisters: (i) field work and sampling; (ii) sample preparation for whole-rock and mineral analyses; (iii) acquisition of mineral chemical data on EMP (apatite, titanite), SEM (zircon) and LA ICP-MS (apatite, titanite); (iv) reduction of mineral chemical LA ICP-MS data in Glitter (apatite, titanite) and Iolite (zircon); (v) generation of the figures; (vi) writing of the manuscript. Apatite Sr isotope data acquisition reduction were done by Cristiano Lana. Zircon mineral chemical LA ICP-MS data acquisition was performed by Riana Rossouw. Whole-rock Sr isotope data acquisition was done by Petrus Le Roux.

Thermometry and trace-element composition of accessory minerals record Mesoarchean short-lived MT metamorphic event in the Stolzburg Block, BGGT, South Africa

Moritz Mühlberg[a,b]*, Emilie Bruand[c], Jean-François Moyen[b], Gary Stevens[a]

[a] Department of Earth Sciences, University of Stellenbosch, Private Bag X1, Matieland 7602, South Africa

[b] Université de Lyon, LGL-TPE, UJM-UCLB-ENSL-CNRS, 23 rue Dr. Paul Michelon, 42023 Saint Etienne, France

[c] Université Clermont Auvergne, Laboratoire Magmas et Volcans, CNRS-IRD, 6 Avenue Blaise Pascal, 63170 Aubière, France

* Corresponding author. moritzmberg@gmail.com

Abstract

The thermal state of the felsic crust during the Archean is a crucial bit of information for reconstructing the geodynamic processes that shaped the first stable continents. Here we report new trace-element data for apatite, titanite and zircon grains as well as Sr isotopic data for apatite grains from granitoid samples from the Stolzburg Block, Barberton Granitoid Greenstone Terrain, South Africa. The apatite grains, for which U-Pb dates ranging from ca. 3.45 Ga down to ca. 2.82 Ga had been previously obtained, yield homogenous REE compositions and $^{87}Sr/^{86}Sr$ ratios that are within uncertainty identical to one another and to the initial $^{87}Sr/^{86}Sr$ ratio of the respective bulk rock. This shows, that the U-Pb isotope systematics in apatite have been decoupled from the REE and Sr isotope systematics, likely through short-lived heating. Thermometry of metamorphic titanite and zircon grains yields temperatures of ca. 650 ± 20 °C and 645 ± 62 °C. Heating to such temperatures while preserving pristine U-Pb (partially) and Sr (completely) isotope characteristics is only possible with a short duration of heating. The results of this study are incompatible with the postulations of the model of partial convective overturn, which has been evoked for the Barberton crust at ca. 3.2 Ga. Instead of prolonged radiogenic heating of the felsic crust and subsequent diapiric rise in a partially molten state, it is more likely that the Stolzburg Block was buried to mid-crustal depths and rapidly exhumed in a compressional tectonic setting.

5.1 Introduction

The Paleo- to Mesoarchean (3600 to 2800 Ma) is a critical time in Earth's history. It was at this time, that the first continents got thick and stable enough to emerge above the ocean (Chowdhury et al., 2021), and from which the first clear sign of life are preserved (e.g. Allwood et al. (2006) and Hickman-Lewis et al. (2018); see also review by Homann (2019)). It is also a period that is characterized by distinctly different lithologies compared to the modern Earth, found in greenstone belts and surrounding tonalite-trondhjemite-granodiorite (TTG) plutons. The lack of modern equivalents of TTG rocks has sparked a debate on the geodynamic processes that produced TTG magmas and shaped the first continents, with uniformitarian (e.g. De Ronde and Kamo, 2000; Furnes et al., 2015; Moyen et al., 2006; Moyen and Laurent, 2018) and unique (e.g. François et al., 2014; Thébaud and Rey, 2013; Van Kranendonk et al., 2015) processes having been suggested. However, not much in the debate is based on constraints from metamorphic rocks but rather on models that are themselves based on assumptions on the thermal state of the crust. While most studies of Archean terranes have focused on the formation of cratons, their lithologies (i.e. greenstone sequences and TTG plutons) and how they were amalgamated, the subsequent metamorphic history has not yet been documented.

Where Archean greenstone sequences are preserved, they are often highly deformed and have experienced subsequent metamorphism, overprinting their older metamorphic signatures and erasing the Archean thermal history. Thus, only a few places exist where the first few 100 Ma of crustal development in early cratonization can be studied. One of them is the Barberton Granitoid Greenstone Terrane (BGGT; Fig. 5.1a) of South Africa and Eswatini. Despite the well-documented greenschist- and amphibolite-facies polymetamorphic history of the greenstone belt rocks bounding them (see below for details), Paleo- and Mesoarchean TTG rocks have experienced little deformation after their emplacement and still show pristine igneous textures (e.g. Moyen et al., 2019). The southern BGGT TTGs give insight into the mid crust of the evolving early Kaapvaal Craton, but because their main mineral assemblage is rather inert to change at the amphibolite-facies conditions that were recorded by the associated felsic schists, metasediments and meta(ultra)mafic rocks of the lower Onverwacht Group (e.g. Diener et al., 2005; Dziggel et al., 2002; Kato et al., 2018), one has to look to the minor phases.

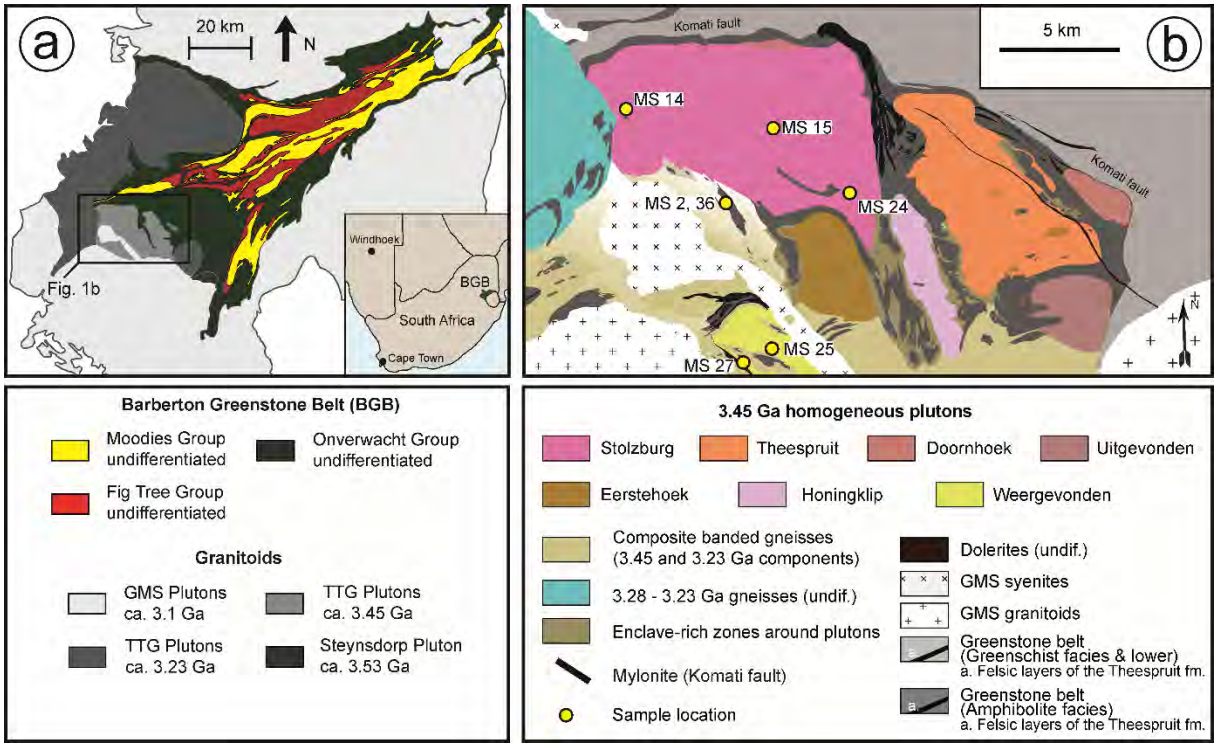

Fig. 5.1. (a) Geological map of the Stolzburg Block, showing the important lithological units and sample localities. Modified after Moyen et al. (2019). (b) Geological sketch map of the Barberton Granitoid Greenstone Terrane (BGGT); inset shows the location of the BGGT in the context of southern Africa. Modified after Anhaeusser et al. (1981).

Accessory minerals such as allanite, apatite, monazite, titanite and zircon account for most of the trace-element budget of a rock, and their chemical characteristics may give insight into the rock's history, as already proven in some Archean terranes (Bruand et al., 2020; Fisher et al., 2020b, 2020a; Hammerli et al., 2019; Iizuka et al., 2011). The most popular of these minerals is zircon, which is a common magmatic mineral in felsic rocks and is widely used to date the

crystallization of igneous rocks. Zircon can also grow as a metamorphic mineral (Rubatto and Hermann, 2007, 2003). The Ti concentration in zircon is dependent on the crystallization temperature and zircon can therefore be used as a thermometer for both magmatic and metamorphic processes (Ferry and Watson, 2007; Fu et al., 2008; Siégel et al., 2018; Watson et al., 2006). Furthermore, the light rare earth element (LREE) composition of zircon might be indicative of hydrothermal alteration (Hoskin, 2005) and the size of the Ce anomaly can be used to infer the redox conditions of the parent magma (Trail et al., 2012). Other accessory minerals have also been proven fruitful to reconstruct the igneous and metamorphic history of old terranes.

For example, apatite can occur both as a magmatic and a metamorphic mineral, with characteristic trace-element signatures allowing to discriminate their nature (Belousova et al., 2002a; Bruand et al., 2014; Hoskin et al., 2000; Sha and Chappell, 1999; Sullivan et al., 2020). Apatite does not take in any Rb into its crystal structure and the $^{87}Sr/^{86}Sr$ ratio of magmatic apatite can be used to retrieve the Sr isotopic composition of the magma at the time of apatite crystallization. Finally, with a typical closure temperature for the U-Pb system of ca. 400-500 °C (Chamberlain and Bowring, 2000; Cherniak et al., 1991; Schoene and Bowring, 2007), apatite is a popular tool to date mid-T processes. Titanite can also grow as a magmatic (Garber et al., 2017; Kirkland et al., 2020, 2017; Kohn, 2017) and a metamorphic (Bruand et al., 2014; Hoskin et al., 2000; Storey et al., 2007) mineral. The Zr concentration in titanite was shown to be dependent on temperature, allowing to estimate the conditions of titanite formation (Hayden et al., 2008).

Interestingly, recent works focusing on multiple analyses in accessory minerals have shown, that the U-Pb and trace-element signatures of apatite (Antoine et al., 2020; C.M. Fisher et al., 2020b) and titanite (Gordon et al., 2021) can be decoupled under certain conditions. For example, Antoine et al. (2020) recently reported that matrix apatite from the Acasta Gneiss Complex, which had their original U-Pb systematics completely reset by a metamorphic event at about 1.8 Ga, could still preserve primary magmatic trace-element characteristics identical to primary apatite inclusions protected in zircon.

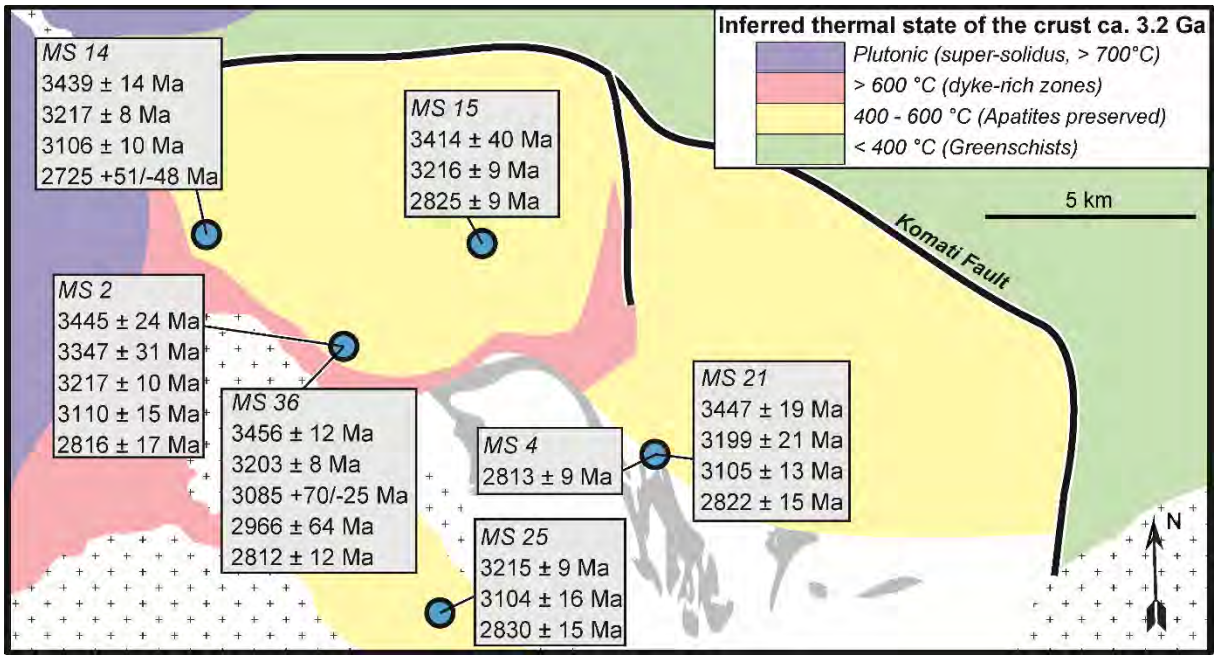

Fig. 5.2. Summary of U-Pb ages determined for apatite grains from granitoid (MS 2, 4, 14, 15, 25, 36) and mafic schist (MS 21) samples from the Stolzburg Block. The map shows the key interpretation derived from the apatite geochronology and the published pressure and temperature estimates for the Stolzburg Block and the Barberton Greenstone Belt. Age data and map from Mühlberg et al. (2021).

The Stolzburg Block in the southern BGGT (Fig. 5.1b) is comprised of metavolcanic and metavolcanosedimentary rocks of the lower Onverwacht Group, yielding U-Pb zircon ages of ca. 3.53 Ga (Kröner et al., 2016, 1996), and TTG plutons, for which magmatic U-Pb zircon ages of ca. 3.45 Ga have been obtained (Kamo and Davis, 1994; Lana et al., 2010; Laurent et al., 2020; Schoene et al., 2008; Wang et al., 2019). The Stolzburg is bordered to the south and cut by granitic plutons with U-Pb zircon ages of ca. 3.1 Ga (e.g. Kamo and Davis, 1994; Murphy, 2015). The supracrustal rocks record peak metamorphic conditions of ca. 550 to 700 °C at ca. 7 to 10 kbar (Cutts et al., 2021, 2014; Diener et al., 2005; Dziggel et al., 2002; Kato et al., 2018; Moyen et al., 2006), and the timing of metamorphism has been constrained to ca. 3.2 Ga (Cutts et al., 2021, 2014; Diener et al., 2005; Dziggel et al., 2005). The constraints on the metamorphism of the TTG rocks have until now been limited to a handful of U-Pb zircon and titanite ages of ca. 3.2 Ga (Kamo and Davis, 1994; Mühlberg et al., 2021).

A recent (thermo)chronological study conducted by Mühlberg et al. (2021) on apatite and zircon grains from Stolzburg Block granitoids found four distinct groups of U-Pb apatite ages ranging from ca. 3.45 Ga down to ca. 2.82 Ga (Fig. 5.2). The 3.45 Ga ages obtained for magmatic zircon indicate that the oldest apatites preserve igneous crystallization ages and this has been interpreted as evidence that the ca. 3.45 Ga rocks of the Stolzburg Block were not heated above ca. 500-600 °C after their emplacement, at least not for a prolonged period. The subsequent younger U-Pb apatite age groups of ca. 3.2 and 3.1 Ga can be linked to amphibolite-facies metamorphism and granite intrusion, respectively, while the event at ca.

2.82 Ga remains cryptic. However, the exact thermal conditions experienced by the Stolzburg Block granitoids are still unknown, as well as what caused the formation of the different U-Pb apatite ages – be it driven solely by thermal pulses, or through the ingress of fluids or grain boundary melts with heat – and also their preservation. To this end, in this paper we aim at studying the relationship between this spread of ages shown by the samples dated by Mühlberg et al. (2021) and their relationship with trace elements by analyzing and interpreting trace-element compositions of apatite, titanite and zircon grains as well as apatite and whole-rock Sr isotope systematics.

5.2 Geological Background

The Barberton Granitoid Greenstone Terrane (BGGT) of South Africa is comprised of two main parts: The Barberton Greenstone Belt (BGB), a succession of volcanic and sedimentary rocks deposited from ca. 3.6 to 3.2 Ga, and the surrounding granitoid plutons (Fig. 5.1a). An in-depth summary of the geology of the BGB is given by Byerly et al. (2019) and will not be detailed here. The granitoid plutons surrounding the BGB can divided into the ca. 3.5 to 3.2 Ga tonalite-trondhjemite-granodiorite (TTG) plutons and the ca. 3.2 to 3.1 Ga granodiorite-monzogranite-syenogranite (GMS) plutons and batholiths. A review on the TTG plutons was recently given by Moyen et al. (2019). The younger GMS suite rocks are found in the Nelspruit Pluton, the Bosmanskop syenite and the large Heerenven, Mpuluzi and Pigg's Peak batholiths (e.g. Clemens et al., 2010; Kröner et al., 2019; Moyen et al., 2021; Murphy, 2015).

The TTG plutons are intruding the rocks of the BGB and in places, the intrusive contact can be seen (see Fig. 3 of Mühlberg et al., 2021). The whole BGGT underwent several low-grade metamorphic events with typical conditions of >300 °C recorded throughout the BGB. In addition, in the southern BGGT the lowermost strata of the BGB, the Theespruit and Sandspruit formations of the Lower Onverwacht Group, and the TTG rocks of the Stolzburg and Theespruit plutons, along with some smaller plutonic bodies, have experienced upper amphibolite-facies metamorphism at ca. 3.2 Ga (Cutts et al., 2014; Diener et al., 2005; Dziggel et al., 2005, 2002; Kato et al., 2018). Those amphibolite-facies rocks of the southern BGGT are collectively referred to as the Stolzburg Block and are separated from the lower grade rocks of the BGB by the Komati fault (Armstrong et al., 1990; Kisters et al., 2003) (Fig. 5.1b). While the mafic to ultra-mafic volcanic and the sedimentary lithologies of the Stolzburg Block underwent a change of mineral assemblage as a result of the amphibolite-facies metamorphism, the TTG plutons remain virtually unchanged due to their mineral assemblage of feldspar, quartz and biotite which is unresponsive to metamorphic change under the recorded conditions. Because of this, the TTG plutons and plutonic cells of the Stolzburg Block represent some of the most pristine

Paleoarchean plutonic felsic rock compositions anywhere on Earth; in the core they display primary igneous textures (REF / Fig.), they experienced little deformation (REF) and their minerals are well preserved for their age of ca. 3.45 Ga. This makes these rocks the ideal target for studying igneous processes in the early Archean.

Samples from the Stolzburg Block were previously analyzed for their major- and trace-element composition and U-Pb geochronology was performed on apatite and zircon grains from those samples (Mühlberg et al., 2021). In this paper, we analyzed trace elements and Sr isotopes (for apatite only) for the same grains and added trace-element analyses of titanite grains. The samples were taken from the Stolzburg (MS 2, 14, 15, 24, 36) and Weergevonden (MS 25, 27) plutons. Sample localities are shown in Fig. 1b and listed in Table 5.1.

Table 5.1. Sample descriptions, localities and age systematics for granitoid samples from the Stolzburg block.

Sample	Mineral Assemblage	Locality	Apatite[a] [Ga]				Zircon[b] [Ga]		
			3.45	3.2	3.1	2.8	3.45_i	3.2_i	3.2_m
Stolzburg pluton									
MS 2 Trondhjemite	Qtz+Plag+Bt+Mkl +Chl+Ap+Zr+Ttn	26.03089 °S 30.71283 °E	x	x	x	x	x	--	i
MS 14 Trondhjemite	Qtz+Plag+Bt+Mkl +Chl+Ap+Zr+Ttn	25.99689 °S 30.67719 °E	x	x	x	x	x	--	x
MS 15 Trondhjemite	Qtz+Plag+Bt+Mkl +Chl+Ap+Zr+Ttn	26.00331 °S 30.73664 °E	x	x	--	x	x	--	i
MS 24 Trondhjemite	Qtz+Plag+Bt+Mkl +Chl+Ttn+Ap+Zr	26.02475 °S 30.76181 °E	--	--	--	--	--	i	--
MS 36 Tonalite	Qtz+Plag+Bt+Mkl +Chl+Ttn+Ap+Zr	26.03120 °S 30.71247 °E	x	x	x	x	i	--	--
Weergevonden pluton									
MS 25 Diorite	Plag+Qtz+Amph+Bt +Chl+Ttn+Zr+Ap	26.09008 °S 30.73336 °E	--	x	x	x	--	x	i
MS 27 Trondhjemite	Qtz+Plag+Bt+Mkl +Chl+Ap+Zr	26.09836 °S 30.72219 °E	--	--	--	--	x	--	--

[a] : Indicates occurrence of apatite domains from the four age groups described by Mühlberg et al., 2021. See Fig. 2 for individual $^{207}Pb/^{206}Pb$ ages.

[b] : An 'x' marks the occurrence of $^{207}Pb/^{206}Pb$ ages in igneous (i) and metamorphic (m) zircon domains (age data from Mühlberg et al., 2021); an 'i' indicates inferred igneous (inferred from field relationships) and metamorphic (inferred from zircon microtexture) ages for sample without sufficient zircon U-Pb data.

5.3 Samples

5.3.1 Ca. 3.45 Ga TTG rocks

Samples MS 2, 14 and 15 are taken from the Main Trondhjemite (Mühlberg et al., 2021) phase of the Stolzburg Pluton and sample MS 27 from a sheared trondhjemite from the Weergevonden Pluton. The Main Trondhjemite shows, depending on the location, varying degrees of deformation (Moyen et al., 2019), but generally the igneous textures are preserved (Cutts et al., 2015; Mühlberg et al., 2021). The mineral assemblage of the Main Trondhjemite is quartz + plagioclase + biotite + microcline + apatite + zircon ± titanite (Figs. 5.3, 5.13); biotite is sometimes (partially) replaced by chlorite (Fig. 5.3), indicating minor alteration. Microcline occurs mostly as small (ca. x µm), interstitial grains, however one thin section of sample MS 15 contains an aggregate of larger (up to ca. 2 mm) microcline grains (Fig. 5.13). Zircon grains from this phase have been dated to ca. 3.45 Ga (Kamo and Davis, 1994; Lana et al., 2010; Laurent et al., 2020; Mühlberg et al., 2021; Schoene et al., 2008; Wang et al., 2019). A summary of the U-Pb apatite and zircon ages obtained for the studied samples is given in Table 5.1.

Sample MS 36 occurs in the vicinity of sample MS 2 as a ca. 10 cm broad tonalite phase within the Main Trondhjemite; no zircon age is available for this sample, but the oldest group of apatite ages of ca. 3.45 Ga indicates, that it is contemporaneous with the Main Trondhjemite (Mühlberg et al., 2021).

Although titanite occurs in all samples presented here, it is generally rare in the 40+ thin sections of ca. 3.45 Ga TTG samples from the Stolzburg Block that were screened for this study. The thin sections from samples MS 2, MS 14, MS 15 and MS 36 in which titanite grains were found contain enough sufficiently large grains to allow for a representative analysis. Two types of titanite grains occur in the ca. 3.45 Ga samples: large, zoned grains (100s µm in size) and small unzoned grains (≤100 µm in size). The larger titanite grains typically show regular core to rim zoning (Figs. 4 and S.2). Many grains exhibit a fir tree zoning in the core (e.g. Fig. 4b, g, h) and a thin BSE-bright rim overgrown by a darker one (e.g. Fig. 5.2a, g). Some titanite grains also show patchy zoning (e.g. Fig. 5.4b). Major- and trace-element analyses were taken from titanite cores and rims as well as from smaller grains with no identifiable zonation; the spots of analysis are shown in Figures 5.4 and 5.13.

Fig. 5.3. Representative thin section photos showing the typical mineral assemblage for granitoid rocks from the Stolzburg Block. (a+b) ca. 3.45 Ga Main Trondhjemite samples MS 2 and MS 15, respectively, from the Stolzburg Pluton, (c) ca. 3.22 Ga diorite sample MS 25 from the Weergevonden Pluton, (d) ca. 3.45 Ga tonalite phase from the south-western margin of the Stolzburg Pluton. See thin section photos of all analyzed samples in Fig. 5.12.

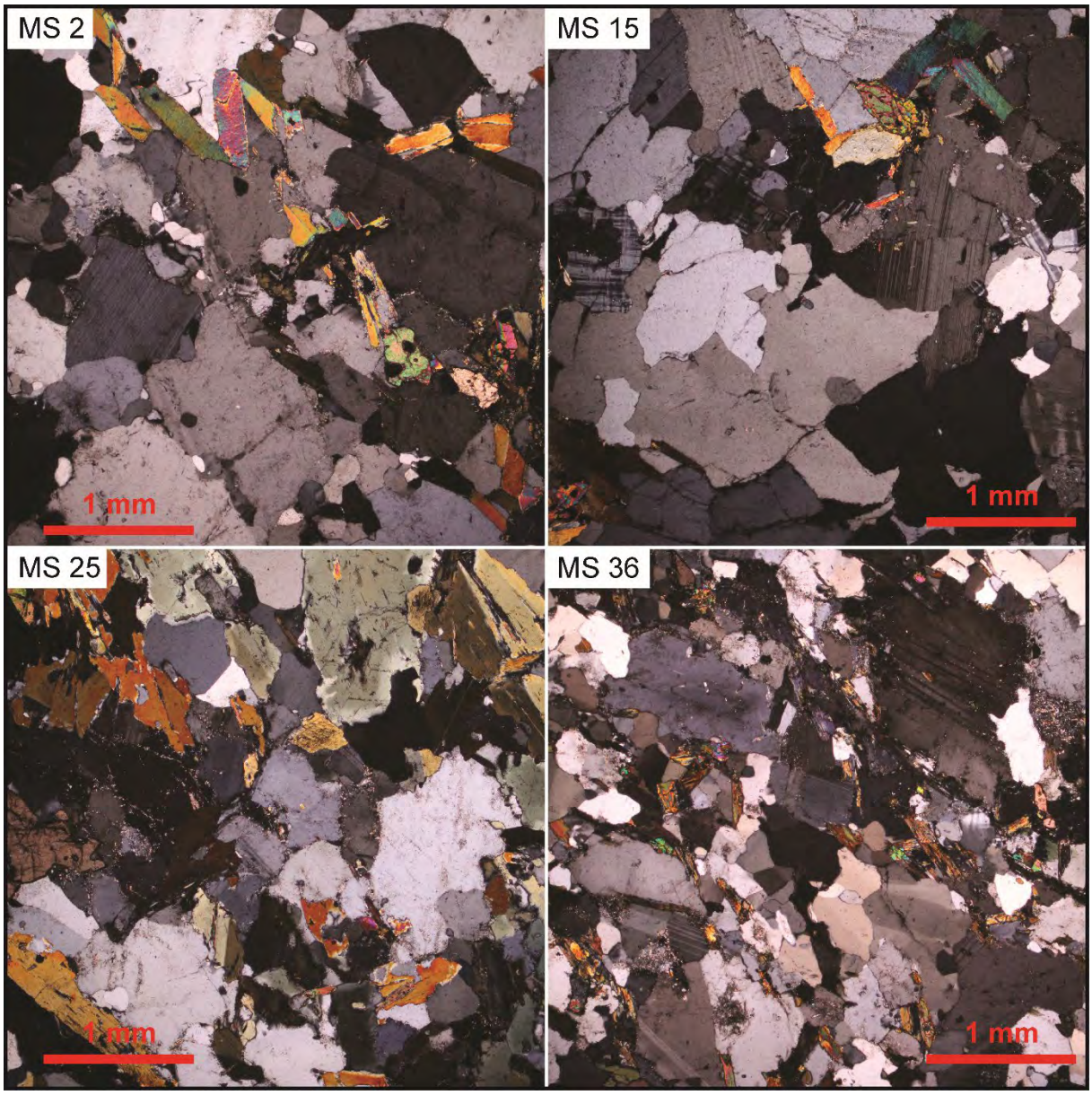

Apatite grains are abundant in the heavy mineral separates from the ca. 3.45 Ga samples. In cathodoluminescence (CL) images, the apatite grains show multiple growth zones. Some zones are idiomorphic, but the majority is xenomorphic and embayed (Fig. 5.14) Grain sizes range typically from 100 to 250 µm. The U-Pb ages obtained for apatite grains from the studied samples fall into four age groups at ca. 3.45, 3.2, 3.1 and 2.8 Ga that are found in all analyzed ca. 3.45 Ga samples (Mühlberg et al., 2021) (Table 5.1). Major- and trace-element and Sr isotope analyses were taken from dated apatite domains as well as from undated domains; the spots of analysis are shown in Figure 5.14.

Zircon grains are common in the analyzed samples and are predominantly opaque brown in color. In the CL images, the zircon grains generally show well preserved igneous textures (Fig. 5.15); the oscillatory zoning is in places recrystallized into broader bands, similar to what has been described by Pidgeon (1992). Inherited cores are rare (Mühlberg et al., 2021). The

igneous zircons are frequently surrounded by featureless metamorphic rims that sometimes protrude into the grain (Fig. 5.15). Major- and trace-element analyses were taken from pristine and recrystallized oscillatory zones as well as from featureless zones and rims; the spots of analysis are shown in Figure 5.15.

5.3.2 Leucocratic dyke sample MS 24

Sample MS 24 was taken from an undeformed, ca. 20 wide fine-grained dyke cutting the Main Trondhjemite on the eastern margin of the Stolzburg Pluton. In hand specimen, the sample is light gray with no visible deformation and titanite grains can be recognized with the naked eye. Sample MS 24 has a trondhjemitic composition (Mühlberg et al., 2021) and its mineral assemblage is quartz + plagioclase + biotite + microcline + apatite + titanite + zircon (Fig. 5.12). Biotite is partially replaced by chlorite; microcline mostly occurs as small (ca. 100 to 200 µm) interstitial grains. The titanite grains in the analyzed thin section are heavily embayed and are large in size (several 100 µm; Fig. 5.4c, d). Sample MS 24 did not yield sufficient zircon grains in the heavy mineral separate to obtain a crystallization age, as is typical for the leucocratic dykes cutting the Main Trondhjemite of the Stolzburg Block (Mühlberg et al., 2021). No apatite grains were analyzed from this sample.

5.3.3 Ca. 3.22 Ga diorite sample MS 25

Diorite sample MS 25 is cutting the Main Trondhjemite of the Weergevonden Pluton (sample MS 26) at a roadcut of the R541 towards Lochiel (Fig. 5.1). It has a dark grey color and titanite grains of ca. 1-2 mm are visible in hand specimen. The main mineral assemblage (Fig. 5.3c) is plagioclase + quartz + amphibole + biotite + chlorite + titanite + zircon + apatite. Titanite grains are ca. 300 to >1000 µm in size with frequent embayment and commonly show sector zoning (Fig. 5.5e+f, Fig. 5.12), one grain displays fir-tree zonation (Fig. 5.4e). Zircon grains have a brown color and are ca. 300 to 800 µm in length; they often have broken terminations and show minor embayment. Zircon grains were dated to ca. 3.22 Ga (Mühlberg et al., 2021; Wang et al., 2020). Apatite grains can be euhedral and anhedral and have a typical size of 100 to 300 µm (Fig. 5.14e). The CL images of apatite grains from sample MS 25 show multiple distinct growth zones, with the inner zones often euhedral, but in some cases also showing different degrees of resorption from rounded terminations to fully rounded zones with embayment (Fig. 9e of Mühlberg et al., 2021). Apatite grains from this sample yield U-Pb ages of ca. 3.2, 3.1 and 2.8 Ga (Mühlberg et al., 2021) (Table 5.1).

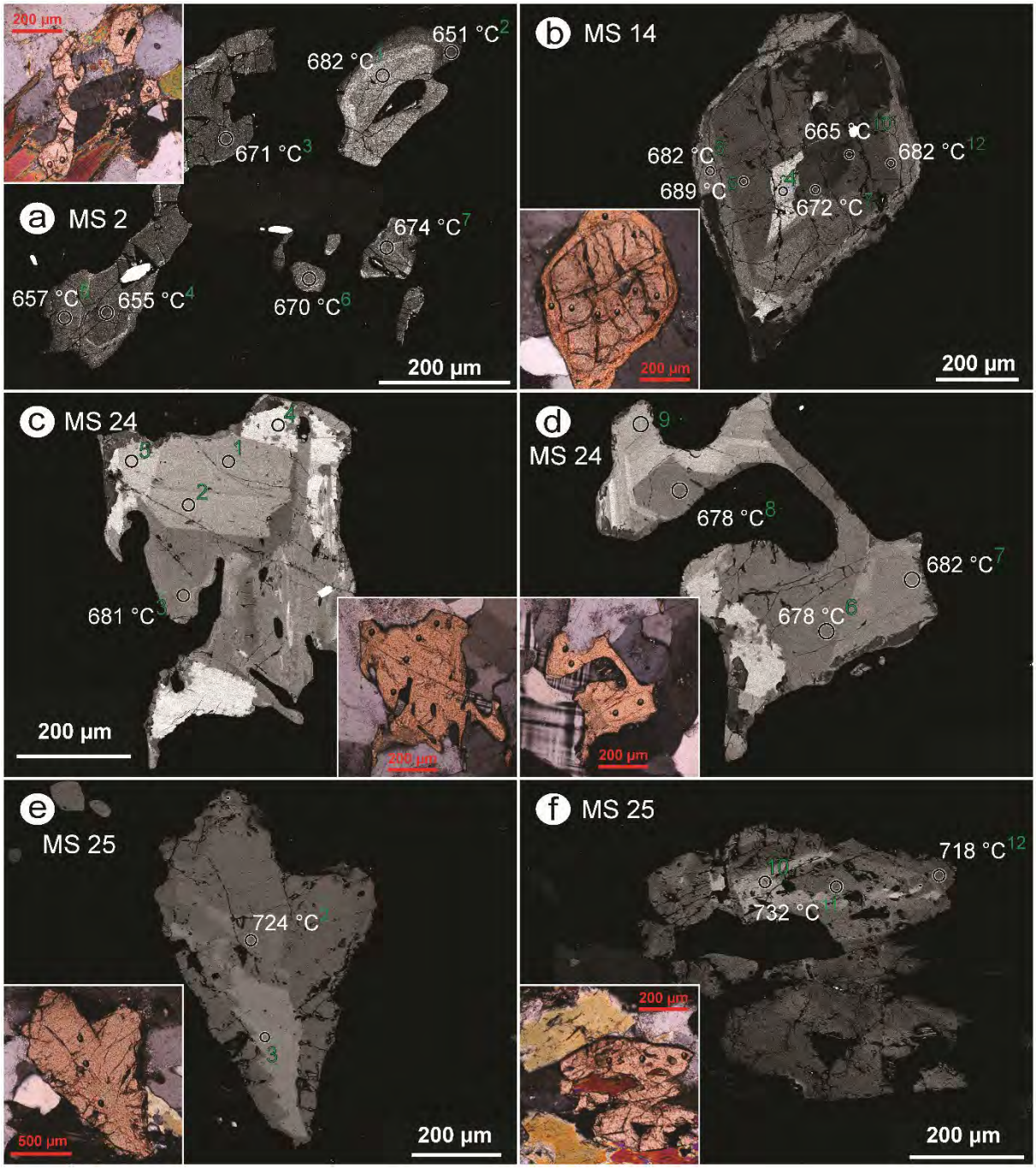

Fig. 5.4. Representative electron and optical (insets; cross-polarized light) microscopy images of titanite grains from granitoid sample MS 2 (a), MS 14 (b), MS 24 (c+d), MS 25 (e+f) and MS 36 (g+h) from the Stolzburg Block. Red and green numerals refer to the spot number of EMPA and LA ICP-MS analyses, respectively (Table 5.5). See Fig. 5.13 for full optical and electron microscopy images of all analyzed titanite grains.

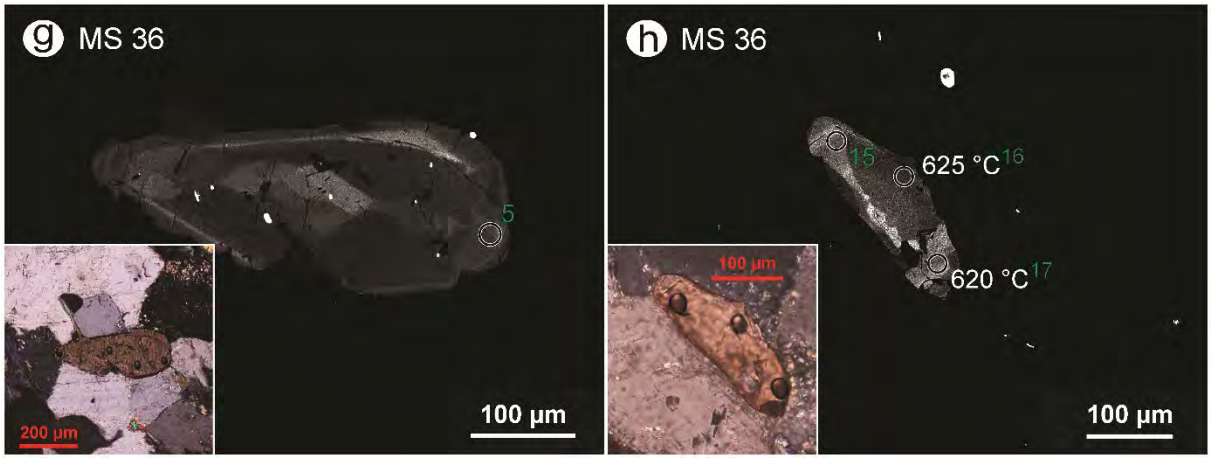

Fig. 5.4, continued.

5.4 Analytical methods

5.4.1 Whole-rock Sr isotope analysis

Whole-rock samples were analyses for their Sr isotopic composition at the University of Cape Town using a NuPlasma HR MC ICP-MS, with the sample being introduced as a solution, obtaining present day 87Sr/86Sr ratio. Reference material JG-2 and NIST987 yield $^{87}Sr/^{86}Sr$ ratios of 0.759423 ± 0.000271 (0.758046 ± 0.000004; Ma et al., 2013) and 0.710255 (0.710250 ± 0.000011; Timm et al., 2016), respectively. Initial Sr ratios were calculated using an in-house spreadsheet and the whole-rock Rb and Sr concentrations and the sample ages published in Mühlberg et al. (2021). Uncertainties on the initial ratios were determined using the uncertainties on the present-day ratios (see Table S.5) and on the whole-rock trace-element analyses (Rb: 2%, Sr: 5%). The whole-rock Sr isotope compositions are given in Table 5.3.

5.4.2 Imaging

Cathodoluminescence (CL) images of apatite and zircon grains were taken at the Central Analytical Facilities (CAF) at Stellenbosch University using a Zeiss Merlin SEM. Beam conditions used for apatite were an accelerating voltage of 20 kV, a beam current of 12 nA at a working distance of 6.1 mm, and for CL images of zircon, an accelerating voltage of 10 kV and a beam current of 12 nA were used at a working distance of 11.3 mm.

Back-scattered electron images of titanite grains were obtained at the University of Clermont-Ferrand in the laboratory Magmas et Volcans (LMV) using a JEOL JSM-5910 LV SEM with an accelerating voltage of 15 kV.

5.4.3 Major-element analyses

Major-element and halogen concentrations of apatite and titanite grains were determined at the University of Clermont-Ferrand in the LMV using a Cameca SX 100 electron microprobe. Apatite grains were analyzed in epoxy mounts with a spot size of 10 µm, an accelerating voltage of 20 kV and a beam current of 10 nA. Titanite grains were analyzed in thin sections with a spot size 1 µm, and accelerating voltage of 20 kV and a beam current of 40 nA. The major-element concentrations as well as detection limits and standard deviations are given in Tables 5.4 (apatite) and 5.5 (titanite).

The major-element compositions of zircon grains were determined at the CAF at Stellenbosch University using a Zeiss EVO MA15 SEM. Full quantitative analyses were obtained using an Oxford Instruments X-Max 20 mm^2 Energy Dispersive X-Ray Spectrometry (EDS) detector and INCA Oxford software. The beam conditions are an accelerating voltage of 20 kV, probe and specimen currents of 1.1 and 19 nA, respectively, and a working distance of 8.5 mm. The results are listed in Table 5.6.

5.3.4 LA ICP-MS analyses

Trace-element concentrations for apatite and titanite grains were determined at the University of Clermont-Ferrand in the LMV using a Thermo Element XR ICP-MS connected to a 193nm Resonetics M-50E laser ablation system. The parameters used are a spot size of 20 µm, a frequency of 2 Hz, fluence of 2.8 Jcm^{-2} and depending on the day of analysis gas flows of 590 and 650 $mlmin^{-1}$ for He and 7.5 and 7 $mlmin^{-1}$ for N_2. Each run lasted 60 s and 30 s of background acquisition. Each sequence was bracketed by two analyses of GSD-1G (Jochum et al., 2005). Internal normalization for LA ICP-MS data was done using ^{43}Ca and data processing was conducted using the GLITTER software (Griffin, 2008). The reference materials Durango apatite (Marks et al., 2012) and Khan titanite (Heaman, 2009) were used for quality control during analysis. The trace-element concentrations as well as their standard deviations and the detection limits are given in Tables 5.4 (apatite) and 5.5 (titanite).

Trace element concentrations in zircon grains mounted in epoxy resin were determined at the CAF at Stellenbosch University using an Agilent 8800 ICP-MS connected to a Resonetics 193nm Excimer laser ablation system. The parameters of analysis are a spot size of 26 µm, a frequency of 7 Hz, fluence of 2.5 Jcm^{-2} and gas flows of 400 mlmin-1 for He, 800 $mlmin^{-1}$ for Ar and 4 $mlmin^{-1}$ for N_2. Each run lasted 30 s and 20 s of background acquisition. Zircon GJ-1 was used as a primary reference material and BCR-2G glass (Jochum et al., 2005) was used for quality control. Data reduction was done using the Iolite software (Paton et al., 2011). Only

data points with stable signal and without spikes were selected to filter for micro-inclusions. The results are given in Table 5.6.

5.3.5 LA-MC-ICP-MS Sr analysis

The Sr isotopic composition of apatite grains was determined at Universidade Federal de Ouro Preto, Brazil, using a ThermoFisher Neptune Plus LA-MC-ICP-MS connected to a 193 nm HelEx Photone Machine laser ablation system, following the methodology proposed by Wilson et al. (2017) and Yang et al. (2014, 2008). The parameters of analysis are a frequency of 6 Hz, fluence of 4 Jcm^{-2} and gas flows of 500 $mlmin^{-1}$ for He, 800 $mlmin^{-1}$ for Ar and 5 $mlmin^{-1}$ for N_2. On the previously dated zones, a variable spot size of ca. 30 to 85 µm was used to accommodate for their varying size, and a spot size of 85 µm was used on apatite grains of unknown age. Each run lasted 60 s and 30 s of background acquisition. The data reduction was performed on an in-house MS Excel spreadsheet modified from Wilson et al. (2017). The raw data for $^{86}Sr/^{87}Sr$ were corrected for isobaric mass interference by ^{84}Kr and ^{86}Kr on ^{84}Sr and ^{86}Sr using a Kr baseline measurement. A NIST 610 glass was used as a primary reference material to determine the $^{87}Rb/^{85}Rb$ mass bias.

Quality control was done using MIR plagioclase (in-house reference material from Dr. A. Gerdes, Frankfurt) and Durango and Madagascar apatite reference materials. Over the course of the analyses, MIR plagioclase yielded an $^{87}Sr/^{86}Sr$ ratio of 0.70303 ± 12 (2SD, n = 19), within uncertainty identical with the published value of 0.703096 ± 70 (2s, Rankenburg et al., 2004). The $^{87}Sr/^{86}Sr$ ratio obtained for Madagascar apatite of 71181 ± 9 (2SD, n = 6) is within uncertainty in agreement with the value of 0.71179 ± 3 (2SD) of Yang et al., (2014), and the $^{87}Sr/^{86}Sr$ ratio obtained for Durango apatite of 0.70632 ± 35 (2SD, n = 7) is within uncertainty in agreement with the published value of 0.706328 ± 23 (2SD, Yang et al., 2014). The Sr isotope systematics of apatite grains are listed in Table 5.8

5.3.6 Thermometry

The Zr-in-titanite and Ti-in-zircon temperatures were calculated using the methods of Hayden et al. (2008) and Ferry and Watson (2007), respectively. Both thermometers require knowledge of the activities of quartz (a_{SiO2}) and rutile (a_{TiO2}), which were obtained using the phase equilibria modeling tool Rcrust (Mayne et al., 2019, 2016) following the methodology described in section 3.6. Calculations were performed assuming closed system crystallization over a pressure-temperature (P-T) range of 550 to 850 °C and 3 to 15 kbar. As all analyzed granitoid samples contain quartz, a_{SiO2} can be assumed to be 1, and this was confirmed by the modeling, which for all samples yielded a_{SiO2} values of 1.00 over the whole modeled P-T range. The calculation

of a_{TiO2} gave values of 0.03 to 1.00 over the modeled P-T range; the a_{TiO2} values for the full P-T range are listed in Table 5.7 and the values used for temperature calculations are outlined in the following. The temperatures are initially calculated using an a_{TiO2} value of 0.5 and are then refined using the values extracted from Rcrust until the calculated $T_{Zr\text{-}in\text{-}titanite}$ / $T_{Ti\text{-}in\text{-}zircon}$ and the temperature corresponding to the used a_{TiO2} value are equal within a reasonable range (± ca. 10 °C). For Zr-in-titanite temperatures, the a_{TiO2} values are in the range of 0.4 to 0.55 for Main Trondhjemite samples MS 2, MS 14 and MS 15, 0.1 for tonalite sample MS 36, 0.6 for trondhjemite dyke sample MS 24 and in the range of 0.6 to 0.9 for diorite sample MS 25. The Zr-in-titanite temperatures are given in Figures 5.4 and 5.13. The uncertainty of the Zr-in-titanite thermometer is given by Hayden et al. (2008) as ca. ± 20 °C. The Ti-in-zircon temperatures are listed in Table 5.2 with the corresponding a_{TiO2} values. Uncertainties on the Ti-in-zircon temperatures have been calculated by propagating the uncertainties on the Ti analyses. Zirconium saturation temperatures were also calculated after Boehnke et al. (2013) in GCDkit (Janoušek et al., 2006) using whole-rock data of Mühlberg et al. (2021) and are listed in Table 5.2.

5.5 Results

5.5.1 Apatite

Major- and trace-element data for apatite grains granitoid rocks from the Stolzburg Block are given in Table 5.4. Apatite grains from the Stolzburg Block are all fluorapatite (F ca. 3.0-4.3 wt. %). In most of the analyzed grains no Cl was detected, only two analyses from sample MS 25 gave Cl concent of ca. 0.03 wt. %. SO_3 concentrations are below detection limits in apatite from sample MS 36; the Trondhjemite samples MS 2, 14 and 15 show SO_3 content from 0.10 to 0.16 wt.% and diorite sample MS 25 shows a larger range of 0.11 to 0.30 wt.%.

In the chondrite-normalized REE diagrams (Fig. 5.5), the general pattern of the studied apatites is a fractionated one, decreasing in enrichment relative to chondrite from La to Lu. In all samples except MS 15, the shapes of the REE patterns are fairly homogenous within a given sample. They all have flat to slightly convex LREE and a slightly positive (samples MS 2, ca. 1.2 to 1.6, and MS 14, ca. 1.4 to 2.1) to slightly negative (samples MS 25, ca. 0.6 to 0.8, and MS 36, ca. 0.7 to 1.2) Eu anomaly. In sample MS 15, two groups of compositions can be distinguished based on their REE patterns. The first group has spectra similar to those of sample MS 25, with $(La/Sm)_N$ values of ca. 1.0 to 1.6 and a negative Eu anomaly (ca. 0.5 to 0.8), while the second group has depleted LREE patterns with lower $(La/Sm)_N$ values (ca. 0.5 to 0.6) and a slightly positive Eu anomaly (ca. 1.3). Ages of the apatites previously published by Mühlberg et al. (2021) obtained on the same zones analyzed in this study are given in

Figure 5.5 and show no correlation between the U-Pb age and the REE contents of the analyzed apatite zone. Generally, no correlation can be seen between the age of an apatite zone and its trace-element composition or the polarity of an Eu anomaly.

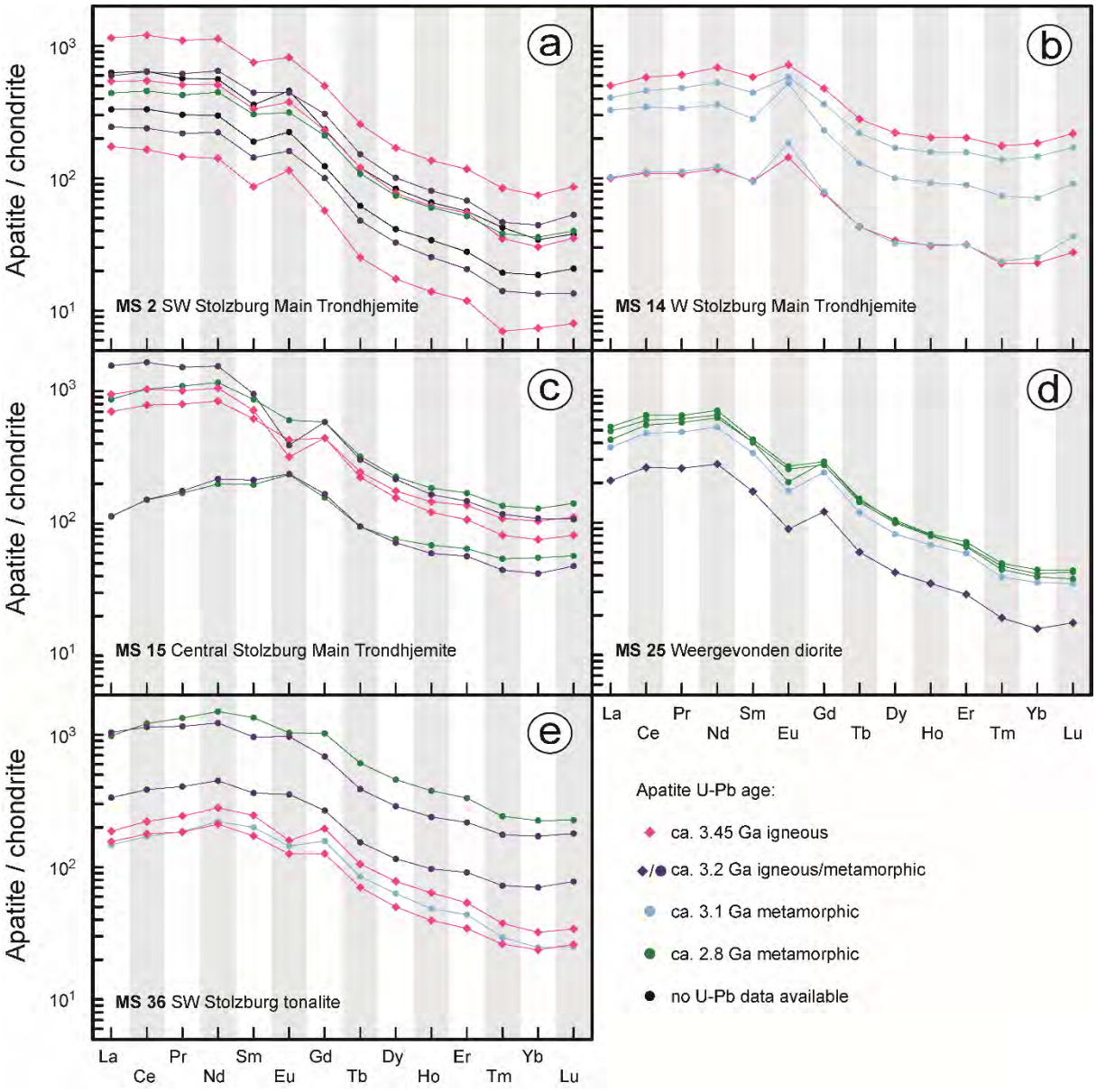

Fig. 5.5. Chondrite-normalized (after McDonough and Sun, 1995) rare-earth-element plots for apatite grains from TTG (a-c, e) and diorite (d) samples from the Stolzburg Block. Uranium-lead age date from Mühlberg et al. (2021).

5.5.2 Titanite

The results of the major- and trace-element analyses of titanite grains from the Stolzburg Block are listed in Table S.2 and shown in Figures 6 and 7. The major- and trace-element characteristics of titanite grains in the different samples are described in the following based on their main lithologies. The Zr concentrations of titanite grains can be used as a thermometer (Hayden et al., 2008). In this study, all zones except Fir-tree features have been used to

calculate temperatures as these features have been shown to be out of equilibrium (see details in Hayden et al., 2008). The Zr-in-titanite thermometer has a minor pressure dependence (Hayden et al., 2008); all temperatures in this section, unless stated otherwise, have been calculated for a pressure of 0.5 GPa.

The major-element concentrations in titanite grains from the Stolzburg Block granitoids are typically ca. 35-38 wt. % TiO2, ca. 30-31 wt. % SiO2, ca. 27.5-29.0 wt. % CaO, ca. 1-3 wt. % Al2O3, ca. 0.5-2.0 wt. % FeO and ca. 0.2-1.0 wt. % F (Table S.2, Fig. 6a+b). Notable is distinction between two types of titanite in sample MS 15, one yielding higher TiO2 concentrations (ca. 36 wt. %) and lower SiO2 (ca. 30 wt. %), CaO (ca. 27.5 wt. %), Al2O3 (ca. 1 wt. %) and F (ca. 0.4-0.6 wt. %) concentrations compared to the second group (TiO2 ca. 35 wt. %, SiO2 ca. 31 wt. %, CaO ca. 28.5-29.0 wt. %, Al2O3 ca. 2.5 wt. %, F ca. 0.8-1.1 wt. %), with both types yielding similar FeO concentrations of ca. 1.5-2.0 wt. %. Furthermore, titanite grains from samples MS 25 and 36 generally show the lowest FeO concentrations (Fig. 6a), though there is significant overlap between sample MS 36 and Main Trondhjemite sample MS 2, which were both taken from the same outcrop; the low FeO concentrations in the titanite grains from the intermediate samples are in contrast to the relatively high whole-rock Fe2O3(t) concentrations of these samples (see inset in Fig. 6a). Sample MS 25 yields the highest TiO2 (ca. 36.5-38 wt. %; Fig. 6a) and the lowest F (ca. 0.2-0.4 wt. %; Fig. 6b) concentrations of the analyzed samples.

Based on the trace-element compositions, several types of titanite can be distinguished. The general REE pattern observed in type 1 and type 2 titanite is fractionated with a convex shape for the LREE and a depleted HREE pattern, decreasing in enrichment relative to chondrite from Gd to Lu (Fig. 7). Type 1 titanite is found in all samples except MS 24. This type of titanite is characterized by high REE enrichment relative to chondrite (∑REE = ca. 3360-18820 ppm in the TTG samples, ca. 1430-10860 ppm in diorite sample MS 25) and by high Th/U ratios of ca. 2.30-4.20, except in tonalite sample MS 36 where type 1 titanite has a Th/U ratio of ca. 0.4-1.6. The polarity and size of the Eu anomaly in type 1 titanite varies from sample to sample, with moderate positive Eu anomalies (ca. 1.9) in titanites from sample MS 2 (Fig. 7a), strong negative Eu anomalies in those from samples MS 14 (ca. 0.5; Fig. 7b) and MS 15 (0.4; Fig. 7c), and moderate negative to positive Eu anomalies in samples MS 25 (ca. 0.8-1.3; Fig. 7e) and MS 36 (ca. 0.8-1.1; Fig. 7f). The Nb/Ta ratios in type 1 titanite are suprachondritic in sample MS 2 (ca. 24-51), subchondritic in samples MS 14 (ca. 6-12) and MS 15 (ca. 10), and sub- to suprachondritic in samples MS 25 (ca. 6-68) and MS 36 (ca. 9-103).

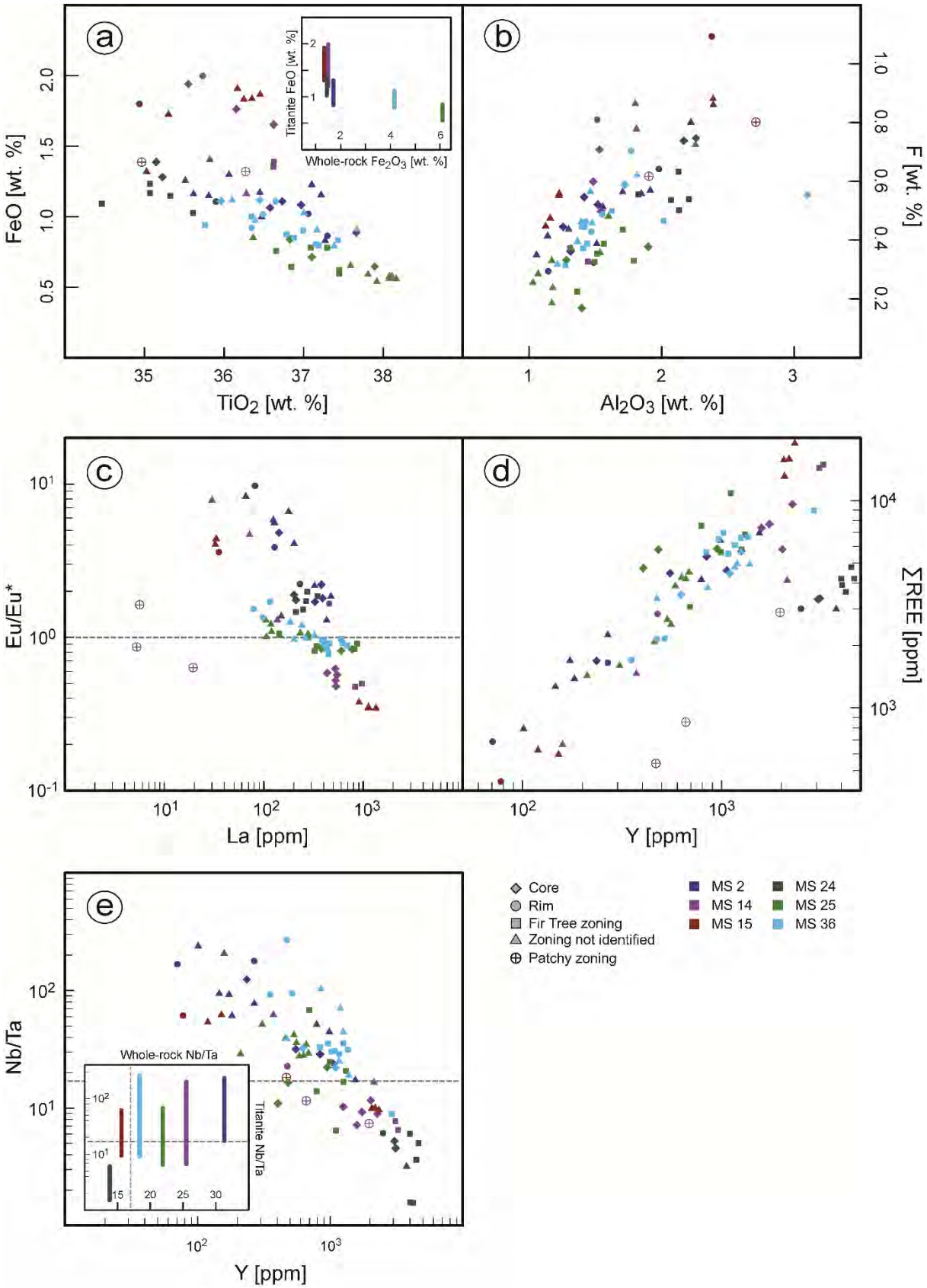

Fig. 5.6. Major- (a+b) and trace-element (c-e) plots for titanite grains from granitoid samples from the Stolzburg Block. Normalization values used for calculation of Eu anomalies are from McDonough and Sun (1995). Whole-rock data used in the insets in (a) and (e) are from Mühlberg et al. (2021).

The Zr concentrations in type 1 titanite are ca. 100-260 ppm for sample MS 2 (TZr-in-titanite ca. 680 ± 20 °C), ca. 250 ppm for sample MS 14 (TZr-in-titanite ca. 690 ± 20 °C), ca. 370 ppm for sample MS 15 (TZr-in-titanite ca. 700 ± 20 °C), ca. 90-190 ppm for sample MS 25 (TZr-in-titanite = 690 ± 20 °C at 0.5 GPa, 720 ± 20 °C at 0.8 GPa) and ca. 190-280 ppm for sample MS 36 (TZr-in-titanite = 620 ± 20 °C).

Type 2 titanite is found in samples MS 2, MS 14, MS 15 and MS 36 and is characterized by a lower enrichment in LREE relative to chondrite (∑REE = ca. 440-2250 ppm) and by low Th/U ratios of ca. 0.19-0.93. In the trondhjemite samples MS 2, MS 14 and MS 15, type 2 titanite shows a strong positive Eu anomaly (ca. 3.9-9.8), while the Eu anomaly is only moderately positive in those from sample MS 36 (ca. 1.3-1.7). The Nb/Ta ratios in type 2 titanite are all suprachondritic, ranging from ca. 54 to 269. The Zr concentrations in this titanite type are ca. 82-104 ppm in sample MS 2 (TZr-in-titanite = 655 ± 20 °C), ca. 95 ppm in sample MS 14 (TZr-in-titanite = 655 ± 20 °C), ca. 70-75 ppm in sample MS 15 (TZr-in-titanite = 645 ± 20 °C) and ca. 95-160 ppm in sample MS 36 (TZr-in-titanite = 600 ± 20 °C).

Type 3 titanite is found in patchy zoned titanite cores from samples MS 14 and MS 15. This type of titanite is characterized by a strongly fractionated LREE pattern with a (La/Sm)N of ca. 0.03-0.06, a flat to slightly fractionated HREE pattern (Fig. 7b, c) and a low Th/U ratio of ca. 0.02-0.04. The Eu anomaly in type 3 titanite is negative in sample MS 14 (ca. 0.7) and positive in sample MS 15 (ca. 1.6). The Nb/Ta ratio is subchondritic in type 3 titanite from

Analyses # MS14-2 and MS14-9 cannot be assigned to any of the three types of titanite. Analysis #MS14-9 lies somewhat in-between type 1 and type 2 titanite, with a depleted LREE pattern compared to type 1 at a (La/Sm)N of ca. 0.19 and with a slightly positive Eu anomaly (ca. 1.3); the HREE pattern of analysis #MS14-9 is similar to that of type 1 titanite. Analysis #MS14-2 has a strongly fractionated LREE pattern at a (La/Sm)N of ca. 2.92, a slightly positive EU anomaly (1.7) and a bulged HREE pattern at a (Dy/Lu)N of ca. 0.40.

In contrast to all other analyzed samples from the Stolzburg Block, titanite grains from trondhjemite dyke sample MS 24 show a ± flat REE pattern with no fractionation from La to Lu (Fig. 7d), with total ∑REE concentrations ranging from ca. 3000 to 4200 ppm. While analyses from fir-tree zoning from sample MS 24 show higher REE concentrations compared to the BSE-dark zones and titanite rims, they all have distinct positive Eu anomalies and form a homogenous group. The Y concentrations in titanite grains from sample MS 24 are generally much higher compared to the other analyzed samples (ca. 2500-4600 ppm vs. typically ca. 100-2000 ppm). On the ∑REE vs. Y plot, the titanite grains from sample MS 24 plot outside of the trend shown by the other samples (Fig. 6d). In contrast to that, the titanite grains from

sample MS 24 follow the general trend in the Nb/Ta vs. Y plot, plotting at the far end of the spectrum, with all analyses showing strongly subchondritic Nb/Ta ratios of ca. 1.5-6 (Fig. 6e). The Th/U ratio of titanite grains from sample MS 24 is ca. 0.27 ± 0.03 (1 SD; n = 4).

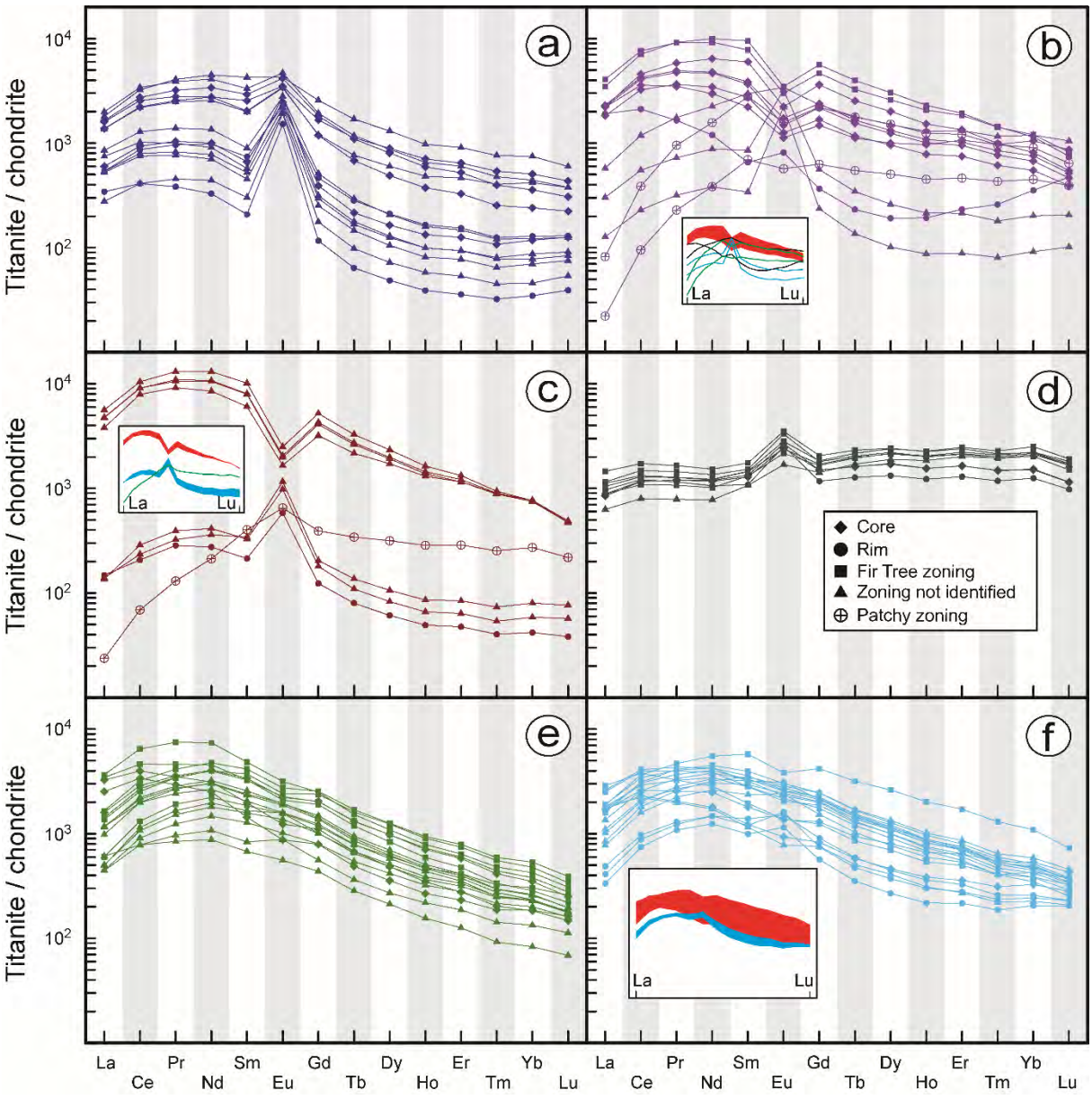

Fig. 5.7. Chondrite-normalized (after McDonough and Sun, 1995) rare-earth-element plots for titanite grains from TTG (a-d, f) samples and diorite sample MS 25 (e) from the Stolzburg Block. The legend in (d) applies to all subfigures. Insets show the different groups of titanite identified in the analyses; see text for details.

5.5.3 Zircon

The major- and trace-element compositions were determined for zircon grains from Stolzburg Block granitoids on which U-Pb analyses had been performed previously (Mühlberg et al., 2021). The major-element compositions were obtained to get the Si content which was used as an internal standard. The data reduction using the Iolite software (Paton et al., 2011) revealed, that many analyses were contaminated by subsurface micro-inclusions within the zircon grains, which will falsify the results as described by Zhong et al. (2018). The contaminated analyses were consequently discarded from the dataset, keeping only analyses that can undoubtedly be considered pure zircon. The results are given in Table 5.6 and are shown in Figure 5.8.

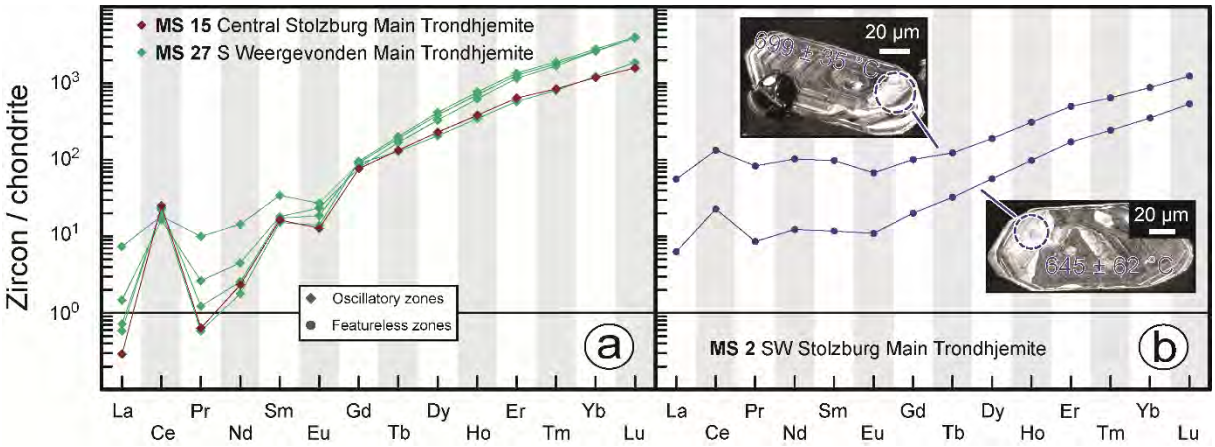

Fig. 5.8. Chondrite-normalized (after McDonough and Sun, 1995) rare-earth element plots for zircon grains from TTG samples from the Stolzburg Block. Legend in (a) applies to both subfigures. See text for discussion.

Analyses from oscillatory zoned igneous zircon grains from samples MS 15 and MS 27 show a fractionated pattern (Sm_N/La_N >10), increasing in enrichment relative to chondrite from La to Lu, with a strong positive Ce anomaly and a negative Eu anomaly (Fig. 5.8a). The titanium concentrations are ca. 1.4 ppm in sample MS 15, with a corresponding Ti-in-zircon temperature of 628 ± 53 °C (propagated uncertainty; a_{TiO2} = 0.60), and ca. 3.8 to 4.5 ppm in zircon grains from sample MS 27, with a corresponding Ti-in-zircon temperature of 852 ± 9 °C (1 SD, n = 4; propagated uncertainty on individual temperatures ~20-30 °C; a_{TiO2} = 0.15). Featureless zircon rims from sample MS 2 yield a flat LREE pattern with a slightly positive Ce anomaly, and a fractionated HREE pattern, increasing in enrichment relative to chondrite from Eu to Lu (Fig. 5.8b). A featureless zircon rim with no indication of contamination (low Sr, Th, U) yields a Ti concentration of ca. 2 ± 0.8 ppm (2σ), with a corresponding Ti-in-zircon temperature of 645 ± 62 °C (propagated uncertainty).

Table 5.2. Titanium-in-zircon and Zr saturation temperatures for trondhjemite samples from the Stolzburg Block.

sample	Ti [ppm]	2σ [ppm]	a_{TiO2}	$T_{Zr\text{-}in\text{-}titanite}$[a] [°C]	2σ [°C]	$T_{Zr\text{-}saturation}$[b]
MS 2 – SW Stolzburg Main Trondhjemite						
MS 2-5	3.0	0.6	0.50	699	35	695
MS 2-9	2.0	0.8	0.65	645	62	695
MS 2 mean				672		
MS 15 – Central Stolzburg Main Trondhjemite						
MS 15-6	1.5	0.5	0.60	628	53	688
MS 27 – S Weergevonden Main Trondhjemite						
MS 27-2	3.8	0.7	0.15	842	24	692
MS 27-3	4.4	0.9	0.15	857	28	692
MS 27-4	4.5	0.8	0.15	862	24	692
MS 27-5	4.0	0.7	0.15	848	24	692
MS 27 mean				852		

[a] : Calculated after Hayden et al. (2008).
[b] : calculated after Boehnke et al. (2013).

5.5.4 Apatite and whole-rock Sr isotope data

Strontium isotope data were determined for apatite grains from two samples from the south-western margin of the Stolzburg Pluton (MS 2, 36) and one from the Weergevonden pluton (MS 25). In the apatite grains, zones dated to ca. 3.45, 3.2, 3.1 and 2.8 Ga were targeted. Additionally, grains of unknown age were also analyzed. The whole-rock Sr isotope data is given in Table 5.3 and the apatite Sr isotope data in Table 5.8. The combined whole-rock and apatite Sr isotope data is shown in Fig. 5.9.

The $^{87}Sr/^{86}Sr$ ratios determined for apatite grains are 0.7002 to 0.7015 for sample MS 2, 0.7014 to 0.7027 for sample MS 25, with an outlier at 0.7042 and 0.7001 to 0.7027 for sample MS 36, with two outliers at 0.6835 and 0.7047. Uncertainties are typically in the range of ca. 0.0001 to 0.0005, with some outliers at ca. 0.002-0.003 and one extreme outlier at ca. 0.03. Apart from the outliers in sample MS 36, all analyses are similar in value and no difference can be seen between the different age groups (Fig. 5.9). The analyses of grains of unknown age – which were taken at a spot size larger than many zones observed in the studied apatite grains and could potentially include mixed analyses – are also within error identical with those of dated apatite grains (Table 5.8). The $^{87}Sr/^{86}Sr$ ratios of apatite are for most data points identical with their respective whole-rock Sr isotopic compositions (Fig. 5.9).

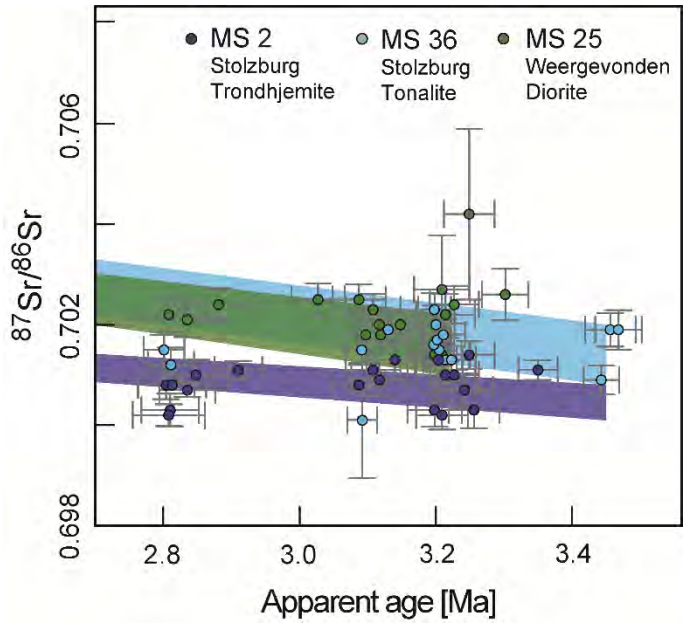

Fig. 5.9. $^{87}Sr/^{86}Sr$ ratios vs age determined for apatite grains from granitoid samples MS 2 (blue), MS 25 (green) and MS 36 (red) from the Stolzburg Block. Shaded areas indicate the evolution of the whole-rock isotope composition, calculated based on the measured present-day $^{87}Sr/^{86}Sr$ ratios and the whole-rock Rb and Sr content (see methods section for details). Age data from Mühlberg et al., 2021.

Table 5.3. Whole-rock Sr isotope systematics for granitoid and mafic schist samples from the Stolzburg Block.

sample	Age[a] [Ga]	Rb[a] [ppm]	Sr[a] [ppm]	$^{87}Sr/^{86}Sr$ (measured)	2σ	$^{87}Sr/^{86}Sr_i$[b] (calculated)	error[b]
MS 2	3.45	54.0	1042	0.703596	0.000012	0.69608	0.00082
MS 25	3.22	34.2	835	0.707141	0.000012	0.70159	0.0006
MS 36	3.45	43.0	949	0.707861	0.000013	0.70129	0.00072

[a] : Ages and whole-rock Rb and Sr concentrations from Mühlberg et al., 2021.
[b] : Initial $^{87}Sr/^{86}Sr$ ratio and uncertainty calculated using the measured present-day ratio and whole-rock Rb and Sr concentrations and their respective uncertainties; calculated for an age of 3445 Ma (ca. 3.45 Ga samples) and 3222 Ma (MS 25), respectively.

5.6 Discussion

5.6.1 Trace-element and isotope characteristics of apatite grains

In the studied granitoid samples, most apatite grains (except for two datapoints in sample MS 15) show similar REE patterns characterized by ± flat LREE patterns that are enriched relative to HREE and by fractionated HREE patterns (Fig. 5). The Eu anomalies are positive in apatite grains from samples MS 2 and MS 14, which also show a strong positive Eu anomaly in their whole-rock composition (ca. 1.76 and 1.64, respectively; Mühlberg et al., 2021) and negative in samples MS 15, MS 25 and MS 36, for which the bulk rock shows a negative (ca. 0.85 for

sample MS 15; Mühlberg et al., 2021) or no Eu anomaly (ca. 1.01 and 1.05 for samples MS 25 and MS 36, respectively; Mühlberg et al., 2021). Texturally, these patterns can be found in both cores and rims of apatite grains (Fig. 5.14). The two “outliers” in sample MS 15 are depleted in REE, particularly in LREE, compared to the other analyses and show a change in polarity of their Eu anomalies from negative to positive (Fig. 5.5c). The general REE pattern observed in the analyzed apatite grains is comparable to those from magmatic apatite from adakite samples and from calc-alkaline arc magmas (Bruand et al., 2020) (Fig. 5.10a). Furthermore, the Sr isotopic composition of apatites from the Stolzburg Block is homogenous and within uncertainties identical with the whole-rock Sr isotopic composition at the time of emplacement (Fig. 5.9). Strontium diffuses more readily in apatite than the REE (Cherniak, 2000; Cherniak and Ryerson, 1993), so if the REE composition had been affected by diffusion after the emplacement, this would also reflect in the Sr isotopic composition. Based on the above, we assume that the REE pattern shown by most apatite analyses represents the primary magmatic apatite REE signature.

The analyzed apatite grains show a wide range of $^{207}Pb/^{206}Pb$ ages, in four distinct groups at ca. 3.45, 3.2, 3.1 and 2.8 Ga (Mühlberg et al., 2021). In contrast to that, the $^{87}Sr/^{86}Sr$ ratios are within error identical for apatite grains of all age groups and are also within error identical with the $^{87}Sr/^{86}Sr$ ratios of their respective host rocks (Fig. 5.9). Furthermore, as outlined above, in all samples except MS 15 the analyzed apatite grains show only primary igneous REE signatures. Diffusion experiments have shown that Pb diffuses more readily in apatite than Sr and especially REE, with closure temperatures for Sr being some 50 °C higher than those for Pb, while those for REE are in the range of 100-200 °C above those for Pb (Cherniak, 2000; Cherniak et al., 1991; Cherniak and Ryerson, 1993), which explains how the U-Pb systematics could have been (partially) reset in the apatite grains, while the REE and Sr isotopes remained mostly unchanged from their primary igneous compositions.

Such a decoupling of U-Pb and REE signatures has been recently described for matrix apatite grains from the ca. 4.0 Ga Acasta gneiss by Antoine et al. (2020), who showed that some of the matrix apatites were able to preserve REE signatures identical to those from primary apatite inclusion protected in zircon grains, while their U-Pb ages were completely reset by a ca. 1.7-1.8 Ga metamorphic event. However, in contrast to the Acasta Gneiss Complex where the matrix apatites were not able to preserve their U-Pb systematics, our samples from the Stolzburg Block still show igneous apatite ages. This can be easily explained by the difference in metamorphic grade between the Acasta Gneiss Complex and the Stolzburg Block. The peak metamorphic conditions reported for the ca. 1.7-1.8 Ga Wopmay orogen which erased the U-Pb systematics in Antoine et al. (2020)’s matrix apatites are ca. 670-745 °C at ca. 5-6 kbar (St-Onge and Davis, 2018) and the rocks of the Acasta Gneiss Complex are highly deformed and

have suffered anatexis (Iizuka et al., 2007). On the other hand, the maximum metamorphic conditions reported for supracrustal lithologies of the Stolzburg Block are ca. 550-650 °C at ca. 7 to >10 kbar for the ca. 3.2 Ga metamorphic event (Cutts et al., 2014; Diener et al., 2005; Dziggel et al., 2002; Kato et al., 2018; Moyen et al., 2006) and the rocks show only minor deformation and no signs of anatexis. The metamorphic REE signature that can only be seen in two analyses from sample MS 15 is likely due to localized higher deformation in this sample as indicated by a more pronounced foliation compared to the other analyzed samples.

Finally, the exceptional preservation of in-situ decoupling between U-Pb and trace elements has been recently reported for titanite (Gordon et al., 2021) and monazite (Weinberg et al., 2020), but from our knowledge has not been clearly reported in matrix apatites so far. This study shows that the exceptional preservation of the Stolzburg Block allows to reconstruct the magmatic and metamorphic histories of the region using apatite crystals only.

Our observations on the U-Pb, Sr and REE characteristics of apatite grains have implications for detrital provenance studies. The decoupling of the U-Pb systematics from the REE and Sr isotope systematics in matrix apatites show, that upmost care needs to be taken when investigating detrital apatite populations. If one were to the Stolzburg Block apatites in a sediment and did trace-element and U-Pb isotope analyses on these apatites, one might come to the conclusion that these apatites record four separate magmatic events, when in they in fact preserved their primary igneous REE composition over multiple heating events that partially reset the U-Pb systematics.

5.6.2 Trace-element characteristics of titanite grains

The titanite analyses obtained in this study generally fall into three groups with unique characteristics that will be discussed in the following.

The first group corresponds to the type 1 titanites of samples MS 2, MS 14, MS 15 and MS 36 and to the titanites of sample MS 25. These titanites all show similar patterns, although with differences in the polarity of the Eu anomaly (positive in sample MS 2, negative in samples MS 14 and MS 15 and slightly positive to slightly negative in samples MS 25 and MS 36). Based on the REE enrichment, the temperature estimates of ca. 680 to 700 °C and the texture (Figs. 5.4, 5.13) we interpret this titanite composition to reflect primary igneous titanite.

Group 2 titanite corresponds to the type 2 titanite of samples MS 2, MS 14 and MS 15, characterized by lower REE enrichment compared to group 1 titanite, distinct positive Eu anomalies and low Th/U ratios, lower than those of group 1 titanite from the same samples. The REE pattern of group 2 titanite bears strong resemblance to hydrothermal metamorphic

titanite previously reported in the literature (Kirkland et al., 2020) (Fig. 5.10b). Low Th/U ratios in titanite have been linked to metamorphic growth, with a suggested threshold of ca. 1.5 discriminating magmatic (>1.5) and metamorphic titanite (<1.5) (Gao et al., 2012). However, this correlation has recently been shown to not always be valid. Recently, Scibiorski et al. (2019) reported metamorphic titanite with Th/U ratios of up to ca. 8.5. Regardless, based on the REE composition, the low Th/U ratios, the temperature estimates of ca. 640 to 650 °C and on the fact that some of the group 2 titanite analyses can be found in the titanite rims, we interpret this composition as metamorphic titanite.

Type 2 titanite of sample MS 36 shows an overall similar REE pattern to group 2 titanite but has a lower Eu anomaly (ca. 1.3 to 1.7) and shows no difference in Th/U ratio compared to type 1 titanite from the same sample. It is likely that the type 2 titanite of sample MS 36 simply represents a later stage of titanite crystallization, when the melt was depleted in REE compared to when the type 1 titanite crystallized and when most if not all plagioclase grains had formed and was not competing for Eu anymore. From a texture point of view, both an interpretation of this type of titanite as metamorphic or as late magmatic are possible, as it is confined to anhedral titanite rims (Fig. 5.13). The temperature estimates for type 2 titanite of sample MS 36 are ca. 600 ± 20 °C, which is within uncertainty identical with the temperature estimate of ca. 620 ± 20 °C for type 1 titanite of the same sample.

Group 3 titanite corresponds to type 3 titanites of samples MS 14 and MS 15 and was only found in three analyses; it is characterized by highly fractionated LREE patterns, increasing in enrichment relative to chondrite from La to Sm, ± flat HREE patterns and very low Th/U ratios of ca. 0.03. Texturally, group 3 titanite is confined to patchy zonation of euhedral grains. This group of titanite likely represents hydrothermal alteration of magmatic titanite.

Titanite grains from sample MS 24 yield a flat REE pattern and elevated Y concentrations that are distinct from the titanites from the other analyzed samples. Based on the microtexture of the titanite grains in sample MS 24, which shows the preservation of oscillatory igneous zoning and also no patchy zoning indicative of alteration in the analyzed zones, we interpret the TE signature of titanites in this sample as primary magmatic. Flat REE patterns in titanite are uncommon, but have been reported for both metamorphic (Storey et al., 2007) and magmatic titanite (Gros et al., 2020). Gros et al. (2020) propose that in their samples early apatite crystallization led to a depletion of the melt in (L)REE, thereby causing the flat, LREE depleted pattern. The apatite saturation temperature calculated for sample MS 24 of. 850 °C is some 170 °C above the Zr-in-titanite temperature of 680 °C, so early apatite crystallization is indeed a possibility for this sample. However, the other analyzed samples from the Stolzburg Block

yield similar apatite saturation in Zr-in-titanite temperatures to sample MS 24, and these samples do not show the same LREE depletion in their titanite grains.

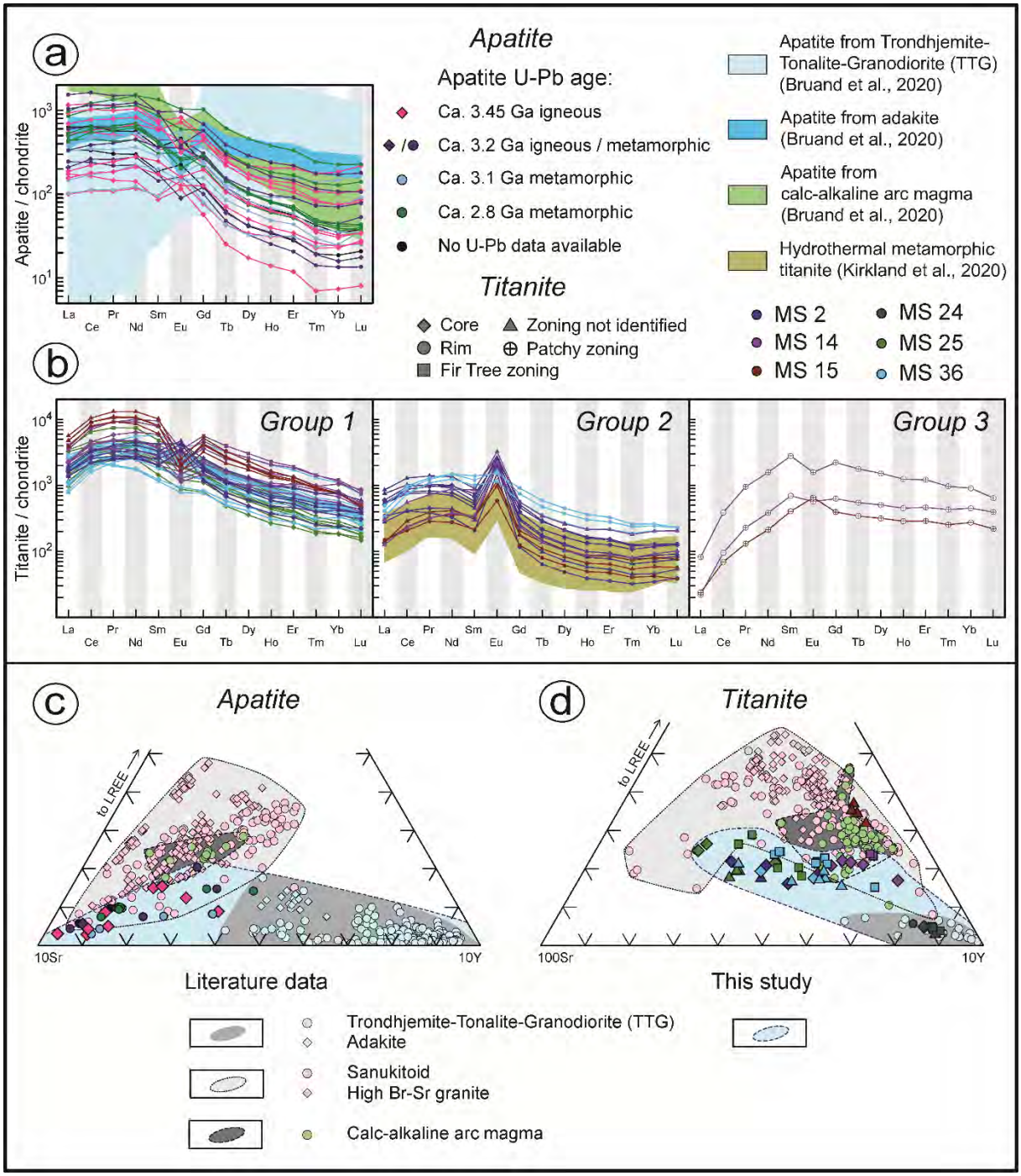

Fig. 5.10. Ternary discrimination diagrams after Bruand et al. (2020) for apatite (a, b) and titanite grains (c) from granitoid samples from the Stolzburg Block. The legend in (a) also applies to the fields in (c).

5.6.3 Trace-element signatures in accessory minerals from TTG

The heavy accessory minerals such as apatite, titanite and zircon are popular in detrital studies. Mineral ages can give a maximum age of deposition of a sedimentary rock and their trace-element composition can give information about the rock types from which the sediments were sourced (Belousova et al., 2002a, 2002b; Bruand et al., 2020, 2014; Joshi et al., 2021) or differentiate igneous and metamorphic growth (Henrichs et al., 2018; Sullivan et al., 2020). In a recent study Bruand et al. (2020) have characterized apatite and titanite analyses from a range of granitoid rocks from the Archean through to the Phanerozoic. Based on their dataset, Bruand et al. (2020) propose ternary discrimination diagrams for apatite (10*Sr – LREE – 10*Y) and titanite (100*Sr – LREE – 10*Y). Figure 10c-e show the data from the Stolzburg Block plotted in these discrimination diagrams.

For apatite, the data from this study plots close to the 10*Sr corner, outside of the defined TTG field in Bruand et al. (2020) (Fig. 5.10c+d). This can be explained by the higher Sr content in bulk rock of the samples from the Stolzburg Block compared to those included in the dataset of Bruand et al. (2020) (ca. 850 vs 300 ppm). Furthermore, the chondrite-normalized REE pattern shown by the apatite grains analyzed in this study is distinct from that of TTG apatites of Bruand et al. (2020). In comparison, the apatites from the Stolzburg Block are more enriched in LREE and more depleted in HREE (Fig. 5.10a). Their pattern is more similar to apatites from adakites and from calc-alkaline arc granites than to those from other TTG samples (Fig. 5.10a). Figure 5.10e shows the group 1 titanites, which we interpret to represent the primary igneous composition, in the 100*Sr-LREE-10*Y diagram of Bruand et al. (2020) with their dataset for comparison. While the titanites from sample MS 24 overlap with their data from TTG titanite, the remaining samples plot at higher Sr and LREE values. The titanite data from this study is still mostly distinct from the sanukitoid and arc granite data of Bruand et al. (2020), but there is some overlap, in particular with the data from sample MS 15.

The findings of this study show that the compositional variety of apatite and titanite grains from TTG samples is larger than previously suggested. Based on the combined data of Bruand et al. (2020) and this study, we propose extended fields for apatites and titanites from TTG rocks which are shown in Figures 5.10c+e.

5.6.4 Duration of the heating event(s)

The Zr-in-titanite temperature estimates for metamorphic titanite analyzed in this study (group 2 titanite, see section 5.6.2) are ca. 640 to 650 °C (ca. 600 °C for type two titanite from sample MS 36, which cannot be confidently interpreted as metamorphic) (Table 5.5). No U-Pb age for metamorphic titanite was obtained as part of this study; however, metamorphic titanite ages of

ca. 3230 Ma have been reported for amphibolite-facies rocks of the Theespruit Formation from the Tjakastad schist belt located between the Stolzburg and Theespruit plutons (Diener et al., 2005) and from greenstone remnants on the south-western edge of the Stolzburg Pluton (Dziggel et al., 2005), and of ca. 3215 Ma for the Doornhoek Pluton in the north-east of the Stolzburg Block (Kamo and Davis, 1994). Furthermore, a Ti-in-zircon temperature of ca. 645 ± 62 °C was obtained for metamorphic zircon from sample MS 2 (Table 5.2). While the age of this zircon itself could not be obtained, it can be inferred that this metamorphic zircon rim grew at ca. 3.2 Ga, based on the age of similar featureless zircon from other samples from the Stolzburg Pluton (Mühlberg et al., 2021).

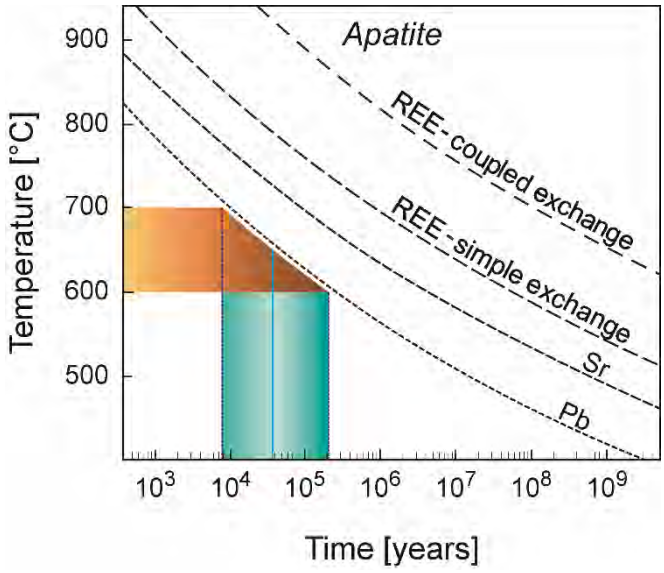

Fig. 5.11. Summary of diffusion constraints for Pb, Sr and REE in apatite (modified after Cherniak et al., 2000). The dashed lines indicate the T-t conditions, above which the original composition of a spherical apatite grain of 250 µm will be lost even at the crystal core. As the apatite grains analyzed in this study typically have a width shorter than 250 µm, these lines represent maximum values. The orange field indicates the metamorphic temperature conditions of ca. 600 to 700 °C recorded by the greenstone (Cutts et al., 2014; Dziggel et al., 2002) and TTG (this study) rocks of the Stolzburg Block. Considering that some apatite grains preserve their ca. 3.45 Ga U-Pb isotopic composition, it can be assumed that the Pb-line was never crossed after TTG emplacement at ca. 3.45 Ga. The blue field shows the inferred duration of heating, ranging from ca. 8000 years at 700 °C to ca. 200,000 years at 600 °C.

The Zr-in-titanite and Ti-in-zircon temperatures obtained for Stolzburg Block granitoids are with uncertainty in agreement with the peak metamorphic grade in the Stolzburg Block of 550-650 °C and 7 to >10 kbar that was achieved at ca. 3230 to 3200 Ma (Cutts et al., 2021, 2014; Diener et al., 2005; Dziggel et al., 2002; Kato et al., 2018; Moyen et al., 2006). The partial preservation of ca. 3.45 Ga U-Pb apatite ages in TTG samples puts an upper limit to the timescale of the ca. 3.2 Ga event. In a ca. 250 µm-sized apatite grains, the original Pb composition in apatite will already be erased during heating to ca. 650 °C for 10^4-10^5 years (Cherniak, 2000). The apatite analyzed in this study are shorter than that with a typical length

of 100 to 200 µm. The fact that both apatite and titanite preserve their primary igneous composition despite being heated to ca. 650 °C indicates, that the duration of the post-3.45 Ga heating events that affected the U-Pb systematics in the Stolzburg Block apatite might have been very short (Fig. 5.11).

While the ca. 3.2 Ga metamorphic event has been well documented in the supracrustal rocks of the Stolzburg Block, the subsequent heating events recorded by the U-Pb systematics of apatite grains are less much well known. Within the Stolzburg Block, these thermal events at ca. 3.1 and 2.8 Ga have so far only been documents in apatite grains (Mühlberg et al., 2021). The time around ca. 3.1 Ga marks the height of granitic (s.l.) intrusions around the BGGT (Kröner et al., 2019). In particular, the Boesmanskop syenite was emplaced on the south-western border of the Stolzburg Pluton at ca. 3105 Ma (Kamo and Davis, 1994), with its “tail” cutting through the south-western part of the Stolzburg Block (Fig. 5.1a). The large Mpuluzi-Piggs Peak batholith was also emplaced directly south of the Stolzburg Block around the same time (Kamo and Davis, 1994; Moyen et al., 2021; Murphy, 2015). These intrusions are within uncertainty overlapping with the ca. 3.1 Ga age group shown by some apatite grains and have likely provided the heat to facilitate Pb diffusion in some apatite grains. However, the exact conditions of the ca. 3.1 Ga heating remain obscure and can only be speculated upon. On the other hand, the ca. 2.8 Ga event has – apart from the U-Pb apatite ages reported by Mühlberg et al. (2021) – not yet been documented in the published geochronological record of the Stolzburg Block and the BGGT as a whole. The U-Pb and trace-element data from apatite grains from the Stolzburg Block show that the conditions were such that not only were the U-Pb systematics affected in all studied samples, but also the REE chemistry in sample MS 15 got partially impacted (Fig. 5.5). But, unlike the ca. 3.1 Ga heating event, there are no reported intrusions of a similar age that could have provided the necessary heat. Hence the cause and conditions of the ca. 2.8 Ga event remain obscure.

5.7 Summary and conclusion

- Combined U-Pb, Sr and REE analyses of matrix apatites show de-coupling of U-Pb, which has been reset during multiple heating events, while Sr isotopes and REE preserve primary igneous composition.

- Preservation of igneous signatures combined with apparent metamorphic temperature of ca. 650 °C indicates very short-lived heating event.

- This short timescale is incompatible with the long-lived radiogenic heating and partial melting of TTG plutons evoked in the partial convective overturn model.

- Instead, we propose that the Stolzburg Block was buried and rapidly exhumed along the Komati fault in a compressional tectonic setting.

Acknowledgments

This research was supported by NRF funding to GS via the SARChI program. The authors thank Jean-Marc Hénot for assistance with the SEM and Jean-Luc Devidal for assistance with the microprobe and LA ICP-MS (both LMV), Madelaine Frazenburg for assistance with SEM major-element analyses of zircon grains and Riana Rossouw for conducting LA ICP-MS trace-element analyses of zircon grains (both CAF Stellenbosch), and Cristiano Lana (UFOP) for providing Sr analyses of apatite. This research was carried out as part of the French-South African collaboration IPR BuCoMO, a collaborative research project funded by the CNRS and the NRF. This is BuCoMO contribution A14. The authors acknowledge financial support from LabEx ClerVolc (ANR-10-LABX-0006).

References

Allwood, A.C., Walter, M.R., Kamber, B.S., Marshall, C.P., Burch, I.W., 2006. Stromatolite reef from the Early Archaean era of Australia. Nature 441, 714–718. https://doi.org/10.1038/nature04764

Anhaeusser, C.R., Robb, L.J., Viljoen, M.J., 1981. Provisional geological map of the Barberton Greenstone Belt and surrounding granitic terrane.

Antoine, C., Bruand, E., Guitreau, M., Devidal, J.L., 2020. Understanding Preservation of Primary Signatures in Apatite by Comparing Matrix and Zircon-Hosted Crystals From the Eoarchean Acasta Gneiss Complex (Canada). Geochemistry, Geophys. Geosystems 21. https://doi.org/10.1029/2020GC008923

Armstrong, R.A., Compston, W., de Wit, M.J., Williams, I.S., 1990. The stratigraphy of the 3.5-3.2 Ga Barberton Greenstone Belt revisited: a single zircon ion microprobe study. Earth Planet. Sci. Lett. 101, 90–106. https://doi.org/10.1016/0012-821X(90)90127-J

Belousova, E.A., Griffin, W.L., O'Reilly, S.Y., Fisher, N.I., 2002a. Apatite as an indicator mineral for mineral exploration: Trace-element compositions and their relationship to host rock type. J. Geochemical Explor. 76, 45–69. https://doi.org/10.1016/S0375-6742(02)00204-2

Belousova, E.A., Griffin, W.L., O'Reilly, S.Y., Fisher, N.I., 2002b. Igneous zircon: Trace element composition as an indicator of source rock type. Contrib. to Mineral. Petrol. 143, 602–622. https://doi.org/10.1007/s00410-002-0364-7

Boehnke, P., Watson, E.B., Trail, D., Harrison, T.M., Schmitt, A.K., 2013. Zircon saturation re-revisited. Chem. Geol. 351, 324–334. https://doi.org/10.1016/j.chemgeo.2013.05.028

Bruand, E., Fowler, M., Storey, C., Laurent, O., Antoine, C., Guitreau, M., Heilimo, E., Nebel, O., 2020. Accessory mineral constraints on crustal evolution: Elemental fingerprints for magma discrimination. Geochemical Perspect. Lett. 13, 7–12. https://doi.org/10.7185/geochemlet.2006

Bruand, E., Storey, C., Fowler, M., 2014. Accessory mineral chemistry of high Ba-Sr granites from Northern Scotland: Constraints on petrogenesis and records of whole-rock Signature. J. Petrol. 55, 1619–1651. https://doi.org/10.1093/petrology/egu037

Byerly, G.R., Lowe, D.R., Heubeck, C., 2019. Geologic Evolution of the Barberton Greenstone Belt - A Unique Record of Crustal Development, Surface Processes, and Early Life 3.55-3.20 Ga, in: Van Kranendonk, M.J., Bennett, V.C., Hoffmann, J.E. (Eds.), Earth's Oldest Rocks. pp. 569–613.

Chamberlain, K.R., Bowring, S.A., 2000. Apatite – feldspar U – Pb thermochronometer : a reliable , mid-range (~ 450°C), diffusion-controlled system. Chem. Geol. 172, 173–200.

Cherniak, D.J., 2000. Rare earth element diffusion in apatite. Geochim. Cosmochim. Acta 64, 3871–3885. https://doi.org/10.1016/S0016-7037(00)00467-1

Cherniak, D.J., Lanford, W.A., Ryerson, F.J., 1991. Lead diffusion in apatite and zircon using ion implantation and Rutherford Backscattering techniques. Geochim. Cosmochim. Acta 55, 1663–1673. https://doi.org/10.1016/0016-7037(91)90137-T

Cherniak, D.J., Ryerson, F.J., 1993. A study of strontium diffusion in apatite using Rutherford backscattering spectroscopy and ion implantation. Geochim. Cosmochim. Acta 57, 4653–4662. https://doi.org/10.1016/0016-7037(93)90190-8

Chowdhury, P., Mulder, J.A., Cawood, P.A., Bhattacharjee, S., Roy, S., Wainwright, A.N., Nebel, O., Mukherjee, S., 2021. Magmatic thickening of crust in non–plate tectonic settings initiated the subaerial rise of Earth's first continents 3.3 to 3.2 billion years ago. Proc. Natl. Acad. Sci. 118, e2105746118. https://doi.org/10.1073/pnas.2105746118

Clemens, J.D., Belcher, R.W., Kisters, A.F.M., 2010. The Heerenveen Batholith , Barberton Mountain Land , South Africa : Mesoarchaean , Potassic , Felsic Magmas Formed by Melting of an Ancient Subduction Complex 0, 1–22. https://doi.org/10.1093/petrology/egq014

Cutts, K.A., Maneiro, K.A., Stevens, G., Baxter, E.F., 2021. Metamorphic evolution for the Inyoni shear zone: Investigating the geodynamic evolution of a 3.20 Ga terrane boundary in the Barberton granitoid greenstone terrane, South Africa. South African J. Geol. 124, 163–180. https://doi.org/10.25131/sajg.124.0009

Cutts, K.A., Stevens, G., Hoffmann, J.E., Buick, I.S., Frei, D., Münker, C., 2014. Paleo- to Mesoarchean polymetamorphism in the Barberton Granite- Greenstone Belt , South Africa : Constraints from U-Pb monazite and Lu- Hf garnet geochronology on the tectonic processes that shaped the belt 251–270. https://doi.org/10.1130/B30807.1

Cutts, K.A., Stevens, G., Kisters, A., 2015. Reply to " Paleo- to Mesoarchean polymetamorphism in the Barberton granite-greenstone belt , South Africa : Constraints from U-Pb monazite and Lu-Hf garnet geochronology on the tectonic processes that shaped the belt : Discussion " by M . Brown 1558–1563. https://doi.org/10.1130/B31304.1

De Ronde, C.E.J., Kamo, S.L., 2000. An Archaean arc-arc collisional event: a short-lived (ca 3 Myr) episode, Weltevreden area, Barberton greenstone belt, South Africa. J. African Earth Sci. 30, 219–248.

Diener, J.F.A., Stevens, G., Kisters, A.F.M., Poujol, M., 2005. Metamorphism and exhumation of the basal parts of the Barberton greenstone belt , South Africa : Constraining the rates of Mesoarchaean tectonism 143, 87–112.

https://doi.org/10.1016/j.precamres.2005.10.001

Dziggel, A., Armstrong, R.A., Stevens, G., Nasdala, L., 2005. Growth of zircon and titanite during metamorphism in the granitoid-gneiss terrane south of the Barberton greenstone belt, South Africa. Mineral. Mag. 69, 1019–1036.

Dziggel, A., Stevens, G., Poujol, M., Anhaeusser, C.R., Armstrong, R.A., 2002. Metamorphism of the granite-greenstone terrane south of the Barberton greenstone belt, South Africa: An insight into the tectono-thermal evolution of the “lower” portions of the Onverwacht Group. Precambrian Res. 114, 221–247. https://doi.org/10.1016/S0301-9268(01)00225-X

Ferry, J.M., Watson, E.B., 2007. New thermodynamic models and revised calibrations for the Ti-in-zircon and Zr-in-rutile thermometers. Contrib. to Mineral. Petrol. 154, 429–437. https://doi.org/10.1007/s00410-007-0201-0

Fisher, C.M., Bauer, A.M., Luo, Y., Sarkar, C., Hanchar, J.M., Vervoort, J.D., Tapster, S.R., Horstwood, M., Pearson, D.G., 2020a. Laser ablation split-stream analysis of the Sm-Nd and U-Pb isotope compositions of monazite, titanite, and apatite – Improvements, potential reference materials, and application to the Archean Saglek Block gneisses. Chem. Geol. 539. https://doi.org/10.1016/j.chemgeo.2020.119493

Fisher, C.M., Bauer, A.M., Vervoort, J.D., 2020b. Disturbances in the Sm–Nd isotope system of the Acasta Gneiss Complex—Implications for the Nd isotope record of the early Earth. Earth Planet. Sci. Lett. 530, 115900. https://doi.org/10.1016/j.epsl.2019.115900

François, C., Philippot, P., Rey, P., Rubatto, D., 2014. Burial and exhumation during Archean sagduction in the East Pilbara Granite-Greenstone Terrane. Earth Planet. Sci. Lett. 396, 235–251. https://doi.org/10.1016/j.epsl.2014.04.025

Fu, B., Page, F.Z., Cavosie, A.J., Fournelle, J., Kita, N.T., Lackey, J.S., Wilde, S.A., Valley, J.W., 2008. Ti-in-zircon thermometry: Applications and limitations. Contrib. to Mineral. Petrol. 156, 197–215. https://doi.org/10.1007/s00410-008-0281-5

Furnes, H., Dilek, Y., De Wit, M., 2015. Precambrian greenstone sequences represent different ophiolite types. Gondwana Res. 27, 649–685. https://doi.org/10.1016/j.gr.2013.06.004

Gao, X.Y., Zheng, Y.F., Chen, Y.X., Guo, J., 2012. Geochemical and U-Pb age constraints on the occurrence of polygenetic titanites in UHP metagranite in the Dabie orogen. Lithos 136–139, 93–108. https://doi.org/10.1016/j.lithos.2011.03.020

Garber, J.M., Hacker, B.R., Kylander-Clark, A.R.C., Stearns, M., Seward, G., 2017. Controls on trace element uptake in metamorphic titanite: Implications for petrochronology. J. Petrol. 58, 1031–1057. https://doi.org/10.1093/petrology/egx046

Gordon, S.M., Kirkland, C.L., Reddy, S.M., Blatchford, H.J., Whitney, D.L., Teyssier, C., Evans, N.J., McDonald, B.J., 2021. Deformation-enhanced recrystallization of titanite drives decoupling between U-Pb and trace elements. Earth Planet. Sci. Lett. 560, 116810. https://doi.org/10.1016/j.epsl.2021.116810

Griffin, W.L., 2008. GLITTER: data reduction software for laser ablation ICP-MS. Laser Ablation ICP-MS Earth Sci. Curr. Pract. Outst. issues 308–311.

Gros, K., Słaby, E., Birski, Ł., Kozub-Budzyń, G., Sláma, J., 2020. Geochemical evolution of a composite pluton: insight from major and trace element chemistry of titanite. Mineral. Petrol. 114, 375–401. https://doi.org/10.1007/s00710-020-00715-x

Hammerli, J., Kemp, A.I.S., Whitehouse, M.J., 2019. In situ trace element and Sm-Nd isotope analysis of accessory minerals in an Eoarchean tonalitic gneiss from Greenland: Implications for Hf and Nd isotope decoupling in Earth’s ancient rocks. Chem. Geol. 524,

394–405. https://doi.org/10.1016/j.chemgeo.2019.06.025

Hayden, L.A., Watson, E.B., Wark, D.A., 2008. A thermobarometer for sphene (titanite). Contrib. to Mineral. Petrol. 155, 529–540. https://doi.org/10.1007/s00410-007-0256-y

Heaman, L.M., 2009. The application of U-Pb geochronology to mafic, ultramafic and alkaline rocks: An evaluation of three mineral standards. Chem. Geol. 261, 43–52. https://doi.org/10.1016/j.chemgeo.2008.10.021

Henrichs, I.A., O'Sullivan, G., Chew, D.M., Mark, C., Babechuk, M.G., McKenna, C., Emo, R., 2018. The trace element and U-Pb systematics of metamorphic apatite. Chem. Geol. 483, 218–238. https://doi.org/10.1016/j.chemgeo.2017.12.031

Hickman-Lewis, K., Cavalazzi, B., Foucher, F., Westall, F., 2018. Most ancient evidence for life in the Barberton greenstone belt: Microbial mats and biofabrics of the ~3.47 Ga Middle Marker horizon. Precambrian Res. 312, 45–67. https://doi.org/10.1016/j.precamres.2018.04.007

Homann, M., 2019. Earliest life on Earth: Evidence from the Barberton Greenstone Belt, South Africa. Earth-Science Rev. 196, 102888. https://doi.org/10.1016/j.earscirev.2019.102888

Hoskin, P.W.O., 2005. Trace-element composition of hydrothermal zircon and the alteration of Hadean zircon from the Jack Hills, Australia. Geochim. Cosmochim. Acta 69, 637–648. https://doi.org/10.1016/j.gca.2004.07.006

Hoskin, P.W.O., Kinny, P.D., Wyborn, D., Chappell, B.W., 2000. Identifying accessory mineral saturation during differentiation in granitoid magmas: An integrated approach. J. Petrol. 41, 1365–1396. https://doi.org/10.1093/petrology/41.9.1365

Iizuka, T., Komiya, T., Ueno, Y., Katayama, I., Uehara, Y., Maruyama, S., Hirata, T., Johnson, S.P., Dunkley, D.J., 2007. Geology and zircon geochronology of the Acasta Gneiss Complex, northwestern Canada: New constraints on its tectonothermal history. Precambrian Res. 153, 179–208. https://doi.org/10.1016/j.precamres.2006.11.017

Iizuka, T., Nebel, O., McCulloch, M.T., 2011. Tracing the provenance and recrystallization processes of the Earth's oldest detritus at Mt. Narryer and Jack Hills, Western Australia: An in situ Sm-Nd isotopic study of monazite. Earth Planet. Sci. Lett. 308, 350–358. https://doi.org/10.1016/j.epsl.2011.06.006

Janoušek, V., Farrow, C.M., Erban, V., 2006. Interpretation of whole-rock geochemical data in igneous geochemistry: Introducing Geochemical Data Toolkit (GCDkit). J. Petrol. 47, 1255–1259. https://doi.org/10.1093/petrology/egl013

Jochum, K.P., Willbold, M., Raczek, I., Stoll, B., Herwig, K., 2005. Chemical characterisation of the USGS reference glasses GSA-1G, GSC-1G, GSD-1G, GSE-1G, BCR-2G, BHVO-2G and BIR-1G using EPMA, ID-TIMS, ID-ICP-MS and LA-ICP-MS. Geostand. Geoanalytical Res. 29, 285–302. https://doi.org/10.1111/j.1751-908x.2005.tb00901.x

Joshi, K.B., Banerji, U.S., Dubey, C.P., Oliveira, E.P., 2021. Heavy minerals in provenance studies: an overview. Arab. J. Geosci. 14. https://doi.org/10.1007/s12517-021-07687-y

Kamo, S.L., Davis, D.W., 1994. Reassessment of Archean crustal development in the Barberton Mountain Land, South Africa, based on U-Pb dating. Tectonics 13, 167–192.

Kato, D., Aoki, K., Komiya, T., Yamamoto, S., Sawaki, Y., Asanuma, H., Sato, T., Tsuchiya, Y., Shozugawa, K., Matsuo, M., Windley, B.F., 2018. Constraints on the P–T conditions of high-pressure metamorphic rocks from the Inyoni shear zone in the mid-Archean Barberton Greenstone Belt, South Africa. Precambrian Res. 315, 1–18. https://doi.org/10.1016/j.precamres.2018.06.018

Kirkland, C.L., Hollis, J., Dani, M., Petersen, J., Evans, N.J., Mcdonald, B.J., 2017. Apatite and titanite from the Karrat Group , Greenland ; implications for charting the thermal evolution of crust from the U-Pb geochronology of common Pb bearing phases 300, 107–120. https://doi.org/10.1016/j.precamres.2017.07.033

Kirkland, C.L., Yakymchuk, C., Gardiner, N.J., Szilas, K., Hollis, J., Olierook, H., Steenfelt, A., 2020. Titanite petrochronology linked to phase equilibrium modelling constrains tectono-thermal events in the Akia Terrane, West Greenland. Chem. Geol. 536. https://doi.org/10.1016/j.chemgeo.2020.119467

Kisters, A.F.M., Stevens, G., Dziggel, A., Armstrong, R.A., 2003. Extensional detachment faulting and core-complex formation in the southern Barberton granite-greenstone terrain, South Africa: Evidence for a 3.2 Ga orogenic collapse. Precambrian Res. https://doi.org/10.1016/j.precamres.2003.08.002

Kohn, M.J., 2017. Titanite Petrochronology. Rev. Mineral. Geochemistry 83, 419–441. https://doi.org/10.2138/rmg.2017.83.13

Kröner, A., Anhaeusser, C.R., Hoffmann, J.E., Wong, J., Geng, H., Hegner, E., Xie, H., Yang, J., Liu, D., 2016. Chronology of the oldest supracrustal sequences in the Palaeoarchaean Barberton Greenstone Belt, South Africa and Swaziland. Precambrian Res. 279, 123–143. https://doi.org/10.1016/J.PRECAMRES.2016.04.007

Kröner, A., Hegner, E., Wendt, J.I., Byerly, G.R., 1996. The oldest part of the Barberton granitoid-greenstone terrain, South Africa: Evidence for crust formation between 3.5 and 3.7 Ga. Precambrian Res. 78, 105–124. https://doi.org/10.1016/0301-9268(95)00072-0

Kröner, A., Hoffmann, J.E., Wong, J.M., Geng, H., 2019. Archaean Crystalline Rocks of the Eastern Kaapvaal Craton.

Lana, C., Kisters, A., Stevens, G., 2010. Exhumation of Mesoarchean TTG gneisses from the middle crust: Insights from the Steynsdorp core complex, Barberton granitoid-greenstone terrain, South Africa. Bull. Geol. Soc. Am. 122, 183–197. https://doi.org/10.1130/B26580.1

Laurent, O., Björnsen, J., Wotzlaw, J.F., Bretscher, S., Pimenta Silva, M., Moyen, J.F., Ulmer, P., Bachmann, O., 2020. Earth's earliest granitoids are crystal-rich magma reservoirs tapped by silicic eruptions. Nat. Geosci. https://doi.org/10.1038/s41561-019-0520-6

Ma, J.L., Wei, G.J., Liu, Y., Ren, Z.Y., Xu, Y.G., Yang, Y.H., 2013. Precise measurement of stable (δ88/86Sr) and radiogenic (87Sr/86Sr) strontium isotope ratios in geological standard reference materials using MC-ICP-MS. Chinese Sci. Bull. 58, 3111–3118. https://doi.org/10.1007/s11434-013-5803-5

Mayne, M.J., Moyen, J.F., Stevens, G., Kaislaniemi, L., 2016. Rcrust: a tool for calculating path-dependent open system processes and application to melt loss. J. Metamorph. Geol. 34, 663–682. https://doi.org/10.1111/jmg.12199

Mayne, M.J., Stevens, G., Moyen, J.-F., Johnson, T., 2019. Performing process-oriented investigations involving mass transfer using Rcrust: a new phase equilibrium modelling tool. Geol. Soc. London, Spec. Publ. SP491-2018–85. https://doi.org/10.1144/sp491-2018-85

McDonough, W.F., Sun, S. s., 1995. The composition of the Earth. Chem. Geol. 120, 223–253. https://doi.org/10.1016/0009-2541(94)00140-4

Moyen, J.-F., Stevens, G., Kisters, A.F.M., Belcher, R.W., Lemirre, B., 2019. TTG Plutons of the Barberton Granitoid-Greenstone Terrain, South Africa, in: Van Kranendonk, M.J., Bennett, V.C., Hoffmann, J.E. (Eds.), Earth's Oldest Rocks. pp. 615–653.

Moyen, J.F., Laurent, O., 2018. Archaean tectonic systems: A view from igneous rocks. Lithos. https://doi.org/10.1016/j.lithos.2017.11.038

Moyen, J.F., Stevens, G., Kisters, A.F.M., 2006. Record of mid-Archaean subduction from metamorphism in the Barberton terrain , South Africa. Nature 442, 559–562. https://doi.org/10.1038/nature04972

Moyen, J.F., Zeh, A., Cuney, M., Dziggel, A., Carrouée, S., 2021. The multiple ways of recycling Archaean crust: A case study from the ca. 3.1 Ga granitoids from the Barberton Greenstone Belt, South Africa. Precambrian Res. 353, 105998. https://doi.org/10.1016/j.precamres.2020.105998

Mühlberg, M., Stevens, G., Moyen, J.F., Kisters, A.F.M., Lana, C., 2021. Thermal evolution of the Stolzburg Block, Barberton granitoid-greenstone terrain, South Africa: Implications for Paleoarchean tectonic processes. Precambrian Res. 359, 106082. https://doi.org/10.1016/j.precamres.2020.106082

Murphy, R., 2015. Stabilizing a Craton: The Origin and Emplacment of the 3.1 Ga Mpuluzi Batholith. Maquarie University.

Paton, C., Hellstrom, J., Paul, B., Woodhead, J., Hergt, J., 2011. Iolite: Freeware for the visualisation and processing of mass spectrometric data. J. Anal. At. Spectrom. 26, 2508–2518. https://doi.org/10.1039/c1ja10172b

Pidgeon, R.T., 1992. Recrystallisation of oscillatory zoned zircon: some geochronological and petrological implications. Contrib. to Mineral. Petrol. 110, 463–472. https://doi.org/10.1007/BF00344081

Rankenburg, K., Lassiter, J.C., Brey, G., 2004. Origin of megacrysts in volcanic rocks of the Cameroon volcanic chain - Constraints on magma genesis and crustal contamination. Contrib. to Mineral. Petrol. 147, 129–144. https://doi.org/10.1007/s00410-003-0534-2

Rubatto, D., Hermann, J., 2007. Zircon behaviour in deeply subducted rocks. Elements 3, 31–35. https://doi.org/10.2113/gselements.3.1.31

Rubatto, D., Hermann, J., 2003. Zircon formation during fluid circulation in eclogites (Monviso, Western Alps): Implications for Zr and Hf budget in subduction zones. Geochim. Cosmochim. Acta 67, 2173–2187. https://doi.org/10.1016/S0016-7037(02)01321-2

Schoene, B., Bowring, S.A., 2007. Determining accurate temperature-time paths from U-Pb thermochronology: An example from the Kaapvaal craton, southern Africa. Geochim. Cosmochim. Acta 71, 165–185. https://doi.org/10.1016/j.gca.2006.08.029

Schoene, B., de Wit, M.J., Bowring, S.A., 2008. Mesoarchean assembly and stabilization of the eastern Kaapvaal craton: A structural-thermochronological perspective. Tectonics 27, 1–27. https://doi.org/10.1029/2008TC002267

Scibiorski, E., Kirkland, C.L., Kemp, A.I.S., Tohver, E., Evans, N.J., 2019. Trace elements in titanite: A potential tool to constrain polygenetic growth processes and timing. Chem. Geol. 509, 1–19. https://doi.org/10.1016/j.chemgeo.2019.01.006

Sha, L.K., Chappell, B.W., 1999. Apatite chemical composition, determined by electron microprobe and laser-ablation inductively coupled plasma mass spectrometry, as a probe into granite petrogenesis. Geochim. Cosmochim. Acta 63, 3861–3881. https://doi.org/10.1016/S0016-7037(99)00210-0

Siégel, C., Bryan, S.E., Allen, C.M., Gust, D.A., 2018. Use and abuse of zircon-based thermometers: A critical review and a recommended approach to identify antecrystic zircons. Earth-Science Rev. 176, 87–116. https://doi.org/10.1016/j.earscirev.2017.08.011

St-Onge, M.R., Davis, W.J., 2018. Wopmay orogen revisited: Phase equilibria modeling, detrital zircon geochronology, and U-Pb monazite dating of a regional Buchan-type metamorphic sequence. Bull. Geol. Soc. Am. 130, 678–704. https://doi.org/10.1130/B31809.1

Storey, C.D., Smith, M.P., Jeffries, T.E., 2007. In situ LA-ICP-MS U-Pb dating of metavolcanics of Norrbotten, Sweden: Records of extended geological histories in complex titanite grains. Chem. Geol. 240, 163–181. https://doi.org/10.1016/j.chemgeo.2007.02.004

Sullivan, G.O., Chew, D., Kenny, G., Henrichs, I., Mulligan, D., 2020. Earth-Science Reviews The trace element composition of apatite and its application to detrital provenance studies. Earth-Science Rev. 201, 103044. https://doi.org/10.1016/j.earscirev.2019.103044

Thébaud, N., Rey, P.F., 2013. Archean gravity-driven tectonics on hot and flooded continents: Controls on long-lived mineralised hydrothermal systems away from continental margins. Precambrian Res. 229, 93–104. https://doi.org/10.1016/j.precamres.2012.03.001

Timm, C., Leybourne, M.I., Hoernle, K., Wysoczanski, R.J., Hauff, F., Handler, M., Tontini, F.C., de Ronde, C.E.J., 2016. Trench-perpendicular geochemical variation between two adjacent Kermadec arc volcanoes Rumble II East and West: The role of the subducted Hikurangi Plateau in element recycling in arc magmas. J. Petrol. 57, 1335–1360. https://doi.org/10.1093/petrology/egw042

Trail, D., Bruce Watson, E., Tailby, N.D., 2012. Ce and Eu anomalies in zircon as proxies for the oxidation state of magmas. Geochim. Cosmochim. Acta 97, 70–87. https://doi.org/10.1016/j.gca.2012.08.032

Van Kranendonk, M.J., Smithies, R.H., Griffin, W.L., Huston, D.L., Hickman, A.H., Champion, D.C., Anhaeusser, C.R., Pirajno, F., 2015. Making it thick: a volcanic plateau origin of Palaeoarchean continental lithosphere of the Pilbara and Kaapvaal cratons. Geol. Soc. London, Spec. Publ. 389, 83–111. https://doi.org/10.1144/SP389.12

Wang, H., Yang, J.H., Kröner, A., Zhu, Y.S., Li, R., 2019. Non-subduction origin for 3.2 Ga high-pressure metamorphic rocks in the Barberton granitoid-greenstone terrane, South Africa. Terra Nov. 31, 373–380. https://doi.org/10.1111/ter.12397

Watson, E.B., Wark, D.A., Thomas, J.B., 2006. Crystallization thermometers for zircon and rutile. Contrib. to Mineral. Petrol. 151, 413–433. https://doi.org/10.1007/s00410-006-0068-5

Weinberg, R.F., Wolfram, L.C., Nebel, O., Hasalová, P., Závada, P., Kylander-Clark, A.R.C., Becchio, R., 2020. Decoupled U-Pb date and chemical zonation of monazite in migmatites: The case for disturbance of isotopic systematics by coupled dissolution-reprecipitation. Geochim. Cosmochim. Acta 269, 398–412. https://doi.org/10.1016/j.gca.2019.10.024

Wilson, A.H., Zeh, A., Gerdes, A., 2017. In situ Sr isotopes in plagioclase and trace element systematics in the lowest part of the eastern Bushveld Complex: Dynamic processes in an evolving magma chamber. J. Petrol. 58, 327–360. https://doi.org/10.1093/petrology/egx018

Yang, Y.H., Sun, J.F., Xie, L.W., Fan, H.R., Wu, F.Y., 2008. In situ Nd isotopic measurement of natural geological materials by LA-MC-ICPMS. Chinese Sci. Bull. 53, 1062–1070. https://doi.org/10.1007/s11434-008-0166-z

Yang, Y.H., Wu, F.Y., Yang, J.H., Chew, D.M., Xie, L.W., Chu, Z.Y., Zhang, Y. Bin, Huang, C., 2014. Sr and Nd isotopic compositions of apatite reference materials used in U-Th-Pb geochronology. Chem. Geol. 385, 35–55. https://doi.org/10.1016/j.chemgeo.2014.07.012

Zhong, S., Feng, C., Seltmann, R., Li, D., Qu, H., 2018. Can magmatic zircon be distinguished from hydrothermal zircon by trace element composition? The effect of mineral inclusions on zircon trace element composition. Lithos 314–315, 646–657. https://doi.org/10.1016/j.lithos.2018.06.029

Chapter 6: Additional results

Not all data obtained during this project was published in the two research papers for because either beyond the scope or does not add anything significant to justify their inclusion. These results will be described and discussed in this chapter.

6.1 Cryo CL images

It has been shown by Higgins (2017) that textures in rock-forming minerals of felsic rocks (feldspars, quartz) can be studied using cathodoluminescence. Following the discovery of cryptic metamorphism of the Stolzburg Block trondhjemites reflected in the apatite U-Pb isotope data, a thin section of trondhjemite sample MS 2 was investigated for signs of post-crystallization alteration of major minerals using Cryo cathodoluminescence (Cryo CL). The images are shown in Figure 6.1. Plagioclase and biotite are unresponsive, but polysynthetic twinning can be identified in the plagioclase grains. Quartz becomes more CL-active with decreasing temperature. Apatite was identified to be occurring both interstitially and as an inclusion in plagioclase. The examination of a thin section of trondhjemite sample MS 2 has revealed no zonation of plagioclase. Overall, the Cryo CL imaging suggests, that the sample has experienced little fluid-rock interaction despite the convoluted thermal history as revealed by the apatite U-Pb thermochronology (chapter 4).

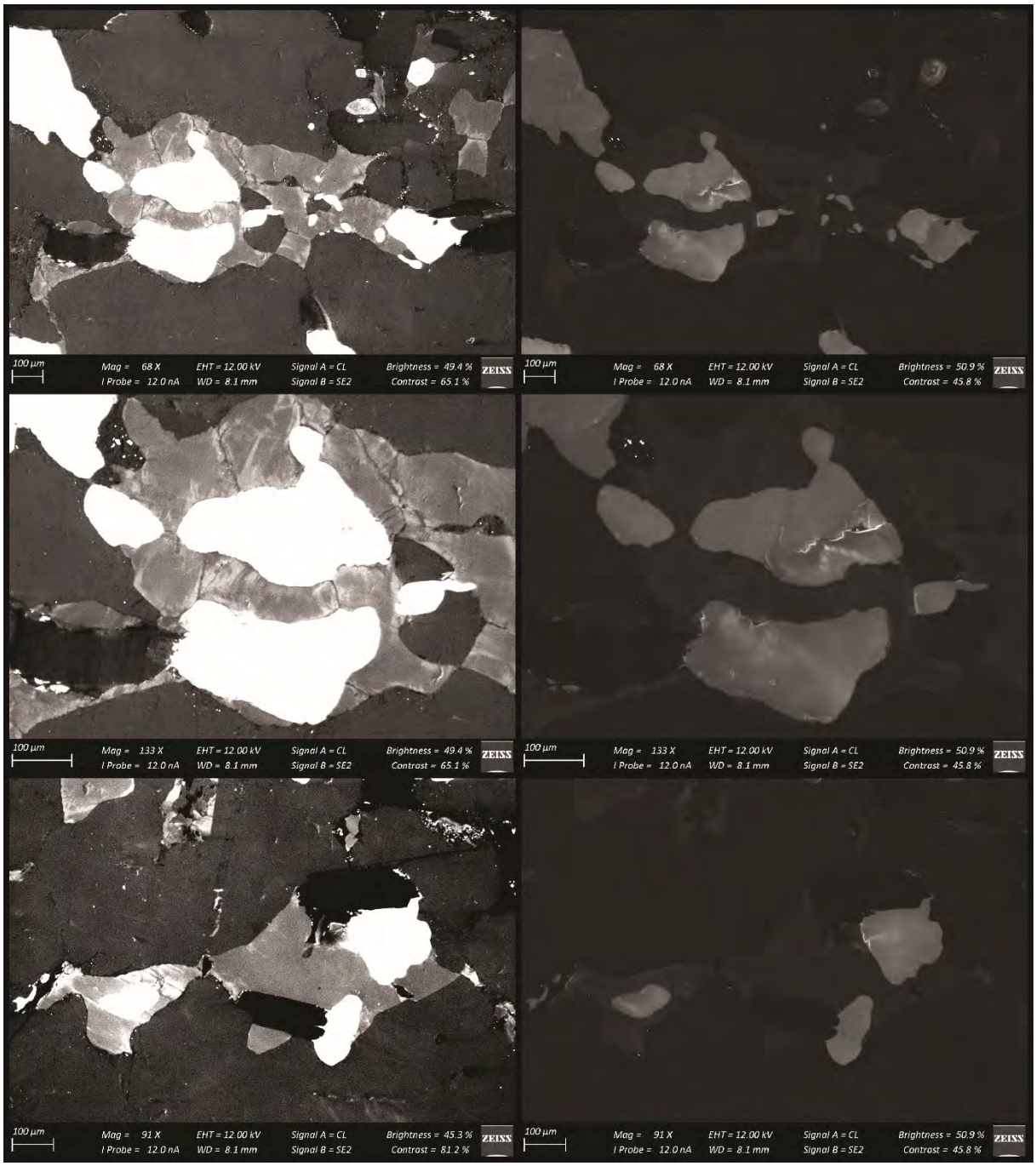

Fig. 6.1. Cathodoluminescence images of mineral grains in trondhjemite sample MS 2, taken with the sample cell cooled down to ca. -196 °C.

6.2 Major- and trace-element data for greenstone samples

In addition to the samples published in research paper 1 (chapter 4), the whole-rock major- and trace-element concentrations were also determined for five metavolcanic and metasedimentary samples from the lower Onverwacht Group. The results are given in Table 6.1 and chondrite-normalized REE diagrams are shown in Figure 6.2. The REE patterns of the greenstone samples fall into three groups, which will be discussed in the following.

Samples MS 5 and MS 39 show a fractionated pattern, decreasing in enrichment relative to chondrite from La to Lu, with no Eu anomaly. This LREE-enriched pattern in Theespruit/Sandspruit fm. mafic rocks has been attributed to crustal contamination from the Ancient Gneiss Complex (Schneider et al., 2019). Sample MS 21, assumed to be taken from the same unit as sample MS 5, is shown in Figure 6.2 for comparison; the REE pattern for sample MS 21 is parallel to those of samples MS 5 and MS 39, though at higher enrichment relative to chondrite.

Felsic volcanosedimentary sample MS 16 has a strongly fractionated LREE pattern, decreasing in enrichment relative to chondrite from La (LaN >200) to Eu (EuN ~10), and a less fractionated, slightly bulged HREE pattern. The REE pattern of sample MS 16 is similar to TTG (Moyen and Martin, 2012) and to felsic volcanic rocks from the Theespruit Formation (Furnes et al., 2013). This sample might represent an eroded older TTG pluton or a metamorphosed felsic volcanic rock. Samples MS 28 and MS 29 show a relatively flat REE pattern, slightly increasing in enrichment from La (LaN ~6.5) to Lu (LuN ~8.5). The fairly flat REE patterns of amphibolite samples MS 28 and MS 29 are comparable to published data on Theespruit and Sandspruit fm. tholeiites (Schneider et al., 2019).

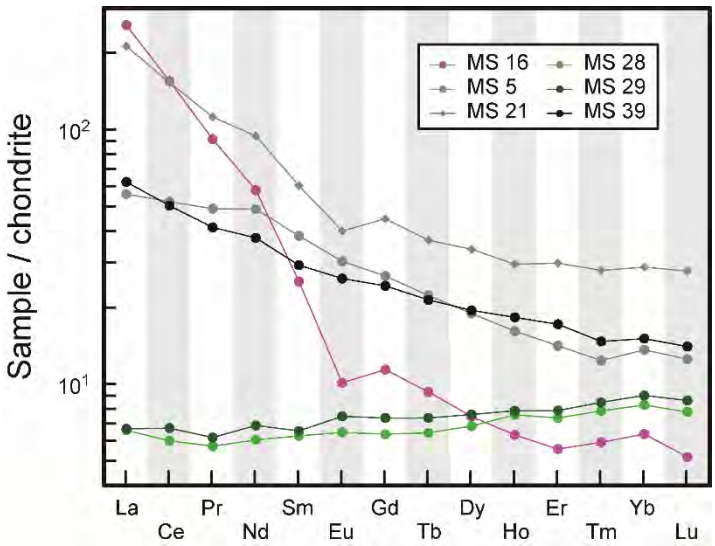

Fig. 6.2. Chondrite-normalized (after McDonough and Sun, 1995) REE diagram for metavolcanic and metasedimentary rocks from the Stolzburg Block. See Table 6.1 for the data for samples MS 5, MS 16, MS 28, MS 29 and MS 39, and Table 4.4 for the data for sample MS 21.

Table 6.1. Major- and trace-element concentrations of metavolcanic and meta-sediment samples from the lower Onverwacht Group, Barberton Greenstone Belt, South Africa.

Sample	MS 5	MS 16	MS 28	MS 29	MS 39
Rock type					
SiO_2	60.67	78.46	51.53	51.35	52.45
TiO_2	1.97	0.16	0.42	0.46	1.01
Al_2O_3	14.39	12.93	15.88	16.36	13.14
Fe_2O_3(t)	11.49	1.26	8.18	7.85	13.04
Cr_2O_3	b.d.	b.d.	0.05	0.05	0.07
MnO	0.29	0.02	0.15	0.11	0.19
MgO	3.99	1.80	9.74	8.45	7.38
CaO	2.87	0.77	8.45	11.67	9.37
Na_2O	1.69	1.52	2.90	2.19	2.40
K_2O	2.53	3.06	2.65	1.47	0.76
P_2O_5	0.10	0.02	0.03	0.04	0.16
Total	100	100	100	100	100
LOI	2.78	1.55	2.18	1.20	1.53
Mg#	41	74	70	68	53
Sc	44.1	8.0	37.5	39.3	31.4
V	340	7.7	209.6	221.9	210.3
Cr	541	9	394.5	394.5	503.0
Co	139	76	47	55	82
Ni	251	14	143	142	191
Cu	358	2.1	17.5	40.2	71.1
Zn	115	33	91	47	101
Rb	86	94	126	93	53
Sr	350	51	284	191	272
Ba	338	754	151	53	200
Ta	0.655	1.34	0.067	0.087	0.292
Cs	4.47	2.03	6.81	1.77	27.26
Mo	2.14	0.63	0.23	0.31	0.85
Y	21.8	9.2	10.2	11.0	24.1
Zr	97	154	23	25	116
Nb	12.2	13.6	1.2	1.2	5.1
Hf	2.92	4.38	0.70	0.78	3.17
Pb	4.26	9.95	4.12	1.77	3.76
Th	0.795	23.4	0.12	0.15	1.33
U	0.303	2.88	0.23	0.16	0.25
La	13.2	61	1.6	1.6	14.7
Ce	31.9	94.9	3.7	4.1	30.8
Pr	4.54	8.51	0.53	0.57	3.83
Nd	22.3	26	2.8	3.1	17.2
Sm	5.66	3.75	0.93	0.97	4.34
Eu	1.71	0.57	0.364	0.421	1.464
Gd	5.29	2.27	1.27	1.47	4.84
Tb	0.805	0.337	0.233	0.266	0.774
Dy	4.66	1.84	1.68	1.87	4.80
Ho	0.882	0.345	0.414	0.430	0.999
Er	2.27	0.89	1.18	1.26	2.75
Tm	0.306	0.146	0.194	0.210	0.364
Yb	2.195	1.03	1.33	1.46	2.43
Lu	0.310	0.128	0.192	0.213	0.347

Major- and trace-element concentrations in wt. % and µg/g, respectively. Mg # = atomic ratio of Mg^{2+}/ (Mg^{2+}+Fe^{2+}) x 100, using FeO = 0.9 of total Fe as Fe_2O_3. LOI = Loss on ignition; b.d. = below detection.

6.3 Apatite U-Pb isotope data from trondhjemite sample MS 27

In addition to the data published in research paper 1 (Chapter 4), the U-Pb composition was also determined for sample MS 27. However, due to an interruption of the run, the numbers of analysis do not correspond to ~~with~~ the spot documentation which had been done prior to the analysis. The analyses cannot be correlated to the microtexture and because of this, the apatite U-Pb isotope data from sample MS 27 was omitted from research paper 1.

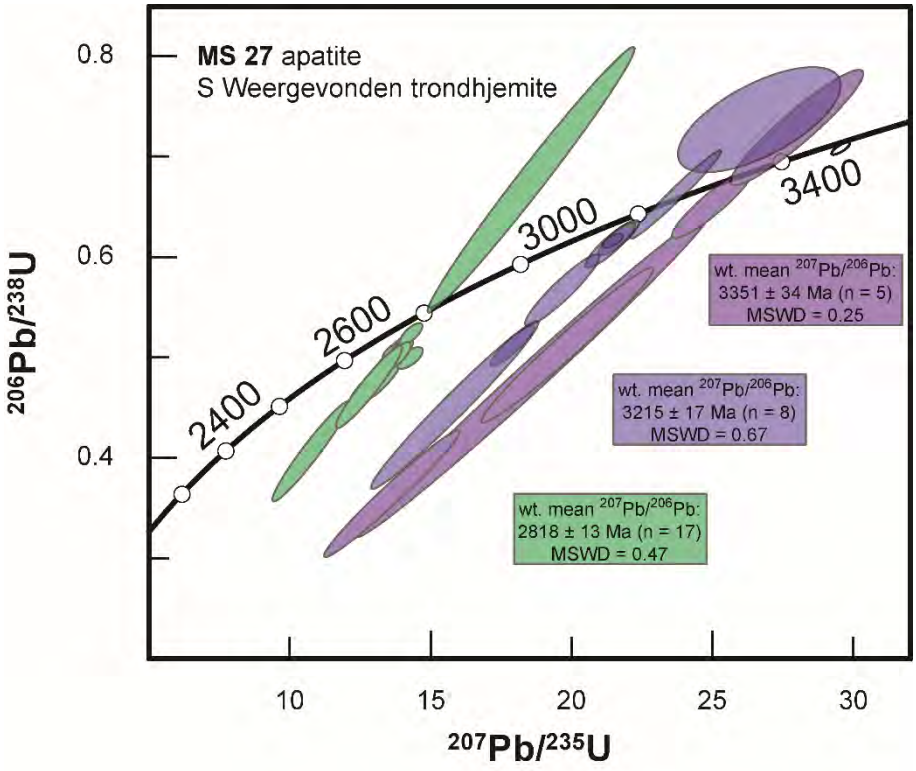

Fig. 6.3. U-Pb Concordia diagram for apatite grains from trondhjemite sample MS 27 from the southern margin of the Weergevonden Pluton. Error ellipses are 2σ.

The results of the U-Pb isotope analysis of apatite grains from sample MS 27 are listed in Table 6.5 and shown in Figure 6.3. Three groups of $^{207}Pb/^{206}Pb$ dates can be recognized in this sample at 3351 ± 34 Ma (n = 5), 3215 ± 17 Ma (n = 8) and 2818 ± 13 Ma (n = 17) (Fig. 6.3). A single concordant analysis gives a date of 3484 ± 8 Ma (Table 6.5). Most data points show varying degrees of Pb loss, with the lower intercepts for all three age groups being around zero (within uncertainties), indicating recent surface alteration as a potential cause for this Pb loss.

The youngest two age groups at ca. 3215 and ca. 2818 Ma are within uncertainties identical with those in the other analyzed samples (c.f. Fig. 4.10), showing once more how pervasive these heating events were in the Stolzburg Block. The ca. 3351 Ma age group is much less prominent, but analyses of similar age were also obtained for some apatites from sample MS 2.

6.4 Apatite major- and trace-element data from sample MS 21

The results of major- and trace-element analyses on apatite grains from mafic schist sample MS 21 was omitted from research paper 2 because this sample is beyond the scope of that paper. The major- and trace-element concentrations of apatite grains from sample MS 21 are listed in Table 6.6 and a chondrite-normalized REE diagram is shown in Figure 6.4. Trace-element characteristics in apatites from sample MS 21 are indistinguishable from one another regardless of apparent age of analyzed zone. The chondrite-normalized REE pattern for apatites from sample MS 21 shows fractionated and depleted LREE, increasing in concentration relative to chondrite from La to Sm, a strong negative Eu anomaly (ca. 0.22 to 0.27) and fractionated HREE, decreasing in concentration relative to chondrite from Gd to Lu (Fig. 6.4).

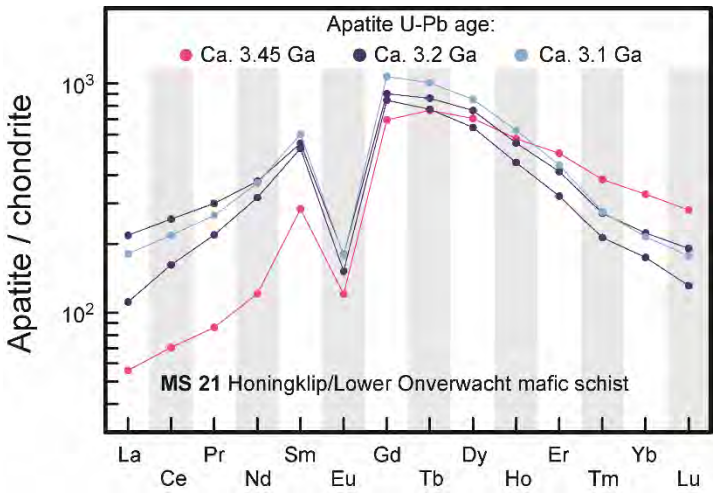

Fig. 6.4. Chondrite-normalized (after McDonough and Sun, 1995) REE plot for apatite grains from mafic schist sample MS 21.

The REE pattern of apatite grains from mafic schist sample MS 21 is distinct from those obtained for granitoid samples from the Stolzburg Block (c.f. Fig. 5.5). The general pattern is similar to those reported for hydrothermal apatite (ref Birski 2018; Chen 2019), apart from the strong negative Eu anomaly. The microtexture of the apatite grains from sample MS 21 does not show any zonation as it can be observed in the granitoid samples (Fig. 4.9). The apatite grains from sample MS 21 yield the same age populations as those from the granitoid samples, the oldest at 3447 ± 19 Ma (Fig. 4.10). This oldest population of U-Pb apatite ages in sample MS 21 is within uncertainty identical to the age of 3462 ± 17 Ma obtained for a sample from the host trondhjemite taken in the proximity of sample MS 21 (Moyen, per. comm.) and the age of 3440 ± 6 Ma obtained for trondhjemite sample MS 4 (Fig. 4.7) taken ca. 420 m from sample MS 21. The 3447 ± 19 Ma age group in apatite grains from sample MS 21 likely represents thermal resetting during the intrusion of the trondhjemite, while the younger populations at 3199 ± 21 Ma, 3103 ± 13 Ma and 2822 ± 15 Ma are most likely related to thermal

resetting of the U-Pb systematics in some apatites in sample MS 21 due to later heating events, as discussed in section 5.6.4.

6.5 Whole-rock isotope data

The Pb isotopic data determined for granitoid samples and mafic schist sample MS 21 from the Stolzburg Block are given in Table 6.2. The whole-rock Sr isotope data for samples that were not included in research paper 2 (chapter 5) are given in Table 6.3. The whole-rock Nd isotope data determined for granitoid samples and mafic schist sample MS 21 from the Stolzburg Block are given in Table 6.4.

Table 6.2. Whole-rock Pb isotope systematics for granitoid and mafic schist samples from the Stolzburg Block.

sample	Age[a] [Ga]	$^{208}Pb/^{204}Pb$	2σ	$^{207}Pb/^{204}Pb$	2σ	$^{206}Pb/^{204}Pb$	2σ
MS 1	3.2	38.7581	0.0029	15.6803	0.0009	18.6022	0.0009
MS 2	3.45	34.6934	0.0026	14.4131	0.0008	13.6544	0.0006
MS 3	3.2	36.7514	0.0032	15.1755	0.0011	16.6466	0.0010
MS 4	3.45	36.2697	0.0032	15.1439	0.0011	16.2091	0.0009
MS 14	3.45	35.5441	0.0028	14.9714	0.0008	15.4543	0.0007
MS 15	3.45	35.3145	0.0029	15.4219	0.0010	17.3014	0.0010
MS 18	3.45	43.5662	0.0038	16.7271	0.0011	21.8284	0.0016
MS 20	3.2	34.0318	0.0021	15.2838	0.0007	16.8218	0.0007
MS 21	>3.45	42.6706	0.0036	17.1487	0.0011	22.5833	0.0012
MS 24	3.45	35.4284	0.0025	15.2396	0.0009	16.7560	0.0007
MS 25	3.22	36.1184	0.0027	15.6791	0.0009	18.3308	0.0009
MS 26	3.45	35.5967	0.0029	14.9957	0.0010	15.8020	0.0009
MS 27	3.45	39.2975	0.0026	17.0605	0.0008	23.8961	0.0011
MS 36	3.45	42.4310	0.0033	15.7130	0.0010	18.6309	0.0010

[a] : See Table 4.2; no U-Pb age data available for sample MS 24, an age of ca. 3.2 Ga is assumed based on field relationships.

Table 6.3. Whole-rock Sr isotope systematics for granitoid and mafic schist samples from the Stolzburg Block.

sample	Age[a] [Ga]	Rb[b] [ppm]	Sr[b] [ppm]	$^{87}Sr/^{86}Sr$ (measured)	2σ	$^{87}Sr/^{86}Sr_i$[c] (calculated)	error[c]
MS 1	3.2	54.0	701	0.711346	0.000015	0.70093	0.00114
MS 3	3.2	45.0	600	0.711909	0.000012	0.70177	0.0011
MS 4	3.45	45.0	708	0.709989	0.000012	0.70077	0.00101
MS 14	3.45	47.0	740	0.706534	0.000011	0.69732	0.001
MS 15	3.45	41.7	656	0.709105	0.000012	0.69989	0.001
MS 18	3.45	31.0	294	0.717457	0.000012	0.70215	0.00166
MS 20	3.2	47.0	261	0.726038	0.000013	0.70166	0.00264
MS 21	>3.45	85.0	359	0.734515	0.000014	0.70009	0.00372
MS 24	3.2?	108.0	461	0.732844	0.000012	0.69878	0.00368
MS 26	3.45	28.0	711	0.706531	0.000011	0.70082	0.00063
MS 27	3.45	72.0	238	0.740650	0.000013	0.69663	0.00475

[a] : See Table 4.2; no U-Pb age data available for sample MS 24, an age of ca. 3.2 Ga is assumed based on field relationships.
[b] : See Table 4.4.
[c] : Initial $^{87}Sr/^{86}Sr$ ratio and uncertainty calculated using the measured present-day ratio and whole-rock Rb and Sr concentrations and their respective uncertainties; calculated for an age of 3445 Ma (ca. 3.45 Ga samples) and 3215 Ma (ca. 3.2 Ga samples), respectively.

Table 6.4. Whole-rock Nd isotope systematics for granitoid and mafic schist samples from the Stolzburg Block.

sample	Age[a] [Ga]	Sm[b] [ppm]	Nd[b] [ppm]	$^{143}Nd/^{144}Nd$ (measured)	2σ	$^{143}Nd/^{144}Nd_i$[c] (calculated)	error[c]	$\varepsilon Nd_{(t)}$[d]	error[d]
MS 1	3.2	3.61	22	0.510552	0.000012	0.50845	0.00016	-0.25	3.22
MS 2	3.45	1.46	8.6	0.510208	0.000013	0.50787	0.00018	-5.60	3.57
MS 3	3.2	2.57	16.1	0.510539	0.000013	0.50849	0.00016	+0.62	3.16
MS 4	3.45	2.75	16.7	0.510448	0.000008	0.50818	0.00017	+0.50	3.37
MS 14	3.45	1.48	10	0.510391	0.000011	0.50835	0.00016	+3.89	3.11
MS 15	3.45	1.73	11	0.510520	0.000012	0.50836	0.00017	+3.92	3.31
MS 18	3.45	2.24	13	0.510412	0.000013	0.50804	0.00018	-2.28	3.62
MS 20	3.2	2.48	7.8	0.511946	0.000009	0.50786	0.00030	-11.7	5.97
MS 21	>3.45	8.91	43	0.510931	0.000009	0.50808	0.00021	-1.52	4.22
MS 24	3.2?	2	9.5	0.510752	0.000011	0.50805	0.00021	-8.04	4.05
MS 25	3.22	6.61	31	0.511057	0.000012	0.50831	0.00021	-2.67	4.13
MS 26	3.45	2.03	12.2	0.510261	0.000012	0.50797	0.00018	-3.64	3.49
MS 27	3.45	2.93	13	0.511301	0.000014	0.50820	0.00024	+0.83	4.68
MS 36	3.45	6.51	42.8	0.510329	0.000014	0.50824	0.00016	+1.56	3.25

[a] : See Table 4.2; no U-Pb age data available for sample MS 24, an age of ca. 3.2 Ga is assumed based on field relationships.
[b] : See Table 4.4.
[c] : Initial $^{143}Nd/^{144}Nd$ ratio and uncertainty calculated using the measured present-day ratio and whole-rock Sm and Nd concentrations and their respective uncertainties.
[d] : εNd value calculated using the calculated initial $^{143}Nd/^{144}Nd$ and a present day $^{143}Nd/^{144}Nd_{CHUR}$ ratio of 0.512638; error on the εNd value calculated from the error on the initial $^{143}Nd/^{144}Nd$ ratio; calculated for an age of 3445 Ma (ca. 3.45 Ga samples), 3222 Ma (MS 25) and 3215 Ma (ca. 3.2 Ga samples), respectively.

References

Birski, Ł., Wirth, E.S.R., Müller, M.K., Wudarska, K.S.A., Lepland, J.G.A., 2019. Archaean phosphates : a case study of transformation processes in apatite from the Barberton greenstone belt. Contrib. to Mineral. Petrol. 174, 1–23. https://doi.org/10.1007/s00410-019-1560-z

Chen, M., Bagas, L., Liao, X., Zhang, Z., Li, Q., 2019. Hydrothermal apatite SIMS Th–Pb dating: Constraints on the timing of low-temperature hydrothermal Au deposits in Nibao, SW China. Lithos 324–325, 418–428. https://doi.org/10.1016/j.lithos.2018.11.018

Furnes, H., de Wit, M., Robins, B., 2013. A review of new interpretations of the tectonostratigraphy, geochemistry and evolution of the Onverwacht Suite, Barberton Greenstone Belt, South Africa. Gondwana Res. 23, 403–428. https://doi.org/10.1016/j.gr.2012.05.007

Higgins, M.D., 2017. Quantitative investigation of felsic rock textures using cathodoluminescence images and other techniques. Lithos 277, 259–268. https://doi.org/10.1016/j.lithos.2016.05.006

McDonough, W.F., Sun, S. s., 1995. The composition of the Earth. Chem. Geol. 120, 223–253. https://doi.org/10.1016/0009-2541(94)00140-4

Moyen, J.F., Martin, H., 2012. Forty years of TTG research. Lithos. https://doi.org/10.1016/j.lithos.2012.06.010

Schneider, K.P., Hoffmann, J.E., Münker, C., Patyniak, M., Sprung, P., Roerdink, D., Garbe-Schönberg, D., Kröner, A., 2019. Petrogenetic evolution of metabasalts and metakomatiites of the lower Onverwacht Group, Barberton Greenstone Belt (South Africa). Chem. Geol. 511, 152–177. https://doi.org/10.1016/j.chemgeo.2019.02.020

Chapter 7: Summary, discussion and conclusion

7.1 Thermal history of the Stolzburg Block

Discussing the magmatic and metamorphic history of the Stolzburg Block and the geodynamic implications that can be drawn from it requires a review of the geochronological data available for the Stolzburg Block and the vicinity, both from the published literature and from this study. In the following, the most important geochronological data for the Stolzburg Block and the vicinity published within the last ca. 30 years will be discussed. A summary of the available geochronological data is given in Table 7.1. It is worth noting that only the most relevant data is included here and that this section by no means intends to be a complete overview.

7.1.1 Pre 3.50 Ga rocks

The (ultra-)mafic and felsic volcanic rocks and volcanosedimentary rocks of the lower Onverwacht Group and the gneisses of the Steynsdorp dome form the “Proto Stolzburg Block”. Robust zircon U-Pb sensitive high resolution ion microprobe (SHRIMP) zircon data for felsic metavolcanic rocks of the Theespruit and Sandspruit formations by Kröner et al. (2016) pinpoint the deposition of the bulk of both units to ca. 3530 Ma. Older ages of ca. 3550-3540 Ma (Kröner et al., 2016) indicate earlier volcanic episodes. Emplacement of the protolith of the Steynsdorp gneisses occurred at ca. 3518 to 3501 Ma (Kamo and Davis, 1994; Kröner et al., 1996; Schoene et al., 2008). The ages obtained for the lower Onverwacht Group and the Steynsdorp dome are within error identical to those from inherited cores in zircon grains from the Stolzburg, Theespruit and Honingklip plutons analyzed in this study which yield ages of 3493 ± 19 Ma (sample ST-J 26, Stolzburg), 3530 ± 19 Ma (sample MS 18, Theespruit) and 3520 ± 8 (sample MS 4, Honingklip) (Table 4.2), and to that of a ca. 3527 Ma gneiss enclave in trondhjemite of the Honingklip Pluton (Moyen, pers. comm.).

7.1.2 Ca. 3.45 Ga plutonism

The emplacement of the two large plutons of the Stolzburg Block is reasonably well constrained, with published ages ranging from ca. 3455 ± 0.5 Ma (Schoene et al., 2008) over ca. 3550-3440 Ma (Kamo and Davis, 1994; Wang et al., 2019) to 3431 ± 11 Ma (Dziggel et al., 2002) for the Stolzburg Pluton and from 3465.7 ± 2.2 Ma (Kröner et al., 2016) over 3456.57 ± 0.11 (Laurent et al., 2020) and 3451 ± 7 Ma (Zeh et al., 2009) to 3441 ± 2.6 Ma (Kamo and Davis, 1994) for the Theespruit Pluton. Less geochronological data is available in the literature for the smaller bodies of the Stolzburg Block. For the Doornhoek Pluton, (Kamo and Davis, 1994) report U-Pb zircon and monazite ages of 3441 ± 2.6 and 3443 ± 1.6 Ma, respectively, while the supplementary data of Laurent et al. (2020) yield an age of 3456.4 ± 16.2 Ma (note

that this age was calculated by myself). An age of 3431.9 ± 9.8 is available for the Uitgevonden (Lana et al., 2010b). Conflicting age data is available for the Honingklip; a trondhjemite sample from the contact with the Tjakastad schist belt on the western margin of the Honingklip yields a U-Pb zircon age of 3462.1 ± 17.2 Ma (Moyen, pers. comm.), while U-Pb zircon ages of 3236.9 ± 7.8 and 3224.6 ± 8.3 Ma (Wang et al., 2020, 2019) and a U-Pb titanite age of 3225.0 ± 3.9 (Wang et al., 2019) have been reported for samples from the northern part of the Honingklip.

The U-Pb zircon data obtained for Stolzburg Block trondhjemites as part of this study complement the existing database. The oldest single dates are found at ca. 3460-3450 Ma, generally with an uncertainty of ± 19 Ma (Table 4.7), while the majority of the data cluster at ca. 3445 to 3430 Ma. The data also show a long, uninterrupted tail of concordant dates from ca. 3440 Ma down to ca. 3300 Ma (Fig. 7.1), with many of these dates taken from seemingly pristine zircon domains. As discussed in section 4.5.1, a protracted buildup of the plutons over such a long period is highly unlikely and an explanation for this phenomenon could be ancient Pb loss. Lead loss in the first few 100 million years after emplacement would produce concordant data points along the line from the magmatic age to the time of Pb loss. This could for example have happened at around ca. 3.2 Ga when a major metamorphic event affects the Stolzburg Block (see below) and which is the time around which the youngest concordant dates are found in the data obtained in this thesis (Table 4.7). The U-Pb apatite chronology yields the oldest age groups at 3445 ± 24 Ma (sample MS 2), 3439 ± 14 (sample MS 14), 3414 ± 40 (sample MS 15) and 3456 ± 12 (sample MS 36), which are within uncertainties identical with range of zircon ages and some 30-50 million years older than the oldest U-Pb apatite date reported by Schoene et al. (2008).

This period is also characterized by metamorphism of the supracrustal rocks of the lower Onverwacht Group, timed to 3436 ± 18 by a monazite U-Pb age obtained for a Theespruit Formation metavolcanic rock (Cutts et al., 2014) and an apatite U-Pb age of ca. 3447 ± 19 Ma for sample MS 21 (Table 4.3). Granitoid sills cutting the rocks of the Sandspruit formation yield U-Pb zircon ages that are within error identical with the emplacement ages of the trondhjemite plutons (Kröner et al., 2016) and a younger felsic rock (3431.4 ± 1.5 Ma) cutting the Theespruit Formation was interpreted by Kröner et al. (2016) to represent a feeder dyke for the Komati Formation volcanism.

7.1.3 Surrounding the ca. 3.2 Ga event

Ages in the range of ca. 3430 to 3230 Ma are rare in the Stolzburg Block. Dates of 3387 ± 36 and 3382.4 ± 13.0 Ma are found in felsic dykes cutting rocks of Theespruit Formation and

Pluton (Moyen, pers. comm.). Apatite grains from two samples analyzed as part of this thesis yield U-Pb dates of 3347 ± 31 Ma (MS 2) and 3351 ± 34 Ma (MS 27). Zircon dates of that time are found in the analyzed samples but those are part of the lead loss “tail” described above and are unlikely to carry any geological siginicance.

A major metamorphic event affects the Stolzburg Block at ca. 3.2 Ga. Metamorphic titanite growths at ca. 3229 ± 25 Ma in the Tjakastad schist belt (Diener et al., 2005), at ca. 3229 ± 9.3 Ma in the Inyoni shear zone (Dziggel et al., 2005), and at 3215 ± 1.6 and 3215 ± 3.2 Ma in the Stolzburg and Doornhoek plutons, respectively (Kamo and Davis, 1994). Growth of metamorphic monazite in Theespruit Formation metavolcanic 3191 ± 9 Ma (Cutts et al., 2014). Garnet in a sample from the Tjakastad schist belt at 3233 ± 17 (Cutts et al., 2014) and in the Inyoni shear zone at ca. 3200 Ma (Cutts et al., 2021).However, as stated by Cutts et al. (2021), “147Sm decay constant uncertainty leaves open the possibility that Inyoni garnet growth could have coincided with the previously recognized 3.23 Ga regional metamorphism”. Metasomatized zircon grows in a Sandspruit Formation metavolcanic rock at 3220.0 ± 1.6 Ma (Kröner et al., 2016). Metamorphic zircon from a trondhjemite sample from the contact zone of the Tjakastad schist belt with the Honingklip that was analyzed as part of this thesis yields an age of 3219.4 ± 6.0 Ma. The apatite samples analyzed as part of this thesis yield U-Pb ages of 3217 ± 10 Ma (MS 2), 3217 ± 9 Ma (MS 14), 3216 ± 9 Ma (MS 15), 3203 ± 8 Ma (MS 36), 3199 ± 21 (MS 21) and 3215 ± 17 Ma (MS 27).

The Stolzburg Block is not only affected by metamorphism at the time, but also by magmatism. For a granodiorite cutting the south-eastern margin of the Stolzburg Block, Wang et al. (2019) report a U-Pb zircon age of 3225.6 ± 3.9 Ma. A diorite cropping out in the Weergevonden was dated to 3224.7 ± 3.7 Ma by Wang et al. (2019) and to 3221.1 ± 1.9 Ma as part of this thesis (sample MS 25); sample MS 25 also yields a U-Pb apatite age of 3215 ± 9 Ma. Wang et al. (2020, 2019) report U-Pb zircon ages of 3224.6 ± 8.3 and 3236.9 ± 7.8 Ma and a U-Pb titanite age of 3225.0 ± 3.9 Ma for trondhjemite samples from the northern Honingklip. For a felsic dykes cross-cutting the southern margin of the Stolzburg Pluton, a precise TIMS U-Pb zircon age of 3212.5 ± 0.8 Ma has been reported by (Schoene et al., 2008); the less precise LA ICP-MS U-Pb zircon ages obtained as part of this thesis for similar dykes cutting the Stolzburg (MS 1, 3204 ± 12 Ma) and Theespruit (MS 19, 3211 ± 13 Ma, and MS 20, 3214 ± 23 Ma) plutons and the Honingklip (MS 3, 3207 ± 7 Ma) are all within uncertainty identical with the ca. 3212 Ma age of Schoene et al. (2008).

The ca. 3.2 Ga event is accompanied by extensive TTG plutonism in the vicinity of the Stolzburg Pluton. The oldest and most prolonged plutonism around that time is building the Badplaas Complex from ca. 3280 to 3230 Ma (Kisters et al., 2010). The Nelshoogte Pluton is

emplaced at ca. 3236 Ma (De Ronde and Kamo, 2000; Schoene et al., 2008; Wang et al., 2020; Zeh et al., 2009) and the Kaap Valley Pluton at ca. 3227 Ma (Kamo and Davis, 1994; Wang et al., 2020). Published ages for the Dalmein Pluton range from 3218 ± 16 Ma (Wang et al., 2020) to 3192 ± 27 Ma (Zeh et al., 2009); precise ID TIMS U-Pb zircon and titanite ages of 3207 ± 2.6 and 3215 ± 1.6 Ma, respectively, reported by Kamo and Davis (1994) remain the best available age constraints for the Dalmein Pluton.

7.1.4 Post ca. 3.2 Ga ages

The time following the ca. 3.2 Ga metamorphic event is once again characterized by "quietness", with no ages appearing in the Stolzburg Block apart from some concordant U-Pb zircon dates of 3186 ± 19 and 3168 ± 19 Ma in sample MS 4 (Table 4.7). It is unclear whether these dates carry any geological significance. At 3107 ± 1.6, the Boesmanskop Pluton intrudes the southern and western section of the Stolzburg Block (Kamo and Davis, 1994) and contemporaneously the large Mpuluzi-Piggs Peak batholith is emplaced to the south of the Stolzburg Block at 3105 ± 1.6 Ma (Kamo and Davis, 1994). This time is also reflected in U-Pb apatite ages from Stolzburg Block rocks. Schoene et al. (2008) report U-Pb apatite date ranging from ca. 3100 to 3080 Ma. Similar dates were also found in apatites from most samples analyzed as part of this study, yielding U-Pb ages of 3110 ± 15 Ma (MS 2), 3106 ± 10 Ma (MS 14), 3085 +70/-25 Ma (MS 36), 3103 ± 13 Ma (MS 21) and 3104 ± 16 Ma (MS 25). Ages younger than that have not been reported for the Stolzburg Block prior to this thesis, which revealed apatite U-Pb ages of 2816 ± 17 Ma (MS 2), 2725 +51/-48 Ma (MS 14), 2825 ± 9 (MS 15), 2812 ± 12 Ma (MS 36), 2822 ± 15 Ma (MS 21), 2813 ± 9 (MS 4), 2830 ± 15 Ma (MS 25) and 2818 ± 13 (MS 27).

Fig. 7.1. Distribution of $^{207}Pb/^{206}Pb$ ages obtained for zircon and apatite grains from granitoid samples and mafic schist sample MS 21 from the Stolzburg Block.

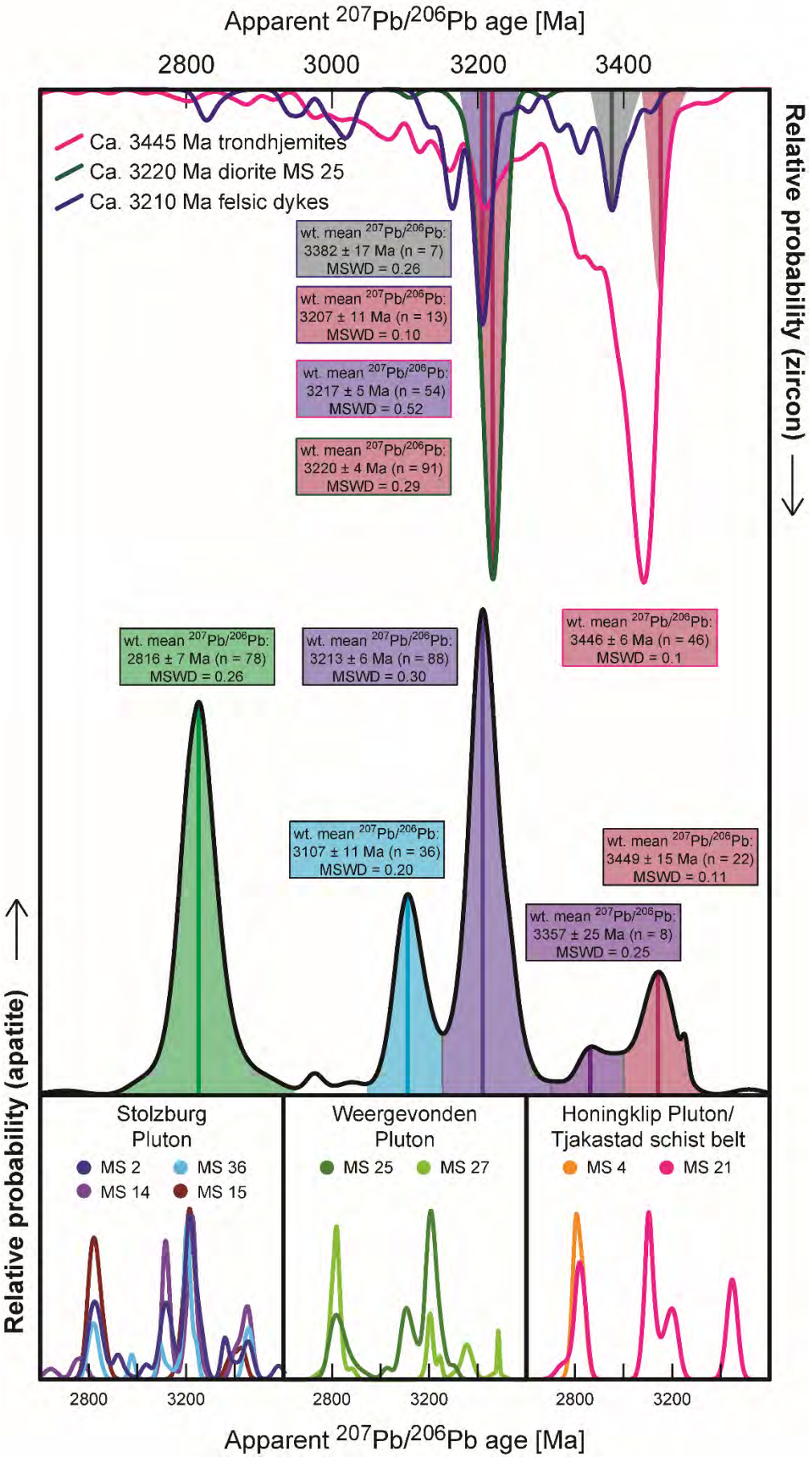

Table 7.1. Summary of the most important geochronological data available for the Stolzburg Block and vicinity

Unit/Sample	Rock type	Mineral	Decay system	Method	Age type	Age [Ma]	Reference	Interpretation
				Granitoids				
Steynsdorp dome								
B	Trondhjemite gneiss	Zircon	U-Pb	ID TIMS	$^{207}Pb/^{206}Pb$	3501 ± 2.6	Kamo and Davis, 1994	
B	Trondhjemite gneiss	Titanite	U-Pb	ID TIMS	$^{207}Pb/^{206}Pb$	3190 ± 1.6	Kamo and Davis, 1994	
EKC02-40	Tonalite/granodiorite	Zircon	U-Pb	ID TIMS	$^{207}Pb/^{206}Pb$	3517.6 ± 0.7	Schoene et al., 2008	
BA 48	Trondhjemite gneiss	Zircon	U-Pb	SHRIMP	$^{207}Pb/^{206}Pb$	3509 ± 4	Kröner et al., 1996	
Stolzburg Block								
Stolzburg Pluton								
D	Trondhjemite	Zircon	U-Pb	ID TIMS	$^{207}Pb/^{206}Pb$	3450 ± 2.9	Kamo and Davis, 1994	
N	Trondhjemite	Zircon	U-Pb	ID TIMS	$^{207}Pb/^{206}Pb$	3207 ± 2.6	Kamo and Davis, 1994	
N	Trondhjemite	Titanite	U-Pb	ID TIMS	$^{207}Pb/^{206}Pb$	3215 ± 1.6	Kamo and Davis, 1994	
Marc2	Trondhjemite	Zircon	U-Pb	ID TIMS	U.I.	3431 ± 11	Dziggel et al., 2002	
EKC03-3	Trondhjemite	Zircon	U-Pb	ID TIMS	$^{207}Pb/^{206}Pb$	3455.9 ± 0.5	Schoene et al., 2008	
EKC03-3	Trondhjemite	Apatite	U-Pb	ID TIMS	$^{207}Pb/^{206}Pb$	3401-3263	Schoene et al., 2008	
KPV99-96	Trondhjemite	Zircon	U-Pb	ID TIMS	$^{207}Pb/^{206}Pb$	3455.5 ± 0.6	Schoene et al., 2008	
KPV99-96	Trondhjemite	Apatite	U-Pb	ID TIMS	$^{207}Pb/^{206}Pb$	3101-3092	Schoene et al., 2008	
EKC03-11	Granite dyke	Zircon	U-Pb	ID TIMS	$^{207}Pb/^{206}Pb$	3212.5 ± 0.8	Schoene et al., 2008	
EKC03-11	Granite dyke	Apatite	U-Pb	ID TIMS	$^{207}Pb/^{206}Pb$	3100-3082	Schoene et al., 2008	
14SA10	Granodiorite	Zircon	U-Pb	SIMS	$^{207}Pb/^{206}Pb$	3225.6 ± 3.9	Wang et al., 2019	
14SA11	Trondhjemite	Zircon	U-Pb	SIMS	$^{207}Pb/^{206}Pb$	3441.7 ± 4.8	Wang et al., 2019	
C5b	Tonalite	Zircon	U-Pb	LA ICP-MS	$^{207}Pb/^{206}Pb$	3453.2 ± 7.3*	Laurent et al., 2020	
C6	Trondhjemite	Zircon	U-Pb	LA ICP-MS	$^{207}Pb/^{206}Pb$	3449.4 ± 3.1*	Laurent et al., 2020	
MS 1	Trondhjemite dyke	Zircon	U-Pb	LA ICP-MS	$^{207}Pb/^{206}Pb$	3204 ± 12	This study (Table 4.2)	
MS 2	Trondhjemite	Zircon	U-Pb	LA ICP-MS	$^{207}Pb/^{206}Pb$	3438.6 ± 4.7	This study (Fig. 4.7)	
MS 2	Trondhjemite	Apatite	U-Pb	LA ICP-MS	$^{207}Pb/^{206}Pb$	3445-2816	This study (Table 4.3)	See text
MS 14	Trondhjemite	Zircon	U-Pb	LA ICP-MS	$^{207}Pb/^{206}Pb$	3439.8 ± 5.7	This study (Fig. 4.7)	
MS 14	Trondhjemite	Apatite	U-Pb	LA ICP-MS	$^{207}/^{206}$, U.I.	3439-2725	This study (Table 4.3)	See text
MS 15	Trondhjemite	Zircon	U-Pb	LA ICP-MS	$^{207}Pb/^{206}Pb$	3432 ± 3	This study (Fig. 4.7)	
MS 15	Trondhjemite	Apatite	U-Pb	LA ICP-MS	$^{207}Pb/^{206}Pb$	3414-2825	This study (Table 4.3)	See text
MS 36	Tonalite	Apatite	U-Pb	LA ICP-MS	$^{207}Pb/^{206}Pb$	3456-2812	This study (Table 4.3)	See text
ST-J 26	Trondhjemite	Zircon	U-Pb	LA ICP-MS	$^{207}Pb/^{206}Pb$	3451.0 ± 8	This study (Fig. 4.7)	

* Age calculated from supplementary data.

Table 7.1, continued.

Unit/Sample	Rock type	Mineral	Decay system	Method	Age type	Age [Ma]	Reference	Interpretation
Theespruit Pluton								
F	Trondhjemite	Zircon	U-Pb	ID TIMS	$^{207}Pb/^{206}Pb$	3441 ± 2.6	Kamo and Davis, 1994	
F	Trondhjemite	Titanite	U-Pb	ID TIMS	$^{207}Pb/^{206}Pb$	3443 ± 1.6	Kamo and Davis, 1994	
C2a	Trondhjemite	Zircon	U-Pb	ID TIMS	$^{207}Pb/^{206}Pb$	3456.33 ± 0.14	Laurent et al., 2020	
C2d	Diorite	Zircon	U-Pb	ID TIMS	$^{207}Pb/^{206}Pb$	3456.57 ± 0.11	Laurent et al., 2020	
BB3	?	Zircon	U-Pb	LA ICP-MS	Concordia	3451 ± 7	Zeh et al., 2009	
BA 115	Tonalitic gneiss	Zircon	U-Pb	SHRIMP	$^{207}Pb/^{206}Pb$	3465.7 ± 2.2	Kröner et al., 2016	
BL13-11	Trondhjemite	Zircon	U-Pb	LA ICP-MS	$^{207}Pb/^{206}Pb$	3382.4 ± 13.0	Moyen, pers. comm.	
BL13-12	Felsic dyke	Zircon	U-Pb	LA ICP-MS	$^{207}Pb/^{206}Pb$	3387 ± 36	Moyen, pers. comm.	
MS 17	Tonalite	Zircon	U-Pb	LA ICP-MS	$^{207}Pb/^{206}Pb$	3444 ± 12	This study (Fig. 4.7)	
MS 18	Trondhjemite	Zircon	U-Pb	LA ICP-MS	$^{207}Pb/^{206}Pb$	3438 ± 19	This study (Fig. 4.7)	
MS 19	Trondhjemite dyke	Zircon	U-Pb	LA ICP-MS	$^{207}Pb/^{206}Pb$	3211 ± 13	This study (Table 4.2)	
MS 20	Trondhjemite dyke	Zircon	U-Pb	LA ICP-MS	$^{207}Pb/^{206}Pb$	3214 ± 23	This study (Table 4.2)	
Honingklip								
14SA14	Trondhjemite	Zircon	U-Pb	SIMS	$^{207}Pb/^{206}Pb$	3224.6 ± 8.3	Wang et al., 2019	
15SA10	Trondhjemite	Titanite	U-Pb	SIMS	$^{207}Pb/^{206}Pb$	3225.0 ± 3.9	Wang et al., 2019	
15SA10	Trondhjemite	Zircon	U-Pb	SIMS	$^{207}Pb/^{206}Pb$	3236.9 ± 7.8	Wang et al., 2020	
BL13-32	Gneiss	Zircon	U-Pb	LA ICP-MS	$^{207}Pb/^{206}Pb$	3526.7 ± 15.4	Moyen, pers. comm.	
BL13-34	Trondhjemite	Zircon	U-Pb	LA ICP-MS	$^{207}Pb/^{206}Pb$	3462.1 ± 17.2	Moyen, pers. comm.	
MS 3	Tonalite	Zircon	U-Pb	LA ICP-MS	$^{207}Pb/^{206}Pb$	3207 ± 7	This study (Table 4.2)	
MS 4	Trondhjemite	Zircon	U-Pb	LA ICP-MS	$^{207}Pb/^{206}Pb$	3439.7 ± 5.7	This study (Fig. 4.7)	
MS 4	Trondhjemite	Zircon	U-Pb	LA ICP-MS	$^{207}Pb/^{206}Pb$	3219.4 ± 6.0	This study (Fig. 4.7)	
MS 4	Trondhjemite	Apatite	U-Pb	LA ICP-MS	$^{207}Pb/^{206}Pb$	2813 ± 9	This study (Table 4.3)	
Weergevonden								
16SA16	Trondhjemite	Zircon	U-Pb	SIMS	$^{207}Pb/^{206}Pb$	3453.9 ± 8.0	Wang et al., 2019	
16SA16	Quartz diorite	Zircon	U-Pb	SIMS	Concordia	3224.7 ± 3.7	Wang et al., 2019	
MS 25	Diorite	Zircon	U-Pb	LA ICP-MS	$^{207}Pb/^{206}Pb$	3221.2 ± 1.9	This study (Fig. 4.7)	
MS 25	Diorite	Apatite	U-Pb	LA ICP-MS	$^{207}Pb/^{206}Pb$	3215-2830	This study (Table 4.3)	
MS 26	Trondhjemite	Zircon	U-Pb	LA ICP-MS	$^{207}Pb/^{206}Pb$	3434.1 ± 4.0	This study (Fig. 4.7)	
MS 27	Trondhjemite	Zircon	U-Pb	LA ICP-MS	$^{207}Pb/^{206}Pb$	3434.2 ± 2.9	This study (Fig. 4.7)	
MS 27	Trondhjemite	Apatite	U-Pb	LA ICP-MS	$^{207}Pb/^{206}Pb$	3484-2818	This study (Table 6.4)	

Table 7.1, continued.

Unit/Sample	Rock type	Mineral	Decay system	Method	Age type	Age [Ma]	Reference	Interpretation
Doornhoek Pluton								
E	Trondhjemite	Zircon	U-Pb	ID TIMS	$^{207}Pb/^{206}Pb$	3439 ± 6.4	Kamo and Davis, 1994	
E	Trondhjemite	Monazite	U-Pb	ID TIMS	$^{207}Pb/^{206}Pb$	3446 ± 3.2	Kamo and Davis, 1994	
E	Trondhjemite	Titanite	U-Pb	ID TIMS	$^{207}Pb/^{206}Pb$	3215 ± 3.2	Kamo and Davis, 1994	
D2a	Granite	Zircon	U-Pb	LA ICP-MS	$^{207}Pb/^{206}Pb$	3456.4 ± 16.2*	Laurent et al., 2020	
Uitgevonden								
GG1	Gneiss	Zircon	U-Pb	LA ICP-MS	Concordia	3431.9 ± 9.8	Lana et al., 2010b	
Vicinity								
Badplaas Complex								
22-06-1A	Trondhjemite gneiss	Zircon	U-Pb	LA ICP-MS	Concordia	3257 ± 13	Kisters et al., 2010	
22-06-1B	Trondhjemite	Zircon	U-Pb	LA ICP-MS	Concordia	3272.2 ± 9.4	Kisters et al., 2010	
26-10-16	Trondhjemite	Zircon	U-Pb	LA ICP-MS	Concordia	3256.0 ± 9.6	Kisters et al., 2010	
23-06-10	Trondhjemite	Zircon	U-Pb	LA ICP-MS	Concordia	3282 ± 14	Kisters et al., 2010	
27-7-02	Trondhjemite	Zircon	U-Pb	LA ICP-MS	Concordia	3256 ± 23	Kisters et al., 2010	
27-7-04	Trondhjemite	Zircon	U-Pb	LA ICP-MS	Concordia	3231 ± 30	Kisters et al., 2010	
16SA08	Trondhjemite	Zircon	U-Pb	SIMS	$^{207}Pb/^{206}Pb$	3240.7 ± 3.7	Wang et al., 2020	
Nelshoogte Pluton								
EKC03-9	Tonalite	Zircon	U-Pb	ID TIMS	$^{207}Pb/^{206}Pb$	3236.0 ± 0.5	Schoene et al., 2008	
EKC03-9	Tonalite	Apatite	U-Pb	ID TIMS	$^{207}Pb/^{206}Pb$	3225-3201	Schoene et al., 2008	
KPV99-94	Tonalite	Zircon	U-Pb	ID TIMS	$^{207}Pb/^{206}Pb$	3236.3 ± 0.4	Schoene et al., 2008	
KPV99-94	Tonalite	Apatite	U-Pb	ID TIMS	$^{207}Pb/^{206}Pb$	>3166	Schoene et al., 2008	
B-90-16	Trondhjemite	Zircon	U-Pb		U.I.?	3236 ± 1	De Ronde and Kamo, 2000	
14SA02	Trondhjemite	Zircon	U-Pb	SIMS	$^{207}Pb/^{206}Pb$	3236.0 ± 1.9	Wang et al., 2020	
KK89		Zircon	U-Pb	LA ICP-MS	Concordia	3238 ± 8	Zeh et al., 2009	
Kaap Valley Pluton								
H	Tonalite	Zircon	U-Pb	ID TIMS	$^{207}Pb/^{206}Pb$	3227 ± 1.6	Kamo and Davis, 1994	
H	Tonalite	Titanite	U-Pb	ID TIMS	$^{207}Pb/^{206}Pb$	3227 ± 1.6	Kamo and Davis, 1994	
I	Tonalite	Zircon	U-Pb	ID TIMS	$^{207}Pb/^{206}Pb$	3228 ± 1.6	Kamo and Davis, 1994	
I	Tonalite	Titanite	U-Pb	ID TIMS	$^{207}Pb/^{206}Pb$	3226 ± 1.6	Kamo and Davis, 1994	
KV01	Tonalite	Zircon	U-Pb	SIMS	$^{207}Pb/^{206}Pb$	3227.3 ± 2.7	Wang et al., 2020	

* Age calculated from supplementary data.

Table 7.1, continued.

Unit/Sample	Rock type	Mineral	Decay system	Method	Age type	Age [Ma]	Reference	Interpretation
Dalmein Pluton								
M	Monzonite	Zircon	U-Pb	ID TIMS	$^{207}Pb/^{206}Pb$	3207 ± 2.6	Kamo and Davis, 1994	
M	Monzonite	Titanite	U-Pb	ID TIMS	$^{207}Pb/^{206}Pb$	3215 ± 1.6	Kamo and Davis, 1994	
DL	Monzonite	Zircon	U-Pb	LA ICP-MS	$^{207}Pb/^{206}Pb$	3201 ± 12	Lana et al., 2010b	
15SA13	Monzogranite	Zircon	U-Pb	SIMS	U.I.	3218 ± 16	Wang et al., 2020	
KK10	?	Zircon	U-Pb	LA ICP-MS	U.I.	3192 ± 27	Zeh et al., 2009	
Mpuluzi-Piggs Peak Batholith								
S	Granodiorite	Zircon	U-Pb	ID TIMS	$^{207}Pb/^{206}Pb$	3105 ± 1.6	Kamo and Davis, 1994	
S	Granodiorite	Titanite	U-Pb	ID TIMS	$^{207}Pb/^{206}Pb$	3092 ± 3.2	Kamo and Davis, 1994	
KK11	?	Zircon	U-Pb	LA ICP-MS	Concordia	3082 ± 6	Zeh et al., 2009	
Boesmanskop Pluton								
T	Syeno-granite	Zircon	U-Pb	ID TIMS	$^{207}Pb/^{206}Pb$	3107 ± 1.6	Kamo and Davis, 1994	
T	Syeno-granite	Titanite	U-Pb	ID TIMS	$^{207}Pb/^{206}Pb$	3108 ± 1.6	Kamo and Davis, 1994	
KK12	?	Zircon	U-Pb	LA ICP-MS	U.I.	3097 ± 11	Zeh et al., 2009	

Table 7.1, continued.

Unit/Sample	Rock type	Mineral	Decay system	Method	Age type	Age [Ma]	Reference	Interpretation
			Supracrustal rocks and cross-cutting intrusives					
Theespruit Formation								
A	Tonalite gneiss	Zircon	U-Pb	ID TIMS	$^{207}Pb/^{206}Pb$	3538 ± 2.9	Kamo and Davis, 1994	
MS 21	Schist	Apatite	U-Pb	LA ICP-MS	$^{207}Pb/^{206}Pb$	3447-2822	This study (Table 4.3)	See text
Tj 3	Metabasite	Titanite	U-Pb	LA ICP-MS	U.I.	3229 ± 25	Diener et al., 2005	
BKC-8	?	Monazite	U-Pb	LA ICP-MS	$^{207}Pb/^{206}Pb$	3436 ± 18	Cutts et al., 2014	
BKC-16	?	Monazite	U-Pb	LA ICP-MS	$^{207}Pb/^{206}Pb$	3191 ± 9	Cutts et al., 2014	
BKC-23	?	Garnet	Lu-Hf	TIMS?	Isochron	3233 ± 17	Cutts et al., 2014	
AGC 496	Felsic metavolcanic	Zircon	U-Pb	SHRIMP	$^{207}Pb/^{206}Pb$	3540.7 ± 1.3	Kröner et al., 2016	
BA 39	Felsic schist	Zircon	U-Pb	Kober	$^{207}Pb/^{206}Pb$	3547 ± 2	Kröner et al., 1996	
BA 40	Felsic tuff	Zircon	U-Pb	Kober	$^{207}Pb/^{206}Pb$	3547 ± 1.7	Kröner et al., 1996	
BA 49	Felsic tuff	Zircon	U-Pb	Kober	$^{207}Pb/^{206}Pb$	3548 ± 3.0	Kröner et al., 1996	
SA 414-2	Felsic tuff	Zircon	U-Pb	Kober	$^{207}Pb/^{206}Pb$	3548 ± 1.3	Kröner et al., 1996	
BA 39	Felsic schist	Zircon	U-Pb	SHRIMP	$^{207}Pb/^{206}Pb$	3552.0 ± 0.5	Kröner et al., 2016	
08-Ver-04	Felsic schist	Zircon	U-Pb	SHRIMP	$^{207}Pb/^{206}Pb$	3537.3 ± 2.6	Kröner et al., 2016	
BA 137&140	Felsic schist	Zircon	U-Pb	SHRIMP	$^{207}Pb/^{206}Pb$	3530.2 ± 0.3	Kröner et al., 2016	
BA 137	Felsic schist	Zircon	U-Pb	LA ICP-MS	U.I.	3527 ± 15	Kröner et al., 2016	
BA 140	Felsic schist	Zircon	U-Pb	LA ICP-MS	U.I.	3528 ± 11	Kröner et al., 2016	
BA 139	Felsic breccia	Zircon	U-Pb	SHRIMP	$^{207}Pb/^{206}Pb$	3521.3 ± 0.9	Kröner et al., 2016	
BA 130	Massive felsic rock	Zircon	U-Pb	SHRIMP	$^{207}Pb/^{206}Pb$	3431.4 ± 1.5	Kröner et al., 2016	Feeder dyke
Sandspruit Formation								
BA 149	Felsic volcanic	Zircon	U-Pb	SHRIMP	$^{207}Pb/^{206}Pb$	3531.5 ± 0.8	Kröner et al., 2016	
BA173	Felsic volcanic	Zircon	U-Pb	SHRIMP	$^{207}Pb/^{206}Pb$	3533.2 ± 0.7	Kröner et al., 2016	
Ba170	Felsic volcanic	Zircon	U-Pb	SHRIMP	$^{207}Pb/^{206}Pb$	3534.4 ± 1.5	Kröner et al., 2016	
BA 116	Felsic volcanic	Zircon	U-Pb	SHRIMP	$^{207}Pb/^{206}Pb$	3220.0 ± 1.6	Kröner et al., 2016	Metasomatism
Ba 118	Granite sill	Zircon	U-Pb	SHRIMP	$^{207}Pb/^{206}Pb$	3445.2 ± 0.4	Kröner et al., 2016	
Ba 117	Leucogranite sill	Zircon	U-Pb	SHRIMP	$^{207}Pb/^{206}Pb$	3535-3221	Kröner et al., 2016	
BA 151	Granitoid sill	Zircon	U-Pb	SHRIMP	$^{207}Pb/^{206}Pb$	3450.2 ± 2.8	Kröner et al., 2016	
BA 167	Granite sill	Zircon	U-Pb	SHRIMP	$^{207}Pb/^{206}Pb$	3446.7 ± 0.8	Kröner et al., 2016	
14SA04	Metavolcanic	Zircon	U-Pb	SIMS	$^{207}Pb/^{206}Pb$	3443 ± 13	Wang et al., 2019	
14SA36	Metavolcanic	Zircon	U-Pb	SIMS	$^{207}Pb/^{206}Pb$	3226.3 ± 5.5	Wang et al., 2019	
15SA36	Metavolcanic	Zircon	U-Pb	SIMS	$^{207}Pb/^{206}Pb$	3418.8 ± 8.1	Wang et al., 2019	
15SA36	Metavolcanic	Zircon	U-Pb	SIMS	$^{207}Pb/^{206}Pb$	3223.3 ± 7.7	Wang et al., 2019	

Table 7.1, continued.

Unit/Sample	Rock type	Mineral	Decay system	Method	Age type	Age [Ma]	Reference	Interpretation
Inyoni Shear Zone								
115-13	Garnet-amphibolite	Garnet	Sm-Nd	ID (?) TIMS	Isochron	3201.6 ± 4.7	Cutts et al., 2021	
21-13	Garnet-amphibolite	Garnet	Sm-Nd	ID (?) TIMS	Isochron	3200.3 ± 5.3	Cutts et al., 2021	
MS	Metasediment	Zircon	U-Pb	SHRIMP	$^{207}Pb/^{206}Pb$	3227 ± 7	Dziggel et al., 2005	
MS	Metasediment	Titanite	U-Pb	SHRIMP	U.I.	3229 ± 9.3	Dziggel et al., 2005	
14SA35	Metavolcanic	Zircon	U-Pb	SIMS	$^{207}Pb/^{206}Pb$	3248.8 ± 5.6	Wang et al., 2019	
15SA30	Metavolcanic	Zircon	U-Pb	SIMS	$^{207}Pb/^{206}Pb$	3249 ± 25	Wang et al., 2019	
15SA31-1	Metavolcanic	Zircon	U-Pb	SIMS	$^{207}Pb/^{206}Pb$	3253 ± 10	Wang et al., 2019	
15SA31-2	Metavolcanic	Zircon	U-Pb	SIMS	$^{207}Pb/^{206}Pb$	3280.9 ± 4.7	Wang et al., 2020	
15SA31-2	Metavolcanic	Zircon	U-Pb	SIMS	$^{207}Pb/^{206}Pb$	3245.8 ± 7.6	Wang et al., 2020	

7.2 Thermal history of the Stolzburg Block

The thermal history of the Stolzburg Block begins with the intrusion of TTG plutons into the supracrustal rock succession of the Theespruit and Sandspruit formations, lower Onverwacht Group. The intrusive relationship between the two can be seen in many outcrops in the Stolzburg Block. Based on U-Pb zircon ages, both published in the literature and as part of this thesis (see section 7.1.2), the emplacement happened between ca. 3460 and 3440 Ma, with the best estimate for the Stolzburg and Theespruit plutons being ca. 3455 Ma (Laurent et al., 2020; Schoene et al., 2008). The oldest population of U-Pb apatite dates obtained in this study for granitoid samples and a mafic schist sample from the Stolzburg Block of ca. 3449 ± 15 Ma (Fig. 7.1) is within uncertainty identical with the U-Pb ages of igneous zircon grains. The only estimate on the metamorphic conditions recorded by the greenstones at that time is ca. 550 °C at ca. 4.5 kbar, reported by Cutts et al. (2014) for a sample from the north-east of the Stolzburg Block, which has been temporally constrained to 3436 ± 18 Ma with a U-Pb monazite age (Cutts et al., 2014), within uncertainty identical with the age of TTG emplacement. Apatite from mafic schist sample MS 21 with a trace-element signature comparable to hydrothermal apatite (see section 6.4) grows at the same time (3447 ± 19 Ma). In the TTG plutons, igneous titanite grains yield Zr-in-titanite temperatures of ca. 680 to 700 °C (see chapter 5).

Prior to this thesis, the constraints on the post-emplacement thermal evolution of the Stolzburg Block were for the most part limited to the supracrustal rocks of the Theespruit and Sandspruit formations. The peak metamorphic P-T conditions recorded by the greenstones are in the range of ca. 7 to 11 kbar and ca. 550 to 700 °C (Cutts et al., 2021, 2014; Diener et al., 2005; Dziggel et al., 2002; Kato et al., 2018; Moyen et al., 2006). The timing of metamorphism is constrained to ca. 3230 Ma to 3200 Ma (see section 7.1.3) (Cutts et al., 2021). The only information available on the post-emplacement history of the TTG plutons were (presumed metamorphic) titanite ages of ca. 3215 ± 3 Ma for the Doornhoek Pluton and ca. 3201 ± 2 Ma for the Stolzburg pluton (Kamo and Davis, 1994) and U-Pb apatite ages of ca. 3400 to 3270 Ma and ca. 3100 to 3080 Ma for samples from the northern and southern margin of the Stolzburg Pluton, respectively (Schoene et al., 2008). With this thesis, I attempt to contribute to the existing constraints on the thermal evolution of the Stolzburg Block and to provide data on the metamorphic history of the TTG plutons that has been lacking so far.

The results of this thesis revealed that the Stolzburg Block has been subject to at least three thermal events after its “formation” at ca. 3450 Ma, which can be seen in the U-Pb apatite thermochronology (section 7.1; Fig. 7.1). The first potential thermal event affecting the Stolzburg Block is only observed in apatite grains from two of the analyzed samples, giving an age of 3357 ± 25 Ma (n = 8). A similar age has already been reported by Moyen et al. (2019)

for felsic dykes cross-cutting the Theespruit Pluton. However, no further information is available regarding a potential thermal event at that time.

The next youngest group of apatite dates at 3213 ± 6 Ma is the largest in the dataset (n = 88) and coincides with the reported ages for the well-documented amphibolite-facies metamorphism of the supracrustal rocks of the Stolzburg Block. As stated above, the reported temperature conditions of the ca. 3230 to 3200 Ma metamorphism are in the range of 550 to 700 °C. Furthermore, the trace-element analyses of metamorphic titanite and zircon give the first temperature constraints for the TTG rocks of the Stolzburg Block, yielding Zr-in-titanite and Ti-in-zircon temperatures of ca. 650 ± 20 °C and 645 ± 62 °C, respectively. Even though there is no geochronological data available for the grains for which these temperatures were obtained, based on the fact that they are within uncertainty identical with the conditions recorded by the associated greenstones and on ages obtained for metamorphic zircon in this study and for metamorphic titanite (Diener et al., 2005; Dziggel et al., 2005; Kamo and Davis, 1994), I assume that these temperatures represent the conditions experienced by the whole Stolzburg Block at ca. 3215 Ma. Even the lower end of this temperature range is well within the typical closure temperature range of U-Pb in apatite (Chamberlain and Bowring, 2000; Cherniak et al., 1991). The preservation of apatite ages older than ca. 3215 Ma and of primary Sr and REE signatures indicates that, despite experiencing temperatures of potentially up to 700 °C, the apatite grains did not have their U-Pb systematics completely reset. In order to achieve this, the duration of peak metamorphism would have to be very short (<100,000 years).

No temperature constraints are available for the ca. 3107 ± 11 Ma event. However, it is contemporaneous with the emplacement of the Boesmanskop syenite (Kamo and Davis, 1994) and the Mpuluzi-Piggs Peak batholith (Moyen et al., 2021; Murphy, 2015). This plutonism has likely heated the neighboring Stolzburg Block lithologies sufficiently, to cause a reset of U-Pb systematics in some apatite domains. There is no temperature and cooling history available for the Boesmanskop syenite. The youngest population of U-Pb apatite dates reveals a previously unknown event at ca. 2816 ± 7 Ma. No similar ages have been reported in the vicinity, however, whatever happened then was hot and/or long enough to reset a fairly large fraction of apatite domains, it being the second largest population of apatite dates after the 3213 ± 6 Ma population (Fig. 7.1). Apatite dated to ca. 2.8 Ga in sample MS 15 shows both igneous and metamorphic REE signature (Fig. 5.5c). The REE are much more resistant to diffusion in apatite than Sr (which has not been reset in the analyzed samples) and Pb (which has been partially reset) (Cherniak, 2000; Cherniak et al., 1991; Cherniak and Ryerson, 1993). This implies that the ca. 2.8 Ga apatite domain showing a metamorphic REE signature does

either represent new metamorphic growth at 2.8 Ga or an older, ca. 3.2 Ga metamorphic domain that had its U-Pb systematics reset at ca. 2.8 Ga.

Figure 7.2 shows the currently known constraints on the thermal evolution of the Stolzburg Block, based on published P-T estimates and geochronology combined with the findings of this thesis. What can be inferred from the data at hand, is that the Stolzburg Block has experienced at least three thermal events following the emplacement of TTG plutons at ca. 3450 Ma. The peak temperature conditions in all of these were sufficiently high to facilitate a partial reset of U-Pb systematics in apatite. At ca. 3215 Ma, the peak temperature was potentially in the range of 600 to 700 °C, implying a very high burial and exhumation rate.

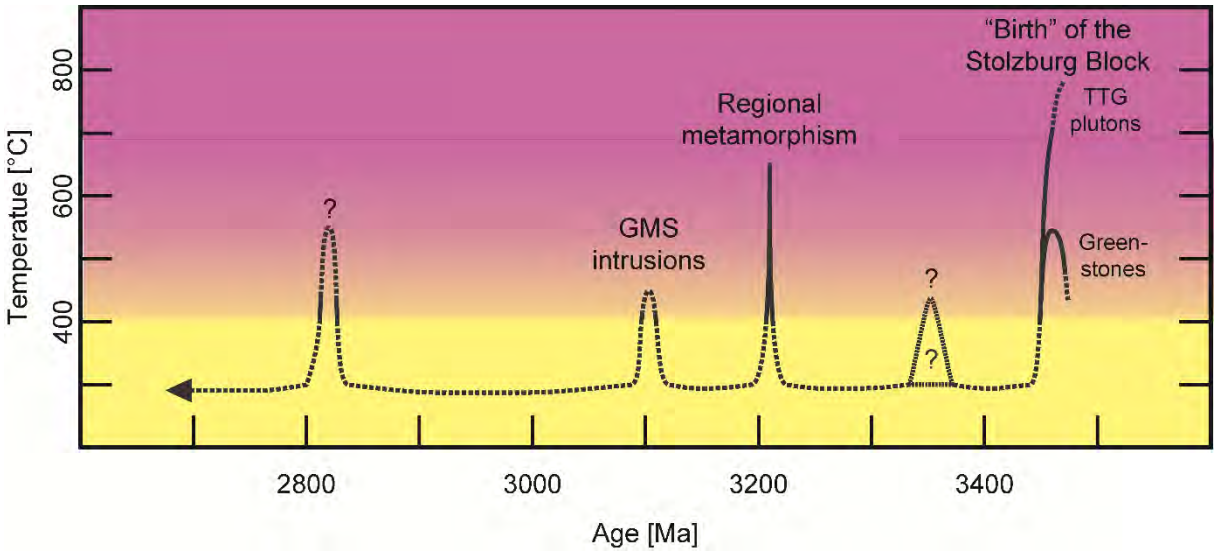

Fig. 7.2. Projected thermal evolution of the Stolzburg Block from the intrusion of TTG plutons into the supracrustal rocks of the lower Onverwacht Group at ca. 3450 Ma to the last heating event discovered by apatite thermochronology at ca. 2820 Ma. The peak temperature of the ca. 3215 Ma metamorphism is given by petrological studies on greenstones (Cutts et al., 2021, 2014; Diener et al., 2005; Dziggel et al., 2002; Kato et al., 2018) and inferred for the TTG rocks from Zr-in-titanite and Ti-in-zircon temperatures from mineral domains that were interpreted as metamorphic (chapter 5).

7.3 Implications for geodynamic models

The current geodynamic models for the Mesoarchean need to be reviewed and revised in the light of the findings of this thesis. As stated in the introduction of this thesis, the ways in which the crust reacts to compressional stress are governed by its thermal state. Through apatite petrochronology, I have provided new constraints on the thermal state of the felsic crust from ca. 3450 down to ca. 2820 Ma. In the following, the implication of the findings of this thesis will be discussed with respect to the consequences for the tectonic evolution of the Stolzburg Block specifically and the BGGT in general.

The ca. 3215 Ma event is a critical point. The exact tectonic setting, both locally and globally, remains unclear. No decisive argument in favor of one of the proposed geotectonic models can be made based on the results of this study. However, the data at hand allows to rule out certain processes and the models which invoke them. Absence of eclogites in the Archean rock record has been used to evoke non-uniformitarian tectonic models for that time. The model of partial convective overturn (PCO) which is regularly proposed for the BGGT (Schmitz and Heubeck, 2021; Van Kranendonk, 2011; Van Kranendonk et al., 2015, 2014; Wang et al., 2019) requires specific and distinct thermal conditions and P-T paths for the “greenstone keels” and “TTG domes” during the PCO event (Van Kranendonk et al., 2015, 2014). In the PCO model, a partial melting of TTG rocks is achieved by radiogenic heating, insulated by the overlying greenstone sequences (“the volcanic plateau”). Such a partial melting would require temperatures of >750 °C (Huang and Wyllie, 1973; Stern and Wyllie, 1973). Such a temperature is already at the upper limit of conditions under which U-Pb apatite ages can be preserved, and that only at very short heating duration (< ca. 50 k.yrs.) (Chamberlain and Bowring, 2000; Cherniak et al., 1991). The proposed partial melting through radiogenic heating cannot be achieved in such a short duration. Hence the PCO model is at odds with the findings of this thesis, which show that apatite U-Pb ages, Sr isotopic and REE signatures older than the proposed PCO event at ca. 3.2 Ga have been preserved, and that the greenstones and TTG plutons have potentially experienced the same metamorphic conditions which were never hot enough to produce the required melting.

The supracrustal rocks of the Stolzburg Block and the Inyoni shear zone record metamorphic conditions of ca. 7-11 kbar and 550-700 °C (Cutts et al., 2021, 2014; Diener et al., 2005; Dziggel et al., 2002; Kato et al., 2018; Moyen et al., 2006). Time estimates for peak metamorphism range from a U-Pb titanite age of 3229 ± 25 Ma (Diener et al., 2005), and a Lu-Hf garnet age of 3233 ± 17 Ma (Cutts et al., 2014) from the Tjakastad schist belt, through U-Pb titanite and zircon ages of 3229 ± 9 and 3227 ± 7 Ma, respectively, for a sample from the Inyoni shear zone (Dziggel et al., 2005) to potentially as late as a Sm-Nd garnet age of 3200 ± 5 Ma, also for the Inyoni Shear Zone (Cutts et al., 2021) – however, as stated by Cutts et al. (2021), “147Sm decay constant uncertainty leaves open the possibility that Inyoni garnet growth could have coincided with the previously recognized 3.23 Ga regional metamorphism”. Combining the available geochronological data for metamorphic minerals (see section 7.1.3) with the results of the apatite thermochronology pinpoints the timing of peak metamorphism to ca. 3220-3210 Ma. The metamorphic ages obtained for the supracrustal rocks are within uncertainty identical with the 3213 ± 6 Ma U-Pb apatite age group shown by Stolzburg Block granitoids (Fig. 7.1). This indicates, that both greenstones and TTG plutons of the Stolzburg Block have experienced a thermal event at roughly the same time. What remains unresolved

is whether both lithologies have experienced the same metamorphic conditions or not, with currently only circumstantial evidence available for a uniform history of the two.

The results of the apatite U-Pb thermochronology show, that ca. 3450 Ma apatite ages have been preserved in the Stolzburg Block TTGs, which puts an upper limit on the temperatures experience by the TTG rocks – or on the heating duration (chapter 4; Figs. 7.1 and 7.2). Metamorphic temperatures in the TTG rocks are ca. 650 °C, as indicated by Zr-in-titanite and Ti-in-zircon thermometry (chapter 5). While no radiometric ages are available for the grains from which these temperatures were obtained, a shared history between the supracrustal and TTG rocks of the Stolzburg Block post ca. 3450 Ma is indicated by the intrusive relationship between the two. If the temperatures recorded by titanite and zircon from the TTG rocks are indeed related to ca. 3.2 Ga metamorphism, then peak temperature conditions were only achieved for no more than 100,000 years (Fig. 5.11). If these temperatures are not related to the ca. 3.2 Ga metamorphism – the growth of “metamorphic” titanite and zircon could for example also be due to hydrothermal activity directly after emplacement – and the TTG rocks have for whatever reason not been heated as much as the greenstones at ca. 3225 Ma, then the maximum duration of peak metamorphism is still confined to ca. 1 million years by the preservation of older U-Pb systematics in apatite (chapter 4, Figs. 5.11 and 7.1).

The PT conditions in the Stolzburg Block at ca. 3.2 Ga indicate that no deep burial to reach eclogite-facies has happened, which is typical for a “hot orogen” (Chardon et al., 2009; Fossen et al., 2017; Gapais et al., 2009). Another feature of “hot orogens” is gravitational collapse of the orogens due to crustal thickening – and the impossibility to substantially thicken a hot and rheologically “weak” crust (Chardon et al., 2009). A “hot orogen” setting for the Barberton crust has for example been evoked by Moyen and Laurent (2018). However, at face value a rapid exhumation of the Stolzburg Block as indicated by the apatite petrochronology seems to be at odds with a “hot orogen”, which typically tend to be long-lasting. In light of this finding, the “hot orogen” model will need to be revised to accommodate for fast processes on a local scale. These new constraints on the thermal state of the Archean crust need to be taken into account in future modelling. Based on my findings and building on previous work, I propose the following evolution for the Stolzburg Block and the southern BGGT:

0. Ca. 3530 Ma to >3450 Ma: Deposition of Theespruit and Sandspruit formations (Fig. 7.3a). Mafic to ultramafic volcanism with subordinate felsic volcanism at ca. 3530 Ma (Kröner et al., 1996; Kröner et al., 2016). Erosion of volcanic rocks and (nearby?) deposition of volcaniclastic sediments, with the minimum age of ca. 3450 Ma given by TTG intrusions into the metasediments (Dziggel et al., 2002). Contemporaneously, the

Steynsdorp Pluton is emplaced (Kamo and Davis, 1994; Kröner et al., 1996), relation to the lower Onverwacht Group rocks unclear (Kisters and Anhaeusser, 1995).

1. Ca. 3450 Ma: “Birth” of the Stolzburg Block (Fig, 7.3b). Intrusion of TTG plutons (Kamo and Davis, 1994; Lana et al., 2010a; Laurent et al., 2020; Schoene et al., 2008) (chapter 4) into the Theespruit and Sandspruit formation supracrustal rocks (Figs. 2.2h+i, 2.3b+c, 2.4b) (Moyen et al., 2019), which have been buried to mid-crustal levels, with peak metamorphic condition of ca. 550 °C at ca. 4.5 kbar recorded by the greenstones (Cutts et al., 2014). Trace-element systematics of apatite grains from the ca. 3450 Ma TTG rocks indicate a high-pressure source of the parent magma (chapter 5), opposed to a uniform source for both medium- and high-pressure TTGs as proposed by Laurent et al. (2020).
2. Ca. 3450 to 3230 Ma: A period of relative quiescence for the Stolzburg Block. Temperatures in the block were generally <400 °C, with potentially some heating at ca. 3350 Ma as seen in the apatite U-Pb thermochronology of samples MS 2 and MS 27 (Fig. 7.1). Meanwhile, (ultra)mafic and subordinate felsic volcanism continues to build the Onverwacht Group, with a potential thrusting of the Kromberg Formation over the Hooggenoeg Formation (Grosch and Slama, 2017).
3. Ca. 3280 to 3230 Ma: Deposition of Fig Tree Group (FTG) sediments (Fig. 7.3c). Sedimentation in the south of the BGB commenced at ca. 3280 Ma with homogenous, regionally sourced sediments, changing to an increasingly local provenance between ca. 3260 and 3240 Ma, as a fold-and-thrust belt develops due to local uplifts caused by an approaching orogenic front (Drabon and Lowe, 2021).
4. Ca. 3230 to 3200 Ma: Major accretion and deformation event. At ca. 3225 Ma, sedimentation of the FTG ceases and Moodies deposition begins (refs). At the same time, the Kaap Valley and Nelshoogte plutons are emplaced (Guitreau et al., 2012; Matsumura, 2014; Schoene et al., 2008; Zeh et al., 2009), intruding the greenstones of the lower Onverwacht Group in the west of the BGB (De Ronde and Kamo, 2000). The Stolzburg Block is subjected to amphibolite-facies metamorphism with rapid burial in a “hot orogen” (Fig. 7.3d) and exhumation (Fig. 7.3e) along the Komati fault due to orogenic collapse (Kisters et al., 2003). Peak temperatures were only reached for <1 million years. Felsic dykes are emplaced on the margins of the TTG plutons syn- to post-tectonically.
5. Ca. 3100 Ma: Intrusion of large granitic plutons and batholiths (Fig. 7.3f). The Stolzburg Block is briefly heated to >400 °C by the intrusion of the Boesmanskop syenite and the Mpuluzi-Piggs Peak batholiths (Kamo and Davis, 1994; Moyen et al., 2021; Murphy, 2015), resetting some U-Pb apatite ages.

6. Ca. 3100 to 2820 Ma: Relative quiescence. Temperatures in the Stolzburg Block do not exceed ca. 400 °C.
7. Ca. 2820 Ma: Unspecified heating event. Stolzburg Block is heated to >>400 °C, resetting some U-Pb apatite ages and potentially affecting the REE composition in apatite from sample MS 15.
8. < ca. 2820 Ma: No more substantial heating of the Stolzburg Block.

Fig. 7.3. Proposed tectonic evolution for the Stolzburg Block from >3450 to <2820 Ma. See text for details. (c) to (e) modified after (Drabon and Lowe, 2021).

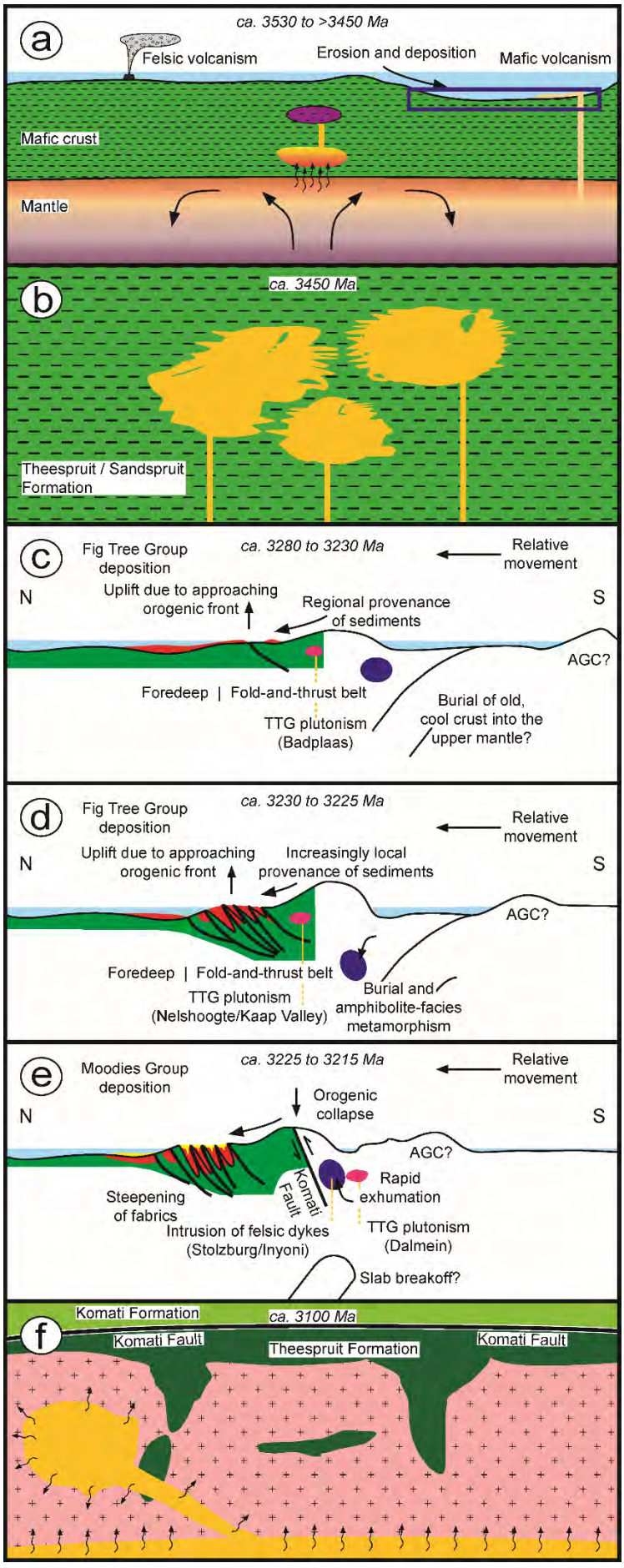

7.4 General conclusion and outlook

The main motivation for this thesis was to improve the current understanding of the thermal state of the Archean crust, in order to provide robust constraints to be taken into account for geodynamic models. This was done in two parts. At first, U-Pb ages were obtained for apatite and zircon grains from a variety of samples from the Stolzburg Block – the zircon ages primarily to map the occurrence of ca. 3.2 Ga igneous ages, the apatite ages for thermochronology. Based on the results of the U-Pb analyses, the first observations on the thermal evolution of the Stolzburg Block were drawn and published in research paper 1 (chapter 4). Then, trace-element analyses of apatite, titanite and zircon and Sr isotope analyses of apatite were performed and combined with the U-Pb age data to get a deeper understanding of the thermal history recorded by the analyzed samples; these results were published in research paper 2 (chapter 5). The implications of my findings are discussed in the two research papers and in sections 7.1 and 7.2 above. The data obtained as part of this thesis have revealed a polymetamorphic history of the Stolzburg Block and given the first constraints on the thermal state of the Archean felsic crust. The scientific contribution of my thesis are primarily these thermal constraints, which will help refine and test the validity of geodynamic models for the Archean. I have also shown that, in addition to the well-documented events at ca. 3225-3200 and 3100 Ma, the Stolzburg Block had been affected by a thermal event at ca. 2820 Ma that has so far not been reported for the BGGT.

However, in light of the previously unknown thermal event at ca. 2820 Ma, more work is necessary to accurately constrain the extent and conditions of the cryptic metamorphism. The first places to look at for this could be extensive in-situ U-Pb isotope analysis of titanite grains throughout the Stolzburg Block and high-resolution in-situ U-Pb analysis of featureless rims that occur in multiple generations around the igneous zircon grains (Fig. 4.14). It can also be expanded to U-Pb apatite thermochronology on samples beyond the Stolzburg Block or even beyond the BGGT. The age of intrusion is still not determined for many of the felsic dykes cross-cutting the Stolzburg Block. During my field work, I have taken samples from these dykes where it was possible using hammer and chisel only, but in many outcrops a sampling drill is necessary to obtain fresh samples. Furthermore, now that the medium- to high-temperature history of the Stolzburg Block has been documented, the next step would be to investigate the further cooling history. This could for example be achieved by Ar-Ar thermochronology of amphibole (present in samples MS 25 and MS 36) and Ar-Ar and/or Rb-Sr thermochronology of micas (readily available in most samples). The application of low-T thermochronology could potentially help resolve the cryptic ca. 2820 Ma heating event.

Another interesting study could be to conduct similarly extensive apatite U-Pb analyses on the supracrustal rocks of the Theespruit and Sandspruit formations, in particular on those for which

P-T estimates have already been calculated. This could provide further proof for or against a uniform thermal history of the different rocks of the Stolzburg Block. The first step in this direction has been taken with sample MS 21, for which I obtained the U-Pb (chapter 4) and trace-element (section 6.4) compositions of apatite. The same lithology had been sampled in the past and U-Pb and trace-element analyses on rutile yielded dates of ca. 3.1 Ga and Zr-in-rutile temperatures of ca. 650-660 °C (Stevens, pers. comm.). This sample also offers potential for garnet geochronology (Sm-Nd or Lu-Hf, potentially U-Pb). Further samples from Stolzburg Block greenstones can be readily sourced from the existing sample collection at Stellenbosch University.

Looking beyond Barberton, a similar study applying apatite petrochronology to rocks from other Archean terranes of similar age (Pilbara in particular, which is often linked and compared to Barberton) could complement the results of this thesis and shed light on whether the thermal conditions observed in the Stolzburg crust were unique to the proto-Kaapvaal craton or if they were unique for the time.

Unrelated to the questions asked in this thesis, the zircon grains from diorite sample MS 25 show potential to be used as a reference material. Based on the abundance and relatively large size (typical length ca. 300 to 500 µm) of the zircon grains in sample MS 25 as well as their fairly homogenous igneous microtexture and last but not least on the homogenous U-Pb and Lu-Hf characteristics determined in this study via LA ICP-MS (Fig. 4.7l and 4.8), I deduce that they can be used as a reference material, at least for in-situ U-Pb and Lu-Hf analyses. The potential for (chemical abrasion) isotope dilution thermal ionization mass spectrometry (ID TIMS) U-Pb analysis and for ion beam O isotope analysis can also be explored. A chemical abrasion is likely necessary prior to any ID TIMS analysis due to the thin featureless, likely metamorphic, rim around many zircon grains from this sample. But it is worth exploring this sample for a potential use as an Archean zircon reference material, of which not many exist (Wall et al., 2016; Wei et al., 2020). Sample MS 25b was taken from what I assume to be the same phase on the opposite side of the outcrop with the aim of determining the zircon density in this phase at outcrop scale.

Finally, the outcome of this thesis emphasizes once more how important and powerful an integrated approach of classic field work, geochronology and petrology can be when dealing with complex metamorphic histories. With relatively cheap and quick in-situ techniques like LA ICP-MS becoming increasingly available and more methods for isotope analyses in a variety of minerals being developed and refined (e.g. Sr in apatite), it should become the standard to combine geochronological studies with other isotopic and trace-element analyses of the same grains.

References

Chamberlain, K.R., Bowring, S.A., 2000. Apatite – feldspar U – Pb thermochronometer : a reliable , mid-range (~ 450°C), diffusion-controlled system. Chem. Geol. 172, 173–200.

Chardon, D., Gapais, D., Cagnard, F., 2009. Flow of ultra-hot orogens: A view from the Precambrian, clues for the Phanerozoic. Tectonophysics 477, 105–118. https://doi.org/10.1016/j.tecto.2009.03.008

Cherniak, D.J., 2000. Rare earth element diffusion in apatite. Geochim. Cosmochim. Acta 64, 3871–3885. https://doi.org/10.1016/S0016-7037(00)00467-1

Cherniak, D.J., Lanford, W.A., Ryerson, F.J., 1991. Lead diffusion in apatite and zircon using ion implantation and Rutherford Backscattering techniques. Geochim. Cosmochim. Acta 55, 1663–1673. https://doi.org/10.1016/0016-7037(91)90137-T

Cherniak, D.J., Ryerson, F.J., 1993. A study of strontium diffusion in apatite using Rutherford backscattering spectroscopy and ion implantation. Geochim. Cosmochim. Acta 57, 4653–4662. https://doi.org/10.1016/0016-7037(93)90190-8

Cutts, K.A., Maneiro, K.A., Stevens, G., Baxter, E.F., 2021. Metamorphic evolution for the Inyoni shear zone: Investigating the geodynamic evolution of a 3.20 Ga terrane boundary in the Barberton granitoid greenstone terrane, South Africa. South African J. Geol. 124, 163–180. https://doi.org/10.25131/sajg.124.0009

Cutts, K.A., Stevens, G., Hoffmann, J.E., Buick, I.S., Frei, D., Münker, C., 2014. Paleo- to Mesoarchean polymetamorphism in the Barberton Granite- Greenstone Belt , South Africa : Constraints from U-Pb monazite and Lu- Hf garnet geochronology on the tectonic processes that shaped the belt 251–270. https://doi.org/10.1130/B30807.1

De Ronde, C.E.J., Kamo, S.L., 2000. An Archaean arc-arc collisional event: a short-lived (ca 3 Myr) episode, Weltevreden area, Barberton greenstone belt, South Africa. J. African Earth Sci. 30, 219–248.

Diener, J.F.A., Stevens, G., Kisters, A.F.M., Poujol, M., 2005. Metamorphism and exhumation of the basal parts of the Barberton greenstone belt , South Africa : Constraining the rates of Mesoarchaean tectonism 143, 87–112. https://doi.org/10.1016/j.precamres.2005.10.001

Drabon, N., Lowe, D.R., 2021. Progressive accretion recorded in sedimentary rocks of the 3.28−3.23 Ga Fig Tree Group, Barberton Greenstone Belt. GSA Bull. 1–19. https://doi.org/10.1130/b35973.1

Dziggel, A., Armstrong, R.A., Stevens, G., Nasdala, L., 2005. Growth of zircon and titanite during metamorphism in the granitoid-gneiss terrane south of the Barberton greenstone belt, South Africa. Mineral. Mag. 69, 1019–1036.

Dziggel, A., Stevens, G., Poujol, M., Anhaeusser, C.R., Armstrong, R.A., 2002. Metamorphism of the granite-greenstone terrane south of the Barberton greenstone belt, South Africa: An insight into the tectono-thermal evolution of the “lower” portions of the Onverwacht Group. Precambrian Res. 114, 221–247. https://doi.org/10.1016/S0301-9268(01)00225-X

Fossen, H., Cavalcante, G.C., de Almeida, R.P., 2017. Hot Versus Cold Orogenic Behavior: Comparing the Araçuaí-West Congo and the Caledonian Orogens. Tectonics 36, 2159–2178. https://doi.org/10.1002/2017TC004743

Gapais, D., Cagnard, F., Gueydan, F., Barbey, P., Ballèvre, M., 2009. Mountain building and exhumation processes through time: Inferences from nature and models. Terra Nov. 21, 188–194. https://doi.org/10.1111/j.1365-3121.2009.00873.x

Grosch, E., Slama, J., 2017. Evidence for 3.3-billion-year-old oceanic crust in the Barberton greenstone belt, South Africa. Geology 45, G39035.1. https://doi.org/10.1130/G39035.1

Guitreau, M., Blichert-Toft, J., Martin, H., Mojzsis, S.J., Albarède, F., 2012. Hafnium isotope evidence from Archean granitic rocks for deep-mantle origin of continental crust. Earth Planet. Sci. Lett. 337–338, 211–223. https://doi.org/10.1016/j.epsl.2012.05.029

Huang, W.L., Wyllie, P.J., 1973. Melting relations of muscovite-granite to 35 kbar as a model for fusion of metamorphosed subducted oceanic sediments. Contrib. to Mineral. Petrol. 42, 1–14. https://doi.org/10.1007/BF00521643

Kamo, S.L., Davis, D.W., 1994. Reassessment of Archean crustal development in the Barberton Mountain Land, South Africa, based on U-Pb dating. Tectonics 13, 167–192.

Kato, D., Aoki, K., Komiya, T., Yamamoto, S., Sawaki, Y., Asanuma, H., Sato, T., Tsuchiya, Y., Shozugawa, K., Matsuo, M., Windley, B.F., 2018. Constraints on the P–T conditions of high-pressure metamorphic rocks from the Inyoni shear zone in the mid-Archean Barberton Greenstone Belt, South Africa. Precambrian Res. 315, 1–18. https://doi.org/10.1016/j.precamres.2018.06.018

Kisters, A.F.M., Anhaeusser, C.R., 1995. The structural significance of the Steynsdorp pluton and anticline within the tectono-magmatic framework of the Barberton Mountain Land. South African J. Geol. 98, 43–51.

Kisters, A.F.M., Belcher, R.W., Poujol, M., Dziggel, A., 2010. Continental growth and convergence-related arc plutonism in the Mesoarchaean : Evidence from the Barberton granitoid-greenstone terrain , South Africa. Precambrian Res. 178, 15–26. https://doi.org/10.1016/j.precamres.2010.01.002

Kisters, A.F.M., Stevens, G., Dziggel, A., Armstrong, R.A., 2003. Extensional detachment faulting and core-complex formation in the southern Barberton granite-greenstone terrain, South Africa: Evidence for a 3.2 Ga orogenic collapse. Precambrian Res. https://doi.org/10.1016/j.precamres.2003.08.002

Kröner, A., Anhaeusser, C.R., Hoffmann, J.E., Wong, J., Geng, H., Hegner, E., Xie, H., Yang, J., Liu, D., 2016. Chronology of the oldest supracrustal sequences in the Palaeoarchaean Barberton Greenstone Belt, South Africa and Swaziland. Precambrian Res. 279, 123–143. https://doi.org/10.1016/J.PRECAMRES.2016.04.007

Kröner, A., Hegner, E., Wendt, J.I., Byerly, G.R., 1996. The oldest part of the Barberton granitoid-greenstone terrain, South Africa: Evidence for crust formation between 3.5 and 3.7 Ga. Precambrian Res. 78, 105–124. https://doi.org/10.1016/0301-9268(95)00072-0

Lana, C., Kisters, A., Stevens, G., 2010a. Exhumation of Mesoarchean TTG gneisses from the middle crust: Insights from the Steynsdorp core complex, Barberton granitoid-greenstone terrain, South Africa. Bull. Geol. Soc. Am. 122, 183–197. https://doi.org/10.1130/B26580.1

Lana, C., Tohver, E., Cawood, P., 2010b. Quantifying rates of dome-and-keel formation in the Barberton granitoid-greenstone belt, South Africa. Precambrian Res. 177, 199–211. https://doi.org/10.1016/j.precamres.2009.12.001

Laurent, O., Björnsen, J., Wotzlaw, J.F., Bretscher, S., Pimenta Silva, M., Moyen, J.F., Ulmer, P., Bachmann, O., 2020. Earth's earliest granitoids are crystal-rich magma reservoirs tapped by silicic eruptions. Nat. Geosci. https://doi.org/10.1038/s41561-019-0520-6

Matsumura, R., 2014. The petrogenesis of the Nelshoogte pluton: The youngest and most compositionally variable TTG plutons in the Barberton Granit-Greenstone Terrain. Stellenbosch University.

Moyen, J.-F., Stevens, G., Kisters, A.F.M., Belcher, R.W., Lemirre, B., 2019. TTG Plutons of the Barberton Granitoid-Greenstone Terrain, South Africa, in: Van Kranendonk, M.J., Bennett, V.C., Hoffmann, J.E. (Eds.), Earth's Oldest Rocks. pp. 615–653.

Moyen, J.F., Laurent, O., 2018. Archaean tectonic systems: A view from igneous rocks. Lithos. https://doi.org/10.1016/j.lithos.2017.11.038

Moyen, J.F., Stevens, G., Kisters, A.F.M., 2006. Record of mid-Archaean subduction from metamorphism in the Barberton terrain , South Africa. Nature 442, 559–562. https://doi.org/10.1038/nature04972

Moyen, J.F., Zeh, A., Cuney, M., Dziggel, A., Carrouée, S., 2021. The multiple ways of recycling Archaean crust: A case study from the ca. 3.1 Ga granitoids from the Barberton Greenstone Belt, South Africa. Precambrian Res. 353, 105998. https://doi.org/10.1016/j.precamres.2020.105998

Murphy, R., 2015. Stabilizing a Craton: The Origin and Emplacment of the 3.1 Ga Mpuluzi Batholith. Maquarie University.

Schmitz, M., Heubeck, C., 2021. Constraints on deformation mechanisms of the Barberton Greenstone Belt from regional stratigraphic and structural data of the synorogenic Moodies Group. Precambrian Res. 362, 106177. https://doi.org/10.1016/j.precamres.2021.106177

Schoene, B., de Wit, M.J., Bowring, S.A., 2008. Mesoarchean assembly and stabilization of the eastern Kaapvaal craton: A structural-thermochronological perspective. Tectonics 27, 1–27. https://doi.org/10.1029/2008TC002267

Stern, C.R., Wyllie, P.J., 1973. Water-saturated and undersaturated melting relations of a granite to 35 kilobars. Earth Planet. Sci. Lett. 18, 163–167. https://doi.org/10.1016/0012-821X(73)90052-6

Van Kranendonk, M.J., 2011. Cool greenstone drips and the role of partial convective overturn in Barberton greenstone belt evolution. J. African Earth Sci. 60, 346–352. https://doi.org/10.1016/j.jafrearsci.2011.03.012

Van Kranendonk, M.J., Kröner, A., Hoffman, J.E., Nagel, T., Anhaeusser, C.R., 2014. Just another drip: Re-analysis of a proposed mesoarchean suture from the Barberton mountain land, South Africa. Precambrian Res. 254, 19–35. https://doi.org/10.1016/j.precamres.2014.07.022

Van Kranendonk, M.J., Smithies, R.H., Griffin, W.L., Huston, D.L., Hickman, A.H., Champion, D.C., Anhaeusser, C.R., Pirajno, F., 2015. Making it thick: a volcanic plateau origin of Palaeoarchean continental lithosphere of the Pilbara and Kaapvaal cratons. Geol. Soc. London, Spec. Publ. 389, 83–111. https://doi.org/10.1144/SP389.12

Wall, C.J., Scoates, J.S., Weis, D., 2016. Zircon from the Anorthosite zone II of the Stillwater Complex as a U-Pb geochronological reference material for Archean rocks. Chem. Geol. 436, 54–71. https://doi.org/10.1016/j.chemgeo.2016.04.027

Wang, H., Yang, J.H., Kröner, A., Zhu, Y.S., Li, R., 2019. Non-subduction origin for 3.2 Ga high-pressure metamorphic rocks in the Barberton granitoid-greenstone terrane, South Africa. Terra Nov. 31, 373–380. https://doi.org/10.1111/ter.12397

Wang, H., Yang, J.H., Kröner, A., Zhu, Y.S., Wei, Q. Di, Li, R., Xu, L., 2020. Extensive magmatism and metamorphism at ca. 3.2 Ga in the eastern Kaapvaal Craton. Precambrian Res. 351. https://doi.org/10.1016/j.precamres.2020.105952

Wei, Q., Wang, H., Yang, Y., Yang, J., Huang, C., Wu, S., Xie, L., 2020. KV01 zircon—A potential New Archean reference material for microbeam U-Pb age and Hf-O isotope

determinations. Sci. China Earth Sci. 63, 1780–1790. https://doi.org/10.1007/s11430-019-9638-y

Zeh, A., Gerdes, A., Barton, J.M., 2009. Archean accretion and crustal evolution of the kalahari craton - The zircon age and Hf isotope record of granitic rocks from barberton/ swaziland to the francistown arc. J. Petrol. 50, 933–966. https://doi.org/10.1093/petrology/egp027

Appendices

Appendix A: Supplementary material for research paper 1 (chapter 4)

Fig. 4.14. Cathodoluminescence images of zircon grains.

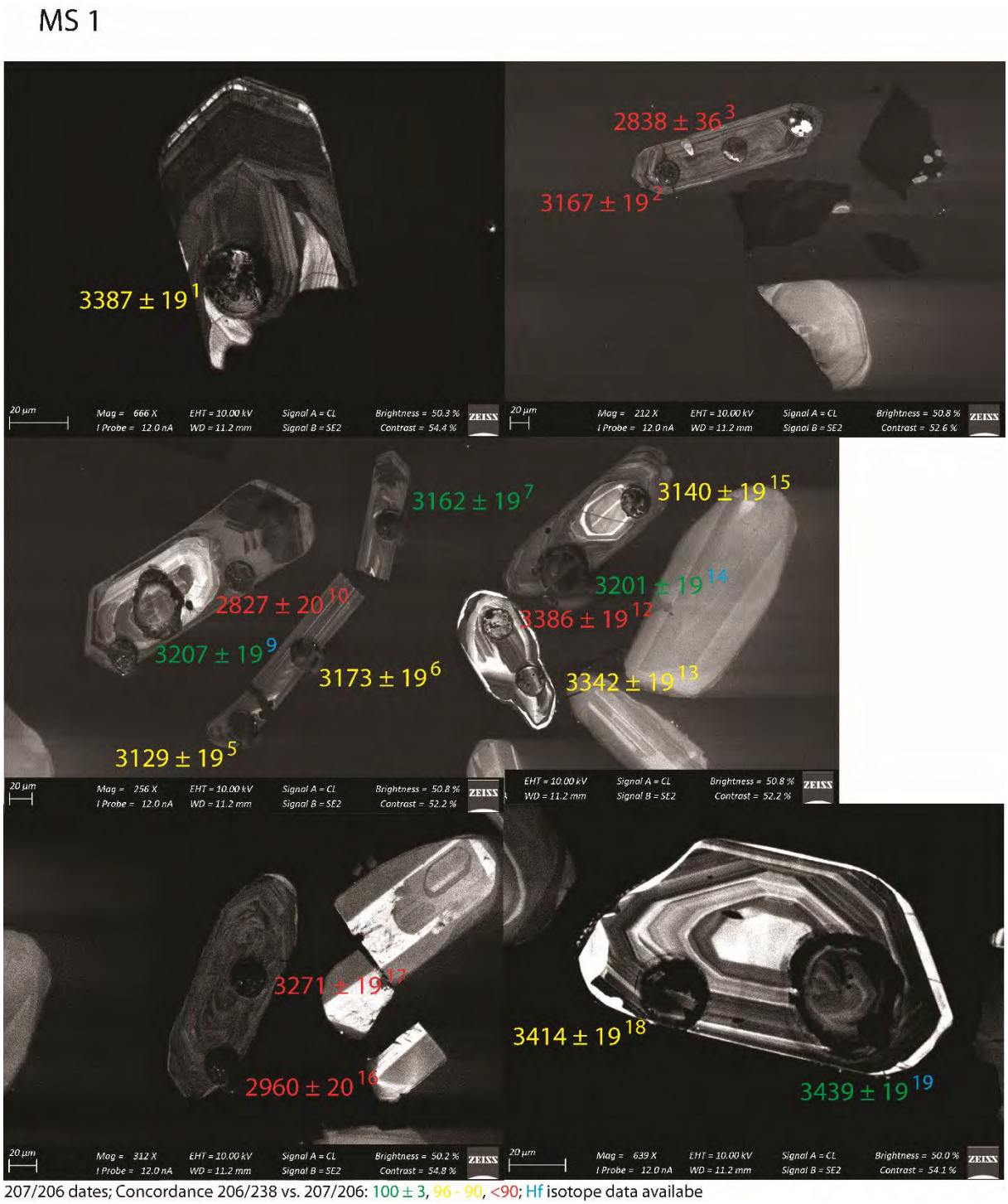

207/206 dates; Concordance 206/238 vs. 207/206: 100 ± 3, 96 - 90, <90; Hf isotope data availabe

Fig. 4.14, continued.

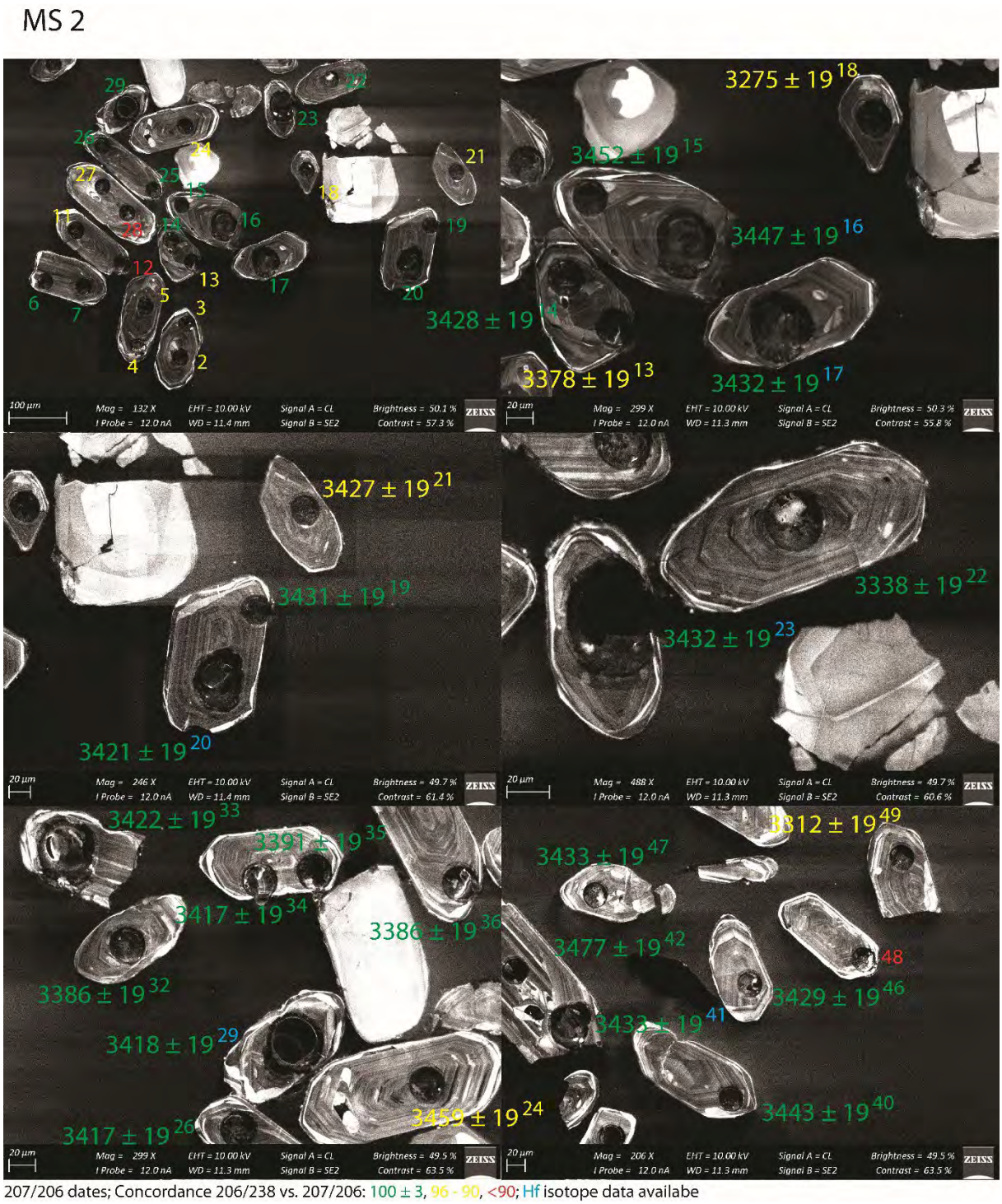

207/206 dates; Concordance 206/238 vs. 207/206: 100 ± 3, 96 - 90, <90; Hf isotope data availabe

Fig. 4.14, continued.

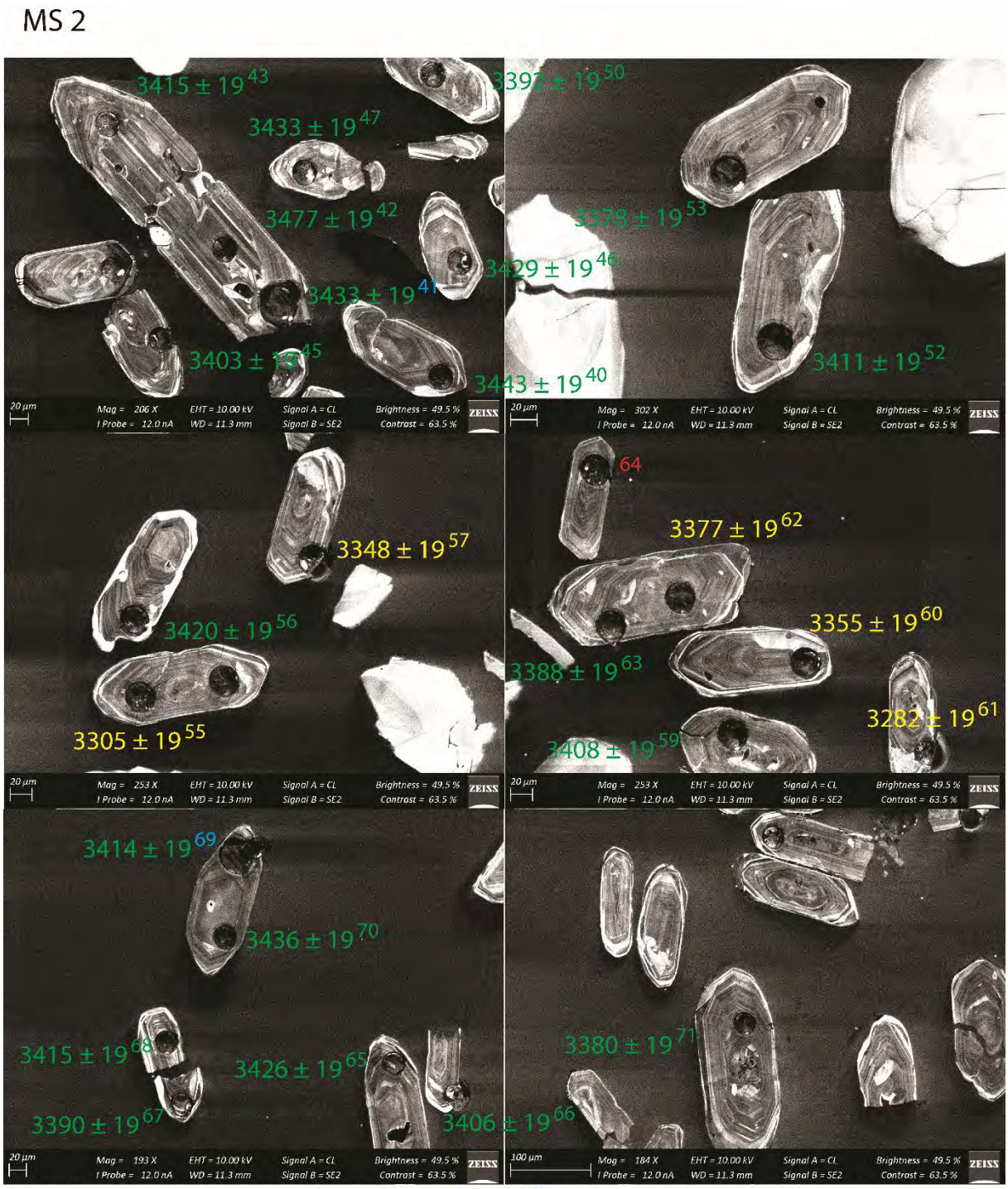

207/206 dates; Concordance 206/238 vs. 207/206: 100 ± 3, 96 - 90, <90; Hf isotope data availabe

Fig. 4.14, continued.

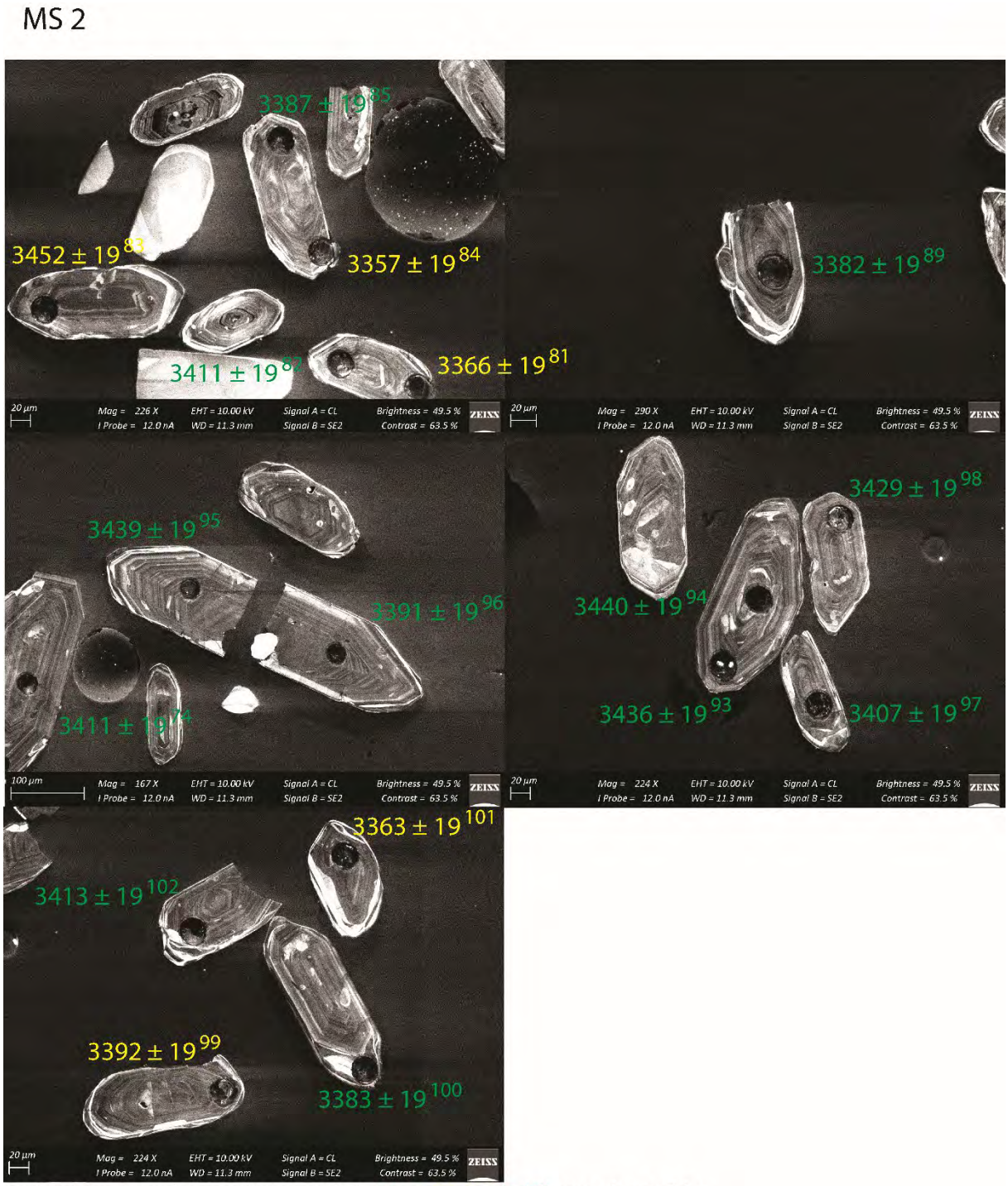

207/206 dates; Concordance 206/238 vs. 207/206: 100 ± 3, 96 - 90, <90; Hf isotope data availabe

Fig. 4.14, continued.

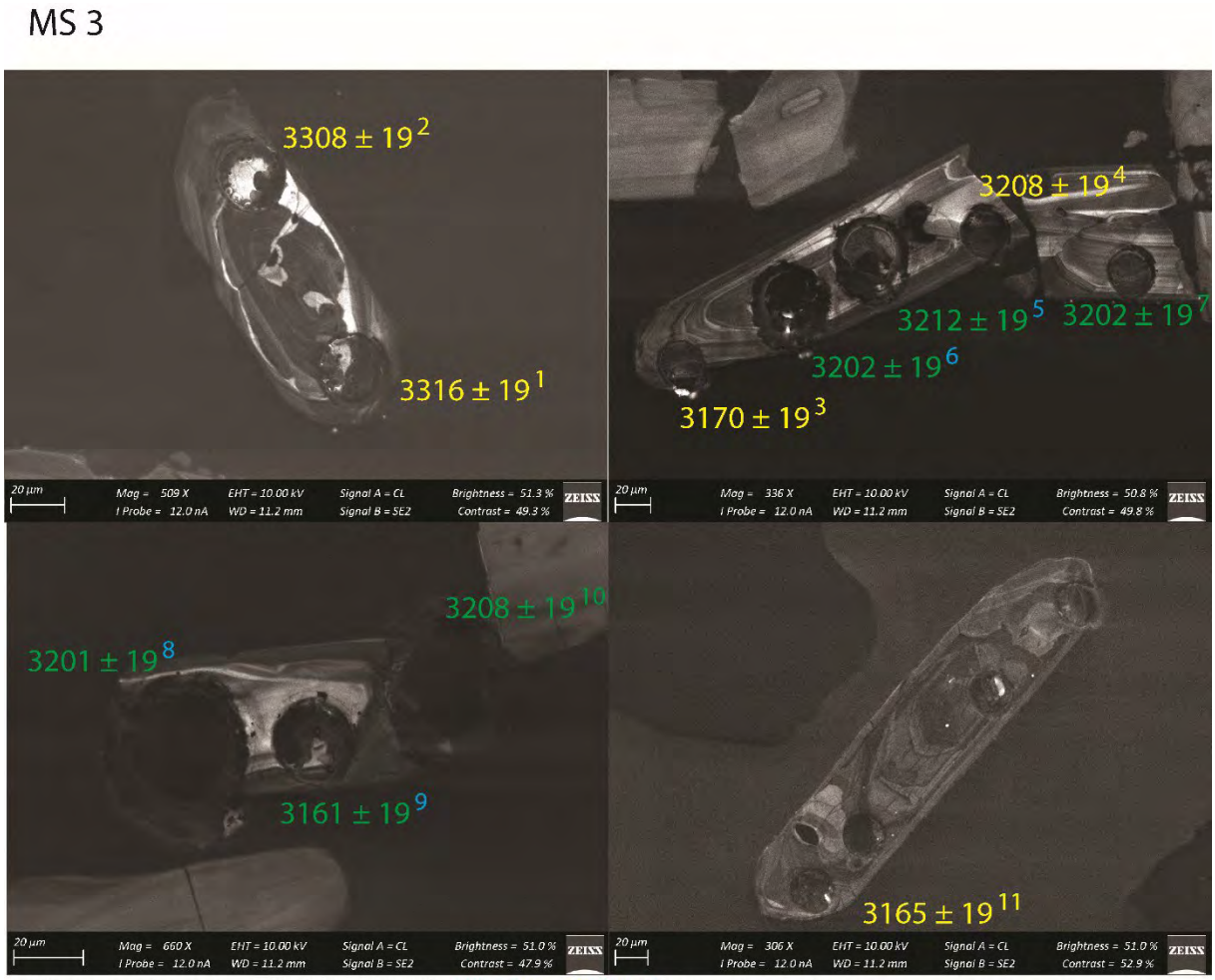

207/206 dates; Concordance 206/238 vs. 207/206: 100 ± 3, 96 - 90, <90; Hf isotope data availabe

Fig. 4.14, continued.

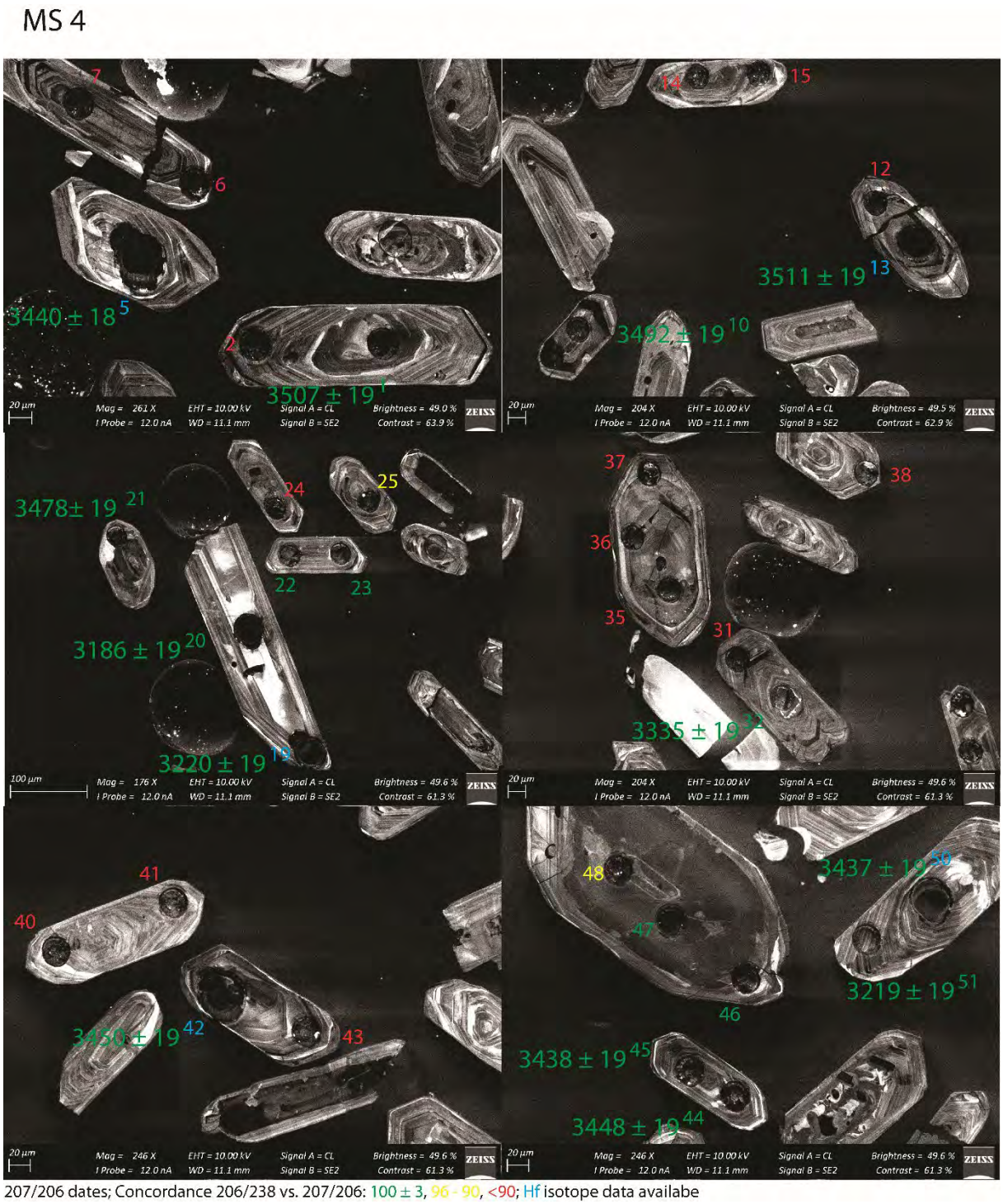

207/206 dates; Concordance 206/238 vs. 207/206: 100 ± 3, 96 - 90, <90; Hf isotope data availabe

Fig. 4.14, continued.

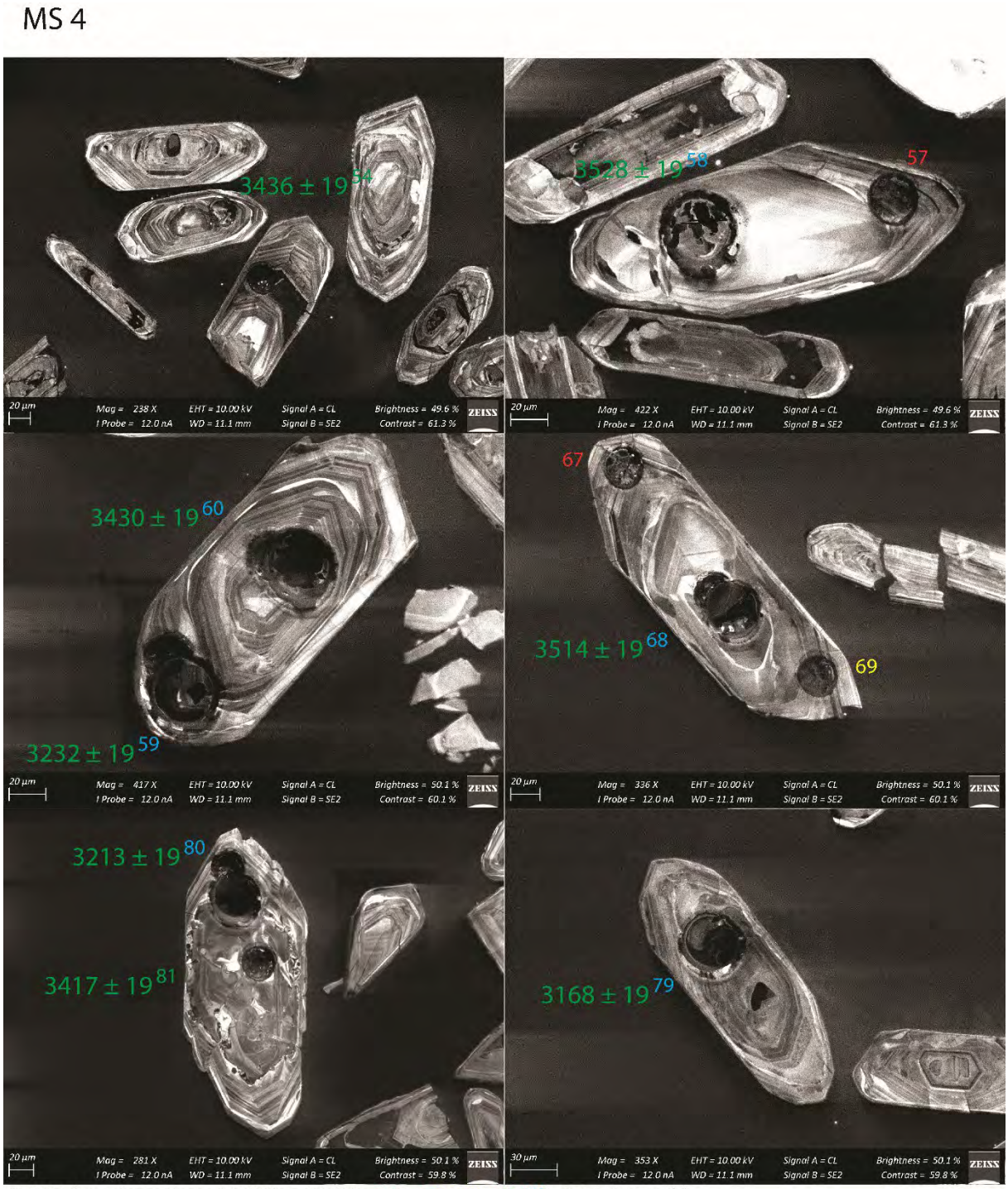

207/206 dates; Concordance 206/238 vs. 207/206: 100 ± 3, 96 - 90, <90; Hf isotope data availabe

Fig. 4.14, continued.

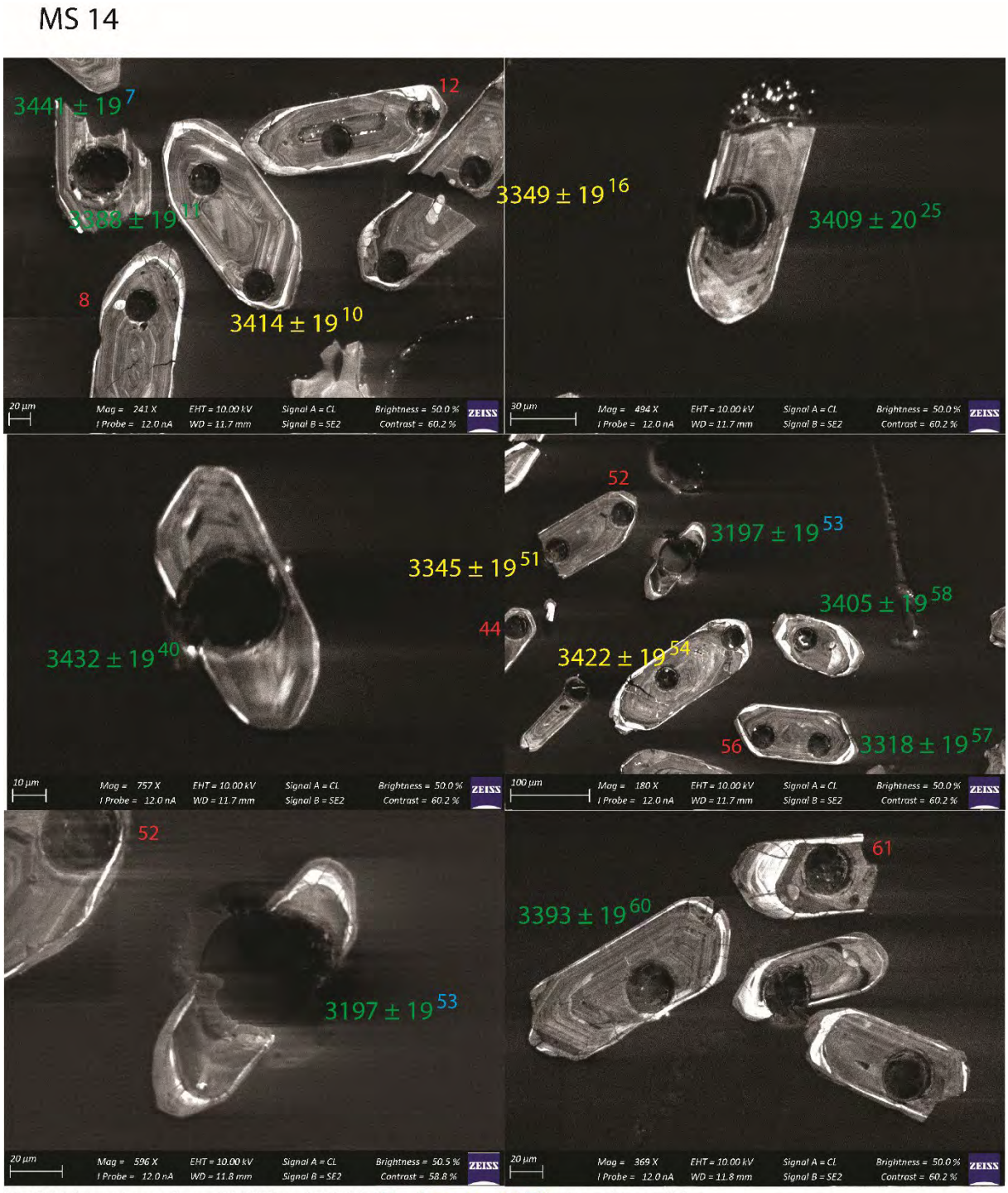

Fig. 4.14, continued.

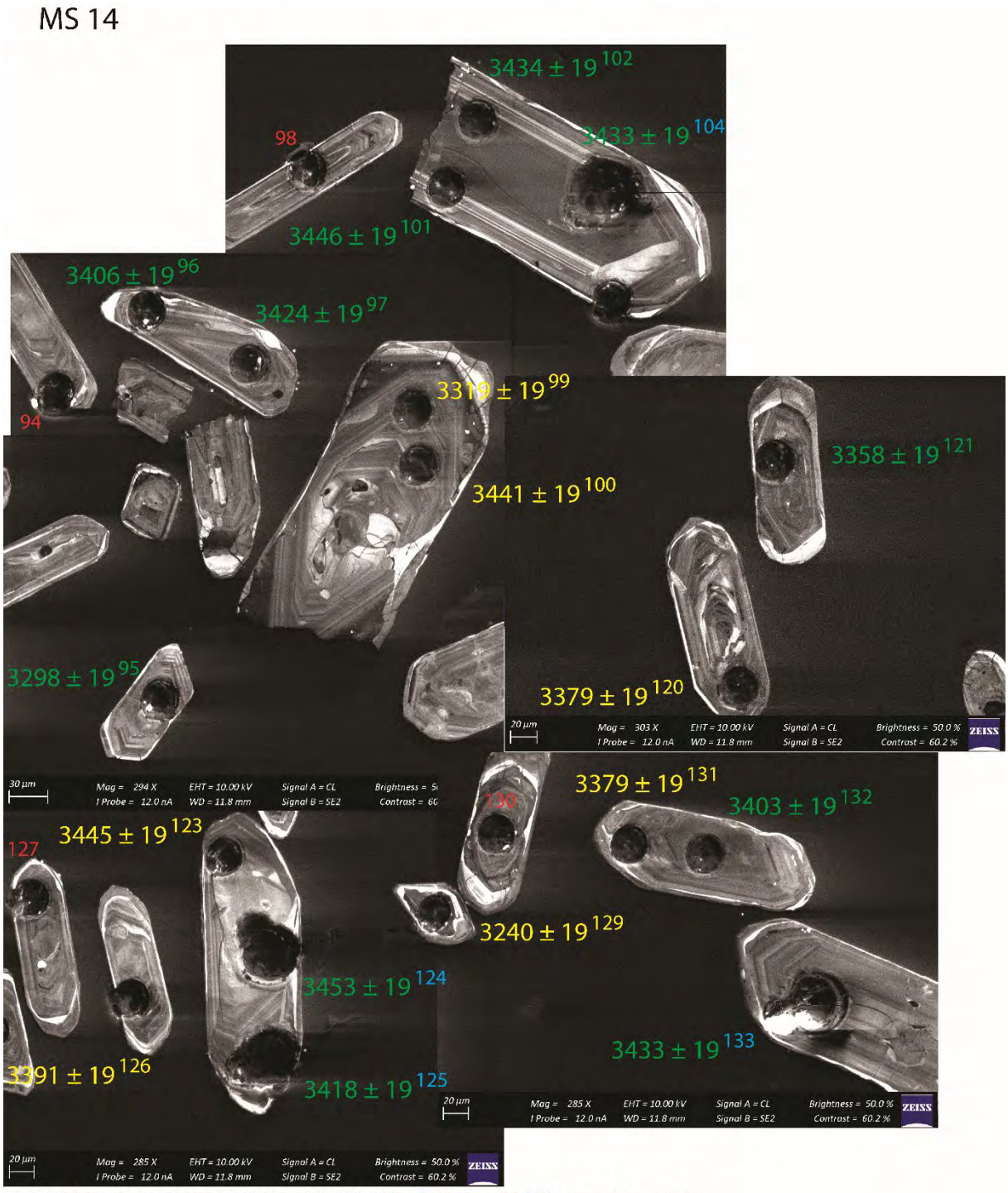

207/206 dates; Concordance 206/238 vs. 207/206: 100 ± 3, 96 - 90, <90; Hf isotope data availabe

Fig. 4.14, continued.

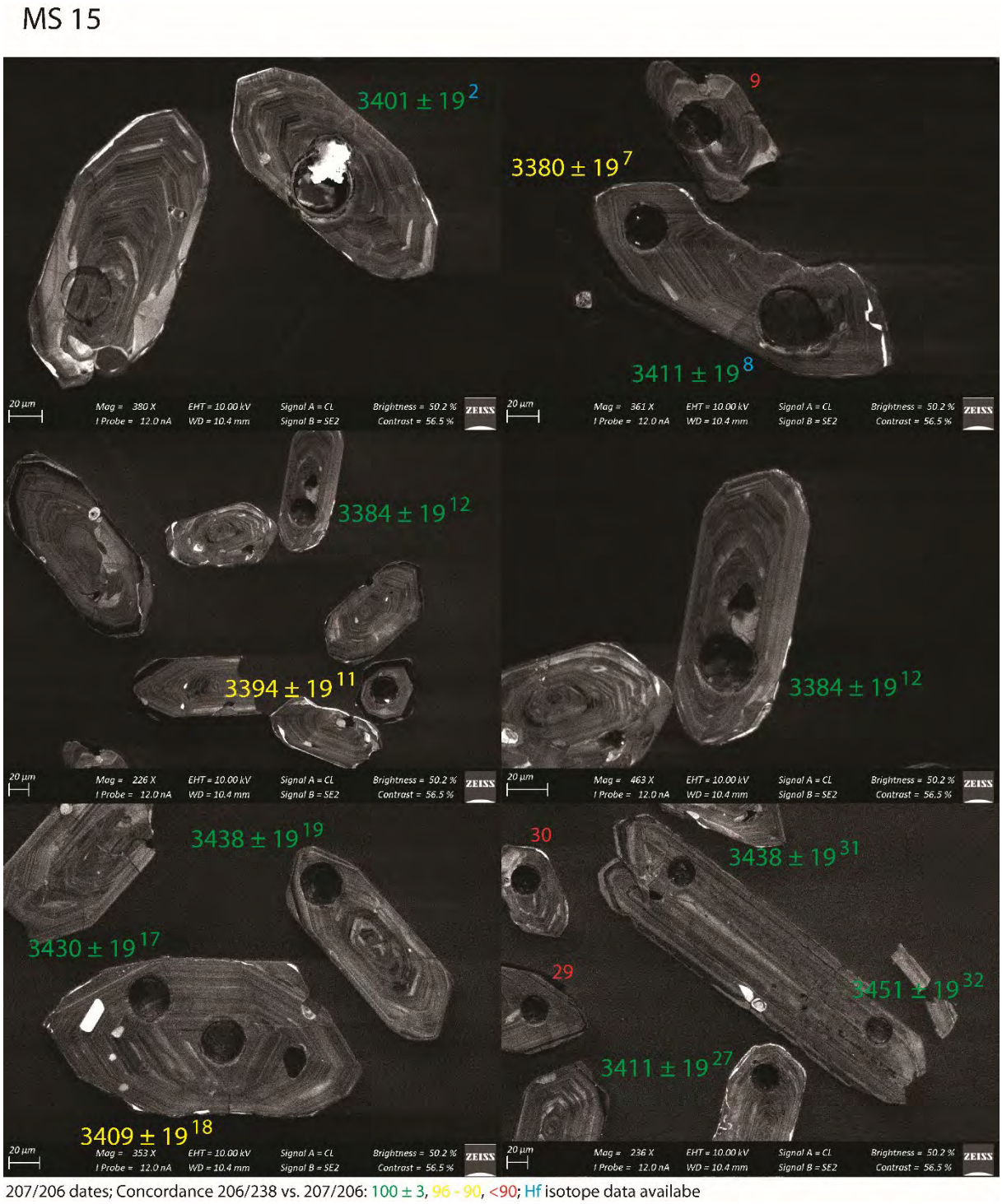

Fig. 4.14, continued.

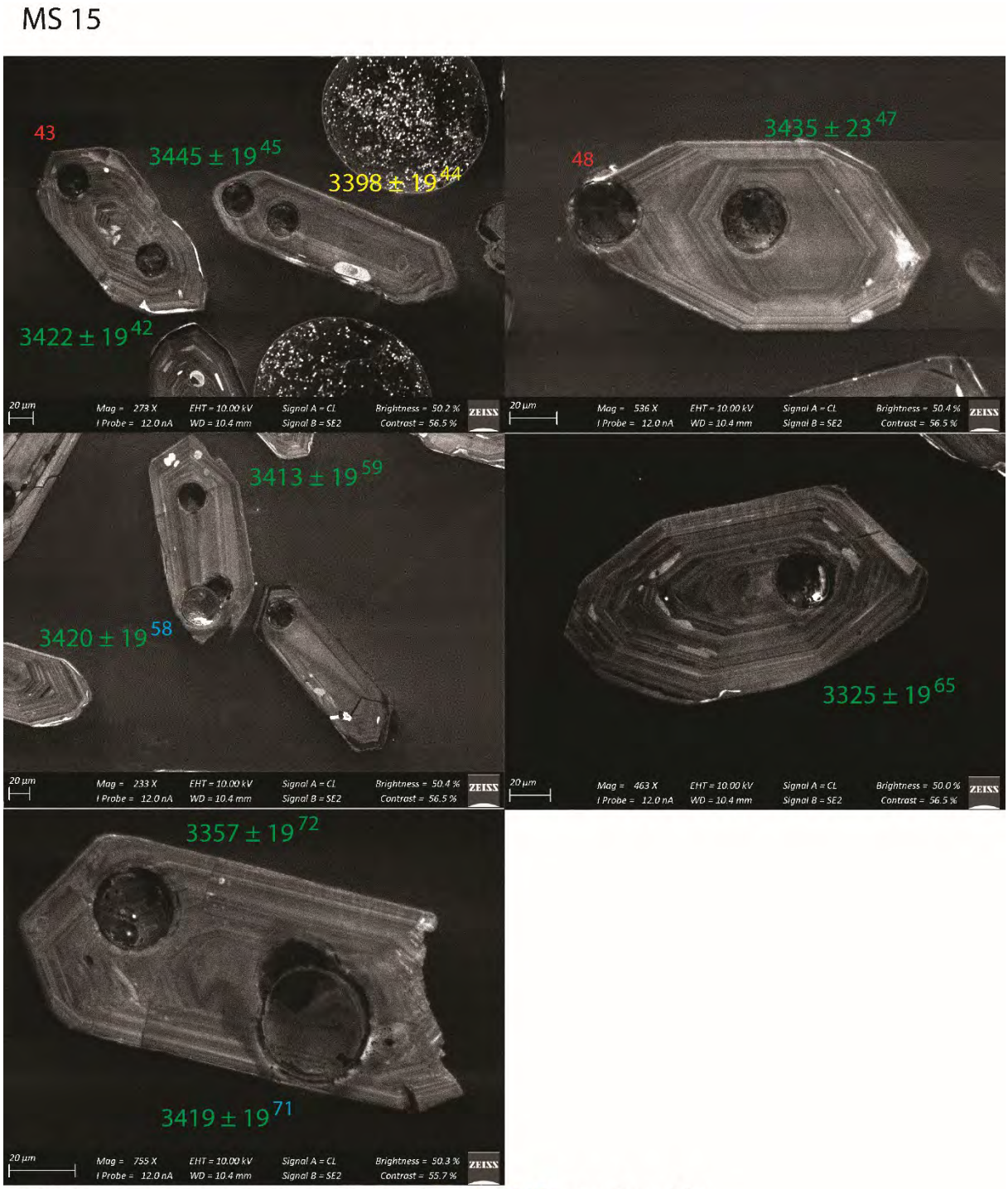

207/206 dates; Concordance 206/238 vs. 207/206: 100 ± 3, 96 - 90, <90; Hf isotope data availabe

Fig. 4.14, continued.

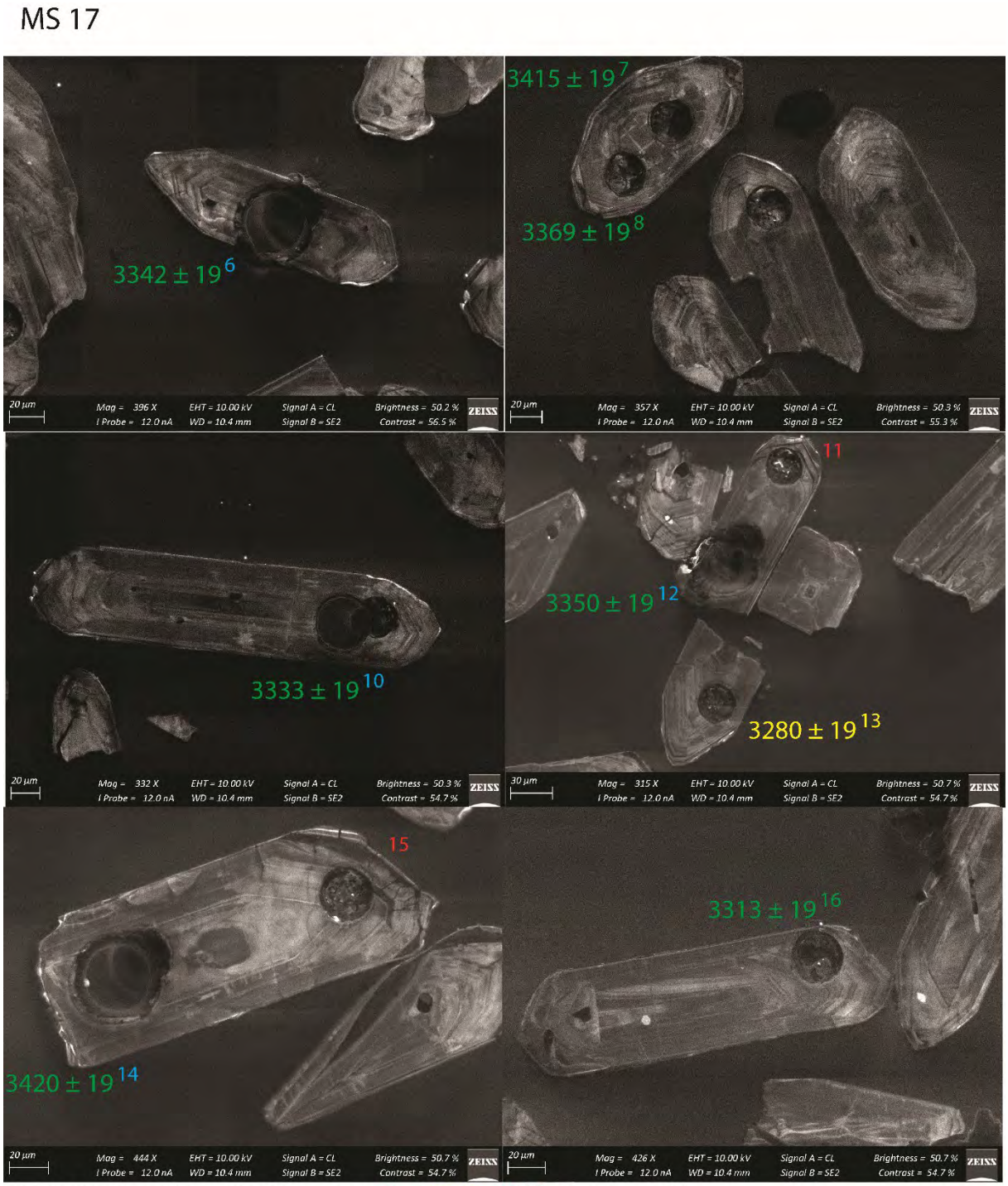

207/206 dates; Concordance 206/238 vs. 207/206: 100 ± 3, 96 - 90, <90; Hf isotope data availabe

Fig. 4.14, continued.

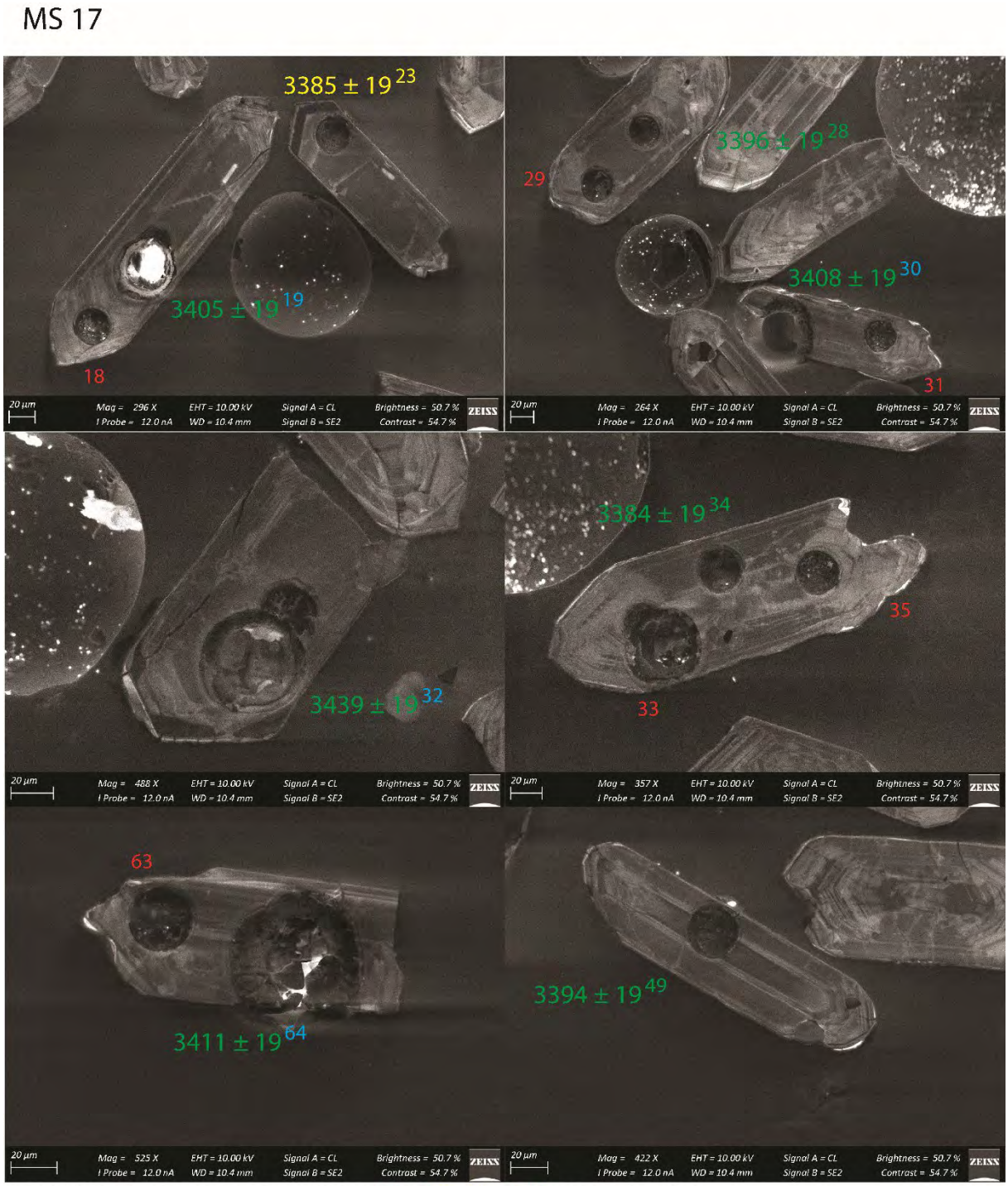

207/206 dates; Concordance 206/238 vs. 207/206: 100 ± 3, 96 - 90, <90; Hf isotope data availabe

Fig. 4.14, continued.

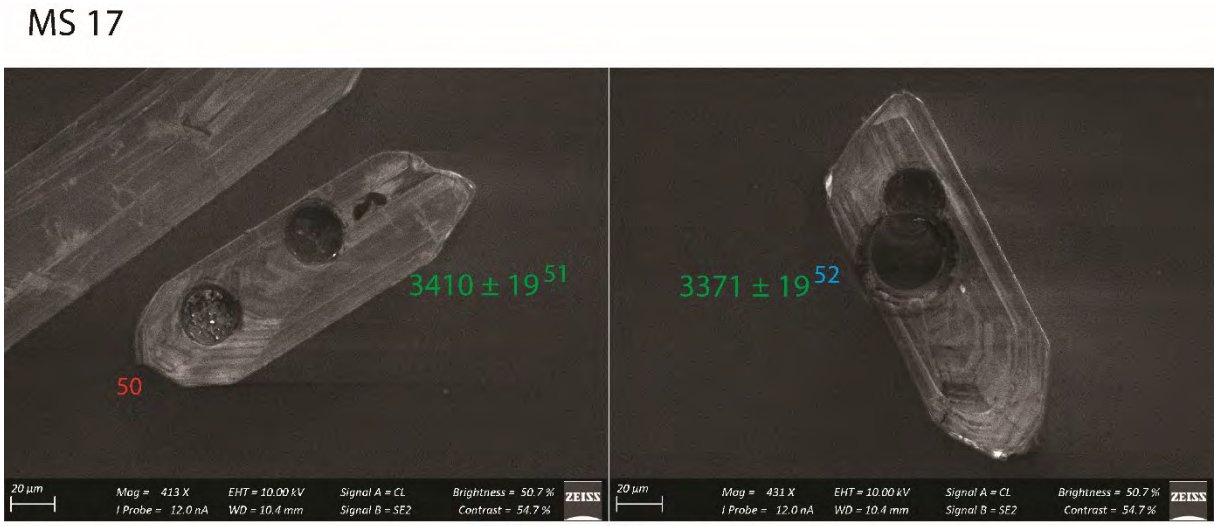

207/206 dates; Concordance 206/238 vs. 207/206: 100 ± 3, 96 - 90, <90; Hf isotope data availabe

Fig. 4.14, continued.

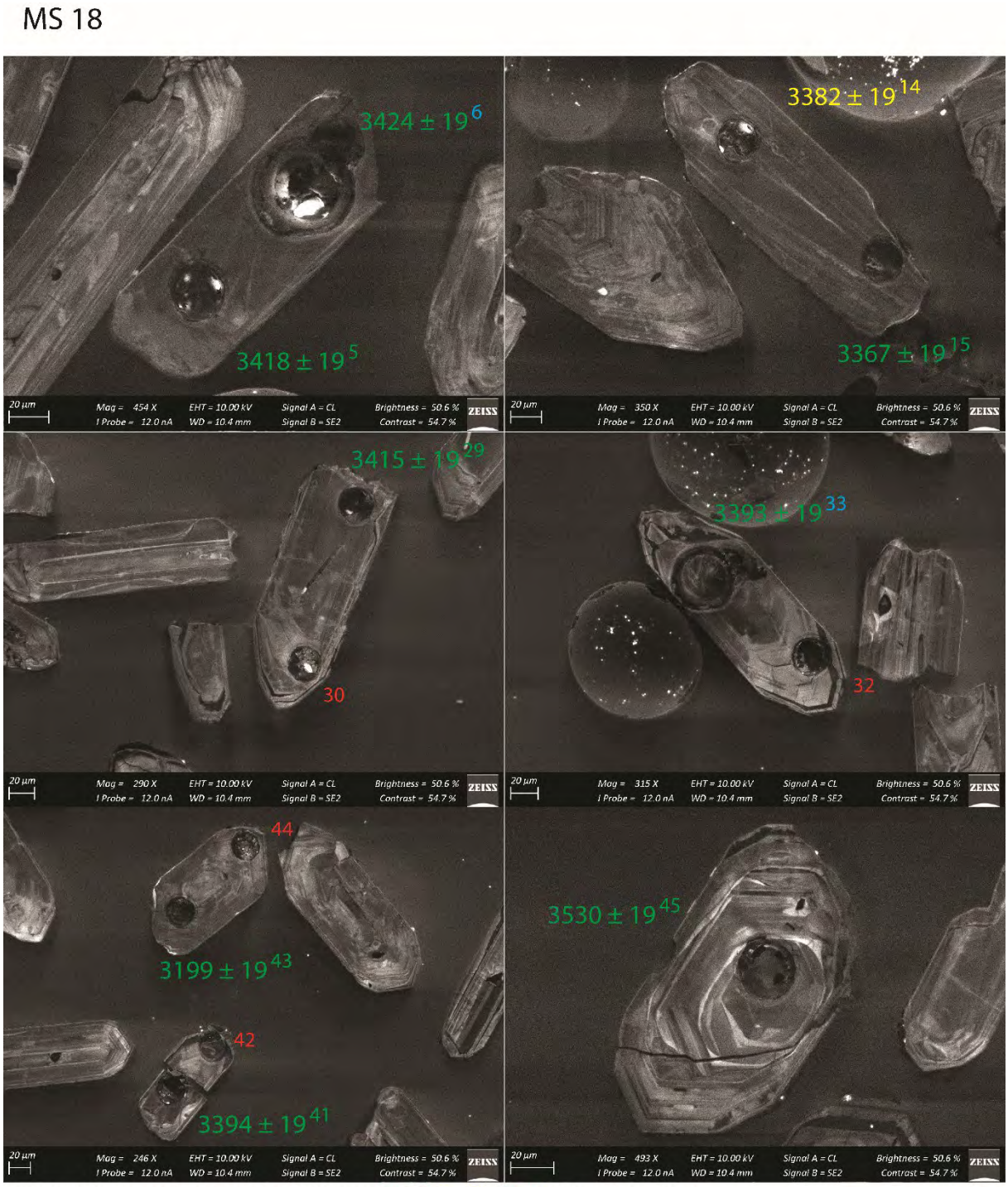

207/206 dates; Concordance 206/238 vs. 207/206: 100 ± 3, 96 - 90, <90; Hf isotope data availabe

Fig. 4.14, continued.

207/206 dates; Concordance 206/238 vs. 207/206: 100 ± 3, 96 - 90, <90; Hf isotope data availabe

Fig. 4.14, continued.

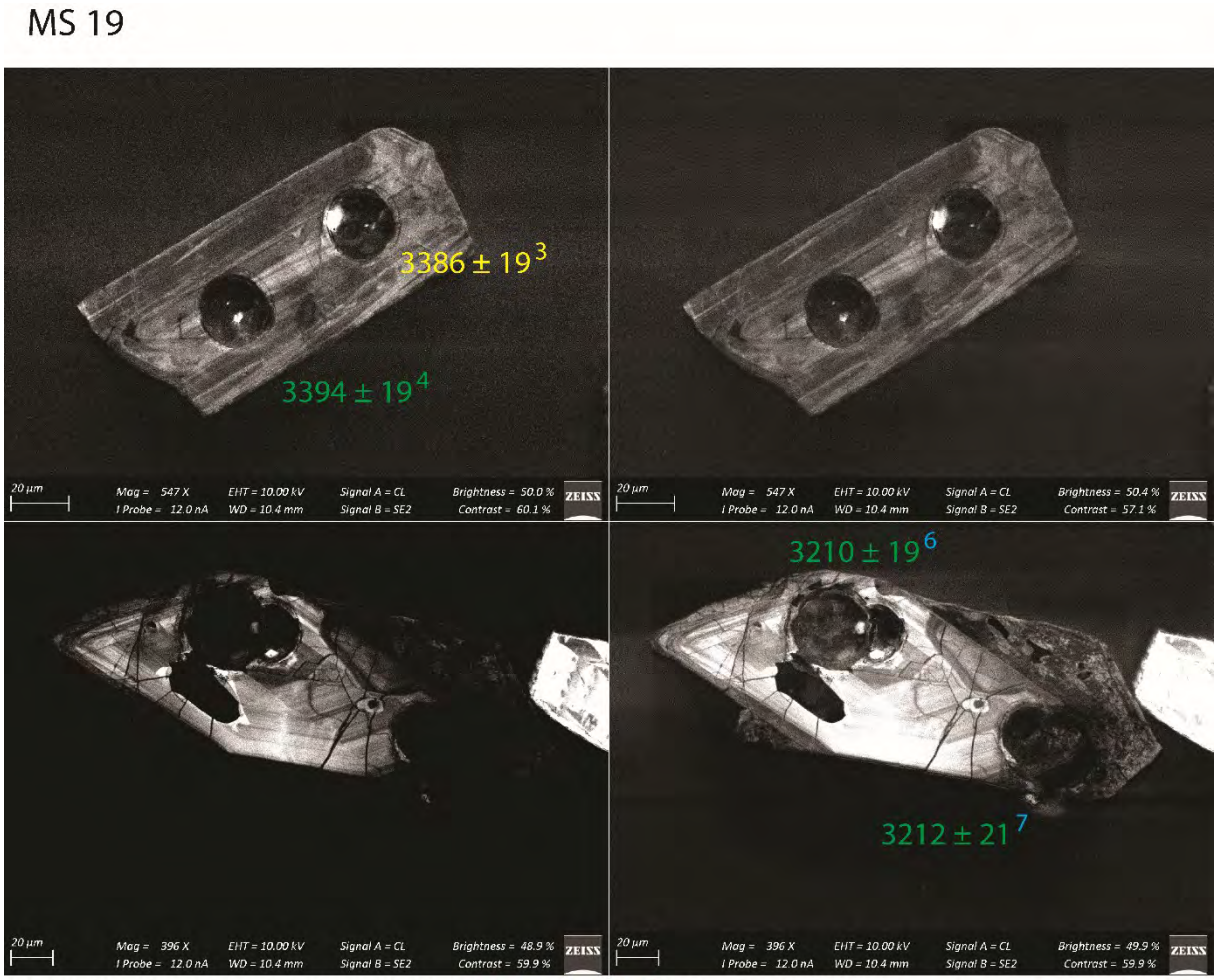

207/206 dates; Concordance 206/238 vs. 207/206: 100 ± 3, 96 - 90, <90; Hf isotope data availabe

Fig. 4.14, continued.

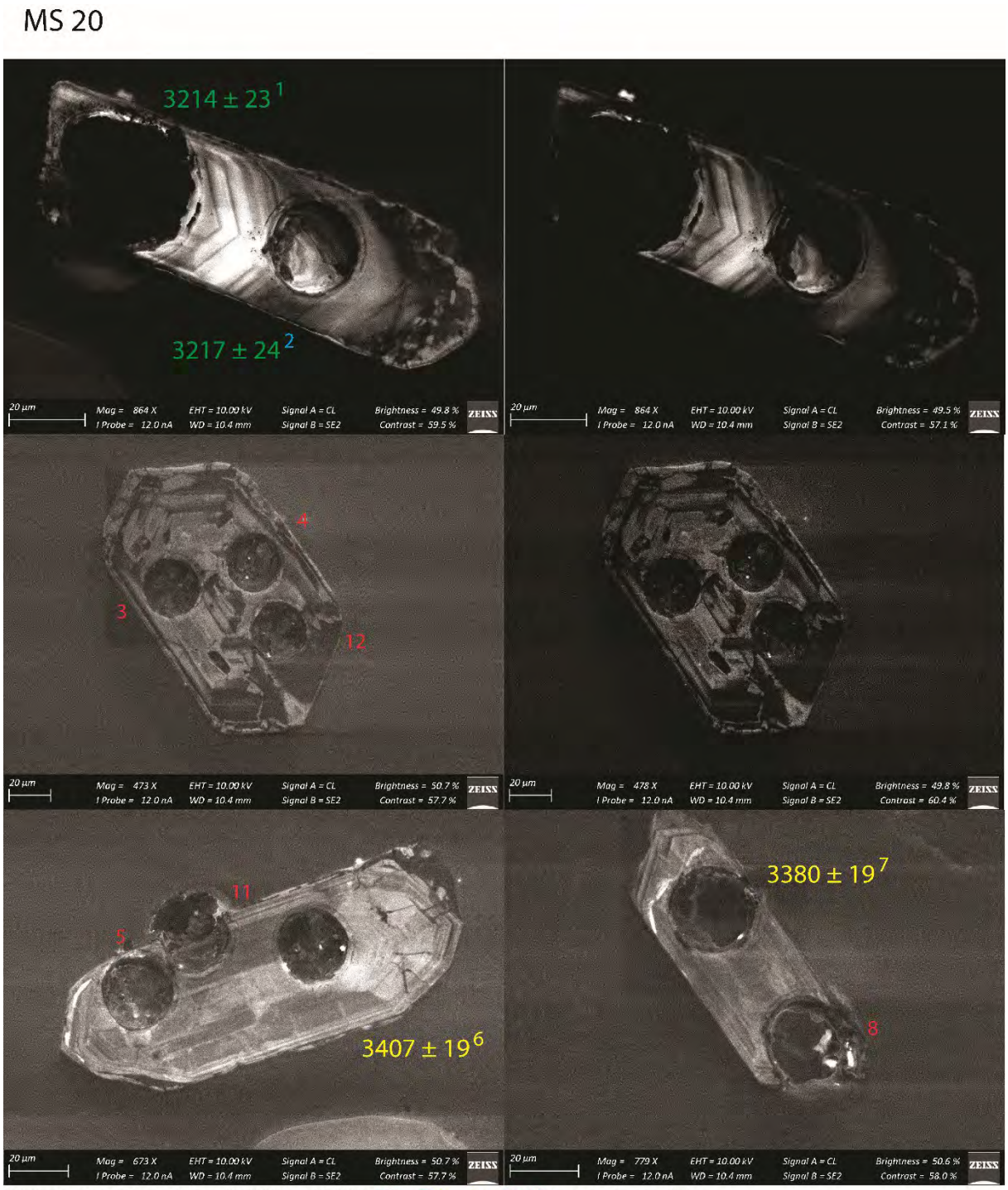

207/206 dates; Concordance 206/238 vs. 207/206: 100 ± 3, 96 - 90, <90; Hf isotope data availabe

Fig. 4.14, continued.

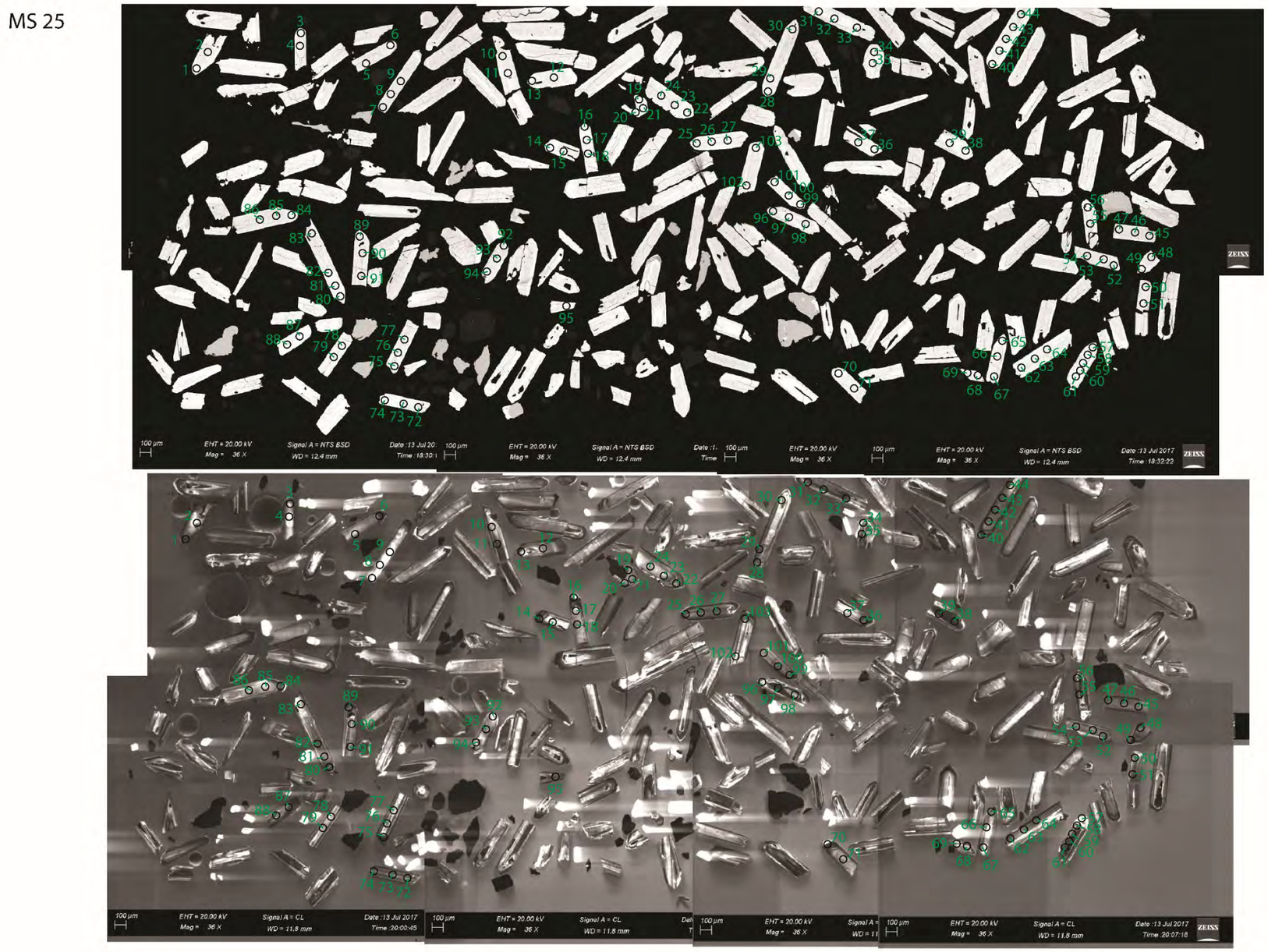

Fig. 4.14, continued.

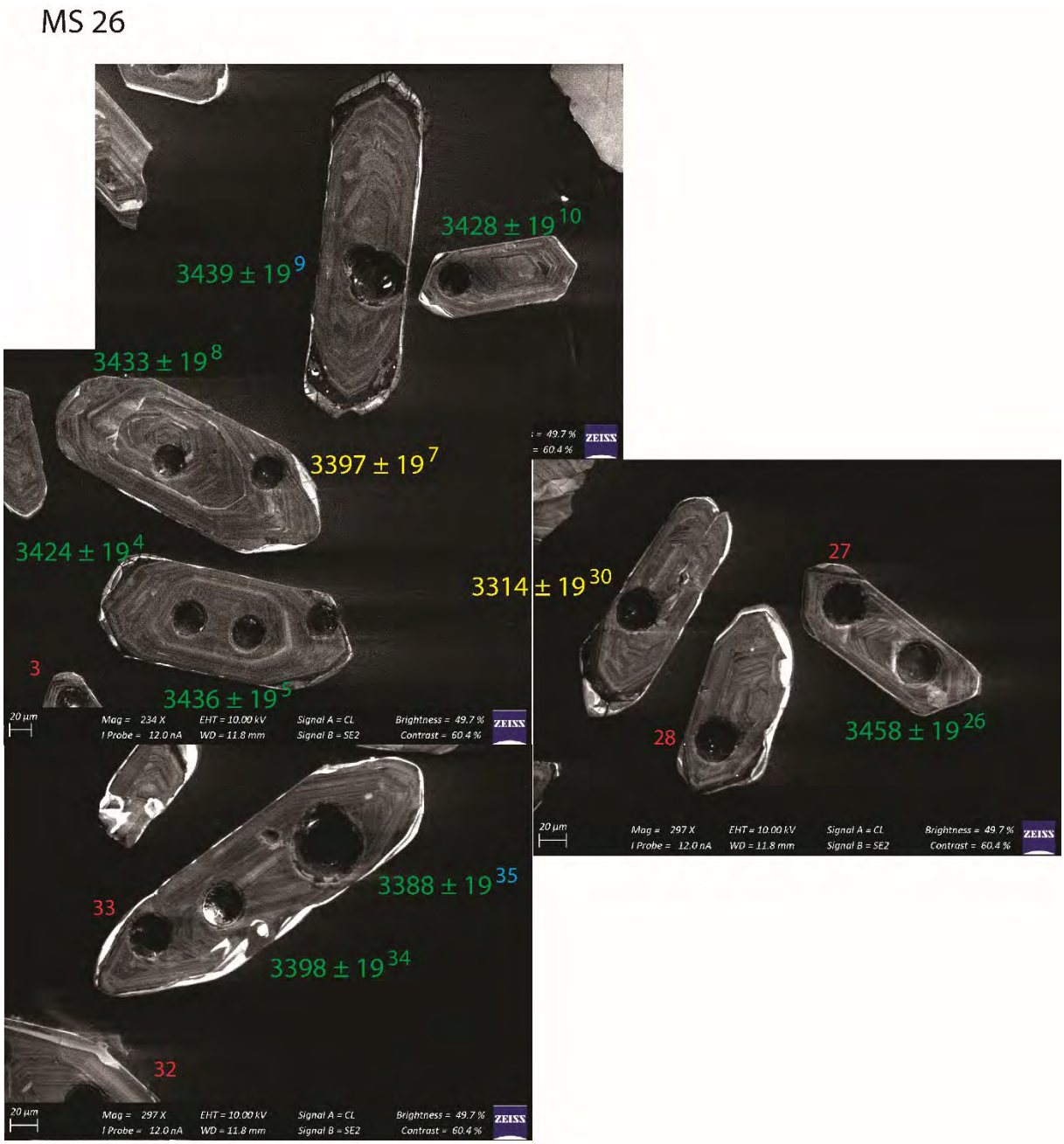

207/206 dates; Concordance 206/238 vs. 207/206: 100 ± 3, 96 - 90, <90; Hf isotope data availabe

Fig. 4.14, continued.

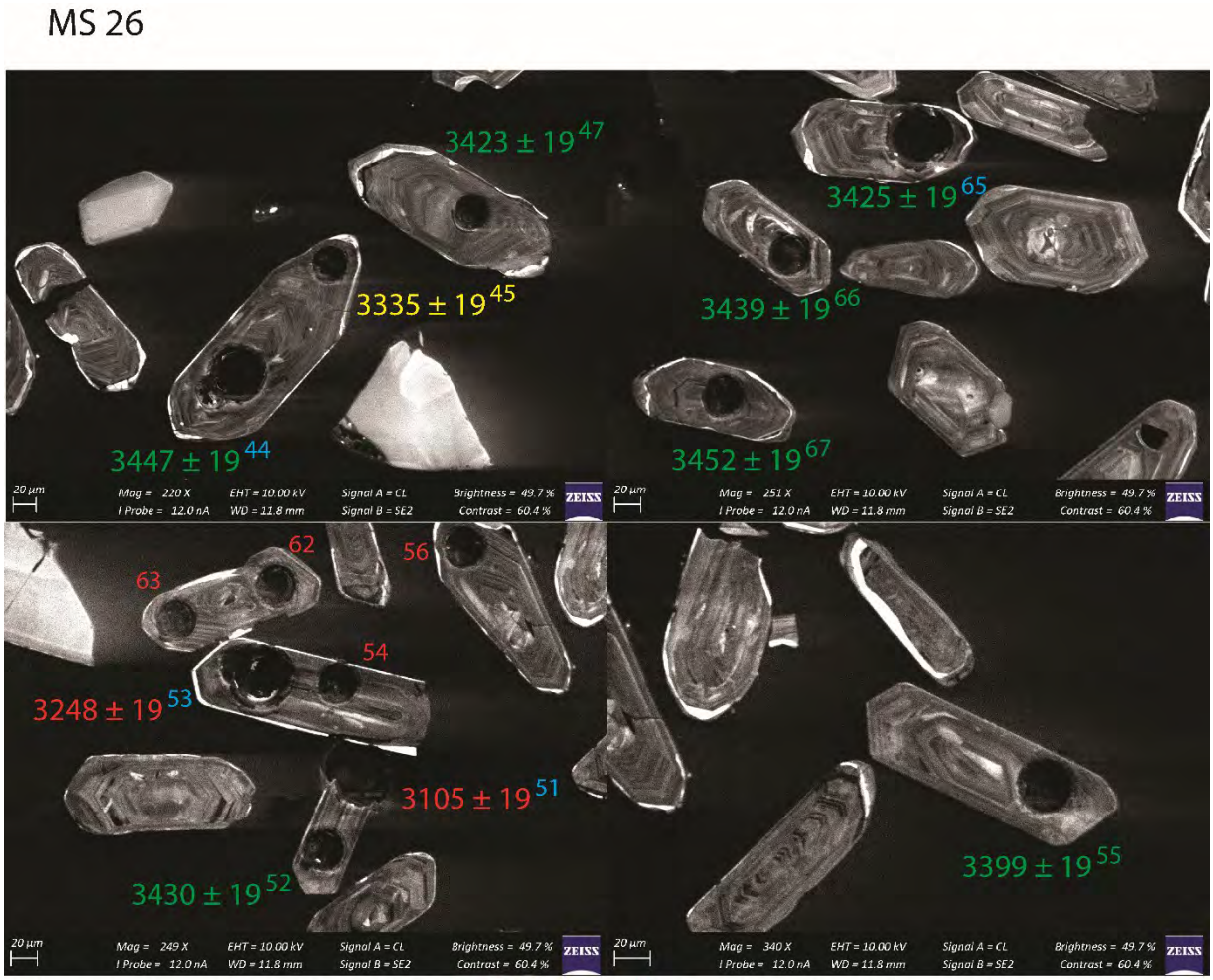

207/206 dates; Concordance 206/238 vs. 207/206: 100 ± 3, 96 - 90, <90; Hf isotope data availabe

Fig. 4.14, continued.

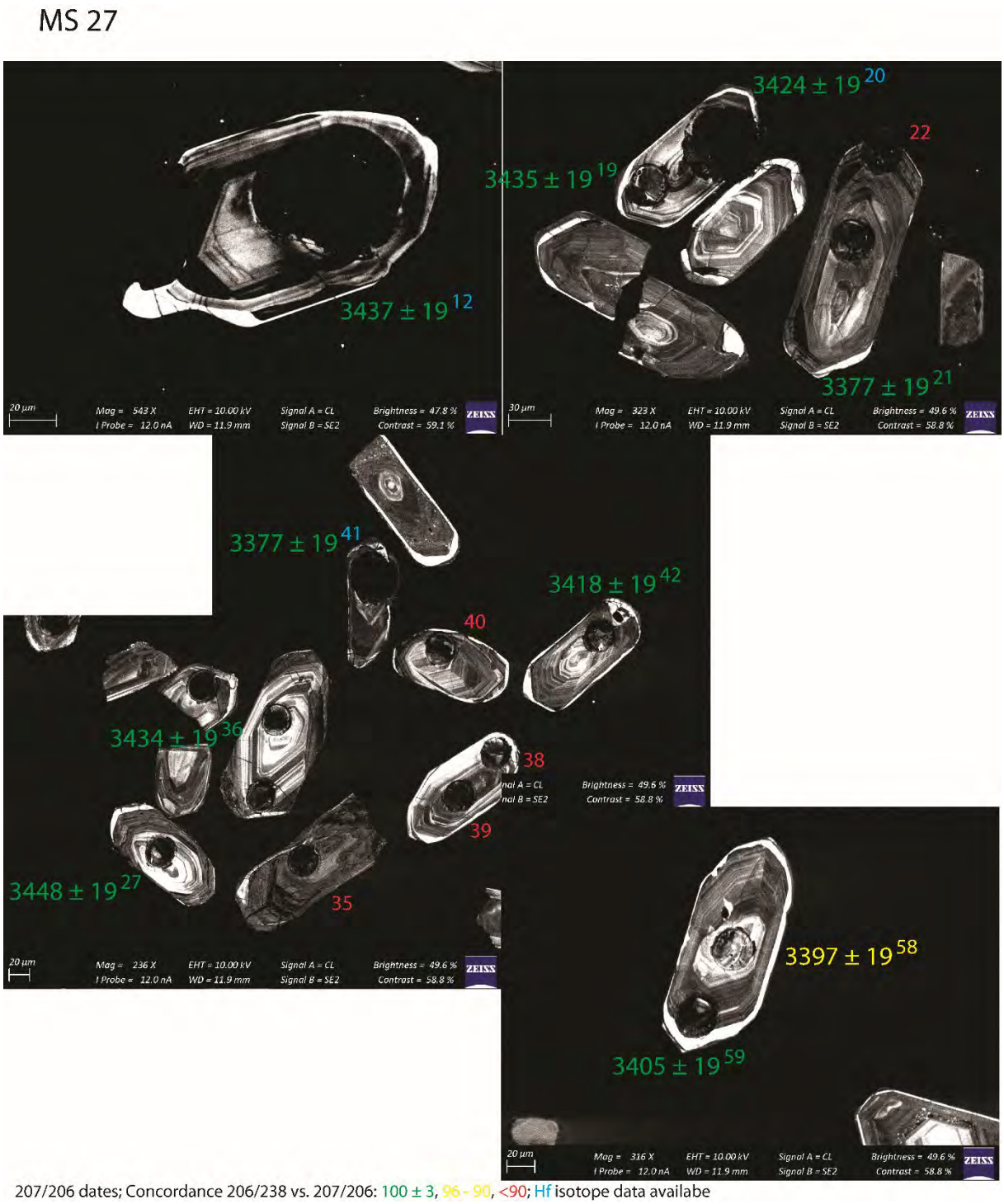

207/206 dates; Concordance 206/238 vs. 207/206: 100 ± 3, 96 - 90, <90; Hf isotope data availabe

Fig. 4.14, continued.

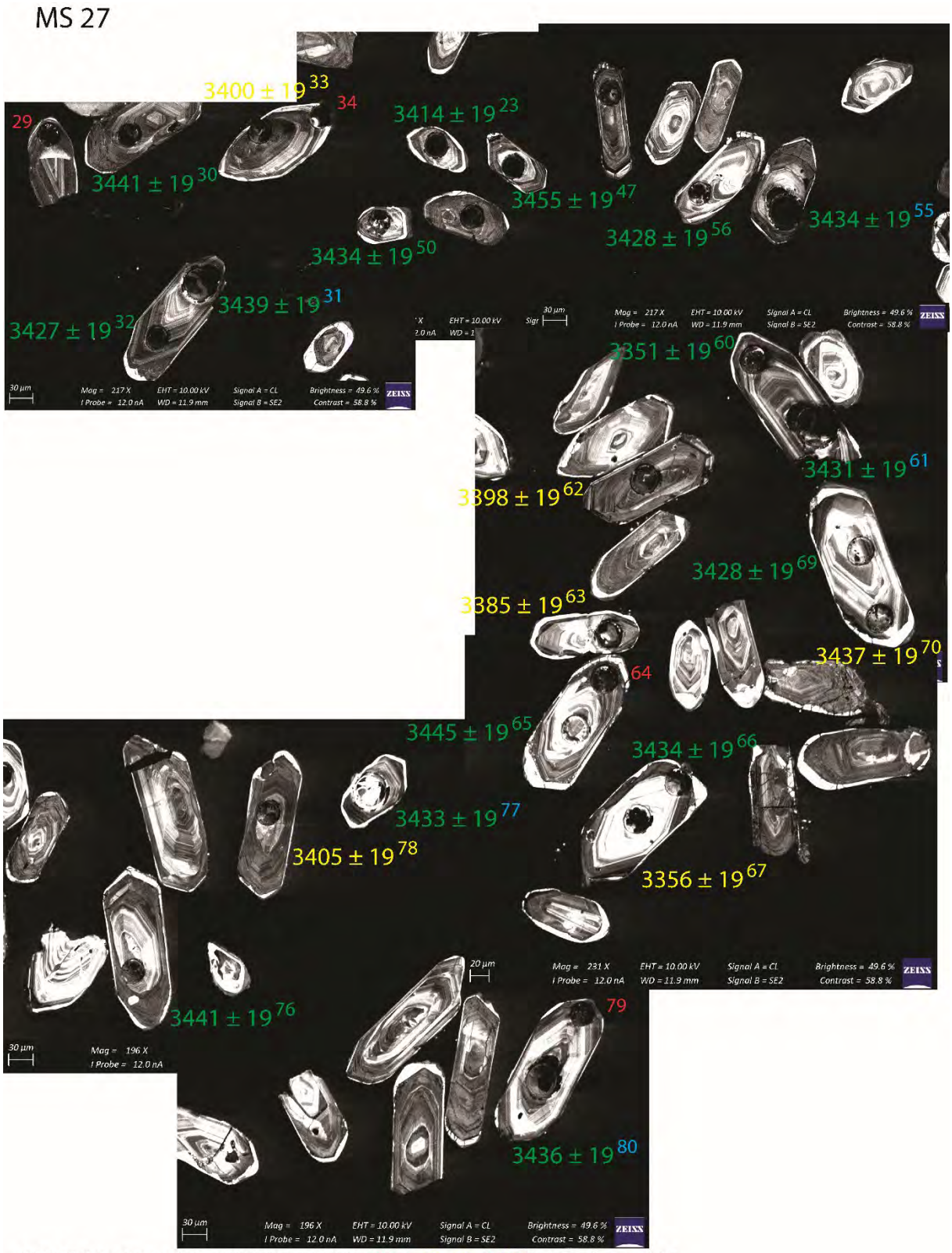

207/206 dates; Concordance 206/238 vs. 207/206: 100 ± 3, 96 - 90, <90; Hf isotope data availabe

Fig. 4.14, continued.

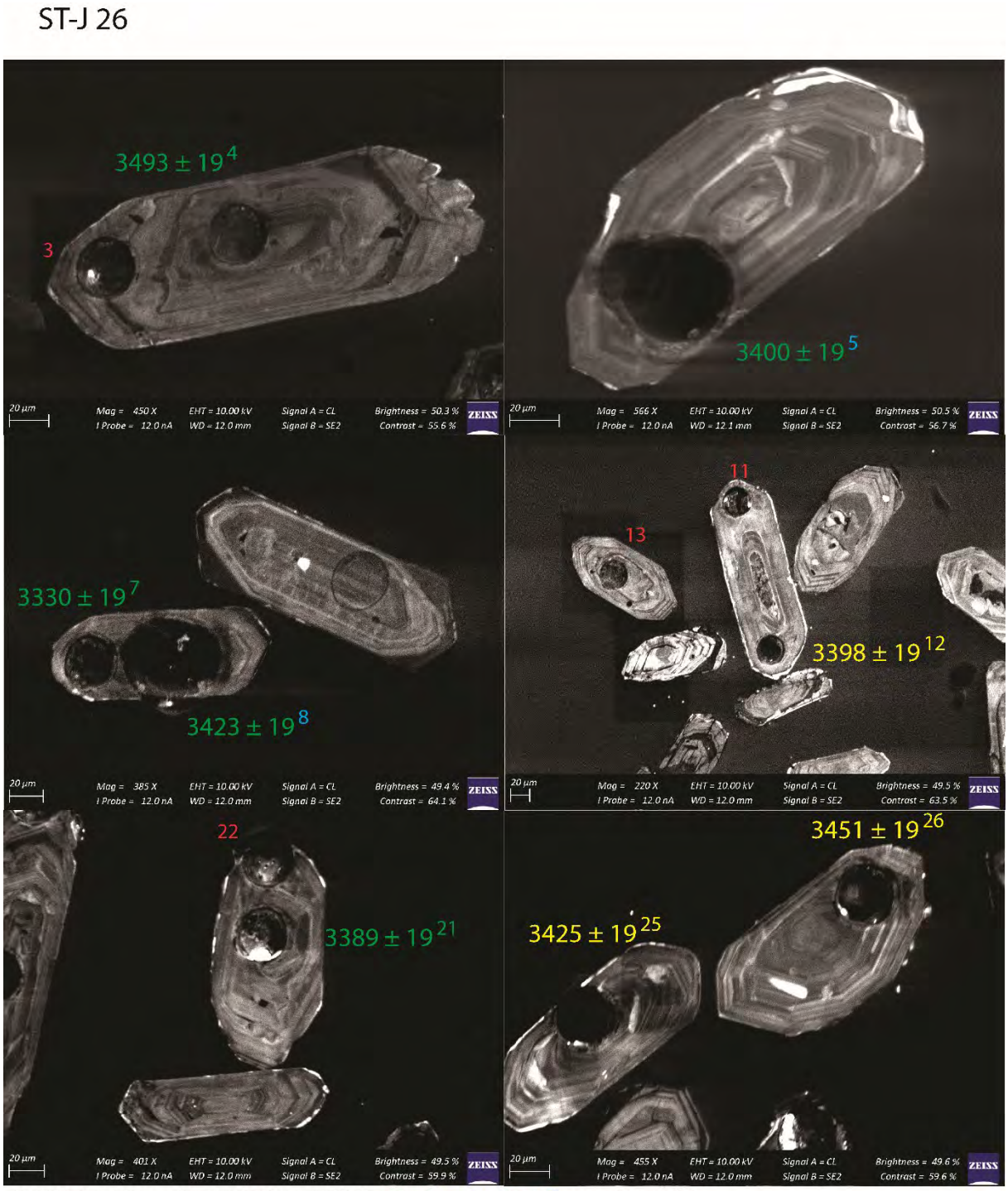

207/206 dates; Concordance 206/238 vs. 207/206: 100 ± 3, 96 - 90, <90; Hf isotope data availabe

Fig. 4.14, continued.

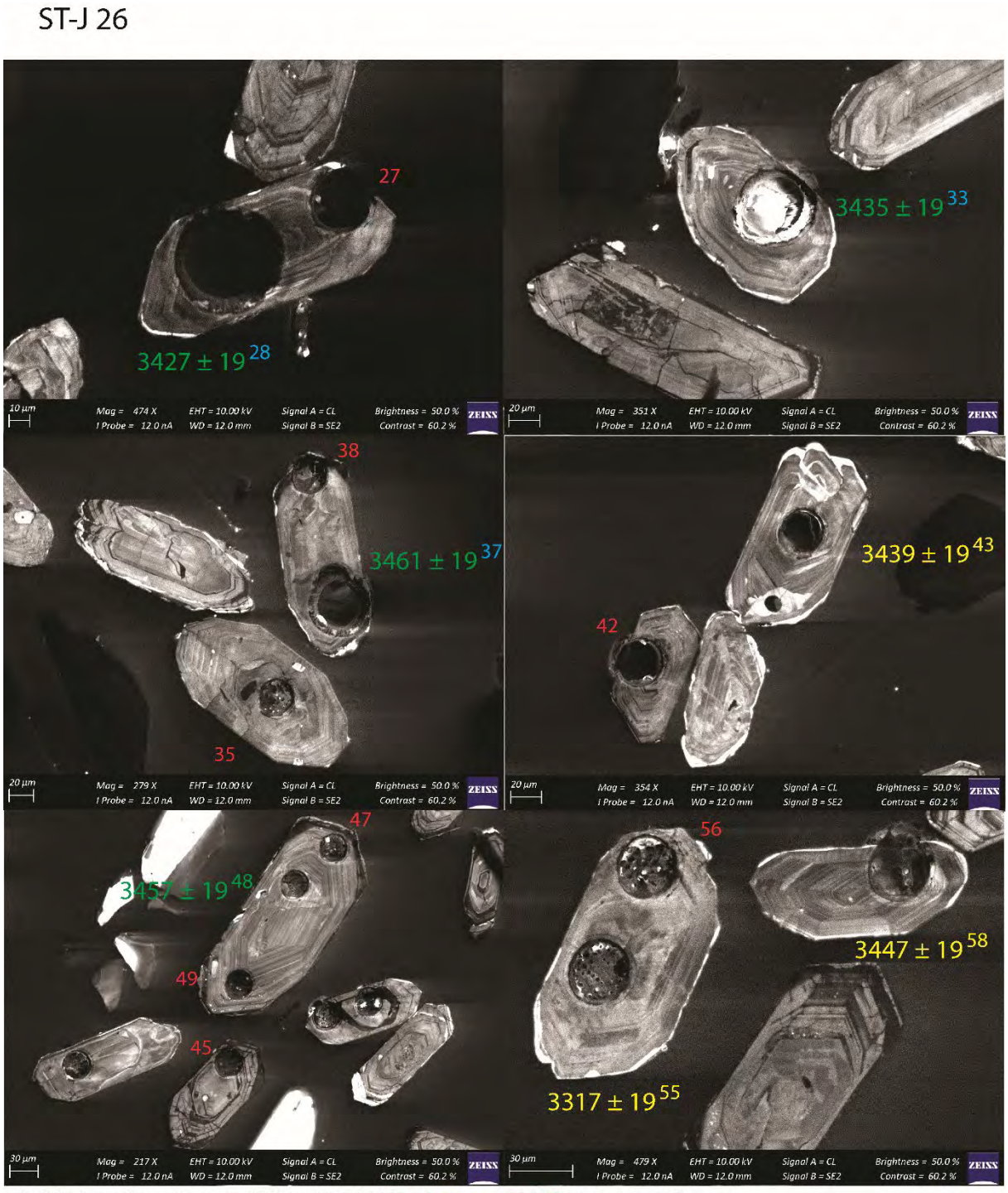

207/206 dates; Concordance 206/238 vs. 207/206: 100 ± 3, 96 - 90, <90; Hf isotope data availabe

Table 4.4. Major- and trace-element concentrations of TTG and meta-sediment samples from the Stolzburg, Theespruit, Honingklip, Eerstehoek and Weergevonden Plutons, Barberton Granitoid Greenstone Terrain, South Africa.

	Stolzburg Pluton						
Sample	MS 1	MS 2	MS 6	MS 7	MS 8	MS 9	MS 10
Rock type	Trondhjemite	Trondhjemite	Trondhjemite	Trondhjemite	Trondhjemite	Trondhjemite	Trondhjemite
SiO_2	69.95	69.93	72.04	72.80	71.77	71.76	72.95
TiO_2	0.34	0.27	0.19	0.27	0.44	0.39	0.27
Al_2O_3	16.63	16.85	16.09	15.24	14.92	15.10	15.44
Fe_2O_3(t)	1.93	1.71	1.31	1.57	2.35	2.22	1.39
Cr_2O_3	b.d.	b.d.	b.d.	b.d.	b.d.	b.d.	b.d.
MnO	0.03	0.02	0.02	0.02	0.03	0.02	0.02
MgO	0.52	0.78	0.47	0.42	0.83	0.76	0.38
CaO	2.34	2.79	1.94	2.14	1.87	1.82	2.25
Na_2O	5.75	6.32	5.80	5.10	4.83	4.97	5.60
K_2O	2.40	1.24	2.10	2.33	2.82	2.85	1.61
P_2O_5	0.11	0.08	0.05	0.09	0.13	0.11	0.08
Total	100	100	100	100	100	100	100
LOI	0.91	0.51	0.47	0.38	0.57	0.36	0.35
Mg#	35	48	41	35	41	40	35
Sc	7.5	7.7	7.1	7.9	6.9	6.7	6.7
V	22.9	20.9	14.2	18.9	27.9	26.6	17.1
Cr	11.8	24	16	13	12.8	18.0	12.3
Co	96	93	86	100	74	187	106
Ni	9	20	16	12	11	51	10
Cu	6.7	2.1	2.0	12.7	2.3	4.6	3.8
Zn	33	38	36	43	90	83	39
Rb	54	22.6	46	44	77	72	41
Sr	701	1042	640	648	571	615	824
Ba	557	425	456	734	681	653	340
Ta	0.235	0.082	0.151	0.106	0.165	0.151	0.119
Cs	1.40	1.16	5.41	1.85	4.50	3.87	2.11
Mo	0.42	0.37	0.31	0.46	0.45	0.55	0.37
Y	7.1	1.9	2.7	4.2	3.0	2.8	3.1
Zr	139	122	97	123	117	115	129
Nb	6.3	2.6	5.7	7.4	3.7	7.7	2.7
Hf	3.55	3.08	2.63	3.10	3.33	3.25	3.46
Pb	5.01	4.59	9.84	8.87	13.44	12.34	8.65
Th	3.19	1.273	2.41	2.23	2.76	2.80	3.14
U	0.728	0.117	0.689	0.471	0.809	0.967	0.623
La	25.5	15.1	12.2	19.9	21.4	18.6	24.3
Ce	49.7	25.3	19.5	36.8	40.7	36.5	44.1
Pr	5.44	2.51	2.12	4.18	4.38	3.81	4.69
Nd	22	8.6	8.0	16	17.6	15.3	18
Sm	3.61	1.46	1.19	3.19	2.78	2.77	2.86
Eu	1.00	0.647	0.54	0.90	0.825	0.793	0.90
Gd	2.22	0.86	0.98	2.05	1.80	1.78	1.60
Tb	0.307	0.085	0.134	0.190	0.190	0.159	0.212
Dy	1.30	0.37	0.44	0.90	0.687	0.62	0.78
Ho	0.264	0.063	0.088	0.169	0.100	0.094	0.116
Er	0.63	0.182	0.191	0.209	0.191	0.151	0.23
Tm	0.086	0.012	b.d.	0.044	b.d.	b.d.	0.033
Yb	0.55	0.085	0.22	0.20	0.071	0.131	b.d.
Lu	0.064	b.d.	b.d.	0.024	b.d.	b.d.	b.d.

Major- and trace-element concentrations in wt. % and µg/g, respectively. Mg # = atomic ratio of Mg^{2+}/ (Mg^{2+}+Fe^{2+}) x 100, using FeO = 0.9 of total Fe as Fe_2O_3. LOI = Loss on ignition; b.d. = below detection.

Table 4.4, continued.

	Stolzburg Pluton						
Sample	MS 11	MS 12	MS 13	MS 14	MS 15	MS 22	MS 23
Rock type	Trondhjemite	Trondhjemite	Trondhjemite	Trondhjemite	Trondhjemite	Trondhjemite	Tonalite
SiO_2	73.43	72.71	73.62	72.33	73.02	73.74	62.57
TiO_2	0.19	0.20	0.19	0.23	0.20	0.16	1.03
Al_2O_3	15.06	15.44	15.30	15.65	15.21	14.99	17.72
Fe_2O_3(t)	1.28	1.23	1.21	1.50	1.34	1.17	3.91
Cr_2O_3	b.d.	b.d.	b.d.	b.d.	b.d.	b.d.	b.d.
MnO	0.02	0.02	0.02	0.03	0.02	0.02	0.04
MgO	0.45	0.47	0.27	0.51	0.46	0.34	1.99
CaO	1.35	1.79	1.25	2.30	1.82	1.28	5.01
Na_2O	6.16	5.72	5.79	5.66	5.58	5.60	5.57
K_2O	2.00	2.37	2.28	1.74	2.29	2.65	1.84
P_2O_5	0.05	0.05	0.06	0.06	0.05	0.04	0.34
Total	100	100	100	100	100	100	100
LOI	0.83	0.4	0.84	0.63	0.4	0.74	1.04
Mg#	41	43	31	40	40	36	50
Sc	6.9	7.7	6.4	7.3	6.9	6.8	10.4
V	14.8	15.0	15.2	16.2	15.5	11.6	76
Cr	15	15	10	12.7	14.6	10.3	31
Co	80	87	102	70	101	125	62.5
Ni	23	14	13	11	15	10	18
Cu	4.5	1.4	8.6	1.9	1.6	3.4	15.0
Zn	13	28	16	33	31	35	75
Rb	36	50	50	28	42	68	59
Sr	521	670	595	740	656	387	1115
Ba	410	488	419	433	550	714	516
Ta	0.305	0.280	0.157	0.254	0.236	0.134	0.300
Cs	0.11	0.87	1.18	0.63	0.84	0.97	3.91
Mo	0.31	0.38	0.30	0.34	0.15	0.17	0.55
Y	4.2	3.2	4.5	3.3	3.1	2.5	8.1
Zr	99	94	104	110	102	86	194
Nb	7.2	4.3	7.6	6.5	3.7	3.7	7.3
Hf	2.95	2.54	2.93	2.87	2.93	2.57	4.33
Pb	4.39	7.70	9.44	7.04	6.67	7.72	7.44
Th	4.43	3.54	2.32	2.47	2.26	2.14	3.02
U	1.95	1.70	1.26	0.532	0.726	0.591	1.33
La	15.2	13.8	17.3	14.1	14.2	11.4	21.4
Ce	25.9	25.9	28.0	24.1	25.8	20.5	43.0
Pr	2.72	2.79	3.30	2.42	2.68	2.35	5.32
Nd	11.7	11	12.7	10	11	8.8	23.9
Sm	1.47	1.50	2.17	1.48	1.73	1.40	4.75
Eu	0.55	0.476	0.66	0.568	0.413	0.47	1.58
Gd	1.23	1.42	1.39	0.75	1.28	1.29	3.74
Tb	0.116	0.120	0.143	0.149	0.117	0.119	0.417
Dy	0.60	0.49	0.61	0.62	0.54	0.63	1.84
Ho	0.092	0.096	0.107	0.100	0.067	0.081	0.290
Er	0.225	0.240	0.298	0.243	0.195	0.145	0.69
Tm	0.044	0.022	b.d.	0.019	0.022	0.024	0.073
Yb	0.22	0.105	0.22	0.263	0.100	b.d.	0.44
Lu	b.d.	b.d.	b.d.	0.035	b.d.	b.d.	0.063

Major- and trace-element concentrations in wt. % and µg/g, respectively. Mg # = atomic ratio of Mg^{2+}/ (Mg^{2+}+Fe^{2+}) x 100, using FeO = 0.9 of total Fe as Fe_2O_3. LOI = Loss on ignition; b.d. = below detection.

Table 4.4, continued.

	Stolzburg Pluton						
Sample	MS 24	MS 36	MS 42	MS 44	MS 45	MS 46	MS 47
Rock type	Trondhjemite	Tonalite	Trondhjemite	Trondhjemite	Granite	Tonalite	Trondhjemite
SiO_2	72.95	65.49	72.65	69.50	75.37	69.84	74.17
TiO_2	0.25	0.92	0.16	0.45	0.11	0.48	0.17
Al_2O_3	15.21	16.90	15.53	16.16	13.85	15.42	15.01
Fe_2O_3(t)	1.45	4.16	1.30	2.75	0.76	2.78	1.13
Cr_2O_3	b.d.	0.02	b.d.	b.d.	b.d.	b.d.	b.d.
MnO	0.02	0.05	0.02	0.04	0.03	0.05	0.03
MgO	0.48	1.60	0.39	0.66	0.11	1.39	0.23
CaO	2.13	3.97	1.90	2.85	1.07	2.96	2.38
Na_2O	5.15	5.32	5.28	5.15	4.15	4.86	5.51
K_2O	2.31	1.31	2.74	2.25	4.53	2.08	1.30
P_2O_5	0.05	0.26	0.05	0.20	0.02	0.14	0.06
Total	100	100	100	100	100	100	100
LOI	0.47	1.40	0.51	0.76	0.73	0.43	0.44
Mg#	39	43	37	32	22	50	29
Sc	7.2	15.3	5.1	4.8	6.0	7.9	4.8
V	17.4	95.5	18.9	33.5	15.6	44.2	19.3
Cr	8.2	295.4	7.7	7.2	5.1	41.1	4.9
Co	79	55	104	73	45	58	76
Ni	8	21	9	7	4	23	5
Cu	5.0	29.3	11.2	10.7	19.7	7.5	4.9
Zn	38	86	47	89	31	67	41
Rb	108	43	56	67	116	94	44
Sr	461	949	585	757	182	525	525
Ba	433	396	1113	1580	434	621	379
Ta	0.381	0.322	0.385	0.529	2.243	0.905	0.280
Cs	7.31	4.11	1.80	2.83	2.46	11.31	2.35
Mo	0.28	0.43	0.39	0.26	0.34	0.25	0.32
Y	4.2	10.7	2.4	4.6	26.7	11.1	6.6
Zr	106	243	94	167	88	207	109
Nb	5.3	5.9	3.1	8.3	16.8	11.5	3.2
Hf	2.83	5.71	2.85	4.52	4.09	5.48	2.98
Pb	9.07	8.90	13.27	15.64	35.60	16.13	12.73
Th	3.02	7.10	3.19	5.14	9.44	11.50	2.58
U	1.05	1.19	0.76	1.26	7.88	2.51	1.31
La	14.1	61.9	20.8	32.2	11.2	54.5	15.6
Ce	24.6	110.8	37.2	62.9	21.3	97.6	30.2
Pr	2.57	11.57	3.78	7.05	2.37	9.54	3.47
Nd	9.5	42.8	13.2	27.1	9.0	32.1	13.2
Sm	2.00	6.51	2.08	5.01	2.51	5.41	2.53
Eu	0.64	1.843	0.664	1.330	0.761	1.300	0.976
Gd	1.34	4.44	1.38	2.95	2.90	3.75	1.89
Tb	0.169	0.536	0.209	0.310	0.634	0.469	0.373
Dy	0.54	2.51	0.62	1.20	3.99	2.42	1.32
Ho	0.132	0.488	0.239	0.177	0.994	0.434	0.305
Er	0.35	1.06	0.31	0.31	2.92	1.12	0.75
Tm	0.037	0.152	0.113	0.039	0.556	0.178	0.196
Yb	0.36	0.98	0.30	0.26	3.71	1.04	0.70
Lu	0.069	0.135	0.090	0.036	0.635	0.145	0.164

Major- and trace-element concentrations in wt. % and µg/g, respectively. Mg # = atomic ratio of Mg^{2+}/ (Mg^{2+}+Fe^{2+}) x 100, using FeO = 0.9 of total Fe as Fe_2O_3. LOI = Loss on ignition; b.d. = below detection.

Table 4.4, continued.

	Honingklip Pluton			Theespruit Pluton			
Sample	MS 3	MS 4	MS 17	MS 18	MS 19	MS 20	MS 31
Rock type	Granodiorite	Trondhjemite	Tonalite	Trondhjemite	Granite	Trondhjemite	Trondhjemite
SiO_2	69.72	70.61	70.99	75.95	74.80	75.18	71.61
TiO_2	0.56	0.43	0.41	0.38	0.19	0.19	0.28
Al_2O_3	16.24	16.19	15.02	13.04	14.42	14.39	15.19
Fe_2O_3(t)	2.65	2.11	2.87	1.90	1.19	1.19	1.99
Cr_2O_3	b.d.	b.d.	b.d.	b.d.	b.d.	b.d.	b.d.
MnO	0.03	0.03	0.04	0.03	0.02	0.03	0.03
MgO	0.81	0.69	1.65	0.89	0.38	0.27	1.19
CaO	3.15	2.64	3.35	2.27	0.97	1.73	2.48
Na_2O	5.15	5.74	3.99	4.70	5.01	5.80	5.33
K_2O	1.55	1.45	1.56	0.75	2.98	1.17	1.82
P_2O_5	0.14	0.12	0.11	0.09	0.05	0.05	0.08
Total	100	100	100	100	100	100	100
LOI	0.71	0.48	1.55	0.89	0.82	0.64	0.79
Mg#	38	39	53	48	39	31	54
Sc	8.1	8.2	9.5	8.0	8.1	7.8	6.2
V	25.9	25.9	38.0	26.5	15.6	14.7	30.3
Cr	13.7	11.3	27	18.9	8	9	25.9
Co	88	93	73	113	92	115	60
Ni	15	10	41	26	11	7	37
Cu	17.3	4.7	4.8	15.9	32	15.3	15.1
Zn	67	58	35	27	14	30	53
Rb	45	45	73	31	74	47	55
Sr	600	708	400	294	173	261	533
Ba	295	322	267	252	461	468	351
Ta	0.293	0.267	0.609	0.641	0.622	0.590	0.453
Cs	5.16	2.49	1.31	0.96	0.82	1.69	1.70
Mo	0.43	0.40	0.41	0.80	0.29	0.60	0.46
Y	5.0	4.4	7.3	6.0	6.8	14.6	5.2
Zr	163	146	184	212	78	76	122
Nb	6.9	5.4	8.5	7.4	8.1	8.9	4.4
Hf	3.67	3.77	4.60	5.28	2.66	2.70	3.26
Pb	6.44	8.60	5.01	7.52	9.63	13.64	12.64
Th	2.68	3.33	2.75	7.76	2.26	2.53	3.43
U	0.651	0.678	0.93	1.48	1.10	1.54	1.66
La	19.2	21.4	12.8	22.8	7.4	8.6	15.7
Ce	36.9	40.0	21.9	36.8	18.8	16.3	26.8
Pr	3.92	4.23	2.36	3.58	1.74	1.92	2.81
Nd	16.1	16.7	9.1	13.0	7.1	7.8	10.6
Sm	2.57	2.75	1.73	2.24	1.49	2.48	2.04
Eu	0.834	0.817	0.600	0.512	0.55	0.53	0.755
Gd	1.64	1.67	1.77	1.71	1.33	2.60	1.50
Tb	0.171	0.186	0.273	0.216	0.199	0.319	0.250
Dy	0.97	0.95	1.27	1.14	1.30	2.52	1.01
Ho	0.181	0.169	0.267	0.209	0.252	0.442	0.225
Er	0.357	0.393	0.712	0.479	0.72	1.29	0.49
Tm	0.045	0.035	0.104	0.081	0.092	0.213	0.130
Yb	0.503	0.22	0.503	0.53	0.63	1.32	0.53
Lu	b.d.	0.023	0.081	0.107	0.086	0.133	0.139

Major- and trace-element concentrations in wt. % and µg/g, respectively. Mg # = atomic ratio of Mg^{2+}/ (Mg^{2+}+Fe^{2+}) x 100, using FeO = 0.9 of total Fe as Fe_2O_3. LOI = Loss on ignition; b.d. = below detection.

Table 4.4, continued.

	Weergevonden Pluton						
Sample	MS 25	MS 25b	MS 26	MS 27	MS 50	MS 51	MS 52
Rock type	Diorite	Diorite	Trondhjemite	Trondhjemite	Trondhjemite	Trondhjemite	Trondhjemite
SiO_2	60.18	60.14	71.60	72.31	72.17	72.68	70.59
TiO_2	1.29	1.01	0.29	0.26	0.22	0.22	0.43
Al_2O_3	15.16	13.18	15.86	14.84	15.84	15.54	15.43
Fe_2O_3(t)	6.10	7.46	1.87	2.04	1.45	1.40	2.55
Cr_2O_3	0.01	0.03	b.d.	b.d.	b.d.	b.d.	b.d.
MnO	0.07	0.09	0.03	0.04	0.02	0.02	0.05
MgO	4.79	6.86	0.82	0.94	0.56	0.56	0.81
CaO	6.45	5.91	2.36	2.75	2.30	1.86	2.64
Na_2O	4.34	3.64	5.57	5.06	5.75	5.66	4.80
K_2O	1.19	1.50	1.51	1.70	1.63	2.01	2.55
P_2O_5	0.42	0.20	0.08	0.07	0.06	0.06	0.14
Total	100	100	100	100	100	100	100
LOI	1.14	1.80	0.78	1.22	0.39	0.78	0.83
Mg#	61	65	47	48	43	44	39
Sc	19.3	21.8	7.3	8.8	5.0	5.0	6.2
V	139	169	16.5	29.0	21.4	21.0	40.1
Cr	98	216	13.2	15.2	10.7	10.0	14.5
Co	68.1	73.9	77	103	76	70	68
Ni	77	154	15	18	10	10	10
Cu	70	58	9.9	8.5	10.0	11.3	12.6
Zn	94	131	47	39	52	47	66
Rb	34.2	46.0	28	72	24	46	53
Sr	835	465	711	238	759	691	662
Ba	270	343	486	255	544	469	782
Ta	0.272	0.161	0.252	0.504	0.380	0.360	0.990
Cs	2.27	1.17	0.94	1.39	0.57	0.48	0.68
Mo	0.38	0.33	0.34	0.29	0.39	0.23	0.23
Y	12.2	12.6	3.0	15.8	2.9	3.0	7.3
Zr	157	101	124	114	117	107	109
Nb	5.9	3.2	4.3	6.5	3.3	3.4	9.7
Hf	3.50	2.91	3.32	3.57	3.73	3.24	3.53
Pb	5.49	4.15	7.28	5.27	10.24	12.86	14.06
Th	2.04	1.72	2.47	3.26	2.33	2.99	4.42
U	0.862	1.215	0.535	1.24	0.68	1.12	3.01
La	22.2	17.4	19.4	14.3	14.1	13.5	22.7
Ce	51.4	41.7	33.0	27.4	25.0	23.1	45.2
Pr	6.70	6.08	3.31	3.18	2.64	2.58	5.15
Nd	31.0	30.0	12.2	13.0	9.4	9.7	20.2
Sm	6.61	6.75	2.03	2.93	1.78	1.79	3.69
Eu	1.90	1.78	0.514	0.769	0.628	0.611	1.133
Gd	4.95	5.42	1.20	3.42	1.11	1.14	2.82
Tb	0.604	0.633	0.111	0.461	0.204	0.252	0.344
Dy	2.97	3.09	0.63	2.78	0.65	0.70	1.45
Ho	0.493	0.522	0.102	0.558	0.175	0.138	0.276
Er	1.112	1.089	0.289	1.51	0.32	0.35	0.64
Tm	0.144	0.149	0.044	0.208	0.088	0.098	0.083
Yb	0.88	0.82	0.130	1.54	0.30	0.33	0.60
Lu	0.117	0.115	0.042	0.237	0.095	0.083	0.078

Major- and trace-element concentrations in wt. % and µg/g, respectively. Mg # = atomic ratio of Mg^{2+}/ (Mg^{2+}+Fe^{2+}) x 100, using FeO = 0.9 of total Fe as Fe_2O_3. LOI = Loss on ignition; b.d. = below detection.

Table 4.4, continued.

	Eerstehoek Pluton			Onverwacht Group
Sample	MS 37	MS 40	MS 41	MS 21
Rock type	Tonalite	Tonalite	Tonalite	Mafic schist
SiO_2	72.92	71.96	69.17	58.08
TiO_2	0.30	0.35	0.65	0.97
Al_2O_3	14.88	15.02	16.00	20.25
Fe_2O_3(t)	2.17	2.52	3.16	6.97
Cr_2O_3	b.d.	b.d.	b.d.	0.01
MnO	0.04	0.05	0.05	0.18
MgO	0.76	0.95	1.11	2.21
CaO	2.84	3.24	3.13	5.79
Na_2O	4.56	4.24	4.83	3.41
K_2O	1.42	1.56	1.72	1.90
P_2O_5	0.09	0.10	0.17	0.24
Total	100	100	100	100
LOI	0.74	0.65	0.94	2.12
Mg#	41	43	41	39
Sc	6.8	7.0	7.0	23.1
V	31.8	35.1	48.4	117
Cr	14.7	19.0	10.2	76
Co	112	80	67	141
Ni	27	19	10	122
Cu	30.4	6.8	21.5	82
Zn	55	45	70	121
Rb	67	62	82	85
Sr	295	254	429	359
Ba	229	227	281	279
Ta	0.879	1.067	1.036	1.073
Cs	7.64	5.71	12.47	2.95
Mo	0.31	0.25	0.31	1.28
Y	16.2	19.0	16.1	46.7
Zr	125	162	190	220
Nb	8.9	10.3	12.0	15.2
Hf	3.43	4.52	4.80	5.69
Pb	8.83	7.01	8.66	10.69
Th	4.03	4.85	6.49	8.46
U	1.32	0.91	0.90	2.24
La	19.2	24.5	32.0	50.3
Ce	36.9	45.3	63.4	93.8
Pr	4.16	5.00	6.51	10.40
Nd	16.0	19.4	24.8	43
Sm	3.59	3.93	4.85	8.91
Eu	1.022	1.155	1.462	2.25
Gd	3.46	3.73	4.00	8.88
Tb	0.558	0.593	0.585	1.326
Dy	3.04	3.81	3.40	8.33
Ho	0.622	0.727	0.595	1.616
Er	1.52	1.98	1.60	4.78
Tm	0.259	0.277	0.211	0.692
Yb	1.53	1.75	1.44	4.64
Lu	0.249	0.254	0.186	0.687

Major- and trace-element concentrations in wt. % and µg/g, respectively. Mg # = atomic ratio of Mg^{2+}/ (Mg^{2+}+Fe^{2+}) x 100, using FeO = 0.9 of total Fe as Fe_2O_3. LOI = Loss on ignition; b.d. = below detection.

Table 4.5. Zircon U-Pb LA ICP-MS analysis metadata

Laboratory & Sample Preparation	
Laboratory name	Central Analytical Facilities, University of Stellenbosch
Sample type/mineral	Igneous zircons
Sample preparation	Conventional mineral separation, 1 inch resin mount, 1 µm polish to finish
Imaging	CL, Zeiss Merlin, 12 nA, 11.8 mm working distance
Laser ablation system	
Make, Model & type	ASI Resolution SE Excimer laser
Ablation cell & volume	Laurin Technic S-155 dual-volume cell
Laser wavelength	193 nm
Pulse width	5 ns
Fluence	1.4 $J.cm^{-2}$
Repetition rate	9 Hz
Ablation duration	21 secs
Ablation pit depth	~ 15 µm
Spot size	30 µm
Sampling mode / pattern	Static spot ablation
Carrier gas	100% He in the cell, Ar make-up gas combined using a Y-piece 50% along the sample transport line to the torch.
Cell carrier gas flow	0.8 l/min
ICP-MS Instrument	
Make, Model & type	Thermo-Fisher, Element2, single collector HR-SF-ICP-MS
Sample introduction	Ablation aerosol via conventional tubing
RF power	1325 W
Make-up gas flow	0.9 l/min Ar
Detection system	Single collector SEM (Secondary Electron Multiplier)
Masses measured	202, 204, 206-208, 232, 235, 238
Integration time per peak/dwell times	202: 7 ms; 204: 14 ms; 206: 15 ms; 207: 18 ms; 208: 8 ms; 232: 8 ms; 235: 1 ms; 238: 13 ms
Total integration time per output datapoint	0.1 s
Sensitivity	0.3% U
IC Dead time	6 ns
Data Processing	
Gas blank	21 s
Calibration strategy	GJ1 used as primary reference material, Plesovice & M127 used as secondaries/validation
Reference Material info	GJ1 (Jackson et al., 2004) Plesovice (Sláma et al., 2008) M127 (Nasdala et al., 2016)
Data processing package used / Correction for LIEF	Iolite reduction software package v.3.5 with VizualAge; LIEF modelled within each analytical session on the basis of combined analyses of the main reference material; LIEF correction assumes reference material and samples behave identically.

Mass discrimination	Reference material-sample bracketing with $^{207}Pb/^{206}Pb$ and $^{206}Pb/^{238}U$ normalized to zircon GJ-1
Common-Pb correction, composition and uncertainty	No common-Pb correction applied to the data.
Uncertainty level & propagation	Ages are quoted at 2*s* absolute, propagation is by quadratic addition. Reproducibility and age uncertainty of reference material and common-Pb composition uncertainty are propagated where appropriate.
Quality control / Validation	Plesovice – Wtd ave $^{206}Pb/^{238}U$ age = 339.6 ± 0.7 (2σ, MSWD = 1.64, n=43) M127 – Wtd ave $^{206}Pb/^{238}U$ age = 531.2 ± 2.1 (2σ, MSWD = 0.31, n=43)

Jackson, S.E., Pearson, N.J., Griffin, W.L., Belousova, E.A., 2004. The application of laser ablation-inductively coupled plasma-mass spectrometry to in situ U-Pb zircon geochronology. Chem. Geol. 211, 47–69. https://doi.org/10.1016/j.chemgeo.2004.06.017

Nasdala, L., Corfu, F., Valley, J.W., Spicuzza, M.J., Wu, F., Kennedy, A.K., Li, Q., Yang, Y., Fisher, C., Carsten, M., Reiners, P.W., Kronz, A., Wiedenbeck, M., Wirth, R., 2016. Zircon M127 – A Homogeneous Reference Material for SIMS U – Pb Geochronology Combined with Hafnium, Oxygen and, Potentially, Lithium Isotope Analysis 40, 457–475. https://doi.org/10.1111/ggr.12123

Sláma, J., Košler, J., Condon, D.J., Crowley, J.L., Gerdes, A., Hanchar, J.M., Horstwood, M.S.A., Morris, G.A., Nasdala, L., Norberg, N., Schaltegger, U., Schoene, B., Tubrett, M.N., Whitehouse, M.J., 2008. Plešovice zircon - A new natural reference material for U-Pb and Hf isotopic microanalysis. Chem. Geol. 249, 1–35. https://doi.org/10.1016/j.chemgeo.2007.11.005

Table 4.6. Apatite U-Pb LA ICP-MS analysis metadata

Laboratory & Sample Preparation	
Laboratory name	Laboratório de Geoquímica Isotópica, Departamento de Geologia, Universidade Federal de Ouro Preto (UFOP)
Sample type/mineral	Apatite
Sample preparation	Conventional mineral separation, 1 inch resin mount, 1 µm polish to finish
Imaging	CL, Zeiss Merlin, 12 nA, 10 mm working distance
Laser ablation system	
Make, Model & type	Photon Machines G2 excimer laser
Ablation cell & volume	Low volume HelEx
Laser wavelength	193 nm
Pulse width	4 ns
Fluence	1-2 $J.cm^{-2}$
Repetition rate	6 Hz
Ablation duration	40 secs
Ablation pit depth	5-10 µm
Spot size	20 µm
Sampling mode / pattern	Static spot ablation
Carrier gas	100% He in the cell, Ar and N_2 make-up gas combined using a Y-piece 50% along the sample transport line to the torch.
Cell carrier gas flow	0.1 l/min
ICP-MS Instrument	
Make, Model & type	Thermo-Fisher, Neptune Plus, MC-ICP-MS
Sample introduction	Ablation aerosol
RF power	1100 W
Make-up gas flow	0.5 l/min Ar
Detection system	SEM (Secondary Electron Multiplier)/compact discrete dynode ion counters/Faraday cups
Masses measured	Faraday; 232 and 238 and IC 202, 204, 206-208
Integration time per peak/dwell times	N.A.
Total integration time per output datapoint	0.131 s
Sensitivity	0.3% U
IC Dead time	IC1-2: 20 ns; IC3-4-5: 70 ns and IC6-7-8: 5ns
Data Processing	
Gas blank	15s

Calibration strategy	GJ1 used as primary reference material, 401, MAD and DUR used as secondaries/validation
Reference Material info	GJ1 (Jackson et al., 2004) 401 (Thompson et al., 2016) MAD (Thomson et al., 2012) DUR (McDowell et al., 2005)
Data processing package used / Correction for LIEF	In-house spreadsheet modified from Gerdes and Zeh (2006)
Common-Pb correction	Common Pb correction by measuring masses 202 and 204 and subtracting both from the apatite analysis on a ratio-by-ratio basis; ^{204}Hg calculated using natural ^{202}Hg/^{204}Hg = 4.36, subtracted from ^{204}total (Pb+Hg); non-radiogenic, common ^{206}Pb and ^{207}Pb calculated following the model of Stacey and Kramers (1975)
Uncertainty propagation	As recommended by Horstwood et al. (2016)
Quality control / Validation	401 – Wtd ave ^{206}Pb/^{238}U age = 531.8 ± 3.5 (2σ, MSWD = 0.72, n=22) MAD – Wtd ave ^{206}Pb/^{238}U age = 481.9 ± 2.7 (2σ, MSWD = 0.54, n=33) DUR - Wtd ave ^{206}Pb/^{238}U age = 31.93 ± 0.22 (2σ, MSWD = 1.68, n=23/25)

Gerdes, A., Zeh, A., 2006. Combined U-Pb and Hf isotope LA-(MC-)ICP-MS analyses of detrital zircons: Comparison with SHRIMP and new constraints for the provenance and age of an Armorican metasediment in Central Germany. Earth Planet. Sci. Lett. 249, 47–61. https://doi.org/10.1016/j.epsl.2006.06.039

Horstwood, M.S.A., Košler, J., Gehrels, G., Jackson, S.E., McLean, N.M., Paton, C., Pearson, N.J., Sircombe, K., Sylvester, P., Vermeesch, P., Bowring, J.F., Condon, D.J., Schoene, B., 2016. Community-Derived Standards for LA-ICP-MS U-(Th-)Pb Geochronology – Uncertainty Propagation, Age Interpretation and Data Reporting. Geostand. Geoanalytical Res. 40, 311–332. https://doi.org/10.1111/j.1751-908X.2016.00379.x

Jackson, S.E., Pearson, N.J., Griffin, W.L., Belousova, E.A., 2004. The application of laser ablation-inductively coupled plasma-mass spectrometry to in situ U-Pb zircon geochronology. Chem. Geol. 211, 47–69. https://doi.org/10.1016/j.chemgeo.2004.06.017

McDowell, F.W., McIntosh, W.C., Farley, K.A., 2005. A precise 40 Ar – 39 Ar reference age for the Durango apatite (U – Th)/ He and fission-track dating standard 214, 249–263. https://doi.org/10.1016/j.chemgeo.2004.10.002

Stacey, J.S., Kramers, J.D., 1975. Approximation of terrestrial lead isotope evolution by a two-stage model. Earth Planet. Sci. Lett. 26, 207–221. https://doi.org/10.1016/0012-821X(75)90088-6

Thompson, J., Meffre, S., Maas, R., Kamenetsky, V., Kamanetsky, M., Goemann, K., Ehrig, K., Danyushevsky, L., 2016. Matrix effects in Pb/U measurements during LA-ICP-MS analysis of the mineral apatite. J. Anal. At. Spectrom. 31, 1206–1215.

Thomson, S.N., Gehrels, G.E., Ruiz, J., Buchwaldt, R., 2012. Routine low-damage apatite U-Pb dating using laser ablation-multicollector- ICPMS. Geochemistry, Geophys. Geosystems 13, 1–23. https://doi.org/10.1029/2011GC003928

Table 4.7. Zircon U-Pb isotope data

17th-19th July 2017, Central Analytical Facilities University of Stellenbosch							Data for Tera-Wasserburg plot [a]				Data for Wetherill plot [a]					Dates (Ma)									Concordance [b]	
Identifier	Comment	^{206}Pb (CPS)	^{204}Pb (CPS)	^{206}Pb/^{204}Pb	U (mg g-1)	Th/U	^{238}U/^{206}Pb	2 s	^{207}Pb/^{206}Pb	2 s	^{207}Pb/^{235}U	2 s	^{206}Pb/^{238}U	2 s	rho	^{207}Pb/^{206}Pb	2 s	2s $_{sys}$	^{206}Pb/^{238}U	2 s	2s $_{sys}$	^{207}Pb/^{235}U	2 s	2s $_{sys}$	6/38 - 7/35	6/38 - 7/6
MS 1: Stolzburg dyke																										
MS 1 - 1		6.0.E+05	b.d.	b.d	181	0.51	1.65	0.03	0.2848	0.00313	23.74	0.43	0.6046	0.0097	0.89	3387	17	19	3045	39	62	3255	18	28	94	90
MS 1 - 2		7.5.E+05	b.d.	b.d	1293	0.87	8.69	0.15	0.2476	0.00272	3.93	0.08	0.1151	0.0020	0.90	3167	17	19	702	11	17	1617	16	25	43	22
MS 1 - 3		1.0.E+06	b.d.	b.d	912	1.24	4.73	0.08	0.2030	0.00430	5.94	0.18	0.2116	0.0034	0.53	2838	34	36	1237	18	28	1959	26	39	63	44
MS 1 - 5		1.3.E+06	b.d.	b.d	424	0.14	1.71	0.03	0.2414	0.00266	19.53	0.33	0.5851	0.0088	0.89	3129	17	19	2967	36	58	3067	16	25	97	95
MS 1 - 6		6.6.E+05	b.d.	b.d	215	0.35	1.65	0.02	0.2485	0.00273	20.76	0.37	0.6046	0.0090	0.84	3173	17	19	3046	36	59	3125	17	27	97	96
MS 1 - 7		7.2.E+05	b.d.	b.d	227	0.22	1.63	0.02	0.2468	0.00271	20.96	0.35	0.6151	0.0086	0.84	3162	17	19	3088	34	58	3134	17	27	99	98
MS 1 - 9		1.6.E+05	b.d.	b.d	49	0.31	1.53	0.02	0.2541	0.00280	22.89	0.39	0.6518	0.0091	0.82	3207	17	19	3232	36	61	3221	16	26	100	101
MS 1 - 10		1.9.E+06	b.d.	b.d	888	0.04	2.41	0.03	0.2004	0.00220	11.48	0.19	0.4148	0.0055	0.80	2827	18	20	2235	25	44	2560	16	26	87	79
MS 1 - 12		3.8.E+05	b.d.	b.d	123	0.58	1.68	0.02	0.2842	0.00313	23.31	0.40	0.5936	0.0085	0.83	3386	17	19	3001	34	58	3237	17	27	93	89
MS 1 - 13		4.5.E+05	b.d.	b.d	142	0.38	1.59	0.02	0.2767	0.00304	23.99	0.43	0.6282	0.0097	0.86	3342	17	19	3139	38	62	3264	17	29	96	94
MS 1 - 14		8.1.E+05	b.d.	b.d	239	0.19	1.54	0.02	0.2530	0.00278	22.67	0.34	0.6496	0.0081	0.83	3201	17	19	3224	32	58	3211	15	25	100	101
MS 1 - 15		5.6.E+05	b.d.	b.d	208	0.18	1.79	0.03	0.2433	0.00268	18.77	0.40	0.5580	0.0100	0.84	3140	17	19	2856	43	61	3028	21	29	94	91
MS 1 - 16		9.8.E+05	b.d.	b.d	585	0.11	3.00	0.05	0.2177	0.00239	10.03	0.21	0.3330	0.0055	0.79	2960	18	20	1852	26	40	2434	19	29	76	63
MS 1 - 17		8.6.E+05	b.d.	b.d	358	0.48	2.16	0.03	0.2644	0.00291	16.86	0.30	0.4620	0.0068	0.83	3271	17	19	2446	30	50	2924	17	27	84	75
MS 1 - 18		3.0.E+05	b.d.	b.d	90	0.38	1.58	0.02	0.2899	0.00319	25.29	0.43	0.6335	0.0090	0.84	3414	17	19	3160	36	61	3316	17	28	95	93
MS 1 - 19		3.4.E+05	b.d.	b.d	95	0.49	1.45	0.02	0.2945	0.00324	28.07	0.46	0.6908	0.0092	0.81	3439	17	19	3383	35	62	3419	16	27	99	98
MS 2: Stolzburg Main Trondhjemite																										
MS 2 - 1		9.3.E+05	b.d.	b.d	316	0.63	1.70	0.03	0.2725	0.00300	22.15	0.45	0.5883	0.0110	0.92	3319	17	19	2979	43	65	3187	20	30	93	90
MS 2 - 2		7.5.E+05	b.d.	b.d	225	0.58	1.53	0.02	0.2868	0.00315	25.86	0.44	0.6529	0.0090	0.81	3399	17	19	3236	35	61	3338	17	28	97	95
MS 2 - 3		8.9.E+05	b.d.	b.d	288	0.41	1.61	0.04	0.2887	0.00318	24.75	0.62	0.6200	0.0140	0.90	3408	17	19	3104	54	77	3292	25	37	94	91
MS 2 - 4		7.0.E+05	b.d.	b.d	212	0.44	1.53	0.02	0.2875	0.00316	25.94	0.45	0.6534	0.0089	0.79	3402	17	19	3238	35	61	3340	17	29	97	95
MS 2 - 5		7.7.E+05	b.d.	b.d	237	0.59	1.58	0.02	0.2792	0.00307	24.51	0.45	0.6348	0.0087	0.75	3356	17	19	3165	34	60	3285	18	29	96	94
MS 2 - 6		6.9.E+05	b.d.	b.d	200	0.49	1.48	0.02	0.2856	0.00314	26.63	0.44	0.6754	0.0089	0.80	3393	17	19	3324	34	61	3367	16	27	99	98
MS 2 - 7		1.1.E+06	b.d.	b.d	299	0.50	1.38	0.02	0.2900	0.00319	28.96	0.43	0.7237	0.0089	0.83	3415	17	19	3507	33	62	3450	15	25	102	103
MS 2 - 8		8.8.E+05	b.d.	b.d	235	0.50	1.39	0.02	0.2922	0.00321	29.10	0.45	0.7217	0.0092	0.82	3427	17	19	3499	34	63	3454	15	27	101	102
MS 2 - 9		8.4.E+05	b.d.	b.d	315	0.51	1.82	0.03	0.2705	0.00320	20.59	0.47	0.5504	0.0100	0.80	3306	19	20	2825	43	60	3117	22	31	91	85
MS 2 - 10		9.3.E+05	b.d.	b.d	305	0.61	1.65	0.03	0.2754	0.00303	23.07	0.43	0.6065	0.0097	0.86	3335	17	19	3053	39	61	3227	18	28	95	92
MS 2 - 11		7.7.E+05	b.d.	b.d	233	0.64	1.52	0.02	0.2887	0.00318	26.20	0.40	0.6578	0.0085	0.85	3408	17	19	3256	33	59	3352	15	25	97	96
MS 2 - 12		6.9.E+05	b.d.	b.d	227	0.51	1.67	0.02	0.2867	0.00315	23.69	0.38	0.5976	0.0077	0.80	3398	17	19	3017	31	56	3253	16	27	93	89
MS 2 - 13		8.3.E+05	b.d.	b.d	250	0.28	1.58	0.02	0.2832	0.00312	24.66	0.41	0.6316	0.0094	0.90	3378	17	19	3152	37	62	3292	16	27	96	93
MS 2 - 14		6.9.E+05	b.d.	b.d	202	0.42	1.43	0.02	0.2923	0.00322	28.20	0.49	0.6982	0.0100	0.82	3428	17	19	3411	38	64	3424	17	27	100	100
MS 2 - 15		5.2.E+05	b.d.	b.d	139	0.39	1.38	0.02	0.2969	0.00327	29.77	0.46	0.7264	0.0088	0.78	3452	17	19	3517	33	62	3477	15	26	101	102
MS 2 - 16		5.4.E+05	b.d.	b.d	149	0.33	1.41	0.02	0.2960	0.00326	29.04	0.43	0.7110	0.0085	0.81	3447	17	19	3459	32	61	3453	15	25	100	100
MS 2 - 17		5.6.E+05	b.d.	b.d	158	0.50	1.42	0.02	0.2916	0.00321	28.37	0.45	0.7050	0.0090	0.80	3424	17	19	3436	34	62	3430	16	26	100	100
MS 2 - 18		1.2.E+06	b.d.	b.d	354	0.96	1.64	0.02	0.2650	0.00292	22.29	0.39	0.6099	0.0089	0.83	3275	17	19	3067	36	59	3194	17	27	96	94
MS 2 - 19		7.8.E+05	b.d.	b.d	220	0.37	1.45	0.02	0.2928	0.00322	27.89	0.42	0.6905	0.0084	0.81	3431	17	19	3382	32	60	3413	15	25	99	99
MS 2 - 20		6.6.E+05	b.d.	b.d	185	0.40	1.43	0.02	0.2911	0.00320	28.02	0.43	0.6976	0.0088	0.82	3421	17	19	3409	34	61	3418	15	25	100	100
MS 2 - 21		1.1.E+06	b.d.	b.d	354	0.84	1.59	0.02	0.2921	0.00321	25.29	0.43	0.6270	0.0096	0.90	3427	17	19	3135	38	61	3317	17	27	95	91
MS 2 - 22		1.0.E+06	b.d.	b.d	314	0.61	1.52	0.02	0.2761	0.00304	25.08	0.41	0.6583	0.0098	0.91	3338	17	19	3258	38	62	3309	16	26	98	98
MS 2 - 23		6.9.E+05	b.d.	b.d	192	0.40	1.42	0.02	0.2932	0.00323	28.46	0.43	0.7032	0.0086	0.81	3432	17	19	3430	32	61	3433	15	25	100	100
MS 2 - 24		1.0.E+06	b.d.	b.d	303	0.77	1.51	0.02	0.2983	0.00328	27.21	0.43	0.6613	0.0091	0.87	3459	17	19	3269	35	61	3388	16	27	96	94
MS 2 - 25		7.7.E+05	b.d.	b.d	221	0.52	1.50	0.02	0.2847	0.00313	26.16	0.41	0.6664	0.0088	0.84	3387	17	19	3289	34	60	3351	15	25	98	97
MS 2 - 26		8.6.E+05	b.d.	b.d	248	0.52	1.44	0.02	0.2902	0.00319	27.82	0.43	0.6939	0.0087	0.81	3417	17	19	3395	33	60	3410	15	26	100	99
MS 2 - 27		4.6.E+05	b.d.	b.d	151	0.47	1.68	0.03	0.2768	0.00304	22.79	0.44	0.5964	0.0097	0.84	3343	17	19	3012	39	62	3215	19	29	94	90
MS 2 - 28		8.9.E+05	b.d.	b.d	402	0.63	2.06	0.05	0.2582	0.00320	17.38	0.51	0.4860	0.0120	0.84	3233	20	21	2550	52	68	2951	29	38	86	79
MS 2 - 29		8.7.E+05	b.d.	b.d	259	0.59	1.43	0.03	0.2905	0.00320	28.04	0.57	0.6990	0.0130	0.91	3418	17	19	3412	50	73	3418	20	29	100	100

Uncertainties quoted without components related to systematic error unless otherwise stated. Total systematic uncertainties (s sys): ^{206}Pb/^{238}U = 1.8 %; ^{207}Pb/^{206}Pb = 0.5 % (2s).

[a] Data not corrected for common Pb

[b] Concordance calculated as: (^{206}Pb-^{238}U date/^{207}Pb-^{235U} date)*100 and (^{206}Pb-^{238}U date/^{207}Pb-^{206}Pb date)*100

Table 4.7, continued.

17th-19th July 2017, Central Analytical Facilities University of Stellenbosch							Data for Tera-Wasserburg plot [a]				Data for Wetherill plot [a]					Dates (Ma)									Concordance [b]	
Identifier	Comment	^{206}Pb (CPS)	^{204}Pb (CPS)	^{206}Pb/^{204}Pb	U (mg g-1)	Th/U	^{238}U/^{206}Pb	2 s	^{207}Pb/^{206}Pb	2 s	^{207}Pb/^{235}U	2 s	^{206}Pb/^{238}U	2 s	rho	^{207}Pb/^{206}Pb	2 s	2s $_{sys}$	^{206}Pb/^{238}U	2 s	2s $_{sys}$	^{207}Pb/^{235}U	2 s	2s $_{sys}$	6/38 - 7/35	6/38 - 7/6
MS 2 - 30		9.1.E+05	b.d.	b.d	285	0.65	1.54	0.02	0.2875	0.00316	25.75	0.45	0.6486	0.0096	0.85	3402	17	19	3220	37	62	3334	17	28	97	95
MS 2 - 31		9.7.E+05	b.d.	b.d	275	0.51	1.41	0.02	0.2903	0.00319	28.51	0.45	0.7115	0.0091	0.81	3417	17	19	3461	34	62	3435	16	26	101	101
MS 2 - 32		9.2.E+05	b.d.	b.d	272	0.65	1.49	0.02	0.2846	0.00313	26.38	0.41	0.6714	0.0083	0.80	3386	17	19	3309	32	59	3358	15	26	99	98
MS 2 - 33		8.7.E+05	b.d.	b.d	244	0.45	1.42	0.02	0.2912	0.00320	28.26	0.44	0.7032	0.0089	0.81	3422	17	19	3430	34	61	3426	15	26	100	100
MS 2 - 34		6.6.E+05	b.d.	b.d	192	0.36	1.44	0.02	0.2864	0.00315	27.54	0.46	0.6963	0.0096	0.83	3396	17	19	3404	36	62	3401	16	26	100	100
MS 2 - 35		8.9.E+05	b.d.	b.d	252	0.54	1.42	0.02	0.2854	0.00314	27.73	0.45	0.7039	0.0095	0.83	3391	17	19	3432	36	63	3407	16	27	101	101
MS 2 - 36		6.5.E+05	b.d.	b.d	199	0.27	1.50	0.02	0.2846	0.00313	26.19	0.41	0.6660	0.0085	0.82	3386	17	19	3288	33	59	3351	15	26	98	97
MS 2 - 37		9.1.E+05	b.d.	b.d	266	0.46	1.45	0.02	0.2900	0.00319	27.62	0.43	0.6903	0.0091	0.85	3415	17	19	3384	35	58	3404	16	25	99	99
MS 2 - 38		8.8.E+05	b.d.	b.d	430	0.95	2.51	0.03	0.2341	0.00258	12.90	0.23	0.3986	0.0055	0.77	3078	18	19	2161	25	43	2669	16	27	81	70
MS 2 - 40		7.8.E+05	b.d.	b.d	224	0.58	1.46	0.02	0.2952	0.00325	27.88	0.44	0.6845	0.0088	0.81	3443	17	19	3359	34	60	3413	15	26	98	98
MS 2 - 41		6.4.E+05	b.d.	b.d	182	0.39	1.42	0.02	0.2931	0.00322	28.45	0.44	0.7032	0.0088	0.81	3433	17	19	3430	33	61	3433	15	25	100	100
MS 2 - 42		8.4.E+05	b.d.	b.d	238	1.08	1.38	0.02	0.3019	0.00332	30.35	0.64	0.7270	0.0120	0.78	3477	17	19	3518	46	70	3494	21	32	101	101
MS 2 - 43		4.3.E+05	b.d.	b.d	129	0.34	1.43	0.02	0.2899	0.00319	28.04	0.51	0.7002	0.0110	0.86	3415	17	19	3418	41	67	3418	18	28	100	100
MS 2 - 45		5.5.E+05	b.d.	b.d	165	0.38	1.45	0.02	0.2877	0.00316	27.46	0.45	0.6913	0.0097	0.86	3403	17	19	3385	37	63	3398	16	26	100	99
MS 2 - 46		7.1.E+05	b.d.	b.d	204	0.42	1.41	0.02	0.2925	0.00322	28.65	0.45	0.7093	0.0092	0.83	3429	17	19	3453	35	62	3440	15	25	100	101
MS 2 - 47		8.8.E+05	b.d.	b.d	254	0.60	1.45	0.02	0.2933	0.00323	27.94	0.45	0.6897	0.0091	0.82	3433	17	19	3379	35	61	3414	16	27	99	98
MS 2 - 48		8.1.E+05	b.d.	b.d	285	0.64	1.71	0.03	0.2847	0.00313	23.05	0.42	0.5860	0.0094	0.88	3387	17	19	2970	38	60	3226	18	28	92	88
MS 2 - 49		1.4.E+06	b.d.	b.d	480	0.61	1.65	0.03	0.2715	0.00299	22.76	0.48	0.6060	0.0110	0.86	3312	17	19	3052	44	64	3214	21	30	95	92
MS 2 - 50		8.3.E+05	b.d.	b.d	251	0.55	1.49	0.02	0.2856	0.00314	26.54	0.42	0.6729	0.0087	0.82	3392	17	19	3315	33	59	3365	16	25	99	98
MS 2 - 51		5.7.E+05	b.d.	b.d	186	0.96	1.74	0.03	0.2891	0.00318	22.91	0.46	0.5749	0.0100	0.87	3410	17	19	2925	41	62	3220	20	30	91	86
MS 2 - 52		1.1.E+06	b.d.	b.d	298	0.53	1.42	0.02	0.2891	0.00318	28.20	0.49	0.7063	0.0096	0.78	3411	17	19	3441	36	64	3423	17	28	101	101
MS 2 - 53		1.2.E+06	b.d.	b.d	354	0.80	1.47	0.02	0.2832	0.00312	26.66	0.42	0.6821	0.0088	0.82	3378	17	19	3350	33	60	3369	15	26	99	99
MS 2 - 55		1.1.E+06	b.d.	b.d	343	0.66	1.58	0.02	0.2700	0.00297	23.63	0.36	0.6334	0.0078	0.81	3305	17	19	3161	31	56	3251	15	26	97	96
MS 2 - 56		9.1.E+05	b.d.	b.d	258	0.60	1.44	0.02	0.2908	0.00320	27.87	0.45	0.6944	0.0097	0.87	3420	17	19	3396	37	63	3412	16	27	100	99
MS 2 - 57		6.4.E+05	b.d.	b.d	253	0.29	1.92	0.03	0.2777	0.00305	19.96	0.37	0.5200	0.0083	0.86	3348	17	19	2697	35	55	3086	18	29	87	81
MS 2 - 58		1.1.E+06	b.d.	b.d	385	0.44	1.73	0.03	0.2652	0.00292	21.11	0.39	0.5765	0.0085	0.80	3276	17	19	2932	35	57	3140	18	29	93	89
MS 2 - 59		7.7.E+05	b.d.	b.d	208	0.59	1.40	0.02	0.2886	0.00317	28.41	0.47	0.7139	0.0099	0.84	3408	17	19	3470	37	64	3431	16	27	101	102
MS 2 - 60		1.0.E+06	b.d.	b.d	318	0.60	1.56	0.02	0.2790	0.00307	24.67	0.45	0.6401	0.0100	0.86	3355	17	19	3186	40	63	3292	18	28	97	95
MS 2 - 61		5.9.E+05	b.d.	b.d	207	0.48	1.73	0.03	0.2663	0.00293	21.32	0.37	0.5796	0.0088	0.87	3282	17	19	2944	36	59	3150	17	28	93	90
MS 2 - 62		7.9.E+05	b.d.	b.d	248	0.49	1.57	0.02	0.2829	0.00311	24.92	0.39	0.6380	0.0083	0.83	3377	17	19	3178	33	59	3303	15	26	96	94
MS 2 - 63		6.8.E+05	b.d.	b.d	191	0.58	1.45	0.03	0.2850	0.00314	27.07	0.56	0.6890	0.0120	0.84	3388	17	19	3374	44	70	3382	21	31	100	100
MS 2 - 64		8.9.E+05	b.d.	b.d	382	0.88	2.09	0.04	0.2611	0.00287	17.29	0.41	0.4776	0.0094	0.83	3251	17	19	2518	42	54	2945	22	35	86	77
MS 2 - 65		8.8.E+05	b.d.	b.d	243	0.53	1.38	0.02	0.2919	0.00321	29.14	0.44	0.7235	0.0090	0.82	3426	17	19	3506	33	62	3456	15	25	101	102
MS 2 - 66		4.4.E+05	b.d.	b.d	129	0.36	1.44	0.02	0.2883	0.00317	27.70	0.49	0.6956	0.0100	0.81	3406	17	19	3401	39	64	3406	17	28	100	100
MS 2 - 67		8.9.E+05	b.d.	b.d	263	0.38	1.43	0.02	0.2852	0.00314	27.49	0.47	0.6977	0.0100	0.84	3390	17	19	3408	39	65	3398	17	28	100	101
MS 2 - 68		9.5.E+05	b.d.	b.d	275	0.44	1.45	0.02	0.2900	0.00319	27.51	0.44	0.6874	0.0093	0.85	3415	17	19	3370	35	62	3399	16	27	99	99
MS 2 - 69		8.1.E+05	b.d.	b.d	232	0.46	1.43	0.02	0.2897	0.00319	27.90	0.44	0.6978	0.0088	0.80	3414	17	19	3409	33	61	3413	15	26	100	100
MS 2 - 70		8.8.E+05	b.d.	b.d	253	0.51	1.43	0.02	0.2938	0.00323	28.38	0.42	0.7000	0.0088	0.85	3436	17	19	3418	33	61	3430	15	25	100	99
MS 2 - 71		9.4.E+05	b.d.	b.d	274	0.46	1.46	0.02	0.2835	0.00312	26.82	0.42	0.6855	0.0086	0.80	3380	17	19	3363	33	60	3375	15	26	100	99
MS 2 - 72		5.4.E+05	b.d.	b.d	153	0.31	1.40	0.02	0.2935	0.00323	28.90	0.46	0.7133	0.0093	0.82	3434	17	19	3468	35	62	3448	16	26	101	101
MS 2 - 73		8.8.E+05	b.d.	b.d	252	0.51	1.46	0.02	0.2906	0.00320	27.52	0.44	0.6864	0.0088	0.80	3419	17	19	3366	34	61	3400	16	26	99	98
MS 2 - 74		7.1.E+05	b.d.	b.d	222	0.42	1.43	0.03	0.2893	0.00330	28.01	0.58	0.7000	0.0140	0.97	3411	18	19	3419	52	73	3417	20	29	100	100
MS 2 - 75		3.4.E+05	b.d.	b.d	128	0.22	1.79	0.03	0.2777	0.00305	21.41	0.45	0.5577	0.0096	0.82	3347	17	19	2854	40	60	3153	21	31	91	85
MS 2 - 76		6.5.E+05	b.d.	b.d	187	0.47	1.44	0.02	0.2956	0.00325	28.30	0.45	0.6940	0.0090	0.82	3445	17	19	3395	34	61	3427	16	26	99	99
MS 2 - 77		1.0.E+06	b.d.	b.d	368	0.70	1.74	0.03	0.2796	0.00308	22.20	0.46	0.5744	0.0093	0.78	3357	17	19	2923	38	60	3189	20	30	92	87
MS 2 - 78		7.8.E+05	b.d.	b.d	222	0.50	1.43	0.02	0.2910	0.00320	28.09	0.42	0.6996	0.0088	0.84	3421	17	19	3416	33	61	3420	15	25	100	100
MS 2 - 79		5.9.E+05	b.d.	b.d	180	0.59	1.53	0.02	0.2836	0.00312	25.58	0.41	0.6543	0.0083	0.79	3381	17	19	3242	32	59	3329	16	25	97	96
MS 2 - 80		6.1.E+05	b.d.	b.d	178	0.39	1.46	0.02	0.2903	0.00319	27.51	0.46	0.6864	0.0090	0.78	3417	17	19	3366	34	61	3399	16	27	99	99

Uncertainties quoted without components related to systematic error unless otherwise stated. Total systematic uncertainties (s sys): ^{206}Pb/^{238}U = 1.8 %; ^{207}Pb/^{206}Pb = 0.5 % (2s).

[a] Data not corrected for common Pb

[b] Concordance calculated as: (^{206}Pb-^{238}U date/^{207}Pb-^{235U} date)*100 and (^{206}Pb-^{238}U date/^{207}Pb-^{206}Pb date)*100

Table 4.7, continued.

17th-19th July 2017, Central Analytical Facilities University of Stellenbosch							Data for Tera-Wasserburg plot [a]				Data for Wetherill plot [a]					Dates (Ma)									Concordance [b]	
Identifier	Comment	^{206}Pb (CPS)	^{204}Pb (CPS)	^{206}Pb/^{204}Pb	U (mg g-1)	Th/U	^{238}U/^{206}Pb	2 s	^{207}Pb/^{206}Pb	2 s	^{207}Pb/^{235}U	2 s	^{206}Pb/^{238}U	2 s	rho	^{207}Pb/^{206}Pb	2 s	2s $_{sys}$	^{206}Pb/^{238}U	2 s	2s $_{sys}$	^{207}Pb/^{235}U	2 s	2s $_{sys}$	6/38 - 7/35	6/38 - 7/6
MS 2 - 81		4.7.E+05	b.d.	b.d	146	0.18	1.54	0.02	0.2807	0.00309	25.11	0.40	0.6485	0.0089	0.86	3366	17	19	3219	35	61	3310	16	26	97	96
MS 2 - 82		9.6.E+05	b.d.	b.d	277	0.73	1.47	0.02	0.2892	0.00318	27.21	0.45	0.6817	0.0089	0.79	3411	17	19	3349	34	60	3389	16	26	99	98
MS 2 - 83		7.0.E+05	b.d.	b.d	217	0.57	1.56	0.02	0.2970	0.00327	26.30	0.47	0.6418	0.0096	0.84	3452	17	19	3193	38	62	3355	17	28	95	92
MS 2 - 84		7.6.E+05	b.d.	b.d	256	0.52	1.68	0.02	0.2793	0.00307	22.96	0.36	0.5958	0.0077	0.82	3357	17	19	3010	31	56	3223	15	26	93	90
MS 2 - 85		1.2.E+06	b.d.	b.d	352	0.84	1.46	0.02	0.2848	0.00313	26.99	0.42	0.6867	0.0087	0.81	3387	17	19	3367	33	61	3381	15	26	100	99
MS 2 - 86		3.6.E+05	b.d.	b.d	167	0.52	2.27	0.03	0.2533	0.00279	15.40	0.27	0.4401	0.0060	0.78	3201	17	19	2352	26	44	2837	17	28	83	73
MS 2 - 87		4.5.E+05	b.d.	b.d	144	0.42	1.66	0.03	0.2810	0.00309	23.34	0.49	0.6020	0.0100	0.79	3366	17	19	3035	40	62	3238	21	30	94	90
MS 2 - 88		9.9.E+05	b.d.	b.d	316	0.57	1.58	0.02	0.2771	0.00305	24.31	0.47	0.6342	0.0090	0.73	3344	17	19	3163	36	60	3275	19	32	97	95
MS 2 - 89		8.9.E+05	b.d.	b.d	263	0.63	1.46	0.02	0.2838	0.00312	26.88	0.44	0.6859	0.0092	0.82	3382	17	19	3364	35	62	3376	16	27	100	99
MS 2 - 90		9.5.E+05	b.d.	b.d	291	0.58	1.51	0.03	0.2813	0.00309	25.76	0.59	0.6620	0.0130	0.86	3368	17	19	3273	49	70	3334	23	32	98	97
MS 2 - 91		1.1.E+06	b.d.	b.d	328	0.58	1.42	0.02	0.2857	0.00314	27.87	0.45	0.7065	0.0090	0.79	3392	17	19	3442	34	62	3412	16	27	101	101
MS 2 - 92		7.3.E+05	b.d.	b.d	322	0.79	2.16	0.04	0.2723	0.00300	17.39	0.34	0.4623	0.0076	0.84	3317	17	19	2446	34	53	2953	19	29	83	74
MS 2 - 93		1.0.E+06	b.d.	b.d	290	0.55	1.39	0.02	0.2938	0.00323	29.12	0.44	0.7172	0.0091	0.84	3436	17	19	3483	34	62	3456	15	25	101	101
MS 2 - 94		9.2.E+05	b.d.	b.d	268	0.68	1.40	0.02	0.2947	0.00324	28.94	0.44	0.7120	0.0091	0.84	3440	17	19	3463	34	62	3450	15	25	100	101
MS 2 - 95		7.8.E+05	b.d.	b.d	229	0.41	1.40	0.02	0.2944	0.00324	29.07	0.47	0.7143	0.0098	0.85	3439	17	19	3473	37	62	3454	16	26	101	101
MS 2 - 96		9.6.E+05	b.d.	b.d	295	0.41	1.47	0.02	0.2853	0.00314	26.83	0.49	0.6804	0.0100	0.80	3391	17	19	3343	39	63	3374	18	29	99	99
MS 2 - 97		6.7.E+05	b.d.	b.d	189	0.49	1.47	0.02	0.2883	0.00317	27.10	0.49	0.6816	0.0110	0.89	3407	17	19	3348	40	65	3385	18	27	99	98
MS 2 - 98		8.2.E+05	b.d.	b.d	252	0.53	1.48	0.02	0.2925	0.00322	27.31	0.44	0.6767	0.0091	0.83	3429	17	19	3328	35	62	3392	16	27	98	97
MS 2 - 99		4.3.E+05	b.d.	b.d	129	0.34	1.56	0.02	0.2857	0.00314	25.25	0.43	0.6418	0.0097	0.89	3392	17	19	3193	38	62	3316	17	26	96	94
MS 2 - 100		6.8.E+05	b.d.	b.d	208	0.04	1.48	0.02	0.2841	0.00313	26.48	0.42	0.6751	0.0083	0.78	3383	17	19	3323	32	59	3362	16	26	99	98
MS 2 - 101		7.9.E+05	b.d.	b.d	262	0.72	1.62	0.02	0.2803	0.00308	23.90	0.39	0.6174	0.0078	0.77	3363	17	19	3097	31	57	3262	16	26	95	92
MS 2 - 102		7.5.E+05	b.d.	b.d	223	0.42	1.45	0.02	0.2896	0.00319	27.61	0.43	0.6904	0.0084	0.78	3413	17	19	3381	32	60	3403	15	26	99	99
MS 2 - 103		9.1.E+05	b.d.	b.d	267	0.54	1.44	0.02	0.2892	0.00318	27.74	0.44	0.6947	0.0091	0.83	3412	17	19	3397	34	62	3409	15	25	100	100
MS 3: Honingklip dyke																										
MS 3 - 1		7.1.E+05	b.d.	b.d	226	0.62	1.66	0.02	0.2722	0.00299	22.71	0.42	0.6040	0.0085	0.76	3316	17	19	3043	34	58	3211	18	29	95	92
MS 3 - 2		3.7.E+05	b.d.	b.d	119	0.49	1.64	0.03	0.2709	0.00298	22.91	0.45	0.6110	0.0110	0.92	3308	17	19	3071	44	65	3223	18	26	95	93
MS 3 - 3		7.8.E+05	b.d.	b.d	252	0.04	1.74	0.02	0.2481	0.00273	19.63	0.33	0.5738	0.0081	0.84	3170	17	19	2921	33	56	3071	16	26	95	92
MS 3 - 4		3.6.E+05	b.d.	b.d	117	0.14	1.67	0.02	0.2542	0.00280	20.96	0.33	0.5978	0.0076	0.81	3208	17	19	3019	31	55	3135	15	25	96	94
MS 3 - 5		2.6.E+05	b.d.	b.d	77	0.38	1.57	0.02	0.2549	0.00280	22.37	0.34	0.6365	0.0081	0.84	3212	17	19	3173	32	57	3198	15	26	99	99
MS 3 - 6		2.3.E+05	b.d.	b.d	70	0.35	1.57	0.02	0.2543	0.00280	22.33	0.37	0.6364	0.0085	0.81	3209	17	19	3172	33	59	3196	16	26	99	99
MS 3 - 7		2.4.E+05	b.d.	b.d	72	0.32	1.52	0.02	0.2532	0.00279	23.07	0.41	0.6600	0.0100	0.85	3202	17	19	3264	39	63	3229	17	26	101	102
MS 3 - 8		4.2.E+05	b.d.	b.d	130	0.50	1.58	0.02	0.2528	0.00278	22.04	0.35	0.6315	0.0083	0.83	3201	17	19	3153	33	58	3183	16	26	99	99
MS 3 - 9		8.3.E+05	b.d.	b.d	271	0.02	1.58	0.03	0.2467	0.00271	21.63	0.47	0.6330	0.0130	0.95	3161	17	19	3159	49	70	3164	21	31	100	100
MS 3 - 10		3.3.E+05	b.d.	b.d	101	0.32	1.49	0.03	0.2541	0.00280	23.53	0.46	0.6690	0.0120	0.92	3208	17	19	3299	45	68	3247	19	28	102	103
MS 3 - 11		8.3.E+05	b.d.	b.d	273	0.06	1.65	0.02	0.2472	0.00272	20.65	0.32	0.6051	0.0078	0.83	3165	17	19	3048	31	56	3121	15	25	98	96
MS 3: Honingklip trondhjemite																										
MS 4 - 1		6.5.E+05	b.d.	b.d	205	0.61	1.44	0.03	0.3076	0.00338	29.43	0.56	0.6930	0.0140	0.79	3507	17	19	3390	52	75	3466	19	28	98	97
MS 4 - 2		8.0.E+05	b.d.	b.d	330	0.08	1.96	0.03	0.2353	0.00259	16.52	0.27	0.5094	0.0086	0.83	3087	18	19	2652	37	56	2904	16	27	91	86
MS 4 - 3		9.0.E+05	b.d.	b.d	337	0.15	1.70	0.03	0.2424	0.00267	19.67	0.36	0.5875	0.0120	0.86	3134	17	19	2977	50	67	3073	18	27	97	95
MS 4 - 4		7.6.E+05	b.d.	b.d	338	0.18	2.14	0.04	0.2392	0.00263	15.32	0.29	0.4663	0.0092	0.89	3112	18	19	2464	40	58	2831	18	29	87	79
MS 4 - 5		5.3.E+05	b.d.	b.d	163	0.72	1.43	0.02	0.2947	0.00324	28.43	0.42	0.7009	0.0120	0.84	3440	17	8	3421	45	69	3432	14	25	100	99
MS 4 - 6		7.0.E+05	b.d.	b.d	347	0.47	2.24	0.05	0.2478	0.00273	15.28	0.30	0.4464	0.0093	0.78	3168	17	19	2378	42	56	2831	19	27	84	75
MS 4 - 7		8.5.E+05	b.d.	b.d	542	0.53	3.17	0.07	0.2268	0.00330	9.86	0.26	0.3158	0.0068	0.81	3024	23	25	1768	33	45	2416	24	35	73	58
MS 4 - 8		5.5.E+05	b.d.	b.d	207	0.30	1.72	0.04	0.2518	0.00277	20.22	0.37	0.5813	0.0120	0.82	3194	17	19	2952	50	67	3100	18	27	95	92
MS 4 - 9		5.4.E+05	b.d.	b.d	194	0.47	1.66	0.03	0.2767	0.00304	22.93	0.33	0.6012	0.0097	0.82	3343	17	19	3032	39	61	3221	14	26	94	91
MS 4 - 10		7.8.E+05	b.d.	b.d	228	0.77	1.42	0.03	0.3047	0.00335	29.46	0.46	0.7035	0.0130	0.86	3492	17	19	3431	47	71	3467	15	26	99	98

Uncertainties quoted without components related to systematic error unless otherwise stated. Total systematic uncertainties (s sys): ^{206}Pb/^{238}U = 1.8 %; ^{207}Pb/^{206}Pb = 0.5 % (2s).

[a] Data not corrected for common Pb

[b] Concordance calculated as: (^{206}Pb-^{238}U date/^{207}Pb-^{235U} date)*100 and (^{206}Pb-^{238}U date/^{207}Pb-^{206}Pb date)*100

Table 4.7, continued.

17th-19th July 2017, Central Analytical Facilities University of Stellenbosch							Data for Tera-Wasserburg plot [a]				Data for Wetherill plot [a]					Dates (Ma)									Concordance [b]	
Identifier	Comment	^{206}Pb (CPS)	^{204}Pb (CPS)	^{206}Pb/^{204}Pb	U (mg g-1)	Th/U	^{238}U/^{206}Pb	2 s	^{207}Pb/^{206}Pb	2 s	^{207}Pb/^{235}U	2 s	^{206}Pb/^{238}U	2 s	rho	^{207}Pb/^{206}Pb	2 s	2s $_{sys}$	^{206}Pb/^{238}U	2 s	2s $_{sys}$	^{207}Pb/^{235}U	2 s	2s $_{sys}$	6/38 - 7/35	6/38 - 7/6
MS 4 - 12		9.9.E+05	b.d.	b.d	854	0.15	3.96	0.08	0.1705	0.00260	5.97	0.18	0.2523	0.0051	0.85	2554	26	27	1449	26	36	1962	25	40	74	57
MS 4 - 13		6.0.E+05	b.d.	b.d	179	0.52	1.37	0.03	0.3083	0.00339	31.19	0.60	0.7320	0.0150	0.88	3511	17	19	3537	56	78	3522	19	29	100	101
MS 4 - 14		1.0.E+06	b.d.	b.d	385	0.79	1.85	0.04	0.2576	0.00283	19.14	0.42	0.5400	0.0120	0.92	3230	17	19	2782	51	66	3044	22	32	91	86
MS 4 - 15		8.3.E+05	b.d.	b.d	344	0.45	1.93	0.03	0.2516	0.00277	17.96	0.28	0.5184	0.0091	0.87	3192	17	19	2690	39	58	2985	15	26	90	84
MS 4 - 16		7.9.E+05	b.d.	b.d	302	0.20	1.81	0.03	0.2343	0.00258	17.86	0.26	0.5530	0.0090	0.82	3079	18	19	2836	37	57	2980	14	25	95	92
MS 4 - 17		6.3.E+05	b.d.	b.d	275	0.07	2.08	0.04	0.2472	0.00272	16.43	0.29	0.4818	0.0086	0.89	3165	17	19	2533	37	55	2898	17	29	87	80
MS 4 - 18		6.8.E+05	b.d.	b.d	311	0.08	2.17	0.04	0.2339	0.00257	14.84	0.27	0.4605	0.0083	0.92	3077	18	19	2439	37	54	2801	17	29	87	79
MS 4 - 19		6.1.E+05	b.d.	b.d	207	0.28	1.55	0.03	0.2560	0.00282	22.85	0.43	0.6460	0.0140	0.81	3220	17	19	3209	53	75	3218	19	28	100	100
MS 4 - 20		3.0.E+05	b.d.	b.d	98	0.22	1.57	0.03	0.2506	0.00276	21.97	0.39	0.6383	0.0130	0.84	3186	17	19	3178	49	72	3179	17	28	100	100
MS 4 - 21		7.3.E+05	b.d.	b.d	209	0.77	1.40	0.03	0.3013	0.00331	29.58	0.53	0.7140	0.0140	0.84	3475	17	19	3472	52	73	3470	18	28	100	100
MS 4 - 22		6.7.E+05	b.d.	b.d	229	0.18	1.58	0.02	0.2540	0.00279	22.13	0.32	0.6327	0.0100	0.83	3208	17	19	3158	41	62	3187	14	25	99	98
MS 4 - 23		7.2.E+05	b.d.	b.d	249	0.23	1.59	0.03	0.2519	0.00277	21.74	0.36	0.6271	0.0120	0.83	3194	17	19	3135	46	68	3169	16	27	99	98
MS 4 - 24		6.5.E+05	b.d.	b.d	322	0.25	2.35	0.04	0.2397	0.00264	14.04	0.24	0.4260	0.0079	0.85	3116	18	19	2286	36	51	2749	16	27	83	73
MS 4 - 25		8.1.E+05	b.d.	b.d	278	0.62	1.65	0.03	0.2757	0.00303	22.95	0.47	0.6056	0.0120	0.88	3336	17	19	3049	49	68	3221	20	31	95	91
MS 4 - 26		6.2.E+05	b.d.	b.d	265	0.27	2.07	0.04	0.2511	0.00276	16.66	0.31	0.4831	0.0098	0.87	3189	17	19	2538	43	60	2913	18	27	87	80
MS 4 - 27		3.8.E+05	b.d.	b.d	184	0.10	2.18	0.06	0.2448	0.00269	15.53	0.44	0.4590	0.0130	0.93	3149	17	19	2431	58	72	2841	27	39	86	77
MS 4 - 28		7.7.E+05	b.d.	b.d	352	0.24	2.12	0.03	0.2438	0.00268	15.89	0.24	0.4727	0.0078	0.89	3143	17	19	2494	34	52	2868	14	25	87	79
MS 4 - 29		5.4.E+05	b.d.	b.d	200	0.13	1.63	0.04	0.2544	0.00280	21.71	0.52	0.6140	0.0150	0.87	3210	17	19	3084	59	76	3167	24	33	97	96
MS 4 - 30		1.1.E+06	b.d.	b.d	427	0.28	1.77	0.03	0.2757	0.00303	21.52	0.40	0.5664	0.0110	0.85	3336	17	19	2890	47	65	3160	18	28	91	87
MS 4 - 31		1.0.E+06	b.d.	b.d	581	0.47	2.51	0.05	0.2245	0.00247	12.39	0.25	0.3978	0.0084	0.86	3011	18	20	2157	39	53	2631	19	29	82	72
MS 4 - 32		5.3.E+05	b.d.	b.d	171	0.42	1.50	0.02	0.2754	0.00303	25.40	0.37	0.6688	0.0110	0.83	3335	17	19	3298	43	66	3321	14	26	99	99
MS 4 - 34		7.7.E+05	b.d.	b.d	272	0.36	1.67	0.03	0.2641	0.00291	21.82	0.36	0.5990	0.0100	0.84	3268	17	19	3023	42	62	3172	16	28	95	93
MS 4 - 35		8.6.E+05	b.d.	b.d	487	0.11	2.48	0.06	0.2624	0.00330	14.67	0.35	0.4026	0.0100	0.79	3259	20	21	2179	48	59	2792	23	31	78	67
MS 4 - 36		6.9.E+05	b.d.	b.d	407	0.14	2.64	0.05	0.2435	0.00268	12.75	0.25	0.3785	0.0078	0.90	3141	17	19	2067	37	51	2657	19	30	78	66
MS 4 - 37		7.0.E+05	b.d.	b.d	693	0.04	4.49	0.08	0.1724	0.00190	5.31	0.09	0.2229	0.0040	0.68	2577	18	20	1297	21	30	1868	14	23	69	50
MS 4 - 38		8.1.E+05	b.d.	b.d	370	0.17	2.19	0.04	0.2524	0.00278	15.84	0.26	0.4564	0.0078	0.82	3197	17	19	2422	35	52	2865	15	26	85	76
MS 4 - 39		7.0.E+05	b.d.	b.d	337	0.16	2.24	0.04	0.2394	0.00263	14.70	0.23	0.4458	0.0076	0.74	3113	18	19	2375	34	51	2794	15	25	85	76
MS 4 - 40		7.6.E+05	b.d.	b.d	381	0.29	2.25	0.05	0.2400	0.00264	14.72	0.30	0.4437	0.0096	0.90	3118	18	19	2364	43	59	2794	19	29	85	76
MS 4 - 41		9.1.E+05	b.d.	b.d	493	0.25	2.50	0.05	0.2303	0.00253	12.69	0.21	0.4002	0.0076	0.85	3052	18	19	2169	35	49	2655	16	25	82	71
MS 4 - 42		6.6.E+05	b.d.	b.d	199	0.54	1.41	0.02	0.2966	0.00326	29.04	0.49	0.7110	0.0120	0.83	3450	17	19	3459	47	69	3452	17	27	100	100
MS 4 - 43		8.6.E+05	b.d.	b.d	413	0.05	2.33	0.05	0.2072	0.00228	12.27	0.31	0.4298	0.0095	0.89	2880	18	20	2302	42	58	2620	23	34	88	80
MS 4 - 44		6.3.E+05	b.d.	b.d	187	0.60	1.39	0.02	0.2962	0.00326	29.40	0.44	0.7208	0.0120	0.84	3448	17	19	3496	47	69	3465	15	25	101	101
MS 4 - 45		8.9.E+05	b.d.	b.d	279	0.69	1.45	0.03	0.2941	0.00324	27.92	0.40	0.6884	0.0120	0.84	3438	17	19	3374	44	68	3414	14	25	99	98
MS 4 - 46		7.9.E+05	b.d.	b.d	249	0.51	1.48	0.02	0.2884	0.00317	26.91	0.37	0.6771	0.0110	0.77	3407	17	19	3331	42	65	3378	14	24	99	98
MS 4 - 47		1.3.E+06	b.d.	b.d	379	0.67	1.37	0.02	0.2955	0.00325	29.83	0.42	0.7320	0.0120	0.84	3445	17	19	3538	44	69	3479	14	25	102	103
MS 4 - 48		1.4.E+06	b.d.	b.d	493	0.98	1.57	0.03	0.2841	0.00313	25.15	0.49	0.6388	0.0130	0.85	3384	17	19	3181	50	71	3311	19	29	96	94
MS 4 - 49		6.5.E+05	b.d.	b.d	203	0.40	1.48	0.02	0.2796	0.00308	25.92	0.39	0.6740	0.0110	0.84	3359	17	19	3319	44	65	3341	15	26	99	99
MS 4 - 50		5.6.E+05	b.d.	b.d	169	0.64	1.41	0.02	0.2941	0.00324	28.80	0.41	0.7098	0.0110	0.79	3437	17	19	3455	43	66	3445	14	25	100	101
MS 4 - 51		5.5.E+05	b.d.	b.d	178	0.12	1.49	0.02	0.2558	0.00281	23.69	0.32	0.6717	0.0110	0.79	3219	17	19	3310	42	65	3254	13	24	102	103
MS 4 - 52		8.4.E+05	b.d.	b.d	502	0.07	2.74	0.05	0.2082	0.00229	10.51	0.20	0.3653	0.0068	0.82	2888	18	20	2006	32	46	2477	18	28	81	69
MS 4 - 54		4.5.E+05	b.d.	b.d	133	0.65	1.38	0.02	0.2939	0.00323	29.48	0.44	0.7271	0.0120	0.83	3436	17	19	3519	46	70	3467	15	26	101	102
MS 4 - 55		4.4.E+05	b.d.	b.d	204	0.26	2.17	0.05	0.2466	0.00271	15.62	0.34	0.4602	0.0110	0.86	3163	17	19	2438	47	63	2850	21	31	86	77
MS 4 - 56		6.3.E+05	b.d.	b.d	325	0.18	2.42	0.04	0.2261	0.00249	12.88	0.20	0.4136	0.0070	0.85	3022	18	20	2230	32	48	2668	15	26	84	74
MS 4 - 57		7.1.E+05	b.d.	b.d	328	0.12	2.09	0.04	0.2412	0.00265	15.95	0.28	0.4789	0.0092	0.87	3126	17	19	2521	40	56	2872	17	26	88	81
MS 4 - 58		2.0.E+05	b.d.	b.d	59	0.52	1.37	0.02	0.3119	0.00343	31.44	0.47	0.7308	0.0120	0.78	3528	17	19	3534	45	69	3530	15	26	100	100
MS 4 - 59		3.8.E+05	b.d.	b.d	122	0.26	1.54	0.04	0.2580	0.00284	23.13	0.56	0.6510	0.0170	0.91	3232	17	19	3227	65	85	3228	24	34	100	100
MS 4 - 60		6.8.E+05	b.d.	b.d	210	0.60	1.41	0.02	0.2926	0.00322	28.73	0.41	0.7110	0.0120	0.84	3430	17	19	3459	44	69	3442	14	25	100	101
MS 4 - 61		5.8.E+05	b.d.	b.d	206	0.44	1.66	0.03	0.2590	0.00285	21.44	0.39	0.6020	0.0120	0.85	3239	17	19	3035	50	68	3156	18	28	96	94
MS 4 - 62		7.5.E+05	b.d.	b.d	306	0.34	1.83	0.04	0.2520	0.00277	19.02	0.35	0.5466	0.0110	0.83	3195	17	19	2809	48	63	3040	18	28	92	88

Uncertainties quoted without components related to systematic error unless otherwise stated. Total systematic uncertainties (s sys): ^{206}Pb/^{238}U = 1.8 %; ^{207}Pb/^{206}Pb = 0.5 % (2s).

[a] Data not corrected for common Pb

[b] Concordance calculated as: (^{206}Pb-^{238}U date/^{207}Pb-^{235U} date)*100 and (^{206}Pb-^{238}U date/^{207}Pb-^{206}Pb date)*100

Table 4.7, continued.

17th-19th July 2017, Central Analytical Facilities University of Stellenbosch							Data for Tera-Wasserburg plot [a]				Data for Wetherill plot [a]					Dates (Ma)								Concordance [b]	
Identifier	Comment	^{206}Pb (CPS)	^{204}Pb (CPS)	^{206}Pb/^{204}Pb	U (mg g-1)	Th/U	^{238}U/^{206}Pb	2 s	^{207}Pb/^{206}Pb	2 s	^{207}Pb/^{235}U	2 s	^{206}Pb/^{238}U	2 s	rho	^{207}Pb/^{206}Pb	2 s	2s $_{sys}$	^{206}Pb/^{238}U	2 s	2s $_{sys}$	^{207}Pb/^{235}U	2 s	2s $_{sys}$	6/38 - 7/35	6/38 - 7/6
MS 4 - 63		7.2.E+05	b.d.	b.d	242	0.53	1.59	0.03	0.2798	0.00308	24.36	0.44	0.6308	0.0120	0.80	3359	17	19	3150	47	68	3282	17	26	96	94
MS 4 - 64		1.0.E+06	b.d.	b.d	367	0.55	1.57	0.03	0.2787	0.00307	24.55	0.56	0.6370	0.0130	0.87	3353	17	19	3174	53	71	3290	22	29	96	95
MS 4 - 66		6.5.E+05	b.d.	b.d	201	0.51	1.41	0.02	0.2902	0.00319	28.52	0.41	0.7111	0.0120	0.84	3417	17	19	3459	45	69	3435	14	25	101	101
MS 4 - 68		4.7.E+05	b.d.	b.d	142	0.62	1.36	0.02	0.3091	0.00340	31.34	0.46	0.7338	0.0120	0.83	3514	17	19	3545	45	69	3527	14	26	101	101
MS 4 - 69		3.0.E+06	b.d.	b.d	1033	0.09	1.59	0.03	0.2257	0.00248	19.62	0.29	0.6292	0.0110	0.84	3020	18	20	3144	42	65	3070	14	26	102	104
MS 4 - 70		1.0.E+06	b.d.	b.d	462	0.80	2.12	0.04	0.2712	0.00298	17.62	0.33	0.4719	0.0090	0.86	3311	17	19	2490	39	56	2966	18	28	84	75
MS 4 - 71		7.0.E+05	b.d.	b.d	249	0.18	1.66	0.03	0.2495	0.00274	20.75	0.30	0.6029	0.0099	0.78	3179	17	19	3039	40	61	3125	14	25	97	96
MS 4 - 72		4.1.E+05	b.d.	b.d	144	0.08	1.65	0.03	0.2567	0.00282	21.44	0.32	0.6065	0.0100	0.81	3224	17	19	3054	40	61	3157	15	25	97	95
MS 4 - 73		4.8.E+05	b.d.	b.d	163	0.18	1.55	0.03	0.2575	0.00283	22.89	0.34	0.6442	0.0110	0.82	3229	17	19	3203	42	65	3220	14	25	99	99
MS 4 - 74		7.3.E+05	b.d.	b.d	234	0.49	1.48	0.02	0.2927	0.00322	27.24	0.41	0.6745	0.0110	0.87	3431	17	19	3320	44	66	3390	15	25	98	97
MS 4 - 76		4.1.E+05	b.d.	b.d	166	0.11	1.84	0.03	0.2489	0.00274	18.73	0.29	0.5445	0.0094	0.78	3177	17	19	2800	39	59	3026	15	25	93	88
MS 4 - 77		9.1.E+05	b.d.	b.d	269	0.52	1.40	0.03	0.3033	0.00334	29.72	0.50	0.7120	0.0140	0.87	3485	17	19	3462	52	75	3475	17	27	100	99
MS 4 - 78		4.5.E+05	b.d.	b.d	190	0.16	2.03	0.04	0.2425	0.00267	16.42	0.28	0.4915	0.0093	0.82	3134	17	19	2575	40	58	2899	17	27	89	82
MS 4 - 79		2.1.E+06	b.d.	b.d	712	0.59	1.58	0.03	0.2477	0.00272	21.66	0.35	0.6347	0.0110	0.87	3168	17	19	3165	44	66	3166	16	26	100	100
MS 4 - 80		5.2.E+05	b.d.	b.d	172	0.09	1.54	0.03	0.2547	0.00280	22.80	0.37	0.6488	0.0120	0.88	3213	17	19	3221	46	68	3215	16	27	100	100
MS 4 - 81		8.6.E+05	b.d.	b.d	271	0.40	1.48	0.03	0.2903	0.00319	27.04	0.41	0.6758	0.0120	0.83	3417	17	19	3326	45	68	3383	15	25	98	97
MS 14: Stolzburg Main Trondhjemite																									
MS 14 - 1		1.1.E+06	b.d.	b.d	309	0.65	1.58	0.02	0.2802	0.00308	24.49	0.38	0.6337	0.0079	0.80	3362	17	19	3162	31	57	3286	15	26	96	94
MS 14 - 2		7.3.E+05	b.d.	b.d	242	0.34	1.88	0.02	0.2672	0.00294	19.54	0.30	0.5308	0.0066	0.81	3287	17	19	2743	28	51	3067	15	25	89	83
MS 14 - 3		7.7.E+05	b.d.	b.d	257	0.41	1.85	0.02	0.2784	0.00306	20.77	0.31	0.5411	0.0065	0.80	3352	17	19	2786	27	51	3126	15	25	89	83
MS 14 - 5		1.1.E+06	b.d.	b.d	370	0.45	1.75	0.03	0.2696	0.00300	21.26	0.55	0.5700	0.0110	0.75	3301	17	19	2905	46	64	3146	25	35	92	88
MS 14 - 6		9.0.E+05	b.d.	b.d	634	0.33	3.77	0.08	0.2404	0.00264	8.84	0.20	0.2654	0.0053	0.88	3121	18	19	1520	28	34	2318	21	30	66	49
MS 14 - 7		5.4.E+05	b.d.	b.d	138	0.47	1.42	0.02	0.2947	0.00324	28.61	0.44	0.7050	0.0088	0.81	3441	17	19	3437	33	61	3439	15	25	100	100
MS 14 - 8		5.3.E+05	b.d.	b.d	345	0.24	3.71	0.05	0.2277	0.00250	8.45	0.15	0.2693	0.0039	0.82	3033	18	19	1537	20	32	2278	16	26	67	51
MS 14 - 9		8.9.E+05	b.d.	b.d	369	0.46	2.34	0.04	0.2557	0.00281	15.10	0.27	0.4281	0.0066	0.86	3218	17	19	2296	30	47	2819	17	27	81	71
MS 14 - 10		6.5.E+05	b.d.	b.d	184	0.42	1.56	0.02	0.2898	0.00319	25.74	0.44	0.6426	0.0086	0.78	3414	17	19	3196	34	60	3335	17	26	96	94
MS 14 - 11		1.3.E+06	b.d.	b.d	362	0.63	1.51	0.02	0.2849	0.00313	26.07	0.40	0.6633	0.0081	0.80	3388	17	19	3277	31	59	3347	15	26	98	97
MS 14 - 12		1.0.E+06	b.d.	b.d	421	0.13	2.28	0.04	0.2286	0.00251	13.81	0.27	0.4377	0.0069	0.81	3039	18	19	2338	31	49	2733	19	29	86	77
MS 14 - 14		1.2.E+06	b.d.	b.d	826	0.41	3.80	0.07	0.2270	0.00250	8.25	0.17	0.2632	0.0046	0.85	3029	18	19	1505	23	35	2256	18	28	67	50
MS 14 - 16		1.1.E+06	b.d.	b.d	295	0.37	1.55	0.02	0.2780	0.00306	24.74	0.45	0.6443	0.0100	0.85	3349	17	19	3204	40	62	3296	18	27	97	96
MS 14 - 17		8.9.E+05	b.d.	b.d	313	0.23	1.83	0.04	0.2722	0.00300	20.53	0.45	0.5460	0.0110	0.92	3316	17	19	2806	44	64	3114	21	30	90	85
MS 14 - 18		6.3.E+05	b.d.	b.d	277	0.43	2.35	0.04	0.2619	0.00288	15.32	0.27	0.4249	0.0066	0.88	3255	17	19	2281	30	47	2833	17	27	81	70
MS 14 - 22		1.1.E+06	b.d.	b.d	428	0.31	2.12	0.04	0.2532	0.00279	16.48	0.31	0.4712	0.0078	0.88	3203	17	19	2487	34	52	2903	18	27	86	78
MS 14 - 24		8.5.E+05	b.d.	b.d	432	0.18	2.60	0.04	0.2489	0.00274	13.21	0.26	0.3841	0.0066	0.87	3176	17	19	2094	31	46	2693	19	27	78	66
MS 14 - 25		1.0.E+06	b.d.	b.d	304	0.35	1.47	0.04	0.2888	0.00340	27.17	0.74	0.6810	0.0170	0.92	3409	18	20	3343	66	85	3386	27	36	99	98
MS 14 - 26		6.6.E+05	b.d.	b.d	242	0.11	2.11	0.03	0.2359	0.00259	15.40	0.27	0.4737	0.0069	0.83	3090	18	19	2498	30	50	2838	17	27	88	81
MS 14 - 27		6.0.E+05	b.d.	b.d	199	0.04	1.79	0.02	0.2523	0.00278	19.41	0.34	0.5582	0.0072	0.74	3196	17	19	2857	30	53	3060	17	27	93	89
MS 14 - 28		7.5.E+05	b.d.	b.d	487	0.11	3.39	0.06	0.2221	0.00244	9.07	0.22	0.2951	0.0055	0.77	2993	18	20	1666	27	39	2340	23	33	71	56
MS 14 - 29		1.4.E+06	b.d.	b.d	608	0.31	2.39	0.04	0.2448	0.00269	14.11	0.25	0.4176	0.0066	0.89	3149	17	19	2248	30	47	2755	17	26	82	71
MS 14 - 30		8.4.E+05	b.d.	b.d	382	0.18	2.39	0.05	0.2594	0.00285	14.99	0.36	0.4180	0.0082	0.82	3240	17	19	2249	37	53	2810	23	33	80	69
MS 14 - 31		1.3.E+06	b.d.	b.d	542	0.61	2.20	0.05	0.2518	0.00360	15.81	0.40	0.4544	0.0098	0.85	3193	23	24	2413	43	58	2863	24	32	84	76
MS 14 - 32		1.3.E+06	b.d.	b.d	397	0.44	1.53	0.03	0.2799	0.00308	25.29	0.52	0.6540	0.0120	0.89	3361	17	19	3240	47	69	3317	20	29	98	96
MS 14 - 34		1.5.E+06	b.d.	b.d	546	0.53	1.89	0.04	0.2552	0.00300	18.66	0.43	0.5290	0.0110	0.90	3215	19	20	2735	48	63	3022	22	31	91	85
MS 14 - 37		7.3.E+05	b.d.	b.d	225	0.35	1.61	0.03	0.2884	0.00317	24.77	0.47	0.6222	0.0099	0.84	3407	17	19	3116	39	62	3297	19	28	95	91
MS 14 - 38		9.0.E+05	b.d.	b.d	406	0.42	2.39	0.04	0.2544	0.00280	14.70	0.25	0.4187	0.0062	0.87	3210	17	19	2253	28	46	2794	16	26	81	70
MS 14 - 40		9.0.E+05	b.d.	b.d	261	0.39	1.48	0.03	0.2931	0.00322	27.43	0.62	0.6770	0.0140	0.91	3432	17	19	3331	55	73	3396	22	31	98	97
MS 14 - 42		8.1.E+05	b.d.	b.d	417	0.50	2.82	0.04	0.2334	0.00257	11.41	0.22	0.3542	0.0047	0.69	3072	18	19	1954	22	38	2554	18	28	77	64
MS 14 - 44		1.1.E+06	b.d.	b.d	447	0.43	2.10	0.03	0.2592	0.00285	17.07	0.29	0.4768	0.0068	0.84	3240	17	19	2511	30	50	2936	16	27	86	78

Uncertainties quoted without components related to systematic error unless otherwise stated. Total systematic uncertainties (s sys): ^{206}Pb/^{238}U = 1.8 %; ^{207}Pb/^{206}Pb = 0.5 % (2s).

[a] Data not corrected for common Pb

[b] Concordance calculated as: (^{206}Pb-^{238}U date/^{207}Pb-^{235U} date)*100 and (^{206}Pb-^{238}U date/^{207}Pb-^{206}Pb date)*100

Table 4.7, continued.

17th-19th July 2017, Central Analytical Facilities University of Stellenbosch							Data for Tera-Wasserburg plot [a]				Data for Wetherill plot [a]					Dates (Ma)								Concordance [b]	
Identifier	Comment	^{206}Pb (CPS)	^{204}Pb (CPS)	^{206}Pb/^{204}Pb	U (mg g-1)	Th/U	^{238}U/^{206}Pb	2 s	^{207}Pb/^{206}Pb	2 s	^{207}Pb/^{235}U	2 s	^{206}Pb/^{238}U	2 s	rho	^{207}Pb/^{206}Pb	2 s	2s $_{sys}$	^{206}Pb/^{238}U	2 s	2s $_{sys}$	^{207}Pb/^{235}U	2 s	2s $_{sys}$	6/38 - 7/35	6/38 - 7/6
MS 14 - 45		1.6.E+06	b.d.	b.d	551	0.92	1.87	0.03	0.2620	0.00288	19.36	0.32	0.5353	0.0073	0.83	3257	17	19	2762	31	52	3058	16	26	90	85
MS 14 - 46		1.2.E+06	b.d.	b.d	359	0.51	1.56	0.02	0.2800	0.00308	24.73	0.44	0.6400	0.0092	0.81	3361	17	19	3186	36	61	3295	17	28	97	95
MS 14 - 49		1.1.E+06	b.d.	b.d	500	0.61	2.47	0.04	0.2446	0.00269	13.65	0.24	0.4044	0.0061	0.86	3148	17	19	2187	28	46	2722	17	28	80	69
MS 14 - 50		1.2.E+06	b.d.	b.d	382	0.27	1.73	0.03	0.2650	0.00292	21.23	0.36	0.5796	0.0088	0.90	3277	17	19	2945	36	58	3147	17	26	94	90
MS 14 - 51		1.2.E+06	b.d.	b.d	369	0.44	1.54	0.02	0.2771	0.00305	24.86	0.49	0.6495	0.0100	0.78	3345	17	19	3223	40	63	3299	19	30	98	96
MS 14 - 52		1.2.E+06	b.d.	b.d	432	0.48	1.86	0.02	0.2616	0.00288	19.41	0.31	0.5379	0.0071	0.83	3254	17	19	2772	29	53	3060	15	26	91	85
MS 14 - 53		1.4.E+06	b.d.	b.d	416	0.32	1.57	0.03	0.2523	0.00278	22.20	0.45	0.6370	0.0110	0.85	3197	17	19	3175	43	65	3189	20	30	100	99
MS 14 - 54		8.4.E+05	b.d.	b.d	248	0.35	1.56	0.02	0.2912	0.00320	25.75	0.46	0.6406	0.0100	0.87	3422	17	19	3189	40	62	3335	18	27	96	93
MS 14 - 56		1.3.E+06	b.d.	b.d	526	0.48	2.12	0.03	0.2419	0.00266	15.74	0.28	0.4712	0.0071	0.85	3130	17	19	2487	31	50	2858	17	28	87	79
MS 14 - 57		9.9.E+05	b.d.	b.d	269	0.41	1.55	0.02	0.2725	0.00300	24.30	0.43	0.6472	0.0099	0.86	3318	17	19	3214	39	63	3278	17	27	98	97
MS 14 - 58		1.0.E+06	b.d.	b.d	300	0.36	1.47	0.03	0.2880	0.00317	27.07	0.54	0.6800	0.0120	0.88	3405	17	19	3343	46	67	3384	19	28	99	98
MS 14 - 59		1.0.E+06	b.d.	b.d	318	0.45	1.65	0.02	0.2758	0.00303	23.14	0.39	0.6079	0.0082	0.80	3337	17	19	3059	33	57	3230	17	27	95	92
MS 14 - 60		6.8.E+05	b.d.	b.d	178	0.31	1.48	0.02	0.2858	0.00314	26.66	0.57	0.6760	0.0110	0.76	3393	17	19	3325	44	67	3367	22	32	99	98
MS 14 - 61		6.3.E+05	b.d.	b.d	199	0.36	1.77	0.04	0.2745	0.00340	21.38	0.57	0.5650	0.0130	0.86	3330	19	21	2884	53	71	3152	26	35	91	87
MS 14 - 64		8.5.E+05	b.d.	b.d	510	0.74	3.42	0.08	0.2232	0.00246	9.00	0.21	0.2920	0.0065	0.95	3005	18	20	1650	32	43	2334	22	31	71	55
MS 14 - 65		1.1.E+06	b.d.	b.d	395	0.33	1.90	0.03	0.2754	0.00303	20.05	0.38	0.5269	0.0086	0.86	3335	17	19	2726	36	56	3091	18	28	88	82
MS 14 - 66		1.4.E+06	b.d.	b.d	484	1.69	1.86	0.03	0.2837	0.00312	21.10	0.43	0.5388	0.0100	0.91	3381	17	19	2775	42	62	3140	20	30	88	82
MS 14 - 67		8.8.E+05	b.d.	b.d	344	0.29	2.17	0.04	0.2544	0.00280	16.18	0.35	0.4611	0.0093	0.93	3210	17	19	2442	41	57	2884	21	31	85	76
MS 14 - 70		8.2.E+05	b.d.	b.d	437	0.67	2.92	0.05	0.2003	0.00320	9.45	0.21	0.3421	0.0053	0.70	2823	26	27	1896	26	40	2382	20	27	80	67
MS 14 - 72		1.0.E+06	b.d.	b.d	296	0.49	1.57	0.02	0.2812	0.00309	24.65	0.42	0.6352	0.0084	0.78	3367	17	19	3168	33	58	3292	16	27	96	94
MS 14 - 75		9.4.E+05	b.d.	b.d	316	0.54	1.83	0.03	0.2709	0.00298	20.39	0.42	0.5453	0.0092	0.82	3309	17	19	2801	39	61	3104	21	33	90	85
MS 14 - 76		1.1.E+06	b.d.	b.d	635	0.54	2.97	0.04	0.2235	0.00246	10.38	0.20	0.3362	0.0050	0.77	3003	18	20	1867	24	39	2467	18	27	76	62
MS 14 - 77		9.2.E+05	b.d.	b.d	270	0.33	1.52	0.03	0.2876	0.00316	26.21	0.52	0.6600	0.0120	0.92	3402	17	19	3263	46	70	3352	20	29	97	96
MS 14 - 82		9.0.E+05	b.d.	b.d	389	0.27	2.24	0.03	0.2402	0.00264	14.80	0.24	0.4466	0.0059	0.81	3119	18	19	2378	26	47	2800	15	26	85	76
MS 14 - 83		1.6.E+06	b.d.	b.d	568	0.55	1.80	0.03	0.2547	0.00280	19.52	0.34	0.5545	0.0084	0.87	3214	17	19	2842	35	56	3066	17	26	93	88
MS 14 - 85		2.8.E+05	b.d.	b.d	100	0.13	1.99	0.03	0.2744	0.00360	19.07	0.38	0.5028	0.0079	0.79	3327	21	22	2624	34	53	3043	20	28	86	79
MS 14 - 88		1.2.E+06	b.d.	b.d	957	0.28	4.19	0.07	0.2189	0.00241	7.20	0.14	0.2385	0.0041	0.88	2970	18	20	1378	21	32	2135	18	25	65	46
MS 14 - 92		7.8.E+05	b.d.	b.d	314	0.50	2.22	0.03	0.2478	0.00273	15.40	0.26	0.4509	0.0064	0.84	3168	17	19	2398	28	47	2838	16	26	84	76
MS 14 - 93		7.1.E+05	b.d.	b.d	200	0.29	1.53	0.02	0.2854	0.00314	25.66	0.42	0.6522	0.0090	0.84	3390	17	19	3234	35	60	3331	16	27	97	95
MS 14 - 94		1.4.E+06	b.d.	b.d	528	0.46	1.98	0.03	0.2528	0.00278	17.63	0.33	0.5060	0.0083	0.88	3200	17	19	2638	35	54	2969	18	26	89	82
MS 14 - 95		1.5.E+06	b.d.	b.d	436	0.43	1.50	0.02	0.2690	0.00296	24.82	0.41	0.6682	0.0094	0.85	3298	17	19	3297	36	61	3299	16	26	100	100
MS 14 - 96		1.1.E+06	b.d.	b.d	289	0.43	1.44	0.02	0.2883	0.00317	27.53	0.44	0.6924	0.0094	0.85	3406	17	19	3389	36	62	3400	16	26	100	100
MS 14 - 97		1.0.E+06	b.d.	b.d	276	0.54	1.41	0.02	0.2915	0.00321	28.51	0.44	0.7077	0.0088	0.81	3424	17	19	3447	33	61	3435	15	26	100	101
MS 14 - 98		9.5.E+05	b.d.	b.d	326	0.30	1.77	0.03	0.2714	0.00299	21.19	0.41	0.5654	0.0085	0.78	3311	17	19	2886	35	57	3143	19	30	92	87
MS 14 - 99		1.3.E+06	b.d.	b.d	387	0.62	1.57	0.02	0.2726	0.00300	23.95	0.41	0.6364	0.0086	0.79	3319	17	19	3172	34	59	3263	17	28	97	96
MS 14 - 100		8.0.E+05	b.d.	b.d	238	0.87	1.57	0.02	0.2949	0.00324	25.94	0.42	0.6378	0.0082	0.79	3441	17	19	3178	32	58	3342	16	26	95	92
MS 14 - 101		4.9.E+05	b.d.	b.d	130	0.28	1.39	0.02	0.2958	0.00325	29.29	0.44	0.7177	0.0088	0.82	3446	17	19	3485	33	61	3461	15	26	101	101
MS 14 - 102		1.1.E+06	b.d.	b.d	279	0.46	1.41	0.02	0.2935	0.00323	28.66	0.43	0.7077	0.0085	0.80	3434	17	19	3447	32	60	3441	15	24	100	100
MS 14 - 104		9.4.E+05	b.d.	b.d	248	0.55	1.41	0.02	0.2933	0.00323	28.72	0.45	0.7096	0.0090	0.81	3433	17	19	3454	34	62	3442	15	26	100	101
MS 14 - 105		1.0.E+06	b.d.	b.d	391	0.41	2.06	0.04	0.2569	0.00283	17.28	0.37	0.4866	0.0083	0.80	3225	17	19	2553	36	55	2945	21	32	87	79
MS 14 - 106		1.1.E+06	b.d.	b.d	416	0.40	1.94	0.03	0.2541	0.00280	18.09	0.32	0.5164	0.0081	0.89	3207	17	19	2681	35	55	2991	17	28	90	84
MS 14 - 107		6.8.E+05	b.d.	b.d	217	0.40	1.78	0.03	0.2688	0.00296	20.85	0.40	0.5614	0.0092	0.85	3297	17	19	2870	38	59	3129	19	28	92	87
MS 14 - 109		9.0.E+05	b.d.	b.d	291	0.21	1.65	0.03	0.2818	0.00310	23.55	0.43	0.6051	0.0095	0.86	3371	17	19	3048	38	60	3247	18	28	94	90
MS 14 - 110		7.8.E+05	b.d.	b.d	269	0.17	1.91	0.03	0.2772	0.00305	19.96	0.40	0.5223	0.0089	0.85	3345	17	19	2707	38	57	3086	19	30	88	81
MS 14 - 111		1.2.E+06	b.d.	b.d	617	0.33	2.66	0.06	0.2224	0.00250	11.55	0.28	0.3758	0.0082	0.90	2996	18	20	2055	39	51	2566	22	31	80	69
MS 14 - 112		1.5.E+06	b.d.	b.d	658	0.75	2.19	0.04	0.2473	0.00272	15.62	0.30	0.4570	0.0080	0.91	3165	17	19	2425	35	52	2851	19	28	85	77
MS 14 - 113		1.1.E+06	b.d.	b.d	446	0.38	1.98	0.04	0.2547	0.00280	17.80	0.44	0.5050	0.0110	0.88	3212	17	19	2634	46	62	2975	24	33	89	82
MS 14 - 114		7.0.E+05	b.d.	b.d	203	0.43	1.59	0.03	0.2784	0.00306	24.21	0.52	0.6300	0.0110	0.81	3352	17	19	3146	43	66	3272	21	32	96	94
MS 14 - 116		8.1.E+05	b.d.	b.d	263	0.42	1.68	0.03	0.2796	0.00308	23.06	0.43	0.5969	0.0093	0.84	3359	17	19	3015	37	60	3226	18	29	93	90

Uncertainties quoted without components related to systematic error unless otherwise stated. Total systematic uncertainties (s sys): ^{206}Pb/^{238}U = 1.8 %; ^{207}Pb/^{206}Pb = 0.5 % (2s).

[a] Data not corrected for common Pb

[b] Concordance calculated as: (^{206}Pb-^{238}U date/^{207}Pb-^{235U} date)*100 and (^{206}Pb-^{238}U date/^{207}Pb-^{206}Pb date)*100

Table 4.7, continued.

17th-19th July 2017, Central Analytical Facilities University of Stellenbosch							Data for Tera-Wasserburg plot [a]				Data for Wetherill plot [a]					Dates (Ma)									Concordance [b]	
Identifier	Comment	^{206}Pb (CPS)	^{204}Pb (CPS)	^{206}Pb/^{204}Pb	U (mg g-1)	Th/U	^{238}U/^{206}Pb	2 s	^{207}Pb/^{206}Pb	2 s	^{207}Pb/^{235}U	2 s	^{206}Pb/^{238}U	2 s	rho	^{207}Pb/^{206}Pb	2 s	2s $_{sys}$	^{206}Pb/^{238}U	2 s	2s $_{sys}$	^{207}Pb/^{235}U	2 s	2s $_{sys}$	6/38 - 7/35	6/38 - 7/6
MS 14 - 117		7.6.E+05	b.d.	b.d	230	0.28	1.61	0.03	0.2817	0.00310	24.13	0.47	0.6211	0.0100	0.83	3370	17	19	3111	40	63	3271	19	29	95	92
MS 14 - 119		5.2.E+05	b.d.	b.d	342	0.41	3.47	0.05	0.2289	0.00252	9.11	0.16	0.2885	0.0041	0.81	3043	18	19	1633	20	34	2347	16	25	70	54
MS 14 - 120		9.3.E+05	b.d.	b.d	280	0.55	1.58	0.02	0.2833	0.00312	24.79	0.38	0.6347	0.0078	0.80	3379	17	19	3166	31	57	3298	15	25	96	94
MS 14 - 121		6.1.E+05	b.d.	b.d	166	0.39	1.49	0.02	0.2797	0.00308	25.86	0.55	0.6700	0.0110	0.77	3358	17	19	3304	43	65	3337	21	32	99	98
MS 14 - 122		1.1.E+06	b.d.	b.d	348	0.44	1.69	0.02	0.2690	0.00296	22.01	0.39	0.5916	0.0084	0.80	3297	17	19	2993	34	58	3181	17	28	94	91
MS 14 - 123		7.5.E+05	b.d.	b.d	227	0.58	1.57	0.03	0.2956	0.00325	25.89	0.51	0.6350	0.0110	0.88	3445	17	19	3163	44	69	3338	19	31	95	92
MS 14 - 124		4.1.E+05	b.d.	b.d	111	0.35	1.39	0.02	0.2972	0.00327	29.48	0.52	0.7182	0.0110	0.87	3453	17	19	3487	40	66	3467	17	28	101	101
MS 14 - 125		1.0.E+06	b.d.	b.d	278	0.53	1.41	0.02	0.2902	0.00319	28.39	0.44	0.7085	0.0089	0.81	3418	17	19	3450	34	61	3431	15	25	101	101
MS 14 - 126		6.9.E+05	b.d.	b.d	205	0.61	1.55	0.02	0.2852	0.00314	25.46	0.43	0.6460	0.0092	0.84	3391	17	19	3210	36	61	3324	16	26	97	95
MS 14 - 127		6.2.E+05	b.d.	b.d	235	0.38	2.11	0.04	0.2800	0.00308	18.26	0.38	0.4734	0.0091	0.92	3361	17	19	2495	39	58	3000	20	30	83	74
MS 14 - 128		1.1.E+06	b.d.	b.d	354	0.47	1.71	0.03	0.2719	0.00299	21.95	0.39	0.5841	0.0098	0.94	3315	17	19	2962	40	62	3179	17	27	93	89
MS 14 - 129		9.8.E+05	b.d.	b.d	317	0.38	1.75	0.03	0.2592	0.00285	20.36	0.35	0.5699	0.0087	0.89	3240	17	19	2905	35	58	3106	17	27	94	90
MS 14 - 130		6.9.E+05	b.d.	b.d	276	0.52	2.21	0.04	0.2624	0.00290	16.36	0.39	0.4523	0.0090	0.83	3258	17	19	2403	40	56	2893	23	34	83	74
MS 14 - 131		9.7.E+05	b.d.	b.d	308	0.33	1.66	0.02	0.2831	0.00311	23.50	0.38	0.6015	0.0083	0.85	3379	17	19	3033	34	58	3245	16	27	93	90
MS 14 - 132		9.8.E+05	b.d.	b.d	272	0.36	1.44	0.02	0.2876	0.00316	27.49	0.42	0.6923	0.0085	0.80	3403	17	19	3389	32	60	3399	15	26	100	100
MS 14 - 133		6.4.E+05	b.d.	b.d	171	0.36	1.43	0.02	0.2933	0.00323	28.33	0.44	0.7004	0.0088	0.81	3433	17	19	3420	33	60	3429	15	25	100	100
MS 14 - 134		7.3.E+05	b.d.	b.d	362	0.26	2.58	0.04	0.2478	0.00273	13.29	0.27	0.3872	0.0059	0.75	3168	17	19	2108	27	44	2695	19	31	78	67
MS 14 - 135		9.9.E+05	b.d.	b.d	442	0.14	2.31	0.04	0.2537	0.00279	15.14	0.32	0.4320	0.0076	0.83	3205	17	19	2312	34	52	2819	20	32	82	72
MS 14 - 136		1.6.E+06	b.d.	b.d	516	0.59	1.72	0.02	0.2437	0.00268	19.55	0.32	0.5820	0.0080	0.84	3142	17	19	2955	33	56	3067	16	26	96	94
MS 14 - 137		1.1.E+06	b.d.	b.d	393	0.46	1.85	0.02	0.2580	0.00284	19.30	0.31	0.5419	0.0071	0.82	3233	17	19	2789	29	53	3054	16	27	91	86
MS 14 - 138		9.4.E+05	b.d.	b.d	297	0.79	1.60	0.02	0.2890	0.00318	24.94	0.42	0.6242	0.0083	0.79	3410	17	19	3127	33	55	3302	17	28	95	92
MS 15: Stolzburg Main Trondhjemite																										
MS 15 - 1		7.3.E+05	b.d.	b.d	250	0.56	1.59	0.03	0.2878	0.00317	24.98	0.48	0.6279	0.0100	0.83	3405	17	19	3139	41	62	3305	19	28	95	92
MS 15 - 2		5.3.E+05	b.d.	b.d	162	0.51	1.42	0.02	0.2872	0.00316	27.93	0.49	0.7034	0.0100	0.81	3401	17	19	3432	38	62	3416	17	26	100	101
MS 15 - 3		6.6.E+05	b.d.	b.d	224	0.62	1.59	0.02	0.2767	0.00304	24.10	0.44	0.6299	0.0098	0.85	3343	17	19	3147	39	61	3271	18	27	96	94
MS 15 - 6		3.8.E+05	b.d.	b.d	123	0.31	1.45	0.02	0.2925	0.00322	27.85	0.48	0.6899	0.0093	0.78	3429	17	19	3380	36	61	3412	17	27	99	99
MS 15 - 7		5.1.E+05	b.d.	b.d	167	0.73	1.54	0.03	0.3010	0.00331	26.97	0.54	0.6477	0.0110	0.85	3473	17	19	3217	42	65	3380	20	29	95	93
MS 15 - 8		6.6.E+05	b.d.	b.d	202	0.41	1.42	0.02	0.2892	0.00318	28.17	0.49	0.7050	0.0098	0.80	3411	17	19	3438	37	62	3423	17	26	100	101
MS 15 - 9		4.2.E+05	b.d.	b.d	157	0.37	1.73	0.04	0.2695	0.00300	21.53	0.55	0.5770	0.0120	0.81	3301	17	19	2933	49	68	3158	25	35	93	89
MS 15 - 10		6.7.E+05	b.d.	b.d	275	0.45	1.75	0.04	0.2803	0.00308	22.05	0.51	0.5710	0.0120	0.91	3363	17	19	2910	49	67	3183	23	31	91	87
MS 15 - 11		5.9.E+05	b.d.	b.d	209	0.46	1.57	0.02	0.2861	0.00315	25.10	0.49	0.6352	0.0100	0.81	3394	17	19	3168	40	62	3310	19	28	96	93
MS 15 - 12		1.1.E+06	b.d.	b.d	354	0.67	1.46	0.02	0.2841	0.00313	26.86	0.46	0.6854	0.0095	0.81	3384	17	19	3363	36	61	3377	17	26	100	99
MS 15 - 13		4.2.E+05	b.d.	b.d	208	0.24	2.26	0.04	0.2955	0.00325	18.02	0.35	0.4421	0.0073	0.85	3445	17	19	2358	33	50	2989	19	27	79	68
MS 15 - 14		4.9.E+05	b.d.	b.d	165	0.37	1.56	0.03	0.2920	0.00321	25.80	0.53	0.6390	0.0110	0.84	3426	17	19	3183	44	65	3337	20	29	95	93
MS 15 - 15		8.0.E+05	b.d.	b.d	314	0.68	1.82	0.03	0.2951	0.00325	22.36	0.41	0.5481	0.0086	0.86	3443	17	19	2815	36	57	3198	18	27	88	82
MS 15 - 16		6.4.E+05	b.d.	b.d	222	0.38	1.43	0.03	0.2930	0.00350	28.07	0.63	0.6970	0.0140	0.89	3431	19	20	3406	53	74	3420	22	30	100	99
MS 15 - 17		5.0.E+05	b.d.	b.d	153	0.36	1.37	0.02	0.2927	0.00322	29.49	0.50	0.7298	0.0099	0.80	3430	17	19	3530	37	64	3468	17	27	102	103
MS 15 - 18		6.6.E+05	b.d.	b.d	242	0.59	1.60	0.02	0.2887	0.00318	24.97	0.47	0.6269	0.0098	0.83	3409	17	19	3135	39	61	3304	18	29	95	92
MS 15 - 19		5.2.E+05	b.d.	b.d	162	0.71	1.45	0.02	0.2942	0.00324	27.96	0.52	0.6876	0.0110	0.86	3438	17	19	3371	42	66	3416	18	27	99	98
MS 15 - 20		8.8.E+05	b.d.	b.d	289	0.51	1.45	0.02	0.2904	0.00319	27.68	0.50	0.6910	0.0100	0.80	3418	17	19	3384	39	63	3405	18	28	99	99
MS 15 - 22		9.9.E+05	b.d.	b.d	351	0.44	1.49	0.03	0.2930	0.00322	27.10	0.60	0.6720	0.0130	0.87	3432	17	19	3312	48	70	3385	22	30	98	97
MS 15 - 23		6.6.E+05	b.d.	b.d	228	0.46	1.53	0.02	0.2909	0.00320	26.28	0.45	0.6540	0.0090	0.80	3420	17	19	3242	35	59	3355	17	27	97	95
MS 15 - 26		6.0.E+05	b.d.	b.d	188	0.41	1.39	0.02	0.2931	0.00322	29.13	0.49	0.7194	0.0100	0.83	3432	17	19	3491	38	64	3456	16	26	101	102
MS 15 - 27		9.1.E+05	b.d.	b.d	288	0.63	1.41	0.02	0.2891	0.00318	28.21	0.48	0.7071	0.0100	0.83	3411	17	19	3445	38	63	3425	17	26	101	101
MS 15 - 28		7.9.E+05	b.d.	b.d	388	0.34	2.06	0.04	0.2859	0.00314	19.10	0.46	0.4849	0.0100	0.86	3393	17	19	2546	43	60	3043	23	33	84	75
MS 15 - 29		6.4.E+05	b.d.	b.d	240	0.45	1.67	0.02	0.2819	0.00310	23.24	0.40	0.5971	0.0083	0.81	3371	17	19	3016	33	57	3235	17	26	93	89
MS 15 - 30		5.7.E+05	b.d.	b.d	225	0.64	1.85	0.03	0.2704	0.00310	20.19	0.42	0.5399	0.0092	0.82	3306	18	20	2781	39	58	3098	20	29	90	84
MS 15 - 31		1.1.E+06	b.d.	b.d	352	0.88	1.43	0.02	0.2943	0.00324	28.44	0.55	0.7004	0.0110	0.81	3438	17	19	3419	43	66	3432	19	28	100	99

Uncertainties quoted without components related to systematic error unless otherwise stated. Total systematic uncertainties (s sys): ^{206}Pb/^{238}U = 1.8 %; ^{207}Pb/^{206}Pb = 0.5 % (2s).

[a] Data not corrected for common Pb

[b] Concordance calculated as: (^{206}Pb-^{238}U date/^{207}Pb-^{235U} date)*100 and (^{206}Pb-^{238}U date/^{207}Pb-^{206}Pb date)*100

Table 4.7, continued.

17th-19th July 2017, Central Analytical Facilities University of Stellenbosch							Data for Tera-Wasserburg plot [a]				Data for Wetherill plot [a]					Dates (Ma)									Concordance [b]	
Identifier	Comment	^{206}Pb (CPS)	^{204}Pb (CPS)	^{206}Pb/^{204}Pb	U (mg g-1)	Th/U	^{238}U/^{206}Pb	2 s	^{207}Pb/^{206}Pb	2 s	^{207}Pb/^{235}U	2 s	^{206}Pb/^{238}U	2 s	rho	^{207}Pb/^{206}Pb	2 s	2s $_{sys}$	^{206}Pb/^{238}U	2 s	2s $_{sys}$	^{207}Pb/^{235}U	2 s	2s $_{sys}$	6/38 - 7/35	6/38 - 7/6
MS 15 - 32		7.2.E+05	b.d.	b.d	234	1.02	1.48	0.02	0.2966	0.00326	27.79	0.51	0.6773	0.0100	0.80	3451	17	19	3331	39	63	3409	18	28	98	97
MS 15 - 33		6.1.E+05	b.d.	b.d	238	0.50	1.59	0.04	0.2936	0.00323	25.33	0.65	0.6270	0.0140	0.87	3435	17	19	3134	57	75	3317	25	35	94	91
MS 15 - 34		7.7.E+05	b.d.	b.d	246	0.53	1.45	0.02	0.2910	0.00320	27.85	0.48	0.6908	0.0096	0.81	3422	17	19	3384	37	61	3412	17	27	99	99
MS 15 - 35		4.9.E+05	b.d.	b.d	157	0.37	1.42	0.02	0.2938	0.00323	28.64	0.48	0.7066	0.0089	0.75	3436	17	19	3444	34	60	3441	17	25	100	100
MS 15 - 36		5.3.E+05	b.d.	b.d	195	0.41	1.56	0.02	0.2909	0.00320	25.62	0.50	0.6390	0.0100	0.80	3420	17	19	3183	40	62	3330	19	28	96	93
MS 15 - 37		8.0.E+05	b.d.	b.d	263	0.30	1.42	0.02	0.2892	0.00318	28.12	0.51	0.7054	0.0100	0.78	3412	17	19	3439	39	63	3422	18	27	100	101
MS 15 - 38		4.5.E+05	b.d.	b.d	141	0.36	1.38	0.02	0.2946	0.00324	29.52	0.49	0.7263	0.0096	0.80	3440	17	19	3517	36	63	3470	16	26	101	102
MS 15 - 39		5.7.E+05	b.d.	b.d	196	0.49	1.57	0.02	0.2819	0.00310	24.79	0.46	0.6360	0.0099	0.84	3372	17	19	3171	39	62	3298	18	27	96	94
MS 15 - 40		9.2.E+05	b.d.	b.d	343	0.61	1.63	0.02	0.2810	0.00309	23.73	0.41	0.6120	0.0085	0.80	3366	17	19	3076	34	58	3256	17	26	94	91
MS 15 - 42		6.4.E+05	b.d.	b.d	217	0.48	1.42	0.02	0.2909	0.00320	28.22	0.56	0.7030	0.0120	0.86	3422	17	19	3430	47	68	3424	19	29	100	100
MS 15 - 43		6.4.E+05	b.d.	b.d	245	0.48	1.68	0.03	0.2941	0.00324	24.19	0.44	0.5959	0.0090	0.83	3437	17	19	3011	37	59	3274	18	27	92	88
MS 15 - 44		4.3.E+05	b.d.	b.d	159	0.41	1.52	0.03	0.2868	0.00315	26.05	0.54	0.6600	0.0120	0.88	3398	17	19	3265	46	68	3346	20	29	98	96
MS 15 - 45		4.8.E+05	b.d.	b.d	148	0.40	1.41	0.02	0.2956	0.00325	28.99	0.56	0.7091	0.0120	0.88	3445	17	19	3452	45	69	3451	19	28	100	100
MS 15 - 46		5.8.E+05	b.d.	b.d	270	0.40	2.02	0.03	0.2905	0.00320	19.82	0.36	0.4950	0.0072	0.80	3420	17	19	2593	30	49	3080	18	28	84	76
MS 15 - 47		6.6.E+05	b.d.	b.d	235	0.36	1.45	0.03	0.2937	0.00400	27.78	0.71	0.6890	0.0160	0.91	3435	21	23	3374	61	82	3409	25	33	99	98
MS 15 - 48		6.6.E+05	b.d.	b.d	231	0.48	1.51	0.03	0.2950	0.00325	26.85	0.52	0.6605	0.0110	0.86	3442	17	19	3266	41	66	3375	19	29	97	95
MS 15 - 49		9.1.E+05	b.d.	b.d	314	0.54	1.44	0.02	0.2910	0.00320	27.74	0.54	0.6925	0.0110	0.82	3421	17	19	3390	44	65	3408	19	28	99	99
MS 15 - 51		4.7.E+05	b.d.	b.d	154	0.42	1.51	0.02	0.2928	0.00322	26.90	0.52	0.6644	0.0110	0.86	3430	17	19	3282	43	65	3378	19	28	97	96
MS 15 - 52		5.2.E+05	b.d.	b.d	192	0.42	1.62	0.03	0.2891	0.00318	24.65	0.48	0.6179	0.0096	0.80	3410	17	19	3099	38	61	3291	19	30	94	91
MS 15 - 54		8.1.E+05	b.d.	b.d	342	0.72	1.82	0.03	0.2918	0.00321	22.18	0.44	0.5508	0.0095	0.87	3426	17	19	2826	39	59	3189	19	29	89	82
MS 15 - 55		5.9.E+05	b.d.	b.d	201	0.45	1.56	0.03	0.2921	0.00321	25.95	0.50	0.6425	0.0110	0.89	3428	17	19	3196	42	65	3342	19	29	96	93
MS 15 - 56		6.5.E+05	b.d.	b.d	237	0.56	1.63	0.02	0.2811	0.00309	23.89	0.43	0.6152	0.0087	0.79	3367	17	19	3088	35	59	3261	18	28	95	92
MS 15 - 58		5.0.E+05	b.d.	b.d	170	0.36	1.43	0.02	0.2909	0.00320	28.04	0.60	0.7000	0.0120	0.80	3420	17	19	3417	47	69	3417	21	31	100	100
MS 15 - 59		5.7.E+05	b.d.	b.d	195	0.46	1.40	0.03	0.2896	0.00319	28.39	0.61	0.7130	0.0130	0.85	3413	17	19	3466	49	72	3430	21	30	101	102
MS 15 - 60		8.0.E+05	b.d.	b.d	280	0.70	1.50	0.02	0.2931	0.00322	26.98	0.48	0.6667	0.0098	0.83	3432	17	19	3290	38	63	3380	18	28	97	96
MS 15 - 61		3.6.E+05	b.d.	b.d	129	0.42	1.54	0.03	0.2952	0.00325	26.44	0.53	0.6495	0.0110	0.84	3443	17	19	3222	43	67	3360	19	29	96	94
MS 15 - 62		4.6.E+05	b.d.	b.d	198	0.61	1.83	0.03	0.2793	0.00307	20.97	0.42	0.5454	0.0089	0.81	3356	17	19	2804	37	57	3136	20	27	89	84
MS 15 - 63		6.2.E+05	b.d.	b.d	209	0.53	1.51	0.02	0.2883	0.00317	26.40	0.47	0.6620	0.0095	0.81	3406	17	19	3272	37	62	3359	17	27	97	96
MS 15 - 65		1.6.E+06	b.d.	b.d	566	0.79	1.53	0.02	0.2733	0.00301	24.71	0.42	0.6547	0.0091	0.82	3325	17	19	3244	35	60	3295	17	26	98	98
MS 15 - 66		6.8.E+05	b.d.	b.d	279	0.49	1.73	0.03	0.2924	0.00322	23.24	0.45	0.5770	0.0100	0.90	3428	17	19	2934	41	61	3235	19	28	91	86
MS 15 - 67		3.7.E+05	b.d.	b.d	125	0.32	1.54	0.02	0.2916	0.00321	26.15	0.49	0.6487	0.0100	0.82	3424	17	19	3221	40	62	3350	19	28	96	94
MS 15 - 68		5.6.E+05	b.d.	b.d	178	0.40	1.39	0.02	0.2918	0.00321	28.93	0.50	0.7181	0.0098	0.79	3425	17	19	3486	37	64	3449	17	27	101	102
MS 15 - 69		6.8.E+05	b.d.	b.d	214	0.42	1.39	0.02	0.2925	0.00322	29.10	0.51	0.7208	0.0100	0.79	3429	17	19	3496	39	64	3455	17	27	101	102
MS 15 - 70		6.4.E+05	b.d.	b.d	251	0.57	1.62	0.03	0.2927	0.00322	24.93	0.49	0.6187	0.0100	0.82	3430	17	19	3102	42	62	3303	19	29	94	90
MS 15 - 71		6.6.E+05	b.d.	b.d	216	0.46	1.42	0.02	0.2906	0.00320	28.26	0.51	0.7045	0.0100	0.79	3419	17	19	3435	38	64	3427	17	26	100	100
MS 15 - 72		8.9.E+05	b.d.	b.d	284	0.53	1.41	0.02	0.2793	0.00307	27.30	0.50	0.7075	0.0100	0.77	3357	17	19	3447	39	63	3392	18	28	102	103
MS 15 - 73		6.7.E+05	b.d.	b.d	226	0.43	1.42	0.02	0.2921	0.00321	28.45	0.52	0.7061	0.0100	0.77	3427	17	19	3441	39	64	3432	18	28	100	100
MS 15 - 74		5.9.E+05	b.d.	b.d	205	0.49	1.44	0.02	0.2904	0.00319	27.70	0.53	0.6930	0.0110	0.83	3418	17	19	3392	43	65	3407	19	27	100	99
MS 15 - 75		4.7.E+05	b.d.	b.d	160	0.48	1.58	0.03	0.2916	0.00330	25.46	0.50	0.6314	0.0110	0.89	3424	18	19	3153	43	64	3324	19	28	95	92
MS 17: Theespruit Main Trondhjemite																										
MS 17 - 1		1.4.E+06	b.d.	b.d	574	0.46	1.87	0.05	0.2594	0.00300	19.26	0.52	0.5360	0.0130	0.87	3241	18	20	2763	55	71	3051	26	35	91	85
MS 17 - 3		1.0.E+06	b.d.	b.d	545	0.68	2.48	0.05	0.1966	0.00290	10.92	0.25	0.4030	0.0076	0.71	2791	24	26	2181	35	50	2511	22	33	87	78
MS 17 - 4		4.6.E+05	b.d.	b.d	127	0.38	1.28	0.02	0.2961	0.00326	31.79	0.55	0.7800	0.0150	0.82	3448	17	19	3714	53	77	3542	17	27	105	108
MS 17 - 5		1.1.E+06	b.d.	b.d	405	0.48	1.61	0.03	0.2748	0.00302	23.54	0.42	0.6195	0.0110	0.85	3331	17	19	3105	45	65	3246	17	28	96	93
MS 17 - 6		1.2.E+06	b.d.	b.d	402	0.50	1.47	0.03	0.2769	0.00305	26.15	0.60	0.6810	0.0140	0.92	3342	17	19	3343	52	76	3343	23	38	100	100
MS 17 - 7		1.3.E+06	b.d.	b.d	382	0.66	1.38	0.02	0.2898	0.00319	29.04	0.41	0.7255	0.0120	0.87	3415	17	19	3513	45	70	3453	14	25	102	103
MS 17 - 8		1.4.E+06	b.d.	b.d	461	0.66	1.49	0.03	0.2814	0.00310	26.19	0.40	0.6724	0.0120	0.88	3369	17	19	3313	46	68	3352	15	25	99	98
MS 17 - 10		1.4.E+06	b.d.	b.d	436	0.62	1.48	0.03	0.2751	0.00303	25.63	0.47	0.6760	0.0140	0.85	3333	17	19	3327	54	73	3330	18	28	100	100

Uncertainties quoted without components related to systematic error unless otherwise stated. Total systematic uncertainties (s sys): ^{206}Pb/^{238}U = 1.8 %; ^{207}Pb/^{206}Pb = 0.5 % (2s).

[a] Data not corrected for common Pb

[b] Concordance calculated as: (^{206}Pb-^{238}U date/^{207}Pb-^{235U} date)*100 and (^{206}Pb-^{238}U date/^{207}Pb-^{206}Pb date)*100

Table 4.7, continued.

17th-19th July 2017, Central Analytical Facilities University of Stellenbosch							Data for Tera-Wasserburg plot [a]				Data for Wetherill plot [a]					Dates (Ma)									Concordance [b]	
Identifier	Comment	^{206}Pb (CPS)	^{204}Pb (CPS)	^{206}Pb/^{204}Pb	U (mg g-1)	Th/U	^{238}U/^{206}Pb	2 s	^{207}Pb/^{206}Pb	2 s	^{207}Pb/^{235}U	2 s	^{206}Pb/^{238}U	2 s	rho	^{207}Pb/^{206}Pb	2 s	2s $_{sys}$	^{206}Pb/^{238}U	2 s	2s $_{sys}$	^{207}Pb/^{235}U	2 s	2s $_{sys}$	6/38 - 7/35	6/38 - 7/6
MS 17 - 11		1.0.E+06	b.d.	b.d	444	0.86	2.02	0.04	0.2406	0.00280	16.42	0.30	0.4953	0.0091	0.69	3120	19	20	2592	39	56	2901	17	25	89	83
MS 17 - 12		1.7.E+06	b.d.	b.d	549	0.57	1.43	0.03	0.2780	0.00306	26.92	0.55	0.6990	0.0150	0.92	3350	17	19	3414	56	77	3376	20	31	101	102
MS 17 - 13		1.2.E+06	b.d.	b.d	401	0.62	1.60	0.03	0.2659	0.00292	22.95	0.37	0.6267	0.0110	0.81	3280	17	19	3134	43	65	3223	16	26	97	96
MS 17 - 14		1.1.E+06	b.d.	b.d	353	0.58	1.42	0.02	0.2908	0.00320	28.35	0.39	0.7060	0.0110	0.83	3420	17	19	3441	42	66	3430	13	24	100	101
MS 17 - 15		8.2.E+05	b.d.	b.d	461	0.67	2.65	0.06	0.2202	0.00320	11.47	0.30	0.3775	0.0079	0.80	2977	23	25	2063	37	50	2557	24	35	81	69
MS 17 - 16		1.4.E+06	b.d.	b.d	462	0.62	1.50	0.02	0.2716	0.00299	25.01	0.39	0.6683	0.0110	0.85	3313	17	19	3297	44	65	3306	15	26	100	100
MS 17 - 18		1.3.E+06	b.d.	b.d	560	0.76	1.87	0.05	0.2593	0.00285	19.30	0.54	0.5360	0.0130	0.91	3243	17	19	2762	55	72	3052	27	37	90	85
MS 17 - 19		1.2.E+06	b.d.	b.d	409	0.58	1.43	0.03	0.2880	0.00317	27.88	0.52	0.6990	0.0140	0.85	3405	17	19	3415	54	73	3415	18	26	100	100
MS 17 - 20		8.0.E+05	b.d.	b.d	280	0.59	1.59	0.03	0.2792	0.00307	24.14	0.46	0.6279	0.0130	0.88	3356	17	19	3138	50	71	3271	19	29	96	94
MS 17 - 21		1.2.E+06	b.d.	b.d	435	0.55	1.58	0.04	0.2751	0.00303	24.19	0.57	0.6320	0.0150	0.88	3333	17	19	3155	58	77	3272	23	33	96	95
MS 17 - 22		8.9.E+05	b.d.	b.d	283	0.68	1.51	0.03	0.2879	0.00317	26.13	0.48	0.6603	0.0130	0.84	3404	17	19	3266	49	70	3352	19	25	97	96
MS 17 - 23		1.0.E+06	b.d.	b.d	361	0.55	1.60	0.03	0.2845	0.00313	24.56	0.37	0.6258	0.0100	0.80	3385	17	19	3130	41	63	3289	15	25	95	92
MS 17 - 24		1.1.E+06	b.d.	b.d	887	0.68	3.40	0.08	0.1962	0.00370	8.04	0.29	0.2941	0.0073	0.86	2787	31	32	1660	37	47	2224	34	48	75	60
MS 17 - 25		1.2.E+06	b.d.	b.d	618	0.85	2.35	0.05	0.2319	0.00255	13.56	0.27	0.4248	0.0083	0.82	3062	18	19	2281	38	52	2717	19	28	84	74
MS 17 - 27		1.6.E+06	b.d.	b.d	601	0.54	1.59	0.04	0.2702	0.00297	23.67	0.63	0.6280	0.0150	0.88	3305	17	19	3138	58	78	3250	26	36	97	95
MS 17 - 28		9.0.E+05	b.d.	b.d	291	0.42	1.39	0.03	0.2866	0.00315	28.43	0.50	0.7174	0.0130	0.87	3396	17	19	3482	48	73	3429	18	30	102	103
MS 17 - 29		1.2.E+06	b.d.	b.d	476	0.56	1.88	0.05	0.2574	0.00283	18.87	0.45	0.5330	0.0130	0.91	3229	17	19	2749	54	73	3031	23	33	91	85
MS 17 - 30		1.1.E+06	b.d.	b.d	338	0.56	1.43	0.02	0.2884	0.00317	27.90	0.43	0.7002	0.0120	0.87	3408	17	19	3418	46	69	3414	15	25	100	100
MS 17 - 31		1.5.E+06	b.d.	b.d	759	0.67	2.19	0.05	0.2306	0.00390	14.66	0.49	0.4557	0.0110	0.84	3051	27	28	2418	47	63	2786	32	43	87	79
MS 17 - 32		1.1.E+06	b.d.	b.d	350	0.51	1.41	0.03	0.2944	0.00324	28.89	0.50	0.7070	0.0140	0.86	3439	17	19	3446	53	72	3448	17	27	100	100
MS 17 - 33		1.0.E+06	b.d.	b.d	655	0.83	3.01	0.05	0.1902	0.00209	8.71	0.15	0.3323	0.0059	0.83	2741	18	20	1848	29	42	2305	16	26	80	67
MS 17 - 34		9.2.E+05	b.d.	b.d	295	0.49	1.45	0.03	0.2842	0.00313	27.14	0.42	0.6917	0.0120	0.86	3384	17	19	3386	45	69	3386	16	26	100	100
MS 17 - 35		1.1.E+06	b.d.	b.d	831	0.95	3.47	0.07	0.1619	0.00260	6.48	0.20	0.2882	0.0060	0.85	2465	27	28	1631	30	41	2031	26	43	80	66
MS 17 - 36		9.1.E+05	b.d.	b.d	377	0.62	1.93	0.04	0.2591	0.00285	18.51	0.40	0.5180	0.0110	0.85	3238	17	19	2688	44	64	3012	21	32	89	83
MS 17 - 38		1.4.E+06	b.d.	b.d	573	0.73	1.92	0.04	0.2470	0.00272	17.74	0.36	0.5217	0.0110	0.88	3163	17	19	2704	44	63	2972	19	30	91	85
MS 17 - 39		1.0.E+06	b.d.	b.d	549	0.73	2.45	0.04	0.2127	0.00234	11.97	0.21	0.4087	0.0075	0.80	2924	18	20	2207	34	50	2599	16	27	85	75
MS 17 - 40		9.7.E+05	b.d.	b.d	571	0.35	2.63	0.05	0.2449	0.00269	12.87	0.23	0.3798	0.0073	0.90	3149	17	19	2073	34	49	2667	18	27	78	66
MS 17 - 42		1.1.E+06	b.d.	b.d	596	0.63	2.51	0.05	0.2359	0.00259	13.03	0.28	0.3984	0.0079	0.92	3090	18	19	2159	36	52	2679	20	29	81	70
MS 17 - 43		1.3.E+06	b.d.	b.d	913	0.79	3.28	0.06	0.1748	0.00220	7.34	0.13	0.3048	0.0058	0.61	2598	21	23	1714	29	40	2150	16	27	80	66
MS 17 - 44		8.3.E+05	b.d.	b.d	310	0.49	1.62	0.04	0.2790	0.00307	23.97	0.66	0.6190	0.0150	0.92	3354	17	19	3100	60	80	3258	27	41	95	92
MS 17 - 45		9.2.E+05	b.d.	b.d	509	0.74	2.51	0.04	0.2191	0.00241	12.02	0.19	0.3981	0.0070	0.86	2972	18	20	2159	32	47	2603	15	26	83	73
MS 17 - 46		8.3.E+05	b.d.	b.d	375	0.48	2.02	0.04	0.2550	0.00281	17.42	0.31	0.4947	0.0095	0.92	3214	17	19	2587	41	60	2954	17	29	88	80
MS 17 - 47		7.7.E+05	b.d.	b.d	594	0.55	3.50	0.07	0.2182	0.00240	8.59	0.18	0.2857	0.0057	0.83	2963	18	20	1619	29	39	2291	19	30	71	55
MS 17 - 48		1.1.E+06	b.d.	b.d	396	0.52	1.66	0.03	0.2658	0.00292	22.00	0.38	0.6007	0.0110	0.88	3279	17	19	3030	44	65	3180	17	28	95	92
MS 17 - 49		1.0.E+06	b.d.	b.d	307	0.51	1.40	0.03	0.2861	0.00315	28.09	0.49	0.7134	0.0130	0.83	3394	17	19	3468	50	72	3420	17	27	101	102
MS 17 - 50		1.1.E+06	b.d.	b.d	557	0.64	2.34	0.04	0.2262	0.00320	13.31	0.27	0.4274	0.0076	0.61	3019	23	24	2293	34	50	2698	19	30	85	76
MS 17 - 51		1.0.E+06	b.d.	b.d	302	0.53	1.39	0.03	0.2890	0.00318	28.76	0.51	0.7210	0.0140	0.88	3410	17	19	3501	51	70	3444	17	26	102	103
MS 17 - 52		1.0.E+06	b.d.	b.d	338	0.56	1.46	0.03	0.2819	0.00310	26.66	0.49	0.6850	0.0120	0.88	3371	17	19	3360	48	69	3366	18	30	100	100
MS 17 - 53		1.0.E+06	b.d.	b.d	520	0.48	2.21	0.05	0.2427	0.00267	15.23	0.36	0.4524	0.0095	0.92	3134	17	19	2402	42	59	2820	23	38	85	77
MS 17 - 55		8.9.E+05	b.d.	b.d	473	0.68	2.42	0.05	0.2299	0.00253	13.12	0.32	0.4132	0.0084	0.90	3047	18	19	2227	38	54	2681	23	36	83	73
MS 17 - 56		1.2.E+06	b.d.	b.d	664	0.69	2.43	0.05	0.2322	0.00255	13.21	0.27	0.4114	0.0085	0.91	3065	18	19	2219	39	54	2691	19	30	82	72
MS 17 - 57		1.1.E+06	b.d.	b.d	510	0.57	2.06	0.03	0.2448	0.00269	16.42	0.26	0.4853	0.0081	0.85	3149	17	19	2548	35	54	2898	15	27	88	81
MS 17 - 58		5.0.E+05	b.d.	b.d	278	0.75	2.56	0.05	0.2801	0.00308	15.04	0.28	0.3903	0.0080	0.88	3361	17	19	2122	37	51	2815	18	28	75	63
MS 17 - 60		8.2.E+05	b.d.	b.d	259	0.48	1.37	0.02	0.2900	0.00319	29.26	0.43	0.7307	0.0120	0.83	3416	17	19	3533	46	69	3460	14	25	102	103
MS 17 - 61		9.5.E+05	b.d.	b.d	683	0.51	3.11	0.06	0.2318	0.00255	10.31	0.18	0.3216	0.0058	0.89	3062	18	19	1796	28	41	2460	16	26	73	59
MS 17 - 62		1.3.E+06	b.d.	b.d	459	0.51	1.53	0.03	0.2741	0.00302	24.87	0.46	0.6553	0.0120	0.82	3328	17	19	3246	49	68	3300	18	29	98	98
MS 17 - 63		1.1.E+06	b.d.	b.d	465	0.56	1.83	0.03	0.2530	0.00278	19.02	0.28	0.5456	0.0094	0.84	3202	17	19	2804	39	59	3041	14	25	92	88
MS 17 - 64		9.2.E+05	b.d.	b.d	298	0.47	1.42	0.02	0.2892	0.00318	28.10	0.39	0.7033	0.0110	0.83	3411	17	19	3431	43	65	3421	14	25	100	101
MS 17 - 65		9.5.E+05	b.d.	b.d	491	0.77	2.27	0.04	0.2337	0.00257	14.20	0.27	0.4403	0.0078	0.84	3074	18	19	2350	35	52	2758	18	30	85	76

Uncertainties quoted without components related to systematic error unless otherwise stated. Total systematic uncertainties (s sys): ^{206}Pb/^{238}U = 1.8 %; ^{207}Pb/^{206}Pb = 0.5 % (2s).

[a] Data not corrected for common Pb

[b] Concordance calculated as: (^{206}Pb-^{238}U date/^{207}Pb-^{235U} date)*100 and (^{206}Pb-^{238}U date/^{207}Pb-^{206}Pb date)*100

Table 4.7, continued.

17th-19th July 2017, Central Analytical Facilities University of Stellenbosch							Data for Tera-Wasserburg plot [a]				Data for Wetherill plot [a]					Dates (Ma)									Concordance [b]	
Identifier	Comment	^{206}Pb (CPS)	^{204}Pb (CPS)	^{206}Pb/^{204}Pb	U (mg g-1)	Th/U	^{238}U/^{206}Pb	2 s	^{207}Pb/^{206}Pb	2 s	^{207}Pb/^{235}U	2 s	^{206}Pb/^{238}U	2 s	rho	^{207}Pb/^{206}Pb	2 s	2s $_{sys}$	^{206}Pb/^{238}U	2 s	2s $_{sys}$	^{207}Pb/^{235}U	2 s	2s $_{sys}$	6/38 - 7/35	6/38 - 7/6
MS 18: Theespruit Main Trondhjemite																										
MS 18 - 1		8.5.E+05	b.d.	b.d	295	1.01	1.53	0.03	0.2943	0.00324	26.49	0.38	0.6523	0.0110	0.83	3438	17	19	3234	42	66	3363	14	25	96	94
MS 18 - 2		9.7.E+05	b.d.	b.d	336	0.64	1.58	0.03	0.2705	0.00298	23.62	0.39	0.6347	0.0120	0.84	3307	17	19	3165	47	68	3251	16	26	97	96
MS 18 - 3		1.2.E+06	b.d.	b.d	606	0.95	2.19	0.04	0.2459	0.00270	15.60	0.35	0.4574	0.0091	0.81	3155	17	19	2426	40	56	2848	21	32	85	77
MS 18 - 5		9.7.E+05	b.d.	b.d	325	0.56	1.48	0.02	0.2904	0.00319	27.18	0.38	0.6778	0.0110	0.82	3418	17	19	3334	41	65	3388	14	25	98	98
MS 18 - 6		1.0.E+06	b.d.	b.d	321	0.57	1.40	0.03	0.2916	0.00321	28.70	0.45	0.7150	0.0130	0.88	3424	17	19	3474	48	72	3440	16	27	101	101
MS 18 - 7		1.2.E+06	b.d.	b.d	669	0.84	2.44	0.04	0.2505	0.00276	14.20	0.23	0.4103	0.0075	0.88	3186	17	19	2215	34	49	2761	16	25	80	70
MS 18 - 8		1.2.E+06	b.d.	b.d	574	1.18	2.06	0.04	0.2503	0.00275	16.73	0.34	0.4856	0.0100	0.90	3184	17	19	2548	44	61	2917	19	29	87	80
MS 18 - 9		1.2.E+06	b.d.	b.d	421	0.94	1.55	0.03	0.2790	0.00307	24.90	0.35	0.6468	0.0110	0.87	3355	17	19	3213	42	65	3302	14	25	97	96
MS 18 - 10		1.2.E+06	b.d.	b.d	531	0.63	1.96	0.03	0.2469	0.00272	17.35	0.27	0.5106	0.0089	0.85	3163	17	19	2657	38	57	2952	15	26	90	84
MS 18 - 11		1.2.E+06	b.d.	b.d	770	0.65	2.70	0.07	0.2313	0.00254	11.84	0.29	0.3698	0.0092	0.90	3059	18	19	2027	43	55	2588	23	32	78	66
MS 18 - 12		9.3.E+05	b.d.	b.d	381	0.75	1.70	0.03	0.2829	0.00311	23.02	0.43	0.5883	0.0120	0.84	3377	17	19	2980	48	67	3224	18	29	92	88
MS 18 - 13		1.1.E+06	b.d.	b.d	441	0.66	1.59	0.04	0.2753	0.00350	24.10	0.66	0.6290	0.0150	0.85	3333	20	21	3142	58	78	3267	28	37	96	94
MS 18 - 14		1.1.E+06	b.d.	b.d	443	0.86	1.60	0.04	0.2838	0.00312	24.60	0.59	0.6240	0.0160	0.91	3382	17	19	3121	63	82	3289	24	33	95	92
MS 18 - 15		1.3.E+06	b.d.	b.d	436	0.62	1.47	0.03	0.2812	0.00309	26.43	0.48	0.6794	0.0130	0.78	3367	17	19	3339	49	71	3360	18	28	99	99
MS 18 - 16		1.7.E+06	b.d.	b.d	767	0.89	1.99	0.03	0.2404	0.00264	16.77	0.30	0.5023	0.0086	0.84	3120	18	19	2622	37	55	2919	17	27	90	84
MS 18 - 17		1.2.E+06	b.d.	b.d	562	0.84	2.03	0.03	0.2309	0.00254	15.75	0.26	0.4934	0.0085	0.81	3057	18	19	2583	36	55	2858	16	27	90	84
MS 18 - 18		1.1.E+06	b.d.	b.d	665	1.02	2.54	0.06	0.2290	0.00252	12.48	0.33	0.3941	0.0097	0.96	3044	18	19	2138	44	59	2640	25	31	81	70
MS 18 - 19		9.7.E+05	b.d.	b.d	375	0.71	1.71	0.03	0.2780	0.00306	22.50	0.34	0.5862	0.0110	0.88	3351	17	19	2971	43	65	3204	15	25	93	89
MS 18 - 20		1.1.E+06	b.d.	b.d	436	1.06	1.83	0.04	0.2611	0.00287	19.61	0.40	0.5459	0.0120	0.89	3251	17	19	2805	49	68	3071	20	28	91	86
MS 18 - 21		1.0.E+06	b.d.	b.d	579	0.95	2.37	0.05	0.2319	0.00255	13.53	0.29	0.4220	0.0084	0.89	3061	18	19	2266	38	55	2710	20	34	84	74
MS 18 - 22		1.0.E+06	b.d.	b.d	520	0.68	2.14	0.04	0.2396	0.00264	15.48	0.26	0.4679	0.0085	0.90	3115	18	19	2475	38	52	2843	16	26	87	79
MS 18 - 24		8.1.E+05	b.d.	b.d	397	0.68	2.24	0.05	0.2470	0.00272	15.15	0.32	0.4456	0.0100	0.89	3164	17	19	2373	45	60	2822	20	29	84	75
MS 18 - 25		8.7.E+05	b.d.	b.d	375	0.93	1.94	0.05	0.2623	0.00289	18.62	0.40	0.5155	0.0120	0.90	3259	17	19	2677	49	67	3019	21	30	89	82
MS 18 - 26		8.8.E+05	b.d.	b.d	377	0.77	1.92	0.04	0.2463	0.00271	17.59	0.32	0.5196	0.0097	0.71	3157	17	19	2695	41	59	2965	17	27	91	85
MS 18 - 27		1.2.E+06	b.d.	b.d	499	0.76	1.78	0.03	0.2657	0.00292	20.60	0.37	0.5620	0.0110	0.90	3279	17	19	2871	43	65	3115	18	30	92	88
MS 18 - 29		1.0.E+06	b.d.	b.d	355	0.46	1.49	0.02	0.2899	0.00319	26.80	0.39	0.6695	0.0110	0.86	3415	17	19	3301	42	66	3374	14	25	98	97
MS 18 - 30		7.5.E+05	b.d.	b.d	559	0.49	3.14	0.06	0.2248	0.00247	9.86	0.17	0.3180	0.0060	0.89	3013	18	20	1778	29	42	2419	16	26	74	59
MS 18 - 31		1.2.E+06	b.d.	b.d	779	0.56	2.79	0.06	0.2209	0.00350	11.00	0.36	0.3584	0.0081	0.86	2981	25	27	1973	38	51	2513	30	45	79	66
MS 18 - 32		9.2.E+05	b.d.	b.d	448	0.46	2.19	0.04	0.2467	0.00271	15.48	0.28	0.4564	0.0089	0.85	3161	17	19	2422	39	55	2843	17	27	85	77
MS 18 - 33		1.0.E+06	b.d.	b.d	353	0.39	1.45	0.02	0.2859	0.00314	27.17	0.39	0.6893	0.0110	0.82	3393	17	19	3378	42	65	3387	14	26	100	100
MS 18 - 34		1.1.E+06	b.d.	b.d	408	0.44	1.65	0.03	0.2787	0.00307	23.29	0.40	0.6077	0.0110	0.84	3353	17	19	3058	43	65	3238	16	26	94	91
MS 18 - 35		1.3.E+06	b.d.	b.d	504	0.47	1.69	0.04	0.2634	0.00290	21.50	0.46	0.5930	0.0130	0.92	3265	17	19	3000	51	69	3157	21	32	95	92
MS 18 - 36		9.1.E+05	b.d.	b.d	322	0.44	1.51	0.03	0.2857	0.00314	26.10	0.38	0.6621	0.0110	0.79	3392	17	19	3273	41	65	3348	14	25	98	96
MS 18 - 37		1.2.E+06	b.d.	b.d	668	0.62	2.38	0.05	0.2332	0.00290	13.65	0.34	0.4199	0.0084	0.85	3068	20	22	2257	38	54	2716	24	39	83	74
MS 18 - 38		1.1.E+06	b.d.	b.d	544	1.05	2.08	0.04	0.2549	0.00280	16.91	0.30	0.4803	0.0082	0.82	3212	17	19	2527	35	53	2925	17	29	86	79
MS 18 - 39		1.1.E+06	b.d.	b.d	508	0.42	1.89	0.03	0.2573	0.00283	18.78	0.30	0.5299	0.0090	0.66	3226	17	19	2739	38	57	3028	15	26	90	85
MS 18 - 40		9.0.E+05	b.d.	b.d	457	0.56	2.26	0.05	0.2219	0.00310	13.51	0.35	0.4420	0.0097	0.82	2990	22	24	2357	43	59	2710	24	36	87	79
MS 18 - 41		1.1.E+06	b.d.	b.d	398	0.38	1.48	0.03	0.2859	0.00314	26.73	0.48	0.6770	0.0140	0.87	3394	17	19	3332	52	72	3371	17	28	99	98
MS 18 - 42		8.0.E+05	b.d.	b.d	1037	0.40	5.41	0.16	0.2473	0.00272	6.31	0.17	0.1849	0.0055	0.94	3164	17	19	1092	30	37	2012	23	36	54	35
MS 18 - 43		1.8.E+06	b.d.	b.d	654	0.63	1.60	0.03	0.2525	0.00278	21.68	0.36	0.6245	0.0110	0.86	3199	17	19	3125	43	65	3167	16	27	99	98
MS 18 - 44		1.3.E+06	b.d.	b.d	531	0.70	1.90	0.04	0.2283	0.00251	16.46	0.34	0.5251	0.0120	0.88	3038	18	19	2717	50	68	2901	19	29	94	89
MS 18 - 45		5.1.E+05	b.d.	b.d	161	0.60	1.35	0.02	0.3124	0.00344	31.88	0.48	0.7414	0.0130	0.80	3530	17	19	3573	47	71	3544	15	26	101	101
MS 18 - 46		1.6.E+06	b.d.	b.d	555	0.48	1.47	0.03	0.2756	0.00303	25.80	0.50	0.6820	0.0140	0.86	3336	17	19	3348	52	75	3336	19	29	100	100
MS 18 - 47		8.8.E+05	b.d.	b.d	279	0.39	1.42	0.03	0.2890	0.00318	27.91	0.51	0.7020	0.0140	0.89	3410	17	19	3425	53	74	3413	18	28	100	100
MS 18 - 48		1.2.E+06	b.d.	b.d	646	0.58	2.35	0.04	0.2409	0.00265	14.14	0.26	0.4256	0.0075	0.78	3123	17	19	2284	34	50	2755	17	29	83	73
MS 18 - 50		9.6.E+05	b.d.	b.d	404	0.68	1.76	0.03	0.2814	0.00310	22.03	0.38	0.5681	0.0100	0.81	3368	17	19	2898	43	61	3182	16	28	91	86
MS 18 - 51		7.8.E+05	b.d.	b.d	401	0.80	2.12	0.04	0.2714	0.00299	17.74	0.39	0.4724	0.0096	0.80	3311	17	19	2492	42	58	2972	21	31	84	75

Uncertainties quoted without components related to systematic error unless otherwise stated. Total systematic uncertainties (s sys): ^{206}Pb/^{238}U = 1.8 %; ^{207}Pb/^{206}Pb = 0.5 % (2s).

[a] Data not corrected for common Pb

[b] Concordance calculated as: (^{206}Pb-^{238}U date/^{207}Pb-^{235U} date)*100 and (^{206}Pb-^{238}U date/^{207}Pb-^{206}Pb date)*100

Table 4.7, continued.

17th-19th July 2017, Central Analytical Facilities University of Stellenbosch							Data for Tera-Wasserburg plot [a]				Data for Wetherill plot [a]					Dates (Ma)									Concordance [b]	
Identifier	Comment	^{206}Pb (CPS)	^{204}Pb (CPS)	^{206}Pb/^{204}Pb	U (mg g-1)	Th/U	^{238}U/^{206}Pb	2 s	^{207}Pb/^{206}Pb	2 s	^{207}Pb/^{235}U	2 s	^{206}Pb/^{238}U	2 s	rho	^{207}Pb/^{206}Pb	2 s	2s $_{sys}$	^{206}Pb/^{238}U	2 s	2s $_{sys}$	^{207}Pb/^{235}U	2 s	2s $_{sys}$	6/38 - 7/35	6/38 - 7/6
MS 18 - 52		8.3.E+05	b.d.	b.d	265	0.55	1.43	0.03	0.2886	0.00317	27.77	0.48	0.7000	0.0140	0.84	3408	17	19	3419	51	73	3409	17	27	100	100
MS 18 - 53		9.4.E+05	b.d.	b.d	830	0.86	3.75	0.07	0.2240	0.00246	8.23	0.14	0.2666	0.0049	0.88	3008	18	20	1522	25	36	2253	16	26	68	51
MS 18 - 54		6.7.E+05	b.d.	b.d	222	0.37	1.43	0.02	0.2922	0.00321	28.06	0.42	0.6993	0.0120	0.81	3427	17	19	3415	44	69	3419	15	25	100	100
MS 18 - 55		9.8.E+05	b.d.	b.d	812	0.56	3.46	0.06	0.1797	0.00198	7.15	0.12	0.2889	0.0053	0.87	2647	18	20	1635	26	38	2128	15	25	77	62
MS 18 - 56		1.0.E+06	b.d.	b.d	356	0.43	1.46	0.03	0.2811	0.00309	26.51	0.49	0.6850	0.0130	0.92	3367	17	19	3357	51	75	3361	18	30	100	100
MS 18 - 57		9.6.E+05	b.d.	b.d	324	0.47	1.47	0.03	0.2836	0.00312	26.58	0.40	0.6815	0.0120	0.83	3381	17	19	3347	45	69	3366	15	25	99	99
MS 18 - 58		7.4.E+05	b.d.	b.d	263	0.47	1.49	0.03	0.2868	0.00315	26.44	0.42	0.6700	0.0120	0.85	3398	17	19	3303	45	68	3360	16	27	98	97
MS 18 - 59		6.4.E+05	b.d.	b.d	460	0.75	3.13	0.06	0.2194	0.00241	9.63	0.20	0.3192	0.0062	0.85	2974	18	20	1785	30	42	2396	19	29	74	60
MS 18 - 60		8.2.E+05	b.d.	b.d	282	0.55	1.43	0.02	0.2898	0.00319	27.88	0.38	0.6993	0.0110	0.80	3414	17	19	3415	43	66	3413	14	24	100	100
MS 18 - 61		8.7.E+05	b.d.	b.d	402	0.71	2.01	0.04	0.2548	0.00280	17.44	0.33	0.4982	0.0092	0.83	3212	17	19	2604	40	57	2956	18	29	88	81
MS 18 - 62		1.1.E+06	b.d.	b.d	423	0.64	1.60	0.04	0.2700	0.00297	23.19	0.48	0.6260	0.0140	0.89	3304	17	19	3131	53	74	3232	20	30	97	95
MS 18 - 63		9.0.E+05	b.d.	b.d	302	0.60	1.40	0.02	0.2903	0.00319	28.66	0.40	0.7165	0.0120	0.85	3417	17	19	3480	43	69	3440	14	25	101	102
MS 18 - 64		1.1.E+06	b.d.	b.d	732	1.00	2.84	0.05	0.2386	0.00262	11.55	0.22	0.3515	0.0065	0.89	3108	18	19	1940	31	45	2564	17	29	76	62
MS 18 - 65		1.0.E+06	b.d.	b.d	398	0.83	1.73	0.04	0.2544	0.00280	20.28	0.52	0.5780	0.0140	0.93	3210	17	19	2946	61	66	3104	26	31	95	92
MS 18 - 66		1.2.E+06	b.d.	b.d	472	0.63	1.77	0.04	0.2532	0.00279	19.62	0.39	0.5644	0.0120	0.91	3203	17	19	2881	48	68	3069	19	30	94	90
MS 19: Theespruit dyke																										
MS 19 - 1		6.6.E+05	b.d.	b.d	673	0.25	5.06	0.12	0.2768	0.00320	7.56	0.19	0.1977	0.0046	0.93	3342	18	20	1162	25	32	2178	22	30	53	35
MS 19 - 2		6.3.E+05	b.d.	b.d	1033	0.37	8.10	0.19	0.2269	0.00300	3.87	0.09	0.1235	0.0029	0.99	3028	21	23	751	16	21	1606	19	26	47	25
MS 19 - 3		1.2.E+06	b.d.	b.d	365	0.45	1.50	0.02	0.2846	0.00313	26.23	0.49	0.6671	0.0110	0.88	3386	17	19	3292	43	65	3353	18	28	98	97
MS 19 - 4		1.2.E+06	b.d.	b.d	355	0.47	1.46	0.03	0.2861	0.00315	27.07	0.53	0.6850	0.0120	0.89	3394	17	19	3360	46	69	3384	19	28	99	99
MS 19 - 5		8.7.E+05	b.d.	b.d	344	0.71	1.94	0.03	0.2803	0.00308	19.99	0.39	0.5160	0.0091	0.90	3363	17	19	2681	39	56	3089	19	28	87	80
MS 19 - 6		2.3.E+05	b.d.	b.d	78	0.80	1.57	0.02	0.2542	0.00280	22.40	0.39	0.6382	0.0090	0.81	3210	17	19	3180	36	59	3200	17	26	99	99
MS 19 - 7		3.1.E+05	b.d.	b.d	110	0.43	1.54	0.04	0.2542	0.00310	22.79	0.70	0.6510	0.0190	0.95	3212	19	21	3224	76	95	3212	32	40	100	100
MS 19 - 8		7.7.E+05	b.d.	b.d	622	0.57	4.00	0.08	0.2219	0.00244	7.68	0.17	0.2500	0.0049	0.89	2994	18	20	1438	25	35	2191	20	29	66	48
MS 20: Theespruit dyke																										
MS 20 - 1		7.1.E+05	b.d.	b.d	252	0.39	1.52	0.03	0.2551	0.00340	23.01	0.54	0.6570	0.0140	0.91	3214	21	23	3252	53	75	3225	23	31	101	101
MS 20 - 2		1.5.E+05	b.d.	b.d	53	0.89	1.57	0.03	0.2557	0.00360	22.37	0.49	0.6360	0.0120	0.86	3217	22	24	3172	47	66	3198	21	30	99	99
MS 20 - 3		8.3.E+05	b.d.	b.d	330	0.31	1.95	0.03	0.2244	0.00247	15.89	0.31	0.5121	0.0085	0.85	3010	18	20	2664	36	55	2868	19	28	93	89
MS 20 - 4		8.5.E+05	b.d.	b.d	435	0.58	2.45	0.04	0.2150	0.00237	12.12	0.25	0.4076	0.0074	0.88	2941	18	20	2202	34	50	2610	19	30	84	75
MS 20 - 5		8.5.E+05	b.d.	b.d	322	0.38	1.79	0.03	0.2835	0.00312	21.92	0.40	0.5600	0.0083	0.81	3380	17	19	2865	34	55	3178	18	27	90	85
MS 20 - 6		9.1.E+05	b.d.	b.d	306	0.47	1.64	0.03	0.2885	0.00317	24.45	0.47	0.6101	0.0097	0.83	3407	17	19	3068	38	61	3284	18	28	93	90
MS 20 - 7		1.1.E+06	b.d.	b.d	373	0.52	1.58	0.02	0.2832	0.00312	24.82	0.50	0.6347	0.0099	0.77	3380	17	19	3166	39	62	3298	20	30	96	94
MS 20 - 8		1.2.E+06	b.d.	b.d	571	0.50	2.14	0.03	0.2601	0.00286	16.77	0.35	0.4675	0.0075	0.77	3245	17	19	2471	33	51	2919	20	29	85	76
MS 20 - 9		1.0.E+06	b.d.	b.d	628	0.72	3.06	0.06	0.2518	0.00280	11.37	0.24	0.3269	0.0062	0.90	3194	18	19	1822	30	43	2552	20	28	71	57
MS 20 - 10		2.1.E+06	b.d.	b.d	1491	0.39	3.19	0.07	0.2260	0.00249	9.78	0.26	0.3134	0.0070	0.84	3022	18	20	1755	34	46	2410	24	34	73	58
MS 20 - 11		8.2.E+05	b.d.	b.d	412	0.27	2.15	0.06	0.2764	0.00380	17.67	0.49	0.4650	0.0120	0.93	3340	21	23	2459	51	67	2968	27	36	83	74
MS 25: Weergevonden diorite																										
MS 25 - 2		1.8.E+05	b.d.	b.d	60	0.11	1.57	0.02	0.2679	0.00295	23.57	0.42	0.6372	0.0086	0.76	3292	17	19	3176	34	58	3248	17	28	98	96
MS 25 - 3		2.0.E+05	b.d.	b.d	65	0.42	1.58	0.02	0.2551	0.00281	22.32	0.37	0.6323	0.0084	0.80	3218	17	19	3157	33	57	3196	16	26	99	98
MS 25 - 4		7.4.E+04	b.d.	b.d	25	0.35	1.56	0.02	0.2579	0.00330	22.82	0.44	0.6416	0.0092	0.74	3228	20	22	3193	36	60	3216	19	29	99	99
MS 25 - 5		1.5.E+05	b.d.	b.d	51	0.43	1.53	0.02	0.2565	0.00282	23.07	0.43	0.6531	0.0094	0.77	3222	17	19	3237	37	62	3227	18	28	100	100
MS 25 - 6		6.2.E+05	b.d.	b.d	209	0.48	1.54	0.02	0.2558	0.00281	22.90	0.38	0.6488	0.0085	0.79	3219	17	19	3222	33	58	3221	16	26	100	100
MS 25 - 7		1.4.E+05	b.d.	b.d	49	0.04	1.56	0.02	0.2559	0.00281	22.61	0.40	0.6410	0.0088	0.78	3217	17	19	3191	34	59	3208	17	27	99	99
MS 25 - 8		1.8.E+05	b.d.	b.d	61	0.19	1.56	0.02	0.2560	0.00282	22.61	0.41	0.6418	0.0089	0.76	3220	17	19	3193	35	60	3207	18	28	100	99
MS 25 - 9		2.2.E+05	b.d.	b.d	73	0.47	1.54	0.02	0.2568	0.00282	22.93	0.40	0.6483	0.0093	0.82	3225	17	19	3219	36	61	3221	17	28	100	100
MS 25 - 10		2.1.E+05	b.d.	b.d	70	0.39	1.56	0.02	0.2573	0.00283	22.74	0.40	0.6408	0.0088	0.78	3227	17	19	3190	35	59	3214	17	27	99	99

Uncertainties quoted without components related to systematic error unless otherwise stated. Total systematic uncertainties (s sys): ^{206}Pb/^{238}U = 1.8 %; ^{207}Pb/^{206}Pb = 0.5 % (2s).

[a] Data not corrected for common Pb

[b] Concordance calculated as: (^{206}Pb-^{238}U date/^{207}Pb-^{235U} date)*100 and (^{206}Pb-^{238}U date/^{207}Pb-^{206}Pb date)*100

Table 4.7, continued.

17th-19th July 2017, Central Analytical Facilities University of Stellenbosch							Data for Tera-Wasserburg plot [a]				Data for Wetherill plot [a]					Dates (Ma)									Concordance [b]	
Identifier	Comment	^{206}Pb (CPS)	^{204}Pb (CPS)	^{206}Pb/^{204}Pb	U (mg g-1)	Th/U	^{238}U/^{206}Pb	2 s	^{207}Pb/^{206}Pb	2 s	^{207}Pb/^{235}U	2 s	^{206}Pb/^{238}U	2 s	rho	^{207}Pb/^{206}Pb	2 s	2s $_{sys}$	^{206}Pb/^{238}U	2 s	2s $_{sys}$	^{207}Pb/^{235}U	2 s	2s $_{sys}$	6/38 - 7/35	6/38 - 7/6
MS 25 - 11		3.8.E+05	b.d.	b.d	127	0.50	1.53	0.02	0.2569	0.00283	23.12	0.41	0.6528	0.0095	0.82	3225	17	19	3236	37	62	3230	17	27	100	100
MS 25 - 12		4.3.E+05	b.d.	b.d	138	0.55	1.54	0.02	0.2568	0.00282	22.97	0.42	0.6482	0.0095	0.80	3224	17	19	3219	37	61	3223	18	28	100	100
MS 25 - 13		1.9.E+05	b.d.	b.d	64	0.41	1.51	0.02	0.2571	0.00283	23.55	0.46	0.6644	0.0099	0.76	3226	17	19	3282	38	62	3249	19	27	101	102
MS 25 - 14		8.8.E+05	b.d.	b.d	310	0.51	1.54	0.03	0.2527	0.00278	22.56	0.46	0.6486	0.0110	0.83	3199	17	19	3220	44	65	3206	20	29	100	101
MS 25 - 15		2.8.E+05	b.d.	b.d	101	0.75	1.67	0.02	0.2556	0.00281	21.12	0.38	0.5982	0.0084	0.78	3219	17	19	3020	34	58	3143	18	26	96	94
MS 25 - 16		1.4.E+05	b.d.	b.d	52	0.01	1.69	0.03	0.2586	0.00310	21.03	0.41	0.5910	0.0089	0.77	3235	19	21	2992	36	58	3139	19	27	95	92
MS 25 - 17		1.1.E+05	b.d.	b.d	35	0.38	1.53	0.02	0.2549	0.00280	22.99	0.44	0.6541	0.0097	0.77	3213	17	19	3245	38	59	3224	19	28	101	101
MS 25 - 18		1.1.E+05	b.d.	b.d	37	0.37	1.56	0.02	0.2586	0.00290	22.84	0.45	0.6414	0.0100	0.79	3233	18	19	3191	40	63	3218	19	28	99	99
MS 25 - 19		1.4.E+05	b.d.	b.d	47	0.03	1.56	0.02	0.2588	0.00285	22.94	0.41	0.6428	0.0088	0.77	3235	17	19	3198	34	59	3222	18	27	99	99
MS 25 - 20		1.6.E+05	b.d.	b.d	56	0.06	1.58	0.02	0.2544	0.00280	22.27	0.40	0.6340	0.0085	0.75	3211	17	19	3163	33	58	3193	17	28	99	99
MS 25 - 21		1.9.E+05	b.d.	b.d	65	0.05	1.54	0.02	0.2561	0.00282	22.93	0.42	0.6491	0.0091	0.77	3221	17	19	3222	35	60	3221	18	28	100	100
MS 25 - 22		2.7.E+05	b.d.	b.d	93	0.43	1.55	0.02	0.2573	0.00283	22.93	0.39	0.6463	0.0087	0.79	3227	17	19	3211	34	60	3222	17	27	100	100
MS 25 - 24		1.7.E+05	b.d.	b.d	56	0.44	1.53	0.02	0.2572	0.00283	23.19	0.46	0.6539	0.0098	0.76	3226	17	19	3241	38	62	3232	19	29	100	100
MS 25 - 25		3.8.E+05	b.d.	b.d	129	0.28	1.55	0.02	0.2570	0.00283	22.94	0.41	0.6463	0.0091	0.79	3227	17	19	3211	35	60	3222	17	27	100	100
MS 25 - 26		2.5.E+05	b.d.	b.d	87	0.68	1.59	0.02	0.2602	0.00286	22.66	0.42	0.6308	0.0098	0.84	3245	17	19	3150	39	62	3210	18	28	98	97
MS 25 - 27		4.1.E+05	b.d.	b.d	140	0.64	1.53	0.03	0.2574	0.00283	23.09	0.48	0.6523	0.0110	0.81	3229	17	19	3234	43	66	3229	21	29	100	100
MS 25 - 28		2.9.E+05	b.d.	b.d	98	0.29	1.56	0.02	0.2558	0.00281	22.68	0.39	0.6424	0.0086	0.78	3218	17	19	3196	34	59	3211	17	27	100	99
MS 25 - 29		2.8.E+05	b.d.	b.d	91	0.54	1.52	0.03	0.2562	0.00282	23.26	0.46	0.6591	0.0110	0.84	3219	17	19	3264	45	62	3234	19	30	101	101
MS 25 - 30		2.1.E+05	b.d.	b.d	74	0.56	1.58	0.02	0.2591	0.00285	22.66	0.41	0.6338	0.0090	0.78	3239	17	19	3162	35	60	3210	18	28	99	98
MS 25 - 31		1.6.E+06	b.d.	b.d	658	1.22	1.77	0.03	0.2385	0.00262	18.58	0.40	0.5665	0.0110	0.90	3108	18	19	2891	45	64	3018	21	29	96	93
MS 25 - 32		1.7.E+06	b.d.	b.d	590	1.26	1.55	0.03	0.2479	0.00273	22.00	0.45	0.6441	0.0110	0.83	3170	17	19	3203	43	65	3181	20	29	101	101
MS 25 - 33		5.3.E+05	b.d.	b.d	177	0.70	1.53	0.02	0.2575	0.00283	23.25	0.43	0.6546	0.0098	0.81	3229	17	19	3243	38	63	3235	18	28	100	100
MS 25 - 34		3.0.E+05	b.d.	b.d	109	0.04	1.65	0.03	0.2580	0.00284	21.58	0.44	0.6066	0.0100	0.81	3232	17	19	3054	41	62	3161	20	31	97	94
MS 25 - 35		5.5.E+05	b.d.	b.d	186	0.72	1.56	0.02	0.2553	0.00281	22.68	0.41	0.6427	0.0094	0.81	3216	17	19	3200	38	58	3210	18	28	100	100
MS 25 - 36		6.6.E+05	b.d.	b.d	231	0.35	1.55	0.02	0.2538	0.00279	22.69	0.45	0.6472	0.0100	0.78	3207	17	19	3213	40	64	3216	18	24	100	100
MS 25 - 37		9.6.E+04	b.d.	b.d	33	0.39	1.55	0.02	0.2561	0.00290	22.74	0.42	0.6444	0.0092	0.77	3220	18	20	3203	36	61	3213	18	28	100	99
MS 25 - 38		3.2.E+05	b.d.	b.d	110	0.48	1.54	0.02	0.2564	0.00282	22.92	0.41	0.6485	0.0095	0.82	3223	17	19	3220	37	61	3221	17	27	100	100
MS 25 - 39		8.4.E+05	b.d.	b.d	273	0.74	1.50	0.02	0.2535	0.00279	23.38	0.40	0.6679	0.0090	0.79	3205	17	19	3296	35	60	3241	17	26	102	103
MS 25 - 40		8.5.E+05	b.d.	b.d	279	0.39	1.54	0.02	0.2533	0.00279	22.72	0.38	0.6497	0.0090	0.83	3204	17	19	3225	35	60	3214	16	26	100	101
MS 25 - 42		2.0.E+05	b.d.	b.d	72	0.48	1.55	0.03	0.2572	0.00290	22.82	0.45	0.6445	0.0110	0.87	3230	18	20	3205	42	64	3220	20	25	100	99
MS 25 - 44		1.2.E+06	b.d.	b.d	389	1.03	1.56	0.03	0.2540	0.00279	22.57	0.45	0.6430	0.0120	0.94	3208	17	19	3199	47	67	3207	19	28	100	100
MS 25 - 45		1.9.E+05	b.d.	b.d	65	0.42	1.56	0.02	0.2538	0.00279	22.46	0.40	0.6422	0.0092	0.80	3205	17	19	3195	36	61	3201	17	28	100	100
MS 25 - 46		2.0.E+05	b.d.	b.d	74	0.46	1.62	0.03	0.2500	0.00290	21.19	0.43	0.6157	0.0100	0.80	3182	18	20	3091	40	61	3145	20	29	98	97
MS 25 - 47		2.0.E+05	b.d.	b.d	71	0.49	1.57	0.02	0.2578	0.00284	22.62	0.43	0.6358	0.0094	0.78	3232	17	19	3171	37	60	3208	18	28	99	98
MS 25 - 48		2.2.E+05	b.d.	b.d	77	0.49	1.54	0.03	0.2574	0.00290	23.06	0.46	0.6507	0.0110	0.85	3228	18	20	3229	41	65	3227	19	29	100	100
MS 25 - 49		4.7.E+05	b.d.	b.d	160	0.47	1.53	0.02	0.2558	0.00281	23.06	0.39	0.6528	0.0086	0.78	3219	17	19	3237	34	59	3227	17	26	100	101
MS 25 - 50		1.5.E+05	b.d.	b.d	49	0.23	1.51	0.02	0.2572	0.00283	23.37	0.42	0.6602	0.0094	0.79	3226	17	19	3265	36	62	3241	18	26	101	101
MS 25 - 51		5.4.E+05	b.d.	b.d	175	0.67	1.54	0.03	0.2554	0.00281	22.88	0.43	0.6477	0.0110	0.90	3217	17	19	3217	41	65	3220	18	27	100	100
MS 25 - 52		2.1.E+05	b.d.	b.d	75	0.50	1.52	0.03	0.2548	0.00300	23.00	0.51	0.6570	0.0120	0.82	3212	19	20	3254	45	67	3224	21	31	101	101
MS 25 - 53		1.7.E+05	b.d.	b.d	58	0.45	1.54	0.02	0.2562	0.00282	23.03	0.41	0.6514	0.0089	0.77	3220	17	19	3231	35	60	3226	17	27	100	100
MS 25 - 54		2.0.E+05	b.d.	b.d	66	0.52	1.54	0.02	0.2564	0.00282	23.05	0.41	0.6500	0.0089	0.77	3224	17	19	3226	35	60	3226	17	28	100	100
MS 25 - 55		1.0.E+06	b.d.	b.d	340	1.03	1.53	0.02	0.2539	0.00279	22.85	0.40	0.6517	0.0090	0.79	3207	17	19	3233	35	59	3219	17	27	100	101
MS 25 - 56		8.3.E+05	b.d.	b.d	279	0.98	1.54	0.02	0.2555	0.00281	22.89	0.39	0.6490	0.0085	0.77	3217	17	19	3222	33	59	3220	17	27	100	100
MS 25 - 57		1.1.E+05	b.d.	b.d	36	0.03	1.55	0.02	0.2528	0.00280	22.52	0.41	0.6468	0.0094	0.80	3198	18	19	3213	37	61	3205	18	27	100	100
MS 25 - 58		1.7.E+05	b.d.	b.d	61	0.04	1.57	0.02	0.2578	0.00284	22.59	0.42	0.6358	0.0093	0.79	3232	17	19	3170	36	60	3207	18	28	99	98
MS 25 - 59		1.1.E+06	b.d.	b.d	344	0.74	1.53	0.02	0.2524	0.00278	22.82	0.39	0.6542	0.0092	0.82	3198	17	19	3242	36	61	3217	17	26	101	101
MS 25 - 60		9.8.E+05	b.d.	b.d	331	0.75	1.54	0.02	0.2548	0.00280	22.80	0.38	0.6481	0.0087	0.81	3213	17	19	3219	34	59	3217	16	26	100	100
MS 25 - 61		9.9.E+05	b.d.	b.d	347	0.81	1.59	0.03	0.2524	0.00278	21.89	0.41	0.6280	0.0100	0.85	3198	17	19	3139	40	62	3176	19	28	99	98
MS 25 - 62		1.9.E+05	b.d.	b.d	64	0.53	1.55	0.02	0.2549	0.00280	22.68	0.41	0.6453	0.0091	0.78	3213	17	19	3210	36	58	3210	18	28	100	100

Uncertainties quoted without components related to systematic error unless otherwise stated. Total systematic uncertainties (s sys): ^{206}Pb/^{238}U = 1.8 %; ^{207}Pb/^{206}Pb = 0.5 % (2s).

[a] Data not corrected for common Pb

[b] Concordance calculated as: (^{206}Pb-^{238}U date/^{207}Pb-^{235U} date)*100 and (^{206}Pb-^{238}U date/^{207}Pb-^{206}Pb date)*100

Table 4.7, continued.

17th-19th July 2017, Central Analytical Facilities University of Stellenbosch							Data for Tera-Wasserburg plot [a]				Data for Wetherill plot [a]					Dates (Ma)									Concordance [b]	
Identifier	Comment	^{206}Pb (CPS)	^{204}Pb (CPS)	^{206}Pb/^{204}Pb	U (mg g-1)	Th/U	^{238}U/^{206}Pb	2 s	^{207}Pb/^{206}Pb	2 s	^{207}Pb/^{235}U	2 s	^{206}Pb/^{238}U	2 s	rho	^{207}Pb/^{206}Pb	2 s	2s $_{sys}$	^{206}Pb/^{238}U	2 s	2s $_{sys}$	^{207}Pb/^{235}U	2 s	2s $_{sys}$	6/38 - 7/35	6/38 - 7/6
MS 25 - 63		1.8.E+05	b.d.	b.d	61	0.63	1.54	0.02	0.2555	0.00281	22.96	0.40	0.6510	0.0088	0.78	3217	17	19	3230	34	59	3223	17	27	100	100
MS 25 - 64		2.0.E+05	b.d.	b.d	69	0.62	1.57	0.02	0.2561	0.00282	22.57	0.40	0.6385	0.0085	0.75	3220	17	19	3181	33	58	3206	17	27	99	99
MS 25 - 65		3.1.E+05	b.d.	b.d	103	0.45	1.53	0.02	0.2561	0.00282	23.07	0.39	0.6535	0.0089	0.81	3220	17	19	3240	35	59	3228	16	26	100	101
MS 25 - 66		1.6.E+05	b.d.	b.d	57	0.46	1.55	0.02	0.2563	0.00282	22.83	0.43	0.6453	0.0098	0.81	3221	17	19	3207	38	62	3217	18	28	100	100
MS 25 - 67		1.9.E+05	b.d.	b.d	64	0.48	1.56	0.02	0.2572	0.00283	22.78	0.41	0.6408	0.0095	0.82	3228	17	19	3190	37	61	3215	18	28	99	99
MS 25 - 68		1.6.E+05	b.d.	b.d	54	0.44	1.53	0.02	0.2566	0.00282	23.21	0.43	0.6545	0.0090	0.74	3224	17	19	3244	35	59	3233	18	28	100	101
MS 25 - 69		1.4.E+05	b.d.	b.d	49	0.41	1.54	0.03	0.2560	0.00350	22.91	0.47	0.6500	0.0120	0.90	3218	22	23	3227	46	66	3221	20	29	100	100
MS 25 - 70		6.4.E+05	b.d.	b.d	217	0.36	1.56	0.02	0.2546	0.00280	22.54	0.38	0.6413	0.0089	0.82	3212	17	19	3192	35	59	3205	17	26	100	99
MS 25 - 71		2.2.E+05	b.d.	b.d	74	0.51	1.56	0.02	0.2567	0.00282	22.68	0.39	0.6397	0.0087	0.79	3223	17	19	3186	34	58	3211	17	27	99	99
MS 25 - 72		2.0.E+05	b.d.	b.d	72	0.66	1.60	0.03	0.2513	0.00310	21.68	0.48	0.6250	0.0120	0.87	3190	20	21	3127	47	68	3166	21	31	99	98
MS 25 - 73		2.3.E+05	b.d.	b.d	85	0.68	1.59	0.03	0.2543	0.00300	21.99	0.43	0.6290	0.0100	0.81	3209	19	20	3144	40	61	3183	20	26	99	98
MS 25 - 74		2.1.E+05	b.d.	b.d	71	0.57	1.53	0.02	0.2569	0.00283	23.19	0.43	0.6544	0.0095	0.78	3225	17	19	3242	37	62	3232	18	28	100	101
MS 25 - 75		6.8.E+05	b.d.	b.d	237	0.50	1.53	0.02	0.2533	0.00279	22.85	0.41	0.6537	0.0098	0.84	3204	17	19	3240	38	62	3219	18	27	101	101
MS 25 - 76		2.4.E+05	b.d.	b.d	81	0.14	1.54	0.02	0.2569	0.00283	23.07	0.40	0.6507	0.0089	0.79	3225	17	19	3229	35	59	3228	17	26	100	100
MS 25 - 77		2.2.E+05	b.d.	b.d	75	0.04	1.56	0.02	0.2552	0.00281	22.59	0.40	0.6414	0.0088	0.77	3214	17	19	3192	34	59	3207	17	27	100	99
MS 25 - 78		2.3.E+05	b.d.	b.d	78	0.60	1.55	0.02	0.2577	0.00283	22.97	0.40	0.6461	0.0089	0.79	3230	17	19	3211	35	59	3224	17	26	100	99
MS 25 - 79		2.4.E+05	b.d.	b.d	84	0.59	1.57	0.02	0.2578	0.00284	22.70	0.39	0.6387	0.0089	0.81	3230	17	19	3181	35	60	3212	17	27	99	98
MS 25 - 80		3.6.E+05	b.d.	b.d	122	0.63	1.50	0.02	0.2565	0.00282	23.63	0.43	0.6678	0.0098	0.81	3223	17	19	3294	38	63	3250	18	28	101	102
MS 25 - 83		1.2.E+05	b.d.	b.d	43	0.42	1.52	0.03	0.2567	0.00350	23.23	0.48	0.6563	0.0110	0.81	3225	22	23	3256	46	59	3234	20	29	101	101
MS 25 - 84		3.2.E+05	b.d.	b.d	110	0.42	1.54	0.02	0.2555	0.00281	22.89	0.39	0.6489	0.0084	0.76	3217	17	19	3222	33	58	3220	17	26	100	100
MS 25 - 85		3.0.E+05	b.d.	b.d	100	0.51	1.53	0.02	0.2561	0.00282	23.11	0.45	0.6527	0.0100	0.79	3220	17	19	3235	39	64	3228	19	30	100	100
MS 25 - 86		4.3.E+05	b.d.	b.d	145	0.57	1.55	0.02	0.2549	0.00280	22.76	0.40	0.6467	0.0091	0.80	3213	17	19	3213	36	60	3214	17	27	100	100
MS 25 - 88		8.0.E+05	b.d.	b.d	275	0.93	1.57	0.02	0.2538	0.00279	22.36	0.38	0.6379	0.0083	0.77	3207	17	19	3179	33	57	3197	17	26	99	99
MS 25 - 89		2.9.E+05	b.d.	b.d	104	0.38	1.53	0.02	0.2581	0.00284	23.28	0.43	0.6546	0.0100	0.83	3233	17	19	3244	40	62	3237	18	27	100	100
MS 25 - 90		2.0.E+05	b.d.	b.d	68	0.43	1.55	0.02	0.2583	0.00284	22.92	0.40	0.6432	0.0087	0.78	3233	17	19	3199	34	59	3221	17	27	99	99
MS 25 - 91		4.7.E+05	b.d.	b.d	154	0.57	1.52	0.02	0.2563	0.00282	23.31	0.41	0.6585	0.0092	0.79	3223	17	19	3262	35	58	3240	17	25	101	101
MS 25 - 92		9.5.E+04	b.d.	b.d	33	0.33	1.53	0.02	0.2547	0.00280	22.98	0.42	0.6545	0.0092	0.77	3216	17	19	3243	36	61	3225	18	26	101	101
MS 25 - 93		2.4.E+05	b.d.	b.d	82	0.49	1.53	0.02	0.2576	0.00283	23.19	0.41	0.6530	0.0090	0.78	3228	17	19	3240	35	58	3233	17	27	100	100
MS 25 - 94		1.9.E+05	b.d.	b.d	68	0.10	1.54	0.02	0.2581	0.00310	23.10	0.46	0.6497	0.0100	0.77	3231	19	21	3225	40	62	3228	20	29	100	100
MS 25 - 95		3.0.E+05	b.d.	b.d	102	0.70	1.52	0.02	0.2585	0.00284	23.43	0.41	0.6569	0.0093	0.81	3235	17	19	3253	36	61	3243	17	27	100	101
MS 25 - 96		2.1.E+05	b.d.	b.d	73	0.29	1.53	0.02	0.2578	0.00284	23.28	0.41	0.6554	0.0090	0.78	3230	17	19	3247	35	60	3237	17	26	100	101
MS 25 - 97		1.1.E+06	b.d.	b.d	376	1.10	1.48	0.02	0.2522	0.00277	23.45	0.39	0.6737	0.0088	0.79	3197	17	19	3318	34	60	3244	16	26	102	104
MS 25 - 98		5.8.E+05	b.d.	b.d	206	0.55	1.56	0.02	0.2520	0.00277	22.25	0.44	0.6404	0.0100	0.79	3195	17	19	3187	40	63	3191	19	30	100	100
MS 25 - 99		6.0.E+05	b.d.	b.d	201	0.53	1.51	0.02	0.2544	0.00280	23.25	0.39	0.6608	0.0090	0.81	3211	17	19	3268	35	60	3236	16	26	101	102
MS 25 - 100		2.5.E+05	b.d.	b.d	92	0.62	1.56	0.02	0.2556	0.00281	22.52	0.43	0.6393	0.0100	0.82	3217	17	19	3184	40	62	3204	19	28	99	99
MS 25 - 101		2.2.E+05	b.d.	b.d	80	0.52	1.57	0.03	0.2550	0.00350	22.37	0.48	0.6380	0.0120	0.88	3212	22	23	3179	45	67	3198	21	29	99	99
MS 25 - 102		1.4.E+05	b.d.	b.d	48	0.59	1.53	0.03	0.2583	0.00340	23.19	0.51	0.6520	0.0120	0.84	3233	21	22	3233	47	68	3232	21	31	100	100
MS 25 - 103		4.0.E+05	b.d.	b.d	135	0.40	1.51	0.02	0.2562	0.00282	23.40	0.40	0.6618	0.0090	0.80	3221	17	19	3272	35	60	3242	17	26	101	102
MS 26: Weergevonden Main Trondhjemite																										
MS 26 - 1		6.2.E+05	b.d.	b.d	175	0.26	1.42	0.02	0.2943	0.00324	28.62	0.59	0.7040	0.0120	0.83	3438	17	19	3432	45	70	3438	20	30	100	100
MS 26 - 2		7.3.E+05	b.d.	b.d	239	0.49	1.66	0.03	0.2750	0.00303	22.90	0.45	0.6033	0.0100	0.84	3335	17	19	3041	40	61	3223	20	26	94	91
MS 26 - 3		1.2.E+06	b.d.	b.d	789	0.53	3.06	0.06	0.2195	0.00241	9.90	0.24	0.3273	0.0068	0.86	2975	18	20	1824	33	45	2426	21	27	75	61
MS 26 - 4		7.0.E+05	b.d.	b.d	218	0.40	1.49	0.02	0.2915	0.00321	27.05	0.46	0.6727	0.0090	0.79	3424	17	19	3314	35	60	3384	16	26	98	97
MS 26 - 5		6.9.E+05	b.d.	b.d	211	0.35	1.44	0.02	0.2938	0.00323	28.10	0.48	0.6933	0.0097	0.82	3436	17	19	3393	37	62	3421	17	26	99	99
MS 26 - 7		9.3.E+05	b.d.	b.d	298	0.37	1.55	0.02	0.2864	0.00315	25.45	0.43	0.6438	0.0086	0.79	3397	17	19	3202	34	58	3324	17	26	96	94
MS 26 - 8		4.7.E+05	b.d.	b.d	138	0.47	1.45	0.03	0.2928	0.00322	28.04	0.60	0.6920	0.0130	0.88	3433	17	19	3387	50	72	3418	21	30	99	99
MS 26 - 9		5.5.E+05	b.d.	b.d	165	0.36	1.42	0.02	0.2945	0.00324	28.55	0.51	0.7034	0.0100	0.80	3439	17	19	3431	39	63	3436	18	27	100	100
MS 26 - 10		8.6.E+05	b.d.	b.d	262	0.36	1.38	0.02	0.2923	0.00322	29.07	0.61	0.7230	0.0130	0.86	3428	17	19	3504	50	72	3454	21	29	101	102

Uncertainties quoted without components related to systematic error unless otherwise stated. Total systematic uncertainties (s sys): ^{206}Pb/^{238}U = 1.8 %; ^{207}Pb/^{206}Pb = 0.5 % (2s).

[a] Data not corrected for common Pb

[b] Concordance calculated as: (^{206}Pb-^{238}U date/^{207}Pb-^{235U} date)*100 and (^{206}Pb-^{238}U date/^{207}Pb-^{206}Pb date)*100

Table 4.7, continued.

17th-19th July 2017, Central Analytical Facilities University of Stellenbosch							Data for Tera-Wasserburg plot [a]				Data for Wetherill plot [a]					Dates (Ma)									Concordance [b]	
Identifier	Comment	^{206}Pb (CPS)	^{204}Pb (CPS)	^{206}Pb/^{204}Pb	U (mg g-1)	Th/U	^{238}U/^{206}Pb	2 s	^{207}Pb/^{206}Pb	2 s	^{207}Pb/^{235}U	2 s	^{206}Pb/^{238}U	2 s	rho	^{207}Pb/^{206}Pb	2 s	2s $_{sys}$	^{206}Pb/^{238}U	2 s	2s $_{sys}$	^{207}Pb/^{235}U	2 s	2s $_{sys}$	6/38 - 7/35	6/38 - 7/6
MS 26 - 11		8.3.E+05	b.d.	b.d	277	0.69	1.66	0.03	0.2756	0.00303	22.91	0.46	0.6014	0.0098	0.81	3336	17	19	3033	39	61	3220	20	30	94	91
MS 26 - 12		9.6.E+05	b.d.	b.d	415	0.43	2.12	0.04	0.2561	0.00282	16.70	0.40	0.4715	0.0094	0.83	3221	17	19	2487	41	58	2913	23	34	85	77
MS 26 - 13		5.4.E+05	b.d.	b.d	221	0.36	2.04	0.03	0.2722	0.00299	18.41	0.37	0.4892	0.0079	0.80	3317	17	19	2565	34	53	3009	19	29	85	77
MS 26 - 14		9.3.E+05	b.d.	b.d	275	0.48	1.40	0.02	0.2941	0.00324	29.04	0.50	0.7163	0.0100	0.81	3437	17	19	3480	38	63	3453	17	26	101	101
MS 26 - 15		6.8.E+05	b.d.	b.d	217	0.51	1.58	0.03	0.2813	0.00309	24.58	0.49	0.6326	0.0110	0.87	3368	17	19	3158	43	64	3290	19	28	96	94
MS 26 - 16		1.0.E+06	b.d.	b.d	714	0.72	3.45	0.05	0.1979	0.00230	7.92	0.16	0.2902	0.0043	0.73	2805	19	21	1642	21	34	2221	19	26	74	59
MS 26 - 18		7.7.E+05	b.d.	b.d	228	0.37	1.43	0.02	0.2893	0.00318	27.93	0.51	0.6990	0.0100	0.78	3412	17	19	3414	39	64	3414	18	28	100	100
MS 26 - 19		6.3.E+05	b.d.	b.d	207	0.42	1.57	0.02	0.2919	0.00321	25.73	0.51	0.6383	0.0098	0.77	3426	17	19	3179	39	63	3334	19	29	95	93
MS 26 - 20		4.5.E+05	b.d.	b.d	172	0.34	1.74	0.03	0.2946	0.00330	23.33	0.50	0.5755	0.0110	0.89	3439	17	19	2928	43	64	3238	21	30	90	85
MS 26 - 21		8.5.E+05	b.d.	b.d	273	0.46	1.59	0.03	0.2886	0.00317	25.04	0.49	0.6278	0.0110	0.90	3408	17	19	3138	42	65	3307	19	29	95	92
MS 26 - 22		9.9.E+05	b.d.	b.d	350	0.63	1.64	0.03	0.2756	0.00303	23.22	0.44	0.6116	0.0100	0.86	3338	17	19	3074	40	62	3234	18	28	95	92
MS 26 - 23		6.8.E+05	b.d.	b.d	258	0.31	1.86	0.03	0.2973	0.00327	22.13	0.42	0.5389	0.0084	0.82	3454	17	19	2777	35	55	3187	18	28	87	80
MS 26 - 24		6.0.E+05	b.d.	b.d	182	0.46	1.43	0.02	0.2937	0.00323	28.34	0.50	0.7000	0.0099	0.80	3435	17	19	3418	38	63	3429	17	27	100	100
MS 26 - 25		1.3.E+06	b.d.	b.d	644	0.56	2.19	0.04	0.2400	0.00264	15.10	0.36	0.4569	0.0087	0.80	3118	18	19	2424	38	55	2818	23	32	86	78
MS 26 - 26		4.4.E+05	b.d.	b.d	132	0.37	1.42	0.02	0.2977	0.00327	28.92	0.52	0.7035	0.0100	0.79	3458	17	19	3431	39	64	3449	18	27	99	99
MS 26 - 27		1.0.E+06	b.d.	b.d	456	0.70	2.14	0.03	0.2464	0.00271	15.88	0.29	0.4665	0.0070	0.82	3159	17	19	2467	31	49	2868	18	26	86	78
MS 26 - 28		1.0.E+06	b.d.	b.d	390	0.56	1.94	0.03	0.2670	0.00294	18.95	0.35	0.5144	0.0092	0.97	3286	17	19	2673	39	58	3037	18	27	88	81
MS 26 - 29		8.9.E+05	b.d.	b.d	304	0.69	1.69	0.03	0.2746	0.00302	22.45	0.42	0.5914	0.0088	0.80	3331	17	19	2993	36	58	3201	18	28	94	90
MS 26 - 30		9.9.E+05	b.d.	b.d	333	0.39	1.63	0.02	0.2711	0.00298	23.03	0.42	0.6133	0.0090	0.80	3314	17	19	3081	36	59	3226	18	27	96	93
MS 26 - 31		9.5.E+05	b.d.	b.d	373	0.37	1.77	0.03	0.2819	0.00310	21.96	0.44	0.5662	0.0098	0.86	3372	17	19	2890	40	60	3180	20	28	91	86
MS 26 - 32		1.2.E+06	b.d.	b.d	773	1.41	3.03	0.07	0.2053	0.00310	9.39	0.29	0.3304	0.0077	0.75	2865	25	26	1839	37	48	2372	28	37	78	64
MS 26 - 33		9.2.E+05	b.d.	b.d	343	0.44	1.83	0.03	0.2682	0.00295	20.27	0.42	0.5467	0.0091	0.80	3293	17	19	2809	38	58	3102	20	29	91	85
MS 26 - 34		5.8.E+05	b.d.	b.d	173	0.36	1.43	0.02	0.2867	0.00315	27.67	0.51	0.6991	0.0100	0.78	3398	17	19	3415	40	63	3405	18	28	100	101
MS 26 - 35		9.8.E+05	b.d.	b.d	295	0.40	1.45	0.02	0.2849	0.00313	27.06	0.46	0.6884	0.0093	0.79	3388	17	19	3374	35	62	3384	17	26	100	100
MS 26 - 36		8.1.E+05	b.d.	b.d	349	0.88	2.02	0.03	0.2713	0.00298	18.51	0.36	0.4948	0.0080	0.83	3312	17	19	2589	35	54	3014	18	28	86	78
MS 26 - 37		1.4.E+06	b.d.	b.d	456	0.48	1.54	0.02	0.2801	0.00308	25.00	0.45	0.6483	0.0100	0.86	3362	17	19	3219	39	63	3307	18	26	97	96
MS 26 - 39		4.7.E+05	b.d.	b.d	169	0.39	1.80	0.03	0.2751	0.00320	21.05	0.43	0.5545	0.0098	0.87	3332	18	20	2841	40	61	3138	20	29	91	85
MS 26 - 40		8.5.E+05	b.d.	b.d	316	0.47	1.86	0.03	0.2580	0.00284	19.16	0.35	0.5375	0.0085	0.87	3232	17	19	2771	36	56	3048	18	27	91	86
MS 26 - 42		1.5.E+06	b.d.	b.d	494	0.53	1.49	0.02	0.2732	0.00301	25.29	0.52	0.6712	0.0110	0.80	3322	17	19	3308	41	65	3316	20	30	100	100
MS 26 - 43		7.2.E+05	b.d.	b.d	301	0.45	2.08	0.03	0.2747	0.00302	18.28	0.38	0.4814	0.0081	0.81	3331	17	19	2531	35	54	3002	20	29	84	76
MS 26 - 44		4.8.E+05	b.d.	b.d	138	0.38	1.42	0.02	0.2959	0.00325	28.74	0.55	0.7029	0.0110	0.82	3447	17	19	3430	43	65	3443	19	28	100	100
MS 26 - 45		1.3.E+06	b.d.	b.d	472	0.51	1.65	0.02	0.2754	0.00303	23.05	0.44	0.6071	0.0091	0.79	3335	17	19	3056	37	59	3227	18	28	95	92
MS 26 - 46		7.1.E+05	b.d.	b.d	223	0.44	1.49	0.02	0.2902	0.00319	26.86	0.45	0.6706	0.0089	0.79	3418	17	19	3306	34	60	3377	17	26	98	97
MS 26 - 47		6.1.E+05	b.d.	b.d	180	0.38	1.40	0.02	0.2914	0.00321	28.71	0.51	0.7137	0.0100	0.79	3423	17	19	3470	38	63	3441	18	28	101	101
MS 26 - 48		8.8.E+05	b.d.	b.d	275	0.41	1.44	0.02	0.2855	0.00314	27.32	0.56	0.6940	0.0120	0.84	3391	17	19	3397	45	67	3393	20	29	100	100
MS 26 - 49		4.2.E+05	b.d.	b.d	129	0.32	1.45	0.02	0.2935	0.00323	27.98	0.50	0.6912	0.0097	0.79	3434	17	19	3385	37	62	3416	17	28	99	99
MS 26 - 50		7.1.E+05	b.d.	b.d	340	0.60	2.33	0.03	0.2574	0.00283	15.30	0.28	0.4301	0.0063	0.80	3229	17	19	2305	28	46	2832	17	27	81	71
MS 26 - 51		9.6.E+05	b.d.	b.d	775	0.62	3.75	0.06	0.2382	0.00262	8.75	0.16	0.2665	0.0041	0.84	3105	18	19	1522	21	33	2310	17	26	66	49
MS 26 - 52		6.5.E+05	b.d.	b.d	187	0.43	1.42	0.02	0.2927	0.00322	28.45	0.50	0.7034	0.0100	0.81	3430	17	19	3431	39	63	3433	17	27	100	100
MS 26 - 53		1.0.E+06	b.d.	b.d	363	0.60	1.77	0.03	0.2606	0.00287	20.34	0.41	0.5645	0.0093	0.82	3248	17	19	2884	38	58	3105	19	29	93	89
MS 26 - 54		8.9.E+05	b.d.	b.d	378	0.77	1.88	0.03	0.2624	0.00289	19.22	0.41	0.5323	0.0099	0.87	3259	17	19	2749	42	60	3053	20	27	90	84
MS 26 - 55		1.0.E+06	b.d.	b.d	300	0.40	1.43	0.02	0.2868	0.00315	27.63	0.53	0.6974	0.0120	0.90	3399	17	19	3408	44	69	3404	19	28	100	100
MS 26 - 56		9.2.E+05	b.d.	b.d	332	0.67	1.71	0.02	0.2855	0.00314	23.05	0.38	0.5854	0.0079	0.82	3391	17	19	2969	32	55	3228	16	26	92	88
MS 26 - 57		1.2.E+06	b.d.	b.d	523	0.33	1.96	0.04	0.2584	0.00284	18.14	0.41	0.5097	0.0094	0.82	3235	17	19	2653	40	58	2994	22	31	89	82
MS 26 - 58		8.4.E+05	b.d.	b.d	412	0.48	2.32	0.04	0.2542	0.00280	15.13	0.28	0.4307	0.0065	0.82	3209	17	19	2310	30	44	2821	17	27	82	72
MS 26 - 60		7.1.E+05	b.d.	b.d	209	0.41	1.42	0.02	0.2924	0.00322	28.38	0.52	0.7028	0.0110	0.85	3428	17	19	3429	41	66	3431	18	27	100	100
MS 26 - 62		7.1.E+05	b.d.	b.d	292	0.78	2.02	0.03	0.2575	0.00340	17.74	0.42	0.4955	0.0076	0.65	3228	21	22	2593	33	52	2972	22	32	87	80
MS 26 - 63		1.2.E+06	b.d.	b.d	471	0.59	1.85	0.03	0.2753	0.00303	20.52	0.37	0.5407	0.0083	0.85	3335	17	19	2785	35	55	3114	18	27	89	84
MS 26 - 64		8.2.E+05	b.d.	b.d	295	0.71	1.61	0.03	0.2916	0.00321	24.85	0.50	0.6192	0.0110	0.88	3424	17	19	3105	43	64	3300	20	29	94	91

Uncertainties quoted without components related to systematic error unless otherwise stated. Total systematic uncertainties (s sys): ^{206}Pb/^{238}U = 1.8 %; ^{207}Pb/^{206}Pb = 0.5 % (2s).

[a] Data not corrected for common Pb

[b] Concordance calculated as: (^{206}Pb-^{238}U date/^{207}Pb-^{235U} date)*100 and (^{206}Pb-^{238}U date/^{207}Pb-^{206}Pb date)*100

Table 4.7, continued.

17th-19th July 2017, Central Analytical Facilities University of Stellenbosch							Data for Tera-Wasserburg plot [a]				Data for Wetherill plot [a]					Dates (Ma)									Concordance [b]	
Identifier	Comment	^{206}Pb (CPS)	^{204}Pb (CPS)	^{206}Pb/^{204}Pb	U (mg g-1)	Th/U	^{238}U/^{206}Pb	2 s	^{207}Pb/^{206}Pb	2 s	^{207}Pb/^{235}U	2 s	^{206}Pb/^{238}U	2 s	rho	^{207}Pb/^{206}Pb	2 s	2s $_{sys}$	^{206}Pb/^{238}U	2 s	2s $_{sys}$	^{207}Pb/^{235}U	2 s	2s $_{sys}$	6/38 - 7/35	6/38 - 7/6
MS 26 - 65		7.8.E+05	b.d.	b.d	229	0.58	1.42	0.02	0.2918	0.00321	28.37	0.51	0.7038	0.0100	0.79	3425	17	19	3433	39	63	3430	17	27	100	100
MS 26 - 66		6.3.E+05	b.d.	b.d	190	0.54	1.42	0.02	0.2943	0.00324	28.52	0.53	0.7021	0.0110	0.84	3439	17	19	3426	41	66	3435	18	28	100	100
MS 26 - 67		1.1.E+06	b.d.	b.d	333	0.77	1.48	0.02	0.2968	0.00326	27.75	0.54	0.6779	0.0110	0.83	3452	17	19	3334	42	65	3408	19	28	98	97
MS 27: Weergevonden Main Trondhjemite																										
MS 27 - 2		3.2.E+05	b.d.	b.d	120	0.31	1.91	0.03	0.2881	0.00317	20.79	0.45	0.5225	0.0095	0.84	3405	17	19	2708	40	58	3126	21	30	87	80
MS 27 - 3		2.9.E+05	b.d.	b.d	137	0.47	2.31	0.04	0.2610	0.00290	15.60	0.35	0.4332	0.0074	0.76	3249	17	19	2318	33	50	2848	22	32	81	71
MS 27 - 6		5.9.E+05	b.d.	b.d	223	0.55	1.88	0.03	0.2542	0.00280	18.65	0.36	0.5310	0.0078	0.76	3208	17	19	2744	33	54	3021	18	29	91	86
MS 27 - 7		7.6.E+05	b.d.	b.d	399	0.27	2.70	0.05	0.2470	0.00272	12.66	0.27	0.3702	0.0063	0.80	3163	17	19	2029	29	44	2652	21	29	77	64
MS 27 - 8		5.5.E+05	b.d.	b.d	175	0.42	1.55	0.02	0.2912	0.00320	25.94	0.43	0.6462	0.0087	0.81	3422	17	19	3211	34	59	3342	16	26	96	94
MS 27 - 9		2.9.E+05	b.d.	b.d	112	0.64	1.97	0.03	0.2853	0.00314	19.98	0.41	0.5072	0.0084	0.81	3389	17	19	2643	36	55	3087	20	30	86	78
MS 27 - 10		5.4.E+05	b.d.	b.d	200	0.35	1.88	0.03	0.2699	0.00297	19.84	0.37	0.5326	0.0081	0.82	3303	17	19	2750	34	55	3081	18	28	89	83
MS 27 - 12		1.6.E+05	b.d.	b.d	45	0.39	1.44	0.02	0.2940	0.00323	28.19	0.51	0.6946	0.0097	0.77	3437	17	19	3398	37	62	3423	18	28	99	99
MS 27 - 13		3.0.E+05	b.d.	b.d	83	0.40	1.39	0.02	0.2937	0.00323	29.10	0.49	0.7179	0.0095	0.79	3435	17	19	3486	36	62	3455	17	26	101	101
MS 27 - 14		5.2.E+05	b.d.	b.d	183	0.32	1.69	0.03	0.2873	0.00316	23.38	0.45	0.5907	0.0097	0.85	3401	17	19	2990	39	60	3241	19	28	92	88
MS 27 - 15		3.7.E+05	b.d.	b.d	138	0.55	1.85	0.03	0.2895	0.00318	21.52	0.42	0.5398	0.0087	0.83	3412	17	19	2780	36	57	3159	19	29	88	81
MS 27 - 16		3.4.E+05	b.d.	b.d	115	0.53	1.61	0.03	0.2857	0.00314	24.48	0.50	0.6224	0.0110	0.87	3392	17	19	3117	43	65	3285	20	29	95	92
MS 27 - 17		6.7.E+05	b.d.	b.d	207	0.46	1.46	0.03	0.2913	0.00320	27.48	0.56	0.6858	0.0120	0.86	3422	17	19	3364	45	68	3398	20	30	99	98
MS 27 - 18		5.3.E+05	b.d.	b.d	151	0.35	1.47	0.03	0.2907	0.00320	27.29	0.62	0.6790	0.0120	0.78	3419	17	19	3339	45	67	3391	22	31	98	98
MS 27 - 19		2.8.E+05	b.d.	b.d	82	0.36	1.43	0.02	0.2937	0.00323	28.29	0.52	0.6996	0.0100	0.78	3435	17	19	3417	39	63	3427	18	28	100	99
MS 27 - 20		2.1.E+05	b.d.	b.d	61	0.37	1.40	0.02	0.2916	0.00321	28.65	0.51	0.7137	0.0100	0.79	3424	17	19	3470	38	63	3440	17	27	101	101
MS 27 - 21		4.7.E+05	b.d.	b.d	140	0.33	1.51	0.02	0.2829	0.00311	25.88	0.46	0.6627	0.0098	0.83	3377	17	19	3275	38	62	3340	17	27	98	97
MS 27 - 22		1.1.E+06	b.d.	b.d	840	0.32	3.84	0.06	0.2206	0.00243	7.90	0.16	0.2601	0.0043	0.82	2983	18	20	1490	22	33	2219	19	25	67	50
MS 27 - 23		5.5.E+05	b.d.	b.d	171	0.79	1.53	0.02	0.2915	0.00321	26.22	0.50	0.6521	0.0097	0.78	3423	17	19	3234	38	62	3352	19	29	96	94
MS 27 - 24		5.7.E+05	b.d.	b.d	234	0.27	2.13	0.04	0.2535	0.00279	16.49	0.39	0.4705	0.0086	0.77	3204	17	19	2484	38	55	2902	23	32	86	78
MS 27 - 25		6.0.E+05	b.d.	b.d	162	0.44	1.34	0.02	0.2905	0.00320	29.85	0.62	0.7440	0.0120	0.78	3418	17	19	3582	45	70	3483	19	26	103	105
MS 27 - 27		2.5.E+05	b.d.	b.d	73	0.45	1.41	0.02	0.2962	0.00326	28.96	0.58	0.7095	0.0110	0.77	3448	17	19	3454	42	66	3449	20	30	100	100
MS 27 - 28		5.3.E+05	b.d.	b.d	150	0.46	1.44	0.02	0.2893	0.00318	27.78	0.51	0.6953	0.0100	0.78	3411	17	19	3401	39	63	3409	18	28	100	100
MS 27 - 29		1.1.E+06	b.d.	b.d	406	0.56	1.72	0.02	0.2732	0.00301	21.90	0.37	0.5817	0.0080	0.81	3322	17	19	2954	32	55	3178	16	26	93	89
MS 27 - 30		4.1.E+05	b.d.	b.d	120	0.33	1.40	0.02	0.2948	0.00324	28.98	0.53	0.7131	0.0110	0.84	3441	17	19	3467	40	67	3450	18	28	100	101
MS 27 - 31		2.5.E+05	b.d.	b.d	72	0.33	1.42	0.02	0.2946	0.00324	28.62	0.50	0.7052	0.0095	0.77	3439	17	19	3438	36	62	3438	17	27	100	100
MS 27 - 32		5.6.E+05	b.d.	b.d	158	0.41	1.38	0.02	0.2922	0.00321	29.27	0.52	0.7268	0.0100	0.77	3427	17	19	3522	40	61	3461	18	27	102	103
MS 27 - 33		4.7.E+05	b.d.	b.d	158	0.32	1.57	0.02	0.2870	0.00316	25.17	0.48	0.6365	0.0099	0.82	3400	17	19	3173	39	62	3313	19	28	96	93
MS 27 - 34		3.7.E+05	b.d.	b.d	254	0.22	3.27	0.07	0.2774	0.00305	11.67	0.28	0.3062	0.0069	0.94	3346	17	19	1720	34	45	2573	22	33	67	51
MS 27 - 35		6.1.E+05	b.d.	b.d	253	0.38	2.10	0.04	0.2656	0.00292	17.49	0.36	0.4768	0.0088	0.90	3278	17	19	2512	38	55	2960	20	29	85	77
MS 27 - 36		2.7.E+05	b.d.	b.d	76	0.53	1.39	0.02	0.2935	0.00323	29.19	0.50	0.7219	0.0097	0.78	3434	17	19	3501	36	63	3458	17	27	101	102
MS 27 - 38		4.4.E+05	b.d.	b.d	166	1.22	1.77	0.03	0.2903	0.00320	22.66	0.51	0.5660	0.0110	0.86	3420	17	19	2889	46	64	3210	22	31	90	84
MS 27 - 39		9.5.E+05	b.d.	b.d	385	0.91	2.05	0.04	0.2832	0.00312	19.07	0.40	0.4877	0.0093	0.91	3380	17	19	2557	40	59	3041	21	31	84	76
MS 27 - 40		4.6.E+05	b.d.	b.d	181	0.44	1.81	0.04	0.2894	0.00318	22.03	0.51	0.5540	0.0120	0.94	3412	17	19	2838	48	68	3182	23	32	89	83
MS 27 - 41		3.9.E+05	b.d.	b.d	112	0.44	1.43	0.03	0.2831	0.00311	27.38	0.57	0.7010	0.0130	0.89	3377	17	19	3421	47	72	3394	21	30	101	101
MS 27 - 42		4.3.E+05	b.d.	b.d	127	0.56	1.47	0.02	0.2905	0.00320	27.36	0.49	0.6821	0.0099	0.81	3418	17	19	3350	38	63	3394	17	28	99	98
MS 27 - 43		2.5.E+05	b.d.	b.d	76	0.41	1.45	0.02	0.2931	0.00322	27.85	0.50	0.6896	0.0100	0.81	3431	17	19	3378	38	64	3412	18	27	99	98
MS 27 - 45		6.3.E+05	b.d.	b.d	208	0.27	1.59	0.03	0.2760	0.00304	23.99	0.54	0.6304	0.0110	0.78	3338	17	19	3148	44	65	3264	22	32	96	94
MS 27 - 47		2.9.E+05	b.d.	b.d	90	0.51	1.45	0.03	0.2971	0.00327	28.12	0.60	0.6900	0.0130	0.88	3455	17	19	3378	49	73	3423	21	28	99	98
MS 27 - 48		3.3.E+05	b.d.	b.d	106	0.35	1.43	0.03	0.2898	0.00410	27.77	0.62	0.6980	0.0140	0.90	3414	22	23	3411	52	73	3409	22	30	100	100
MS 27 - 50		5.0.E+05	b.d.	b.d	153	0.37	1.45	0.03	0.2935	0.00323	27.99	0.57	0.6910	0.0120	0.85	3434	17	19	3385	46	67	3416	20	30	99	99
MS 27 - 51		3.4.E+05	b.d.	b.d	103	0.43	1.46	0.02	0.2962	0.00326	27.95	0.52	0.6845	0.0110	0.86	3448	17	19	3359	40	66	3415	18	28	98	97
MS 27 - 52		4.2.E+05	b.d.	b.d	117	0.47	1.42	0.02	0.2928	0.00322	28.54	0.52	0.7061	0.0100	0.78	3431	17	19	3441	39	64	3435	18	28	100	100
MS 27 - 53		6.1.E+05	b.d.	b.d	237	0.36	1.94	0.03	0.2650	0.00292	18.83	0.34	0.5145	0.0076	0.82	3275	17	19	2674	32	53	3031	18	27	88	82

Uncertainties quoted without components related to systematic error unless otherwise stated. Total systematic uncertainties (s sys): ^{206}Pb/^{238}U = 1.8 %; ^{207}Pb/^{206}Pb = 0.5 % (2s).

[a] Data not corrected for common Pb

[b] Concordance calculated as: (^{206}Pb-^{238}U date/^{207}Pb-^{235U} date)*100 and (^{206}Pb-^{238}U date/^{207}Pb-^{206}Pb date)*100

Table 4.7, continued.

17th-19th July 2017, Central Analytical Facilities University of Stellenbosch							Data for Tera-Wasserburg plot [a]				Data for Wetherill plot [a]					Dates (Ma)									Concordance [b]	
Identifier	Comment	^{206}Pb (CPS)	^{204}Pb (CPS)	^{206}Pb/^{204}Pb	U (mg g-1)	Th/U	^{238}U/^{206}Pb	2 s	^{207}Pb/^{206}Pb	2 s	^{207}Pb/^{235}U	2 s	^{206}Pb/^{238}U	2 s	rho	^{207}Pb/^{206}Pb	2 s	2s $_{sys}$	^{206}Pb/^{238}U	2 s	2s $_{sys}$	^{207}Pb/^{235}U	2 s	2s $_{sys}$	6/38 - 7/35	6/38 - 7/6
MS 27 - 54		6.6.E+05	b.d.	b.d	288	1.01	2.01	0.04	0.2900	0.00319	19.79	0.44	0.4963	0.0100	0.91	3416	17	19	2596	45	59	3079	21	30	84	76
MS 27 - 55		2.5.E+05	b.d.	b.d	74	0.49	1.42	0.02	0.2935	0.00323	28.45	0.49	0.7030	0.0095	0.78	3434	17	19	3430	36	62	3433	17	27	100	100
MS 27 - 56		2.2.E+05	b.d.	b.d	65	0.45	1.45	0.02	0.2925	0.00322	27.73	0.48	0.6874	0.0096	0.81	3428	17	19	3370	37	62	3407	17	27	99	98
MS 27 - 57		5.5.E+05	b.d.	b.d	159	0.58	1.44	0.02	0.2940	0.00323	28.25	0.48	0.6954	0.0092	0.78	3437	17	19	3401	35	61	3426	17	26	99	99
MS 27 - 58		2.7.E+05	b.d.	b.d	83	0.75	1.54	0.02	0.2866	0.00315	25.73	0.48	0.6505	0.0099	0.82	3397	17	19	3227	39	63	3335	18	27	97	95
MS 27 - 59		7.9.E+05	b.d.	b.d	238	0.56	1.45	0.03	0.2881	0.00317	27.43	0.56	0.6910	0.0130	0.92	3405	17	19	3383	49	72	3397	20	29	100	99
MS 27 - 60		1.0.E+06	b.d.	b.d	302	0.56	1.49	0.02	0.2783	0.00306	25.78	0.44	0.6715	0.0094	0.82	3351	17	19	3309	36	62	3337	17	26	99	99
MS 27 - 61		4.7.E+05	b.d.	b.d	140	0.47	1.41	0.02	0.2930	0.00322	28.64	0.52	0.7087	0.0100	0.78	3431	17	19	3451	39	64	3439	18	28	100	101
MS 27 - 62		4.7.E+05	b.d.	b.d	155	0.34	1.55	0.02	0.2867	0.00315	25.43	0.50	0.6433	0.0100	0.79	3398	17	19	3199	40	63	3322	19	29	96	94
MS 27 - 63		3.1.E+05	b.d.	b.d	102	0.34	1.55	0.02	0.2845	0.00313	25.28	0.50	0.6442	0.0100	0.78	3385	17	19	3203	40	62	3316	19	29	97	95
MS 27 - 64		7.0.E+05	b.d.	b.d	333	0.31	2.26	0.04	0.2635	0.00290	16.23	0.39	0.4427	0.0081	0.76	3267	17	19	2360	36	53	2884	22	35	82	72
MS 27 - 65		2.2.E+05	b.d.	b.d	67	0.46	1.45	0.02	0.2957	0.00325	28.20	0.51	0.6916	0.0095	0.76	3445	17	19	3386	36	62	3423	18	28	99	98
MS 27 - 66		1.8.E+05	b.d.	b.d	53	0.44	1.44	0.02	0.2938	0.00323	28.19	0.50	0.6965	0.0099	0.80	3434	17	19	3405	38	63	3424	17	27	99	99
MS 27 - 67		5.3.E+05	b.d.	b.d	174	0.53	1.56	0.03	0.2792	0.00307	24.67	0.50	0.6408	0.0110	0.85	3356	17	19	3190	44	65	3296	19	26	97	95
MS 27 - 68		1.8.E+05	b.d.	b.d	51	0.32	1.40	0.02	0.2904	0.00319	28.51	0.51	0.7122	0.0100	0.78	3416	17	19	3464	37	64	3434	18	28	101	101
MS 27 - 69		2.7.E+05	b.d.	b.d	81	0.53	1.47	0.02	0.2924	0.00322	27.52	0.48	0.6825	0.0095	0.80	3428	17	19	3352	36	61	3400	17	27	99	98
MS 27 - 70		3.7.E+05	b.d.	b.d	116	0.51	1.52	0.02	0.2938	0.00323	26.70	0.48	0.6578	0.0094	0.79	3437	17	19	3256	36	61	3370	18	28	97	95
MS 27 - 71		5.0.E+05	b.d.	b.d	170	0.95	1.63	0.02	0.2920	0.00321	24.72	0.46	0.6137	0.0094	0.82	3426	17	19	3082	38	61	3295	18	28	94	90
MS 27 - 72		1.6.E+05	b.d.	b.d	47	0.48	1.40	0.02	0.2951	0.00325	29.11	0.51	0.7158	0.0098	0.78	3441	17	19	3478	37	63	3455	17	27	101	101
MS 27 - 73		4.3.E+05	b.d.	b.d	129	0.56	1.37	0.02	0.2926	0.00322	29.39	0.60	0.7290	0.0120	0.81	3430	17	19	3529	46	67	3464	20	30	102	103
MS 27 - 74		2.5.E+05	b.d.	b.d	71	0.45	1.38	0.02	0.2944	0.00324	29.40	0.53	0.7242	0.0100	0.77	3438	17	19	3509	38	64	3464	18	28	101	102
MS 27 - 75		2.5.E+05	b.d.	b.d	81	0.58	1.54	0.02	0.2941	0.00324	26.31	0.47	0.6488	0.0094	0.81	3437	17	19	3221	37	61	3356	18	27	96	94
MS 27 - 76		5.4.E+05	b.d.	b.d	167	0.70	1.48	0.02	0.2948	0.00324	27.45	0.47	0.6752	0.0090	0.78	3441	17	19	3324	35	60	3398	17	26	98	97
MS 27 - 77		2.7.E+05	b.d.	b.d	79	0.50	1.44	0.02	0.2934	0.00323	28.19	0.48	0.6968	0.0094	0.79	3433	17	19	3406	36	62	3424	17	26	99	99
MS 27 - 78		5.1.E+05	b.d.	b.d	169	0.44	1.55	0.03	0.2881	0.00317	25.66	0.51	0.6457	0.0110	0.86	3405	17	19	3209	42	65	3331	19	29	96	94
MS 27 - 79		7.8.E+05	b.d.	b.d	385	0.86	2.45	0.04	0.2364	0.00260	13.32	0.24	0.4085	0.0062	0.84	3094	18	19	2207	28	45	2701	17	26	82	71
MS 27 - 80		3.6.E+05	b.d.	b.d	102	0.33	1.42	0.02	0.2939	0.00323	28.60	0.54	0.7059	0.0110	0.83	3436	17	19	3440	42	66	3440	19	26	100	100
MS 27 - 83		2.4.E+05	b.d.	b.d	77	0.37	1.57	0.02	0.2923	0.00322	25.70	0.44	0.6376	0.0085	0.78	3427	17	19	3177	34	59	3333	17	27	95	93
MS 27 - 84		1.1.E+06	b.d.	b.d	402	0.44	1.69	0.03	0.2750	0.00303	22.37	0.47	0.5910	0.0110	0.89	3333	17	19	2992	46	63	3198	20	29	94	90
MS 27 - 85		6.3.E+05	b.d.	b.d	408	0.57	3.17	0.05	0.2560	0.00282	11.13	0.20	0.3150	0.0047	0.83	3219	17	19	1764	23	37	2532	17	26	70	55
MS 27 - 86		4.0.E+05	b.d.	b.d	127	0.60	1.51	0.02	0.2923	0.00322	26.63	0.46	0.6609	0.0092	0.81	3428	17	19	3269	35	60	3368	17	26	97	95
ST-J 26: Stolzburg Main Trondhjemite																										
ST-J 26 - 1		1.6.E+06	b.d.	b.d	939	0.83	2.89	0.05	0.2075	0.00270	9.92	0.27	0.3460	0.0065	0.69	2883	21	23	1914	31	45	2423	25	34	79	66
ST-J 26 - 2		7.9.E+05	b.d.	b.d	363	1.08	2.40	0.04	0.2536	0.00300	14.58	0.37	0.4160	0.0077	0.73	3204	19	20	2240	35	51	2786	24	32	80	70
ST-J 26 - 4		1.1.E+06	b.d.	b.d	310	0.74	1.37	0.02	0.3048	0.00335	30.51	0.56	0.7274	0.0110	0.82	3493	17	19	3521	41	66	3501	18	28	101	101
ST-J 26 - 5		9.0.E+05	b.d.	b.d	254	0.46	1.43	0.02	0.2872	0.00316	27.67	0.48	0.6986	0.0098	0.81	3400	17	19	3413	37	63	3405	17	27	100	100
ST-J 26 - 6		1.1.E+06	b.d.	b.d	548	0.52	2.52	0.04	0.2379	0.00262	13.02	0.26	0.3962	0.0060	0.76	3103	18	19	2150	28	45	2677	19	30	80	69
ST-J 26 - 7		1.5.E+06	b.d.	b.d	445	0.55	1.46	0.02	0.2745	0.00302	25.82	0.44	0.6827	0.0093	0.80	3330	17	19	3352	36	62	3338	17	27	100	101
ST-J 26 - 8		2.4.E+06	b.d.	b.d	673	1.32	1.42	0.02	0.2914	0.00321	28.26	0.51	0.7036	0.0100	0.79	3423	17	19	3431	39	64	3426	18	27	100	100
ST-J 26 - 9		8.5.E+05	b.d.	b.d	380	0.65	2.27	0.04	0.2347	0.00258	14.27	0.32	0.4402	0.0073	0.74	3081	18	19	2349	33	51	2762	21	33	85	76
ST-J 26 - 11		9.6.E+05	b.d.	b.d	468	0.71	2.54	0.04	0.2404	0.00264	13.08	0.28	0.3939	0.0065	0.77	3120	18	19	2139	30	46	2681	20	31	80	69
ST-J 26 - 12		1.2.E+06	b.d.	b.d	359	0.97	1.54	0.02	0.2868	0.00315	25.73	0.49	0.6499	0.0093	0.75	3398	17	19	3225	36	61	3333	19	29	97	95
ST-J 26 - 13		1.5.E+06	b.d.	b.d	562	1.03	1.85	0.03	0.2768	0.00304	20.65	0.42	0.5415	0.0094	0.85	3345	17	19	2787	39	59	3119	20	30	89	83
ST-J 26 - 14		7.9.E+05	b.d.	b.d	476	0.53	3.06	0.05	0.2121	0.00233	9.57	0.18	0.3271	0.0049	0.80	2919	18	20	1823	24	38	2392	18	26	76	62
ST-J 26 - 15		9.2.E+05	b.d.	b.d	640	0.65	3.52	0.05	0.2044	0.00225	8.01	0.15	0.2843	0.0042	0.79	2859	18	20	1612	21	34	2230	17	26	72	56
ST-J 26 - 16		8.5.E+05	b.d.	b.d	292	1.08	1.74	0.02	0.2813	0.00309	22.25	0.39	0.5738	0.0081	0.81	3368	17	19	2921	33	56	3192	17	27	92	87
ST-J 26 - 17		1.1.E+06	b.d.	b.d	474	0.62	2.13	0.03	0.2357	0.00270	15.25	0.35	0.4688	0.0075	0.70	3086	18	20	2476	33	52	2826	22	33	88	80
ST-J 26 - 18		1.5.E+06	b.d.	b.d	667	1.24	2.42	0.04	0.1978	0.00250	11.26	0.24	0.4124	0.0070	0.80	2805	21	22	2224	32	48	2543	20	28	87	79

Uncertainties quoted without components related to systematic error unless otherwise stated. Total systematic uncertainties (s sys): ^{206}Pb/^{238}U = 1.8 %; ^{207}Pb/^{206}Pb = 0.5 % (2s).

[a] Data not corrected for common Pb

[b] Concordance calculated as: (^{206}Pb-^{238}U date/^{207}Pb-^{235U} date)*100 and (^{206}Pb-^{238}U date/^{207}Pb-^{206}Pb date)*100

Table 4.7, continued.

17th-19th July 2017, Central Analytical Facilities University of Stellenbosch							Data for Tera-Wasserburg plot [a]				Data for Wetherill plot [a]					Dates (Ma)									Concordance [b]	
Identifier	Comment	^{206}Pb (CPS)	^{204}Pb (CPS)	^{206}Pb/^{204}Pb	U (mg g-1)	Th/U	^{238}U/^{206}Pb	2 s	^{207}Pb/^{206}Pb	2 s	^{207}Pb/^{235}U	2 s	^{206}Pb/^{238}U	2 s	rho	^{207}Pb/^{206}Pb	2 s	2s $_{sys}$	^{206}Pb/^{238}U	2 s	2s $_{sys}$	^{207}Pb/^{235}U	2 s	2s $_{sys}$	6/38 - 7/35	6/38 - 7/6
ST-J 26 - 19		1.7.E+06	b.d.	b.d	837	0.67	2.41	0.05	0.2558	0.00300	14.62	0.40	0.4148	0.0088	0.78	3219	19	20	2235	40	54	2787	26	35	80	69
ST-J 26 - 20		1.5.E+06	b.d.	b.d	784	0.58	2.45	0.06	0.2527	0.00278	14.21	0.37	0.4084	0.0092	0.87	3200	17	19	2206	42	55	2761	24	33	80	69
ST-J 26 - 21		1.5.E+06	b.d.	b.d	455	0.81	1.46	0.02	0.2850	0.00314	26.87	0.51	0.6841	0.0110	0.85	3389	17	19	3357	41	66	3376	19	29	99	99
ST-J 26 - 22		1.1.E+06	b.d.	b.d	429	0.84	2.02	0.04	0.2635	0.00290	18.03	0.41	0.4954	0.0087	0.77	3265	17	19	2591	38	57	2985	22	34	87	79
ST-J 26 - 23		8.7.E+05	b.d.	b.d	330	0.71	1.92	0.03	0.2848	0.00313	20.46	0.41	0.5211	0.0088	0.84	3388	17	19	2700	37	58	3109	19	31	87	80
ST-J 26 - 24		1.2.E+06	b.d.	b.d	892	0.63	3.83	0.05	0.1848	0.00203	6.65	0.12	0.2608	0.0035	0.74	2692	18	20	1494	18	30	2063	16	25	72	55
ST-J 26 - 25		5.2.E+05	b.d.	b.d	162	0.48	1.56	0.02	0.2919	0.00321	25.79	0.45	0.6417	0.0089	0.79	3425	17	19	3194	35	59	3337	17	26	96	93
ST-J 26 - 26		7.9.E+05	b.d.	b.d	249	0.66	1.57	0.02	0.2965	0.00326	26.04	0.46	0.6367	0.0091	0.81	3451	17	19	3174	36	60	3346	17	27	95	92
ST-J 26 - 27		9.0.E+05	b.d.	b.d	479	0.46	2.51	0.04	0.2456	0.00270	13.46	0.28	0.3988	0.0067	0.81	3154	17	19	2162	31	47	2711	20	28	80	69
ST-J 26 - 28		8.2.E+05	b.d.	b.d	237	0.52	1.43	0.02	0.2921	0.00321	28.17	0.50	0.6998	0.0098	0.79	3427	17	19	3417	37	63	3422	17	28	100	100
ST-J 26 - 29		1.0.E+06	b.d.	b.d	411	0.48	1.99	0.03	0.2617	0.00288	18.12	0.37	0.5020	0.0084	0.82	3255	17	19	2620	36	55	2992	20	30	88	80
ST-J 26 - 30		1.0.E+06	b.d.	b.d	416	0.42	1.99	0.03	0.2629	0.00289	18.20	0.36	0.5019	0.0078	0.79	3262	17	19	2619	33	54	2996	19	30	87	80
ST-J 26 - 32		8.6.E+05	b.d.	b.d	285	0.92	1.63	0.03	0.2755	0.00303	23.34	0.47	0.6148	0.0100	0.81	3335	17	19	3091	39	58	3238	20	30	95	93
ST-J 26 - 33		6.4.E+05	b.d.	b.d	179	0.45	1.42	0.02	0.2936	0.00323	28.60	0.51	0.7064	0.0100	0.79	3435	17	19	3442	39	64	3437	18	28	100	100
ST-J 26 - 34		1.6.E+06	b.d.	b.d	759	0.68	2.30	0.04	0.2448	0.00269	14.72	0.31	0.4350	0.0069	0.75	3150	17	19	2326	31	49	2793	20	31	83	74
ST-J 26 - 35		1.3.E+06	b.d.	b.d	520	1.04	1.97	0.03	0.2749	0.00302	19.21	0.33	0.5071	0.0070	0.80	3332	17	19	2643	30	50	3051	17	26	87	79
ST-J 26 - 36		1.5.E+06	b.d.	b.d	688	1.02	2.29	0.03	0.2438	0.00268	14.67	0.27	0.4368	0.0065	0.81	3143	17	19	2335	29	47	2792	18	27	84	74
ST-J 26 - 37		1.8.E+06	b.d.	b.d	506	1.08	1.42	0.02	0.2986	0.00328	29.02	0.54	0.7054	0.0110	0.84	3461	17	19	3439	41	65	3452	18	28	100	99
ST-J 26 - 38		7.1.E+05	b.d.	b.d	508	0.50	3.78	0.06	0.2071	0.00280	7.57	0.17	0.2647	0.0043	0.72	2879	22	24	1513	22	34	2179	20	28	69	53
ST-J 26 - 39		5.8.E+05	b.d.	b.d	173	0.43	1.55	0.02	0.2852	0.00314	25.43	0.48	0.6458	0.0100	0.82	3389	17	19	3209	40	63	3323	18	28	97	95
ST-J 26 - 40		6.3.E+05	b.d.	b.d	243	0.49	2.02	0.04	0.2704	0.00297	18.53	0.47	0.4957	0.0098	0.78	3306	17	19	2593	42	59	3013	24	35	86	78
ST-J 26 - 41		1.1.E+06	b.d.	b.d	585	0.61	2.64	0.04	0.2346	0.00258	12.24	0.23	0.3787	0.0056	0.79	3082	18	19	2069	26	42	2621	18	27	79	67
ST-J 26 - 42		1.2.E+06	b.d.	b.d	435	0.60	1.87	0.04	0.2638	0.00340	19.52	0.52	0.5361	0.0110	0.77	3267	20	22	2765	46	63	3064	26	35	90	85
ST-J 26 - 43		8.6.E+05	b.d.	b.d	263	0.70	1.49	0.02	0.2944	0.00324	27.27	0.54	0.6726	0.0110	0.83	3439	17	19	3314	44	65	3391	19	29	98	96
ST-J 26 - 44		8.0.E+05	b.d.	b.d	314	0.77	1.95	0.03	0.2751	0.00303	19.50	0.35	0.5141	0.0072	0.78	3333	17	19	2672	30	52	3064	18	28	87	80
ST-J 26 - 45		8.7.E+05	b.d.	b.d	714	0.66	4.23	0.06	0.2111	0.00232	6.90	0.13	0.2365	0.0034	0.76	2912	18	20	1368	18	29	2096	17	25	65	47
ST-J 26 - 47		8.7.E+05	b.d.	b.d	410	0.57	2.44	0.04	0.2397	0.00264	13.58	0.30	0.4099	0.0067	0.74	3115	18	19	2213	31	47	2717	21	31	81	71
ST-J 26 - 48		5.2.E+05	b.d.	b.d	148	0.52	1.45	0.02	0.2973	0.00327	28.35	0.51	0.6904	0.0100	0.81	3457	17	19	3382	40	63	3429	18	27	99	98
ST-J 26 - 49		1.0.E+06	b.d.	b.d	475	0.54	2.22	0.04	0.2460	0.00271	15.24	0.32	0.4506	0.0086	0.91	3158	17	19	2396	38	54	2830	21	27	85	76
ST-J 26 - 52		6.4.E+05	b.d.	b.d	222	0.48	1.79	0.03	0.2744	0.00302	21.17	0.41	0.5586	0.0092	0.85	3329	17	19	2859	38	58	3144	19	28	91	86
ST-J 26 - 53		8.1.E+05	b.d.	b.d	535	0.41	3.47	0.06	0.2325	0.00330	9.24	0.20	0.2879	0.0047	0.75	3065	23	24	1630	24	36	2360	20	28	69	53
ST-J 26 - 55		1.2.E+06	b.d.	b.d	413	0.45	1.70	0.03	0.2723	0.00300	22.06	0.43	0.5882	0.0096	0.84	3317	17	19	2980	39	60	3184	19	28	94	90
ST-J 26 - 56		1.3.E+06	b.d.	b.d	621	0.58	2.51	0.04	0.2170	0.00239	11.93	0.23	0.3982	0.0064	0.83	2956	18	20	2159	29	46	2597	18	27	83	73
ST-J 26 - 58		8.5.E+05	b.d.	b.d	269	0.65	1.52	0.02	0.2956	0.00325	26.83	0.48	0.6588	0.0100	0.85	3447	17	19	3261	39	62	3376	18	26	97	95
ST-J 26 - 59		8.7.E+05	b.d.	b.d	618	0.43	3.60	0.07	0.1947	0.00300	7.48	0.23	0.2778	0.0056	0.66	2777	25	27	1579	28	39	2166	27	36	73	57
ST-J 26 - 60		8.7.E+05	b.d.	b.d	391	0.48	2.10	0.04	0.2687	0.00296	17.64	0.38	0.4767	0.0081	0.79	3298	17	19	2511	36	53	2967	21	30	85	76
ST-J 26 - 61		9.3.E+05	b.d.	b.d	682	0.46	3.60	0.06	0.2348	0.00270	8.99	0.22	0.2780	0.0049	0.72	3081	18	20	1580	25	37	2332	24	33	68	51

Uncertainties quoted without components related to systematic error unless otherwise stated. Total systematic uncertainties (s sys): ^{206}Pb/^{238}U = 1.8 %; ^{207}Pb/^{206}Pb = 0.5 % (2s).

[a] Data not corrected for common Pb

[b] Concordance calculated as: (^{206}Pb-^{238}U date/^{207}Pb-^{235U} date)*100 and (^{206}Pb-^{238}U date/^{207}Pb-^{206}Pb date)*100

Table 4.7, continued.

17th-19th July 2017, Central Analytical Facilities University of Stellenbosch							Data for Tera-Wasserburg plot [a]				Data for Wetherill plot [a]					Dates (Ma)									Concordance [b]	
Identifier	Comment	^{206}Pb (CPS)	^{204}Pb (CPS)	^{206}Pb/^{204}Pb	U (mg g-1)	Th/U	^{238}U/^{206}Pb	2 s	^{207}Pb/^{206}Pb	2 s	^{207}Pb/^{235}U	2 s	^{206}Pb/^{238}U	2 s	rho	^{207}Pb/^{206}Pb	2 s	2s $_{sys}$	^{206}Pb/^{238}U	2 s	2s $_{sys}$	^{207}Pb/^{235}U	2 s	2s $_{sys}$	6/38 - 7/35	6/38 - 7/6
Reference Materials:																										
M127																										
M127 - 1		3.9.E+05	b.d.	b.d	774	0.52	11.61	0.13	0.0584	0.00064	0.69	0.01	0.0861	0.0010	0.66	535	24	27	532	6	11	534	7	11	100	100
M127 - 2		3.9.E+05	b.d.	b.d	773	0.53	11.51	0.13	0.0587	0.00065	0.70	0.01	0.0869	0.0010	0.72	547	24	27	537	6	11	539	7	11	100	98
M127 - 3		3.8.E+05	b.d.	b.d	766	0.53	11.54	0.13	0.0581	0.00064	0.69	0.01	0.0867	0.0010	0.65	530	24	27	536	6	11	535	7	11	100	101
M127 - 4		3.8.E+05	b.d.	b.d	771	0.53	11.58	0.13	0.0582	0.00064	0.69	0.01	0.0864	0.0010	0.67	531	24	27	534	6	11	534	7	11	100	101
M127 - 5		3.8.E+05	b.d.	b.d	776	0.53	11.64	0.13	0.0581	0.00064	0.69	0.01	0.0859	0.0010	0.71	529	24	27	531	6	11	531	7	10	100	100
M127 - 6		3.7.E+05	b.d.	b.d	771	0.53	11.54	0.13	0.0581	0.00064	0.69	0.01	0.0867	0.0010	0.73	529	24	27	536	6	11	534	7	10	100	101
M127 - 7		3.6.E+05	b.d.	b.d	770	0.53	11.61	0.13	0.0584	0.00064	0.70	0.01	0.0862	0.0010	0.67	538	24	27	533	6	11	535	7	11	99	99
M127 - 8		3.6.E+05	b.d.	b.d	771	0.53	11.64	0.13	0.0580	0.00064	0.69	0.01	0.0859	0.0010	0.71	528	24	27	531	6	11	531	7	11	100	101
M127 - 9		3.5.E+05	b.d.	b.d	775	0.53	11.67	0.14	0.0581	0.00064	0.69	0.01	0.0857	0.0010	0.73	528	24	27	530	6	11	531	7	11	100	100
M127 - 10		3.5.E+05	b.d.	b.d	771	0.53	11.61	0.15	0.0580	0.00064	0.69	0.01	0.0861	0.0011	0.73	522	24	27	532	6	11	531	7	11	100	102
M127 - 11		3.4.E+05	b.d.	b.d	775	0.52	11.70	0.15	0.0579	0.00064	0.68	0.01	0.0855	0.0011	0.73	515	24	27	529	6	11	528	7	11	100	103
M127 - 12		3.4.E+05	b.d.	b.d	773	0.52	11.56	0.13	0.0582	0.00064	0.69	0.01	0.0865	0.0010	0.67	529	24	27	535	6	11	535	7	11	100	101
M127 - 13		3.4.E+05	b.d.	b.d	778	0.52	11.58	0.15	0.0584	0.00064	0.70	0.01	0.0864	0.0011	0.74	538	24	27	534	6	11	536	7	11	100	99
M127 - 14		3.3.E+05	b.d.	b.d	774	0.53	11.50	0.15	0.0577	0.00063	0.69	0.01	0.0869	0.0011	0.73	508	24	27	537	6	12	533	7	11	101	106
M127 - 15		3.3.E+05	b.d.	b.d	778	0.52	11.58	0.13	0.0578	0.00064	0.69	0.01	0.0863	0.0010	0.66	515	24	27	534	6	11	532	7	11	100	104
M127 - 16		3.3.E+05	b.d.	b.d	789	0.53	11.50	0.15	0.0580	0.00064	0.70	0.01	0.0869	0.0011	0.73	525	24	27	537	6	11	536	7	11	100	102
M127 - 1		3.4.E+05	b.d.	b.d	765	0.53	11.53	0.16	0.0588	0.00065	0.70	0.01	0.0867	0.0012	0.75	552	24	27	536	7	12	540	8	12	99	97
M127 - 2		3.3.E+05	b.d.	b.d	772	0.53	11.70	0.15	0.0584	0.00070	0.69	0.01	0.0855	0.0011	0.68	539	26	29	529	7	11	532	8	12	99	98
M127 - 3		3.2.E+05	b.d.	b.d	761	0.52	11.74	0.15	0.0581	0.00065	0.68	0.01	0.0852	0.0011	0.68	531	24	27	527	7	11	528	8	11	100	99
M127 - 4		3.2.E+05	b.d.	b.d	766	0.53	11.66	0.15	0.0576	0.00063	0.68	0.01	0.0857	0.0011	0.73	509	24	27	530	7	11	527	8	11	101	104
M127 - 5		3.1.E+05	b.d.	b.d	754	0.52	11.66	0.15	0.0582	0.00067	0.69	0.01	0.0858	0.0011	0.68	529	25	28	530	7	11	531	8	12	100	100
M127 - 6		3.2.E+05	b.d.	b.d	759	0.53	11.64	0.15	0.0580	0.00068	0.69	0.01	0.0859	0.0011	0.68	519	26	28	531	7	11	530	8	12	100	102
M127 - 7		3.1.E+05	b.d.	b.d	760	0.53	11.70	0.15	0.0573	0.00065	0.68	0.01	0.0855	0.0011	0.67	506	25	27	529	7	11	526	8	12	101	104
M127 - 8		3.0.E+05	b.d.	b.d	757	0.53	11.72	0.15	0.0581	0.00064	0.68	0.01	0.0853	0.0011	0.68	527	24	27	528	7	11	528	8	12	100	100
M127 - 9		3.0.E+05	b.d.	b.d	766	0.52	11.91	0.16	0.0579	0.00065	0.67	0.01	0.0840	0.0011	0.73	520	25	27	520	7	11	522	7	10	100	100
M127 - 10		3.0.E+05	b.d.	b.d	754	0.53	11.70	0.16	0.0581	0.00068	0.68	0.01	0.0855	0.0012	0.74	525	26	28	529	7	12	529	8	12	100	101
M127 - 11		2.9.E+05	b.d.	b.d	758	0.53	11.71	0.15	0.0580	0.00069	0.68	0.01	0.0854	0.0011	0.68	521	26	28	528	7	11	528	8	12	100	101
M127 - 12		2.9.E+05	b.d.	b.d	747	0.53	11.68	0.15	0.0580	0.00065	0.68	0.01	0.0856	0.0011	0.68	520	25	27	530	7	11	529	8	11	100	102
M127 - 13		2.9.E+05	b.d.	b.d	753	0.53	11.62	0.15	0.0582	0.00065	0.69	0.01	0.0861	0.0011	0.68	529	24	27	532	6	11	533	8	12	100	101
M127 - 14		2.8.E+05	b.d.	b.d	757	0.53	11.65	0.15	0.0576	0.00074	0.68	0.01	0.0859	0.0011	0.67	501	28	30	531	7	11	527	8	12	101	106
M127 - 15		2.8.E+05	b.d.	b.d	732	0.53	11.54	0.15	0.0578	0.00074	0.69	0.01	0.0866	0.0011	0.67	515	28	30	536	7	11	533	8	11	101	104
M127 - 16		2.8.E+05	b.d.	b.d	749	0.53	11.68	0.15	0.0576	0.00076	0.68	0.01	0.0856	0.0011	0.67	508	29	31	529	7	11	526	8	12	101	104
M127 - 1		3.1.E+05	b.d.	b.d	770	0.53	11.78	0.19	0.0584	0.00065	0.68	0.01	0.0849	0.0014	0.49	535	24	27	525	8	12	528	6	11	100	98
M127 - 2		3.1.E+05	b.d.	b.d	769	0.53	11.76	0.19	0.0584	0.00064	0.68	0.01	0.0850	0.0014	0.59	535	24	27	526	8	12	529	7	11	99	98
M127 - 3		3.0.E+05	b.d.	b.d	766	0.51	11.62	0.19	0.0582	0.00066	0.69	0.01	0.0861	0.0014	0.56	528	25	27	532	8	13	533	7	11	100	101
M127 - 4		3.0.E+05	b.d.	b.d	770	0.55	11.67	0.19	0.0581	0.00064	0.69	0.01	0.0857	0.0014	0.61	528	24	27	530	8	12	532	7	11	100	100
M127 - 5		2.9.E+05	b.d.	b.d	756	0.53	11.73	0.19	0.0579	0.00064	0.68	0.01	0.0852	0.0014	0.57	515	24	27	527	8	12	526	7	11	100	102
M127 - 6		2.8.E+05	b.d.	b.d	760	0.55	11.73	0.19	0.0581	0.00064	0.68	0.01	0.0853	0.0014	0.54	523	24	27	527	8	12	528	7	11	100	101
M127 - 7		2.8.E+05	b.d.	b.d	763	0.48	11.79	0.19	0.0580	0.00064	0.68	0.01	0.0848	0.0014	0.62	520	24	27	525	8	12	524	7	11	100	101
M127 - 8		2.7.E+05	b.d.	b.d	754	0.55	11.65	0.18	0.0580	0.00064	0.69	0.01	0.0858	0.0013	0.60	523	24	27	531	8	12	531	7	11	100	101
M127 - 9		2.7.E+05	b.d.	b.d	753	0.55	11.70	0.18	0.0589	0.00066	0.69	0.01	0.0855	0.0013	0.60	555	24	27	529	8	12	534	7	11	99	95
M127 - 10		2.7.E+05	b.d.	b.d	759	0.55	11.73	0.18	0.0580	0.00066	0.68	0.01	0.0853	0.0013	0.52	527	25	27	527	8	12	527	7	11	100	100
M127 - 11		2.7.E+05	b.d.	b.d	753	0.55	11.75	0.19	0.0583	0.00064	0.68	0.01	0.0851	0.0014	0.61	532	24	27	526	8	12	528	7	10	100	99

Uncertainties quoted without components related to systematic error unless otherwise stated. Total systematic uncertainties (s sys): ^{206}Pb/^{238}U = 1.8 %; ^{207}Pb/^{206}Pb = 0.5 % (2s).

[a] Data not corrected for common Pb

[b] Concordance calculated as: (^{206}Pb-^{238}U date/^{207}Pb-^{235U} date)*100 and (^{206}Pb-^{238}U date/^{207}Pb-^{206}Pb date)*100

Table 4.7, continued.

17th-19th July 2017, Central Analytical Facilities University of Stellenbosch							Data for Tera-Wasserburg plot [a]				Data for Wetherill plot [a]					Dates (Ma)									Concordance [b]	
Identifier	Comment	^{206}Pb (CPS)	^{204}Pb (CPS)	^{206}Pb/^{204}Pb	U (mg g-1)	Th/U	^{238}U/^{206}Pb	2 s	^{207}Pb/^{206}Pb	2 s	^{207}Pb/^{235}U	2 s	^{206}Pb/^{238}U	2 s	rho	^{207}Pb/^{206}Pb	2 s	2s $_{sys}$	^{206}Pb/^{238}U	2 s	2s $_{sys}$	^{207}Pb/^{235}U	2 s	2s $_{sys}$	6/38 - 7/35	6/38 - 7/6
Plesovice																										
PLES - 1		1.9.E+05	b.d.	b.d	607	0.09	18.38	0.21	0.0534	0.00068	0.40	0.01	0.0544	0.0006	0.61	334	29	31	342	4	7	343	5	8	100	102
PLES - 2		2.1.E+05	b.d.	b.d	670	0.09	18.34	0.22	0.0538	0.00067	0.40	0.01	0.0545	0.0006	0.63	353	28	30	342	4	7	344	5	8	99	97
PLES - 3		1.5.E+05	b.d.	b.d	476	0.09	18.35	0.22	0.0532	0.00084	0.40	0.01	0.0545	0.0007	0.58	320	36	38	342	4	7	341	6	9	100	107
PLES - 4		1.2.E+05	b.d.	b.d	399	0.09	18.20	0.22	0.0532	0.00083	0.40	0.01	0.0550	0.0007	0.62	319	35	37	345	4	7	342	6	8	101	108
PLES - 5		1.8.E+05	b.d.	b.d	585	0.09	18.26	0.22	0.0528	0.00071	0.40	0.01	0.0548	0.0007	0.62	306	31	33	344	4	7	339	6	8	101	112
PLES - 6		1.8.E+05	b.d.	b.d	596	0.09	18.69	0.22	0.0535	0.00068	0.39	0.01	0.0535	0.0006	0.65	339	29	31	336	4	7	337	5	8	100	99
PLES - 7		1.3.E+05	b.d.	b.d	459	0.09	18.67	0.23	0.0532	0.00082	0.39	0.01	0.0536	0.0007	0.63	321	35	37	336	4	7	335	6	8	100	105
PLES - 8		1.2.E+05	b.d.	b.d	401	0.09	18.53	0.23	0.0529	0.00081	0.39	0.01	0.0540	0.0007	0.58	317	35	37	339	4	7	337	6	9	101	107
PLES - 9		1.6.E+05	b.d.	b.d	564	0.09	18.49	0.23	0.0531	0.00078	0.40	0.01	0.0541	0.0007	0.63	319	33	35	339	4	7	338	6	8	100	106
PLES - 10		1.3.E+05	b.d.	b.d	468	0.09	18.55	0.23	0.0537	0.00082	0.40	0.01	0.0539	0.0007	0.61	347	34	36	339	4	7	341	6	9	99	98
PLES - 11		1.8.E+05	b.d.	b.d	647	0.09	18.34	0.22	0.0528	0.00076	0.40	0.01	0.0545	0.0007	0.64	304	33	35	342	4	7	338	6	8	101	113
PLES - 12		1.6.E+05	b.d.	b.d	556	0.09	18.29	0.23	0.0530	0.00072	0.40	0.01	0.0547	0.0007	0.66	315	31	33	343	4	7	341	6	8	101	109
PLES - 13		1.3.E+05	b.d.	b.d	479	0.09	18.37	0.24	0.0528	0.00082	0.40	0.01	0.0544	0.0007	0.62	308	35	37	342	4	7	339	6	9	101	111
PLES - 14		1.6.E+05	b.d.	b.d	597	0.09	18.40	0.22	0.0529	0.00080	0.40	0.01	0.0543	0.0007	0.60	308	34	36	341	4	7	339	6	8	101	111
PLES - 15		1.2.E+05	b.d.	b.d	449	0.09	18.46	0.24	0.0539	0.00090	0.40	0.01	0.0542	0.0007	0.60	351	38	39	340	4	7	343	6	9	99	97
PLES - 16		1.2.E+05	b.d.	b.d	441	0.09	18.31	0.23	0.0532	0.00084	0.40	0.01	0.0546	0.0007	0.60	318	36	38	343	4	7	342	6	9	100	108
PLES - 1		1.8.E+05	b.d.	b.d	637	0.09	18.28	0.25	0.0532	0.00083	0.40	0.01	0.0547	0.0008	0.65	327	35	37	343	5	8	342	6	9	100	105
PLES - 2		1.5.E+05	b.d.	b.d	556	0.09	18.31	0.24	0.0533	0.00087	0.40	0.01	0.0546	0.0007	0.60	329	37	39	343	4	7	342	7	8	100	104
PLES - 3		1.9.E+05	b.d.	b.d	717	0.10	18.71	0.27	0.0541	0.00071	0.40	0.01	0.0535	0.0008	0.69	366	30	32	336	5	8	341	6	8	98	92
PLES - 4		2.0.E+05	b.d.	b.d	775	0.10	18.58	0.25	0.0531	0.00074	0.39	0.01	0.0538	0.0007	0.67	321	32	34	338	4	7	337	6	8	100	105
PLES - 5		1.6.E+05	b.d.	b.d	616	0.12	18.59	0.25	0.0530	0.00086	0.39	0.01	0.0538	0.0007	0.60	316	37	39	338	4	7	336	7	8	101	107
PLES - 6		1.5.E+05	b.d.	b.d	593	0.10	18.55	0.24	0.0535	0.00084	0.40	0.01	0.0539	0.0007	0.61	334	35	37	338	4	7	338	6	9	100	101
PLES - 7		1.5.E+05	b.d.	b.d	581	0.10	18.46	0.24	0.0530	0.00079	0.40	0.01	0.0542	0.0007	0.63	318	34	36	340	4	7	338	6	8	101	107
PLES - 8		1.5.E+05	b.d.	b.d	581	0.11	18.61	0.24	0.0531	0.00083	0.39	0.01	0.0537	0.0007	0.60	323	35	37	337	4	7	337	6	9	100	104
PLES - 9		1.6.E+05	b.d.	b.d	631	0.11	18.49	0.25	0.0529	0.00078	0.39	0.01	0.0541	0.0007	0.65	310	33	35	339	5	8	337	6	8	101	109
PLES - 10		2.0.E+05	b.d.	b.d	810	0.09	18.71	0.25	0.0529	0.00073	0.39	0.01	0.0535	0.0007	0.65	311	31	33	336	4	7	334	6	8	101	108
PLES - 11		1.6.E+05	b.d.	b.d	668	0.09	18.63	0.25	0.0539	0.00084	0.40	0.01	0.0537	0.0007	0.61	349	35	37	337	4	7	341	6	9	99	97
PLES - 12		2.0.E+05	b.d.	b.d	809	0.10	18.70	0.24	0.0533	0.00071	0.39	0.01	0.0535	0.0007	0.68	332	30	32	336	4	7	336	5	8	100	101
PLES - 13		1.4.E+05	b.d.	b.d	594	0.12	18.26	0.24	0.0532	0.00083	0.40	0.01	0.0548	0.0007	0.62	323	35	37	344	5	8	343	6	9	100	106
PLES - 14		1.4.E+05	b.d.	b.d	598	0.11	18.53	0.25	0.0519	0.00087	0.39	0.01	0.0540	0.0007	0.60	269	38	40	339	5	8	332	7	8	102	126
PLES - 15		1.2.E+05	b.d.	b.d	528	0.10	18.53	0.25	0.0531	0.00091	0.40	0.01	0.0540	0.0007	0.57	313	39	41	339	4	7	338	7	9	100	108
PLES - 16		1.4.E+05	b.d.	b.d	588	0.10	18.72	0.25	0.0532	0.00092	0.39	0.01	0.0534	0.0007	0.59	320	39	41	335	4	7	335	7	9	100	105
PLES - 1		1.6.E+05	b.d.	b.d	625	0.13	18.50	0.30	0.0529	0.00078	0.39	0.01	0.0541	0.0009	0.89	317	33	35	339	5	8	337	5	7	101	107
PLES - 2		1.5.E+05	b.d.	b.d	605	0.13	18.45	0.29	0.0538	0.00086	0.40	0.01	0.0542	0.0009	0.82	344	36	38	340	5	8	342	6	8	99	99
PLES - 3		1.5.E+05	b.d.	b.d	597	0.12	18.49	0.30	0.0533	0.00076	0.40	0.01	0.0541	0.0009	0.87	330	32	34	340	5	8	340	5	8	100	103
PLES - 4		1.4.E+05	b.d.	b.d	576	0.12	18.36	0.30	0.0531	0.00079	0.40	0.01	0.0545	0.0009	0.84	322	34	36	342	5	8	341	6	8	100	106
PLES - 5		1.4.E+05	b.d.	b.d	569	0.11	18.33	0.30	0.0533	0.00080	0.40	0.01	0.0546	0.0009	0.85	328	34	36	342	5	8	343	6	8	100	104
PLES - 6		1.4.E+05	b.d.	b.d	600	0.12	18.55	0.30	0.0533	0.00073	0.40	0.01	0.0539	0.0009	0.82	328	31	33	338	5	8	339	6	8	100	103
PLES - 7		1.4.E+05	b.d.	b.d	588	0.11	18.59	0.30	0.0537	0.00077	0.40	0.01	0.0538	0.0009	0.87	347	32	34	338	5	8	340	5	8	99	97
PLES - 8		1.3.E+05	b.d.	b.d	585	0.12	18.67	0.31	0.0529	0.00085	0.39	0.01	0.0536	0.0009	0.82	306	37	38	336	5	8	334	6	8	101	110
PLES - 9		1.1.E+05	b.d.	b.d	502	0.11	18.74	0.31	0.0533	0.00090	0.39	0.01	0.0534	0.0009	0.80	324	38	40	335	5	8	334	6	9	100	103
PLES - 10		8.4.E+04	b.d.	b.d	375	0.10	18.50	0.30	0.0530	0.00100	0.39	0.01	0.0541	0.0009	0.74	310	43	44	339	6	8	337	6	9	101	109
PLES - 11		1.3.E+05	b.d.	b.d	600	0.13	18.64	0.30	0.0538	0.00089	0.40	0.01	0.0537	0.0009	0.82	342	37	39	337	5	8	339	6	8	99	99

Uncertainties quoted without components related to systematic error unless otherwise stated. Total systematic uncertainties (s sys): ^{206}Pb/^{238}U = 1.8 %; ^{207}Pb/^{206}Pb = 0.5 % (2s).

[a] Data not corrected for common Pb

[b] Concordance calculated as: (^{206}Pb-^{238}U date/^{207}Pb-^{235U} date)*100 and (^{206}Pb-^{238}U date/^{207}Pb-^{206}Pb date)*100

Table 4.8. Zircon Lu-Hf isotope data.

	Corresponding # of U-Pb analysis	Comment	$^{176}Yb/^{177}Hf$ [a]	±2σ	$^{176}Lu/^{177}Hf$ [a]	±2σ	$^{178}Hf/^{177}Hf$	$^{180}Hf/^{177}Hf$	Sig_{Hf} [b] (V)	$^{176}Hf/^{177}Hf$	±2σ [c]	$^{176}Hf/^{177}Hf_{(t)}$ [d]	εHf(t) [d]	±2σ [c]	Avg MORB [e] (Ga)	T_{DM2} [f] (Ga)	T_{DM2} [g] (Ga)	age [h] (Ma)
Sample MS 1																		
seq_20180315-115547\seq158.dat	19		0.0355	29	0.00115	7	1.46711	1.88682	12	0.280685	15	0.28060903	1.9	0.91292	3.5	3.59	3.3	3440
seq_20180315-115547\seq159.dat	14		0.0439	36	0.00132	8	1.46712	1.88675	13	0.280770	16	0.280688364	-1.0	0.93680	3.4	3.6	3.3	3201
seq_20180315-115547\seq160.dat	9		0.0035	3	0.00007	0	1.46709	1.88681	11	0.280710	16	0.280705438	-0.2	0.86727	3.4	3.5	3.3	3207
average 3.2			0.0237	19	0.00070	4	1.46710	1.88678	12	0.280740	16	0.28069685	-0.6	0.88777	3.4	3.54	3.3	3205
Sample MS 2																		
seq_20180315-115547\seq147.dat	16		0.0172	14	0.00052	3	1.46710	1.88690	12	0.280575	24	0.280540887	-0.4	0.87784	3.6	3.7	3.5	3447
seq_20180315-115547\seq148.dat	17		0.0196	16	0.00057	3	1.46705	1.88687	13	0.280580	17	0.280542384	-0.9	0.88101	3.6	3.7	3.5	3424
seq_20180315-115547\seq149.dat	20		0.0144	12	0.00043	3	1.46711	1.88677	14	0.280571	19	0.28054233	-0.9	0.87452	3.6	3.7	3.5	3421
seq_20180315-115547\seq150.dat	23		0.0122	10	0.00037	2	1.46709	1.88663	14	0.280579	24	0.280554703	-0.2	0.87236	3.6	3.7	3.4	3432
seq_20180315-115547\seq146.dat	29		0.0160	13	0.00048	3	1.46719	1.88676	15	0.280570	18	0.280537709	-1.2	0.87630	3.6	3.7	3.5	3418
seq_20180315-115547\seq145.dat	33		0.0148	12	0.00045	3	1.46711	1.88680	12	0.280579	17	0.280549204	-0.7	0.87490	3.6	3.7	3.4	3422
seq_20180315-115547\seq151.dat	41		0.0114	11	0.00034	3	1.46712	1.88668	13	0.280560	21	0.280536924	-0.9	0.87330	3.6	3.7	3.5	3433
seq_20180315-115547\seq152.dat	69		0.0150	12	0.00045	3	1.46709	1.88684	12	0.280570	19	0.280540787	-1.2	0.87529	3.6	3.7	3.5	3414
average 3.4			0.0151	12	0.00045	3	1.4671	1.88678	13	0.280573	20	0.280543083	-0.7	0.87553	3.6	3.73	3.5	3430
Sample MS 3																		
seq_20180315-115547\seq154.dat	8	Core (9)	0.0111	10	0.00032	2	1.46712	1.88679	9	0.280738	15	0.28071899	0.1	0.87238	3.4	3.5	3.2	3201
seq_20180315-115547\seq156.dat	6	Duplicate (5)	0.0125	10	0.00035	2	1.46701	1.88676	9	0.280758	16	0.280736115	0.9	0.87268	3.3	3.5	3.2	3209
seq_20180315-115547\seq157.dat	5		0.0176	14	0.00050	3	1.46702	1.88678	8	0.280741	21	0.280710027	0.1	0.87834	3.4	3.5	3.2	3212
average 3.2			0.0137	11	0.00039	2	1.46705	1.88678	9	0.280746	17	0.280721665	0.5	0.87426	3.3	3.49	3.2	3214
seq_20180315-115547\seq155.dat	9	Tip (8/10)	0.0100	8	0.00032	2	1.46710	1.88655	11	0.280729	16	0.280709504	-1.2	0.87054	3.4	3.54	3.3	3161
Sample MS 4																		
seq_20180315-115547\seq134.dat	13		0.0271	23	0.00091	6	1.46718	1.88674	13	0.280664	19	0.280602294	3.3	0.89696	3.4	3.6	3.3	3511
seq_20180315-115547\seq139.dat	58		0.0346	28	0.00102	6	1.46705	1.88681	9	0.280576	18	0.280506758	0.3	0.91134	3.6	3.7	3.5	3528
seq_20180315-115547\seq142.dat	68		0.0502	41	0.00139	9	1.46706	1.88685	11	0.280653	17	0.280558806	1.9	0.95825	3.5	3.6	3.4	3514
average 3.5			0.0373	31	0.00111	7	1.46710	1.88680	11	0.280631	18	0.280556008	1.8	0.91949	3.5	3.65	3.4	3515
seq_20180315-115547\seq138.dat	50		0.0186	21	0.00063	6	1.46717	1.88660	8	0.280607	18	0.280565242	0.2	0.89101	3.5	3.7	3.4	3437
seq_20180315-115547\seq141.dat	60	Core (59)	0.0204	17	0.00065	4	1.46711	1.88681	12	0.280616	16	0.280572745	0.3	0.88267	3.5	3.7	3.4	3430
seq_20180315-115547\seq132.dat	5		0.0166	16	0.00052	5	1.46716	1.88660	13	0.280626	20	0.280591809	1.3	0.88208	3.5	3.6	3.4	3440
seq_20180315-115547\seq137.dat	42		0.0484	49	0.00138	12	1.46707	1.88673	12	0.280646	68	0.280554651	0.2	0.99734	3.6	3.7	3.4	3450
average 3.4			0.0260	26	0.00079	6	1.46713	1.88668	11	0.280624	30	0.280571139	0.5	0.90419	3.5	3.66	3.4	3440
seq_20180315-115547\seq140.dat	59	Rim (60)	0.0116	9	0.00034	2	1.46709	1.88674	14	0.280689	18	0.280668048	-1.0	0.87177	3.4	3.6	3.3	3232
seq_20180315-115547\seq135.dat	19		0.0223	19	0.00060	4	1.46718	1.88683	14	0.280720	18	0.280682582	-0.7	0.88669	3.4	3.6	3.3	3221
seq_20180315-115547\seq143.dat	80		0.0213	17	0.00071	4	1.46710	1.88658	12	0.280658	20	0.28061437	-3.3	0.88337	3.6	3.7	3.4	3213
average 3.2			0.0184	15	0.00055	3	1.46712	1.88672	13	0.280689	19	0.280654987	-1.7	0.87968	3.5	3.62	3.3	3221
seq_20180315-115547\seq136.dat	20	Duplicate (19)	0.0191	16	0.00056	4	1.46709	1.88691	12	0.280692	21	0.280657691	-2.4	0.88107	3.5	3.6	3.4	3186
seq_20180315-115547\seq144.dat	79		0.0419	34	0.00139	8	1.46711	1.88673	14	0.280643	20	0.280558277	-6.4	0.93014	3.7	3.8	3.6	3168
seq_20180315-115547\seq133.dat	3		0.0138	12	0.00038	2	1.46713	1.88667	13	0.280673	17	0.2806504	-3.9	0.87504	3.5	3.7	3.4	3134
average 3.1			0.0249	21	0.00078	5	1.46711	1.88677	13	0.280669	19	0.280622074	-4.1	0.89076	3.6	3.71	3.4	3170
Sample MS 14																		
seq_20180315-115547\seq105.dat	124	Core (125)	0.0165	13	0.00053	3	1.46720	1.88667	13	0.280629	17	0.280594288	1.7	0.87717	3.5	3.6	3.3	3453
seq_20180315-115547\seq106.dat	104		0.0327	26	0.00105	6	1.46718	1.88686	10	0.280650	21	0.280580485	0.7	0.90556	3.5	3.7	3.4	3433
seq_20180315-115547\seq108.dat	7		0.0176	14	0.00055	3	1.46718	1.88682	14	0.280603	19	0.280566773	0.4	0.87826	3.5	3.7	3.4	3441
seq_20180315-115547\seq103.dat	133		0.0301	24	0.00099	6	1.46720	1.88681	13	0.280611	27	0.28054531	-0.6	0.89995	3.6	3.7	3.5	3433
seq_20180315-115547\seq104.dat	125	Rim (124)	0.0163	13	0.00051	3	1.46717	1.88679	13	0.280594	26	0.280559738	-0.4	0.87657	3.6	3.7	3.4	3418
average 3.4			0.0226	18	0.00073	4	1.46719	1.88679	13	0.280617	22	0.280569246	0.5	0.88572	3.5	3.67	3.4	3440
seq_20180315-115547\seq107.dat	53		0.0184	15	0.00081	5	1.46724	1.88654	9	0.280512	17	0.280462286	-9.1	0.87839	3.9	4.01	3.7	3197

For legend and references, see page 244

Table 4.8, continued.

	Corresponding # of U-Pb analysis	Comment	$^{176}Yb/^{177}Hf$ [a]	±2σ	$^{176}Lu/^{177}Hf$ [a]	±2σ	$^{178}Hf/^{177}Hf$	$^{180}Hf/^{177}Hf$	Sig_{Hf} [b] (V)	$^{176}Hf/^{177}Hf$	±2σ [c]	$^{176}Hf/^{177}Hf_{(t)}$ [d]	εHf(t) [d]	±2σ [c]	Avg MORB [e] (Ga)	T_{DM2} [f] (Ga)	T_{DM2} [g] (Ga)	age [h] (Ma)
Sample MS 15																		
seq_20180315-115547\seq072.dat	74	Duplicate (73)	0.0107	9	0.00033	2	1.46722	1.88688	14	0.280585	17	0.280563881	-0.3	0.87104	3.6	3.7	3.4	3418
seq_20180315-115547\seq068.dat	2		0.0136	11	0.00043	3	1.46717	1.88687	11	0.280569	21	0.280540715	-1.5	0.87359	3.6	3.7	3.5	3401
seq_20180315-115547\seq069.dat	8		0.0173	14	0.00053	3	1.46718	1.88678	12	0.280590	18	0.280554773	-0.7	0.87824	3.6	3.7	3.4	3411
seq_20180315-115547\seq070.dat	58		0.0153	12	0.00046	3	1.46719	1.88671	11	0.280586	29	0.280555732	-0.5	0.87540	3.6	3.7	3.4	3420
seq_20180315-115547\seq071.dat	71		0.0182	15	0.00056	3	1.46718	1.88689	12	0.280584	17	0.280547437	-0.8	0.87884	3.6	3.7	3.5	3419
average 3.4			0.0150	12	0.00046	3	1.46719	1.88682	12	0.280583	21	0.280552359	-0.4	0.87519	3.6	3.71	3.4	3430
Sample MS 17																		
seq_20180315-115547\seq078.dat	32		0.0450	37	0.00135	8	1.46722	1.88691	12	0.280652	22	0.280562825	0.2	0.94169	3.5	3.7	3.4	3439
seq_20180315-115547\seq076.dat	14		0.0296	24	0.00093	6	1.46717	1.88680	13	0.280620	17	0.280559461	-0.4	0.89935	3.6	3.7	3.4	3420
seq_20180315-115547\seq077.dat	19		0.0352	28	0.00109	7	1.46724	1.88668	11	0.280643	15	0.280571935	-0.3	0.91178	3.5	3.7	3.4	3405
seq_20180315-115547\seq079.dat	30		0.0281	23	0.00093	6	1.46723	1.88666	13	0.280629	19	0.280568133	-0.3	0.89570	3.6	3.7	3.4	3408
seq_20180315-115547\seq081.dat	64		0.0408	33	0.00123	7	1.46719	1.88674	12	0.280642	21	0.280561535	-0.5	0.92713	3.6	3.7	3.4	3411
average 3.4			0.0357	29	0.00110	7	1.46721	1.88676	12	0.280638	19	0.28056499	-0.5	0.91371	3.6	3.69	3.4	3408
seq_20180315-115547\seq082.dat	52		0.0335	28	0.00108	7	1.46720	1.88683	11	0.280620	20	0.280550281	-1.9	0.91016	3.6	3.7	3.5	3371
seq_20180315-115547\seq073.dat	6		0.0321	26	0.00100	6	1.46725	1.88667	11	0.280661	16	0.280596429	-0.9	0.90467	3.5	3.7	3.4	3342
seq_20180315-115547\seq075.dat	12		0.0331	27	0.00103	6	1.46724	1.88676	13	0.280635	23	0.280568876	-1.7	0.90630	3.6	3.7	3.5	3350
seq_20180315-115547\seq074.dat	10		0.0383	45	0.00119	12	1.46720	1.88675	12	0.280645	18	0.280568742	-2.1	0.97755	3.6	3.7	3.5	3333
average 3.3			0.0342	31	0.00107	8	1.46722	1.88675	12	0.280640	20	0.280570926	-1.5	0.92170	3.6	3.71	3.4	3356
Sample MS 18																		
seq_20180315-115547\seq067.dat	6		0.0303	24	0.00095	6	1.46721	1.88678	13	0.280622	21	0.280558884	-0.3	0.89997	3.6	3.7	3.4	3424
seq_20180315-115547\seq063.dat	54		0.0263	21	0.00088	5	1.46724	1.88683	11	0.280595	19	0.280536454	-1.0	0.89202	3.6	3.7	3.5	3427
seq_20180315-115547\seq065.dat	47		0.0340	27	0.00106	6	1.46718	1.88688	13	0.280607	28	0.28053743	-1.4	0.90838	3.6	3.7	3.5	3410
seq_20180315-115547\seq064.dat	52		0.0363	29	0.00108	6	1.46720	1.88672	14	0.280645	19	0.280573737	-0.1	0.91420	3.5	3.7	3.4	3408
average 3.4			0.0317	25	0.00099	6	1.46720	1.88680	13	0.280617	22	0.280551559	-0.6	0.90318	3.6	3.71	3.4	3420
seq_20180315-115547\seq066.dat	33		0.0309	25	0.00098	6	1.46720	1.88677	12	0.280649	20	0.280585056	-0.1	0.90148	3.5	3.7	3.4	3393
seq_20180315-115547\seq062.dat	56		0.0445	36	0.00131	8	1.46717	1.88685	12	0.280611	19	0.280525985	-2.6	0.93691	3.7	3.8	3.5	3376
average 3.3			0.0377	30	0.00115	7	1.46718	1.88681	12	0.280630	20	0.280555596	-1.5	0.91776	3.6	3.73	3.5	3380
seq_20180315-115547\seq061.dat	61	90% conc.!	0.0330	30	0.00105	7	1.46723	1.88670	13	0.280630	23	0.280565272	-5.1	0.91596	3.7	3.80	3.5	3212
Sample MS 19																		
seq_20180315-115547\seq059.dat	7		0.0541	49	0.00174	13	1.46719	1.88679	20	0.280783	20	0.280675593	-1.2	0.99524	3.4	3.6	3.3	3212
seq_20180315-115547\seq060.dat	6	Duplicate (7)	0.0298	25	0.00093	6	1.46724	1.88691	12	0.280739	18	0.280681704	-1.0	0.90123	3.4	3.6	3.3	3210
average 3.2			0.0420	37	0.00133	9	1.46722	1.88685	16	0.280761	19	0.28067863	-1.1	0.94165	3.4	3.58	3.3	3212
Sample MS 20																		
seq_20180315-115547\seq058.dat	2		0.0425	43	0.00115	10	1.46723	1.88664	11	0.280721	21	0.280650123	-2.0	0.96783	3.5	3.63	3.4	3214

For legend and references, see page 244

Table 4.8, continued.

	Corresponding # of U-Pb analysis	Comment	$^{176}Yb/^{177}Hf$ [a]	±2σ	$^{176}Lu/^{177}Hf$ [a]	±2σ	$^{178}Hf/^{177}Hf$	$^{180}Hf/^{177}Hf$	Sig_{Hf} [b] (V)	$^{176}Hf/^{177}Hf$	±2σ [c]	$^{176}Hf/^{177}Hf_{(t)}$ [d]	εHf(t) [d]	±2σ [c]	Avg MORB [e] (Ga)	T_{DM2} [f] (Ga)	T_{DM2} [g] (Ga)	age [h] (Ma)
Sample MS 25																		
seq_20180315-115547\seq036.dat	25	Duplicate (27)	0.0192	16	0.00065	4	1.46716	1.88683	9	0.280698	17	0.280654522	3.7	0.88152	3.4	3.5	3.2	3450
seq_20180315-115547\seq033.dat	32	Duplicate (33)	0.0379	30	0.00116	7	1.46725	1.88691	7	0.280738	21	0.280661111	4.0	0.91871	3.3	3.5	3.2	3450
seq_20180315-115547\seq026.dat	53	Duplicate (54)	0.0084	7	0.00028	2	1.46709	1.88694	5	0.280674	27	0.280655386	3.8	0.86974	3.4	3.5	3.2	3450
seq_20180315-115547\seq028.dat	55	Duplicate (56)	0.0416	33	0.00120	7	1.46721	1.88688	9	0.280724	21	0.280644438	3.4	0.92887	3.4	3.5	3.2	3450
seq_20180315-115547\seq042.dat	5	Duplicate (6)	0.0227	18	0.00072	4	1.46724	1.88685	9	0.280697	20	0.280649492	3.6	0.88613	3.4	3.5	3.2	3450
seq_20180315-115547\seq020.dat	57	Duplicate (60)	0.0018	1	0.00009	1	1.46721	1.88678	12	0.280668	24	0.280662256	4.0	0.86729	3.3	3.5	3.2	3450
seq_20180315-115547\seq022.dat	63	Duplicate (62)	0.0028	2	0.00011	1	1.46721	1.88689	14	0.280662	26	0.280654429	3.7	0.86743	3.4	3.5	3.2	3450
seq_20180315-115547\seq044.dat	86	Duplicate (84)	0.0287	31	0.00096	9	1.46730	1.88672	5	0.280726	19	0.280662271	4.0	0.92106	3.3	3.5	3.2	3450
seq_20180315-115547\seq041.dat	6		0.0265	30	0.00084	8	1.46721	1.88684	11	0.280700	17	0.28064802	-2.0	0.91793	3.5	3.6	3.4	3219
seq_20180315-115547\seq043.dat	9		0.0121	12	0.00043	3	1.46727	1.88691	10	0.280668	18	0.280641631	-2.1	0.87436	3.5	3.6	3.4	3225
seq_20180315-115547\seq039.dat	11		0.0163	18	0.00054	5	1.46711	1.88658	7	0.280699	21	0.280664963	-1.2	0.88433	3.5	3.6	3.3	3225
seq_20180315-115547\seq038.dat	21		0.0112	9	0.00039	2	1.46719	1.88680	10	0.280693	17	0.280668398	-1.2	0.87148	3.4	3.6	3.3	3221
seq_20180315-115547\seq037.dat	24		0.0126	10	0.00042	3	1.46722	1.88669	10	0.280703	24	0.280677333	-0.8	0.87301	3.4	3.6	3.3	3226
seq_20180315-115547\seq035.dat	27		0.0433	35	0.00134	8	1.46713	1.88680	9	0.280742	22	0.28065852	-1.4	0.93348	3.5	3.6	3.3	3229
seq_20180315-115547\seq032.dat	36		0.0227	18	0.00073	4	1.46719	1.88658	10	0.280695	17	0.280650251	-2.2	0.88546	3.5	3.6	3.4	3207
seq_20180315-115547\seq031.dat	38		0.0162	13	0.00053	3	1.46725	1.88683	10	0.280700	18	0.280667124	-1.2	0.87632	3.5	3.6	3.3	3223
seq_20180315-115547\seq030.dat	40		0.0206	17	0.00068	4	1.46724	1.88667	12	0.280700	23	0.280657999	-2.0	0.88228	3.5	3.6	3.4	3204
seq_20180315-115547\seq025.dat	45		0.0201	16	0.00066	4	1.46715	1.88683	9	0.280704	24	0.280663523	-1.8	0.88151	3.5	3.6	3.3	3205
seq_20180315-115547\seq027.dat	54		0.0141	11	0.00045	3	1.46727	1.88680	9	0.280676	26	0.280648174	-1.9	0.87408	3.5	3.6	3.4	3224
seq_20180315-115547\seq029.dat	56		0.0373	30	0.00108	6	1.46721	1.88681	10	0.280708	25	0.280640969	-2.3	0.91671	3.5	3.6	3.4	3217
seq_20180315-115547\seq019.dat	60		0.0325	26	0.00102	6	1.46720	1.88675	9	0.280739	25	0.280675551	-1.1	0.90497	3.4	3.6	3.3	3213
seq_20180315-115547\seq021.dat	62		0.0033	3	0.00012	1	1.46721	1.88662	11	0.280685	21	0.280677103	-1.1	0.86713	3.4	3.6	3.3	3213
seq_20180315-115547\seq023.dat	68		0.0106	9	0.00035	2	1.46719	1.88685	9	0.280684	20	0.280662494	-1.4	0.87088	3.5	3.6	3.3	3224
seq_20180315-115547\seq024.dat	74		0.0150	12	0.00047	3	1.46718	1.88681	9	0.280691	21	0.280662302	-1.3	0.87502	3.5	3.6	3.3	3225
seq_20180315-115547\seq045.dat	84		0.0209	26	0.00069	8	1.46722	1.88672	10	0.280714	20	0.280671725	-1.2	0.90424	3.4	3.6	3.3	3217
seq_20180315-115547\seq040.dat	92		0.0126	10	0.00042	3	1.46724	1.88684	9	0.280685	19	0.280659067	-1.7	0.87279	3.5	3.6	3.3	3216
seq_20180315-115547\seq034.dat	96		0.0088	7	0.00030	2	1.46720	1.88689	11	0.280678	18	0.280659359	-1.3	0.86959	3.5	3.6	3.3	3230
average			0.0188	16	0.00060	4	1.46720	1.88677	10	0.280698	21	0.280660711	-1.4	0.88202	3.5	3.61	3.3	3223
Sample MS 26																		
seq_20180315-115547\seq116.dat	44		0.0144	12	0.00045	3	1.46719	1.88681	13	0.280604	26	0.28057423	0.8	0.87580	3.5	3.7	3.4	3447
seq_20180315-115547\seq114.dat	9		0.0231	19	0.00070	4	1.46713	1.88675	13	0.280615	25	0.280568624	0.4	0.88749	3.5	3.7	3.4	3439
seq_20180315-115547\seq117.dat	65		0.0208	17	0.00066	4	1.46719	1.88672	11	0.280602	17	0.280558527	-0.3	0.88347	3.6	3.7	3.4	3425
seq_20180315-115547\seq118.dat	51		0.0244	23	0.00084	5	1.46741	1.88660	5	0.280559	17	0.280503231	-2.1	0.89556	3.7	3.8	3.5	3430
average 3.4			0.0194	16	0.00061	4	1.46717	1.88676	12	0.280607	23	0.280567078	0.4	0.88184	3.5	3.67	3.4	3440
seq_20180315-115547\seq119.dat	53	90% conc.!	0.0272	24	0.00082	6	1.46714	1.88679	12	0.280618	15	0.280566553	-4.2	0.89785	3.6	3.78	3.5	3248
seq_20180315-115547\seq115.dat	35		0.0211	17	0.00065	4	1.46720	1.88677	13	0.280587	17	0.280545051	-1.6	0.88317	3.6	3.74	3.5	3388
Sample MS 27																		
seq_20180315-115547\seq098.dat	31		0.0417	33	0.00149	9	1.46717	1.88684	10	0.280701	18	0.280601772	1.6	0.92898	3.5	3.6	3.3	3439
seq_20180315-115547\seq100.dat	61		0.0317	25	0.00113	7	1.46716	1.88675	12	0.280666	22	0.280591204	1.0	0.90319	3.5	3.6	3.4	3431
seq_20180315-115547\seq096.dat	20		0.0359	29	0.00129	8	1.46719	1.88664	14	0.280672	18	0.280587451	0.7	0.91337	3.5	3.6	3.4	3424
seq_20180315-115547\seq099.dat	55		0.0347	28	0.00114	7	1.46721	1.88690	13	0.280643	24	0.280567516	0.3	0.91012	3.5	3.7	3.4	3434
seq_20180315-115547\seq101.dat	77		0.0404	32	0.00140	8	1.46715	1.88675	9	0.280689	19	0.280596664	1.3	0.92537	3.5	3.6	3.3	3433
seq_20180315-115547\seq102.dat	80		0.0267	22	0.00096	6	1.46718	1.88669	10	0.280655	24	0.28059131	1.2	0.89429	3.5	3.6	3.4	3436
seq_20180315-115547\seq095.dat	12		0.0262	25	0.00093	7	1.46718	1.88679	12	0.280652	19	0.28059	1.1	0.90093	3.5	3.6	3.4	3437
average 3.4			0.0339	28	0.00119	7	1.46718	1.88677	12	0.280668	20	0.280589283	1.2	0.91017	3.5	3.63	3.4	3439
seq_20180315-115547\seq097.dat	41		0.0633	51	0.00225	13	1.46718	1.88669	13	0.280723	22	0.28057651	-0.8	1.00378	3.6	3.69	3.4	3377

For legend and references, see page 244

Table 4.8, continued.

	Corresponding # of U-Pb analysis	Comment	$^{176}Yb/^{177}Hf$ [a]	±2σ	$^{176}Lu/^{177}Hf$ [a]	±2σ	$^{178}Hf/^{177}Hf$	$^{180}Hf/^{177}Hf$	Sig_{Hf} [b] (V)	$^{176}Hf/^{177}Hf$	±2σ [c]	$^{176}Hf/^{177}Hf_{(t)}$ [d]	εHf(t) [d]	±2σ [c]	Avg MORB [e] (Ga)	T_{DM2} [f] (Ga)	T_{DM2} [g] (Ga)	age [h] (Ma)
Sample ST J26																		
seq_20180315-115547\seq113.dat	37		0.0379	31	0.00111	7	1.46721	1.88672	13	0.280617	23	0.280542941	0.0	0.91946	3.6	3.7	3.4	3461
seq_20180315-115547\seq112.dat	33		0.0150	16	0.00048	4	1.46721	1.88658	11	0.280596	18	0.280564997	0.2	0.88145	3.5	3.7	3.4	3435
seq_20180315-115547\seq110.dat	8		0.0432	35	0.00122	7	1.46711	1.88650	12	0.280637	19	0.280556202	-0.4	0.93335	3.6	3.7	3.4	3423
seq_20180315-115547\seq111.dat	28		0.0190	15	0.00059	4	1.46721	1.88662	11	0.280610	21	0.2805703	0.2	0.88027	3.5	3.7	3.4	3427
seq_20180315-115547\seq109.dat	5		0.0211	19	0.00063	4	1.46716	1.88678	12	0.280607	18	0.280565269	-0.6	0.88705	3.6	3.70	3.4	3400
average 3.4			0.0272	23	0.00081	5	1.46718	1.88664	12	0.280613	20	0.280559795	0.2	0.89706	3.6	3.69	3.4	3441
Reference Materials:																		
seq_20180315-115547\seq009.dat			0.0058	5	0.00016	1	1.46720	1.88675	14	0.281662	19	0.281660697	-27.30447	0.86570	2.7	2.9	2.7	560
seq_20180315-115547\seq010.dat			0.0054	4	0.00015	1	1.46721	1.88681	14	0.281655	20	0.281653787	-27.54914	0.86557	2.7	2.9	2.7	560
seq_20180315-115547\seq011.dat			0.0054	4	0.00015	1	1.46722	1.88665	14	0.281667	17	0.28166542	-27.13726	0.86560	2.7	2.9	2.7	560
seq_20180315-115547\seq012.dat			0.0055	4	0.00015	1	1.46721	1.88684	14	0.281646	19	0.281644569	-27.87552	0.86556	2.7	2.9	2.7	560
seq_20180315-115547\seq013.dat			0.0055	4	0.00015	1	1.46720	1.88688	14	0.281653	23	0.281651051	-27.64600	0.86555	2.7	2.9	2.7	560
seq_20180315-115547\seq050.dat			0.0053	5	0.00015	1	1.46720	1.88682	11	0.281671	17	0.281669533	-26.99164	0.86596	2.7	2.9	2.6	560
seq_20180315-115547\seq051.dat			0.0054	4	0.00015	1	1.46715	1.88681	13	0.281660	16	0.281658923	-27.36728	0.86555	2.7	2.9	2.7	560
seq_20180315-115547\seq052.dat			0.0053	5	0.00015	1	1.46725	1.88689	12	0.281672	18	0.281670634	-26.95265	0.86617	2.7	2.9	2.6	560
seq_20180315-115547\seq053.dat			0.0054	4	0.00015	1	1.46719	1.88681	12	0.281663	21	0.281661612	-27.27208	0.86553	2.7	2.9	2.7	560
seq_20180315-115547\seq087.dat			0.0054	5	0.00015	1	1.46718	1.88665	13	0.281674	16	0.281672881	-26.87310	0.86573	2.7	2.9	2.6	560
seq_20180315-115547\seq088.dat			0.0057	5	0.00015	1	1.46720	1.88684	13	0.281685	16	0.281683246	-26.50610	0.86609	2.6	2.9	2.6	560
seq_20180315-115547\seq089.dat			0.0056	5	0.00015	1	1.46719	1.88663	11	0.281683	22	0.281680992	-26.58591	0.86569	2.7	2.9	2.6	560
seq_20180315-115547\seq090.dat			0.0056	5	0.00015	1	1.46719	1.88690	12	0.281677	21	0.281675479	-26.78108	0.86589	2.7	2.9	2.6	560
seq_20180315-115547\seq124.dat			0.0053	4	0.00015	1	1.46710	1.88673	12	0.281669	20	0.281667284	-27.07125	0.86562	2.7	2.9	2.6	560
seq_20180315-115547\seq125.dat			0.0055	6	0.00015	1	1.46713	1.88678	13	0.281698	20	0.281696109	-26.05065	0.86656	2.6	2.9	2.6	560
seq_20180315-115547\seq126.dat			0.0054	5	0.00015	1	1.46713	1.88680	12	0.281686	22	0.281684659	-26.45607	0.86569	2.6	2.9	2.6	560
seq_20180315-115547\seq127.dat			0.0054	4	0.00015	1	1.46716	1.88682	13	0.281676	19	0.281674244	-26.82481	0.86555	2.7	2.9	2.6	560
seq_20180315-115547\seq165.dat			0.0055	4	0.00015	1	1.46678	1.88675	12	0.281664	23	0.281662558	-27.23857	0.86560	2.7	2.9	2.7	560
seq_20180315-115547\seq166.dat			0.0053	4	0.00014	1	1.46683	1.88683	12	0.281681	22	0.281679747	-26.62998	0.86558	2.7	2.9	2.6	560
seq_20180315-115547\seq167.dat			0.0055	4	0.00015	1	1.46686	1.88690	13	0.281668	24	0.281666021	-27.11598	0.86557	2.7	2.9	2.7	560
seq_20180315-115547\seq168.dat			0.0054	4	0.00015	1	1.46690	1.88673	13	0.281669	21	0.281667019	-27.08063	0.86557	2.7	2.9	2.6	560
BB (560Ma): 176Hf/177Hf=0.281674±0.0000028; Santos et al. (2017)									Average:	**0.281670**								
seq_20180315-115547\seq014.dat			0.0076	8	0.00025	2	1.46729	1.88689	9	0.281990	17	0.281987205	-14.80223	0.86940	2.1	2.3	2.0	602
seq_20180315-115547\seq015.dat			0.0076	6	0.00025	2	1.46722	1.88678	9	0.281987	20	0.281983872	-14.92025	0.86770	2.1	2.3	2.0	602
seq_20180315-115547\seq016.dat			0.0076	8	0.00025	2	1.46726	1.88673	9	0.282018	21	0.282015007	-13.81775	0.86908	2.0	2.2	2.0	602
seq_20180315-115547\seq018.dat			0.0076	6	0.00025	1	1.46722	1.88676	8	0.282008	21	0.282004823	-14.17839	0.86770	2.0	2.2	2.0	602
seq_20180315-115547\seq054.dat			0.0079	6	0.00025	2	1.46721	1.88678	10	0.282017	18	0.282014615	-13.83166	0.86805	2.0	2.2	2.0	602
seq_20180315-115547\seq057.dat			0.0077	13	0.00025	4	1.46718	1.88681	9	0.281993	13	0.281989839	-14.70896	0.87471	2.0	2.3	2.0	602
seq_20180315-115547\seq092.dat			0.0077	6	0.00025	2	1.46713	1.88686	9	0.282009	15	0.282005807	-14.14355	0.86796	2.0	2.2	2.0	602
seq_20180315-115547\seq093.dat			0.0077	7	0.00025	2	1.46717	1.88687	9	0.282016	18	0.282012863	-13.89367	0.86820	2.0	2.2	2.0	602
seq_20180315-115547\seq129.dat			0.0077	9	0.00024	2	1.46715	1.88683	9	0.282008	21	0.282005114	-14.16809	0.87020	2.0	2.2	2.0	602
seq_20180315-115547\seq130.dat			0.0077	7	0.00025	2	1.46716	1.88677	9	0.281972	28	0.281969338	-15.43489	0.86803	2.1	2.3	2.1	602
seq_20180315-115547\seq131.dat			0.0078	7	0.00025	2	1.46711	1.88673	9	0.282006	23	0.282003654	-14.21976	0.86802	2.0	2.2	2.0	602
seq_20180315-115547\seq169.dat			0.0078	7	0.00025	2	1.46691	1.88665	9	0.282035	18	0.282032493	-13.19857	0.86848	2.0	2.2	1.9	602
Gj-1(602Ma): 176Hf/177Hf=0.2820000±0.0000005; Morel et al. (2008)									Average:	**0.282005**								

For legend and references, see page 244

Table 4.8, continued.

Corresponding # of U-Pb analysis	Comment	$^{176}Yb/^{177}Hf$ [a]	±2σ	$^{176}Lu/^{177}Hf$ [a]	±2σ	$^{178}Hf/^{177}Hf$	$^{180}Hf/^{177}Hf$	Sig_{Hf} [b] (V)	$^{176}Hf/^{177}Hf$	±2σ [c]	$^{176}Hf/^{177}Hf_{(t)}$ [d]	εHf(t) [d]	±2σ [c]	Avg MORB [e] (Ga)	T_{DM2} [f] (Ga)	T_{DM2} [g] (Ga)	age [h] (Ma)
seq_20180315-115547\seq004.dat		0.0011	1	0.00003	0	1.46720	1.88682	12	0.282476	19	0.282476013	5.43200	0.86734	1.0	1.3	1.0	732
seq_20180315-115547\seq005.dat		0.0012	1	0.00003	0	1.46720	1.88678	13	0.282498	24	0.282497898	6.20717	0.86741	1.0	1.2	1.0	732
seq_20180315-115547\seq006.dat		0.0012	1	0.00003	0	1.46721	1.88681	13	0.282486	19	0.282485915	5.78274	0.86737	1.0	1.3	1.0	732
seq_20180315-115547\seq007.dat		0.0012	1	0.00003	0	1.46722	1.88675	13	0.282497	24	0.28249706	6.17750	0.86741	1.0	1.2	1.0	732
seq_20180315-115547\seq008.dat		0.0012	1	0.00003	0	1.46721	1.88663	13	0.282504	23	0.282503614	6.40963	0.86743	1.0	1.2	1.0	732
seq_20180315-115547\seq046.dat		0.0012	1	0.00003	0	1.46722	1.88678	14	0.282494	20	0.282493576	6.05408	0.86744	1.0	1.2	1.0	732
seq_20180315-115547\seq047.dat		0.0013	1	0.00003	0	1.46716	1.88674	12	0.282492	22	0.282491199	5.96989	0.86740	1.0	1.2	1.0	732
seq_20180315-115547\seq048.dat		0.0012	1	0.00003	0	1.46720	1.88681	12	0.282488	13	0.282487945	5.85464	0.86738	1.0	1.3	1.0	732
seq_20180315-115547\seq049.dat		0.0011	1	0.00003	0	1.46716	1.88680	13	0.282485	18	0.282485005	5.75050	0.86738	1.0	1.3	1.0	732
seq_20180315-115547\seq083.dat		0.0012	1	0.00003	0	1.46717	1.88678	14	0.282512	16	0.282511352	6.68372	0.86748	1.0	1.2	0.9	732
seq_20180315-115547\seq084.dat		0.0012	2	0.00003	0	1.46720	1.88682	13	0.282504	22	0.282503251	6.39679	0.86755	1.0	1.2	1.0	732
seq_20180315-115547\seq085.dat		0.0012	1	0.00003	0	1.46721	1.88686	14	0.282504	25	0.282503919	6.42043	0.86748	1.0	1.2	1.0	732
seq_20180315-115547\seq086.dat		0.0012	1	0.00003	0	1.46719	1.88671	13	0.282521	20	0.28252065	7.01306	0.86749	1.0	1.2	0.9	732
seq_20180315-115547\seq120.dat		0.0012	1	0.00003	0	1.46716	1.88672	13	0.282537	21	0.282537028	7.59319	0.86754	0.9	1.2	0.9	732
seq_20180315-115547\seq121.dat		0.0011	1	0.00003	0	1.46713	1.88679	13	0.282515	20	0.28251509	6.81610	0.86746	1.0	1.2	0.9	732
seq_20180315-115547\seq122.dat		0.0011	1	0.00003	0	1.46718	1.88674	13	0.282520	21	0.282519628	6.97685	0.86747	1.0	1.2	0.9	732
seq_20180315-115547\seq123.dat		0.0012	1	0.00003	0	1.46717	1.88686	13	0.282510	14	0.282509841	6.63021	0.86746	1.0	1.2	0.9	732
seq_20180315-115547\seq161.dat		0.0013	1	0.00003	0	1.46707	1.88676	15	0.282505	15	0.282504964	6.45746	0.86744	1.0	1.2	1.0	732
seq_20180315-115547\seq162.dat		0.0012	1	0.00003	0	1.46699	1.88671	15	0.282488	18	0.28248768	5.84526	0.86738	1.0	1.3	1.0	732
seq_20180315-115547\seq163.dat		0.0012	1	0.00003	0	1.46699	1.88678	15	0.282511	15	0.2825105	6.65355	0.86745	1.0	1.2	0.9	732
seq_20180315-115547\seq164.dat		0.0013	1	0.00003	0	1.46694	1.88676	15	0.282514	15	0.282513407	6.75651	0.86747	1.0	1.2	0.9	732
Mudtank(732Ma): 176Hf/177Hf = **0.282507 ± 0.000006 Woodhead and Hergt 2005**								Average:	**0.282503**								
seq_20180315-115547\seq001.dat		0.0217	18	0.00080	4.8	1.46718	1.88686	17	0.282680	15	0.282673705	5.35586	0.43668	0.8	1.0	0.8	417
seq_20180315-115547\seq002.dat		0.0210	18	0.00076	4.8	1.46721	1.88691	32	0.282649	19	0.282642883	4.26490	0.43712	0.9	1.1	0.8	417
seq_20180315-115547\seq003.dat		0.0256	12	0.00167	1.1	1.46723	1.88694	19	0.282685	11	0.282672026	5.29644	0.54789	0.8	1.0	0.8	416
seq_20180315-115547\seq166.dat		0.0494	10	0.00119	4.2	1.46296	1.88195	17	0.282701	98	0.282691295	5.95609	0.10306	0.8	1.0	0.7	416
seq_20180315-115547\seq169.dat		0.0201	16	0.00064	4.0	1.46726	1.88675	19	0.282657	18	0.28265201	4.56557	0.16007	0.8	1.1	0.8	416
seq_20180315-115547\seq171.dat		0.0148	16	0.00062	5.0	1.46721	1.88678	16	0.282674	22	0.282669166	5.17281	0.16008	0.8	1.0	0.8	416
seq_20180315-115547\seq172.dat		0.0233	19	0.00085	5.0	1.46526	1.88874	15	0.282703	16	0.282696373	6.13580	0.19012	0.7	1.0	0.7	416
Temora (416 Ma): 176Hf/177Hf=0.282686 ±0.000007 Woodhead et al. (2004)								Average:	**0.282678**								

Quoted uncertainties (absolute) relate to the last quoted figure. The effect of the inter-element fractionation on the Lu/Hf was estimated to be about 6 % or less based on analyses of the GJ-1 zircon. Accuracy and reproducibilty was checked by repeated analyses of reference zircon GJ-1 (data given as mean with 2 standard deviation uncertainties)

a: $^{176}Yb/^{177}Hf = (^{176}Yb/^{173}Yb)_{true} \times (^{173}Yb/^{177}Hf)_{meas} \times (M_{173(Yb)}/M_{177(Hf)})^{b(Hf)}$, $b(Hf) = \ln(^{179}Hf/^{177}Hf_{true} / {}^{179}Hf/^{177}Hf_{meas}) / \ln(M_{179(Hf)}/M_{177(Hf)})$, M=mass of respective isotope. The $^{176}Lu/^{177}Hf$ were calculated in a similar way by using the $^{175}Lu/^{177}Hf$ and b(Yb);

b: Mean Hf signal in volt;

c: Uncertainties are quadratic additions of the within-run precision and the daily reproducibility of the zircon standards;

d: Initial $^{176}Hf/^{177}Hf$ and ε_{Hf} calculated using the apparent U-Pb age determined by LA-ICP-MS dating (see column f), and the CHUR parameters: $^{176}Lu/^{177}Hf = 0.0336$, and $^{176}Hf/^{177}Hf = 0.282785$ (Bouvier et al., 2008);

e: Avg MORB - Chauvel et al. 2008

f: BLIC TDM - Blichert-Toft & Albarède 2008

g: NC TDM - Dhuime et al. (2011)

h: Apparent U-Pb age determined by LA-ICP-MS;

Blichert-Toft J. & Albarède F. 2008. Hafnium isotopes in Jack Hills zircons and the formation of the Hadean crust. Earth Planet. Sci. Lett. 265: 686-702.

Bouvier A., Vervoort J.D., Patchett P.J. 2008. The Lu-Hf and Sm-Nd isotopic composition of CHUR: Constraints from unequilibrated chondrites and implications for the bulk composition of terrestrial planets. Earth Planet. Sci. Lett. 273: 48-57.

Chauvel C., Lewin E., Carpentier M., Arndt N.T., Marini, J.-C. 2008. Role of recycled oceanic basalt and sediment in generating the Hf-Nd mantle array. Nature Geoscience 1: 64-67.

Dhuime B., Hawkesworth C., Cawood P. 2011. When Continents Formed. Science 311: 154-155.

Morel M.L.A., Nebel O., Nebel-Jacobsen Y.J., Miller J.S., Vroon P.Z. 2008. Hafnium isotope characterization of the GJ-1 zircon reference material by solution and laser-ablation MC-ICPMS. Chem. Geol., 255: 231-235.

Santos, M.M.; Lana, C.; Scholz, R.; Buick, I.; Schmitz, M.D.; Kamo, S.L.; Gerdes, A.; Corfu, F.; Tapster, S.; Lancaster, P.; et al. A New Appraisal of Sri Lankan BB Zircon as a Reference Material for LA-ICP-MS U–Pb Geochronology and Lu–Hf Isotope Tracing. Geostand. Geoanal. Res. 2017, 41, 335–358.

Woodhead J.D., Hergt J.M., Shelley M., Eggins S., Kemp R. 2004. Zircon Hf-isotope analysis with an excimer laser, depth profiling, ablation of complex geometries and concomitant age estimation. Chem. Geol., 209: 121-135.

Woodhead J.D. & Hergt J.M. 2005. Preliminary appraisal of seven natural zircon reference materials for in situ Hf isotope determination. Geostand. Geoanal. Res., 29: 183–195.

Table 4.9. Apatite U-Pb isotope data

	Ub (ppm)	Th[b] U	^{202}Hg	^{204}Hg raw counts (CPS)	^{204}Pb	^{206}Pb	^{238}U	^{206}Pb[a] (cps)	^{238}U[a] (cps)	^{207}Pb[a] (cps)	^{206}Pb[c] / ^{204}Pb	206Pbc[c] (%)	206Pb[d] 238U	±2s[f] (%)	207Pbd 235U	±2s[f] (%)	207Pbd 206Pb	±2s[f] (%)	rho[e]	206Pb 238U	±2s[f] (Ma)	207Pb 235U	±2s[f] (Ma)	207Pb 206Pb	±2s[f] (Ma)	disc (%)
MS 2: Stolzburg Main Trondhjemite																										
Run number: 19	2	5	10919	2535	393	19028	25716	14555	25327	3680	140	31	0.575	7.6	20.032	8.1	0.253	2.7	0.9	2927	181	3093	81	3202	43	91
Run number: 20	4	3	7616	1768	383	25533	40044	20782	39438	4180	212	23	0.527	3.4	14.614	4.2	0.201	2.5	0.8	2729	76	2790	41	2835	41	96
Run number: 22	3	4	9320	2164	355	18693	24551	14726	24179	3738	150	27	0.609	5.6	21.315	6.2	0.254	2.6	0.9	3066	138	3153	62	3209	41	96
Run number: 25	3	3	8034	1865	402	25630	41378	20570	40752	4073	209	25	0.505	4.0	13.780	4.7	0.198	2.6	0.8	2634	86	2735	46	2810	42	94
Run number: 27	3	3	8174	1898	291	18511	27575	14998	27158	3923	140	23	0.552	4.2	19.917	4.8	0.262	2.4	0.9	2835	98	3087	48	3256	37	87
Run number: 30	3	5	8885	2063	376	20369	27013	16146	26604	4069	166	26	0.607	4.7	21.090	5.3	0.252	2.5	0.9	3058	115	3143	53	3198	40	96
Run number: 31	1	1	24281	5638	814	11338	4783	7476	4710	2965	126	52	1.587	9.3	86.788	9.9	0.397	3.4	0.9	6128	378	4544	104	3896	51	157
Run number: 32	2	1	12996	3018	442	14622	14792	10676	14568	3133	118	37	0.733	10.1	29.653	10.5	0.293	3.0	1.0	3544	282	3475	109	3436	47	103
Run number: 33	2	3	12838	2981	416	20171	35237	14744	34704	2916	130	37	0.425	12.9	11.586	13.3	0.198	3.2	1.0	2283	253	2572	133	2808	53	81
Run number: 36	2	4	10542	2448	369	18025	24365	13823	23996	3480	137	30	0.576	8.9	19.995	9.3	0.252	2.8	1.0	2933	213	3091	94	3196	44	92
Run number: 37	3	5	8091	1879	347	20107	26504	16224	26102	4118	169	24	0.622	4.4	21.754	5.0	0.254	2.4	0.9	3116	109	3173	50	3209	38	97
Run number: 38	4	5	7027	1632	315	20267	26531	16751	26129	4238	180	21	0.641	3.9	22.366	4.5	0.253	2.2	0.9	3193	99	3200	45	3204	35	100
Run number: 40	4	4	7382	1714	301	20308	31261	16614	30788	4266	158	22	0.540	3.0	19.106	3.8	0.257	2.3	0.8	2782	68	3047	37	3227	36	86
Run number: 41	1	0	18745	4353	286	10628	16187	7131	15942	2813	46	49	0.447	28.3	24.326	28.5	0.394	3.2	1.0	2383	591	3282	325	3888	49	61
Run number: 42	2	5	10862	2522	393	19079	25350	14659	24966	3734	140	30	0.587	6.3	20.622	6.8	0.255	2.7	0.9	2978	151	3121	68	3214	43	93
Run number: 43	3	4	10269	2384	448	25234	41395	19558	40769	3835	181	29	0.480	4.9	12.969	5.6	0.196	2.8	0.9	2526	103	2677	54	2794	46	90
Run number: 44	4	3	8684	2016	435	27475	44330	22005	43659	4341	209	25	0.504	3.7	13.711	4.5	0.197	2.6	0.8	2631	80	2730	44	2804	42	94
Run number: 45	3	5	10609	2463	510	27658	45433	21195	44745	4236	192	30	0.474	6.2	13.052	6.8	0.200	2.9	0.9	2500	129	2683	66	2825	47	88
Run number: 46	3	4	9661	2243	420	22559	31458	17678	30982	4235	171	28	0.571	4.2	18.846	4.9	0.240	2.6	0.8	2910	99	3034	49	3117	41	93
Run number: 48	4	3	10924	2536	395	18723	24564	14312	24192	3709	139	31	0.592	16.4	21.141	16.6	0.259	2.7	1.0	2996	406	3145	176	3242	42	92
Run number: 49	3	5	8348	1938	394	22582	31036	18045	30566	4300	187	25	0.590	4.1	19.395	4.8	0.238	2.5	0.9	2991	99	3062	47	3108	40	96
Run number: 50	2	4	10409	2417	463	21325	30565	15865	30102	3764	167	34	0.527	7.6	17.242	8.1	0.237	2.9	0.9	2729	171	2948	81	3102	47	88
Run number: 69	3	4	6885	1599	239	15788	23542	12897	23185	3359	138	22	0.556	6.3	19.973	6.7	0.260	2.3	0.9	2851	147	3090	67	3249	37	88
Run number: 72	2	4	9377	2177	349	18612	30732	14171	30267	3386	140	31	0.468	6.3	15.425	6.8	0.239	2.7	0.9	2476	130	2842	67	3113	44	80
Run number: 74	2	5	8967	2082	255	12983	17728	10061	17459	2970	106	29	0.576	8.4	23.454	8.8	0.295	2.6	1.0	2933	202	3246	90	3445	41	85
Run number: 76	3	4	6612	1535	276	19169	31880	15645	31397	3542	168	23	0.498	4.3	15.553	4.9	0.226	2.4	0.9	2606	93	2850	48	3027	39	86
Run number: 77	2	5	10351	2403	421	22372	44870	16571	44190	3288	150	35	0.375	13.3	10.260	13.6	0.198	3.1	1.0	2053	238	2459	135	2813	50	73
Run number: 78	3	4	6511	1512	263	17656	26611	14458	26208	3664	159	22	0.552	3.9	19.278	4.6	0.253	2.5	0.8	2832	89	3056	46	3206	40	88
Run number: 79	2	2	10457	2428	269	13717	21682	10365	21354	3074	92	32	0.485	13.9	19.846	14.1	0.297	2.7	1.0	2551	299	3084	147	3452	42	74
Run number: 80	3	2	5925	1376	242	18111	27486	15162	27070	3826	163	19	0.560	4.1	19.487	4.6	0.252	2.2	0.9	2867	94	3066	45	3199	34	90
Run number: 81	2	4	8197	1903	372	20921	39045	15941	38454	3231	172	31	0.415	11.2	11.586	11.5	0.203	2.9	1.0	2236	215	2572	114	2848	47	78
Run number: 82	1	2	10524	2444	622	18737	17659	13628	17392	2891	213	37	0.784	12.9	22.919	13.5	0.212	4.0	1.0	3730	376	3223	141	2922	65	128
Run number: 83	3	3	7128	1655	286	19035	30587	15449	30124	3631	160	23	0.513	5.5	16.621	6.0	0.235	2.4	0.9	2669	122	2913	60	3087	39	86
Run number: 84	2	4	10391	2413	281	12511	15924	9443	15683	3025	97	32	0.602	9.3	26.594	9.7	0.320	2.7	1.0	3038	229	3369	99	3571	41	85
Run number: 85	2	3	8014	1861	271	16944	28315	13474	27886	3206	133	26	0.483	7.8	15.853	8.2	0.238	2.6	1.0	2541	167	2868	82	3106	41	82
Run number: 86	2	4	8377	1945	289	16734	26625	13120	26222	3189	135	28	0.500	8.1	16.770	8.6	0.243	2.6	1.0	2615	178	2922	86	3140	42	83
Run number: 87	2	5	9552	2218	295	15426	24523	11750	24151	2968	117	31	0.487	10.5	16.942	10.9	0.253	2.8	1.0	2556	226	2932	110	3201	45	80
Run number: 88	3	5	5593	1299	233	18153	27532	15318	27115	3883	167	19	0.565	4.3	19.744	4.8	0.253	2.1	0.9	2887	101	3079	47	3207	33	90
Run number: 89	2	4	8814	2047	242	14425	24018	11335	23654	3224	101	27	0.479	10.1	18.790	10.4	0.284	2.5	1.0	2524	215	3031	106	3387	39	75
Run number: 90	3	3	2294	533	94	12188	12302	11354	12116	3953	153	7	0.937	4.4	44.991	4.6	0.348	1.3	1.0	4262	140	3887	47	3699	20	115
Run number: 91	5	6	4118	956	376	30569	43567	26146	42907	5506	350	17	0.609	3.1	17.693	3.8	0.211	2.1	0.8	3067	76	2973	37	2910	35	105
Run number: 92	3	2	4626	1074	226	17528	20160	15241	19855	4234	193	15	0.768	3.8	29.406	4.2	0.278	1.8	0.9	3672	108	3467	42	3351	28	110
Run number: 93	0	3	4753	1104	225	18952	25159	16421	24778	4559	186	15	0.663	4.3	25.371	4.7	0.278	1.9	0.9	3278	112	3323	47	3350	29	98

^{207}Pb /^{235}U error is the quadratic addition of the ^{207}Pb/^{206}Pb and ^{206}Pb /^{238}U uncertainty.

[a] Within run background-corrected mean signal in cps (counts per second).

[b] U content and Th/U ratio were calculated relative to reference

[c] Pb 206/204 ratios measured and percentage of common Pb on the ^{206}Pb. b.d. = below dectection limit.

[d] corrected for background, within-run Pb/U fractionation (in case of ^{206}Pb/^{238}U) and common Pb using Stacy and Kramers (1975) model Pb and subsequently normalised to reference material used;

[e] rho is the ^{206}Pb/^{238}U/^{207}Pb/^{235}U error correlation coefficient.

[f] Accuracy and reproducibilty was checked by repeated analyses (n = 16) of reference zircon Plesovice, Griedel, and 91500; data given as mean with 2 standard deviation uncertainties

Table 4.9, continued.

	Ub (ppm)	Th[b]/U	^{202}Hg	^{204}Hg	^{204}Pb	^{206}Pb	^{238}U	^{206}Pb[a] (cps)	^{238}U[a] (cps)	^{207}Pb[a] (cps)	^{206}Pb[c]/^{204}Pb	206Pbc[c] (%)	206Pb[d]/238U	±2s[f] (%)	207Pbd/235U	±2s[f] (%)	207Pbd/206Pb	±2s[f] (%)	rho[e]	206Pb/238U	±2s[f] (Ma)	207Pb/235U	±2s[f] (Ma)	207Pb/206Pb	±2s[f] (Ma)	disc (%)
				raw counts (CPS)																						
MS 4: Honingklip trondhjemite																										
Run number: 119	3	1	2080	483	333	42956	107971	38044	106336	7619	420	13	0.358	2.0	9.879	2.7	0.200	1.8	0.7	1972	34	2424	25	2828	30	70
Run number: 120	1	0	4025	935	342	30162	77506	25080	76333	4950	260	20	0.329	5.4	8.942	5.8	0.197	2.3	0.9	1831	86	2332	55	2805	37	65
Run number: 121	2	0	2766	642	364	38837	100175	33429	98658	6533	363	16	0.339	2.9	9.131	3.5	0.195	2.1	0.8	1881	47	2351	33	2789	34	67
Run number: 124	3	0	2211	513	279	37336	104206	33103	102628	6551	343	13	0.323	2.5	8.802	3.1	0.198	1.8	0.8	1802	40	2318	29	2809	30	64
Run number: 127	8	0	345	80	447	86195	239317	79427	235693	15653	858	9	0.337	0.9	9.157	1.7	0.197	1.4	0.5	1872	15	2354	15	2802	23	67
Run number: 129	3	0	2230	518	382	44485	114276	38818	112546	7728	427	15	0.345	2.3	9.468	3.0	0.199	1.9	0.8	1910	38	2384	28	2819	31	68
Run number: 132	3	0	3115	723	311	33152	99250	28360	97747	5733	268	17	0.290	2.9	8.087	3.6	0.202	2.1	0.8	1642	42	2241	33	2844	34	58
Run number: 133	4	0	2043	474	373	47329	143768	41567	141591	8177	403	14	0.294	2.6	7.963	3.3	0.197	2.0	0.8	1659	39	2227	30	2799	33	59
Run number: 135	5	0	1718	399	300	44627	131512	40017	129520	8005	405	12	0.309	1.5	8.521	2.3	0.200	1.7	0.7	1736	23	2288	21	2826	28	61
Run number: 139	6	0	1812	421	411	53631	177147	47182	174464	9322	427	14	0.270	2.2	7.368	2.9	0.198	1.9	0.8	1543	30	2157	27	2806	31	55
Run number: 146	10	0	1504	349	329	52174	185660	46938	182849	9389	402	11	0.257	1.6	7.080	2.3	0.200	1.7	0.7	1473	22	2122	21	2826	27	52
Run number: 147	14	1	652	151	267	65054	234521	60792	230969	11983	548	7	0.263	0.4	7.153	1.2	0.197	1.1	0.3	1506	5	2131	11	2802	18	54
Run number: 148	5	0	3474	807	305	31253	112872	26387	111163	5194	215	18	0.237	3.6	6.442	4.2	0.197	2.2	0.9	1373	45	2038	38	2800	36	49
Run number: 149	6	0	3138	729	217	29298	102351	25848	100801	5211	189	13	0.256	2.7	7.127	3.3	0.202	1.9	0.8	1472	36	2127	30	2839	31	52
MS 14: Stolzburg Main Trondhjemite																										
Run number: 11	1	2	55296	12840	-6177	14248	7257	9848	7147	1753	140	45	1.378	16.9	33.807	17.2	0.178	3.3	1.0	5584	663	3604	185	2634	55	212
Run number: 13	4	2	9728	2259	172	15019	23575	12885	23218	3327	77	17	0.555	4.4	19.755	4.8	0.258	2.1	0.9	2846	102	3079	48	3236	32	88
Run number: 14	1	2	15281	3548	118	6572	8861	5231	8727	1503	33	26	0.599	13.0	23.740	13.3	0.287	2.8	1.0	3027	321	3258	138	3403	43	89
Run number: 15	3	4	10812	2511	171	13458	21550	11318	21224	2864	69	19	0.533	8.8	18.606	9.0	0.253	2.2	1.0	2755	199	3022	91	3204	35	86
Run number: 17	12	1	3874	900	175	31591	53351	29338	52544	6996	193	8	0.558	1.7	18.358	2.2	0.238	1.4	0.8	2860	40	3009	21	3110	22	92
Run number: 18	4	0	7807	1813	146	15331	25335	13474	24951	3247	84	14	0.540	3.8	17.944	4.3	0.241	1.9	0.9	2783	87	2987	42	3127	31	89
Run number: 19	3	2	8730	2027	128	11742	17023	10223	16766	3004	63	15	0.610	4.0	24.703	4.4	0.294	1.8	0.9	3069	98	3297	44	3438	29	89
Run number: 20	12	2	2002	465	58	21847	34802	21127	34275	5409	132	3	0.616	2.2	21.759	2.5	0.256	1.1	0.9	3096	55	3173	24	3222	17	96
Run number: 21	5	1	7697	1787	158	17556	28860	15546	28423	3960	90	13	0.547	3.2	19.212	3.7	0.255	1.8	0.9	2813	73	3053	36	3215	28	87
Run number: 23	4	2	12926	3001	191	9511	9580	7815	9435	2228	61	22	0.828	7.6	32.560	7.9	0.285	2.4	1.0	3890	225	3567	81	3391	37	115
Run number: 30	4	0	8439	1959	165	15683	24108	13653	23743	3489	87	15	0.575	3.7	20.259	4.2	0.256	1.9	0.9	2928	89	3104	42	3219	31	91
Run number: 43	4	4	8230	1911	158	15531	24574	13567	24202	3208	88	14	0.561	3.8	18.275	4.3	0.236	2.0	0.9	2869	89	3004	42	3096	33	93
Run number: 44	3	3	9124	2119	126	11611	18475	10035	18195	2526	62	16	0.552	5.4	19.140	5.8	0.252	2.1	0.9	2832	126	3049	58	3195	33	89
Run number: 49	2	4	#VALUE!	#VALUE!	#VALUE!	#VALUE!	4180	2744	4117	657	46	b.d.	0.666	9.8	21.994	10.0	0.239	2.0	1.0	3292	258	3183	102	3116	32	106
Run number: 50	3	3	10444	2425	151	11919	18364	10061	18086	2543	64	18	0.556	5.9	19.388	6.3	0.253	2.2	0.9	2851	136	3061	62	3202	35	89
Run number: 52	1	3	11910	2766	116	6822	8044	5625	7922	1464	44	21	0.710	13.2	25.480	13.4	0.260	2.5	1.0	3459	362	3327	140	3248	40	106
Run number: 55	11	1	2803	651	104	25611	44515	24254	43841	6171	159	6	0.553	1.6	19.407	2.0	0.254	1.2	0.8	2839	37	3062	19	3213	18	88
Run number: 56	4	2	9491	2204	175	14281	22080	12123	21746	3050	81	18	0.557	4.4	19.340	4.9	0.252	2.1	0.9	2856	102	3059	48	3195	34	89
Run number: 57	4	3	6811	1581	116	11754	16122	10425	15878	3092	74	13	0.657	4.7	26.851	5.0	0.297	1.7	0.9	3254	121	3378	50	3453	27	94
Run number: 58	6	2	5789	1344	146	17852	27183	16070	26772	4111	113	11	0.600	3.4	21.171	3.8	0.256	1.7	0.9	3031	82	3146	37	3221	27	94
Run number: 59	2	2	10256	2381	89	6448	8907	5422	8773	1587	38	19	0.618	11.6	24.943	11.9	0.293	2.3	1.0	3102	293	3306	123	3432	36	90
Run number: 71	2	4	14359	3334	229	13438	21866	10547	21535	2510	67	27	0.490	14.0	16.071	14.3	0.238	2.7	1.0	2570	305	2881	147	3107	43	83
Run number: 73	7	2	4900	1138	142	19637	31077	17868	30606	4267	132	10	0.584	2.9	19.223	3.3	0.239	1.6	0.9	2964	69	3053	32	3112	26	95
Run number: 79	2	4	11241	2610	154	10061	13803	8289	13593	2462	57	21	0.610	8.4	24.970	8.7	0.297	2.6	1.0	3069	207	3307	89	3455	40	89
Run number: 81	11	3	2608	606	118	27465	44181	25988	43512	6149	199	6	0.597	2.2	19.484	2.6	0.237	1.2	0.9	3019	54	3066	25	3097	19	97
Run number: 82	6	1	3588	833	86	16096	25709	15015	25319	3573	114	7	0.593	1.9	19.457	2.4	0.238	1.4	0.8	3002	47	3065	24	3106	23	97
Run number: 83	2	0	14088	3271	190	8675	9807	6788	9659	1991	54	28	0.703	8.1	28.426	8.7	0.293	3.2	0.9	3431	219	3434	89	3436	50	100
Run number: 84	5	1	7271	1688	199	20678	39218	17989	38624	3406	128	15	0.466	3.1	12.158	3.8	0.189	2.2	0.8	2465	64	2617	36	2736	36	90
Run number: 87	25	2	6534	1517	463	50286	125260	43470	123363	8396	242	16	0.352	2.6	9.384	3.4	0.193	2.1	0.8	1946	44	2376	31	2769	35	70

^{207}Pb /^{235}U error is the quadratic addition of the ^{207}Pb/^{206}Pb and ^{206}Pb /^{238}U uncertainty.

[a] Within run background-corrected mean signal in cps (counts per second).

[b] U content and Th/U ratio were calculated relative to reference

[c] Pb 206/204 ratios measured and percentage of common Pb on the ^{206}Pb. b.d. = below dectection limit.

[d] corrected for background, within-run Pb/U fractionation (in case of ^{206}Pb/^{238}U) and common Pb using Stacy and Kramers (1975) model Pb and subsequently normalised to reference material used;

[e] rho is the ^{206}Pb/^{238}U/^{207}Pb/^{235}U error correlation coefficient.

[f] Accuracy and reproducibilty was checked by repeated analyses (n = 16) of reference zircon Plesovice, Griedel, and 91500; data given as mean with 2 standard deviation uncertainties

Table 4.9, continued.

	Ub (ppm)	Th/U [b]	^{202}Hg raw counts (CPS)	^{204}Hg raw counts (CPS)	^{204}Pb raw counts (CPS)	^{206}Pb raw counts (CPS)	^{238}U raw counts (CPS)	^{206}Pb [a] (cps)	^{238}U [a] (cps)	^{207}Pb [a] (cps)	^{206}Pb/^{204}Pb [c]	206Pbc [c] (%)	206Pb/238U [d]	±2s [f] (%)	207Pb/235U [d]	±2s [f] (%)	207Pb/206Pb [d]	±2s [f] (%)	rho [e]	206Pb/238U age (Ma)	±2s [f] (Ma)	207Pb/235U age (Ma)	±2s [f] (Ma)	207Pb/206Pb age (Ma)	±2s [f] (Ma)	disc (%)
MS 15: Stolzburg Main Trondhjemite																										
Run number: 19	3	4	7420	1723	231	14793	22336	11985	21998	3062	125	23	0.545	4.9	19.194	5.4	0.256	2.4	0.9	2804	112	3052	54	3219	37	87
Run number: 20	4	5	7413	1721	251	16101	24877	13015	24500	3322	134	24	0.531	6.4	18.695	6.8	0.255	2.4	0.9	2747	144	3026	68	3217	37	85
Run number: 21	11	1	2489	578	291	36205	65778	32343	64782	6490	410	12	0.499	2.1	13.812	2.8	0.201	1.8	0.8	2611	46	2737	26	2831	29	92
Run number: 22	4	5	6067	1409	227	15414	20653	12845	20340	3765	144	20	0.632	5.0	25.519	5.4	0.293	2.1	0.9	3156	126	3328	54	3434	32	92
Run number: 24	5	0	4788	1112	196	17635	26671	15250	26267	3872	168	16	0.581	3.5	20.326	4.0	0.254	1.9	0.9	2951	84	3107	40	3209	30	92
Run number: 25	3	6	8515	1977	297	16597	24629	13025	24256	3402	134	27	0.537	15.2	19.341	15.4	0.261	2.5	1.0	2771	351	3059	161	3254	40	85
Run number: 28	4	2	5523	1282	198	15736	23347	13349	22993	3450	147	18	0.581	3.8	20.689	4.4	0.258	2.1	0.9	2951	92	3124	43	3237	32	91
Run number: 29	4	3	7115	1652	330	22338	40867	17953	40248	3639	185	24	0.446	7.2	12.467	7.6	0.203	2.5	0.9	2378	144	2640	74	2848	41	83
Run number: 30	2	0	12053	2799	316	12758	17040	9193	16782	2295	101	39	0.548	15.1	18.853	15.5	0.250	3.0	1.0	2816	355	3034	161	3182	48	88
Run number: 32	5	4	7169	1665	392	27113	54391	21715	53567	4400	202	25	0.405	8.9	11.326	9.4	0.203	3.0	0.9	2194	168	2550	92	2848	50	77
Run number: 33	2	3	10691	2482	307	15225	23744	11429	23385	2884	109	33	0.489	11.3	17.005	11.6	0.252	2.8	1.0	2565	243	2935	118	3200	44	80
Run number: 41	6	0	3890	903	199	21178	32180	18755	31692	4767	205	13	0.592	4.0	20.740	4.3	0.254	1.7	0.9	2997	96	3127	43	3211	26	93
Run number: 42	6	3	5432	1261	368	28544	52324	23652	51532	4684	260	21	0.459	4.3	12.531	4.9	0.198	2.3	0.9	2435	88	2645	47	2810	38	87
Run number: 44	3	2	11932	2771	304	16442	35687	12136	35147	3058	84	35	0.345	32.2	11.995	32.4	0.252	3.3	1.0	1912	556	2604	360	3197	52	60
Run number: 47	5	3	7271	1688	320	22205	39389	18010	38793	3574	183	23	0.464	4.4	12.704	5.1	0.198	2.5	0.9	2458	90	2658	49	2814	42	87
Run number: 48	3	5	10626	2467	355	19284	36295	14507	35745	2958	130	33	0.406	11.5	11.410	11.9	0.204	2.9	1.0	2196	219	2557	118	2858	47	77
Run number: 49	11	3	2869	666	252	33234	59775	29901	58870	5927	342	11	0.508	2.4	13.882	2.9	0.198	1.7	0.8	2648	52	2742	28	2812	28	94
Run number: 50	2	0	12547	2914	287	12169	17058	8829	16800	2515	84	38	0.526	19.2	20.642	19.4	0.285	3.0	1.0	2723	440	3122	208	3390	47	80
Run number: 72	9	0	2610	606	274	32058	58946	28414	58054	5603	380	13	0.489	2.6	13.308	3.2	0.197	1.9	0.8	2568	55	2702	31	2803	31	92
Run number: 73	4	5	6508	1511	281	18825	28624	15398	28190	3875	168	22	0.546	4.1	18.953	4.8	0.252	2.4	0.9	2809	95	3039	47	3195	38	88
Run number: 74	6	3	5165	1199	300	26281	47863	22296	47138	4413	236	18	0.473	3.6	12.907	4.2	0.198	2.2	0.9	2497	74	2673	40	2809	36	89
Run number: 80	2	2	9499	2206	367	18677	32556	13889	32063	2782	153	34	0.433	26.5	11.963	26.7	0.200	3.2	1.0	2320	539	2601	288	2829	53	82
Run number: 81	3	3	6707	1557	376	24137	45225	19091	44540	3762	214	26	0.429	12.5	11.645	12.7	0.197	2.6	1.0	2299	246	2576	127	2802	43	82
Run number: 83	8	0	3823	888	373	33201	57932	28338	57054	5777	351	17	0.497	2.8	13.961	3.5	0.204	2.1	0.8	2600	60	2747	34	2857	34	91
Run number: 84	18	5	1607	373	461	59581	107854	53478	106221	10762	678	11	0.503	1.5	13.970	2.3	0.201	1.7	0.7	2629	33	2748	22	2836	27	93
Run number: 85	2	2	10310	2394	354	13205	15406	9586	15172	2720	123	38	0.632	12.5	24.723	12.8	0.284	2.9	1.0	3157	320	3297	134	3384	46	93
Run number: 86	10	2	2577	598	269	34144	61546	30584	60614	6105	383	12	0.505	2.4	13.887	3.0	0.200	1.7	0.8	2633	53	2742	29	2823	28	93
Run number: 87	3	5	8337	1936	310	16398	25762	12557	25372	3185	138	31	0.495	7.3	17.307	7.8	0.254	2.7	0.9	2592	159	2952	78	3208	43	81
Run number: 88	3	6	10187	2365	403	23805	46002	18335	45305	3610	155	30	0.405	8.9	10.987	9.3	0.197	2.8	1.0	2191	167	2522	90	2801	46	78
Run number: 89	3	3	7762	1802	260	16726	27555	13419	27138	3371	130	25	0.494	7.6	17.128	8.0	0.251	2.5	0.9	2590	164	2942	80	3193	40	81
Run number: 92	5	2	4416	1026	205	19053	28564	16566	28131	4234	187	15	0.589	3.8	20.755	4.2	0.256	1.8	0.9	2985	92	3127	42	3220	29	93
Run number: 93	1	3	4439	1031	212	20600	35646	17849	35106	4559	182	15	0.508	4.3	17.907	4.7	0.255	1.9	0.9	2650	95	2985	46	3219	29	82
Run number: 95	0	4	6859	1593	246	15735	22926	12809	22579	3285	143	23	0.567	6.4	20.057	6.9	0.256	2.4	0.9	2897	152	3094	69	3225	38	90
Run number: 97	0	1	7044	1636	187	14106	29280	11500	28836	2975	96	23	0.399	12.3	14.225	12.6	0.259	2.5	1.0	2163	230	2765	127	3239	40	67
Run number: 98	0	4	10167	2361	242	13037	23115	9857	22765	2870	83	32	0.433	21.4	17.384	21.6	0.291	2.8	1.0	2319	432	2956	232	3424	44	68

^{207}Pb /^{235}U error is the quadratic addition of the ^{207}Pb/^{206}Pb and ^{206}Pb /^{238}U uncertainty.

[a] Within run background-corrected mean signal in cps (counts per second).

[b] U content and Th/U ratio were calculated relative to reference

[c] Pb 206/204 ratios measured and percentage of common Pb on the ^{206}Pb. b.d. = below dectection limit.

[d] corrected for background, within-run Pb/U fractionation (in case of ^{206}Pb/^{238}U) and common Pb using Stacy and Kramers (1975) model Pb and subsequently normalised to reference material used;

[e] rho is the ^{206}Pb/^{238}U/^{207}Pb/^{235}U error correlation coefficient.

[f] Accuracy and reproducibilty was checked by repeated analyses (n = 16) of reference zircon Plesovice, Griedel, and 91500; data given as mean with 2 standard deviation uncertainties

Table 4.9, continued.

	Ub (ppm)	Th[b] U	^{202}Hg	^{204}Hg raw counts (CPS)	^{204}Pb	^{206}Pb	^{238}U	^{206}Pb[a] (cps)	^{238}U[a] (cps)	^{207}Pb[a] (cps)	^{206}Pb[c] / ^{204}Pb	206Pbc[c] (%)	206Pb[d] 238U	±2s[f] (%)	207Pbd 235U	±2s[f] (%)	207Pbd 206Pb	±2s[f] (%)	rho[e]	206Pb 238U	±2s[f] (Ma)	207Pb 235U	±2s[f] (Ma)	207Pb 206Pb	±2s[f] (Ma)	disc (%)
MS 21: Tjakastad/Honingklip mafic schist																										
Run number: 119	0	0	342977	79639	13992	196050	145448	120873	143245	25270	109	62	0.844	8.8	24.324	16.1	0.209	13.4	0.5	3944	266	3281	170	2898	218	136
Run number: 123	1	0	11915	2767	397	30936	53135	25798	52331	5147	149	20	0.493	4.1	13.560	5.1	0.200	2.9	0.8	2584	88	2719	49	2822	48	92
Run number: 124	2	0	6219	1444	410	44159	73132	38936	72025	7835	277	13	0.541	1.6	14.998	2.5	0.201	1.9	0.6	2786	37	2815	24	2836	31	98
Run number: 127	1	0	12204	2834	382	24074	35023	19532	34492	4653	131	23	0.566	8.4	18.598	8.9	0.238	2.8	0.9	2892	199	3021	90	3108	45	93
Run number: 128	0	0	17306	4018	412	20508	30839	15508	30372	3704	96	32	0.511	10.0	16.817	10.5	0.239	3.0	1.0	2659	223	2924	106	3113	47	85
Run number: 129	1	0	12324	2862	310	20100	29537	16386	29089	3889	109	23	0.563	4.4	18.434	5.0	0.237	2.4	0.9	2880	103	3013	49	3102	38	93
Run number: 131	1	0	16089	3736	327	16990	24443	13117	24073	3266	84	30	0.545	5.3	18.703	5.9	0.249	2.7	0.9	2804	121	3027	59	3178	43	88
Run number: 132	2	1	19905	4622	414	14622	15754	10676	15515	3133	77	37	0.688	10.1	27.843	10.5	0.293	3.0	1.0	3375	271	3414	109	3436	47	98
Run number: 132	1	0	13967	3243	278	16485	25128	13089	24748	3092	85	26	0.529	5.8	17.226	6.3	0.236	2.6	0.9	2737	131	2947	63	3095	41	88
Run number: 135	1	0	15211	3532	314	17088	25554	13291	25167	3161	87	29	0.528	5.1	17.316	5.7	0.238	2.7	0.9	2733	114	2953	56	3105	43	88
Run number: 136	1	0	11788	2737	371	23651	34746	19214	34220	4569	132	23	0.561	3.5	18.408	4.2	0.238	2.4	0.8	2873	82	3011	42	3105	38	93
Run number: 138	0	0	24182	5615	364	14880	24082	10293	23717	2524	57	45	0.434	19.4	14.672	19.7	0.245	3.2	1.0	2324	391	2794	207	3154	50	74
Run number: 140	1	0	16010	3718	427	20807	28721	15879	28286	4024	107	31	0.561	5.0	19.617	5.8	0.253	2.8	0.9	2872	118	3073	57	3206	44	90
Run number: 141	1	0	13719	3186	349	19380	27053	15320	26643	3902	105	27	0.575	8.6	20.193	9.0	0.255	2.6	1.0	2928	206	3101	91	3214	41	91
Run number: 144	4	0	3273	760	182	35610	61423	33251	60492	7891	228	7	0.550	1.1	17.987	1.7	0.237	1.3	0.7	2824	26	2989	17	3102	20	91
Run number: 145	2	0	12152	2822	417	27304	46279	21937	45578	4355	149	24	0.481	3.8	13.174	4.6	0.199	2.6	0.8	2533	81	2692	45	2814	42	90
Run number: 149	2	0	10314	2395	340	25388	42533	21035	41889	4224	147	21	0.502	4.0	13.902	4.7	0.201	2.4	0.9	2623	88	2743	45	2833	39	93
Run number: 150	2	0	13705	3182	463	27850	48525	21817	47791	4308	143	28	0.457	3.6	12.430	4.5	0.197	2.7	0.8	2424	73	2637	43	2805	44	86
Run number: 170	1	0	27460	6376	529	15894	18793	10425	18508	1992	83	52	0.563	14.3	14.836	14.7	0.191	3.5	1.0	2880	341	2805	151	2751	58	105
Run number: 172	39	1	3689	856	456	62570	106076	56708	104470	11239	444	10	0.543	1.1	14.834	2.0	0.198	1.6	0.6	2795	26	2805	19	2811	26	99
Run number: 173	6	0	14232	3305	309	17102	27200	13247	26788	3337	86	29	0.495	6.6	17.174	7.1	0.252	2.8	0.9	2590	142	2945	71	3197	44	81
Run number: 174	2	5	14385	3340	270	12983	16309	10061	16062	2970	74	29	0.626	8.4	25.494	8.8	0.295	2.6	1.0	3135	213	3327	90	3445	41	91
Run number: 179	2	2	15785	3665	282	13717	19948	10365	19646	3074	67	32	0.528	13.9	21.572	14.1	0.297	2.7	1.0	2731	316	3165	147	3452	42	79
Run number: 193	0	4	14540	3376	308	14699	18954	11302	18667	3337	82	30	0.605	7.2	24.650	7.6	0.295	2.7	0.9	3052	177	3294	77	3446	41	89
Run number: 194	0	5	14836	3445	219	12951	24809	9987	24433	2963	52	30	0.409	13.6	16.719	13.9	0.297	2.7	1.0	2209	259	2919	142	3453	42	64

^{207}Pb /^{235}U error is the quadratic addition of the ^{207}Pb/^{206}Pb and ^{206}Pb /^{238}U uncertainty.

[a] Within run background-corrected mean signal in cps (counts per second).

[b] U content and Th/U ratio were calculated relative to reference

[c] Pb 206/204 ratios measured and percentage of common Pb on the ^{206}Pb. b.d. = below dectection limit.

[d] corrected for background, within-run Pb/U fractionation (in case of ^{206}Pb/^{238}U) and common Pb using Stacy and Kramers (1975) model Pb and subsequently normalised to reference material used;

[e] rho is the ^{206}Pb/^{238}U/^{207}Pb/^{235}U error correlation coefficient.

[f] Accuracy and reproducibilty was checked by repeated analyses (n = 16) of reference zircon Plesovice, Griedel, and 91500;
data given as mean with 2 standard deviation uncertainties

Table 4.9, continued.

	Ub (ppm)	Th[b] / U	^{202}Hg	^{204}Hg	^{204}Pb	^{206}Pb	^{238}U	^{206}Pb[a] (cps)	^{238}U[a] (cps)	^{207}Pb[a] (cps)	^{206}Pb[c] / ^{204}Pb	206Pbc[c] (%)	206Pb[d] / 238U	±2s[f] (%)	207Pbd / 235U	±2s[f] (%)	207Pbd / 206Pb	±2s[f] (%)	rho[e]	206Pb / 238U	±2s[f] (Ma)	207Pb / 235U	±2s[f] (Ma)	207Pb / 206Pb	±2s[f] (Ma)	disc (%)
				raw counts (CPS)																						
MS 25: Weergevonden diorite																										
Run number: 19	2	5	12537	2911	378	19028	27388	14555	26973	3680	118	31	0.540	7.6	18.810	8.1	0.253	2.7	0.9	2782	174	3032	81	3202	43	87
Run number: 20	4	3	8877	2061	372	25533	42647	20782	42001	4180	178	23	0.495	3.4	13.722	4.2	0.201	2.5	0.8	2591	73	2731	41	2835	41	91
Run number: 22	3	4	10681	2480	341	18693	26147	14726	25751	3738	128	27	0.572	5.6	20.014	6.2	0.254	2.6	0.9	2915	133	3092	62	3209	41	91
Run number: 24	2	4	9397	2182	315	18441	24176	14928	23810	3647	140	24	0.627	4.6	21.119	5.1	0.244	2.2	0.9	3138	116	3144	51	3148	34	100
Run number: 25	3	3	9624	2235	391	25630	44068	20570	43401	4073	172	25	0.474	4.0	12.939	4.7	0.198	2.6	0.8	2501	83	2675	46	2810	42	89
Run number: 27	3	3	10130	2352	282	18511	29368	14998	28923	3923	110	23	0.519	4.2	18.702	4.8	0.262	2.4	0.9	2693	94	3027	48	3256	37	83
Run number: 30	3	5	10332	2399	361	20369	28769	16146	28333	4069	139	26	0.570	4.7	19.803	5.3	0.252	2.5	0.9	2907	110	3082	53	3198	40	91
Run number: 33	2	3	17352	4029	405	20171	37528	14744	36959	2916	94	37	0.399	12.9	10.879	13.3	0.198	3.2	1.0	2164	242	2513	132	2808	53	77
Run number: 35	4	4	10429	2422	325	20458	28800	16666	28364	4190	129	23	0.588	3.5	20.368	4.2	0.251	2.3	0.8	2980	85	3109	42	3194	37	93
Run number: 36	2	4	14266	3313	355	18025	25949	13823	25556	3480	100	30	0.541	8.9	18.774	9.3	0.252	2.8	1.0	2787	204	3030	94	3196	44	87
Run number: 37	3	5	10943	2541	333	20107	28226	16224	27799	4118	125	24	0.584	4.4	20.427	5.0	0.254	2.4	0.9	2964	105	3112	49	3209	38	92
Run number: 38	4	5	9558	2219	303	20267	28255	16751	27827	4238	132	21	0.602	3.9	21.001	4.5	0.253	2.2	0.9	3038	95	3139	45	3204	35	95
Run number: 40	4	4	10243	2378	292	20308	33293	16614	32789	4266	113	22	0.507	3.0	17.940	3.8	0.257	2.3	0.8	2643	65	2987	37	3227	36	82
Run number: 42	2	5	13907	3229	377	19079	26998	14659	26589	3734	108	30	0.551	6.3	19.363	6.8	0.255	2.7	0.9	2831	145	3060	68	3214	43	88
Run number: 43	3	4	13429	3118	435	25234	44086	19558	43419	3835	137	29	0.450	4.9	12.178	5.6	0.196	2.8	0.9	2397	98	2618	54	2794	46	86
Run number: 44	4	3	11064	2569	422	27475	47212	22005	46497	4341	163	25	0.473	3.7	12.874	4.5	0.197	2.6	0.8	2498	77	2670	43	2804	42	89
Run number: 45	3	5	13548	3146	495	27658	48387	21195	47654	4236	149	30	0.445	6.2	12.255	6.8	0.200	2.9	0.9	2372	124	2624	66	2825	47	84
Run number: 46	3	4	12330	2863	405	22559	33503	17678	32995	4235	133	28	0.536	4.2	17.696	4.9	0.240	2.6	0.8	2766	95	2973	48	3117	41	89
Run number: 48	4	3	14051	3263	379	18723	26160	14312	25764	3709	106	31	0.555	16.4	19.851	16.6	0.259	2.7	1.0	2848	389	3084	175	3242	42	88
Run number: 49	3	5	11143	2587	380	22582	33053	18045	32553	4300	140	25	0.554	4.1	18.212	4.8	0.238	2.5	0.9	2843	95	3001	47	3108	40	91
Run number: 50	2	4	15559	3613	447	21325	32552	15865	32059	3764	112	34	0.495	7.6	16.190	8.1	0.237	2.9	0.9	2592	164	2888	81	3102	47	84
Run number: 69	3	4	10238	2377	251	15788	21658	12897	21330	3359	103	22	0.605	6.3	21.709	6.7	0.260	2.3	0.9	3049	155	3171	67	3249	37	94
Run number: 72	2	4	14343	3330	364	18612	28274	14171	27845	3386	102	31	0.509	6.3	16.767	6.8	0.239	2.7	0.9	2652	138	2922	68	3113	44	85
Run number: 76	3	4	10091	2343	288	19169	29330	15645	28886	3542	123	23	0.542	4.3	16.905	4.9	0.226	2.4	0.9	2790	98	2929	48	3027	39	92
Run number: 77	2	5	15686	3642	435	22372	41280	16571	40655	3288	111	35	0.408	13.3	11.152	13.6	0.198	3.1	1.0	2204	253	2536	136	2813	50	78
Run number: 78	3	4	9922	2304	276	17656	24482	14458	24111	3664	117	22	0.600	3.9	20.955	4.6	0.253	2.5	0.8	3028	94	3136	46	3206	40	94
Run number: 80	3	2	8656	2010	254	18111	25287	15162	24904	3826	125	19	0.609	4.1	21.182	4.6	0.252	2.2	0.9	3065	100	3147	46	3199	34	96
Run number: 81	2	4	14782	3432	385	20921	35922	15941	35378	3231	110	31	0.451	11.2	12.593	11.5	0.203	2.9	1.0	2398	228	2650	115	2848	47	84
Run number: 82	1	2	16668	3870	700	18737	16247	13628	16001	2891	152	37	0.852	12.9	24.912	13.5	0.212	4.0	1.0	3972	394	3305	141	2922	65	136
Run number: 83	3	3	10899	2531	298	19035	28140	15449	27714	3631	117	23	0.557	5.5	18.066	6.0	0.235	2.4	0.9	2856	129	2993	60	3087	39	93
Run number: 85	2	3	12233	2840	283	16944	26050	13474	25655	3206	97	26	0.525	7.8	17.231	8.2	0.238	2.6	1.0	2721	176	2948	82	3106	41	88
Run number: 86	2	4	13001	3019	302	16734	24495	13120	24124	3189	97	28	0.544	8.1	18.228	8.6	0.243	2.6	1.0	2800	188	3002	86	3140	42	89
Run number: 87	2	5	14933	3467	308	15426	22561	11750	22219	2968	83	31	0.529	10.5	18.415	10.9	0.253	2.8	1.0	2736	239	3012	111	3201	45	85
Run number: 88	3	5	8612	2000	244	18153	25329	15318	24946	3883	122	19	0.614	4.3	21.461	4.8	0.253	2.1	0.9	3086	106	3160	47	3207	33	96
Run number: 89	2	4	12107	2811	306	16132	23632	12472	23274	3165	101	29	0.536	10.5	18.752	10.8	0.254	2.7	1.0	2766	240	3029	110	3209	42	86
Run number: 90	2	2	12234	2841	259	15549	30187	12022	29730	3057	78	29	0.404	20.2	14.177	20.4	0.254	2.7	1.0	2189	386	2762	214	3212	42	68
Run number: 91	3	3	8274	1921	272	19065	28056	15800	27631	3737	140	21	0.572	4.0	18.649	4.6	0.237	2.3	0.9	2915	94	3024	45	3097	37	94
Run number: 92	3	3	11101	2578	333	17680	24546	13828	24175	3534	120	28	0.572	5.1	20.155	5.7	0.256	2.6	0.9	2916	120	3099	57	3219	41	91
Run number: 96	0	4	16176	3756	551	23066	33917	16465	33403	3406	137	40	0.493	8.9	14.060	9.4	0.207	3.1	0.9	2583	193	2754	94	2881	50	90
Run number: 97	0	6	18155	4216	619	21749	24776	15541	24401	3162	143	40	0.637	5.9	17.869	6.7	0.203	3.2	0.9	3177	151	2983	67	2854	52	111
Run number: 99	0	3	8249	1915	257	17192	23127	14277	22776	3844	128	20	0.627	4.1	23.271	4.6	0.269	2.2	0.9	3137	102	3238	46	3302	34	95

[207]Pb /[235]U error is the quadratic addition of the [207]Pb/[206]Pb and [206]Pb /[238]U uncertainty.

[a] Within run background-corrected mean signal in cps (counts per second).

[b] U content and Th/U ratio were calculated relative to reference

[c] Pb 206/204 ratios measured and percentage of common Pb on the [206]Pb. b.d. = below dectection limit.

[d] corrected for background, within-run Pb/U fractionation (in case of [206]Pb/[238]U) and common Pb using Stacy and Kramers (1975) model Pb and subsequently normalised to reference material used;

[e] rho is the [206]Pb/[238]U/[207]Pb/[235]U error correlation coefficient.

[f] Accuracy and reproducibilty was checked by repeated analyses (n = 16) of reference zircon Plesovice, Griedel, and 91500; data given as mean with 2 standard deviation uncertainties

Table 4.9, continued.

	Ub (ppm)	Th[b]/U	^{202}Hg	^{204}Hg raw counts (CPS)	^{204}Pb	^{206}Pb	^{238}U	^{206}Pb[a] (cps)	^{238}U[a] (cps)	^{207}Pb[a] (cps)	^{206}Pb[c]/^{204}Pb	206Pbc[c] (%)	206Pb[d]/238U	±2s[f] (%)	207Pbd/235U	±2s[f] (%)	207Pbd/206Pb	±2s[f] (%)	rho[e]	206Pb/238U	±2s[f] (Ma)	207Pb/235U	±2s[f] (Ma)	207Pb/206Pb	±2s[f] (Ma)	disc (%)
MS 36: Stolzburg tonalite																										
Run number: 19	4	0	4426	1028	119	14400	19561	13041	19265	3843	115	10	0.677	3.1	27.507	3.5	0.295	1.7	0.9	3333	80	3402	35	3443	26	97
Run number: 21	10	0	2784	646	171	31331	51016	29168	50243	6878	253	7	0.581	1.5	18.875	2.0	0.236	1.4	0.7	2951	35	3035	19	3092	22	95
Run number: 22	8	1	3710	861	200	29124	47453	26597	46734	6267	224	10	0.569	1.7	18.491	2.3	0.236	1.5	0.7	2904	40	3016	22	3091	24	94
Run number: 23	6	1	7433	1726	383	30405	50288	25536	49526	6069	199	19	0.516	2.7	16.896	3.5	0.238	2.1	0.8	2681	60	2929	34	3104	34	86
Run number: 24	7	1	4625	1074	250	28058	41475	25050	40847	6399	218	12	0.613	2.0	21.600	2.5	0.255	1.6	0.8	3083	48	3166	25	3219	26	96
Run number: 25	11	1	2956	686	222	36038	56038	33302	55190	8389	287	8	0.603	1.3	20.959	1.9	0.252	1.4	0.7	3044	31	3137	18	3197	22	95
Run number: 27	1	0	13494	3133	1220	10733	6549	7689	6450	2644	96	40	1.192	20.8	56.514	21.1	0.344	3.5	1.0	5059	775	4114	236	3680	54	137
Run number: 28	11	1	5105	1185	487	49908	97043	43281	95573	8605	339	15	0.453	2.4	12.414	3.4	0.199	2.4	0.7	2408	49	2636	33	2817	39	85
Run number: 29	6	2	734	170	21	14934	23505	14679	23149	3807	131	2	0.634	2.8	22.678	3.0	0.259	1.1	0.9	3166	70	3213	30	3243	17	98
Run number: 30	2	0	10538	2447	211	12443	17145	10013	16885	2978	79	24	0.593	8.0	24.314	8.3	0.297	2.4	1.0	3002	194	3281	85	3456	37	87
Run number: 31	25	2	860	200	183	66759	103876	64502	102303	16430	578	3	0.631	0.7	22.144	1.3	0.255	1.0	0.6	3152	18	3190	12	3214	16	98
Run number: 32	6	0	6698	1555	356	29049	43981	24713	43315	6329	205	18	0.571	2.6	20.147	3.5	0.256	2.3	0.7	2910	61	3098	34	3223	36	90
Run number: 33	11	1	3445	800	300	41348	64366	37640	63391	9491	317	10	0.594	1.3	20.643	2.0	0.252	1.5	0.6	3005	31	3122	19	3198	24	94
Run number: 34	5	1	5442	1264	217	22349	34305	19686	33785	5007	166	14	0.583	2.4	20.436	3.0	0.254	1.8	0.8	2960	57	3112	29	3212	28	92
Run number: 35	13	1	1931	448	185	41558	64959	39264	63976	9903	349	6	0.614	0.9	21.342	1.5	0.252	1.2	0.6	3085	23	3154	15	3199	19	96
Run number: 36	11	1	1970	457	133	32866	54736	31162	53907	7843	265	5	0.578	1.3	20.060	1.7	0.252	1.1	0.8	2941	30	3094	17	3195	18	92
Run number: 37	3	1	7196	1671	283	24397	44387	20646	43714	4130	169	18	0.472	12.3	13.025	12.5	0.200	2.3	1.0	2494	259	2681	125	2826	38	88
Run number: 38	4	0	6579	1528	259	20376	27186	17448	26774	5227	153	17	0.652	3.1	26.918	3.8	0.300	2.2	0.8	3235	80	3380	38	3468	34	93
Run number: 39	4	0	6762	1570	229	19365	29723	16555	29273	4207	141	17	0.566	3.3	19.816	3.9	0.254	2.1	0.8	2890	77	3082	38	3211	32	90
Run number: 41	11	1	2515	584	214	36981	56153	34373	55303	8686	318	8	0.622	1.3	21.656	1.8	0.253	1.3	0.7	3116	31	3168	18	3202	20	97
Run number: 42	27	0	1589	369	520	90115	165187	83196	162686	16640	733	8	0.511	0.9	14.103	1.7	0.200	1.5	0.5	2663	20	2757	16	2826	24	94
Run number: 43	5	1	4066	944	173	20175	27370	18202	26955	5435	170	11	0.675	3.7	27.798	4.0	0.299	1.6	0.9	3326	98	3412	40	3463	24	96
Run number: 44	16	2	1633	379	204	46912	71367	44423	70286	11244	421	6	0.632	0.9	22.058	1.4	0.253	1.1	0.6	3158	22	3186	14	3204	18	99
Run number: 45	2	1	14831	3444	338	13277	15948	9738	15707	3730	76	36	0.620	8.0	32.742	8.5	0.383	2.9	0.9	3110	200	3573	87	3844	44	81
Run number: 46	8	1	4854	1127	309	33085	56034	29110	55185	6407	254	14	0.527	2.0	16.007	2.8	0.220	1.9	0.7	2731	46	2877	27	2981	30	92
Run number: 47	7	0	7330	1702	733	43476	57415	35260	56546	10507	305	23	0.624	1.9	25.620	2.8	0.298	2.2	0.7	3124	46	3332	28	3460	33	90
Run number: 48	4	2	8758	2034	431	30347	56543	24572	55687	4907	196	24	0.441	4.1	12.149	4.8	0.200	2.5	0.9	2356	81	2616	46	2824	41	83
Run number: 49	5	2	6911	1605	350	26668	39386	22470	38790	5799	196	19	0.579	3.2	20.612	3.9	0.258	2.2	0.8	2946	76	3121	38	3235	35	91
Run number: 50	6	0	4813	1118	219	23534	36224	20849	35675	5264	186	13	0.584	2.9	20.344	3.4	0.252	1.7	0.9	2967	68	3108	33	3200	28	93
Run number: 69	19	1	3120	725	858	86770	160131	75325	157706	15235	640	15	0.478	1.2	13.319	2.4	0.202	2.1	0.5	2517	25	2703	23	2844	35	88
Run number: 70	5	0	7083	1645	309	24436	38829	20579	38241	4970	175	19	0.538	3.4	17.920	4.1	0.242	2.1	0.8	2776	78	2985	40	3130	34	89
Run number: 71	5	1	7748	1799	400	26391	36279	21790	35729	6446	186	21	0.610	2.6	24.876	3.3	0.296	2.1	0.8	3069	64	3303	33	3449	33	89
Run number: 72	7	1	6550	1521	465	38730	71772	32517	70685	6417	272	19	0.460	2.3	12.516	3.3	0.197	2.3	0.7	2440	46	2644	31	2804	38	87
Run number: 73	7	1	5678	1319	296	29465	53938	25525	53121	5059	220	15	0.481	2.0	13.130	2.9	0.198	2.1	0.7	2529	43	2689	28	2811	34	90
Run number: 74	14	1	3617	840	435	53536	98421	47744	96931	9401	419	12	0.493	1.2	13.372	2.2	0.197	1.8	0.6	2582	27	2706	21	2801	30	92
Run number: 75	3	2	10941	2541	384	21786	33928	17039	33414	4312	135	28	0.510	5.0	17.793	5.7	0.253	2.7	0.9	2656	111	2979	56	3204	43	83
Run number: 76	9	1	4105	953	258	30955	48418	27758	47685	6871	246	12	0.582	1.5	19.866	2.2	0.248	1.6	0.7	2957	37	3085	22	3169	25	93
Run number: 77	23	1	1734	403	401	73109	125690	67916	123787	14890	612	8	0.549	0.8	16.585	1.5	0.219	1.3	0.5	2820	17	2911	14	2975	21	95
Run number: 78	11	0	2999	696	254	37774	58498	34645	57612	8771	312	9	0.601	1.4	20.992	2.0	0.253	1.4	0.7	3035	35	3138	19	3205	22	95

^{207}Pb /^{235}U error is the quadratic addition of the ^{207}Pb/^{206}Pb and ^{206}Pb /^{238}U uncertainty.

[a] Within run background-corrected mean signal in cps (counts per second).

[b] U content and Th/U ratio were calculated relative to reference

[c] Pb 206/204 ratios measured and percentage of common Pb on the ^{206}Pb. b.d. = below dectection limit.

[d] corrected for background, within-run Pb/U fractionation (in case of ^{206}Pb/^{238}U) and common Pb using Stacy and Kramers (1975) model Pb and subsequently normalised to reference material used;

[e] rho is the ^{206}Pb/^{238}U/^{207}Pb/^{235}U error correlation coefficient.

[f] Accuracy and reproducibilty was checked by repeated analyses (n = 16) of reference zircon Plesovice, Griedel, and 91500; data given as mean with 2 standard deviation uncertainties

Table 4.9, continued.

	Ub (ppm)	Thb U	207Pba (cps)	206Pbcc (%)	207Pbd / 235U	±2s (%)	206Pbd / 238U	±2s (%)	rhoe	207Pbd / 206Pb	±2s (%)	206Pb / 238U	±2s (Ma)	207Pb / 235U	±2s (Ma)	207Pb / 206Pb	±2s (Ma)	disc (%)
DURANGO																		
DURANGO 1	14	19.23	139	11.4	0.0331	6.5	0.0	3.1	0.49	0.0513	5.7	30	1	33	2	255	130	91
DURANGO 2	14	19.28	148	12.2	0.0334	7.8	0.0	4.1	0.52	0.0516	6.7	30	1	33	3	268	154	91
DURANGO 3	13	19.16	132	10.7	0.0343	7.3	0.0	3.2	0.44	0.0513	6.6	31	1	34	2	255	151	91
DURANGO 4	14	19.15	142	11.3	0.0343	7.2	0.0	2.8	0.39	0.0512	6.7	31	1	34	2	252	153	91
DURANGO 5	14	18.90	132	10.4	0.0347	6.7	0.0	2.6	0.39	0.0509	6.2	32	1	35	2	234	143	92
DURANGO 6	14	18.83	144	10.5	0.0347	6.6	0.0	4.1	0.62	0.0514	5.2	32	1	35	2	258	119	91
DURANGO 7	13	18.88	136	10.8	0.0348	8.0	0.0	5.4	0.68	0.0516	5.8	31	2	35	3	268	134	91
DURANGO 8	14	19.19	130	11.2	0.0349	6.5	0.0	2.3	0.36	0.0514	6.1	32	1	35	2	258	140	91
DURANGO 9	14	19.22	126	10.0	0.0350	6.3	0.0	3.4	0.54	0.0509	5.3	32	1	35	2	238	122	92
DURANGO 10	14	19.18	138	10.6	0.0350	7.7	0.0	5.3	0.69	0.0511	5.6	32	2	35	3	247	128	91
DURANGO 11	14	19.02	140	8.9	0.0350	7.3	0.0	5.9	0.80	0.0514	4.4	32	2	35	3	259	100	91
DURANGO 12	14	19.17	132	10.7	0.0350	6.9	0.0	2.4	0.34	0.0509	6.4	32	1	35	2	234	149	92
DURANGO 13	14	19.03	148	11.5	0.0351	7.1	0.0	2.9	0.41	0.0514	6.5	32	1	35	2	259	148	91
DURANGO 14	14	19.20	135	10.5	0.0353	7.4	0.0	4.1	0.56	0.0513	6.1	32	1	35	3	253	141	91
DURANGO 15	13	19.15	132	10.9	0.0353	7.9	0.0	4.3	0.55	0.0514	6.6	32	1	35	3	259	153	91
DURANGO 16	14	18.85	139	11.6	0.0357	6.8	0.0	2.4	0.36	0.0517	6.3	32	1	36	2	271	145	90
DURANGO 17	14	19.20	151	11.9	0.0357	6.9	0.0	2.5	0.36	0.0518	6.4	32	1	36	2	277	147	90
DURANGO 18	14	19.06	145	12.1	0.0358	7.5	0.0	3.6	0.48	0.0519	6.6	32	1	36	3	280	150	90
DURANGO 19	14	19.13	134	10.8	0.0359	7.0	0.0	2.7	0.39	0.0511	6.4	33	1	36	2	247	147	91
DURANGO 20	13	19.24	138	11.8	0.0360	7.0	0.0	2.9	0.41	0.0518	6.4	32	1	36	2	277	146	90
DURANGO 21	14	19.27	138	10.7	0.0363	7.0	0.0	3.4	0.48	0.0515	6.1	33	1	36	2	263	140	91
DURANGO 22	14	19.14	139	10.7	0.0363	6.6	0.0	2.5	0.38	0.0511	6.1	33	1	36	2	246	140	91
DURANGO 23	8	21.05	199	34.6	0.0456	12.4	0.0	10.2	0.82	0.0693	7.1	31	3	45	6	906	146	68
DURANGO 24	7	21.35	56	13.6	0.0437	8.0	0.0	5.3	0.66	0.0531	6.0	38	2	43	3	335	136	88
DURANGO 25	11	21.76	129	19.7	0.0410	9.6	0.0	6.7	0.70	0.0593	6.8	32	2	41	4	577	148	79

^{207}Pb /^{235}U error is the quadratic addition of the $^{207}Pb/^{206}Pb$ and ^{206}Pb /^{238}U uncertainty.

[a] Within run background-corrected mean signal in cps (counts per second).

[b] U content and Th/U ratio were calculated relative to reference

[c] Pb 206/204 ratios measured and percentage of common Pb on the ^{206}Pb. b.d. = below dectection limit.

[d] corrected for background, within-run Pb/U fractionation (in case of $^{206}Pb/^{238}U$) and common Pb using Stacy and Kramers (1975) model Pb and subsequently normalised to reference material used;

[e] rho is the $^{206}Pb/^{238}U/^{207}Pb/^{235}U$ error correlation coefficient.

[f] Accuracy and reproducibilty was checked by repeated analyses (n = 16) of reference zircon Plesovice, Griedel, and 91500; data given as mean with 2 standard deviation uncertainties

Table 4.9, continued.

	Ub (ppm)	Thb U	207Pba (cps)	206Pbcc (%)	207Pbd / 235U	±2s (%)	206Pbd / 238U	±2s (%)	rhoe	207Pbd / 206Pb	±2s (%)	206Pb / 238U	±2s (Ma)	207Pb / 235U	±2s (Ma)	207Pb / 206Pb	±2s (Ma)	disc (%)
MADAGASCAR																		
MADAGASCAR 1	20	24.88	1615	2.5	0.6221	4.8	0.1	3.7	0.76	0.0575	3.1	487	17	491	19	510	68	96
MADAGASCAR 2	20	24.39	1527	2.3	0.6248	4.8	0.1	3.5	0.73	0.0572	3.3	491	17	493	19	499	73	98
MADAGASCAR 3	22	26.48	1824	3.2	0.6251	4.8	0.1	3.5	0.73	0.0575	3.3	489	17	493	19	513	73	95
MADAGASCAR 4	22	26.48	1824	3.2	0.6251	4.8	0.1	3.5	0.73	0.0575	3.3	489	17	493	19	513	73	95
MADAGASCAR 5	22	25.59	1718	2.5	0.6268	4.4	0.1	3.5	0.78	0.0576	2.7	490	16	494	17	515	60	95
MADAGASCAR 6	24	24.68	1812	2.6	0.6231	4.5	0.1	3.5	0.77	0.0574	2.9	488	16	492	18	507	63	96
MADAGASCAR 7	23	25.54	1761	2.7	0.6158	4.7	0.1	3.5	0.75	0.0571	3.1	485	16	487	18	496	68	98
MADAGASCAR 8	25	24.00	1872	2.3	0.6144	4.4	0.1	3.5	0.80	0.0571	2.6	484	16	486	17	496	58	98
MADAGASCAR 9	27	25.45	2107	2.8	0.6184	4.7	0.1	3.5	0.74	0.0573	3.2	486	16	489	18	504	70	96
MADAGASCAR 10	27	25.45	2107	2.8	0.6184	4.7	0.1	3.5	0.74	0.0573	3.2	486	16	489	18	504	70	96
MADAGASCAR 11	24	24.97	1955	2.5	0.6120	4.4	0.1	3.5	0.81	0.0573	2.6	481	16	485	17	505	57	95
MADAGASCAR 12	24	24.68	1959	2.9	0.6165	4.7	0.1	3.5	0.74	0.0574	3.2	484	16	488	18	506	69	96
MADAGASCAR 13	25	24.46	1829	2.3	0.6162	4.3	0.1	3.5	0.80	0.0571	2.6	485	16	487	17	497	58	98
MADAGASCAR 14	25	24.46	1829	2.3	0.6162	4.3	0.1	3.5	0.80	0.0571	2.6	485	16	487	17	497	58	98
MADAGASCAR 15	23	25.62	1893	2.7	0.6186	4.6	0.1	3.5	0.76	0.0575	2.9	484	16	489	18	511	65	95
MADAGASCAR 16	23	25.62	1893	2.7	0.6186	4.6	0.1	3.5	0.76	0.0575	2.9	484	16	489	18	511	65	95
MADAGASCAR 17	24	25.40	1994	3.0	0.6161	4.6	0.1	3.5	0.76	0.0575	3.0	482	16	487	18	510	67	95
MADAGASCAR 18	22	26.05	1804	2.7	0.6015	4.6	0.1	3.5	0.77	0.0571	2.9	475	16	478	18	495	64	96
MADAGASCAR 19	25	25.21	1975	2.9	0.6110	4.6	0.1	3.5	0.76	0.0574	3.0	480	16	484	18	505	67	95
MADAGASCAR 20	25	24.80	1902	2.4	0.6068	4.5	0.1	3.5	0.78	0.0571	2.8	478	16	482	17	496	61	96
MADAGASCAR 21	24	25.52	1812	3.0	0.6005	4.8	0.1	3.5	0.73	0.0570	3.2	475	16	478	18	491	72	97
MADAGASCAR 22	25	25.25	2195	3.7	0.6027	5.2	0.1	3.5	0.67	0.0575	3.9	472	16	479	20	511	85	93
MADAGASCAR 23	25	24.34	1982	2.7	0.6029	4.5	0.1	3.5	0.77	0.0572	2.9	475	16	479	17	499	63	95
MADAGASCAR 24	26	25.44	1958	2.6	0.5987	4.6	0.1	3.5	0.76	0.0569	3.0	474	16	476	18	489	66	97
MADAGASCAR 25	26	25.40	2003	2.5	0.5989	4.5	0.1	3.5	0.77	0.0571	2.9	473	16	477	17	496	64	95
MADAGASCAR 26	22	25.61	1581	2.3	0.5932	4.3	0.1	3.5	0.81	0.0568	2.5	471	16	473	16	484	56	97
MADAGASCAR 27	18	26.32	921	4.3	0.6294	5.6	0.1	3.1	0.55	0.0583	4.7	486	14	496	22	541	103	90
MADAGASCAR 28	20	26.57	1060	4.8	0.6331	5.2	0.1	3.0	0.58	0.0585	4.3	487	14	498	21	548	93	89
MADAGASCAR 29	20	26.55	1292	6.7	0.6229	6.3	0.1	3.1	0.49	0.0595	5.5	472	14	492	25	586	118	80
MADAGASCAR 30	26	24.77	1056	2.6	0.6145	4.1	0.1	2.9	0.71	0.0572	2.9	483	14	486	16	501	64	96
MADAGASCAR 31	22	26.90	995	3.8	0.6223	4.8	0.1	2.9	0.61	0.0579	3.8	484	14	491	19	526	84	92
MADAGASCAR 32	20	27.08	874	3.6	0.6180	4.9	0.1	2.9	0.60	0.0576	3.9	483	14	489	19	515	86	94
MADAGASCAR 33	19	26.73	831	3.3	0.6094	4.4	0.1	2.9	0.66	0.0575	3.3	478	13	483	17	510	74	94

$^{207}Pb/^{235}U$ error is the quadratic addition of the $^{207}Pb/^{206}Pb$ and $^{206}Pb/^{238}U$ uncertainty.

[a] Within run background-corrected mean signal in cps (counts per second).

[b] U content and Th/U ratio were calculated relative to reference

[c] Pb 206/204 ratios measured and percentage of common Pb on the ^{206}Pb. b.d. = below dectection limit.

[d] corrected for background, within-run Pb/U fractionation (in case of $^{206}Pb/^{238}U$) and common Pb using Stacy and Kramers (1975) model Pb and subsequently normalised to reference material used;

[e] rho is the $^{206}Pb/^{238}U/^{207}Pb/^{235}U$ error correlation coefficient.

[f] Accuracy and reproducibilty was checked by repeated analyses (n = 16) of reference zircon Plesovice, Griedel, and 91500; data given as mean with 2 standard deviation uncertainties

Table 4.9, continued.

	Ub (ppm)	Thb U	207Pba (cps)	206Pbcc (%)	207Pbd / 235U	±2s (%)	206Pbd / 238U	±2s (%)	rhoe	207Pbd / 206Pb	±2s (%)	206Pb / 238U	±2s (Ma)	207Pb / 235U	±2s (Ma)	207Pb / 206Pb	±2s (Ma)	disc (%)
401 APATITE																		
401 APATITE 1	10	9.31	610	0.5	0.6721	4.3	0.1	3.6	0.85	0.0571	2.3	528	18	522	18	494	50	107
402 APATITE 2	11	10.16	638	0.1	0.7078	4.0	0.1	3.5	0.88	0.0576	1.9	551	18	543	17	513	41	107
402 APATITE 1	11	10.15	657	0.0	0.7050	3.8	0.1	3.5	0.91	0.0576	1.6	548	18	542	16	516	35	106
403 APATITE 2	9	9.10	646	1.2	0.6865	4.9	0.1	3.6	0.72	0.0577	3.4	534	18	531	21	517	75	103
403 APATITE 1	11	10.32	636	0.1	0.6901	4.1	0.1	3.5	0.85	0.0572	2.2	541	18	533	17	498	47	109
404 APATITE 2	20	25.31	1816	3.6	0.7019	5.2	0.1	3.5	0.68	0.0591	3.8	533	18	540	22	569	82	94
404 APATITE 1	11	10.39	676	0.3	0.6871	4.1	0.1	3.5	0.86	0.0573	2.1	537	18	531	17	504	45	107
405 APATITE 2	19	26.47	1777	3.9	0.7009	5.3	0.1	3.5	0.67	0.0593	3.9	531	18	539	22	577	85	92
405 APATITE 1	12	10.32	746	0.1	0.6841	4.4	0.1	3.5	0.80	0.0574	2.7	534	18	529	18	508	58	105
406 APATITE 2	10	9.10	635	0.6	0.6716	4.1	0.1	3.5	0.85	0.0572	2.2	527	18	522	17	497	48	106
406 APATITE 1	20	25.88	1649	2.7	0.6859	4.8	0.1	3.5	0.74	0.0585	3.2	526	18	530	20	549	71	96
407 APATITE 2	10	8.97	560	0.0	0.6679	4.6	0.1	3.5	0.75	0.0569	3.1	526	18	519	19	489	67	108
407 APATITE 1	11	10.29	709	0.2	0.6722	4.5	0.1	3.5	0.77	0.0571	2.9	528	18	522	19	497	64	106
408 APATITE 2	20	25.52	1764	3.6	0.6763	5.2	0.1	3.5	0.68	0.0585	3.8	519	17	525	21	550	83	94
408 APATITE 1	12	10.07	758	1.7	0.6961	5.0	0.1	2.9	0.58	0.0580	4.1	538	15	536	21	530	90	101
409 APATITE 2	12	10.09	846	2.5	0.6827	8.2	0.1	3.0	0.36	0.0579	7.6	529	15	528	34	526	167	100
409 APATITE 1	12	10.12	1006	3.7	0.6813	4.5	0.1	2.9	0.65	0.0581	3.4	527	15	528	19	532	75	99
410 APATITE 2	12	10.03	993	3.8	0.6901	4.5	0.1	2.9	0.64	0.0582	3.4	532	15	533	19	537	75	99
410 APATITE 1	12	10.70	901	2.1	0.6856	3.6	0.1	2.8	0.79	0.0578	2.2	532	14	530	15	522	48	102
411 APATITE 2	12	9.99	984	3.4	0.6784	4.2	0.1	2.8	0.66	0.0579	3.2	526	14	526	18	526	70	100
411 APATITE 1	12	10.74	931	2.2	0.6877	3.5	0.1	2.7	0.78	0.0581	2.2	531	14	531	15	533	48	100
412 APATITE 2	12	10.75	898	2.5	0.6857	3.7	0.1	2.7	0.73	0.0580	2.5	530	14	530	15	529	56	100

^{207}Pb /^{235}U error is the quadratic addition of the $^{207}Pb/^{206}Pb$ and ^{206}Pb /^{238}U uncertainty.

[a] Within run background-corrected mean signal in cps (counts per second).

[b] U content and Th/U ratio were calculated relative to reference

[c] Pb 206/204 ratios measured and percentage of common Pb on the ^{206}Pb. b.d. = below dectection limit.

[d] corrected for background, within-run Pb/U fractionation (in case of $^{206}Pb/^{238}U$) and common Pb using Stacy and Kramers (1975) model Pb and subsequently normalised to reference material used;

[e] rho is the $^{206}Pb/^{238}U/^{207}Pb/^{235}U$ error correlation coefficient.

[f] Accuracy and reproducibilty was checked by repeated analyses (n = 16) of reference zircon Plesovice, Griedel, and 91500; data given as mean with 2 standard deviation uncertainties

Appendix B: Supplementary material for research paper 2 (chapter 5)

Fig. 5.12, Thin section images.

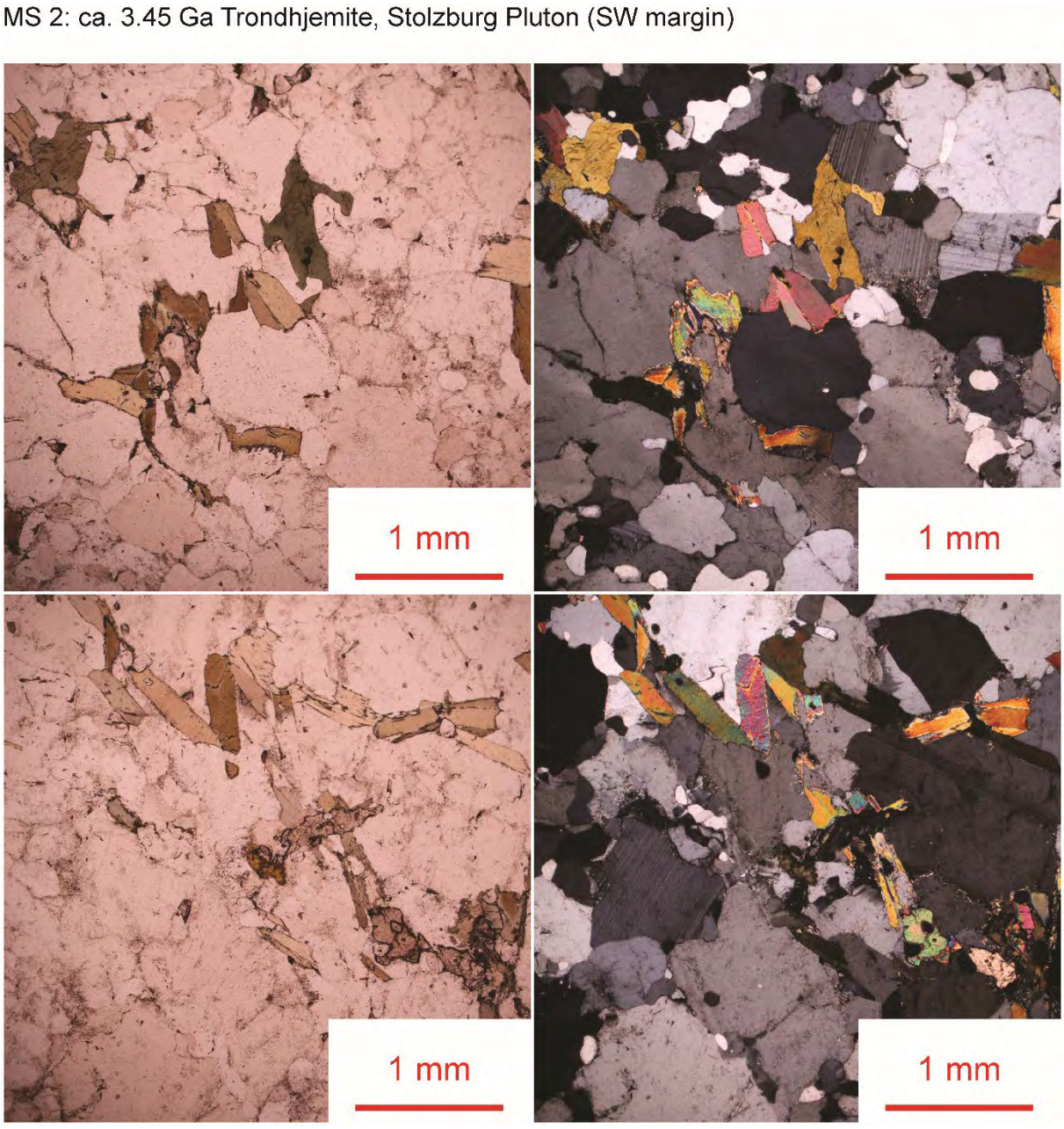

Fig. 5.12, continued.

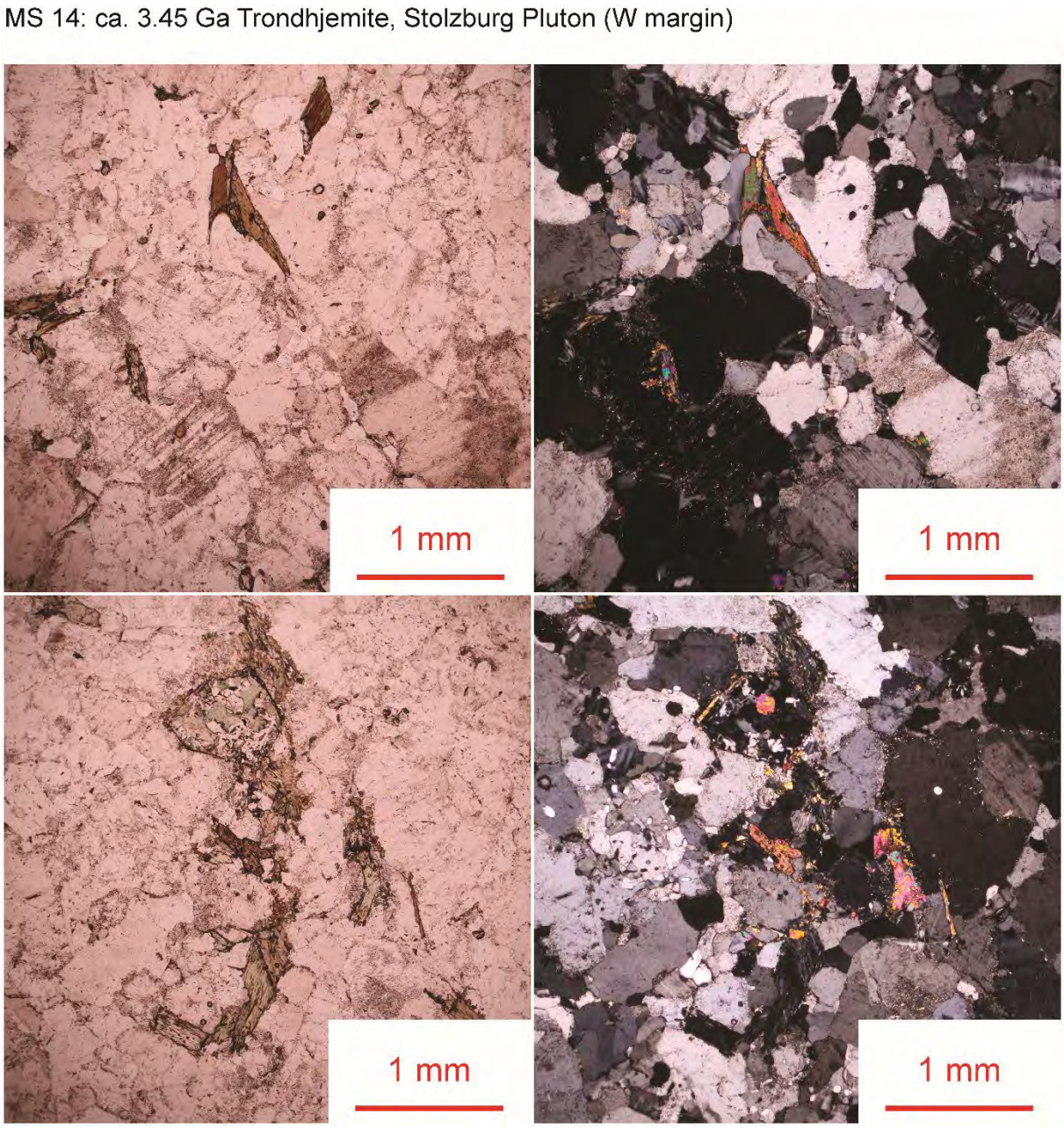

Fig. 5.12, continued.

MS 15: ca. 3.45 Ga Trondhjemite, Stolzburg Pluton (center)

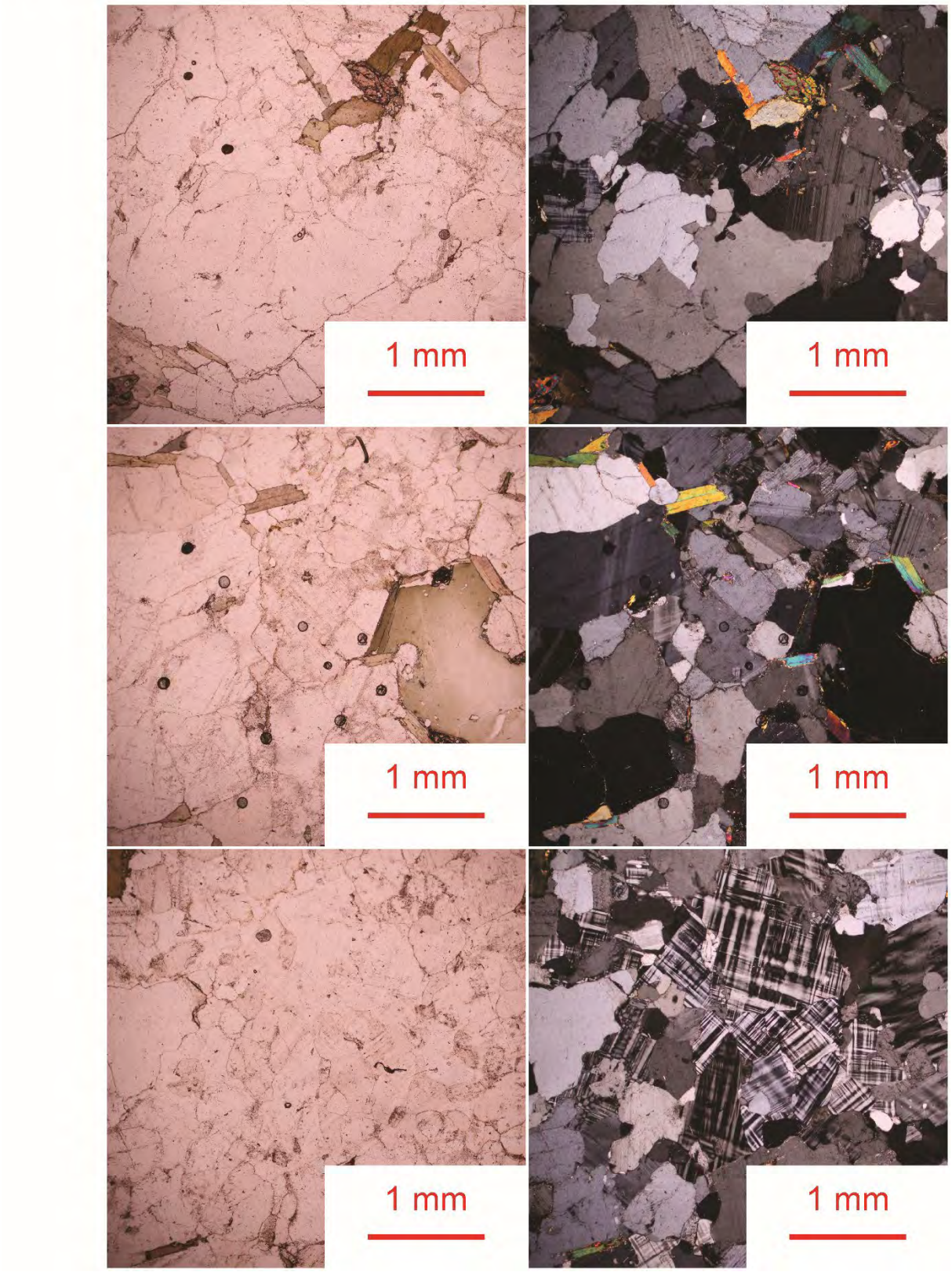

Fig. 5.12, continued.

MS 24: ca. 3.2 Ga* Trondhjemite dyke, Stolzburg Pluton (E margin)

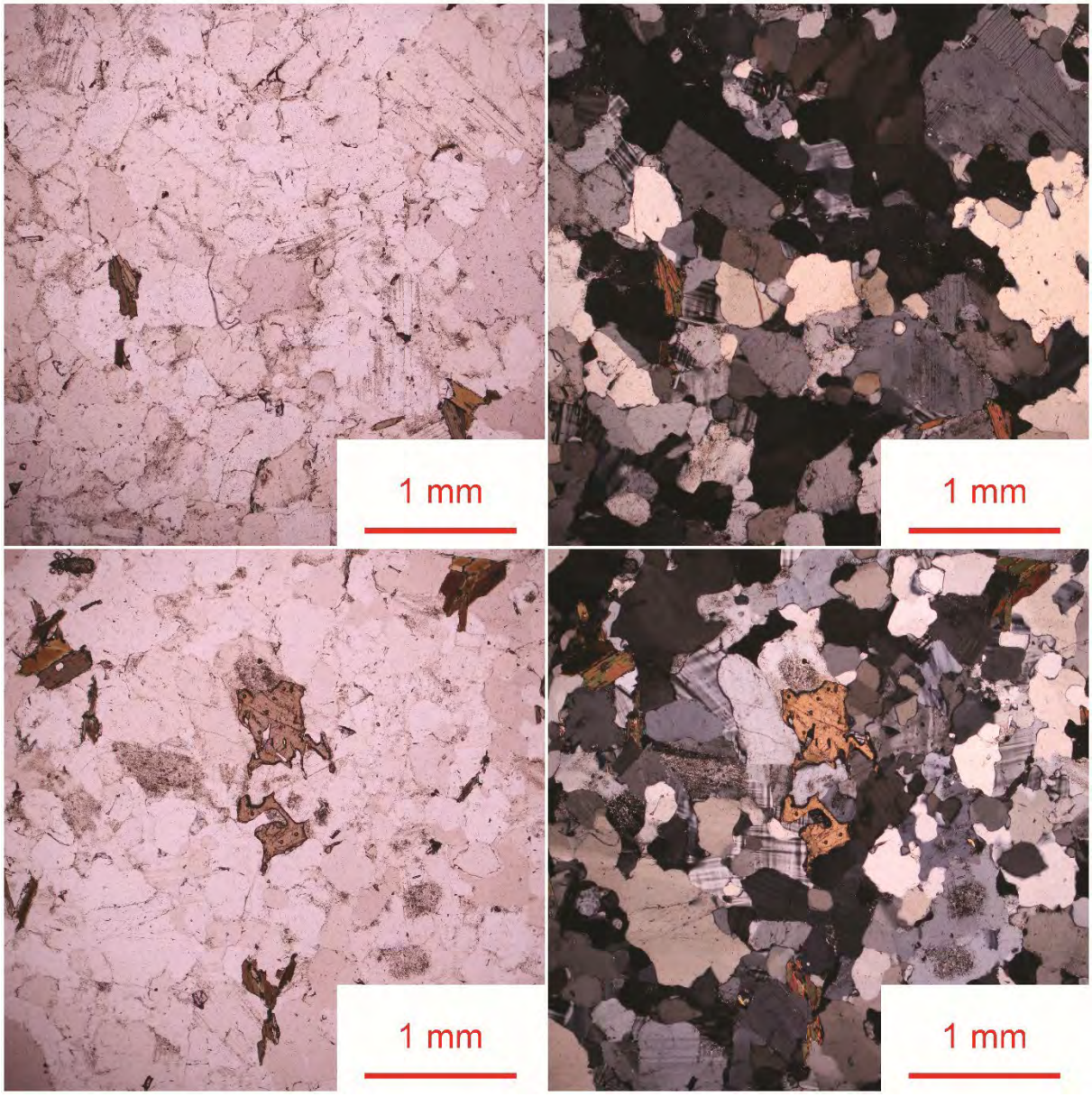

Fig. 5.12, continued.

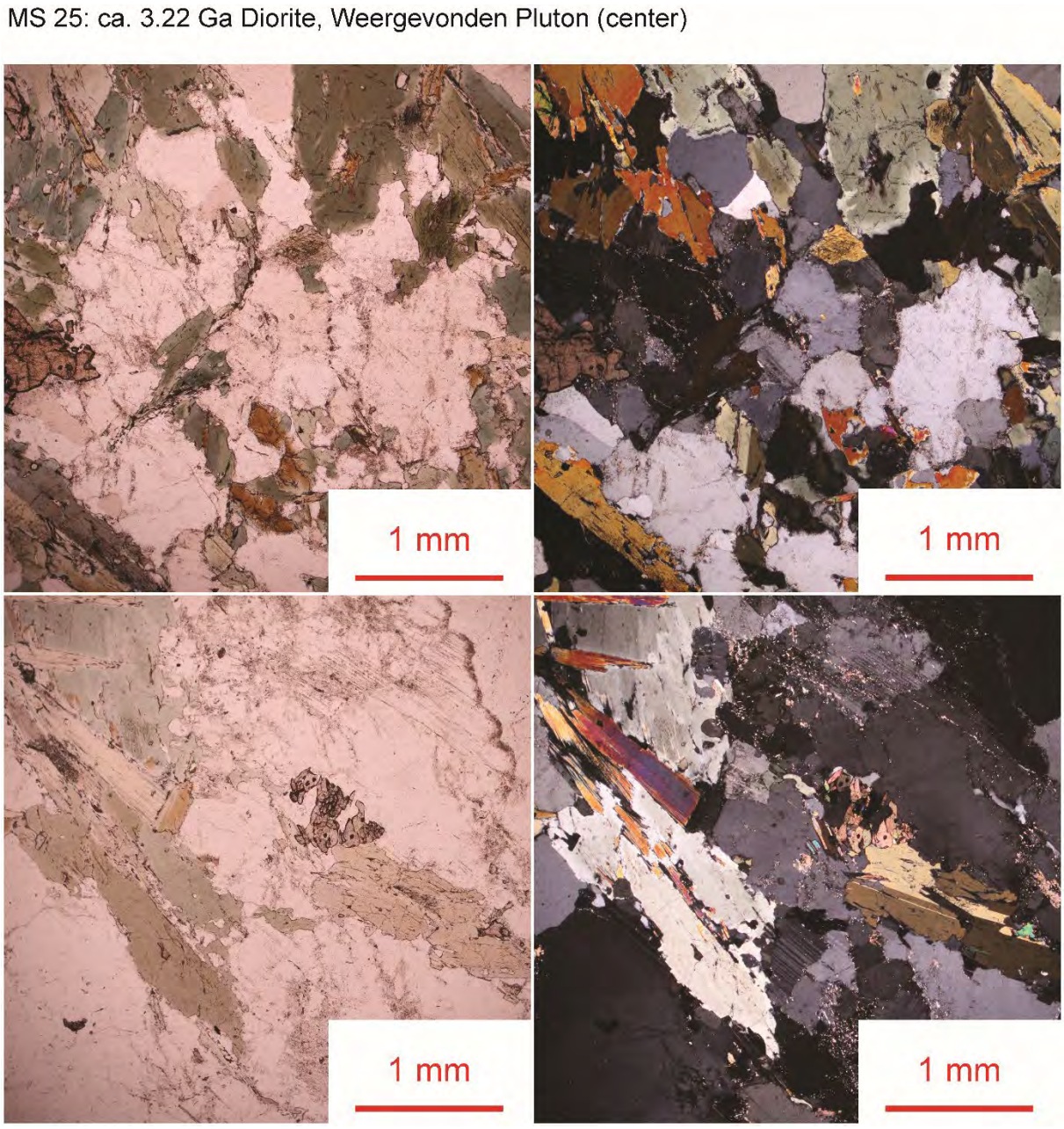

Fig. 5.12, continued.

MS 36: ca. 3.45 Ga Tonalite, Stolzburg Pluton (SW margin)

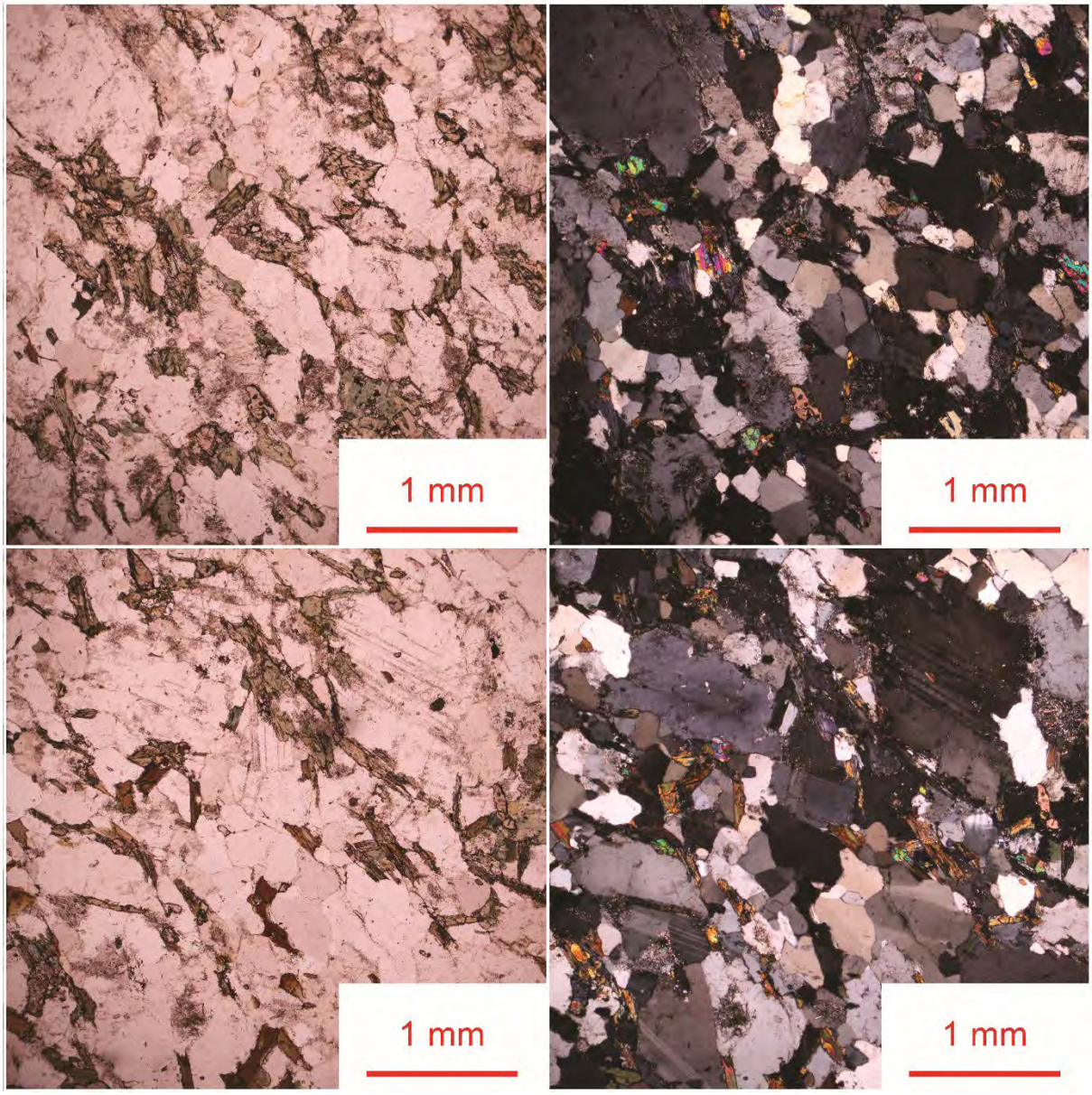

Fig. 5.13, Titanite electron and light microscope images.

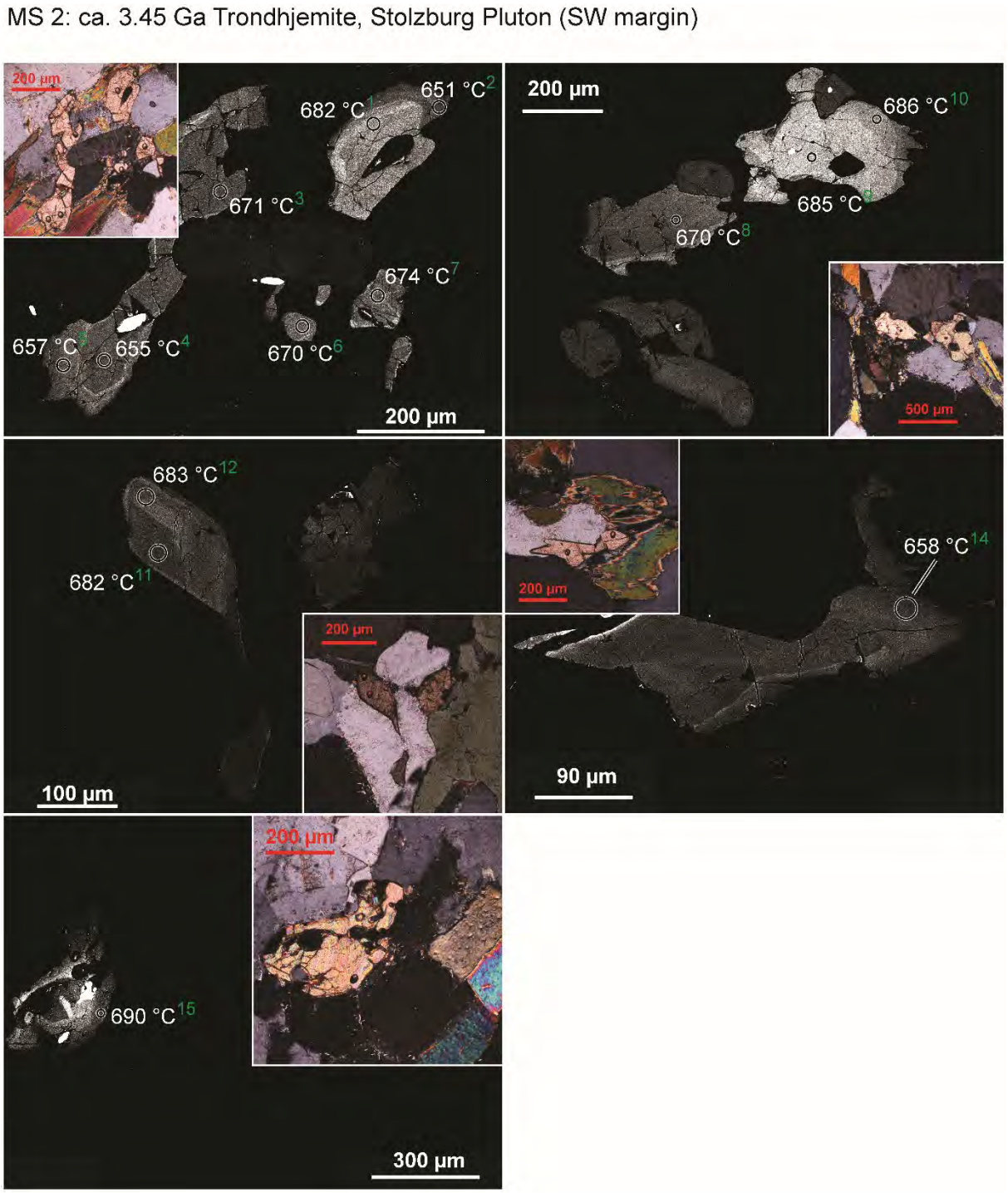

Fig. 5.13, continued.

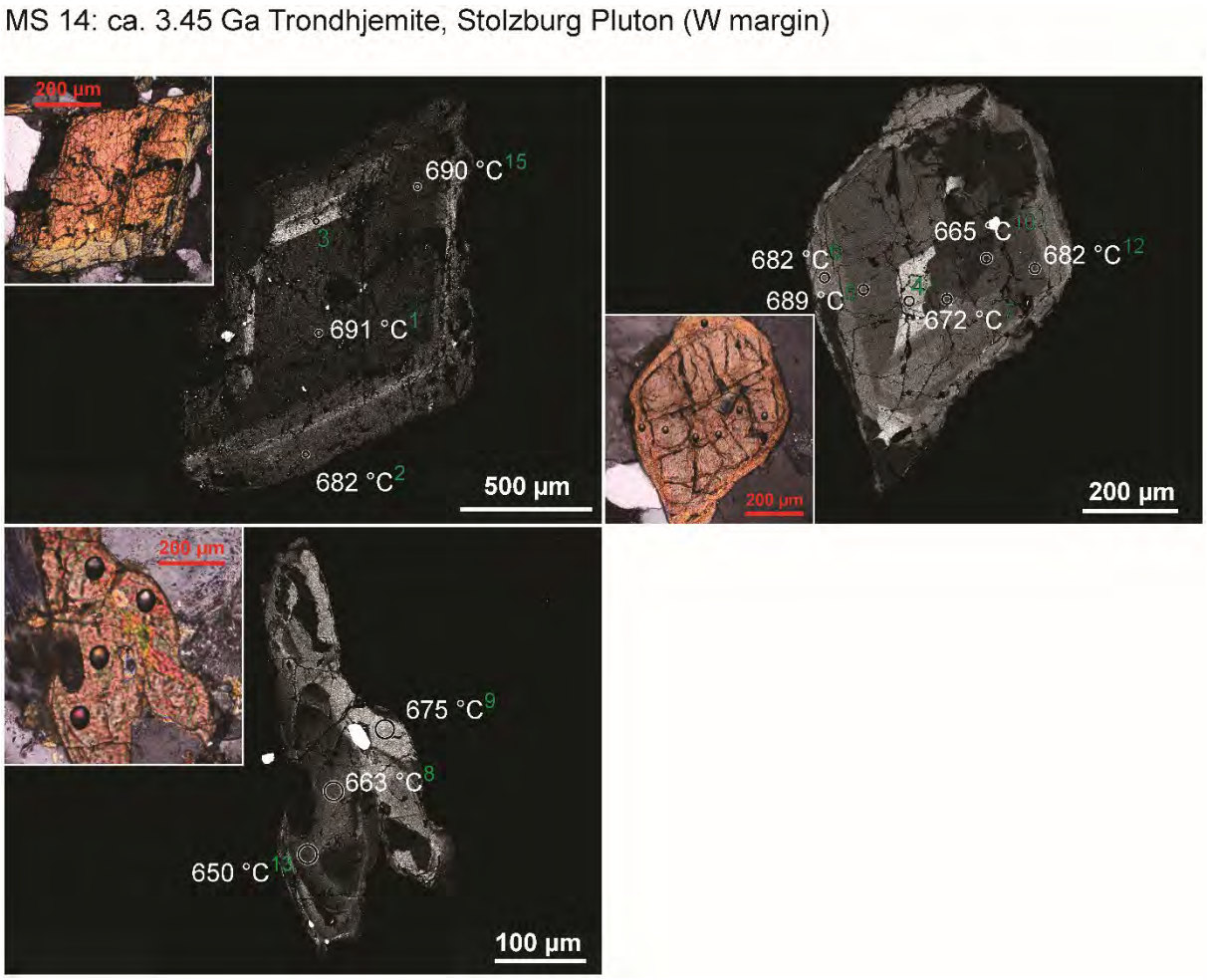

Fig. 5.13, continued.

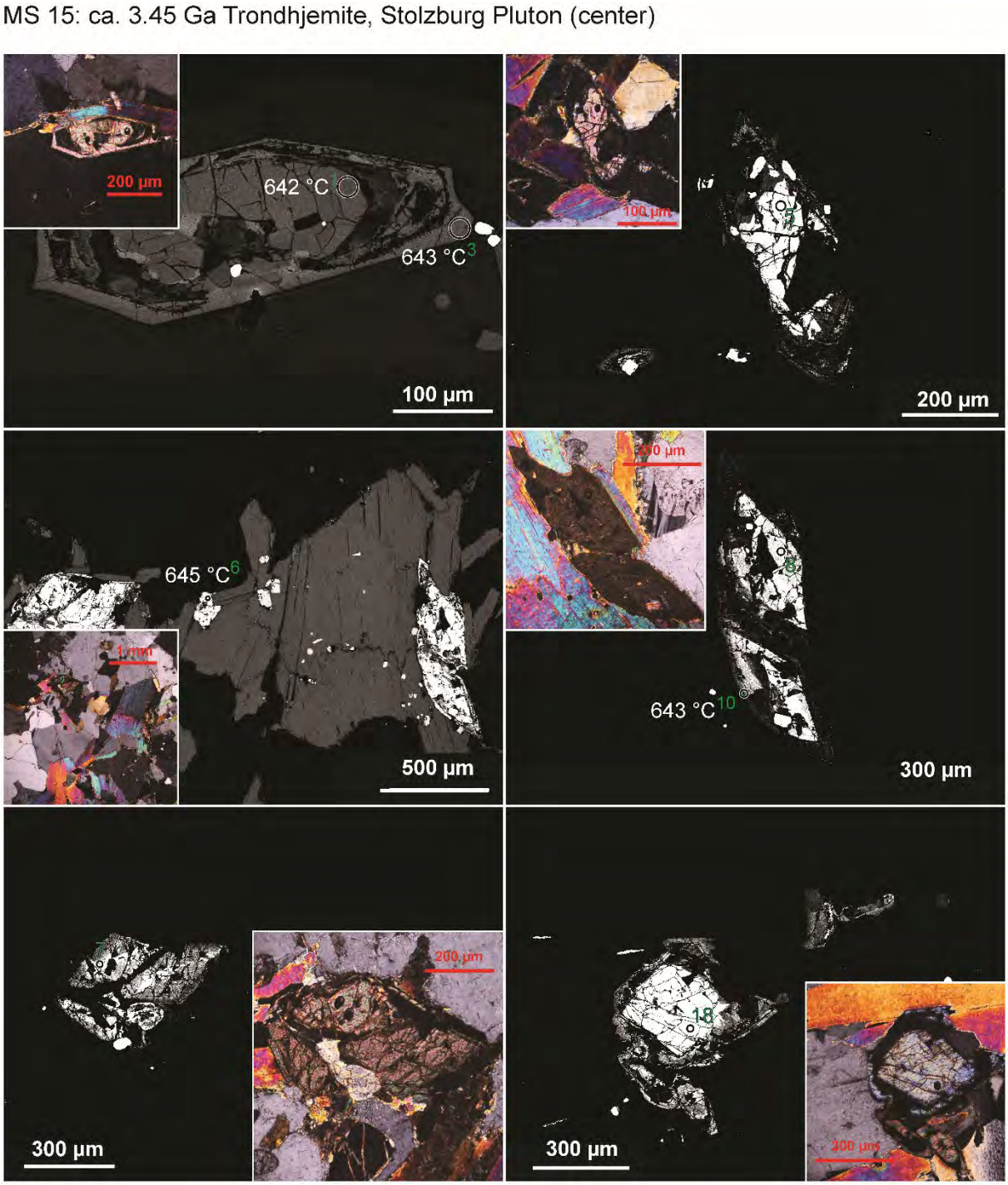

Fig. 5.13, continued.

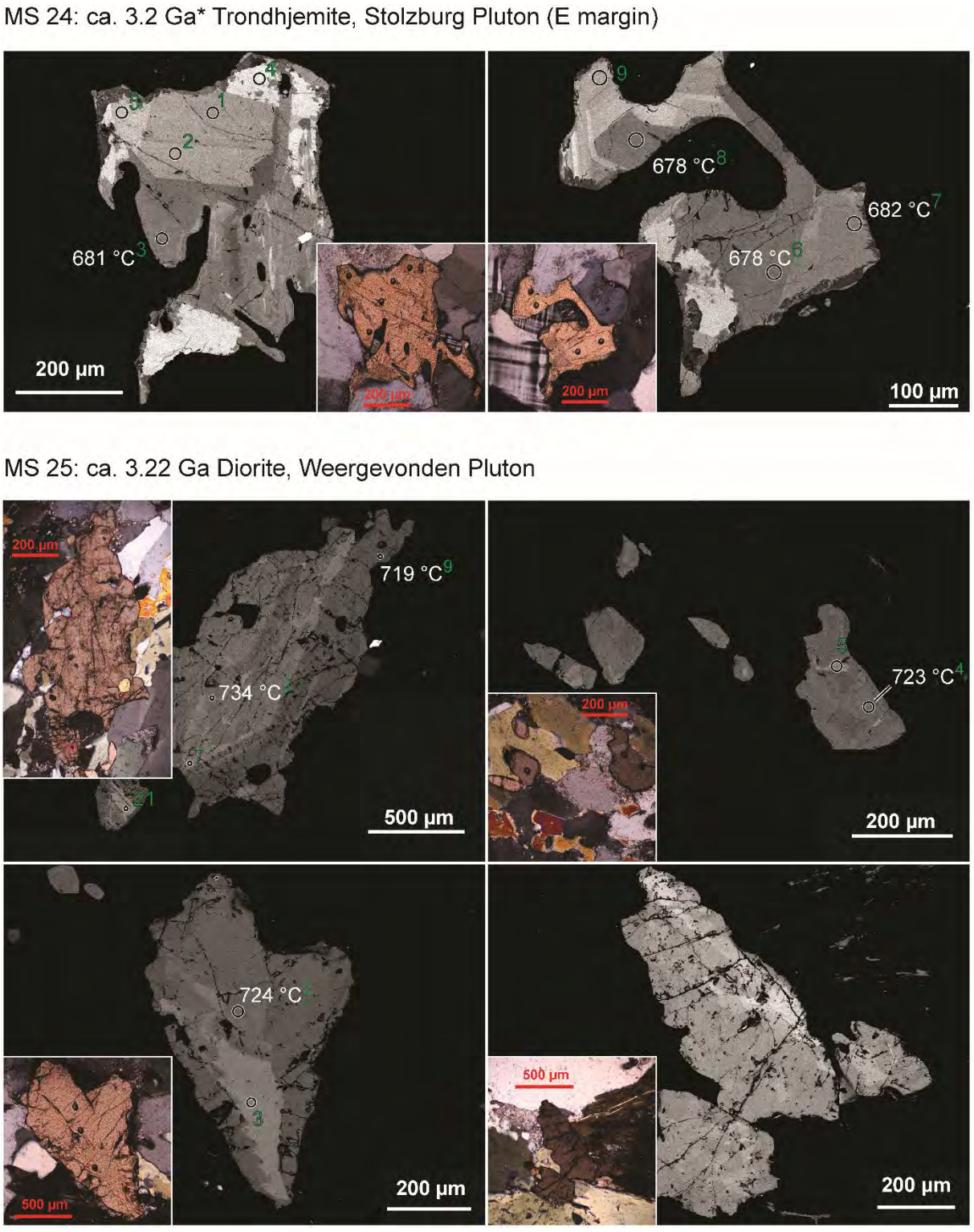

Fig. 5.13, continued.

MS 25: ca. 3.22 Ga Diorite, Weergevonden Pluton, continued

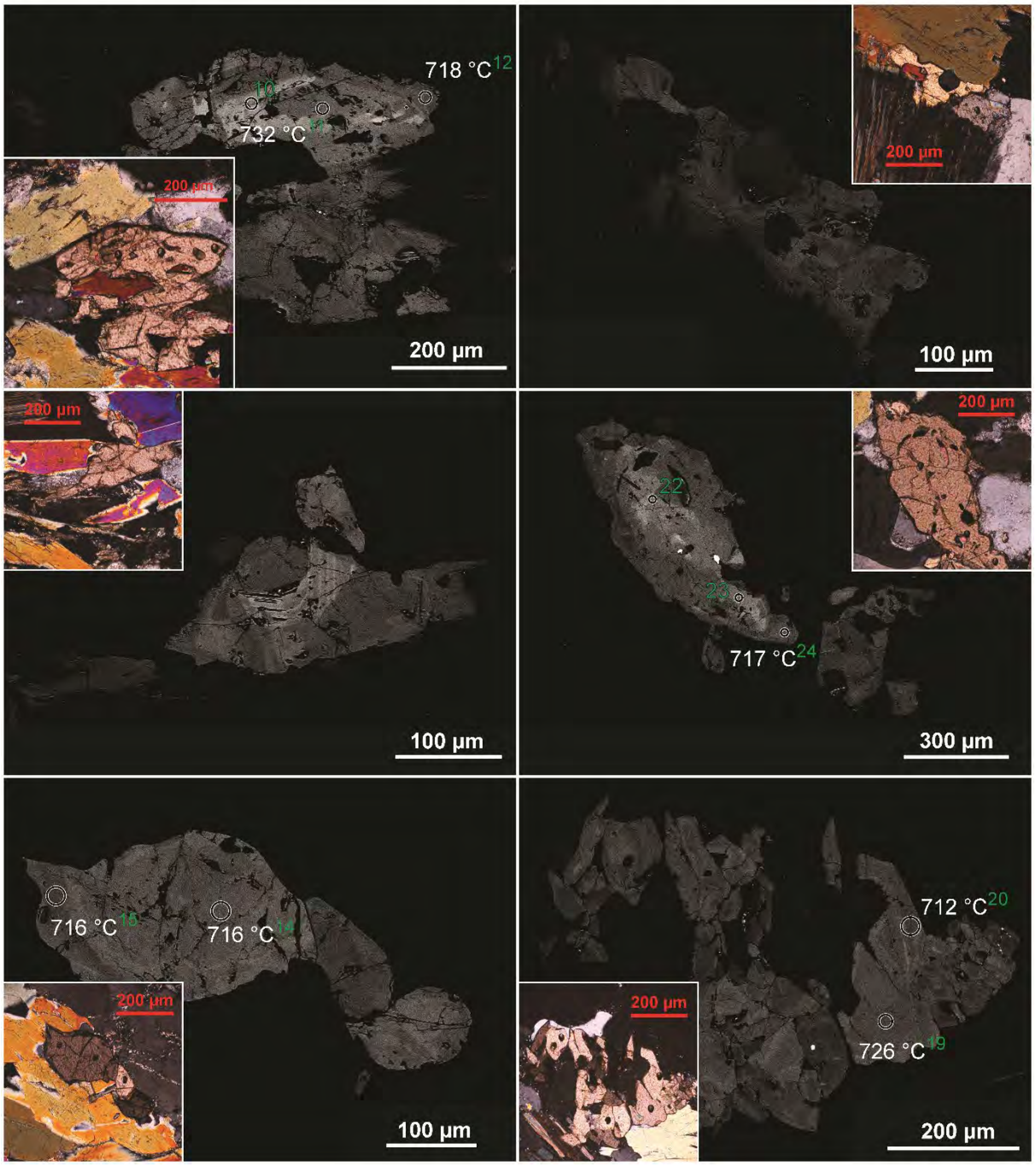

Fig. 5.13, continued.

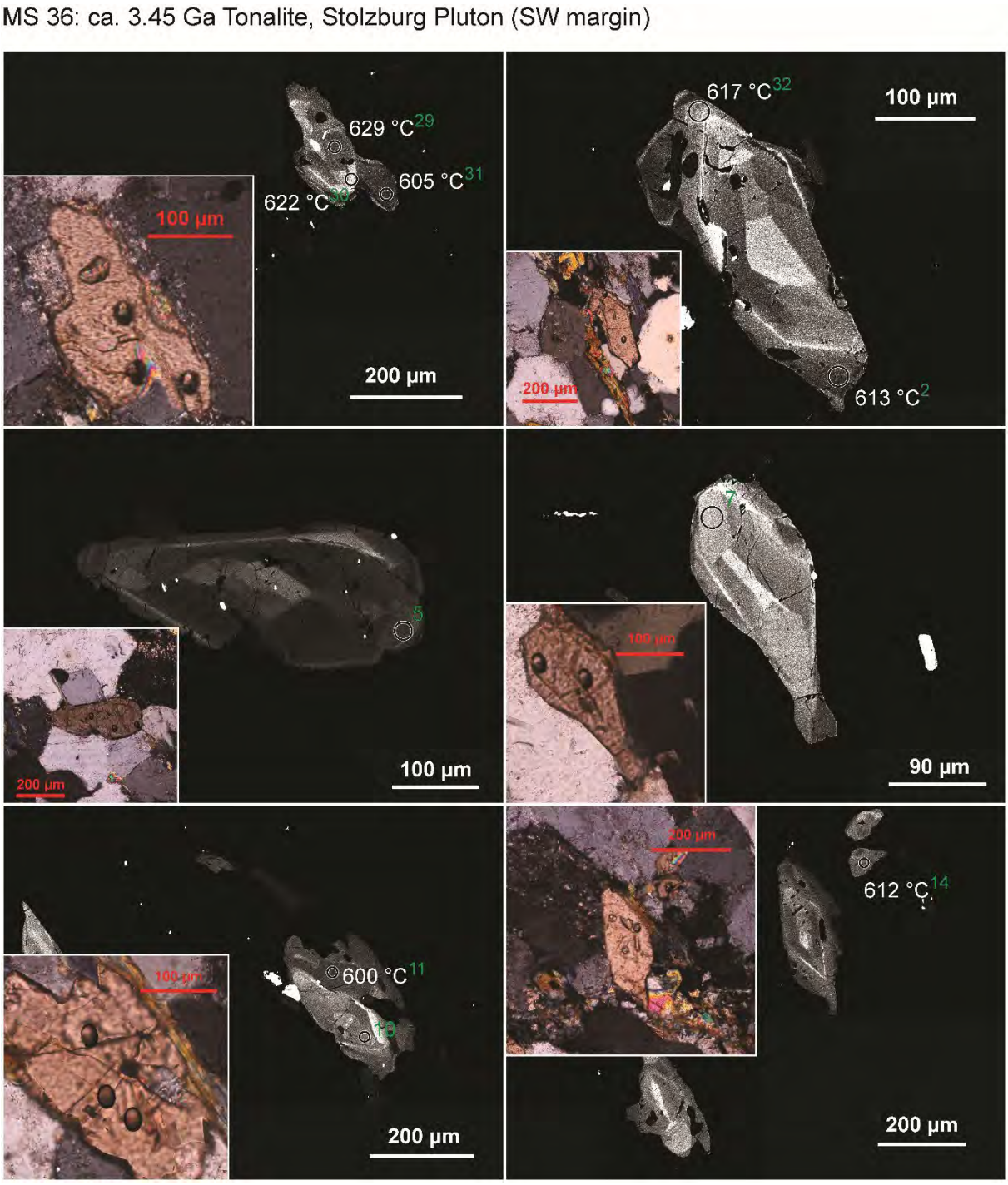

Fig. 5.13, continued.

MS 36: ca. 3.45 Ga Tonalite, Stolzburg Pluton (SW margin), continued

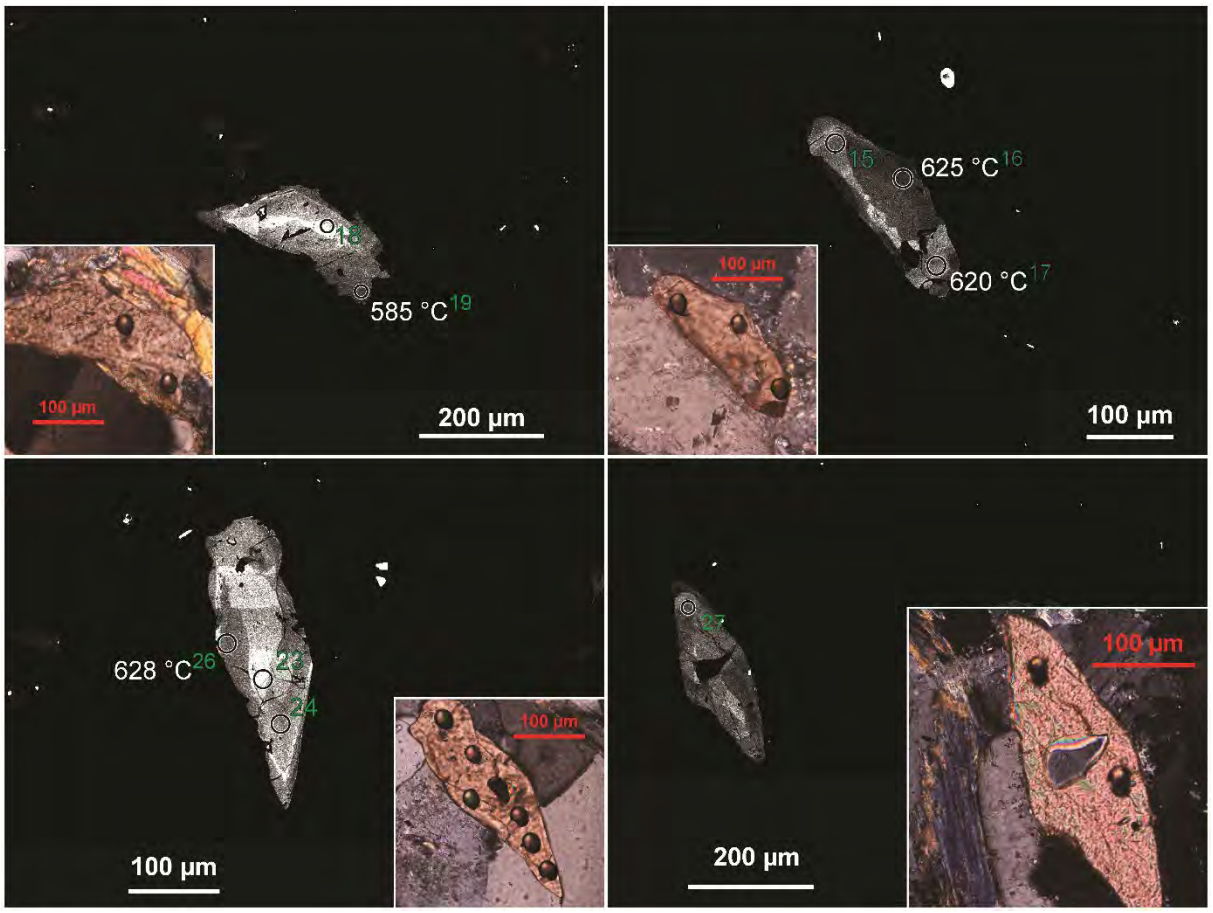

Fig. 5.14. Cathodoluminescence images of apatite grains.

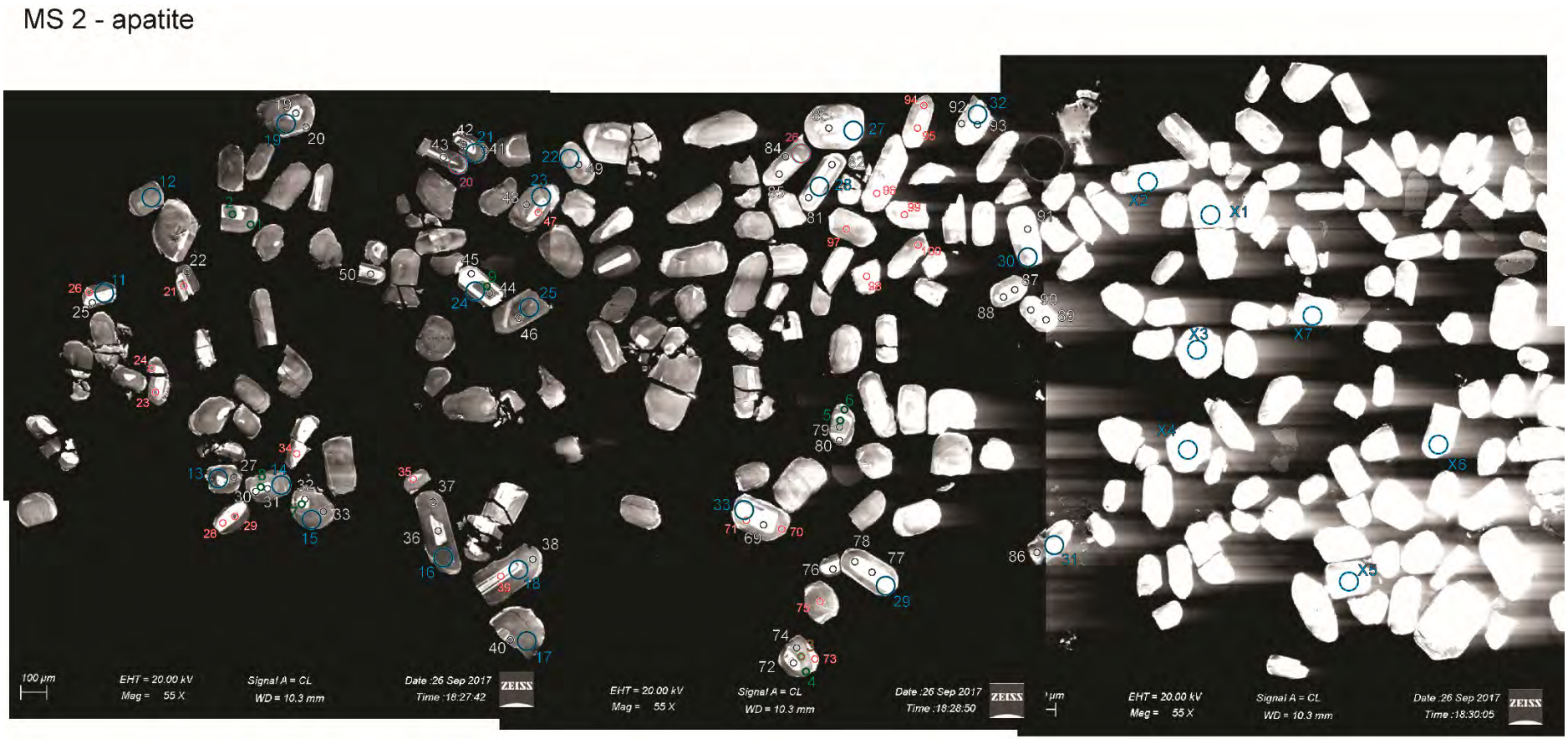

White outlines and numbers indicate the location of U-Pb isotope analyses, green circles and numbers the location of trace-element analyses and blue circles and numbers the location of Sr isotope analyses. Discarded analyses are marked by red outlines around the numbers and by red circles. See Table 4.9 for U-Pb isotope data, Table 5.4 for trace-element data and Table 5.8 for Sr isotope data.

Fig. 5.14, continued.

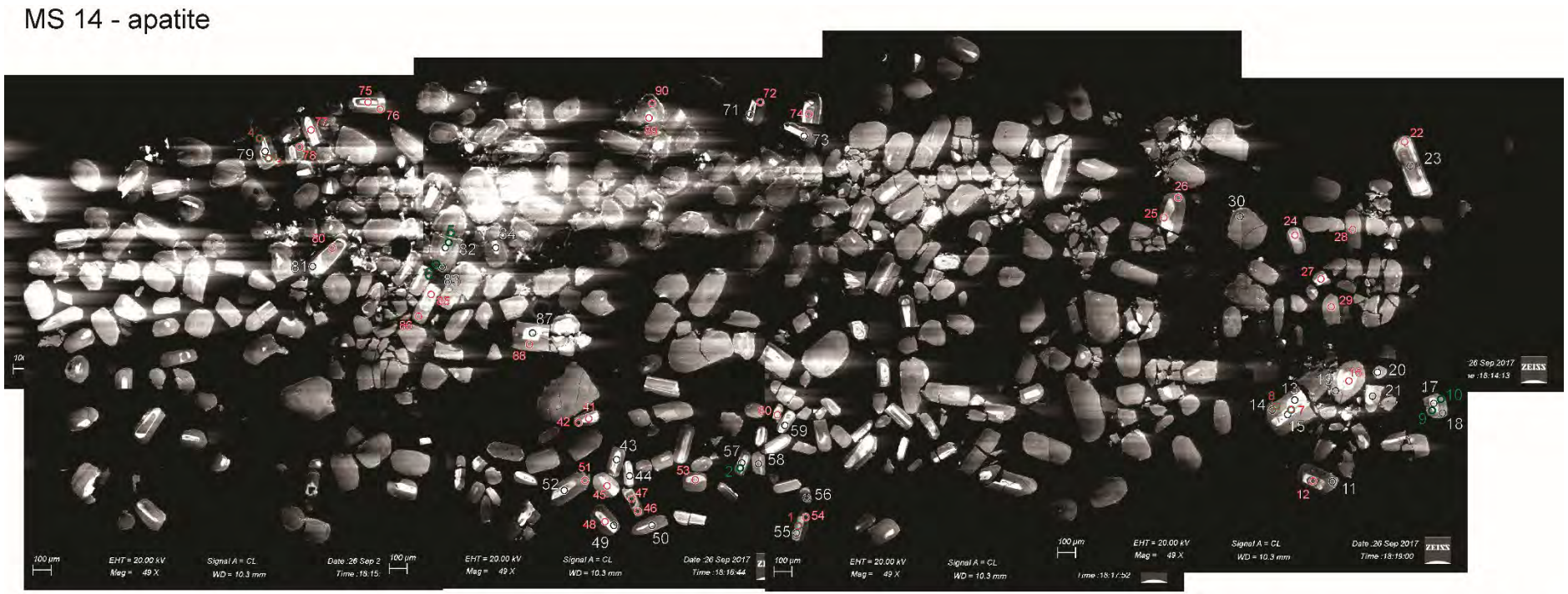

White outlines and numbers indicate the location of U-Pb isotope analyses and green circles and numbers the location of trace-element analyses. Discarded analyses are marked by red outlines around the numbers and by red circles. See Table 4.9 for U-Pb isotope data and Table 5.4 for trace-element data.

Fig. 5.14, continued.

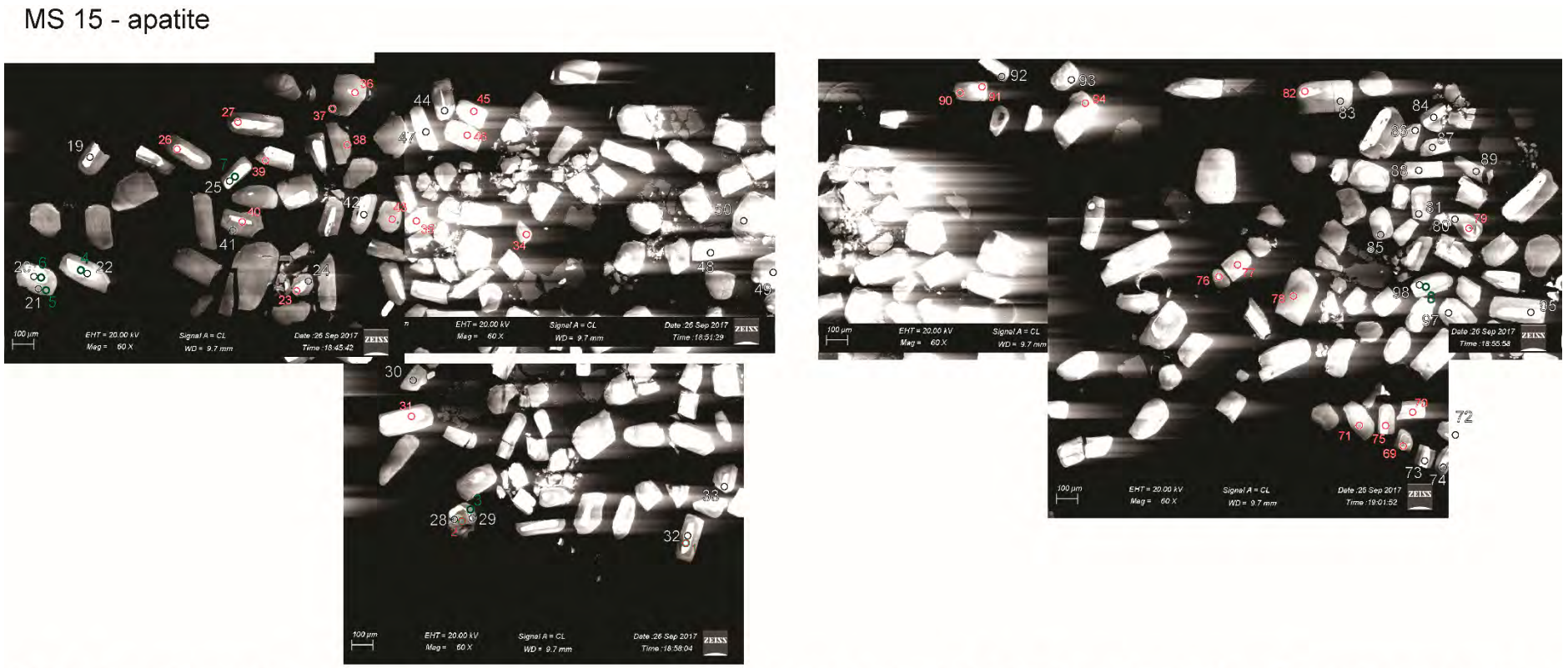

White outlines and numbers indicate the location of U-Pb isotope analyses and green circles and numbers the location of trace-element analyses. Discarded analyses are marked by red outlines around the numbers and by red circles. See Table 4.9 for U-Pb isotope data and Table 5.4 for trace-element data.

Fig. 5.14, continued.

MS 25 - apatite

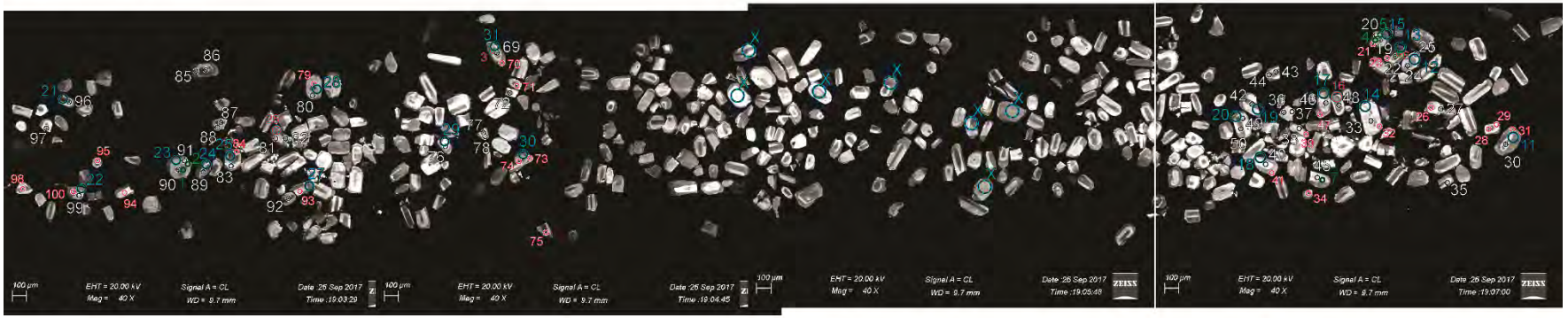

MS 36 - apatite

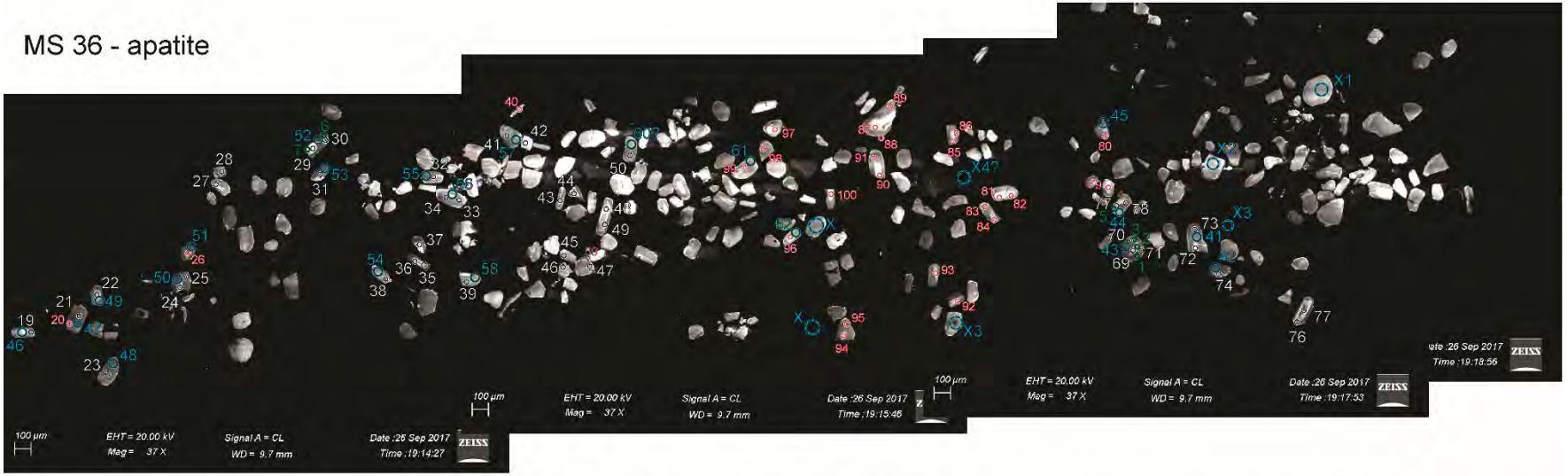

White outlines and numbers indicate the location of U-Pb isotope analyses, green circles and numbers the location of trace-element analyses and blue circles and numbers the location of Sr isotope analyses. Discarded analyses are marked by red outlines around the numbers and by red circles. See Table 4.9 for U-Pb isotope data, Table 5.4 for trace-element data and Table 5.8 for Sr isotope data.

Table 5.4. Major- and trace-element compositions of apatite grains from granitoid samples from the Stolzburg Block.

Sample								**MS 2**									**MS 14**															**MS 15**		
# of analysis EMP	1	2	3	4	5	6	7	8	9	10	11	12	13	14	15	16	17	18	19	20	21	22	23	24	25	26	27	28	29	30	31	32	33
# of analysis ICP MS		4		7	8			2	1		9			5	6	9	10					5	6						2		4	5	6
Weight%																																	
Na	b.d.	b.d.	b.d.	b.d.	b.d.	b.d.	b.d.	b.d.	b.d.	b.d.	b.d.	b.d.	b.d.	b.d.	b.d.	b.d.	b.d.	b.d.	b.d.	b.d.	b.d.	b.d.	b.d.	b.d.	b.d.	b.d.	b.d.	b.d.	b.d.	b.d.	b.d.	b.d.	b.d.
Si	0.04	b.d.	0.05	b.d.	b.d.	b.d.	0.03	0.08	0.03	0.05	0.10	0.07	b.d.	0.04	b.d.	1.92	b.d.	0.05	0.67	0.04	b.d.	b.d.	b.d.	0.05	b.d.	b.d.	b.d.	0.05	0.04	0.05	0.04	0.07	0.03
F	3.38	3.49	3.22	3.70	3.71	3.69	3.44	3.52	3.56	3.52	3.46	3.13	3.47	3.18	3.50	3.05	3.73	3.53	3.42	3.36	3.63	3.75	3.36	3.64	3.63	3.53	3.59	3.62	3.68	3.42	3.41	3.47	3.48
P	17.92	18.10	17.73	17.81	18.20	17.62	18.00	17.58	17.63	18.09	17.84	17.92	17.80	17.89	17.99	15.94	18.13	17.97	17.06	17.88	18.04	17.91	17.90	17.92	17.74	17.97	18.17	17.82	17.77	17.91	17.75	17.75	17.80
Cl	b.d.	b.d.	b.d.	b.d.	b.d.	b.d.	b.d.	b.d.	b.d.	b.d.	b.d.	b.d.	b.d.	b.d.	b.d.	b.d.	b.d.	b.d.	b.d.	b.d.	b.d.	b.d.	b.d.	b.d.	b.d.	b.d.	b.d.	b.d.	b.d.	b.d.	b.d.	b.d.	b.d.
Ca	40.68	40.56	39.72	40.13	40.37	39.92	39.86	40.20	40.60	40.35	40.12	40.34	40.88	40.30	40.69	34.81	40.99	40.61	38.30	40.50	40.60	40.36	40.76	40.45	40.33	40.53	41.10	40.45	40.48	40.27	40.18	39.71	40.58
Ce	b.d.	b.d.	b.d.	b.d.	b.d.	b.d.	b.d.	b.d.	b.d.	0.10	b.d.	b.d.	b.d.	b.d.	b.d.	b.d.	b.d.	b.d.	b.d.	b.d.	b.d.	b.d.	b.d.	b.d.	b.d.	b.d.	b.d.	b.d.	b.d.	b.d.	b.d.	0.10	b.d.
S	b.d.	b.d.	b.d.	b.d.	b.d.	b.d.	b.d.	0.07	0.05	b.d.	0.06	0.06	0.04	b.d.	b.d.	b.d.	0.04	b.d.	b.d.	b.d.	b.d.	b.d.	0.05	b.d.	0.04	b.d.	b.d.	b.d.	b.d.	b.d.	b.d.	b.d.	b.d.
La	b.d.	b.d.	b.d.	b.d.	b.d.	b.d.	b.d.	b.d.	b.d.	b.d.	b.d.	b.d.	b.d.	b.d.	b.d.	b.d.	b.d.	b.d.	b.d.	b.d.	b.d.	b.d.	b.d.	b.d.	b.d.	b.d.	b.d.	b.d.	b.d.	b.d.	b.d.	b.d.	b.d.
Sr	0.07	0.07	0.08	0.07	0.09	0.08	0.05	0.06	0.07	0.10	0.06	0.08	0.08	0.07	0.08	b.d.	0.06	b.d.	b.d.	0.06	0.06	b.d.	b.d.	b.d.	b.d.	0.06	b.d.	0.05	0.05	0.06	0.06	0.06	b.d.
Y	b.d.	b.d.	b.d.	b.d.	b.d.	b.d.	b.d.	b.d.	b.d.	b.d.	b.d.	b.d.	b.d.	b.d.	b.d.	b.d.	b.d.	b.d.	b.d.	b.d.	b.d.	b.d.	b.d.	b.d.	b.d.	b.d.	b.d.	b.d.	0.05	b.d.	b.d.	b.d.	b.d.
O	38.94	38.79	38.52	38.54	39.20	38.81	39.12	38.57	38.80	38.94	39.24	38.78	40.02	38.99	39.22	39.17	38.55	39.31	41.02	38.94	39.14	38.37	38.89	38.61	38.41	38.87	39.16	38.57	38.12	38.40	38.22	37.76	38.71
Total	101.12	101.05	99.46	100.40	101.61	100.19	100.62	100.22	100.79	101.26	100.98	100.51	102.34	100.59	101.59	95.02	101.57	101.57	100.56	100.91	101.56	100.52	101.08	100.81	100.26	101.06	102.14	100.70	100.22	100.27	99.78	99.00	100.70
Weight% Oxides																																	
CaO	56.92	56.75	55.57	56.15	56.49	55.86	55.78	56.24	56.81	56.46	56.14	56.45	57.19	56.38	56.94	48.70	57.35	56.82	53.59	56.67	56.81	56.46	57.03	56.60	56.43	56.71	57.50	56.60	56.63	56.34	56.22	55.55	56.77
SrO	0.08	0.08	0.10	0.09	0.10	0.09	0.06	0.07	0.08	0.12	0.07	0.10	0.09	0.08	0.09	0.00	0.07	0.00	0.00	0.07	0.07	0.00	0.00	0.00	0.00	0.07	0.00	0.06	0.06	0.07	0.08	0.07	0.00
Ce_2O_3	0.00	0.00	0.00	0.00	0.00	0.00	0.00	0.00	0.00	0.11	0.00	0.00	0.00	0.00	0.00	0.00	0.00	0.00	0.00	0.00	0.00	0.00	0.00	0.00	0.00	0.00	0.00	0.00	0.00	0.00	0.00	0.00	0.00
P_2O_5	41.05	41.48	40.63	40.81	41.71	40.37	41.25	40.28	40.40	41.46	40.88	41.07	40.79	40.98	41.23	36.52	41.54	41.18	39.10	40.98	41.34	41.03	41.01	41.06	40.65	41.17	41.64	40.83	40.72	41.03	40.68	40.67	40.78
SiO_2	0.08	0.00	0.11	0.00	0.00	0.00	0.07	0.17	0.06	0.11	0.22	0.15	0.00	0.08	0.00	4.11	0.00	0.10	1.44	0.09	0.00	0.00	0.00	0.10	0.00	0.00	0.00	0.12	0.08	0.11	0.07	0.14	0.06
SO_3								0.18	0.13		0.16	0.15	0.10				0.10						0.11			0.11								
Atoms p.f.u. [a]																																	
Ca	10.30	10.23	10.21	10.26	10.16	10.29	10.15	10.33	10.38	10.18	10.22	10.23	10.37	10.25	10.28	9.47	10.28	10.27	10.04	10.28	10.25	10.27	10.33	10.26	10.32	10.27	10.29	10.29	10.32	10.23	10.28	10.20	10.33
Sr	0.01	0.01	0.01	0.01	0.01	0.01	0.01	0.01	0.01	0.01	0.01	0.01	0.01	0.01	0.01	0.00	0.01	0.00	0.00	0.01	0.01	0.00	0.00	0.00	0.00	0.01	0.00	0.01	0.01	0.01	0.01	0.01	0.00
Ce	0.00	0.00	0.00	0.00	0.00	0.00	0.00	0.00	0.00	0.01	0.00	0.00	0.00	0.00	0.00	0.00	0.00	0.00	0.00	0.00	0.00	0.00	0.00	0.00	0.00	0.00	0.00	0.00	0.00	0.00	0.00	0.00	0.00
∑	10.30	10.23	10.22	10.27	10.17	10.30	10.15	10.33	10.39	10.20	10.23	10.24	10.38	10.26	10.29	9.47	10.29	10.27	10.04	10.29	10.26	10.27	10.33	10.26	10.32	10.27	10.29	10.30	10.32	10.24	10.29	10.20	10.33
P	5.87	5.91	5.90	5.89	5.93	5.88	5.93	5.84	5.84	5.91	5.88	5.88	5.85	5.89	5.88	5.61	5.88	5.88	5.79	5.87	5.90	5.89	5.87	5.88	5.87	5.89	5.89	5.87	5.86	5.89	5.88	5.90	5.86
Si	0.01	0.00	0.02	0.00	0.00	0.00	0.01	0.03	0.01	0.02	0.04	0.02	0.00	0.01	0.00	0.75	0.00	0.02	0.25	0.01	0.00	0.00	0.00	0.02	0.00	0.00	0.00	0.02	0.01	0.02	0.01	0.02	0.01
∑	5.88	5.91	5.92	5.89	5.93	5.88	5.94	5.87	5.85	5.92	5.92	5.91	5.85	5.90	5.88	6.36	5.88	5.90	6.04	5.89	5.90	5.89	5.87	5.90	5.87	5.89	5.89	5.89	5.87	5.91	5.89	5.92	5.87
F	1.80	1.86	1.75	1.99	1.97	2.01	1.85	1.91	1.92	1.87	1.86	1.67	1.86	1.71	1.86	1.75	1.97	1.88	1.89	1.80	1.94	2.01	1.80	1.95	1.96	1.89	1.89	1.94	1.98	1.83	1.84	1.88	1.87
Cl	0.00	0.00	0.00	0.00	0.00	0.00	0.00	0.00	0.00	0.00	0.00	0.00	0.00	0.00	0.00	0.00	0.00	0.00	0.00	0.00	0.00	0.00	0.00	0.00	0.00	0.00	0.00	0.00	0.00	0.00	0.00	0.00	0.00
OH	0.20	0.14	0.25	0.01	0.03	-0.01	0.15	0.09	0.08	0.13	0.14	0.33	0.14	0.29	0.14	0.25	0.03	0.12	0.11	0.20	0.06	-0.01	0.20	0.05	0.04	0.11	0.11	0.06	0.02	0.17	0.16	0.12	0.13
spot#		**MS2-4**		**MS2-7**	**MS2-8**			**MS2-2**	**MS2-1**		**MS2-9**			**MS2-5**	**MS2-6**	**MS14-9**	**MS14-10**					**MS14-5**	**MS14-6**						**MS14-2**		**MS15-4**	**MS15-5**	**MS15-6**
^{6}Li		<2.76		<3.25	<2.88			6.03	<3.23		<2.44			<2.83	<2.56	3.34	<2.54					3.77	<2.56						<2.42		2.75	5.73	<2.33
^{7}Li		<1.57		<1.93	<1.77			3.46	<1.84		<1.53			<1.71	<1.58	<1.28	<1.67					3.06	<1.63						<1.55		<1.62	3.23	<1.65
^{43}Ca		405235.4		401661.9	404520.7			401661.9	405950		400947.2			403091.3	406664.8	348059.4	410238.3					403806	407379.5						404520.7		401661.8	397373.6	405950
^{44}Ca		434958.3		425706.1	427778.4			430562.2	439976.7		420433.8			435291.3	439523.9	375534.7	450910.7					433669.8	440192.5						440605.7		431567.6	423668.8	443265
^{47}Ti		25.49		12.17	11.25			16.5	13.95		<8.59			14.14	19.5	14.46	14.41					13.17	20.17						17.01		21.65	12.22	14.61
^{49}Ti		<6.70		<8.26	<7.50			<7.42	<7.82		<6.50			<7.28	<6.66	<5.20	<6.87					<6.93	<6.84						<6.51		<6.62	<6.23	<6.63
^{51}V		1.34		2.74	2.3			9.03	2.98		6.85			6.54	2.48	1.2	2.23					1.63	1.91						2.69		1.61	2.54	2.88
^{53}Cr		<7.69		<9.31	<8.56			<8.56	<8.99		<7.35			<8.27	<7.57	<5.64	<7.74					<7.94	<8.04						<7.59		9.83	9.87	<7.12
^{88}Sr		717		769.96	755.93			741.68	723.34		741.51			736.6	722.13	503.08	501.51					472.25	522.64						576.15		575.14	584.92	571.15
^{89}Y		22.08		215.44	126.75			107.36	52.9		95.32			99.79	40.71	315.83	61.6					171.33	57.72						382.08		260.1	329.89	116.24
^{91}Zr		<0.96		<1.18	<1.09			<1.06	<1.10		<0.94			<1.05	<0.96	<0.78	<1.02					<1.01	<1.02						<0.96		<1.02	<0.96	<1.04
^{93}Nb		<0.031		<0.037	<0.031			<0.031	<0.036		<0.030			<0.028	<0.0263	<0.0212	<0.030					<0.029	<0.0268						<0.028		<0.0259	<0.0246	<0.030
^{139}La		41.12		273.04	141.09			148.99	78.74		104.51			128.18	57.92	96.37	24.13					77.56	23.7						118.84		163.8	202.9	26.45
^{140}Ce		100.71		739.42	390.98			394.46	204.1		280.55			334.78	146.32	281.58	68.67					212.33	67.14						355.51		473.73	628.06	91.53
^{141}Pr		13.53		102.24	57.29			52.77	28.11		39.6			47.29	20.27	44.74	10.44					31.43	10.06						56.27		73.16	100.1	16.15
^{146}Nd		64.7		517.03	296.13			256.44	136.2		204.61			232.48	101.68	242.13	56					165.28	53.83						314.14		378.83	524.07	97.84
^{147}Sm		12.8		111.45	65.75			53.29	28.02		45.07			49.62	21.26	65.46	13.93					41.64	14.09						86.16		90.33	126.52	31.06
^{153}Eu		6.47		46.13	25.01			25.82	12.6		17.7			21.21	9.05	32.84	10.4					29.29	8.12						40.56		23.74	33.51	13.18
^{157}Gd		11.33		99.42	61.14			46.68	24.54		41.97			45.87	19.98	72.48	15.76					45.88	15.31						95.16		86.74	114.82	32.76
^{159}Tb		0.914		9.27	5.49			4.34	2.239		3.92			4.35	1.728	7.93	1.562					4.7	1.554						10.13		8.73	11.44	3.38
^{163}Dy		4.27		41.88	24.8			20.53	10.18		18.18			18.97	8.03	41.88	7.96					24.66	8.37						54.3		42.68	54.69	17.38
^{165}Ho		0.76		7.44	4.4			3.59	1.861		3.28			3.37	1.386	8.64	1.727					5.03	1.695						11.08		7.87	9.98	3.2
^{166}Er		1.899		18.82	10.89			9.01	4.46		8.29			8.78	3.3	25.18	5.01					14.31	5.04						32.46		21.62	26.83	8.94
^{169}Tm		0.173		2.083	1.15			1.051	0.478		0.943			0.867	0.348	3.43	0.585					1.814	0.562						4.34		2.659	3.31	1.085
^{172}Yb		1.186		12	7.14			5.54	3		5.79			4.89	2.16	23.51	4.05					11.44	3.69						29.56		16.59	20.62	6.65
^{175}Lu		0.198		2.129	1.312			0.937	0.514		0.989			0.872	0.334	4.23	0.899					2.242	0.68						5.38		2.718	3.46	1.161
^{178}Hf		<0.091		<0.134	<0.100			<0.090	<0.079		<0.098			<0.088	<0.106	<0.088	<0.125					<0.101	<0.118						<0.106		<0.110	<0.090	<0.095
^{181}Ta		<0.0149		<0.0240	<0.0218			<0.0215	<0.0199		<0.0224			<0.0215	<0.0191	<0.0164	<0.0207					0.0167	<0.0211						0.0183		<0.0191	<0.0171	<0.0221
^{208}Pb		1.295		3.07	2.174			2.458	1.706		2.152			2.001	1.302	2.395	1.484					2.429	1.603						3.2		2.86	3.37	2.193
^{232}Th		0.154		6.26	3.87			3.55	1.285		2.538			2.67	0.305	3.65	0.598					4.38	0.208						5.87		3.75	5.77	2.08
^{238}U		0.358		6.69	4.66			**6.56**	1.935		2.314			2.99	0.594	3.76	4.19					12.49	2.75						4.1		3.05	3.91	9.59
Th/U		0.43		0.94	0.83			0.54	0.66		1.10			0.89	0.51	0.97	0.14					0.35	0.08						1.43		1.23	1.48	0.22
Sr/Y		32		3.6	6.0			6.9	14		7.8			7.4	18	1.6	8.1					2.8	9.1						1.5		2.2	1.8	4.9
ASI [b]	1.002	1.002	1.002	1.002	1.002	1.002	1.002	1.002	1.002	1.002	1.002	1.002	1.002	1.002	1.002	1.019	1.019	1.019	1.019	1.019	1.019	1.019	1.019	1.019	1.019	1.019	1.019	1.019	1.019	1.019	1.015	1.015	1.015
$^{207}Pb/^{206}Pb$ age [Ma] [c]		3445 ± 41		3436 ± 47	3198 ± 40			n/a	n/a		2804 ± 42			3452 ± 42	3199 ± 34	3110 ± 22	3127 ± 31					3106 ± 23	3436 ± 50						3453 ± 27		3434 ± 32	2831 ± 29	3217 ± 37

[a] : Mineral formula calculation using Appoach 2 of Ketcham (2015).

[b] : ASI .= Alumina Saturation Index "Al_2O_3 / ($CaO+Na_2O+K_2O$)", using whole-rock compositions of Mühlberg et al. (2021).

[c] : Approximate age of targeted apatite zone; U-Pb data from Mühlberg et al. (2021).

Ketcham, R.A., 2015. Technical Note: Calculation of stoichiometry from EMP data for apatite and other phases with mixing on monovalent anion sites †. Am. Mineral. 100, 1620–1623.

Mühlberg, M., Stevens, G., Moyen, J.-F., Kisters, A.F.M., Lana, C., 2021. Thermal evolution of the Stolzburg Block, Barberton granitoid-greenstone terrain, South Africa: Implications for Paleoarchean tectonic processes. Prec. Research

Table 5.4, continued.

Sample	**MS 15**												**MS 25**														**MS 36**					
# of analysis EMP	34	35	36	37	38	39	40	41	42	43	44	45	61	62	63	64	65	66	67	68	69	70	71	72	73	74	75	76	77	78	79	80	81
# of analysis ICP MS	7			3				8					1	2						4	5						7	5		3	2	1	
Weight%																																	
Na	b.d.	b.d.	b.d.	b.d.	b.d.	b.d.	b.d.	b.d.	b.d.	b.d.	b.d.	b.d.	b.d.	b.d.	b.d.	b.d.	b.d.	b.d.	b.d.	b.d.	b.d.	b.d.	b.d.	b.d.	b.d.	b.d.	b.d.	b.d.	b.d.	b.d.	b.d.	b.d.
Si	0.08	b.d.	b.d.	b.d.	0.09	0.08	b.d.	0.07	b.d.	0.04	b.d.	0.04	0.03	0.03	0.06	b.d.	0.04	0.04	0.02	0.03	0.03	0.04	b.d.	0.04	0.03	b.d.	0.03	0.03	0.02	b.d.	0.04	b.d.	0.04
F	3.47	3.50	4.27	3.85	3.26	3.40	3.47	3.52	3.56	3.52	3.77	3.39	3.45	3.35	3.10	3.12	3.18	3.30	3.23	3.25	3.18	3.25	3.13	3.21	3.27	3.20	3.35	3.37	3.31	3.34	3.35	3.40	3.41
P	18.06	18.28	17.82	17.90	17.77	17.77	18.34	17.95	18.02	17.70	17.79	17.75	18.39	17.93	17.77	17.87	18.06	17.90	18.06	17.64	17.88	17.97	18.08	17.74	18.20	18.25	17.71	18.05	17.84	18.18	18.21	17.81	17.89
Cl	b.d.	b.d.	b.d.	b.d.	b.d.	b.d.	b.d.	b.d.	b.d.	b.d.	b.d.	b.d.	b.d.	b.d.	b.d.	b.d.	b.d.	0.02	b.d.	b.d.	0.03	b.d.	b.d.	b.d.	b.d.	b.d.	b.d.	b.d.	b.d.	b.d.	b.d.	b.d.	b.d.
Ca	40.38	40.28	40.29	39.77	40.23	39.81	40.73	40.29	40.30	40.29	40.08	40.18	40.53	40.07	39.97	40.08	40.98	39.96	40.87	40.13	40.25	40.27	41.07	40.32	40.05	40.81	40.57	40.89	40.52	40.84	41.09	40.63	40.06
Ce	0.10	b.d.	b.d.	b.d.	0.11	b.d.	b.d.	0.12	b.d.	b.d.	b.d.	b.d.	b.d.	b.d.	b.d.	b.d.	b.d.	b.d.	b.d.	b.d.	b.d.	b.d.	b.d.	b.d.	b.d.	b.d.	b.d.	b.d.	b.d.	b.d.	b.d.	b.d.	b.d.
S	b.d.	b.d.	b.d.	b.d.	b.d.	b.d.	b.d.	b.d.	0.04	b.d.	0.05	b.d.	b.d.	b.d.	0.12	b.d.	b.d.	0.05	b.d.	0.08	b.d.	0.05	b.d.	0.09	b.d.	0.04	b.d.	b.d.	b.d.	b.d.	b.d.	b.d.	b.d.
La	b.d.	b.d.	b.d.	b.d.	b.d.	b.d.	b.d.	b.d.	b.d.	b.d.	b.d.	b.d.	b.d.	b.d.	b.d.	b.d.	b.d.	b.d.	b.d.	b.d.	b.d.	b.d.	b.d.	b.d.	b.d.	b.d.	b.d.	b.d.	b.d.	b.d.	b.d.	b.d.	b.d.
Sr	b.d.	0.05	0.07	0.07	0.06	0.06	0.08	b.d.	0.06	0.06	0.05	0.06	0.06	0.07	0.06	0.08	0.06	0.05	0.07	0.07	0.09	0.09	0.06	0.09	0.07	b.d.	0.09	b.d.	0.06	0.05	b.d.	0.06	0.07
Y	b.d.	b.d.	b.d.	b.d.	b.d.	0.05	b.d.	b.d.	b.d.	b.d.	b.d.	b.d.	b.d.	b.d.	b.d.	b.d.	b.d.	b.d.	b.d.	b.d.	b.d.	b.d.	b.d.	b.d.	b.d.	b.d.	b.d.	b.d.	b.d.	b.d.	b.d.	b.d.	b.d.
O	38.47	38.96	37.70	37.63	38.88	38.34	38.30	38.04	37.57	38.24	38.43	37.94	39.18	38.57	38.59	38.41	39.26	38.51	38.56	37.60	38.27	39.28	39.44	38.88	38.25	39.14	38.51	39.47	38.99	38.56	38.67	37.96	38.83
Total	100.70	101.12	100.26	99.34	100.49	99.64	101.00	100.14	99.62	100.04	100.21	99.47	101.75	100.09	99.74	99.69	101.69	99.92	100.91	98.84	99.88	101.01	101.93	100.42	99.97	101.57	100.43	101.98	100.77	101.04	101.56	99.94	100.33
Weight% Oxides																																	
CaO	56.50	56.36	56.38	55.65	56.28	55.70	56.98	56.38	56.39	56.38	56.08	56.22	56.71	56.07	55.93	56.07	57.33	55.92	57.18	56.15	56.32	56.34	57.46	56.41	56.04	57.10	56.76	57.21	56.69	57.14	57.50	56.84	56.05
SrO	0.00	0.06	0.08	0.08	0.08	0.07	0.10	0.00	0.07	0.07	0.06	0.07	0.07	0.08	0.07	0.09	0.07	0.06	0.08	0.08	0.10	0.11	0.07	0.10	0.08	0.00	0.11	0.00	0.08	0.06	0.00	0.07	0.08
Ce_2O_3	0.11	0.00	0.00	0.00	0.00	0.00	0.00	0.14	0.00	0.00	0.00	0.00	0.00	0.00	0.00	0.00	0.00	0.00	0.00	0.00	0.00	0.00	0.00	0.00	0.00	0.00	0.00	0.00	0.00	0.00	0.00	0.00	0.00
P_2O_5	41.37	41.89	40.82	41.01	40.73	40.72	42.02	41.12	41.29	40.55	40.77	40.67	42.15	41.09	40.71	40.95	41.37	41.02	41.38	40.42	40.98	41.18	41.43	40.64	41.71	41.83	40.58	41.35	40.88	41.65	41.72	40.80	41.00
SiO_2	0.17	0.00	0.00	0.00	0.18	0.18	0.00	0.16	0.00	0.08	0.00	0.09	0.05	0.06	0.13	0.00	0.08	0.09	0.05	0.07	0.07	0.09	0.00	0.08	0.06	0.00	0.07	0.05	0.05	0.00	0.09	0.00	0.07
SO_3									0.10		0.11				0.30			0.13		0.19		0.11		0.23		0.11							
Atoms p.f.u. [a]																																	
Ca	10.19	10.13	10.28	10.18	10.26	10.20	10.17	10.22	10.22	10.31	10.26	10.28	10.12	10.20	10.23	10.23	10.29	10.19	10.28	10.31	10.24	10.21	10.31	10.30	10.11	10.22	10.35	10.29	10.30	10.24	10.26	10.34	10.21
Sr	0.00	0.01	0.01	0.01	0.01	0.01	0.01	0.00	0.01	0.01	0.01	0.01	0.01	0.01	0.01	0.01	0.01	0.01	0.01	0.01	0.01	0.01	0.01	0.01	0.01	0.00	0.01	0.00	0.01	0.01	0.00	0.01	0.01
Ce	0.01	0.00	0.00	0.00	0.00	0.00	0.00	0.01	0.00	0.00	0.00	0.00	0.00	0.00	0.00	0.00	0.00	0.00	0.00	0.00	0.00	0.00	0.00	0.00	0.00	0.00	0.00	0.00	0.00	0.00	0.00	0.00	0.00
∑	10.20	10.13	10.29	10.18	10.27	10.21	10.18	10.22	10.22	10.32	10.27	10.28	10.13	10.21	10.24	10.24	10.30	10.20	10.29	10.32	10.25	10.23	10.32	10.31	10.12	10.22	10.36	10.29	10.31	10.25	10.26	10.34	10.22
P	5.90	5.95	5.88	5.93	5.87	5.89	5.93	5.89	5.91	5.86	5.89	5.87	5.94	5.91	5.89	5.90	5.87	5.91	5.88	5.86	5.89	5.90	5.87	5.86	5.95	5.91	5.85	5.88	5.87	5.90	5.88	5.86	5.90
Si	0.03	0.00	0.00	0.00	0.03	0.03	0.00	0.03	0.00	0.01	0.00	0.02	0.01	0.01	0.02	0.00	0.01	0.02	0.01	0.01	0.01	0.01	0.00	0.01	0.01	0.00	0.01	0.01	0.01	0.00	0.01	0.00	0.01
∑	5.92	5.95	5.88	5.93	5.90	5.92	5.93	5.91	5.91	5.88	5.89	5.89	5.95	5.92	5.91	5.90	5.88	5.92	5.89	5.88	5.90	5.91	5.87	5.88	5.96	5.91	5.86	5.89	5.88	5.90	5.90	5.86	5.91
F	1.85	1.86	2.30	2.08	1.75	1.84	1.83	1.88	1.90	1.90	2.04	1.83	1.82	1.80	1.67	1.68	1.69	1.77	1.71	1.76	1.71	1.74	1.66	1.73	1.74	1.69	1.80	1.79	1.78	1.77	1.77	1.82	1.83
Cl	0.00	0.00	0.00	0.00	0.00	0.00	0.00	0.00	0.00	0.00	0.00	0.00	0.00	0.00	0.00	0.00	0.00	0.01	0.00	0.00	0.01	0.00	0.00	0.00	0.00	0.00	0.00	0.00	0.00	0.00	0.00	0.00	0.00
OH	0.15	0.14	-0.30	-0.08	0.25	0.16	0.17	0.12	0.10	0.10	-0.04	0.17	0.18	0.20	0.33	0.32	0.31	0.22	0.29	0.24	0.28	0.26	0.34	0.27	0.26	0.31	0.20	0.21	0.22	0.23	0.23	0.18	0.17
spot#	**MS15-7**			**MS15-3**				**MS15-8**					**MS25-1**	**MS25-2**						**MS25-4**	**MS25-5**						**MS25-7**	**MS36-5**		**MS36-3**	**MS36-2**	**MS36-1**	
^{6}Li	<1.71			<2.40				2.39					<2.05	<2.11						<2.19	<2.19						<2.19	<1.97		<2.00	2.32	<1.97	
^{7}Li	2.15			<1.71				<1.58					<1.43	<1.41						<1.54	<1.48						<1.57	<1.44		<1.45	<1.37	<1.45	
^{43}Ca	403805.9			398088.4				403091.2					405235.3	400947.1						401661.8	402376.5						405950.1	408808.8		408094.2	410953	405950.1	
^{44}Ca	430280.4			432027.7				424257.2					432242.6	421724.7						429844.7	421219.5						424392	439029.2		437947.6	456653.4	439393	
^{47}Ti	10.95			17.39				13.45					8.98	16.36						14.21	17.07						17.9	11.84		15.71	12.37	11.71	
^{49}Ti	<4.78			<7.00				<6.46					<5.92	<5.87						<6.40	<6.12						<6.51	<6.05		<5.93	<5.59	<6.07	
^{51}V	2.31			1.92				3.86					4.36	2.64						2.81	2.77						3.18	3.03		1.77	2.74	2.32	
^{53}Cr	11.48			<7.60				<6.67					<6.08	<5.95						<6.45	8.17						<6.53	<6.67		<5.88	6.34	<5.96	
^{88}Sr	616.4			595.48				633.56					607.19	560.71						739.44	690.36						681.92	593.71		555.94	619.15	599.26	
^{89}Y	295.69			123.09				201.17					51.53	104.11						127.79	124.05						120.61	164.01		78.14	582.43	98.13	
^{91}Zr	<0.74			<1.08				<0.99					<0.92	1.23						1.07	<0.95						1.3	<0.96		<0.92	1.33	<0.94	
^{93}Nb	0.0292			<0.027				<0.0256					0.0253	0.0267						<0.0238	<0.0272						<0.029	<0.0253		<0.0249	<0.0238	<0.0260	
^{139}La	364.38			26.62				220.99					49.35	87.96						125.8	116.66						100.54	79.39		34.81	232.44	44.32	
^{140}Ce	997.45			91.25				626.49					160.21	291.93						397.94	364.96						335.13	236.16		104.51	745.08	135.62	
^{141}Pr	138.65			15.56				92.23					23.95	44.99						60.17	56.66						53.05	37.68		17.26	124.14	22.58	
^{146}Nd	696.76			89.52				475.43					126.61	240.27						322.16	297.17						283.54	205.64		100.95	684.85	128.2	
^{147}Sm	139.09			28.71				104.53					25.53	49.69						63.17	59.86						60.08	53.67		29.57	199.51	36.4	
^{153}Eu	21.67			13.01				17.71					5.05	9.75						15.02	14.3						11.44	19.94		8.11	58.2	8.94	
^{157}Gd	114.92			30.8				86.91					24.09	47.8						57.68	54.46						57.28	53.31		31.34	203.98	38.98	
^{159}Tb	10.81			3.37				7.96					2.162	4.3						5.31	5.17						5.48	5.57		3.07	22.02	3.81	
^{163}Dy	52.4			18.5				38					10.38	20.26						25.76	24.52						25.03	28.43		15.54	112.69	19.16	
^{165}Ho	8.91			3.69				6.55					1.897	3.71						4.47	4.32						4.4	5.3		2.646	20.63	3.49	
^{166}Er	23.31			10.18				16.87					4.6	9.42						11.46	10.73						10.53	14.59		7	53.22	8.6	
^{169}Tm	2.87			1.318				1.987					0.471	0.961						1.217	1.16						1.094	1.791		0.728	5.98	0.927	
^{172}Yb	17.3			8.76				12					2.55	5.7						7.11	6.61						6.27	11.31		3.97	36.17	5.18	
^{175}Lu	2.625			1.389				1.986					0.433	0.858						1.075	1.049						0.932	1.924		0.618	5.6	0.841	
^{178}Hf	<0.084			<0.121				<0.091					<0.099	<0.096						<0.110	<0.108						<0.110	<0.124		<0.110	<0.096	<0.114	
^{181}Ta	<0.0140			<0.0213				0.0273					<0.0192	<0.0160						<0.0231	<0.0202						<0.0180	<0.0183		<0.0154	<0.0176	<0.0210	
^{208}Pb	3.73			2.097				3.3					2.038	2.536						3.78	3.64						3.66	2.638		1.689	3.92	1.934	
^{232}Th	6.19			1.645				4.71					1.133	3.37						6.59	6.73						6.23	3.31		0.445	8.13	0.966	
^{238}U	2.463			1.978				2.496					2.112	5.28						4.31	3.41						2.849	14.16		3.25	14.29	4.49	
Th/U	2.51			0.83				1.89					0.54	0.64						1.53	1.97						2.19	0.23		0.14	0.57	0.22	
Sr/Y	2.1			4.8				3.1					12	5.4						5.8	5.6						5.7	3.6		7.1	1.1	6.1	
ASI [b]	1.015	1.015	1.015	1.015	1.015	1.015	1.015	1.015	1.015	1.015	1.015	1.015	0.752	0.752	0.752	0.752	0.752	0.752	0.752	0.752	0.752	0.752	0.752	0.752	0.752	0.752	0.752	0.971	0.971	0.971	0.971	0.971	0.971
$^{207}Pb/^{206}Pb$ age [Ma] [c]	3254 ± 40			2848 ± 41				3424 ± 44					3212 ± 42	3097 ± 37						2835 ± 41	2835 ± 41						2825 ± 47	3205 ± 22		3130 ± 34	2844 ± 35	3449 ± 33	

[a] : Mineral formula calculation using Appoach 2 of Ketcham (2015).

[b] : ASI .= Alumina Saturation Index "Al_2O_3 / ($CaO+Na_2O+K_2O$)", using whole-rock compositions of Mühlberg et al. (2021).

[c] : Approximate age of targeted apatite zone; U-Pb data from Mühlberg et al. (2021).

Ketcham, R.A., 2015. Technical Note: Calculation of stoichiometry from EMP data for apatite and other phases with mixing on monovalent anion sites †. Am. Mineral. 100, 1620–1623.

Mühlberg, M., Stevens, G., Moyen, J.-F., Kisters, A.F.M., Lana, C., 2021. Thermal evolution of the Stolzburg Block, Barberton granitoid-greenstone terrain, South Africa: Implications for Paleoarchean tectonic processes. Prec. Research

Table 5.4, continued.

Sample					**MS 36**				
# of analysis EMP	82	83	84	85	86	87	88	89	90
# of analysis ICP MS					7	6			
Weight%									
Na	b.d.	b.d.	b.d.	b.d.	b.d.	b.d.	b.d.	b.d.	b.d.
Si	b.d.	0.03	0.03	0.05	0.06	0.04	b.d.	0.02	0.06
F	3.29	3.39	3.51	3.27	3.47	3.32	3.36	3.46	3.23
P	17.90	18.10	17.96	17.79	18.23	17.67	17.84	18.20	17.79
Cl	b.d.	b.d.	b.d.	b.d.	b.d.	b.d.	b.d.	b.d.	b.d.
Ca	40.19	40.21	40.16	39.90	40.68	40.40	40.59	41.04	40.03
Ce	b.d.	b.d.	b.d.	b.d.	b.d.	b.d.	b.d.	b.d.	b.d.
S	b.d.	b.d.	b.d.	b.d.	b.d.	b.d.	b.d.	b.d.	b.d.
La	b.d.	b.d.	b.d.	b.d.	b.d.	b.d.	b.d.	b.d.	b.d.
Sr	b.d.	0.07	0.08	0.07	0.06	0.07	b.d.	0.07	0.06
Y	b.d.	b.d.	b.d.	0.04	b.d.	b.d.	b.d.	b.d.	b.d.
O	38.49	39.14	38.72	38.19	38.98	38.48	37.97	38.90	38.53
Total	100.04	101.06	100.54	99.42	101.67	100.10	99.86	101.77	99.87
Weight% Oxides									
CaO	56.24	56.26	56.20	55.83	56.92	56.53	56.79	57.43	56.01
SrO	0.00	0.08	0.10	0.08	0.07	0.09	0.00	0.09	0.07
Ce_2O_3	0.00	0.00	0.00	0.00	0.00	0.00	0.00	0.00	0.00
P_2O_5	41.01	41.46	41.14	40.75	41.77	40.49	40.88	41.70	40.75
SiO_2	0.00	0.07	0.07	0.11	0.13	0.08	0.00	0.05	0.12
SO_3									
Atoms p.f.u. [a]									
Ca	10.24	10.17	10.21	10.22	10.19	10.34	10.32	10.26	10.24
Sr	0.00	0.01	0.01	0.01	0.01	0.01	0.00	0.01	0.01
Ce	0.00	0.00	0.00	0.00	0.00	0.00	0.00	0.00	0.00
∑	10.24	10.17	10.22	10.23	10.19	10.35	10.32	10.27	10.24
P	5.90	5.92	5.90	5.89	5.91	5.85	5.87	5.89	5.89
Si	0.00	0.01	0.01	0.02	0.02	0.01	0.00	0.01	0.02
∑	5.90	5.93	5.92	5.91	5.93	5.86	5.87	5.89	5.91
F	1.77	1.81	1.88	1.77	1.84	1.79	1.80	1.82	1.74
Cl	0.00	0.00	0.00	0.00	0.00	0.00	0.00	0.00	0.00
OH	0.23	0.19	0.12	0.23	0.16	0.21	0.20	0.18	0.26
spot#					**MS36-7**	**MS36-6**			
^{6}Li					4.33	<1.88			
^{7}Li					<1.50	<1.40			
^{43}Ca					406664.7	403805.9			
^{44}Ca					436638.4	437161.4			
^{47}Ti					<8.52	19.99			
^{49}Ti					<6.12	<5.76			
^{51}V					2.22	1.05			
^{53}Cr					7.71	<6.50			
^{88}Sr					624.17	578.89			
^{89}Y					395.77	61.55			
^{91}Zr					<0.99	<0.93			
^{93}Nb					<0.0236	<0.0218			
^{139}La					246.69	36.97			
^{140}Ce					702.28	109.21			
^{141}Pr					107.43	17.11			
^{146}Nd					561.15	96.48			
^{147}Sm					142.26	25.49			
^{153}Eu					54.55	7.09			
^{157}Gd					136.24	25.16			
^{159}Tb					14.02	2.542			
^{163}Dy					70.99	12.3			
^{165}Ho					13.07	2.163			
^{166}Er					34.86	5.5			
^{169}Tm					4.34	0.647			
^{172}Yb					27.58	3.82			
^{175}Lu					4.43	0.644			
^{178}Hf					<0.105	<0.100			
^{181}Ta					<0.0201	<0.0177			
^{208}Pb					3.57	1.729			
^{232}Th					5.65	0.348			
^{238}U					7.96	1.729			
Th/U					0.71	0.20			
Sr/Y					1.6	9.4			
ASI [b]	0.971	0.971	0.971	0.971	0.971	0.971	0.971	0.971	0.971
$^{207}Pb/^{206}Pb$ age [Ma] [c]					3243 ± 17	3456 ± 37			

[a] : Mineral formula calculation using Appoach 2 of Ketcham (2015).

[b] : ASI .= Alumina Saturation Index "Al_2O_3 / ($CaO+Na_2O+K_2O$)", using whole-rock compositions of Mühlberg et al. (2021).

[c] : Approximate age of targeted apatite zone; U-Pb data from Mühlberg et al. (2021).

Ketcham, R.A., 2015. Technical Note: Calculation of stoichiometry from EMP data for apatite and other phases with mixing on monovalent anion sites †. Am. Mineral. 100, 1620–1623.

Mühlberg, M., Stevens, G., Moyen, J.-F., Kisters, A.F.M., Lana, C., 2021. Thermal evolution of the Stolzburg Block, Barberton granitoid-greenstone terrain, South Africa: Implications for Paleoarchean tectonic processes. Prec. Research

Table 5.4, continued.

Sample								**MS2**											**MS14**				
# of analysis EMP	1	2	3	4	5	6	7	8	9	10	11	12	13	14	15	16	17	18	19	20	21	22	23
Uncertainty [3 S.D. wt. %]																							
Na	0	0.0562	0.0606	0.0561	-0.0001	0	0.0589	0.0624	-0.0004	0.0519	0.0605	0.0561	0.0544	0.0594	0.0585	0	0.0592	0	0.0599	0	0.0603	0.0598	0.0557
Si	0.0182	0.0175	0.0202	0.0194	0.0173	0.0182	0.0194	0.0206	0.0189	0.0195	0.1862	0.0208	0.0178	0.0194	0.0181	0.0671	0.0182	0.0194	0.0392	0.0196	-0.0001	0.0186	0.0179
F	0.5142	0.5246	0.511	0.5613	0.549	0.5567	0.5342	0.5368	0.5446	0.5276	0.5318	0.5021	0.5262	0.4952	0.5246	0.49	0.5496	0.5302	0.5409	0.5241	0.5422	0.5621	0.5154
P	0.5045	0.5092	0.5118	0.5128	0.5104	0.5078	0.5167	0.5046	0.5082	0.5081	0.5124	0.5152	0.502	0.5043	0.5065	0.4753	0.51	0.5053	0.4975	0.5115	0.5071	0.5139	0.5045
Cl	0.018	0.0179	0.018	0.0167	-0.0004	0.017	0	0.0188	0.0189	0.0174	0.0172	0.019	0.0159	0.0178	0.0168	0.0181	0.0172	0.0169	0.0179	0.0175	0.0161	0.0172	0.0172
Ca	0.6778	0.6778	0.69	0.6922	0.6733	0.689	0.6898	0.6874	0.6966	0.6733	0.6908	0.6952	0.6797	0.6744	0.6785	0.634	0.683	0.676	0.673	0.6912	0.6761	0.694	0.6793
Ce	0.0612	0	0.0645	0.0618	-0.0002	0.0624	0.0627	0.0616	0.0624	0.0616	0	0.0627	0.0594	0.0605	0.0602	0.0634	0.0584	0.0594	0.0621	0.0618	0.058	0.0615	-0.0001
S	0.0318	0.0291	0.0314	0.031	0.029	0.0294	0.0293	0.0365	0.032	0.0273	0.0377	0.0365	0.0311	0.0327	0.0303	0.0292	0.0322	0.026	0.0315	0.0276	0.0287	0.0307	0.0329
La	0.051	0	0.055	0.0525	0.0499	0.0519	0.0528	0.052	-0.0001	0.0516	0.0516	0.0535	0	0.0516	0.0515	0.0529	-0.0002	0.0499	0.0531	0.0531	0.0495	0	-0.0001
Sr	0.0394	0.0429	0.0439	0.0437	0.039	0.0427	0.0409	0.0426	0.0422	0.0399	0.0422	0.0423	0.0406	0.041	0.0393	0.0439	0.0384	0.0398	0.0397	0.041	0.0407	0.0403	0.0383
Y	0.0345	0	0.0361	0	-0.0001	0	0.0358	-0.0001	0	0.0342	0.0354	-0.0001	0	0	0.0347	0.0376	0	0.0347	0.0356	0.0357	0	-0.0001	0
O	2.0908	2.0852	2.0952	2.0935	2.0995	2.1057	2.1172	2.0891	2.106	2.0873	2.1227	2.1068	2.1388	2.0915	2.1023	2.1163	2.0736	2.1046	2.202	2.1071	2.0967	2.084	2.089
Detection limit [ppm]																							
Na		668	694	667			693	707		609	674	657	641	650	703		657		729		656	700	595
Si	199	208	217	222	203	216	217	206	211	209	2094	215	210	214	206	236	213	210	208	215		211	207
F	2355	2306	2466	2547	2388	2411	2502	2403	2467	2353	2388	2513	2434	2377	2286	2377	2329	2390	2725	2509	2425	2416	2442
P	292	318	309	356	312	327	320	325	314	321	324	339	315	334	304	501	326	312	326	331	334	295	323
Cl	208	215	209	181		182		219	214	203	208	218	175	209	196	211	205	201	212	201	191	200	203
Ca	567	591	600	542	565	603	623	590	535	598	633	601	593	614	576	560	615	588	577	599	564	611	575
Ce	719		742	722		735	731	715	730	699		719	706	713	710	745	696	705	739	710	694	722	
S	351	314	375	360	334	349	348	343	310	327	373	361	320	340	314	350	331	307	353	327	323	350	336
La	606		651	608	599	624	620	604		597	602	631		618	619	633		592	636	634	592		
Sr	416	467	459	465	395	447	449	466	452	393	458	438	426	439	406	502	413	439	449	446	441	447	421
Y	410		433				428			401	422				417	439		415	427	423			
O	3314	3318	3297	3334	3266	3461	3158	3290	3392	3235	3346	3429	3344	3101	3204	3242	3207	3231	3367	3354	3204	3232	3230

Sample															**MS15**								**MS25**
# of analysis EMP	24	25	26	27	28	29	30	31	32	33	34	35	36	37	38	39	40	41	42	43	44	45	61
Uncertainty [3 S.D. wt. %]																							
Na	0.0553	0.0658	0.0582	0.0575	0.0567	-0.0003	0.052	0.0575	0.0584	-0.0001	0.0566	-0.0016	0.0626	0.0589	0.0603	0	0.0577	0.0559	0.0603	0.0604	0.0639	0.0576	0.0551
Si	0.019	0.0186	0.0173	0.0179	0.0202	0.0193	0.0196	0.0196	0.0203	0.0183	0.0204	0.0181	0.019	0.0183	0.0215	0.0213	0.0183	0.0208	0.0187	0.0202	0.018	0.0201	0.0182
F	0.5426	0.553	0.5355	0.5334	0.5429	0.5536	0.5184	0.5254	0.5345	0.5249	0.5205	0.5282	0.6185	0.5717	0.5179	0.5268	0.5168	0.5331	0.5375	0.5393	0.5583	0.5294	0.52
P	0.5047	0.5098	0.5054	0.5108	0.5097	0.5119	0.5039	0.5113	0.5124	0.5022	0.5074	0.5135	0.5126	0.5145	0.5112	0.5117	0.5135	0.5126	0.5142	0.509	0.511	0.5111	0.5158
Cl	0.0185	0	-0.0001	0.0167	0	0.0174	0.0164	0.017	0.0198	0.0168	0.0172	0.0176	0.0183	0.0174	0.018	0	0.0169	0	0.0198	0.0175	0.0179	0.0176	0.0179
Ca	0.6753	0.6926	0.6755	0.6837	0.6902	0.6966	0.6724	0.6929	0.6898	0.677	0.6744	0.6756	0.6944	0.689	0.6924	0.6887	0.6781	0.6884	0.6896	0.6923	0.6902	0.6929	0.6777
Ce	0.0605	0.0603	0.0591	0.0607	0.0627	0.0628	0.0613	0.0644	0.0661	-0.0001	0.062	0.0583	0.0595	0.0603	0.0642	0.0625	0.0591	0.0656	-0.0001	0.0644	0.0622	0.0612	0.0595
S	-0.0001	0.0351	0.0286	0.0297	0.029	-0.0002	0.028	0.0314	0.026	0.0304	0.0275	0.0295	0.0324	0.033	-0.0001	0.0323	0.0311	0.0298	0.0309	0.0304	0.0321	0.0281	0.0304
La	0.0508	0.053	0.0495	0	0.0532	0.0533	0.051	0.052	0.0538	-0.0001	0.0514	0	0.0514	0.0514	0.0536	0.0533	0	0.0532	0.0515	0.0535	0.0512	0.0535	0.0498
Sr	0.0395	0.0403	0.0386	0.0413	0.042	0.0429	0.0376	0.0419	0.0431	0.0382	0.0379	0.0394	0.041	0.04	0.0402	0.0417	0.0391	0.0424	0.0405	0.0404	0.0428	0.0419	0.0403
Y	0.0347	0	0	0	0.0366	0.0359	0.0348	-0.0001	0.036	0.0342	0.035	0	0	0	0.0363	0.0364	0	0.0365	0	0.036	0	0.0365	0
O	2.0748	2.086	2.0838	2.102	2.0878	2.0766	2.0649	2.0812	2.0613	2.0805	2.0683	2.091	2.0547	2.0538	2.1084	2.0851	2.0615	2.0648	2.0457	2.0785	2.0875	2.0697	2.1017
Detection limit [ppm]																							
Na	648	762	671	682	687		615	690	637		635		701	638	684		654	640	678	718	758	694	612
Si	204	215	197	213	215	212	211	217	208	206	207	214	218	212	214	214	211	213	216	222	212	220	206
F	2399	2526	2538	2264	2290	2327	2390	2351	2422	2355	2267	2386	2476	2366	2594	2429	2157	2304	2323	2446	2207	2527	2274
P	332	333	339	315	296	354	312	345	369	327	275	317	317	301	329	343	281	312	280	296	312	334	321
Cl	203			193		203	178	203	222	201	201	212	209	207	204		197		222	205	204	205	200
Ca	583	615	592	546	608	578	570	590	586	577	586	604	610	609	616	580	560	554	619	576	646	567	569
Ce	714	717	695	716	726	750	713	756	751		704	696	706	719	722	718	706	734		746	748	727	706
S		366	317	324	331		303	368	305	323	317	323	361	362		355	337	337	313	346	320	301	340
La	603	634	592		625	638	600	592	643		600		615	610	637	618		627	613	618	616	632	591
Sr	451	447	414	462	462	471	402	451	469	425	417	432	434	419	427	453	398	478	440	435	471	455	441
Y	412				431	417	408		427	405	417				427	423		428		421		429	
O	3240	3323	3076	3345	3223	3367	3268	3419	3332	3219	3262	3137	3299	3406	3349	3373	3274	3271	3296	3291	3410	3447	3276

Table 5.4, continued.

Sample							**MS 25**												**MS36**			
# of analysis EMP	62	63	64	65	66	67	68	69	70	71	72	73	74	75	76	77	78	79	80	81	82	83	84
Uncertainty [3 S.D. wt. %]																							
Na	0	0.0646	0.0588	0	0	0.054	0.0653	0.0594	0.0612	0.0594	0.0626	0.0605	0.055	0.059	0.0603	-0.0001	0.0585	0.0566	0.0567	0.0552	0.0547	0.0628	0
Si	0.0191	0.0204	0.0185	0.0183	0.0191	0.0181	0.0197	0.0197	0.0198	0.0182	0.0198	0.0194	0.0181	0.0193	0.0185	0.0197	0.0178	0.0191	0.0189	0.0191	0.0189	0.0193	0.0187
F	0.5236	0.4895	0.4999	0.4949	0.5182	0.4962	0.5059	0.5027	0.5131	0.4887	0.5061	0.5106	0.4958	0.518	0.5147	0.515	0.5096	0.5069	0.521	0.5285	0.5168	0.5308	0.5357
P	0.515	0.5106	0.5135	0.5083	0.5152	0.5076	0.5086	0.5139	0.5153	0.509	0.5102	0.5207	0.5131	0.5075	0.5083	0.5126	0.5111	0.5117	0.5117	0.5125	0.5138	0.5171	0.5153
Cl	0.0191	0.0187	0.0184	0.0182	0.0189	0.0182	0.0185	0.0194	0.0181	0.0185	-0.0001	0.0195	0.0185	0.0192	0.0178	0.0176	0.0162	0.0177	0.0172	0	-0.0002	0.0179	0.017
Ca	0.6916	0.6887	0.6916	0.6824	0.6926	0.6796	0.6927	0.6933	0.6931	0.6835	0.6934	0.6912	0.6818	0.6916	0.6819	0.696	0.6813	0.6842	0.6966	0.6882	0.6923	0.6903	0.6917
Ce	0.0614	-0.0001	0.0605	0.0606	0.0625	0.0593	0	0.0605	0.0611	0.0609	0.0621	0.0618	0	0.0614	0.0609	0.062	0.06	0.0602	0.0613	0.0626	0.062	0.0611	0.0627
S	0.0299	0.0411	0.0314	0.0303	0.0325	0.0302	0.0367	0.0311	0.0339	0.0309	0.0382	0.0324	0.0298	0.0327	0.0297	0.0292	0	0.0288	0.029	0.0285	0.0282	0.0305	0.0289
La	0.0513	0.0528	0.0509	0.0518	0	0.051	0.0526	0.0518	0.0519	-0.0001	0.0515	0.0529	0.0488	0.0521	0.0508	0.0532	0.0499	0.0501	0.0529	-0.0001	0.0523	0.0539	0.0518
Sr	0.0425	0.0401	0.041	0.0402	0.0425	0.0405	0.043	0.0427	0.0424	0.0378	0.0413	0.0414	0.041	0.0436	0.0396	0.0427	0.0372	0.0374	0.0425	0.0431	0.0391	0.042	0.0417
Y	-0.0001	0	-0.0002	-0.0001	0.0359	0	0	0	0.0359	0	0	0.0356	-0.0005	0	-0.0001	0.036	0.0345	0.0348	0	-0.0001	0.0354	0	0.0359
O	2.0967	2.0946	2.0887	2.1061	2.0957	2.0741	2.0556	2.0841	2.1261	2.1141	2.1088	2.0825	2.1016	2.0879	2.1137	2.1134	2.0762	2.0795	2.0687	2.104	2.0917	2.1169	2.0998
Detection limit [ppm]																							
Na		731	632			641	766	704	725	661	714	720	623	691	689		690	651	669	658	663	749	
Si	213	214	216	200	206	205	220	221	217	207	220	218	214	216	209	224	210	209	216	211	219	214	205
F	2468	2244	2480	2365	2460	2283	2249	2376	2476	2336	2379	2344	2324	2366	2360	2330	2301	2197	2252	2479	2467	2624	2366
P	330	362	288	298	294	336	301	334	313	337	351	314	329	318	312	307	323	291	313	317	324	308	354
Cl	222	215	205	211	198	207	215	191	201	205		208	205	217	195	213	195	212	206			206	203
Ca	610	616	583	548	612	567	575	555	654	576	635	610	597	575	600	591	564	592	546	586	636	621	589
Ce	722		716	703	717	694		709	719	716	742	735		711	723	745	707	696	729	751	722	710	741
S	331	341	327	320	310	311	334	319	345	331	338	343	296	343	307	317		316	335	305	307	341	324
La	617	623	612	613		613	621	596	624		612	628	574	610	598	640	596	589	624		625	631	611
Sr	453	434	427	439	470	430	464	439	433	402	422	439	455	450	439	461	399	416	463	465	428	450	431
Y					431				431			428				432	414	416			420		430
O	3454	3265	3273	3212	3412	3252	3407	3443	3382	3188	3341	3480	3238	3343	3112	3260	3314	3196	3346	3363	3337	3339	3250

Sample			**MS36**			
# of analysis EMP	85	86	87	88	89	90
Uncertainty [3 S.D. wt. %]						
Na	0.0627	0.0565	0.0615	0.0565	0	0.0589
Si	0.0205	0.0198	0.019	0.0184	0.0188	0.0193
F	0.5101	0.5237	0.5187	0.5215	0.5225	0.508
P	0.5111	0.5124	0.5088	0.5121	0.5113	0.5103
Cl	0.0171	0.0184	0.0179	0	0.0175	0.0186
Ca	0.6884	0.6796	0.6941	0.6959	0.6827	0.688
Ce	0.064	0.0611	0.0618	0.0611	0.0608	0.0635
S	0.0313	0.0276	0.0293	0.0274	0.0268	0.0274
La	0	0.0507	0.0531	0	0.0505	0.052
Sr	0.0419	0.0398	0.0422	0.0411	0.0397	0.0404
Y	0.0362	0.0351	-0.0001	0.0353	0.035	0.0364
O	2.0764	2.0934	2.0918	2.0695	2.0889	2.0914
Detection limit [ppm]						
Na	690	657	708	678		620
Si	221	209	209	216	214	201
F	2343	2332	2449	2414	2360	2405
P	338	318	329	327	320	326
Cl	194	208	209		209	208
Ca	623	579	575	622	574	554
Ce	752	695	727	723	718	745
S	361	319	302	328	314	303
La		593	622		597	622
Sr	445	427	445	453	415	437
Y	422	416		422	416	427
O	3266	3326	3400	3441	3223	3377

Table 5.4, continued.

Sample	MS 2								MS 14					MS 15						MS 25					MS 36					
# of analysis ICP MS	MS2-1	MS2-2	MS2-4	MS2-5	MS2-6	MS2-7	MS2-8	MS2-9	MS14-2	MS14-5	MS14-6	MS14-9	MS14-10	MS15-3	MS15-4	MS15-5	MS15-6	MS15-7	MS15-8	MS25-1	MS25-2	MS25-4	MS25-5	MS25-7	MS36-1	MS36-2	MS36-3	MS36-5	MS36-6	MS36-7
Uncertainty [1σ ppm]																														
^{6}Li	1.17	1.18	1.01	1.04	0.93	1.16	1.07	0.88	0.88	0.98	0.92	0.83	0.92	0.91	0.83	0.88	0.85	0.74	0.84	0.75	0.76	0.79	0.79	0.78	0.71	0.75	0.72	0.73	0.72	0.8
^{7}Li	0.66	0.66	0.58	0.61	0.58	0.68	0.64	0.59	0.58	0.62	0.59	0.5	0.6	0.63	0.59	0.58	0.59	0.51	0.59	0.52	0.51	0.55	0.53	0.56	0.53	0.52	0.52	0.52	0.53	0.54
^{43}Ca	12854.18	12718.83	12830.5	12762.71	12874.18	12719.79	12809.04	12692.7	12808.02	12784.32	12897.15	11021.11	12987.21	12605.75	12715.89	12580.37	12851.71	12784.72	12764.45	12826.88	12691.07	12715.39	12736.79	12851	12849.9	13011.24	12917.68	12940.31	12786.08	12873.32
^{44}Ca	13803.14	13508.9	13647.91	13659.44	13792.42	13362.17	13428.94	13197.9	13835.23	13623.13	13829.61	11804.16	14173.85	14444.19	14454.08	14259.71	14964.75	14576.88	14428.9	14759.17	14465.47	14894.64	14676.39	15063.51	15700.9	16433.99	15874.22	13802.9	13746.78	13729.09
^{47}Ti	3.71	3.62	3.39	3.5	3.24	3.88	3.65	3.1	3.28	3.33	3.35	2.82	3.38	3.49	3.27	3.1	3.28	2.79	3.29	2.88	2.87	3.11	2.99	3.21	2.95	2.94	2.97	2.95	3.09	3.08
^{49}Ti	2.8	2.7	2.48	2.61	2.4	2.92	2.72	2.33	2.41	2.49	2.46	2.03	2.48	2.58	2.38	2.28	2.39	2	2.42	2.12	2.1	2.3	2.19	2.34	2.17	2.13	2.14	2.17	2.18	2.2
^{51}V	0.21	0.37	0.17	0.29	0.18	0.21	0.2	0.3	0.19	0.17	0.18	0.14	0.19	0.18	0.17	0.18	0.19	0.16	0.22	0.22	0.17	0.19	0.19	0.21	0.18	0.19	0.16	0.19	0.16	0.18
^{53}Cr	3.23	3.19	2.84	3.07	2.76	3.3	3.22	2.69	2.84	2.91	2.93	2.26	2.87	2.83	2.66	2.53	2.56	2.09	2.55	2.21	2.16	2.35	2.28	2.34	2.15	2.18	2.14	2.49	2.58	2.72
^{88}Sr	24.86	25.54	24.82	25.59	25.19	27	26.81	26.47	20.88	17.72	19.81	19.68	19.83	18.84	18.21	18.55	18.14	19.6	20.17	19.36	17.91	23.7	22.17	22.06	19.43	20.14	18.13	18.68	18.23	19.67
^{89}Y	1.72	3.48	0.72	3.25	1.33	7.04	4.16	3.14	12.65	5.76	1.95	10.82	2.13	3.88	8.19	10.4	3.67	9.33	6.36	1.63	3.3	4.05	3.94	3.84	3.13	18.59	2.5	5.13	1.93	12.36
^{91}Zr	0.39	0.38	0.35	0.38	0.35	0.42	0.39	0.34	0.35	0.36	0.37	0.3	0.37	0.4	0.37	0.36	0.37	0.31	0.38	0.33	0.33	0.36	0.35	0.37	0.34	0.35	0.34	0.34	0.35	0.35
^{93}Nb	0.013	0.011	0.011	0.01	0.0096	0.013	0.011	0.011	0.01	0.01	0.0098	0.0084	0.011	0.01	0.0094	0.0092	0.011	0.008	0.0097	0.0083	0.0089	0.009	0.0096	0.01	0.0091	0.0091	0.0088	0.0088	0.0085	0.0089
^{139}La	2.57	4.86	1.35	4.2	1.91	8.99	4.68	3.48	3.99	2.66	0.82	3.39	0.86	0.85	5.18	6.43	0.84	11.56	7.02	1.57	2.81	4.02	3.74	3.24	1.44	7.53	1.13	2.48	1.16	7.7
^{140}Ce	6.31	12.19	3.12	10.35	4.53	22.86	12.09	8.68	11	6.57	2.08	8.72	2.13	2.92	15.16	20.16	2.95	32.13	20.23	5.19	9.47	12.99	11.95	11.1	4.51	24.87	3.51	7.94	3.69	23.83
^{141}Pr	0.94	1.77	0.46	1.6	0.69	3.47	1.97	1.37	1.97	1.13	0.37	1.67	0.4	0.5	2.33	3.2	0.52	4.44	2.96	0.77	1.45	1.95	1.85	1.75	0.75	4.12	0.58	1.19	0.55	3.41
^{146}Nd	4.26	8	2.04	7.26	3.19	16.11	9.25	6.4	9.83	5.2	1.72	7.64	1.79	2.86	11.98	16.59	3.13	22.1	15.12	4.05	7.67	10.32	9.54	9.17	4.17	22.23	3.31	6.46	3.06	17.6
^{147}Sm	0.92	1.71	0.44	1.59	0.7	3.53	2.1	1.45	2.75	1.35	0.48	2.12	0.48	0.97	2.96	4.15	1.05	4.59	3.47	0.87	1.67	2.14	2.03	2.07	1.27	6.88	1.05	1.83	0.9	4.85
^{153}Eu	0.42	0.84	0.22	0.7	0.3	1.51	0.83	0.59	1.35	0.99	0.28	1.13	0.37	0.46	0.82	1.17	0.47	0.77	0.63	0.19	0.35	0.55	0.53	0.44	0.35	2.23	0.32	0.71	0.26	1.96
^{157}Gd	0.82	1.51	0.4	1.48	0.67	3.17	1.97	1.36	3.04	1.49	0.53	2.34	0.54	1.12	3.06	4.07	1.19	4.12	3.15	0.9	1.76	2.15	2.05	2.22	1.53	7.98	1.27	1.87	0.92	4.78
^{159}Tb	0.08	0.15	0.036	0.15	0.063	0.32	0.19	0.14	0.35	0.17	0.06	0.29	0.062	0.12	0.3	0.4	0.12	0.38	0.29	0.081	0.16	0.2	0.19	0.21	0.15	0.84	0.12	0.18	0.087	0.44
^{163}Dy	0.35	0.68	0.16	0.63	0.28	1.37	0.82	0.61	1.78	0.83	0.3	1.4	0.29	0.61	1.36	1.74	0.57	1.67	1.22	0.35	0.66	0.83	0.79	0.81	0.63	3.57	0.51	0.91	0.42	2.25
^{165}Ho	0.066	0.12	0.031	0.11	0.05	0.24	0.15	0.11	0.36	0.17	0.061	0.29	0.062	0.13	0.27	0.34	0.11	0.3	0.23	0.069	0.13	0.16	0.15	0.16	0.13	0.73	0.099	0.18	0.079	0.44
^{166}Er	0.18	0.34	0.09	0.33	0.14	0.69	0.42	0.32	1.22	0.57	0.22	1.04	0.22	0.35	0.7	0.86	0.3	0.76	0.56	0.17	0.32	0.38	0.36	0.35	0.29	1.7	0.24	0.54	0.22	1.29
^{169}Tm	0.021	0.04	0.012	0.034	0.016	0.073	0.043	0.036	0.14	0.063	0.024	0.12	0.025	0.05	0.093	0.11	0.042	0.1	0.073	0.021	0.037	0.047	0.044	0.043	0.037	0.21	0.03	0.063	0.028	0.14
^{172}Yb	0.13	0.21	0.067	0.19	0.098	0.42	0.26	0.21	0.98	0.4	0.15	0.8	0.16	0.33	0.58	0.72	0.25	0.62	0.44	0.11	0.22	0.27	0.25	0.25	0.21	1.31	0.17	0.4	0.16	0.95
^{175}Lu	0.023	0.038	0.012	0.035	0.017	0.077	0.05	0.038	0.18	0.08	0.029	0.15	0.036	0.053	0.096	0.12	0.045	0.095	0.074	0.02	0.035	0.043	0.041	0.038	0.035	0.2	0.027	0.069	0.029	0.15
^{178}Hf	0.031	0.033	0.035	0.034	0.038	0.047	0.037	0.036	0.038	0.036	0.041	0.034	0.043	0.043	0.04	0.035	0.036	0.036	0.036	0.036	0.034	0.04	0.038	0.04	0.041	0.039	0.039	0.043	0.039	0.039
^{181}Ta	0.0072	0.0077	0.0057	0.0076	0.007	0.0085	0.0077	0.0076	0.0063	0.0063	0.0074	0.0064	0.0074	0.0075	0.0067	0.0065	0.0076	0.0059	0.0062	0.0067	0.0059	0.0079	0.0071	0.0065	0.0073	0.0066	0.0059	0.0065	0.0069	0.007
^{208}Pb	0.068	0.093	0.055	0.077	0.054	0.11	0.085	0.081	0.12	0.092	0.065	0.092	0.061	0.086	0.11	0.13	0.087	0.14	0.13	0.081	0.099	0.14	0.14	0.14	0.081	0.16	0.073	0.098	0.072	0.13
^{232}Th	0.051	0.13	0.011	0.098	0.017	0.22	0.14	0.094	0.21	0.16	0.013	0.14	0.028	0.082	0.18	0.28	0.1	0.31	0.24	0.061	0.17	0.35	0.36	0.36	0.06	0.49	0.031	0.14	0.021	0.24
^{238}U	0.068	0.22	0.017	0.1	0.024	0.22	0.16	0.081	0.14	0.43	0.099	0.14	0.15	0.068	0.1	0.13	0.3	0.084	0.085	0.071	0.17	0.14	0.11	0.095	0.15	0.46	0.11	0.45	0.061	0.25
Detection limit [ppm]																														
^{6}Li	3.23	2.88	2.76	2.83	2.56	3.25	2.88	2.44	2.42	2.45	2.56	1.84	2.54	2.4	2.2	2.12	2.33	1.71	2.13	2.05	2.11	2.19	2.19	2.19	1.97	1.87	2	1.97	1.88	1.91
^{7}Li	1.84	1.73	1.57	1.71	1.58	1.93	1.77	1.53	1.55	1.61	1.63	1.28	1.67	1.71	1.62	1.53	1.65	1.19	1.58	1.43	1.41	1.54	1.48	1.57	1.45	1.37	1.45	1.44	1.4	1.5
^{43}Ca	732.53	702.86	631.5	681.92	623.41	762.6	697.74	597.47	613.71	641.68	643.79	458.5	626.26	657.87	623.2	587.98	633.66	414.94	608.61	553.46	545.36	601.22	572.12	617.31	571.61	538.8	571.25	573.1	560.12	603.32
^{44}Ca	103.46	98.65	89.01	96.36	88.35	108.06	99.56	85.69	88.04	92.29	92.92	70.73	93.97	96.12	91.2	85.89	92.49	65.3	88.75	81.39	80.08	87.91	84.33	90.62	83.82	78.68	83.68	85.68	83.21	88.78
^{47}Ti	10.27	9.83	8.82	9.63	8.75	10.85	9.97	8.59	8.73	9.12	9.09	7.07	9.29	9.27	8.79	8.34	8.97	6.53	8.63	7.96	7.76	8.49	8.12	8.72	8.09	7.61	8.04	8.11	7.89	8.52
^{49}Ti	7.82	7.42	6.7	7.28	6.66	8.26	7.5	6.5	6.51	6.93	6.84	5.2	6.87	7	6.62	6.23	6.63	4.78	6.46	5.92	5.87	6.4	6.12	6.51	6.07	5.59	5.93	6.05	5.76	6.12
^{51}V	0.496	0.474	0.427	0.458	0.424	0.52	0.48	0.408	0.425	0.445	0.446	0.328	0.444	0.448	0.431	0.401	0.435	0.293	0.42	0.384	0.38	0.413	0.398	0.432	0.397	0.371	0.396	0.403	0.393	0.419
^{53}Cr	8.99	8.56	7.69	8.27	7.57	9.31	8.56	7.35	7.59	7.94	8.04	5.64	7.74	7.6	7.14	6.62	7.12	4.56	6.67	6.08	5.95	6.45	6.09	6.53	5.96	5.54	5.88	6.67	6.5	6.9
^{88}Sr	0.158	0.15	0.139	0.158	0.14	0.176	0.166	0.141	0.143	0.151	0.151	0.118	0.154	0.158	0.154	0.145	0.154	0.109	0.147	0.138	0.138	0.149	0.14	0.153	0.141	0.136	0.142	0.143	0.139	0.149
^{89}Y	0.064	0.0567	0.0513	0.0557	0.0515	0.0663	0.0573	0.0537	0.0539	0.058	0.0573	0.0433	0.063	0.0558	0.0559	0.0522	0.0569	0.0395	0.0531	0.0483	0.0505	0.0553	0.0551	0.058	0.0534	0.0488	0.0562	0.0555	0.0516	0.0569
^{91}Zr	1.1	1.06	0.959	1.05	0.959	1.18	1.09	0.94	0.957	1.01	1.02	0.781	1.02	1.08	1.02	0.959	1.04	0.741	0.993	0.916	0.89	0.981	0.948	1.01	0.938	0.87	0.92	0.956	0.925	0.986
^{93}Nb	0.0358	0.0314	0.031	0.0285	0.0263	0.0366	0.0312	0.0302	0.0283	0.029	0.0268	0.0212	0.0299	0.0269	0.0259	0.0246	0.0298	0.0165	0.0256	0.0213	0.0233	0.0238	0.0272	0.0294	0.026	0.0238	0.0249	0.0253	0.0218	0.0236
^{139}La	0.0233	0.023	0.0183	0.0164	0.0229	0.0316	0.0243	0.0221	0.0207	0.022	0.0249	0.0201	0.0295	0.0215	0.022	0.0269	0.0291	0.0168	0.0282	0.021	0.0224	0.02	0.0191	0.0251	0.0253	0.0225	0.0226	0.0225	0.0226	0.0251
^{140}Ce	0.0298	0.0213	0.0245	0.0284	0.0207	0.0327	0.0297	0.0244	0.0258	0.029	0.0269	0.0229	0.031	0.0284	0.0283	0.0277	0.0298	0.0212	0.0271	0.026	0.024	0.0289	0.0288	0.0318	0.0286	0.027	0.0276	0.0301	0.027	0.0261
^{141}Pr	0.0162	0.00975	0.00986	0.0127	0.0149	0.0174	0.00691	0.0112	0.00887	0.0131	0.0118	0.00992	0.0147	0.0149	0.014	0.0166	0.0117	0.00985	0.0119	0.0152	0.00947	0.015	0.0119	0.0132	0.0131	0.0103	0.0158	0.0122	0.0114	0.0148
^{146}Nd	0.117	0.118	0.0957	0.11	0.0882	0.104	0.1	0.111	0.0986	0.0914	0.102	0.0912	0.112	0.123	0.116	0.106	0.123	0.0869	0.121	0.123	0.0884	0.101	0.108	0.13	0.109	0.0969	0.11	0.117	0.0987	0.126
^{147}Sm	0.11	0.0948	0.118	0.116	0.0817	0.113	0.0893	0.071	0.0784	0.108	0.0854	0.0728	0.114	0.0757	0.0758	0.0729	0.111	0.0802	0.0919	0.096	0.0642	0.0911	0.0936	0.103	0.103	0.0917	0.0895	0.0711	0.0841	0.105
^{153}Eu	0.0222	0.03	0.034	0.0262	0.0281	0.0279	0.0328	0.0224	0.028	0.0272	0.0282	0.0216	0.0295	0.0355	0.0255	0.0323	0.0243	0.0235	0.0241	0.0281	0.0302	0.0246	0.028	0.0301	0.0284	0.0283	0.0205	0.0252	0.0289	0.0271
^{157}Gd	0.183	0.15	0.166	0.158	0.149	0.209	0.185	0.142	0.155	0.167	0.191	0.12	0.183	0.178	0.17	0.162	0.188	0.134	0.174	0.152	0.154	0.169	0.172	0.173	0.173	0.156	0.178	0.176	0.175	0.182
^{159}Tb	0.0162	0.0136	0.0156	0.0171	0.0142	0.0211	0.0187	0.0212	0.02	0.0174	0.0186	0.0164	0.0208	0.0265	0.0217	0.0176	0.0244	0.0166	0.0195	0.0162	0.0184	0.0246	0.0171	0.0259	0.0227	0.0205	0.0236	0.0226	0.0195	0.0198
^{163}Dy	0.0964	0.0897	0.0699	0.112	0.0835	0.115	0.0877	0.0893	0.0941	0.0932	0.103	0.0953	0.115	0.129	0.116	0.104	0.122	0.0845	0.112	0.103	0.102	0.0992	0.118	0.104	0.109	0.0875	0.122	0.0973	0.0944	0.116
^{165}Ho	0.0094	0.0156	0.00885	0.00958	0.0143	0.0127	<0.00000	0.0138	0.0101	0.0106	0.0151	0.00892	0.0135	0.00737	0.00977	0.0144	0.015	0.00865	0.0108	0.0114	0.0122	0.0101	0.0133	0.0128	0.0132	0.0102	0.00969	0.00838	0.0125	0.0124
^{166}Er	0.109	0.117	0.0819	0.0935	0.0952	0.0981	0.0952	0.101	0.0899	0.116	0.097	0.0858	0.103	0.118	0.105	0.103	0.106	0.0771	0.129	0.0973	0.104	0.0935	0.116	0.122	0.107	0.102	0.103	0.109	0.105	0.121
^{169}Tm	0.00853	0.0131	0.014	0.0125	0.00362	0.0154	0.0056	0.011	0.00951	<0.00000	0.012	0.0093	0.0146	0.0139	0.0105	0.0129	0.0131	0.0101	0.0145	0.00937	0.00923	0.0148	0.00969	0.0143	0.0136	0.012	0.0102	0.017	0.0132	0.00962
^{172}Yb	0.0626	0.0614	0.0575	0.0583	0.0689	0.0956	0.101	0.0666	0.0792	0.1	0.0937	0.0629	0.101	0.0861	0.0712	0.0822	0.0876	0.0646	0.0842	0.0945	0.0687	0.0503	0.066	0.0902	0.0681	0.068	0.0853	0.105	0.0809	0.0937
^{175}Lu	0.00983	0.0137	0.00781	0.0145	0.00935	0.0195	0.0138	0.0107	0.0138	0.0138	0.017	0.0144	0.0107	0.0105	0.0122	0.0149	0.0186	0.0151	0.0146	0.0149	0.0174	0.0167	0.0126	0.0172	0.0178	0.0154	0.0169	0.0196	0.0124	0.0206
^{178}Hf	0.079	0.09	0.091	0.0885	0.106	0.134	0.1	0.0985	0.106	0.101	0.118	0.088	0.125	0.121	0.11	0.0899	0.0945	0.0835	0.0909	0.099	0.0956	0.11	0.108	0.11	0.114	0.0965	0.11	0.124	0.0997	0.105
^{181}Ta	0.0199	0.0215	0.0149	0.0215	0.0191	0.024	0.0218	0.0224	0.0151	0.0158	0.0211	0.0164	0.0207	0.0213	0.0191	0.0171	0.0221	0.014	0.013	0.0192	0.016	0.0231	0.0202	0.018	0.021	0.0176	0.0154	0.0183	0.0177	0.0201
^{208}Pb	<0.00000	0.0124	<0.00000	<0.00000	0.0228	0.0287	0.0234	<0.00000	<0.00000	0.0169	0.0242	0.00976	0.0209	0.0276	<0.00000	0.0269	0.00849	0.00758	0.0216	0.0198	0.0209	0.00811	0.028	0.0206	0.019	0.0207	0.0135	0.0208	0.0109	0.0184
^{232}Th	0.00791	0.0147	<0.00000	0.0052	0.0117	0.00906	0.00905	0.0046	0.00474	0.00497	<0.00000	0.00572	0.00707	<0.00000	0.0108	0.00431	<0.00000	0.00667	0.0094	0.00744	0.00733	0.00929	0.00444	0.00676	0.00625	0.00415	<0.00000	0.00619	0.0121	0.00649
^{238}U	0.00519	<0.00000	<0.00000	0.00343	<0.00000	0.00423	<0.00000	0.00306	<0.00000	<0.00000	0.00674	0.00315	0.00478	<0.00000	0.00471	0.00298	<0.00000	<0.00000	0.00461	0.00517	0.00416	<0.00000	0.0031	0.00474	0.00537	<0.00000	0.0044	0.00764	<0.00000	0.00568

Table 5.4, continued.

Reference material	**Durango**		
# of analysis EMP	101	102	103
Concentrations [wt. %]			
Na	0.1807	0.2056	0.1592
Si	0.1782	0.16	0.1657
F	3.0627	3.3788	3.4097
P	17.4075	17.7692	17.4396
Cl	0.4229	0.4497	0.4426
Ca	39.0807	39.8271	38.9706
Ce	0.4657	0.4367	0.4551
S	0.1763	0.1544	0.1777
La	0.3689	0.3811	0.3712
Sr	0.0412	0.031	0.0521
Y	b.d.	b.d.	0.0571
O	38.2919	38.5024	37.5062
Total	99.7178	101.3216	99.207
Uncertainty [3 S.D. wt. %]			
Na	0.0808	0.0763	0.0749
Si	0.0252	0.024	0.0248
F	0.4963	0.5149	0.526
P	0.5051	0.503	0.5048
Cl	0.0452	0.0455	0.0462
Ca	0.6829	0.6704	0.6792
Ce	0.0776	0.0737	0.0752
S	0.047	0.0418	0.0471
La	0.0681	0.0637	0.0669
Sr	0.0422	0.0386	0.0427
Y	0.0374	0.0359	0.0373
O	2.0793	2.0656	2.0425
Detection limit [ppm]			
Na	728	640	673
Si	217	216	218
F	2557	2404	2425
P	283	335	338
Cl	207	227	215
Ca	601	561	569
Ce	739	711	709
S	353	311	355
La	655	598	637
Sr	473	440	470
Y	438	424	432
O	3181	3047	3290

Table 5.4, continued.

Reference material	GSD												Average GSD	Durango					Average DUR
Concentrations [ppm]																			
^{6}Li	43.27	42.59	45.2	40.9	43.69	42.34	42.2	43.78	44.9	40.75	43.93	42.3	42.99	<2.19	<1.93	<2.06	<1.86	<1.72	b.d.
^{7}Li	41.84	44.13	44.22	41.76	42.34	43.66	42.8	43.16	43.88	42.08	42.7	43.34	42.99	<1.34	<1.31	<1.43	<1.43	<1.39	b.d.
^{43}Ca	51457.96	51457.96	51457.98	51457.98	51457.96	51457.96	51457.97	51457.96	51457.96	51457.96	51457.97	51457.98	51457.97	387367.9	387367.9	387367.8	387367.8	387367.8	387367.84
^{44}Ca	51462.15	51456.1	51404.87	51509.78	50908.75	52034.27	51399.68	51488.76	51521.33	51385.48	51508.06	51417.22	51458.04	422120.7	417103.6	423721.9	425084	419371.1	421480.26
^{47}Ti	7481.91	7382.83	7438.89	7427.49	7339.02	7531.93	7388.28	7469.96	7432.04	7430.64	7449.77	7415.83	7432.38	11.36	8.13	14.66	13.01	14.39	12.31
^{49}Ti	7459.7	7402.79	7474.48	7392.93	7434.28	7431.1	7398.91	7463.84	7475.24	7381.9	7487.98	7385.38	7432.38	<5.71	<5.42	<5.92	<5.82	<5.73	b.d.
^{51}V	44.54	43.46	44.43	43.62	43.24	44.8	44.12	43.85	44.39	43.53	44.77	43.35	44.01	40.55	44.03	40.66	39.89	39.94	41.01
^{53}Cr	38.61	45.38	42.27	41.59	39.64	44.33	41.46	42.42	46.04	37.91	38.68	45.28	41.97	10.88	11.03	<6.39	<6.08	<6.45	10.96
^{88}Sr	70.15	68.65	70.1	68.78	69.21	69.61	69.01	69.76	69.32	69.46	69.76	69.07	69.41	475.04	467.56	468.97	468.73	466.39	469.34
^{89}Y	42.24	41.75	42.28	41.75	42.16	41.84	42.06	41.95	42.06	41.94	42	42	42.00	590.76	587.34	593.07	597.85	588.43	591.49
^{91}Zr	41.1	42.95	41.62	42.32	40.18	43.84	41.94	41.98	41.22	42.87	41.72	42.2	42.00	<0.83	0.86	<0.91	1.3	1.34	1.17
^{93}Nb	42.32	41.68	42.1	41.91	41.86	42.16	41.66	42.33	42.33	41.61	42.52	41.57	42.00	<0.028	<0.0236	0.0317	<0.0241	<0.0229	0.03
^{139}La	39.28	38.9	39.45	38.78	38.9	39.31	38.99	39.2	39.1	39.11	38.97	39.22	39.10	3675.47	3347.09	3825.83	3699.53	3689.99	3647.58
^{140}Ce	41.44	41.36	41.37	41.43	41.31	41.5	41.08	41.7	41.65	41.1	41.87	41	41.40	4367.98	4075.76	4501.28	4468.93	4376.27	4358.04
^{141}Pr	45.54	44.49	44.82	45.19	44.67	45.34	45	44.98	44.99	44.99	45.32	44.72	45.00	326.71	305.84	331.59	332.03	324.74	324.18
^{146}Nd	44.81	44.58	44.81	44.6	44.54	44.86	44.93	44.48	44.53	44.88	44.81	44.59	44.70	1060.7	1001.15	1071.17	1062.93	1051.38	1049.47
^{147}Sm	47.58	48.02	47.8	47.79	47.86	47.76	47.36	48.23	48.15	47.46	47.33	48.27	47.80	146.89	138.92	151.62	148.45	148.67	146.91
^{153}Eu	41.35	40.66	41.08	40.94	40.5	41.55	40.78	41.19	41.26	40.68	41.63	40.47	41.01	15.94	16.05	15.9	15.9	15.86	15.93
^{157}Gd	50.86	50.55	50.72	50.69	50.32	51.13	50.08	51.29	50.19	51.24	51.15	50.25	50.71	134.02	129.58	141.18	138.27	134.97	135.60
^{159}Tb	47.39	46.63	46.69	47.32	46.41	47.62	47.17	46.82	46.98	47.03	46.89	47.1	47.00	16.27	15.48	16.7	16.35	16.39	16.24
^{163}Dy	51.09	51.32	50.9	51.49	51.28	51.12	51.16	51.24	51.1	51.3	51.27	51.13	51.20	92.94	89.15	95.83	98.07	95.26	94.25
^{165}Ho	48.79	49.2	49.15	48.84	48.58	49.45	48.8	49.17	49.15	48.8	49.48	48.58	49.00	18.63	18.12	19.24	18.84	18.7	18.71
^{166}Er	40.62	39.59	40.45	39.79	40.08	40.13	40.07	40.13	39.5	40.77	40.29	39.88	40.11	52.26	50.03	53.31	52.71	51.9	52.04
^{169}Tm	48.93	49.07	48.91	49.08	48.77	49.25	48.63	49.35	48.8	49.2	49.19	48.81	49.00	6.33	6.06	6.34	6.35	6.27	6.27
^{172}Yb	50.82	50.99	50.66	51.12	50.91	50.87	51.43	50.42	50.74	51.11	50.45	51.31	50.90	35.45	33.77	36.28	35.84	36.04	35.48
^{175}Lu	51.73	51.27	51.47	51.54	51.14	51.88	51.41	51.57	51.26	51.76	51.48	51.5	51.50	4.63	4.31	4.68	4.46	4.56	4.53
^{178}Hf	39.02	38.96	39.44	38.59	38.72	39.29	39.01	38.98	39.1	38.87	39.28	38.75	39.00	<0.097	<0.095	<0.095	<0.108	<0.111	b.d.
^{181}Ta	40.35	39.64	40.46	39.59	40.11	39.91	39.45	40.55	40.14	39.82	40.4	39.65	40.01	<0.0172	<0.0158	<0.0209	<0.0184	<0.0203	b.d.
^{208}Pb	49.94	50.06	49.88	50.11	50.49	49.52	49.8	50.21	49.79	50.23	50.04	49.94	50.00	0.8	0.605	0.743	0.745	0.726	0.72
^{232}Th	41.02	41	40.59	41.4	40.15	41.97	40.1	41.87	40.66	41.32	41.92	40.18	41.02	271.02	239.19	268.83	261.07	257.7	259.56
^{238}U	41.24	40.75	41.28	40.75	40.91	41.09	41.08	40.92	40.97	41.02	41.11	40.9	41.00	13.93	11.98	14.73	14.57	14.53	13.95
Uncertainty [1σ ppm]																			
^{6}Li	3.39	3.37	4.85	4.53	2.56	2.49	2.87	2.98	3.35	3.12	4.53	4.54		0.8	0.73	0.75	0.69	0.64	
^{7}Li	2.49	2.61	3.58	3.46	2.05	2.1	2.24	2.28	2.21	2.13	2.51	2.59		0.5	0.51	0.51	0.52	0.5	
^{43}Ca	1690.54	1688.28	1689.57	1690.38	1689.01	1686.54	1689.92	1689.12	1688.58	1689.35	1690.77	1690.33		12262.23	12261.28	12261.82	12262.06	12261.85	
^{44}Ca	1646.31	1645	1647.71	1651.74	1725.5	1762.75	1919.03	1936.93	1651.21	1647.18	1654.72	1652.12		13248	13099.66	14222.63	14898.33	13190.04	
^{47}Ti	249.57	246.11	257.64	258.14	261.47	268.26	302.04	308.57	243.27	243.25	244.67	243.66		2.8	2.72	2.86	2.89	2.86	
^{49}Ti	247	244.98	257.76	255.89	243.03	242.78	246.6	249.11	252.85	249.84	271.63	270.64		2.09	2	2.12	2.09	2.05	
^{51}V	1.62	1.59	1.9	1.89	1.63	1.69	2.03	2.05	1.71	1.68	2.08	2.06		1.5	1.72	1.54	1.65	1.61	
^{53}Cr	4.96	5.35	7.26	7.35	4.35	4.45	4.83	4.93	7.18	6.22	8.86	10.58		2.61	2.58	2.3	2.4	2.44	
^{88}Sr	2.46	2.4	2.84	2.82	2.24	2.25	2.31	2.34	2.23	2.23	2.3	2.28		16.75	17.38	14.86	15.09	14.77	
^{89}Y	1.4	1.38	1.49	1.48	1.36	1.35	1.38	1.38	1.35	1.34	1.35	1.35		19.32	19.65	18.67	18.98	18.39	
^{91}Zr	1.7	1.77	2.24	2.32	2.26	2.45	3.46	3.54	1.66	1.72	2.04	2.11		0.31	0.3	0.33	0.34	0.33	
^{93}Nb	1.4	1.38	1.47	1.47	1.39	1.4	1.48	1.51	1.49	1.46	1.72	1.71		0.01	0.0089	0.0085	0.009	0.0087	
^{139}La	1.31	1.29	1.43	1.42	1.26	1.27	1.3	1.31	1.25	1.25	1.26	1.27		121.34	113.97	120.95	118.67	115.31	
^{140}Ce	1.31	1.31	1.31	1.32	1.35	1.35	1.42	1.45	1.42	1.41	1.61	1.61		134.97	126.03	144.19	146.78	152.35	
^{141}Pr	1.55	1.51	1.73	1.76	1.45	1.47	1.54	1.55	1.45	1.45	1.52	1.51		11.12	10.89	10.56	10.83	10.38	
^{146}Nd	1.46	1.45	1.48	1.47	1.47	1.48	1.53	1.52	1.46	1.47	1.5	1.49		33.01	31.3	33.83	34.11	33.08	
^{147}Sm	1.56	1.57	1.6	1.6	1.61	1.61	1.72	1.76	1.68	1.66	1.84	1.91		4.64	4.42	4.95	5.01	5.19	
^{153}Eu	1.36	1.34	1.45	1.46	1.41	1.45	1.63	1.67	1.48	1.46	1.76	1.75		0.53	0.54	0.56	0.59	0.6	
^{157}Gd	1.68	1.66	1.69	1.69	1.81	1.84	2.08	2.15	1.8	1.84	2.08	2.08		4.25	4.12	4.96	5.2	4.87	
^{159}Tb	1.59	1.56	1.73	1.77	1.61	1.65	1.88	1.88	1.5	1.5	1.51	1.52		0.55	0.54	0.58	0.6	0.52	
^{163}Dy	1.68	1.69	1.74	1.77	1.66	1.66	1.67	1.67	1.66	1.67	1.68	1.68		2.99	2.91	3.02	3.1	3.01	
^{165}Ho	1.58	1.59	1.64	1.63	1.63	1.65	1.78	1.8	1.65	1.64	1.8	1.79		0.6	0.59	0.64	0.65	0.64	
^{166}Er	1.46	1.42	1.71	1.71	1.31	1.31	1.31	1.31	1.46	1.51	1.77	1.79		1.9	1.93	1.69	1.67	1.99	
^{169}Tm	1.57	1.57	1.58	1.58	1.62	1.64	1.73	1.77	1.59	1.6	1.65	1.65		0.2	0.2	0.21	0.22	0.21	
^{172}Yb	1.68	1.68	1.72	1.74	1.75	1.74	1.92	1.89	1.74	1.75	1.85	1.9		1.16	1.11	1.23	1.26	1.24	
^{175}Lu	1.69	1.67	1.72	1.72	1.7	1.72	1.8	1.81	1.68	1.7	1.73	1.74		0.15	0.15	0.16	0.16	0.15	
^{178}Hf	1.35	1.35	1.51	1.49	1.31	1.33	1.39	1.39	1.33	1.32	1.4	1.39		0.034	0.034	0.034	0.038	0.039	
^{181}Ta	1.41	1.38	1.63	1.62	1.4	1.39	1.6	1.66	1.35	1.34	1.48	1.47		0.006	0.0059	0.007	0.0068	0.0072	
^{208}Pb	1.63	1.63	1.65	1.66	1.73	1.7	1.89	1.92	1.65	1.66	1.69	1.69		0.037	0.03	0.036	0.037	0.035	
^{232}Th	1.41	1.41	1.52	1.56	1.83	1.91	2.55	2.72	1.64	1.67	2.16	2.13		9.24	8.39	12.5	14.24	11.14	
^{238}U	1.36	1.34	1.47	1.46	1.31	1.31	1.33	1.32	1.31	1.31	1.33	1.32		0.46	0.41	0.46	0.46	0.46	
Detection limit [ppm]																			
^{6}Li	3.43	3.65	2.88	3.09	3.05	2.91	2.72	2.65	2.67	2.97	2.61	2.63		2.19	1.93	2.06	1.86	1.72	
^{7}Li	1.98	1.94	2.01	2.07	2.1	1.99	2.01	1.99	2.02	2.03	2	1.98		1.34	1.31	1.43	1.43	1.39	
^{43}Ca	809.42	799.58	798.51	815.72	797.63	761.06	801.47	799.23	794.44	800.41	811.19	807.96		528.07	476.66	554.53	558.3	558.18	
^{44}Ca	113.8	111.37	116.43	119.51	118.08	111.44	117.16	117.55	119.63	119.64	119.36	119.78		75.44	72.73	81.08	81.64	82.52	
^{47}Ti	11.27	10.85	11.39	11.58	11.61	10.75	11.31	11.1	11.36	11.37	11.3	11.14		7.55	7.32	7.8	7.91	7.83	
^{49}Ti	8.55	8.28	8.61	8.86	8.74	8.05	8.38	8.3	8.35	8.32	8.31	8.22		5.71	5.42	5.92	5.82	5.73	
^{51}V	0.535	0.532	0.557	0.574	0.546	0.517	0.558	0.557	0.565	0.567	0.561	0.551		0.363	0.337	0.381	0.387	0.394	
^{53}Cr	9.93	9.75	9.93	10.18	9.53	9	8.11	7.99	9.48	9.5	8.98	8.82		6.45	5.94	6.39	6.08	6.45	
^{88}Sr	0.183	0.171	0.191	0.196	0.197	0.182	0.202	0.199	0.202	0.197	0.202	0.193		0.123	0.116	0.136	0.132	0.141	
^{89}Y	0.0623	0.0678	0.0686	0.0745	0.0737	0.0699	0.0789	0.0741	0.0748	0.0757	0.0749	0.0738		0.0438	0.0446	0.0491	0.049	0.0549	
^{91}Zr	1.18	1.17	1.27	1.3	1.33	1.24	1.3	1.29	1.35	1.33	1.31	1.31		0.827	0.795	0.91	0.905	0.912	
^{93}Nb	0.033	0.0375	0.0354	0.0388	0.0349	0.0355	0.0312	0.0337	0.0343	0.0414	0.0328	0.0303		0.0276	0.0236	0.0216	0.0241	0.0229	
^{139}La	0.0273	0.0246	0.028	0.0295	0.0333	0.027	0.0307	0.0286	0.0383	0.0303	0.0303	0.0372		0.0187	0.0172	0.0185	0.0203	0.0178	
^{140}Ce	0.032	0.0323	0.038	0.0347	0.0375	0.0352	0.0369	0.0418	0.0394	0.0366	0.041	0.0408		0.0248	0.0234	0.0229	0.0287	0.0259	
^{141}Pr	0.0158	0.0134	0.0192	0.0123	0.0158	0.018	0.0154	0.0175	0.0153	0.0186	0.0204	0.0196		0.00855	0.0105	0.0092	0.0113	0.0127	
^{146}Nd	0.116	0.113	0.164	0.152	0.141	0.114	0.115	0.154	0.172	0.147	0.133	0.156		0.0828	0.0889	0.0974	0.103	0.126	
^{147}Sm	0.12	0.0864	0.125	0.125	0.11	0.0995	0.15	0.147	0.12	0.123	0.118	0.136		0.0758	0.0921	0.0561	0.089	0.0901	
^{153}Eu	0.0307	0.0285	0.0305	0.0343	0.0351	0.0349	0.0318	0.0381	0.0302	0.0334	0.0259	0.0448		0.0243	0.0268	0.024	0.0283	0.0293	
^{157}Gd	0.216	0.173	0.237	0.236	0.226	0.201	0.251	0.252	0.192	0.185	0.219	0.255		0.146	0.155	0.14	0.167	0.171	
^{159}Tb	0.0226	0.0153	0.0285	0.018	0.0366	0.0246	0.0312	0.0278	0.0308	0.0309	0.0329	0.0325		0.013	0.015	0.0186	0.0205	0.0202	
^{163}Dy	0.118	0.11	0.155	0.148	0.146	0.128	0.148	0.148	0.153	0.145	0.168	0.177		0.074	0.0806	0.105	0.115	0.11	
^{165}Ho	0.0112	0.0144	0.0133	0.0121	0.0132	0.0175	0.00959	0.0173	0.0126	0.0203	0.0162	0.0154		0.00821	0.008	0.00734	0.012	0.0082	
^{166}Er	0.103	0.104	0.141	0.155	0.136	0.131	0.17	0.154	0.155	0.155	0.163	0.149		0.0832	0.0914	0.0963	0.0957	0.115	
^{169}Tm	0.0162	0.0113	0.0141	0.0131	0.0106	0.0176	0.0213	0.0151	0.0187	0.0175	0.0177	0.017		0.00508	0.00849	0.0136	0.00815	0.00829	
^{172}Yb	0.0911	0.0875	0.105	0.105	0.116	0.121	0.129	0.107	0.117	0.0932	0.138	0.109		0.0706	0.0622	0.0849	0.0663	0.0733	
^{175}Lu	0.00759	0.0119	0.0134	0.02	0.025	0.0204	0.0193	0.0279	0.0185	0.0217	0.0263	0.0287		0.0127	0.00881	0.0184	0.0155	0.0157	
^{178}Hf	0.136	0.0957	0.135	0.151	0.143	0.0991	0.16	0.163	0.142	0.141	0.126	0.187		0.0967	0.0949	0.0945	0.108	0.111	
^{181}Ta	0.0302	0.0287	0.0193	0.0288	0.0229	0.0309	0.0251	0.0305	0.0266	0.0218	0.0271	0.0323		0.0172	0.0158	0.0209	0.0184	0.0203	
^{208}Pb	0.0291	0.0177	0.0151	0.0299	0.0211	0.0345	0.0244	0.0218	0.0219	0.033	0.0313	0.0191		0.0113	0.0171	0.0223	0.0131	0.0264	
^{232}Th	0.0106	<0.00000	0.0125	0.0114	0.0106	0.0136	<0.00000	0.0138	0.0149	0.00612	<0.00000	0.0139		0.00773	0.00502	0.00429	0.00431	0.00427	
^{238}U	<0.00000	<0.00000	<0.00000	0.00448	<0.00000	0.00661	<0.00000	0.00616	<0.00000	<0.00000	0.00638	<0.00000		<0.00000	0.00336	<0.00000	0.00301	<0.00000	

Table 5.5. Major- and trace-element compositions of titanite grains from granitoid samples from the Stolzburg Block.

Sample	**MS 2**														**MS 14**										
# of analysis EMP	4 / 1 .	3 / 1 .	8 / 1 .	7 / 1 .	9 / 1 .	10 / 1 .	12 / 1 .	16 / 1 .	15 / 1 .	13 / 1 .	20 / 1 .	22 / 1 .	25 / 1 .	29 / 1 .	31 / 1 .	32 / 1 .	30 / 1 .	34 / 1 .	35 / 1 .	36 / 1 .	33 / 1 .	37 / 1 .	38 / 1 .	33 / 1 .	35 / 1 .	37 / 1 .	31 / 1 .
# of analysis ICP MS	1	2	3	4	5	6	7	8	9	10	11	12	14	15	1	2	3	4	5	6	7	8	9	10	12	13	15
Domain	Core	Rim	Core	Core	Rim	Small grair	Small grair	Core	n/d	n/d	Core	Core	Rim	Rim	Core	Rim	Rim	Core	Core	Rim	Core	Core	Rim	Core	Core	Core	Core
Zoning															Core	Rim	Fir tree	Fir tree	Core	Rim	Patchy	Core	?	Patchy	Core	Core	Core
Group	1	2	2	2	2	2	2	2	1	1	1	1	2	1	1	?	1	1	1	1	3	2	?	3	1	2	1
Weight%																											
SiO_2	29.96	31.00	30.48	30.35	30.42	30.83	30.26	30.54	30.24	30.49	30.44	30.31	31.34	30.30	30.15	30.73	29.87	30.07	30.46	30.49	30.58	30.65	30.30	30.58	30.46	30.65	30.15
CaO	27.93	28.23	28.15	28.27	28.25	28.10	28.28	28.76	28.09	28.15	28.22	28.17	28.61	27.98	28.01	28.37	27.46	27.57	28.00	28.05	28.48	28.58	28.06	28.48	28.00	28.58	28.01
Al_2O_3	1.31	1.14	1.85	1.91	1.56	1.14	1.51	1.42	1.30	1.71	1.52	1.26	1.49	1.59	1.54	1.51	1.44	1.31	1.48	1.53	1.90	1.80	1.81	1.90	1.48	1.80	1.54
F	0.36	0.29	0.56	0.57	0.51	0.41	0.39	0.55	0.44	0.56	0.52	0.45	0.32	0.45	0.50	0.81	0.33	0.37	0.60	0.71	0.62	0.86	0.78	0.62	0.60	0.86	0.50
TiO_2	36.58	37.30	35.62	35.81	36.45	37.27	36.47	37.66	37.22	36.06	36.73	36.97	37.06	36.32	36.62	35.73	36.62	36.62	36.15	35.55	36.27	36.28	35.82	36.27	36.15	36.28	36.62
La_2O_3	0.04	0.00	0.00	0.02	0.00	0.00	0.02	0.01	0.07	0.03	0.05	0.02	0.02	0.02	0.04	0.06	0.12	0.12	0.06	0.03	0.00	0.00	0.02	0.00	0.06	0.00	0.04
Nb_2O_5	0.10	0.03	0.04	0.02	0.02	0.05	0.09	0.06	0.11	0.08	0.07	0.13	0.01	0.09	0.11	0.29	0.30	0.25	0.10	0.18	0.35	0.10	0.20	0.35	0.10	0.10	0.11
ZrO_2	0.01	0.01	0.00	0.00	0.02	0.02	0.02	0.00	0.02	0.01	0.03	0.03	0.01	0.02	0.03	0.02	0.04	0.06	0.03	0.03	0.00	0.02	0.03	0.00	0.03	0.02	0.03
P_2O_5	0.05	0.02	0.03	0.02	0.01	0.02	0.04	0.03	0.07	0.04	0.04	0.05	0.00	0.05	0.04	0.02	0.15	0.11	0.05	0.02	0.05	0.02	0.03	0.05	0.05	0.02	0.04
Y_2O_3	0.07	0.00	0.01	0.00	0.03	0.01	0.04	0.03	0.15	0.09	0.13	0.12	0.00	0.19	0.24	0.08	0.43	0.36	0.18	0.24	0.24	0.07	0.28	0.24	0.18	0.07	0.24
FeO	1.06	0.86	1.16	1.15	1.17	0.83	1.00	0.89	1.15	1.30	1.11	1.08	1.02	1.30	1.65	2.00	1.39	1.35	1.76	1.94	1.32	1.16	1.40	1.32	1.76	1.16	1.65
MnO	0.07	0.05	0.07	0.04	0.05	0.05	0.04	0.05	0.08	0.08	0.07	0.07	0.03	0.09	0.11	0.15	0.11	0.12	0.12	0.14	0.16	0.10	0.12	0.16	0.12	0.10	0.11
Ta_2O_5	0.01	0.02	0.03	0.00	0.00	0.00	0.00	0.00	0.02	0.03	0.00	0.01	0.00	0.00	0.03	0.00	0.06	0.04	0.01	0.01	0.03	0.00	0.02	0.03	0.01	0.00	0.03
Total	97.55	98.97	98.01	98.16	98.49	98.72	98.17	100.00	98.97	98.61	98.93	98.66	99.90	98.40	99.08	99.77	98.30	98.34	99.01	98.92	100.00	99.65	98.87	100.00	99.01	99.65	99.08
Atoms p.f.u. [a]																											
Si	1.01	1.03	1.02	1.02	1.02	1.02	1.01	1.01	1.01	1.02	1.01	1.01	1.03	1.01	1.01	1.02	1.00	1.01	1.02	1.02	1.01	1.02	1.02	1.01	1.02	1.02	1.01
Ti	0.93	0.93	0.90	0.90	0.92	0.93	0.92	0.93	0.93	0.91	0.92	0.93	0.91	0.91	0.92	0.90	0.92	0.92	0.91	0.90	0.90	0.91	0.90	0.90	0.91	0.91	0.92
Al	0.05	0.04	0.07	0.08	0.06	0.04	0.06	0.06	0.05	0.07	0.06	0.05	0.06	0.06	0.06	0.06	0.06	0.05	0.06	0.06	0.07	0.07	0.07	0.07	0.06	0.07	0.06
La	0.00	0.00	0.00	0.00	0.00	0.00	0.00	0.00	0.00	0.00	0.00	0.00	0.00	0.00	0.00	0.00	0.00	0.00	0.00	0.00	0.00	0.00	0.00	0.00	0.00	0.00	0.00
Fe+3	0.03	0.02	0.03	0.03	0.03	0.02	0.03	0.02	0.03	0.04	0.03	0.03	0.03	0.04	0.05	0.06	0.04	0.04	0.05	0.05	0.04	0.03	0.04	0.04	0.05	0.03	0.05
Mn	0.00	0.00	0.00	0.00	0.00	0.00	0.00	0.00	0.00	0.00	0.00	0.00	0.00	0.00	0.00	0.00	0.00	0.00	0.00	0.00	0.00	0.00	0.00	0.00	0.00	0.00	0.00
Nb	0.00	0.00	0.00	0.00	0.00	0.00	0.00	0.00	0.00	0.00	0.00	0.00	0.00	0.00	0.00	0.00	0.00	0.00	0.00	0.00	0.01	0.00	0.00	0.01	0.00	0.00	0.00
Ca	1.01	1.00	1.01	1.02	1.01	1.00	1.01	1.02	1.00	1.01	1.01	1.01	1.00	1.00	1.00	1.01	0.99	0.99	1.00	1.01	1.01	1.02	1.01	1.01	1.00	1.02	1.00
P	0.00	0.00	0.00	0.00	0.00	0.00	0.00	0.00	0.00	0.00	0.00	0.00	0.00	0.00	0.00	0.00	0.01	0.01	0.00	0.00	0.00	0.00	0.00	0.00	0.00	0.00	0.00
Y	0.00	0.00	0.00	0.00	0.00	0.00	0.00	0.00	0.00	0.00	0.00	0.00	0.00	0.00	0.00	0.00	0.01	0.01	0.00	0.00	0.00	0.00	0.00	0.00	0.00	0.00	0.00
Ta	0.00	0.00	0.00	0.00	0.00	0.00	0.00	0.00	0.00	0.00	0.00	0.00	0.00	0.00	0.00	0.00	0.00	0.00	0.00	0.00	0.00	0.00	0.00	0.00	0.00	0.00	0.00
Zr	0.00	0.00	0.00	0.00	0.00	0.00	0.00	0.00	0.00	0.00	0.00	0.00	0.00	0.00	0.00	0.00	0.00	0.00	0.00	0.00	0.00	0.00	0.00	0.00	0.00	0.00	0.00
F	0.02	0.02	0.03	0.03	0.03	0.02	0.02	0.03	0.02	0.03	0.03	0.02	0.02	0.02	0.03	0.04	0.02	0.02	0.03	0.04	0.03	0.05	0.04	0.03	0.03	0.05	0.03
Total	3.04	3.03	3.05	3.05	3.04	3.03	3.04	3.04	3.04	3.05	3.04	3.04	3.03	3.04	3.04	3.06	3.03	3.03	3.05	3.05	3.05	3.06	3.06	3.05	3.05	3.06	3.04
spot#	**MS2-1**	**MS2-2**	**MS2-3**	**MS2-4**	**MS2-5**	**MS2-6**	**MS2-7**	**MS2-8**	**MS2-9**	**MS2-10**	**MS2-11**	**MS2-12**	**MS2-14**	**MS2-15**	**MS14-1**	**MS14-2**	**MS14-3**	**MS14-4**	**MS14-5**	**MS14-6**	**MS14-7**	**MS14-8**	**MS14-9**	**MS14-10**	**MS14-12**	**MS14-13**	**MS14-15**
^{6}Li	4.93	<3.10	<2.73	<3.28	3.89	<3.26	3.79	<3.83	<3.11	<3.14	<3.56	<3.49	<3.96	<3.14	<3.47	<3.92	<3.42	<2.86	<3.08	4.11	3.75	<2.95	<2.95	<2.72	<2.81	<3.05	<3.31
^{7}Li	2.88	2.65	<1.49	2.02	3.58	<1.67	<1.73	<2.12	<1.73	<1.70	<1.94	<1.86	<2.15	<1.73	<1.81	<2.10	<1.83	<1.54	<1.61	<1.57	<1.39	<1.60	<1.59	<1.48	<1.55	<1.68	<1.86
^{43}Ca	199401.6	201545.7	201545.7	202260.4	201545.7	200831	202260.4	205833.9	200831	200831	201545.7	201545.7	204404.5	196542.8	200116.3	202975.1	196542.8	197257.5	200116.3	200116.3	203689.8	204404.5	200831	203689.8	200116.3	204404.5	200116.3
^{44}Ca	210363.5	215988.3	220338.9	213324.1	215043.3	209454.6	212944.3	217377	212188.7	220453.8	220349.3	218746.1	221684.7	209737.1	215632.6	218065.9	214384.2	214592.1	213253.4	218850.2	220349.2	219401.3	220877.8	224880.3	219395.4	217658.7	212025.8
^{47}Ti	214757.8	216376.3	211195.8	211302.8	216546.3	208848.2	215423.1	207870	220562.2	218638.5	221589.2	226811.1	218674.3	212655.5	221968.8	207546.2	224214.1	215393.1	214367.8	215049.1	212453.5	216805.9	216409.8	214715.9	216715.4	213722.3	211634.4
^{49}Ti	212320.1	213070.7	207754.6	209103.6	210809.8	210975.2	214485.2	208347.7	218532.1	215310.2	222112.6	223172.7	217236.1	210419.6	215794.1	204711.1	215886.6	213587.3	211249.5	212832.3	210709.5	214583	211342.5	209552.2	212382.2	212838.2	209038.9
^{51}V	411.42	453.68	466.44	450	438.5	400.52	407.3	475.13	424.3	466.85	433.62	415.27	431.05	438.43	323.29	345.59	305.82	322.56	326.69	347.99	312.68	313.74	349.82	317.56	359.23	322.92	348.95
^{53}Cr	71.99	54.8	87.23	65.95	85.06	67.2	77.34	108.36	72.78	90.28	106.19	60.84	123.09	58.02	27.94	14.03	37.78	21.2	24.08	21.19	18.84	21.29	32.57	25.28	26.69	8.77	29.98
^{88}Sr	79.04	49.08	67.16	62.98	51.84	71.11	70.87	68.7	83.82	80.01	80.24	80.3	50.84	81.78	60.84	38.17	67.9	67.85	57.93	30.37	74.06	51.91	58.09	64.87	54.64	48.87	56.21
^{89}Y	551.13	70.65	182.12	101.15	145.99	172.84	267.78	235.19	986.74	791.31	1061.94	842.33	267.96	1549.26	2272.64	475.73	3255.62	3104.03	1589.48	2023.09	1968.6	372.84	2140.34	660.22	1257.25	158.73	1739.96
^{90}Zr	219.52	82.33	139.62	100.46	103.95	136.69	165.09	151.96	235.18	224.28	222.28	227.58	95.57	260.27	267.45	222.18	353.12	388.95	257.18	221.6	144.72	108.14	169.59	111.72	219.43	80.13	258.63
^{93}Nb	684.13	186.28	258.86	267.5	210.62	534.48	554.25	237.32	881.78	520.08	555.44	761.64	171.06	720.98	764.13	1647.58	2253.72	1906.57	656.42	1396.44	1500.05	796.61	1197.23	1319.61	736.76	540.47	628.83
^{139}La	378.98	81.43	127.64	65.83	124.62	177.04	201.9	142.02	472.24	324.24	326.93	389.15	127.97	427.81	531	453.21	824.93	966.77	526.92	523.82	19.47	71.81	136.66	5.27	432.22	30.14	546.66
^{140}Ce	1565.06	251.55	487.29	251.88	460.49	625.47	788.8	573.72	2087.6	1340.92	1360.99	1676.2	532.2	1984.3	2807.22	1295.27	4336.33	4662.62	2504.78	2197.32	237.85	337.98	728.24	58.28	1988.31	140.89	2598.51
^{141}Pr	258.81	35.55	76.5	42.19	71.19	92.54	129.03	96.39	359.38	229.87	236.88	297.26	89.42	377.08	541.72	153.07	851.84	846.19	439.15	323.88	88.44	67.29	162.93	21.27	338.43	29.5	456.83
^{146}Nd	1260.38	150.28	355.13	201.51	322.01	414.05	617.46	458.2	1872.47	1170.56	1261.69	1549.41	447.4	2050.8	2921.61	546.05	4550.77	4216.34	2137.09	1360.39	718.3	401.5	1029.85	175.58	1568.51	174.61	2178.61
^{147}Sm	300.51	30.83	77.41	44.78	67.03	84.74	132.95	98.49	492.12	295.97	377.31	432.38	109.86	631.32	885.37	96.91	1406.91	1150.57	543.28	327.27	412.13	126.25	440.77	102.55	405.89	50.45	572.08
^{153}Eu	193.04	85.6	123.72	107.91	110.77	158.02	156.56	138.44	264.17	189.55	197.27	234.18	127.94	240.45	125.46	45.74	195.55	168.78	83.25	63.45	88.58	181.66	191.9	32.12	70.65	124.98	97.12
^{157}Gd	236.5	23.22	58.85	35.11	50.2	62.7	102.14	78	385.05	239.66	330.99	363.47	92.4	511.26	719.03	72.96	1117.03	928.09	433.29	294.13	440.5	111.29	463.44	125.05	334.22	46.91	474.43
^{159}Tb	24.59	2.314	6.03	3.55	5.29	6.43	10.61	7.8	42.61	27.65	40.46	39.6	10.2	61.35	91.55	8.36	143.67	117.93	55.87	40.32	64.16	12.44	64.71	19.74	42.26	4.92	59.88
^{163}Dy	120.41	11.98	30.74	17.78	25.88	31.83	50.9	40.41	214.46	147.8	219.39	197.98	51.99	321.33	494.98	47.11	748.04	637.34	305.51	245.96	373.51	64.18	369.47	124.46	235.69	24.98	325.61
^{165}Ho	20.45	2.133	5.43	3.17	4.44	5.43	8.71	7.28	35.75	26.35	38.54	32.35	9.04	53.25	83.28	10.54	125.47	112.98	55	52.88	68	11.74	70.76	24.62	42.8	4.77	59.07
^{166}Er	52.47	5.72	15.03	8.57	12.41	14.97	23.59	20.07	96.27	74.19	103.13	83.63	24.68	145.37	214.67	37.28	309.24	294.48	152.01	170.61	194.34	34.15	210.45	74.12	119.82	14.17	163.2
^{169}Tm	6.26	0.797	1.987	1.113	1.596	1.933	2.99	2.658	11.79	9.98	13.31	9.81	3.09	18.79	24.6	6.41	35.43	35.05	18.94	24.04	23.82	4.45	28.65	10.64	15.12	1.99	20.93
^{172}Yb	38.73	5.6	14.06	7.4	11.26	12.56	19.64	19.01	71.43	67.32	81.54	57.59	20.72	120.33	131.03	57.04	184.7	193.8	108.51	169.13	145.85	32.56	191.99	72.4	88.45	14.79	121.53
^{175}Lu	5.52	0.97	2.25	1.326	1.859	2.07	3.09	3.11	9.33	9.3	10.75	7.58	3.21	14.77	13.48	11.71	18.5	20.25	11.47	21.4	15.89	5.08	25.93	9.73	9.7	2.51	12.78
^{178}Hf	13.95	4.56	7.65	6.05	6.25	8.89	10.77	7.76	13.59	12	12.01	14.28	6.04	14.19	22.24	64.58	29.41	32.86	23.08	35.05	14.98	9.63	12.03	9.37	16.68	7.29	20.19
^{181}Ta	21.66	1.115	4.25	1.12	2.243	5.8	7.17	1.918	19.85	10.13	23.31	26.52	0.959	41.81	85.66	72.71	347.51	246.63	91.83	120.03	203.14	12.82	72.59	114.59	72	2.62	67.97
^{208}Pb	16.35	1.319	1.888	3.64	2.013	2.81	3.47	2.64	18.25	11.67	10.91	14.35	2.165	16.87	22.62	41.12	50.91	66.08	19.23	73.41	2.9	16.22	16.53	1.745	17.84	5.46	24.85
^{232}Th	49.82	2.167	3.81	1.117	4.93	6.23	9.35	6.29	56.22	35.17	34.69	44.97	4.57	53.66	68.8	120.19	156.18	201.78	58.07	220.02	3.78	47.04	50.5	1.14	50.4	14.54	73.36
^{238}U	17.73	2.074	4.5	1.693	4.5	5.55	9.63	6.54	21.9	14.38	14.69	20.73	5.95	37.45	20.83	155.55	36.83	47.35	18	67.69	89.92	178.43	266.93	39.42	19.58	126.81	21.9
Eu/Eu* [b]	2.2	9.8	5.6	8.4	5.9	6.7	4.1	4.9	1.9	2.2	1.7	1.8	3.9	1.3	0.5	1.7	0.5	0.5	0.5	0.6	0.6	4.7	1.3	0.9	0.6	7.9	0.6
$T_{Zr\text{-}in\text{-}titanite}$ calculation [c]																											
P = 4 kbar	671	640	660	649	646	660	668	664	674	672	677	678	642	679	680	677			678	677	661	648	669	649	676	639	678
P = 5 kbar	682	651	671	655	657	670	674	670	685	686	682	683	658	690	691	682			689	682	672	663	675	665	682	650	690
P = 6 kbar	693	662	677	671	668	681	685	681	696	694	694	695	668	701	703	699			707	693	684	670	686	671	699	660	707
P = 7 kbar	704	672	688	677	679	687	696	692	708	705	705	706	675	713	714	716			723	716	690	681	697	682	704	671	712
P = 8 kbar	727	694	704	697	690	703	712	708	725	722	722	723	694	730	725	716			723	716	701	692	708	693	715	682	724
P = 9 kbar	726	692	710	699	701	709	718	714	730	728	727	728	697	735	737	727			735	727	712	703	719	704	726	688	735
P = 10 kbar	731	695	715	705	706	714	723	719	734	732	732	733	702	740	748	738			746	738	723	713	731	715	738	699	746

[a] : Calculated by charge balance to 5 oxygen atoms.
[b] : Normalization values from McDonough and Sun (1995)
[c] : Calculated according to the method of Hayden et al. (2008).

Hayden, L.A., Watson, E.B., Wark, D.A., 2008. A thermobarometer for sphene (titanite). Contrib. to Mineral. Petrol. 155, 529–540. https://doi.org/10.1007/s00410-007-0256-y
McDonough, W.F., Sun, S. s., 1995. The composition of the Earth. Chem. Geol. 120, 223–253. https://doi.org/10.1016/0009-2541(94)00140-4

Table 5.5, continued.

Sample	**MS 15**								**MS 24**									**MS 25**									
# of analysis EMP	2 / 1 .	5 / 1 .	6 / 1 .	12 / 1 .	10 / 1 .	14 / 1 .	16 / 1 .	26 / 1 .	31 / 1 .	30 / 1 .	33 / 1 .	32 / 1 .	29 / 1 .	37 / 1 .	36 / 1 .	35 / 1 .	34 / 1 .	71 / 1 .	72 / 1 .	66 / 1 .	67 / 1 .	62 / 1 .	63 / 1 .	65 / 1 .	73 / 1 .	74 / 1 .	76 / 1 .
# of analysis ICP MS	1	3	5	6	7	8	10	18	1	2	3	4	5	6	7	8	9	2	3	4	5	7	8	9	10	11	12
Domain	Core	Rim	Core	Small grair	Core	Core	Rim	Core	Core	Core	Rim	Core	Core	Core	Rim	Core	Rim	Core	Core	n/d	n/d	Core	Core	Rim	Core	Core	Rim
Zoning	n/d	n/d	Fir tree	n/d	Fir tree	Fir tree	Rim	Fir tree	Fir Tree	Fir Tree	?	Fir Tree	Fir Tree	Core	Rim	Core	Fir Tree	Core	Fir tree		Fir tree	Fir tree	Core	Rim	Fir tree	Core	Rim
Group	3	2	1	2	1	1	2	1										1	1	1	2 ?		3	2	1	3	1
Weight%																											
SiO_2	31.21	30.99	29.69	30.92	30.14	29.89	31.22	30.27	30.61	30.39	30.59	30.16	30.32	30.57	30.68	30.50	30.26	30.18	30.35	30.28	30.62	30.27	30.14	30.24	30.29	30.41	30.65
CaO	28.45	28.88	27.62	28.60	27.71	27.45	28.47	27.75	28.08	28.09	28.13	27.70	27.96	28.22	28.31	28.25	27.83	28.17	28.24	28.34	28.69	27.88	28.09	28.24	28.23	28.13	28.54
Al_2O_3	2.71	2.39	1.12	2.39	1.23	1.16	2.38	1.22	2.13	2.13	2.22	2.20	2.07	2.26	1.98	2.17	1.83	1.28	1.57	1.18	2.25	1.36	1.40	1.03	1.79	1.90	1.17
F	0.80	0.86	0.45	0.88	0.56	0.47	1.09	0.55	0.63	0.50	0.80	0.54	0.54	0.75	0.64	0.74	0.56	0.33	0.39	0.24	0.73	0.23	0.17	0.26	0.33	0.38	0.19
TiO_2	34.97	35.30	36.45	35.03	36.35	36.25	34.94	36.17	35.07	35.07	35.51	34.46	35.32	35.15	35.90	35.22	35.61	37.89	37.09	38.09	36.37	37.45	37.10	38.11	36.66	36.83	38.08
La_2O_3	0.00	0.00	0.13	0.00	0.11	0.14	0.01	0.11	0.02	0.02	0.00	0.02	0.01	0.01	0.00	0.01	0.04	0.06	0.03	0.03	0.00	0.09	0.06	0.02	0.05	0.06	0.02
Nb_2O_5	0.17	0.05	0.12	0.14	0.09	0.14	0.06	0.13	0.67	0.67	0.29	1.47	0.81	0.28	0.38	0.29	0.76	0.04	0.10	0.01	0.03	0.05	0.05	0.02	0.06	0.03	0.02
ZrO_2	0.00	0.02	0.05	0.00	0.05	0.05	0.01	0.02	0.04	0.04	0.01	0.03	0.03	0.01	0.02	0.02	0.02	0.04	0.05	0.03	0.01	0.01	0.03	0.02	0.03	0.03	0.01
P_2O_5	0.02	0.00	0.03	0.01	0.03	0.04	0.01	0.04	0.04	0.04	0.02	0.07	0.06	0.02	0.03	0.03	0.04	0.20	0.17	0.08	0.04	0.24	0.13	0.06	0.13	0.11	0.07
Y_2O_3	0.06	0.03	0.26	0.00	0.22	0.26	0.01	0.23	0.45	0.49	0.43	0.55	0.52	0.35	0.31	0.33	0.46	0.09	0.18	0.06	0.06	0.07	0.06	0.08	0.13	0.04	0.04
FeO	1.39	1.73	1.87	1.32	1.84	1.83	1.80	1.91	1.23	1.17	1.25	1.09	1.15	1.39	1.11	1.28	1.02	0.65	0.78	0.56	0.85	0.62	0.71	0.58	0.76	0.84	0.56
MnO	0.09	0.08	0.09	0.05	0.09	0.09	0.08	0.09	0.14	0.15	0.14	0.17	0.15	0.14	0.15	0.17	0.16	0.05	0.05	0.05	0.03	0.06	0.07	0.03	0.04	0.04	0.04
Ta_2O_5	0.00	0.01	0.05	0.02	0.00	0.01	0.00	0.00	0.34	0.42	0.06	0.32	0.18	0.03	0.05	0.07	0.09	0.00	0.01	0.00	0.00	0.00	0.00	0.00	0.00	0.00	0.00
Total	99.86	100.33	97.93	99.35	98.41	97.79	100.08	98.49	99.46	99.19	99.47	98.79	99.12	99.16	99.56	99.07	98.69	99.00	98.99	98.94	99.69	98.33	98.00	98.69	98.50	98.78	99.37
Atoms p.f.u. [a]																											
Si	1.03	1.02	1.00	1.03	1.01	1.01	1.04	1.02	1.02	1.01	1.02	1.01	1.01	1.02	1.02	1.02	1.01	1.00	1.01	1.00	1.02	1.01	1.01	1.00	1.01	1.01	1.01
Ti	0.87	0.88	0.93	0.88	0.92	0.92	0.87	0.91	0.88	0.88	0.89	0.87	0.89	0.88	0.90	0.89	0.90	0.95	0.93	0.95	0.91	0.94	0.93	0.95	0.92	0.92	0.94
Al	0.11	0.09	0.04	0.09	0.05	0.05	0.09	0.05	0.08	0.08	0.09	0.09	0.08	0.09	0.08	0.09	0.07	0.05	0.06	0.05	0.09	0.05	0.05	0.04	0.07	0.07	0.05
La	0.00	0.00	0.00	0.00	0.00	0.00	0.00	0.00	0.00	0.00	0.00	0.00	0.00	0.00	0.00	0.00	0.00	0.00	0.00	0.00	0.00	0.00	0.00	0.00	0.00	0.00	0.00
Fe+3	0.04	0.05	0.05	0.04	0.05	0.05	0.05	0.05	0.03	0.03	0.04	0.03	0.03	0.04	0.03	0.04	0.03	0.02	0.02	0.02	0.02	0.02	0.02	0.02	0.02	0.02	0.02
Mn	0.00	0.00	0.00	0.00	0.00	0.00	0.00	0.00	0.00	0.00	0.00	0.00	0.00	0.00	0.00	0.00	0.00	0.00	0.00	0.00	0.00	0.00	0.00	0.00	0.00	0.00	0.00
Nb	0.00	0.00	0.00	0.00	0.00	0.00	0.00	0.00	0.01	0.01	0.00	0.02	0.01	0.00	0.01	0.00	0.01	0.00	0.00	0.00	0.00	0.00	0.00	0.00	0.00	0.00	0.00
Ca	1.01	1.02	1.00	1.02	1.00	0.99	1.01	1.00	1.00	1.00	1.01	1.00	1.00	1.01	1.01	1.01	1.00	1.00	1.00	1.01	1.02	0.99	1.00	1.01	1.01	1.00	1.01
P	0.00	0.00	0.00	0.00	0.00	0.00	0.00	0.00	0.00	0.00	0.00	0.00	0.00	0.00	0.00	0.00	0.00	0.01	0.01	0.00	0.00	0.01	0.01	0.00	0.01	0.00	0.00
Y	0.00	0.00	0.00	0.00	0.00	0.00	0.00	0.00	0.01	0.01	0.01	0.01	0.01	0.01	0.00	0.01	0.01	0.00	0.00	0.00	0.00	0.00	0.00	0.00	0.00	0.00	0.00
Ta	0.00	0.00	0.00	0.00	0.00	0.00	0.00	0.00	0.00	0.00	0.00	0.00	0.00	0.00	0.00	0.00	0.00	0.00	0.00	0.00	0.00	0.00	0.00	0.00	0.00	0.00	0.00
Zr	0.00	0.00	0.00	0.00	0.00	0.00	0.00	0.00	0.00	0.00	0.00	0.00	0.00	0.00	0.00	0.00	0.00	0.00	0.00	0.00	0.00	0.00	0.00	0.00	0.00	0.00	0.00
F	0.04	0.04	0.02	0.05	0.03	0.03	0.06	0.03	0.03	0.03	0.04	0.03	0.03	0.04	0.03	0.04	0.03	0.02	0.02	0.01	0.04	0.01	0.01	0.01	0.02	0.02	0.01
Total	3.06	3.07	3.04	3.07	3.04	3.04	3.07	3.04	3.05	3.05	3.06	3.04	3.04	3.06	3.05	3.06	3.04	3.03	3.04	3.03	3.06	3.02	3.03	3.02	3.04	3.04	3.02
spot#	**MS15-1**	**MS15-3**	**MS15-5**	**MS15-6**	**MS15-7**	**MS15-8**	**MS15-10**	**MS15-18**	**MS24-1**	**MS24-2**	**MS24-3**	**MS24-4**	**MS24-5**	**MS24-6**	**MS24-7**	**MS24-8**	**MS24-9**	**MS25-2**	**MS25-3**	**MS25-4**	**MS25-5**	**MS25-7**	**MS25-8**	**MS25-9**	**MS25-10**	**MS25-11**	**MS25-12**
^{6}Li	<2.20	9.78	3.2	25.28	<1.98	<2.01	93.21	<2.05	<2.60	<2.65	3.86	6.28	<2.63	<2.65	<2.63	<2.65	<2.72	<2.61	<2.66	<2.23	<2.30	<2.39	<2.45	2.97	<2.20	<2.05	<2.27
^{7}Li	<1.52	6.35	<1.31	24.81	<1.43	<1.44	93.82	<1.55	<1.50	<1.53	<1.51	4.74	<1.58	<1.58	<1.54	<1.55	<1.53	<1.59	<1.59	<1.41	<1.47	<1.53	<1.53	<1.53	<1.46	<1.36	<1.47
^{43}Ca	205833.9	206548.6	197257.4	204404.5	197972.1	196542.7	203689.8	192969.2	200831	200831	200831	197972.1	200116.2	201545.7	202260.4	201545.7	198686.8	201545.6	201545.6	202260.3	205119.1	199401.5	200830.9	201545.6	201545.6	200830.9	203689.7
^{44}Ca	225917.7	219635.1	217815.7	214833.2	218618.4	218407.1	220873.5	211638.8	218075.5	222240.5	216486.3	216224.2	219771.7	221960.6	221843.5	223795.6	217445.5	214679.8	214505.5	218639.2	221805	217519	218441.3	218708.1	216640.5	216357.5	220326.5
^{47}Ti	213211	220210.8	219804.7	203920.3	224162.6	222653	216613.8	210918.4	208716.9	209400.4	218795.7	210297.8	211454.2	212105.3	217580.2	213963.9	212990.3	228253.1	218361.8	227496.4	219791.1	227250.2	227705.3	226052.4	224954.2	218562.7	232520.4
^{49}Ti	210694.4	221511.8	219949.4	200096.8	219724	216708.9	209155.2	213614	208960.7	207623.4	213211.4	206022	212294.1	214761.4	219310.9	212958.2	209181.5	221670.3	215508.7	225398.5	216346.1	223853.8	223134.5	223681.8	219244.5	217191.6	231760.4
^{51}V	386.5	472.43	438.64	444.71	443.35	442.65	530.42	428.41	259.1	256.29	319.96	273.05	305.94	309.41	280.4	323.58	300.58	526.3	556.34	570.15	668.16	497.64	476.85	666.47	584.71	514.45	588.58
^{53}Cr	38.91	69.95	80.21	88.86	88.83	79.77	141.27	75.23	12.42	12	17.9	<8.78	<8.10	30.98	<8.09	15	10.04	76.51	45.68	87.51	108.84	61.13	74.15	82.48	74.44	132.03	114.26
^{88}Sr	56.35	43.11	45.49	41.35	48.44	47.5	41.53	38.23	43.24	43.29	40.53	47.89	41.38	40.19	40.32	40.1	42.29	81.63	86.17	88.7	92.9	106.12	98.09	59.98	80.83	90.8	77.71
^{89}Y	467.47	151.42	2184.81	119.45	2334.78	2057.31	77.69	2070.9	4038.14	4218.02	3770.1	4488.03	4644.24	3116.75	2506.6	3057.27	4000.55	949.77	1312.4	686.44	459.7	792.07	481.64	557.3	1261.38	404.25	585.66
^{90}Zr	68.14	69.8	376.68	73.23	403.93	375.4	69.14	325.6	346.23	403.77	145.46	278.89	295.76	136.65	146.13	136.66	280.77	172.36	415.98	147.22	176.75	208.36	193.21	133.88	256.33	186.36	131.27
^{93}Nb	1237.03	597.32	777.63	525.59	692.91	902.23	358.65	743.91	4663.85	4924.16	2286.35	10230.97	5738.9	1905.13	3224.9	2332.88	5365	326.58	793.67	172.02	91	400.01	287.69	108.66	470.65	160.77	157.25
^{139}La	5.64	33.23	1128.42	32.39	1340.17	1137.24	35.28	906.65	248.24	211.08	149.79	346.75	266.79	201.37	230.49	210.63	274.3	378.32	392.45	273.49	106.05	817.13	773.13	119.54	323.22	599.27	276.9
^{140}Ce	42.4	144.41	5574.12	176.74	6421.28	5602.56	127.36	4871.89	796.06	667.85	491.55	1061.4	814.7	715.34	745.08	719.01	911.53	1767.03	1971.59	1358.52	557.53	2831.9	2442.88	655.27	1556.13	2078.65	1217.19
^{141}Pr	12.15	30.12	1018.89	36.56	1218.74	984.83	26.49	854.36	117.86	99.89	73.18	153.77	118.87	112.06	107.36	111.57	134.57	331.18	383.94	264.86	115.24	427.48	324.98	141.12	317.43	273.1	225.35
^{146}Nd	97.41	165.39	4924.92	189.62	5995.87	4833.17	126.17	3902.46	556.12	466.19	356.67	700.27	559.78	547.6	484.64	537.2	620.76	1851	2176.49	1476.06	673.14	2084.54	1431.67	823.75	1825.2	1148.04	1214.76
^{147}Sm	59.85	50.74	1194.79	48.71	1506.49	1178.91	31.74	899.42	215.07	195.26	158.59	259.73	216.99	198.65	161.55	190.98	226.54	501.44	613.85	380.19	189.09	485.43	291.96	234.18	550.41	212.81	302.48
^{153}Eu	36.67	65.51	116.05	55.33	141.21	111.52	32.96	93.61	135.09	122.17	95.41	198.52	158.98	151.21	142.32	136.93	186.72	125.39	154.46	108.91	57.12	118.23	69.52	77.25	136.41	49.18	89.58
^{157}Gd	78.45	40.9	855.82	35.87	1038.18	817.37	24.65	638.32	340.51	330.9	283.59	410.92	365.5	298.98	234.49	298	359.68	406.25	507.53	296.5	159.04	378.26	220.42	200.23	474.07	157.92	245.43
^{159}Tb	12.4	4.95	98.96	3.96	118.76	95.27	2.9	78.45	71.75	70.71	61.86	83.88	78.57	58.42	46.1	58.9	73.71	47.25	61.22	34.18	19.58	42.97	24.48	24.42	58.22	17.63	28.63
^{163}Dy	78.04	26.18	489.06	20.43	576.48	473.46	15.06	424.73	527.01	533.05	467.37	596.28	588.6	426.48	327.36	419.89	545.87	240.99	309.66	171.19	102.75	205.62	119.29	126.1	303.89	87.71	142.29
^{165}Ho	15.64	4.7	78.99	3.62	89.63	75.62	2.7	71.53	110.63	111.89	101.16	123.18	124.28	85.14	67.06	85.22	109.98	38.56	51.3	27.73	17.58	32.37	18.91	21.16	49.27	14.62	23.92
^{166}Er	46.12	13.52	195.1	10.23	213.12	185.09	7.63	185.16	344.07	357.2	323.38	383.25	395.76	263.03	207.72	263.54	340.46	92.81	126.39	66.21	44.83	76.34	44.37	53.7	119.25	37.14	56.37
^{169}Tm	6.27	1.819	22.34	1.333	23.28	21.89	1	22.14	50.33	51.88	48.4	53.18	56.47	36.9	29.25	36.73	48.16	10.23	14.6	7.3	5.33	8.29	5	6.27	13.69	4.62	6.21
^{172}Yb	43.97	12.93	124.47	9.47	123.79	120.89	6.76	120.93	349.56	359.28	340.63	354.53	404.34	246.64	202.11	243.3	327.07	56.3	86.29	42.29	32.25	45.93	29.53	37.48	76.9	29.81	36.49
^{175}Lu	5.42	1.893	12.13	1.411	11.72	11.67	0.95	12.1	41.66	44.9	41.27	42.85	47.54	28.57	24.24	28.34	37.21	6.18	9.63	4.83	3.95	5.44	3.65	4.43	8.42	4.02	4.36
^{178}Hf	5.82	5.83	27.38	6.18	28.36	25.5	5.47	24.95	51.39	58.76	17.68	26.39	28.75	12.13	14.1	13.74	29.65	14.75	40.81	10.85	11.19	16.75	14.45	11.13	26.99	13.58	10.95
^{181}Ta	68.04	9.63	78	9.8	72.19	91.76	5.86	75.46	2950.34	3155.73	718.5	2828.29	1142.18	418.9	528.81	446.42	888.79	14.75	38.46	5.88	2.354	28.93	17.49	3.03	28.31	14.75	5.69
^{208}Pb	1.192	6.28	26.67	4.6	26.73	25.54	17.81	26.16	22.78	20.81	12.03	41.4	35.85	15.4	19.73	16.71	34.1	23.7	34.07	5.57	18.97	55.95	36.1	2.47	24.9	24.03	5.37
^{232}Th	0.724	4.45	80.95	7.16	82.04	75.6	3.49	74.19	70.16	63.42	34.88	126.11	111.32	47.18	60.33	51.43	104.77	71.71	103.1	13.72	1.656	177.28	114.41	4.7	73.22	75.2	13.51
^{238}U	42.97	67.48	18.97	51.05	18.38	19.2	31.98	17.99	204.05	204.29	150.97	345.99	343.87	177.63	213.46	169.63	292.84	74.78	188.58	28.63	91.03	81.82	50.27	43.89	162.17	35.07	21.35
Eu/Eu* [b]	1.6	4.4	0.4	4.1	0.3	0.3	3.6	0.4	1.5	1.5	1.4	1.9	1.7	1.9	2.2	1.8	2.0	0.9	0.9	1.0	1.0	0.8	0.8	1.1	0.8	0.8	1.0
$T_{Zr\text{-}in\text{-}titanite}$ calculation [c]																											
P = 4 kbar	632	633	690	635	694	690	632	683			674			671	674	671		689		682			695	677		693	676
P = 5 kbar	642	643	702	645	705	702	643	694			681			678	682	678		697		693			703	688		701	687
P = 6 kbar	653	654	713	656	717	713	654	706			693			690	693	690		712		704			714	700		713	699
P = 7 kbar	664	665	725	667	728	724	664	717			704			701	704	701		712		716			726	714		724	713
P = 8 kbar	674	676	736	678	740	736	675	729			715			712	715	712		724		723	733		734	719		732	718
P = 9 kbar	685	686	747	689	751	747	686	740			722			719	722	719		753		745			752	740		754	739
P = 10 kbar	696	697	759	699	763	759	697	751			733			730	733	730		771		765			774	757		777	756

[a] : Calculated by charge balance to 5 oxygen atoms.
[b] : Normalization values from McDonough and Sun (1995)
[c] : Calculated according to the method of Hayden et al. (2008).

Hayden, L.A., Watson, E.B., Wark, D.A., 2008. A thermobarometer for sphene (titanite). Contrib. to Mineral. Petrol. 155, 529–540. https://doi.org/10.1007/s00410-007-0256-y
McDonough, W.F., Sun, S. s., 1995. The composition of the Earth. Chem. Geol. 120, 223–253. https://doi.org/10.1016/0009-2541(94)00140-4

Table 5.5, continued.

Sample	**MS 25**								**MS 36**																					
# of analysis EMP	92 / 1 .	90 / 1 .	99 / 1 .	100 / 1 .	109 / 1 .	82 / 1 .	84 / 1 .	85 / 1 .	38 / 1 .	49 / 1 .	50 / 1 .	52 / 1 .	54 / 1 .	57 / 1 .	115 / 1 .	114 / 1 .	113 / 1 .	58 / 1 .	59 / 1 .	123 / 1 .	124 / 1 .	126 / 1 .	60 / 1 .	44 / 1 .	43 / 1 .	42 / 1 .	41 / 1 .				
# of analysis ICP MS	14	15	19	20	21	22	23	24	2	5	7	10	11	14	15	16	17	18	19	23	24	26	27	29	30	31	32			
Domain	Core	Rim	n/d	n/d	n/d	Core	Core	Rim	Rim	Rim	Core	Core	Rim	Small grair	Core	Core	Rim	Core	Rim	Core	Core	Core	Core	Core	Rim	n/d	Rim			
Zoning	Core	Rim	n/d	n/d	Fir tree	Fir tree	Fir tree	Rim	Rim	Fir tree	Fir tree	Fir tree	Rim	n/d	Fir tree	Core	Rim	Fir tree	Rim	Fir tree	Fir tree	Core	Fir tree	Core	?	Rim	Rim			
Group	2	1	2	2	2	1	1	1	1	1	1	1	2	1	3	3	1	1	2	1	1	1	1	3	1	2	1			
Weight%																														
SiO_2	30.54	30.13	30.44	30.38	30.49	30.06	30.39	30.32	30.54	30.62	30.59	30.26	30.95	30.94	30.57	30.27	30.50	30.46	30.73	29.92	30.05	30.30	30.38	30.58	30.34	30.54	30.30			
CaO	28.21	28.21	28.47	28.61	28.21	27.75	28.35	28.52	28.17	28.06	28.00	28.11	28.46	28.50	28.31	28.23	28.21	27.83	28.25	27.85	28.03	28.15	27.77	28.22	27.93	28.22	28.26			
Al_2O_3	1.32	1.07	1.54	1.60	1.71	1.49	1.51	1.17	1.39	1.41	1.42	1.63	1.77	1.21	1.40	3.10	1.36	2.02	1.43	1.44	1.47	1.72	1.28	1.81	1.47	1.55	1.46			
F	0.37	0.29	0.36	0.48	0.44	0.33	0.35	0.33	0.46	0.37	0.44	0.50	0.70	0.32	0.45	0.55	0.40	0.47	0.46	0.39	0.43	0.59	0.31	0.62	0.46	0.49	0.57			
TiO_2	37.92	38.08	37.59	37.81	36.84	37.30	37.44	38.16	37.17	36.99	37.16	36.34	36.49	37.67	37.43	35.96	37.38	35.76	36.65	36.79	36.88	36.45	37.19	36.10	36.39	36.35	37.00			
La_2O_3	0.01	0.00	0.01	0.00	0.00	0.14	0.02	0.03	0.02	0.06	0.06	0.06	0.00	0.00	0.05	0.03	0.04	0.02	0.00	0.06	0.06	0.02	0.08	0.01	0.02	0.00	0.00			
Nb_2O_5	0.02	0.01	0.00	0.02	0.06	0.04	0.05	0.01	0.05	0.10	0.09	0.07	0.01	0.05	0.13	0.05	0.11	0.22	0.01	0.27	0.11	0.04	0.13	0.04	0.07	0.04	0.05			
ZrO_2	0.01	0.01	0.03	0.00	0.02	0.05	0.04	0.01	0.02	0.04	0.04	0.05	0.01	0.02	0.06	0.05	0.03	0.05	0.03	0.06	0.07	0.02	0.02	0.04	0.05	0.01	0.02			
P_2O_5	0.08	0.04	0.12	0.04	0.13	0.28	0.14	0.08	0.04	0.10	0.07	0.06	0.02	0.02	0.09	0.05	0.08	0.12	0.01	0.12	0.09	0.05	0.09	0.03	0.04	0.03	0.05			
Y_2O_3	0.09	0.05	0.03	0.03	0.08	0.11	0.13	0.07	0.11	0.21	0.15	0.10	0.04	0.17	0.10	0.10	0.16	0.39	0.05	0.31	0.10	0.06	0.19	0.10	0.18	0.07	0.15			
FeO	0.54	0.58	0.65	0.59	0.64	0.78	0.60	0.56	0.90	0.90	0.81	1.00	1.02	0.91	0.83	1.11	0.79	0.94	1.11	0.87	0.85	1.12	0.80	1.12	0.97	0.92	1.03			
MnO	0.06	0.05	0.05	0.05	0.03	0.05	0.04	0.05	0.07	0.09	0.12	0.09	0.05	0.06	0.13	0.10	0.10	0.05	0.06	0.12	0.10	0.09	0.11	0.10	0.09	0.08	0.09			
Ta_2O_5	0.00	0.04	0.00	0.02	0.00	0.02	0.01	0.01	0.00	0.00	0.00	0.04	0.00	0.00	0.00	0.00	0.01	0.01	0.00	0.00	0.00	0.03	0.00	0.01	0.00	0.00	0.00			
Total	99.15	98.56	99.28	99.63	98.66	98.41	99.07	99.32	98.96	98.95	98.94	98.30	99.53	99.87	99.55	99.61	99.18	98.34	98.78	98.19	98.24	98.63	98.34	98.78	98.02	98.30	98.97			
Atoms p.f.u. [a]																														
Si	1.01	1.00	1.01	1.00	1.01	1.00	1.01	1.00	1.02	1.02	1.02	1.01	1.03	1.02	1.01	1.00	1.01	1.02	1.02	1.00	1.01	1.01	1.01	1.02	1.02	1.02	1.01			
Ti	0.94	0.95	0.93	0.94	0.92	0.94	0.93	0.95	0.93	0.92	0.93	0.92	0.91	0.93	0.93	0.89	0.93	0.90	0.92	0.93	0.93	0.92	0.93	0.91	0.92	0.92	0.93			
Al	0.05	0.04	0.06	0.06	0.07	0.06	0.06	0.05	0.05	0.06	0.06	0.06	0.07	0.05	0.05	0.12	0.05	0.08	0.06	0.06	0.06	0.07	0.05	0.07	0.06	0.06	0.06			
La	0.00	0.00	0.00	0.00	0.00	0.00	0.00	0.00	0.00	0.00	0.00	0.00	0.00	0.00	0.00	0.00	0.00	0.00	0.00	0.00	0.00	0.00	0.00	0.00	0.00	0.00	0.00			
Fe+3	0.01	0.02	0.02	0.02	0.02	0.02	0.02	0.02	0.03	0.03	0.02	0.03	0.03	0.02	0.02	0.03	0.02	0.03	0.03	0.02	0.02	0.03	0.02	0.03	0.03	0.03	0.03			
Mn	0.00	0.00	0.00	0.00	0.00	0.00	0.00	0.00	0.00	0.00	0.00	0.00	0.00	0.00	0.00	0.00	0.00	0.00	0.00	0.00	0.00	0.00	0.00	0.00	0.00	0.00	0.00			
Nb	0.00	0.00	0.00	0.00	0.00	0.00	0.00	0.00	0.00	0.00	0.00	0.00	0.00	0.00	0.00	0.00	0.00	0.00	0.00	0.00	0.00	0.00	0.00	0.00	0.00	0.00	0.00			
Ca	1.00	1.01	1.01	1.01	1.01	0.99	1.01	1.01	1.00	1.00	1.00	1.01	1.01	1.00	1.00	1.00	1.00	1.00	1.01	1.00	1.01	1.01	0.99	1.01	1.00	1.01	1.01			
P	0.00	0.00	0.01	0.00	0.01	0.01	0.01	0.00	0.00	0.00	0.00	0.00	0.00	0.00	0.00	0.00	0.00	0.01	0.00	0.01	0.00	0.00	0.00	0.00	0.00	0.00	0.00			
Y	0.00	0.00	0.00	0.00	0.00	0.00	0.00	0.00	0.00	0.00	0.00	0.00	0.00	0.00	0.00	0.00	0.00	0.01	0.00	0.00	0.00	0.00	0.00	0.00	0.00	0.00	0.00			
Ta	0.00	0.00	0.00	0.00	0.00	0.00	0.00	0.00	0.00	0.00	0.00	0.00	0.00	0.00	0.00	0.00	0.00	0.00	0.00	0.00	0.00	0.00	0.00	0.00	0.00	0.00	0.00			
Zr	0.00	0.00	0.00	0.00	0.00	0.00	0.00	0.00	0.00	0.00	0.00	0.00	0.00	0.00	0.00	0.00	0.00	0.00	0.00	0.00	0.00	0.00	0.00	0.00	0.00	0.00	0.00			
F	0.02	0.02	0.02	0.03	0.02	0.02	0.02	0.02	0.02	0.02	0.02	0.03	0.04	0.02	0.02	0.03	0.02	0.02	0.02	0.02	0.02	0.03	0.02	0.03	0.02	0.03	0.03			
Total	3.03	3.03	3.04	3.04	3.04	3.03	3.03	3.03	3.04	3.03	3.03	3.04	3.05	3.03	3.04	3.05	3.03	3.04	3.04	3.03	3.04	3.05	3.03	3.05	3.04	3.04	3.04			
spot#	**MS25-14**	**MS25-15**	**MS25-19**	**MS25-20**	**MS25-21**	**MS25-22**	**MS25-23**	**MS25-24**	**MS36-2**	**MS36-5**	**MS36-7**	**MS36-10**	**MS36-11**	**MS36-14**	**MS36-15**	**MS36-16**	**MS36-17**	**MS36-18**	**MS36-19**	**MS36-23**	**MS36-24**	**MS36-26**	**MS36-27**	**MS36-29**	**MS36-30**	**MS36-31**	**MS36-32**			
^{6}Li	<2.26	<2.25	<2.19	<1.99	<2.20	8.49	<2.22	<2.23	<3.09	<3.48	<3.35	<3.02	<3.13	<2.91	<2.34	<2.31	<2.42	5.17	<2.46	<2.43	2.83	<2.52	3.57	<2.42	2.33	<2.27	<2.53			
^{7}Li	<1.53	<1.56	<1.56	<1.52	<1.61	5.95	<1.62	<1.65	<1.55	<1.72	<1.62	<1.51	<1.54	<1.58	<1.30	<1.32	<1.35	<1.45	<1.46	<1.47	<1.49	<1.51	1.97	<1.52	<1.43	<1.51	<1.63			
^{43}Ca	201545.6	201545.6	203689.7	204404.4	201545.6	198686.8	202260.3	203689.7	201545.7	200831	200116.3	200831	203689.8	203689.8	202260.4	201545.7	201545.7	198686.9	201545.7	198686.9	200116.3	200831	198686.9	201545.7	199401.6	201545.7	202260.4			
^{44}Ca	213059.8	215467.7	217238.2	221101.4	214822.2	211734.1	215080.1	219623.5	220670.7	218804.8	218237	214519.6	225420.3	220805.4	216224.2	217351.8	213408.8	212492.5	213168.8	209732	212346.5	214931.3	211922.9	222328.1	212475.7	209376.9	213563.4			
^{47}Ti	223245.9	228160	218351.6	224354.1	222644.3	220567.1	221042.7	228651	217508.5	219478.2	218348.4	218041.9	225925.9	228057.7	226404	226139.9	221598.9	222455.3	217043.6	217935.5	215254.5	214227.7	219310.8	218448.7	226817	216273	224386.8			
^{49}Ti	223483.5	224469.1	219206.1	220969.3	218913.2	212939	220118.1	226037.1	214525.6	222168.4	221565.3	217841.2	222732.6	227779.2	217842.9	223143.2	221096.1	225552.4	214531.6	214491.3	212491.6	217287.3	217536	219542.3	224937.1	213151	223639.7			
^{51}V	556.24	542.69	695.64	654.43	620.11	525.7	593.54	545.06	430.39	406.76	410.68	420.91	434.74	463.43	399.66	456.7	407.16	381.3	493.28	405.05	431.8	447.52	412.22	433.32	441.87	440.29	425.31			
^{53}Cr	37.46	27.94	49.11	62.48	51.65	139.12	75.94	56.79	64.06	48.23	36.62	57.03	28.8	43.85	60.53	108.47	32.01	46.97	59.65	45.55	45.51	125.09	30.89	75.29	43.55	40.13	46.28			
^{88}Sr	91.86	83.93	112.2	68.88	95.14	126.03	83.16	94.97	61.79	58.12	82.05	83.47	56.31	55.92	68.21	63.44	56.71	72.99	40.8	60.51	57.2	61.41	62	61.98	61.12	58.38	62.72			
^{89}Y	533.97	630.62	210.89	307.18	694.26	1110.16	992.57	661	853.68	1253.25	1022.28	965.4	517.83	1385.42	836.83	624.87	1166.57	2921.3	353.05	1167.42	1080.78	1098.69	1357.36	472.11	1256.17	471.98	1197.72			
^{90}Zr	111.38	119.81	155.65	91.88	254.26	221.96	221.8	121.85	189.69	280.32	273.5	329.87	138.73	185.65	586.15	253.72	223.31	445.62	94.32	262.3	287.57	272.69	255.01	277.43	235.44	157.22	209.15			
^{93}Nb	169.85	161.86	101.48	51.08	430.77	149.5	324.66	165.48	344	521.37	733.11	737.68	196.28	391.16	967.6	429.57	600.71	1578.32	157.58	539.23	333.73	611.02	579.57	340.02	474.72	240.1	446.71			
^{139}La	118.02	278.81	144.71	104.95	142.25	868.48	337.84	232.84	184.23	452.65	619.32	599.23	97.29	201.38	684.74	408.98	262.28	448.37	79.29	404.72	428.81	402.45	382.25	436.45	322.44	116.09	241.13			
^{140}Ce	702.37	1307.59	479.88	479.93	807.49	3963.9	1647.99	1219.91	980.16	2106.75	2519.69	2429.83	542.17	1112.36	2330.28	1412.11	1291.11	2243.76	458.9	1878.19	1794.19	1589.73	1908.7	1360.66	1580.37	596.49	1245.55			
^{141}Pr	154.62	253.77	78.34	89.53	177.67	693.99	320.67	247.96	208.76	376.77	402.35	369.24	114.47	240.46	303.23	189.97	250.09	436.07	101.21	343.18	301.23	237.41	384.38	183.47	312.9	120.94	262.27			
^{146}Nd	899.92	1376.4	401.01	491.53	1014.8	3387.02	1818.73	1392.53	1200.74	1943.84	1943.3	1778.82	674.88	1468.25	1304.5	821.59	1405.51	2532.17	569.71	1847.66	1573.81	1137.95	2061.04	792.05	1746.74	677.66	1535.4			
^{147}Sm	245.4	344.64	99.95	123.67	274.04	715.04	482.23	353.94	351.5	531.61	472.28	418.94	206.38	521.09	289.86	181.91	437.7	856.9	147.41	491.1	416.58	266.57	586.21	170.66	488.27	178.21	474.35			
^{153}Eu	88.67	105.91	31.4	49.59	88.08	177.8	127.1	110.55	135.34	146.2	130.41	122.81	85.43	160.96	77.71	52.59	136.4	215.72	64.86	144.67	115.94	77.11	170.74	44.09	155.71	91.16	175.49			
^{157}Gd	201.77	274.5	86.87	111.13	235.82	497.77	403.99	282.81	305.96	447.75	397	349.79	181.29	492.46	247.11	165.36	404.85	836.37	113	423.38	372.45	258.89	490.87	150.97	433.16	148.67	424.16			
^{159}Tb	23.5	31.07	10.26	13.16	28.29	55.28	47.79	32.53	37.31	55.77	47.73	43.41	21.38	61.63	30.89	21.01	50.1	115.1	12.8	52.35	46.52	34.04	60.6	18.33	54.47	17.17	52.91			
^{163}Dy	118.98	152.7	52.24	66.75	149.67	268.37	240.43	160.32	190.41	298.87	245.64	224.45	110.5	330.64	172.07	114.11	269.46	645.39	66.38	272.35	247.38	197.42	314.87	101.09	287.21	91.62	280.35			
^{165}Ho	19.97	25.33	8.49	11.94	25.57	43	39.74	26.21	32.76	48.48	40.03	37.4	19.77	55.58	29.46	21.04	45	110.66	11.93	45.13	41.18	36.25	53.1	17.04	48.25	16.53	47.11			
^{166}Er	50.32	60.26	20.16	29.97	66.41	102.36	95.86	63.35	85.72	118.88	96.68	89.13	52.57	138.55	79.8	57.5	114.19	275.33	34.61	111.68	103.09	102.63	127.8	43.72	120.76	44.67	115.49			
^{169}Tm	6.1	6.78	2.277	3.52	8.02	11.86	10.92	7.29	10.14	13.27	10.95	10.04	6.39	15.97	10.04	7.71	13.15	32.23	4.64	12.61	11.62	13.44	14.8	5.47	14.07	5.85	13.12			
^{172}Yb	36.78	37.78	13.37	21.48	48.91	68.31	61.07	41.35	62.2	74.73	61.95	56.21	41.58	94.96	69.34	52.75	77.98	176.6	33.15	72.05	68.24	86.13	83.66	36.47	80.4	39.24	76.87			
^{175}Lu	4.49	4.42	1.697	2.788	6.37	7.63	6.86	4.88	8.05	8.56	7.14	6.27	5.71	11.27	9.29	6.97	9.2	18.09	5.06	8.29	7.93	10.6	9.34	5.15	9	5.7	9.09			
^{178}Hf	7.49	9.03	8.98	6.91	17.98	16.38	19.42	8.38	10.88	18.83	19.89	21.9	8.2	13.28	41.61	19.98	18.61	45.36	6.17	18.9	19.54	21.39	18.68	22.17	16.67	9.54	13.13			
^{181}Ta	4.07	5.81	3.52	0.992	6.3	23.19	13.15	4.77	3.33	14.68	24.33	20.85	2.073	20.7	29.45	13.28	23.93	178.07	1.711	18.71	10.91	27.66	18.53	8.77	10.72	0.891	6.33			
^{208}Pb	2.213	6.18	6.67	1.753	4.26	51.03	23.92	4.65	7.12	18.3	21.91	22.96	3.97	7.52	26.42	11.68	11.75	16.86	3.11	15.86	15.77	14.07	16.42	12.27	11.84	4.27	9.46			
^{232}Th	1.613	15.82	3.64	1.493	2.73	154.84	68.42	9.57	19.31	55.94	65.86	69.56	9.07	21.29	85.1	35.77	36.13	52.8	7.97	48.27	47.85	43.04	50.1	38.62	36.04	11.6	27.65			
^{238}U	11.73	26.52	19.55	4.23	460.5	55.9	100.61	21.73	28.58	36.93	38.79	34.7	15.58	60.46	58.7	28.4	45.02	40.71	12.39	45.27	31.8	31.4	79.07	24.55	87.13	12.95	43.03			
Eu/Eu* [b]	1.2	1.1	1.0	1.3	1.1	0.9	0.9	1.1	1.3	0.9	0.9	1.0	1.4	1.0	0.9	0.9	1.0	0.8	1.5	1.0	0.9	0.9	1.0	0.8	1.0	1.7	1.2			
$T_{Zr\text{-}in\text{-}titanite}$ calculation [c]																														
P = 4 kbar	671	675	684	662				676	603				590	602		615	609		575			618		618	612	595	607			
P = 5 kbar	682	683	696	673				684	613				600	612		625	620		585			628		629	622	605	617			
P = 6 kbar	694	697	704	684				695	623				610	622		636	630		595			639		640	633	616	627			
P = 7 kbar	705	708	715	698				709	634				621	633		646	641		605			649		650	643	626	638			
P = 8 kbar	716	716	726	712				717	662				661	674		675	669		654			678		679	672	666	666			
P = 9 kbar	730	734	748	723				735	673				659	672		686	680		654			689		690	682	664	677			
P = 10 kbar	750	754	765	740				755	665				669	664		678	672		652			681		682	675	657	669			

[a] : Calculated by charge balance to 5 oxygen atoms.
[b] : Normalization values from McDonough and Sun (1995)
[c] : Calculated according to the method of Hayden et al. (2008).

Hayden, L.A., Watson, E.B., Wark, D.A., 2008. A thermobarometer for sphene (titanite). Contrib. to Mineral. Petrol. 155, 529–540. https://doi.org/10.1007/s00410-007-0256-y
McDonough, W.F., Sun, S. s., 1995. The composition of the Earth. Chem. Geol. 120, 223–253. https://doi.org/10.1016/0009-2541(94)00140-4

Table 5.5, continued.

Sample	MS 2																									MS 14				
# of analysis EMP	3 / 1 .	4 / 1 .	5 / 1 .	6 / 1 .	7 / 1 .	8 / 1 .	9 / 1 .	10 / 1 .	11 / 1 .	12 / 1 .	13 / 1 .	14 / 1 .	15 / 1 .	16 / 1 .	17 / 1 .	18 / 1 .	19 / 1 .	20 / 1 .	21 / 1 .	22 / 1 .	23 / 1 .	24 / 1 .	25 / 1 .	26 / 1 .	27 / 1 .	28 / 1 .	29 / 1 .	30 / 1 .	31 / 1 .	32 / 1 .	33 / 1 .	34 / 1 .
Uncertainty [3 S.D. wt. %]																														
Si	0.1261	0.124	0.1249	0.1231	0.125	0.1254	0.1252	0.1259	0.1287	0.1247	0.1254	0.1245	0.1246	0.1254	0.1253	0.1246	0.1263	0.1253	0.1251	0.1249	0.1255	0.1253	0.1273	0.1252	0.1241	0.1242	0.1251	0.124	0.1246	0.1261	0.1255	0.1245
Ca	0.2777	0.2757	0.2787	0.2763	0.2782	0.2775	0.2781	0.2769	0.2755	0.2784	0.2775	0.2764	0.2768	0.2818	0.2808	0.2779	0.2825	0.2781	0.2773	0.2777	0.2797	0.278	0.2808	0.2773	0.2756	0.2721	0.2764	0.2726	0.2765	0.2792	0.2798	0.2734
O																																
Al	0.0306	0.0322	0.0338	0.03	0.038	0.0376	0.0346	0.0305	0.0384	0.0342	0.0358	0.0322	0.0322	0.0336	0.0339	0.0306	0.0406	0.0347	0.0333	0.0319	0.0337	0.0343	0.0339	0.037	0.0291	0.0297	0.0348	0.0338	0.0347	0.0344	0.0379	0.0325
F	0.1305	0.1313	0.1299	0.1249	0.1356	0.1347	0.1332	0.1305	0.1319	0.1306	0.1384	0.1299	0.1326	0.1326	0.1364	0.1309	0.1457	0.1375	0.1366	0.1298	0.1298	0.1323	0.132	0.1386	0.1275	0.1263	0.1346	0.1278	0.1361	0.1441	0.1418	0.1335
Ti	0.2483	0.2454	0.2455	0.2478	0.242	0.2414	0.2449	0.2483	0.2444	0.2451	0.2433	0.247	0.248	0.25	0.2486	0.2508	0.2417	0.2463	0.2458	0.2472	0.2461	0.2446	0.2476	0.2425	0.2486	0.2473	0.2446	0.2459	0.2456	0.2419	0.2439	0.2459
La	0.0343	0.0349	0.0347	0.0338	0.0335	0	-0.0003	-0.0001	0	0.0346	0.0347	0.0354	0.0353	0.0348	-0.0001	0.0354	0	0.0348	0.0348	0.0354	0	0	0.0345	0.0346	0.0363	0.0362	0.0356	0.0364	0.0357	0.0354	-0.0001	0.0362
Nb	0.0201	0.0217	0.0223	0.0203	0.0195	0.02	0.0201	0.0209	0.0204	0.0215	0.0211	0.0224	0.0229	0.0215	0.0197	0.0215	0.0198	0.0209	0.0219	0.0229	0.0213	0.02	0.019	0.0209	0.0219	0.0249	0.0216	0.0273	0.0226	0.0277	0.0279	0.0266
Zr	0.0226	0.0238	0.0235	0.0226	-0.0001	0.0232	0.0224	0.0236	0.0231	0.0235	0.0241	0.0248	0.0233	-0.0001	-0.0001	0.0237	0.0224	0.0241	0.024	0.0243	0.0223	0.022	0.0224	0.0237	0.024	0.0257	0.0235	0.0252	0.0235	0.0236	-0.0001	0.0244
P	0.0077	0.0083	0.0085	0.0076	0.0077	0.008	0.0076	0.0078	0.0085	0.0081	0.0081	0.0085	0.0092	0.0081	0.0079	0.0081	0.0077	0.0081	0.0081	0.0086	0.0076	0.0076	0.0074	0.0079	0.0085	0.0091	0.0086	0.0103	0.0082	0.0078	0.0083	0.0096
Y	-0.0002	0.028	0.0285	0.0273	0	0.0252	0.0258	0.026	0.0263	0.0264	0.0301	0.0313	0.0306	0.0261	0.0261	0.0306	0.0271	0.031	0.0295	0.0307	0.0275	0.0273	-0.0003	0.0269	0.0295	0.0321	0.0336	0.0428	0.0354	0.0297	0.035	0.0402
Fe	0.0551	0.0597	0.0625	0.0571	0.0623	0.0623	0.0631	0.0541	0.0602	0.0589	0.0658	0.0612	0.0624	0.0558	0.0554	0.0583	0.065	0.0615	0.0618	0.0606	0.0567	0.0626	0.0599	0.0576	0.0611	0.0649	0.0662	0.0688	0.0741	0.0811	0.0659	0.0676
Mn	0.0248	0.0254	0.0269	0.0257	0.0251	0.0251	0.0252	0.025	0.0264	0.0259	0.0261	0.027	0.0265	0.0255	0.0257	0.0254	0.0259	0.0269	0.0269	0.0262	0.0258	0.0262	0.025	0.0251	0.0257	0.0273	0.027	0.0288	0.0287	0.0285	0.0287	0.0289
Ta																																
Detection limit [ppm]																																
Si	178	180	181	179	179	180	181	185	183	179	182	181	181	188	176	185	182	180	182	185	184	180	185	180	180	187	185	179	179	182	183	184
Ca	240	242	238	241	236	235	235	241	241	242	246	247	232	238	231	241	242	246	237	245	245	237	232	233	236	248	237	238	243	241	237	241
O																																
Al	187	182	185	180	190	195	185	186	186	185	180	184	187	192	182	191	189	196	188	190	181	185	184	181	188	186	180	190	189	188	191	190
F	1432	1408	1377	1392	1362	1355	1356	1370	1380	1386	1405	1362	1389	1328	1396	1327	1438	1412	1377	1343	1413	1437	1437	1352	1408	1348	1409	1379	1405	1362	1427	1433
Ti	301	283	292	288	281	284	283	283	292	293	293	285	294	289	287	288	285	294	290	286	296	281	296	283	306	296	286	294	289	292	292	296
La	412	413	409	404	399					414	412	418	415	417		419		411	414	422			412	415	420	414	425	422	424	417		418
Nb	231	223	235	230	225	226	234	234	229	225	225	219	237	235	220	236	231	225	234	228	238	235	225	242	224	236	226	228	231	239	221	238
Zr	265	284	279	270		277	261	276	274	273	288	283	272			273	268	279	276	278	264	260	267	273	279	277	273	287	269	272		267
P	87	88	91	89	88	87	90	90	89	87	89	88	95	89	87	91	89	88	85	90	89	88	89	89	90	91	91	92	89	90	87	92
Y		301	315	302		299	290	310	310	296	317	313	285	299	309	306	306	307	315	308	310	312		308	319	302	311	329	307	318	299	318
Fe	328	317	343	337	335	323	340	324	331	335	335	337	333	327	326	337	325	334	322	326	333	316	348	327	328	356	345	360	353	353	324	348
Mn	271	268	282	284	280	262	279	273	289	289	275	287	275	281	285	277	291	286	283	282	283	285	287	282	253	293	281	296	294	269	267	291
Ta	643	647	650			636			641	655	642		642			642				660					656	649		660	645		646	668

Sample	MS 14				MS 24																									
# of analysis EMP	35 / 1 .	36 / 1 .	37 / 1 .	38 / 1 .	2 / 1 .	3 / 1 .	4 / 1 .	5 / 1 .	6 / 1 .	7 / 1 .	8 / 1 .	9 / 1 .	10 / 1 .	11 / 1 .	12 / 1 .	13 / 1 .	14 / 1 .	15 / 1 .	16 / 1 .	17 / 1 .	18 / 1 .	19 / 1 .	20 / 1 .	21 / 1 .	22 / 1 .	23 / 1 .	24 / 1 .	25 / 1 .	26 / 1 .	27 / 1 .	127 / 1 .	128 / 1 .
Uncertainty [3 S.D. wt. %]																														
Si	0.1254	0.1254	0.1258	0.125	0.1279	0.1262	0.1	0.1265	0.1232	0.1261	0.0115	0.1257	0.125	0.1234	0.1262	0.1264	0.1235	0.1226	0.1277	0.0885	0.1254	0.1265	0.1264	0.126	0.1255	0.1263	0.1258	0.127	0.1246	0.1268	0.0871	0.015
Ca	0.2764	0.2767	0.2806	0.2771	0.2806	0.2815	0.0539	0.2826	0.2731	0.2786	0.0118	0.2768	0.2748	0.2702	0.2805	0.2801	0.2718	0.2669	0.2805	0.0532	0.2796	0.2817	0.281	0.2792	0.2764	0.2801	0.2788	0.2798	0.2741	0.2689	0.0503	0.4757
O																																
Al	0.034	0.0348	0.0372	0.0371	0.0447	0.0418	0.0305	0.0419	0.0307	0.046	0.01	0.0432	0.0319	0.0307	0.042	0.04	0.0309	0.0295	0.0421	0.0362	0.0441	0.0449	0.0457	0.038	0.0407	0.0429	0.0411	0.0421	0.0316	0.0481	0.0383	-0.0001
F	0.1382	0.1412	0.146	0.1423	0.149	0.1421	0.1131	0.1463	0.1353	0.1548	0.0502	0.1438	0.1376	0.1307	0.1425	0.1468	0.1357	0.1288	0.1557	0.1214	0.1367	0.1433	0.1501	0.1436	0.1404	0.1379	0.1502	0.1531	0.1374	0.1503	0.1233	0.2455
Ti	0.2436	0.2409	0.2442	0.2423	0.2394	0.2402	0.3479	0.2395	0.2443	0.2361	0.0156	0.2366	0.2451	0.2442	0.2383	0.2408	0.2433	0.243	0.2389	0.368	0.2386	0.2343	0.2372	0.2413	0.2357	0.2391	0.2383	0.2378	0.2432	0.2299	0.3689	0.026
La	0.0352	0.0353	0.035	0.0345	0.0347	0.0344	0.0387	0	0.0364	0	-0.0001	0	0.0372	0.0374	0	0.0338	0.0363	0.038	0.0345	0.0389	0.0342	-0.0002	0.0339	0.0341	0	0.0341	0.0345	-0.0001	0.036	0	0.0374	-0.001
Nb	0.0217	0.0245	0.0227	0.0249	0.0245	0.0221	0.0258	0.021	0.0231	0.0247	0	0.0206	0.0229	0.0236	0.0227	0.0208	0.023	0.0231	0.021	0.0396	0.0204	0.0197	0.0249	0.0224	0.0219	0.025	0.024	0.0209	0.0232	0.0242	0.0261	0
Zr	0.0234	0.0238	0.0231	0.0241	-0.0001	-0.0001	0.0234	0.0227	0.0252	0.0229	0.0163	0.0229	0.0256	0.0255	0	-0.0002	0.0241	0.0257	0.0227	0.0263	0.0222	0.0219	-0.0001	-14.1267	0.0229	-0.0004	0.0239	0.0228	0.0243	0.0226	0.0234	0
P	0.0082	0.0081	0.0077	0.0081	0.0078	0.0075	0.0084	0.0075	0.0081	0.0081	0.0044	0.0075	0.0081	0.0083	0.0076	0.0072	0.008	0.0093	0.0073	0.0091	0.0073	0.0075	0.0079	0.0077	0.0075	0.0076	0.008	0.0074	0.0082	0.0078	0.0106	0.3398
Y	0.0343	0.0355	0.0271	0.0378	0.0279	0.0256	0.0293	0.0253	0.0359	0.0293	0.0182	0.0258	0.0353	0.0387	-0.0001	0.0256	0.0359	0.0393	0.0255	0.0302	0.0283	0	0.0289	0.0282	0.028	0.0304	0.0354	0.0261	0.0344	0.0285	0.0278	0.02
Fe	0.0758	0.0792	0.0626	0.0688	0.0677	0.0652	0.128	0.075	0.0778	0.0654	0.0187	0.0758	0.0783	0.0756	0.0658	0.0687	0.0772	0.0733	0.0768	0.1248	0.0574	0.0753	0.0623	0.0685	0.0757	0.0566	0.075	0.0741	0.0786	0.0803	0.1247	0.0293
Mn	0.0288	0.0286	0.0276	0.0282	0.0266	0.0273	0.0255	0.0255	0.0279	0.0269	0.014	0.026	0.0276	0.028	0.0257	0.0258	0.0281	0.0281	0.0262	0.027	0.0261	0.0256	0.027	0.0268	0.0262	0.0268	0.0282	0.0254	0.0274	0.0282	0.0252	0.024
Ta																																
Detection limit [ppm]																																
Si	178	181	182	182	185	182	172	178	182	180	119	183	185	187	179	179	175	182	186	179	180	186	178	186	183	186	187	180	182	183	173	150
Ca	248	233	232	253	245	239	200	238	234	236	130	242	243	236	240	245	242	234	241	202	240	232	238	234	237	238	241	239	241	232	194	276
O																																
Al	186	194	194	188	189	188	211	190	194	185	108	185	193	188	194	190	189	183	192	225	188	187	191	187	187	192	193	182	191	188	219	
F	1384	1372	1359	1349	1437	1402	1295	1372	1422	1403	604	1399	1394	1366	1300	1372	1415	1351	1392	1346	1374	1397	1325	1360	1403	1349	1412	1349	1399	1388	1323	1473
Ti	290	291	287	284	291	292	309	287	292	286	151	294	293	299	287	291	290	294	287	306	281	281	290	284	275	278	289	291	303	296	305	266
La	414	420	420	412	417	413	437		420				432	427		406	418	427	413	431	409		406	409		410	413		417		430	
Nb	224	234	239	231	236	234	251	234	236	230		224	244	239	223	231	226	237	232	246	222	227	223	237	228	220	236	234	233	233	241	
Zr	265	270	267	276			265	266	283	275	189	272	288	271			268	295	268	284	264	263			271		275	264	285	267	273	
P	87	93	88	90	87	88	79	89	90	93	52	88	90	88	88	87	87	92	86	78	84	89	89	92	90	90	90	89	90	87	78	210
Y	324	308	283	322	304	291	302	287	303	303	209	305	318	320		297	304	331	301	299	305		320	296	312	311	308	305	296	301	298	229
Fe	336	330	329	352	325	338	346	340	340	331	191	319	361	346	325	342	344	358	337	353	334	342	330	334	340	338	328	338	338	326	337	329
Mn	287	275	283	282	276	290	288	266	293	263	166	284	287	281	285	278	294	305	276	295	284	267	276	270	284	286	282	274	287	287	280	267
Ta	653	662		654		650		638	640	640			668	658	635	648	655		653	664		635				642	640		655	644		586

Table 5.5, continued.

Sample	**MS 24**										**MS 25**																		
# of analysis EMP	28 / 1 .	29 / 1 .	30 / 1 .	31 / 1 .	32 / 1 .	33 / 1 .	34 / 1 .	35 / 1 .	36 / 1 .	37 / 1 .	62 / 1 .	63 / 1 .	64 / 1 .	65 / 1 .	66 / 1 .	67 / 1 .	68 / 1 .	69 / 1 .	70 / 1 .	71 / 1 .	72 / 1 .	73 / 1 .	74 / 1 .	75 / 1 .	76 / 1 .	77 / 1 .	78 / 1 .	79 / 1 .	80 / 1 .	81 / 1 .
Uncertainty [3 S.D. wt. %]																													
Si	0.1249	0.1246	0.1248	0.1253	0.1243	0.1254	0.1246	0.1254	0.1255	0.1254	0.1241	0.1235	0.124	0.1243	0.1243	0.1255	0.1246	0.1251	0.1245	0.1242	0.1242	0.1246	0.1246	0.1245	0.1254	0.1251	0.1259	0.1252	0.1257	0.1251
Ca	0.2535	0.2759	0.2769	0.2768	0.2744	0.2772	0.2751	0.2782	0.2783	0.2779	0.2745	0.2757	0.2776	0.2776	0.2781	0.2812	0.2793	0.2798	0.2789	0.2771	0.2771	0.2777	0.2765	0.2796	0.2799	0.2813	0.2807	0.2821	0.2777	0.2811
O																													
Al	0.0388	0.0392	0.0397	0.0396	0.0403	0.0407	0.037	0.0401	0.0384	0.041	0.0325	0.0332	0.0343	0.0293	0.0309	0.0407	0.0331	0.0318	0.0366	0.0321	0.0346	0.0366	0.0377	0.0318	0.031	0.032	0.0328	0.0382	0.039	0.0312
F	0.1312	0.1356	0.1358	0.1374	0.1327	0.1462	0.1349	0.1429	0.1377	0.1415	0.1247	0.12	0.127	0.1241	0.1286	0.1413	0.1336	0.1263	0.1322	0.1242	0.1283	0.1302	0.1289	0.1259	0.1239	0.1283	0.1326	0.1305	0.1346	0.1279
Ti	0.238	0.2395	0.2386	0.2383	0.2362	0.2404	0.241	0.2394	0.242	0.2389	0.2481	0.2463	0.2487	0.2514	0.2513	0.2442	0.2499	0.2515	0.246	0.2505	0.2464	0.2454	0.2457	0.2509	0.2516	0.2513	0.2518	0.245	0.243	0.2515
La	0.0357	0.0352	0.0348	0.0351	0.0353	0	0.0346	0.0346	0.0348	0.0344	0.0357	0.0354	0.0346	0.0346	0.0348	-0.0004	0.0345	0.0346	0.0348	0.0361	0.0349	0.0348	0.035	0.0345	0.0351	0.035	0.0349	0.034	-0.0002	0
Nb	0.0342	0.038	0.0358	0.0351	0.0497	0.0269	0.0373	0.0265	0.0298	0.0277	0.0202	0.0201	0.0205	0.0191	0.0194	0.0196	0.0195	0.0192	0.0191	0.0199	0.0214	0.0208	0.0203	0.02	0.0195	0.0189	0.0192	0.019	0.0188	0
Zr	0.0361	0.0243	0.0246	0.0247	0.0248	0.0234	0.0242	0.0229	0.0243	0.0235	0.0237	0.0234	0.0231	0.0229	0.0234	0.0231	-0.0001	0.023	0.0235	0.0239	0.0244	0.024	0.0236	0.0226	0.0232	0.0224	0.0229	-0.0002	0.0231	0.0225
P	0.0087	0.0086	0.0085	0.0082	0.0089	0.008	0.0086	0.0082	0.0081	0.0081	0.0115	0.0098	0.0097	0.0082	0.009	0.008	0.0091	0.0089	0.0089	0.0108	0.0106	0.0098	0.0093	0.009	0.0084	0.0085	0.0087	0.0085	0.0084	0.0082
Y	0.0427	0.0453	0.0447	0.0435	0.0468	0.0423	0.0437	0.0386	0.0382	0.0391	0.0299	0.0269	0.0303	0.0278	0.0282	0.0275	0.0292	0.0283	0.0296	0.0296	0.0322	0.0306	0.0265	0.0287	0.0268	0.0283	0.0288	0.0269	0.0284	0.0275
Fe	0.0601	0.0625	0.0635	0.0637	0.0605	0.0648	0.0595	0.0654	0.0612	0.0679	0.0495	0.0502	0.0492	0.0478	0.0468	0.0547	0.0479	0.0485	0.0526	0.0489	0.0525	0.0531	0.0541	0.0465	0.0468	0.0495	0.0478	0.0557	0.0558	0.0477
Mn	0.0301	0.0294	0.0306	0.0293	0.0299	0.0293	0.0297	0.0296	0.0291	0.0295	0.0265	0.0256	0.025	0.0251	0.0249	0.0245	0.0259	0.0255	0.0255	0.0253	0.0263	0.0261	0.0254	0.025	0.0251	0.026	0.0253	0.0248	0.0242	0.0254
Ta																														
Detection limit [ppm]																													
Si	179	186	182	186	180	179	185	184	184	182	182	182	182	183	176	179	177	178	176	182	185	179	178	180	181	185	180	181	182	182
Ca	247	238	232	240	243	235	243	244	235	248	235	240	246	240	233	243	235	250	245	244	239	239	230	236	239	240	233	233	240	243
O																														
Al	189	190	191	190	191	195	186	190	188	194	182	193	186	186	185	186	190	196	190	190	188	184	188	184	190	189	192	179	188	185
F	1343	1383	1403	1361	1342	1401	1361	1382	1356	1358	1391	1360	1377	1367	1434	1363	1389	1390	1357	1329	1357	1410	1370	1397	1399	1414	1416	1351	1358	1371
Ti	290	286	293	277	302	280	292	289	293	292	284	293	290	282	287	283	283	290	290	292	292	291	293	295	289	298	290	284	276	291
La	415	422	416	419	422		410	415	418	412	417	417	412	413	414		415	413	416	426	416	411	413	413	420	419	417	404		
Nb	234	231	240	226	244	225	235	220	244	245	223	225	225	220	230	223	227	221	218	224	221	229	234	225	228	221	226	228	222	
Zr	295	277	277	281	285	278	281	267	284	278	282	270	255	265	269	271		268	280	270	274	278	272	268	276	267	270		273	265
P	92	91	92	88	91	91	94	91	91	92	89	89	88	83	89	87	85	89	87	86	91	87	88	88	85	86	88	89	88	89
Y	329	320	328	328	333	317	324	307	314	309	325	292	305	292	310	296	313	308	304	308	298	298	293	301	303	290	304	303	307	298
Fe	344	345	357	322	324	338	339	337	332	342	346	311	335	336	324	326	327	329	354	319	321	345	320	339	324	337	329	326	318	337
Mn	287	283	297	287	277	284	280	274	278	288	292	272	284	288	271	276	292	283	274	278	292	293	284	273	279	289	297	269	271	292
Ta	658	642	646	658	662	660	658	652	663	650			646				652		631	653	649					656	639		634	

Sample	**MS 25**																												
# of analysis EMP	82 / 1 .	83 / 1 .	84 / 1 .	85 / 1 .	86 / 1 .	87 / 1 .	88 / 1 .	89 / 1 .	90 / 1 .	91 / 1 .	92 / 1 .	93 / 1 .	94 / 1 .	95 / 1 .	96 / 1 .	97 / 1 .	98 / 1 .	99 / 1 .	100 / 1 .	101 / 1 .	102 / 1 .	103 / 1 .	104 / 1 .	105 / 1 .	106 / 1 .	107 / 1 .	108 / 1 .	109 / 1 .	110 / 1 .	111 / 1 .
Uncertainty [3 S.D. wt. %]																													
Si	0.1238	0.1248	0.1247	0.1246	0.1246	0.1242	0.1253	0.1245	0.1239	0.1236	0.1251	0.1246	0.1246	0.1241	0.1245	0.1245	0.1248	0.1247	0.1246	0.1243	0.1247	0.1242	0.1251	0.1242	0.1244	0.1248	0.1243	0.1251	0.1232	0.1247
Ca	0.2738	0.2803	0.2784	0.2797	0.2782	0.279	0.2792	0.2754	0.2772	0.2786	0.2774	0.28	0.279	0.2777	0.2799	0.2789	0.2817	0.2791	0.2803	0.2811	0.2785	0.2737	0.2794	0.2774	0.2792	0.281	0.2803	0.2777	0.2774	0.2788
O																													
Al	0.0344	0.0337	0.0343	0.0308	0.0296	0.0309	0.032	0.0309	0.0297	0.0305	0.0324	0.0366	0.0327	0.031	0.0343	0.034	0.0331	0.0344	0.0352	0.031	0.0312	0.0362	0.0373	0.035	0.037	0.0375	0.0295	0.0361	0.0374	0.0313
F	0.1297	0.1329	0.1304	0.1253	0.1271	0.1274	0.1304	0.1257	0.1268	0.1263	0.1297	0.1333	0.1284	0.1247	0.1309	0.1301	0.1339	0.1333	0.1333	0.1279	0.1292	0.1298	0.134	0.1276	0.1332	0.1382	0.1276	0.1358	0.1267	0.1303
Ti	0.2477	0.25	0.2487	0.252	0.252	0.2503	0.2516	0.2478	0.2513	0.2518	0.2508	0.2468	0.2494	0.251	0.2486	0.2498	0.2493	0.2489	0.2502	0.2526	0.2529	0.2477	0.2456	0.2479	0.2464	0.247	0.2527	0.2464	0.2446	0.2505
La	0.0362	0.0347	0.0353	0.0352	0.0351	0	-0.0001	0.035	0	0	0.0349	-0.0002	-0.0001	-0.0001	-0.0001	-0.0001	0.0348	0.0343	0	0.0347	0.0348	0.0355	0.0354	0.0343	0.035	0.0348	0	0	0.0346	-0.0002
Nb	0.0205	0.0195	0.0202	0.0192	0.0199	0.019	0.0195	0.0191	0.0191	0.0183	0.0196	0.0205	0.0193	0.0198	0.0184	0.0191	0.0191	0.0183	0.0191	0.0194	0.0192	0.022	0.0197	0.0198	0.021	0.0192	0.0193	0.0207	0.0224	0.0195
Zr	0.0246	0.0236	0.0244	0.0229	0.0231	0.0233	0.0224	0.0223	0.0236	0.0221	0.0227	0.0238	0.0222	0.0234	0.0226	0.0232	0.024	0.0231	0.0237	-0.0001	-0.0004	0.0247	0.0236	0.0233	0.025	0.024	-0.0001	0.024	0.0251	-0.0004
P	0.0123	0.0091	0.0099	0.0091	0.0093	0.0092	0.0088	0.0087	0.0081	0.0079	0.009	0.0093	0.0082	0.0096	0.0082	0.0078	0.0087	0.0095	0.0082	0.0092	0.0092	0.0107	0.0096	0.0089	0.0104	0.0091	0.0078	0.01	0.01	0.0087
Y	0.0308	0.0273	0.0308	0.029	0.0279	0.0284	0.0282	0.0289	0.0279	0.0274	0.0285	0.0281	0.0262	0.0286	0.0288	0	0.0256	0.0258	0.026	0.0295	0.029	0.0305	0.0268	0.034	0.0298	0.0276	0.0276	0.0286	0.03	0.0286
Fe	0.0531	0.0509	0.0493	0.0475	0.0477	0.047	0.0467	0.0475	0.0472	0.0462	0.046	0.052	0.05	0.0476	0.0494	0.0476	0.046	0.0499	0.048	0.048	0.0473	0.0542	0.0566	0.0536	0.0524	0.0522	0.049	0.0498	0.0485	0.0495
Mn	0.0263	0.025	0.0257	0.0258	0.0255	0.0257	0.0256	0.0252	0.0248	0.0246	0.0257	0.0253	0.0252	0.0253	0.0254	0.0244	0.0247	0.0248	0.0252	0.0254	0.0256	0.0257	0.0252	0.026	0.0256	0.0246	0.026	0.0255	0.0259	0.0261
Ta																														
Detection limit [ppm]																													
Si	182	180	182	184	181	172	183	177	179	177	184	176	182	182	180	177	180	184	178	181	183	179	178	184	179	180	181	180	182	178
Ca	232	243	239	237	245	243	233	243	233	240	249	243	238	237	235	234	242	240	242	245	233	242	234	231	242	239	239	244	241	234
O																														
Al	197	190	191	186	184	192	189	190	186	193	188	193	190	183	191	193	184	188	192	188	189	187	190	192	183	187	187	190	193	187
F	1406	1395	1400	1343	1404	1343	1397	1421	1387	1326	1381	1415	1421	1381	1419	1367	1409	1438	1374	1403	1411	1416	1380	1349	1409	1370	1363	1432	1434	1433
Ti	298	286	288	292	288	287	281	286	292	277	299	285	294	283	280	284	291	288	290	290	287	284	299	285	292	285	285	284	279	285
La	415	413	421	419	416			419	1.#INF		418						418	411		414	413	425	414	409	420	418			414	
Nb	231	232	224	226	230	227	224	223	226	216	229	230	227	224	220	225	225	221	222	230	224	230	235	224	226	217	223	226	228	224
Zr	272	279	275	270	270	279	259	266	279	262	270	282	260	272	266	268	280	264	285			284	276	275	284	272		278	288	
P	94	88	89	90	91	88	87	92	87	89	91	86	90	89	87	87	86	86	88	88	91	91	92	90	90	89	88	91	88	90
Y	313	296	301	314	306	294	306	312	310	307	296	309	295	304	315		302	294	299	315	302	306	313	316	311	294	304	298	290	313
Fe	333	326	356	339	342	330	333	340	324	339	321	348	318	322	328	320	319	337	333	331	333	336	328	321	335	349	317	338	332	336
Mn	290	283	290	282	282	282	279	286	273	279	277	273	288	286	286	268	272	271	279	287	285	289	290	274	278	277	294	292	280	291
Ta	643		648	651	637				644						648	644			640	641		641		649	625	629			640	

Table 5.5, continued.

Sample	MS 25																				MS 36									
# of analysis EMP	111 / 2 .	111 / 3 .	111 / 4 .	111 / 5 .	111 / 6 .	111 / 7 .	111 / 8 .	111 / 9 .	111 / 10 .	111 / 11 .	111 / 12 .	111 / 13 .	112 / 1 .	112 / 2 .	112 / 3 .	112 / 4 .	112 / 5 .	112 / 6 .	112 / 7 .	112 / 8 .	38 / 1 .	39 / 1 .	40 / 1 .	41 / 1 .	42 / 1 .	43 / 1 .	44 / 1 .	45 / 1 .	46 / 1 .	47 / 1 .
Uncertainty [3 S.D. wt. %]																														
Si	0.1253	0.1253	0.1254	0.119	0.1258	0.1233	0.1246	0.1249	0.1248	0.125	0.1254	0.1251	0.1243	0.1246	0.1266	0.1247	0.1256	0.1254	0.1247	0.1256	0.1254	0.1248	0.1269	0.1251	0.1231	0.1247	0.1252	0.1251	0.1222	0.1244
Ca	0.2804	0.2799	0.2786	0.276	0.2793	0.2771	0.2772	0.2786	0.2777	0.2788	0.2796	0.2784	0.2777	0.2793	0.278	0.2785	0.2799	0.2807	0.279	0.28	0.2777	0.2769	0.2772	0.2785	0.2746	0.2755	0.2774	0.2781	0.273	0.2761
O																														
Al	0.0378	0.0364	0.0387	0.0358	0.0325	0.0334	0.0355	0.0357	0.0358	0.0362	0.0365	0.0352	0.0357	0.0358	0.0345	0.0322	0.0384	0.0386	0.0405	0.0318	0.0331	0.0338	0.0373	0.034	0.0337	0.0338	0.0369	0.0312	0.032	0.0353
F	0.1397	0.1339	0.1321	0.1301	0.1272	0.1269	0.1291	0.1297	0.1311	0.1281	0.1343	0.1366	0.1311	0.1319	0.129	0.1281	0.1347	0.1354	0.1346	0.1322	0.1354	0.1304	0.14	0.1357	0.1345	0.1349	0.142	0.1286	0.1251	0.1307
Ti	0.2477	0.2478	0.2453	0.2449	0.2521	0.2489	0.2471	0.2478	0.2472	0.2469	0.2474	0.2498	0.2472	0.2473	0.2499	0.2512	0.2454	0.2463	0.245	0.2519	0.248	0.2464	0.2434	0.2477	0.2405	0.2443	0.2427	0.249	0.2441	0.2454
La	-0.0001	0	0.035	0.0354	0.0351	0.035	0.0356	0.0352	0.035	0.0349	0.0353	0.0352	0.0349	0.0349	0.036	0.0352	0.0351	0.0343	-0.0005	0.0349	0.0346	0.036	0.0352	0.0352	0.0338	0.0348	0.0349	0.0346	0.0347	0.0354
Nb	0.0195	0.0195	0.0192	0.0192	0.0201	0.0207	0.0231	0.0224	0.0227	0.0217	0.0218	0.0211	0.0222	0.0191	0.0212	0.02	0.0196	0.02	0.0193	0.0188	0.0206	0.0252	0.0211	0.0209	0.0199	0.0213	0.0205	0.0205	0.0231	0.0241
Zr	0.0232	0.0231	0.024	0.024	0.0229	0.0242	0.0245	0.0247	0.0256	0.0254	0.0252	0.0246	0.0248	0.0236	0.0239	-0.0009	0.0239	0.0231	0.0233	0.0239	0.0237	0.0247	0.0244	0.024	0.0226	0.024	0.0237	0.0229	0.0251	0.0246
P	0.0085	0.0088	0.0086	0.0095	0.0097	0.0095	0.011	0.0109	0.0109	0.0109	0.0108	0.01	0.0108	0.0104	0.0117	0.01	0.0091	0.0088	0.0085	0.0089	0.0083	0.0096	0.008	0.0084	0.0079	0.0082	0.0084	0.0079	0.0091	0.0099
Y	0.029	0.0298	0.03	0.027	0.0309	0.0311	0.033	0.0314	0.0323	0.0316	0.0307	0.0308	0.0312	0.0296	0.0298	0.0277	0.0299	0.0299	0.0292	0.0295	0.03	0.0305	0.032	0.0324	0.0275	0.0328	0.0287	0.0324	0.0324	0.0363
Fe	0.053	0.053	0.0569	0.0537	0.0482	0.0518	0.0538	0.0519	0.0542	0.0524	0.051	0.0506	0.0504	0.0543	0.0496	0.0481	0.0569	0.0565	0.0564	0.0495	0.0555	0.0563	0.0636	0.0599	0.0556	0.0581	0.0614	0.0561	0.0545	0.0579
Mn	0.0248	0.0258	0.0253	0.0259	0.0261	0.0262	0.0253	0.0259	0.0253	0.0264	0.0252	0.0252	0.0254	0.0264	0.0268	0.0259	0.0258	0.026	0.0253	0.0254	0.0277	0.0281	0.0267	0.0277	0.0269	0.0273	0.0267	0.0264	0.0275	0.0278
Ta																														
Detection limit [ppm]																														
Si	180	186	180	177	185	177	184	179	179	184	179	184	185	181	181	186	179	185	179	184	183	184	189	183	180	182	182	180	173	180
Ca	244	227	241	232	235	250	242	247	237	228	243	252	240	243	238	230	237	230	240	246	250	236	242	238	216	241	236	243	234	240
O																														
Al	187	189	188	184	193	189	189	192	193	191	193	193	191	186	193	196	191	194	187	190	186	190	198	190	180	185	187	187	185	190
F	1363	1407	1379	1380	1385	1374	1372	1401	1404	1336	1403	1450	1422	1400	1420	1377	1398	1419	1398	1433	1413	1404	1397	1362	1398	1410	1428	1380	1354	1399
Ti	286	284	294	285	294	295	304	291	291	286	286	290	290	291	289	294	298	286	284	291	283	299	281	287	287	292	290	280	290	290
La			421	418	416	413	420	417	415	415	421	420	413	412	421	412	420	409		416	413	420	422	423	406	415	418	414	408	420
Nb	232	230	220	226	226	238	225	234	224	231	228	224	230	225	232	228	228	232	227	218	228	234	233	231	224	230	232	227	221	226
Zr	269	273	280	281	266	284	266	265	278	284	280	277	287	270	279		277	274	261	287	276	270	282	278	266	268	269	270	287	263
P	91	89	87	89	93	90	89	88	88	95	87	86	89	90	93	93	89	90	91	90	89	90	90	90	88	89	94	88	85	89
Y	294	314	310	301	311	317	314	325	296	301	309	297	319	312	306	304	305	308	300	319	304	308	306	316	294	306	292	317	300	310
Fe	338	331	340	334	330	336	338	316	335	338	328	333	344	339	330	332	326	322	348	338	310	333	332	341	325	335	332	345	322	339
Mn	268	290	276	276	288	282	275	286	276	276	285	283	280	281	288	282	283	277	272	289	297	281	268	290	285	283	272	274	278	283
Ta		652		636		634	650		650	648	652			641	654	649	644	642				638				646	635	641	644	

Sample	MS 36																													
# of analysis EMP	48 / 1 .	49 / 1 .	50 / 1 .	51 / 1 .	52 / 1 .	53 / 1 .	54 / 1 .	55 / 1 .	56 / 1 .	57 / 1 .	58 / 1 .	59 / 1 .	60 / 1 .	61 / 1 .	113 / 1 .	114 / 1 .	115 / 1 .	116 / 1 .	117 / 1 .	118 / 1 .	119 / 1 .	120 / 1 .	121 / 1 .	122 / 1 .	123 / 1 .	124 / 1 .	125 / 1 .	126 / 1 .
Uncertainty [3 S.D. wt. %]																														
Si	0.1239	0.1252	0.123	0.1233	0.1243	0.1244	0.126	0.1246	0.1259	0.126	0.1245	0.125	0.1244	0.1253	0.125	0.1251	0.1253	0.125	0.1269	0.1255	0.125	0.1249	0.1249	0.1256	0.1236	0.124	0.1265	0.1249
Ca	0.2754	0.2762	0.2728	0.2739	0.2765	0.2772	0.2791	0.2752	0.2793	0.2796	0.2741	0.277	0.2739	0.2776	0.2774	0.278	0.2784	0.2795	0.2825	0.2758	0.2775	0.277	0.2758	0.2755	0.2748	0.2762	0.276	0.2773
O																														
Al	0.0361	0.0331	0.0323	0.0358	0.0354	0.0342	0.0365	0.0361	0.0308	0.0316	0.0385	0.0332	0.032	0.0361	0.0331	0.0475	0.0331	0.0308	0.0378	0.0322	0.0302	0.0327	0.0339	0.0377	0.0336	0.0338	0.0384	0.0363
F	0.1351	0.1329	0.1279	0.1325	0.1358	0.1347	0.1414	0.1314	0.1332	0.1288	0.132	0.1312	0.1319	0.136	0.1328	0.1368	0.1324	0.1344	0.1472	0.1299	0.1322	0.1318	0.131	0.1322	0.1286	0.1309	0.1371	0.1363
Ti	0.2411	0.2466	0.2437	0.2395	0.2436	0.2449	0.2443	0.2435	0.2479	0.2496	0.2406	0.2444	0.2471	0.2435	0.2483	0.2427	0.2487	0.2496	0.244	0.2483	0.2487	0.2482	0.2471	0.245	0.246	0.2463	0.2435	0.2448
La	0.0338	0.0356	0.0349	0.034	0.0346	0.0353	0.034	0.0355	0.0347	0	0.0347	-0.0001	0.0349	0.0346	0.0353	0.0349	0.0355	-0.0001	0	0.0361	0.0346	0.0348	0.0358	0.0354	0.0355	0.0358	0.035	0.0353
Nb	0.0203	0.0222	0.0211	0.0205	0.0206	0.0243	0.0199	0.0277	0.0201	0.021	0.0253	0.0194	0.0227	0.0212	0.0224	0.0213	0.0233	0.0205	0.019	0.0229	0.0201	0.0211	0.024	0.0239	0.0263	0.0224	0.0197	0.0202
Zr	0.0233	0.0247	0.0234	0.0232	0.0241	0.0259	0.0227	0.0253	0.0228	0.0237	0.0241	0.0226	0.0235	0.0236	0.0244	0.0235	0.0254	0.0222	0.0231	0.025	0.0233	0.0238	0.0244	0.0249	0.0255	0.0253	0.0243	0.0236
P	0.0082	0.0094	0.0085	0.0082	0.0082	0.0098	0.0075	0.0097	0.0075	0.0079	0.0095	0.0076	0.0091	0.0084	0.0087	0.0084	0.0092	0.0077	0.0074	0.0091	0.0075	0.0085	0.0097	0.0094	0.0094	0.0091	0.008	0.0085
Y	0.0267	0.0336	0.0306	0.0295	0.0306	0.0297	0.0273	0.0393	0.027	0.0327	0.0407	0.0271	0.0332	0.029	0.0316	0.0295	0.0295	0.031	0.0274	0.0329	0.0294	0.0321	0.0294	0.0344	0.038	0.0297	0.0313	0.0274
Fe	0.0594	0.0564	0.0536	0.0612	0.058	0.055	0.0587	0.0579	0.0568	0.0561	0.0573	0.0609	0.0533	0.0606	0.0538	0.0623	0.0547	0.0542	0.064	0.0571	0.0546	0.0542	0.0537	0.0571	0.0554	0.0549	0.0605	0.0618
Mn	0.0271	0.0281	0.0273	0.0273	0.0269	0.0279	0.0264	0.0284	0.0263	0.0262	0.0262	0.0258	0.0279	0.0262	0.0279	0.028	0.0279	0.0268	0.0265	0.0284	0.0259	0.0278	0.0288	0.0284	0.0279	0.0275	0.0282	0.028
Ta																														
Detection limit [ppm]																														
Si	178	182	179	182	184	181	180	184	182	179	180	180	179	180	187	181	182	177	181	179	181	182	179	180	180	187	181	182		
Ca	243	243	222	225	240	242	230	238	238	238	234	235	245	236	246	236	240	245	233	237	237	238	235	242	232	240	241	240		
O																														
Al	189	185	177	185	193	193	187	190	190	194	188	186	190	185	196	191	186	189	191	192	188	190	186	189	189	186	187	191		
F	1416	1426	1329	1371	1402	1413	1377	1365	1370	1397	1369	1358	1442	1400	1412	1388	1380	1416	1443	1390	1406	1380	1415	1362	1358	1368	1350	1361		
Ti	288	298	290	281	287	291	290	288	285	284	282	292	290	287	293	285	276	286	277	295	292	285	285	289	297	284	291	293		
La	400	419	411	406	408	411	409	419	417		413		409	410	419	416	420			428	415	414	418	418	419	422	418	422		
Nb	224	230	223	221	222	232	235	235	230	233	229	231	225	233	230	237	233	230	228	229	222	225	229	227	225	230	232	228		
Zr	268	281	262	268	268	280	267	277	273	278	269	259	275	279	282	258	279	261	267	281	275	286	273	276	281	274	279	275		
P	88	89	87	89	85	89	86	91	86	89	87	90	89	88	86	89	89	86	86	91	87	88	88	93	86	89	87	90		
Y	299	297	294	293	317	317	306	316	304	306	314	300	305	308	300	300	305	305	303	302	296	301	310	318	313	307	311	297		
Fe	320	338	346	342	317	341	326	340	328	323	340	331	328	322	340	356	335	332	335	332	328	341	332	350	329	330	331	339		
Mn	268	294	269	273	281	289	291	286	279	282	293	279	281	277	285	290	271	281	286	289	279	281	294	279	276	279	290	292		
Ta	626				646	649		654			658		654		651					650		641	645	651			642	643		

Table 5.5, continued.

Sample	MS 2														MS 14												
# of analysis ICP MS	MS2-1	MS2-2	MS2-3	MS2-4	MS2-5	MS2-6	MS2-7	MS2-8	MS2-9	MS2-10	MS2-11	MS2-12	MS2-14	MS2-15	MS14-1	MS14-2	MS14-3	MS14-4	MS14-5	MS14-6	MS14-7	MS14-8	MS14-9	MS14-10	MS14-12	MS14-13	MS14-15
Uncertainty [1σ ppm]																											
^{6}Li	1.11	1.14	1.1	1.19	1.06	1.17	1.16	1.35	1.13	1.13	1.27	1.25	1.42	1.13	1.24	1.44	1.22	1.04	1.11	1.08	1.05	1.08	1.07	1.02	1.01	1.11	1.2
^{7}Li	0.57	0.58	0.58	0.62	0.58	0.61	0.62	0.77	0.62	0.61	0.72	0.67	0.78	0.64	0.66	0.76	0.65	0.56	0.58	0.56	0.54	0.57	0.57	0.57	0.56	0.6	0.67
^{43}Ca	6323.56	6392.14	6396.01	6416.23	6390.49	6372.09	6417.27	6530.71	6370.77	6370.68	6395.63	6395.58	6493.44	6235.07	6349.03	6442.07	6236.43	6254.42	6345.56	6345.31	6462.24	6480.85	6368.2	6459.14	6344.62	6482.17	6350.14
^{44}Ca	7855.94	8101.19	8314.68	8107.86	8243.53	8112.67	8342.14	8742.68	8660.23	9139.77	9288.78	9382.14	9865.2	9510.11	7805.6	7921.03	7822.66	7874.33	7881.49	8155.7	8291.07	8436.37	8599.01	8871.18	8905.11	8971.02	9025.17
^{47}Ti	7878.53	7966.19	7814.43	7864.19	8115.95	7894.67	8220.04	8107.05	8708.18	8746.65	8990.25	9338.04	9291.41	9181.75	8897.33	8360.87	9093.03	8808.67	8857.87	8992.58	9005.57	9476.05	9622.5	9721.83	10198.83	10265.08	10603.36
^{49}Ti	7389.22	7435.02	7276.8	7354.93	7452.41	7505.73	7683.28	7584.82	8028.35	7988.44	8329.18	8462.79	8441.16	8277.74	8260.54	7871.19	8349.81	8321.34	8305.39	8455.79	8472.67	8865.6	8866.37	8935.09	9376.37	9571.94	9771.01
^{51}V	14.45	15.97	16.49	15.97	15.64	14.38	14.73	17.46	15.74	17.49	16.42	15.91	16.93	17.43	14.12	15.19	13.56	14.46	14.84	16.05	14.67	15.29	17.41	16.16	19.15	17.64	20.03
^{53}Cr	12.99	10.25	16.21	12.77	16.67	13.79	16.32	24.4	17.18	22.04	26.93	16.3	35.25	17.48	6	4.08	8.03	4.97	5.7	5.28	4.93	5.85	8.78	7.23	8.26	3.9	10.57
^{88}Sr	2.67	1.66	2.29	2.15	1.78	2.45	2.46	2.42	2.98	2.87	2.9	2.94	1.91	3.09	2.3	1.46	2.6	2.62	2.26	1.2	2.96	2.13	2.43	2.76	2.41	2.2	2.63
^{89}Y	18.89	2.43	6.29	3.51	5.09	6.07	9.46	8.45	35.77	28.98	39.32	31.55	10.3	60.27	90.08	18.96	130.69	125.73	65.11	83.93	82.87	16.22	94.8	29.81	59.14	7.63	87.44
^{91}Zr	7.18	2.72	4.6	3.33	3.45	4.54	5.5	5.11	7.93	7.61	7.59	7.82	3.37	9.13	14.69	12.33	19.86	22.24	15.01	13.23	8.86	7	11.3	7.68	16.04	6.06	20.82
^{93}Nb	23.59	6.44	8.99	9.33	7.38	18.85	19.68	8.57	32.14	19.16	20.69	28.69	6.61	28.2	30.72	66.6	91.79	78.38	27.3	58.85	64.17	35.25	53.98	60.68	35.33	26.5	32.27
^{139}La	12.12	2.61	4.1	2.12	4.02	5.72	6.54	4.63	15.45	10.65	10.79	12.91	4.3	14.42	20.83	17.88	32.77	38.75	21.35	21.5	0.82	3.09	5.99	0.24	20.09	1.43	27.13
^{140}Ce	55.7	8.99	17.51	9.11	16.77	22.99	29.28	21.79	80.32	52.32	53.89	67.41	22.13	83.92	107.56	49.88	168.1	182.24	98.91	87.79	9.64	14.11	30.92	2.52	89.27	6.46	124.15
^{141}Pr	8.13	1.12	2.42	1.33	2.25	2.93	4.09	3.07	11.46	7.35	7.6	9.57	2.91	12.27	23.04	6.56	36.81	36.98	19.46	14.58	4.06	3.21	7.94	1.06	17.69	1.58	25.76
^{146}Nd	44.69	5.37	12.74	7.28	11.71	15.19	22.86	17.37	71.86	45.57	49.87	62.21	18.61	86.64	101.79	19.12	159.77	148.82	75.95	48.74	25.99	14.83	38.45	6.66	60.92	6.9	88.58
^{147}Sm	9.58	1.02	2.52	1.47	2.18	2.76	4.31	3.22	15.99	9.67	12.37	14.23	3.69	21.06	30.5	3.38	48.76	40.05	19.04	11.56	14.68	4.59	16.12	3.82	15.36	1.96	22.53
^{153}Eu	6.03	2.68	3.88	3.38	3.48	4.96	4.92	4.36	8.32	5.98	6.24	7.42	4.08	7.66	4.06	1.49	6.35	5.49	2.72	2.08	2.92	6.01	6.37	1.08	2.39	4.25	3.35
^{157}Gd	7.9	0.81	2.02	1.22	1.73	2.17	3.52	2.73	13.4	8.42	11.71	12.97	3.41	18.77	28.77	2.97	45.31	38.01	17.98	12.38	18.82	4.94	20.89	5.78	16.06	2.33	24.43
^{159}Tb	0.8	0.08	0.2	0.12	0.18	0.22	0.35	0.26	1.42	0.93	1.36	1.34	0.36	2.11	3.38	0.32	5.35	4.43	2.12	1.55	2.49	0.5	2.61	0.81	1.79	0.22	2.68
^{163}Dy	3.85	0.41	1.02	0.59	0.85	1.05	1.66	1.33	6.96	4.82	7.17	6.49	1.75	10.64	16.37	1.59	24.81	21.19	10.2	8.25	12.59	2.2	12.64	4.3	8.24	0.9	11.67
^{165}Ho	0.7	0.078	0.19	0.11	0.16	0.19	0.31	0.26	1.28	0.95	1.41	1.19	0.35	2.03	3.08	0.4	4.68	4.24	2.08	2.02	2.63	0.47	2.85	1.01	1.81	0.21	2.63
^{166}Er	2.13	0.25	0.64	0.37	0.53	0.65	1.04	0.92	4.42	3.48	4.95	4.11	1.29	7.68	7.83	1.38	11.38	10.9	5.68	6.43	7.41	1.34	8.32	2.98	4.96	0.61	7.11
^{169}Tm	0.21	0.031	0.073	0.042	0.058	0.07	0.1	0.095	0.4	0.34	0.46	0.34	0.11	0.66	1.03	0.27	1.5	1.5	0.82	1.06	1.07	0.21	1.36	0.52	0.77	0.11	1.14
^{172}Yb	1.32	0.21	0.51	0.28	0.41	0.46	0.7	0.69	2.51	2.38	2.91	2.08	0.79	4.44	4.75	2.09	6.74	7.1	4.02	6.3	5.51	1.27	7.48	2.88	3.61	0.63	5.2
^{175}Lu	0.2	0.039	0.087	0.052	0.071	0.08	0.12	0.12	0.34	0.35	0.4	0.29	0.13	0.58	0.47	0.41	0.65	0.71	0.41	0.76	0.57	0.19	0.94	0.36	0.37	0.1	0.5
^{178}Hf	0.52	0.19	0.31	0.25	0.25	0.36	0.43	0.32	0.55	0.49	0.5	0.6	0.29	0.62	0.87	2.51	1.16	1.3	0.93	1.41	0.63	0.42	0.52	0.42	0.76	0.35	0.97
^{181}Ta	0.76	0.044	0.16	0.045	0.085	0.21	0.26	0.076	0.74	0.38	0.89	1.02	0.045	1.68	4.03	3.45	16.65	11.98	4.54	6.04	10.43	0.69	4	6.49	4.31	0.16	4.43
^{208}Pb	0.54	0.055	0.079	0.13	0.078	0.11	0.13	0.1	0.61	0.4	0.38	0.49	0.091	0.58	0.96	1.76	2.19	2.87	0.85	3.28	0.14	0.77	0.8	0.096	0.93	0.3	1.39
^{232}Th	1.67	0.08	0.14	0.045	0.17	0.22	0.33	0.22	1.95	1.23	1.22	1.59	0.17	1.94	2.25	3.92	5.1	6.58	1.9	7.19	0.14	1.55	1.66	0.046	1.66	0.49	2.43
^{238}U	0.62	0.077	0.17	0.065	0.17	0.2	0.35	0.25	0.82	0.55	0.57	0.81	0.25	1.53	0.9	6.74	1.62	2.1	0.81	3.09	4.18	8.64	13.21	2	1.05	6.93	1.27
Detection limit [ppm]																											
^{6}Li	2.93	3.1	2.73	3.28	2.75	3.26	3.08	3.83	3.11	3.14	3.56	3.49	3.96	3.14	3.47	3.92	3.42	2.86	3.08	2.88	2.55	2.95	2.95	2.72	2.81	3.05	3.31
^{7}Li	1.51	1.57	1.49	1.69	1.46	1.67	1.73	2.12	1.73	1.7	1.94	1.86	2.15	1.73	1.81	2.1	1.83	1.54	1.61	1.57	1.39	1.6	1.59	1.48	1.55	1.68	1.86
^{43}Ca	622.75	649.61	552.15	686.16	561.01	668.71	690.42	759.08	688.96	669.23	718.37	723.6	844.78	671.92	689.69	752.06	707.11	594.44	619.95	602.89	535.59	612.7	611.11	559.31	592.29	637.45	714.34
^{44}Ca	84.21	87.29	79.4	92.2	77.89	89.75	92.75	109.55	92.92	91.01	100.57	97.76	114.88	91.26	97.17	109.26	97.44	81.56	84.8	82.88	73	83.85	83.81	76.87	80.81	87.2	98.12
^{47}Ti	7.81	8.29	7.82	8.98	7.71	8.81	9.22	11.16	9.3	9.22	10.4	10.18	11.78	9.38	8.46	9.89	8.72	7.42	7.77	7.71	6.86	7.9	7.92	7.37	7.85	8.59	9.68
^{49}Ti	5.48	5.83	5.36	6.41	5.53	6.57	6.77	8	6.86	6.77	7.74	7.54	8.96	7.09	4.91	5.76	5.35	4.72	5.09	5.01	4.55	5.17	5.37	4.98	5.52	6.01	6.83
^{51}V	0.417	0.433	0.377	0.463	0.382	0.452	0.464	0.535	0.465	0.459	0.499	0.497	0.579	0.461	0.468	0.513	0.476	0.397	0.419	0.409	0.36	0.411	0.413	0.378	0.401	0.431	0.486
^{53}Cr	7.68	8.08	6.67	8.44	6.95	8.36	8.6	9.39	8.71	8.63	9.04	9.24	10.97	8.71	7.82	8.51	8.09	6.79	7.22	7.02	6.27	7.18	7.27	6.65	7.17	7.83	8.91
^{88}Sr	0.128	0.136	0.128	0.143	0.121	0.138	0.143	0.168	0.147	0.141	0.161	0.152	0.183	0.143	0.153	0.168	0.154	0.129	0.13	0.127	0.117	0.13	0.133	0.121	0.129	0.138	0.156
^{89}Y	0.05	0.0517	0.0425	0.0467	0.0459	0.0543	0.0544	0.0613	0.0526	0.0569	0.0623	0.0607	0.0605	0.0513	0.0502	0.057	0.0528	0.0437	0.0429	0.0425	0.0427	0.0463	0.0443	0.0375	0.0454	0.0477	0.052
^{91}Zr	0.863	0.904	0.83	0.964	0.825	0.946	0.991	1.2	0.999	0.993	1.09	1.07	1.26	1	0.94	1.08	0.964	0.811	0.854	0.836	0.745	0.864	0.87	0.809	0.856	0.932	1.06
^{93}Nb	0.0288	0.0279	0.0193	0.0277	0.0277	0.0243	0.0263	0.0315	0.0284	0.0297	0.0309	0.0312	0.0353	0.027	0.0255	0.0321	0.0214	0.0233	0.0254	0.0235	0.0178	0.0271	0.0245	0.0216	0.0275	0.027	0.0305
^{139}La	0.0166	0.02	0.0145	0.0167	0.0182	0.0215	0.0195	0.0196	0.0264	0.0235	0.0209	0.0232	0.0253	0.0222	0.0189	0.0221	0.0198	0.019	0.0296	0.0144	0.0138	0.0219	0.0198	0.0148	0.0189	0.0166	0.0242
^{140}Ce	0.0201	0.0241	0.0188	0.0227	0.0198	0.0245	0.0266	0.0345	0.024	0.0234	0.0283	0.0284	0.0322	0.027	0.0219	0.0365	0.0249	0.0201	0.0228	0.0236	0.0161	0.0238	0.0199	0.0177	0.0208	0.0193	0.0308
^{141}Pr	0.0115	0.0106	0.013	0.012	0.0101	0.0093	0.0125	0.0133	0.0117	0.0115	0.013	0.0136	0.015	0.012	0.00438	0.0104	0.0117	0.0119	0.00942	0.0105	0.00631	0.0119	0.00907	0.00665	0.0127	0.0134	0.0116
^{146}Nd	0.0701	0.0991	0.0506	0.105	0.0837	0.0858	0.0848	0.114	0.0895	0.096	0.111	0.105	0.146	0.107	0.0879	0.0981	0.104	0.0755	0.0731	0.0656	0.0696	0.0797	0.0727	0.0593	0.081	0.0783	0.084
^{147}Sm	0.0715	0.101	0.0754	0.0954	0.0848	0.0858	0.0769	0.125	0.0758	0.0972	0.0891	0.12	0.146	0.0904	0.0815	0.0975	0.116	0.082	0.0746	0.081	0.0736	0.0686	0.0743	0.0605	0.0769	0.0951	0.105
^{153}Eu	0.0229	0.0268	0.0225	0.0229	0.0251	0.0272	0.0214	0.0245	0.0354	0.0355	0.0328	0.0267	0.0272	0.0289	0.0316	0.0337	0.0285	0.0246	0.0242	0.0199	0.019	0.0233	0.0286	0.0214	0.0179	0.0237	0.0331
^{157}Gd	0.136	0.135	0.144	0.144	0.133	0.136	0.147	0.198	0.155	0.17	0.158	0.166	0.222	0.155	0.157	0.186	0.124	0.128	0.127	0.123	0.125	0.114	0.114	0.135	0.129	0.141	0.162
^{159}Tb	0.0182	0.0144	0.00775	0.0116	0.0125	0.0142	0.0143	0.0202	0.0133	0.0165	0.0159	0.0147	0.0232	0.0167	0.0127	0.0147	0.0149	0.0109	0.0112	0.0111	0.00851	0.0162	0.0113	0.012	0.0127	0.0141	0.0102
^{163}Dy	0.0644	0.0658	0.0833	0.0665	0.073	0.0826	0.074	0.106	0.0937	0.0963	0.106	0.088	0.124	0.104	0.0633	0.0706	0.0805	0.0644	0.0563	0.0627	0.0373	0.0633	0.0703	0.0569	0.06	0.0749	0.106
^{165}Ho	0.00962	0.00871	0.00889	0.00997	0.00507	0.0098	0.0121	0.00685	0.0105	0.00999	0.0101	0.0122	0.0135	0.0101	0.0118	0.00978	0.0123	0.0106	0.00805	0.0108	0.00677	0.00774	0.0104	0.00713	0.00953	0.00814	0.00581
^{166}Er	0.0717	0.0851	0.0766	0.0795	0.0596	0.0799	0.0782	0.104	0.0883	0.084	0.105	0.0996	0.127	0.102	0.0536	0.0714	0.0857	0.0716	0.0598	0.0617	0.0537	0.0729	0.0739	0.0584	0.0634	0.0741	0.0965
^{169}Tm	0.0119	0.00949	0.0114	0.012	0.0118	<0.00000	0.00548	0.00979	0.0113	0.00661	0.0103	0.017	0.0103	0.0134	0.013	0.00872	0.0136	0.0106	0.0114	0.0118	0.01	0.0098	0.0104	0.00783	0.00894	0.0116	0.00826
^{172}Yb	0.0655	0.0729	0.052	0.0751	0.0438	0.0555	0.0636	0.0874	0.0795	0.0656	0.0832	0.105	0.0851	0.0386	0.0549	0.0945	0.0736	0.0528	0.0253	0.051	0.0451	0.0689	0.0489	0.055	0.0751	0.068	0.0681
^{175}Lu	0.00396	0.011	0.0097	0.00439	0.0102	0.00863	0.00893	0.00977	0.008	0.00439	0.00834	0.0116	0.0103	0.0161	0.00459	0.0177	0.0048	0.00785	0.0042	0.00978	0.00499	0.00698	0.00904	0.00742	0.0111	0.00598	0.0117
^{178}Hf	0.0646	0.0754	0.081	0.0956	0.071	0.0733	0.0855	0.13	0.0999	0.1	0.121	0.109	0.135	0.0958	0.0333	0.087	0.0461	0.0712	0.0628	0.0724	0.0443	0.0716	0.0687	0.0571	0.0585	0.0782	0.0946
^{181}Ta	0.017	0.0193	0.016	0.0188	0.0176	0.0181	0.0153	0.0256	0.0181	0.0239	0.0222	0.0157	0.0272	0.0219	0.0192	0.0222	0.0212	0.0146	0.0153	0.0159	0.0198	0.0193	0.0199	0.0187	0.0203	0.0173	0.0209
^{208}Pb	0.0188	0.0113	0.0174	0.00849	0.0228	0.0236	0.0273	0.0393	0.02	0.0294	0.0263	0.029	0.0256	0.0228	0.0251	0.0198	0.0361	0.0275	0.0231	0.0191	0.00974	0.0262	0.0327	0.0219	0.0204	0.0373	0.0231
^{232}Th	0.00806	<0.00000	0.00609	<0.00000	0.00401	0.00508	0.00913	0.00666	<0.00000	0.0052	0.014	0.00797	0.0122	0.00749	0.0095	<0.00000	0.00813	0.00665	<0.00000	0.00677	<0.00000	0.00484	0.00842	<0.00000	0.00471	0.00884	<0.00000
^{238}U	<0.00000	<0.00000	<0.00000	<0.00000	<0.00000	0.00329	<0.00000	<0.00000	<0.00000	0.00581	<0.00000	<0.00000	0.00784	<0.00000	<0.00000	<0.00000	<0.00000	<0.00000	<0.00000	<0.00000	<0.00000	<0.00000	<0.00000	0.00408	<0.00000	<0.00000	0.00373

Table 5.5, continued.

Sample	MS 15									MS 24									MS 25									
# of analysis ICP MS	MS15-1	MS15-3	MS15-5	MS15-6	MS15-7	MS15-8	MS15-9	MS15-10	MS15-18	MS24-1	MS24-2	MS24-3	MS24-4	MS24-5	MS24-6	MS24-7	MS24-8	MS24-9	MS25-2	MS25-3	MS25-4	MS25-5	MS25-7	MS25-8	MS25-9	MS25-10	MS25-11	MS25-12
Uncertainty [1σ ppm]																												
^{6}Li	0.84	1.03	0.74	1.66	0.76	0.75	17.2	5.08	0.78	0.95	0.97	1	1.28	0.98	0.99	0.95	1.01	1	0.94	0.98	0.83	0.85	0.89	0.88	0.85	0.82	0.75	0.82
^{7}Li	0.56	0.64	0.49	1.28	0.53	0.53	12.1	4.4	0.59	0.54	0.55	0.54	0.72	0.56	0.6	0.56	0.55	0.56	0.57	0.57	0.51	0.53	0.56	0.55	0.55	0.52	0.5	0.53
^{43}Ca	6526.37	6550.34	6252.47	6481.97	6276.69	6229.8	9205.28	6465.72	6121.78	6367.61	6367.38	6367.19	6286.62	6345.5	6391.98	6412.18	6390.09	6299.43	6390.27	6390.52	6410.21	6500.87	6322.3	6366.41	6388.85	6387.72	6364.82	6455.88
^{44}Ca	8260.22	8077.81	8083.83	8021.58	8217.03	8337.87	8580.75	8593.69	9189.8	8105.66	8330.89	8209.96	8324.75	8603.61	9056.04	9265.57	9584.6	9561.22	6787.52	6782.89	6912.91	7014.24	6885.07	6915.63	6926.23	6868.18	6862.19	6991.7
^{47}Ti	7023.51	7264.28	7264.43	6750.02	7430.84	7407.15	426240.5	7243.18	7257.95	7763.7	7848.85	8287.54	8075.85	8244.19	8588.28	9001.38	9058.92	9240.06	7310.99	6994.31	7285.27	7038.62	7279.43	7293.53	7240.71	7205.84	7001.34	7449.14
^{49}Ti	7304.41	7708.27	7696.98	7029.61	7751.17	7720.58	437318.3	7544.95	8294.28	9103.23	9172.68	9598.9	9496.54	10049.36	10824.75	11442.89	11520.61	11745.25	7144.82	6947.93	7267.21	6977.79	7231.49	7211.8	7234.02	7106.14	7045.66	7525.57
^{51}V	13.11	16.08	14.99	15.25	15.25	15.35	928.59	18.58	15.91	10.06	10.04	12.7	11.03	12.59	13.33	12.39	14.7	14.06	17.87	18.91	19.39	22.76	17.05	16.37	22.93	20.3	17.92	20.57
^{53}Cr	3.63	5.92	6.78	7.7	7.76	7.3	281.46	13.36	9.17	3.14	3.18	3.68	3.39	3.04	6.11	2.93	4.15	3.59	5.93	3.93	6.7	8.31	5.11	6.11	6.82	6.48	11.36	10.07
^{88}Sr	2.12	1.64	1.75	1.6	1.89	1.89	124.07	1.69	1.77	1.66	1.68	1.6	1.93	1.7	1.73	1.78	1.83	1.99	2.54	2.68	2.75	2.89	3.3	3.05	1.87	2.51	2.82	2.42
^{89}Y	15.95	5.19	75.26	4.14	81.11	72.23	547.21	2.77	79.65	146.66	154.46	139.6	168.61	177.28	123.8	101.84	127.27	170.87	29.63	40.94	21.41	14.34	24.71	15.03	17.39	39.35	12.62	18.28
^{91}Zr	2.63	2.71	14.54	2.88	15.8	14.92	690.37	2.85	14.76	14.48	17.11	6.29	12.32	13.39	6.58	7.27	7.05	14.98	6.36	15.35	5.46	6.57	7.85	7.32	5.11	9.97	7.31	5.2
^{93}Nb	39.79	19.25	25.11	17	22.45	29.34	3718.49	11.74	25.11	202.44	216.93	102.74	471.19	271.74	96.3	168.97	126.9	303.3	10.25	24.89	5.4	2.86	12.56	9.03	3.42	14.79	5.06	4.95
^{139}La	0.19	1.07	36.31	1.05	43.29	36.89	1189.52	1.16	30.66	11.21	9.69	7.03	16.72	13.26	10.75	12.79	12.17	16.52	11.87	12.32	8.59	3.33	25.69	24.32	3.77	10.19	18.91	8.75
^{140}Ce	1.4	4.78	184.99	5.89	214.48	188.61	2527.9	4.34	175.95	32.28	27.44	20.56	45.37	35.7	33.26	35.79	35.76	46.98	56.26	62.81	43.29	17.78	90.56	78.2	21.01	50.09	67.03	39.32
^{141}Pr	0.39	0.97	32.62	1.18	39.16	31.78	445.2	0.87	28.75	4.79	4.12	3.07	6.6	5.23	5.23	5.18	5.57	6.97	10.46	12.13	8.37	3.65	13.55	10.31	4.48	10.12	8.72	7.21
^{146}Nd	3.48	5.92	176.8	6.87	217.85	178.23	1875.7	4.78	162.89	22.69	19.3	15.05	30.23	24.8	25.82	23.65	27.18	32.62	58.81	69.18	46.94	21.43	66.51	45.73	26.36	58.61	36.94	39.15
^{147}Sm	2.11	1.81	41.92	1.75	53.4	42.33	427.9	1.21	36.06	7.21	6.57	5.37	8.88	7.47	6.99	5.76	6.9	8.31	16.38	20.07	12.45	6.21	15.98	9.64	7.76	18.32	7.12	10.14
^{153}Eu	1.41	2.54	4.55	2.19	5.63	4.54	162.17	1.39	4.52	6.56	6.04	4.83	10.36	8.58	8.81	8.65	8.69	12.38	4.28	5.27	3.72	1.96	4.09	2.41	2.69	4.81	1.75	3.19
^{157}Gd	2.68	1.43	29.07	1.26	35.52	28.22	257.16	0.92	23.87	17	16.86	14.83	22.19	20.44	18.14	14.87	19.77	24.99	14.11	17.65	10.34	5.57	13.34	7.81	7.13	17.08	5.74	8.96
^{159}Tb	0.43	0.18	3.46	0.14	4.2	3.41	36.53	0.11	3.12	2.83	2.83	2.51	3.48	3.33	2.62	2.13	2.81	3.64	1.49	1.93	1.08	0.62	1.36	0.77	0.77	1.84	0.56	0.91
^{163}Dy	2.53	0.87	15.76	0.68	18.64	15.37	185.63	0.53	14.31	22.2	22.78	20.36	26.6	26.96	20.81	16.54	22.01	29.71	8.52	10.96	6.08	3.66	7.39	4.31	4.58	11.18	3.26	5.31
^{165}Ho	0.52	0.16	2.64	0.13	3.02	2.57	32.09	0.1	2.6	4.51	4.62	4.25	5.29	5.46	3.96	3.22	4.23	5.66	1.24	1.65	0.89	0.57	1.05	0.61	0.69	1.6	0.48	0.78
^{166}Er	1.52	0.47	6.41	0.36	7.04	6.14	89.16	0.28	6.46	17.35	18.36	17.06	20.86	22.3	16.06	13.25	17.57	23.76	2.96	4.03	2.12	1.44	2.45	1.43	1.73	3.82	1.2	1.82
^{169}Tm	0.21	0.066	0.73	0.049	0.76	0.72	12.45	0.041	0.75	2.13	2.22	2.11	2.38	2.59	1.81	1.49	1.93	2.64	0.33	0.47	0.24	0.17	0.27	0.16	0.2	0.44	0.15	0.2
^{172}Yb	1.53	0.48	4.31	0.36	4.32	4.26	90.96	0.28	4.64	16.82	17.61	17.11	18.37	21.65	14.28	12.21	15.35	21.57	1.81	2.75	1.36	1.05	1.48	0.96	1.21	2.46	0.97	1.18
^{175}Lu	0.19	0.07	0.41	0.054	0.4	0.4	10.82	0.041	0.43	1.81	1.98	1.85	1.97	2.25	1.44	1.27	1.54	2.1	0.2	0.31	0.16	0.13	0.18	0.12	0.15	0.28	0.13	0.15
^{178}Hf	0.22	0.22	0.92	0.23	0.95	0.86	85.33	0.22	0.88	1.94	2.23	0.7	1.06	1.16	0.52	0.61	0.62	1.34	0.5	1.34	0.37	0.38	0.57	0.49	0.38	0.9	0.46	0.38
^{181}Ta	2.21	0.32	2.55	0.33	2.37	3.03	64.17	0.2	2.63	114.2	123.53	28.56	114.56	47.27	18.26	23.73	20.66	42.47	0.47	1.21	0.19	0.079	0.91	0.55	0.1	0.89	0.47	0.18
^{208}Pb	0.053	0.23	0.91	0.17	0.92	0.88	644.33	0.63	0.96	1.01	0.94	0.56	1.96	1.75	0.81	1.07	0.95	2.01	0.86	1.24	0.21	0.7	2.06	1.34	0.1	0.94	0.92	0.21
^{232}Th	0.034	0.17	3.03	0.28	3.11	2.9	206.88	0.15	3.2	3.08	2.83	1.59	5.89	5.35	2.43	3.22	2.86	6.06	2.54	3.65	0.49	0.065	6.33	4.1	0.18	2.66	2.74	0.5
^{238}U	1.36	2.13	0.6	1.62	0.59	0.61	373.67	1.02	0.59	7.85	7.95	5.97	13.95	14.18	7.73	9.57	7.85	14.01	2.34	5.88	0.9	2.84	2.56	1.57	1.37	5.07	1.1	0.67
Detection limit [ppm]																												
^{6}Li	2.2	2.09	1.85	2.37	1.98	2.01	38.8	2.58	2.05	2.6	2.65	2.54	2.84	2.63	2.65	2.63	2.65	2.72	2.61	2.66	2.23	2.3	2.39	2.45	2.23	2.2	2.05	2.27
^{7}Li	1.52	1.5	1.31	1.64	1.43	1.44	28.48	1.77	1.55	1.5	1.53	1.51	1.7	1.58	1.58	1.54	1.55	1.53	1.59	1.59	1.41	1.47	1.53	1.53	1.53	1.46	1.36	1.47
^{43}Ca	554.04	538.14	470.67	594.65	512.22	513.68	10257.69	634.35	555.54	586.22	602.54	588.99	666.72	615.5	604.58	593.37	600.55	590.49	590.37	593.17	516.31	537.05	560.81	558.21	555.98	524.6	501.42	532.3
^{44}Ca	79.48	77.4	67.16	84.65	72.96	73.32	1457.34	90.48	78.97	83.11	85.06	82.67	94.08	86.07	85.54	83.83	84.39	83.53	85.57	84.81	74.82	77.45	80.58	80.12	79.59	75.55	71.86	75.7
^{47}Ti	7.35	7.33	6.41	8.25	7.16	7.21	144.69	9.13	8.23	8.26	8.37	8.08	9.29	8.62	8.59	8.47	8.57	8.55	7.72	7.73	6.93	7.19	7.64	7.65	7.79	7.14	6.87	7.34
^{49}Ti	5.4	5.51	4.78	6.26	5.39	5.56	110.31	6.98	6.48	6.39	6.14	6.28	7.06	6.61	6.54	6.5	6.68	6.88	4.96	5.27	4.58	4.82	5.36	5.29	5.27	5.03	4.83	5.36
^{51}V	0.381	0.374	0.328	0.413	0.354	0.366	7.25	0.448	0.399	0.398	0.406	0.398	0.449	0.411	0.409	0.406	0.41	0.4	0.411	0.416	0.364	0.382	0.394	0.388	0.39	0.373	0.354	0.376
^{53}Cr	5.26	5.18	4.51	5.73	4.86	4.93	98.34	6.1	5.37	7.49	7.72	7.58	8.78	8.1	7.96	8.09	8.19	8.16	5.59	5.65	4.95	5.15	5.35	5.31	5.3	5.03	4.82	5.09
^{88}Sr	0.131	0.126	0.11	0.136	0.117	0.122	2.4	0.151	0.131	0.131	0.129	0.129	0.141	0.134	0.133	0.129	0.132	0.135	0.144	0.144	0.126	0.127	0.134	0.13	0.134	0.128	0.117	0.128
^{89}Y	0.0466	0.0494	0.039	0.055	0.0456	0.0444	0.991	0.0591	0.0528	0.053	0.0456	0.0547	0.0563	0.0815	0.0517	0.0478	0.0515	0.0544	0.0551	0.0539	0.0451	0.0473	0.0507	0.0515	0.0497	0.0481	0.045	0.0505
^{91}Zr	0.967	0.954	0.823	1.05	0.892	0.9	17.99	1.11	0.942	0.859	0.897	0.877	0.993	0.923	0.921	0.902	0.922	0.91	0.982	0.98	0.859	0.904	0.937	0.938	0.926	0.885	0.843	0.892
^{93}Nb	0.0245	0.0229	0.0178	0.0239	0.0174	0.0247	0.45	0.0268	0.0238	0.0463	0.0272	0.0541	0.0308	0.127	0.0328	0.0344	0.0258	0.027	0.0235	0.0306	0.019	0.0192	0.0268	0.0235	0.021	0.0209	0.022	0.0235
^{139}La	0.0224	0.0197	0.0186	0.0211	0.0201	0.0211	0.432	0.0228	0.019	0.0207	0.0187	0.0199	0.0229	0.0268	0.0201	0.0247	0.0193	0.0191	0.0216	0.0234	0.0217	0.0199	0.0188	0.0217	0.0244	0.0193	0.0184	0.0205
^{140}Ce	0.0227	0.0252	0.0202	0.0239	0.0222	0.0273	0.528	0.0334	0.0304	0.0209	0.0188	0.0242	0.0242	0.0213	0.0259	0.0251	0.0254	0.0339	0.0274	0.0377	0.0246	0.0306	0.0256	0.0272	0.0437	0.0251	0.024	0.0463
^{141}Pr	0.0123	0.00992	0.00759	0.0131	0.0127	0.0104	0.196	0.0142	0.012	0.00911	0.00878	0.0121	0.0134	0.009	0.0129	0.0118	0.0101	0.0139	0.0128	0.0127	0.0112	0.0116	0.0103	0.0118	0.0192	0.0106	0.01	0.0123
^{146}Nd	0.0915	0.105	0.0852	0.1	0.0872	0.0992	2.05	0.119	0.0997	0.0884	0.0787	0.0714	0.118	0.0947	0.0838	0.116	0.103	0.0982	0.114	0.108	0.0933	0.117	0.112	0.116	0.127	0.109	0.092	0.105
^{147}Sm	0.074	0.0912	0.0798	0.0773	0.0955	0.0458	1.43	0.0939	0.0641	0.0848	0.058	0.0972	0.0699	0.0888	0.0902	0.0933	0.0713	0.0977	0.0826	0.0564	0.0659	0.0893	0.0761	0.0928	0.088	0.0798	0.0683	0.0915
^{153}Eu	0.0216	0.0271	0.02	0.028	0.0284	0.0233	0.499	0.0334	0.0279	0.0316	0.0287	0.018	0.0289	0.026	0.034	0.0224	0.0278	0.0255	0.0267	0.0278	0.0292	0.0302	0.0254	0.024	0.0291	0.0277	0.0204	0.0201
^{157}Gd	0.176	0.13	0.147	0.137	0.143	0.139	2.94	0.172	0.162	0.159	0.16	0.0971	0.155	0.21	0.153	0.171	0.143	0.116	0.14	0.159	0.128	0.126	0.15	0.134	0.141	0.127	0.124	0.151
^{159}Tb	0.0155	0.0138	0.0115	0.0163	0.0103	0.0124	0.297	0.0147	0.014	0.0151	0.0137	0.0134	0.0153	0.016	0.0155	0.0146	0.014	0.0126	0.0152	0.0097	0.0121	0.0129	0.0166	0.0141	0.0122	0.0159	0.0157	0.0165
^{163}Dy	0.0928	0.0901	0.071	0.0808	0.1	0.0819	1.67	0.118	0.106	0.13	0.0912	0.077	0.0997	0.0856	0.0861	0.0883	0.0916	0.0816	0.0915	0.091	0.0855	0.0859	0.101	0.107	0.0996	0.0849	0.0847	0.0952
^{165}Ho	0.0092	0.00601	0.00644	0.00838	0.0125	0.00729	0.187	0.0111	0.00642	0.0101	0.0113	0.00956	0.00941	0.0109	0.0127	0.0128	0.0119	0.00712	0.0104	0.00914	0.00747	0.00774	0.00873	0.0114	0.0103	0.0112	0.00839	0.00936
^{166}Er	0.0912	0.0898	0.0679	0.104	0.0853	0.0912	1.9	0.106	0.109	0.1	0.0872	0.0961	0.0974	0.091	0.0922	0.0998	0.0888	0.0828	0.0962	0.106	0.0901	0.0923	0.0907	0.097	0.1	0.0904	0.0828	0.0986
^{169}Tm	0.00925	0.01	0.0102	0.00486	0.00886	0.00668	0.149	0.0111	0.00906	0.0101	0.0113	0.00829	0.0109	0.0151	0.01	0.0125	0.00965	0.00808	0.0115	0.00976	0.0106	0.0109	0.0057	0.00656	0.0117	0.00927	0.00881	0.0116
^{172}Yb	0.0899	0.0701	0.0551	0.0834	0.0716	0.0622	1.24	0.0818	0.0822	0.0585	0.0668	0.0815	0.0988	0.061	0.0819	0.0512	0.0821	0.0815	0.063	0.065	0.0703	0.098	0.0684	0.0757	0.0881	0.0679	0.0806	0.0586
^{175}Lu	0.0107	0.00492	0.0101	0.00969	0.0068	0.00687	0.184	0.00605	0.00903	0.00785	0.00829	0.0118	0.011	0.00951	0.00582	0.00416	0.0133	0.00934	0.00974	0.0112	0.00605	0.00724	0.00928	0.00755	0.00748	0.00797	0.00719	0.00802
^{178}Hf	0.0861	0.0905	0.0836	0.106	0.0859	0.0784	1.83	0.141	0.117	0.0873	0.0717	0.0932	0.109	0.0934	0.0827	0.0962	0.0791	0.103	0.105	0.0881	0.0883	0.0847	0.0894	0.103	0.105	0.0999	0.0747	0.0881
^{181}Ta	0.0175	0.0171	0.0127	0.0134	0.0166	0.0161	0.3	0.0194	0.0163	0.0165	0.0203	0.0171	0.0182	0.0179	0.0176	0.0193	0.0201	0.0199	0.0163	0.0196	0.0173	0.017	0.0169	0.0174	0.0197	0.0174	0.0129	0.0165
^{208}Pb	0.0101	0.007	0.0123	<0.00000	0.00685	<0.00000	0.293	0.015	0.0183	0.0271	0.0263	0.0185	0.0211	0.0246	0.0211	0.014	0.0184	0.0163	0.0141	<0.00000	0.0202	0.0209	0.019	0.0189	0.0132	0.0163	0.0114	0.0164
^{232}Th	0.00422	0.0092	<0.00000	0.0104	0.00979	0.00986	0.17	0.00865	0.00423	0.00929	0.011	0.00469	<0.00000	<0.00000	0.00859	0.0101	<0.00000	0.0114	0.00691	<0.00000	<0.00000	0.00767	<0.00000	0.0103	0.00642	0.0043	0.00387	0.0061
^{238}U	0.00395	0.00387	0.0024	0.00313	0.00381	<0.00000	<0.00000	<0.00000	0.00512	0.00293	<0.00000	0.00295	0.00336	<0.00000	0.00311	0.00315	0.00452	0.00317	0.00323	0.00321	<0.00000	0.00294	0.00436	<0.00000	0.00431	<0.00000	<0.00000	0.00414

Table 5.5, continued.

Sample	MS 25								MS 36																			
# of analysis ICP MS	MS25-14	MS25-15	MS25-19	MS25-20	MS25-21	MS25-22	MS25-23	MS25-24	MS36-2	MS36-5	MS36-7	MS36-10	MS36-11	MS36-14	MS36-15	MS36-16	MS36-17	MS36-18	MS36-19	MS36-23	MS36-24	MS36-26	MS36-27	MS36-29	MS36-30	MS36-31	MS36-32
Uncertainty [1σ ppm]																											
^{6}Li	0.8	0.81	0.78	0.74	0.81	1.18	0.81	0.8	1.15	1.25	1.22	1.08	1.12	1.05	0.89	0.86	0.87	0.91	0.9	0.89	0.88	0.92	0.96	0.92	0.82	0.82	0.92
^{7}Li	0.55	0.57	0.56	0.57	0.58	0.71	0.59	0.59	0.57	0.62	0.59	0.54	0.55	0.58	0.49	0.49	0.48	0.52	0.53	0.53	0.54	0.55	0.57	0.57	0.54	0.55	0.59
^{43}Ca	6388.52	6389.32	6456.5	6480.12	6389.35	6301.71	6412.69	6457.59	6390.07	6368.51	6345.3	6365.52	6455.81	6456.73	6410.45	6387.3	6385.24	6296.04	6387.22	6296.61	6342.03	6365.51	6299.48	6390.69	6319.82	6386.68	6412
^{44}Ca	6768.61	6849.48	6928.37	7057.46	6862.34	6770.84	6882.37	7033.65	7032.23	6973.37	6954.97	6835.17	7182.29	7498.62	7353.29	7406.71	7290.78	7283.95	7335.62	7417.46	7562.41	7772.34	7727.78	8251.12	8034.54	7995.57	8239.91
^{47}Ti	7153.26	7311.69	6999.93	7193.61	7139.44	7075.25	7090.03	7334.69	7529.41	7598.15	7558.76	7546.93	7819.64	7479.74	7427.69	7422.91	7278.23	7314.01	7144.5	7234.62	7161.57	7163.19	7354.15	7369.01	7699.86	7366.99	7672.53
^{49}Ti	7272	7312.62	7186.56	7255.36	7198.55	7014.55	7261.45	7468.87	8538.48	8843.16	8818.91	8669.62	8864.14	7716.77	7388.01	7579.79	7525.04	7697.33	7343.95	7505.4	7477.42	7741.73	7803.72	7990.14	8313.6	7942.33	8405.09
^{51}V	19.59	19.2	25.18	23.82	22.69	19.35	21.96	20.29	17.13	16.19	16.35	16.75	17.3	14.93	12.87	14.71	13.11	12.28	15.89	13.07	13.94	14.46	13.33	14.03	14.32	14.28	13.81
^{53}Cr	3.88	3.22	5.36	6.77	5.83	15.22	8.63	6.72	3	2.77	2.47	2.75	2.18	3.34	4.06	6.81	2.63	3.48	4.23	3.71	3.81	9.78	3.16	6.6	4.22	4.05	4.79
^{88}Sr	2.85	2.61	3.49	2.14	2.96	3.92	2.59	2.95	2.19	2.06	2.9	2.95	1.99	1.85	2.26	2.11	1.89	2.44	1.37	2.07	1.97	2.14	2.18	2.21	2.21	2.13	2.31
^{89}Y	16.67	19.69	6.59	9.6	21.69	34.69	31.02	20.66	32.21	47.28	38.57	36.42	19.53	44.02	26.6	19.87	37.11	93.01	11.26	37.46	34.75	35.47	43.92	15.36	41.06	15.47	39.38
^{91}Zr	4.49	4.88	6.66	3.99	11.11	9.81	9.92	5.52	8.89	13.13	12.81	15.45	6.51	7	22.14	9.64	8.53	17.13	3.67	10.76	11.95	11.68	11.09	12.46	10.94	7.44	10.07
^{93}Nb	5.35	5.1	3.21	1.62	13.6	4.73	10.27	5.24	13.13	19.9	27.98	28.15	7.49	12.79	31.64	14.07	19.69	51.83	5.19	18.02	11.2	20.68	19.71	11.69	16.49	8.39	15.71
^{139}La	3.74	8.83	4.61	3.35	4.55	27.77	10.82	7.47	7.94	19.5	26.68	25.82	4.19	6.56	22.32	13.35	8.58	14.69	2.61	13.53	14.4	13.65	13.04	15.06	11.27	4.09	8.55
^{140}Ce	22.78	42.51	15.8	15.84	26.73	131.59	54.87	40.74	38.56	82.87	99.11	95.57	21.33	38.56	80.93	49.18	45.12	78.75	16.19	68.67	66.19	59.81	72.57	52.9	62.9	24.04	50.83
^{141}Pr	4.96	8.16	2.55	2.92	5.8	22.7	10.52	8.15	8.16	14.72	15.71	14.42	4.47	8.35	10.55	6.63	8.76	15.34	3.58	12.61	11.18	9	14.73	7.2	12.59	4.93	10.83
^{146}Nd	29.13	44.63	13.18	16.19	33.49	112.06	60.35	46.36	53.1	85.95	85.93	78.65	29.85	72.39	64.71	41.1	71.03	129.54	29.57	105.14	91.53	69.27	128.46	51.82	120.01	47.73	110.84
^{147}Sm	8.29	11.68	3.48	4.32	9.57	25.06	16.99	12.54	12.76	19.28	17.13	15.2	7.5	19.44	10.86	6.85	16.52	32.52	5.66	19.75	16.96	11.16	24.86	7.48	22	8.17	22.08
^{153}Eu	3.19	3.84	1.18	1.88	3.35	6.81	4.91	4.31	5.38	5.81	5.19	4.88	3.4	5.35	2.59	1.76	4.55	7.21	2.18	4.96	4	2.7	6.01	1.58	5.64	3.33	6.47
^{157}Gd	7.46	10.21	3.37	4.35	9.26	19.68	16.11	11.39	10.95	16.01	14.2	12.51	6.5	17.58	8.86	5.96	14.58	30.24	4.13	16	14.21	10.1	19.34	6.11	17.91	6.24	18
^{159}Tb	0.75	0.99	0.33	0.42	0.91	1.77	1.53	1.04	1.32	1.97	1.69	1.53	0.76	2.08	1.05	0.72	1.7	3.92	0.44	1.84	1.65	1.22	2.19	0.68	2.04	0.65	2.02
^{163}Dy	4.5	5.82	2.08	2.68	6.04	10.92	9.88	6.65	6	9.41	7.73	7.07	3.49	10.48	5.47	3.63	8.55	20.46	2.13	8.69	7.91	6.33	10.11	3.28	9.28	2.98	9.1
^{165}Ho	0.65	0.83	0.28	0.4	0.85	1.43	1.32	0.88	1.32	1.96	1.62	1.51	0.8	2.1	1.12	0.8	1.72	4.26	0.47	1.85	1.71	1.55	2.3	0.76	2.23	0.78	2.25
^{166}Er	1.63	1.95	0.67	0.99	2.16	3.33	3.12	2.07	3.83	5.31	4.32	3.98	2.35	4.83	2.8	2.02	4.01	9.68	1.24	4.08	3.79	3.84	4.83	1.7	4.75	1.78	4.64
^{169}Tm	0.2	0.22	0.078	0.12	0.26	0.38	0.35	0.24	0.39	0.5	0.42	0.38	0.24	0.51	0.33	0.25	0.42	1.03	0.15	0.41	0.38	0.44	0.48	0.18	0.46	0.2	0.43
^{172}Yb	1.19	1.22	0.45	0.71	1.58	2.2	1.97	1.34	2.54	3.05	2.53	2.3	1.7	3.13	2.29	1.75	2.57	5.8	1.11	2.41	2.29	2.91	2.84	1.27	2.77	1.37	2.67
^{175}Lu	0.15	0.15	0.061	0.097	0.21	0.25	0.23	0.17	0.3	0.31	0.26	0.23	0.21	0.37	0.31	0.23	0.3	0.59	0.17	0.28	0.27	0.36	0.32	0.18	0.31	0.2	0.31
^{178}Hf	0.27	0.32	0.32	0.26	0.62	0.57	0.67	0.31	0.5	0.85	0.9	0.98	0.38	0.45	1.36	0.67	0.62	1.48	0.22	0.63	0.65	0.72	0.63	0.75	0.57	0.33	0.46
^{181}Ta	0.13	0.19	0.12	0.037	0.2	0.74	0.42	0.16	0.12	0.52	0.86	0.73	0.077	0.69	0.97	0.44	0.79	5.89	0.062	0.64	0.37	0.95	0.64	0.31	0.38	0.036	0.23
^{208}Pb	0.095	0.25	0.28	0.083	0.19	2.14	1.02	0.21	0.32	0.81	0.96	1.01	0.18	0.28	0.94	0.42	0.42	0.61	0.12	0.59	0.59	0.54	0.63	0.49	0.48	0.18	0.39
^{232}Th	0.066	0.59	0.15	0.064	0.11	6.05	2.69	0.39	0.77	2.21	2.6	2.74	0.36	0.71	2.8	1.18	1.19	1.74	0.27	1.6	1.59	1.44	1.68	1.3	1.22	0.4	0.94
^{238}U	0.37	0.83	0.62	0.14	14.43	1.76	3.16	0.69	1.15	1.48	1.55	1.39	0.63	1.96	1.9	0.92	1.46	1.33	0.41	1.5	1.06	1.05	2.66	0.84	2.99	0.45	1.49
Detection limit [ppm]																											
^{6}Li	2.26	2.25	2.19	1.99	2.2	2.46	2.22	2.23	3.09	3.48	3.35	3.02	3.13	2.91	2.34	2.31	2.42	2.35	2.46	2.43	2.35	2.52	2.51	2.42	2.14	2.27	2.53
^{7}Li	1.53	1.56	1.56	1.52	1.61	1.81	1.62	1.65	1.55	1.72	1.62	1.51	1.54	1.58	1.3	1.32	1.35	1.45	1.46	1.47	1.49	1.51	1.55	1.52	1.43	1.51	1.63
^{43}Ca	553.23	563.17	560.28	535.76	568.99	640.81	574.2	581.06	562.15	622.72	585.83	540.86	545.04	544.73	449.14	457.13	464.11	497.14	496.75	486.06	500.35	512.2	532.03	527.79	456.02	488.71	570.98
^{44}Ca	79.55	80.79	79.49	76.32	80.49	91.13	80.81	82.2	80.34	88.35	83.2	76.83	77.29	78.65	64.54	65.22	66.27	70.65	71.08	71.05	72.22	73.82	75.86	74.79	67.71	71.95	80.81
^{47}Ti	10.37	10.14	9.36	7.74	8.23	11.28	8.22	8.39	6.13	7.02	6.72	6.39	6.5	6.49	5.4	5.57	5.77	6.26	6.34	6.61	6.75	6.9	7.05	7.06	6.59	6.92	7.76
^{49}Ti	9.81	9.17	7.4	5.72	6.09	9.25	6.19	6.32	2.38	3.23	3.27	3.48	3.67	3.31	3.02	3.17	3.4	3.72	3.86	4.08	4.31	4.45	4.61	4.64	4.43	4.7	5.25
^{51}V	0.401	0.407	0.398	0.384	0.408	0.462	0.403	0.409	0.379	0.422	0.39	0.361	0.371	0.384	0.319	0.321	0.327	0.35	0.355	0.353	0.356	0.359	0.373	0.373	0.323	0.353	0.402
^{53}Cr	5.26	5.34	5.33	5.14	5.44	6.06	5.46	5.53	5.55	6.16	5.81	5.35	5.38	5.69	4.73	4.83	4.84	5.18	5.18	4.99	5.15	5.27	5.41	5.43	4.7	4.99	5.84
^{88}Sr	0.136	0.138	0.136	0.136	0.134	0.158	0.141	0.142	0.13	0.143	0.131	0.124	0.121	0.133	0.108	0.109	0.108	0.117	0.12	0.116	0.124	0.125	0.127	0.124	0.119	0.124	0.137
^{89}Y	0.0801	0.081	0.0591	0.0498	0.0539	0.109	0.0537	0.0533	0.0404	0.0465	0.0461	0.0424	0.0409	0.048	0.0399	0.0385	0.0398	0.0453	0.0444	0.0447	0.0449	0.0461	0.0444	0.0468	0.0445	0.046	0.0463
^{91}Zr	0.93	0.942	0.93	0.9	0.951	1.07	0.963	0.979	0.863	0.969	0.927	0.866	0.875	0.934	0.762	0.77	0.785	0.832	0.846	0.839	0.862	0.882	0.906	0.893	0.819	0.861	0.969
^{93}Nb	0.0385	0.0402	0.0362	0.0272	0.0222	0.0708	0.0248	0.0242	0.0178	0.0216	0.021	0.0202	0.0208	0.0268	0.0165	0.0159	0.0159	0.0188	0.0206	0.0191	0.0264	0.0197	0.0195	0.0254	0.0227	0.0204	0.0199
^{139}La	0.0395	0.0276	0.0312	0.0208	0.022	0.0403	0.0225	0.0202	0.0164	0.0199	0.0168	0.0166	0.0154	0.0157	0.0144	0.015	0.0143	0.0115	0.0184	0.0179	0.0181	0.0224	0.0201	0.0176	0.0175	0.0192	0.0196
^{140}Ce	0.0844	0.0798	0.0622	0.0271	0.027	0.0783	0.0293	0.0264	0.0185	0.018	0.0221	0.0183	0.0232	0.0188	0.0189	0.0175	0.0184	0.0202	0.0241	0.0217	0.0259	0.0236	0.0253	0.0219	0.0222	0.0224	0.026
^{141}Pr	0.0433	0.0306	0.0202	0.0095	0.0131	0.0375	0.0118	0.0126	<0.00000	0.00282	0.0104	0.00851	0.00429	0.0105	0.00761	0.00908	0.00617	0.00839	0.00574	0.00807	0.00982	0.0103	0.00687	0.0128	0.012	0.0123	0.0105
^{146}Nd	0.154	0.218	0.158	0.0893	0.109	0.196	0.108	0.103	0.0693	0.0645	0.0895	0.0794	0.0694	0.0896	0.0634	0.0732	0.0402	0.0729	0.0967	0.0538	0.0735	0.0826	0.0908	0.0915	0.0754	0.0915	0.109
^{147}Sm	0.121	0.158	0.0842	0.106	0.105	0.148	0.103	0.113	0.0429	0.0764	0.0899	0.0665	0.0311	0.1	0.0436	0.0383	0.0528	0.0701	0.0617	0.0761	0.0716	0.0562	0.0927	0.0686	0.0627	0.112	0.0653
^{153}Eu	0.0468	0.0436	0.0283	0.0278	0.0245	0.0565	0.0253	0.0271	0.0224	0.0344	0.019	0.0128	0.0235	0.025	0.0192	0.0178	0.0243	0.0173	0.0194	0.0217	0.021	0.0255	0.0192	0.0237	0.0189	0.028	0.0288
^{157}Gd	0.164	0.156	0.138	0.155	0.162	0.201	0.146	0.146	0.119	0.109	0.104	0.0906	0.0998	0.117	0.106	0.124	0.101	0.115	0.111	0.144	0.148	0.152	0.13	0.163	0.129	0.147	0.161
^{159}Tb	0.0158	0.02	0.0165	0.0126	0.0143	0.0189	0.013	0.0128	0.00487	0.0123	0.00902	0.00755	0.0144	0.00941	0.0116	0.01	0.0092	0.00981	0.0125	0.0139	0.0118	0.0114	0.0121	0.012	0.0121	0.0153	0.0109
^{163}Dy	0.108	0.107	0.104	0.0946	0.0957	0.125	0.0962	0.105	0.0333	0.0514	0.0787	0.0746	0.0671	0.0791	0.0622	0.0721	0.0702	0.0615	0.0875	0.0614	0.0815	0.0734	0.0997	0.0767	0.0844	0.0829	0.0957
^{165}Ho	0.0145	0.0109	0.0143	0.011	0.0116	0.015	0.00984	0.0133	0.00604	0.00705	0.00647	0.00531	<0.00000	0.00956	0.00836	0.00889	0.00818	0.013	0.00414	0.0108	0.00725	0.00605	0.0091	0.0052	0.00823	0.0113	0.00883
^{166}Er	0.103	0.0974	0.108	0.0969	0.102	0.109	0.11	0.104	0.0631	0.0611	0.0698	0.0532	0.0689	0.0776	0.07	0.0601	0.0712	0.0707	0.0752	0.0829	0.0799	0.0834	0.0875	0.0812	0.0785	0.097	0.0931
^{169}Tm	0.00913	0.015	0.0103	0.0118	0.012	0.0175	0.00976	0.0113	0.00899	<0.00000	0.00453	0.0043	0.00868	0.0032	0.0065	0.0111	0.00908	0.00292	0.00777	0.0105	0.0084	0.00304	0.00914	0.00739	0.0103	0.011	0.0075
^{172}Yb	0.0763	0.064	0.0697	0.0614	0.0803	0.094	0.0544	0.0595	0.0426	0.0583	0.0603	0.0306	0.0655	0.0558	0.055	0.0469	0.0435	0.0549	0.0708	0.0584	0.0649	0.0819	0.0705	0.0755	0.0551	0.0761	0.0803
^{175}Lu	0.0106	0.0107	0.00535	0.00817	0.0109	0.0115	0.00928	0.0137	0.0049	0.00404	<0.00000	0.00497	<0.00000	0.00521	0.00432	0.00537	0.00834	0.00475	0.00478	<0.00000	<0.00000	0.00779	0.00907	0.00598	0.0063	0.00474	0.00542
^{178}Hf	0.0856	0.0988	0.107	0.0999	0.112	0.117	0.104	0.106	0.0574	0.0547	0.0629	0.0673	0.0715	0.0713	0.0828	0.062	0.0681	0.0795	0.0941	0.0573	0.0925	0.0743	0.0691	0.0669	0.0808	0.0776	0.0898
^{181}Ta	0.0205	0.0158	0.0155	0.0171	0.0205	0.0217	0.0199	0.0233	0.0146	0.0164	0.0164	0.014	0.0155	0.0189	0.0143	0.0124	0.0145	0.0164	0.0144	0.0134	0.0142	0.0173	0.0208	0.0157	0.0132	0.0108	0.0151
^{208}Pb	0.00765	0.0206	0.0135	0.015	0.0224	0.0252	0.0174	0.0244	0.0121	0.0182	0.0183	<0.00000	0.0101	<0.00000	0.0106	0.0124	0.0127	0.0179	0.0136	0.00679	0.0139	0.0225	0.0185	<0.00000	0.0183	0.0119	0.0193
^{232}Th	0.00775	<0.00000	<0.00000	0.0075	<0.00000	0.00512	0.00631	<0.00000	0.00927	0.00483	<0.00000	0.0094	0.00424	0.00443	<0.00000	0.00529	0.00538	0.00574	0.00579	0.00577	0.00417	0.00604	0.00643	0.0113	0.0039	0.00719	<0.00000
^{238}U	0.00915	0.0082	0.00619	<0.00000	<0.00000	0.0482	<0.00000	<0.00000	<0.00000	<0.00000	0.00293	0.00278	<0.00000	<0.00000	<0.00000	<0.00000	0.00441	0.00666	0.00387	0.00272	0.00278	0.00493	0.00303	<0.00000	<0.00000	0.00276	0.00316

Table 5.5, continued.

Sample	**Khan**
# of analysis EMP	1 / 1 .
Concentrations [wt. %]	
SiO2	29.89
Al2O3	2.54
F	0.65
CaO	26.85
TiO2	33.62
La2O3	0.23
Nb2O5	0.96
ZrO2	0.04
P2O5	0.04
Y2O3	0.43
FeO	1.32
MnO	0.12
Ta2O5	0.15
Total	96.83
Uncertainty [3 S.D. wt. %]	
Si	0.1242
Ca	0.2684
O	
Al	0.0434
F	0.1392
Ti	0.233
La	0.038
Nb	0.0411
Zr	0.0257
P	0.0085
Y	0.0426
Fe	0.0671
Mn	0.0292
Ta	
Detection limit [ppm]	
Si	182
Ca	241
O	
Al	199
F	1378
Ti	299
La	425
Nb	239
Zr	291
P	92
Y	321
Fe	356
Mn	296
Ta	670

Table 5.5, continued.

Reference material	BCR			Average	St.Dev	Durango			Average	St.Dev	Khan							Average	St.Dev
Concentrations [ppm]																			
^{6}Li	9.9	11.43	9.27	**10.2**	1.1	<2.77	<2.42	<2.31			<1.98	<1.92	<2.14	<1.79	<2.89	<2.49	<2.24		
^{7}Li	5.73	7.6	6.12	**6.5**	1.0	<1.43	<1.33	<1.45			<1.33	<1.37	<1.33	<1.34	<1.44	<1.45	<1.38		
^{43}Ca	50900.01	50900.01	50886.69	**50895.6**	7.7	387368	387368	387367.9	**387367.9**	0.1	195113.3	195113.3	195113.3	195113.3	195113.4	195113.4	195113.4	**195113.3**	0.04
^{44}Ca	49097.26	51089.55	49849.13	**50012.0**	1006.1	416772.8	443655.9	423090.6	**427839.8**	14056.7	208850.3	212715.3	208906.6	210416.1	207620.6	211779.1	204990.2	**209325.5**	2607.8
^{47}Ti	12035.59	12722.15	12539.21	**12432.3**	355.5	13.59	6.7	<8.19	**10.1**	4.9	204725.8	207075.8	199849.5	200029.6	197395.2	203763.3	200485.3	**201903.5**	3372.5
^{49}Ti	12378.88	12600.98	12512.5	**12497.5**	111.8	<5.66	<4.36	<6.21			201907.8	200070.7	199791.6	195456.5	194228.8	202255.6	203299.8	**199573.0**	3472.2
^{51}V	409.36	418.3	422.71	**416.8**	6.8	49.47	48.4	48.44	**48.8**	0.6	1182.1	1230.72	1190.53	1181.05	1141.33	1202.97	1185.05	**1187.7**	26.8
^{53}Cr	18.16	19.31	19.3	**18.9**	0.7	<7.18	<5.73	<7.79			88.55	81.62	82.5	81.29	81.43	89.38	88.22	**84.7**	3.8
^{88}Sr	315.12	325.76	318.9	**319.9**	5.4	467.43	467.62	468.06	**467.7**	0.3	32.35	32.84	32.52	32.14	31.28	32.75	31.74	**32.2**	0.6
^{89}Y	31.56	32.94	32.72	**32.4**	0.7	586.76	559.67	582.58	**576.3**	14.6	3797.8	3913.9	3819.15	3782.48	3748.35	3924.11	3747.8	**3819.1**	72.9
^{91}Zr	174.59	179.37	168.87	**174.3**	5.3	1.53	<0.71	<0.86	**1.5**		538.82	531.57	498.8	494.47	513.15	526.19	500.39	**514.8**	17.6
^{93}Nb	10.8	11.27	11.09	**11.1**	0.2	<0.0245	0.0201	<0.047	**0.0**		6998.36	6942.37	6953.92	6960.99	6674.53	7059.91	6794.96	**6912.1**	132.0
^{139}La	22.92	23.93	23.68	**23.5**	0.5	3544.27	3556.74	3617.69	**3572.9**	39.3	2214.18	2275.86	2206.96	2201.16	2194.05	2304.01	2212.13	**2229.8**	42.4
^{140}Ce	48.81	50.65	49.44	**49.6**	0.9	4226.05	4193.53	4230.17	**4216.6**	20.1	6479.5	6653.37	6379.18	6290.5	6394.6	6674.54	6376.58	**6464.0**	147.3
^{141}Pr	6.12	6.49	6.16	**6.3**	0.2	321.31	314.13	320.93	**318.8**	4.0	776.29	799.04	771.37	773.05	772.76	797.34	776.94	**781.0**	11.9
^{146}Nd	27.06	27.7	27.06	**27.3**	0.4	1053.48	1022.33	1030.83	**1035.5**	16.1	2907.7	2976.4	2925.85	2891.92	2869.6	3038.33	2949.12	**2937.0**	57.0
^{147}Sm	6.19	6.22	6.26	**6.2**	0.0	148.7	145.21	147.99	**147.3**	1.8	590.82	605.94	586.85	579.68	577.84	602.03	584.37	**589.6**	10.8
^{153}Eu	1.793	1.873	1.861	**1.8**	0.0	16.3	16.17	16.52	**16.3**	0.2	62.99	66.24	63.9	63.61	62.35	65.45	63.46	**64.0**	1.4
^{157}Gd	6.61	6.75	6.12	**6.5**	0.3	135.82	128.74	137.2	**133.9**	4.5	542.19	563.98	537.54	529.11	543.77	564.19	543.14	**546.3**	13.2
^{159}Tb	0.913	0.921	0.916	**0.9**	0.0	16.1	15.39	16.62	**16.0**	0.6	86.68	88.97	86.67	87.89	87.9	89.31	87.9	**87.9**	1.0
^{163}Dy	5.8	6.01	5.79	**5.9**	0.1	94.64	90.48	94.72	**93.3**	2.4	575.36	594.65	573.93	570.49	576.93	596.12	564.54	**578.9**	12.0
^{165}Ho	1.201	1.161	1.194	**1.2**	0.0	18.53	17.58	18.5	**18.2**	0.5	116.41	120.84	116.73	116.31	115.63	122.18	115.33	**117.6**	2.7
^{166}Er	3.66	3.36	3.58	**3.5**	0.2	52.36	49.68	53.82	**52.0**	2.1	382.9	386.11	378.9	370.08	372.39	391.58	371.57	**379.1**	8.2
^{169}Tm	0.484	0.463	0.459	**0.5**	0.0	6.27	5.89	6.28	**6.1**	0.2	60.41	61.39	60.52	58.56	58.34	60.24	58.95	**59.8**	1.2
^{172}Yb	3.23	3.33	3.32	**3.3**	0.1	36.73	33.95	37.62	**36.1**	1.9	449.14	462.37	437.16	437.51	438.93	455.39	428.69	**444.2**	11.8
^{175}Lu	0.465	0.459	0.452	**0.5**	0.0	4.55	4.41	4.7	**4.6**	0.1	57.36	58.79	57.33	57.16	57.8	58.8	56.02	**57.6**	1.0
^{178}Hf	4.56	4.41	4.36	**4.4**	0.1	<0.058	<0.049	<0.084			44.67	46.65	43.03	42.78	41.5	43.91	40.73	**43.3**	2.0
^{181}Ta	0.648	0.721	0.636	**0.7**	0.0	<0.0189	<0.0145	<0.079			1526.43	1616.23	1466.87	1468.33	1330.65	1334.81	1289.49	**1433.3**	119.3
^{208}Pb	9.78	10.33	10.46	**10.2**	0.4	0.613	0.622	0.718	**0.7**	0.1	26.14	26.3	25.5	25.54	26.36	26.53	26.6	**26.1**	0.4
^{232}Th	5.34	5.56	5.42	**5.4**	0.1	234.5	226.24	241.93	**234.2**	7.8	528.01	537.71	539.28	524.02	527.74	554.42	529.87	**534.4**	10.4
^{238}U	1.504	1.605	1.568	**1.6**	0.1	12.49	12.49	12.76	**12.6**	0.2	674.37	700.98	690.75	679.58	660.93	707.26	671.27	**683.6**	16.7
Uncertainty [1σ ppm]																			
^{6}Li	1.32	1.34	1.31			0.99	0.91	0.87			0.73	0.7	0.78	0.67	1.03	0.91	0.81		
^{7}Li	0.68	0.73	0.76			0.52	0.49	0.52			0.49	0.49	0.48	0.48	0.52	0.53	0.5		
^{43}Ca	1650.8	1653.52	1661.31			12262.08	12262.23	12262.33			6184.63	6183.03	6182.98	6182.73	6183.85	6184.37	6182.53		
^{44}Ca	1583.07	1648.66	1603.77			16521.35	16855.42	16881.41			7908	8645.73	6608.83	6700.19	6615.11	7356.93	7676.74		
^{47}Ti	420.79	445.1	407.72			2.83	2.49	2.94			6797.65	6996.34	6399.84	6410.41	6832.1	6726.86	6782.6		
^{49}Ti	496.44	505.62	410.96			2.03	1.62	2.23			7155.81	7425.26	6449.09	6389.57	7729.73	6976.19	7453.89		
^{51}V	16.42	16.79	14.78			1.81	2.32	2.04			40.8	44.05	40.68	42.33	45.42	38.76	38.36		
^{53}Cr	2.27	2.36	2.92			2.9	2.2	4.21			7.87	8.62	6.5	8.11	3.32	6.2	7.75		
^{88}Sr	11.23	11.62	10.05			16.28	18.87	19.57			1.27	1.41	1.01	1	1.11	1.11	1.14		
^{89}Y	1.21	1.26	1.04			20.87	23.92	22.65			132.59	143.49	119.1	118.06	141.38	125.36	122.13		
^{91}Zr	8.23	8.46	6.56			0.3	0.27	0.31			21.23	22.53	18.67	20.67	24.02	20.79	22.84		
^{93}Nb	0.42	0.44	0.36			0.009	0.0078	0.017			227.07	229.6	218.1	219.27	254.69	233.52	234.63		
^{139}La	1	1.04	0.76			114.93	150.29	185.95			71.66	75.25	69.32	69.9	94.51	76.12	76.77		
^{140}Ce	1.94	2.01	1.62			158.44	172.18	190.58			217.22	231.47	203.72	205.88	251.49	238.39	250.74		
^{141}Pr	0.25	0.26	0.2			10.19	14.66	14.51			25	26.29	24.41	24.98	30.17	28.58	30.85		
^{146}Nd	1.23	1.26	0.92			39.39	37.3	47.01			106.4	116.55	93.22	94.36	126.86	162.94	197.67		
^{147}Sm	0.26	0.26	0.25			4.82	5.23	5.15			21.09	22.94	19.27	19.85	20.95	23.43	25.91		
^{153}Eu	0.081	0.085	0.077			0.52	0.54	0.93			2.54	2.94	2.2	2.35	2.48	2.22	2.28		
^{157}Gd	0.28	0.29	0.27			4.68	5.61	7.99			18.65	20.22	18.86	20.07	19.43	20.79	22.16		
^{159}Tb	0.038	0.039	0.036			0.53	0.61	0.73			3.08	3.35	2.73	2.79	3.1	3.08	3.26		
^{163}Dy	0.21	0.22	0.24			3.06	3.08	4.48			18.63	19.62	20.5	22.19	18.13	18.95	18.18		
^{165}Ho	0.054	0.053	0.046			0.65	0.69	0.84			3.93	4.23	3.75	3.81	4.66	4.83	5.23		
^{166}Er	0.18	0.17	0.14			2.31	1.92	3.16			12.65	13.09	12.05	11.9	16.61	13.97	14.42		
^{169}Tm	0.024	0.023	0.021			0.21	0.27	0.3			1.96	2.03	1.91	1.86	2.2	1.93	1.92		
^{172}Yb	0.16	0.16	0.14			1.28	1.31	2.11			15.67	16.87	13.82	13.87	17.79	15.01	14.58		
^{175}Lu	0.023	0.023	0.022			0.17	0.16	0.23			1.92	2.02	1.83	1.84	2.08	1.92	1.88		
^{178}Hf	0.23	0.22	0.18			0.023	0.02	0.03			1.49	1.58	1.41	1.43	1.85	1.44	1.35		
^{181}Ta	0.029	0.032	0.027			0.0065	0.0055	0.035			50.22	54.69	45.85	46.16	46.48	44.54	45.33		
^{208}Pb	0.44	0.46	0.41			0.031	0.038	0.044			0.9	0.93	0.94	1.02	1.15	0.96	1.05		
^{232}Th	0.22	0.23	0.21			8.01	7.4	12			20.09	21.82	19.18	19.8	20.76	18.29	17.76		
^{238}U	0.066	0.07	0.056			0.46	0.6	0.54			21.32	22.4	21.53	21.26	26.38	23.13	22.85		
Detection limit [ppm]																			
^{6}Li	3.18	3.16	2.99			2.77	2.42	2.31			1.98	1.92	2.14	1.79	2.89	2.49	2.24		
^{7}Li	1.67	1.72	1.97			1.43	1.33	1.45			1.33	1.37	1.33	1.34	1.44	1.45	1.38		
^{43}Ca	590	617.89	717.03			571.66	483.21	570.91			475.19	493.17	490.97	478.82	513.18	496.03	480.17		
^{44}Ca	84.18	87.42	102.79			77.3	68.69	79.99			68.09	70.02	70.05	68.14	72.94	70.6	67.71		
^{47}Ti	7.28	7.38	9.89			7.73	6.61	8.19			6.65	7.36	6.6	6.8	5.98	6.38	6.36		
^{49}Ti	4.19	4.13	6.87			5.66	4.36	6.21			5.05	5.58	4.59	4.95	3.14	4.08	4.33		
^{51}V	0.403	0.42	0.502			0.385	0.335	0.387			0.337	0.35	0.343	0.339	0.348	0.351	0.339		
^{53}Cr	5.83	6.07	6.83			7.18	5.73	7.79			4.58	4.72	4.69	4.58	5.1	5.13	4.93		
^{88}Sr	0.13	0.14	0.171			0.121	0.105	0.122			0.111	0.119	0.118	0.113	0.116	0.119	0.114		
^{89}Y	0.0454	0.0501	0.0641			0.044	0.0394	0.0538			0.046	0.0491	0.0402	0.0428	0.038	0.0403	0.0397		
^{91}Zr	0.963	1.01	1.2			0.82	0.714	0.857			0.832	0.857	0.817	0.803	0.818	0.835	0.806		
^{93}Nb	0.0243	0.0275	0.0279			0.0245	0.0194	0.0466			0.0193	0.0215	0.0218	0.0221	0.0183	0.0181	0.02		
^{139}La	0.0199	0.019	0.024			0.0174	0.0189	0.0169			0.0162	0.0174	0.0196	0.0199	0.0145	0.0163	0.0156		
^{140}Ce	0.0218	0.0166	0.0388			0.0221	0.0186	0.023			0.0251	0.0235	0.0196	0.0252	0.0141	0.0188	0.0198		
^{141}Pr	0.00809	0.0109	0.0155			0.0116	0.00745	0.00926			0.0108	0.0103	0.00832	0.0096	0.00572	0.00873	0.0108		
^{146}Nd	0.0932	0.0937	0.156			0.0614	0.0717	0.0913			0.0807	0.107	0.0956	0.098	0.0807	0.0747	0.084		
^{147}Sm	0.0704	0.0759	0.0899			0.0713	0.0519	0.0866			0.0644	0.087	0.0778	0.0687	0.0757	0.0295	0.0807		
^{153}Eu	0.0206	0.0245	0.0307			0.0228	0.0138	0.0277			0.0258	0.0278	0.0257	0.0212	0.0238	0.0239	0.021		
^{157}Gd	0.127	0.108	0.201			0.127	0.104	0.126			0.132	0.134	0.119	0.129	0.105	0.123	0.136		
^{159}Tb	0.00829	0.0134	0.0214			0.0103	0.0112	0.0138			0.0124	0.0129	0.015	0.00988	0.00543	0.00667	0.012		
^{163}Dy	0.0601	0.0771	0.134			0.0732	0.0533	0.0865			0.0761	0.0956	0.0805	0.0907	0.044	0.0636	0.0771		
^{165}Ho	0.00476	0.00699	0.013			0.00637	0.00473	0.0114			0.00553	0.00817	0.0091	0.00692	<0.00000	0.0065	0.0074		
^{166}Er	0.0696	0.0885	0.117			0.0744	0.0588	0.0967			0.0811	0.0905	0.0858	0.0952	0.0749	0.0613	0.075		
^{169}Tm	<0.00000	0.0125	0.0114			0.00911	0.0109	0.0148			0.01	0.00818	0.00908	0.0129	0.00647	0.0109	0.0105		
^{172}Yb	0.0336	0.0428	0.0996			0.0781	0.0359	0.0708			0.0561	0.0652	0.0578	0.0663	0.0545	0.0688	0.0769		
^{175}Lu	<0.00000	0.00567	0.0149			0.00742	0.0045	0.0109			0.00553	0.00998	0.00808	0.00325	<0.00000	0.0106	0.00787		
^{178}Hf	0.0803	0.106	0.121			0.0585	0.0489	0.0845			0.0935	0.0838	0.0761	0.0686	0.0555	0.0951	0.0789		
^{181}Ta	0.0168	0.0163	0.0222			0.0189	0.0145	0.079			0.0128	0.0158	0.0163	0.0159	0.0133	0.0155	0.0168		
^{208}Pb	0.0135	0.0161	0.0288			0.0287	0.0241	0.0149			<0.00000	0.00952	0.00953	0.0149	<0.00000	0.0192	0.0132		
^{232}Th	0.0103	0.00831	0.00851			<0.00000	<0.00000	0.00654			0.0053	0.00862	0.00402	0.00387	0.004	0.00912	0.0105		
^{238}U	<0.00000	<0.00000	<0.00000			<0.00000	<0.00000	<0.00000			0.00438	0.0103	<0.00000	<0.00000	0.00375	0.00472	0.00264		

Reference material	GSD													
Concentrations [ppm]														
^{6}Li	43.01	43.06	42.07	44	43.94	42.04	43.53	42.54	42.57	43.39	43.89	42.15	43.57	42.17
^{7}Li	41.85	44.29	41.85	44.1	41.92	43.97	44.14	41.92	43.19	42.76	43.68	42.34	43.29	42.86
^{43}Ca	51458.02	51458.01	51458.01	51458.01	51458	51458	51458	51458	51458	51457.99	51458	51458	51457.99	51457.99
^{44}Ca	50508.94	52511.5	51370.26	51499.09	51663.45	51218	52354.73	50695.45	51283.09	51599.7	52394.57	50604.2	51990.74	51008.86
^{47}Ti	7350.89	7524.93	7343.86	7521.36	7457.12	7399	7610.55	7282.86	7408.15	7454.83	7483.99	7382.12	7560.8	7313.61
^{49}Ti	7457.1	7412.64	7341.57	7529.41	7413.82	7440.88	7590.29	7296.73	7380.31	7483.5	7517.9	7350.58	7639.33	7248.33
^{51}V	43.65	44.4	43.53	44.47	44.22	43.72	45.29	42.9	44.21	43.75	44.45	43.59	44.64	43.43
^{53}Cr	43	41.41	35.25	48.85	48.79	35.31	45.67	38.92	44.82	39.02	42.15	41.98	39.79	43.89
^{88}Sr	68.68	70.2	68.95	69.82	69.51	69.21	70.9	68.12	69.36	69.37	70.88	68.08	70.17	68.76
^{89}Y	41.6	42.45	41.62	42.37	42.14	41.81	43.03	41.13	41.89	42.09	42.58	41.47	42.49	41.57
^{91}Zr	41.66	42.36	41.83	42.16	40.17	43.8	41.79	42.09	41.16	42.9	42.15	41.82	40.96	43.08
^{93}Nb	41.53	42.53	41.69	42.29	42.01	41.93	43.08	41.09	41.69	42.34	41.96	42.02	42.7	41.41
^{139}La	38.97	39.25	38.84	39.36	38.84	39.31	40.01	38.31	39.28	38.9	39.36	38.86	40.01	38.32
^{140}Ce	40.89	41.98	40.97	41.82	41.32	41.43	42.34	40.59	41.31	41.47	41.86	40.97	42.07	40.83
^{141}Pr	44.83	45.19	44.79	45.2	45.03	44.9	46.34	43.88	44.94	45.05	45.36	44.66	45.7	44.4
^{146}Nd	44.61	44.84	43.98	45.45	44.78	44.58	45.42	44.06	44.81	44.55	45.49	44.01	45.72	43.78
^{147}Sm	47.67	47.96	47.49	48.11	48.06	47.5	48.46	47.21	47.8	47.76	48.57	47.12	48	47.64
^{153}Eu	41.03	40.98	40.84	41.17	40.84	41.14	41.34	40.69	41.21	40.74	41.92	40.2	42.23	39.93
^{157}Gd	50.76	50.67	50.15	51.27	50.94	50.39	51.96	49.61	50.62	50.76	51.35	50.12	52.54	49.05
^{159}Tb	46.69	47.34	46.77	47.22	47.14	46.82	47.92	46.21	47.09	46.87	47.71	46.37	47.85	46.25
^{163}Dy	51.47	50.93	51.03	51.38	51.33	51.04	51.73	50.72	50.97	51.43	51.51	50.91	52.39	50.14
^{165}Ho	48.7	49.35	48.5	49.51	49.03	48.92	49.96	48.17	48.58	49.44	49.32	48.68	49.68	48.43
^{166}Er	39.63	40.66	39.29	40.93	39.79	40.38	40.77	39.49	40.08	40.11	40.47	39.76	41.08	39.27
^{169}Tm	48.69	49.34	48.74	49.25	48.93	49	50.36	47.85	49.36	48.63	49.06	48.96	50.11	48.03
^{172}Yb	50.73	51.11	50.4	51.41	51.38	50.39	51.65	50.25	51.47	50.3	51.22	50.64	51.93	50.04
^{175}Lu	51.38	51.67	50.89	52.14	51.44	51.52	52.19	50.89	51.9	51.08	51.75	51.28	52.5	50.64
^{178}Hf	38.39	39.65	39.14	38.82	38.6	39.37	39.73	38.33	38.78	39.23	39.19	38.82	39.71	38.34
^{181}Ta	39.7	40.35	39.53	40.48	39.96	39.96	41.45	38.81	40.22	39.76	40.3	39.73	40.76	39.32
^{208}Pb	50.09	49.92	49.7	50.32	50.59	49.37	51.26	48.94	50.44	49.53	50.24	49.8	51.27	48.89
^{232}Th	40.8	41.23	40.71	41.29	40.89	41.1	41.12	40.89	40.32	41.76	40.93	41.03	41.83	40.29
^{238}U	40.47	41.59	40.71	41.28	41.03	40.9	42.24	39.96	41.19	40.8	41.09	40.92	41.58	40.5
Uncertainty [1σ ppm]														
^{6}Li	2.55	2.58	2.89	3.09	2.7	2.59	2.95	2.94	2.51	2.53	2.8	2.73	3.79	3.7
^{7}Li	2.48	2.62	3.46	3.74	2.44	2.53	3.35	3.26	2.06	2.05	2.31	2.26	2.65	2.63
^{43}Ca	1691.81	1689.91	1681.54	1685.51	1691.74	1685.37	1684.7	1683.03	1674.16	1674.22	1670.95	1671.53	1702.5	1697.54
^{44}Ca	1904.76	1981.72	2392.76	2447.75	1892.39	1874.29	2286.1	2250.44	1890.03	1902.96	2355.57	2308.52	1950.83	1915.25
^{47}Ti	272.69	279.29	325.16	338.95	301.33	298.88	392.13	383.37	247.01	248.61	262.38	259.95	284.18	275
^{49}Ti	263.03	261.55	295.63	307.53	286.51	287.42	364.59	357.45	258.44	262.18	300.23	296.6	332.89	316.61
^{51}V	1.57	1.6	1.79	1.85	1.96	1.93	2.69	2.61	1.53	1.52	1.71	1.69	1.77	1.72
^{53}Cr	8.3	8.07	11.43	16.1	9.6	7.31	16.4	14.68	4.2	3.85	5.76	5.89	6.36	6.76
^{88}Sr	2.35	2.41	2.67	2.74	2.65	2.64	3.41	3.35	2.63	2.63	3.4	3.32	2.71	2.66
^{89}Y	1.45	1.48	1.66	1.72	1.69	1.67	2.23	2.18	1.45	1.46	1.69	1.67	1.57	1.53
^{91}Zr	1.45	1.47	1.56	1.59	2.24	2.44	3.51	3.64	1.65	1.71	2.02	2.03	1.79	1.87
^{93}Nb	1.46	1.49	1.68	1.72	1.71	1.7	2.28	2.22	1.36	1.38	1.45	1.46	1.86	1.81
^{139}La	1.27	1.28	1.34	1.37	1.54	1.56	2.05	2	1.28	1.27	1.36	1.35	1.8	1.73
^{140}Ce	1.48	1.52	1.78	1.86	1.6	1.61	2.09	2.04	1.38	1.39	1.56	1.54	1.72	1.67
^{141}Pr	1.44	1.45	1.49	1.51	1.93	1.92	2.7	2.62	1.45	1.46	1.56	1.55	1.87	1.82
^{146}Nd	1.63	1.64	1.93	2.04	1.61	1.6	1.92	1.89	1.63	1.62	1.99	1.95	1.9	1.82
^{147}Sm	1.58	1.59	1.65	1.69	1.71	1.69	1.99	1.96	1.7	1.7	2.04	2	1.68	1.66
^{153}Eu	1.32	1.31	1.33	1.35	1.35	1.36	1.46	1.45	1.59	1.58	2.11	2.06	2.04	1.94
^{157}Gd	1.76	1.76	1.92	1.99	2.09	2.07	2.78	2.72	1.76	1.77	2.01	1.98	2.63	2.47
^{159}Tb	1.54	1.56	1.65	1.68	1.76	1.75	2.21	2.17	1.65	1.64	1.96	1.93	1.9	1.84
^{163}Dy	1.69	1.68	1.75	1.77	1.75	1.74	1.92	1.89	1.68	1.69	1.79	1.78	2.23	2.14
^{165}Ho	1.68	1.7	1.9	1.96	1.83	1.83	2.29	2.25	1.63	1.66	1.84	1.83	2.03	1.99
^{166}Er	1.62	1.67	2.15	2.3	1.48	1.51	1.84	1.81	1.34	1.34	1.46	1.44	2.07	1.99
^{169}Tm	1.61	1.63	1.73	1.76	2.05	2.05	2.83	2.76	1.61	1.59	1.69	1.7	2.12	2.03
^{172}Yb	1.75	1.76	1.92	1.98	1.9	1.87	2.29	2.26	1.8	1.76	2.04	2.03	2.5	2.42
^{175}Lu	1.79	1.8	2.02	2.1	1.8	1.8	2.06	2.03	1.73	1.71	1.87	1.87	2.27	2.2
^{178}Hf	1.42	1.47	1.73	1.75	1.51	1.54	1.94	1.91	1.3	1.32	1.39	1.38	1.53	1.47
^{181}Ta	1.4	1.42	1.63	1.69	1.88	1.89	2.79	2.69	1.33	1.31	1.44	1.43	1.59	1.54
^{208}Pb	1.66	1.66	1.72	1.75	2.15	2.1	2.94	2.88	1.72	1.69	1.87	1.87	2.26	2.17
^{232}Th	1.39	1.41	1.5	1.54	1.36	1.37	1.39	1.38	1.51	1.56	1.83	1.86	1.83	1.77
^{238}U	1.43	1.47	1.71	1.77	1.78	1.77	2.52	2.44	1.32	1.31	1.36	1.36	1.61	1.57
Detection limit [ppm]														
^{6}Li	3.6	3.73	3.35	3.6	3.97	3.76	3.38	3.42	3.08	2.86	2.26	2.41	3.66	3.64
^{7}Li	1.94	1.9	1.88	1.92	2.13	1.96	2.01	1.97	1.88	1.88	1.74	1.82	2.22	2.15
^{43}Ca	827.71	805.93	721.34	747.74	839.9	773.13	767.5	750.82	692.46	682.43	631.29	659.32	885.55	858.91
^{44}Ca	112.25	108.5	99.16	102.19	118.11	106.9	105.29	103.05	101	99.45	89.66	93.78	127.25	121.91
^{47}Ti	10.39	9.88	10.16	10.45	10.22	9.18	10.45	10.12	9.54	9.29	9.37	9.63	12.08	11.46
^{49}Ti	6.97	6.83	7.73	7.87	5.96	5.35	7.44	7.04	7.06	6.96	7.36	7.56	8.82	8.35
^{51}V	0.545	0.538	0.503	0.514	0.56	0.525	0.521	0.513	0.465	0.47	0.459	0.479	0.591	0.575
^{53}Cr	10.28	10.02	9.6	9.86	9.33	8.8	9.52	9.5	6.51	6.51	6.15	6.4	11.16	10.96
^{88}Sr	0.165	0.157	0.156	0.159	0.186	0.166	0.168	0.16	0.16	0.169	0.151	0.152	0.201	0.18
^{89}Y	0.0621	0.0569	0.0583	0.0586	0.0621	0.053	0.0612	0.0599	0.0634	0.0622	0.0567	0.0653	0.0629	0.063
^{91}Zr	1.1	1.08	1.09	1.13	1.12	1	1.14	1.1	1.23	1.23	1.06	1.11	1.29	1.23
^{93}Nb	0.0344	0.0296	0.033	0.031	0.0297	0.0259	0.0344	0.0303	0.0338	0.0302	0.0286	0.0326	0.0384	0.0324
^{139}La	0.0254	0.0263	0.0218	0.0236	0.0224	0.026	0.0252	0.0221	0.0258	0.0284	0.0241	0.0293	0.0294	0.0289
^{140}Ce	0.025	0.0226	0.0283	0.034	0.029	0.0273	0.0312	0.029	0.0308	0.0292	0.0309	0.0332	0.0281	0.0291
^{141}Pr	0.0111	0.0153	0.0124	0.0181	0.0147	0.0133	0.0138	0.0209	0.014	0.0135	0.0182	0.0163	0.013	0.0153
^{146}Nd	0.0981	0.113	0.107	0.136	0.0787	0.0747	0.104	0.0883	0.127	0.128	0.145	0.141	0.0997	0.0864
^{147}Sm	0.111	0.0924	0.115	0.121	0.0952	0.115	0.109	0.107	0.11	0.0875	0.0986	0.111	0.139	0.0941
^{153}Eu	0.0311	0.0276	0.0283	0.0359	0.0251	0.0263	0.0361	0.0308	0.0341	0.0309	0.021	0.0361	0.0429	0.0369
^{157}Gd	0.153	0.148	0.17	0.152	0.153	0.162	0.166	0.168	0.185	0.173	0.183	0.187	0.169	0.154
^{159}Tb	0.0136	0.0196	0.0122	0.012	0.0147	0.0157	0.0165	0.0207	0.0135	0.0145	0.0119	0.0171	0.0209	0.0189
^{163}Dy	0.113	0.0736	0.0943	0.103	0.0729	0.045	0.0949	0.0749	0.128	0.0949	0.119	0.121	0.102	0.09
^{165}Ho	0.0146	0.00878	0.0168	0.00408	0.00861	0.00434	0.0124	0.0114	0.012	0.0134	0.0143	0.00787	0.01	0.013
^{166}Er	0.107	0.0986	0.121	0.0997	0.0897	0.0609	0.119	0.0977	0.125	0.122	0.111	0.115	0.126	0.127
^{169}Tm	0.0123	0.014	0.0144	0.0149	0.0164	0.00966	0.014	0.0157	0.0114	0.022	0.00617	0.0118	0.00998	0.012
^{172}Yb	0.0688	0.0926	0.0772	0.0825	0.0921	0.0775	0.101	0.0863	0.106	0.0903	0.112	0.0737	0.079	0.101
^{175}Lu	0.0108	0.00512	0.0103	0.0106	0.013	0.0088	0.0088	0.0132	0.00928	0.00775	0.01	0.0135	0.00823	0.0128
^{178}Hf	0.0943	0.0855	0.105	0.119	0.0968	0.0803	0.0782	0.0811	0.133	0.122	0.127	0.111	0.119	0.0989
^{181}Ta	0.029	0.0263	0.02	0.0196	0.0268	0.0241	0.0235	0.0209	0.0264	0.025	0.0196	0.0248	0.0262	0.0249
^{208}Pb	0.0295	0.0198	0.0294	0.0259	0.0405	0.034	0.0225	0.0298	0.0132	0.0254	0.0235	0.0243	0.0368	0.0189
^{232}Th	<0.00000	0.0085	0.00546	0.0126	0.012	0.00606	<0.00000	0.0121	0.0156	0.00752	0.00937	0.0115	0.00684	<0.00000
^{238}U	0.00712	<0.00000	0.00607	0.00362	0.00891	0.00389	<0.00000	0.00785	<0.00000	<0.00000	<0.00000	<0.00000	<0.00000	<0.00000

Reference material	GSD (continued)													Average	St.Dev
Concentrations [ppm]															
^{6}Li	45.76	40.28	44.61	41.35	44.32	42.06	43.86	43.13	42.91	43.7	42.21	43.48	42.63	**43.05**	1.11
^{7}Li	41.34	44.65	43.5	42.45	39.7	43.19	42.85	42.01	43.73	43.23	42.68	43.04	42.99	**42.87**	1.06
^{43}Ca	51457.99	51458	51457.98	51457.98	51458.45	51457.99	51457.99	51458	51458.01	51458	51458	51458	51458	**51458.02**	0.09
^{44}Ca	50693.9	52283.73	51421.71	51504.27	51121.01	51263.75	51641.54	51790.4	51214.27	52049.62	50749.3	51522.7	51441.35	**51459.26**	559.14
^{47}Ti	7391.51	7481.78	7436.75	7427.18	7372.92	7421.91	7441.67	7548.45	7348.75	7478.19	7376.22	7433.04	7433.93	**7432.83**	77.77
^{49}Ti	7372.43	7506.83	7459.04	7403.98	7293.75	7403.52	7460.02	7647	7284.35	7509.17	7340.99	7429.86	7438.3	**7431.54**	102.31
^{51}V	43.36	44.69	44.28	43.71	43.66	43.6	44.4	45.23	43.11	43.96	44.06	43.83	44.14	**44.01**	0.58
^{53}Cr	46.57	37.36	44.51	39.2	44.29	42.37	41.74	41.47	42.38	42.88	40.6	44.4	40.2	**42.10**	3.44
^{88}Sr	68.2	70.69	69.39	69.4	68.75	69.43	69.37	70.78	68.39	70.02	68.69	69.91	69.02	**69.41**	0.84
^{89}Y	41.47	42.57	42.06	41.93	41.85	42.02	41.99	43.04	41.23	41.81	42.21	42.18	41.84	**42.02**	0.48
^{91}Zr	41.7	42.2	41.58	42.45	41.86	42.7	41.34	40.32	43.27	41.82	42.27	40.89	42.89	**41.97**	0.85
^{93}Nb	41.08	43.01	41.9	42.1	41.36	42.08	41.92	43.08	41.21	42.37	41.6	42.1	41.94	**42.00**	0.56
^{139}La	38.32	39.98	39.12	39.09	38.87	38.91	39.28	40.49	38.11	39.43	38.74	39.3	38.95	**39.12**	0.56
^{140}Ce	40.65	42.22	41.11	41.72	40.21	41.44	41.35	42.58	40.54	41.85	40.9	41.93	41	**41.38**	0.61
^{141}Pr	44.16	45.92	45.29	44.7	44.27	44.95	45.06	46.27	44.08	45.65	44.29	45.21	44.86	**45.00**	0.62
^{146}Nd	44.19	45.28	44.39	45.03	44.08	44.72	44.67	46.3	43.45	46.39	43.25	44.11	45.32	**44.71**	0.79
^{147}Sm	47.29	48.32	48.27	47.31	47.06	47.79	47.82	48.8	46.99	48.39	47.23	48.69	47.07	**47.79**	0.54
^{153}Eu	40.22	41.88	41.51	40.48	41.26	40.78	41.22	42.18	40.12	41.42	40.57	41.24	40.82	**41.04**	0.60
^{157}Gd	50.2	51.33	51.39	50.01	48.55	50.43	50.98	51.66	49.91	51.58	49.91	50.78	50.66	**50.65**	0.87
^{159}Tb	46.35	47.72	46.84	47.17	46.75	47.11	46.89	47.91	46.32	47.52	46.43	47.31	46.78	**47.01**	0.52
^{163}Dy	50.51	51.98	51.89	50.48	51.61	51.65	50.81	51.42	51.02	51.38	51.02	51.41	51.02	**51.23**	0.50
^{165}Ho	48.05	50.03	48.91	49.1	48.63	48.68	49.31	50.47	47.94	49.94	48	49.36	48.76	**49.02**	0.66
^{166}Er	39.01	41.3	39.91	40.3	40.28	40.12	40.07	41.55	38.99	40.69	39.54	40.23	40.02	**40.14**	0.66
^{169}Tm	48.3	49.79	49.19	48.8	48.51	48.98	49.03	50.2	48.12	49.23	48.75	48.85	49.14	**49.01**	0.61
^{172}Yb	49.54	52.38	50.89	50.9	50.89	51.02	50.79	52.36	49.74	51.19	50.64	50.56	51.22	**50.93**	0.70
^{175}Lu	50.51	52.6	51.55	51.45	50.51	51.28	51.71	52.53	50.74	51.84	51.13	51.42	51.59	**51.49**	0.59
^{178}Hf	38.78	39.27	39.18	38.82	38.76	38.81	39.19	40.36	37.93	39.16	38.85	38.85	39.15	**39.01**	0.51
^{181}Ta	39.56	40.49	40.08	39.91	39.51	40.11	39.9	40.74	39.44	40.39	39.58	40.12	39.92	**40.00**	0.53
^{208}Pb	49.27	50.83	49.31	50.79	48.9	49.65	50.31	51.72	48.72	50.49	49.53	49.42	50.54	**49.99**	0.80
^{232}Th	40.22	41.85	40.85	41.19	42.07	40.46	41.53	42.07	40.2	41.15	40.85	40.81	41.17	**41.06**	0.54
^{238}U	40.36	41.69	41.01	40.98	40.35	41.1	40.91	42.21	40.12	41.33	40.64	40.93	41.08	**41.00**	0.55
Uncertainty [1σ ppm]															
^{6}Li	6	5.63	3.08	2.91	3.23	3.82	4	2.44	2.26	2.39	2.36	2.68	2.61		
^{7}Li	3.42	3.83	1.95	1.92	1.86	2.19	2.18	2.06	2.09	1.89	1.91	2.01	1.98		
^{43}Ca	1693.44	1697.02	1672.24	1674.64	1672.7	1673.87	1672.48	1680.89	1667.54	1659.75	1666.45	1681.01	1672.57		
^{44}Ca	2313.23	2453.95	1646.71	1650.62	1641.53	1664.95	1678.02	1676.07	1650.58	1779.81	1738.87	2029.67	2044.16		
^{47}Ti	332.25	345.26	241.27	241.13	239.28	241.3	241.87	264.78	256.88	247.39	244.45	258.59	259.03		
^{49}Ti	432.5	457.5	243.41	241.8	239.28	248.15	250.38	307.45	292.1	256.32	251.04	284.83	287.13		
^{51}V	2.12	2.25	1.54	1.52	1.54	1.66	1.7	1.83	1.74	1.44	1.45	1.46	1.47		
^{53}Cr	11.16	9.83	3.95	3.7	4.31	5.42	5.42	2.95	2.63	3.21	3.38	5.05	4.65		
^{88}Sr	3.34	3.57	2.19	2.19	2.17	2.19	2.19	2.54	2.44	2.34	2.3	2.62	2.61		
^{89}Y	1.84	1.95	1.34	1.33	1.33	1.34	1.34	1.65	1.57	1.35	1.36	1.42	1.41		
^{91}Zr	2.37	2.49	1.6	1.64	1.69	2.01	1.97	1.95	2.07	1.62	1.65	2.07	2.19		
^{93}Nb	2.43	2.65	1.34	1.34	1.32	1.36	1.35	1.67	1.59	1.4	1.38	1.51	1.51		
^{139}La	2.42	2.63	1.25	1.25	1.25	1.27	1.28	1.76	1.66	1.3	1.28	1.42	1.42		
^{140}Ce	2.19	2.36	1.33	1.35	1.31	1.41	1.41	1.7	1.61	1.47	1.43	1.75	1.73		
^{141}Pr	2.39	2.58	1.45	1.43	1.43	1.5	1.51	1.83	1.74	1.6	1.55	1.91	1.92		
^{146}Nd	2.45	2.61	1.46	1.48	1.46	1.54	1.54	2.09	1.96	2.31	2.15	3.29	3.46		
^{147}Sm	1.82	1.89	1.63	1.6	1.62	1.75	1.76	1.83	1.75	1.85	1.8	2.34	2.3		
^{153}Eu	2.8	3.05	1.44	1.4	1.47	1.62	1.65	1.7	1.61	1.4	1.37	1.56	1.55		
^{157}Gd	3.69	3.95	1.84	1.79	1.79	2.1	2.14	1.91	1.84	1.89	1.83	2.23	2.25		
^{159}Tb	2.39	2.55	1.49	1.51	1.5	1.53	1.52	1.72	1.65	1.62	1.58	1.85	1.84		
^{163}Dy	2.89	3.09	1.87	1.82	1.93	2.2	2.18	1.67	1.65	1.67	1.65	1.72	1.7		
^{165}Ho	2.58	2.79	1.59	1.6	1.59	1.65	1.68	2.06	1.95	1.9	1.83	2.41	2.42		
^{166}Er	2.87	3.18	1.3	1.32	1.32	1.34	1.34	1.88	1.76	1.44	1.4	1.66	1.67		
^{169}Tm	2.77	2.97	1.58	1.56	1.56	1.59	1.6	1.91	1.83	1.58	1.57	1.63	1.64		
^{172}Yb	3.45	3.82	1.66	1.66	1.66	1.67	1.67	2.17	2.05	1.72	1.7	1.8	1.83		
^{175}Lu	2.98	3.23	1.67	1.67	1.64	1.69	1.71	1.92	1.84	1.7	1.68	1.77	1.78		
^{178}Hf	1.82	1.9	1.31	1.3	1.3	1.34	1.36	1.82	1.71	1.3	1.29	1.33	1.33		
^{181}Ta	1.97	2.09	1.27	1.27	1.26	1.29	1.28	1.45	1.4	1.34	1.32	1.47	1.48		
^{208}Pb	3.04	3.27	1.8	1.85	1.85	2.16	2.21	2.28	2.14	1.79	1.76	2.05	2.12		
^{232}Th	2.44	2.65	1.46	1.48	1.54	1.63	1.69	1.68	1.6	1.37	1.36	1.41	1.42		
^{238}U	2.02	2.16	1.3	1.3	1.28	1.31	1.31	1.71	1.62	1.35	1.33	1.45	1.46		
Detection limit [ppm]															
^{6}Li	3.55	3.96	3.08	3.2	2.78	2.73	2.4	3.97	3.04	2.31	3.11	3.25	2.81		
^{7}Li	2.15	2.2	1.71	1.81	1.84	1.94	1.87	1.96	1.58	1.26	1.79	2.21	1.91		
^{43}Ca	829.83	855.63	655.09	681.5	665.47	675.22	657.42	724.87	585.14	440.31	620.97	768.37	668.07		
^{44}Ca	117.23	120.48	95.82	99.25	95.12	96.31	93.21	104.69	83.71	63.42	89.65	107.47	94.61		
^{47}Ti	12.06	12.31	8.38	8.71	9.06	9.88	9.38	7.99	6.25	5.25	7.43	10.25	8.93		
^{49}Ti	9.4	9.55	5.41	5.63	6.39	7.41	7.07	2.37	1.93	2.71	3.79	7.07	6.07		
^{51}V	0.568	0.58	0.463	0.482	0.474	0.483	0.471	0.478	0.39	0.312	0.445	0.536	0.471		
^{53}Cr	11.52	11.98	6.21	6.52	6.34	6.46	6.27	7.04	5.75	4.6	6.57	7.84	6.84		
^{88}Sr	0.188	0.196	0.161	0.163	0.167	0.165	0.16	0.176	0.133	0.106	0.148	0.182	0.162		
^{89}Y	0.0776	0.0775	0.0584	0.061	0.0582	0.0619	0.0613	0.0533	0.0417	0.0368	0.0486	0.0702	0.0626		
^{91}Zr	1.27	1.31	1.09	1.14	1.11	1.14	1.11	1.11	0.873	0.738	1.04	1.3	1.12		
^{93}Nb	0.0443	0.0421	0.0263	0.0309	0.0272	0.0338	0.0285	0.024	0.0194	0.0175	0.0269	0.0316	0.0313		
^{139}La	0.0331	0.0273	0.0257	0.0241	0.022	0.0301	0.0257	0.02	0.0178	0.0152	0.0226	0.0248	0.0253		
^{140}Ce	0.0322	0.036	0.0295	0.0314	0.0332	0.0327	0.0297	0.0123	0.0153	0.0171	0.0259	0.03	0.03		
^{141}Pr	0.0195	0.0175	0.0104	0.0111	0.0166	0.017	0.0148	0.00913	0.00863	0.00652	0.00997	0.0142	0.0155		
^{146}Nd	0.133	0.164	0.11	0.118	0.137	0.138	0.123	0.0763	0.0526	0.0588	0.0975	0.119	0.106		
^{147}Sm	0.0789	0.128	0.0941	0.0896	0.0843	0.0944	0.0891	0.0873	0.0714	0.0539	0.0906	0.112	0.103		
^{153}Eu	0.042	0.0406	0.0333	0.03	0.0293	0.0324	0.0268	0.0168	0.0183	0.0209	0.031	0.0275	0.0337		
^{157}Gd	0.192	0.237	0.167	0.163	0.177	0.215	0.192	0.0936	0.0694	0.0774	0.107	0.23	0.209		
^{159}Tb	0.0221	0.0195	0.0168	0.0184	0.0223	0.0201	0.0197	0.00919	<0.00000	0.00764	0.0145	0.0171	0.0164		
^{163}Dy	0.0999	0.117	0.114	0.121	0.115	0.127	0.113	0.0496	0.0533	0.0596	0.0936	0.138	0.113		
^{165}Ho	0.012	0.0112	0.0124	0.012	0.0152	0.004	0.0136	0.00569	0.00596	0.00669	0.0136	0.00714	0.00873		
^{166}Er	0.129	0.133	0.118	0.124	0.0974	0.126	0.123	0.0832	0.0677	0.0665	0.0918	0.113	0.11		
^{169}Tm	0.0172	0.0144	0.00989	0.0139	0.0123	0.0148	0.0106	<0.00000	0.00662	0.00671	0.0136	0.0101	0.0118		
^{172}Yb	0.106	0.0773	0.111	0.11	0.0761	0.12	0.0844	0.0402	0.0595	0.0535	0.0763	0.11	0.0897		
^{175}Lu	0.00574	0.0132	0.00605	0.00648	0.00778	0.0113	0.00872	0.00462	0.00484	0.00742	0.00757	0.00819	0.00633		
^{178}Hf	0.141	0.124	0.116	0.104	0.123	0.126	0.106	0.0728	0.0711	0.0663	0.0828	0.139	0.138		
^{181}Ta	0.0261	0.0313	0.02	0.025	0.0194	0.0192	0.0194	0.0218	0.0172	0.0133	0.0185	0.0228	0.0169		
^{208}Pb	0.0112	0.0463	0.0174	0.0209	0.0184	0.0135	0.0201	0.0131	0.0195	0.0126	0.0247	0.0267	0.0278		
^{232}Th	0.00992	0.00722	0.0118	<0.00000	0.00768	0.0154	0.0114	0.00781	0.00579	0.00536	<0.00000	0.0125	0.0125		
^{238}U	0.00437	0.009	0.00601	0.00372	0.00518	0.00758	0.00357	0.00365	<0.00000	<0.00000	0.00497	0.0253	0.0037		

Table 5.6. Major- and trace-element compositions of zircon grains from trondhjemite samples from the Stolzburg Block.

Sample	**MS 2**		**MS 15**		**MS 27**		
# of analysis SEM	27	32	92	61	62	64	66
# of analysis ICP MS	5	9	6	2	3	4	5
Weight%							
Si	14.95	15.13	15.18	14.90	14.84	15.06	14.93
Ti	b.d.	b.d.	b.d.	b.d.	0.09	b.d.	b.d.
Zr	49.35	49.50	49.67	49.37	49.42	49.39	49.08
Hf	1.88	1.88	1.51	1.50	1.03	0.98	1.42
Pb	b.d.	b.d.	b.d.	b.d.	b.d.	b.d.	b.d.
U	b.d.	b.d.	b.d.	b.d.	b.d.	b.d.	b.d.
O	34.68	34.94	34.99	34.56	34.49	34.66	34.49
Total	100.86	101.45	101.35	100.33	99.87	100.09	99.92
Weight% Oxides							
SiO_2	31.98	32.37	32.47	31.88	31.75	32.22	31.95
ZrO_2	66.66	66.86	67.10	66.68	66.75	66.72	66.30
HfO_2	2.21	2.22	1.78	1.77	1.22	1.15	1.68
Total	100.86	101.45	101.35	100.33	99.71	100.09	99.92
Atoms p.f.u. [a]							
Si	0.98	0.99	0.99	0.98	0.98	0.99	0.99
Zr	1.00	0.99	1.00	1.00	1.01	1.00	1.00
Hf	0.02	0.02	0.02	0.02	0.01	0.01	0.01
Total	2.00	2.00	2.00	2.00	2.00	2.00	2.00
spot#	**MS2 - 5**	**MS2 - 9**	**MS15 - 6**	**MS27 - 2**	**MS27 - 3**	**MS27 - 4**	**MS27 - 5**
Weight% Si	14.9	15.1	15.2	14.9	14.8	15.1	14.9
Integration time	21.287	12.897	14.737	19.983	14.557	19.983	17.928
^{45}Sc	323	316.4	398	384.5	334.1	376	353
^{49}Ti	2.98	1.98	1.45	3.83	4.35	4.54	4.03
^{51}V	3.93	0.82	b.d.	0.25	0.43	0.128	b.d.
^{53}Cr	b.d.	b.d.	b.d.	b.d.	b.d.	b.d.	b.d.
^{55}Mn	24.5	6.8	b.d.	b.d.	1.67	2.9	2.95
^{59}Co	b.d.	b.d.	b.d.	b.d.	b.d.	b.d.	b.d.
^{60}Ni	1.88	4.74	b.d.	b.d.	b.d.	b.d.	b.d.
^{63}Cu	1.33	0.72	b.d.	0.58	0.27	b.d.	0.39
^{66}Zn	2	b.d.	b.d.	1.15	0.94	b.d.	b.d.
^{85}Rb	0.06	0.091	0.175	0.311	0.169	0.276	0.351
^{88}Sr	4.04	0.64	0.53	0.56	0.56	0.96	0.55
^{89}Y	60.5	172.5	685	1268	599	1154	1318
^{91}Zr	430000	435000	452000	434000	433200	439000	432000
^{93}Nb	0.367	0.582	1.194	3.54	1.44	2.56	4.6
^{95}Mo	1.32	1.23	1.47	1.26	1.21	1.3	1.08
^{133}Cs	b.d.	b.d.	b.d.	b.d.	b.d.	b.d.	b.d.
^{137}Ba	0.7	0.52	b.d.	b.d.	0.14	0.28	b.d.
^{139}La	12.98	1.41	0.051	0.139	1.63	0.349	0.165
^{140}Ce	98.1	13.8	15.7	14.41	10.69	10	13.01
^{141}Pr	7.65	0.754	0.061	0.114	0.85	0.245	0.045
^{143}Nd	48	5.34	0.86	1.28	5.82	2.04	0.92
^{146}Nd	48.7	5.26	1.02	1.17	5.88	2.07	0.83
^{147}Sm	13.8	1.59	2.46	2.57	4.57	2.69	2.16
^{149}Sm	13.4	1.72	2.44	2.48	4.73	3.08	2.16
^{153}Eu	4.23	0.56	0.72	1.05	1.4	1.32	0.755
^{157}Gd	8.96	3.95	15.4	18.1	17.1	15.7	18.58
^{159}Tb	0.771	1.17	4.92	6.86	4.41	6.09	7.04
^{163}Dy	5.2	14.22	57.1	95	48.9	81.3	98.9
^{165}Ho	1.68	5.52	21.17	38.71	18.32	34.19	40.6
^{166}Er	10.03	28.06	103.9	204.1	90.8	185.7	209
^{169}Tm	2.55	6.16	21.1	44.5	19.54	41.8	45.2
^{172}Yb	29.6	56.2	193.8	428.5	194.4	422	432
^{175}Lu	9.52	12.71	39.4	96.8	45.8	96.9	94.3
^{178}Hf	11450	11190	10510	9330	9330	9170	10360
^{181}Ta	0.074	0.237	0.342	0.998	0.562	0.761	1.725
^{208}Pb	2.62	5.89	23.8	15.79	6.19	10.99	22.6
^{232}Th	8.94	16.16	68.3	43	20.13	33.21	65.7
^{238}U	202.4	88.8	191.1	131.3	57.2	120.7	171.2
LREE-I	0	12	90	111	19	70	153
U/Yb	6.8	1.6	1.0	0.3	0.3	0.3	0.4
Zr/Hf	38	39	43	47	46	48	42
Ti/Mn	0.12	0.29			2.60	1.57	1.37
Th/U	0.04	0.18	0.36	0.33	0.35	0.28	0.38
Th/U age spots [b]	--	--	0.36	0.31	0.39	0.32	0.47
Diff TE vs age spots	--	--	0.00	-0.02	0.04	0.04	0.09

[a] : Calculated by charge balance to 4 oxygen atoms

[b] : Data from Mühlberg et al. (2020)

Mühlberg, M., Stevens, G., Moyen, J.-F., Kisters, A.F.M., Lana, C., 2020. Thermal evolution of the Stolzburg Block, Barnerton granitoid-greenstone terrain, South Africa: Implications for Paleoarchean tectonic processes. Prec. Research

Table 5.7. TiO2-activities calculated for granitoid samples from the Stolzburg Block

MS 2 – SW Stolzburg Main Trondhjemite

P [kbar] \ T [°C]	500	510	520	530	540	550	560	570	580	590	600	610	620	630	640	650	660	670	680	690	700	710	720	730	740	750	760	770	780	790	800	810	820	830	840	850	860	870	880	890	900
15	0.74	0.76	0.79	0.81	0.83	0.86	0.88	0.95	1.00	1.00	1.00	1.00	1.00	1.00	1.00	1.00	1.00	1.00	1.00	1.00	1.00	1.00	1.00	1.00	1.00	1.00	1.00	1.00	1.00	1.00	1.00	1.00	1.00	1.00	1.00	1.00	1.00	1.00	1.00	1.00	1.00
14.75	0.72	0.74	0.76	0.79	0.81	0.84	0.86	0.94	1.00	1.00	1.00	1.00	1.00	1.00	1.00	1.00	1.00	1.00	1.00	1.00	1.00	1.00	1.00	1.00	1.00	1.00	1.00	1.00	1.00	1.00	1.00	1.00	1.00	1.00	1.00	1.00	1.00	1.00	1.00	1.00	0.89
14.5	0.70	0.72	0.74	0.77	0.79	0.81	0.84	0.92	1.00	1.00	1.00	1.00	1.00	1.00	1.00	1.00	1.00	1.00	1.00	1.00	1.00	1.00	1.00	1.00	1.00	1.00	1.00	1.00	1.00	1.00	1.00	1.00	1.00	1.00	1.00	1.00	1.00	1.00	0.98	0.70	0.67
14.25	0.68	0.70	0.72	0.75	0.77	0.79	0.82	0.94	1.00	1.00	1.00	1.00	1.00	1.00	1.00	1.00	1.00	1.00	1.00	1.00	1.00	1.00	1.00	1.00	1.00	1.00	1.00	1.00	1.00	1.00	1.00	1.00	1.00	1.00	1.00	1.00	0.88	0.73	0.65	0.55	0.47
14	0.66	0.68	0.70	0.72	0.75	0.77	0.80	0.93	1.00	1.00	1.00	1.00	1.00	1.00	1.00	1.00	1.00	1.00	1.00	1.00	1.00	1.00	1.00	1.00	1.00	1.00	1.00	1.00	1.00	1.00	1.00	1.00	1.00	1.00	0.87	0.73	0.64	0.57	0.44	0.41	0.43
13.75	0.64	0.66	0.68	0.70	0.73	0.75	0.79	0.91	1.00	1.00	0.99	1.00	1.00	1.00	1.00	1.00	1.00	1.00	1.00	1.00	1.00	1.00	1.00	1.00	1.00	1.00	1.00	1.00	1.00	1.00	1.00	1.00	0.95	0.80	0.65	0.59	0.47	0.42	0.34	0.27	0.28
13.5	0.62	0.64	0.66	0.69	0.71	0.73	0.80	0.90	0.94	0.90	0.94	1.00	1.00	1.00	1.00	1.00	1.00	1.00	1.00	1.00	1.00	1.00	1.00	1.00	1.00	1.00	1.00	1.00	1.00	1.00	0.97	0.82	0.62	0.52	0.47	0.54	0.37	0.28	0.25	0.22	0.22
13.25	0.60	0.62	0.64	0.67	0.69	0.73	0.79	0.82	0.83	0.90	0.98	1.00	1.00	1.00	1.00	1.00	1.00	1.00	1.00	1.00	1.00	1.00	1.00	1.00	1.00	1.00	1.00	1.00	1.00	0.85	0.59	0.64	0.48	0.46	0.35	0.37	0.31	0.23	0.21	0.22	0.10
13	0.58	0.60	0.63	0.65	0.67	0.71	0.73	0.80	0.87	0.94	1.00	1.00	1.00	1.00	1.00	1.00	1.00	1.00	1.00	1.00	1.00	1.00	1.00	1.00	1.00	1.00	1.00	1.00	0.82	0.69	0.50	0.52	0.44	0.35	0.26	0.20	0.21	0.16	0.12	0.31	0.05
12.75	0.57	0.59	0.61	0.63	0.67	0.69	0.76	0.83	0.90	0.98	1.00	1.00	1.00	1.00	1.00	1.00	1.00	1.00	1.00	1.00	1.00	1.00	1.00	1.00	1.00	1.00	0.90	0.71	0.49	0.54	0.38	0.36	0.26	0.22	0.25	0.19	0.24	0.10	0.24	0.33	0.33
12.5	0.55	0.57	0.59	0.61	0.66	0.73	0.79	0.87	0.94	1.00	1.00	1.00	1.00	1.00	1.00	1.00	1.00	1.00	1.00	1.00	1.00	1.00	1.00	1.00	1.00	0.80	0.64	0.53	0.48	0.36	0.22	0.27	0.30	0.29	0.28	0.27	0.22	0.22	0.27	0.32	0.31
12.25	0.54	0.56	0.58	0.63	0.69	0.76	0.83	0.91	0.99	1.00	1.00	1.00	1.00	1.00	1.00	1.00	1.00	1.00	1.00	1.00	1.00	1.00	1.00	1.00	0.85	0.74	0.44	0.33	0.31	0.37	0.35	0.32	0.30	0.29	0.28	0.26	0.25	0.23	0.28	0.31	0.31
12	0.52	0.54	0.60	0.66	0.73	0.79	0.87	0.95	1.00	1.00	1.00	1.00	1.00	1.00	1.00	1.00	1.00	1.00	1.00	1.00	1.00	1.00	1.00	1.00	0.80	0.56	0.43	0.41	0.38	0.36	0.34	0.32	0.30	0.28	0.27	0.25	0.24	0.24	0.28	0.30	0.30
11.75	0.51	0.57	0.63	0.69	0.76	0.83	0.91	0.99	1.00	1.00	1.00	1.00	1.00	1.00	1.00	1.00	1.00	1.00	1.00	1.00	1.00	1.00	1.00	1.00	0.82	0.48	0.44	0.42	0.39	0.37	0.35	0.33	0.31	0.29	0.28	0.26	0.25	0.23	0.24	0.30	0.30
11.5	0.54	0.60	0.66	0.72	0.80	0.87	0.95	1.00	1.00	1.00	1.00	1.00	1.00	1.00	1.00	1.00	1.00	1.00	1.00	1.00	1.00	1.00	1.00	0.92	0.71	0.45	0.44	0.41	0.39	0.37	0.34	0.32	0.30	0.29	0.27	0.26	0.24	0.23	0.25	0.31	0.30
11.25	0.57	0.63	0.69	0.76	0.84	0.91	1.00	1.00	1.00	1.00	1.00	1.00	1.00	1.00	1.00	1.00	1.00	1.00	1.00	1.00	1.00	1.00	1.00	0.72	0.44	0.46	0.43	0.41	0.39	0.36	0.34	0.31	0.29	0.28	0.26	0.25	0.23	0.22	0.26	0.29	0.29
11	0.60	0.66	0.73	0.80	0.87	0.95	1.00	1.00	1.00	1.00	1.00	1.00	1.00	1.00	1.00	1.00	1.00	1.00	1.00	1.00	1.00	0.81	0.52	0.33	0.45	0.43	0.39	0.37	0.34	0.32	0.31	0.29	0.27	0.25	0.24	0.23	0.23	0.28	0.28	0.29	0.29
10.75	0.63	0.69	0.76	0.84	0.91	1.00	1.00	1.00	1.00	1.00	1.00	1.00	1.00	1.00	1.00	1.00	1.00	1.00	1.00	1.00	0.89	0.71	0.41	0.46	0.44	0.41	0.39	0.36	0.34	0.31	0.29	0.28	0.26	0.25	0.23	0.22	0.23	0.29	0.28	0.28	0.28
10.5	0.66	0.73	0.80	0.88	0.96	1.00	1.00	1.00	1.00	1.00	1.00	1.00	1.00	1.00	1.00	1.00	1.00	1.00	1.00	1.00	0.79	0.53	0.49	0.45	0.43	0.40	0.37	0.35	0.33	0.31	0.29	0.28	0.25	0.24	0.23	0.22	0.25	0.28	0.28	0.28	0.28
10.25	0.69	0.76	0.84	0.91	1.00	1.00	1.00	1.00	1.00	1.00	1.00	1.00	1.00	1.00	1.00	1.00	1.00	1.00	1.00	1.00	0.81	0.64	0.52	0.49	0.45	0.42	0.39	0.36	0.34	0.32	0.30	0.28	0.27	0.25	0.23	0.22	0.21	0.25	0.28	0.28	0.27	0.27
10	0.73	0.80	0.87	0.96	1.00	1.00	1.00	1.00	1.00	1.00	1.00	1.00	1.00	1.00	1.00	1.00	1.00	1.00	0.90	0.69	0.53	0.50	0.46	0.44	0.41	0.38	0.35	0.34	0.31	0.29	0.28	0.26	0.24	0.23	0.22	0.21	0.26	0.27	0.27	0.27	0.27
9.75	0.76	0.83	0.91	1.00	1.00	1.00	1.00	1.00	1.00	1.00	1.00	1.00	1.00	1.00	1.00	1.00	1.00	1.00	0.76	0.54	0.52	0.49	0.46	0.43	0.39	0.37	0.35	0.33	0.31	0.29	0.27	0.25	0.24	0.23	0.21	0.23	0.27	0.27	0.26	0.27	0.27
9.5	0.80	0.87	0.96	1.00	1.00	1.00	1.00	1.00	1.00	1.00	1.00	1.00	1.00	1.00	1.00	1.00	1.00	1.00	0.51	0.55	0.52	0.49	0.45	0.42	0.39	0.37	0.34	0.32	0.30	0.28	0.26	0.25	0.24	0.22	0.21	0.25	0.27	0.27	0.27	0.27	0.26
9.25	0.83	0.92	1.00	1.00	1.00	1.00	1.00	1.00	1.00	1.00	1.00	1.00	1.00	1.00	1.00	1.00	1.00	0.79	0.57	0.54	0.51	0.47	0.44	0.41	0.39	0.36	0.33	0.31	0.29	0.28	0.26	0.24	0.23	0.22	0.21	0.25	0.27	0.26	0.27	0.26	0.26
9	0.87	0.96	1.00	1.00	1.00	1.00	1.00	1.00	1.00	1.00	1.00	1.00	1.00	1.00	1.00	1.00	1.00	0.61	0.57	0.53	0.49	0.46	0.43	0.40	0.37	0.35	0.32	0.31	0.29	0.27	0.26	0.24	0.22	0.22	0.22	0.27	0.26	0.26	0.26	0.26	0.26
8.75	0.92	1.00	1.00	1.00	1.00	1.00	1.00	1.00	1.00	1.00	1.00	1.00	1.00	1.00	1.00	1.00	0.74	0.59	0.55	0.52	0.49	0.45	0.42	0.39	0.37	0.34	0.32	0.30	0.28	0.26	0.25	0.23	0.22	0.21	0.22	0.27	0.26	0.26	0.26	0.26	0.26
8.5	0.96	1.00	1.00	1.00	1.00	1.00	1.00	1.00	1.00	1.00	1.00	1.00	1.00	1.00	1.00	1.00	0.65	0.59	0.54	0.52	0.48	0.44	0.41	0.39	0.36	0.33	0.31	0.29	0.27	0.26	0.24	0.23	0.22	0.20	0.23	0.26	0.26	0.26	0.26	0.26	0.26
8.25	1.00	1.00	1.00	1.00	1.00	1.00	1.00	1.00	1.00	1.00	1.00	1.00	1.00	1.00	1.00	0.87	0.65	0.59	0.54	0.50	0.47	0.44	0.41	0.38	0.35	0.33	0.31	0.29	0.27	0.25	0.24	0.22	0.21	0.20	0.25	0.26	0.26	0.26	0.26	0.26	0.26
8	1.00	1.00	1.00	1.00	1.00	1.00	1.00	1.00	1.00	1.00	1.00	1.00	1.00	1.00	0.85	0.69	0.65	0.57	0.53	0.49	0.46	0.43	0.40	0.37	0.33	0.32	0.30	0.27	0.27	0.25	0.23	0.22	0.20	0.21	0.25	0.25	0.25	0.26	0.26	0.25	0.25
7.75	1.00	1.00	1.00	1.00	1.00	1.00	1.00	1.00	1.00	1.00	1.00	1.00	1.00	1.00	0.73	0.68	0.63	0.57	0.51	0.47	0.44	0.42	0.39	0.36	0.33	0.31	0.29	0.27	0.26	0.24	0.23	0.21	0.20	0.23	0.25	0.25	0.25	0.25	0.26	0.26	0.25
7.5	1.00	1.00	1.00	1.00	1.00	1.00	1.00	1.00	1.00	1.00	1.00	1.00	0.76	0.75	0.71	0.68	0.62	0.56	0.50	0.46	0.43	0.41	0.38	0.35	0.33	0.30	0.28	0.27	0.25	0.23	0.22	0.21	0.20	0.25	0.25	0.25	0.25	0.24	0.25	0.25	0.25
7.25	1.00	1.00	1.00	1.00	1.00	1.00	1.00	1.00	1.00	1.00	1.00	0.80	0.75	0.75	0.71	0.66	0.60	0.55	0.50	0.45	0.43	0.40	0.37	0.35	0.32	0.30	0.28	0.26	0.24	0.23	0.22	0.20	0.21	0.25	0.25	0.25	0.25	0.25	0.25	0.25	0.25
7	1.00	1.00	1.00	1.00	1.00	1.00	1.00	1.00	1.00	1.00	0.83	0.78	0.74	0.73	0.70	0.65	0.60	0.54	0.49	0.45	0.42	0.39	0.36	0.33	0.32	0.30	0.28	0.25	0.24	0.22	0.21	0.20	0.22	0.25	0.25	0.25	0.25	0.24	0.24	0.25	0.24
6.75	1.00	1.00	1.00	1.00	1.00	1.00	1.00	1.00	1.00	0.87	0.82	0.77	0.74	0.72	0.68	0.64	0.58	0.52	0.48	0.44	0.41	0.38	0.35	0.33	0.30	0.28	0.26	0.25	0.23	0.22	0.20	0.20	0.23	0.25	0.25	0.24	0.24	0.24	0.24	0.24	0.24
6.5	1.00	1.00	1.00	1.00	1.00	1.00	1.00	1.00	0.93	0.85	0.80	0.75	0.75	0.70	0.67	0.63	0.58	0.52	0.47	0.43	0.41	0.37	0.34	0.32	0.30	0.28	0.26	0.24	0.23	0.21	0.20	0.20	0.31	0.25	0.24	0.24	0.24	0.24	0.24	0.24	0.24
6.25	1.00	1.00	1.00	1.00	1.00	1.00	1.00	0.98	0.91	0.83	0.78	0.75	0.73	0.69	0.65	0.62	0.58	0.51	0.46	0.43	0.39	0.37	0.34	0.31	0.29	0.28	0.26	0.24	0.22	0.21	0.20	0.22	0.25	0.25	0.24	0.24	0.24	0.24	0.24	0.24	0.23
6	1.00	1.00	1.00	1.00	1.00	1.00	1.00	0.93	0.87	0.81	0.78	0.73	0.72	0.68	0.64	0.62	0.57	0.51	0.46	0.41	0.38	0.35	0.33	0.31	0.28	0.27	0.25	0.23	0.21	0.20	0.20	0.24	0.25	0.24	0.24	0.24	0.24	0.24	0.24	0.23	0.23
5.75	1.00	1.00	1.00	1.00	1.00	1.00	0.99	0.91	0.85	0.82	0.76	0.71	0.70	0.66	0.63	0.59	0.55	0.50	0.45	0.40	0.37	0.35	0.33	0.30	0.29	0.26	0.24	0.23	0.21	0.20	0.21	0.26	0.24	0.24	0.24	0.24	0.24	0.24	0.23	0.23	0.25
5.5	1.00	1.00	1.00	1.00	1.00	1.00	0.96	0.89	0.83	0.80	0.74	0.75	0.69	0.65	0.62	0.58	0.54	0.50	0.44	0.40	0.36	0.33	0.31	0.29	0.28	0.26	0.24	0.22	0.21	0.20	0.21	0.25	0.24	0.24	0.24	0.24	0.24	0.24	0.24	0.24	0.24
5.25	1.00	1.00	1.00	0.98	0.99	1.00	0.95	0.87	0.83	0.78	0.73	0.73	0.67	0.64	0.61	0.57	0.54	0.49	0.43	0.38	0.35	0.33	0.30	0.28	0.26	0.25	0.24	0.22	0.21	0.19	0.23	0.24	0.24	0.24	0.24	0.24	0.24	0.23	0.23	0.24	0.24
5	0.97	0.95	0.94	0.94	0.97	1.00	0.93	0.85	0.82	0.76	0.71	0.70	0.66	0.63	0.60	0.56	0.53	0.48	0.43	0.38	0.35	0.32	0.30	0.28	0.26	0.24	0.22	0.21	0.20	0.20	0.24	0.24	0.24	0.24	0.24	0.24	0.23	0.23	0.24	0.24	0.23
4.75	0.90	0.90	0.97	0.93	0.95	0.96	0.89	0.85	0.79	0.75	0.70	0.68	0.66	0.62	0.60	0.55	0.52	0.47	0.42	0.38	0.34	0.32	0.29	0.27	0.25	0.24	0.22	0.21	0.20	0.22	0.24	0.24	0.24	0.24	0.24	0.23	0.23	0.24	0.24	0.23	0.24
4.5	0.85	0.96	0.97	0.96	0.94	0.94	0.89	0.83	0.78	0.73	0.68	0.67	0.64	0.62	0.58	0.54	0.51	0.47	0.42	0.38	0.34	0.31	0.29	0.27	0.25	0.23	0.21	0.20	0.19	0.29	0.24	0.24	0.24	0.23	0.24	0.24	0.24	0.24	0.23	0.23	0.24
4.25	0.91	1.00	0.99	0.97	0.92	0.91	0.87	0.81	0.77	0.72	0.67	0.67	0.63	0.60	0.57	0.53	0.50	0.47	0.42	0.37	0.33	0.30	0.28	0.26	0.25	0.23	0.21	0.19	0.20	0.24	0.24	0.24	0.24	0.24	0.23	0.24	0.24	0.23	0.23	0.24	0.24
4	1.00	1.00	0.96	0.96	0.91	0.91	0.85	0.81	0.76	0.70	0.69	0.65	0.62	0.59	0.56	0.51	0.51	0.44	0.41	0.37	0.33	0.30	0.27	0.26	0.24	0.22	0.21	0.19	0.21	0.24	0.24	0.24	0.24	0.23	0.24	0.24	0.23	0.23	0.23	0.23	0.23
3.75	1.00	1.00	0.97	0.93	0.89	0.89	0.83	0.79	0.74	0.69	0.67	0.64	0.61	0.57	0.54	0.54	0.47	0.44	0.40	0.37	0.34	0.29	0.27	0.25	0.23	0.21	0.20	0.19	0.25	0.23	0.23	0.23	0.23	0.23	0.24	0.23	0.23	0.23	0.23	0.23	0.23
3.5	1.00	1.00	0.99	0.91	0.88	0.87	0.82	0.77	0.72	0.68	0.66	0.63	0.59	0.55	0.53	0.49	0.47	0.44	0.39	0.38	0.33	0.29	0.27	0.24	0.23	0.21	0.19	0.19	0.22	0.23	0.23	0.23	0.23	0.24	0.24	0.23	0.23	0.22	0.23	0.23	0.23
3.25	1.00	1.00	0.96	0.90	0.86	0.85	0.79	0.75	0.70	0.67	0.65	0.61	0.58	0.55	0.51	0.48	0.45	0.42	0.43	0.40	0.33	0.30	0.27	0.24	0.22	0.20	0.19	0.20	0.23	0.23	0.23	0.23	0.23	0.24	0.23	0.23	0.23	0.23	0.23	0.23	0.22
3	1.00	1.00	0.96	0.90	0.85	0.82	0.78	0.72	0.67	0.65	0.64	0.60	0.56	0.54	0.50	0.47	0.44	0.44	0.41	0.37	0.35	0.30	0.26	0.24	0.22	0.21	0.19	0.21	0.23	0.23	0.23	0.23	0.24	0.24	0.23	0.23	0.23	0.23	0.23	0.22	0.22

Table 5.7, continued.

MS 14 – W Stolzburg Main Trondhjemite

P [kbar] \ T [°C]	550	560	570	580	590	600	610	620	630	640	650	660	670	680	690	700	710	720	730	740	750	760	770	780	790	800	810	820	830	840	850
15	1.00	1.00	1.00	1.00	1.00	1.00	1.00	1.00	1.00	1.00	1.00	1.00	1.00	1.00	1.00	1.00	1.00	1.00	1.00	1.00	1.00	1.00	1.00	1.00	1.00	1.00	1.00	1.00	1.00	1.00	1.00
14.75	1.00	1.00	1.00	1.00	1.00	1.00	1.00	1.00	1.00	1.00	1.00	1.00	1.00	1.00	1.00	1.00	1.00	1.00	1.00	1.00	1.00	1.00	1.00	1.00	1.00	1.00	1.00	1.00	1.00	1.00	1.00
14.5	1.00	1.00	1.00	1.00	1.00	1.00	1.00	1.00	1.00	1.00	1.00	1.00	1.00	1.00	1.00	1.00	1.00	1.00	1.00	1.00	1.00	1.00	1.00	1.00	1.00	1.00	1.00	1.00	1.00	1.00	1.00
14.25	1.00	1.00	1.00	1.00	1.00	1.00	1.00	1.00	1.00	1.00	1.00	1.00	1.00	1.00	1.00	1.00	1.00	1.00	1.00	1.00	1.00	1.00	1.00	1.00	1.00	1.00	1.00	1.00	1.00	0.89	0.72
14	1.00	1.00	1.00	1.00	1.00	1.00	1.00	1.00	1.00	1.00	1.00	1.00	1.00	1.00	1.00	1.00	1.00	1.00	1.00	1.00	1.00	1.00	1.00	1.00	1.00	1.00	1.00	0.99	0.82	0.65	0.55
13.75	1.00	1.00	1.00	1.00	1.00	1.00	1.00	1.00	1.00	1.00	1.00	1.00	1.00	1.00	1.00	1.00	1.00	1.00	1.00	1.00	1.00	1.00	1.00	1.00	1.00	1.00	0.83	0.74	0.53	0.46	0.46
13.5	1.00	1.00	1.00	1.00	1.00	1.00	1.00	1.00	1.00	1.00	1.00	1.00	1.00	1.00	1.00	1.00	1.00	1.00	1.00	1.00	1.00	1.00	1.00	1.00	1.00	0.81	0.68	0.52	0.45	0.36	0.36
13.25	1.00	1.00	1.00	1.00	1.00	1.00	1.00	1.00	1.00	1.00	1.00	1.00	1.00	1.00	1.00	1.00	1.00	1.00	1.00	1.00	1.00	1.00	1.00	1.00	0.81	0.57	0.42	0.41	0.36	0.26	0.22
13	1.00	1.00	1.00	1.00	1.00	1.00	1.00	1.00	1.00	1.00	1.00	1.00	1.00	1.00	1.00	1.00	1.00	1.00	1.00	1.00	1.00	1.00	1.00	0.91	0.58	0.40	0.30	0.36	0.23	0.27	0.26
12.75	1.00	1.00	1.00	1.00	1.00	1.00	1.00	1.00	1.00	1.00	1.00	1.00	1.00	1.00	1.00	1.00	1.00	1.00	1.00	1.00	1.00	1.00	1.00	0.63	0.40	0.23	0.31	0.29	0.28	0.26	0.26
12.5	1.00	1.00	1.00	1.00	1.00	1.00	1.00	1.00	1.00	1.00	1.00	1.00	1.00	1.00	1.00	1.00	1.00	1.00	1.00	1.00	1.00	1.00	0.78	0.54	0.35	0.32	0.30	0.28	0.27	0.26	0.25
12.25	1.00	1.00	1.00	1.00	1.00	1.00	1.00	1.00	1.00	1.00	1.00	1.00	1.00	1.00	1.00	1.00	1.00	1.00	1.00	1.00	1.00	0.76	0.59	0.39	0.34	0.32	0.30	0.28	0.26	0.25	0.24
12	1.00	1.00	1.00	1.00	1.00	1.00	1.00	1.00	1.00	1.00	1.00	1.00	1.00	1.00	1.00	1.00	1.00	1.00	1.00	1.00	1.00	0.62	0.44	0.36	0.33	0.32	0.29	0.28	0.26	0.25	0.23
11.75	1.00	1.00	1.00	1.00	1.00	1.00	1.00	1.00	1.00	1.00	1.00	1.00	1.00	1.00	1.00	1.00	1.00	1.00	1.00	1.00	0.61	0.49	0.37	0.35	0.33	0.31	0.28	0.27	0.26	0.24	0.23
11.5	1.00	1.00	1.00	1.00	1.00	1.00	1.00	1.00	1.00	1.00	1.00	1.00	1.00	1.00	1.00	1.00	1.00	1.00	1.00	0.74	0.48	0.39	0.37	0.34	0.32	0.31	0.29	0.27	0.25	0.24	0.22
11.25	1.00	1.00	1.00	1.00	1.00	1.00	1.00	1.00	1.00	1.00	1.00	1.00	1.00	1.00	1.00	1.00	1.00	1.00	0.81	0.60	0.42	0.38	0.36	0.34	0.31	0.29	0.28	0.26	0.25	0.23	0.22
11	1.00	1.00	1.00	1.00	1.00	1.00	1.00	1.00	1.00	1.00	1.00	1.00	1.00	1.00	1.00	1.00	1.00	1.00	0.72	0.48	0.39	0.38	0.36	0.33	0.32	0.29	0.28	0.26	0.25	0.23	0.21
10.75	1.00	1.00	1.00	1.00	1.00	1.00	1.00	1.00	1.00	1.00	1.00	1.00	1.00	1.00	1.00	1.00	1.00	1.00	0.71	0.54	0.41	0.39	0.38	0.36	0.33	0.30	0.29	0.27	0.26	0.24	0.23	0.21
10.5	1.00	1.00	1.00	1.00	1.00	1.00	1.00	1.00	1.00	1.00	1.00	1.00	1.00	1.00	1.00	1.00	1.00	0.85	0.61	0.44	0.41	0.40	0.37	0.34	0.32	0.30	0.29	0.27	0.25	0.24	0.22	0.21
10.25	1.00	1.00	1.00	1.00	1.00	1.00	1.00	1.00	1.00	1.00	1.00	1.00	1.00	1.00	1.00	1.00	0.55	0.47	0.44	0.42	0.40	0.36	0.34	0.31	0.29	0.28	0.26	0.25	0.23	0.22	0.20
10	1.00	1.00	1.00	1.00	1.00	1.00	1.00	1.00	1.00	1.00	1.00	1.00	1.00	1.00	1.00	0.71	0.35	0.46	0.44	0.42	0.40	0.37	0.33	0.31	0.29	0.27	0.26	0.24	0.23	0.21	0.20
9.75	1.00	1.00	1.00	1.00	1.00	1.00	1.00	1.00	1.00	1.00	1.00	1.00	1.00	1.00	0.70	0.53	0.49	0.46	0.43	0.41	0.38	0.36	0.33	0.30	0.28	0.27	0.25	0.24	0.22	0.21	0.20
9.5	1.00	1.00	1.00	1.00	1.00	1.00	1.00	1.00	1.00	1.00	1.00	1.00	1.00	0.98	0.56	0.51	0.48	0.45	0.43	0.41	0.38	0.35	0.32	0.29	0.28	0.26	0.25	0.23	0.22	0.20	0.19
9.25	1.00	1.00	1.00	1.00	1.00	1.00	1.00	1.00	1.00	1.00	1.00	1.00	1.00	0.64	0.53	0.50	0.48	0.45	0.43	0.39	0.38	0.35	0.32	0.29	0.27	0.26	0.24	0.23	0.21	0.20	0.19
9	1.00	1.00	1.00	1.00	1.00	1.00	1.00	1.00	1.00	1.00	1.00	1.00	0.79	0.44	0.53	0.50	0.47	0.45	0.42	0.40	0.38	0.34	0.32	0.28	0.27	0.26	0.24	0.22	0.21	0.20	0.18
8.75	1.00	1.00	1.00	1.00	1.00	1.00	1.00	1.00	1.00	1.00	1.00	0.93	0.44	0.55	0.52	0.49	0.47	0.44	0.41	0.38	0.37	0.33	0.31	0.28	0.26	0.25	0.23	0.22	0.20	0.19	0.18
8.5	1.00	1.00	1.00	1.00	1.00	1.00	1.00	1.00	1.00	1.00	1.00	0.60	0.59	0.55	0.52	0.49	0.46	0.44	0.40	0.37	0.35	0.33	0.30	0.28	0.26	0.25	0.23	0.21	0.20	0.19	0.18
8.25	1.00	1.00	1.00	1.00	1.00	1.00	1.00	1.00	1.00	1.00	0.63	0.60	0.58	0.54	0.51	0.49	0.46	0.43	0.40	0.37	0.35	0.32	0.30	0.28	0.26	0.24	0.22	0.21	0.20	0.18	0.17
8	1.00	1.00	1.00	1.00	1.00	1.00	1.00	1.00	1.00	0.65	0.62	0.59	0.58	0.54	0.51	0.48	0.45	0.41	0.39	0.37	0.34	0.31	0.29	0.28	0.25	0.24	0.22	0.20	0.19	0.18	0.17
7.75	1.00	1.00	1.00	1.00	1.00	1.00	1.00	0.53	0.68	0.64	0.61	0.59	0.58	0.56	0.50	0.48	0.44	0.41	0.38	0.36	0.34	0.31	0.29	0.27	0.25	0.23	0.21	0.20	0.19	0.18	0.18
7.5	1.00	1.00	1.00	1.00	1.00	1.00	0.60	0.71	0.67	0.64	0.61	0.58	0.58	0.55	0.48	0.47	0.43	0.40	0.37	0.35	0.33	0.30	0.29	0.27	0.25	0.23	0.21	0.20	0.19	0.18	0.19
7.25	1.00	1.00	1.00	1.00	1.00	0.96	0.74	0.70	0.66	0.63	0.60	0.58	0.55	0.52	0.48	0.45	0.42	0.39	0.37	0.35	0.32	0.29	0.27	0.27	0.25	0.23	0.21	0.19	0.18	0.18	0.21
7	1.00	1.00	1.00	1.00	1.00	0.78	0.73	0.69	0.66	0.63	0.60	0.57	0.55	0.54	0.49	0.45	0.41	0.38	0.36	0.34	0.31	0.29	0.28	0.25	0.24	0.23	0.20	0.19	0.18	0.17	0.21
6.75	1.00	1.00	1.00	1.00	0.82	0.78	0.73	0.69	0.65	0.62	0.59	0.57	0.53	0.52	0.48	0.44	0.41	0.38	0.36	0.33	0.30	0.28	0.27	0.25	0.23	0.22	0.20	0.18	0.18	0.18	0.21
6.5	1.00	1.00	1.00	0.85	0.81	0.77	0.73	0.68	0.65	0.62	0.59	0.55	0.53	0.51	0.47	0.43	0.41	0.37	0.35	0.32	0.30	0.28	0.26	0.24	0.24	0.22	0.20	0.18	0.17	0.18	0.20
6.25	1.00	1.00	0.92	0.85	0.80	0.74	0.72	0.68	0.64	0.60	0.57	0.55	0.52	0.50	0.46	0.44	0.39	0.37	0.34	0.31	0.29	0.27	0.26	0.24	0.23	0.21	0.19	0.18	0.17	0.20	0.20
6	1.00	0.96	0.91	0.83	0.78	0.77	0.73	0.66	0.63	0.61	0.59	0.54	0.51	0.49	0.45	0.43	0.40	0.36	0.33	0.30	0.28	0.26	0.25	0.23	0.22	0.20	0.19	0.18	0.16	0.21	0.20
5.75	0.98	0.95	0.87	0.82	0.78	0.72	0.68	0.67	0.63	0.62	0.57	0.54	0.51	0.47	0.45	0.42	0.39	0.36	0.32	0.30	0.28	0.26	0.24	0.23	0.21	0.20	0.19	0.17	0.17	0.20	0.20
5.5	0.99	0.91	0.86	0.81	0.77	0.73	0.69	0.66	0.63	0.61	0.58	0.54	0.50	0.46	0.44	0.41	0.38	0.35	0.32	0.29	0.27	0.25	0.24	0.22	0.21	0.19	0.18	0.17	0.20	0.20	0.20
5.25	0.95	0.90	0.85	0.80	0.76	0.72	0.69	0.66	0.63	0.61	0.58	0.53	0.49	0.45	0.43	0.40	0.37	0.34	0.31	0.28	0.26	0.25	0.23	0.21	0.20	0.19	0.18	0.17	0.20	0.20	0.20
5	0.94	0.89	0.84	0.80	0.75	0.72	0.68	0.65	0.61	0.60	0.58	0.55	0.48	0.44	0.42	0.39	0.37	0.34	0.31	0.28	0.27	0.24	0.23	0.21	0.20	0.18	0.17	0.17	0.20	0.20	0.20
4.75	0.93	0.88	0.83	0.79	0.75	0.71	0.68	0.63	0.60	0.57	0.55	0.53	0.48	0.43	0.40	0.38	0.36	0.33	0.30	0.27	0.25	0.23	0.22	0.21	0.19	0.18	0.16	0.18	0.19	0.19	0.19
4.5	0.92	0.87	0.82	0.78	0.74	0.70	0.65	0.62	0.59	0.57	0.54	0.52	0.50	0.43	0.40	0.37	0.35	0.32	0.30	0.27	0.25	0.23	0.22	0.20	0.18	0.17	0.16	0.20	0.19	0.19	0.19
4.25	0.88	0.86	0.81	0.77	0.73	0.69	0.65	0.62	0.59	0.56	0.54	0.52	0.46	0.42	0.39	0.36	0.34	0.31	0.29	0.27	0.24	0.22	0.21	0.19	0.18	0.17	0.16	0.20	0.19	0.19	0.19
4	0.90	0.85	0.80	0.76	0.72	0.67	0.64	0.61	0.58	0.56	0.53	0.51	0.48	0.41	0.38	0.35	0.33	0.30	0.28	0.26	0.24	0.22	0.20	0.19	0.17	0.17	0.18	0.19	0.19	0.19	0.19
3.75	0.89	0.84	0.79	0.75	0.69	0.67	0.64	0.60	0.58	0.55	0.54	0.50	0.49	0.41	0.37	0.34	0.31	0.30	0.27	0.25	0.24	0.22	0.20	0.19	0.17	0.16	0.19	0.19	0.19	0.19	0.19
3.5	0.86	0.81	0.75	0.71	0.69	0.66	0.63	0.60	0.58	0.55	0.52	0.48	0.48	0.40	0.36	0.33	0.30	0.29	0.26	0.24	0.23	0.21	0.19	0.18	0.17	0.16	0.19	0.19	0.19	0.19	0.19
3.25	0.85	0.80	0.75	0.71	0.68	0.65	0.62	0.60	0.57	0.55	0.50	0.49	0.46	0.40	0.36	0.32	0.30	0.28	0.26	0.24	0.22	0.20	0.19	0.18	0.16	0.17	0.19	0.19	0.19	0.19	0.18
3	0.83	0.81	0.75	0.71	0.68	0.65	0.62	0.59	0.56	0.52	0.48	0.48	0.44	0.42	0.36	0.31	0.29	0.27	0.25	0.23	0.21	0.20	0.19	0.17	0.16	0.19	0.19	0.18	0.18	0.18	0.18

Table 5.7, continued.

MS 15 – Central Stolzburg Main Trondhjemite

P [kbar] \ T [°C]	550.00	560.00	570.00	580.00	590.00	600.00	610.00	620.00	630.00	640.00	650.00	660.00	670.00	680.00	690.00	700.00	710.00	720.00	730.00	740.00	750.00	760.00	770.00	780.00	790.00	800.00	810.00	820.00	830.00	840.00	850.00
15.00	1.00	1.00	1.00	1.00	1.00	1.00	1.00	1.00	1.00	1.00	1.00	1.00	1.00	1.00	1.00	1.00	1.00	1.00	1.00	1.00	1.00	1.00	1.00	1.00	1.00	1.00	1.00	1.00	1.00	1.00	1.00
14.75	1.00	1.00	1.00	1.00	1.00	1.00	1.00	1.00	1.00	1.00	1.00	1.00	1.00	1.00	1.00	1.00	1.00	1.00	1.00	1.00	1.00	1.00	1.00	1.00	1.00	1.00	1.00	1.00	1.00	1.00	0.92
14.50	1.00	1.00	1.00	1.00	1.00	1.00	1.00	1.00	1.00	1.00	1.00	1.00	1.00	1.00	1.00	1.00	1.00	1.00	1.00	1.00	1.00	1.00	1.00	1.00	1.00	1.00	1.00	1.00	0.99	0.73	0.65
14.25	1.00	1.00	1.00	1.00	1.00	1.00	1.00	1.00	1.00	1.00	1.00	1.00	1.00	1.00	1.00	1.00	1.00	1.00	1.00	1.00	1.00	1.00	1.00	1.00	1.00	1.00	1.00	0.74	0.70	0.64	0.58
14.00	1.00	1.00	1.00	1.00	1.00	1.00	1.00	1.00	1.00	1.00	1.00	1.00	1.00	1.00	1.00	1.00	1.00	1.00	1.00	1.00	1.00	1.00	1.00	1.00	1.00	1.00	0.82	0.58	0.52	0.56	0.44
13.75	1.00	1.00	1.00	1.00	1.00	1.00	1.00	1.00	1.00	1.00	1.00	1.00	1.00	1.00	1.00	1.00	1.00	1.00	1.00	1.00	1.00	1.00	1.00	1.00	1.00	0.85	0.55	0.56	0.43	0.39	0.37
13.50	1.00	1.00	1.00	1.00	1.00	1.00	1.00	1.00	1.00	1.00	1.00	1.00	1.00	1.00	1.00	1.00	1.00	1.00	1.00	1.00	1.00	1.00	1.00	1.00	1.00	0.61	0.40	0.40	0.33	0.21	0.19
13.25	1.00	1.00	1.00	1.00	1.00	1.00	1.00	1.00	1.00	1.00	1.00	1.00	1.00	1.00	1.00	1.00	1.00	1.00	1.00	1.00	1.00	1.00	1.00	1.00	0.68	0.46	0.29	0.27	0.30	0.28	0.27
13.00	1.00	1.00	1.00	1.00	1.00	1.00	1.00	1.00	1.00	1.00	1.00	1.00	1.00	1.00	1.00	1.00	1.00	1.00	1.00	1.00	1.00	1.00	1.00	1.00	0.48	0.27	0.16	0.30	0.30	0.27	0.26
12.75	1.00	1.00	1.00	1.00	1.00	1.00	1.00	1.00	1.00	1.00	1.00	1.00	1.00	1.00	1.00	1.00	1.00	1.00	1.00	1.00	1.00	1.00	1.00	0.52	0.28	0.32	0.31	0.30	0.28	0.27	0.26
12.50	1.00	1.00	1.00	1.00	1.00	1.00	1.00	1.00	1.00	1.00	1.00	1.00	1.00	1.00	1.00	1.00	1.00	1.00	1.00	1.00	1.00	1.00	0.64	0.38	0.34	0.32	0.30	0.29	0.28	0.27	0.25
12.25	1.00	1.00	1.00	1.00	1.00	1.00	1.00	1.00	1.00	1.00	1.00	1.00	1.00	1.00	1.00	1.00	1.00	1.00	1.00	1.00	1.00	0.99	0.35	0.35	0.33	0.31	0.29	0.28	0.28	0.25	0.24
12.00	1.00	1.00	1.00	1.00	1.00	1.00	1.00	1.00	1.00	1.00	1.00	1.00	1.00	1.00	1.00	1.00	1.00	1.00	1.00	1.00	1.00	0.43	0.37	0.35	0.33	0.31	0.29	0.28	0.26	0.25	0.23
11.75	1.00	1.00	1.00	1.00	1.00	1.00	1.00	1.00	1.00	1.00	1.00	1.00	1.00	1.00	1.00	1.00	1.00	1.00	1.00	1.00	1.00	0.53	0.38	0.36	0.34	0.33	0.31	0.28	0.27	0.25	0.24	0.23
11.50	1.00	1.00	1.00	1.00	1.00	1.00	1.00	1.00	1.00	1.00	1.00	1.00	1.00	1.00	1.00	1.00	1.00	1.00	1.00	1.00	0.56	0.35	0.38	0.36	0.34	0.32	0.30	0.28	0.27	0.25	0.24	0.22
11.25	1.00	1.00	1.00	1.00	1.00	1.00	1.00	1.00	1.00	1.00	1.00	1.00	1.00	1.00	1.00	1.00	1.00	1.00	0.60	0.32	0.40	0.38	0.35	0.33	0.32	0.30	0.28	0.27	0.25	0.23	0.22
11.00	1.00	1.00	1.00	1.00	1.00	1.00	1.00	1.00	1.00	1.00	1.00	1.00	1.00	1.00	1.00	1.00	1.00	0.81	0.41	0.42	0.39	0.37	0.35	0.34	0.31	0.29	0.28	0.26	0.25	0.23	0.21
10.75	1.00	1.00	1.00	1.00	1.00	1.00	1.00	1.00	1.00	1.00	1.00	1.00	1.00	1.00	1.00	1.00	1.00	0.43	0.43	0.41	0.39	0.37	0.34	0.33	0.31	0.29	0.28	0.26	0.24	0.23	0.21
10.50	1.00	1.00	1.00	1.00	1.00	1.00	1.00	1.00	1.00	1.00	1.00	1.00	1.00	1.00	1.00	1.00	0.39	0.44	0.43	0.41	0.39	0.36	0.34	0.32	0.30	0.29	0.27	0.26	0.24	0.22	0.21
10.25	1.00	1.00	1.00	1.00	1.00	1.00	1.00	1.00	1.00	1.00	1.00	1.00	1.00	1.00	1.00	0.54	0.25	0.45	0.42	0.41	0.38	0.36	0.34	0.32	0.30	0.28	0.27	0.25	0.24	0.22	0.20
10.00	1.00	1.00	1.00	1.00	1.00	1.00	1.00	1.00	1.00	1.00	1.00	1.00	1.00	1.00	0.72	0.51	0.48	0.45	0.42	0.40	0.37	0.35	0.33	0.31	0.29	0.28	0.26	0.25	0.23	0.21	0.20
9.75	1.00	1.00	1.00	1.00	1.00	1.00	1.00	1.00	1.00	1.00	1.00	1.00	1.00	0.73	0.62	0.51	0.47	0.45	0.43	0.39	0.37	0.35	0.33	0.31	0.29	0.28	0.26	0.25	0.23	0.21	0.20
9.50	1.00	1.00	1.00	1.00	1.00	1.00	1.00	1.00	1.00	1.00	1.00	1.00	1.00	0.51	0.51	0.49	0.46	0.45	0.42	0.40	0.37	0.34	0.32	0.30	0.30	0.28	0.25	0.24	0.22	0.21	0.20
9.25	1.00	1.00	1.00	1.00	1.00	1.00	1.00	1.00	1.00	1.00	1.00	1.00	0.61	0.54	0.51	0.48	0.47	0.44	0.42	0.39	0.36	0.34	0.32	0.30	0.29	0.27	0.25	0.24	0.22	0.21	0.19
9.00	1.00	1.00	1.00	1.00	1.00	1.00	1.00	1.00	1.00	1.00	1.00	0.62	0.57	0.54	0.50	0.48	0.46	0.44	0.41	0.39	0.35	0.34	0.31	0.29	0.28	0.27	0.25	0.23	0.21	0.20	0.19
8.75	1.00	1.00	1.00	1.00	1.00	1.00	1.00	1.00	1.00	1.00	0.59	0.59	0.55	0.53	0.50	0.48	0.46	0.43	0.40	0.38	0.35	0.34	0.31	0.29	0.28	0.26	0.25	0.23	0.21	0.20	0.18
8.50	1.00	1.00	1.00	1.00	1.00	1.00	1.00	1.00	1.00	0.67	0.63	0.59	0.56	0.52	0.50	0.48	0.45	0.42	0.40	0.37	0.34	0.33	0.30	0.29	0.27	0.25	0.24	0.22	0.21	0.20	0.18
8.25	1.00	1.00	1.00	1.00	1.00	1.00	1.00	1.00	0.69	0.66	0.63	0.60	0.56	0.52	0.50	0.47	0.45	0.42	0.39	0.37	0.34	0.32	0.30	0.29	0.27	0.26	0.24	0.22	0.20	0.20	0.18
8.00	1.00	1.00	1.00	1.00	1.00	1.00	1.00	0.80	0.69	0.65	0.62	0.59	0.56	0.54	0.49	0.47	0.44	0.41	0.38	0.36	0.34	0.32	0.29	0.28	0.26	0.25	0.24	0.22	0.20	0.19	0.18
7.75	1.00	1.00	1.00	1.00	1.00	1.00	1.00	0.71	0.68	0.65	0.62	0.59	0.55	0.52	0.49	0.46	0.43	0.40	0.38	0.36	0.33	0.31	0.29	0.28	0.26	0.25	0.23	0.21	0.20	0.19	0.17
7.50	1.00	1.00	1.00	1.00	1.00	1.00	0.75	0.71	0.67	0.64	0.61	0.58	0.54	0.52	0.49	0.45	0.42	0.40	0.38	0.35	0.33	0.31	0.29	0.27	0.26	0.24	0.22	0.21	0.19	0.18	0.17
7.25	1.00	1.00	1.00	1.00	1.00	0.78	0.74	0.70	0.67	0.63	0.61	0.58	0.54	0.50	0.49	0.45	0.42	0.39	0.37	0.35	0.32	0.30	0.28	0.27	0.25	0.24	0.22	0.20	0.19	0.17	0.16
7.00	1.00	1.00	1.00	1.00	0.83	0.78	0.73	0.69	0.66	0.63	0.60	0.57	0.53	0.51	0.48	0.44	0.41	0.39	0.36	0.35	0.32	0.30	0.28	0.26	0.25	0.23	0.21	0.20	0.19	0.18	0.17
6.75	1.00	1.00	1.00	0.85	0.80	0.78	0.74	0.69	0.65	0.62	0.60	0.57	0.53	0.51	0.47	0.43	0.40	0.38	0.35	0.34	0.32	0.29	0.27	0.25	0.24	0.22	0.21	0.20	0.18	0.17	0.19
6.50	1.00	1.00	0.91	0.84	0.80	0.77	0.73	0.68	0.65	0.62	0.59	0.55	0.53	0.50	0.46	0.43	0.39	0.37	0.36	0.33	0.30	0.28	0.27	0.25	0.23	0.22	0.20	0.19	0.18	0.17	0.23
6.25	1.00	0.95	0.90	0.85	0.80	0.74	0.72	0.69	0.63	0.61	0.58	0.55	0.53	0.48	0.45	0.42	0.39	0.37	0.35	0.33	0.30	0.28	0.27	0.24	0.23	0.21	0.20	0.19	0.17	0.16	0.21
6.00	1.00	0.91	0.89	0.81	0.77	0.75	0.72	0.66	0.63	0.60	0.58	0.55	0.53	0.47	0.44	0.41	0.38	0.36	0.34	0.32	0.29	0.28	0.26	0.24	0.22	0.21	0.19	0.18	0.17	0.16	0.21
5.75	0.98	0.90	0.85	0.80	0.76	0.73	0.67	0.65	0.62	0.60	0.58	0.55	0.50	0.47	0.43	0.40	0.38	0.35	0.34	0.32	0.29	0.27	0.25	0.24	0.22	0.20	0.19	0.18	0.17	0.19	0.20
5.50	0.97	0.89	0.84	0.80	0.75	0.72	0.68	0.65	0.62	0.60	0.56	0.54	0.49	0.46	0.44	0.40	0.37	0.35	0.33	0.31	0.29	0.27	0.25	0.23	0.21	0.20	0.19	0.17	0.16	0.21	0.20
5.25	0.96	0.90	0.83	0.79	0.76	0.73	0.68	0.64	0.62	0.59	0.57	0.54	0.48	0.45	0.43	0.40	0.36	0.35	0.32	0.30	0.28	0.26	0.24	0.23	0.21	0.19	0.18	0.17	0.16	0.20	0.20
5.00	0.95	0.89	0.83	0.78	0.76	0.72	0.68	0.64	0.59	0.57	0.55	0.54	0.47	0.45	0.42	0.39	0.35	0.34	0.32	0.30	0.27	0.26	0.24	0.22	0.20	0.19	0.17	0.16	0.17	0.20	0.20
4.75	0.93	0.88	0.83	0.79	0.75	0.71	0.68	0.63	0.59	0.56	0.54	0.50	0.46	0.44	0.40	0.38	0.36	0.33	0.31	0.29	0.27	0.25	0.23	0.21	0.20	0.19	0.17	0.16	0.20	0.20	0.20
4.50	0.92	0.87	0.82	0.78	0.74	0.70	0.66	0.62	0.59	0.55	0.53	0.50	0.47	0.43	0.39	0.37	0.35	0.33	0.30	0.29	0.27	0.25	0.23	0.21	0.20	0.18	0.17	0.16	0.20	0.19	0.20
4.25	0.91	0.86	0.81	0.77	0.73	0.70	0.65	0.62	0.59	0.56	0.53	0.50	0.47	0.42	0.40	0.38	0.34	0.32	0.29	0.27	0.26	0.24	0.22	0.20	0.19	0.18	0.17	0.17	0.20	0.20	0.19
4.00	0.90	0.85	0.81	0.76	0.73	0.67	0.64	0.61	0.59	0.56	0.53	0.50	0.46	0.42	0.38	0.36	0.34	0.31	0.29	0.27	0.25	0.24	0.22	0.20	0.18	0.17	0.16	0.27	0.19	0.20	0.19
3.75	0.89	0.84	0.80	0.72	0.69	0.67	0.64	0.61	0.58	0.56	0.53	0.50	0.49	0.38	0.39	0.36	0.33	0.30	0.28	0.26	0.24	0.23	0.21	0.19	0.18	0.17	0.16	0.19	0.19	0.19	0.19
3.50	0.84	0.80	0.76	0.72	0.69	0.66	0.63	0.60	0.58	0.56	0.53	0.48	0.48	0.39	0.38	0.35	0.32	0.29	0.27	0.26	0.24	0.22	0.20	0.19	0.17	0.16	0.18	0.19	0.19	0.19	0.19
3.25	0.85	0.80	0.75	0.71	0.69	0.65	0.63	0.60	0.58	0.55	0.50	0.47	0.46	0.40	0.37	0.35	0.31	0.28	0.26	0.25	0.23	0.21	0.20	0.18	0.17	0.16	0.19	0.19	0.19	0.19	0.19
3.00	0.84	0.79	0.75	0.71	0.68	0.65	0.62	0.60	0.57	0.52	0.49	0.48	0.44	0.40	0.36	0.33	0.31	0.28	0.25	0.24	0.22	0.21	0.19	0.18	0.17	0.16	0.19	0.19	0.19	0.18	0.18

Table 5.7, continued.

MS 24 – SE Stolzburg trondhjemite dyke

P [kbar] \ T [°C]	550.00	560.00	570.00	580.00	590.00	600.00	610.00	620.00	630.00	640.00	650.00	660.00	670.00	680.00	690.00	700.00	710.00	720.00	730.00	740.00	750.00	760.00	770.00	780.00	790.00	800.00	810.00	820.00	830.00	840.00	850.00
15.00	1.00	1.00	1.00	1.00	1.00	1.00	1.00	1.00	1.00	1.00	1.00	1.00	1.00	1.00	1.00	1.00	1.00	1.00	1.00	1.00	1.00	1.00	1.00	1.00	1.00	1.00	1.00	1.00	1.00	1.00	1.00
14.75	1.00	1.00	1.00	1.00	1.00	1.00	1.00	1.00	1.00	1.00	1.00	1.00	1.00	1.00	1.00	1.00	1.00	1.00	1.00	1.00	1.00	1.00	1.00	1.00	1.00	1.00	1.00	1.00	1.00	1.00	1.00
14.50	1.00	1.00	1.00	1.00	1.00	1.00	1.00	1.00	1.00	1.00	1.00	1.00	1.00	1.00	1.00	1.00	1.00	1.00	1.00	1.00	1.00	1.00	1.00	1.00	1.00	1.00	1.00	1.00	1.00	1.00	1.00
14.25	1.00	1.00	1.00	1.00	1.00	1.00	1.00	1.00	1.00	1.00	1.00	1.00	1.00	1.00	1.00	1.00	1.00	1.00	1.00	1.00	1.00	1.00	1.00	1.00	1.00	1.00	1.00	1.00	1.00	1.00	1.00
14.00	1.00	1.00	1.00	1.00	1.00	1.00	1.00	1.00	1.00	1.00	1.00	1.00	1.00	1.00	1.00	1.00	1.00	1.00	1.00	1.00	1.00	1.00	1.00	1.00	1.00	1.00	1.00	1.00	1.00	0.98	0.78
13.75	1.00	1.00	1.00	1.00	1.00	1.00	1.00	1.00	1.00	1.00	1.00	1.00	1.00	1.00	1.00	1.00	1.00	1.00	1.00	1.00	1.00	1.00	1.00	1.00	1.00	1.00	1.00	1.00	0.88	0.69	0.56
13.50	1.00	1.00	1.00	1.00	1.00	1.00	1.00	1.00	1.00	1.00	1.00	1.00	1.00	1.00	1.00	1.00	1.00	1.00	1.00	1.00	1.00	1.00	1.00	1.00	1.00	1.00	0.84	0.75	0.59	0.51	0.49
13.25	1.00	1.00	1.00	1.00	1.00	1.00	1.00	1.00	1.00	1.00	1.00	1.00	1.00	1.00	1.00	1.00	1.00	1.00	1.00	1.00	1.00	1.00	1.00	1.00	1.00	0.74	0.73	0.55	0.46	0.40	0.32
13.00	1.00	1.00	1.00	1.00	1.00	1.00	1.00	1.00	1.00	1.00	1.00	1.00	1.00	1.00	1.00	1.00	1.00	1.00	1.00	1.00	1.00	1.00	1.00	1.00	0.89	0.47	0.57	0.39	0.31	0.21	0.34
12.75	1.00	1.00	1.00	1.00	1.00	1.00	1.00	1.00	1.00	1.00	1.00	1.00	1.00	1.00	1.00	1.00	1.00	1.00	1.00	1.00	1.00	1.00	1.00	1.00	0.56	0.38	0.26	0.40	0.38	0.36	0.33
12.50	1.00	1.00	1.00	1.00	1.00	1.00	1.00	1.00	1.00	1.00	1.00	1.00	1.00	1.00	1.00	1.00	1.00	1.00	1.00	1.00	1.00	1.00	1.00	0.63	0.44	0.43	0.41	0.38	0.37	0.35	0.33
12.25	1.00	1.00	1.00	1.00	1.00	1.00	1.00	1.00	1.00	1.00	1.00	1.00	1.00	1.00	1.00	1.00	1.00	1.00	1.00	1.00	1.00	1.00	0.76	0.45	0.44	0.42	0.40	0.38	0.37	0.35	0.32
12.00	1.00	1.00	1.00	1.00	1.00	1.00	1.00	1.00	1.00	1.00	1.00	1.00	1.00	1.00	1.00	1.00	1.00	1.00	1.00	1.00	1.00	0.89	0.60	0.48	0.44	0.42	0.41	0.38	0.36	0.34	0.32
11.75	1.00	1.00	1.00	1.00	1.00	1.00	1.00	1.00	1.00	1.00	1.00	1.00	1.00	1.00	1.00	1.00	1.00	1.00	1.00	1.00	1.00	0.58	0.50	0.46	0.44	0.42	0.40	0.38	0.36	0.33	0.32
11.50	1.00	1.00	1.00	1.00	1.00	1.00	1.00	1.00	1.00	1.00	1.00	1.00	1.00	1.00	1.00	1.00	1.00	1.00	1.00	1.00	0.77	0.52	0.48	0.46	0.43	0.41	0.39	0.37	0.35	0.33	0.30
11.25	1.00	1.00	1.00	1.00	1.00	1.00	1.00	1.00	1.00	1.00	1.00	1.00	1.00	1.00	1.00	1.00	1.00	1.00	1.00	0.79	0.39	0.51	0.49	0.45	0.43	0.40	0.39	0.37	0.34	0.33	0.30
11.00	1.00	1.00	1.00	1.00	1.00	1.00	1.00	1.00	1.00	1.00	1.00	1.00	1.00	1.00	1.00	1.00	1.00	1.00	0.83	0.47	0.53	0.51	0.49	0.46	0.42	0.39	0.39	0.36	0.34	0.32	0.30
10.75	1.00	1.00	1.00	1.00	1.00	1.00	1.00	1.00	1.00	1.00	1.00	1.00	1.00	1.00	1.00	1.00	1.00	1.00	0.52	0.55	0.53	0.51	0.49	0.45	0.41	0.40	0.38	0.35	0.33	0.32	0.30
10.50	1.00	1.00	1.00	1.00	1.00	1.00	1.00	1.00	1.00	1.00	1.00	1.00	1.00	1.00	1.00	1.00	1.00	0.77	0.58	0.55	0.53	0.50	0.48	0.45	0.41	0.39	0.37	0.35	0.32	0.31	0.30
10.25	1.00	1.00	1.00	1.00	1.00	1.00	1.00	1.00	1.00	1.00	1.00	1.00	1.00	1.00	1.00	1.00	0.67	0.61	0.57	0.55	0.52	0.50	0.48	0.44	0.41	0.39	0.36	0.35	0.32	0.30	0.29
10.00	1.00	1.00	1.00	1.00	1.00	1.00	1.00	1.00	1.00	1.00	1.00	1.00	1.00	1.00	1.00	0.73	0.64	0.59	0.57	0.54	0.52	0.50	0.47	0.44	0.40	0.37	0.36	0.34	0.31	0.30	0.29
9.75	1.00	1.00	1.00	1.00	1.00	1.00	1.00	1.00	1.00	1.00	1.00	1.00	1.00	1.00	1.00	0.47	0.64	0.60	0.56	0.54	0.52	0.49	0.46	0.43	0.40	0.38	0.35	0.33	0.31	0.30	0.28
9.50	1.00	1.00	1.00	1.00	1.00	1.00	1.00	1.00	1.00	1.00	1.00	1.00	1.00	1.00	0.75	0.67	0.64	0.61	0.56	0.54	0.51	0.48	0.45	0.42	0.39	0.37	0.35	0.32	0.31	0.29	0.28
9.25	1.00	1.00	1.00	1.00	1.00	1.00	1.00	1.00	1.00	1.00	1.00	1.00	1.00	0.65	0.69	0.66	0.63	0.59	0.56	0.53	0.51	0.47	0.44	0.42	0.39	0.36	0.34	0.32	0.30	0.29	0.27
9.00	1.00	1.00	1.00	1.00	1.00	1.00	1.00	1.00	1.00	1.00	1.00	1.00	0.74	0.72	0.69	0.66	0.63	0.58	0.55	0.53	0.50	0.47	0.44	0.41	0.38	0.36	0.33	0.32	0.30	0.28	0.27
8.75	1.00	1.00	1.00	1.00	1.00	1.00	1.00	1.00	1.00	1.00	1.00	0.63	0.75	0.72	0.68	0.65	0.62	0.58	0.55	0.53	0.49	0.46	0.43	0.41	0.37	0.35	0.33	0.31	0.29	0.27	0.26
8.50	1.00	1.00	1.00	1.00	1.00	1.00	1.00	1.00	1.00	1.00	0.63	0.79	0.75	0.71	0.68	0.65	0.62	0.59	0.55	0.52	0.48	0.45	0.42	0.41	0.37	0.34	0.32	0.31	0.29	0.27	0.25
8.25	1.00	1.00	1.00	1.00	1.00	1.00	1.00	1.00	1.00	0.99	0.82	0.78	0.74	0.71	0.68	0.65	0.62	0.57	0.54	0.51	0.47	0.44	0.41	0.39	0.36	0.34	0.32	0.30	0.28	0.27	0.25
8.00	1.00	1.00	1.00	1.00	1.00	1.00	1.00	1.00	1.00	0.85	0.84	0.77	0.74	0.70	0.67	0.64	0.60	0.57	0.54	0.52	0.46	0.43	0.41	0.38	0.36	0.33	0.32	0.29	0.27	0.26	0.24
7.75	1.00	1.00	1.00	1.00	1.00	1.00	1.00	1.00	0.90	0.87	0.80	0.80	0.73	0.70	0.67	0.61	0.59	0.57	0.54	0.49	0.45	0.43	0.40	0.39	0.35	0.32	0.31	0.29	0.27	0.25	0.24
7.50	1.00	1.00	1.00	1.00	1.00	1.00	1.00	0.96	0.91	0.87	0.80	0.78	0.73	0.69	0.64	0.62	0.59	0.55	0.53	0.48	0.45	0.42	0.40	0.38	0.35	0.33	0.31	0.28	0.28	0.25	0.23
7.25	1.00	1.00	1.00	1.00	1.00	1.00	1.00	0.95	0.90	0.86	0.80	0.76	0.72	0.67	0.64	0.61	0.58	0.54	0.52	0.47	0.44	0.41	0.39	0.37	0.34	0.33	0.30	0.28	0.26	0.25	0.23
7.00	1.00	1.00	1.00	1.00	1.00	1.00	0.99	0.94	0.89	0.85	0.81	0.78	0.69	0.67	0.64	0.61	0.57	0.55	0.51	0.46	0.43	0.40	0.39	0.37	0.33	0.32	0.30	0.28	0.26	0.24	0.22
6.75	1.00	1.00	1.00	1.00	1.00	1.00	0.98	0.93	0.88	0.84	0.79	0.76	0.70	0.66	0.63	0.60	0.56	0.54	0.50	0.45	0.42	0.39	0.38	0.36	0.33	0.30	0.30	0.28	0.26	0.23	0.22
6.50	1.00	1.00	1.00	1.00	1.00	1.00	0.94	0.92	0.87	0.81	0.77	0.75	0.69	0.66	0.63	0.59	0.55	0.51	0.49	0.44	0.41	0.39	0.37	0.35	0.33	0.30	0.29	0.27	0.25	0.22	0.22
6.25	1.00	1.00	1.00	1.00	1.00	0.98	0.96	0.88	0.84	0.80	0.78	0.75	0.68	0.65	0.62	0.58	0.54	0.52	0.48	0.43	0.41	0.38	0.37	0.34	0.32	0.31	0.28	0.26	0.24	0.22	0.21
6.00	1.00	1.00	1.00	1.00	1.00	1.00	0.92	0.87	0.84	0.80	0.77	0.74	0.68	0.65	0.61	0.57	0.53	0.51	0.47	0.43	0.40	0.39	0.36	0.33	0.31	0.29	0.28	0.26	0.24	0.22	0.22
5.75	1.00	1.00	1.00	1.00	1.00	0.96	0.91	0.87	0.83	0.80	0.77	0.73	0.68	0.63	0.60	0.56	0.52	0.50	0.46	0.42	0.39	0.38	0.35	0.33	0.30	0.29	0.27	0.25	0.24	0.22	0.25
5.50	1.00	1.00	1.00	1.00	1.00	0.95	0.90	0.86	0.82	0.79	0.76	0.73	0.67	0.62	0.59	0.55	0.53	0.49	0.46	0.41	0.39	0.37	0.34	0.32	0.30	0.28	0.26	0.24	0.22	0.21	0.26
5.25	1.00	1.00	1.00	1.00	0.99	0.94	0.89	0.85	0.83	0.79	0.75	0.72	0.67	0.62	0.57	0.54	0.51	0.48	0.45	0.40	0.38	0.36	0.34	0.31	0.29	0.27	0.25	0.23	0.22	0.21	0.26
5.00	1.00	1.00	1.00	1.00	0.98	0.93	0.89	0.83	0.79	0.75	0.72	0.69	0.66	0.61	0.56	0.52	0.50	0.47	0.44	0.39	0.38	0.34	0.32	0.31	0.28	0.27	0.25	0.23	0.21	0.24	0.25
4.75	1.00	1.00	1.00	1.00	0.97	0.92	0.88	0.82	0.78	0.74	0.71	0.68	0.66	0.59	0.55	0.51	0.49	0.46	0.43	0.39	0.36	0.34	0.31	0.30	0.28	0.25	0.24	0.22	0.21	0.25	0.25
4.50	1.00	1.00	1.00	1.00	0.96	0.91	0.85	0.81	0.77	0.74	0.71	0.68	0.64	0.58	0.54	0.50	0.48	0.45	0.42	0.39	0.36	0.33	0.31	0.29	0.27	0.25	0.23	0.22	0.20	0.25	0.25
4.25	1.00	1.00	1.00	1.00	0.95	0.90	0.84	0.80	0.76	0.73	0.70	0.67	0.64	0.57	0.53	0.49	0.47	0.44	0.41	0.38	0.35	0.32	0.30	0.28	0.26	0.24	0.22	0.21	0.25	0.25	0.25
4.00	1.00	1.00	1.00	0.99	0.94	0.87	0.83	0.79	0.76	0.72	0.70	0.68	0.65	0.57	0.52	0.50	0.46	0.44	0.41	0.37	0.34	0.31	0.29	0.27	0.26	0.23	0.22	0.21	0.25	0.24	0.24
3.75	1.00	1.00	1.00	0.97	0.91	0.86	0.82	0.78	0.75	0.73	0.70	0.68	0.63	0.56	0.51	0.48	0.45	0.42	0.40	0.37	0.33	0.30	0.28	0.26	0.25	0.23	0.22	0.20	0.25	0.24	0.24
3.50	1.00	1.00	1.00	0.96	0.90	0.86	0.82	0.78	0.75	0.72	0.70	0.65	0.63	0.54	0.51	0.48	0.44	0.41	0.38	0.36	0.32	0.29	0.28	0.26	0.24	0.23	0.21	0.23	0.24	0.24	0.24
3.25	1.00	1.00	1.00	0.95	0.92	0.85	0.80	0.78	0.75	0.74	0.68	0.63	0.61	0.54	0.51	0.47	0.43	0.41	0.37	0.35	0.32	0.29	0.27	0.25	0.23	0.22	0.20	0.24	0.24	0.24	0.24
3.00	1.00	1.00	0.99	0.96	0.91	0.85	0.81	0.77	0.76	0.70	0.65	0.63	0.59	0.55	0.50	0.45	0.41	0.38	0.36	0.34	0.31	0.28	0.26	0.24	0.23	0.21	0.22	0.23	0.23	0.23	0.23

Table 5.7, continued.

MS 25 – Weergevonden diorite

P [kbar] \ T [°C]	550.00	560.00	570.00	580.00	590.00	600.00	610.00	620.00	630.00	640.00	650.00	660.00	670.00	680.00	690.00	700.00	710.00	720.00	730.00	740.00	750.00	760.00	770.00	780.00	790.00	800.00	810.00	820.00	830.00	840.00	850.00
15.00	1.00	1.00	1.00	1.00	1.00	1.00	1.00	1.00	1.00	1.00	1.00	1.00	1.00	1.00	1.00	1.00	1.00	1.00	1.00	1.00	1.00	1.00	1.00	1.00	1.00	1.00	1.00	1.00	1.00	1.00	1.00
14.75	1.00	1.00	1.00	1.00	1.00	1.00	1.00	1.00	1.00	1.00	1.00	1.00	1.00	1.00	1.00	1.00	1.00	1.00	1.00	1.00	1.00	1.00	1.00	1.00	1.00	1.00	1.00	1.00	1.00	1.00	1.00
14.50	1.00	1.00	1.00	1.00	1.00	1.00	1.00	1.00	1.00	1.00	1.00	1.00	1.00	1.00	1.00	1.00	1.00	1.00	1.00	1.00	1.00	1.00	1.00	1.00	1.00	1.00	1.00	1.00	1.00	1.00	1.00
14.25	1.00	1.00	1.00	1.00	1.00	1.00	1.00	1.00	1.00	1.00	1.00	1.00	1.00	1.00	1.00	1.00	1.00	1.00	1.00	1.00	1.00	1.00	1.00	1.00	1.00	1.00	1.00	1.00	1.00	1.00	1.00
14.00	1.00	1.00	1.00	1.00	1.00	1.00	1.00	1.00	1.00	1.00	1.00	1.00	1.00	1.00	1.00	1.00	1.00	1.00	1.00	1.00	1.00	1.00	1.00	1.00	1.00	1.00	1.00	1.00	1.00	1.00	1.00
13.75	1.00	1.00	1.00	1.00	1.00	1.00	1.00	1.00	1.00	1.00	1.00	1.00	1.00	1.00	1.00	1.00	1.00	1.00	1.00	1.00	1.00	1.00	1.00	1.00	1.00	1.00	1.00	1.00	1.00	1.00	1.00
13.50	1.00	1.00	1.00	1.00	1.00	1.00	1.00	1.00	1.00	1.00	1.00	1.00	1.00	1.00	1.00	1.00	1.00	1.00	1.00	1.00	1.00	1.00	1.00	1.00	1.00	1.00	1.00	1.00	1.00	1.00	1.00
13.25	1.00	1.00	1.00	1.00	1.00	1.00	1.00	1.00	1.00	1.00	1.00	1.00	1.00	1.00	1.00	1.00	1.00	1.00	1.00	1.00	1.00	1.00	1.00	1.00	1.00	1.00	1.00	1.00	1.00	1.00	1.00
13.00	1.00	1.00	1.00	1.00	1.00	1.00	1.00	1.00	1.00	1.00	1.00	1.00	1.00	1.00	1.00	1.00	1.00	1.00	1.00	1.00	1.00	1.00	1.00	1.00	1.00	1.00	1.00	1.00	1.00	1.00	1.00
12.75	1.00	1.00	1.00	1.00	1.00	1.00	1.00	1.00	1.00	1.00	1.00	1.00	1.00	1.00	1.00	1.00	1.00	1.00	1.00	1.00	1.00	1.00	1.00	1.00	1.00	1.00	1.00	1.00	1.00	1.00	1.00
12.50	1.00	1.00	1.00	1.00	1.00	1.00	1.00	1.00	1.00	1.00	1.00	1.00	1.00	1.00	1.00	1.00	1.00	1.00	1.00	1.00	1.00	1.00	1.00	1.00	1.00	1.00	1.00	1.00	1.00	1.00	1.00
12.25	1.00	1.00	1.00	1.00	1.00	1.00	1.00	1.00	1.00	1.00	1.00	1.00	1.00	1.00	1.00	1.00	1.00	1.00	1.00	1.00	1.00	1.00	1.00	1.00	1.00	1.00	1.00	1.00	1.00	1.00	1.00
12.00	1.00	1.00	1.00	1.00	1.00	1.00	1.00	1.00	1.00	1.00	1.00	1.00	1.00	1.00	1.00	1.00	1.00	1.00	1.00	1.00	1.00	1.00	1.00	1.00	1.00	1.00	1.00	1.00	1.00	1.00	1.00
11.75	1.00	1.00	1.00	1.00	1.00	1.00	1.00	1.00	1.00	1.00	1.00	1.00	1.00	1.00	1.00	1.00	1.00	1.00	1.00	1.00	1.00	1.00	1.00	1.00	1.00	1.00	1.00	1.00	1.00	1.00	1.00
11.50	1.00	1.00	1.00	1.00	1.00	1.00	1.00	1.00	1.00	1.00	1.00	1.00	1.00	1.00	1.00	1.00	1.00	1.00	1.00	1.00	1.00	1.00	1.00	1.00	1.00	1.00	1.00	1.00	1.00	1.00	1.00
11.25	1.00	1.00	1.00	1.00	1.00	1.00	1.00	1.00	1.00	1.00	1.00	1.00	1.00	1.00	1.00	1.00	1.00	1.00	1.00	1.00	1.00	1.00	1.00	1.00	1.00	1.00	1.00	1.00	1.00	1.00	1.00
11.00	1.00	1.00	1.00	1.00	1.00	1.00	1.00	1.00	1.00	1.00	1.00	1.00	1.00	1.00	1.00	1.00	1.00	1.00	1.00	1.00	1.00	1.00	1.00	1.00	1.00	1.00	1.00	0.95	0.89	0.95	1.00
10.75	1.00	1.00	1.00	1.00	1.00	1.00	1.00	1.00	1.00	1.00	1.00	1.00	1.00	1.00	1.00	1.00	1.00	1.00	1.00	1.00	1.00	1.00	1.00	1.00	1.00	1.00	0.99	0.93	1.00	0.92	0.83
10.50	1.00	1.00	1.00	1.00	1.00	1.00	1.00	1.00	1.00	1.00	1.00	1.00	1.00	1.00	1.00	1.00	1.00	1.00	1.00	1.00	1.00	1.00	1.00	1.00	1.00	0.96	0.77	0.77	0.91	0.86	0.88
10.25	1.00	1.00	1.00	1.00	1.00	1.00	1.00	1.00	1.00	1.00	1.00	1.00	1.00	1.00	1.00	1.00	1.00	1.00	1.00	1.00	1.00	1.00	1.00	1.00	0.91	0.81	0.73	0.68	0.81	0.85	0.83
10.00	1.00	1.00	1.00	1.00	1.00	1.00	1.00	1.00	1.00	1.00	1.00	1.00	1.00	1.00	1.00	1.00	1.00	1.00	1.00	1.00	1.00	1.00	0.99	0.97	0.77	0.67	0.62	0.75	0.60	0.77	0.69
9.75	1.00	1.00	1.00	1.00	1.00	1.00	1.00	1.00	1.00	1.00	1.00	1.00	1.00	1.00	1.00	1.00	1.00	1.00	1.00	1.00	1.00	0.97	0.95	0.86	0.75	0.48	0.51	0.59	0.72	0.66	0.82
9.50	1.00	1.00	1.00	1.00	1.00	1.00	1.00	1.00	1.00	1.00	1.00	1.00	1.00	1.00	1.00	1.00	1.00	1.00	1.00	1.00	1.00	0.87	0.68	0.83	0.66	0.48	0.69	0.71	0.61	0.76	0.81
9.25	1.00	1.00	1.00	1.00	1.00	1.00	1.00	1.00	1.00	1.00	1.00	1.00	1.00	1.00	1.00	1.00	1.00	1.00	1.00	0.96	0.66	0.63	0.68	0.51	0.47	0.51	0.50	0.55	0.49	0.64	0.84
9.00	1.00	1.00	1.00	1.00	1.00	1.00	1.00	1.00	1.00	1.00	1.00	1.00	1.00	1.00	1.00	1.00	1.00	0.98	0.83	0.88	0.85	0.52	0.68	0.48	0.49	0.49	0.54	0.51	0.57	0.55	0.83
8.75	1.00	1.00	1.00	1.00	1.00	1.00	1.00	1.00	1.00	1.00	1.00	1.00	1.00	1.00	1.00	1.00	1.00	0.95	0.74	0.69	0.74	0.66	0.57	0.48	0.49	0.50	0.55	0.50	0.66	0.69	0.79
8.50	1.00	1.00	1.00	1.00	1.00	1.00	1.00	1.00	1.00	1.00	1.00	1.00	1.00	1.00	1.00	1.00	1.00	0.91	0.83	0.54	0.51	0.49	0.58	0.50	0.49	0.49	0.50	0.50	0.62	0.62	0.83
8.25	1.00	1.00	1.00	1.00	1.00	1.00	1.00	1.00	1.00	1.00	1.00	1.00	1.00	1.00	1.00	1.00	0.99	0.82	0.74	0.53	0.51	0.48	0.57	0.45	0.49	0.53	0.48	0.49	0.50	0.56	0.86
8.00	1.00	1.00	1.00	1.00	1.00	1.00	1.00	1.00	1.00	1.00	1.00	1.00	1.00	1.00	1.00	1.00	0.94	0.61	0.67	0.53	0.50	0.49	0.49	0.45	0.50	0.49	0.49	0.50	0.56	0.60	0.86
7.75	1.00	1.00	1.00	1.00	1.00	1.00	1.00	1.00	1.00	1.00	1.00	1.00	1.00	1.00	1.00	0.97	0.89	0.63	0.55	0.52	0.49	0.48	0.48	0.45	0.49	0.49	0.47	0.48	0.59	0.71	1.00
7.50	1.00	1.00	1.00	1.00	1.00	1.00	1.00	1.00	1.00	1.00	1.00	1.00	1.00	1.00	0.99	0.93	0.87	0.71	0.64	0.58	0.52	0.49	0.43	0.44	0.48	0.49	0.48	0.49	0.58	0.65	0.90
7.25	1.00	1.00	1.00	1.00	1.00	1.00	1.00	1.00	1.00	1.00	1.00	1.00	1.00	1.00	0.92	0.80	0.81	0.67	0.54	0.51	0.48	0.49	0.43	0.44	0.48	0.47	0.48	0.48	0.61	0.74	1.00
7.00	1.00	1.00	1.00	1.00	1.00	1.00	1.00	1.00	1.00	1.00	1.00	1.00	1.00	0.89	0.88	0.85	0.79	0.69	0.53	0.50	0.49	0.48	0.43	0.47	0.48	0.48	0.47	0.48	0.52	0.73	1.00
6.75	1.00	1.00	1.00	1.00	1.00	1.00	1.00	1.00	1.00	1.00	1.00	1.00	1.00	0.95	0.85	0.83	0.78	0.69	0.52	0.49	0.49	0.48	0.43	0.47	0.47	0.47	0.47	0.55	0.66	0.79	1.00
6.50	1.00	1.00	1.00	1.00	1.00	1.00	1.00	1.00	1.00	1.00	1.00	1.00	0.92	0.92	0.87	0.79	0.74	0.68	0.55	0.48	0.47	0.47	0.44	0.47	0.46	0.48	0.46	0.47	0.64	0.97	1.00
6.25	1.00	1.00	1.00	1.00	1.00	1.00	1.00	1.00	1.00	1.00	1.00	0.98	0.98	0.89	0.83	0.77	0.74	0.69	0.54	0.47	0.46	0.47	0.46	0.43	0.46	0.47	0.47	0.47	0.81	0.99	1.00
6.00	1.00	1.00	1.00	1.00	1.00	1.00	1.00	1.00	1.00	1.00	1.00	1.00	0.93	0.87	0.82	0.75	0.72	0.66	0.55	0.47	0.47	0.47	0.46	0.44	0.46	0.46	0.46	0.58	0.81	1.00	1.00
5.75	1.00	1.00	1.00	1.00	1.00	1.00	1.00	1.00	1.00	1.00	1.00	0.99	0.93	0.86	0.80	0.75	0.69	0.66	0.56	0.48	0.46	0.46	0.46	0.45	0.46	0.44	0.46	0.61	0.86	1.00	1.00
5.50	1.00	1.00	1.00	1.00	1.00	1.00	1.00	1.00	1.00	1.00	1.00	0.96	0.87	0.84	0.79	0.74	0.67	0.65	0.57	0.46	0.46	0.46	0.46	0.45	0.45	0.46	0.52	0.65	1.00	1.00	1.00
5.25	1.00	1.00	1.00	1.00	1.00	1.00	1.00	1.00	1.00	1.00	1.00	0.96	0.88	0.81	0.77	0.72	0.69	0.63	0.58	0.46	0.45	0.45	0.45	0.45	0.46	0.45	0.53	0.75	1.00	1.00	1.00
5.00	1.00	1.00	1.00	1.00	1.00	1.00	1.00	1.00	1.00	1.00	1.00	0.92	0.86	0.79	0.75	0.70	0.66	0.62	0.58	0.47	0.46	0.45	0.44	0.45	0.45	0.45	0.58	0.95	1.00	1.00	1.00
4.75	1.00	1.00	1.00	1.00	1.00	1.00	1.00	1.00	1.00	1.00	0.97	0.90	0.83	0.78	0.74	0.69	0.63	0.60	0.57	0.48	0.44	0.44	0.44	0.44	0.46	0.46	0.57	0.93	1.00	1.00	1.00
4.50	1.00	1.00	1.00	1.00	1.00	1.00	1.00	1.00	1.00	0.99	0.94	0.87	0.82	0.76	0.70	0.66	0.67	0.64	0.57	0.48	0.44	0.45	0.44	0.45	0.44	0.45	0.75	1.00	1.00	1.00	1.00
4.25	1.00	1.00	1.00	1.00	1.00	1.00	1.00	1.00	1.00	0.98	0.92	0.86	0.78	0.72	0.74	0.70	0.67	0.62	0.57	0.49	0.44	0.44	0.43	0.45	0.44	0.46	0.76	1.00	1.00	1.00	1.00
4.00	1.00	1.00	1.00	1.00	1.00	1.00	1.00	1.00	1.00	0.95	0.90	0.83	0.83	0.78	0.73	0.69	0.65	0.61	0.57	0.50	0.43	0.43	0.44	0.43	0.45	0.70	0.97	1.00	1.00	1.00	1.00
3.75	1.00	1.00	1.00	1.00	1.00	1.00	1.00	1.00	1.00	0.97	0.92	0.86	0.81	0.75	0.70	0.67	0.63	0.51	0.47	0.45	0.43	0.42	0.43	0.43	0.45	0.68	1.00	1.00	1.00	1.00	1.00
3.50	1.00	1.00	1.00	1.00	1.00	1.00	1.00	1.00	1.00	0.97	0.90	0.85	0.79	0.74	0.70	0.65	0.62	0.49	0.46	0.43	0.40	0.42	0.43	0.44	0.45	0.78	1.00	1.00	1.00	1.00	1.00
3.25	1.00	1.00	1.00	1.00	1.00	1.00	1.00	1.00	1.00	0.94	0.88	0.82	0.77	0.73	0.68	0.66	0.51	0.47	0.44	0.42	0.40	0.42	0.43	0.45	0.53	0.87	1.00	1.00	1.00	1.00	1.00
3.00	1.00	1.00	1.00	1.00	1.00	1.00	1.00	1.00	0.99	0.92	0.87	0.80	0.76	0.71	0.66	0.62	0.58	0.46	0.44	0.41	0.40	0.41	0.44	0.44	0.64	1.00	1.00	1.00	1.00	1.00	0.99

Table 5.7, continued.

MS 27 – Weergevonden Main Trondhjemite

P [kbar] \ T [°C]	550.00	560.00	570.00	580.00	590.00	600.00	610.00	620.00	630.00	640.00	650.00	660.00	670.00	680.00	690.00	700.00	710.00	720.00	730.00	740.00	750.00	760.00	770.00	780.00	790.00	800.00	810.00	820.00	830.00	840.00	850.00
15.00	1.00	1.00	1.00	1.00	1.00	1.00	1.00	1.00	1.00	1.00	1.00	1.00	1.00	1.00	1.00	1.00	1.00	1.00	1.00	1.00	1.00	1.00	1.00	1.00	1.00	1.00	1.00	1.00	1.00	1.00	1.00
14.75	1.00	1.00	1.00	1.00	1.00	1.00	1.00	1.00	1.00	1.00	1.00	1.00	1.00	1.00	1.00	1.00	1.00	1.00	1.00	1.00	1.00	1.00	1.00	1.00	1.00	1.00	1.00	1.00	1.00	1.00	1.00
14.50	1.00	1.00	1.00	1.00	1.00	1.00	1.00	1.00	1.00	1.00	1.00	1.00	1.00	1.00	1.00	1.00	1.00	1.00	1.00	1.00	1.00	1.00	1.00	1.00	1.00	1.00	1.00	1.00	1.00	1.00	1.00
14.25	1.00	1.00	1.00	1.00	1.00	1.00	1.00	1.00	1.00	1.00	1.00	1.00	1.00	1.00	1.00	1.00	1.00	1.00	1.00	1.00	1.00	1.00	1.00	1.00	1.00	1.00	1.00	1.00	1.00	0.90	0.82
14.00	1.00	1.00	1.00	1.00	1.00	1.00	1.00	1.00	1.00	1.00	1.00	1.00	1.00	1.00	1.00	1.00	1.00	1.00	1.00	1.00	1.00	1.00	1.00	1.00	1.00	1.00	1.00	1.00	0.77	0.67	0.68
13.75	1.00	1.00	1.00	1.00	1.00	1.00	1.00	1.00	1.00	1.00	1.00	1.00	1.00	1.00	1.00	1.00	1.00	1.00	1.00	1.00	1.00	1.00	1.00	1.00	1.00	1.00	0.88	0.89	0.63	0.47	0.55
13.50	1.00	1.00	1.00	1.00	1.00	1.00	1.00	1.00	1.00	1.00	1.00	1.00	1.00	1.00	1.00	1.00	1.00	1.00	1.00	1.00	1.00	1.00	1.00	1.00	1.00	0.79	1.00	0.90	0.89	0.82	0.44
13.25	1.00	1.00	1.00	1.00	1.00	1.00	1.00	1.00	1.00	1.00	1.00	1.00	1.00	1.00	1.00	1.00	1.00	1.00	1.00	1.00	1.00	1.00	1.00	1.00	1.00	1.00	1.00	0.98	0.37	0.35	0.31
13.00	1.00	1.00	1.00	1.00	1.00	1.00	1.00	1.00	1.00	1.00	1.00	1.00	1.00	1.00	1.00	1.00	1.00	1.00	1.00	1.00	1.00	1.00	1.00	1.00	1.00	1.00	0.43	0.34	0.30	0.29	0.29
12.75	1.00	1.00	1.00	1.00	1.00	1.00	1.00	1.00	1.00	1.00	1.00	1.00	1.00	1.00	1.00	1.00	1.00	1.00	1.00	1.00	1.00	1.00	1.00	1.00	0.45	0.37	0.33	0.26	0.28	0.27	0.14
12.50	1.00	1.00	1.00	1.00	1.00	1.00	1.00	1.00	1.00	1.00	1.00	1.00	1.00	1.00	1.00	1.00	1.00	1.00	1.00	1.00	0.90	0.54	0.63	0.37	0.26	0.32	0.28	0.17	0.20	0.21	0.20
12.25	1.00	1.00	1.00	1.00	1.00	1.00	1.00	1.00	1.00	1.00	1.00	1.00	1.00	1.00	1.00	1.00	1.00	1.00	1.00	1.00	0.80	0.64	0.38	0.37	0.25	0.25	0.23	0.22	0.21	0.19	0.18
12.00	1.00	1.00	1.00	1.00	1.00	1.00	1.00	1.00	1.00	1.00	1.00	1.00	1.00	1.00	1.00	1.00	1.00	1.00	1.00	0.87	0.67	0.48	0.39	0.27	0.25	0.24	0.23	0.22	0.20	0.19	0.18
11.75	1.00	1.00	1.00	1.00	1.00	1.00	1.00	1.00	1.00	1.00	1.00	1.00	1.00	1.00	1.00	1.00	1.00	1.00	0.93	0.75	0.57	0.40	0.28	0.27	0.25	0.23	0.22	0.21	0.19	0.19	0.18
11.50	1.00	1.00	1.00	1.00	1.00	1.00	1.00	1.00	1.00	1.00	1.00	1.00	1.00	1.00	1.00	1.00	1.00	1.00	0.78	0.61	0.42	0.31	0.28	0.27	0.24	0.22	0.21	0.20	0.19	0.18	0.16
11.25	1.00	1.00	1.00	1.00	1.00	1.00	1.00	1.00	1.00	1.00	1.00	1.00	1.00	1.00	1.00	1.00	1.00	0.86	0.60	0.51	0.34	0.29	0.27	0.25	0.24	0.22	0.21	0.19	0.18	0.17	0.16
11.00	1.00	1.00	1.00	1.00	1.00	1.00	1.00	1.00	1.00	1.00	1.00	1.00	1.00	1.00	1.00	1.00	0.95	0.61	0.54	0.34	0.30	0.28	0.26	0.24	0.23	0.21	0.20	0.19	0.18	0.17	0.16
10.75	1.00	1.00	1.00	1.00	1.00	1.00	1.00	1.00	1.00	1.00	1.00	1.00	1.00	1.00	1.00	0.97	0.77	0.53	0.42	0.32	0.30	0.27	0.25	0.23	0.23	0.21	0.20	0.18	0.17	0.16	0.16
10.50	1.00	1.00	1.00	1.00	1.00	1.00	1.00	1.00	1.00	1.00	1.00	1.00	1.00	1.00	1.00	0.84	0.48	0.39	0.33	0.31	0.29	0.26	0.25	0.24	0.22	0.21	0.19	0.18	0.17	0.16	0.15
10.25	1.00	1.00	1.00	1.00	1.00	1.00	1.00	1.00	1.00	1.00	1.00	1.00	1.00	1.00	0.92	0.71	0.47	0.37	0.31	0.29	0.28	0.26	0.24	0.23	0.21	0.20	0.19	0.18	0.17	0.16	0.15
10.00	1.00	1.00	1.00	1.00	1.00	1.00	1.00	1.00	1.00	1.00	1.00	1.00	1.00	0.99	0.78	0.47	0.27	0.33	0.31	0.29	0.27	0.25	0.24	0.22	0.21	0.20	0.19	0.18	0.16	0.15	0.15
9.75	1.00	1.00	1.00	1.00	1.00	1.00	1.00	1.00	1.00	1.00	1.00	1.00	1.00	0.86	0.60	0.48	0.35	0.32	0.30	0.28	0.26	0.25	0.24	0.22	0.20	0.19	0.17	0.17	0.16	0.15	0.14
9.50	1.00	1.00	1.00	1.00	1.00	1.00	1.00	1.00	1.00	1.00	1.00	1.00	0.93	0.70	0.50	0.36	0.33	0.32	0.30	0.27	0.26	0.25	0.23	0.22	0.20	0.18	0.17	0.16	0.16	0.15	0.14
9.25	1.00	1.00	1.00	1.00	1.00	1.00	1.00	1.00	1.00	1.00	1.00	1.00	0.76	0.52	0.36	0.35	0.34	0.31	0.29	0.27	0.26	0.24	0.22	0.21	0.20	0.18	0.17	0.16	0.15	0.14	0.14
9.00	1.00	1.00	1.00	1.00	1.00	1.00	1.00	1.00	1.00	1.00	1.00	1.00	0.52	0.47	0.37	0.35	0.33	0.31	0.28	0.27	0.25	0.23	0.22	0.20	0.20	0.18	0.17	0.16	0.15	0.14	0.13
8.75	1.00	1.00	1.00	1.00	1.00	1.00	1.00	1.00	1.00	1.00	1.00	0.66	0.34	0.39	0.36	0.35	0.32	0.30	0.28	0.26	0.24	0.22	0.21	0.19	0.18	0.17	0.16	0.15	0.14	0.13	0.14
8.50	1.00	1.00	1.00	1.00	1.00	1.00	1.00	1.00	1.00	1.00	1.00	0.53	0.37	0.39	0.36	0.34	0.31	0.29	0.28	0.26	0.24	0.22	0.20	0.19	0.18	0.17	0.16	0.15	0.14	0.13	0.14
8.25	1.00	1.00	1.00	1.00	1.00	1.00	1.00	1.00	1.00	1.00	0.68	0.43	0.40	0.38	0.36	0.33	0.30	0.29	0.27	0.25	0.23	0.22	0.20	0.19	0.17	0.16	0.15	0.15	0.14	0.13	0.17
8.00	1.00	1.00	1.00	1.00	1.00	1.00	1.00	1.00	1.00	0.80	0.44	0.42	0.39	0.38	0.35	0.32	0.30	0.28	0.26	0.24	0.23	0.21	0.20	0.18	0.17	0.16	0.15	0.14	0.13	0.13	0.17
7.75	1.00	1.00	1.00	1.00	1.00	1.00	1.00	1.00	0.74	0.46	0.43	0.41	0.39	0.37	0.34	0.31	0.29	0.27	0.25	0.24	0.22	0.21	0.19	0.18	0.17	0.16	0.15	0.14	0.13	0.14	0.18
7.50	1.00	1.00	1.00	1.00	1.00	1.00	1.00	0.62	0.48	0.45	0.43	0.41	0.38	0.36	0.33	0.31	0.29	0.27	0.24	0.23	0.21	0.20	0.18	0.17	0.16	0.16	0.14	0.14	0.13	0.17	0.17
7.25	1.00	1.00	1.00	1.00	1.00	1.00	0.62	0.51	0.47	0.44	0.42	0.39	0.37	0.35	0.32	0.31	0.28	0.26	0.24	0.22	0.21	0.19	0.18	0.17	0.16	0.15	0.14	0.13	0.12	0.20	0.18
7.00	1.00	1.00	1.00	1.00	1.00	0.72	0.53	0.49	0.46	0.44	0.41	0.39	0.37	0.34	0.32	0.30	0.27	0.26	0.24	0.22	0.20	0.19	0.18	0.17	0.16	0.15	0.14	0.13	0.14	0.17	0.17
6.75	1.00	1.00	1.00	1.00	0.75	0.54	0.51	0.48	0.45	0.43	0.40	0.38	0.36	0.33	0.31	0.28	0.27	0.25	0.23	0.22	0.20	0.19	0.17	0.16	0.16	0.15	0.14	0.13	0.15	0.17	0.17
6.50	1.00	1.00	1.00	0.91	0.58	0.53	0.50	0.47	0.45	0.42	0.39	0.37	0.35	0.33	0.30	0.28	0.26	0.24	0.23	0.21	0.20	0.18	0.17	0.16	0.15	0.14	0.13	0.12	0.17	0.17	0.17
6.25	1.00	1.00	0.59	0.61	0.57	0.52	0.49	0.47	0.44	0.41	0.39	0.37	0.35	0.32	0.30	0.28	0.25	0.24	0.22	0.21	0.19	0.18	0.17	0.16	0.15	0.14	0.13	0.13	0.17	0.16	0.16
6.00	1.00	0.89	0.64	0.60	0.56	0.51	0.47	0.45	0.43	0.40	0.38	0.36	0.34	0.31	0.29	0.27	0.25	0.22	0.21	0.20	0.19	0.18	0.16	0.15	0.14	0.13	0.12	0.14	0.16	0.16	0.16
5.75	1.00	0.67	0.61	0.57	0.54	0.50	0.46	0.44	0.42	0.39	0.37	0.35	0.33	0.31	0.28	0.26	0.24	0.22	0.21	0.19	0.18	0.17	0.16	0.15	0.14	0.13	0.12	0.17	0.16	0.16	0.16
5.50	0.70	0.65	0.59	0.55	0.53	0.50	0.45	0.44	0.41	0.38	0.36	0.34	0.33	0.30	0.27	0.25	0.24	0.22	0.20	0.19	0.18	0.17	0.16	0.14	0.14	0.13	0.13	0.27	0.16	0.16	0.16
5.25	0.68	0.64	0.58	0.56	0.52	0.48	0.45	0.43	0.40	0.38	0.35	0.33	0.32	0.29	0.27	0.25	0.23	0.22	0.20	0.19	0.17	0.16	0.15	0.14	0.13	0.13	0.13	0.16	0.16	0.16	0.16
5.00	0.67	0.62	0.57	0.54	0.51	0.47	0.44	0.42	0.40	0.37	0.35	0.33	0.31	0.29	0.26	0.24	0.23	0.21	0.20	0.18	0.17	0.16	0.15	0.14	0.13	0.13	0.15	0.16	0.16	0.16	0.16
4.75	0.64	0.59	0.57	0.53	0.49	0.47	0.43	0.41	0.39	0.36	0.34	0.32	0.31	0.28	0.26	0.24	0.22	0.21	0.19	0.18	0.17	0.15	0.14	0.13	0.13	0.14	0.16	0.16	0.16	0.16	0.16
4.50	0.62	0.58	0.54	0.50	0.49	0.45	0.42	0.41	0.37	0.35	0.34	0.32	0.30	0.28	0.25	0.23	0.22	0.20	0.19	0.18	0.16	0.15	0.14	0.13	0.12	0.15	0.16	0.16	0.16	0.16	0.16
4.25	0.61	0.57	0.54	0.50	0.47	0.44	0.41	0.39	0.36	0.35	0.33	0.31	0.30	0.28	0.25	0.23	0.21	0.20	0.18	0.17	0.16	0.15	0.14	0.13	0.13	0.19	0.16	0.16	0.16	0.16	0.15
4.00	0.59	0.57	0.53	0.49	0.46	0.43	0.40	0.38	0.36	0.34	0.31	0.30	0.28	0.28	0.25	0.22	0.20	0.19	0.18	0.17	0.15	0.15	0.14	0.13	0.18	0.16	0.16	0.16	0.16	0.16	0.16
3.75	0.59	0.55	0.52	0.48	0.45	0.43	0.40	0.37	0.35	0.33	0.31	0.29	0.28	0.26	0.24	0.21	0.20	0.19	0.17	0.16	0.15	0.14	0.13	0.12	0.15	0.16	0.16	0.16	0.16	0.15	0.15
3.50	0.58	0.55	0.51	0.47	0.44	0.42	0.38	0.36	0.34	0.32	0.30	0.28	0.27	0.26	0.24	0.21	0.20	0.18	0.17	0.16	0.14	0.13	0.13	0.12	0.15	0.16	0.16	0.16	0.16	0.15	0.15
3.25	0.56	0.53	0.50	0.46	0.43	0.41	0.38	0.35	0.33	0.32	0.29	0.28	0.27	0.25	0.23	0.22	0.20	0.18	0.17	0.16	0.14	0.13	0.12	0.14	0.16	0.15	0.15	0.16	0.15	0.15	0.15
3.00	0.56	0.52	0.49	0.44	0.41	0.40	0.37	0.35	0.33	0.31	0.29	0.28	0.26	0.25	0.23	0.21	0.19	0.18	0.16	0.15	0.14	0.13	0.12	0.19	0.15	0.15	0.15	0.15	0.15	0.15	0.15

Table 5.7, continued.

MS 36 – SW Stolzburg tonalite

P [kbar] \ T [°C]	550.00	560.00	570.00	580.00	590.00	600.00	610.00	620.00	630.00	640.00	650.00	660.00	670.00	680.00	690.00	700.00	710.00	720.00	730.00	740.00	750.00	760.00	770.00	780.00	790.00	800.00	810.00	820.00	830.00	840.00	850.00
15.00	1.00	1.00	1.00	1.00	1.00	1.00	1.00	1.00	1.00	1.00	1.00	1.00	1.00	1.00	1.00	1.00	1.00	1.00	1.00	1.00	1.00	1.00	1.00	1.00	1.00	1.00	1.00	1.00	1.00	0.91	0.77
14.75	1.00	1.00	1.00	1.00	1.00	1.00	1.00	1.00	1.00	1.00	1.00	1.00	1.00	1.00	1.00	1.00	1.00	1.00	1.00	1.00	1.00	1.00	1.00	1.00	1.00	1.00	1.00	0.98	0.85	0.72	0.63
14.50	1.00	1.00	1.00	1.00	1.00	1.00	1.00	1.00	1.00	1.00	1.00	1.00	1.00	1.00	1.00	1.00	1.00	1.00	1.00	1.00	1.00	1.00	1.00	1.00	1.00	1.00	0.98	0.82	0.72	0.63	0.53
14.25	1.00	1.00	1.00	1.00	1.00	1.00	1.00	1.00	1.00	1.00	1.00	1.00	1.00	1.00	1.00	1.00	1.00	1.00	1.00	1.00	1.00	1.00	1.00	1.00	1.00	1.00	0.78	0.67	0.51	0.50	0.44
14.00	1.00	1.00	1.00	1.00	1.00	1.00	1.00	1.00	1.00	1.00	1.00	1.00	1.00	1.00	1.00	1.00	1.00	1.00	1.00	1.00	1.00	1.00	1.00	1.00	0.92	0.76	0.62	0.55	0.43	0.39	0.33
13.75	1.00	1.00	1.00	1.00	1.00	1.00	1.00	1.00	1.00	1.00	1.00	1.00	1.00	1.00	1.00	1.00	1.00	1.00	1.00	1.00	1.00	1.00	1.00	0.87	0.72	0.61	0.49	0.44	0.37	0.34	0.28
13.50	1.00	1.00	1.00	1.00	1.00	1.00	1.00	1.00	1.00	1.00	1.00	1.00	1.00	1.00	1.00	1.00	1.00	1.00	1.00	1.00	1.00	0.98	0.82	0.69	0.60	0.49	0.40	0.34	0.30	0.27	0.21
13.25	1.00	1.00	1.00	1.00	1.00	1.00	1.00	1.00	1.00	1.00	1.00	1.00	1.00	1.00	1.00	1.00	1.00	1.00	1.00	1.00	0.96	0.77	0.66	0.54	0.45	0.38	0.27	0.21	0.23	0.21	0.20
13.00	1.00	1.00	1.00	1.00	1.00	1.00	1.00	1.00	1.00	1.00	1.00	1.00	1.00	1.00	1.00	1.00	1.00	1.00	1.00	0.90	0.72	0.60	0.52	0.41	0.36	0.29	0.26	0.22	0.19	0.15	0.11
12.75	1.00	1.00	1.00	1.00	1.00	1.00	1.00	1.00	1.00	1.00	1.00	1.00	1.00	1.00	1.00	1.00	1.00	0.99	0.82	0.68	0.55	0.49	0.41	0.34	0.27	0.22	0.19	0.16	0.15	0.13	0.13
12.50	1.00	1.00	1.00	1.00	1.00	1.00	1.00	1.00	1.00	1.00	1.00	1.00	1.00	1.00	1.00	1.00	0.95	0.77	0.65	0.55	0.45	0.39	0.31	0.26	0.22	0.17	0.16	0.13	0.12	0.11	0.09
12.25	1.00	1.00	1.00	1.00	1.00	1.00	1.00	1.00	1.00	1.00	1.00	1.00	1.00	1.00	1.00	0.89	0.73	0.61	0.53	0.39	0.31	0.27	0.24	0.19	0.14	0.14	0.12	0.10	0.08	0.06	0.05
12.00	1.00	1.00	1.00	1.00	1.00	1.00	1.00	1.00	1.00	1.00	1.00	1.00	1.00	1.00	0.88	0.70	0.57	0.48	0.41	0.34	0.28	0.22	0.17	0.14	0.12	0.11	0.11	0.08	0.08	0.05	0.05
11.75	1.00	1.00	1.00	1.00	1.00	1.00	1.00	1.00	1.00	1.00	1.00	1.00	1.00	0.87	0.64	0.54	0.46	0.41	0.23	0.25	0.20	0.16	0.13	0.12	0.10	0.07	0.07	0.06	0.05	0.05	0.03
11.50	1.00	1.00	1.00	1.00	1.00	1.00	1.00	1.00	1.00	1.00	1.00	1.00	0.92	0.65	0.51	0.44	0.35	0.23	0.19	0.18	0.14	0.11	0.09	0.08	0.07	0.06	0.06	0.05	0.04	0.04	0.04
11.25	1.00	1.00	1.00	1.00	1.00	1.00	1.00	1.00	1.00	1.00	1.00	0.99	0.67	0.48	0.39	0.30	0.28	0.20	0.17	0.15	0.11	0.08	0.07	0.06	0.05	0.05	0.05	0.05	0.04	0.04	0.04
11.00	1.00	1.00	1.00	1.00	1.00	1.00	1.00	1.00	1.00	1.00	1.00	0.71	0.51	0.32	0.31	0.25	0.20	0.16	0.13	0.10	0.08	0.07	0.06	0.06	0.05	0.05	0.05	0.04	0.04	0.04	0.04
10.75	1.00	1.00	1.00	1.00	1.00	1.00	1.00	1.00	1.00	1.00	0.77	0.54	0.36	0.24	0.20	0.20	0.13	0.11	0.09	0.07	0.07	0.06	0.06	0.06	0.05	0.05	0.05	0.04	0.04	0.04	0.04
10.50	1.00	1.00	1.00	1.00	1.00	1.00	1.00	1.00	1.00	0.81	0.57	0.38	0.21	0.18	0.16	0.13	0.11	0.09	0.08	0.07	0.07	0.06	0.06	0.06	0.05	0.05	0.05	0.04	0.04	0.04	0.04
10.25	1.00	1.00	1.00	1.00	1.00	1.00	1.00	1.00	0.86	0.60	0.40	0.21	0.19	0.17	0.14	0.11	0.10	0.08	0.08	0.07	0.07	0.06	0.06	0.06	0.05	0.05	0.04	0.04	0.04	0.04	0.04
10.00	1.00	1.00	1.00	1.00	1.00	1.00	1.00	0.92	0.64	0.43	0.22	0.19	0.17	0.15	0.13	0.11	0.09	0.08	0.07	0.07	0.06	0.06	0.06	0.05	0.05	0.05	0.04	0.04	0.04	0.04	0.04
9.75	1.00	1.00	1.00	1.00	1.00	1.00	0.98	0.67	0.47	0.25	0.20	0.17	0.16	0.15	0.12	0.10	0.08	0.08	0.07	0.07	0.06	0.06	0.06	0.05	0.05	0.05	0.04	0.04	0.04	0.04	0.04
9.50	1.00	1.00	1.00	1.00	1.00	1.00	0.72	0.49	0.27	0.21	0.17	0.17	0.15	0.15	0.10	0.09	0.08	0.07	0.07	0.07	0.06	0.06	0.05	0.05	0.05	0.04	0.04	0.04	0.04	0.04	0.04
9.25	1.00	1.00	1.00	1.00	1.00	0.79	0.52	0.28	0.21	0.18	0.17	0.16	0.15	0.14	0.09	0.08	0.08	0.07	0.07	0.06	0.06	0.06	0.05	0.05	0.04	0.04	0.04	0.04	0.04	0.04	0.05
9.00	1.00	1.00	1.00	1.00	0.83	0.56	0.29	0.22	0.20	0.18	0.17	0.16	0.15	0.12	0.09	0.08	0.08	0.07	0.07	0.06	0.06	0.05	0.05	0.05	0.04	0.04	0.04	0.04	0.04	0.04	0.05
8.75	1.00	1.00	1.00	0.88	0.61	0.32	0.23	0.22	0.19	0.17	0.16	0.15	0.15	0.10	0.09	0.08	0.08	0.07	0.07	0.06	0.06	0.05	0.05	0.05	0.04	0.04	0.04	0.03	0.04	0.04	0.05
8.50	1.00	1.00	0.89	0.63	0.34	0.24	0.21	0.19	0.18	0.18	0.16	0.15	0.14	0.09	0.08	0.08	0.08	0.07	0.07	0.06	0.06	0.06	0.05	0.05	0.05	0.04	0.04	0.04	0.03	0.04	0.05	0.05
8.25	1.00	0.98	0.66	0.48	0.27	0.22	0.20	0.20	0.19	0.18	0.16	0.15	0.10	0.09	0.08	0.08	0.07	0.07	0.06	0.06	0.06	0.05	0.05	0.04	0.04	0.04	0.03	0.03	0.04	0.05	0.05
8.00	1.00	0.68	0.41	0.29	0.22	0.22	0.21	0.19	0.18	0.17	0.16	0.13	0.10	0.09	0.08	0.08	0.07	0.07	0.06	0.06	0.05	0.05	0.05	0.04	0.04	0.04	0.03	0.04	0.04	0.05	0.05
7.75	0.75	0.52	0.33	0.23	0.22	0.21	0.20	0.19	0.17	0.15	0.15	0.11	0.10	0.09	0.08	0.08	0.07	0.07	0.06	0.05	0.05	0.05	0.04	0.04	0.04	0.04	0.03	0.04	0.04	0.05	0.05
7.50	0.55	0.36	0.24	0.23	0.22	0.20	0.20	0.18	0.17	0.15	0.11	0.11	0.10	0.09	0.08	0.07	0.07	0.06	0.06	0.05	0.05	0.05	0.04	0.04	0.04	0.04	0.03	0.04	0.04	0.05	0.05
7.25	0.40	0.26	0.24	0.24	0.22	0.21	0.19	0.17	0.17	0.12	0.11	0.10	0.10	0.09	0.08	0.07	0.06	0.06	0.06	0.05	0.05	0.05	0.04	0.04	0.04	0.04	0.03	0.04	0.05	0.05	0.05
7.00	0.30	0.25	0.24	0.23	0.21	0.21	0.18	0.13	0.12	0.11	0.11	0.10	0.10	0.08	0.07	0.07	0.06	0.06	0.05	0.05	0.05	0.04	0.04	0.04	0.04	0.03	0.04	0.04	0.05	0.05	0.05
6.75	0.26	0.25	0.24	0.22	0.22	0.20	0.15	0.13	0.12	0.11	0.10	0.10	0.09	0.08	0.07	0.07	0.06	0.06	0.05	0.05	0.05	0.04	0.04	0.04	0.04	0.03	0.04	0.04	0.05	0.05	0.05
6.50	0.26	0.25	0.23	0.22	0.21	0.15	0.13	0.12	0.12	0.11	0.10	0.09	0.09	0.08	0.07	0.07	0.06	0.06	0.05	0.05	0.04	0.04	0.04	0.04	0.04	0.03	0.04	0.04	0.05	0.05	0.05
6.25	0.26	0.25	0.24	0.22	0.16	0.13	0.13	0.12	0.11	0.10	0.10	0.09	0.09	0.08	0.07	0.07	0.06	0.06	0.05	0.05	0.04	0.04	0.04	0.04	0.03	0.03	0.04	0.05	0.05	0.05	0.05
6.00	0.26	0.25	0.23	0.15	0.14	0.13	0.13	0.12	0.11	0.10	0.10	0.09	0.09	0.08	0.07	0.07	0.06	0.06	0.05	0.05	0.04	0.04	0.04	0.04	0.03	0.03	0.04	0.05	0.05	0.05	0.05
5.75	0.26	0.25	0.17	0.15	0.14	0.13	0.13	0.12	0.11	0.10	0.10	0.09	0.09	0.08	0.07	0.06	0.06	0.05	0.05	0.05	0.04	0.04	0.04	0.04	0.03	0.04	0.04	0.05	0.05	0.05	0.05
5.50	0.26	0.18	0.16	0.14	0.14	0.13	0.12	0.11	0.11	0.10	0.09	0.09	0.09	0.08	0.07	0.06	0.05	0.05	0.05	0.04	0.04	0.04	0.04	0.03	0.03	0.04	0.04	0.04	0.05	0.05	0.05
5.25	0.17	0.16	0.15	0.14	0.14	0.13	0.12	0.11	0.11	0.10	0.09	0.09	0.08	0.07	0.06	0.06	0.05	0.05	0.05	0.04	0.04	0.04	0.04	0.03	0.04	0.04	0.04	0.04	0.05	0.04	0.05
5.00	0.17	0.16	0.15	0.14	0.13	0.12	0.12	0.11	0.10	0.09	0.09	0.08	0.08	0.07	0.06	0.06	0.05	0.05	0.05	0.04	0.04	0.04	0.04	0.03	0.04	0.04	0.04	0.04	0.04	0.04	0.04
4.75	0.16	0.15	0.15	0.14	0.13	0.12	0.11	0.10	0.10	0.09	0.08	0.08	0.08	0.07	0.06	0.06	0.05	0.05	0.04	0.04	0.04	0.04	0.03	0.03	0.04	0.04	0.04	0.04	0.04	0.04	0.04
4.50	0.16	0.15	0.14	0.13	0.12	0.11	0.11	0.10	0.10	0.09	0.08	0.08	0.08	0.07	0.06	0.06	0.05	0.05	0.04	0.04	0.04	0.03	0.03	0.03	0.04	0.04	0.04	0.04	0.04	0.04	0.04
4.25	0.16	0.15	0.14	0.13	0.12	0.11	0.11	0.10	0.10	0.09	0.08	0.08	0.08	0.07	0.06	0.06	0.05	0.05	0.04	0.04	0.04	0.03	0.03	0.03	0.04	0.04	0.04	0.04	0.04	0.04	0.04
4.00	0.15	0.15	0.14	0.13	0.12	0.11	0.10	0.10	0.09	0.09	0.08	0.08	0.08	0.07	0.06	0.06	0.05	0.05	0.04	0.04	0.04	0.03	0.03	0.04	0.04	0.04	0.04	0.04	0.04	0.04	0.04
3.75	0.15	0.14	0.14	0.13	0.11	0.11	0.10	0.10	0.09	0.09	0.08	0.08	0.07	0.07	0.06	0.06	0.05	0.05	0.04	0.04	0.03	0.03	0.03	0.04	0.04	0.04	0.04	0.04	0.04	0.04	0.04
3.50	0.15	0.14	0.13	0.12	0.11	0.11	0.10	0.09	0.09	0.08	0.08	0.08	0.07	0.07	0.06	0.05	0.05	0.05	0.04	0.04	0.03	0.03	0.03	0.04	0.04	0.04	0.04	0.04	0.04	0.04	0.04
3.25	0.15	0.14	0.13	0.12	0.11	0.10	0.10	0.09	0.09	0.08	0.07	0.08	0.07	0.07	0.06	0.05	0.05	0.05	0.04	0.04	0.03	0.03	0.04	0.04	0.04	0.04	0.04	0.04	0.04	0.04	0.04
3.00	0.14	0.13	0.13	0.12	0.11	0.10	0.10	0.09	0.08	0.08	0.07	0.07	0.07	0.06	0.06	0.05	0.05	0.05	0.04	0.04	0.03	0.03	0.04	0.04	0.04	0.04	0.04	0.04	0.04	0.04	0.04

Table 5.8. Strontium isotope data for apatite grains from granitoid samples from the Stolzburg Block.

sample	88Sr		$^{87}Sr/^{86}Sr_{raw}$	$^{87}Sr/^{86}Sr_{Kr}$	$^{87}Sr/^{86}Sr_{REE}$	$^{87}Sr/^{86}Sr_{Ca}$	$^{87}Sr/^{86}Sr_{Rb}$	$^{87}Sr/^{86}Sri$	± 2 S.E.	$^{84}Sr/^{86}Sr_{raw}$	$^{84}Sr/^{86}Sr_{Kr}$	$^{84}Sr/^{86}Sr_{Ree}$	$^{84}Sr/^{86}Sr$	± 2 S.E.	84Sr/88Sr	± 2 S.E.	$^{87}Rb/^{86}Sr$	± 2 S.E.	$\beta^{86}Sr/^{88}Sr$	$\beta^{87}Rb/^{85}Rb$	83Kr	167Er	84Sr	85Rb	171Yb	86Sr	173Yb	87Sr	88Sr
MS 2																													
\Sr011.dat	42	0.43	0.67736	0.689461	0.689023	0.689023	0.700367	**0.7004**	**0.000332**	0.184917	0.059854	0.058492	0.05853	0.000324	0.006988	3.87E-05	**-0.01205**	0.00205	-1.70831	-1.74318	0.001137	-0.000002	0.006308	0.002094	0.000021	0.002112	0.000006	0.000847	0.000935
\Sr010.dat	43	0.88	0.694861	0.701196	0.700162	0.700162	0.706224	**0.7062**	**0.000172**	0.125604	0.06298	0.057636	0.057627	0.000161	0.006881	1.92E-05	**-0.00639**	9.86E-05	-1.66585	-1.55687	0.001137	-0.000002	0.006308	0.002094	0.000021	0.002112	0.000006	0.000847	0.000935
\Sr011.dat	42	0.43	0.67736	0.689461	0.689023	0.689023	0.700328	**0.7003**	**0.000330**	0.184917	0.059854	0.058492	0.05853	0.000324	0.006988	3.87E-05	**-0.01201**	0.002043	-1.70831	-1.59655	0.001137	-0.000002	0.006308	0.002094	0.000021	0.002112	0.000006	0.000847	0.000935
\Sr012.dat	43	0.44	0.676433	0.688286	0.688154	0.688154	0.700394	**0.7004**	**0.000305**	0.181927	0.05917	0.058589	0.058624	0.000302	0.007	3.61E-05	**-0.01292**	0.000382	-1.69235	-1.58163	0.001137	-0.000002	0.006308	0.002094	0.000021	0.002112	0.000006	0.000847	0.000935
\Sr013.dat	44	0.41	0.675799	0.688664	0.688422	0.688422	0.700342	**0.7003**	**0.000363**	0.192246	0.058955	0.058338	0.058314	0.000401	0.006963	4.79E-05	**-0.01262**	0.000583	-1.69959	-1.5884	0.001137	-0.000002	0.006308	0.002094	0.000021	0.002112	0.000006	0.000847	0.000935
\Sr014.dat	42	0.42	0.675496	0.688047	0.68778	0.68778	0.700284	**0.7003**	**0.000332**	0.190984	0.060115	0.059563	0.059518	0.000427	0.007106	5.1E-05	**-0.01312**	0.000406	-1.68811	-1.57768	0.001137	-0.000002	0.006308	0.002094	0.000021	0.002112	0.000006	0.000847	0.000935
\Sr015.dat	42	0.43	0.676158	0.688544	0.688355	0.688355	0.700227	**0.7002**	**0.000217**	0.187122	0.061073	0.060521	0.060455	0.000355	0.007218	4.24E-05	**-0.01258**	0.002049	-1.67781	-1.56805	0.001137	-0.000002	0.006308	0.002094	0.000021	0.002112	0.000006	0.000847	0.000935
\Sr016.dat	44	0.43	0.677066	0.689182	0.688899	0.688899	0.700216	**0.7002**	**0.000285**	0.186083	0.060376	0.059828	0.059785	0.000353	0.007138	4.22E-05	**-0.01199**	0.001604	-1.6841	-1.57393	0.001137	-0.000002	0.006308	0.002094	0.000021	0.002112	0.000006	0.000847	0.000935
\Sr017.dat	43	1.34	0.697386	0.701593	0.701448	0.701448	0.701037	**0.7010**	**0.000103**	0.099489	0.057828	0.057456	0.057448	0.000101	0.006859	1.2E-05	**0.000604**	0.000893	-1.69369	-1.58289	0.001137	-0.000002	0.006308	0.002094	0.000021	0.002112	0.000006	0.000847	0.000935
\Sr018.dat	43	1.27	0.699441	0.703897	0.703704	0.703704	0.701297	**0.7013**	**0.000111**	0.101765	0.058048	0.057105	0.057113	9.66E-05	0.006819	1.15E-05	**0.003013**	0.002056	-1.70184	-1.59051	0.001137	-0.000002	0.006308	0.002094	0.000021	0.002112	0.000006	0.000847	0.000935
\Sr019.dat	42	1.23	0.692115	0.696619	0.696245	0.696245	0.700712	**0.7007**	**0.000137**	0.103071	0.057804	0.056719	0.056719	0.0001	0.006772	1.19E-05	**-0.00468**	0.000108	-1.71334	-1.60125	0.001137	-0.000002	0.006308	0.002094	0.000021	0.002112	0.000006	0.000847	0.000935
\Sr021.dat	41	0.40	0.675987	0.689089	0.688935	0.688935	0.700954	**0.7010**	**0.000266**	0.19346	0.057429	0.056738	0.056716	0.000488	0.006772	5.83E-05	**-0.01273**	0.002494	-1.71605	-1.60379	0.001137	-0.000002	0.006308	0.002094	0.000021	0.002112	0.000006	0.000847	0.000935
\Sr022.dat	43	0.37	0.672022	0.686127	0.68588	0.68588	0.701133	**0.7011**	**0.000315**	0.206167	0.059022	0.058427	0.058362	0.000457	0.006968	5.46E-05	**-0.01609**	0.000583	-1.71437	-1.60221	0.001137	-0.000002	0.006308	0.002094	0.000021	0.002112	0.000006	0.000847	0.000935
\Sr023.dat	44	0.42	0.675319	0.687815	0.687511	0.687511	0.700732	**0.7007**	**0.000336**	0.189751	0.060586	0.05925	0.05918	0.000424	0.007066	5.06E-05	**-0.01393**	0.000399	-1.68099	-1.57102	0.001137	-0.000002	0.006308	0.002094	0.000021	0.002112	0.000006	0.000847	0.000935
\Sr024.dat	43	0.42	0.676635	0.689133	0.688822	0.688822	0.700752	**0.7008**	**0.000280**	0.188256	0.059821	0.058901	0.058901	0.000265	0.007033	3.16E-05	**-0.01261**	0.001806	-1.68789	-1.57746	0.001137	-0.000002	0.006308	0.002094	0.000021	0.002112	0.000006	0.000847	0.000935
\Sr025.dat	44	0.35	0.670024	0.684848	0.684621	0.684621	0.700866	**0.7009**	**0.000321**	0.215624	0.059897	0.058674	0.058681	0.000388	0.007007	4.63E-05	**-0.0171**	0.000557	-1.67009	-1.59056	0.001137	-0.000002	0.006308	0.002094	0.000021	0.002112	0.000006	0.000847	0.000935
\Sr027.dat	43	1.23	0.692712	0.697215	0.697124	0.697124	0.700792	**0.7008**	**0.000119**	0.101957	0.05689	0.056639	0.056652	0.000105	0.006764	1.25E-05	**-0.00388**	0.000316	-1.72107	-1.63911	0.001137	-0.000002	0.006308	0.002094	0.000021	0.002112	0.000006	0.000847	0.000935
\Sr028.dat	42	0.44	0.676235	0.68834	0.688008	0.688008	0.700982	**0.7010**	**0.000302**	0.18334	0.058338	0.056871	0.056871	0.000416	0.00679	4.96E-05	**-0.01371**	0.00065	-1.73224	-1.64975	0.001137	-0.000002	0.006308	0.002094	0.000021	0.002112	0.000006	0.000847	0.000935
\Sr029.dat	43	1.21	0.692237	0.696767	0.696468	0.696468	0.700815	**0.7008**	**0.000090**	0.10369	0.057997	0.056759	0.056743	0.000165	0.006775	1.97E-05	**-0.00459**	0.000132	-1.71279	-1.63123	0.001137	-0.000002	0.006308	0.002094	0.000021	0.002112	0.000006	0.000847	0.000935
\Sr030.dat	43	1.02	0.690909	0.696727	0.696439	0.696439	0.701109	**0.7011**	**0.000178**	0.116801	0.057947	0.05686	0.05686	0.000187	0.006789	2.23E-05	**-0.00508**	0.000792	-1.67545	-1.59567	0.001137	-0.000002	0.006308	0.002094	0.000021	0.002112	0.000006	0.000847	0.000935
\Sr031.dat	45	0.38	0.680447	0.694497	0.694117	0.694117	0.701301	**0.7013**	**0.000391**	0.200422	0.059785	0.058478	0.058459	0.000307	0.00698	3.66E-05	**-0.00779**	0.00225	-1.69363	-1.61298	0.001137	-0.000002	0.006308	0.002094	0.000021	0.002112	0.000006	0.000847	0.000935
\Sr032.dat	42	0.45	0.677127	0.68881	0.688596	0.688596	0.701095	**0.7011**	**0.000197**	0.179659	0.058581	0.057367	0.057384	0.000284	0.006852	3.39E-05	**-0.01321**	0.000548	-1.71198	-1.63046	0.001137	-0.000002	0.006308	0.002094	0.000021	0.002112	0.000006	0.000847	0.000935
\Sr033.dat	42	0.47	0.678093	0.689538	0.689197	0.689197	0.701377	**0.7014**	**0.000274**	0.175995	0.058425	0.056566	0.056589	0.000306	0.006757	3.65E-05	**-0.01287**	0.000538	-1.72781	-1.64554	0.001137	-0.000002	0.006308	0.002094	0.000021	0.002112	0.000006	0.000847	0.000935
\Sr008.dat	43	1.30	0.692732	0.696979	0.696911	0.696911	0.70093	**0.7009**	**0.000086**	0.099108	0.056342	0.05606	0.056056	0.000124	0.006693	1.48E-05	**-0.00428**	8.69E-05	-1.71648	-1.61932	0.001137	-0.000002	0.006308	0.002094	0.000021	0.002112	0.000006	0.000847	0.000935
\Sr009.dat	43	0.81	0.691418	0.698494	0.698311	0.698311	0.701469	**0.7015**	**0.000187**	0.126769	0.057015	0.055871	0.055878	0.000281	0.006672	3.36E-05	**-0.00348**	0.001818	-1.71052	-1.6137	0.001137	-0.000002	0.006308	0.002094	0.000021	0.002112	0.000006	0.000847	0.000935
\Sr010.dat	43	1.03	0.690499	0.695809	0.695628	0.695628	0.700817	**0.7008**	**0.000154**	0.110751	0.057213	0.05677	0.056746	0.000186	0.006775	2.22E-05	**-0.00554**	0.000136	-1.69526	-1.59931	0.001137	-0.000002	0.006308	0.002094	0.000021	0.002112	0.000006	0.000847	0.000935
\Sr011.dat	43	1.25	0.691995	0.696416	0.696328	0.696328	0.700831	**0.7008**	**0.000106**	0.101447	0.057031	0.056749	0.056731	0.000131	0.006774	1.56E-05	**-0.00479**	0.000128	-1.7017	-1.60537	0.001137	-0.000002	0.006308	0.002094	0.000021	0.002112	0.000006	0.000847	0.000935
\Sr012.dat	43	1.31	0.692556	0.696775	0.696618	0.696618	0.700875	**0.7009**	**0.000118**	0.099914	0.057375	0.056824	0.056824	8.87E-05	0.006785	1.06E-05	**-0.00453**	9.67E-05	-1.70149	-1.60518	0.001137	-0.000002	0.006308	0.002094	0.000021	0.002112	0.000006	0.000847	0.000935
\Sr013.dat	43	1.29	0.692948	0.697253	0.697143	0.697143	0.700973	**0.7010**	**0.000124**	0.100059	0.056896	0.056614	0.056623	0.000113	0.006761	1.35E-05	**-0.00411**	9.4E-05	-1.70183	-1.6055	0.001137	-0.000002	0.006308	0.002094	0.000021	0.002112	0.000006	0.000847	0.000935
MS 25																													
\Sr011.dat	44	0.45	0.677595	0.689265	0.689055	0.689055	0.701423	**0.7014**	**0.000313**	0.178307	0.057921	0.057434	0.057459	0.000343	0.006861	4.1E-05	**-0.01304**	0.00039	-1.73216	-1.64968	0.001137	-0.000002	0.006308	0.002094	0.000021	0.002112	0.000006	0.000847	0.000935
\Sr012.dat	41	0.41	0.675845	0.688751	0.68855	0.68855	0.701958	**0.7020**	**0.000292**	0.191577	0.057257	0.056243	0.056243	0.000388	0.006715	4.64E-05	**-0.0141**	0.000817	-1.73901	-1.6562	0.001137	-0.000002	0.006308	0.002094	0.000021	0.002112	0.000006	0.000847	0.000935
\Sr013.dat	42	0.12	0.619978	0.655544	0.655095	0.655095	0.702651	**0.7027**	**0.001081**	0.481498	0.05462	0.053631	0.053803	0.001203	0.006424	0.000144	**-0.05137**	0.004793	-1.76855	-1.68433	0.001137	-0.000002	0.006308	0.002094	0.000021	0.002112	0.000006	0.000847	0.000935
\Sr014.dat	44	0.45	0.678793	0.690533	0.690225	0.690225	0.702185	**0.7022**	**0.000342**	0.178736	0.056318	0.055555	0.055548	0.000256	0.006632	3.06E-05	**-0.01271**	0.000574	-1.75052	-1.66716	0.001137	-0.000002	0.006308	0.002094	0.000021	0.002112	0.000006	0.000847	0.000935
\Sr015.dat	44	0.35	0.670064	0.685506	0.685196	0.685196	0.702131	**0.7021**	**0.000346**	0.208547	0.056477	0.05605	0.05605	0.000582	0.006692	6.95E-05	**-0.0178**	0.00142	-1.7372	-1.65448	0.001137	-0.000002	0.006308	0.002094	0.000021	0.002112	0.000006	0.000847	0.000935
\Sr017.dat	44	0.38	0.674223	0.688263	0.687969	0.687969	0.702036	**0.7020**	**0.000334**	0.202549	0.057365	0.056666	0.056593	0.000437	0.006757	5.22E-05	**-0.01505**	0.001941	-1.70883	-1.62745	0.001137	-0.000002	0.006308	0.002094	0.000021	0.002112	0.000006	0.000847	0.000935
\Sr018.dat	43	0.28	0.664881	0.683252	0.683101	0.683101	0.702423	**0.7024**	**0.000372**	0.254126	0.058526	0.057976	0.057976	0.000559	0.006922	6.68E-05	**-0.02072**	0.00292	-1.68905	-1.60862	0.001137	-0.000002	0.006308	0.002094	0.000021	0.002112	0.000006	0.000847	0.000935
\Sr019.dat	41	0.26	0.656537	0.678153	0.677742	0.677742	0.702212	**0.7022**	**0.000406**	0.293584	0.056658	0.056049	0.056011	0.000508	0.006688	6.07E-05	**-0.02573**	0.004823	-1.74081	-1.65792	0.001137	-0.000002	0.006308	0.002094	0.000021	0.002112	0.000006	0.000847	0.000935
\Sr020.dat	44	0.43	0.676964	0.689374	0.689119	0.689119	0.702277	**0.7023**	**0.000307**	0.182884	0.055749	0.055092	0.055116	0.000305	0.006581	3.64E-05	**-0.01399**	0.000665	-1.75939	-1.67561	0.001137	-0.000002	0.006308	0.002094	0.000021	0.002112	0.000006	0.000847	0.000935
\Sr021.dat	44	0.37	0.675597	0.689637	0.689396	0.689396	0.702405	**0.7024**	**0.000331**	0.199042	0.054805	0.054082	0.054136	0.00043	0.006464	5.14E-05	**-0.01385**	0.002997	-1.77263	-1.68822	0.001137	-0.000002	0.006308	0.002094	0.000021	0.002112	0.000006	0.000847	0.000935
\Sr022.dat	44	0.29	0.66483	0.683107	0.682545	0.682545	0.702614	**0.7026**	**0.000512**	0.244215	0.053684	0.052959	0.052832	0.000742	0.006308	8.86E-05	**-0.02174**	0.002538	-1.79089	-1.70561	0.001137	-0.000002	0.006308	0.002094	0.000021	0.002112	0.000006	0.000847	0.000935
\Sr023.dat	43	0.41	0.675322	0.688141	0.687806	0.687806	0.701844	**0.7018**	**0.000316**	0.1879	0.056084	0.055326	0.055326	0.000631	0.006606	7.53E-05	**-0.0149**	0.000694	-1.76942	-1.68516	0.001137	-0.000002	0.006308	0.002094	0.000021	0.002112	0.000006	0.000847	0.000935
\Sr024.dat	43	0.40	0.675427	0.68858	0.688	0.688	0.701445	**0.7014**	**0.000419**	0.193915	0.058047	0.056837	0.056837	0.000349	0.006786	4.17E-05	**-0.01414**	0.001644	-1.74102	-1.65812	0.001137	-0.000002	0.006308	0.002094	0.000021	0.002112	0.000006	0.000847	0.000935
\Sr025.dat	44	0.41	0.677576	0.690523	0.690273	0.690273	0.70251	**0.7025**	**0.000309**	0.190508	0.057832	0.056909	0.056865	0.000295	0.00679	3.52E-05	**-0.01299**	0.002727	-1.7381	-1.65533	0.001137	-0.000002	0.006308	0.002094	0.000021	0.002112	0.000006	0.000847	0.000935
\Sr027.dat	43	0.37	0.675229	0.689175	0.688941	0.688941	0.702147	**0.7021**	**0.000328**	0.199625	0.055814	0.055323	0.0553	0.000382	0.006603	4.57E-05	**-0.01408**	0.003368	-1.74073	-1.65784	0.001137	-0.000002	0.006308	0.002094	0.000021	0.002112	0.000006	0.000847	0.000935
\Sr028.dat	43	0.44	0.682777	0.695226	0.694972	0.694972	0.7018	**0.7018**	**0.000320**	0.181123	0.055875	0.055341	0.055356	0.000306	0.006609	3.66E-05	**-0.00742**	0.008525	-1.75304	-1.66957	0.001137	-0.000002	0.006308	0.002094	0.000021	0.002112	0.000006	0.000847	0.000935
\Sr029.dat	43	0.39	0.676348	0.689668	0.689333	0.689333	0.702537	**0.7025**	**0.000323**	0.193632	0.05523	0.054203	0.054244	0.000441	0.006477	5.27E-05	**-0.014**	0.002659	-1.76299	-1.67904	0.001137	-0.000002	0.006308	0.002094	0.000021	0.002112	0.000006	0.000847	0.000935
\Sr030.dat	42	0.37	0.671687	0.686197	0.685889	0.685889	0.702139	**0.7021**	**0.000319**	0.207931	0.056242	0.055369	0.05532	0.000577	0.006605	6.89E-05	**-0.01737**	0.001204	-1.75808	-1.67436	0.001137	-0.000002	0.006308	0.002094	0.000021	0.002112	0.000006	0.000847	0.000935
\Sr031.dat	44	0.12	0.611331	0.646608	0.645493	0.645493	0.704169	**0.7042**	**0.001699**	0.522105	0.056488	0.054392	0.054392	0.001859	0.006494	0.000222	**-0.06169**	0.014366	-1.75341	-1.66992	0.001137	-0.000002	0.006308	0.002094	0.000021	0.002112	0.000006	0.000847	0.000935
\Sr015.dat	42	0.74	0.687999	0.695376	0.695225	0.695225	0.702123	**0.7021**	**0.000185**	0.131416	0.056515	0.055532	0.055549	0.000197	0.006633	2.35E-05	**-0.00733**	0.00086	-1.74593	-1.6471	0.001137	-0.000002	0.006308	0.002094	0.000021	0.002112	0.000006	0.000847	0.000935
\Sr016.dat	44	1.03	0.691503	0.696836	0.696692	0.696692	0.70219	**0.7022**	**0.000140**	0.110289	0.056557	0.055857	0.055835	0.000131	0.006667	1.56E-05	**-0.00589**	0.000141	-1.72069	-1.62329	0.001137	-0.000002	0.006308	0.002094	0.000021	0.002112	0.000006	0.000847	0.000935
\Sr017.dat	43	1.36	0.693836	0.697923	0.697804	0.697804	0.701708	**0.7017**	**0.000097**	0.09764	0.056698	0.056062	0.056044	0.000181	0.006692	2.16E-05	**-0.00416**	0.000369	-1.74583	-1.64701	0.001137	-0.000002	0.006308	0.002094	0.000021	0.002112	0.000006	0.000847	0.000935
\Sr018.dat	43	1.08	0.692017	0.697155	0.697047	0.697047	0.702108	**0.7021**	**0.000145**	0.108314	0.0569	0.056428	0.056428	0.000179	0.006737	2.14E-05	**-0.0054**	0.000422	-1.70054	-1.60428	0.001137	-0.000002	0.006308	0.002094	0.000021	0.002112	0.000006	0.000847	0.000935

Table 5.8, continued.

sample	88Sr		$^{87}Sr/^{86}Sr_{raw}$	$^{87}Sr/^{86}Sr_{Kr}$	$^{87}Sr/^{86}Sr_{REE}$	$^{87}Sr/^{86}Sr_{Ca}$	$^{87}Sr/^{86}Sr_{Rb}$	$^{87}Sr/^{86}Sri$	± 2 S.E.	$^{84}Sr/^{86}Sr_{raw}$	$^{84}Sr/^{86}Sr_{Kr}$	$^{84}Sr/^{86}Sr_{Ree}$	$^{84}Sr/^{86}Sr$	± 2 S.E.	84Sr/88Sr	± 2 S.E.	$^{87}Rb/^{86}Sr$	± 2 S.E.	$\beta^{86}Sr/^{88}Sr$	$\beta^{87}Rb/^{85}Rb$	83Kr	167Er	84Sr	85Rb	171Yb	86Sr	173Yb	87Sr	88Sr
MS 36																												
\Sr041.dat	43	0.42	0.676743	0.689234	0.688991	0.688991	0.701225	**0.7012**	**0.000348**	0.187393	0.058179	0.057285	0.057295	0.00038	0.006841	4.54E-05	**-0.01297**	0.001992	-1.72365	-1.64157	0.001137	-0.000002	0.006308	0.002094	0.000021	0.002112	0.000006	0.000847	0.000935
\Sr042.dat	41	0.39	0.674196	0.687452	0.687148	0.687148	0.701463	**0.7015**	**0.000298**	0.19574	0.058204	0.056408	0.05644	0.000507	0.006739	6.05E-05	**-0.01505**	0.000305	-1.72121	-1.63924	0.001137	-0.000002	0.006308	0.002094	0.000021	0.002112	0.000006	0.000847	0.000935
\Sr043.dat	42	0.33	0.672673	0.688136	0.687827	0.687827	0.701854	**0.7019**	**0.000327**	0.217689	0.057618	0.056627	0.056689	0.000344	0.006769	4.1E-05	**-0.01492**	0.004564	-1.71848	-1.63665	0.001137	-0.000002	0.006308	0.002094	0.000021	0.002112	0.000006	0.000847	0.000935
\Sr044.dat	43	0.34	0.672473	0.687464	0.686983	0.686983	0.701521	**0.7015**	**0.000298**	0.214819	0.058487	0.056783	0.056796	0.000539	0.006781	6.43E-05	**-0.01543**	0.002212	-1.72766	-1.64539	0.001137	-0.000002	0.006308	0.002094	0.000021	0.002112	0.000006	0.000847	0.000935
\Sr045.dat	43	0.34	0.669696	0.685281	0.684329	0.684329	0.701506	**0.7015**	**0.000459**	0.22242	0.061968	0.057609	0.057527	0.000509	0.006869	6.08E-05	**-0.01829**	0.001218	-1.70533	-1.62413	0.001137	-0.000002	0.006308	0.002094	0.000021	0.002112	0.000006	0.000847	0.000935
\Sr046.dat	43	0.39	0.675592	0.689015	0.688177	0.688177	0.700936	**0.7009**	**0.000287**	0.197962	0.060437	0.057612	0.057579	0.00038	0.006875	4.53E-05	**-0.01362**	0.002388	-1.71224	-1.63071	0.001137	-0.000002	0.006308	0.002094	0.000021	0.002112	0.000006	0.000847	0.000935
\Sr047.dat	43	0.11	0.612588	0.649365	0.648428	0.648428	0.7001	**0.7001**	**0.001146**	0.506171	0.064809	0.063707	0.06383	0.001149	0.007621	0.000137	**-0.05483**	0.00305	-1.69857	-1.61769	0.001137	-0.000002	0.006308	0.002094	0.000021	0.002112	0.000006	0.000847	0.000935
\Sr048.dat	43	0.07	0.40295	0.124337	0.093946	0.093946	0.683501	**0.6835**	**0.033001**	1.540573	0.131387	0.126637	0.130287	0.025016	0.015556	0.002987	**-0.65102**	0.178214	-1.91766	-1.82634	0.001137	-0.000002	0.006308	0.002094	0.000021	0.002112	0.000006	0.000847	0.000935
\Sr049.dat	42	0.40	0.676341	0.689494	0.688817	0.688817	0.701527	**0.7015**	**0.000297**	0.194399	0.059776	0.056948	0.056999	0.000402	0.006806	4.8E-05	**-0.01346**	0.001375	-1.70263	-1.62155	0.001137	-0.000002	0.006308	0.002094	0.000021	0.002112	0.000006	0.000847	0.000935
\Sr050.dat	42	0.38	0.672915	0.686725	0.686341	0.686341	0.701601	**0.7016**	**0.000336**	0.201545	0.058634	0.056865	0.056908	0.000405	0.006795	4.83E-05	**-0.01608**	0.000597	-1.71719	-1.63542	0.001137	-0.000002	0.006308	0.002094	0.000021	0.002112	0.000006	0.000847	0.000935
\Sr051.dat	44	0.22	0.761991	0.792458	0.791952	0.791952	0.704685	**0.7047**	**0.000554**	0.291705	0.056788	0.05558	0.055664	0.000675	0.006646	8.06E-05	**0.090601**	0.010638	-1.7299	-1.64753	0.001137	-0.000002	0.006308	0.002094	0.000021	0.002112	0.000006	0.000847	0.000935
\Sr052.dat	43	0.37	0.673147	0.686989	0.686498	0.686498	0.701875	**0.7019**	**0.000333**	0.202912	0.058308	0.056705	0.05669	0.000536	0.006769	6.4E-05	**-0.01619**	0.000455	-1.72532	-1.64317	0.001137	-0.000002	0.006308	0.002094	0.000021	0.002112	0.000006	0.000847	0.000935
\Sr053.dat	44	0.35	0.671069	0.685627	0.685205	0.685205	0.701268	**0.7013**	**0.000438**	0.210907	0.058624	0.057334	0.057245	0.000622	0.006835	7.43E-05	**-0.01481**	0.003635	-1.70564	-1.62442	0.001137	-0.000002	0.006308	0.002094	0.000021	0.002112	0.000006	0.000847	0.000935
\Sr054.dat	44	0.39	0.674431	0.687978	0.686908	0.686908	0.701858	**0.7019**	**0.000391**	0.202177	0.062456	0.057567	0.057481	0.000615	0.006863	7.34E-05	**-0.01579**	0.000592	-1.70509	-1.6239	0.001137	-0.000002	0.006308	0.002094	0.000021	0.002112	0.000006	0.000847	0.000935
\Sr055.dat	43	0.37	0.672323	0.686233	0.685852	0.685852	0.701344	**0.7013**	**0.000274**	0.203927	0.058236	0.057364	0.057364	0.000262	0.006849	3.13E-05	**-0.01641**	0.000615	-1.70835	-1.627	0.001137	-0.000002	0.006308	0.002094	0.000021	0.002112	0.000006	0.000847	0.000935
\Sr056.dat	42	0.35	0.676226	0.691342	0.6908	0.6908	0.702322	**0.7023**	**0.000327**	0.214227	0.058715	0.056107	0.056086	0.000427	0.006697	5.1E-05	**-0.01227**	0.001889	-1.73117	-1.64873	0.001137	-0.000002	0.006308	0.002094	0.000021	0.002112	0.000006	0.000847	0.000935
\Sr057.dat	44	0.39	0.680508	0.694045	0.693648	0.693648	0.701655	**0.7017**	**0.000355**	0.193573	0.056104	0.055264	0.055328	0.000446	0.006606	5.32E-05	**-0.00863**	0.000915	-1.77445	-1.68995	0.001137	-0.000002	0.006308	0.002094	0.000021	0.002112	0.000006	0.000847	0.000935
\Sr058.dat	42	0.40	0.678177	0.691204	0.690586	0.690586	0.701795	**0.7018**	**0.000313**	0.190239	0.056657	0.054459	0.054459	0.000377	0.006502	4.5E-05	**-0.01193**	0.003605	-1.77607	-1.69149	0.001137	-0.000002	0.006308	0.002094	0.000021	0.002112	0.000006	0.000847	0.000935
\Sr060.dat	43	0.38	0.673307	0.687156	0.686671	0.686671	0.701965	**0.7020**	**0.000384**	0.201808	0.056277	0.054097	0.054065	0.000442	0.006455	5.28E-05	**-0.01612**	0.000479	-1.75141	-1.66801	0.001137	-0.000002	0.006308	0.002094	0.000021	0.002112	0.000006	0.000847	0.000935
\Sr061.dat	42	0.33	0.671578	0.687094	0.686605	0.686605	0.702222	**0.7022**	**0.000377**	0.218425	0.057234	0.054914	0.054805	0.00067	0.006544	8E-05	**-0.01654**	0.002232	-1.72114	-1.63918	0.001137	-0.000002	0.006308	0.002094	0.000021	0.002112	0.000006	0.000847	0.000935
\Sr062.dat	44	0.39	0.67545	0.688966	0.687918	0.687918	0.701757	**0.7018**	**0.000430**	0.19988	0.060303	0.055629	0.055585	0.000305	0.006637	3.64E-05	**-0.01454**	0.001312	-1.72455	-1.64243	0.001137	-0.000002	0.006308	0.002094	0.000021	0.002112	0.000006	0.000847	0.000935
\Sr021.dat	43	1.26	0.693442	0.697814	0.69773	0.69773	0.701883	**0.7019**	**0.000113**	0.10029	0.056461	0.056216	0.056216	0.000105	0.006712	1.26E-05	**-0.00443**	0.000502	-1.71696	-1.61977	0.001137	-0.000002	0.006308	0.002094	0.000021	0.002112	0.000006	0.000847	0.000935
\Sr022.dat	44	1.16	0.691726	0.696481	0.696289	0.696289	0.701204	**0.7012**	**0.000110**	0.104172	0.056388	0.055733	0.055747	0.000118	0.006656	1.41E-05	**-0.00522**	6.03E-05	-1.73787	-1.6395	0.001137	-0.000002	0.006308	0.002094	0.000021	0.002112	0.000006	0.000847	0.000935
\Sr023.dat	43	0.90	0.69029	0.696376	0.696172	0.696172	0.701938	**0.7019**	**0.000153**	0.117736	0.056447	0.055512	0.055491	0.000139	0.006626	1.65E-05	**-0.00613**	0.00026	-1.73595	-1.63769	0.001137	-0.000002	0.006308	0.002094	0.000021	0.002112	0.000006	0.000847	0.000935
\Sr024.dat	44	0.10	0.645675	0.690549	0.646359	0.646359	0.701569	**0.7016**	**0.001701**	0.656365	0.217557	0.049199	0.048968	0.001511	0.005847	0.00018	**-0.05886**	0.001057	-2.10712	-1.98785	0.001137	-0.000002	0.006308	0.002094	0.000021	0.002112	0.000006	0.000847	0.000935
\Sr026.dat	41	1.05	0.6928	0.698103	0.697846	0.697846	0.702743	**0.7027**	**0.000146**	0.110473	0.057807	0.056543	0.056543	0.000214	0.006751	2.56E-05	**-0.00525**	0.000197	-1.68919	-1.59357	0.001137	-0.000002	0.006308	0.002094	0.000021	0.002112	0.000006	0.000847	0.000935
\Sr027.dat	41	0.99	0.690626	0.696155	0.695905	0.695905	0.701501	**0.7015**	**0.000148**	0.113006	0.057168	0.056157	0.056135	0.000148	0.006703	1.76E-05	**-0.00596**	0.000106	-1.72883	-1.63097	0.001137	-0.000002	0.006308	0.002094	0.000021	0.002112	0.000006	0.000847	0.000935
MADAGASCAR																													
\Sr007.dat	43	3.83	0.709014	0.710528	0.710407	0.710407	0.711736	**0.7117**	**0.000060**	0.072071	0.057459	0.056886	0.056886	5.13E-05	0.006792	6.13E-06	**-0.00141**	3.77E-05	-1.67126	-1.56193	0.001137	-0.000002	0.006308	0.002094	0.000021	0.002112	0.000006	0.000847	0.000935
\Sr008.dat	45	3.87	0.709033	0.710534	0.710435	0.710435	0.711786	**0.7118**	**0.000072**	0.071945	0.057514	0.056905	0.056903	4.18E-05	0.006794	5E-06	**-0.00143**	2.57E-05	-1.6688	-1.55963	0.001137	-0.000002	0.006308	0.002094	0.000021	0.002112	0.000006	0.000847	0.000935
\Sr040.dat	44	3.92	0.709272	0.71076	0.710655	0.710655	0.711857	**0.7119**	**0.000059**	0.071639	0.057323	0.056712	0.056717	4.96E-05	0.006772	5.92E-06	**-0.00127**	0.000273	-1.6774	-1.58245	0.001137	-0.000002	0.006308	0.002094	0.000021	0.002112	0.000006	0.000847	0.000935
\Sr041.dat	43	3.81	0.709178	0.710704	0.710591	0.710591	0.711857	**0.7119**	**0.000056**	0.071891	0.057185	0.056598	0.0566	3.55E-05	0.006758	4.24E-06	**-0.00133**	0.000258	-1.68179	-1.5866	0.001137	-0.000002	0.006308	0.002094	0.000021	0.002112	0.000006	0.000847	0.000935
\Sr007.dat	42	3.75	0.708997	0.710539	0.710421	0.710421	0.711833	**0.7118**	**0.000055**	0.07207	0.057212	0.056618	0.056613	4.25E-05	0.00676	5.07E-06	**-0.0015**	2.9E-05	-1.67983	-1.59984	0.001137	-0.000002	0.006308	0.002094	0.000021	0.002112	0.000006	0.000847	0.000935
\Sr008.dat	43	3.77	0.709309	0.710849	0.710729	0.710729	0.711819	**0.7118**	**0.000069**	0.072025	0.057194	0.056597	0.056587	6.23E-05	0.006757	7.44E-06	**-0.00117**	0.000597	-1.67713	-1.59726	0.001137	-0.000002	0.006308	0.002094	0.000021	0.002112	0.000006	0.000847	0.000935
								0.71181	**0.00009**	n = 6																		
DURANGO																													
\Sr009.dat	42	0.88	0.695709	0.702029	0.700863	0.700863	0.705984	**0.7060**	**0.000111**	0.125581	0.063303	0.057991	0.057991	0.000133	0.006924	1.59E-05	**-0.00542**	0.001597	-1.66581	-1.55683	0.001137	-0.000002	0.006308	0.002094	0.000021	0.002112	0.000006	0.000847	0.000935
\Sr010.dat	43	0.88	0.694861	0.701196	0.700162	0.700162	0.706245	**0.7062**	**0.000172**	0.125604	0.06298	0.057636	0.057627	0.000161	0.006881	1.92E-05	**-0.00641**	9.89E-05	-1.66585	-1.69985	0.001137	-0.000002	0.006308	0.002094	0.000021	0.002112	0.000006	0.000847	0.000935
\Sr009.dat	44	0.84	0.695238	0.701876	0.700628	0.700628	0.706365	**0.7064**	**0.000181**	0.12776	0.062342	0.057014	0.056987	0.000175	0.006804	2.09E-05	**-0.00603**	0.001089	-1.68743	-1.60708	0.001137	-0.000002	0.006308	0.002094	0.000021	0.002112	0.000006	0.000847	0.000935
\Sr010.dat	44	0.83	0.694195	0.700841	0.69974	0.69974	0.70632	**0.7063**	**0.000219**	0.128177	0.062446	0.057227	0.057203	0.000142	0.00683	1.7E-05	**-0.00692**	0.000132	-1.68316	-1.60301	0.001137	-0.000002	0.006308	0.002094	0.000021	0.002112	0.000006	0.000847	0.000935
\Sr038.dat	44	0.85	0.694678	0.701181	0.699969	0.699969	0.706379	**0.7064**	**0.000205**	0.126119	0.061876	0.056671	0.056641	0.00021	0.006763	2.51E-05	**-0.00674**	0.000143	-1.69976	-1.61882	0.001137	-0.000002	0.006308	0.002094	0.000021	0.002112	0.000006	0.000847	0.000935
\Sr039.dat	44	0.86	0.694756	0.701226	0.700059	0.700059	0.706533	**0.7065**	**0.000194**	0.12629	0.062473	0.057196	0.057183	0.000154	0.006828	1.84E-05	**-0.00682**	0.000114	-1.68695	-1.60662	0.001137	-0.000002	0.006308	0.002094	0.000021	0.002112	0.000006	0.000847	0.000935
\Sr040.dat	42	0.85	0.694919	0.701413	0.700177	0.700177	0.706435	**0.7064**	**0.000163**	0.126624	0.062515	0.057267	0.057262	0.000173	0.006837	2.06E-05	**-0.00662**	0.000397	-1.68179	-1.60171	0.001137	-0.000002	0.006308	0.002094	0.000021	0.002112	0.000006	0.000847	0.000935
								0.70632	**0.00035**	n = 7																		

Table 5.8, continued.

sample	88Sr		$^{87}Sr/^{86}Sr_{raw}$	$^{87}Sr/^{86}Sr_{Kr}$	$^{87}Sr/^{86}Sr_{REE}$	$^{87}Sr/^{86}Sr_{Ca}$	$^{87}Sr/^{86}Sr_{Rb}$	$^{87}Sr/^{86}Sri$	± 2 S.E.	$^{84}Sr/^{86}Sr_{raw}$	$^{84}Sr/^{86}Sr_{Kr}$	$^{84}Sr/^{86}Sr_{Ree}$	$^{84}Sr/^{86}Sr$	± 2 S.E.	84Sr/88Sr	± 2 S.E.	$^{87}Rb/^{86}Sr$	± 2 S.E.	$\beta^{86}Sr/^{88}Sr$	$\beta^{87}Rb/^{85}Rb$	83Kr	167Er	84Sr	85Rb	171Yb	86Sr	173Yb	87Sr	88Sr
NIST 610																													
\Sr001.dat	42	0.78	3.279706	3.346346	3.395104	3.395104	0.709255	**0.7092**	**0.000645**	0.173927	0.105119	0.055644	0.055672	0.000257	0.006647	3.07E-05	**2.822213**	0.013852	-1.83089	-1.71111	0.001137	-0.000002	0.006308	0.002094	0.000021	0.002112	0.000006	0.000847	0.000935
\Sr002.dat	43	0.80	3.282946	3.348625	3.396325	3.396325	0.709431	**0.7094**	**0.000609**	0.172195	0.104927	0.057314	0.057328	0.000189	0.006845	2.25E-05	**2.824944**	0.005528	-1.79582	-1.67834	0.001137	-0.000002	0.006308	0.002094	0.000021	0.002112	0.000006	0.000847	0.000935
\Sr003.dat	42	0.79	3.23319	3.299203	3.345746	3.345746	0.708546	**0.7085**	**0.000629**	0.172327	0.104447	0.057099	0.057112	0.000264	0.006819	3.15E-05	**2.772183**	0.0054	-1.80141	-1.68356	0.001137	-0.000002	0.006308	0.002094	0.000021	0.002112	0.000006	0.000847	0.000935
\Sr034.dat	43	0.80	3.268692	3.334382	3.380876	3.380876	0.70981	**0.7098**	**0.000527**	0.172286	0.104684	0.05591	0.05591	0.000139	0.006676	1.66E-05	**2.807702**	0.006535	-1.80076	-1.69883	0.001137	-0.000002	0.006308	0.002094	0.000021	0.002112	0.000006	0.000847	0.000935
\Sr035.dat	44	0.80	3.26688	3.332668	3.378807	3.378807	0.710389	**0.7104**	**0.000575**	0.172496	0.104827	0.05608	0.05608	0.000205	0.006696	2.45E-05	**2.8047**	0.008866	-1.7879	-1.6867	0.001137	-0.000002	0.006308	0.002094	0.000021	0.002112	0.000006	0.000847	0.000935
\Sr036.dat	45	0.78	3.289212	3.356551	3.404334	3.404334	0.710117	**0.7101**	**0.000719**	0.173998	0.106121	0.056541	0.056537	0.000254	0.00675	3.03E-05	**2.831747**	0.00872	-1.79201	-1.69057	0.001137	-0.000002	0.006308	0.002094	0.000021	0.002112	0.000006	0.000847	0.000935
\Sr001.dat	42	0.75	3.304343	3.374764	3.420462	3.420462	0.710078	**0.7100**	**0.000663**	0.174534	0.102219	0.054849	0.054847	0.00016	0.006549	1.91E-05	**2.848236**	0.010495	-1.80251	-1.71667	0.001137	-0.000002	0.006308	0.002094	0.000021	0.002112	0.000006	0.000847	0.000935
\Sr002.dat	44	0.78	3.346142	3.415119	3.460942	3.460942	0.708968	**0.7089**	**0.000829**	0.169996	0.102014	0.056943	0.056937	0.000131	0.006798	1.56E-05	**2.891541**	0.013691	-1.77072	-1.6864	0.001137	-0.000002	0.006308	0.002094	0.000021	0.002112	0.000006	0.000847	0.000935
\Sr003.dat	45	0.78	3.34785	3.416762	3.46192	3.46192	0.709359	**0.7093**	**0.000759**	0.17108	0.102224	0.057228	0.057236	0.000221	0.006834	2.63E-05	**2.892489**	0.01383	-1.76031	-1.67648	0.001137	-0.000002	0.006308	0.002094	0.000021	0.002112	0.000006	0.000847	0.000935
\Sr063.dat	43	0.80	3.30217	3.368199	3.413979	3.413979	0.709298	**0.7093**	**0.000615**	0.169797	0.102854	0.055988	0.055977	0.000184	0.006684	2.19E-05	**2.842751**	0.009729	-1.77562	-1.69106	0.001137	-0.000002	0.006308	0.002094	0.000021	0.002112	0.000006	0.000847	0.000935
\Sr064.dat	41	0.80	3.312498	3.378399	3.423886	3.423886	0.709806	**0.7098**	**0.000662**	0.169289	0.10194	0.055683	0.055706	0.000182	0.006651	2.17E-05	**2.852036**	0.009713	-1.77519	-1.69066	0.001137	-0.000002	0.006308	0.002094	0.000021	0.002112	0.000006	0.000847	0.000935
\Sr065.dat	44	0.81	3.282725	3.347748	3.393199	3.393199	0.709186	**0.7091**	**0.000789**	0.168434	0.102168	0.055376	0.055388	0.00016	0.006613	1.91E-05	**2.821261**	0.008868	-1.79065	-1.70538	0.001137	-0.000002	0.006308	0.002094	0.000021	0.002112	0.000006	0.000847	0.000935
\Sr032.dat	42	0.79	3.340617	3.40792	3.453731	3.453731	0.709543	**0.7095**	**0.000805**	0.170128	0.10213	0.056574	0.056541	0.00017	0.006751	2.03E-05	**2.884382**	0.013469	-1.77839	-1.69371	0.001137	-0.000002	0.006308	0.002094	0.000021	0.002112	0.000006	0.000847	0.000935
\Sr033.dat	44	0.80	3.292945	3.358913	3.403602	3.403602	0.709652	**0.7096**	**0.000797**	0.169069	0.101936	0.056234	0.056258	0.000169	0.006717	2.02E-05	**2.832488**	0.011339	-1.77736	-1.69272	0.001137	-0.000002	0.006308	0.002094	0.000021	0.002112	0.000006	0.000847	0.000935
\Sr034.dat	43	0.80	3.27505	3.340527	3.385155	3.385155	0.709664	**0.7096**	**0.000713**	0.168909	0.10173	0.05609	0.056114	0.00023	0.0067	2.75E-05	**2.814311**	0.010503	-1.7962	-1.71066	0.001137	-0.000002	0.006308	0.002094	0.000021	0.002112	0.000006	0.000847	0.000935
\Sr029.dat	44	0.79	3.291727	3.358452	3.40326	3.40326	0.709739	**0.7097**	**0.000777**	0.169388	0.101047	0.055045	0.055053	0.000145	0.006573	1.73E-05	**2.860347**	0.010068	-1.80129	-1.69933	0.001137	-0.000002	0.006308	0.002094	0.000021	0.002112	0.000006	0.000847	0.000935
\Sr030.dat	42	0.78	3.305547	3.373689	3.418978	3.418978	0.709877	**0.7098**	**0.000578**	0.16931	0.100494	0.054603	0.054578	0.000187	0.006517	2.23E-05	**2.876469**	0.012185	-1.80774	-1.70542	0.001137	-0.000002	0.006308	0.002094	0.000021	0.002112	0.000006	0.000847	0.000935
\Sr031.dat	42	0.78	3.306469	3.374758	3.420269	3.420269	0.710003	**0.7100**	**0.000573**	0.170323	0.100591	0.054164	0.054164	0.000177	0.006467	2.11E-05	**2.877847**	0.011016	-1.80583	-1.70361	0.001137	-0.000002	0.006308	0.002094	0.000021	0.002112	0.000006	0.000847	0.000935
\Sr001.dat	44	0.77	3.253735	3.322008	3.366711	3.366711	0.709411	**0.7094**	**0.000786**	0.172132	0.101809	0.054934	0.054937	0.000213	0.00656	2.55E-05	**2.822068**	0.006354	-1.79621	-1.69454	0.001137	-0.000002	0.006308	0.002094	0.000021	0.002112	0.000006	0.000847	0.000935
\Sr002.dat	43	0.80	3.250937	3.316463	3.361195	3.361195	0.709904	**0.7099**	**0.000737**	0.170426	0.102549	0.055496	0.055496	0.000315	0.006626	3.77E-05	**2.815954**	0.008134	-1.78258	-1.68168	0.001137	-0.000002	0.006308	0.002094	0.000021	0.002112	0.000006	0.000847	0.000935
\Sr003.dat	43	0.79	3.253767	3.319469	3.363841	3.363841	0.709889	**0.7099**	**0.000667**	0.170085	0.102233	0.055635	0.05559	0.000271	0.006638	3.23E-05	**2.818978**	0.006716	-1.78978	-1.68847	0.001137	-0.000002	0.006308	0.002094	0.000021	0.002112	0.000006	0.000847	0.000935
								0.70958	**0.00086**																				
MIR																													
\Sr037.dat	44	2.43	0.701424	0.70375	0.703719	0.703719	0.702992	**0.7030**	**0.000066**	0.079744	0.056901	0.056858	0.056853	7.18E-05	0.006788	8.58E-06	**0.000763**	0.000304	-1.65595	-1.56221	0.001137	-0.000002	0.006308	0.002094	0.000021	0.002112	0.000006	0.000847	0.000935
\Sr038.dat	44	2.36	0.701035	0.703416	0.703376	0.703376	0.702947	**0.7029**	**0.000077**	0.080562	0.057072	0.057019	0.057015	5.36E-05	0.006808	6.4E-06	**0.000456**	5.21E-05	-1.65463	-1.56097	0.001137	-0.000002	0.006308	0.002094	0.000021	0.002112	0.000006	0.000847	0.000935
\Sr039.dat	43	2.56	0.701413	0.703612	0.703583	0.703583	0.703053	**0.7031**	**0.000081**	0.07869	0.057005	0.056964	0.056963	3.71E-05	0.006801	4.43E-06	**0.000561**	2.09E-05	-1.64344	-1.55042	0.001137	-0.000002	0.006308	0.002094	0.000021	0.002112	0.000006	0.000847	0.000935
\Sr004.dat	44	2.37	0.701019	0.70341	0.703373	0.703373	0.702946	**0.7029**	**0.000088**	0.080376	0.056852	0.056802	0.056809	5.74E-05	0.006783	6.86E-06	**0.000456**	4.41E-05	-1.65281	-1.54468	0.001137	-0.000002	0.006308	0.002094	0.000021	0.002112	0.000006	0.000847	0.000935
\Sr005.dat	42	2.46	0.701382	0.70368	0.703644	0.703644	0.702991	**0.7030**	**0.000065**	0.079534	0.056856	0.056809	0.056813	4.82E-05	0.006783	5.76E-06	**0.000792**	0.000458	-1.65474	-1.54649	0.001137	-0.000002	0.006308	0.002094	0.000021	0.002112	0.000006	0.000847	0.000935
\Sr006.dat	44	2.35	0.701296	0.703693	0.703645	0.703645	0.702924	**0.7029**	**0.000096**	0.080516	0.056984	0.056927	0.056928	6.8E-05	0.006797	8.12E-06	**0.000764**	0.000497	-1.64951	-1.5416	0.001137	-0.000002	0.006308	0.002094	0.000021	0.002112	0.000006	0.000847	0.000935
\Sr004.dat	45	2.18	0.700728	0.70333	0.703285	0.703285	0.702979	**0.7030**	**0.000098**	0.082583	0.057004	0.056944	0.056947	4.43E-05	0.006799	5.29E-06	**0.000323**	0.00013	-1.65976	-1.58073	0.001137	-0.000002	0.006308	0.002094	0.000021	0.002112	0.000006	0.000847	0.000935
\Sr005.dat	44	2.18	0.700605	0.703188	0.703154	0.703154	0.702957	**0.7030**	**0.000081**	0.082372	0.05686	0.056789	0.056802	8.69E-05	0.006782	1.04E-05	**0.000221**	6.23E-05	-1.66066	-1.58158	0.001137	-0.000002	0.006308	0.002094	0.000021	0.002112	0.000006	0.000847	0.000935
\Sr006.dat	44	2.22	0.70097	0.703506	0.70347	0.70347	0.703001	**0.7030**	**0.000070**	0.08189	0.056791	0.056747	0.056755	5.28E-05	0.006777	6.31E-06	**0.00049**	0.000443	-1.66416	-1.58491	0.001137	-0.000002	0.006308	0.002094	0.000021	0.002112	0.000006	0.000847	0.000935
\Sr035.dat	43	2.23	0.700987	0.703519	0.703492	0.703492	0.703033	**0.7030**	**0.000086**	0.081605	0.056606	0.056571	0.056569	4.69E-05	0.006754	5.61E-06	**0.000476**	0.000241	-1.67163	-1.59203	0.001137	-0.000002	0.006308	0.002094	0.000021	0.002112	0.000006	0.000847	0.000935
\Sr036.dat	43	2.33	0.701259	0.703687	0.703655	0.703655	0.703014	**0.7030**	**0.000052**	0.080256	0.056522	0.056495	0.05649	5.43E-05	0.006745	6.48E-06	**0.000667**	0.000466	-1.67035	-1.59081	0.001137	-0.000002	0.006308	0.002094	0.000021	0.002112	0.000006	0.000847	0.000935
\Sr037.dat	43	2.36	0.701052	0.703441	0.703411	0.703411	0.703078	**0.7031**	**0.000065**	0.079982	0.056478	0.056431	0.05642	9.56E-05	0.006737	1.14E-05	**0.000343**	3.56E-05	-1.67072	-1.59116	0.001137	-0.000002	0.006308	0.002094	0.000021	0.002112	0.000006	0.000847	0.000935
\Sr032.dat	45	2.54	0.701554	0.703784	0.70376	0.70376	0.703042	**0.7030**	**0.000072**	0.077918	0.056006	0.05596	0.055951	6.1E-05	0.006681	7.28E-06	**0.000647**	2.55E-05	-1.68024	-1.58513	0.001137	-0.000002	0.006308	0.002094	0.000021	0.002112	0.000006	0.000847	0.000935
\Sr033.dat	43	2.51	0.701381	0.70364	0.703615	0.703615	0.70314	**0.7031**	**0.000073**	0.078448	0.056254	0.056206	0.056197	0.000102	0.00671	1.21E-05	**0.000498**	2.6E-05	-1.67048	-1.57593	0.001137	-0.000002	0.006308	0.002094	0.000021	0.002112	0.000006	0.000847	0.000935
\Sr034.dat	43	2.64	0.701685	0.703838	0.703804	0.703804	0.703076	**0.7031**	**0.000074**	0.07739	0.056304	0.056254	0.056254	6.41E-05	0.006717	7.65E-06	**0.000669**	2.88E-05	-1.66905	-1.57457	0.001137	-0.000002	0.006308	0.002094	0.000021	0.002112	0.000006	0.000847	0.000935
\Sr004.dat	44	2.56	0.701531	0.703743	0.703706	0.703706	0.703062	**0.7031**	**0.000061**	0.078285	0.056539	0.056488	0.056488	4.48E-05	0.006745	5.35E-06	**0.000684**	2.17E-05	-1.65402	-1.5604	0.001137	-0.000002	0.006308	0.002094	0.000021	0.002112	0.000006	0.000847	0.000935
\Sr005.dat	44	2.55	0.701507	0.703723	0.703676	0.703676	0.703076	**0.7031**	**0.000071**	0.07834	0.056536	0.056494	0.056503	6.58E-05	0.006746	7.85E-06	**0.000634**	1.79E-05	-1.66336	-1.56921	0.001137	-0.000002	0.006308	0.002094	0.000021	0.002112	0.000006	0.000847	0.000935
\Sr006.dat	42	2.46	0.701197	0.703492	0.703472	0.703472	0.703048	**0.7030**	**0.000059**	0.078972	0.056403	0.056372	0.056379	6.78E-05	0.006732	8.09E-06	**0.000444**	2.4E-05	-1.66591	-1.57161	0.001137	-0.000002	0.006308	0.002094	0.000021	0.002112	0.000006	0.000847	0.000935
\Sr007.dat	44	2.52	0.701376	0.703626	0.703604	0.703604	0.703131	**0.7031**	**0.000065**	0.078511	0.056342	0.056298	0.0563	4.26E-05	0.006722	5.09E-06	**0.000501**	2.11E-05	-1.67686	-1.58194	0.001137	-0.000002	0.006308	0.002094	0.000021	0.002112	0.000006	0.000847	0.000935
								0.70303	**0.00012**																				

Appendix C: Supplementary material for chapter 6.

Table 6.5. Uranium-lead isotope data for apatite grains from trondhjemite sample MS 27.

	207Pb[a] (cps)	U[b] (ppm)	Pb[b] (ppm)	Thb U	206Pbc[c] (%)	206Pbd 238U	±2s[f] (%)	207Pbd 235U	±2s[f] (%)	207Pbd 206Pb	±2s[f] (%)	rho[e]	206Pb 238U	±2s[f] (Ma)	207Pb 235U	±2s[f] (Ma)	207Pb 206Pb	±2s[f] (Ma)	disc (%)
MS 27 Weergevonden Main Tronhjemite																			
Run number: 12	5812	9	5	0.29	12.0	0.5	1.8	13.9031	2.6	0.1990	1.9	0.69	2642	40	2743	25	2818	31	94
Run number: 13	1778	1	1	0.65	38.5	0.5	27.3	18.6303	27.5	0.2802	3.3	0.99	2537	600	3023	307	3364	51	75
Run number: 16	5343	8	5	0.17	12.1	0.5	2.5	13.8288	3.1	0.1996	1.9	0.79	2624	54	2738	30	2823	31	93
Run number: 17	3479	6	3	0.32	13.2	0.5	2.4	13.4453	3.1	0.1977	2.0	0.77	2585	52	2711	30	2807	32	92
Run number: 20	4021	6	3	0.30	13.8	0.5	3.9	13.5248	4.4	0.1998	2.0	0.89	2575	84	2717	43	2825	32	91
Run number: 28	4786	6	5	0.33	7.5	0.6	2.3	21.6751	2.7	0.2539	1.4	0.86	3107	57	3169	27	3209	22	97
Run number: 30	3849	5	3	0.29	17.0	0.5	4.0	13.3031	4.6	0.2007	2.3	0.87	2530	84	2701	44	2832	37	89
Run number: 45	5215	9	5	0.14	8.6	0.5	1.5	13.9338	2.1	0.1972	1.6	0.68	2667	32	2745	20	2803	26	95
Run number: 49	2287	2	1	0.03	26.8	0.4	10.0	10.7501	10.4	0.1917	2.8	0.96	2200	190	2502	102	2757	47	80
Run number: 50	6530	8	5	0.30	15.1	0.5	1.8	14.2496	2.7	0.2070	2.0	0.66	2611	38	2766	26	2882	33	91
Run number: 51	822	1	1	-0.11	12.5	0.7	16.0	18.5674	16.2	0.1990	2.6	0.99	3332	430	3020	169	2818	42	118
Run number: 52	4294	5	3	0.33	18.0	0.5	3.4	12.7074	4.2	0.1971	2.4	0.82	2473	71	2658	40	2802	39	88
Run number: 55	3808	5	4	0.16	9.1	0.6	3.0	21.3680	3.4	0.2533	1.5	0.89	3077	74	3155	33	3206	24	96
Run number: 56	3560	5	3	0.15	9.1	0.5	3.2	17.9040	3.6	0.2537	1.5	0.90	2664	71	2985	35	3208	24	83
Run number: 58	17126	30	17	0.26	7.3	0.5	1.0	14.1064	1.6	0.2001	1.3	0.60	2662	21	2757	15	2827	21	94
Run number: 59	1875	1	2	0.06	39.3	0.9	13.3	37.4461	13.7	0.3014	3.3	0.97	4141	419	3705	145	3477	51	119
Run number: 60	1629	1	1	-0.19	30.9	0.4	14.2	13.6313	14.5	0.2711	3.0	0.98	2004	249	2724	147	3313	46	60
Run number: 72	39402	46	39	0.67	b.d.	0.7	0.7	29.5503	0.9	0.3028	0.5	0.80	3450	19	3472	9	3484	8	99
Run number: 74	2190	3	2	0.32	13.8	0.6	5.1	19.6722	5.5	0.2516	2.0	0.93	2896	121	3075	55	3195	31	91
Run number: 75	4330	3	3	-0.01	29.0	0.7	5.8	26.6707	8.9	0.2626	6.7	0.65	3558	161	3371	91	3262	105	109
Run number: 76	1108	1	1	-0.14	17.5	0.5	15.1	15.8532	15.4	0.2541	2.9	0.98	2407	310	2868	158	3210	47	75
Run number: 77	5528	9	5	0.33	9.4	0.5	1.4	13.6678	2.2	0.1960	1.7	0.64	2639	31	2727	21	2793	28	94
Run number: 81	7490	12	7	0.31	8.9	0.5	1.8	13.8499	2.4	0.1983	1.5	0.76	2642	39	2739	23	2812	25	94
Run number: 82	6891	11	6	0.14	9.1	0.5	1.7	14.3079	2.3	0.1983	1.6	0.73	2713	37	2770	22	2812	25	96
Run number: 85	4026	7	5	0.20	3.1	0.7	5.4	23.7076	5.5	0.2597	1.1	0.98	3276	141	3256	55	3245	17	101
Run number: 87	4403	6	4	0.27	11.5	0.5	2.2	13.8099	2.9	0.1999	1.9	0.77	2619	49	2737	28	2825	30	93
Run number: 88	2214	3	2	0.07	17.3	0.5	7.1	12.8167	7.5	0.1975	2.3	0.95	2486	149	2666	73	2806	38	89
Run number: 90	37216	52	37	0.84	6.8	0.6	0.9	21.4615	1.4	0.2527	1.0	0.66	3094	22	3160	13	3202	16	97
Run number: 91	9493	409	51	0.04	b.d.	0.1	0.7	3.2820	1.1	0.1992	0.8	0.68	728	5	1477	8	2820	13	26
Run number: 93	4559	0	0	2.47	15.4	0.7	4.3	25.0025	4.7	0.2776	1.9	0.92	3240	111	3308	47	3350	29	97
Run number: 95	3285	0	0	3.60	22.8	0.7	6.4	28.0053	6.9	0.2787	2.4	0.94	3529	177	3419	70	3356	38	105
Run number: 97	2975	0	0	1.21	22.7	0.5	12.3	19.8618	12.6	0.2812	2.5	0.98	2666	274	3085	129	3370	40	79

$^{207}Pb/^{235}U$ error is the quadratic addition of the $^{207}Pb/^{206}Pb$ and $^{206}Pb/^{238}U$ uncertainty.

[a] Within run background-corrected mean signal in cps (counts per second).

[b] U content and Th/U ratio were calculated relative to reference

[c] Pb 206/204 ratios measured and percentage of common Pb on the ^{206}Pb. b.d. = below dectection limit.

[d] corrected for background, within-run Pb/U fractionation (in case of $^{206}Pb/^{238}U$) and common Pb using Stacy and Kramers (1975) model Pb and subsequently normalised to reference material used;

[e] rho is the $^{206}Pb/^{238}U/^{207}Pb/^{235}U$ error correlation coefficient.

[f] Accuracy and reproducibilty was checked by repeated analyses (n = 16) of reference zircon Plesovice, Griedel, and 91500; data given as mean with 2 standard deviation uncertainties

Table 6.6. Major- and trace-element concentrations of apatite grains from mafic schist sample MS 21.

Sample							**MS 21**								
# of analysis EMP	46	47	48	49	50	51	52	53	54	55	56	57	58	59	60
# of analysis ICP MS				2				3	6						1
Weight%															
Na	b.d.	b.d.	b.d.	b.d.	b.d.	b.d.	b.d.	b.d.	b.d.	b.d.	b.d.	b.d.	b.d.	b.d.	b.d.
Si	b.d.	0.21	b.d.	b.d.	0.04	b.d.	0.08	b.d.	0.05	0.05	0.02	b.d.	b.d.	b.d.	b.d.
F	3.49	3.66	3.47	3.79	3.70	3.60	3.59	3.56	3.59	3.42	3.40	3.76	3.72	3.76	3.42
P	18.00	17.53	17.67	17.73	17.89	18.34	17.98	18.12	17.74	17.70	17.97	18.20	18.12	18.27	17.83
Cl	b.d.	b.d.	b.d.	b.d.	b.d.	b.d.	b.d.	b.d.	b.d.	b.d.	b.d.	b.d.	b.d.	b.d.	b.d.
Ca	40.04	39.76	39.95	39.98	40.09	40.91	40.83	40.63	39.89	39.98	40.16	40.79	39.67	40.68	40.11
Ce	b.d.	b.d.	b.d.	b.d.	b.d.	b.d.	b.d.	b.d.	b.d.	b.d.	b.d.	b.d.	b.d.	b.d.	b.d.
S	b.d.	b.d.	b.d.	b.d.	b.d.	b.d.	b.d.	b.d.	b.d.	b.d.	b.d.	b.d.	b.d.	b.d.	b.d.
La	b.d.	b.d.	b.d.	b.d.	b.d.	b.d.	b.d.	b.d.	b.d.	b.d.	b.d.	b.d.	b.d.	b.d.	b.d.
Sr	b.d.	b.d.	b.d.	b.d.	b.d.	b.d.	b.d.	b.d.	b.d.	b.d.	b.d.	b.d.	b.d.	b.d.	b.d.
Y	0.08	0.07	0.06	0.09	0.16	0.09	0.07	0.09	0.08	0.06	0.08	0.07	0.05	0.08	0.07
O	37.63	38.15	38.12	38.27	38.26	38.71	38.58	38.81	37.77	38.45	37.97	38.85	38.40	39.07	38.23
Total	99.36	99.42	99.35	99.94	100.21	101.76	101.17	101.28	99.15	99.71	99.70	101.71	100.01	101.91	99.74
Weight% Oxides															
CaO	56.02	55.63	55.90	55.93	56.09	57.24	57.13	56.85	55.82	55.94	56.19	57.07	55.51	56.92	56.12
SrO	0.00	0.00	0.00	0.00	0.00	0.00	0.00	0.00	0.00	0.00	0.00	0.00	0.00	0.00	0.00
Ce_2O_3	0.00	0.00	0.00	0.00	0.00	0.00	0.00	0.00	0.00	0.00	0.00	0.00	0.00	0.00	0.00
P_2O_5	41.25	40.16	40.48	40.62	40.98	42.03	41.19	41.52	40.66	40.57	41.18	41.71	41.53	41.87	40.84
SiO_2	0.00	0.44	0.00	0.00	0.09	0.00	0.18	0.00	0.11	0.10	0.05	0.00	0.00	0.00	0.00
SO_3															
Atoms p.f.u. [a]															
Ca	10.19	10.24	10.29	10.27	10.22	10.20	10.29	10.23	10.24	10.26	10.21	10.23	10.09	10.19	10.26
Sr	0.00	0.00	0.00	0.00	0.00	0.00	0.00	0.00	0.00	0.00	0.00	0.00	0.00	0.00	0.00
Ce	0.00	0.00	0.00	0.00	0.00	0.00	0.00	0.00	0.00	0.00	0.00	0.00	0.00	0.00	0.00
∑	10.19	10.24	10.29	10.27	10.22	10.20	10.29	10.23	10.24	10.26	10.21	10.23	10.09	10.19	10.26
P	5.93	5.84	5.89	5.89	5.90	5.92	5.86	5.91	5.89	5.88	5.91	5.91	5.96	5.92	5.90
Si	0.00	0.08	0.00	0.00	0.02	0.00	0.03	0.00	0.02	0.02	0.01	0.00	0.00	0.00	0.00
∑	5.93	5.92	5.89	5.89	5.92	5.92	5.89	5.91	5.91	5.90	5.92	5.91	5.96	5.92	5.90
F	1.87	1.99	1.89	2.05	1.99	1.89	1.91	1.89	1.94	1.85	1.82	1.99	1.99	1.99	1.84
Cl	0.00	0.00	0.00	0.00	0.00	0.00	0.00	0.00	0.00	0.00	0.00	0.00	0.00	0.00	0.00
OH	0.13	0.01	0.11	-0.05	0.01	0.11	0.09	0.11	0.06	0.15	0.18	0.01	0.01	0.01	0.16
spot#				**MS21-2**				**MS21-3**	**MS21-6**						**MS21-1**
^{6}Li				<1.97				<1.74	<1.74						<2.15
^{7}Li				<1.41				<1.33	<1.37						<1.61
^{43}Ca				399517.8				406664.8	398803.1						400947.1
^{44}Ca				444179.1				445003	433015.2						439430.1
^{47}Ti				14.75				12.09	13.71						12.91
^{49}Ti				<5.82				<5.44	<5.63						<6.76
^{51}V				0.57				0.48	0.96						0.54
^{53}Cr				<6.49				9.34	<6.21						8.63
^{88}Sr				135.9				125.76	117.31						124.74
^{89}Y				876.8				885.52	704.34						824.01
^{91}Zr				<0.93				<0.86	<0.90						<1.07
^{93}Nb				<0.0240				<0.0199	<0.0280						<0.0286
^{139}La				51.59				42.81	26.39						13.26
^{140}Ce				157.07				133.44	99.09						43.19
^{141}Pr				27.84				24.69	20.29						8
^{146}Nd				171.22				168.05	145.47						55.32
^{147}Sm				81.24				88.96	77.16						41.99
^{153}Eu				10.09				10.01	8.54						6.78
^{157}Gd				179.86				213.74	168.33						138.16
^{159}Tb				31.16				36.4	27.89						27.61
^{163}Dy				187.84				209.97	158.37						173.31
^{165}Ho				30.07				34.1	24.69						31.4
^{166}Er				66.09				70.48	51.64						79.35
^{169}Tm				6.71				6.8	5.25						9.42
^{172}Yb				35.88				34.53	28.05						52.95
^{175}Lu				4.71				4.37	3.24						6.94
^{178}Hf				<0.110				<0.091	<0.114						<0.130
^{181}Ta				<0.0238				<0.0156	<0.0173						<0.0240
^{208}Pb				1.81				1.922	1.855						**1.431**
^{232}Th				0.315				0.307	0.161						0.0692
^{238}U				2.359				3.58	1.383						1.102
Th/U				0.13				0.09	0.12						0.06
Sr/Y				0.2				0.1	0.2						0.2
ASI [b]	1.1	1.1	1.1	1.1	1.1	1.1	1.1	1.1	1.1	1.1	1.1	1.1	1.1	1.1	1.1
$^{207}Pb/^{206}Pb$ age [Ga] [c]				3.2				3.1	3.2						3.5

[a] : Mineral formula calculation using Appoach 2 of Ketcham (2015).
[b] : ASI .= Alumina Saturation Index "Al_2O_3 / ($CaO+Na_2O+K_2O$)", using whole-rock compositions of Mühlberg et al. (2021).
[c] : Approximate age of targeted apatite zone; age data from Mühlberg et al. (2021).

Ketcham, R.A., 2015. Technical Note: Calculation of stoichiometry from EMP data for apatite and other phases with mixing on monovalent anion sites †. Am. Mineral. 100, 1620–1623.
Mühlberg, M., Stevens, G., Moyen, J.-F., Kisters, A.F.M., Lana, C., 2020. Thermal evolution of the Stolzburg Block, Barnerton granitoid-greenstone terrain, South Africa: Implications for Paleoarchean tectonic processes. Prec. Research

Appendix D: Abstracts presented at conferences.

Poster presentation at Goldschmid2018, 11-17 August 2019, Boston, MA, United States of America.

New insights on the thermal evolution of the Stolzburg Pluton, Barberton granitoid greenstone terrain, South Africa, by U-Pb apatite and zircon ages

M. MÜHLBERG[1,2]*, G. STEVENS[1], J.F. MOYEN[2], C. LANA[3], A.F.M. KISTERS[1] AND L. BRACCIALI[4]

[1]Department of Earth Sciences, University of Stellenbosch, Priate Bag X1, Matieland 7602, South Africa (*correspondence: moritzm@sun.ac.za; gs@sun.ac.za)

[2]Université de Lyon, Laboratoire Magmas et Volcans, UJM-UCA-CNRS-IRD, 23 rue Dr. Paul Michelon, 42023 Saint Etienne, France (jean.francois.moyen@univ-st-etienne.fr)

[3]Departamento de Geologia (DEGEO), Universidade Federal de Ouro Preto, Morro do Cruzeiro, Ouro Preto, Minas Gerais, 35400000, Brazil (cristianodeclana@gmail.com)

[4]Central Analytical Facilities, Stellenbosch University, Stellenbosch, South Africa (bracciali@sun.ac.za)

Two different models currently prevail to explain ca. 3.23 Ga garnet-amphibolite facies metamorphism to the south of the Barberton greenstone belt: A sagduction model involving ca. 3.23 Ga diapiric rise of partially molten tonalite-trondhjemite-granodiorite (TTG) plutons and sinking of more dense greenstone keels [1], and thickening of cool proto-continental crust due to lateral plate tectonics, followed by orogenic collapse and long-lived shortening to steepen fabrics [2]. We report new U-Pb apatite and zircon ages, as well as Lu-Hf zircon data for the Paleoarchean Stolzburg and Theespruit plutons which are proposed to represent the anatectic domes. Zircons from the Stolzburg and Theespruit plutons provide a crystallization age of ca. 3.45 Ga, confirming earlier studies, and εHft values of +1.2 to -3.3. Felsic dykes cross-cutting the 3.45 Ga plutons yielded a crystallization age of ca. 3.23 Ga and εHft values of +0.4 to -2.1. U-Pb apatite ages determined for both plutons and cross-cutting felsic dykes are ca. 3.45, 3.35, 3.21, 3.11 and 2.82 Ga. The preservation of the apatite ages indicates that no prolonged heating of the granitoids above ca. 550 °C has occurred after crystallization and cooling of the plutons. The Hf isotopic data show that the ca. 3.23 Ga dykes are less evolved than the host TTG plutons and are not produced by melt extraction following anatexis of the latter or their equivalents. This argues for metamorphism due to orogenic thickening of cool felsic crust at ca. 3.23 Ga.

[1] Van Kranendonk (2015) *Geol. Soc. London Spec. Pub.* **389**, 83-111. [2] Stevens & Moyen (2007) *Dev. Prec. Geol.* **15**, 669-698.

New Insights on the Thermal Evolution of the Stolzburg Pluton, Barberton Granitoid Greenstone Terrain, South Africa

M. Mühlberg[a,b], G. Stevens[a], J.F. Moyen[b], C. Lana[c], A.F.M. Kisters[a]

[a]Department of Earth Sciences, University of Stellenbosch, Private Bag X1, Matieland 7602, South Africa
[b]Université de Lyon, Laboratoire Magmas et Volcas, UJM-UCA-CNRS-IRD, 23 rue Dr. Paul Michelon, 42023 Saint Etienne, France
[c]Departamento de Geologia (DEGEO), Universidade Federal de Ouro Preto, Morro do Cruzeiro, Ouro Preto, Minas Gerais,, Brazil
[d]Central Analytical Facilities, University of Stellenbosch, Private Bag X1, Matieland 7602, South Africa

Introduction:

The Barberton Granitoid Greenstone Terrain (BGGT), containing some of the Earth's oldest rocks, is comprised of deformed supracrustal rocks and surrounding tonalite-trondhjemite-granodiorite (TTG) plutons. It was formed during two accretionary events, D_1 at ca. 3.45 Ga and D_2 at ca. 3.23 Ga, accompanied by TTG plutonism. In the south of the BGGT, the lowermost units of the supracrustal greenstones have experienced amphibolite-facies metamorphism contemporaneous with the D_2 event. Two different models currently prevail for this event: A model of sagduction via partial convective overturn involving diapiric rise of paritally molten TTG plutons and sinking of more dense greenstone keels [1], and thickening of cool proto-continental crust due to lateral plate tectonics followed by orogenic collapse and long-lived shortening to steepen fabrics [2].

Methods:

Samples of Trondhjemitic gneiss, which, in the model of partial convective overturn, are proposed to represent the anatectic domes, and of cross-cutting felsic dykes were taken from the Stolzburg domain, comprised of the Stolzburg, Theespruit and several smaller plutons (Fig 1). The U-Pb and Lu-Hf isotopic composition of zircon grains and the U-Pb isotopic composition of apatite grains were determined using LA ICP-MS. The aim of this study is to constrain the thermal history of the TTG rocks in order to asses the viability of the different tectonic models.

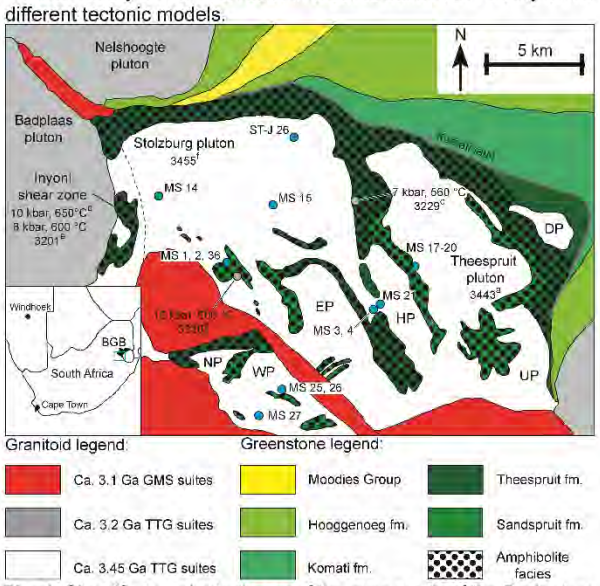

Fig. 1. Simplified geological map of the area south of the Barberton Greenstone Belt. Emplacement respectively metamorphic ages in Ma.

Results:

The U-Pb zircon dates obtained for the Trondhjemitic gneisses of the Stolzburg pluton yielded ages of ca. 3.43 - 3.45 Ga, confirming the emplacement ages of ca. 3.45 Ga suggested by earlier studies. There is a spread of near-concordant data points down to ca. 3.3 Ga in many of the samples (Fig. 2). It is interpreted to be the result of Pb loss or partial resetting, as this spread is most pronounced in the proximity of later cross-cutting dykes, though a few concordant points younger than ca. 3.4 Ga also suggest new zircon growth. Rims of ca. 3.2 Ga in sample MS 4 have significantly lower Th/U ratios (0.08 - 0.30) compared to ca. 3.44 Ga oscillatory zoned cores from the same sample (0.40 - 0.77), indicating metamorphic growth. This likely happened at ca. 3.23 Ga, for which amphibolite-facies metamorphic conditions have been reported (see Fig. 1). The cross-cutting dykes, except for sample MS 25, yielded only a handful of zircon grains. Most concordant points are aged around ca. 3.2 Ga, though some older, likely inherited grains, are also present. MS 25 gave a Concordia age of 3223 ± 4 Ma.

The Hf isotopic data obtained on spots with concordant U-Pb dates show, that the ca. 3.2 Ga felsic dykes cross-cutting the Trondhjemitic gneisses are less evolved compared to the host TTGs (Fig. 3). The later dykes yielded εHf(3.2 Ga) values of +0.4 to -2.1, the inherited grain of ca. 3.44 Ga giving an εHf(3.44 Ga) value of +1.9. Model ages range from 3.49 to 3.63 Ga. The εHf(t) values of the main Trondhjemites range from +1.8 to -4.1 with model ages of 3.62 - 3.74 Ga. A single spot in sample MS 14 of ca. 3.2 Ga yielded an ε Hf(3.2 Ga) value of -9.1 with a model age of 4.01 Ga, indicating a possible old component in this sample.

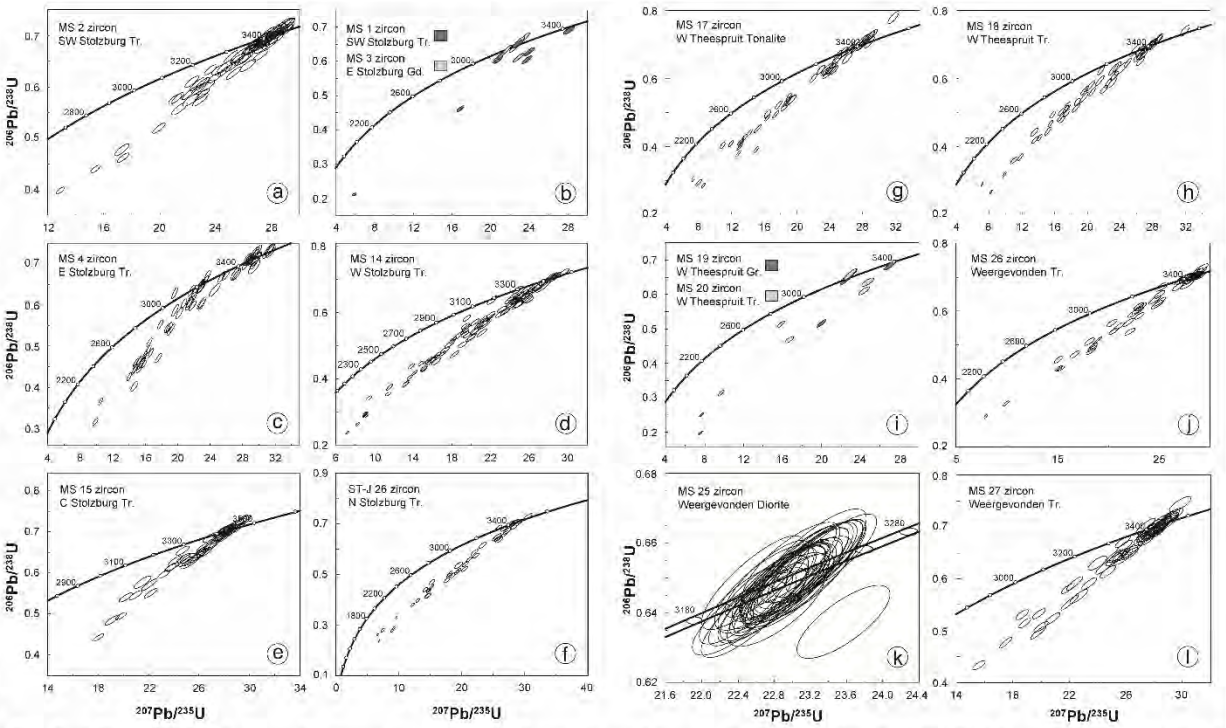

Fig. 2. U-Pb concordia diagrams for zircon grains from TTG samples and cross-cutting felsic dykes from the Stolzburg (a-f), Theespruit (g-i) and Weergevonden (j-l) plutons. Error ellipses are 2σ. Tr. = Trondhjemite, Gd. = Granodiorite, Gr. = Granite.

The mostly discordant U-Pb apatite spots (Fig. 4) seem to show distinct trends pointing towards upper intercepts at ca. 3.45, 3.35, 3.21, 3.11 and 2.82 Ga, that can bee seen in most of the samples. The preservation of pre-3.23 Ga apatite dates indicates, that no prolonged heating of the granitoids above ca. 550 °C has occurred after crystallisation and cooling of the plutons. This is at odds with a suggested diapiric rise of the plutons at ca. 3.23 Ga, as the required temperatures and timescales would lead to a reset of the U-Pb apatite ages. The preservation of ca. 3.45 Ga apatite dates also supports an interpretation of concordant zircon dates younger than ca. 3.4 Ga as the result of metamorphic rather than igneous growth.

The metamorphic conditions reported for the ca. 3.2 Ga event also exceed the closure temperature of apatite by some 100 °C. Taking the reported pressure and temperature conditions, along with the closure temperature of the U-Pb system in apatite, at face value would imply geothermal gradients and exhumation rates comparable to modern orogens, favouring metamorphism due to orogenic thickening of cool felsic crust.

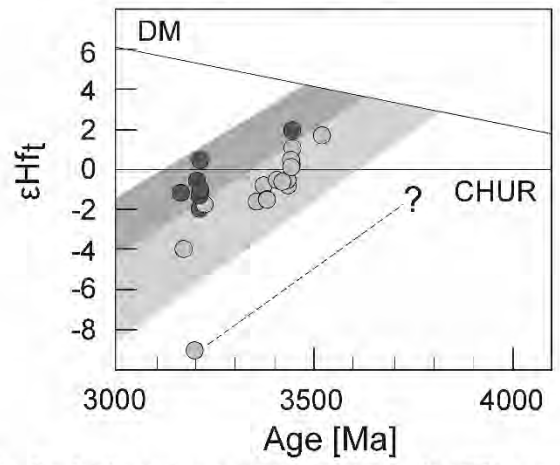

Top: **Fig. 3.** Hf isotopic evolution for zircon grains from TTG samples (light grey) and cross-cutting felsic dykes (dark grey) from the Stolzburg, Theespruit and Weergevonden plutons. CHUR = chondritic uniform reservoir; DM = depleted mantle, after [3]. *Right:* **Fig. 4.** U-Pb concordia diagrams for apatite grains from granitoid (a-c, e, f) and meta-sedimenary (d) samples from the Stolzburg domain. Error circles are 2σ.

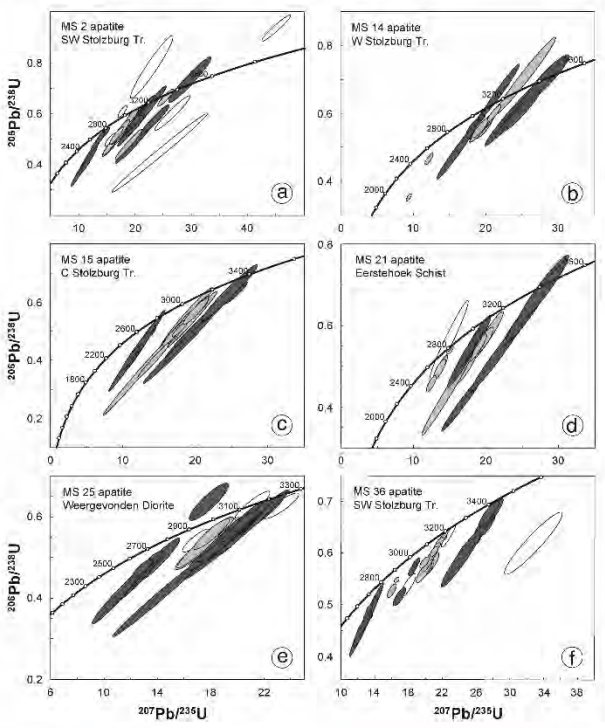

Summary:

- U-Pb zircon dates suggest emplacement of the Stolzburg domain at ca. 3.45 Ga. Younger dates likely represent metamorphic growth.
- Hf isotopic zircon data suggest a more juvenile source for the ca. 3.2 Ga felsic dykes compared to the host TTGs, indicating that those dykes are not the melting product of the host rocks or their equivalent.
- U-Pb apatite dating revealed a range of dates from ca. 3.45 down to ca. 2.82 Ga.
- Preservation of ca. 3.45 Ga apatite dates obtained at the emplacement of TTG plutons argues against partial convective overturn at ca 3.23 Ga, and for accretion through lateral tectonics.

[1] Van Kranendonk (2015) *Geol. Soc. London Spec. Pub.* **389**, 83-111.
[2] Stevens & Moyen (2007) *Dev. Prec. Geol.* **15**, 669-698.
[3] Blichert-Toft & Albarède (2008) *EPSL* **265**, 686-702.

Oral presentation at the 11th Igneous & Metamorphic Studies Group Meeting, 13-16 January 2019, Parys, Freestate, South Africa.

New insights on the thermal evolution of the Stolzburg Pluton, Barberton granitoid greenstone terrain, South Africa, by U-Pb apatite and zircon ages

M. MÜHLBERG[1,2]*, G. STEVENS[1], J.F. MOYEN[2], C. LANA[3], A.F.M. KISTERS[1] AND L. BRACCIALI[4]

[1]Department of Earth Sciences, University of Stellenbosch, Priate Bag X1, Matieland 7602, South Africa (*correspondence: moritzm@sun.ac.za; gs@sun.ac.za)

[2]Université de Lyon, Laboratoire Magmas et Volcans, UJM-UCA-CNRS-IRD, 23 rue Dr. Paul Michelon, 42023 Saint Etienne, France (jean.francois.moyen@univ-st-etienne.fr)

[3]Departamento de Geologia (DEGEO), Universidade Federal de Ouro Preto, Morro do Cruzeiro, Ouro Preto, Minas Gerais, 35400000, Brazil (cristianodeclana@gmail.com)

[4]Central Analytical Facilities, Stellenbosch University, Stellenbosch, South Africa (bracciali@sun.ac.za)

The geodynamic processes that led to the juxtaposition of tonalite-trondhjemite-granodiorite (TTG) plutons, high-pressure amphibolite-facies metavolcanic and metasedimentary rocks of the Theespruit and Sandspruit Formations and the lower greenschist-facies supracrustal rock of the Barberton Greenstone Belt (BGB are to this day subject of debate. Two different "end-member" models currently prevail: A sagduction model involving ca. 3.23 Ga diapiric rise of partially molten TTG plutons and sinking of more dense greenstone keels [1], and thickening of cool proto-continental crust due to lateral plate tectonics, followed by orogenic collapse and long-lived shortening to steepen fabrics [2]. Deciphering the metamorphic history of the gneissic TTG plutons is a crucial step in reconstructing the geodynamic setting, as both models involve distinct pressure-temperature-time paths. This is difficult to do by conventional metamorphic studies as the biotite-quartz-plagioclase assemblage of the plutons is unresponsive to metamorphic change in the relevant pressure-temperature range. We report new U-Pb apatite and zircon ages, as well as Lu-Hf zircon data for the Paleoarchean Stolzburg and Theespruit plutons which are proposed to represent the anatectic domes. Zircons from trondhjemite samples from the Stolzburg and Theespruit plutons provide a crystallization age of ca. 3.44 Ga with $\varepsilon Hf_{3.44\ Ga}$ values of +1.2 to -0.5. The zircon grains contain inheritance of ca. 3.51 to 3.53 Ga with $\varepsilon Hf_{3.52\ Ga}$ values of +1.9. Rare younger dates down to ca. 3.20 Ga are likely due to post-crystallization recrystallization. Felsic dykes cross-cutting the 3.45 Ga plutons yielded an intrusion age of ca. 3.22 Ga and $\varepsilon Hf_{3.22\ Ga}$ values of +0.7 to -1.5. U-Pb apatite ages determined for both plutons and cross-cutting felsic dykes are ca. 3.45, 3.35, 3.21, 3.11 and 2.82 Ga. The preservation of the ca. 3.45 Ga apatite ages indicates that no prolonged heating of the granitoids above ca. 400 – 500 °C has occurred after crystallization and cooling of the plutons. The Hf isotopic data show that the cross-cutting dykes are less evolved than the host TTG plutons and are not produced by melt extraction following anatexis of the latter or their equivalents. This argues against partial melting of the TTG plutons at ca. 3.23 Ga and rather for metamorphism due to orogenic thickening of cool felsic crust.

[1] Van Kranendonk (2015) *Geol. Soc. London Spec. Pub.* **389**, 83-111. [2] Stevens & Moyen (2007) *Dev. Prec. Geol.* **15**, 669-698.

Poster presentation at Petrochro-2019, 3-5 June 2019, Potsdam, Brandenburg, Germany.

The assembly, metamorphic and deformation history of the Stolzburg pluton and surrounding rocks, Kaapvaal craton, South Africa

Moritz Mühlberg[1], Gary Stevens[1], Jean-François Moyen[2] and Alex Kisters[1]

Contact author: Moritz Mühlberg (moritzm@sun.ac.za)
[1] Department of Earth Sciences, Stellenbosch University (South Africa)
[2] Laboratoire Magmas et Volcans, University of Lyon (France)

The tonalite-trondhjemite-granodiorite (TTG) rocks developed to the South and West of the Barberton Greenstone Belt (BGB) possibly represent some of the best preserved TTG plutons in the world. The origin and evolution of these plutons has come to be a central issue in the understanding of the Paleo- to Mesoarchean evolution of the proto-Kaapvaal-craton crust. The models seeking to explain the tectonic processes of the early Archean can be summarized into two end-member models dominated by vertical and horizontal tectonics, respectively.

In the vertical tectonic model, the BGB is assembled as a single vertically stacked sequence. The TTG plutons are interpreted to have crystallized below the greenstone sequence at ca. 3.45 Ga and are proposed to have the undergone anatexis at ca. 3.23 Ga, resulting in the emplacement of the plutons as diapiric domes that ascended simultaneously with gravity-driven sinking of keels of greenstone belt rocks. Metamorphism of greenstone belt rocks in contact with the plutons is considered to be a consequence of increasing pressure due to sinking, combined with heating by the rising anatectic diapirs [1]. The horizontal tectonic model involves ca. 3.23 Ga metamorphism of greenstone belt rocks and ca. 3.45 Ga TTG plutons, as well as formation of ca. 3.23 Ga TTG rocks during accretionary tectonics, with partial subduction of the ca. 3.45 TTG plutons and associated greenstone belt rocks, resulting in high pressure lower- to mid-amphibolite-facies metamorphism. In this model, the TTG plutons and the amphibolite-facies lower sequences of the BGB were exhumed and brought into contact with the lower greenschist-facies rocks of the BGB along a detachment by syn-orogenic extensional collapse. The syn-metamorphic ca. 3.23 Ga TTG magmas are regarded products of melting of metamafic rocks rather than anatexis of older TTG rocks [2].

Because both models outlined above predict different P-T paths for plutons and greenstones, deciphering the thermal history of each is crucial for the reconstruction of the geodynamic setting in the early to middle Archean. This has previously been done through P-T work on the metamafic lithologies, but is difficult to do on the TTG plutons, because their mineral assemblage is unresponsive to change in metamorphic grade. This project aims to contribute to the understanding of the geodynamic evolution of the BGB and related rocks using thermochronology. The chosen field area is the Stolzburg block, which is comprised of a series of Trondhjemite plutons and amphibolite-facies rocks from the lowermost strata of the BGB. The timing of emplacement and of any potential consequent re-melting or fluid penetration of the Trondhjemite plutons is investigated using U-Pb and Lu-Hf LA ICP-MS analyses of zircon grains from both the main plutonic bodies and cross-cutting felsic dykes, giving emplacement ages of ca. 3.45 Ga for the plutons and ca. 3.2 Ga for the later dykes. The thermal evolution of the Stolzburg block post-emplacement is studied by U-Pb and Rb-Sr LA ICP-MS analyses of apatite, combined with trace-element analyses of (igneous and metamorphic) accessory minerals, revealing a polymetamorphic history of the Stolzburg block with heating events at ca. 3.2, 3.1 and 2.8 Ga.

[1] Van Kranendonk (2015) Geol. Sco. London Spec. Pub. **389**, 83-111. [2] Stevens & Moyen (2007) Dev. Prec. Geol. **15** 669-698

Thermal History of the Stolzburg Pluton, Barberton Granitoid Greenstone Terrain, South Africa

M. Mühlberg[a,b], G. Stevens[a], J.F. Moyen[b], C. Lana[c], A.F.M. Kisters[a], E. Bruand[d]

[a]Department of Earth Sciences, University of Stellenbosch, Private Bag X1, Matieland 7602, South Africa
[b]Université de Lyon, Laboratoire Magmas et Volcans, UJM-UCA-CNRS-IRD, 23 rue Dr. Paul Michelon, 42023 Saint Etienne, France
[c]Departamento de Geologia (DEGEO), Universidade Federal de Ouro Preto, Morro do Cruzeiro, Ouro Preto, Minas Gerais, Brazil
[d]Université de Lyon, Laboratoire Magmas et Volcans, UJM-UCA-CNRS-IRD, 6 avenue Blaise Pascal, 63178 Aubiere, France

Geology of the BGGT

- Deformed sequence of mafic-ultramafic and subordinate felsic (meta-) volcanic rocks and (meta-) sedimentary rocks (Fig. 1)
- Surrounded by ca. 3.5 to 3.2 Ga Tonalite-Trondhjemite-Granodiorite (TTG) and ca. 3.1 Granodiorite-Monzogranite-Syenogranite (GMS) plutons
- Study area: Stolzburg block; ca. 3.45 Ga Trondhjemite plutons and ca. 3.5 Ga ultramafic metavolcanic rocks (Fig. 2)
- Reported metamorphic conditions: Amphibolite facies (e.g. [1])

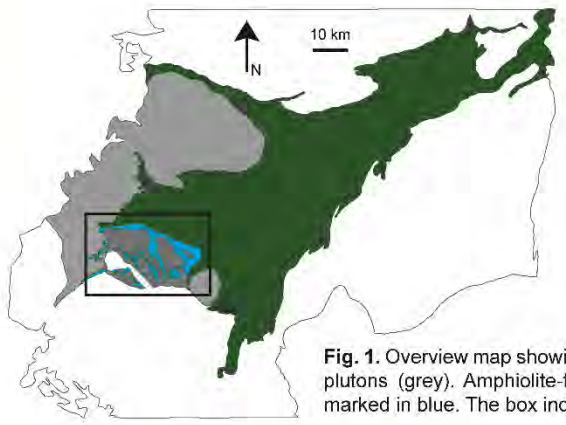

Fig. 1. Overview map showing the Barberton Greenstone Belt (BGB; green) and adjecent TTG plutons (grey). Amphiolite-facies metamorphic rocks of the Lower Onverwacht Group are marked in blue. The box indicated the study area shown in Figure 2.

Geodynamic debate

- Nature of Archean geodynamic process subject of debate
- End-member models:
  - Vertical tectonics / partial convective overturn (e.g. [2])
  - Early plate tectonics (e.g. [3])
- Thermal history crucial for understanding the geodynamic setting

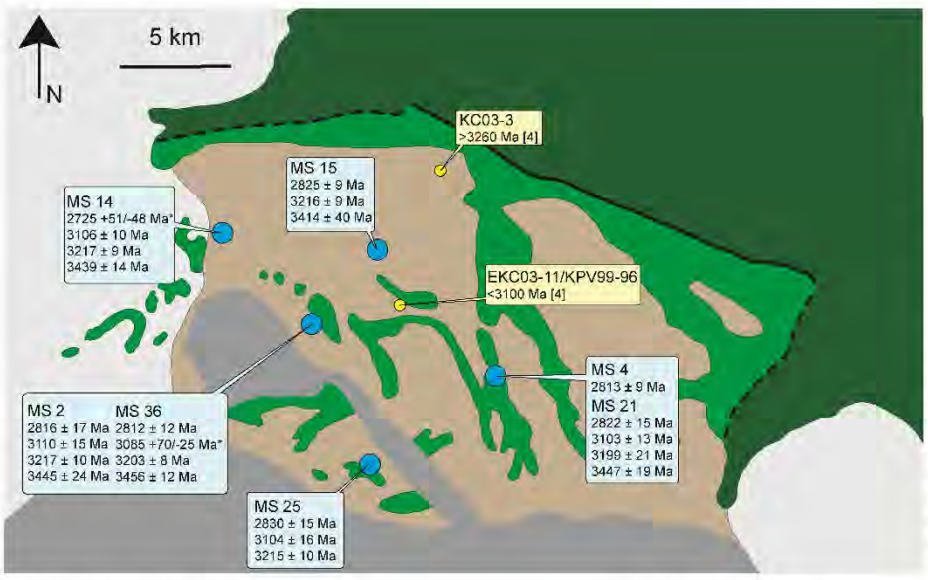

Samples

- Main Trondhjemite of the Stolzburg (MS 2, 14, 15) and Honingklip (MS 4) plutons
- Thin Tonalite phase of the Stolzburg pluton (MS 36)
- Mafic schist enclave within the Honingklip pluton (MS 21)
- Diorite cutting the Weergevonden pluton (MS 25)

Left: **Fig. 2.** Geological map of the Stolzburg block. Legend: BGB undifferentiated (dark green), lower Onverwacht formation (light green), ca. 3.45 TTG (brown), ca. 3.2 TTG (light grey), ca. 3.1 GMS (dark grey). Dates are weighted mean $^{207}Pb/^{206}Pb$ apatite dates (*upper intercept age)

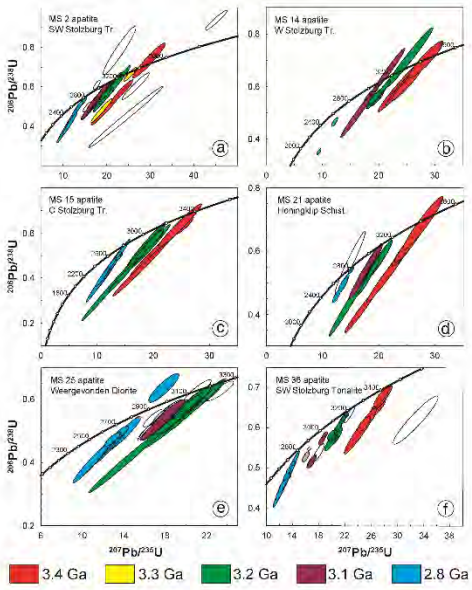

Right: **Fig. 3.** U-Pb concordia diagrams for apatite grains from granitoid (a-c, e, f) and meta-sedimentary (d) samples from the Stolzburg block. Error circles are 2σ.

U-Pb apatite dates

- Previous study: only whole-grain analyses
- CL-imaging revealed internal zoning in apatite grains
- At least four distinct age populations identifiable throughout the Stolzburg block (Figs. 2 and 3)
- Includes dates overlapping within error with emplacement age of the Trondhjemite plutons of ca. 3.45 Ga

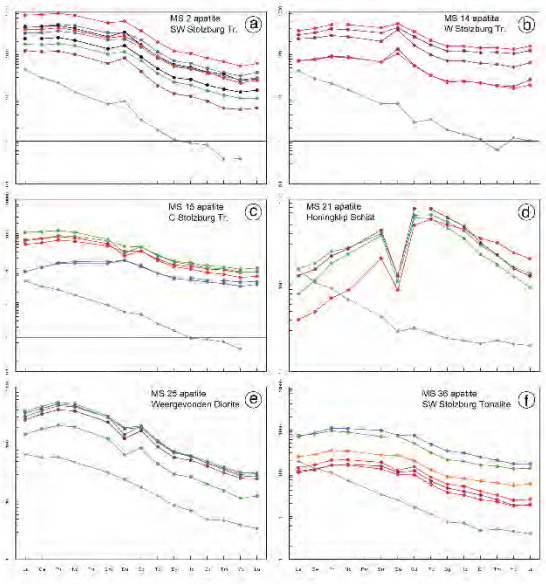

Apatite trace-element analyses

- REE patterns: no differences between the age populations within one samples, slight differences between Trondhjemite samples and Diorite MS25 and mafic schist MS21 (Fig. 4)

Apatite Sr isotopes

- Homogenous within the samples and (±) throughout the Stolzburg block (Fig. 5)

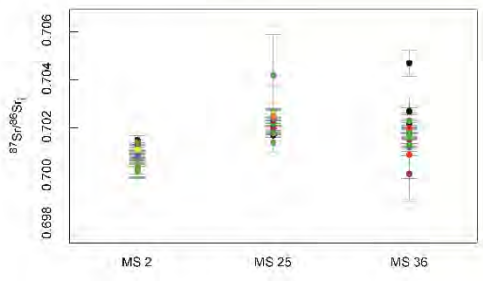

Left: **Fig. 4** Chondrite-normalized rare earth element patterns for apatite grains from the Stolzburg block.
Top: **Fig. 5.** Initial $^{87}Sr/^{86}Sr$ ratios for apatite grains from granitoid samples from the Stolzburg block.
Color coding corresponds to the age populations shown in Fig. 3. Grey circles indicate whole-rock data and back circles analyses that can not be correlated to an age group.

Conclusions

- Preservation of emplacement ages in apatite: No heating above 350-550 °C after emplacement
-> no partial melting of the granitoids of the Stolzburg block post ca. 3.45 Ga

- Apatite grains visibly zoned, age groups distinct
-> Growth by dissolution-precipitation below closure temperature rather than (partial) thermal resetting

- Trace-elements, Sr isotopes: Different age groups indistinguishable from one another
-> "closed" system, not grown from new material brought in post-emplacement

- Ca. 3.2 and 3.1 Ga age populations contemporaneous with local metamorphic (e.g. [1]) and magmatic (e.g. [4, 5]) events
-> Potential water source

- Hydrothermal alteration in agreement with other petrological observations (chloritization of biotite...)

[1] Cutts et al. (2014) *Geol Soc Am Bull* **126** 251-270.
[2] Van Kranendonk (2015) *Geol Soc London Spec Pub* **389**, 83-111.
[3] Stevens & Moyen (2007) *Dev Prec Geol* **15**, 669-698.
[4] Schoene et al. (2008) *Tectonics* **27**, TC5010.
[5] Clemens et al. (2010) *J Petrol* **51** 1099-1120.

UNIVERSITEIT iYUNIVESITHI STELLENBOSCH UNIVERSITY 100 1918 · 2018
saam vorentoe · masiye phambili · forward together

Laboratoire Magmas & Volcans

1876 CUM MENTE ET MALLEO UFOP Universidade Federal de Ouro Preto

CAF Central Analytical Facilities STELLENBOSCH UNIVERSITY

Poster presentation at the (virtual) Journée de la recherche, École Doctorale Sciences Ingénierie Santé (EDSIS), Université de Lyon, June 2020. Englisch version.

The backbone of Earth's first continents

M. Mühlberg[a,b], G. Stevens[a], J.F. Moyen[b], C. Lana[c], A.F.M. Kisters[a]

[a] Department of Earth Sciences, University of Stellenbosch, Private Bag X1, Matieland 7602, South Africa
[b] Université de Lyon, LGL-TPE, UJM-UCLB-ENSL-CNRS, 23 rue Dr. Paul Michelon, 42023 Saint Etienne, France
[c] Departamento de Geologia (DEGEO), Universidade Federal de Ouro Preto, Morro do Cruzeiro, Ouro Preto, Minas Gerais, Brazil

Fig. 1 (above). From makro to micro: (a) location of the Kaapvaal Craton and the study area -> (b) study area, the Stolzburg Block -> (b) outcrop -> (c) sample -> (d) thin section -> (e) apatite and (f) zircon crystals

Fig. 2 (right). The principle behind thermochronology of apatite $[Ca_5(PO_4)_3(OH,F,Cl]$ and zircon $[ZrSiO_4]$, the closure temperature (Tc). Some Ca in apatite and some Zr in zircon can be replaced by U, which decays into lead at a half life of ca. 4.47 billion years for ^{238}U and ca. 704 million years (Ma) for ^{235}U. Above Tc, the crystals equilibrate with their surroundings and Pb is lost. When a crystal cools below Tc, the isotopic clock starts ticking, and the age obtained by isotope analysis reflects that time. Metamorphic crystals can grow beneath Tc, but can be identified with the electron microscope (Fig. 1f+g).

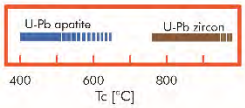

Fig. 3 (below). (a) Results of the U-Pb isotope analyses of apatite and zircon crystals. Zircon ages are ca. 3450 Ma for magmatic grains and ca. 3200 Ma for metamorphic grains. Apatite ages occur in four groups at ca. 3450, 3210, 3105 and 2820 Ma. (b) Interpretation of the apatite thermochronology: After crystallization at ca. 3450 Ma, the apatite grains record multiple heating events, but never did the temperatures exceed ca. 600 °C. Modified after Mühlberg et al., 2021.

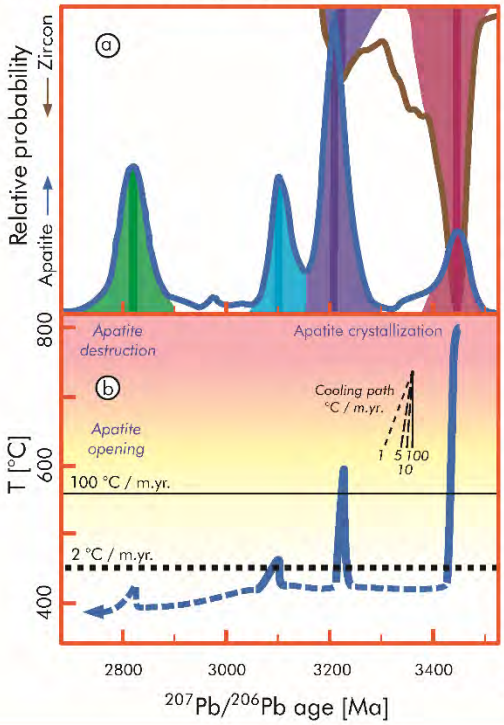

The processes that build the Earth's first continents are still disputed amongst geologists. The ways in which the Earth's crust can deform is controlled by its thermal state. In this study, the thermal state of one of the oldest parts of Earth's continental crust - the Kaapvaal Craton, which now forms part of southern Africa (Fig. 1) - is investigated using uranium-lead (U-Pb) thermochronology of apatite and zircon (Fig. 2).

The results of the U-Pb isotope analyses show, that after crystallization of the rock from a magma at ca. 3450 Ma, the rocks have experienced multiple heating events crystallizing apatite (Fig. 3a). The preservation of magmatic apatite indicates, that the rocks have not been heated above ca. 600 °C after ca. 3450 Ma (Fig. 3b). The Stolzburg Block stayed moderately cool (Figs. 3b, 4), forming a rigid nucleus - the stiff backbone - around which the Kaapvaal Craton was built. The findings of this study help to understand the processes on the early Earth and evaluate the validity of geotectonic models.

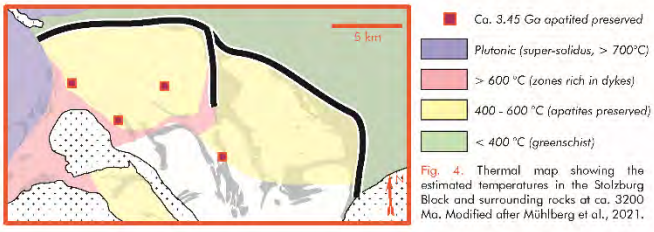

Fig. 4. Thermal map showing the estimated temperatures in the Stolzburg Block and surrounding rocks at ca. 3200 Ma. Modified after Mühlberg et al., 2021.

Mühlberg, M., Stevens, G., Moyen, J.-F., Kisters, A.F.M., Lana, C., 2021. Thermal evolution of the Stolzburg Block, Barberton granitoid-greenstone terrain, South Africa: Implications for Paleoarchean tectonic processes. Precambrian Research 359C, 106082.

Poster presentation at the (virtual) Journée de la recherche, École Doctorale Sciences Ingénierie Santé (EDSIS), Université de Lyon, June 2020. French version.

L'épine dorsale des premiers continents apparus sur Terre

M. Mühlberg [a,b], G. Stevens [a], J.F. Moyen [b], C. Lana [c], A.F.M. Kisters [a]

[a] Department of Earth Sciences, University of Stellenbosch, Private Bag X1, Matieland 7602, South Africa
[b] Université de Lyon, LGL-TPE, UJM-UCLB-ENSL-CNRS, 23 rue Dr. Paul Michelon, 42023 Saint Etienne, France
[c] Departamento de Geologia (DEGEO), Universidade Federal de Ouro Preto, Morro do Cruzeiro, Ouro Preto, Minas Gerais, Brazil

Fig. 1 (dessus). Du macro au micro: (a) localisation du Kaapvaal Craton et de la zone d'étude -> (b) zone d'étude, le Stolzburg Block -> (c) affleurement -> (d) échantillon -> (e) lame mince -> cristaux d'apatite (f) et de zircon (g)

Fig. 2 (à droite). Thermochronologie: température de fermeture ("closure temperature", Tc) pour l'apatite [$Ca_5(PO_4)_3(OH,F,Cl)$] et le zircon [$ZrSiO_4$]. Le Ca dans l'apatite et le Zr dans le zircon sont remplacés par l'uranium (U), qui se désintègre en plomb (Pb) à une demi-vie d'environ 4,47 milliards d'années (Ga) pour ^{238}U (-> ^{206}Pb) et d'environ 704 millions d'années (Ma) pour ^{235}U (-> ^{207}Pb). Au-dessus de Tc, les cristaux s'équilibrent avec leur environnement et le Pb est perdu. Lorsqu'un cristal se refroidit en dessous de Tc, l'horloge isotopique est remise à zéro et l'âge obtenu par l'analyse isotopique reflète ce temps. Les cristaux métamorphiques peuvent se développer en-dessous de Tc et peuvent être identifier au microscope électronique (Fig. 1f, g).

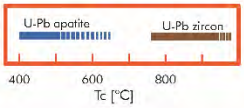

Fig. 3 (dessous). (a) Résultats des analyses isotopiques U-Pb des cristaux d'apatite et de zircon. Les âges du zircon sont d'environ 3450 Ma pour les grains magmatiques et d'environ 3200 Ma pour les grains métamorphiques. Les âges de l'apatite définissent quatre groupes à env. 3450, 3210, 3105 et 2820 Ma. (b) Interprétation de la thermochronologie sur apatite: après cristallisation à env. 3450 Ma, les grains d'apatite enregistrent de multiples événements thermiques, mais les températures ne dépassent jamais env. 600 °C. Modifié d'après Möhlberg et al., 2021.

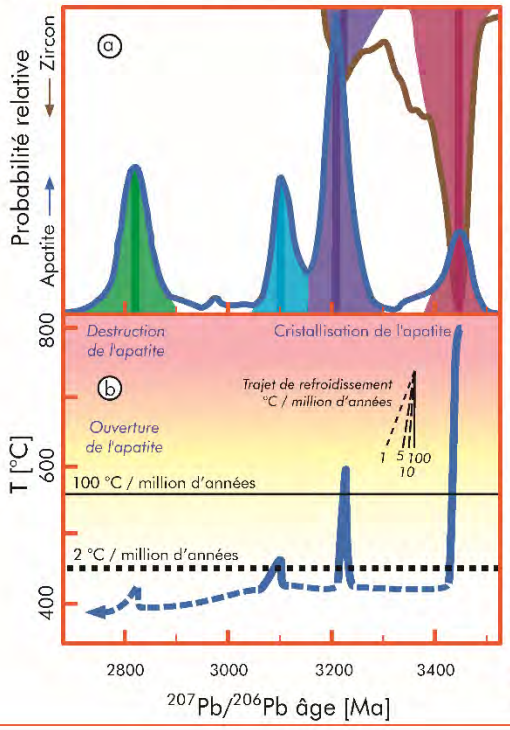

Les processus qui construisent les premiers continents terrestres sont toujours sujet à débat. La façon dont la croûte terrestre peut se déformer est contrôlée par son état thermique. Dans cette étude, l'état thermique de l'une des parties les plus anciennes de la croûte continentale de la Terre - le Kaapvaal Craton, qui fait maintenant partie de l'Afrique australe (Fig. 1) - est étudiée à l'aide de la thermochronologie uranium-plomb (U-Pb) sur apatite et zircon (Fig. 2).

Les résultats des analyses isotopiques U-Pb montrent qu'après cristallisation des roches magmatiques à env. 3450 Ma, les roches ont subi de multiples événements thermiques favorisant la croissance de l'apatite (Fig. 3a). La préservation de l'apatite magmatique indique que les roches n'ont pas allées au-delà d'un maximum d'env. 600 °C après la cristallisation (Fig. 3b). Le Stolzburg Block est resté modérément froid (Figs. 3b, 4), formant un noyau rigide - l'épine dorsale rigide - autour duquel le Kaapvaal Craton s'est construit. Les résultats de cette étude aident à comprendre les processus de la Terre primitive et à évaluer la validité des modèles géotectoniques.

Fig. 4. Carte thermique montrant les températures estimées dans le Stolzburg Block et les roches environnantes à env. 3200 Ma. Modifié d'après Möhlberg et al., 2021.

Möhlberg, M., Stevens, G., Moyen, J.-F., Kisters, A.F.M., Lana, C., 2021. Thermal evolution of the Stolzburg Block, Barberton granitoid-greenstone terrain, South Africa: Implications for Paleoarchean tectonic processes. Precambrian Research 359C, 106082.